



INSIGHTS INTO NEW STRATEGIES TO COMBAT BIOFILMS

EDITED BY: Sujogya Kumar Panda, Silvia Buroni,
Luis Cláudio Nascimento da Silva and Vishvanath Tiwari
PUBLISHED IN: Frontiers in Microbiology



frontiers

Frontiers eBook Copyright Statement

The copyright in the text of individual articles in this eBook is the property of their respective authors or their respective institutions or funders. The copyright in graphics and images within each article may be subject to copyright of other parties. In both cases this is subject to a license granted to Frontiers.

The compilation of articles constituting this eBook is the property of Frontiers.

Each article within this eBook, and the eBook itself, are published under the most recent version of the Creative Commons CC-BY licence.

The version current at the date of publication of this eBook is CC-BY 4.0. If the CC-BY licence is updated, the licence granted by Frontiers is automatically updated to the new version.

When exercising any right under the CC-BY licence, Frontiers must be attributed as the original publisher of the article or eBook, as applicable.

Authors have the responsibility of ensuring that any graphics or other materials which are the property of others may be included in the CC-BY licence, but this should be checked before relying on the CC-BY licence to reproduce those materials. Any copyright notices relating to those materials must be complied with.

Copyright and source acknowledgement notices may not be removed and must be displayed in any copy, derivative work or partial copy which includes the elements in question.

All copyright, and all rights therein, are protected by national and international copyright laws. The above represents a summary only. For further information please read Frontiers' Conditions for Website Use and Copyright Statement, and the applicable CC-BY licence.

ISSN 1664-8714

ISBN 978-2-88971-617-3

DOI 10.3389/978-2-88971-617-3

About Frontiers

Frontiers is more than just an open-access publisher of scholarly articles: it is a pioneering approach to the world of academia, radically improving the way scholarly research is managed. The grand vision of Frontiers is a world where all people have an equal opportunity to seek, share and generate knowledge. Frontiers provides immediate and permanent online open access to all its publications, but this alone is not enough to realize our grand goals.

Frontiers Journal Series

The Frontiers Journal Series is a multi-tier and interdisciplinary set of open-access, online journals, promising a paradigm shift from the current review, selection and dissemination processes in academic publishing. All Frontiers journals are driven by researchers for researchers; therefore, they constitute a service to the scholarly community. At the same time, the Frontiers Journal Series operates on a revolutionary invention, the tiered publishing system, initially addressing specific communities of scholars, and gradually climbing up to broader public understanding, thus serving the interests of the lay society, too.

Dedication to Quality

Each Frontiers article is a landmark of the highest quality, thanks to genuinely collaborative interactions between authors and review editors, who include some of the world's best academicians. Research must be certified by peers before entering a stream of knowledge that may eventually reach the public - and shape society; therefore, Frontiers only applies the most rigorous and unbiased reviews.

Frontiers revolutionizes research publishing by freely delivering the most outstanding research, evaluated with no bias from both the academic and social point of view. By applying the most advanced information technologies, Frontiers is catapulting scholarly publishing into a new generation.

What are Frontiers Research Topics?

Frontiers Research Topics are very popular trademarks of the Frontiers Journals Series: they are collections of at least ten articles, all centered on a particular subject. With their unique mix of varied contributions from Original Research to Review Articles, Frontiers Research Topics unify the most influential researchers, the latest key findings and historical advances in a hot research area! Find out more on how to host your own Frontiers Research Topic or contribute to one as an author by contacting the Frontiers Editorial Office: frontiersin.org/about/contact

INSIGHTS INTO NEW STRATEGIES TO COMBAT BIOFILMS

Topic Editors:

Sujogya Kumar Panda, KU Leuven, Belgium

Silvia Buroni, University of Pavia, Italy

Luis Cláudio Nascimento da Silva, Universidade Ceuma, Brazil

Vishvanath Tiwari, Central University of Rajasthan, India

Citation: Panda, S. K., Buroni, S., Nascimento da Silva, L. C., Tiwari, V., eds. (2021).
Insights into New Strategies to Combat Biofilms. Lausanne: Frontiers Media SA.
doi: 10.3389/978-2-88971-617-3

Table of Contents

- 06 Editorial: Insights Into New Strategies to Combat Biofilms**
Sujogya Kumar Panda, Silvia Buroni, Vishvanath Tiwari and Luis Cláudio Nascimento da Silva
- 11 RAFT-Derived Polymethacrylates as a Superior Treatment for Recurrent Vulvovaginal Candidiasis by Targeting Biotic Biofilms and Persister Cells**
Xueqing Wu, Sisi Zhang, Xinxin Xu, Laien Shen, Boyun Xu, Wenzhen Qu, Wenyi Zhuang, Katherine Locock, Margaret Deighton and Yue Qu
- 22 A New Antibiotic-Loaded Sol-Gel Can Prevent Bacterial Prosthetic Joint Infection: From in vitro Studies to an in vivo Model**
John Jairo Aguilera-Correa, Amaya Garcia-Casas, Aranzazu Mediero, David Romera, Francisca Mulero, Irene Cuevas-López, Antonia Jiménez-Morales and Jaime Esteban
- 36 The β -Lactamase Inhibitor Boronic Acid Derivative SM23 as a New Anti-Pseudomonas aeruginosa Biofilm**
Samuele Peppoloni, Eva Pericolini, Bruna Colombari, Diego Pinetti, Claudio Cermelli, Francesco Fini, Fabio Prati, Emilia Caselli and Elisabetta Blasi
- 47 In vitro Mixed Biofilm of Streptococcus suis and Actinobacillus pleuropneumoniae Impacts Antibiotic Susceptibility and Modulates Virulence Factor Gene Expression**
Yang Wang, Shenglong Gong, Xiao Dong, Jinpeng Li, Daniel Grenier and Li Yi
- 55 Effect of Dalbavancin on Staphylococcal Biofilms When Administered Alone or in Combination With Biofilm-Detaching Compounds**
Miglė Žiemytė, Juan C. Rodríguez-Díaz, María P. Ventero, Alex Mira and María D. Ferrer
- 66 Cannabigerol Prevents Quorum Sensing and Biofilm Formation of Vibrio harveyi**
Muna Aqawi, Ruth Gallily, Ronit Vogt Sionov, Batya Zaks, Michael Friedman and Doron Steinberg
- 79 Hyperosmotic Infusion and Oxidized Surfaces Are Essential for Biofilm Formation of Staphylococcus capitis From the Neonatal Intensive Care Unit**
Yue Qu, Yali Li, David R. Cameron, Christopher D. Easton, Xuebo Zhu, Minli Zhu, Mario Salwiczek, Benjamin W. Muir, Helmut Thissen, Andrew Daley, John S. Forsythe, Anton Y. Peleg and Trevor Lithgow
- 91 A Rational Designed PslG With Normal Biofilm Hydrolysis and Enhanced Resistance to Trypsin-Like Protease Digestion**
Tiantian Su, Jing He, Ningna Li, Shiheng Liu, Sujuan Xu and Lichuan Gu
- 100 Piperine Impedes Biofilm Formation and Hyphal Morphogenesis of Candida albicans**
Arumugam Priya and Shunmugiah Karutha Pandian
- 118 Fighting Mixed-Species Microbial Biofilms With Cold Atmospheric Plasma**
Yifan Rao, Weilong Shang, Yi Yang, Renjie Zhou and Xiancai Rao

- 129 ***Innovative Strategies Toward the Disassembly of the EPS Matrix in Bacterial Biofilms***
Rita M. Pinto, Filipa A. Soares, Salette Reis, Cláudia Nunes and Patrick Van Dijck
- 149 ***Anti-biofilm and Antibacterial Activities of Silver Nanoparticles Synthesized by the Reducing Activity of Phytoconstituents Present in the Indian Medicinal Plants***
Yugal Kishore Mohanta, Kunal Biswas, Santosh Kumar Jena, Abeer Hashem, Elsayed Fathi Abd_Allah and Tapan Kumar Mohanta
- 164 ***Corrigendum: Anti-biofilm and Antibacterial Activities of Silver Nanoparticles Synthesized by the Reducing Activity of Phytoconstituents Present in the Indian Medicinal Plants***
Yugal Kishore Mohanta, Kunal Biswas, Santosh Kumar Jena, Abeer Hashem, Elsayed Fathi Abd_Allah and Tapan Kumar Mohanta
- 165 ***Monoclonal Antibodies Specific to the Extracellular Domain of Histidine Kinase YycG of Staphylococcus epidermidis Inhibit Biofilm Formation***
Zhihui Lyu, Yongpeng Shang, Xiaofei Wang, Yang Wu, Jinxin Zheng, Huayong Liu, Ting Gong, Lina Ye and Di Qu
- 178 ***Antimicrobial Peptide Cec4 Eradicates the Bacteria of Clinical Carbapenem-Resistant Acinetobacter baumannii Biofilm***
Weiwei Liu, Zhaoying Wu, Chengju Mao, Guo Guo, Zhu Zeng, Ying Fei, Shan Wan, Jian Peng and Jianwei Wu
- 191 ***Sodium New Houttuynia Inhibits Candida albicans Biofilm Formation by Inhibiting the Ras1-cAMP-Efg1 Pathway Revealed by RNA-seq***
Jiadi Wu, Daqiang Wu, Yeye Zhao, Yuanqing Si, Longfei Mei, Jing Shao, Tianming Wang, Guiming Yan and Changzhong Wang
- 212 ***Antifungal Photodynamic Activity of Hexyl-Aminolevulinate Ethosomes Against Candida albicans Biofilm***
Yingzhe Wang, Jinru Song, Feiyin Zhang, Kang Zeng and Xiaoliang Zhu
- 219 ***Glabridin Averts Biofilms Formation in Methicillin-Resistant Staphylococcus aureus by Modulation of the Surfaceome***
Bhavana Gangwar, Santosh Kumar and Mahendra P. Darokar
- 234 ***Antimicrobial Hypochlorous Wound Irrigation Solutions Demonstrate Lower Anti-biofilm Efficacy Against Bacterial Biofilm in a Complex in-vitro Human Plasma Biofilm Model (hpBIOM) Than Common Wound Antimicrobials***
Julian-Dario Rembe, Lioba Huelsboemer, Isabell Plattfaut, Manuela Besser and Ewa K. Stuermer
- 247 ***Antimicrobial Potential of Streptomyces ansochromogenes (PB₃) Isolated From a Plant Native to the Amazon Against Pseudomonas aeruginosa***
Erika Alves da Fonseca Amorim, Erima Jousiely Mendonça Castro, Viviane da Silva Souza, Mateus Silva Alves, Léo Ruben Lopes Dias, Maycon Henrique Franzi Melo, Ilana Mirian Almeida da Silva, Paulo Cesar Mendes Villis, Maria Rosa Quaresma Bonfim, Angela Falcai, Maria Raimunda Chagas Silva, Valério Monteiro-Neto, Amanda Aliança, Luís Cláudio Nascimento da Silva and Rita de Cássia Mendonça de Miranda
- 258 ***Natural Anti-biofilm Agents: Strategies to Control Biofilm-Forming Pathogens***
Rojita Mishra, Amrita Kumari Panda, Surajit De Mandal, Muhammad Shakeel, Satpal Singh Bisht and Junaid Khan

- 281 Antibacterial Activity of Cinnamomum camphora Essential Oil on Escherichia coli During Planktonic Growth and Biofilm Formation**
Lei Wang, Kang Zhang, Kai Zhang, Jingyan Zhang, Jingjing Fu, Jie Li, Guibo Wang, Zhengying Qiu, Xuezhi Wang and Jianxi Li
- 292 Maipomycin A, a Novel Natural Compound With Promising Anti-biofilm Activity Against Gram-Negative Pathogenic Bacteria**
Junliang Zhang, Xiaoyan Liang, Shiling Zhang, Zhiman Song, Changyun Wang and Ying Xu
- 302 Recent Advances in a Polydopamine-Mediated Antimicrobial Adhesion System**
Indu Singh, Gagan Dhawan, Seema Gupta and Pradeep Kumar
- 319 A Study of the Disruptive Effect of the Acetate Fraction of Punica granatum Extract on Cryptococcus Biofilms**
Paulo C. M. Villis, Alessandra T. de Macedo, Haryne L. A. Furtado, Pedro H. C. Fontenelle, Ingrid S. Gonçalves, Thayariane L. Mendes, Brenda L. A. Motta, Pedro L. L. Marinho, Aruanã J. M. C. R. Pinheiro, Lídio G. Lima-Neto, Cristina A. Monteiro, Luís C. N. da Silva, Gabriella F. Ferreira, Rodrigo A. Holanda and Julliana R. A. Santos
- 332 Antibiofilm Activity of Small-Molecule ZY-214-4 Against Staphylococcus aureus**
Jingyi Yu, Lulin Rao, Lingling Zhan, Yan Zhou, Yinjuan Guo, Xiaocui Wu, Zengqiang Song and Fangyou Yu
- 341 The Bactericidal Tandem Drug, AB569: How to Eradicate Antibiotic-Resistant Biofilm Pseudomonas aeruginosa in Multiple Disease Settings Including Cystic Fibrosis, Burns/Wounds and Urinary Tract Infections**
Daniel J. Hassett, Rhett A. Kovall, Michael J. Schurr, Nalinikanth Kotagiri, Harshita Kumari and Latha Satish
- 358 Characterization of Binary Biofilms of Listeria monocytogenes and Lactobacillus and Their Response to Chlorine Treatment**
Magdalena A. Olszewska and Francisco Diez-Gonzalez



Editorial: Insights Into New Strategies to Combat Biofilms

Sujogya Kumar Panda^{1*}, Silvia Buroni², Vishvanath Tiwari³ and Luis Cláudio Nascimento da Silva⁴

¹ Center of Environment Climate Change and Public Health, RUSA 2.0, Utkal University, Bhubaneswar, India, ² Department of Biology and Biotechnology, University of Pavia, Pavia, Italy, ³ Department of Biochemistry, Central University of Rajasthan, Ajmer, India, ⁴ Laboratory of Microbial Pathogenesis, Universidade Ceuma, São Luis, Brazil

Keywords: antimicrobials, biofilm, drug discovery, EPS matrix, ESKAPE, peptides, quorum sensing

Editorial on the Research Topic

Insights Into New Strategies to Combat Biofilms

Biofilms form a complex layer with defined structures, that attach on biotic or abiotic surfaces, are tough to eradicate and tend to cause some resistance against most antibiotics (Sahoo et al., 2021). Although they occur on all kinds of surfaces in the outside environment, biofilms become problematic due to their ability to colonize the human body (60–80% of all infections are due to biofilm). Several studies confirmed that biofilm-producing bacteria are typically much less sensitive to antimicrobials than planktonic cells (Sahoo et al., 2021; Van Puyvelde et al., 2021). The rapid rising of antimicrobial resistance, and the need for new approaches to fill the gap in antimicrobial drug discovery are alarming (Jouneghani et al., 2020) due to the scarcity of effective drugs to combat the formation of biofilm infections and the need for drug discovery efforts to overcome this challenge (Kipanga et al., 2020). One of the strategies is to increase multi-targeted or combinatorial therapies to fight the multifactorial nature of biofilm development. Among bacteria, several pathogenic species are highlighted by their biofilm potential, such as those belonging to the genus *Acinetobacter*, *Pseudomonas*, *Vibrio*, *Listeria*, *Staphylococcus*, *Streptococcus*, *Streptomyces*, etc. Similarly, fungi, such as *Candida* and *Cryptococcus*, are also capable of forming biofilms. The focus of this Research Topic is to make a special contribution to the discovery of novel compounds to combat biofilm both for bacteria and fungi. This special issue consists of 27 articles covering diverse topics.

OPEN ACCESS

Edited by:

Natalia V. Kirienko,
Rice University, United States

Reviewed by:

Sang-Do Ha,
Chung-Ang University, South Korea

*Correspondence:

Sujogya Kumar Panda
sujogypanda@utkaluniversity.ac.in

Specialty section:

This article was submitted to
Antimicrobials, Resistance and
Chemotherapy,
a section of the journal
Frontiers in Microbiology

Received: 16 July 2021

Accepted: 30 August 2021

Published: 23 September 2021

Citation:

Panda SK, Buroni S, Tiwari V and
Nascimento da Silva LC (2021)
Editorial: Insights Into New Strategies
to Combat Biofilms.
Front. Microbiol. 12:742647.
doi: 10.3389/fmicb.2021.742647

ANTI-STAPHYLOCOCCAL AND ANTI-BIOFILM COMPOUNDS

Staphylococcus aureus is a very common pathogen and the evolution of antibiotic resistance in this bacterium has shown that there is no long-lasting remedy especially for hospital-acquired infections. A wound infection by methicillin-resistant *S. aureus* (MRSA) may lead to sepsis and even to death (Panda et al., 2020).

Biofilm-associated infections are one of the major concerns for the healthcare system. Most of the current therapies available are mainly focused on the biocidal approach. Pinto et al. highlighted the strategies to target and disrupt extracellular polymeric substances (EPS). They suggested to use matrix disruptive agents, nanocarriers, magnetic fields, photodynamic therapy, and ultrasounds to control the EPS of biofilms. They propose that a synergistic approach between antibiotics and EPS disruptors can completely eradicate biofilms.

Rembe et al. studied the efficacy of three hypochlorous irrigation solutions against bacteria such as *S. aureus*, Methicillin-Resistant *S. aureus* (MRSA) and *Pseudomonas aeruginosa* using an

advanced complex *in-vitro* human plasma biofilm model (hpBIOM). With the help of scanning electron microscopy (SEM), these authors concluded that both reference agents (polyhexanide and octenidine dihydrochloride/phenoxyethanol) induced complete eradication of *P. aeruginosa* and MRSA biofilms after 72 h compared to other tested hypochlorous wound irrigation solutions. The complex hpBIOM model mimics the highly challenging clinical wound micro-environment, providing a profound base for future clinical translation (Rembe et al.).

In a very elegant research, Gangwar et al. studied for the first time the activity of glabridin (C₂₀H₂₀O₄, an isoflavane commonly present on *Glycyrrhiza glabra* root) against biofilm formation of MRSA strains. Crystal violet assay and SEM results suggested that glabridin prevents the formation of cell clusters and the attachment of MRSA to the surface in a dose dependent manner. Further studies on proteomic analysis of biofilm matrix by LC-ESI-QTOF confirmed the involvement of several proteins in cells adhesion, such as fibronectin binding proteins (FnBA, FnBB), serine-aspartate repeat-containing protein D (SdrD), immunoglobulin-binding protein G (Sbi), and other virulence factors. Moreover, several moonlighting proteins, such as translation elongation factors (EF-Tu, EF-G), chaperone protein (DnaK), glyceraldehyde 3-phosphate dehydrogenase (GAPDH), and pyruvate kinase (PK) were detected on the cell surface, while their presence was inversely proportional to surface-associated adhesins. The results obtained from this interesting study suggested that glabridin prevents biofilm formation in *S. aureus* through modulation of the cell surface proteins (Gangwar et al.).

Another study conducted by Yu et al. investigated the inhibitory effect of the novel small-molecule ZY-214-4 (C₁₉H₁₁BrNO₄) on a clinical *S. aureus* isolates having biofilm formation ability (confirmed by SEM). This compound significantly suppressed the production of polysaccharides, intercellular adhesion, cell aggregation, as well as inhibited the expression of *icaA* and other biofilm-related genes (*eno*, *clfA/B*, *fnbB*, *fib*, *ebpS*, *psmA*, and *psmβ*). Authors claim ZY-214-4 as a potent antimicrobial compound highlighting its clinical potential for preventing or treating *S. aureus* infections.

Staphylococcus epidermidis is a Gram-positive bacterium frequently associated with biofilm-related infections. The biofilm formation in this bacterium is mediated by the YycG/YycF two-component system, making YycG kinase an attractive therapeutic target. Lyu et al. developed monoclonal antibodies toward to the extracellular domain of the histidine kinase YycG. Both mAbs exhibited dose-dependent inhibition of *S. epidermidis* biofilm formation. The antibodies induced a marked decrease in the synthesis of polysaccharide intercellular adhesin and in the transcriptional level of genes encoding proteins involved in biofilm formation (Lyu et al.).

Dalbavancin (a recently developed lipoglycopeptide antibiotic), is highly effective to prevent staphylococcal (*S. aureus* and *S. epidermidis*) biofilm formation compared to other four antibiotics (linezolid, vancomycin, cloxacillin, and rifampicin). Further experiments were undertaken to check whether biofilm-detaching compounds, such as *N*-acetylcysteine (NAC) and ficin could enhance dalbavancin efficiency. Real-time dose-response experiments showed that dalbavancin is a potent

compound preventing staphylococcal biofilm formation. Other exciting results showed that the addition of NAC decreased the efficacy of dalbavancin, while the addition of ficin enhanced its efficacy (Žiemyte et al.). The authors conclude their data support the use of dalbavancin as a favorable antimicrobial compound to treat staphylococcal biofilm infections.

As regarding other Gram-positive bacteria, the work by Qu et al. studied the ability of *Staphylococcus capitis*, an opportunistic pathogen responsible for bloodstream infections in the neonatal intensive care units and able to grow on indwelling central venous catheters, to form biofilms. The authors showed that this bacterium initiated biofilm formation only in response to hyperosmotic conditions. Biofilm development was strongly influenced by the presence of the element oxygen on the surface. On the other hand, a lack of oxidized carbon species on the surface prevented the formation of mature biofilms. Together, this information will be used to suggest guidelines for the preparation of hyperosmolar parenteral nutrition and the engineering of surfaces to minimize the risk of catheter-mediated infections due to *S. capitis*.

ANTI-PSEUDOMONAL AND ANTI-BIOFILM COMPOUNDS

Among pathogens able to form biofilm, *Pseudomonas aeruginosa* is one of the most life-threatening, being able to colonize both biotic and abiotic surfaces, including contact lenses, catheters and various medical implants (O'Toole et al., 2000). Interestingly, Su et al. reported that a glycosyl hydrolase produced by this microorganism itself is able to inhibit and disperse biofilms. In particular, they described a mutated version of the hydrolase which is resistant to the action of human secreted proteases, such as trypsin-like serine proteases. Promising effects against both *P. aeruginosa* biofilm formation and virulence factors production were observed by Peppoloni et al. who described a boronic acid derivative designed as a β-lactamase inhibitor. It showed interesting results also against the production of quorum sensing signal molecules, important global regulator of the expression of virulence factors and of biofilm production. Moreover, the achieved data were confirmed also in a model mimicking clinical settings.

It was seen that *P. aeruginosa* was susceptible to the innate immune response molecule nitric oxide (NO). Hassett et al. discussed the NO-based therapeutics. They explain that AB569 can produce NO and can be an alternative or addition to conventional antibiotic regimens to treat highly problematic MDR bacterial infections. The result shows that NO mediate inactivation of the 4Fe-4S cluster of the master regulator, ANR, and NO or its chemical generators have the ability to kill biofilms. RNA sequencing results showed that exposure to AB569 leads to the decrease in transcription of genes involved in the DNA, RNA, proteins, and ATP synthesis. Antimicrobial tolerance of biofilms has emerged as a significant challenge to healthcare sectors as most synthetic drugs and combination therapy fail to inhibit it. Mishra et al. pointed out that natural product-based anti-biofilm agents like phytochemicals, antimicrobial peptides,

and microbial enzymes can be an option as they interfere in quorum sensing pathways, disrupting EPS and adhesion mechanisms. It is also seen that most natural product fails in phase II and phase III clinical trials due to the limited availability of the compound in humans. Failure of natural medicine in clinical trials can be checked by rigorous quality control, pharmacokinetics and pharmacodynamics, and metabolomics of host before clinical trials.

ANTIBIOFILM COMPOUNDS FROM ENDOPHYTES

Among natural products, a metabolite produced by the endophytic bacterium *Streptomyces ansochromogenes* has been shown to own both antibacterial and anti-biofilm activity against *P. aeruginosa* (Alves da Fonseca Amorim et al.). Maipomycin A (MaiA) is a novel antibiofilm compound purified from *Kibdelosporangium phytohabitans* XY-R10 through a bio-guided assay. This rare actinomycete strain was isolated from the root sediments of a mangrove plant, *Kandelia candel* (L.) Druce. The authors observed that MaiA has anti-biofilm activities against *Acinetobacter baumannii* and *P. aeruginosa*, and these effects were partially related to its iron chelator property. Although MaiA has weak antimicrobial effects, it is able to enhance the efficacy of colistin against *A. baumannii*. The authors conclude that MaiA is an interesting candidate to prevent Gram-negative biofilms (Zhang et al.). It was seen that pathogens that can present either in planktonic form or as biofilms in water-carrying pipelines are the source accountable for the cause of water-borne infections. Protein-based adhesives from marine mussels, a catecholic amino acid i.e., 3,4-dihydroxyphenylalanine (DOPA) can adhere to almost all substances. A novel catechol derivative, dopamine-based coating material, i.e., polydopamine (PDA), has been designed. Singh et al. discussed the potential of PDA to be used as antibacterial nanocoating and explain its various antimicrobial mechanisms. It was seen that antibacterial activity of PDA is due to the catechol that produces semiquinone and quinone that get auto-oxidized in the presence of oxygen, generation of ROS which causes ROS dependent antibacterial activity (Singh et al.).

IN VIVO MODELS AND ANTI-BIOFILM COMPOUNDS

Another interesting study is completed by Wang, Gong et al. who investigate the biological impacts of the interactions between two important pathogens (*Streptococcus suis* and *Actinobacillus pleuropneumoniae*) isolated from pigs suffering from severe respiratory disease. More precisely, the authors described that, when grown in dual-species biofilms, *A. pleuropneumoniae* genes associated with virulence factors, including exotoxins and adhesins, were significantly upregulated, while *S. suis* virulence factor-related genes (*cps2*, *gdh*, *mrp*, and *sly*) were highly induced. The authors conclude that the interspecies interactions between *S. suis* and *A. pleuropneumoniae* may be achieved under specific

conditions and may play a vital role in the disease progression and persistent infection (Wang, Gong et al.).

Aguilera-Correa et al. evaluated the effect of a moxifloxacin-loaded organic-inorganic sol-gel *in vitro* against the formation of different biofilms (*S. aureus*, *S. epidermidis*, and *Escherichia coli*) and *in vivo* in a murine model. The microbiological studies revealed that sol-gel coatings inhibited the biofilm development and were able to treat mature biofilms of all the three bacterial species. In the *in vivo* study, mice weight increased over time, except in the *E. coli*-infected group without coating. Authors conclude that moxifloxacin-loaded sol-gel coating is capable of preventing both *Staphylococcal* and *E. coli* biofilms in prosthetic joint infection.

ANTI-FUNGAL AND ANTI-BIOFILM COMPOUNDS

The development of chronic and recurrent infections by *Candida albicans* is also attributed to biofilm formation and *C. albicans* is the most prevalent human fungal pathogen in both immunocompetent and immunocompromised individuals (Kerkoub et al., 2018). Despite advances in antifungal therapy, *Candida* infections continue to have a major impact on mortality and morbidity, as well as on the duration and cost of hospitalization (Tanwar et al., 2014). In this special issue, some agents targeting *Candida* biofilm and other virulence determinants were also reported, including RAFT-derived polymethacrylates (Wu et al.), sodium new houttuynfonate (SNH) (Wu et al.), and piperine (Priya and Pandian). In another elegant paper, the activity of Hexyl-aminolevulinic acid ethosomes system (HAL-ES) as photosensitizer for antimicrobial photodynamic therapy against *C. albicans* (Wang, Song et al.) was reported. The RAFT-Derived Polymethacrylates were effective in two mouse models of Candidiasis: Vulvovaginal candidiasis (VVC) and recurrent VVC (Wu et al.). The SNH showed *in vitro* anti-*Candida* and anti-biofilm activity, inducing morphological changes during the transition from yeast to hypha. These effects are linked to the down-regulation of several biofilm formation related genes from Ras1-cAMP-Efg1 pathway and up-regulation of in yeast form-associated genes (Wu et al.). SNH also has *in vivo* activity in the infection model using *Galleria mellonella*. Similarly, the piperine, a plant-derived alkaloid molecule, displayed antibiofilm activities against *C. albicans* (shown by confocal laser-scanning microscopy and scanning electron microscopy) and modulated the expression of several biofilm related and hyphal-specific genes. In addition, piperine reduced *in vivo* colonization and prolonged the lifespan of *Caenorhabditis elegans* infected by *C. albicans* without any acute toxicity (Priya and Pandian). Transcriptomic analysis revealed that piperine significantly downregulated the expression of several biofilm related and hyphal-specific genes (*ALS3*, *HWPI*, *EFG1*, *CPH1*, etc.).

Cryptococcus neoformans is another yeast capable of causing life threatening meningoencephalitis in patients with impaired immunity. In a very elegant study, Villis et al. focused on fungal infections caused by *Cryptococcus* genus. Natural products

achieved from the plant *Punica granatum* were investigated for their potential to kill various *Cryptococcus* clinical and environmental isolates and for their activity against pre-formed biofilms, with promising results.

ANTI-QUORUM SENSING AND ANTI-BIOFILM COMPOUNDS

The ability to inhibit the biofilm of *A. baumannii* was also evaluated for Cec4, an antimicrobial peptide known to have antibacterial and immunomodulatory activities (Liu et al.). Cec4 could inhibit the growth and biofilm formation of a set of 200 carbapenem-resistant *A. baumannii* (CRAB). Importantly, the peptide eradicated the formed biofilm by impairing its structure. Further, Cec4 modulated the expression of 185 genes in CRAB biofilm affecting multiple metabolic pathways, such as two-component regulation systems, quorum sensing, and antibiotic synthesis-related pathways (Liu et al.).

As regarding *E. coli*, another main biofilm-associated opportunistic pathogen, the *Cinnamomum camphora* essential oil was shown to be able to kill clinical strains isolated from dairy cows suffering from endometritis, in either planktonic or biofilm growth conditions, during the first 30 min of exposure (Wang, Zhang et al.). Gram-negative bacterium, *Vibrio harveyi*, has been shown to be subjected to the effect of a natural product, Cannabigerol, which is a non-psychoactive cannabinoid naturally present in the Cannabis plant (Aqawi et al.). Indeed, Aqawi et al. described a reduction in the QS-regulated bioluminescence and biofilm formation of *V. harveyi*. In another work, silver nanoparticles (AgNPs) were produced from leaf extracts of *Semecarpus anacardium*, *Glochidion lanceolarium*, and *Bridelia retusa* as new approach to eradicate biofilm formed by *P. aeruginosa*, *E. coli*, and *S. aureus* (Mohanta et al.).

In addition, mixed species biofilms display greater resistance to antibiotics and disinfectants due to physical matrix barrier and physiological interaction. This is one of the major threats to different industries like food and human health. Rao et al. has highlighted the use of cold atmospheric plasma (CAP) to eliminate microbial biofilms by applying it on biotic or abiotic surfaces. They also explain that different microbial factors such as peptidoglycan layer thickness, biofilm thickness, matrix production, etc. affecting the efficacy of the CAP procedure.

REFERENCES

- Jouneghani, R. S., Castro, A. H. F., Panda, S. K., Swennen, R., and Luyten, W. (2020). Antimicrobial activity of selected banana cultivars against important human pathogens, including candida biofilm. *Foods* 9:435. doi: 10.3390/foods9040435
- Kerkoub, N., Panda, S. K., Yang, M.-R., Lu, J.-G., Jiang, Z.-H., Nasri, H., et al. (2018). Bioassay-guided isolation of anti-Candida biofilm compounds from methanol extracts of the aerial parts of *Salvia officinalis* (Annaba, Algeria). *Front. Pharmacol.* 9:1418. doi: 10.3389/fphar.2018.01418
- Kipanga, P. N., Liu, M., Panda, S. K., Mai, A. H., Veryser, C., Van Puyvelde, L., et al. (2020). Biofilm inhibiting properties

To conclude, the present Research Topic includes interdisciplinary research work highlighting the use of several natural derived compounds as future drug candidate. This Research Topic successfully gathered comprehensive interdisciplinary information in the field of drug discovery related to biofilm infections caused by multiple microbial species, such as *S. aureus*, MRSA, *S. capitis*, *S. epidermidis*, *S. suis* (as regarding the Gram-positives); *A. baumannii*, *A. pleuropneumoniae*, *E. coli*, *P. aeruginosa*, *V. harveyi* (for the Gram-negatives). Several studies also include the treatment of fungal biofilm caused by *Candida* and *Cryptococcus* genera. Further, several bioactive compounds were described, as well as *in vivo* studies (*Caenorhabditis elegans*, *Galleria mellonella* and mice models).

This unique collection of articles in the present Research Topic gives new insights into the characterization of biofilm and drug resistance mechanisms as well as provides novel strategies to fight several notorious pathogens.

We would like to thank all the reviewers for their comments that improved our manuscripts, and the authors for their excellent contributions.

Finally, we hope that this collection will further inspire scientists from different research fields to make use of the gathered information to combat biofilm.

AUTHOR CONTRIBUTIONS

All authors listed have made a substantial, direct and intellectual contribution to the work, and approved it for publication.

FUNDING

SB was supported by the Italian Ministry of Education, University and Research (MIUR) (Dipartimenti di Eccellenza, Program 2018–2022) L. Spallanzani, University of Pavia.

ACKNOWLEDGMENTS

SP is thankful to the RUSA 2.0 for supporting ECCPH, Utkal University. VT would also like to thank the SERB, India for EMR grant EMR/2017/001854. LN would like to thank the CNPq (Conselho Nacional de Desenvolvimento Científico e Tecnológico, process number: 312349/2020-3) for the support.

- of compounds from the leaves of *Warburgia ugandensis* Sprague subsp *ugandensis* against *Candida* and *Staphylococcal* biofilms. *J. Ethnopharmacol.* 248:112352. doi: 10.1016/j.jep.2019.112352
- O'Toole, G., Kaplan, H. B., and Kolter, R. (2000). Biofilm formation as microbial development. *Annu. Rev. Microbiol.* 54, 49–79. doi: 10.1146/annurev.micro.54.1.49
- Panda, S. K., Das, R., Lavigne, R., and Luyten, W. (2020). Indian medicinal plant extracts to control multidrug-resistant *S. aureus*, including in biofilms. *South Afr. J. Bot.* 128, 283–291. doi: 10.1016/j.sajb.2019.11019
- Sahoo, A., Swain, S. S., Behera, A., Sahoo, G., Mahapatra, P. K., and Panda, S. K. (2021). Antimicrobial peptides derived from insects offer a novel therapeutic option to combat biofilm: a

- review. *Front. Microbiol.* 12:1077. doi: 10.3389/fmicb.2021.661195
- Tanwar, J., Das, S., Fatima, Z., and Hameed, S. (2014). Multidrug resistance: an emerging crisis. *Interdiscip. Perspect. Infect. Dis.* 2014:541340. doi: 10.1155/2014/541340
- Van Puyvelde, L., Aissa, A., Panda, S. K., De Borggraeve, W. M., Mukazayire, M. J., and Luyten, W. (2021). Bioassay-guided isolation of antibacterial compounds from the leaves of *Tetradenia riparia* with potential bactericidal effects on food-borne pathogens. *J. Ethnopharmacol.* 273:113956. doi: 10.1016/j.jep.2021.113956

Conflict of Interest: The authors declare that the research was conducted in the absence of any commercial or financial relationships that could be construed as a potential conflict of interest.

Publisher's Note: All claims expressed in this article are solely those of the authors and do not necessarily represent those of their affiliated organizations, or those of the publisher, the editors and the reviewers. Any product that may be evaluated in this article, or claim that may be made by its manufacturer, is not guaranteed or endorsed by the publisher.

Copyright © 2021 Panda, Buroni, Tiwari and Nascimento da Silva. This is an open-access article distributed under the terms of the Creative Commons Attribution License (CC BY). The use, distribution or reproduction in other forums is permitted, provided the original author(s) and the copyright owner(s) are credited and that the original publication in this journal is cited, in accordance with accepted academic practice. No use, distribution or reproduction is permitted which does not comply with these terms.



RAFT-Derived Polymethacrylates as a Superior Treatment for Recurrent Vulvovaginal Candidiasis by Targeting Biotic Biofilms and Persister Cells

Xueqing Wu^{1,2†}, Sisi Zhang^{2†}, Xinxin Xu², Laien Shen², Boyun Xu², Wenzhen Qu², Wenyi Zhuang¹, Katherine Locock^{3,4}, Margaret Deighton⁵ and Yue Qu^{6,7*}

¹ The Division of Gynecology, Shenzhen University General Hospital, Shenzhen, China, ² Department of Obstetrics and Gynecology, Wenzhou Medical University, Wenzhou, China, ³ CSIRO Manufacturing Flagship, Clayton, VIC, Australia, ⁴ School of Chemical and Biomedical Engineering, The University of Melbourne, Melbourne, VIC, Australia, ⁵ School of Applied Sciences, RMIT University, Bundoora, VIC, Australia, ⁶ Neonatal Intensive Care Unit, The Second Affiliated Hospital and Yuying Children's Hospital of Wenzhou Medical University, Wenzhou, China, ⁷ Department of Microbiology, Monash University, Clayton, VIC, Australia

OPEN ACCESS

Edited by:

Sujogya Kumar Panda,
KU Leuven, Belgium

Reviewed by:

Melyssa Negri,
State University of Maringá, Brazil
Renátó Kovács,
University of Debrecen, Hungary

*Correspondence:

Yue Qu
yue.qu@monash.edu

[†]These authors have contributed
equally to this work

Specialty section:

This article was submitted to
Antimicrobials, Resistance
and Chemotherapy,
a section of the journal
Frontiers in Microbiology

Received: 20 August 2019

Accepted: 25 October 2019

Published: 07 November 2019

Citation:

Wu X, Zhang S, Xu X, Shen L,
Xu B, Qu W, Zhuang W, Locock K,
Deighton M and Qu Y (2019)
RAFT-Derived Polymethacrylates as
a Superior Treatment for Recurrent
Vulvovaginal Candidiasis by Targeting
Biotic Biofilms and Persister Cells.
Front. Microbiol. 10:2592.
doi: 10.3389/fmicb.2019.02592

Background: Vulvovaginal candidiasis (VVC) is a common infection in need of more effective treatment. Formation of epithelium-associated *Candida* biofilms and the presence of persister cells are among the major contributing factors to the recurrence of this condition. We have previously developed RAFT-derived polymethacrylates that are effective in killing *C. albicans* biofilms *in vitro*. This study aimed to examine the clinical potential of polymethacrylates as antifungals for treatment of recurrent VVC (RVVC).

Methods: A mouse model of VVC was used to establish vaginal epithelium-associated biofilms, using *C. albicans* isolates from VVC/RVVC patients. A comparison was made of the efficacies of polymethacrylates and conventional antifungals, clotrimazole and nystatin, in killing *Candida* in epithelium-associated biofilms *in vivo*. *Ex vivo* biofilms were used for *Candida* population profiling and to quantify persister cells in vaginal epithelia. The potency of polymethacrylates and conventional antifungals against persister cells, either as sole agents or in combination, was assessed.

Results: Polymethacrylates showed negligible local toxicity, resistance to vaginal acidity, and outstanding *in vivo* activity against vaginal epithelium-associated *C. albicans* biofilms. *In vivo* tests polymethacrylates outperformed the conventional antifungals, nystatin and clotrimazole at concentrations 50 times below the over-the-counter concentrations. Using polymethacrylates was associated with fewer persister cells, and better eradication of persister cells pre-selected by conventional antifungals.

Conclusion: This study systematically assessed the clinical potential of RAFT-derived polymethacrylates as an effective treatment for VVC/RVVC in a mouse model. Polymethacrylates effectively killed vaginal epithelium-related *C. albicans* *in vivo* by specially targeting biotic biofilms and persister cells. Treatment presented negligible local toxicity.

Keywords: RVVC, mouse model, antifungal treatment, RAFT-derived polymethacrylates, biotic biofilms, persister cells, population analysis

INTRODUCTION

Vulvovaginal candidiasis (VVC) is one of the most common infections in women, affecting up to 75% of those of reproductive age. A 5–8% subset of these women suffer from the very stubborn recurrent VVC (RVVC, at least 3–4 episodes within a 12-month period), which is resistant to currently available treatment (Sobel, 2016). Topical preparations, such as clotrimazole cream or nystatin suppositories are used as first-line antifungals for VVC and RVVC (Wächter et al., 2011; Choukri et al., 2014). Fluconazole is also recommended by CDC as an effective oral antifungal for induction and maintenance therapy of RVVC. Although most *C. albicans* isolates from RVVC patients remain sensitive to many azoles (Gamarra et al., 2014; Adjapong et al., 2017), suppressive maintenance therapies using azoles often fail to eradicate the pathogen or completely cure the infection (Fan et al., 2015a; Mendling et al., 2015; Grinceviciene et al., 2017), suggesting microbial strategies other than intrinsic resistance might be involved.

Biofilm formation by *C. albicans* on vaginal epithelia has been long recognized as a specific fungal self-protective strategy that leads to antifungal resistance and infection recurrence (Harriott et al., 2010; Muzny and Schwebke, 2015), although its physical presence in the vagina of VVC/RVVC patients was recently questioned (Sobel, 2016; Swidsinski et al., 2019). Persister cells are a small population of “transiently resistant” cells that are often associated with the specific mode of biofilm growth (Lafleur et al., 2006; Lafleur et al., 2010; Yang et al., 2015). It is reasonable to hypothesize that epithelium-associated *C. albicans* biofilms involved in RVVC may harbor persister cells. Treatment of persister cells is known to be troublesome (Lewis, 2010). Conventional antimicrobials, unless used at the very high doses for an extended period, often fail to eradicate persister cells residing in biofilms (Yang et al., 2015).

Fluconazole maintenance suppressive therapy is still a preferred option to treat RVVC caused by fluconazole-sensitive *C. albicans* (Mikamo et al., 2015; Dennerstein, 2017). Other conventional antifungals that have a broad spectrum of activity, such as imidazole and nystatin, have been recommended for RVVC caused by fluconazole-resistant *C. albicans* and other *Candida* species (Fan et al., 2015a,b). Several limitations of using conventional agents to treat RVVC have been reported, including low efficacy in curing RVVC, possible systemic side-effects, and the development of antifungal resistance (Howley et al., 2016; Molgaard-Nielsen et al., 2016). The biofilm growth model of *Candida* species around vaginal epithelia, the possible involvement of persister cells, and the acidic condition of the human vagina, have been shown to reduce the effectiveness of some conventional and newly developed antifungals against *Candida* spp. (Kasper et al., 2015; Muzny and Schwebke, 2015). These factors highlight the importance of developing new, effective and safe antifungal drugs that are able to overcome such hurdles for the treatment of VVC/RVVC.

We have previously developed biocompatible RAFT-derived cationic polymethacrylates and demonstrated their efficacy against *in vitro* biofilms formed by *C. albicans* (Qu et al., 2016). The aim of this study was to systematically evaluate the potential

of the polymethacrylates for the treatment of VVC/RVVC, by examining their local toxicity, *in vivo* efficacy in killing biotic biofilms and persister cells, and tolerance to acidic conditions encountered in the human vagina, using a mouse model.

MATERIALS AND METHODS

C. albicans Strains, Antifungal Agents and Ethical Approval

Two *C. albicans* clinical isolates and DAY185, a well-known biofilm-producing laboratory strain, were used in this study. The clinical isolates were from patients who visited the first Affiliated Hospital, Wenzhou Medical University with clinically diagnosed uncomplicated VVC and RVVC and were designated as isolates VVC2 and VVC4, respectively. The clinical isolates were identified to a species level using CHROMagar *Candida* medium (CHROMagar, Paris, France) and MALDI Biotyper Identification System (MALDI-TOF MS, BioMérieux, Craponne, France). All strains were stored at -80°C in 15% (v/v) glycerol and streaked onto yeast-peptone-dextrose plates (YPD, 2% peptone, 1% yeast extract, 2% glucose and 80 mg/L uridine) as working stocks. The conventional antifungals for laboratory use, nystatin, clotrimazole, and amphotericin B, were purchased from Merck Pty Ltd. (Nantong, China). The clinically used antifungal preparations, nystatin vaginal suppository and clotrimazole cream were purchased from Polichem S.R.L (Barcelona, Spain) and Bayer Schering Parma AG (Berlin, Germany), respectively. Two polymethacrylates, designated as KL706 and KL708 and with similar compositions to those described previously, were used in this study (Table 1; Qu et al., 2016). The Ethics Review Boards of Wenzhou Medical University approved this study (wydw2016-0214). All animal experiments were carried out in accordance with the National Institutes of Health guide for the care and use of Laboratory animals.

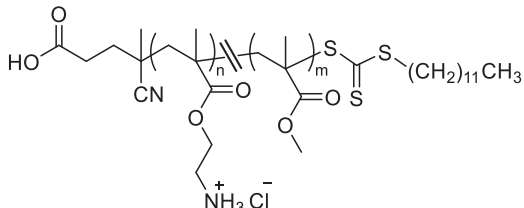
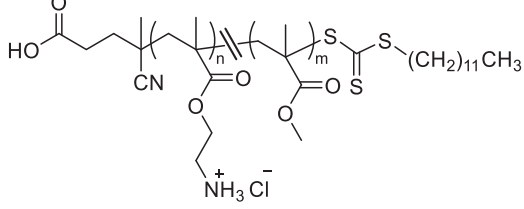
Formulation of Antimicrobial Polymethacrylate Hydrogels

Both polymethacrylates were formulated to final concentrations of 20, 40, and 80 mg/L, respectively in hydrogel preparations using a proprietary Carbopol® 940 polymer as follows: Synperonic™ PE/F 127 emulsifier (10 g) was dissolved in water (429 mL) with heating and then cooled to room temperature before the addition of a stock solution of polymethacrylate (0.01–0.04 g) in ethanol (5 mL) and wetted out completely. To do this, the solution was stirred vigorously before the addition of propylene glycol (50.0 g), followed by the slow addition of Carbopol® 940 polymer (5.00 g). The final mixture was brought to pH 7.0 using triethanolamine (0.75 g).

Qualitative Determination of the Intravaginal Dynamics of Polymethacrylates

Release of polymethacrylates from the formulated hydrogel in the mouse vagina over a time course was determined,

TABLE 1 | Details of antimicrobial polymethacrylates used in this study, KL-706 and KL-708 (Locock et al., 2014).

Polymer	Structure	M_n (g/mol)	DP	MP _{methyl} (%)
KL-706		3900	24	29
KL-708		3100	20	48

M_n denotes the number average molecular weight of the polymer, DP the degree of polymerization, or the average monomer units in a polymer chain, and MP_{methyl}, the mole percentage of methyl side chains in the molecule, in this case compared with amino side chains.

using a previously published method (Zhang et al., 2017). Hydrogel loaded with rhodamine-labeled KL708 at 80 mg/L was administered to mice via an intravaginal pathway. Animals were sacrificed at 1, 2, 8, 12, 24, and 48 h and the entire vagina was collected and washed with saline. Fluorescent images of the vagina were taken using an IVIS spectrum *in vivo* imaging system at 550 nm.

***In vivo* Cervicovaginal Toxicity and Inflammation Assessment**

A mouse model was used to assess cervicovaginal toxicity and local inflammation after polymethacrylate exposure (Catalone et al., 2004). BABL/C female mice of 6–8 weeks old were hormonally synchronized 3 days prior to the experiment with a subcutaneous injection of 0.1 mg of estrogen (17 β -estradiol; Sigma) dissolved in 0.1 mL sesame oil. Anesthetized mice received an intravaginal treatment (100 μ L) of either unformulated hydrogels (negative control) or KL708-hydrogel. PBS was used as the second negative control to document the normal tissue architecture and inflammation status in the cervicovaginal mucosa. Mouse vaginal lavage fluids were collected and the vaginal tissue was surgically excised after sacrificing the animals at 48 h post-treatment. Tissues were formalin-fixed and embedded in paraffin using standard procedures. Gross morphological analyses of the cervicovaginal mucosa were performed on tissues stained with hematoxylin and eosin (H&E) using an Olympus IX81 microscope. Concentrations of two representative inflammatory effectors in vaginal lavage fluids, the innate cytokine IL-1 β (Netea et al., 2010) and the alarmin S100A8 (Vogl et al., 2014), were analyzed using commercially available enzyme-linked immunosorbent assay (ELISA) kits per manufacturers' instructions. All samples were measured in duplicate, and the assay was repeated three times.

***In vivo* VVC Model and Cultivation of Mouse Vaginal Epithelium-Associated *Candida* Biofilms**

Vulvovaginal candidiasis was induced in mice essentially as described by Harriott et al. (2010). *C. albicans* cells were grown for 20 h in YPD (200 rpm, 30°C) and resuspended to a density of $\sim 7 \times 10^6$ CFU/mL. One-hundred microliters of *Candida* suspension was used to infect mice via the intravaginal pathway. Infected vaginal tissue was surgically collected after euthanizing animals 3 days post-infection. *C. albicans* biofilms that formed on vaginal epithelia were qualitatively examined using scanning electronic microscopy (SEM).

Antifungal Susceptibility Tests for Planktonic Cells and Cells Residing in Epithelium-Associated Biofilms

Broth dilution susceptibility testing was carried out for *C. albicans* cells grown as planktonic cultures, by following the CLSI guideline M27-A3, except RPMI-1640 at pH 4.0 and pH 7.2 were used respectively, as growth media. Polymethacrylate solutions at concentrations ranging from 1 to 128 mg/L were tested. For *in vivo* biofilm antifungal susceptibility testing, *C. albicans* epithelium-associated biofilms were established in the mouse vagina as described above. Nystatin vaginal suppository and clotrimazole cream at 4000 mg/L (OTC preparations), and hydrogels loaded with KL706 and KL708 respectively, at 20, 40, and 80 mg/L were delivered as a single dose to infected vagina via an intravaginal pathway. Treatment lasted for 24 h before infected animals were sacrificed, and the entire vagina was surgically excised. The vaginal tissues were weighted with a Mettler Toledo PB603-S milligram balance, washed three times with PBS, and homogenized with a tissue homogenizer. Viable counts were performed for tissue suspensions by plating an aliquot onto YPD plates followed by further incubation at 35°C for 48 h.

Colony-forming-unit (CFU) of *Candida* cells per gram of vaginal tissue (CFU/g) was calculated for quantitative assessment of fungal biofilm survivors after antifungal treatment. Mouse vagina treated with PBS and blank hydrogels served as negative controls. Six biological repeats were carried out for this experiment.

Population Profiling of Infected Vaginal Tissues and *ex vivo* Quantification of Persister Cells

Profiling the population of *C. albicans* cells within infected tissues was carried out using a previously published method, with modification (Yang et al., 2015). Approximately 0.3 g of infected vaginal tissues were homogenized with a tissue homogenizer in 1 mL of RPMI-1640. Suspensions of *Candida* cells were adjusted to a density of $\sim 1 \times 10^8$ CFU/mL with RPMI-1640 and a hemocytometer, and further confirmed with CFU-based viable counts. One-hundred microliters of fungal suspension was challenged with nystatin, clotrimazole, and KL706 prepared in RPMI-1640 at increasing concentrations ranging from planktonic MIC to 1024 mg/L for clotrimazole, 2048 mg/L for nystatin, and 256 mg/L for KL706. Our preliminary study found such high concentrations were effective against vaginal epithelium-associated *C. albicans* biofilms *ex vivo*. Viable counts were performed after exposing fungal suspensions to antifungal agents at various concentrations for 24 h, and the highest concentrations for an extra 24 h (48 h in total) and 48 h (72 h in total). To avoid antifungal carryover, the antifungal treated suspensions were centrifuged at 3000 g for 5 min, washed with PBS, and resuspended to the same volume of YPD broth. Viable counts were performed by plating serially diluted aliquots onto YPD plates followed by incubation at 35°C for 72 h to maximize the recovery of persister cells. The lowest concentration of antifungals and the shortest treatment duration that led to the lowest number of fungal survivors were chosen as the antifungal regimens for persister cell quantification. The percentage of persister cells were calculated as follows: (fungal density after antifungal treatment)/(fungal density before antifungal treatment) \times (100%).

Potency of Polymethacrylates in Further Killing Persister Cells Pre-selected by Conventional Antifungals

As persister cells residing in biofilms might be antimicrobial-dependent (Yang et al., 2015), we further evaluated the effectiveness of polymethacrylates in killing persister cells that have been pre-selected by conventional antifungals. A population of $\sim 1 \times 10^8$ CFU/mL of fungal cells from infected vaginal tissues were treated with amphotericin B at 100 mg/L for 24 h, washed with PBS to remove the amphotericin B, and then subjected to treatment using nystatin (2048 mg/L), or clotrimazole (1024 mg/L), or KL706 (80 mg/L) or KL708 (80 mg/L) for another 24 h. Viable counts were carried out to recover and quantify survivor persister cells as described earlier. To increase the detection sensitivity, a one mL volume of the treated suspension was pelleted, washed three times with PBS, and resuspended into 100 μ L of PBS, followed by spreading and

recovering on YPD plates. The experiment was repeated three times in duplicate.

Data Analysis and Statistical Methods

One-way ANOVA or a non-parametric test (Mann-Whitney *U* test) was carried out to compare two means, depending upon the data distribution. Statistical significance was assumed at the *p*-value of less than 0.05. Data analysis was performed using Minitab 16 (Minitab, State College PA, United States).

RESULTS

Formulation of Polymer Loaded Hydrogels and Intravaginal Sustainability of RAFT-Derived Polymethacrylates

Figure 1A is an example of a formulated hydrogel of polymethacrylate KL708. Figure 1B showed a gradual diminution of rhodamine-labeled KL708 from the hydrogel for a 48-h period after infusion into the mouse vagina. The slow decay of fluorescence intensity in the vagina supported the stability, for at least 48 h, of such a drug delivery system in the vaginal environment and a prolonged contact between polymethacrylate and the vaginal epithelia, paving the foundation for intravaginal application of this system.

Minimum Cervicovaginal Toxicity of RAFT-Derived Polymethacrylates

Toxicity of polymethacrylates to cervicovaginal tissues was determined by examining the morphology of vaginal epithelia and local inflammation. Hematoxylin and eosin staining showed no significant change in the gross appearance of the vaginal mucosa after exposure to hydrogels loaded with KL708 at 40 mg/L or 80 mg/L, or KL706 at 40 mg/L for 48 h, when compared with hydrogel or non-hydrogel PBS controls (Figure 2A). No apparent epithelial disruption in the mouse vagina was noticed when challenged with these products. Vaginal epithelia remained protected by a covering of keratin, and the integrity of the squamous epithelia appeared intact (Figure 2A). Minor sloughing was observed when KL-706 was used at 80 mg/L, however this involved only the upper epithelia (Figure 2A). No significant inflammatory responses were induced in mouse vagina by polymethacrylate-loaded hydrogels, even at a high polymer concentration of 80 mg/L, as indicated by the level of inflammatory cytokine IL-1 β and alarmin S100A8 (Figure 2B).

Acidic Vaginal Environment Did Not Compromise Anti-candida Activity of Polymethacrylates

Minimum inhibitory concentrations were determined for both conventional antifungals and polymethacrylates, using the standard broth-dilution method but with RPMI prepared at a neutral pH (7.2) and a pH comparable to that in the human vagina (4.0) respectively. All but one of the MICs

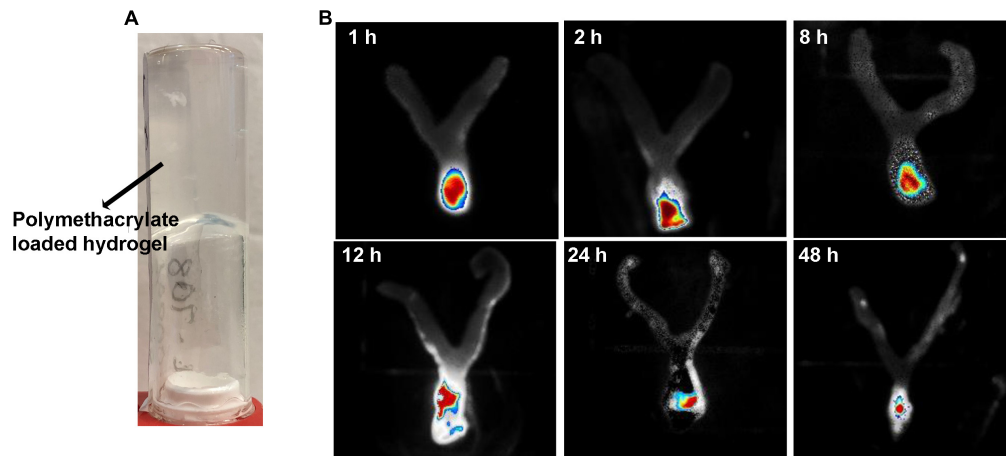


FIGURE 1 | Intravaginal retention and slow decay of polymethacrylates formulated as hydrogel *in vivo*. Fluorescence-labeled polymethacrylate KL-708 was formulated into hydrogels (A) and administered intravaginally to mice. Retention of guanylated polymer in mouse vagina was monitored *in situ*, using an *in vivo* IVIS spectrum imaging system at different time points of 0, 2, 8, 12, 24, and 48 h (B). Substantial amounts of polymethacrylates were found in mouse vagina even at 48 h post-administration.

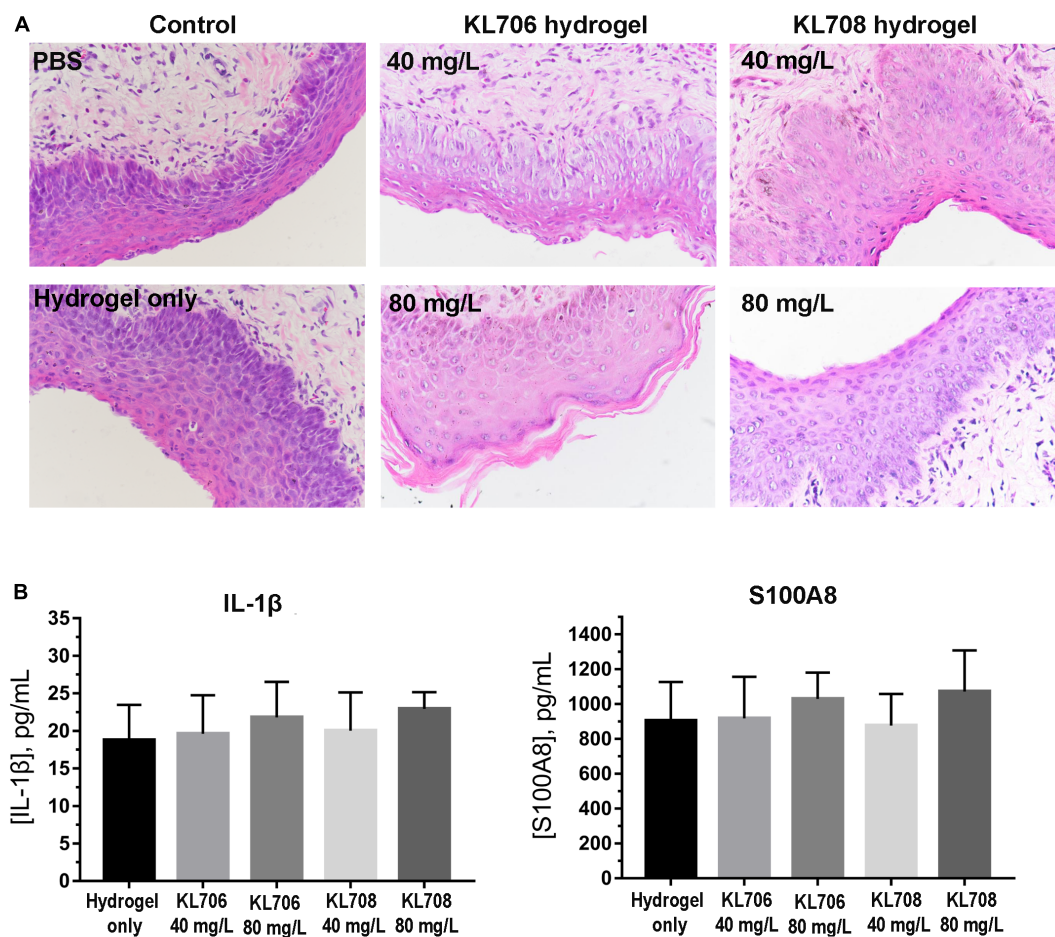


FIGURE 2 | Cervicovaginal toxicity of polymethacrylates and local inflammation. (A) Histopathological presentation of mouse vaginal tissues after exposure to polymethacrylate at 40 and 80 mg/L for 48 h. HE staining showed neglectable morphological changes of vaginal epithelia and underlying tissues. (B) Inflammation responses induced by polymethacrylate-loaded hydrogels. Inflammatory cytokine IL-1 β and alarmin S100A8 were used as indicators.

derived for the polymethacrylates were identical under acidic conditions, indicating a high tolerance of these polymers to acidic conditions found within the human vagina (Table 2). The acidic condition, however, significantly compromised antifungal activities of conventional drugs, by increasing their MICs by 4–16-fold (Table 2).

Polymethacrylates Were Superior to Conventional Antifungals in Killing Epithelium-Associated Biofilms in the Vagina

We first examined *in vivo* biofilm formation of *C. albicans* on mouse vaginal epithelia at 48 h post-infection. A characteristic epithelium-associated biofilm structure was observed with SEM, consisting of yeast and hyphal cells embedded in vaginal mucosae (Figure 3A, with the clinical isolate VVC4 as an example). We further examined the antifungal efficacy of all agents against such epithelium-associated biofilms formed by VVC4 and laboratory strain DAY185. KL706 and KL708 at 40 mg/L were effective in killing epithelium-associated biofilms formed by either *C. albicans* DAY185 or VVC4 (Figures 3A,B). KL706 at 80 mg/L, a concentration 50 times less compared to that of conventional antifungals tested, killed significantly more biofilms than either nystatin or clotrimazole at 4000 mg/L ($p < 0.05$ and $p < 0.01$, respectively). KL708 at 80 mg/L also showed a higher potency than clotrimazole at 4000 mg/L in killing epithelium-associated *C. albicans* biofilms in the mouse vagina (Figure 3B, $p < 0.05$).

Polymethacrylate Treatment of Epithelium-Associated *C. albicans* Biofilms Resulted in Fewer Persister Cells Than Conventional Antifungals

Population analysis profiling was performed to determine antifungal regimens (concentration and duration) that can be used to successfully isolate and quantify persister cells residing

in epithelium-associated *C. albicans* biofilms. Typical three-subpopulation patterns were established when nystatin and KL706 were used as the selecting agents (Figure 4A): Over 99.9% of biofilm cells were susceptible and responded to both agents at 16 mg/L; a small population of cells demonstrated tolerance to nystatin and KL706 at higher concentrations (16–1024 mg/L for nystatin, and 16–128 mg/L for KL706) but could be killed if antifungal concentration and/or exposure time were further increased; a very small population of cells survived the most potent antifungal regimens, such as nystatin at 2048 mg/L and KL706 at 256 mg/L for 48 or 72 h. In contrast; a gradually descending pattern was found when fungistatic clotrimazole was used to select biofilm persister cells (Figure 4A). Thus, the regimens chosen to isolate persister cells in epithelium-based biofilms grown in the mouse vagina were 2048 mg/L \times 48 h for nystatin, 256 mg/L \times 48 h for KL706 and KL708, and 1024 mg/L \times 72 h for clotrimazole.

In general, fewer persister cells were detected after exposing vaginal epithelium-associated biofilm cells to KL706 or KL708 than to clotrimazole or nystatin (Figure 4B and Supplementary Table S1). When epithelium-associated biofilms formed by *C. albicans* VVC4 and VVC2 were studied, average proportions of persister cell selected by KL706 and KL708 reached $0.08 \pm 0.03\%$ (mean \pm SEM) and $0.10 \pm 0.01\%$, and $0.17 \pm 0.02\%$ and $0.21 \pm 0.02\%$, respectively. Conventional antifungal drugs nystatin isolated $0.16 \pm 0.02\%$ and $0.28 \pm 0.02\%$ persister cells, and clotrimazole selected $0.43 \pm 0.02\%$ and $0.51 \pm 0.02\%$ from biofilms formed by VVC4 and VVC2 respectively (Figure 4B). The same trend was noticed when *C. albicans* laboratory reference strain DAY185 was studied. It was also noticed that vaginal epithelium-based biofilms formed by clinical isolates VVC4 and VVC2 harbored more persister cells than *C. albicans* DAY185, a clinically relevant isolate related to systemic infections, regardless of selecting antifungals used.

Polymethacrylates Demonstrate Activity Against Persister Cells Following Conventional Antifungal Treatment

Ex vivo biofilms were used to examine the effectiveness of polymethacrylates in killing persister cells pre-selected by conventional antifungal agent amphotericin B. When challenging persister cells preselected with amphotericin B at 100 mg/L, polymethacrylates at 128 mg/L showed a significantly higher fungicidal activity relative to the conventional agents, nystatin and clotrimazole at 1024 mg/L (Figure 5). KL706 further killed 75, 94, and 82% of pre-selected persister cells of DAY185, VVC2, and VVC4, and KL708 eradicated 64, 90, and 75% of these persister cells. This opens the door for novel and more efficient combination therapies for RVVC, using conventional antifungals sequentially combined with polymethacrylates.

DISCUSSION

The current antifungal regimens for VVC/RVVC, recommended by CDC and based on 2015 Sexually Transmitted Diseases (STD) Treatment Guidelines, have been widely followed by

TABLE 2 | *In vitro* susceptibility of *C. albicans* strains to conventional antifungals and polymethacrylates at different pHs.

Antifungals	MIC (mg/L) for <i>C. albicans</i> isolates					
	DAY185	Fold change	VVC2	Fold change	VVC4	Fold change
pH = 7.2						
Nystatin	4		2		4	
Clotrimazole	0.5		2		1	
KL706	16		16		16	
KL708	16		16		32	
pH = 4.0						
Nystatin	16	4	32	16	32	8
Clotrimazole	8	14	8	4	16	16
KL706	32	2	32	2	32	2
KL708	32	2	32	2	32	1

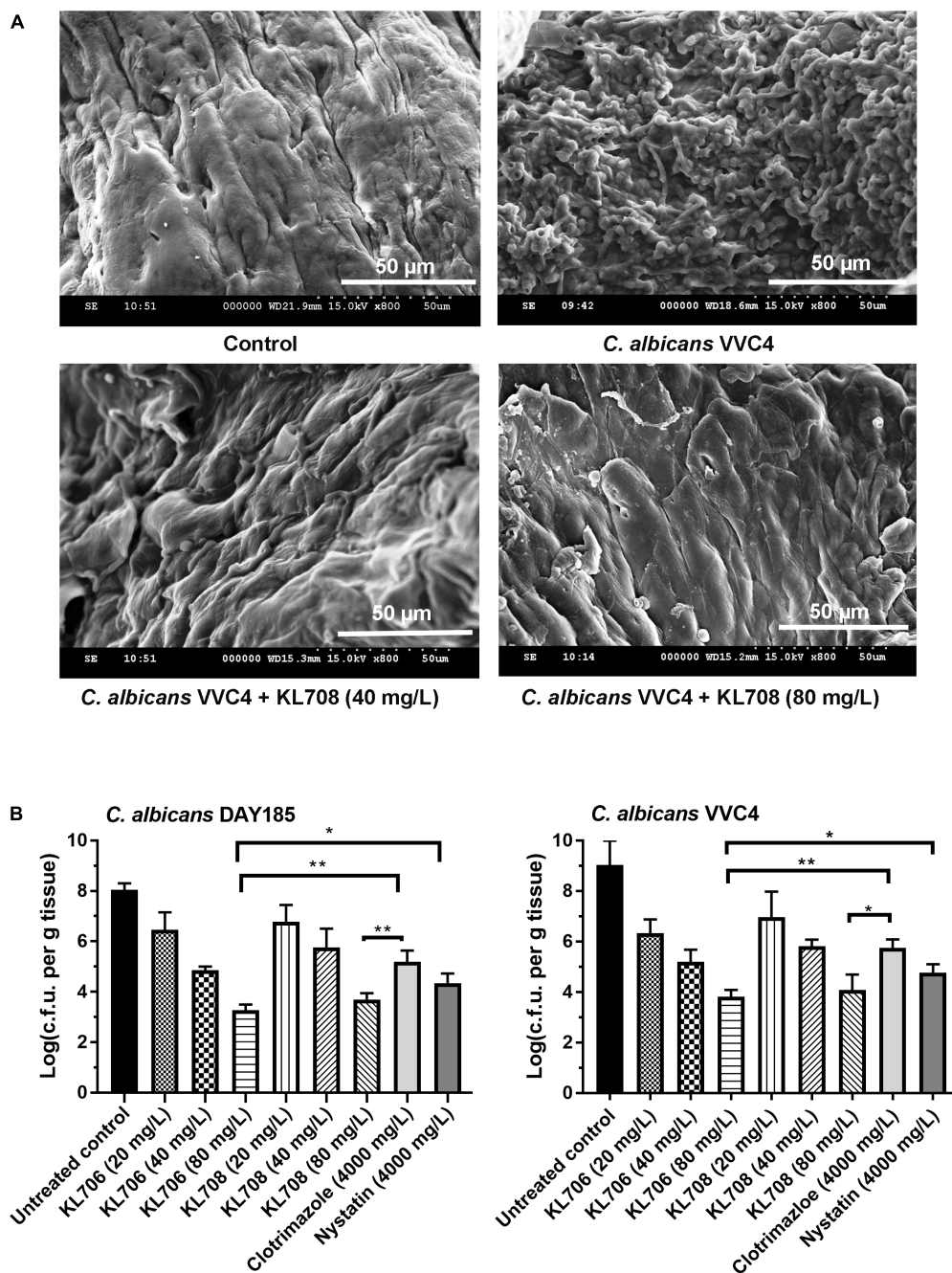


FIGURE 3 | Antifungal activities of polymethacrylates against *C. albicans* grown as vaginal epithelium-associated biofilms. **(A)** Scanning electron microscopy of epithelium-associated biofilms formed by *C. albicans* VVC4 in the mouse vagina, before and after treatment with KL708 at 40 and 80 mg/L. **(B)** Quantitative assessment of anti-infective efficacy of polymethacrylates against vaginal epithelium-associated *C. albicans* biofilms. *C. albicans* cells grown as biotic biofilms on mouse vaginal epithelia were treated with polymethacrylates at 40 and 80 mg/L and conventional antifungal drugs at clinical doses. Mouse vaginal tissue was removed after treatment and homogenized for viable counts. Survivors were recovered after 72 h incubation on YPD plates. Polymethacrylates at non-toxic concentrations (80 µg/mL) demonstrated a significantly higher activities in killing epithelium-associated biotic *C. albicans* biofilms than conventional antifungals. No difference was found between the two negative controls (PBS control and hydrogel-only control) and only that of hydrogel-only was shown. * $p < 0.05$, ** $p < 0.01$.

general practitioners and gynecologists. Among the conventional antifungals recommended by CDC, imidazoles (including clotrimazole, miconazole and econazole), the polyene nystatin, and fluconazole have been on the market for more than 35 years

and still remain effective against acute VVC. Their effectiveness for RVVC, however, are suboptimal, as recurrence of infection is common after an initial course of fluconazole or clotrimazole and ongoing antifungal maintenance therapy is often required

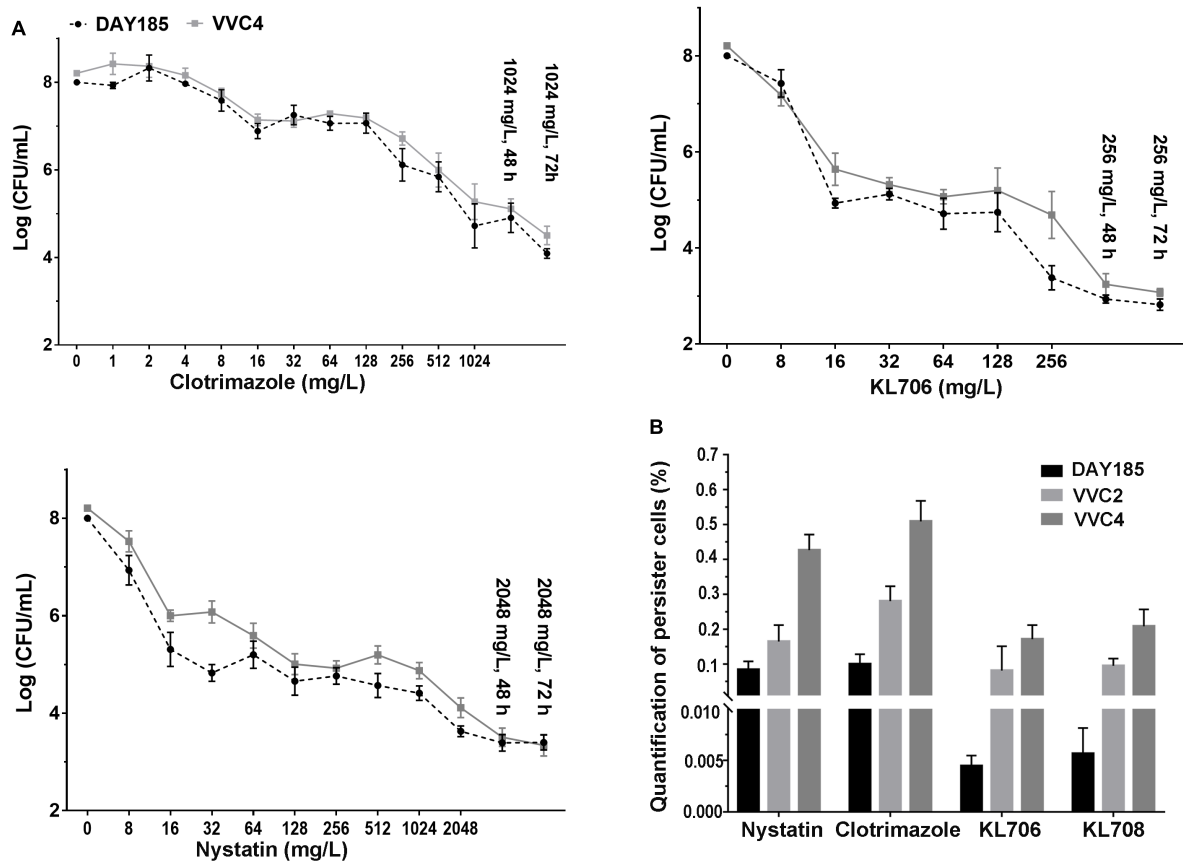


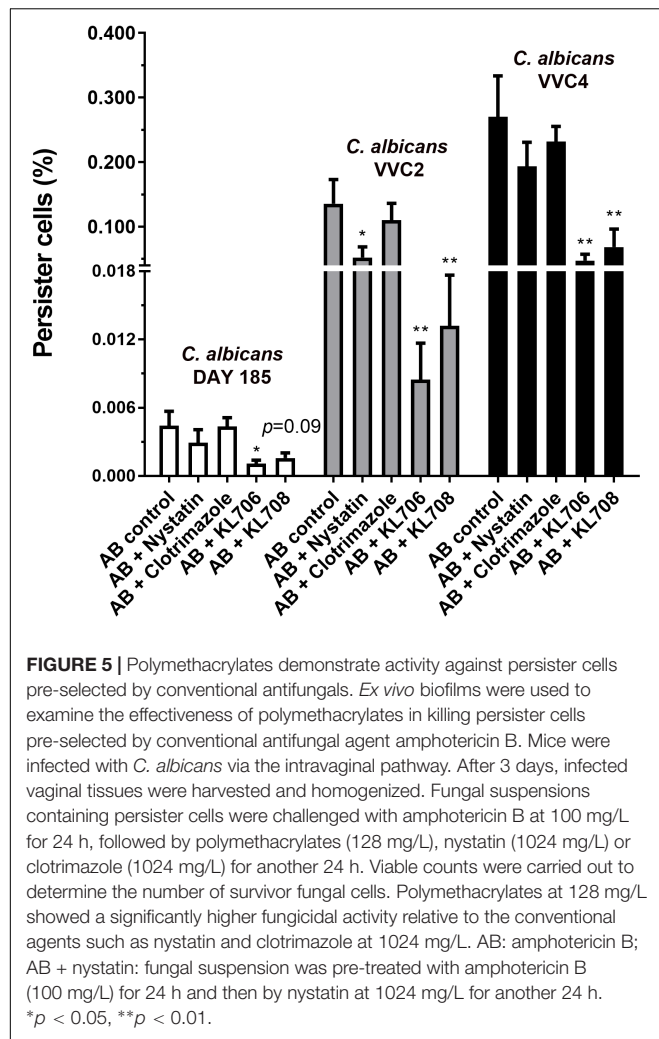
FIGURE 4 | (A) *Ex vivo* population profiling of vagina epithelium-associated *C. albicans* biofilms using different antifungal agents. Mice were infected with *C. albicans* via the intravaginal pathway. After 3 days, infected vaginal tissues were harvested and homogenized. Fungal suspensions containing persister cells were challenged with antifungals at increasing concentrations for 24, 48, and 72 h. Experimental results identified a small population remaining tolerant to antifungals at very high concentration, even for an extended treatment period (48 or 72 h). Polymers KL706 only required a relatively low concentration of 256 mg/L and 24–48 h to reach the persister cell plateau, however the conventional antifungal agents need a higher concentration of 1024 mg/L or 2048 mg/L to reach this plateau. **(B)** Proportions of *C. albicans* persister cells in epithelium-associated biofilms selected by different antifungal agents. Total persister cells were isolated by exposing homogenized mouse vaginal tissues infected with *C. albicans* to antifungal agents at a specific concentration (1024 mg/L for clotrimazole, 2048 mg/L for nystatin, and 256 mg/L for KL706 and KL708, based on population analysis data). Such regimens have been found to be able to isolate persister cells from infected vaginal tissues. The proportion of persister cells was calculated as the proportion of survivor cells out of total population. Shown are the average of three to four biological repeats in duplicate.

(Tapia et al., 2017; Couss et al., 2018). This is possibly due to the low efficacy of conventional antifungals in eradicating biotic biofilms and persister cells that have grown on vaginal epithelia and in underlying tissues.

We have recently developed a new class of antimicrobial polymethacrylates that have shown high potency against *in vitro* *C. albicans* biofilms (Qu et al., 2016). This study was designed to examine clinical potential of polymethacrylates as an effective treatment for VVC/RVVC. In the current study, polymethacrylates demonstrated several properties as topical agents for VVC/RVVC, including high efficacy in killing epithelia-based *C. albicans* biofilms and persister cells, ease of formulation as a hydrogel for topical application, and low toxicity to local vaginal tissue. Unlike other newly proposed antifungal substances from natural sources that often need to be combined with conventional agents such as fluconazole or miconazole for high *in vivo* effectiveness (Gao et al., 2016; Esposito et al.,

2018; Fernandes Costa et al., 2019), polymethacrylates provide a distinct advantage as they can be used as a sole therapy. They also outperformed clotrimazole and nystatin, two market leading antifungals, at 50 times less the equivalent clinical concentration in killing biotic *C. albicans* biofilms grown on vaginal epithelia. Moreover, polymethacrylates were able to maintain their activity in the acidic human vaginal environment, a major hurdles for drug development, since antifungals are often less effective under acid conditions (Ilkit and Guzel, 2011). Similar to valproic acid (Chaillot et al., 2017), both KL706 and KL708 demonstrated pH-independent antifungal efficacy, exhibiting only a 2-fold shift at pH 4.0 compared with pH 7.2, superior to many conventional antifungals and even the newly developed antifungal CD101 (Boikov et al., 2017).

The *in vivo* efficacy of polymethacrylates for VVC/RVVC found in this study is thought to be based on their unique activity against biotic biofilms and persister cells formed by *C. albicans*.



Antifungal resistance stemming from the formation of *Candida* biofilms in VVC has been noted by several studies, mostly based on antifungal susceptibility tests using 96-well microplate biofilm assays (Gao et al., 2016; Sherry et al., 2017). Abiotic biofilms developed in 96-well microplates, however, might differ from biotic epithelium-based biofilms in many aspects, including their resistance to antimicrobial agents (Bjarnsholt et al., 2013). We carried out antifungal susceptibility testing on *Candida* biofilms established in a mammalian vagina that closely mimic the clinical environment of human VVC. Though the mouse vagina differs from that of women in various physical aspects and may have different responses to *Candida* infections, it is still the preferred *in vivo* model for drug development, in the context of cost-effectiveness and labor-intensity (Vecchiarelli et al., 2015).

Harriott et al. (2010) successfully demonstrated vaginal epithelium-based *Candida* biofilms using a mouse VVC model and raised the hypothesis that biofilm formation by *Candida* might be an initiating event for VVC (Harriott et al., 2010). The role of biofilms in the pathogenesis of VVC/RVVC was recently challenged by Swidsinski et al. (2019). Swidsinski et al. (2019) used fluorescent *in situ* hybridization (FISH) on

vaginal biopsies from VVC patients and found no evidence of typical biofilm structures on vaginal epithelia or underlying tissues. It should be noted that biotic biofilms found *in vivo* often fail to present the typical three-dimensional mushroom structure, a biofilm morphology frequently reported by *in vitro* studies. *In vivo* biofilms uniquely grow as monolayers or microcolonies (Bjarnsholt et al., 2013), and detections of such structures often require experimental methods of higher resolutions such as SEM. From microbiological and clinical aspects, it is also reasonable to assume the involvement of *Candida* biofilms and persister cells in VVC/RVVC, as the recurrence pattern of RVVC coincides with the model of recurrent biofilm infections and persister cells proposed by Lewis (2010). Clinical isolates of *C. albicans* from the same RVVC patients over different periods of time, despite therapy, were found to be genetically identical, supporting the possible involvement of persister cells in the recurrence of RVVC (Fodor et al., 2002).

One of the major limitations of this study is that no other *Candida* species were included. Non-*C. albicans* *Candida* species have recently emerged as important etiological agents of VVC/RVVC (Richter et al., 2005; Gamarra et al., 2014). In contrast to *C. albicans*, some non-*C. albicans* *Candida* species are unable to form typical biofilms *in vitro* or *in vivo*, or are intrinsically resistant to many conventional antifungals (Guzel et al., 2013). A future study is required to examine the effect of polymers against VVC/RVVC caused by other *Candida* species.

CONCLUSION

This study systematically assessed the clinical potential of RAFT-derived polymethacrylates as an effective treatment for VVC/RVVC in a mouse model. Polymethacrylates effectively killed vaginal epithelium-related *C. albicans* *in vivo* by specially targeting biotic biofilms and persister cells, outperforming other market leading antifungals. Treatment presented negligible local toxicity.

DATA AVAILABILITY STATEMENT

The datasets generated for this study are available on request to the corresponding author.

ETHICS STATEMENT

The Ethics Review Boards of Wenzhou Medical University approved this study (wydw2016-0214). All animal experiments were carried out in accordance with the National Institutes of Health guide for the care and use of Laboratory animals.

AUTHOR CONTRIBUTIONS

YQ and XW conceived and designed the study. SZ, XX, LS, BX, WQ, WZ, KL, and YQ carried out the experiments. YQ, SZ, XW, and MD performed the data

analysis. YQ wrote the manuscript. YQ, MD, and XW edited the manuscript. All authors reviewed the manuscript and provided critical comments.

FUNDING

This work was supported by the National Natural Science Foundation of China (Grant Number 81772241 to YQ); the National Natural Science Foundation of China (Grant Number 81873822 to XW); the 551 Talent Program of Wenzhou (to XW); and the Shenzhen Science and Technology Innovation Project (Grant Number JCY20170818100355168 to XW).

REFERENCES

- Adjapong, G., Hale, M., and Garrill, A. (2017). A comparative investigation of azole susceptibility in *Candida* isolates from vulvovaginal candidiasis and recurrent vulvovaginal candidiasis patients in Ghana. *Med. Mycol.* 55, 686–689. doi: 10.1093/mmy/myw122
- Bjarnsholt, T., Alhede, M., Alhede, M., Eickhardt-Sorensen, S. R., Moser, C., Kuhl, M., et al. (2013). The *in vivo* biofilm. *Trends Microbiol.* 21, 466–474. doi: 10.1016/j.tim.2013.06.002
- Boikov, D. A., Locke, J. B., James, K. D., Bartizal, K., and Sobel, J. D. (2017). In vitro activity of the novel echinocandin CD101 at pH 7 and 4 against *Candida* spp. isolates from patients with vulvovaginal candidiasis. *J. Antimicrob. Chemother.* 72, 1355–1358. doi: 10.1093/jac/dkx008
- Catalone, B. J., Kish-Catalone, T. M., Budgeon, L. R., Neely, E. B., Ferguson, M., Krebs, F. C., et al. (2004). Mouse model of cervicovaginal toxicity and inflammation for preclinical evaluation of topical vaginal microbicides. *Antimicrob. Agents Chemother.* 48, 1837–1847. doi: 10.1128/aac.48.5.1837-1847.2004
- Chaillot, J., Tebbij, F., Garcia, C., Wurtele, H., Pelletier, R., and Sellam, A. (2017). pH-dependent antifungal activity of valproic acid against the human fungal pathogen *Candida albicans*. *Front. Microbiol.* 8:1956. doi: 10.3389/fmicb.2017.01956
- Choukri, F., Benderdouche, M., and Sednaoui, P. (2014). In vitro susceptibility profile of 200 recent clinical isolates of *Candida* spp. to topical antifungal treatments of vulvovaginal candidiasis, the imidazoles and nystatin agents. *J. Mycol. Med.* 24, 303–307. doi: 10.1016/j.mycmed.2014.05.001
- Crouss, T., Sobel, J. D., Smith, K., and Nyirjesy, P. (2018). Long-term outcomes of women with recurrent vulvovaginal candidiasis after a course of maintenance antifungal therapy. *J. Low Genit. Tract Dis.* 22, 382–386. doi: 10.1097/LGT.0000000000000413
- Dennerstein, G. J. (2017). Recurrent vulvovaginal candidiasis: a review of guidelines and recommendations. *Aust. N. Z. J. Obstet. Gynaecol.* 57, E12–E13.
- Esposito, E., Campolo, M., Casili, G., Lanza, M., Filippone, A., Peritore, A. F., et al. (2018). Effect of pea protein plus grape seed dry extract on a murine model of *Candida albicans* induced vaginitis. *Future Microbiol.* 13, 1375–1382. doi: 10.2217/fmb-2018-0102
- Fan, S., Liu, X., and Liang, Y. (2015a). Miconazole nitrate vaginal suppository 1,200 mg versus oral fluconazole 150 mg in treating severe vulvovaginal candidiasis. *Gynecol. Obstet. Invest.* 80, 113–118. doi: 10.1159/000371759
- Fan, S., Liu, X., Wu, C., Xu, L., and Li, J. (2015b). Vaginal nystatin versus oral fluconazole for the treatment for recurrent vulvovaginal candidiasis. *Mycopathologia* 179, 95–101. doi: 10.1007/s11046-014-9827-4
- Fernandes Costa, A., Evangelista Araujo, D., Santos Cabral, M., Teles Brito, I., Borges De Menezes Leite, L., Pereira, M., et al. (2019). Development, characterization, and in vitro-in vivo evaluation of polymeric nanoparticles containing miconazole and farnesol for treatment of vulvovaginal candidiasis. *Med. Mycol.* 57, 52–62. doi: 10.1093/mmy/myx155
- Fodor, E., Dosa, E., Nagy, E., and Ferenczy, L. (2002). Karyotyping of *Candida albicans* and *Candida glabrata* isolates from recurrent vaginal

ACKNOWLEDGMENTS

KL wishes to acknowledge the CSIRO Julius Career Development Award for funding. The authors also would like to thank Margaret Smith and her team at Syndet Works, Australia for their assistance with preparing polymer gel formulations.

SUPPLEMENTARY MATERIAL

The Supplementary Material for this article can be found online at: <https://www.frontiersin.org/articles/10.3389/fmicb.2019.02592/full#supplementary-material>

- infections by pulsed-field gel electrophoresis. *Acta Microbiol. Immunol. Hung.* 49, 59–68. doi: 10.1556/amcr.49.2002.1.6
- Gamarra, S., Morano, S., Dudiuk, C., Mancilla, E., Nardin, M. E., De Los Angeles Mendez, E., et al. (2014). Epidemiology and antifungal susceptibilities of yeasts causing vulvovaginitis in a teaching hospital. *Mycopathologia* 178, 251–258. doi: 10.1007/s11046-014-9780-2
- Gao, M., Wang, H., and Zhu, L. (2016). Quercetin assists fluconazole to inhibit biofilm formations of fluconazole-resistant *Candida albicans* in in vitro and in vivo antifungal managements of vulvovaginal candidiasis. *Cell Physiol. Biochem.* 40, 727–742. doi: 10.1159/000453134
- Grinceviciene, S., Bellen, G., Ruban, K., and Donders, G. (2017). Non-response to fluconazole maintenance treatment (ReCiDiF regimen) for recurrent vulvovaginal candidosis is not related to impaired glucose metabolism. *Mycoses* 60, 546–551. doi: 10.1111/myc.12626
- Guzel, A. B., Aydin, M., Meral, M., Kalkanci, A., and Ilkit, M. (2013). Clinical characteristics of Turkish women with *Candida krusei* vaginitis and antifungal susceptibility of the *C. krusei* isolates. *Infect. Dis. Obstet. Gynecol.* 2013:698736. doi: 10.1155/2013/698736
- Harriott, M. M., Lilly, E. A., Rodriguez, T. E., Fidel, P. L. Jr., and Noverr, M. C. (2010). *Candida albicans* forms biofilms on the vaginal mucosa. *Microbiology* 156, 3635–3644. doi: 10.1099/mic.0.039354-0
- Howley, M. M., Carter, T. C., Browne, M. L., Romitti, P. A., Cuniff, C. M., and Druschel, C. M. (2016). Fluconazole use and birth defects in the national birth defects prevention study. *Am. J. Obstet. Gynecol.* 214, e651–e659. doi: 10.1016/j.ajog.2015.11.022
- Ilkit, M., and Guzel, A. B. (2011). The epidemiology, pathogenesis, and diagnosis of vulvovaginal candidosis: a mycological perspective. *Crit. Rev. Microbiol.* 37, 250–261. doi: 10.3109/1040841X.2011.576332
- Kasper, L., Miramon, P., Jablonowski, N., Wisgott, S., Wilson, D., Brunke, S., et al. (2015). Antifungal activity of clotrimazole against *Candida albicans* depends on carbon sources, growth phase and morphology. *J. Med. Microbiol.* 64, 714–723. doi: 10.1099/jmm.0.000082
- Lafleur, M. D., Kumamoto, C. A., and Lewis, K. (2006). *Candida albicans* biofilms produce antifungal-tolerant persister cells. *Antimicrob. Agents Chemother.* 50, 3839–3846. doi: 10.1128/aac.00684-06
- Lafleur, M. D., Qi, Q., and Lewis, K. (2010). Patients with long-term oral carriage harbor high-persister mutants of *Candida albicans*. *Antimicrob. Agents Chemother.* 54, 39–44. doi: 10.1128/AAC.00860-09
- Lewis, K. (2010). Persister cells. *Annu. Rev. Microbiol.* 64, 357–372. doi: 10.1146/annurev.micro.112408.134306
- Locock, K. E., Meagher, L., and Haeussler, M. (2014). Oligomeric cationic polymethacrylates: a comparison of methods for determining molecular weight. *Anal. Chem.* 86, 2131–2137. doi: 10.1021/ac403735n
- Mendling, W., Brasch, J., Cornely, O. A., Effendy, I., Friese, K., Ginter-Hanselmayer, G., et al. (2015). Guideline: vulvovaginal candidosis (AWMF 015/072), S2k (excluding chronic mucocutaneous candidosis). *Mycoses* 58(Suppl. 1), 1–15. doi: 10.1111/myc.12292
- Mikamo, H., Matsumizu, M., Nakazuru, Y., Okayama, A., and Nagashima, M. (2015). Efficacy and safety of a single oral 150 mg dose of fluconazole for

- the treatment of vulvovaginal candidiasis in Japan. *J. Infect. Chemother.* 21, 520–526. doi: 10.1016/j.jiac.2015.03.011
- Molgaard-Nielsen, D., Svanstrom, H., Melbye, M., Hviid, A., and Pasternak, B. (2016). Association between use of oral fluconazole during pregnancy and risk of spontaneous abortion and stillbirth. *JAMA* 315, 58–67.
- Muzny, C. A., and Schwabke, J. R. (2015). Biofilms: an underappreciated mechanism of treatment failure and recurrence in vaginal infections. *Clin. Infect. Dis.* 61, 601–606. doi: 10.1093/cid/civ353
- Netea, M. G., Simon, A., Van De Veerdonk, F., Kullberg, B. J., Van Der Meer, J. W., and Joosten, L. A. (2010). IL-1 β processing in host defense: beyond the inflammasomes. *PLoS Pathog.* 6:e1000661. doi: 10.1371/journal.ppat.1000661
- Qu, Y., Locock, K., Verma-Gaur, J., Hay, I. D., Meagher, L., and Traven, A. (2016). Searching for new strategies against polymicrobial biofilm infections: guanlylated polymethacrylates kill mixed fungal/bacterial biofilms. *J. Antimicrob. Chemother.* 71, 413–421. doi: 10.1093/jac/dkv334
- Richter, S. S., Galask, R. P., Messer, S. A., Hollis, R. J., Diekema, D. J., and Pfaller, M. A. (2005). Antifungal susceptibilities of *Candida* species causing vulvovaginitis and epidemiology of recurrent cases. *J. Clin. Microbiol.* 43, 2155–2162. doi: 10.1128/jcm.43.5.2155-2162.2005
- Sherry, L., Kean, R., Mckloud, E., O'donnell, L. E., Metcalfe, R., Jones, B. L., et al. (2017). Biofilms formed by isolates from recurrent vulvovaginal candidiasis patients are heterogeneous and insensitive to fluconazole. *Antimicrob. Agents Chemother.* 61:e1065-17. doi: 10.1128/AAC.01065-17
- Sobel, J. D. (2016). Recurrent vulvovaginal candidiasis. *Am. J. Obstet. Gynecol.* 214, 15–21. doi: 10.1016/j.ajog.2015.06.067
- Swidsinski, A., Guschin, A., Tang, Q., Dorffle, Y., Verstraelen, H., Tertychnyy, A., et al. (2019). Vulvovaginal candidiasis: histologic lesions are primarily polymicrobial and invasive and do not contain biofilms. *Am. J. Obstet. Gynecol.* 220:e91. doi: 10.1016/j.ajog.2018.10.023
- Tapia, C. V., Hermosilla, G., Fortes, P., Alburquenque, C., Bucarey, S., Salinas, H., et al. (2017). Genotyping and persistence of *Candida albicans* from pregnant women with vulvovaginal candidiasis. *Mycopathologia* 182, 339–347. doi: 10.1007/s11046-016-0095-3
- Vecchiarelli, A., Gabrielli, E., and Pericolini, E. (2015). Experimental models of vaginal candidiasis and inflammation. *Future Microbiol.* 10, 1265–1268. doi: 10.2217/fmb.15.52
- Vogl, T., Eisenblatter, M., Voller, T., Zenker, S., Hermann, S., Van Lent, P., et al. (2014). Alarmin S100A8/S100A9 as a biomarker for molecular imaging of local inflammatory activity. *Nat. Commun.* 5:4593. doi: 10.1038/ncomms5593
- Wächter, B., Wilson, D., and Hube, B. (2011). *Candida albicans* adhesion to and invasion and damage of vaginal epithelial cells: stage-specific inhibition by clotrimazole and biconazole. *Antimicrob. Agents Chemother.* 55, 4436–4439. doi: 10.1128/AAC.00144-11
- Yang, S., Hay, I. D., Cameron, D. R., Speir, M., Cui, B., Su, F., et al. (2015). Antibiotic regimen based on population analysis of residing persister cells eradicates *Staphylococcus epidermidis* biofilms. *Sci. Rep.* 5:18578. doi: 10.1038/srep18578
- Zhang, S. S., Xia, W. T., Xu, J., Xu, H. L., Lu, C. T., Zhao, Y. Z., et al. (2017). Three-dimensional structure micelles of heparin-polyoxamer improve the therapeutic effect of 17 β -estradiol on endometrial regeneration for intrauterine adhesions in a rat model. *Int. J. Nanomed.* 12, 5643–5657. doi: 10.2147/IJN.S137237

Conflict of Interest: The authors declare that the research was conducted in the absence of any commercial or financial relationships that could be construed as a potential conflict of interest.

Copyright © 2019 Wu, Zhang, Xu, Shen, Xu, Qu, Zhuang, Locock, Deighton and Qu. This is an open-access article distributed under the terms of the Creative Commons Attribution License (CC BY). The use, distribution or reproduction in other forums is permitted, provided the original author(s) and the copyright owner(s) are credited and that the original publication in this journal is cited, in accordance with accepted academic practice. No use, distribution or reproduction is permitted which does not comply with these terms.



A New Antibiotic-Loaded Sol-Gel Can Prevent Bacterial Prosthetic Joint Infection: From *in vitro* Studies to an *in vivo* Model

John Jairo Aguilera-Correa^{1*}, Amaya Garcia-Casas², Aranzazu Mediero³, David Romera¹, Francisca Mulero⁴, Irene Cuevas-López⁵, Antonia Jiménez-Morales^{2,6} and Jaime Esteban^{1*}

OPEN ACCESS

Edited by:

Sujogya Kumar Panda,
KU Leuven, Belgium

Reviewed by:

Livia Visai,
University of Pavia, Italy
Paul M. Tulkens,
Catholic University of Louvain,
Belgium

*Correspondence:

John Jairo Aguilera-Correa
john_j2a@hotmail.com
Jaime Esteban
jestebanmoreno@gmail.com

Specialty section:

This article was submitted to
Antimicrobials, Resistance
and Chemotherapy,
a section of the journal
Frontiers in Microbiology

Received: 27 September 2019

Accepted: 06 December 2019

Published: 17 January 2020

Citation:

Aguilera-Correa JJ,
Garcia-Casas A, Mediero A,
Romera D, Mulero F, Cuevas-López I,
Jiménez-Morales A and Esteban J
(2020) A New Antibiotic-Loaded
Sol-Gel Can Prevent Bacterial
Prosthetic Joint Infection: From
in vitro Studies to an *in vivo* Model.
Front. Microbiol. 10:2935.
doi: 10.3389/fmicb.2019.02935

¹ Clinical Microbiology Department, IIS-Fundacion Jimenez Diaz, UAM, Madrid, Spain, ² Department of Materials Science and Engineering, University Carlos III of Madrid, Madrid, Spain, ³ Bone and Joint Research Unit, IIS-Fundacion Jimenez Diaz, UAM, Madrid, Spain, ⁴ Molecular Imaging Unit, Spanish National Cancer Research Centre (CNIO), Madrid, Spain, ⁵ Experimental Surgery and Animal Research Service, IIS-Fundacion Jimenez Diaz, UAM, Madrid, Spain, ⁶ Álvaro Alonso Barba Technological Institute of Chemistry and Materials, Carlos III University of Madrid, Madrid, Spain

The aim of this study was to evaluate the effect of a moxifloxacin-loaded organic-inorganic sol-gel with different antibiotic concentration in the *in vitro* biofilm development and treatment against *Staphylococcus aureus*, *S. epidermidis*, and *Escherichia coli*, cytotoxicity and cell proliferation of MC3T3-E1 osteoblasts; and its efficacy in preventing the prosthetic joint infection (PJI) caused by clinical strains of *S. aureus* and *E. coli* using an *in vivo* murine model. Three bacterial strains, *S. epidermidis* ATCC 35984, *S. aureus* 15981, and, *E. coli* ATCC 25922, were used for microbiological studies. Biofilm formation was induced using tryptic-soy supplemented with glucose for 24 h, and then, adhered and planktonic bacteria were estimated using drop plate method and absorbance, respectively. A 24-h-mature biofilm of each species growth in a 96-well plate was treated for 24 h using a MBECTM biofilm Incubator lid with pegs coated with the different types of sol-gel, after incubation, biofilm viability was estimated using alamarBlue. MC3T3-E1 cellular cytotoxicity and proliferation were evaluated using CytoTox 96 Non-Radioactive Cytotoxicity Assay and alamarBlue, respectively. The microbiological studies showed that sol-gel coatings inhibited the biofilm development and treated to a mature biofilm of three evaluated bacterial species. The cell studies showed that the sol-gel both with and without moxifloxacin were non-cytotoxic and that cell proliferation was inversely proportional to the antibiotic concentration containing by sol-gel. In the *in vivo* study, mice weight increased over time, except in the *E. coli*-infected group without coating. The most frequent symptoms associated with infection were limping and piloerection; these symptoms were more frequent in infected groups

with non-coated implants than infected groups with coated implants. The response of moxifloxacin-loaded sol-gel to infection was either total or completely absent. No differences in bone mineral density were observed between groups with coated and non-coated implants and macrophage presence lightly increased in the bone grown directly in contact with the antibiotic-loaded sol-gel. In conclusion, moxifloxacin-loaded sol-gel coating is capable of preventing PJI caused by both Gram-positive and Gram-negative species.

Keywords: sol-gel, moxifloxacin, prosthetic joint infection, *Staphylococcus epidermidis*, *Staphylococcus aureus*, *Escherichia coli*

INTRODUCTION

Prosthetic joint infection (PJI) occurs rarely (1–2% of all cases), though its effects are often devastating due to the high associated morbidity and substantial costs of this kind of surgical complication (Tande and Patel, 2014). Additionally, the economic burden of PJI is expected to rise in the coming years with the increase in the life expectancy and number of patients undergoing arthroplasty replacements (Anagnostakos et al., 2009).

Gram-positive cocci are the most frequent microorganisms isolated from PJIs, representing up to 77% of all PJIs; of these, the most common species are *Staphylococcus aureus* and coagulase-negative staphylococci (Benito et al., 2016). However, Gram-negative bacilli can be isolated from 27–45% of all infections (Cobo et al., 2011; Benito et al., 2016) and the most commonly isolated species belong to the *Enterobacteriaceae* family, mainly *Escherichia coli*, and several non-fermenting Gram-negative bacilli. These organisms are gaining in importance given their increasing incidence and antibiotic resistance (Rodriguez-Pardo et al., 2014; Benito et al., 2016; Papadopoulos et al., 2019; Pfang et al., 2019).

Systemic and prophylactic treatment of PJIs may be ineffective, because antibiotics are unable to reach the prosthesis-tissue interface due to necrotic and/or avascular tissue that remains after surgery (Popat et al., 2007). Therefore, local antibiotic therapy was proposed as an alternative and/or adjuvant to systemic prophylaxis or treatment, preventing systemic toxicity and favoring drug release directly within the implant site (Zhao et al., 2009). Additionally, if the infection probability is reduced, the osteointegration would be improved (Gristina, 1987; Zhao et al., 2014; Martinez-Perez et al., 2017).

We recently demonstrated in an *in vitro* study that an intermediate quantity of organophosphite, [tris(trimethylsilyl) phosphite] in a sol-gel made of two silanes (3-methacryloxypropyl trimethoxysilane and 2-tetramethyl orthosilane) enhanced sol-gel adhesion on metallic surfaces and increased cell proliferation (Garcia-Casas et al., 2019).

The aim of this study was to evaluate the effect of a moxifloxacin-loaded organic-inorganic sol-gel in the *in vitro* biofilm development and treatment, cytotoxicity and cell proliferation. Finally, the efficacy of a moxifloxacin-loaded organic-inorganic sol-gel in preventing PJI caused by *S. aureus* and *E. coli* was evaluated using an *in vivo* murine model for this purpose.

MATERIALS AND METHODS

In vitro Studies

Materials Synthesis

Titanium substrates for microbiological studies were prepared by a conventional powder metallurgy route applying a cold uniaxial charge of 7.9 tn/cm² followed by a sintering step at 1,250°C for 120 min under high vacuum (10^{−5} mbar), as described elsewhere by Bolzoni et al. (2017). The starting Ti powders with a particle size below 75 μm were supplied by AP&C Inc., (Canada). The metallic substrates were ground with SiC paper of 1,000 grit and cleaned with ethanol in an ultrasonic bath.

Sol-gel was prepared as described elsewhere (El hadad et al., 2011) starting with a mixture of γ-methacryloxypropyltrimethoxysilane 98% (Acros Organics, Thermo Fisher Scientific, United States) and tetramethyl orthosilane 98% (Acros Organics, Thermo Fisher Scientific, United States) with a molar ratio of 1:2. Later, tris(trimethylsilyl) phosphite 92% (Sigma-Aldrich, United States) was added at a molar ratio of 1:52 with regard to the silanes (P2) (Figure 1a). Moxifloxacin (Sigma-Aldrich, United States) dissolved in water (Varanda et al., 2006) was added at two concentration: a concentration of 25 mg (A25) (Figure 1b) and a concentration of 50 mg per 20.3 mL of sol-gel (A50) (Figure 1c). These concentrations have been intentionally chosen because they represent 50% and maximum amount of this antibiotic which sol-gel can contain without compromising its stability, durability and adherence on titanium substrates.

Antibiotic Release From Sol-Gel

Moxifloxacin release from sol-gels coating Ti samples was evaluated by introducing in a polypropylene container containing 5 mL of phosphate bufferr saline (bioMérieux, France) previously tempered at 37°C. The antibiotic concentration was periodically measured at 1, 3, 6, 12, 24, and 48 h. The fluorimetric method previously described (Ocana et al., 2000) using an excitation/emission wavelength of 287/465 nm and a standard curve with known concentrations of antibiotic were used to estimate the antibiotic concentration at each time using 300 μL in a Polypropylene 96-well MicroWell™ Plate (Thermo Fisher Scientific, United States). This experiment was performed in triplicate.

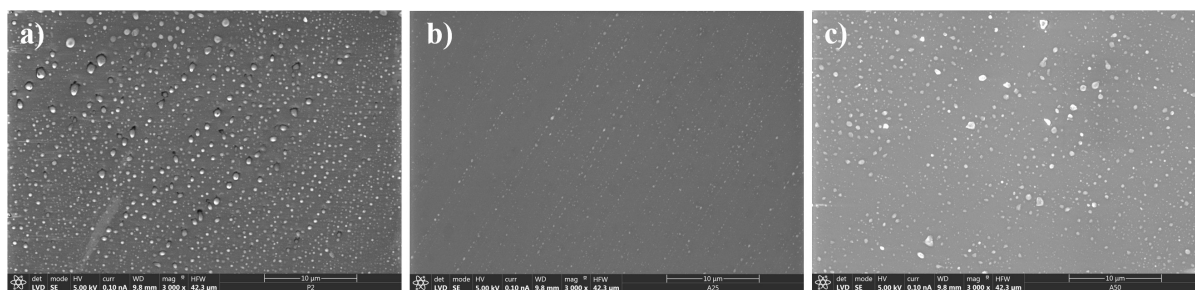


FIGURE 1 | Scanning electron microscopy micrograph of different sol-gel surfaces: P2 (a), A25 (b), and A50 (c).

Microbiological Study

The biofilm formation studies were carried out using three bacterial strains: *S. epidermidis* ATCC 35984, *S. aureus* 15981 (Valle et al., 2003), and *E. coli* ATCC 25922. These species represent the most common pathogens relate to this kind of infection and serve as an example of strains susceptible to this antibiotic. All the strains were kept frozen at -80°C until experiments were performed. Overnight culture of each bacterium was grown in blood tryptic-soy agar (bioMérieux, France) at 37°C in 5% CO_2 . For each species 10^6 colony forming units (CFU/ml) in tryptic soy broth with 1% glucose as biofilm inductive growth medium were inoculated. After incubation, the coatings were washed three times with 0.9% NaCl sterile saline (SS) (B. Braun, Germany). Adhered CFU were estimated by scraping the top disk surface with sterile wooden sticks to corroborate the viability differences on each coating. These wooden sticks with scrapped bacteria were sonicated in a 50-mL FalconTM conical tube (Thermo Fisher Scientific, United States) with 10 mL of SS, with an Ultrasons-H 3000840 low-power bath sonicator (J. P. Selecta, Spain) at 22°C for 5 min (Esteban et al., 2008). This sonicated SS was serially diluted with SS and adhered CFU were estimated using the drop plate method (Herigstad et al., 2001). Supernatant absorbance was measured at 600 nm in eight replicates in a NuncTM 96-Well Polypylene MicroWellTM Plate for estimating planktonic bacterial concentration. This experiment was performed by triplicate for each strain.

Each type of sol-gel incubated with *S. aureus* 15981 were then stained with the Live/Dead BactLight[®] bacterial viability kit (Thermo Fisher Scientific, Waltham, MA, United States) to support visually the numerical results. Photographs (40 \times magnification) were taken in a DM 2000 fluorescence microscope (Leica Microsystems, Germany) for each sample. This strain was the only one which was able to be stained and photographed on sol-gels.

Mature biofilm was grown on black NuncTM F96 MicroWellTM (Thermo Fisher Scientific, United States) using 100 μL per well of an inoculum of 10^6 CFU/mL of brain heart infusion (BHI) at 1% (wt./vol.) (BD, United States) plus 0.03% of fetal bovine serum (Sigma-Aldrich, United States), a culture medium that induces the formation of bacterial biofilm (Perez-Jorge et al., 2017), incubated at 37°C and 5% CO_2 for 24 h. After incubation, the mature biofilm of each well was rinsed twice with 100 μL of SS and

200 μL of BHI at 1% (wt./vol.) with 0.03% of bovine fetal serum (Sigma-Aldrich, United States) were added. The lid of the plate was replaced by a MBECTM biofilm Incubator lid (Innovotech, Canada) whose pegs were coated twice by dipping in wells filled with 200 μL of each treatment (uncoated, P2, A25, and A50) followed by incubation at 37°C and 5% CO_2 at 80 rpm for 48 h. Viable bacteria concentration of the grown biofilm was estimated by adding 10 μL of alamarBlue[®] (BIO-RAD, United States) per well and was incubated at 37°C and 5% CO_2 at 80 rpm for 1 h (Pettit et al., 2005). The fluorescence was measured using an excitation wavelength of 560 nm and an emission wavelength of 590 nm after incubation. The pegs of the uncoated material were used as positive control. This experiment was performed in eight wells per coating by triplicate for each strain.

Cell Study

MC3T3-E1 cells were seeded in a concentration of 10,000 cells/ cm^2 on 96-well plates with α -minimum essential medium with 10% bovine fetal serum and 1% penicillin-streptomycin (α MEM, Invitrogen, Thermo Fisher Scientific Inc., United States) and were incubated at 37°C and 5% CO_2 overnight. After cell adherence, medium was replaced by α MEM with 50 mg/mL ascorbic acid (Sigma-Aldrich, United States), 10 mM β -glycerol-2-phosphate (Sigma-Aldrich, United States) and different treatments: negative control, P2, A25, and A50 ($n = 8$ each) for promoting osteoblastic differentiation, and the lid of the plate was replaced by a MBECTM biofilm Incubator lid (Innovotech, Canada) whose pegs were coated by dipping in wells filled with 200 μL of each treatment (negative control, P2, A25, and A50) followed by incubation at 37°C in 5% CO_2 for 48 h. After incubation, cytotoxicity was tested by CytoTox 96[®] Non-Radioactive Cytotoxicity Assay (Promega, United States). Cell proliferation was determined by addition of alamarBlue[®] solution (BIO-RAD, United States) at 10% (v/v) to the cell culture at 48 h of growth. Absorbance was measured with excitation and emission wavelengths of 570 and 600 nm, respectively, in a Tecan Infinite 200 Reader (Life Sciences, Switzerland).

In vivo Model

Sol-Gel Synthesis and Coating of Titanium Implants

The Ti-6Al-4V implants were prepared from 0.6-mm thick Kirschner wires supplied by Depuy Synthes (Johnson & Johnson, United States). Each wire was cut into implants measuring 1 cm

in length. Next, these were chemically polished (CP) as described previously (Arenas et al., 2013) to achieve a surface finish more closely resembling that used in routine clinical practice (Figures 2a,b). Finally, the Ti-6Al-4V implants for *in vivo* model were coated by dipping in A50 and allowed to dry for at least 1 h at 60°C (CP+A50) (Figures 2c,d).

Animal Surgical Model and Monitoring

We used two clinical strains isolated in the Clinical Microbiology department of the Fundación Jiménez Díaz University Hospital: a strain of *S. aureus* from a 62-year-old man with an acute infection of a hip prosthesis (Sa5) and a strain of *E. coli* from a 61-year-old man with another acute infection, also in a hip prosthesis (Ec30).

This study uses strains obtained from PJIs. The Instituto de Investigación Sanitaria Fundación Jiménez Díaz (IIS-FJD) Research Commission did not require the study to be reviewed or approved by an ethics committee because no clinical, demographical, analytical nor any other data from the patients were included, and bacterial strains do not need such approval according to the present legislation.

Surgical intervention of the *in vivo* model was based on a modified model previously described by Lovati et al. (2013). The intervention consisted of placing the implant into the right femur of SWISS RjOrl:SWISS (CD1®) mice (Janvier Labs, France)

through the knee using an aseptic surgical technique (Figure 3). The main modifications consisted of: (1) replacing phosphate buffer saline with saline, (2) using inhaled isoflurane (3.5%) as the only anesthesia used, and finally, and (3) using chemically polished, 1-cm-long implants made with Ti-6Al-4V instead of a 25-gauge needle, thereby simulating more realistic conditions.

Sixteen-week-old male mice with femoral implants were distributed into six groups: one group with a CP implant without infection (CP group, $n = 8$), a second group with a CP implant with infection induced by Sa5 *S. aureus* (CP Sa5 group, $n = 5$), a third group with a CP implant with infection induced by Ec30 *E. coli* (CP Ec30 group, $n = 5$), a fourth group with a CP implant coated with moxifloxacin-loaded sol-gel without infection (CP+A50 group, $n = 8$), a fifth group with a CP implant coated with moxifloxacin-loaded sol-gel with infection induced by Sa5 (CP+A50 Sa5 group, $n = 5$), and a sixth group with a CP implant coated with moxifloxacin-loaded sol-gel with infection induced by Ec30 *E. coli* (CP+A50 Ec30 group, $n = 5$).

We assessed the pain-stress and weight of each animal every 48 h on weekdays to ensure physical status. Evaluation of pain-stress consisted of the presence or absence of six behaviors directly related to pain or stress in this species and for the surgical procedure the animals had undergone: limping, piloerection, lack of grooming, wound presence, passivity, and aggressiveness. In

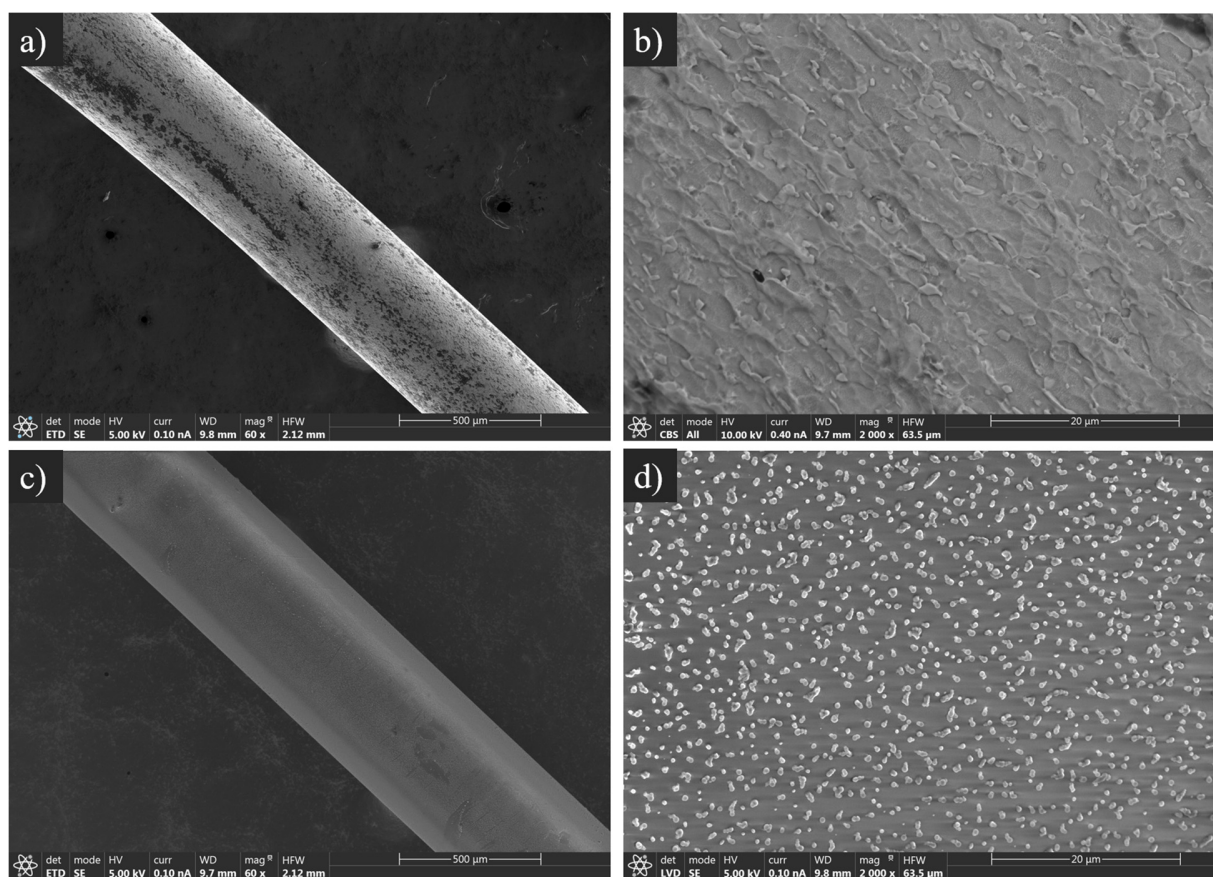


FIGURE 2 | Scanning electron microscopy micrograph of CP (a,b) and CP+A50 surfaces (c,d) at 60 (a,c) and 2,000 (b,d) magnifications.

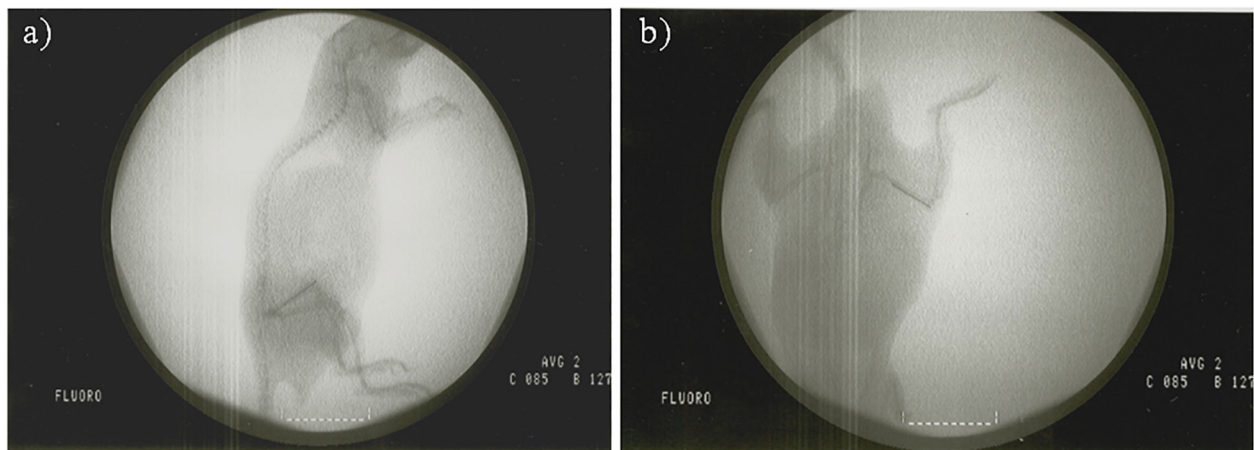


FIGURE 3 | Fluoroscopy of a mouse with an implant placed in the femur in lateral (a) and dorsoventral (b) position.

cases of sustained weight loss over time, the most appropriate refinement measures were taken to encourage the animal to eat. For this, they were offered an additional mixture of grains and vegetables (Vitakraft, Bremen, Deutschland). At 15 days postsurgically, a urine sample was taken from all infected animals, and bacteria presence was evaluated qualitatively.

Five weeks after surgery, the animals were euthanized using hypercapnia. The entire femur of each animal was then recovered through sterile preparation of the knee, including surgical field isolation.

Microbiological Study

The biofilm formation ability of the different clinical strains was evaluated according to a widely accepted published protocol (Stepanovic et al., 2007). The strains were transferred from stock culture into blood tryptic-soy agar and incubated at 37°C overnight under aerobic conditions. The next day, colonies were suspended in TSB until a turbidity comparable to 0.5 MacFarland scale ($\sim 10^8$ CFU/mL) was reached. This suspension was diluted 1:100 in TSB+1% glucose to reach a bacterial concentration of approximately 10^6 CFU/mL. Then, 200 μ L from the diluted suspension was aliquoted into 96-well untreated microtiter plate

and incubated at 37°C and 5% CO₂ for 24 h under static aerobic conditions. The next day, the wells were aspirated, and each well was washed three times with 200 μ L SS. After washing, the remaining attached bacteria were fixed with 200 μ L of methanol, and incubated at room temperature for 20 min. The methanol was discarded and plates were left to dry in at 60°C. Finally, the biofilm formed was stained with 200 μ L of 2% crystal violet for Sa5 and of 1% safranin for Ec30 for 15 min. Plates were washed two times with 250 μ L of sterile distilled water, and dye bound to the cells was eluted with 250 μ L of absolute ethanol. The absorbance was measured at 570 nm for crystal violet and at 492 nm for safranin using a microplate reader. Experiments were performed in eight wells and repeated three times. The cut-off value (optical density control, ODC) was defined as three standard deviations above the mean OD of the negative control. The strains were classified according to its optical density (OD) per well within of the following categories: non-biofilm former ($OD \leq ODC$), weak biofilm former ($ODC < OD < 2 \times ODC$), moderate biofilm former ($2 \times ODC < OD < 4 \times ODC$) and strong biofilm former ($OD > 4 \times ODC$).

The urine samples were seeded in CHROMID® CPS® Elite (bioMérieux, France) to diagnose possible bacteriuria.

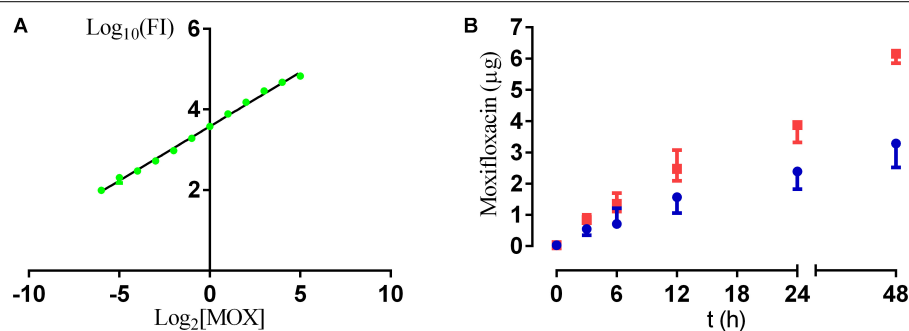


FIGURE 4 | Calibration curve resulting from known concentrations of moxifloxacin (MOX) and their fluorescence intensity (FI) (A); and amount of moxifloxacin released from A25 (blue) and A50 (red) over time (B).

Using a hammer, each femur was divided into two samples on a sterile surface: (1) bone and adnexa, and (2) implant.

The bone was immersed in 2 mL of SS and sonicated using an sonicator at 22°C for 5 min (Esteban et al., 2008). The resulting sonicate was diluted in a 10-fold dilution bank and seeded on blood-chocolate agar (bioMérieux, France) using the plaque extension method, which consists of seeding 100 μ L/plate of each dilution. The concentration of bacteria was estimated as CFU/g of bone and adnexa.

The implant was sonicated in 2 mL of saline for 5 min to release the adhered biofilm bacteria and estimated their concentration, measured as CFU/cm² of implant. All plates were checked at 24 and 48 h.

Microcomputed Tomography

Three bone samples from each non-infected control group included in the aforementioned model were fixed in 10% formaldehyde for 48 h at 4°C. After fixation, they were dehydrated in 96% ethanol for 48 h, changing the ethanol every 24 h, and in 100% ethanol for 48 h, changing the ethanol every 24 h.

Three-dimensional microcomputed tomography was performed with a CompaCT scanner (Sedecal, Spain). Data were acquired with 720 projections by 360-degree scan, having an integration time of 100 ms with three frames, photon energy of 50 KeV, and a current of 100 μ A. The duration of imaging was 20 min per scan. Three-dimensional renderings of the hind paws were generated using original volumetric images reconstructed with MicroView software (GE Healthcare). Bone mass (BM, mg), bone volume (BM, cm³), and bone mineral density

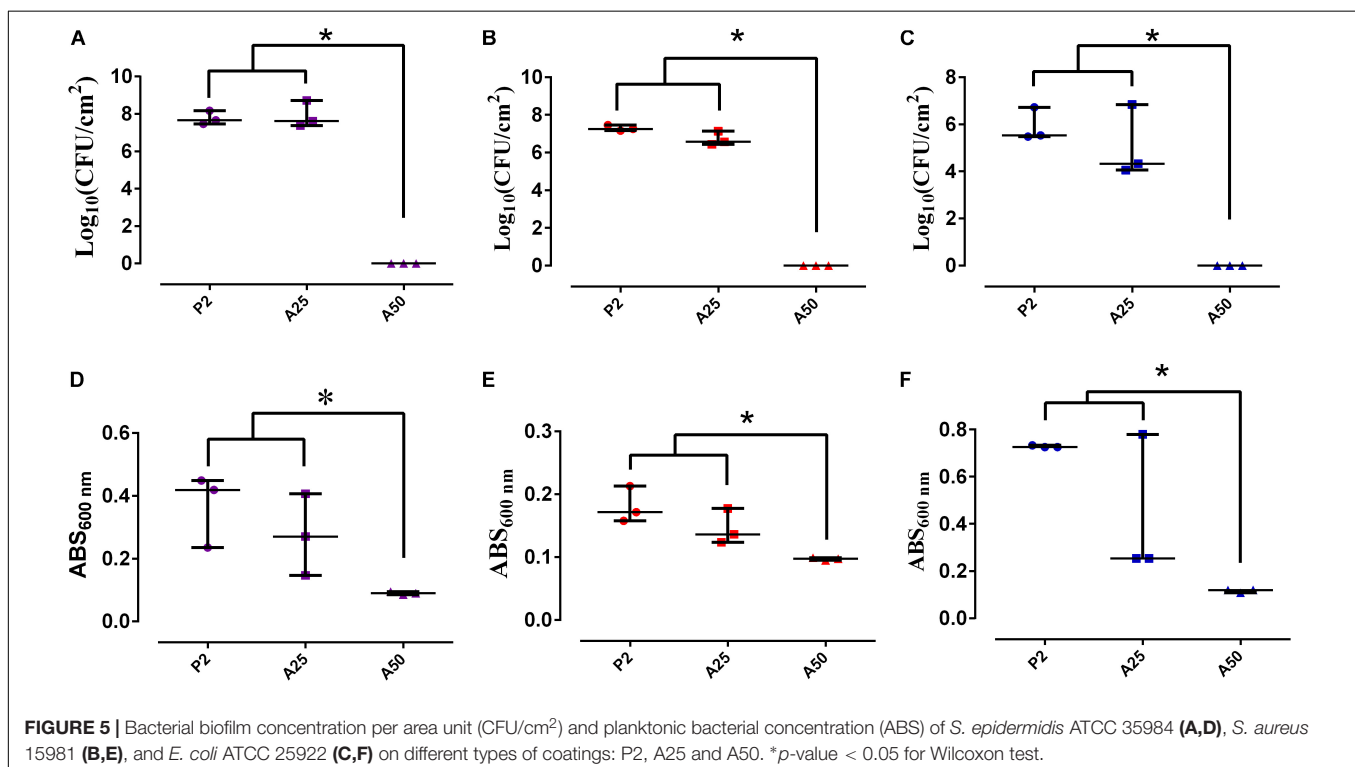
(BMD = BM/BV, mg/cm³) were quantified from MicroCT scans using GE MicroView software 2.2.

Histological Studies

Three femurs of CP group and CP+A50 group were fixed in 4% paraformaldehyde for 48 h, decalcified in 10% EDTA for 4 weeks, paraffin-infiltrated, and stained with hematoxylin-eosin. Implants were removed and transversal sections in the knee condyles (5 μ m) were done.

Tartrate-resistant acid phosphatase (TRAP) staining was carried out in paraffin sections with a homemade TRAP buffer (0.1 M acetate buffer, 0.3 M Sodium Tartrate 10 mg/ml Naphthol AS-MX phosphate, 0.1% Triton X-100, 0.3 mg/ml Fast Red Violet LB (Sigma-Aldrich, United States). After deparaffinization and acetate buffer washing processes, samples were incubated in TRAP buffer for 30 min and counterstained with Fast Green.

Immunohistochemistry analysis was carried out as previously described (Mediero et al., 2012). Briefly, sections were incubated with proteinase K Solution (20 μ g/mL in TE Buffer, pH 8.0) for 15 min in water bath at 37°C for antigen retrieval after deparaffinization and re-hydration. Blocking of non-specific binding was performed with PBS 3% BSA and 0.1% Triton X-100 for 1 h, and primary antibodies anti-cathepsin K (1:25), CD68 (1:200) and alkaline phosphatase (ALP) 1:200 (all antibodies from Santa Cruz Biotechnology, United States) were incubated overnight at 4°C in a humidifying chamber. Secondary antibodies goat anti-rabbit-FITC (1:200), goat anti-mouse-FITC (1:200) (Invitrogen, Life Technologies, United States) were incubated for 1 h in the dark. Slides were mounted



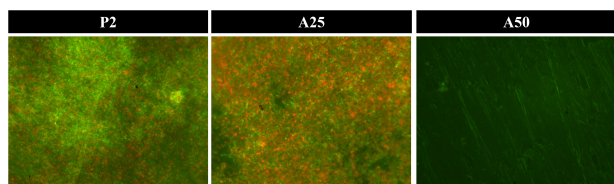


FIGURE 6 | *Staphylococcus aureus* biofilm grown on each sol-gel and stained using Live/Dead Bactlight to 40× magnification. Green bacteria are viable and red ones are dead.

with Fluoroshield with DAPI mounting media (Sigma-Aldrich, United States). Images were taken with the iScan Coreo Au scanner (Ventana Medical Systems, Roche diagnostics, Spain) and visualized with Image Viewer v.3.1 software (Ventana Medical Systems, Roche diagnostics, Spain). Images were taken at 4× or 10× magnifications.

Statistical Analysis

Statistical analyses were performed using Stata Statistical Software, Release 11 (StataCorp, United States). Data were evaluated using a one-sided Wilcoxon non-parametric test to compare two groups. Statistical significance was set at

p -values ≤ 0.05 . Body weight was evaluated over time using a linear regression model. Microbiological, cellular results and weight values are represented as median and interquartile range. Other behavioral variables are represented as relative frequencies at each time point.

RESULTS

In vitro Studies

Antibiotic Release From Sol-Gel

Figure 4A represents the standard curve with known concentrations of antibiotic and their respective fluorescence intensity. The regression coefficients (R^2) was 0.9918. The antibiotic release shows a linear release over time both from A25 and from A50 (Figure 4B), and maximum release values were obtained at 48 h for both sol-gels. The moxifloxacin release rate from A50 (120 ng/h) was significantly higher than the rate from A25 (60.6 ng/h) (p -value < 0.0001 for t -Student test).

Microbiological Studies

Figures 5A–C shows plots of the bacteria concentration per area unit that are attached to the surface by means of colony forming units (CFU). CFU per square centimetre significantly decreased only on A50 for the three strains used (p -value < 0.05). Plots of

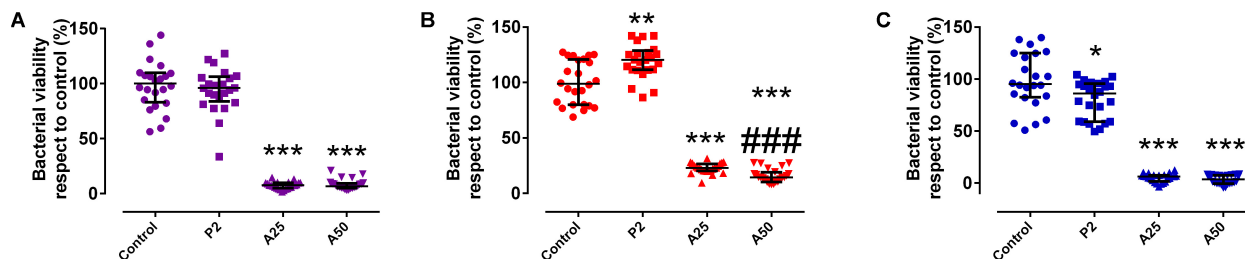


FIGURE 7 | Percentage of biofilm growth respect to the control of *S. epidermidis* ATCC 35984 (A), *S. aureus* 15981 (B), and *E. coli* ATCC 25922 (C) on different types of coatings: P2, A25 and A50. * p -value < 0.05 , ** p -value < 0.01 , *** p -value < 0.001 for Wilcoxon test between biofilm growth on the control and on coatings loaded with MOX. ### p -value < 0.001 for Wilcoxon test between biofilm growth on A25 and A50.

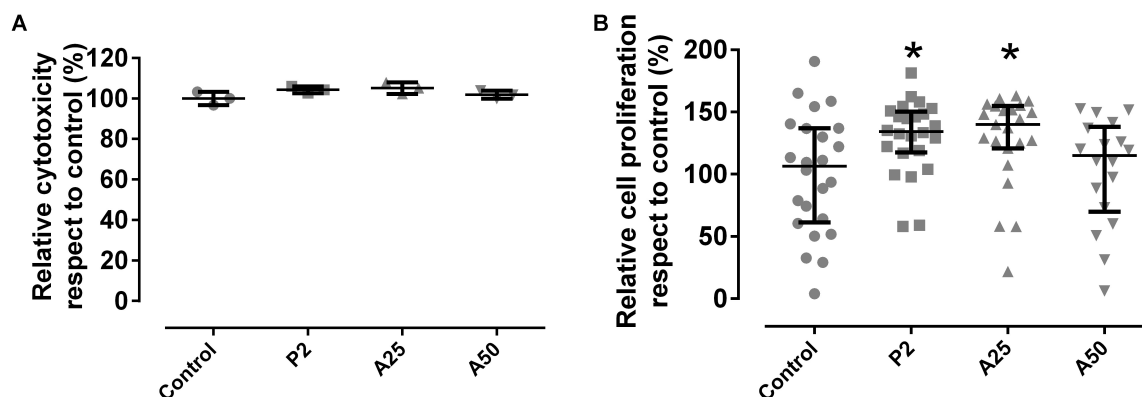


FIGURE 8 | Cytotoxicity (A) and cell proliferation (B) of MC3T3-E1 cells when growing in presence of each coating. Control was considered in the presence of any coating. * p -value < 0.05 for Wilcoxon test between cell proliferation on control and on different coatings loaded with MOX.

Figures 5D–F show that the planktonic bacterial concentration is proportional to the absorbance of the supernatant measured at 600 nm. Bacterial absorbance was inversely proportional to moxifloxacin concentration. The microbiological study revealed two responses for the biofilm development and for the planktonic bacterial concentration. The biofilm development response was all-or-nothing for the staphylococci when their biofilms grow in presence of P2 or A25 (all) and A50 (nothing) (**Figures 5A,B, 6**). *E. coli* ATCC 25922 biofilm development showed a lower development which was influenced by the concentration of

antibiotic (**Figure 5C**). On the contrast, the planktonic bacterial concentration was gradually and inversely proportional to the moxifloxacin coating concentration for all the tested strains (**Figures 5D–F**).

Coatings containing antibiotic behaved as inhibitors of the growth of a mature biofilm (**Figure 7**). The unloaded coating (P2) did not show an inhibitor behavior in the presence of staphylococci mature biofilms (**Figures 7A,B**) (p -value > 0.05) but showed, however, a slightly inhibitor behavior in the presence of a mature biofilm *E. coli* (p -value = 0.0088) (**Figure 7C**). Though

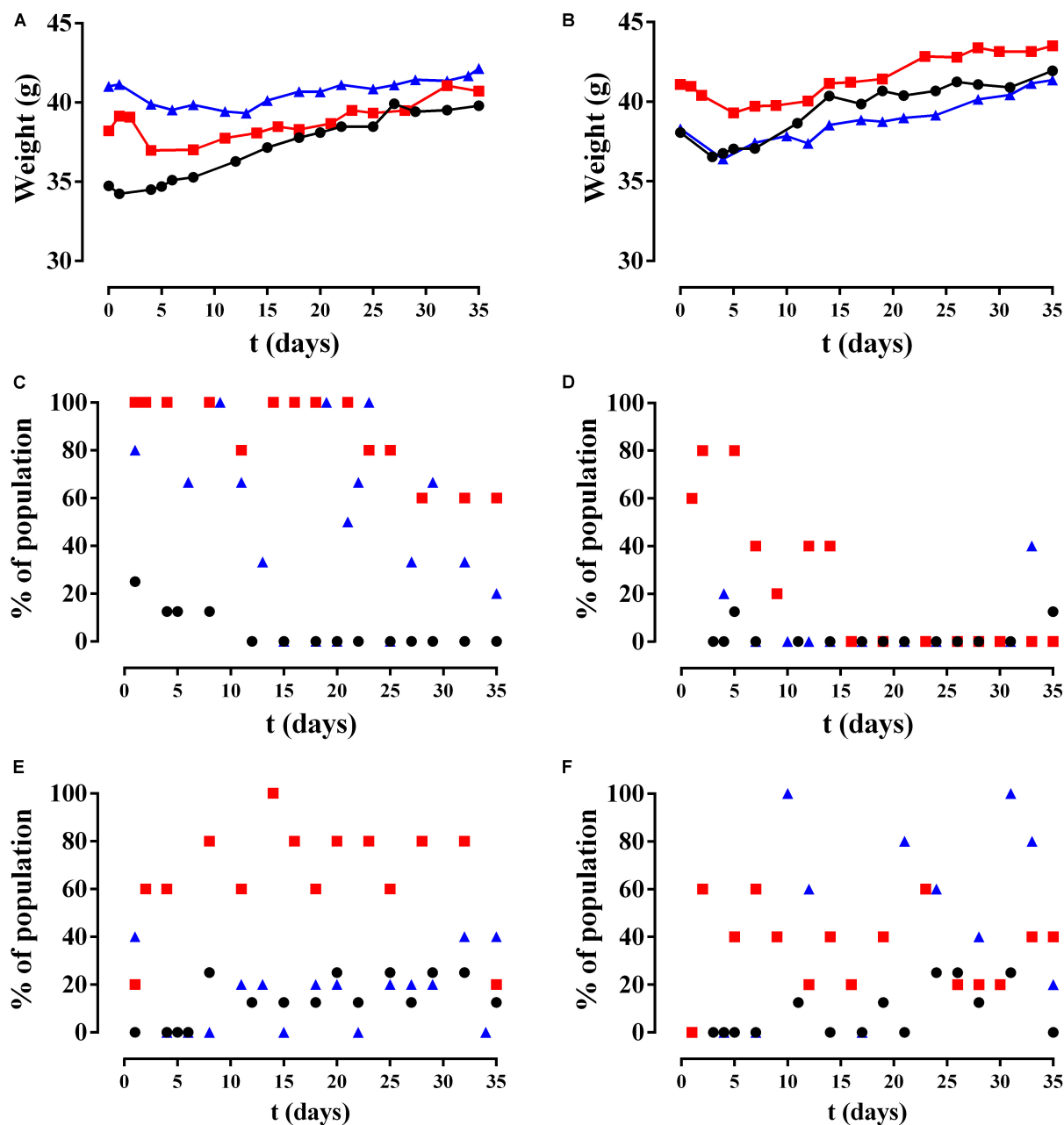


FIGURE 9 | Results of animal monitoring over time. (A,B) Mean weight, (C,D) limping, and (E,F) piloerection in different non-infected groups (circles), Sa5-infected group (squares), and Ec30-infected group (triangles) with CP (left column) and CP+A50 (right column).

A25 and A50 are able to inhibit in a similar way the mature biofilm growth of *S. epidermidis* ATCC 35984 and *E. coli* ATCC 25922, A50 showed the highest inhibitor behavior on the mature biofilm of *S. aureus* 15981 compared to A25 (p -value < 0.001).

Cellular Studies

Cytotoxicity was not detected in the presence of the coatings tested respect to the control used (p -value > 0.05) (Figure 8A).

This explains why P2 stimulates significantly up to 30% the cell proliferation compared to the other coatings and the control (Figure 8B). However, cell proliferation was also influenced by the antibiotic added to the coatings. A50 showed a lower percentage of cell proliferation than the control, meaning the high quantity of antibiotic added on A50 acted against cells although only in the first 48 h.

In vivo Studies

Animal Monitoring

The mean weight over time of the mice is shown by group in Figures 9A,B. All groups significantly increased their weight over time (p -value < 0.001) except CP Ec30 (p -value = 0.1196).

Only two of the six behavioral variables evaluated showed a modification during the study: limping and piloerection (Figures 9C,D). Limping was significantly more frequent in the CP Sa5 group than the CP+A50 Sa5 groups (p -value < 0.0001) and was significantly higher in the CP Ec30 group compared to the CP+A50 Ec30 group (p -value < 0.0001) (Figure 9C). Piloerection was observed with significantly greater frequency in the CP Sa5 group than in the CP+A50 Sa5 groups (p -value = 0.0004) and increased significantly over time in the CP+A50 Ec30 group compared to the CP Ec30 group (p -value = 0.0073) (Figures 9E,F).

Microbiological Study

Both of the clinical bacterial strains used were strong biofilm former: 12.2 (9.3 – 15.5) \times ODC for Sa5 and 4.3 (4.2 – 4.8) \times ODC for Ec30.

Bacteriuria was only detected in nine of the Ec30-infected mice: four from the CP Ec30 group and five from the CP+A50 Ec30 group. The antibiotype of *E. coli* strains isolated from urine was identical to that of Ec30 strains inoculated during surgery.

Of all the femurs studied, seven showed macroscopic deformation consistent with osteomyelitis (Figure 10): five animals in the CP Sa5 group and two in the CP Ec30 group. Deformation was higher in CP Sa5 than in CP Ec30.

Statistically significant differences were observed between the quantity of bacteria in bone and adnexa (p -value = 0.0027 for CP and CP Sa5, and p = 0.0027 for CP and CP Ec30) and implants (p -value = 0.0093 for CP and CP Sa5, and p = 0.0275 for CP and CP Ec30) between the CP groups (Figures 11A,B).

No differences were observed in the number of bacteria in bone and adnexa and implants (p -value = 1.0000 for CP+A50 and CP+A50 Sa5, and p = 1.000 for CP+A50 and CP+A50 Ec30) between the CP+A50 groups (Figures 11C,D).

Microcomputed Tomography

No differences were observed between the BMC and BMD of non-infected CP and non-infected CP+A50 (p -value = 0.1376 and p = 0.4137, respectively) (Figure 12). The BMD results were perfectly comparable, since BMC was no different between the groups compared.

Histology

Hematoxylin-eosin staining showed that mice with CP implant presented fibrous tissue in the area where implant was present (arrow) (Figure 13). CP+A50 showed absence of tissue what correlated with the area occupied by the implant (arrow) (Figure 13). When bone markers were studied, no many changes were found among different animals. Both groups showed similar number of TRAP positive cells (arrow), and immunostaining for cathepsin K (cysteine protease, osteoclast marker) did not showed any difference, ALP (alkaline phosphatase) positive cells were similar in CP and CP+A50, but macrophages (CD68 + cells) were increased in CP+A50.

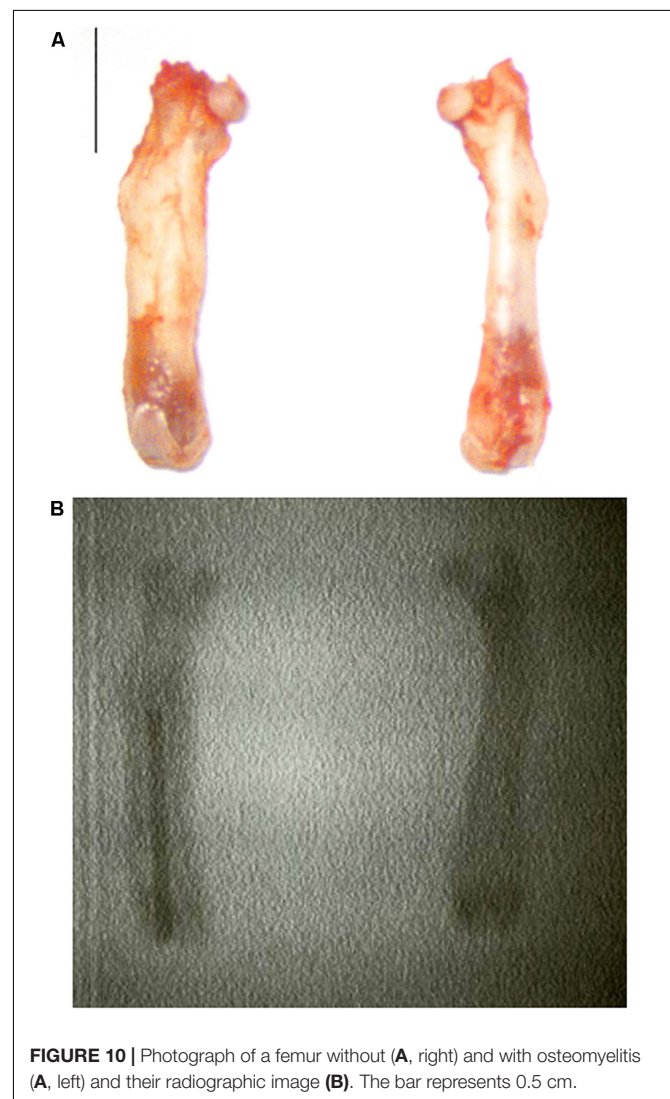


FIGURE 10 | Photograph of a femur without (A, right) and with osteomyelitis (A, left) and their radiographic image (B). The bar represents 0.5 cm.

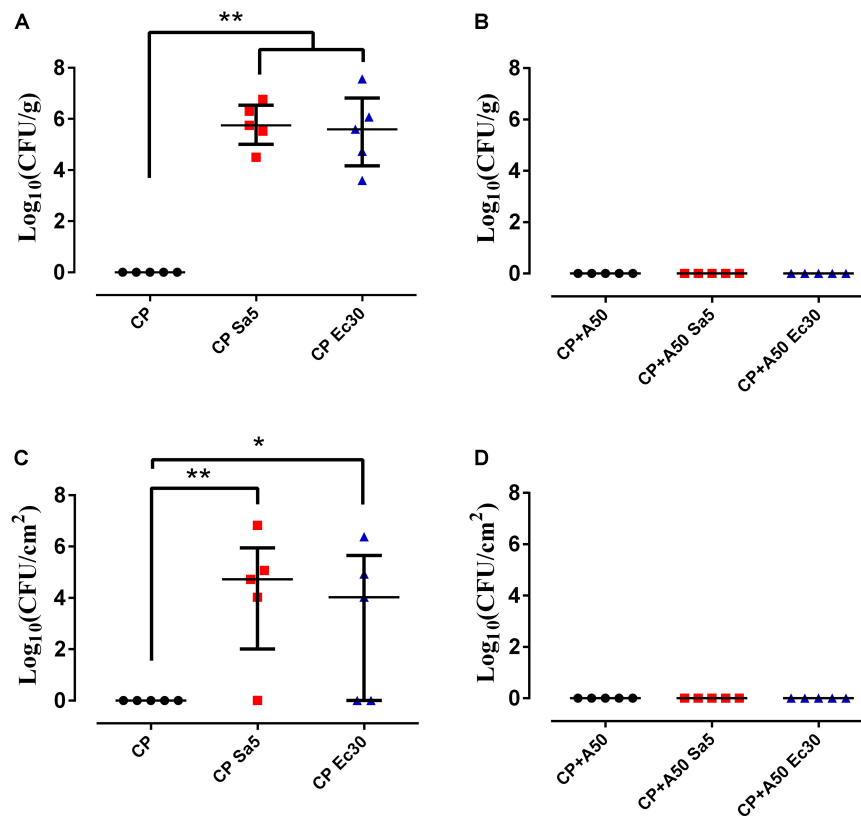


FIGURE 11 | Quantity of bacteria in bone and adnexa (left column) and on recovered implant (right column) with CP (A,B) and CP+A50 (C,D). **p*-value < 0.05, ***p*-value < 0.01 for Wilcoxon test between non-infected group and infected groups by *S. aureus* (Sa5) or *E. coli* (Ec30).

DISCUSSION

In this study, we report the efficacy of a novel approach of sol-gel coatings containing moxifloxacin, that was demonstrated to provide an anti-infective surface to Ti-based materials both *in vitro* and *in vivo*. The active surfaces prevented locally the biofilm development and treated mature biofilms of different clinically important bacterial species. Finally, we demonstrated the *in vivo* efficacy of moxifloxacin-loaded sol-gel in preventing PJI caused by Gram-positive *S. aureus* and Gram-negative *E. coli*.

The microbiological study revealed that only A50 completely inhibited the formation of biofilm on the coated surface and was the best treatment for a mature biofilm of the three bacterial species. Hence, A50 was the most appropriate coating to use in the *in vivo* model and would be the best prophylactic treatment in the clinical practise. The moxifloxacin release rate of A50 was almost two-fold higher than A25 and showed a lineal trend over time as other antibiotics (e.g., vancomycin) loaded in sol-gels made of tetraethyl orthosilicate (Radin and Ducheyne, 2007).

Commonly reported symptoms of PJI include pain, joint swelling or effusion, erythema or warmth around the joint, fever, drainage, or the presence of a sinus tract communicating with the arthroplasty (Tande and Patel, 2014). The joint pain in our *in vivo* model was monitored by observing limping, and generalized malaise was monitored by observing evidence of

piloerection often associated with infection (Campos et al., 2016). Infected animals with A50-coated implants showed significantly less limping and piloerection over time than infected animals with non-coated implants, with the exception of piloerection in *E. coli*-infected animals with coated implants (Figure 9). In these cases of *E. coli*-infected animals with coated implants, piloerection was higher in those animals with coated implant compared to animals with non-coated implants; this may be due to the bacteriuria observed in these animals. We cannot completely explain this apparently symptomatic bacteriuria, though it may be caused by bacterial concentration in the bladder due to transient bacteraemia (Wang et al., 2017) during surgery as well as the motility of *E. coli* (Kaya and Koser, 2012), which allows the bacteria to migrate and colonize a new niche with lower hostility than the interior of the bone when it contains an antibiotic-coated implant. The microbiological results from the *in vivo* study revealed that moxifloxacin-loaded sol-gel showed an all-or-nothing response when used to coat the implant and *S. aureus* or *E. coli* infection is induced (Figure 11) as expected. The femoral deformation observed in *S. aureus*-infected groups with non-coated implants is consistent with the ability of *S. aureus* to internalize in osteoblasts (Cremet et al., 2015) and cause deforming osteomyelitis in chronic bone infections (de Mesy Bentley et al., 2017) (Figure 10). In the case of *E. coli*, the bone deformation observed in infected groups

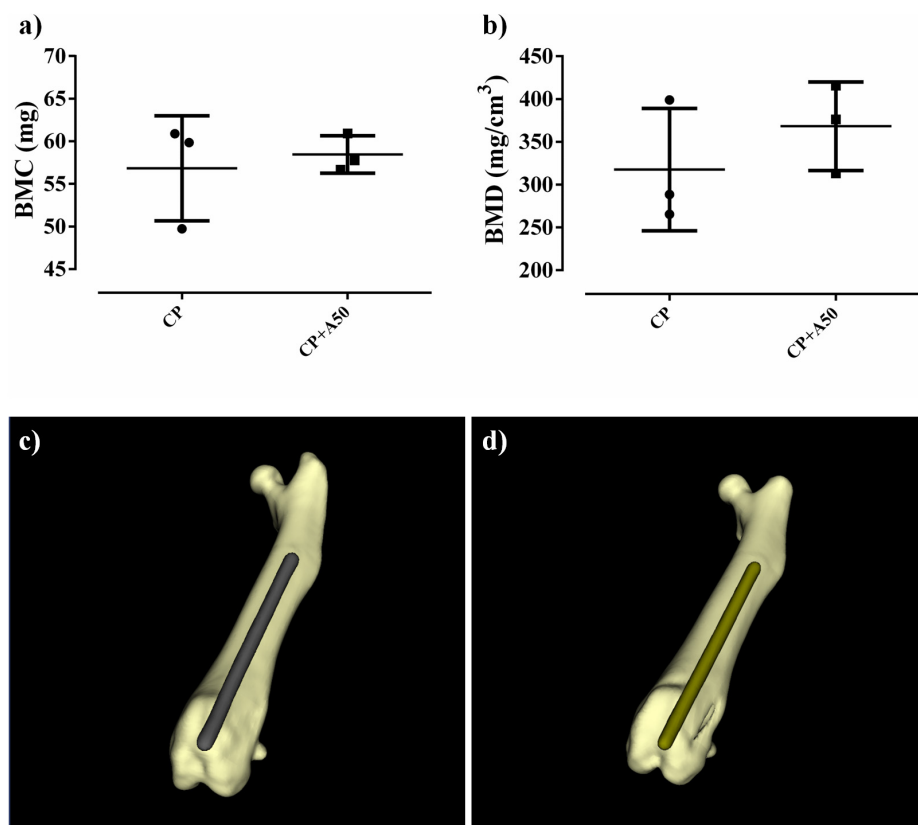


FIGURE 12 | Bone mineral content (BMC) (a) and bone mineral density (BMD) (b) and their three-dimensional reconstructions of a representative sample of the CP group (c) and CP+A50 group (d).

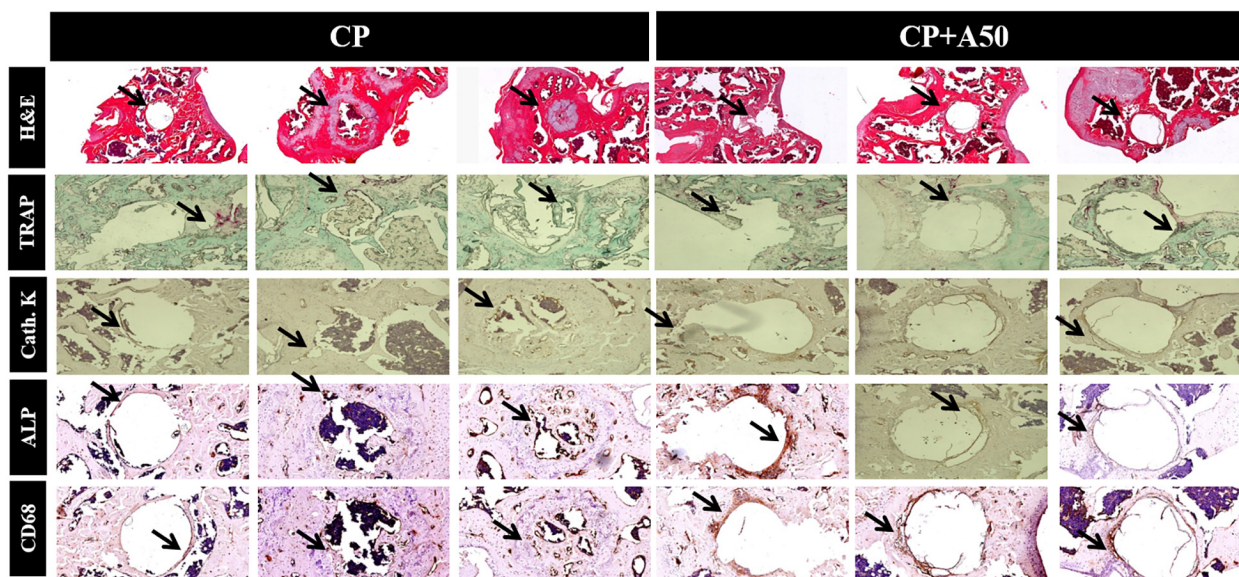


FIGURE 13 | Immunohistochemistry for markers of different bone cells. Long bones were processed and immunohistologic staining carried out. Shown are representative images stained for haematoxylin-eosin (H&E), tartrate-resistant acid phosphatase (TRAP) staining, cathepsin K (cath. K), alkaline phosphatase (ALP) and macrophages (CD68). H&E images were taken at 4× magnification. All immunostaining images were taken at 10× magnification.

with non-coated implants may be due to osteoblastic cytotoxicity (Cremet et al., 2015).

The non-cytotoxicity of these coatings was validated and the cellular proliferation was slightly favored in presence of P2 and A25. The addition of tris(trimethylsilyl) phosphite to the sol-gel formulation created localized areas with higher phosphorus content that is released in form of phosphate when sol-gel is degraded over time. This inorganic phosphorus compound significantly stimulates the growth and osteogenic differentiation of the bone cells (Liu et al., 2009). This cell proliferation increase was absent in presence of A50, this may be due to that the proliferative effect exerted by the phosphate released from sol-gel degradation would be counteracted by the high moxifloxacin concentration, an fluoroquinolone antibiotic which has been frequently associated with a wide spectrum of musculoskeletal complications that involve not only tendon but also cartilage, bone, and muscle (Hall et al., 2011; Jacobs et al., 2014). Due to the degradation of sol-gel would take place after 48–72 h of surgery, this potential local cytotoxicity would be a assumable and transient complication by taking into account the benefit of prophylaxis. Moreover, moxifloxacin-loaded coating showed a non-harmful effect on bone mineralization according to the microcomputed tomographic images (Figure 12) and no changes in bone markers were found among groups (Figure 13), what correlates with micro-CT data. The increased in macrophages in CP+A50 group might be indicating that the local antibiotic delivery from sol-gel is recruiting macrophages at site of surgery what would impede the bacterial proliferation, since it has been also found previously that a multifunctional nanogel for targeted vancomycin delivery provides macrophage targeting and lesion site—activatable drug release properties, which enhances bacterial growth inhibition in a zebra fish *in vivo* model (Xiong et al., 2012).

In recent years, different types of coating have been introduced for clinical use: natural, peptide, ceramic, and synthetic coatings (Civantos et al., 2017). Most have been designed with osteointegration (Civantos et al., 2017; Haimov et al., 2017) and antibacterial purposes (Zhao et al., 2009; Swartjes et al., 2015; Kulkarni Aranya et al., 2017). To date, antibacterial, biodegradable perioperative coatings are designed to be loaded with gentamicin or vancomycin (Romanò et al., 2015) and are already on the market. One example is a fast-resorbable, antibiotic-loadable hydrogel composed of covalently linked hyaluronan and poly-D,L-lactide, whose efficacy has been proven *in vitro* (Drago et al., 2014) and in a multicentre randomized controlled trial (Malizos et al., 2017). Thus, the moxifloxacin-loaded sol-gel used in our study is a new, cost-effective alternative for locally preventing and without significant compromising the bone mineralization. Nevertheless, moxifloxacin can be replaced by a broad spectrum of antibiotics according to the clinical need. The use of this biomaterial and its versatility represent an important advance in Traumatology and Orthopedics field.

In conclusion, coating loaded with higher concentration of moxifloxacin (A50) showed excellent bactericidal and broad-spectrum anti-biofilm response since it showed the highest inhibitor behavior on the biofilm development (local prevention) and on mature bacterial biofilm (local treatment).

DATA AVAILABILITY STATEMENT

The datasets generated for this study are available on request to the corresponding author.

ETHICS STATEMENT

This study was approved by the Instituto de Investigación Sanitaria Fundación Jiménez Díaz (IIS-FJD) Animal Care and Use Committee, which includes *ad hoc* members for ethical issues. Animal care and maintenance complied with institutional guidelines as defined in national and international laws and policies (Spanish Royal Decree 53/2013, authorization reference PROEX019/18 March 8, 2018 granted by the Counsel for the Environment, Local Administration and Territorial Planning of the Community of Madrid and, Directive 2010/63/EU of the European Parliament and of the Council of September 22, 2010).

AUTHOR CONTRIBUTIONS

JA-C, AG-C, AM, AJ-M, and JE made substantial contributions to the research design, acquisition, analysis, interpretation of the data, drafting the manuscript and revising it critically, and approved the submitted and final versions of the manuscript. DR, IC-L, and FM made substantial contributions to the research design, acquisition, analysis and interpretation of data and approved the submitted and final versions of the manuscript.

FUNDING

The authors acknowledge the financial support from the Regional Government of Madrid through the program MULTIMAT-CHALLENGE (S2013/MIT-2862), and from the Mutua Madrileña Foundation (04078/001). JA-C was funded by an FPI grant from the Spanish Ministry of Economics and Competitiveness (BES-2014-069007). AM was funded by grants from Instituto de Salud Carlos III through the “Miguel Servet” program (CP15/00053). DR was funded by a grant from the Fundación Conchita Rábago.

ACKNOWLEDGMENTS

The authors are grateful to Experimental Surgery and Animal Research Service, concretely to Dr. Carlos Castilla-Reparaz and Mr. Carlos Carnero-Guerrero. Parts of this work were previously presented at the 25th European Orthopedic Research Annual Meeting, the 28th and 29th European Congress of Clinical Microbiology and Infectious Diseases, 22nd and 23rd Spanish Congress of Clinical Microbiology and Infectious Diseases and awarded as one of the best six scientific communications in the 23rd Spanish Congress of Clinical Microbiology and Infectious Diseases.

REFERENCES

- Anagnostakos, K., Schmid, N. V., Kelm, J., Grun, U., and Jung, J. (2009). Classification of hip joint infections. *Int. J. Med. Sci.* 6, 227–233. doi: 10.7150/ijms.6.227
- Arenas, M. A., Perez-Jorge, C., Conde, A., Matykina, E., Hernandez-Lopez, J. M., Perez-Tanoira, R., et al. (2013). Doped TiO₂ anodic layers of enhanced antibacterial properties. *Colloids Surf. B Biointerf.* 105, 106–112. doi: 10.1016/j.colsurfb.2012.12.051
- Benito, N., Franco, M., Ribera, A., Soriano, A., Rodriguez-Pardo, D., Sorli, L., et al. (2016). Time trends in the aetiology of prosthetic joint infections: a multicentre cohort study. *Clin. Microbiol. Infect.* 22, e731–e738. doi: 10.1016/j.cmi.2016.05.004
- Bolzoni, L., Ruiz-Navas, E. M., and Gordo, E. (2017). Evaluation of the mechanical properties of powder metallurgy Ti-6Al-7Nb alloy. *J. Mech. Behav. Biomed. Mater.* 67, 110–116. doi: 10.1016/j.jmbbm.2016.12.005
- Campos, J. D., Hoppe, L. Y., Duque, T. L., de Castro, S. L., and Oliveira, G. M. (2016). Use of noninvasive parameters to evaluate swiss webster mice during trypanosoma cruzi experimental acute infection. *J. Parasitol.* 102, 280–285. doi: 10.1645/15-884
- Civantos, A., Martínez-Campos, E., Ramos, V., Elvira, C., Gallardo, A., and Abarrategi, A. (2017). Titanium coatings and surface modifications: toward clinically useful bioactive implants. *ACS Biomater. Sci. Eng.* 3, 1245–1261. doi: 10.1021/acsbomaterials.6b00604
- Cobo, J., Miguel, L. G., Euba, G., Rodriguez, D., Garcia-Lechuz, J. M., Riera, M., et al. (2011). Early prosthetic joint infection: outcomes with debridement and implant retention followed by antibiotic therapy. *Clin. Microbiol. Infect.* 17, 1632–1637. doi: 10.1111/j.1469-0691.2010.03333.x
- Crement, L., Broquet, A., Brulin, B., Jacqueline, C., Dauvergne, S., Brion, R., et al. (2015). Pathogenic potential of *Escherichia coli* clinical strains from orthopedic implant infections towards human osteoblastic cells. *Pathog. Dis.* 73:ftv065. doi: 10.1093/femspd/ftv065
- Drago, L., Boot, W., Dimas, K., Malizos, K., Hansch, G. M., Stuyck, J., et al. (2014). Does implant coating with antibacterial-loaded hydrogel reduce bacterial colonization and biofilm formation in vitro? *Clin. Orthop. Relat. Res.* 472, 3311–3323. doi: 10.1007/s11999-014-3558-1
- de Mesy Bentley, K. L., Trombetta, R., Nishitani, K., Bello-Irizarry, S. N., Ninomiya, M., Zhang, L., et al. (2017). Evidence of *Staphylococcus aureus* deformation, proliferation, and migration in canaliculi of live cortical bone in murine models of osteomyelitis. *J. Bone Miner. Res.* 32, 985–990. doi: 10.1002/jbmr.3055
- El hadad, A. A., Carbonell, D., Barranco, V., Jiménez-Morales, A., Casal, B., and Galván, J. C. (2011). Preparation of sol-gel hybrid materials from γ -methacryloxypropyltrimethoxysilane and tetramethyl orthosilicate: study of the hydrolysis and condensation reactions. *Colloid Polymer Sci.* 289, 1875–1883. doi: 10.1007/s00396-011-2504-y
- Esteban, J., Gomez-Barrena, E., Cordero, J., Martin-de-Hijas, N. Z., Kinnari, T. J., and Fernandez-Roblas, R. (2008). Evaluation of quantitative analysis of cultures from sonicated retrieved orthopedic implants in diagnosis of orthopedic infection. *J. Clin. Microbiol.* 46, 488–492. doi: 10.1128/jcm.01762-07
- Garcia-Casas, A., Aguilera-Correa, J. J., Mediero, A., Esteban, J., and Jimenez-Morales, A. (2019). Functionalization of sol-gel coatings with organophosphorus compounds for prosthetic devices. *Colloids Surf. B* 181, 973–980. doi: 10.1016/j.colsurfb.2019.06.042
- Gristina, A. G. (1987). Biomaterial-centered infection: microbial adhesion versus tissue integration. *Science* 237, 1588–1595. doi: 10.1126/science.3629258
- Haimov, H., Yosupov, N., Pinchasov, G., and Juodzbals, G. (2017). Bone morphogenetic protein coating on titanium implant surface: a systematic review. *J. Oral. Maxillofac. Res.* 8:e1. doi: 10.5037/jomr.2017.8201
- Hall, M. M., Finnoff, J. T., and Smith, J. (2011). Musculoskeletal complications of fluoroquinolones: guidelines and precautions for usage in the athletic population. *PM R* 3, 132–142. doi: 10.1016/j.pmrj.2010.10.003
- Herigstad, B., Hamilton, M., and Heersink, J. (2001). How to optimize the drop plate method for enumerating bacteria. *J. Microbiol. Methods* 44, 121–129. doi: 10.1016/S0167-7012(00)00241-4
- Jacobs, J. C., Shea, K. G., Oxford, J. T., and Carey, J. L. (2014). Fluoroquinolone use in a child associated with development of osteochondritis dissecans. *BMJ Case Rep.* 2014, 1–4. doi: 10.1136/bcr-2014-204544
- Kaya, T., and Koser, H. (2012). Direct upstream motility in *Escherichia coli*. *Biophys. J.* 102, 1514–1523. doi: 10.1016/j.bpj.2012.03.001
- Kulkarni Aranya, A., Pushalkar, S., Zhao, M., LeGeros, R. Z., Zhang, Y., and Saxena, D. (2017). Antibacterial and bioactive coatings on titanium implant surfaces. *J. Biomed. Mater. Res. A* 105, 2218–2227. doi: 10.1002/jbm.a.36081
- Liu, Y. K., Lu, Q. Z., Pei, R., Ji, H. J., Zhou, G. S., Zhao, X. L., et al. (2009). The effect of extracellular calcium and inorganic phosphate on the growth and osteogenic differentiation of mesenchymal stem cells *in vitro*: implication for bone tissue engineering. *Biomed. Mater.* 4:25004. doi: 10.1088/1748-6041/4/2/025004
- Lovati, A. B., Drago, L., Monti, L., De Vecchi, E., Previdi, S., Banfi, G., et al. (2013). Diabetic mouse model of orthopaedic implant-related *Staphylococcus aureus* infection. *PLoS One* 8:e67628. doi: 10.1371/journal.pone.0067628
- Malizos, K., Blauth, M., Danita, A., Capuano, N., Mezzoprete, R., Logoluso, N., et al. (2017). Fast-resorbable antibiotic-loaded hydrogel coating to reduce post-surgical infection after internal osteosynthesis: a multicenter randomized controlled trial. *J. Orthop. Traumatol.* 18, 159–169. doi: 10.1007/s10195-017-0442-2
- Martinez-Perez, M., Perez-Jorge, C., Lozano, D., Portal-Nunez, S., Perez-Tanoira, R., Conde, A., et al. (2017). Evaluation of bacterial adherence of clinical isolates of *Staphylococcus* sp. using a competitive model: an in vitro approach to the "race for the surface" theory. *Bone Joint Res.* 6, 315–322. doi: 10.1302/2046-3758.65.BJR-2016-0226.R2
- Mediero, A., Frenkel, S. R., Wilder, T., He, W., Mazumder, A., and Cronstein, B. N. (2012). Adenosine A2A receptor activation prevents wear particle-induced osteolysis. *Sci. Transl. Med.* 4, 135–165.
- Ocana, J. A., Barragan, F. J., and Callejon, M. (2000). Spectrofluorimetric determination of moxifloxacin in tablets, human urine and serum. *Analyst* 125, 2322–2325. doi: 10.1039/b005991i
- Papadopoulos, A., Ribera, A., Mavrogenis, A. F., Rodriguez-Pardo, D., Bonnet, E., Salles, M. J., et al. (2019). Multidrug-resistant and extensively drug-resistant Gram-negative prosthetic joint infections: role of surgery and impact of colistin administration. *Int. J. Antimicrob. Agents* 53, 294–301. doi: 10.1016/j.ijantimicag.2018.10.018
- Perez-Jorge, C., Arenas, M. A., Conde, A., Hernández-Lopez, J. M., de Damborenea, J. J., Fisher, S., et al. (2017). Bacterial and fungal biofilm formation on anodized titanium alloys with fluorine. *J. Mater. Sci. Mater. Med.* 28:8.
- Pettit, R. K., Weber, C. A., Kean, M. J., Hoffmann, H., Pettit, G. R., Tan, R., et al. (2005). Microplate alamar blue assay for *Staphylococcus epidermidis* biofilm susceptibility testing. *Antimicrob. Agents Chemother.* 49, 2612–2617. doi: 10.1128/AAC.49.7.2612-2617.2005
- Pfang, B. G., Garcia-Canete, J., Garcia-Lasheras, J., Blanco, A., Aunon, A., Parron-Camero, R., et al. (2019). Orthopedic implant-associated infection by multidrug resistant Enterobacteriaceae. *J. Clin. Med.* 8:220. doi: 10.3390/jcm8020220
- Popat, K. C., Eltgroth, M., LaTempa, T. J., Grimes, C. A., and Desai, T. A. (2007). Titania nanotubes: a novel platform for drug-eluting coatings for medical implants? *Small* 3, 1878–1881. doi: 10.1002/smll.200700412
- Radin, S., and Ducheyne, P. (2007). Controlled release of vancomycin from thin sol-gel films on titanium alloy fracture plate material. *Biomaterials* 28, 1721–1729. doi: 10.1016/j.biomaterials.2006.11.035
- Rodriguez-Pardo, D., Pigrau, C., Lora-Tamayo, J., Soriano, A., del Toro, M. D., Cobo, J., et al. (2014). Gram-negative prosthetic joint infection: outcome of a debridement, antibiotics and implant retention approach. A large multicentre study. *Clin. Microbiol. Infect.* 20:O911. doi: 10.1111/1469-0691.12649
- Romanò, C. L., Scarponi, S., Gallazzi, E., Romano, D., and Drago, L. (2015). Antibacterial coating of implants in orthopaedics and trauma: a classification proposal in an evolving panorama. *J. Orthop. Surg. Res.* 10:157. doi: 10.1186/s13018-015-0294-5
- Stepanovic, S., Vukovic, D., Hola, V., Di Bonaventura, G., Djukic, S., Cirkovic, I., et al. (2007). Quantification of biofilm in microtiter plates: overview of testing conditions and practical recommendations for assessment of biofilm production by staphylococci. *APMIS* 115, 891–899. doi: 10.1111/j.1600-0463.2007.apm_630.x
- Swartjes, J. J., Sharma, P. K., van Kooten, T. G., van der Mei, H. C., Mahmoudi, M., Busscher, H. J., et al. (2015). Current developments in antimicrobial surface coatings for biomedical applications. *Curr. Med. Chem.* 22, 2116–2129. doi: 10.2174/0929867321666140916121355

- Tande, A. J., and Patel, R. (2014). Prosthetic joint infection. *Clin. Microbiol. Rev.* 27, 302–345. doi: 10.1128/CMR.00111-13
- Valle, J., Toledo-Arana, A., Berasain, C., Ghigo, J. M., Amorena, B., Penadés J. R., et al. (2003). SarA and not σ^B is essential for biofilm development by *Staphylococcus aureus*. *Mol. Microbiol.* 48, 1075–1087. doi: 10.1046/j.1365-2958.2003.03493.x
- Varanda, F., Pratas de Melo, M. J., Caço, A. I., Dohrn, R., Makrydaki, F. A., Voutsas, E., et al. (2006). Solubility of antibiotics in different solvents. 1. hydrochloride forms of tetracycline, moxifloxacin, and ciprofloxacin. *Indus. Eng. Chem. Res.* 45, 6368–6374. doi: 10.1021/ie060055v
- Wang, Y., Cheng, L. I., Helfer, D. R., Ashbaugh, A. G., Miller, R. J., Tzomides, A. J., et al. (2017). Mouse model of hematogenous implant-related *Staphylococcus aureus* biofilm infection reveals therapeutic targets. *Proc. Natl. Acad. Sci. U.S.A.* 114, E5094–E5102. doi: 10.1073/pnas.1703427114
- Xiong, M.-H., Li, Y. J., Bao, Y., Yang, X.-Z., Hu, B., and Wang, J. (2012). Bacteria responsive multifunctional nanogel for targeted antibiotic delivery. *Adv. Mater.* 24, 6175–6180. doi: 10.1002/adma.201202847
- Zhao, B., van der Mei, H. C., Subbiahdoss, G., de Vries, J., Rustema-Abbing, M., Kuijter, R., et al. (2014). Soft tissue integration versus early biofilm formation on different dental implant materials. *Dent Mater* 30, 716–727. doi: 10.1016/j.dental.2014.04.001
- Zhao, L., Chu, P. K., Zhang, Y., and Wu, Z. (2009). Antibacterial coatings on titanium implants. *J. Biomed. Mater. Res. B Appl. Biomater.* 91, 470–480. doi: 10.1002/jbm.b.31463

Conflict of Interest: JE received travel grants from Pfizer and conference fees from bioMérieux and Heraeus.

The remaining authors declare that the research was conducted in the absence of any commercial or financial relationships that could be construed as a potential conflict of interest.

Copyright © 2020 Aguilera-Correa, Garcia-Casas, Mediero, Romera, Mulero, Cuevas-López, Jiménez-Morales and Esteban. This is an open-access article distributed under the terms of the Creative Commons Attribution License (CC BY). The use, distribution or reproduction in other forums is permitted, provided the original author(s) and the copyright owner(s) are credited and that the original publication in this journal is cited, in accordance with accepted academic practice. No use, distribution or reproduction is permitted which does not comply with these terms.



The β -Lactamase Inhibitor Boronic Acid Derivative SM23 as a New Anti-*Pseudomonas aeruginosa* Biofilm

Samuele Peppoloni^{1†}, Eva Pericolini^{1†}, Bruna Colombari¹, Diego Pinetti², Claudio Cermelli¹, Francesco Fini³, Fabio Prati³, Emilia Caselli^{3*} and Elisabetta Blasi^{1*}

¹ Department of Surgical, Medical, Dental and Morphological Sciences With Interest in Transplant, Oncological and Regenerative Medicine, University of Modena and Reggio Emilia, Modena, Italy, ² Centro Interdipartimentale "Grandi Strumenti" (CIGS), University of Modena and Reggio Emilia, Modena, Italy, ³ Department of Life Sciences, University of Modena and Reggio Emilia, Modena, Italy

OPEN ACCESS

Edited by:

Silvia Buroni,
University of Pavia, Italy

Reviewed by:

Mona I. Shaaban,
Mansoura University, Egypt
Rodolfo García-Contreras,
National Autonomous University of
Mexico, Mexico

*Correspondence:

Emilia Caselli
emilia.caselli@unimore.it
Elisabetta Blasi
elisabetta.blasi@unimore.it

[†]These authors have contributed
equally to this work

Specialty section:

This article was submitted to
Antimicrobials, Resistance and
Chemotherapy,
a section of the journal
Frontiers in Microbiology

Received: 16 September 2019

Accepted: 09 January 2020

Published: 07 February 2020

Citation:

Peppoloni S, Pericolini E,
Colombari B, Pinetti D, Cermelli C,
Fini F, Prati F, Caselli E and Blasi E
(2020) The β -Lactamase Inhibitor
Boronic Acid Derivative SM23 as a
New Anti-*Pseudomonas*
aeruginosa Biofilm.
Front. Microbiol. 11:35.
doi: 10.3389/fmicb.2020.00035

Pseudomonas aeruginosa is a Gram-negative nosocomial pathogen, often causative agent of severe device-related infections, given its great capacity to form biofilm. *P. aeruginosa* finely regulates the expression of numerous virulence factors, including biofilm production, by Quorum Sensing (QS), a cell-to-cell communication mechanism used by many bacteria. Selective inhibition of QS-controlled pathogenicity without affecting bacterial growth may represent a novel promising strategy to overcome the well-known and widespread drug resistance of *P. aeruginosa*. In this study, we investigated the effects of SM23, a boronic acid derivate specifically designed as β -lactamase inhibitor, on biofilm formation and virulence factors production by *P. aeruginosa*. Our results indicated that SM23: (1) inhibited biofilm development and production of several virulence factors, such as pyoverdine, elastase, and pyocyanin, without affecting bacterial growth; (2) decreased the levels of 3-oxo-C₁₂-HSL and C₄-HSL, two QS-related autoinducer molecules, in line with a dampened *lasR/lasI* system; (3) failed to bind to bacterial cells that had been preincubated with *P. aeruginosa*-conditioned medium; and (4) reduced both biofilm formation and pyoverdine production by *P. aeruginosa* onto endotracheal tubes, as assessed by a new *in vitro* model closely mimicking clinical settings. Taken together, our results indicate that, besides inhibiting β -lactamase, SM23 can also act as powerful inhibitor of *P. aeruginosa* biofilm, suggesting that it may have a potential application in the prevention and treatment of biofilm-associated *P. aeruginosa* infections.

Keywords: boronic acids, *Pseudomonas aeruginosa* biofilm, quorum sensing, virulence factors, inhibitors

INTRODUCTION

Pseudomonas aeruginosa is a Gram-negative opportunistic pathogen, causing nosocomial infections in more than 2 million patients every year (Cross et al., 1983; Rossolini and Mantengoli, 2005). Such infections are particularly frequent in immunocompromised patients, such as those with cancer, AIDS, burn wounds, and indwelling devices (Vandeputte et al., 2010; Sarabhai et al., 2015).

Notably, *P. aeruginosa* infections are associated with unfavorable outcome in individuals with cystic fibrosis (CF), the most common life-limiting genetic disorder in the U.S. (Lyczak et al., 2002). These patients, indeed, show abnormalities in their lung tissue that promote bacterial colonization, which in turn causes long-lasting inflammation, lung injury, and eventually respiratory failure.

P. aeruginosa has a uniquely large genome, whose genes encode for several virulence factors (including LasA protease, LasB elastase, pyoverdine, pyocyanin, alginate, and exotoxin A) and regulatory mechanisms, allowing microbial adaptation to many hostile environments (Stover et al., 2000). As a consequence, *P. aeruginosa* is ubiquitous in nature and almost impossible to eliminate from hospitals. As many other microorganisms, besides living in a planktonic form, *P. aeruginosa* is able to form biofilm on medical implants or damaged tissues (Xu et al., 2013). Particularly, more than 70% of hospital-acquired infections are associated with biofilm on catheters, ventilator tubes, implants, and medical prosthetic devices (Brooun et al., 2000). Unlike planktonic cell counterpart, bacterial communities structured as biofilms exhibit an altered phenotype, with respect to growth rate, expression of virulence factors, and cell-to-cell communication system (Qu et al., 2016). Thus, when enclosed in a self-produced extracellular polymeric matrix, *P. aeruginosa* is protected from patient's immune system and becomes up to 1,000 times more antibiotic resistant than the planktonic counterpart (Mah and O'Toole, 2001).

The expression of many virulence factors in *P. aeruginosa* is controlled by the Quorum Sensing (QS) system (Venturi, 2006), an intercellular communication mechanism that coordinates bacterial behavior and gene expression by means of signaling molecules in a cell density-dependent manner (Schuster and Greenberg, 2006). The transcriptional regulation of numerous virulence genes in *Pseudomonas* is under the control of two N-acyl homoserine lactone (AHL)-dependent QS systems, named *lasI/lasR* and *rhlI/rhlR*. In the *lasI/lasR* system, *lasI* encodes the synthesis of N-(3-oxo-dodecanoyl)-homoserine lactone (3-oxo-C₁₂-HSL), which binds and activates the cognate response regulator LasR, leading to regulation of gene expression. Differently, in the *rhlI/rhlR* system, *rhlI* synthesizes the N-(butanoyl)-homoserine lactone (C₄-HSL), which, in turn, by interacting with the cognate RhlR, influences the transcription of target genes. Importantly, the two QS systems are hierarchically organized, with the *lasI/lasR* system in turn regulating the transcription of *rhlI/rhlR*.

These QS systems are among the most studied in bacteria and their regulons are essential for the pathogenicity of *P. aeruginosa* (Schuster and Greenberg, 2006; Girard and Bloemberg, 2008; Zou and Nair, 2009). There is also a third self-inducing signal, referred to as *Pseudomonas* quinolone signal, that plays an integral role in the QS system (Pesci et al., 1999). Such complicated communication systems coordinate/regulate several virulence traits in *P. aeruginosa*, including motility, toxin production, and biofilm formation (Fuqua and Greenberg, 1998; de Kievit and Iglewski, 2000; Dong et al., 2001; Donabedian, 2003; Jakobsen et al., 2013). Recently, a fourth intercellular communication signal has been discovered, as being capable of integrating environmental stress cues with the QS network.

Named as IQS, it belongs to a new class of QS signal molecules and has structurally been established to be 2-(2-hydroxyphenyl)-thiazole-4-carbaldehyde (Lee and Zhang, 2015).

The difficulty in treating biofilm-associated *P. aeruginosa* infections has encouraged the extensive use of antibiotics, in turn facilitating the development of multiple drug-resistant strains. Among several mechanisms of antibiotic resistance, the production of β -lactamases, enzymes able to hydrolyze β -lactams, is consistently the most concerning one (Bush and Bradford, 2016). In *Pseudomonas*, class C β -lactamases confer high level of resistance to penicillins, cephalosporins, and monobactams (Berrazeg et al., 2015). Besides modifying the structure of β -lactams, leading to generation of several new penicillins and cephalosporins, another relevant strategy to overcome resistance to these drugs is the co-administration of the β -lactam antibiotic together with a β -lactamase inhibitor (Bush and Bradford, 2019). Accordingly, in the last decade, new classes of β -lactamase inhibitors have entered the market giving the opportunity to restore the activity of several β -lactams (Bush and Bradford, 2019). One of the most promising class of new β -lactamase inhibitors are the boronic acids transition state analog inhibitors (BATSI), which are known to restore the β -lactam activity both *in vitro* and *in vivo* (Drawz et al., 2011; Eidam et al., 2012; Barnes et al., 2018). Recently, a new combination of a boronic acid and the β -lactam meropenem (Vabomere®) has entered the market for treatment of infections caused by carbapenem-resistant *Enterobacteriaceae* and multidrug-resistant (MDR) *Pseudomonas* (Griffith et al., 2019). In order to obtain highly active BATSI, we have undertaken a biomimetic approach: the boronic acid structure was decorated with chemical groups arranged in a specific stereochemistry resembling that of the natural substrate β -lactam. Among different synthesized BATSI, one of the best inhibitors ever tested was the SM23 (Morandi et al., 2003). This compound has an R1 acylamino side chain of the β -lactam cephalothin on the boron carbon α (red colored in **Supplementary Material**), and a meta-carboxybenzyl side chain, that mimics the 6-carboxyhydrothiazine ring of the antibiotic (blue colored in **Supplementary Material**). Few commercially available phenylboronic acids have also been investigated in *Vibrio harveyi*, where they act as QS inhibitors with IC₅₀ values in the low to sub-micromolar range (Ni et al., 2009).

In this study, we investigated the effects of the β -lactamase inhibitor boronic acid derivative SM23 on biofilm formation and production of QS-dependent virulence factors as well as autoinducer molecules by *P. aeruginosa* during biofilm formation. Overall, our results provide the first evidence on the efficacy of SM23 as a remarkable anti-biofilm agent and QS inhibitor, envisaging its use in the prevention and treatment of biofilm-associated *P. aeruginosa* infections.

MATERIALS AND METHODS

SM23

The boronic acid SM23 was synthesized as previously described (Morandi et al., 2003). The compound was dissolved in DMSO

and the different working concentrations were prepared by diluting each stock solution in PBS. In all experiments, the final DMSO concentration was less than 0.1%.

Microbial Strain

We used the bioluminescent *Pseudomonas aeruginosa* strain (P1242), previously engineered to express both the luciferase gene and substrate under the control of a constitutive P1 integron promoter, in order to constitutively produce a detectable bioluminescent signal (Choi and Schweizer, 2006).

Bacterial cells from -80°C glycerol stocks were initially seeded onto Tryptic Soy Agar (TSA) plates and incubated overnight at 37°C ; isolated colonies were then collected, added to 10 ml of Tryptic Soil Broth (TSB), and allowed to grow overnight at 37°C with gentle shaking. Bacterial concentrations were assessed by the McFarland standard curve and diluted to the required experimental concentration.

Biofilm Formation and Quantification

To investigate the effect of SM23 on *Pseudomonas* biofilm formation, a bacterial cell suspension (10^8 cells/ml in TSB plus 2% sucrose) was seeded (100 μl /well) in a 96-well microtiter plate (Sarstedt, Nümbrecht, Germany), treated or not with 100 μl of scalar doses of SM23 (range concentrations from 0.390 to 25.0 μM) and incubated for 24 h at 37°C to allow biofilm formation. After incubation, each well was gently washed to remove planktonic cells, then crystal violet (CV) staining was performed to quantify biofilm formation as previously described (Stepanovic et al., 2000). The absorbance at 570 nm was spectrophotometrically measured by the Sunrise Microplate Reader (Tecan Group Ltd., Männedorf Switzerland). The results were expressed as optical density (OD_{570}) mean \pm SEM of the biofilm biomass. In order to evaluate the metabolic activity of *Pseudomonas* biofilm, 100 μl of bacterial culture in TSB + 2% sucrose (5×10^4 cells/ml) were seeded (100 μl /well) in a 96-black well microtiter plate, treated or not with scalar doses of SM23 at concentrations ranging from 0.390 to 25.0 μM (100 μl /well) and then incubated for 24 h at 37°C to allow biofilm formation. After incubation, each well was gently washed twice with PBS (EuroClone, Whetstereby, UK) to remove planktonic cells and then bioluminescence signal was measured by Viktor Luminescence reader (Perkin Elmer). The results were expressed as Relative Luminescence Units (RLU) mean \pm SEM of metabolically active biofilm.

Confocal Microscopy Analysis of *P. aeruginosa* Biofilm

The fluorescence property of *Pseudomonas* spp. (Meyer, 2000; Cornelis and Matthijs, 2002) was exploited to perform confocal microscopy imaging. Briefly, bacterial suspensions (1×10^5 cells/ml in TSB plus 2% sucrose) were seeded on coverslips (1,000 μl /well) inserted into 24-microplate (Sarstedt, Nümbrecht Germany) and treated or not with SM23 at 0.780 and 3.125 μM . The plates were then incubated for 24 h at 37°C to allow biofilm formation. After incubation, the coverslips were washed twice with PBS, fixed with 4% paraformaldehyde (PFA) (Sigma-Aldrich, Darmstadt) for 30 min at 4°C , washed again and

then analyzed by confocal microscope Leica TCS SP8 (Wetzlar, Germany) at excitation/emission wavelength 492/517 nm.

Evaluation of Live or Dead Bacterial Cells in Biofilm

In order to evaluate the live or dead cells in *Pseudomonas* biofilm, the bacterial cells (1×10^8 cells/ml) were seeded in 96-well black-plates and treated or not with 0.780 and 3.125 μM of SM23 for 24 h at 37°C to allow biofilm formation. After incubation, the samples were stained with the “live/dead cells stain kit” (Thermo Fisher Scientific, Waltham, Massachusetts, USA), using 5(6)-carboxyfluorescein diacetate (CFDA) to label alive cells (30 min at 37°C plus 5% CO_2) and propidium iodide (PI) to stain the dead cells (15 min at 37°C plus 5% CO_2). The staining procedure was conducted according to the manufacturer’s instructions. After incubation, the samples were washed twice with PBS and the fluorescence emission (CFDA excitation/emission: 485/528; PI excitation/emission: 528/645) was analyzed using a multi-well fluorescence plate reader (Synergy HTX, BIOTEK, Winooski, Vermont, USA). The results were expressed as Relative Fluorescence Units (RFU) mean \pm SEM of alive/dead biofilm cells.

Elastase Activity

Elastase activity was measured in cell-free supernatants from SM23 *Pseudomonas* cells, treated or not with the compound (concentration range from 0.780 to 3.125 μM), during biofilm formation. After 6, 12, and 24 h of culture, the elastase activity was measured as described by (Ohman et al., 1980) using Elastin-Congo Red (ECR) (Sigma, St. Louis, USA) as a substrate. Briefly, 100 μl of untreated or SM23-treated supernatants were mixed with 900 μl of ECR buffer (100 mM Tris, 1 mM CaCl_2 , pH 7.5) containing 20 mg of ECR and then incubated for 3 h at 37°C . The reaction was terminated by adding 1 ml of 0.7 M sodium phosphate buffer (pH 6.0) and the tubes were placed in cold water bath. The insoluble ECR was removed by centrifugation at 10,000 rpm for 10 min and then the absorbance was measured at 495 nm by a Sunrise Microplate Reader. The elastase activity was expressed as the optical density (OD_{495}) mean \pm SEM.

High-Performance Liquid Chromatography-Mass Spectrometric Analysis

Pyoverdine, pyocyanin, 3-oxo- C_{12} -HSL and C_4 -HSL molecules were assessed in culture supernatants of *P. aeruginosa* during biofilm formation after 6, 12, and 24 h of SM23 treatment. All supernatants for the high-performance liquid chromatography-mass spectrometric (HPLC-MS) analysis were filtered on Amicon Ultra-0.5 10 K centrifugal filter devices and 1:5 diluted with 5% methanol - 0.2% formic acid in MilliQ water. The HPLC-MS instrument used was an UltiMate 3,000 system, consisting of an online degasser, a Binary Pump HPG 3400RS, a Well Plate Autosampler WPS 3000RS, and a Thermostatted Column Compartment TCC 3000RS coupled to a Q-Exactive hybrid quadrupole – orbitrap mass analyzer via a HESI-II heated electrospray ion source (Thermo Scientific). Chromatographic separation of a 5 μl sample injection was performed on a Poroshell 120 SB-C18 100 \times 2.1 mm ID, 2.7

μm ps column (Agilent) at 30°C and a 0.4 ml/min flow rate. A linear gradient elution scheme was used with mobile phase components being 0.1% formic acid in water (A) and methanol (B). The gradient started at 2% B which was maintained for 0.5 min, then raised up to 30% B in 30 min, and up again to 98% B in 24.5 min. The column was then kept at 98% B for 17.9 min, then starting conditions were restored in 0.1 min and maintained for 19 min pending a successive injection. Electrospray ionization was operated in positive ion mode, using nitrogen as sheath gas (50 arbitrary units), auxiliary gas (290°C, 40 arbitrary units), and sweep gas (3 arbitrary units). The sprayer voltage was kept at 3.8 kV and the transfer capillary temperature was set at 320°C. The Q-Exactive was operated in Full MS/dd-MS2 mode. The Full MS scan range was set from m/z 170 to 1,000 at 70,000 FWHM resolution (m/z 200). The automatic gain control (AGC) target was set at 1.0×10^6 with a maximum injection time (IT) of 200 ms. Data-dependent MS2 (dd-MS2) acquisitions at 17,500 FWHM resolution (m/z 200) were triggered for the Top 3 precursor ions following each Full MS scan. The intensity threshold for precursor ion selection was set to 1.0×10^5 , then dynamic exclusion was active for 20.0 s. AGC target and maximum IT for the MS2 experiments were set to 2.0×10^5 and 50 ms. Each precursor ion was fragmented using stepped normalized collision energy (NCE) values at 28, 50, and 75.

lasI/lasR Gene Transcription Analysis

A qRT-PCR was used to investigate SM23-induced changes in transcription levels of selected QS genes. Briefly, *Pseudomonas* cells (1×10^7 cells/ml) were seeded in 24-well flat-bottom plates (Becton Dickinson Labware Europe, Meylan Cedex, France) and untreated or treated with SM23 (1.56 μM) for 24 h at 37°C to allow biofilm formation. After incubation, each well was washed twice with PBS to remove the no-adherent bacterial cells; then, biofilm was recovered by scraping and subsequent centrifugation at +4°C; the pellet was dried and stocked at -80°C until qRT-PCR analysis. Total RNA was extracted using the HiPurA Bacterial RNA Purification (Himedia) kit and treated with DNase I on a column to remove the DNA. RNA was quantified by MaestroNano spectrophotometer readings for microvolumes. Two micrograms of total RNA and random primers were used for cDNA synthesis using EasyScript cDNA Synthesis (Abm) kit. Expression of *lasI*, *lasR*, and 16S rRNA genes was performed in triplicate by real-time PCR using 20 ng of cDNA, 0.5 μM of forward and reverse primers and BrightGreen 2x qPCR MasterMix (Abm). The primers list is shown in **Supplementary Material**. The amplification conditions were the following: 1 cycle for 10 min at 95°C; 40 cycles for 15 s at 95°C, 1 min at 60°C; melting curve for 30 s at 95°C, 30 s at 65°C, and 30 s at 95°C. The expression levels of the target genes in treated samples were normalized to the expression of the reference 16S rRNA gene and then compared to the control samples. The relative expression levels were calculated using the $2^{-\Delta\Delta C_t}$ method.

SM23 Interaction With Bacterial Cells

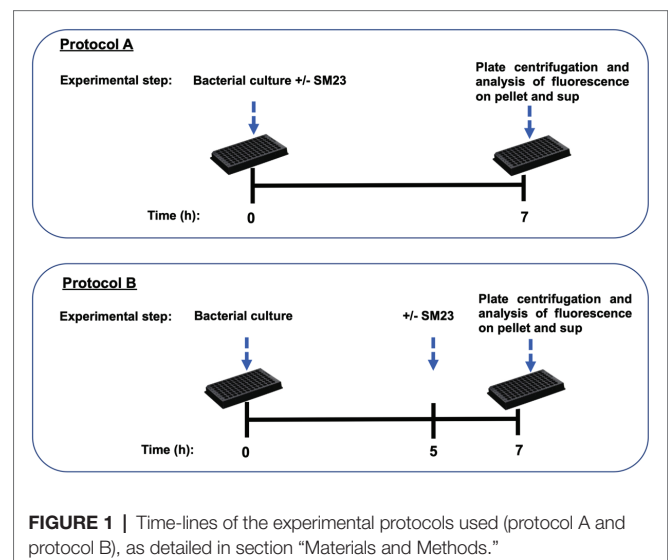
Two experimental protocols, A and B, were used. Bacterial cell cultures (1×10^8 cells/ml; 200 μl /well) were seeded in a 96-black microtiter plate and incubated for 7 h at 37°C and

5% CO₂, in the presence of SM23 (12.5 μM), as illustrated by the time-line of protocol A (**Figure 1**). In parallel experiments, microbial cells were seeded in a 96-black well microtiter plate and incubated for 5 h at 37°C and 5% CO₂; then, SM23 was added to the cells and the plates were further incubated for 2 h, according to the time-line of protocol B (**Figure 1**).

In selected experiments, fresh bacterial cells were suspended at the concentration of 1×10^8 cells/ml and pre-treated for 30 min with cell-free supernatants (*P. aeruginosa*-conditioned medium, recovered from an overnight culture of *Pseudomonas* at the starting concentration of 1×10^8 cells/ml). To exclude residual viable bacteria in such *P. aeruginosa*-conditioned medium, 50 μl of the supernatants was seeded onto TSA plates and incubated for 48 h at 37°C under aerobic conditions; no bacterial CFUs on TSA plates were ever observed. Bacterial cells were then incubated for 7 h with the SM23 (12.5 μM), as described in protocol A. Control wells (namely, medium alone, medium plus SM23, and untreated microbial culture) were also included in the assay to evaluate the SM23 fluorescent signal. In all the experimental protocols, at the end of the incubation period (7 h), the plates were centrifuged for 10 min at 5,000 rpm. The recovered supernatants were then collected, transferred in new wells, and the fluorescent signal in both pellets and supernatants was measured by a multi-well fluorescence plate reader (Synergy HTX, BIOTEK, Winooski, Vermont, USA). The residual fluorescence of SM23 in the cell pellets and cell-free supernatants was defined as the fluorescence values obtained by subtracting, respectively, the fluorescence of the pellet or supernatant, observed in the untreated control groups, from the fluorescence values of the corresponding treated samples. The resulting values were expressed as % of residual fluorescence of SM23 detected in the pellet versus the supernatant.

Biofilm Formation on Endotracheal Tubes and Quantification of Pyoverdine Release

Two-hundred microliter of overnight culture of *Pseudomonas* (5×10^4 /ml) in TSB with 2% sucrose were seeded in 96-well



black-plates, containing 1 endotracheal tube (ETT) piece/well; the plates were then incubated for 90 min at 37°C (adhesion period). After incubation, the ETT pieces were washed twice with PBS, transferred into new wells, and incubated for further 24 h at 37°C in fresh TSB medium in the presence of SM23 (1.560 and 3.150 μ M) to allow biofilm formation. At the end of incubation, the ETT pieces were removed, washed twice with PBS, and the bioluminescence signal was measured by Viktor Luminescence reader (Perkin Elmer). The values were expressed as Relative Luminescence Units (RLU). In parallel, after removing ETT pieces, the supernatants were recovered and centrifuged twice (10,000 rpm for 15 min) to remove the remaining bacteria. Pyoverdine release was quantified in 100 μ l of culture supernatants and fluorescence emission was measured with a multi-well fluorescence plate reader (excitation/emission: 360/460), according to a standard protocol (Das et al., 2016). The values were expressed as RFU.

Statistical Analysis

Quantitative variables were tested for normal distribution. Statistical differences between groups were analyzed according to one-way ANOVA or Kruskal-Wallis followed by Dunnett's multiple comparisons tests by using GraphPad prism 8. A value of $p \leq 0.05$ was considered significant.

RESULTS

Inhibitory Effects of SM23 on *Pseudomonas aeruginosa* Biofilm Formation

Dose-dependent experiments were performed to assess the ability of SM23 to interfere with the biofilm formation by *P. aeruginosa*. Microbial cells were grown in a 96-well microtiter plate in medium only or in the presence of scalar doses of SM23 and then incubated for 24 h to allow biofilm formation. After incubation, each well was gently washed to remove planktonic cells and then CV staining was performed to quantify

the biofilm biomass. The results shown in **Figure 2** (left panel) indicated that the SM23, at the dose of 0.390 μ M, was already able to significantly inhibit biofilm formation (about 40% of biofilm biomass), achieving its greatest effect in the dose range of 0.780–6.250 μ M (about 50% of biomass reduction observed). Next, we analyzed the inhibitory effect of SM23 on biofilm, exploiting the bioluminescent properties of *P. aeruginosa* strain P1242, a model that allows to evaluate the effects of a given compound directly on the metabolically active biofilm (Pericolini et al., 2018). Thus, bacterial biofilm was allowed to form in 96-black well microtiter plates without or with SM23 at different concentrations. After 24 h of incubation, each well was gently washed to remove planktonic cells and, then, the RLU emitted by the metabolically active bacteria embedded in biofilm were measured. Results in **Figure 2** (right panel) indicated that SM23 significantly reduced biofilm formation in a dose-dependent manner (from 0.390 to 25 μ M concentration). In particular, 1.560 and 3.125 μ M were the lowest SM23 doses still capable of reducing biofilm by 50–60%. Thus, from now on, we mainly used these two concentrations.

In parallel experiments, the influence of SM23 was evaluated on the growth of *P. aeruginosa*, cultured in planktonic form for 7 and 24 h. We found that SM23 failed to induce any change on bacterial growth capacity and viability as well, up to the concentration of 25.0 μ M; also, the bacterial doubling times were found to be comparable, in SM23-treated and untreated controls (data not shown).

Morphological Observation of SM23-Treated Biofilm

We next performed confocal analysis in a 24 h-old biofilm, produced in medium alone or in the presence of SM23, at 0.780 and 3.125 μ M. As expected, both doses strongly affected biofilm development and its morphology. Indeed, as shown in **Figure 3** (left panel), unlike controls, SM23-treated biofilms showed large zones with few or no bacteria and scant extracellular matrix onto the well surface. Moreover, the residual biofilm

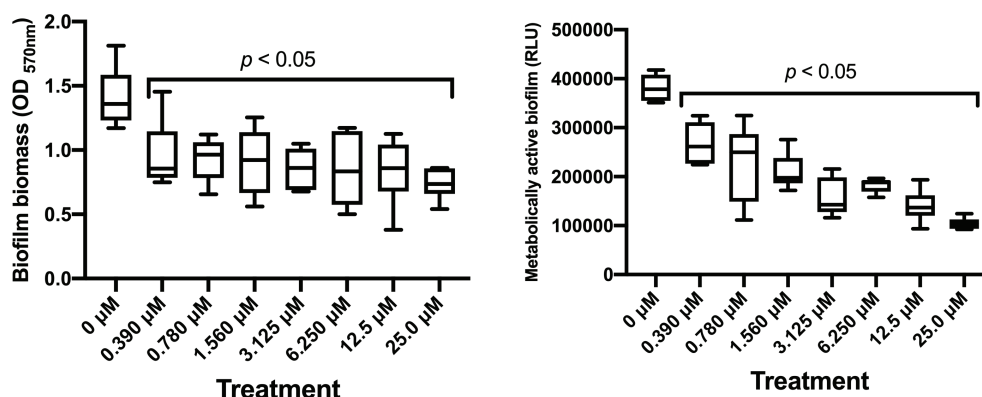


FIGURE 2 | Dose-dependent effect of SM23 on *P. aeruginosa* biofilm formation. Both box-plot graphs show the mean \pm SEM of microbial biofilm produced after 24 h of incubation in medium or in the presence of scalar doses of SM23. Left panel: mean \pm SEM of the OD_{570nm} (biofilm biomass) of triplicate samples from two different experiments. Right panel: mean \pm SEM of the Relative Luminescence Units (RLU) of triplicate samples from two different experiments. $p < 0.05$; SM23-treated vs. untreated according to one-way ANOVA followed by Dunnett's multiple comparisons test.

showed drastic alterations in its architecture (**Figure 3**, left panel). In parallel experiments, a 24 h-old biofilm generated in the presence or absence of SM23 was stained with CFDA and PI, to discriminate live from dead cells, as detailed in section “Materials and Methods.” As shown in **Figure 3** (right panel), a significant reduction of viable bacterial cells was observed in biofilms treated with SM23, irrespective of the dose used.

Inhibition of *Pseudomonas aeruginosa* Quorum Sensing-Related Virulence Factors by SM23

P. aeruginosa elastase is a zinc metalloprotease encoded by *lasB* gene, capable of inactivating a wide range of biological tissues and immunological agents (Preston et al., 1997; Li et al., 2019). Thus, we evaluated the elastase activity in supernatants of biofilm producing *P. aeruginosa*, after 6, 12 or 24 h of culture in the presence or absence of scalar doses of SM23. Our results showed a consistent elastase activity by the untreated control cells, already at 6 h persisting up to 24 h of incubation. Such activity was significantly dampened (about 45% of reduction) by SM23 treatment at all the doses tested (**Table 1**).

It is widely accepted that pyoverdine, the most potent iron-gathering siderophore in *P. aeruginosa*, is an important virulence factor playing an important role in biofilm formation (Meyer et al., 1996).

HPLC-MS analysis was performed to evaluate the levels of pyoverdines, pyocyanin, 3-oxo- C_{12} -HSL and C_4 -HSL under the same experimental conditions used for elastase activity. Pyoverdines, in the form of doubly charged protonated molecular ions, were revealed by the presence of the specific chromophore core (P) fragment ion at m/z 204.0768 in their MS/MS spectra (Budzikiewicz et al., 2007; Wei and Aristilde, 2015). The identification of the four most intensely detected pyoverdines, achieved using their MS/MS spectra, revealed serine (Ser) as the first amino acid of the peptide sequence and either a succinyl amide (Succa, A1+ fragment ion at m/z 416.1565 Th) or a succinic acid (Succ, A1+ fragment ion at m/z 417.1405 Th) moiety as side chain of the chromophore. Two pyoverdines, with their $[M + 2H]^{2+}$ ions being respectively at m/z 667.8015

and 667.3104 Th, were unambiguously identified, as previously reported for Pyoverdine D (Py D) and E (Py E) (Kilz et al., 1999); differently, other two pyoverdines, portrayed by their respective $[M + 2H]^{2+}$ ions at m/z 644.7997 and 645.2914 Th, were not yet completely identified and hereinafter referred to as Succ-P-Ser-Y and Succa-P-Ser-Y, with Y being their unidentified peptide sequence side-chain.

Pyocyanin was detected as mono charged protonated ion $[M + H]^+$ at m/z 211.0866 and its identification possibly confirmed by fragments $[M + H-CH_3]^+$ at m/z 196.0631, $[M + H-CO]^+$ at m/z 183.0917 and $[M + H-CH_3-CO]^+$ at m/z 168.0682 appearing in its MS/MS spectrum (Watson et al., 1986). Both 3-oxo- C_{12} -HSL and C_4 -HSL were revealed by the presence of their respective $[M + H]^+$ and $[M + Na]^+$ molecular ions (at m/z 172.0968 and 194.0788 for C_4 -HSL and at m/z 298.2013 and 320.1832 for 3-oxo- C_{12} -HSL). Their identification was possibly confirmed by the fragments $[M + H-C_4H_7NO_2]^+$ at 71.0491 for C_4 -HSL and at 197.1536 for 3-oxo- C_{12} -HSL and $[C_4H_7NO_2 + H]^+$ at 102.05496 appearing in their respective MS/MS spectra; these data closely recalled the profile previously established (Churchill et al., 2011).

Compounds elution provided peaks appearing in their specific chromatographic traces, showing the abundance of their respective doubly charged ions over the chromatographic run (mass range chromatograms). Peak areas were used for semi-quantitative evaluation, as previously established (Kapoor and Vaidyanathan, 2016). As depicted in **Table 2**, we found

TABLE 1 | Elastase activity of *P. aeruginosa* in response to SM23 treatment: time- and dose-dependence.

Groups	Elastase activity (OD ₄₉₅)		
	6 h	12 h	24 h
Untreated	0.142 ± 0.030	0.114 ± 0.017	0.155 ± 0.013
SM23 (0.780 μM)	0.114 ± 0.011	0.128 ± 0.018	0.092 ± 0.004*
SM23 (1.560 μM)	0.103 ± 0.011	0.134 ± 0.018	0.088 ± 0.003*
SM23 (3.125 μM)	0.106 ± 0.013	0.109 ± 0.015	0.087 ± 0.006*

* $p < 0.05$; SM23-treated vs. untreated group, according to Kruskal-Wallis followed by Dunnett's multiple comparisons test.

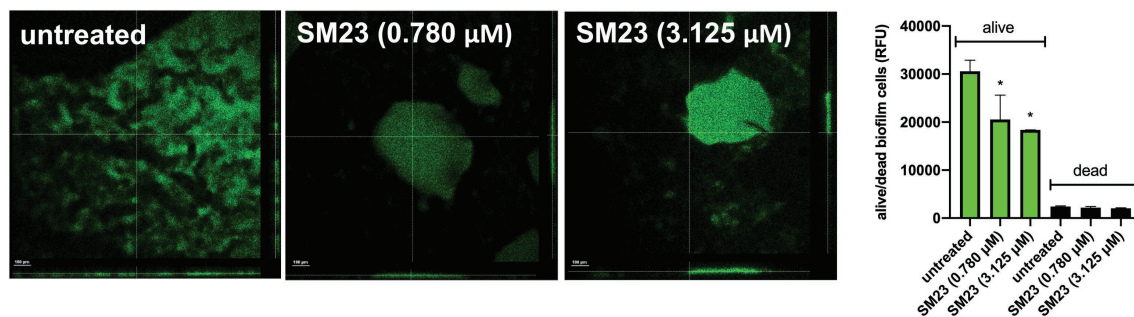


FIGURE 3 | Confocal analysis of SM23-treated biofilm and evaluation of dead/alive cells. **Left panel:** confocal microscope images of a 24 h-old biofilm, untreated or treated with SM23 (0.780 and 3.125 μM). The large images illustrate three representative horizontal sections (X and Y axes) of biofilms, while the small images show biofilm sections observed along the Z axis. The micrographs are representative of two independent experiments. Scale bar: 100 μm. Magnification: 20x. **Right panel:** mean ± SEM of the Relative Fluorescence Units (RFU) of alive (green columns) and dead (black column) cells in a 24 h-old *Pseudomonas* biofilm treated with SM23 (0.780 and 3.125 μM). * $p < 0.05$; SM23-treated vs. untreated according to one-way ANOVA followed by Dunnett's multiple comparisons test.

consistent levels of pyoverdines only after 24 h of *P. aeruginosa* culture. SM23 markedly reduced PyD and PyE production at all the three doses tested, whereas no effect was observed in terms of Py Succ-P-Ser-Y_{isom1/2} or Py Succa-P-Ser-Y_{isom1/2} levels. Under the same experimental conditions, we analyzed also the release of pyocyanin, another key virulence factor involved in *P. aeruginosa* biofilm formation (Li et al., 2015). Again, we found consistent levels of pyocyanin only after 24 h of *P. aeruginosa* culture, while the treatment with SM23, at 0.780, 1.560, and 3.125 μ M, significantly impaired the pyocyanin production.

Inhibition of *Pseudomonas aeruginosa* Quorum Sensing Molecules by SM23

The results in Table 3 show the levels of both 3-oxo-C₁₂-HSL and C₄-HSL autoinducers in supernatants of *P. aeruginosa*

producing biofilm, after 6, 12, and 24 h of SM23 treatment. A consistent presence of 3-oxo-C₁₂-HSL was measured already after 12 h that persisted up to 24 h, while C₄-HSL was detectable only after 24 h of culture. All the SM23 doses significantly reduced 3-oxo-C₁₂-HSL after 12 h of treatment; moreover, both the autoinducer molecules resulted significantly inhibited after 24 h of SM23 treatment at the highest dose (3.125 μ M).

Finally, we tested the effects of SM23 on *P. aeruginosa* expression of *lasI/lasR* genes, known to be crucially involved in QS system, biofilm formation, and virulence (Moghaddam, 2014). Our results showed that, in a 24 h-old biofilm treated with 1.560 μ M SM23, both *lasI* and *lasR* gene transcript levels were downregulated by 36 and 25%, respectively (untreated vs. SM23-treated cells: *lasI* returned 1.0 vs. 0.644 fold change; *lasR* returned 1.0 vs. 0.750 fold change).

TABLE 2 | Mass spectrometry analysis of *P. aeruginosa* pyoverdine and pyocyanin release in response to SM23 treatment: time- and dose-dependence.

	Py D			Py E		
Groups	6 h	12 h	24 h	6 h	12 h	24 h
Untreated	n.f.	n.f.	21.636.937,83 ± 2.064.621,26	n.f.	n.f.	107.118.272,50 ± 6.827.575,27
SM23 (0.780 μM)	n.f.	n.f.	12.791.348,09 ± 3.054.805,04	n.f.	n.f.	89.272.480,54 ± 9.299.967,42
SM23 (1.560 μM)	n.f.	n.f.	13.394.820,07 ± 3.644.560,57	n.f.	n.f.	78.809.117,60 ± 15.530.420,87
SM23 (3.125 μM)	n.f.	n.f.	11.863.503,70 ± 2.030.689,62	n.f.	n.f.	68.465.442,68 ± 8.162.020,46
Py Succ-P-Ser-Y_isom1				Py Succ-P-Ser-Y_isom2		
Groups	6 h	12 h	24 h	6 h	12 h	24 h
Untreated	n.f.	n.f.	12.195.698,41 ± 694.005,68	n.f.	n.f.	13.864.633,08 ± 890.328,25
SM23 (0.780 μM)	n.f.	n.f.	17.853.144,48 ± 1.894.407,84	n.f.	n.f.	20.815.367,39 ± 1.882.888,28
SM23 (1.560 μM)	n.f.	n.f.	17.177.294,38 ± 1.481.504,17	n.f.	n.f.	17.219.927,21 ± 2.725.080,39
SM23 (3.125 μM)	n.f.	n.f.	15.410.576,46 ± 33.533,32	n.f.	n.f.	15.854.231,57 ± 1.705.318,16
Py Succa-P-Ser-Y_isom1				Py Succa-P-Ser-Y_isom2		
Groups	6 h	12 h	24 h	6 h	12 h	24 h
Untreated	n.f.	n.f.	1.443.163,09 ± 118.385,60	n.f.	n.f.	2.740.841,46 ± 256.622,87
SM23 (0.780 μM)	n.f.	n.f.	1.745.369,67 ± 327.147,82	n.f.	n.f.	2.791.882,23 ± 154.538,85
SM23 (1.560 μM)	n.f.	n.f.	846.415,5 ± 400.566,41	n.f.	n.f.	2.853.552,30 ± 557.608,16
SM23 (3.125 μM)	n.f.	n.f.	1.133.441,13 ± 30.587,47	n.f.	n.f.	2.205.285,65 ± 499.846,96
Pyocyanin						
Groups	6 h	12 h	24 h			
Untreated	n.f.	n.f.	1.604.817.246,57 ± 56.645.573,69			
SM23 (0.780 μM)	n.f.	n.f.	804.321.499,25 ± 71.053.820,19*			
SM23 (1.560 μM)	n.f.	n.f.	945.605.723,51 ± 50.626.110,98*			
SM23 (3.125 μM)	n.f.	n.f.	696.891.913,37 ± 34.697.351,25*			

n.f., not found. * $p < 0.001$ SM23 treated vs untreated group according to one-way ANOVA followed by Dunnett's multiple comparisons test.

TABLE 3 | Mass spectrometry analysis of *P. aeruginosa* 3-oxo-C₁₂-HSL and C₄-HSL QS molecules release in response to SM23 treatment: time- and dose-dependence.

Groups	3-oxo-C12-HSL			C4-HSL		
	6 h	12 h	24 h	6 h	12 h	24 h
Untreated	n.f.	37.575.520,70 \pm 2.315.838,91	201.150.062,20 \pm 23.359.699,90	n.f.	n.f.	69.707.031,01 \pm 1.143.025,45
SM23 (0.780 μ M)	n.f.	23.645.421,84 \pm 980.613,63*	55.787.081,98 \pm 5.098.512,17	n.f.	n.f.	56.319.203,07 \pm 2.121.398,89
SM23 (1.560 μ M)	n.f.	24.783.514,13 \pm 339.890,28*	51.160.160,28 \pm 1.534.757,47	n.f.	n.f.	57.213.308,48 \pm 1.431.287,96
SM23 (3.125 μ M)	n.f.	26.816.303,02 \pm 1.469.095,35*	45.531.599,65 \pm 4.653.861,29*	n.f.	n.f.	48.215.432,52 \pm 3.107.395,93*

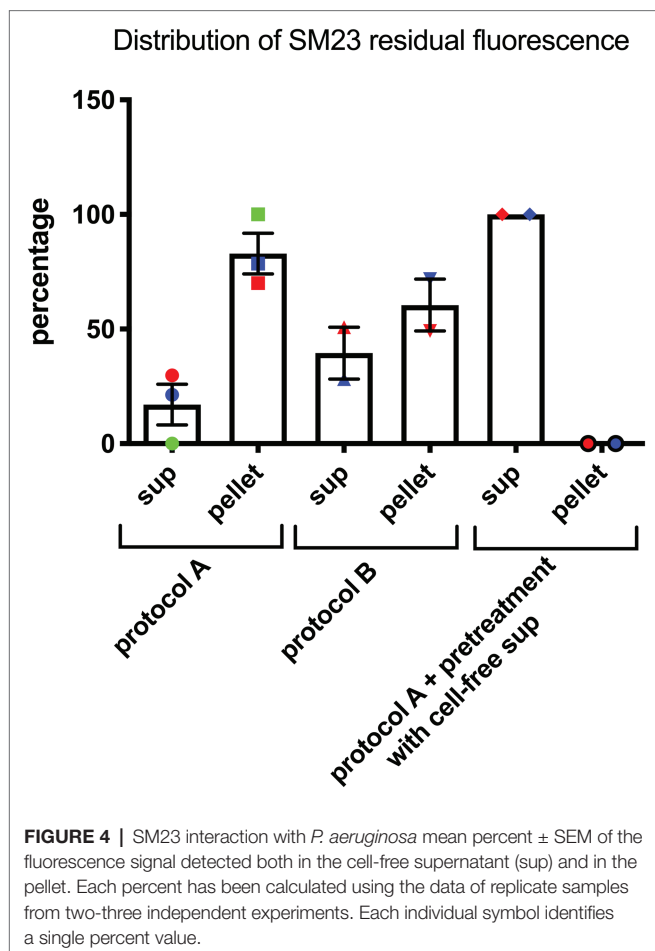
n.f., not found. 12 h: * $p \leq 0.05$ SM23 treated vs untreated group according to ANOVA followed by Dunnett's multiple comparisons test.

24 h: * $p \leq 0.05$ SM23 treated vs untreated group according to Kruskal-Wallis followed by Dunnett's multiple comparisons test.

SM23 Interaction With *Pseudomonas aeruginosa*

Given the effects of the SM23 on *P. aeruginosa* biofilm formation and *lasI/lasR* system, we next investigated its possible mechanism of action. Thus, we developed two different experimental protocols to assess the localization of SM23 on bacterial surface, by exploiting the natural green auto-fluorescence of this compound, as detailed in section “Materials and Methods” and in **Figure 1**. The results, depicted in **Figure 4**, showed that, when the SM23 was added at Time 0 (protocol A), most of the fluorescence was associated to the cell pellet, with a minimal residual fluorescence being detectable in the supernatant. In contrast, when the SM23 was added at Time 5 h (protocol B), the fluorescence signal was detected at comparable levels both on the bacterial cell pellet and on the cell-free supernatants.

Finally, a *Pseudomonas*-conditioned medium (from an overnight culture at 37°C) was used to pre-treat the bacterial cells for 30 min; then, the SM23 was added and the plates were further incubated for additional 7 h, as described in protocol A, prior to assessing the levels of free and cell-associated fluorescence. The results, depicted in **Figure 4**, showed that the fluorescence signal was not cell-associated, but rather only detectable into culture supernatants.



SM23 Inhibitory Effects on Endotracheal Tubes-Associated Biofilm: Impairment of Biofilm Formation and Pyoverdine Release by *Pseudomonas aeruginosa*

We have recently described a rapid and easy-to-perform *in vitro* model for the real-time monitoring of *P. aeruginosa* biofilm formation on endotracheal tube (ETT) pieces (Pericolini et al., 2018). Accordingly, we evaluated the effect of SM23 on a 24 h-old *Pseudomonas* biofilm produced on ETT pieces. As shown in **Figure 5**, the treatment with SM23 significantly decreased the amounts of biofilm associated with the ETT, at both the doses used, as indicated by the significant reduction in RLU (**Figure 5**,

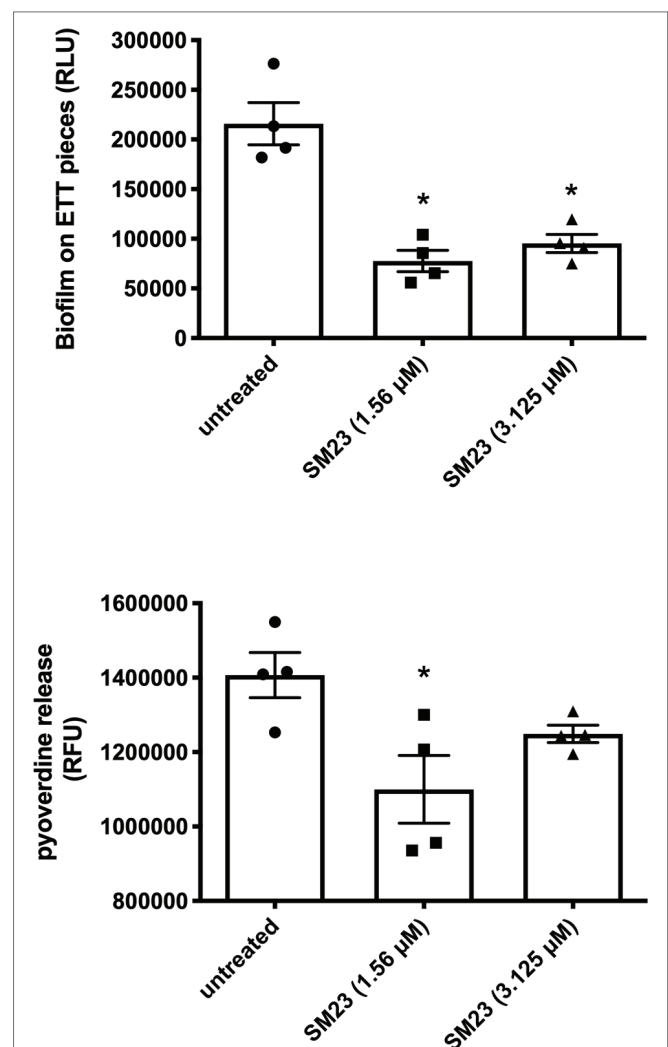


FIGURE 5 | SM23 effects on medical device-associated biofilm by *P. aeruginosa*: impairment of pyoverdine release and biofilm formation. Biofilm mass (upper panel), expressed as mean RLU \pm SEM, and pyoverdine release (lower panel), expressed as mean RFU \pm SEM, by a 24 h-old *Pseudomonas* biofilm produced on ETT pieces, in the absence and in the presence of SM23. In the figure, each individual symbol identifies the value corresponding to a single ETT piece. Data represent the mean values from two independent experiments, with duplicate samples. * $p < 0.05$; SM23-treated samples vs. untreated samples according to ANOVA followed by Dunnett's multiple comparisons test.

upper panel); in addition, the pyoverdine release by such ETT-associated biofilm was also impaired, reaching statistically significant differences at the dose of 1.56 μM (Figure 5, lower panel).

DISCUSSION

P. aeruginosa is a ubiquitous environmental bacterium, responsible for a wide range of severe opportunistic infections, characterized by intense neutrophil activation and significant tissue damage. Clearance is often a serious clinical challenge due to host immunodeficiency and bacterial multidrug resistance, including third-generation cephalosporin (Tenover, 2006; Moghaddam et al., 2012). Moreover, the treatment of chronic *P. aeruginosa* infections is further hampered by adaptive resistance, facilitated also by bacterial ability to form biofilm *in vivo* (Mulcahy et al., 2014). Indeed, bacteria growing as a biofilm have characteristics distinct from their planktonic cell counterpart, including an increased tolerance to antimicrobial agents and host immune response (Costerton, 1999). Furthermore, biofilm is an example of microbial community finely coordinating its behavior through QS. In this study, we provide the first evidence that, SM23, known to be a potent β -lactamase inhibitor, also impairs biofilm formation by *P. aeruginosa* and its production of some QS-dependent virulence factors as well as autoinducer molecules.

The boronic acid derivative SM23 has been described as a strong inhibitor of the *Pseudomonas*-derived cephalosporinase-3 (PDC-3), a class C β -lactamase which represents one of the major antibiotic-resistance determinants in *P. aeruginosa* ($K_i = 4 \text{ nM}$) (Drawz et al., 2011). Such a boronic acid derivative is also able to lower the MIC values of cefotaxime in PDC-3 expressing *E. coli*, to a concentration of 4 $\mu\text{g/ml}$. Subsequent studies demonstrate that SM23 is highly active against other class C (K_i of 1 and 20 nM vs. AmpC and ADC-7, respectively) and class A (β -lactamases K_i of 420 and 64 nM vs. CTXM-16 and TEM-1, respectively), qualifying it as one of the best inhibitors of serine β -lactamase (Caselli et al., 2018). Our present results indicate that SM23 significantly inhibits *P. aeruginosa* biofilm formation, as established by measuring total biomass and metabolic activity of a 24 h-old biofilm. In particular, about 50% reduction in biofilm biomass occurs as assessed by CV assay (Figure 2, left panel), while a clear dose-dependent inhibition is detected by bioluminescence analysis; the latter, known to measure metabolic activity, allows to detect a gradual and consistent effect within the range of 0.390–25.0 μM (Figure 2, right panel). The impact of SM23 on biofilm is also evident by exploring its morphological structure by confocal microscopy. Indeed, unlike the control, SM23-treated biofilm is characterized by large zones with few or no bacteria and scant extracellular polymeric matrix attached to the well surface; accordingly, a noticeable reduction of viable bacteria is detected, as measured by the alive/dead cells assay.

Interestingly, the exposure of *P. aeruginosa* to SM23 significantly inhibits the production of some key QS-controlled virulence factors, namely pyoverdine, pyocyanin, and elastase. As a yellow-green fluorescent pigment, pyoverdine is a strong iron scavenger/iron transporter that promotes *Pseudomonas* pathogenicity stimulating its growth (Meyer et al., 1996). To date, about 40

structurally different pyoverdines have been identified, each one characterized by a distinct peptide chain and a specificity, peculiar to *Pseudomonas* species (Meyer, 2000). Pyoverdine production may also be accompanied by the appearance of related compounds, which are considered as biosynthetic precursors or later modifications; such compounds have the same peptide chain of pyoverdine, but a different chromophore group (Budzikiewicz, 2004). Another key pigment strictly regulated by *Pseudomonas* QS system, in particular by *rhII/rhlR*, is pyocyanin. Here, we show that SM23 strongly inhibits pyocyanin production by *Pseudomonas*, in line with the marked reduction of pyoverdine production also observed after SM23 treatment.

For the determination of both pyoverdines and pyocyanin in culture supernatants, we have employed HPLC-MS analysis, that unambiguously identified (1) four chromophores belonging to the pyoverdine siderophore family and (2) one chromophore for pyocyanin. Interestingly, all of them happen to be markedly affected by SM23 treatment (see Table 2). Similarly, the elastase activity of *P. aeruginosa* is also significantly inhibited by SM23 during biofilm production. In line with these findings, the SM23 is shown to downregulate the expression of the QS-associated autoinducers 3-oxo- C_{12} -HSL and C_4 -HSL during biofilm formation by dampened *lasI/lasR* gene expression, further suggesting that QS pathways are affected by SM23.

As described previously (Schuster and Greenberg, 2006; Girard and Bloemberg, 2008; Zou and Nair, 2009), the QS system of *P. aeruginosa* is mainly composed of two sets of genes. The first consists of *lasI* and *lasR* genes, encoding for HSL autoinducer synthase and R protein, respectively; the second system, named Rhl, comprises the *rhII* and *rhlR* genes, which in turn encode for synthase and R protein. The two systems are strictly connected and hierarchically organized, with the *lasI/lasR* regulating the transcription of *rhII/rhlR* (Schuster and Greenberg, 2006; Zou and Nair, 2009). Our present data, obtained through HPLC-MS analysis, show a significant downregulation of both the autoinducers, 3-oxo- C_{12} -HSL and C_4 -HSL, in the supernatants of SM23-treated biofilm (at the dose of 3.125 μM), as compared to the untreated biofilm. These results indicate that SM23 significantly affects the synthesis of both 3-oxo- C_{12} -HSL and C_4 -HSL; in line with others (Zou and Nair, 2009), we favor the idea that it may compete with the 3-oxo- C_{12} -HSL autoinducer, likely for the same binding site on the LasR receptor. Many efforts will be necessary to deeply understand the molecular mechanisms underlying such a complex phenomenon.

By the experiments aimed at assessing SM23 interaction with bacterial cells, we demonstrate that most of its fluorescence appears to be bacteria-associated when the compound is added to a planktonic *P. aeruginosa* culture. Unexpectedly, such phenomenon is fully prevented once planktonic cells have been pre-incubated with a *Pseudomonas*-conditioned medium, prior to being exposed to SM23; in this case, the compound fluorescence is indeed detectable only in the supernatants. Also, when the compound is added to an early biofilm, approximately half of the SM23-related fluorescence signal remains unbound in the supernatant. Taken together, these data open to the hypothesis that *Pseudomonas* may counteract the activity of SM23 by producing something that prevents its binding to the same bacterial cell.

It should be noted that, though strongly associated with the compound, planktonic cells are not affected by SM23 in their viability or rate of growth. Although remaining widely unexplained, these findings may envisage the possibility that, because of its unique mechanism of action, SM23 might be a novel compound likely insensitive to the well-known drug-resistance mechanisms.

Finally, we provide evidence that SM23 is effective also in reducing *Pseudomonas* biofilm biomass produced on a medical device, such as the ETT; importantly, also the release of pyoverdine by such sessile bacterial community is significantly affected by SM23. In our opinion, these data strengthen the interest on SM23, showing that it acts as anti-*P. aeruginosa* compound also under conditions closely mimicking biofilm infection in patients.

Overall, our results demonstrate that the boronic acid derivative SM23, besides being a strong inhibitor of β -lactamase, is able to drastically reduce biofilm formation and QS-related virulence factors in *Pseudomonas*. This *in vitro* evidence opens to future applications of SM23 in the prevention and treatment of biofilm-associated *P. aeruginosa* infections.

DATA AVAILABILITY STATEMENT

The datasets generated for this study are available on request to the corresponding author.

REFERENCES

- Barnes, M. D., Taracila, M. A., Rutter, J. D., Bethel, C. R., Galdadas, I., Hujer, A. M., et al. (2018). Deciphering the evolution of cephalosporin resistance to ceftolozane-tazobactam in *Pseudomonas aeruginosa*. *MBio* 9, 1–19. doi: 10.1128/mBio.02085-18
- Berrazeg, M., Jeannot, K., Ntsogo Enguéné, V. Y., Broutin, I., Loeffert, S., Fournier, D., et al. (2015). Mutations in β -lactamase AmpC increase resistance of *Pseudomonas aeruginosa* isolates to antipseudomonal cephalosporins. *Antimicrob. Agents Chemother.* 59, 6248–6255. doi: 10.1128/AAC.00825-15
- Brooun, A., Liu, S., and Lewis, K. (2000). A dose-response study of antibiotic resistance in *Pseudomonas aeruginosa* biofilms. *Antimicrob. Agents Chemother.* 44, 640–646. doi: 10.1128/AAC.44.3.640-646.2000
- Budzikiewicz, H. (2004). Siderophores of the Pseudomonadaceae sensu stricto (fluorescent and non-fluorescent *Pseudomonas* spp.). *Fortschr. Chem. Org. Naturst.* 87, 81–237. doi: 10.1007/978-3-7091-0581-8_2
- Budzikiewicz, H., Schäfer, M., Fernández, D. U., Matthijs, S., and Cornelis, P. (2007). Characterization of the chromophores of pyoverdins and related siderophores by electrospray tandem mass spectrometry. *Biomaterials* 20, 135–144. doi: 10.1007/s10534-006-9021-3
- Bush, K., and Bradford, P. A. (2016). β -Lactams and β -lactamase inhibitors: an overview. *Cold Spring Harb. Perspect. Med.* 6, 295–306. doi: 10.1101/cshperspect.a025247
- Bush, K., and Bradford, P. A. (2019). Interplay between β -lactamases and new β -lactamase inhibitors. *Nat. Rev. Microbiol.* 17, 295–306. doi: 10.1038/s41579-019-0159-8
- Caselli, E., Romagnoli, C., Powers, R. A., Taracila, M. A., Bouza, A. A., Swanson, H. C., et al. (2018). Inhibition of *Acinetobacter*-derived cephalosporinase: exploring the carboxylate recognition site using novel β -lactamase inhibitors. *ACS Infect. Dis.* 4, 337–348. doi: 10.1021/acsinfecdis.7b00153
- Choi, K.-H., and Schweizer, H. P. (2006). Mini-Tn7 insertion in bacteria with single attTn7 sites: example *Pseudomonas aeruginosa*. *Nat. Protoc.* 1, 153–161. doi: 10.1038/nprot.2006.24
- Churchill, M. E. A., Sibhatu, H. M., and Uhelson, C. L. (2011). Defining the structure and function of acyl-homoserine lactone autoinducers. *Methods Mol. Biol.* 692, 159–171. doi: 10.1007/978-1-60761-971-0_12

AUTHOR CONTRIBUTIONS

SP, EP, FP, EC, and EB contributed to the conception and design of the study, revised the manuscript critically for important intellectual content, and provided approval for publication of the content. SP, EP, BC, DP, CC, and FF performed experiments and organized the results. EP performed the statistical analysis. SP wrote the first draft of the manuscript. SP, EP, EC, and DP wrote sections of the manuscript. All authors contributed to manuscript revision, read and approved the submitted version.

FUNDING

EC was supported by the Department of Life Science, FAR2016DIP. EP was supported by Department of Diagnostic, Clinical and Public Health Medicine, FAR2017DIP.

SUPPLEMENTARY MATERIAL

The Supplementary Material for this article can be found online at: <https://www.frontiersin.org/articles/10.3389/fmicb.2020.00035/full#supplementary-material>

- Cornelis, P., and Matthijs, S. (2002). Diversity of siderophore-mediated iron uptake systems in fluorescent pseudomonads: not only pyoverdines. *Environ. Microbiol.* 4, 787–798. doi: 10.1046/j.1462-2920.2002.00369.x
- Costerton, J. W. (1999). Introduction to biofilm. *Int. J. Antimicrob. Agents* 11, 217–221; discussion 237–239. doi: 10.1016/S0924-8579(99)00018-7
- Cross, A., Allen, J. R., Burke, J., Duce, G., Harris, A., John, J., et al. (1983). Nosocomial infections due to *Pseudomonas aeruginosa*: review of recent trends. *Rev. Infect. Dis.* 5(Suppl. 5), S837–S845.
- Das, M. C., Sandhu, P., Gupta, P., Rudrapaul, P., De, U. C., Tribedi, P., et al. (2016). Attenuation of *Pseudomonas aeruginosa* biofilm formation by vitexin: a combinatorial study with azithromycin and gentamicin. *Sci. Rep.* 6:23347. doi: 10.1038/srep23347
- de Kievit, T. R., and Iglewski, B. H. (2000). Bacterial quorum sensing in pathogenic relationships. *Infect. Immun.* 68, 4839–4849. doi: 10.1128/IAI.68.9.4839-4849.2000
- Donabedian, H. (2003). Quorum sensing and its relevance to infectious diseases. *J. Infect.* 46, 207–214. doi: 10.1053/jinf.2002.1120
- Dong, Y. H., Wang, L. H., Xu, J. L., Zhang, H. B., Zhang, X. F., and Zhang, L. H. (2001). Quenching quorum-sensing-dependent bacterial infection by an N-acyl homoserine lactonase. *Nature* 411, 813–817. doi: 10.1038/35081101
- Drawz, S. M., Taracila, M., Caselli, E., Prati, F., and Bonomo, R. A. (2011). Exploring sequence requirements for C₃/C₄ carboxylate recognition in the *Pseudomonas aeruginosa* cephalosporinase: insights into plasticity of the AmpC β -lactamase. *Protein Sci.* 20, 941–958. doi: 10.1002/pro.612
- Eidam, O., Romagnoli, C., Dalmasso, G., Barel, S., Caselli, E., Bonnet, R., et al. (2012). Fragment-guided design of subnanomolar β -lactamase inhibitors active in vivo. *Proc. Natl. Acad. Sci. USA* 109, 17448–17453. doi: 10.1073/pnas.1208337109
- Fuqua, C., and Greenberg, E. P. (1998). Self perception in bacteria: quorum sensing with acylated homoserine lactones. *Curr. Opin. Microbiol.* 1, 183–189. doi: 10.1016/S1369-5274(98)80009-X
- Girard, G., and Bloemberg, G. V. (2008). Central role of quorum sensing in regulating the production of pathogenicity factors in *Pseudomonas aeruginosa*. *Future Microbiol.* 3, 97–106. doi: 10.2217/17460913.3.1.97
- Griffith, D. C., Sabet, M., Tarazi, Z., Lomovskaya, O., and Dudley, M. N. (2019). Pharmacokinetics/pharmacodynamics of vaborbactam, a novel

- beta-lactamase inhibitor, in combination with meropenem. *Antimicrob. Agents Chemother.* 63, 1–9. doi: 10.1128/AAC.01659-18
- Jakobsen, T. H., Bjarnsholt, T., Jensen, P. Ø., Givskov, M., and Høiby, N. (2013). Targeting quorum sensing in *Pseudomonas aeruginosa* biofilms: current and emerging inhibitors. *Future Microbiol.* 8, 901–921. doi: 10.2217/fmb.13.57
- Kapoor, R. V., and Vaidyanathan, S. (2016). Towards quantitative mass spectrometry-based metabolomics in microbial and mammalian systems. *Philos. Transact. A Math. Phys. Eng. Sci.* 374, 1–14. doi: 10.1098/rsta.2015.0363
- Kilz, S., Lenz, C., Fuchs, R., and Budzikiewicz, H. (1999). A fast screening method for the identification of siderophores from fluorescent *Pseudomonas* spp. by liquid chromatography/electrospray mass spectrometry. *J. Mass Spectrom.* 34, 281–290. doi: 10.1002/(SICI)1096-9888(199904)34:4<281::AID-JMS750>3.0.CO;2-M
- Lee, J., and Zhang, L. (2015). The hierarchy quorum sensing network in *Pseudomonas aeruginosa*. *Protein Cell* 6, 26–41. doi: 10.1007/s13238-014-0100-x
- Li, H., Li, X., Wang, Z., Fu, Y., Ai, Q., Dong, Y., et al. (2015). Autoinducer-2 regulates *Pseudomonas aeruginosa* PAO1 biofilm formation and virulence production in a dose-dependent manner. *BMC Microbiol.* 15:192. doi: 10.1186/s12866-015-0529-y
- Li, J., Ramezani, M., Fong, S. A., Cooksley, C., Murphy, J., Suzuki, M., et al. (2019). *Pseudomonas aeruginosa* exoprotein-induced barrier disruption correlates with elastase activity and marks chronic rhinosinusitis severity. *Front. Cell. Infect. Microbiol.* 9:38. doi: 10.3389/fcimb.2019.00038
- Lyczak, J. B., Cannon, C. L., and Pier, G. B. (2002). Lung infections associated with cystic fibrosis. *Clin. Microbiol. Rev.* 15, 194–222. doi: 10.1128/CMR.15.2.194-222.2002
- Mah, T. F., and O'Toole, G. A. (2001). Mechanisms of biofilm resistance to antimicrobial agents. *Trends Microbiol.* 9, 34–39. doi: 10.1016/S0966-842X(00)01913-2
- Meyer, J. M. (2000). Pyoverdines: pigments, siderophores and potential taxonomic markers of fluorescent *Pseudomonas* species. *Arch. Microbiol.* 174, 135–142. doi: 10.1007/s002030000188
- Meyer, J. M., Neely, A., Stintzi, A., Georges, C., and Holder, I. A. (1996). Pyoverdine is essential for virulence of *Pseudomonas aeruginosa*. *Infect. Immun.* 64, 518–523. doi: 10.1128/IAI.64.2.518-523.1996
- Moghaddam, M. M. (2014). Quorum sensing in bacteria and a glance on *Pseudomonas aeruginosa*. *Clin. Microbiol. Open Access* 3, 133–139. doi: 10.4172/2327-5073.1000156
- Moghaddam, M. M., Abolhassani, F., Babavalian, H., Mirnejad, R., Azizi Barjini, K., and Amani, J. (2012). Comparison of in vitro antibacterial activities of two cationic peptides CM15 and CM11 against five pathogenic bacteria: *Pseudomonas aeruginosa*, *Staphylococcus aureus*, *Vibrio cholerae*, *Acinetobacter baumannii*, and *Escherichia coli*. *Probiotics Antimicrob. Proteins* 4, 133–139. doi: 10.1007/s12602-012-9098-7
- Morandi, F., Caselli, E., Morandi, S., Focia, P. J., Blázquez, J., Shoichet, B. K., et al. (2003). Nanomolar inhibitors of AmpC beta-lactamase. *J. Am. Chem. Soc.* 125, 685–695. doi: 10.1021/ja0288338
- Mulcahy, L. R., Isabella, V. M., and Lewis, K. (2014). *Pseudomonas aeruginosa* biofilms in disease. *Microb. Ecol.* 68, 1–12. doi: 10.1007/s00248-013-0297-x
- Ni, N., Choudhary, G., Peng, H., Li, M., Chou, H.-T., Lu, C.-D., et al. (2009). Inhibition of quorum sensing in *Vibrio harveyi* by boronic acids. *Chem. Biol. Drug Des.* 74, 51–56. doi: 10.1111/j.1747-0285.2009.00834.x
- Ohman, D. E., Cryz, S. J., and Iglewski, B. H. (1980). Isolation and characterization of *Pseudomonas aeruginosa* PAO mutant that produces altered elastase. *J. Bacteriol.* 142, 836–842. doi: 10.1128/JB.142.3.836-842.1980
- Pericolini, E., Colombari, B., Ferretti, G., Iseppi, R., Ardizzoni, A., Girardis, M., et al. (2018). Real-time monitoring of *Pseudomonas aeruginosa* biofilm formation on endotracheal tubes in vitro. *BMC Microbiol.* 18:84. doi: 10.1186/s12866-018-1224-6
- Pesci, E. C., Milbank, J. B., Pearson, J. P., McKnight, S., Kende, A. S., Greenberg, E. P., et al. (1999). Quinolone signaling in the cell-to-cell communication system of *Pseudomonas aeruginosa*. *Proc. Natl. Acad. Sci. USA* 96, 11229–11234. doi: 10.1073/pnas.96.20.11229
- Preston, M. J., Seed, P. C., Toder, D. S., Iglewski, B. H., Ohman, D. E., Gustin, J. K., et al. (1997). Contribution of proteases and LasR to the virulence of *Pseudomonas aeruginosa* during corneal infections. *Infect. Immun.* 65, 3086–3090. doi: 10.1128/IAI.65.8.3086-3090.1997
- Qu, L., She, P., Wang, Y., Liu, F., Zhang, D., Chen, L., et al. (2016). Effects of norspermidine on *Pseudomonas aeruginosa* biofilm formation and eradication. *MicrobiologyOpen* 5, 402–412. doi: 10.1002/mbo3.338
- Rossolini, G. M., and Mantengoli, E. (2005). Treatment and control of severe infections caused by multiresistant *Pseudomonas aeruginosa*. *Clin. Microbiol. Infect.* 11(Suppl. 4), 17–32. doi: 10.1111/j.1469-0691.2005.01161.x
- Sarabhai, S., Harjai, K., Sharma, P., and Capalash, N. (2015). Ellagic acid derivatives from *Terminalia chebula* Retz. increase the susceptibility of *Pseudomonas aeruginosa* to stress by inhibiting polyphosphate kinase. *J. Appl. Microbiol.* 118, 817–825. doi: 10.1111/jam.12733
- Schuster, M., and Greenberg, E. P. (2006). A network of networks: quorum-sensing gene regulation in *Pseudomonas aeruginosa*. *Int. J. Med. Microbiol.* 296, 73–81. doi: 10.1016/j.ijmm.2006.01.036
- Stepanovic, S., Vukovic, D., Dakic, I., Savic, B., and Svabic-Vlahovic, M. (2000). A modified microtiter-plate test for quantification of staphylococcal biofilm formation. *J. Microbiol. Methods* 40, 175–179. doi: 10.1016/S0167-7012(00)00122-6
- Stover, C. K., Pham, X. Q., Erwin, A. L., Mizoguchi, S. D., Warrener, P., Hickey, M. J., et al. (2000). Complete genome sequence of *Pseudomonas aeruginosa* PAO1, an opportunistic pathogen. *Nature* 406, 959–964. doi: 10.1038/35023079
- Tenover, F. C. (2006). Mechanisms of antimicrobial resistance in bacteria. *Am. J. Infect. Control* 34, S3–S10; discussion S64–73. doi: 10.1016/j.ajic.2006.05.219
- Vandeputte, O. M., Kiendrebeogo, M., Rajaonson, S., Diallo, B., Mol, A., El Jaziri, M., et al. (2010). Identification of catechin as one of the flavonoids from *Combretum albiflorum* bark extract that reduces the production of quorum-sensing-controlled virulence factors in *Pseudomonas aeruginosa* PAO1. *Appl. Environ. Microbiol.* 76, 243–253. doi: 10.1128/AEM.01059-09
- Venturi, V. (2006). Regulation of quorum sensing in *Pseudomonas*. *FEMS Microbiol. Rev.* 30, 274–291. doi: 10.1111/j.1574-6976.2005.00012.x
- Watson, D., MacDermot, J., Wilson, R., Cole, P. J., and Taylor, G. W. (1986). Purification and structural analysis of pyocyanin and 1-hydroxyphenazine. *Eur. J. Biochem.* 159, 309–313. doi: 10.1111/j.1432-1033.1986.tb09869.x
- Wei, H., and Aristilde, L. (2015). Structural characterization of multiple pyoverdines secreted by two *Pseudomonas* strains using liquid chromatography-high resolution tandem mass spectrometry with varying dissociation energies. *Anal. Bioanal. Chem.* 407, 4629–4638. doi: 10.1007/s00216-015-8659-5
- Xu, Z., Fang, X., Wood, T. K., and Huang, Z. J. (2013). A systems-level approach for investigating *Pseudomonas aeruginosa* biofilm formation. *PLoS One* 8:e57050. doi: 10.1371/journal.pone.0057050
- Zou, Y., and Nair, S. K. (2009). Molecular basis for the recognition of structurally distinct autoinducer mimics by the *Pseudomonas aeruginosa* LasR quorum-sensing signaling receptor. *Chem. Biol.* 16, 961–970. doi: 10.1016/j.chembiol.2009.09.001

Conflict of Interest: The authors declare that the research was conducted in the absence of any commercial or financial relationships that could be construed as a potential conflict of interest.

Copyright © 2020 Peppoloni, Pericolini, Colombari, Pinetti, Cermelli, Fini, Prati, Caselli and Blasi. This is an open-access article distributed under the terms of the Creative Commons Attribution License (CC BY). The use, distribution or reproduction in other forums is permitted, provided the original author(s) and the copyright owner(s) are credited and that the original publication in this journal is cited, in accordance with accepted academic practice. No use, distribution or reproduction is permitted which does not comply with these terms.



***In vitro* Mixed Biofilm of *Streptococcus suis* and *Actinobacillus pleuropneumoniae* Impacts Antibiotic Susceptibility and Modulates Virulence Factor Gene Expression**

Yang Wang^{1,2*}, Shenglong Gong^{1,2}, Xiao Dong^{1,2}, Jinpeng Li^{1,2}, Daniel Grenier³ and Li Yi^{2,4*}

¹ College of Animal Science and Technology, Henan University of Science and Technology, Luoyang, China, ² Key Laboratory of Molecular Pathogen and Immunology of Animal of Luoyang, Luoyang, China, ³ Groupe de Recherche en Écologie Buccale, Faculté de Médecine Dentaire, Université Laval, Quebec, QC, Canada, ⁴ College of Life Science, Luoyang Normal University, Luoyang, China

OPEN ACCESS

Edited by:

Sujogya Kumar Panda,
KU Leuven, Belgium

Reviewed by:

Rubén León,
Dentaid S.L., Spain
Xiuzhu Dong,
Institute of Microbiology (CAS), China

*Correspondence:

Yang Wang
wangyocan@163.com
Li Yi
lilili123168@163.com

Specialty section:

This article was submitted to
Antimicrobials, Resistance
and Chemotherapy,
a section of the journal
Frontiers in Microbiology

Received: 05 November 2019

Accepted: 09 March 2020

Published: 07 April 2020

Citation:

Wang Y, Gong S, Dong X, Li J,
Grenier D and Yi L (2020) *In vitro*
Mixed Biofilm of *Streptococcus suis*
and *Actinobacillus pleuropneumoniae*
Impacts Antibiotic Susceptibility
and Modulates Virulence Factor Gene
Expression. *Front. Microbiol.* 11:507.
doi: 10.3389/fmicb.2020.00507

Streptococcus suis (*S. suis*) and *Actinobacillus pleuropneumoniae* (*A. pleuropneumoniae*) are primary swine pathogens that have been frequently co-isolated from pigs suffering from severe respiratory disease. The purpose of this study was to investigate the biological impacts of the interactions between *S. suis* and *A. pleuropneumoniae*. A single- and dual-species culture model was established *in vitro* via *S. suis* HA9801 (serotype 2) and *A. pleuropneumoniae* CVCC265 (serotype 1). The single or mixed biofilms were imaged by confocal laser scanning microscopy. The biomass and viable cells in biofilms were quantified by crystal violet staining and determination of colony-forming units. The antibiotic susceptibility was determined by a microdilution broth method. The differences in gene transcription in pure- or mixed-species biofilms of *S. suis* and *A. pleuropneumoniae* was evaluated by quantitative PCR. *S. suis* and *A. pleuropneumoniae* formed two-species biofilms when co-cultured *in vitro*. When co-cultured with *S. suis*, biofilm formation by *A. pleuropneumoniae* was significantly increased with the absence of NAD that is necessary for the growth of *A. pleuropneumoniae*. Moreover, compared with monocultures, the antibiotic resistance of *S. suis* and *A. pleuropneumoniae* was both enhanced in the co-culture model. When grown in dual-species biofilms, for *A. pleuropneumoniae*, genes associated with virulence factors, including exotoxins and adhesins, were significantly upregulated. For *S. suis*, virulence factor-related genes *cps2*, *gdh*, *mrp*, and *sly* were highly induced. These results suggest that the interspecies interactions between *S. suis* and *A. pleuropneumoniae* may be cooperative under specific conditions and may play an important role in the disease progression and persistent infection.

Keywords: *Streptococcus suis*, *Actinobacillus pleuropneumoniae*, mixed biofilm, antibiotic susceptibility, swine

INTRODUCTION

Respiratory diseases constitute the most important health issues affecting the swine industry worldwide and are often referred to as the porcine respiratory disease complex (PRDC) (Qiao et al., 2011). In general, PRDC causes lung lesions, which, in turn, results in substantial economic losses and impaired animal welfare (Fablet et al., 2012). PRDC is multifactorial in nature and is triggered by mixed infections involving primary and secondary pathogens (Cheong et al., 2017). Clinically, *Streptococcus suis* (*S. suis*) and *Actinobacillus pleuropneumoniae* (*A. pleuropneumoniae*) are two important respiratory pathogens frequently detected in the PRDC (Opriessnig et al., 2011). In recent years, there have been many cases of mixed infections associated with the presence of *S. suis* and *A. pleuropneumoniae* in China. It is more than likely that the different bacteria or viruses coexisting in PRDC interact and exacerbate the pathogenesis of the disease. However, few research groups investigated the interactions between *S. suis* and *A. pleuropneumoniae*, except for a study reporting that these two bacterial species form polymicrobial biofilms *in vitro* (Ramirez-Castillo et al., 2018).

The formation of biofilm is considered as a survival strategy for bacterial pathogens. Bacteria in biofilms are embedded in an extracellular matrix, which reduces their susceptibility to antibiotic and host immune system (Vuotto and Donelli, 2019). This is a major reason why biofilm-related infections are difficult to eradicate. During a chronic infection, bacteria are able to switch between planktonic and biofilm lifestyle (Kathju et al., 2009; Lister and Horswill, 2014). The key role of biofilms have been confirmed in many diseases such as endocarditis, periodontitis, and otitis media (Kobayashi et al., 2005). Multi-species biofilms may be the most significant lifestyle of microbes *in vivo* and bacteria in such polymicrobial biofilms are more difficult to eradicate (Wang et al., 2018). In multi-species biofilms, microorganisms will enhance and ensure their survival and reproduction through communication, competition, or cooperation (Yang et al., 2011). In the present study, we hypothesized that there are synergistic interactions between *S. suis* and *A. pleuropneumoniae* in dual-species biofilms, resulting in enhanced biofilm formation ability, enhanced antibiotic resistance, and upregulated virulence factor gene expression.

MATERIALS AND METHODS

Bacterial Strains and Growth Conditions

S. suis HA9801 (SS) was isolated from a diseased pig in Jiangsu Province, China, and identified to be *S. suis* serotype 2. All experiments in this study were approved by the Experimental Animal Monitoring Committee of Henan University of Science and Technology and carried out accordingly. *A. pleuropneumoniae* CVCC 265 (APP) was purchased from China Veterinary Culture Collection Center (CVCC).

S. suis was grown in tryptic soy broth (TSB) or plated on TSA. *A. pleuropneumoniae* was cultivated in the same media supplemented with 0.1 µg/mL of β-nicotinamide-adenine-dinucleotide (NAD). Bacterial cultures were incubated at 37°C. All experiments described below were replicated in biological triplicate.

Planktonic Growth Assays of Mono- and co-Cultures

Bacterial colonies of *S. suis* and *A. pleuropneumoniae* were inoculated separately in solid media and grown overnight to mid-exponential phase in TSB + 0.1% NAD medium. The bacterial cultures were diluted in fresh medium to obtain an optical density at 660 (OD₆₆₀) of 0.03. Mono-culture of *S. suis* or *A. pleuropneumoniae* and co-culture of mixture (1:1 ratio) were inoculated in TSB + 0.1% NAD medium for 24 h. Samples were taken at 0, 2, 4, 6, 8, 10, 12, and 24 h, serially diluted in sterile PBS, and then plated on TSA or TSA + 0.1% NAD medium to discriminate *S. suis* or *A. pleuropneumoniae*, respectively, and the viable cell counts were enumerated.

For the mixed culture, the Competitive Index (CI) was calculated according to the formula: $(A. pleuropneumoniae/S. suis)_{\text{output}} / (A. pleuropneumoniae/S. suis)_{\text{input}}$. The output and input samples were assessed by plating onto selective medium at different time points, respectively. The Relative Increase Ratio (RIR) was similar to CI, and was calculated from the corresponding growth results obtained from single cultures of each strain (Macho et al., 2007). A positive CI value suggests a competitive advantage for *A. pleuropneumoniae* and vice versa. Only CIs that are statistically different from the RIRs at the same growth stages can be recognized as the result of prominent competition between species (Macho et al., 2007).

Biofilm Formation by Single and Mixed Cultures

Biofilm production was quantified by crystal violet staining as described previously (Bragonzi et al., 2012). Briefly, overnight cultures of *S. suis* and *A. pleuropneumoniae* were diluted 1/100 in fresh TSB broth supplemented with NAD, and inoculated individually or at several different ratios in 96-well plates. After 24 h incubation, the medium and planktonic bacteria were removed, and each well was gently washed twice with sterile PBS. Methanol was used to fix the attached bacteria for 15 min. The plates were then air-dried and the biofilms were stained with crystal violet (0.1%). After 20 min, the excess dye was discarded and plates were washed twice with sterile PBS prior to adding 200 µl of 95% ethanol to the wells to dissolve the biofilms. The optical density at 620 nm (OD₆₂₀) was measured using a microplate reader.

Biofilms were prepared in the 96-well plates as described above. Biofilms were washed twice with sterile PBS, and then bacteria were detached and homogenized in 100 µl of sterile PBS by weak sonication for 4 min. TSA or TSA + 0.1% NAD medium was used to discriminate *S. suis* or *A. pleuropneumoniae*, respectively, and then viable cells were enumerated (Chan et al., 2017).

TABLE 1 | The primers used in this study for qRT-PCR.

Primer	Forward primer	Reverse primer
APP		
16S rRNA	GGAGCTTGCTTTCTTGCCGACG	TAACCTTGCGGCCGTACTCCC
Apx-I	TTGAAGCGGAGAAACAGCTT	TGACCGACCTCGATAAAACC
Apx-II	GGTCAAGGAAAT GGAGTTCAAGAT	GCTAGTTTTT GCAATGTCCAA
afuB	TGGTTTTTAACGAACCTGCCTTT	CTTTAATGATGCGCCAATGT
hgbA	CGGATCCGTTTAGCTTCTTG	TAATGCGGCTTCTTTCGTCT
Pga	GATAAAGCAAGCCAG TTCTTAGGT	GCTGTTTGATGAG AAATACCGA
Apa-I	TTGCAGCAGGTGACGTGAA	TCGCTGACCGCGTATAATT
SS		
16S rRNA	GTTGCGAACGGGTGAGTAA	TCTCAGGTCGGCTATGTATCG
cps2	ATTGGTAGGCACTGTCGTTGGTC	AGAACTTAGCATTGTTGCGGTGG
fbps	AACCATCTTGCCAGGCTCCAC	CAGTTCAGAAGCCGTATCCCGAC
gdh	CACCTTTACCACCGCCGATTG	GGAAATGTTCAAGTCAACCGTGG
mrp	CAGGTAACATCAGAATCACCA CTTTT	AAGTTTTGTTGAGCATCCT CTATAGC
sly	TCATTAGGTGCTTATGTTGCG	GAAGA TTGCG AGCAT TTCCT GG

Confocal Laser Scanning Microscopy

Chamber slides were inoculated with bacterial suspension (*S. suis* alone, *A. pleuropneumoniae* alone and combination in 1:1 ratio) for 24 h at 37°C. The slides were washed twice with PBS to remove the medium and unattached bacteria. Samples was stained with SYTO 9 solution following the manufacturer’s instructions from LIVE/DEAD™ BacLight™ Bacterial Viability Kit (Thermo Fischer Scientific, Inc., Waltham, MA, United States), and then washed with PBS (Tawakoli et al., 2013). Biofilms were observed using a Zeiss LSM800 CLSM (Carl Zeiss, Jena, Germany).

Antibiotic Susceptibility Testing

The *in vitro* antibiotic susceptibility of *S. suis* and *A. pleuropneumoniae* was determined by a twofold dilution method in microplates following the guidelines of Clinical and Laboratory Standards Institute. Antibiotic serial dilutions were made up in culture medium, and 100 µl was transferred to the wells. Overnight cultures of *S. suis* and *A. pleuropneumoniae* were diluted at 1:100 with TSB contain in 0.1% NAD, and 100 µl of *S. suis*, *A. pleuropneumoniae*, or combination in 1:1 were added to 96-well plates and incubated at 37°C for 24 h. The minimum inhibitory concentration (MIC) values were determined by reading the optical density and visual observation of the turbidity.

The minimum biofilm eradication concentration (MBEC) values were also determined. Biofilms were prepared in the 96-well plates as described above. Wells were washed twice with PBS and antibiotic serial dilutions made up in TSB containing 0.1% NAD were transferred (200 µl) to the wells. The plates were incubated for another 24 h.

TABLE 2 | *In vitro* susceptibility of pure culture and co-culture of *S. suis* and *A. pleuropneumoniae* in planktonic growth and biofilm to seven clinically relevant antibiotics.

Antibiotic	<i>Streptococcus suis</i>	<i>Actinobacillus pleuropneumoniae</i>	<i>S. suis</i> + <i>A. pleuropneumoniae</i>
Tylosin tartrate			
MIC	<0.3125	20	20
MBEC	1.25	40	80
Gentamicin			
MIC	10	10	10
MBEC	10	10	10
Amoxicillin			
MIC	<0.3125	160	> 160
MBEC	0.625	160	> 160
Apramycin			
MIC	40	80	80
MBEC	40	80	> 160
Tilmicosin			
MIC	5	5	10
MBEC	80	80	160
Spectinomycin			
MIC	40	80	80
MBEC	80	80	160
Fosfomycin			
MIC	80	20	20
MBEC	> 160	40	> 160

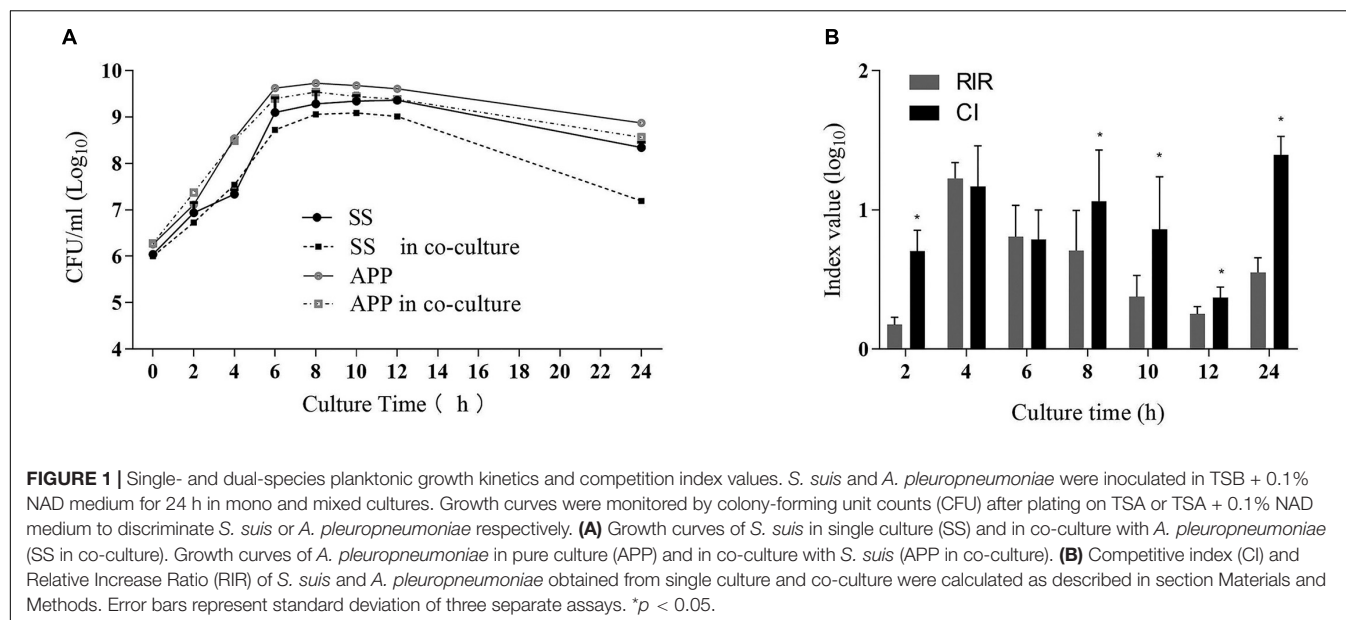
The MBEC values were determined by plating samples on culture medium plates.

Virulence Factor Gene Expression in Mixed Biofilm

Real-time PCR was used to assess the relative expression of virulence factor genes in *A. pleuropneumoniae* or *S. suis* when grown alone or in mixed biofilms. Biofilms were prepared in 24-well plates as described above, washed twice with PBS, detached by sonicating, and then collected. RNA was extracted by the Trizol method (Pompilio et al., 2015). gDNA removal and cDNA synthesis were performed using PrimeScript™ RT reagent Kit with gDNA Eraser (TaKaRa) according to the manufacturer’s protocol. Real-time PCR assay was performed with TB Green® Premix Ex Taq™ (TaKaRa) following the manufacturer’s instructions. The primers used are listed in **Table 1**. The 16S rRNA was used as the house-keeping gene for normalization. Relative expression levels were determined by the ($\Delta\Delta C_t$) method.

Statistical Analysis

GraphPad Prism version 7.0 (GraphPad Software, San Diego, CA, United States) was used for data analysis. Results were obtained from three independent experiments and all values were expressed as means \pm standard deviation. Differences between mean values were evaluated by Student’s *t*-test. *P*-value of 0.05 or less was considered statistically significant.



RESULTS

Competition Between *S. suis* and *A. pleuropneumoniae* in Planktonic co-Cultures

To study the interactions between *S. suis* and *A. pleuropneumoniae* in planktonic co-cultures, the growth curves of single and mixed cultures were compared, and the results are shown in **Figure 1A**. The kinetics analysis showed that the growth of *S. suis* in mixed culture was negatively affected from 8 to 24 h, while *A. pleuropneumoniae* growth was not clearly affected when co-cultured with *S. suis*. To further estimate the differences in growth kinetics between *S. suis* and *A. pleuropneumoniae* in single or mixed cultures, CI and RIR indexes were calculated. As shown in **Figure 1B**, a positive CI index of *A. pleuropneumoniae* versus *S. suis* was always observed, indicating a competitive advantage for *A. pleuropneumoniae* over *S. suis* in co-cultures. The CI was significantly higher than the RIR between 8 and 24 h ($p < 0.05$), suggesting a noticeable negative effect of *A. pleuropneumoniae* on *S. suis* growth.

Formation of Mixed Biofilm of *S. suis* and *A. pleuropneumoniae*

Biofilm formation by *S. suis* and *A. pleuropneumoniae* in single and dual culture in 96-well plate was assessed by crystal violet staining and viable count, and the results are shown in **Figure 2**. Both *S. suis* and *A. pleuropneumoniae* formed important biofilms when grown in TSB supplemented with NAD (**Figure 2A**). However, in the absence of NAD, *A. pleuropneumoniae* couldn't form biofilms (**Figure 2B**). Under favorable growth conditions (supplement with NAD) for *A. pleuropneumoniae*, mixed biofilms with *S. suis* were formed (**Figure 2C**). Moreover, based on results of crystal violet staining and determination of CFU, *A. pleuropneumoniae* was able to

grow and form a dual-species biofilm without the addition of NAD when grown in the presence of *S. suis* (**Figure 2D**).

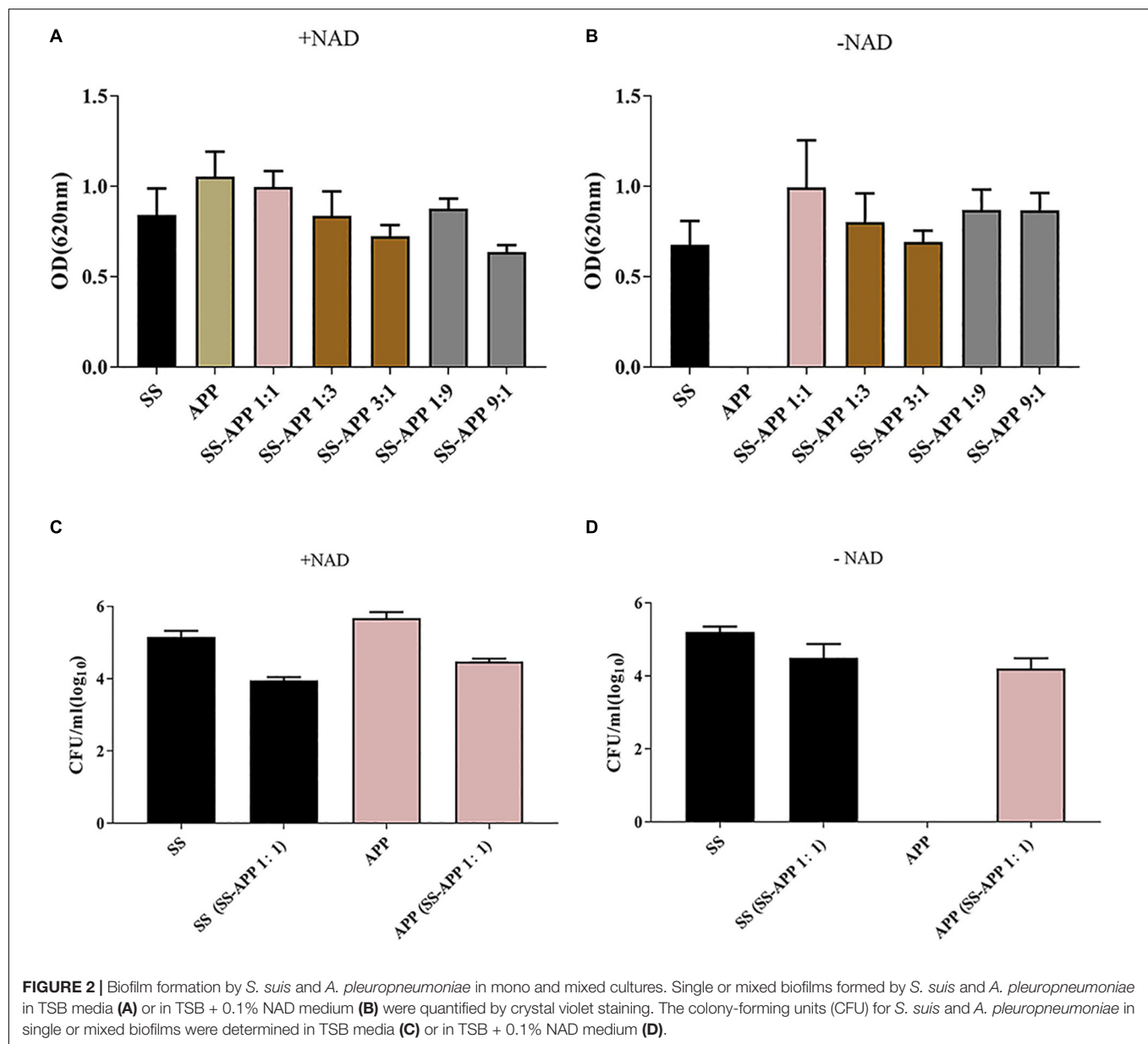
By using confocal laser scanning microscopy (**Figure 3**), it could be confirmed that both *S. suis* and *A. pleuropneumoniae* were able to form robust single- and dual-species biofilms *in vitro*.

Antibiotic Susceptibility

The *in vitro* antibiotic susceptibility of *S. suis* and *A. pleuropneumoniae*, individually and in combination to several antimicrobial drugs, was determined (**Table 2**). For tylosin tartrate, when in co-culture with the other, the MBEC of *S. suis* increased from 1.25 to 80 $\mu\text{g/ml}$, and the MBEC of *A. pleuropneumoniae* increased from 40 to 80 $\mu\text{g/ml}$. For tilmicosin, when in co-culture, the MIC and MBEC of *S. suis* or *A. pleuropneumoniae* were twice as high as that in pure culture. In general, *S. suis* and *A. pleuropneumoniae* in mixed biofilms showed increased resistance to tylosin tartrate and tilmicosin with higher values of MBEC in comparison to single-species biofilms.

Differential Gene Expression in Mono- and Dual-Species Biofilms

As shown in **Figure 4**, in comparison with the single species biofilms, the virulence factor genes in the two-species biofilms were overall upregulated. For *A. pleuropneumoniae*, compared with mono-species biofilms, *ApxI* and *ApxII*, coding for exotoxin, were upregulated by 10.65- and 22.58-fold, respectively, *afuB* involved in biofilm formation was upregulated by 8.69-fold, *apaI* associated with adhesin was upregulated by 5.73-fold, and *hgbA* involved in iron uptake was upregulated by 18.3-fold (**Figure 4A**). For *S. suis*, virulence factor related genes *cps2*, *gdh*, *mrp*, and *sly* were significantly upregulated by 2.61-, 2.23-, 3.81-, and 2.26-fold, respectively, with no statistical differences of



fbps gene (Figure 4B). The results may indicate that co-culture may modulate the bacterial virulence in mixed biofilm.

DISCUSSION

Polymicrobial respiratory diseases remain a major threat in the swine industry worldwide. Pathogens associated with PRDC include swine influenza virus (SIV), porcine circovirus type 2 (PCV2), porcine reproductive and respiratory syndrome virus (PRRSV), *S. suis*, *A. pleuropneumoniae*, *Mycoplasma hyopneumoniae*, and *Haemophilus parasuis*. Bacterial-viral co-infections were reported to exacerbate the pathogenicity (Opriessnig et al., 2011). For instance, co-infections of *M. hyopneumoniae* and SIV lead to the

exacerbation of the clinical signs (Thacker et al., 1999), and during the co-infection of PRRSV and *S. suis*, the virulence of PRRSV was enhanced by *S. suis* and PRRSV increased the susceptibility of pigs to *S. suis* infection (Thanawongnuwech et al., 2000). *S. suis* and *A. pleuropneumoniae* are two important pathogens associated with PRDC, and their co-occurrence in the same site of infection has been frequently reported (Opriessnig et al., 2011), although the interactions between them and the host during coinfection have not been previously investigated. The present study examined the interactions between *S. suis* and *A. pleuropneumoniae* in planktonic and biofilm cultures, and specifically explored whether these interactions provide greater fitness than single cultures, which is helpful to better understand the possible role of coinfection in the pathogenesis.

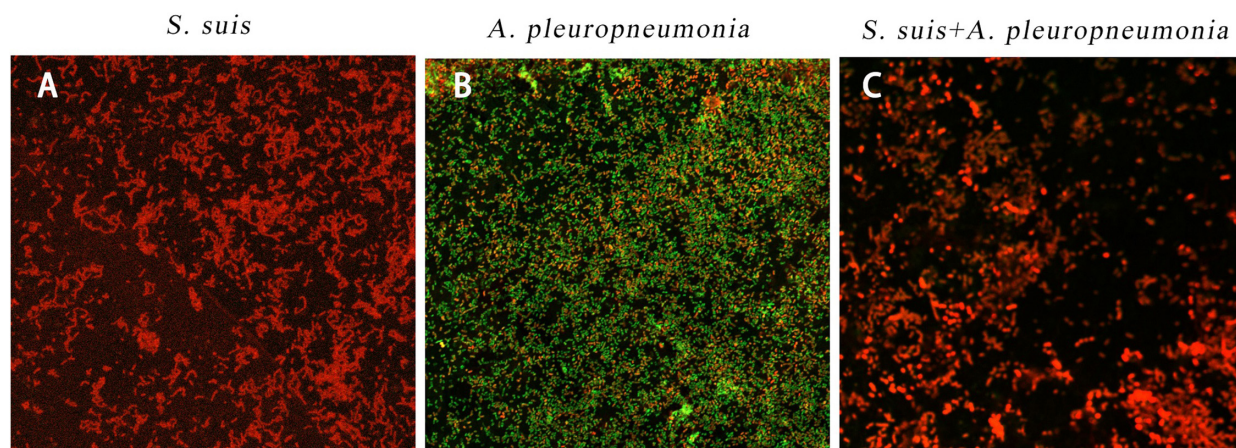


FIGURE 3 | Biofilm formation of single and mixed species imaged by confocal laser scanning microscopy at $\times 63$ magnification after 24 h inoculation. *S. suis* alone (A), *A. pleuropneumoniae* alone (B), or *S. suis* and *A. pleuropneumoniae* together (C).

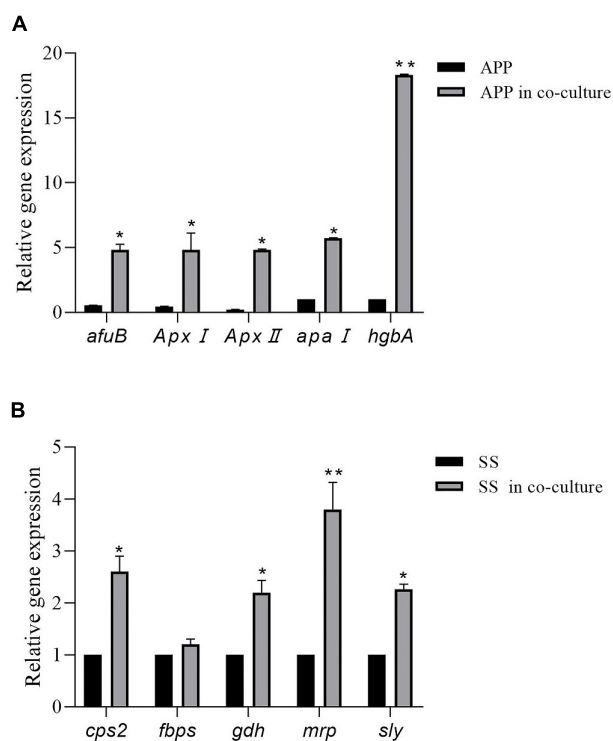


FIGURE 4 | Relative expression levels of *A. pleuropneumoniae* virulence factor genes (*ApxI*, *ApxII*, *afuB*, *apaI*, and *hgbA*) in mixed biofilm (A). Relative expression levels of *S. suis* virulence factor genes (*cps2*, *fbps*, *gdh*, *mrp*, and *sly*) in mixed biofilm (B). Error bars represent standard deviation of three separate assays. * $p < 0.05$; ** $p < 0.01$.

Studies on microbial interactions under planktonic growth conditions have shown that species can coexist with other microbes competing in the same repository through multiple mechanisms (Hibbing et al., 2010). It was reported that the consumption of limited nutrients may impact the interactions

process between species in co-culture models (Sibley et al., 2008). We demonstrated that *S. suis* has no effect on the growth of *A. pleuropneumoniae* in planktonic culture, while a significant negative impact of *A. pleuropneumoniae* on *S. suis* growth was found during the stationary phase of bacterial growth.

When grown in mixed cultures, the exoproducts of *A. pleuropneumoniae* may be the disadvantageous cause of *S. suis* in planktonic bacteria. The CI and RIR indicated that *A. pleuropneumoniae* surpasses *S. suis* in exponential and stationary phases of bacterial growth. The competition for limited nutrients and space may lead to the antagonistic effects among microorganisms within a community (Harrison, 2007).

Crystal violet staining and colony-forming unit results showed that both *S. suis* and *A. pleuropneumoniae* formed strong biofilms when grown in single or mixed culture, and the CSLM images provided additional evidence. Interestingly, *A. pleuropneumoniae* was able to grow in the absence of NAD when co-cultured with *S. suis*. Our results confirm that the presence of *S. suis* promoted *A. pleuropneumoniae* biofilm growth under a hostile condition for *A. pleuropneumoniae* (without NAD supplementation). A variety of animal or human pathogens, such as *Streptococcus mutans*, *Pseudomonas aeruginosa*, *Legionella pneumophila*, *Stenotrophomonas maltophilia*, and *Escherichia coli*, have been reported that to form mixed biofilms, which help to improve their resistance, persistence, and pathogenicity (Yang et al., 2011). Recent studies on multi-species community behavior have shown that the presence of other bacterial species can modulate the virulence and the gene expression of pathogens. In the respiratory tract, the NAD supply, which is essential for *A. pleuropneumoniae* growth, is rather limited. However, *A. pleuropneumoniae* has overcome this deficiency in various ways, such as cell lysis, which releases nutrients into the surrounding environment (Chiers et al., 2010). In addition, polymicrobial biofilm formation with *S. suis* enables *A. pleuropneumoniae* to acquire this compound by cross-feeding. We showed that a mixed biofilm of *S. suis* and *A. pleuropneumoniae* has an increased resistance to several

antibiotics. In fact, it is well known that bacteria residing in biofilms have an increased resistance to antibiotics (Assavacheep and Rycroft, 2013), and multi-species biofilm is believed to provide an enhanced protection against antibiotic and host immune system (Armbruster et al., 2010). Some well-known mechanisms for enhancing multi-microbial biofilm resistance include upregulation and transfer of drug resistance genes, increased responsiveness through quorum sensing, and increased mutation level in antibiotic target molecules (Hoiby et al., 2010). Recent research of multi-species community behavior have reported that the virulence, biofilm formation, and the gene expression level of pathogens can be regulated by the presence of other species (Duan et al., 2003). To investigate this, quantitative PCR was performed to analyze differential gene expression in mixed biofilms. The RT-PCR results showed that genes of *A. pleuropneumoniae*, coding for exotoxin, biofilm formation, or iron uptake, respectively, were highly induced. Further, genes of *cps2*, *gdh*, *mrp*, and *sly* associated with virulence factors of *S. suis* were significantly upregulated. The result suggests that mixed biofilms may reinforce bacteria pathogenicity.

In conclusion, we found that co-culture may result in increased antibiotic resistance and upregulated virulence gene expression for *S. suis* and *A. pleuropneumoniae* in biofilms. It is likely that the interspecies interactions between *S. suis* and *A. pleuropneumoniae* are synergetic under specific conditions. Therefore, the interactions between the species in the biofilm

community potentially influence the clinical course of disease. Our findings provide some relevant information that may affect the choice of antibiotics, and shed light on a new perspective for the treatment of mixed infection.

DATA AVAILABILITY STATEMENT

All datasets generated for this study are included in the article/supplementary material.

AUTHOR CONTRIBUTIONS

YW and LY conceived and designed the experiments. SG, XD, and JL performed the experiments. YW, XD, and DG analyzed the data. LY and JL contributed reagents, materials, and analysis tools. YW and SG wrote the manuscript.

FUNDING

This work was supported by the National Key Research and Development Program of China (2018YFD0500100), the National Natural Science Foundation of China (31902309 and 31772761), Luoyang Normal University National project cultivation program, and Young Teacher Foundation of Luoyang Normal University.

REFERENCES

- Armbruster, C. E., Hong, W., Pang, B., Weimer, K. E., Juneau, R. A., Turner, J., et al. (2010). Indirect pathogenicity of *Haemophilus influenzae* and *Moraxella catarrhalis* in polymicrobial otitis media occurs via interspecies quorum signaling. *mBio* 1:e00102-10. doi: 10.1128/mBio.00102-10
- Assavacheep, P., and Rycroft, A. N. (2013). Survival of *Actinobacillus pleuropneumoniae* outside the pig. *Res. Vet. Sci.* 94, 22–26. doi: 10.1016/j.rvsc.2012.07.024
- Bragonzi, A., Farulla, I., Paroni, M., Twomey, K. B., Pirone, L., Lore, N. I., et al. (2012). Modelling co-infection of the cystic fibrosis lung by *Pseudomonas aeruginosa* and *Burkholderia cenocepacia* reveals influences on biofilm formation and host response. *PLoS One* 7:e52330. doi: 10.1371/journal.pone.0052330
- Chan, C. L., Richter, K., Wormald, P. J., Psaltis, A. J., and Vreugde, S. (2017). *Alloiococcus otitidis* forms multispecies biofilm with *Haemophilus influenzae*: effects on antibiotic susceptibility and growth in adverse conditions. *Front. Cell. Infect. Microbiol.* 7:344. doi: 10.3389/fcimb.2017.00344
- Cheong, Y., Oh, C., Lee, K., and Cho, K. H. (2017). Survey of porcine respiratory disease complex-associated pathogens among commercial pig farms in Korea via oral fluid method. *J. Vet. Sci.* 18, 283–289. doi: 10.4142/jvs.2017.18.3.283
- Chiers, K., De Waele, T., Pasmans, F., Ducatelle, R., and Haesebrouck, F. (2010). Virulence factors of *Actinobacillus pleuropneumoniae* involved in colonization, persistence and induction of lesions in its porcine host. *Vet. Res.* 41:65. doi: 10.1051/vetres/2010037
- Duan, K., Dammel, C., Stein, J., Rabin, H., and Surette, M. G. (2003). Modulation of *Pseudomonas aeruginosa* gene expression by host microflora through interspecies communication. *Mol. Microbiol.* 50, 1477–1491. doi: 10.1046/j.1365-2958.2003.03803.x
- Fablet, C., Marois-Crehan, C., Simon, G., Grasland, B., Jestin, A., Kobisch, M., et al. (2012). Infectious agents associated with respiratory diseases in 125 farrow-to-finish pig herds: a cross-sectional study. *Vet. Microbiol.* 157, 152–163. doi: 10.1016/j.vetmic.2011.12.015
- Harrison, F. (2007). Microbial ecology of the cystic fibrosis lung. *Microbiology* 153(Pt 4), 917–923. doi: 10.1099/mic.0.2006/004077-0
- Hibbing, M. E., Fuqua, C., Parsek, M. R., and Peterson, S. B. (2010). Bacterial competition: surviving and thriving in the microbial jungle. *Nat. Rev. Microbiol.* 8, 15–25. doi: 10.1038/nrmicro2259
- Hoiby, N., Bjarnsholt, T., Givskov, M., Molin, S., and Ciofu, O. (2010). Antibiotic resistance of bacterial biofilms. *Int. J. Antimicrob. Agents* 35, 322–332. doi: 10.1016/j.ijantimicag.2009.12.011
- Kathju, S., Nistico, L., Hall-Stoodley, L., Post, J. C., Ehrlich, G. D., and Stoodley, P. (2009). Chronic surgical site infection due to suture-associated polymicrobial biofilm. *Surg. Infect.* 10, 457–461. doi: 10.1089/sur.2008.062
- Kobayashi, Y., Sunobe, T., Kobayashi, T., Nagahama, Y., and Nakamura, M. (2005). Gonadal structure of the serial-sex changing gobiid fish *Trimma okinawae*. *Dev. Growth Differ.* 47, 7–13. doi: 10.1111/j.1440-169x.2004.00774.x
- Lister, J. L., and Horswill, A. R. (2014). *Staphylococcus aureus* biofilms: recent developments in biofilm dispersal. *Front. Cell. Infect. Microbiol.* 4:178. doi: 10.3389/fcimb.2014.00178
- Macho, A. P., Zumaquero, A., Ortiz-Martin, I., and Beuzon, C. R. (2007). Competitive index in mixed infections: a sensitive and accurate assay for the genetic analysis of *Pseudomonas syringae*-plant interactions. *Mol. Plant Pathol.* 8, 437–450. doi: 10.1111/j.1364-3703.2007.00404.x
- Opriessnig, T., Gimenez-Lirola, L. G., and Halbur, P. G. (2011). Polymicrobial respiratory disease in pigs. *Anim. Health Res. Rev.* 12, 133–148. doi: 10.1017/S1466252311000120
- Pompilio, A., Crocetta, V., De Nicola, S., Verginelli, F., Fiscarelli, E., and Di Bonaventura, G. (2015). Cooperative pathogenicity in cystic fibrosis: *Stenotrophomonas maltophilia* modulates *Pseudomonas aeruginosa*

- virulence in mixed biofilm. *Front. Microbiol.* 6:951. doi: 10.3389/fmicb.2015.00951
- Qiao, S., Feng, L., Bao, D., Guo, J., Wan, B., Xiao, Z., et al. (2011). Porcine reproductive and respiratory syndrome virus and bacterial endotoxin act in synergy to amplify the inflammatory response of infected macrophages. *Vet. Microbiol.* 149, 213–220. doi: 10.1016/j.vetmic.2010.11.006
- Ramirez-Castillo, F. Y., Loera-Muro, A., Vargas-Padilla, N. D., Moreno-Flores, A. C., Avelar-Gonzalez, F. J., Harel, J., et al. (2018). Incorporation of *Actinobacillus pleuropneumoniae* in preformed biofilms by *Escherichia coli* isolated from drinking water of swine farms. *Front. Vet. Sci.* 5:184. doi: 10.3389/fvets.2018.00184
- Sibley, C. D., Duan, K., Fischer, C., Parkins, M. D., Storey, D. G., Rabin, H. R., et al. (2008). Discerning the complexity of community interactions using a *Drosophila* model of polymicrobial infections. *PLoS Pathog.* 4:e1000184. doi: 10.1371/journal.ppat.1000184
- Tawakoli, P. N., Al-Ahmad, A., Hoth-Hannig, W., Hannig, M., and Hannig, C. (2013). Comparison of different live/dead stainings for detection and quantification of adherent microorganisms in the initial oral biofilm. *Clin. Oral Investig.* 17, 841–850. doi: 10.1007/s00784-012-0792-3
- Thacker, E. L., Halbur, P. G., Ross, R. F., Thanawongnuwech, R., and Thacker, B. J. (1999). *Mycoplasma hyopneumoniae* potentiation of porcine reproductive and respiratory syndrome virus-induced pneumonia. *J. Clin. Microbiol.* 37, 620–627. doi: 10.1128/jcm.37.3.620-627.1999
- Thanawongnuwech, R., Brown, G. B., Halbur, P. G., Roth, J. A., Royer, R. L., and Thacker, B. J. (2000). Pathogenesis of porcine reproductive and respiratory syndrome virus-induced increase in susceptibility to *Streptococcus suis* infection. *Vet. Pathol.* 37, 143–152.
- Vuotto, C., and Donelli, G. (2019). Novel treatment strategies for biofilm-based infections. *Drugs* 79, 1635–1655. doi: 10.1007/s40265-019-01184-z
- Wang, L., Li, Y., Wang, L., Zhang, H., Zhu, M., Zhang, P., et al. (2018). Extracellular polymeric substances affect the responses of multi-species biofilms in the presence of sulfamethizole. *Environ. Pollut.* 235, 283–292. doi: 10.1016/j.envpol.2017.12.060
- Yang, L., Liu, Y., Wu, H., Hoiby, N., Molin, S., and Song, Z. J. (2011). Current understanding of multi-species biofilms. *Int. J. Oral Sci.* 3, 74–81. doi: 10.4248/IJOS11027

Conflict of Interest: The authors declare that the research was conducted in the absence of any commercial or financial relationships that could be construed as a potential conflict of interest.

Copyright © 2020 Wang, Gong, Dong, Li, Grenier and Yi. This is an open-access article distributed under the terms of the Creative Commons Attribution License (CC BY). The use, distribution or reproduction in other forums is permitted, provided the original author(s) and the copyright owner(s) are credited and that the original publication in this journal is cited, in accordance with accepted academic practice. No use, distribution or reproduction is permitted which does not comply with these terms.



Effect of Dalbavancin on Staphylococcal Biofilms When Administered Alone or in Combination With Biofilm-Detaching Compounds

Miglė Žiemytė¹, Juan C. Rodríguez-Díaz², María P. Ventero², Alex Mira^{1,3*} and María D. Ferrer^{1,3}

¹ Genomics and Health Department, FISABIO Foundation, Valencia, Spain, ² Servicio de Microbiología, Hospital General Universitario de Alicante, ISABIAL, Alicante, Spain, ³ CIBER Epidemiología y Salud Pública, Madrid, Spain

OPEN ACCESS

Edited by:

Sujogya Kumar Panda,
KU Leuven, Belgium

Reviewed by:

Pilar Teixeira,
University of Minho, Portugal
Fernanda Gomes,
University of Minho, Portugal

*Correspondence:

Alex Mira
mira_ale@gva.es

Specialty section:

This article was submitted to
Antimicrobials, Resistance
and Chemotherapy,
a section of the journal
Frontiers in Microbiology

Received: 20 December 2019

Accepted: 13 March 2020

Published: 17 April 2020

Citation:

Žiemytė M, Rodríguez-Díaz JC, Ventero MP, Mira A and Ferrer MD (2020) Effect of Dalbavancin on Staphylococcal Biofilms When Administered Alone or in Combination With Biofilm-Detaching Compounds. *Front. Microbiol.* 11:553. doi: 10.3389/fmicb.2020.00553

Microorganisms grown in biofilms are more resistant to antimicrobial treatment and immune system attacks compared to their planktonic forms. In fact, infections caused by biofilm-forming *Staphylococcus aureus* and *Staphylococcus epidermidis* are a large threat for public health, including patients with medical devices. The aim of the current manuscript was to test the effect of dalbavancin, a recently developed lipoglycopeptide antibiotic, alone or in combination with compounds contributing to bacterial cell disaggregation, on staphylococcal biofilm formation and elimination. We used real-time impedance measurements in microtiter plates to study biofilm growth dynamics of *S. aureus* and *S. epidermidis* strains, in the absence or presence of dalbavancin, linezolid, vancomycin, cloxacillin, and rifampicin. Further experiments were undertaken to check whether biofilm-detaching compounds such as *N*-acetylcysteine (NAC) and ficin could enhance dalbavancin efficiency. Real-time dose-response experiments showed that dalbavancin is a highly effective antimicrobial, preventing staphylococcal biofilm formation at low concentrations. Minimum biofilm inhibitory concentrations were up to 22 higher compared to standard *E*-test values. Dalbavancin was the only antimicrobial that could halt new biofilm formation on established biofilms compared to the other four antibiotics. The addition of NAC decreased dalbavancin efficacy while the combination of dalbavancin with ficin was more efficient than antibiotic alone in preventing growth once the biofilm was established. Results were confirmed by classical biofilm quantification methods such as crystal violet (CV) staining and viable colony counting. Thus, our data support the use of dalbavancin as a promising antimicrobial to treat biofilm-related infections. Our data also highlight that synergistic and antagonistic effects between antibiotics and biofilm-detaching compounds should be carefully tested in order to achieve an efficient treatment that could prevent both biofilm formation and disruption.

Keywords: dalbavancin, *E*-test, biofilm, *Staphylococcus*, ficin, *N*-acetylcysteine, xCELLigence

INTRODUCTION

Increased drug resistance of bacteria is significantly reducing the therapeutic efficacy of antibiotics (Stewart and Costerton, 2001). Commonly, this resistance is augmented in bacterial biofilms, which can be described as bacterial communities adhering to abiotic or biotic surfaces and encased in a self-produced extracellular matrix (Chung and Toh, 2014; Hall and Mah, 2017). This matrix is composed of polysaccharides, proteins, and extracellular DNAs and plays an important role in persistent chronic infections, resulting in serious health complications. In fact, bacterial cells embedded in a matrix are up to 1,000 times more resistant to antibacterial compounds compared to their planktonic form, leading to increased morbidity and mortality rates of various diseases, like those associated with implantable medical devices (Flemming and Wingender, 2010; Rodrigues, 2011).

A major cause of medical device-associated and chronic infections, resulting in both economical and clinical burden, is the biofilm formation capacity of *Staphylococcus aureus* and *Staphylococcus epidermidis* bacteria (Otto, 2013; Moormeier and Bayles, 2017). This capacity, in addition to the widespread dissemination of methicillin-resistant *S. aureus* (MRSA) and *S. epidermidis* (MRSE), emphasizes the necessity to investigate new antimicrobial compounds and combine different treatment strategies for increasing the therapeutic potential of conventional antibiotics (Bjarnsholt et al., 2013). For instance, several agents for cell detachment and breaking down of biofilm matrix have already been reported. Some of them cleave the essential components of the biofilm matrix, like polysaccharides, proteins, or extracellular DNAs, destroying its architecture (Kaplan, 2010; Fleming and Rumbaugh, 2017). Ficin, a non-specific fig tree plant protease, belongs to this group of anti-biofilm compounds and is able to disperse staphylococcal biofilms via enzymatic lysis (Baidamshina et al., 2017). Others employ microbial signals that disperse bacterial cells embedded inside the biofilm exopolymeric matrix, like nitric oxide in *Pseudomonas* biofilms or certain quorum sensing inhibitors (Brackman and Coenye, 2015; Zhu et al., 2019). Other anti-biofilm agents, like *N*-acetyl-L-cysteine (NAC), besides the ability to impair matrix architecture, have also antimicrobial properties against different pathogenic bacteria, making this molecule an interesting tool to confront biofilms (Dinicola et al., 2014; Blasi et al., 2016; Costa et al., 2017). In addition, a combination of biofilm-detaching compounds together with antibiotics could represent an alternative strategy for the effective treatment of biofilm-associated infections.

Dalbavancin is a new lipoglycopeptide class antibiotic used against many gram-positive pathogens including staphylococcal strains in clinical practice (Chen et al., 2007). It is also a long-action antibiotic that interferes with bacterial cell wall synthesis and does not require frequent administration, allowing weekly dosing and earlier patient discharge from the hospital (Seltzer et al., 2003). Although dalbavancin has been proposed as a promising agent in biofilm-mediated infections, susceptibility to this antibiotic has mainly been tested using traditional microbiological tests such as microdilution or agar-based tests. However, it is well established that bacteria behave differently in a

planktonic state or when forming biofilms, and there is currently limited information on its efficacy on biofilm-embedded bacteria, with only a few studies available (Meeker et al., 2016; Knafl et al., 2017; Di Pilato et al., 2020), some of them in animal models (Darouiche and Mansouri, 2005; Baldoni et al., 2013). In some cases, the efficacy of dalbavancin or vancomycin has been shown to be low, with less than an order-of-magnitude decrease in viable counts of staphylococci (Kusmann et al., 2018). Thus, recent work has proposed the combination of antibiotics and biofilm-detaching compounds to treat biofilm-mediated infections (Chen et al., 2013; Roy et al., 2018), but this strategy has currently not been tested with dalbavancin. In addition, there is conflicting evidence about the comparative efficacy of dalbavancin and other antibiotics of common clinical use in staphylococcal infections, such as vancomycin (Darouiche and Mansouri, 2005; Kusmann et al., 2018).

Recently, we evaluated biofilm inhibition and induction in *S. aureus* and *S. epidermidis* strains using 10 conventional antibiotics and suggested that impedance-based real-time cell analysis (RTCA) could facilitate determination of antibiotic sensitivity when bacteria grow in biofilms, resulting in faster and more accurate assays and therefore more efficient antimicrobial therapy (Ferrer et al., 2017b). The aim of the current study was to describe the effectiveness of dalbavancin to prevent *in vitro* biofilm formation of staphylococcal strains (both sensitive and methicillin-resistant isolates) and compare its effect with other antibiotics that are frequently used in clinical practice against indwelling device-related infections. Our biofilm growth measurements were performed by impedance-based cell analysis and confirmed by more classical tests such as crystal violet (CV) staining and counting of colony-forming units (CFUs). In addition, the effect of two biofilm-disaggregating molecules, NAC and ficin, was tested in combination with the antibiotic, to evaluate the potential synergy of a combined therapy to treat staphylococcal biofilm infections.

MATERIALS AND METHODS

Bacterial Strains and Growth Conditions

Supplementary Table S1 lists bacterial strains used for this study. Staphylococcal strains were grown on tryptic soy agar (TSA) plates and tryptic soy broth (TSB) at 37°C at 120 r.c.f. *S. epidermidis* strain 43040 was isolated at the Microbiology Department of the University of Elche (Spain), MRSA strains were isolated at the Microbiology Department of the Alicante General Hospital (Spain) from a catheter tip in patients diagnosed with indwelling device-related bacteremia. *S. aureus* CETC 240 (*S. aureus* ssp. *aureus* Rosenbach 1884) is a biofilm-positive strain isolated by FDA, which is methicillin susceptible, and a reference strain recommended to test antibiotic resistance.

RTCA-Based Biofilm Analysis

Real-time biofilm analysis was performed using xCELLigence RTCA SP equipment (ACEA Biosciences) according to the manufacturer's instructions. For biofilm formation assays, bacterial strains were grown overnight in TSB and diluted with

filter-sterilized TSB supplemented with 0.25% of D-glucose (TSB-glu). The experiments were performed as previously described by Ferrer et al. (2017b). Impedance data were registered at 10-min time intervals for 20 h, and they were transformed into cell index (CI) values, which accurately correlate with biofilm mass (Ferrer et al., 2017a,b).

To evaluate antimicrobial efficiency on bacterial biofilms, five antibiotics with different mechanisms of action were tested: linezolid (Accordpharma), vancomycin (Pfizer), cloxacillin (Normon), rifampicin (Mavi), and dalbavancin (Angelini). One hundred microliters of each antibiotic diluted in TSB-glu (twofold dilutions to final concentrations from 32 to 0.0625 mg/L) was used as background for impedance measurements. Further, 100 μ l of bacterial cell suspension ($OD_{600} = 0.175$) was added, reaching a final optical density of 0.0875. This optical density corresponds to 10^7 – 10^8 cells, depending on the strain. The lowest antibiotic concentration required to inhibit bacterial growth with a CI value ≤ 0.05 was considered as the minimum biofilm inhibitory concentration (MBIC) (Bjarnsholt et al., 2013; Ferrer et al., 2017b).

To test the antibiotic effect on already-formed bacterial biofilms, the experiments were performed as previously described (Ferrer et al., 2017a). Briefly, 100 μ l of cell suspension ($OD_{600} = 0.153$) was used as background. Then, 75 μ l of TSB-glu was added to each well, reaching a final $OD_{600} = 0.0875$, and biofilms were grown for 6 h (*S. aureus* 240), 7 h (*S. aureus* MRSA4), or 9 h (*S. epidermidis* 43040), corresponding to the exponential phase of biofilm growth of each strain at which time the antibiotics were added (25 μ l of each dilution, reaching final concentrations from 32 to 0.0625 mg/L for each tested antibiotic). After the addition of antibiotics, CI was monitored for a further 20 h. Two replicates of each antibiotic concentration sample and two negative controls were included in each experiment.

Antibiofilm Compounds Assays

For RTCA experiments, ficin (Sigma) at concentrations of 10, 100, and 1,000 mg/L and NAC (Sandoz) at final concentrations of 0.5, 1, 2, 4, and 8 g/L were used alone and in combination with dalbavancin (0.5, 4, and 32 mg/L). In short, ficin and NAC were diluted in TSB-glu to the corresponding concentrations, and 100 μ l of each dilution was used as background when anti-biofilm substances were added at the beginning of the experiment. After the background was measured, 100 μ l of cell suspensions ($OD_{600} = 0.175$) was added into the corresponding wells, and biofilm formation was monitored for 20 h.

When NAC and ficin were added at the exponential biofilm growth phase, 100 μ l of corresponding cell suspensions was used as background as described above. After that, 75 μ l of the TSB-glu was added, reaching a final OD_{600} of 0.0875. When bacterial biofilm growth reached an exponential growth phase, 25 μ l of the different concentrations tested for NAC or ficin and their combinations with dalbavancin was added into the corresponding wells. After the addition of biofilm-detaching compounds, biofilm growth was registered for 20 h more. Two replicates of each condition and their respective controls were tested in each experiment.

The effect of NAC and ficin on planktonic bacterial growth was also measured, by means of an absorbance plate reader Infinite M200 (Tecan, Durham, NC, United States). Briefly, overnight bacterial cultures were diluted to $OD_{600} = 0.175$, and 100 μ l of each cell suspension was added into the corresponding wells of 96-well plates. Then, 100 μ l of biofilm-detaching substances was added to the final concentrations of 10, 100, and 1,000 mg/L for ficin and 0.5, 1, 2, 4, 8, 16, and 32 g/L for NAC. Ninety-six-well plates were incubated at 37°C with orbital shaking at 120 rpm, and bacterial planktonic growth dynamics were monitored for 20 h. Two replicates of each concentration were included as well as their respective controls.

MIC Determination

To determine minimum inhibitory concentrations (MICs) of the tested antibiotics on *S. aureus* and *S. epidermidis* strains on solid media, the E-test (bioMérieux) method was used according to the manufacturer's instructions, following Baldoni et al. (2013). Broth microdilution assays were performed in accordance with the European Committee on Antimicrobial Susceptibility Testing (EUCAST, 2018). MBIC (or BIC) was calculated following Bjarnsholt et al. (2013) and Ferrer et al. (2017b).

Biofilm Quantification

In order to determine dalbavancin and ficin effect alone and in combination on preformed MRSA4 biofilms, 175 μ l of bacterial suspension ($OD_{600} = 0.0875$) was inoculated in TSB-glu and grown in 96-well flat-bottom Ibidi ibiTreat μ -plates 89626 (Ibidi, Germany). These plates are coated with a thin polymer layer in order to assure better biofilm attachment. After 7 h of growth, 25 μ l of dalbavancin, ficin, or the combination of these two compounds was added, reaching final concentrations of 32 mg/L and 1 g/L, and the biofilms were grown for an additional 24 h. After that, the supernatant was discarded, bacterial cells were washed using phosphate buffer saline (PBS, pH = 7.4) to remove unadhered cells, and bacterial biofilms were stained using 0.1% CV as previously described (Stepanovic et al., 2000). Biofilm mass was quantified by an absorbance plate reader, Infinite M200 (Tecan, Durham, NC, United States), at 610 nm.

Viable Count Assay

To assess the number of viable unadhered, planktonic bacteria and biofilm-embedded bacteria, 175 μ l of MRSA4 suspension ($OD_{600} = 0.0875$) was grown for 7 h in triplicate in the xCELLigence system. After that, 25 μ l of ficin and dalbavancin at the corresponding concentrations was added as described above, and the biofilms were cultivated for an additional 24 h. The supernatant was then collected, and serial dilutions were prepared, using 100 μ l of each dilution for plating onto TSA plates in triplicate.

To evaluate viable cell number in bacterial biofilms, biofilms were carefully rinsed using PBS buffer to eliminate non-adhered cells, resuspended with 200 μ l of PBS and sonicated for 5 min in order to disrupt biofilm matrix, and the serial dilutions of each sample were plated on TSA plates in triplicate as described above and incubated at 37°C overnight. After that, CFUs were counted, averaged, and expressed as \log_{10} .

Statistical Analysis

To study differences in the biofilm CI values, regression analysis was performed by a linear model, using the function `lm` (library `stats`) in the R statistical package (Calcagno, 2013) between 10 and 20 h of biofilm formation time. For biofilm inhibition/induction analyses of CFUs and CV staining, experiments were performed in triplicate with three independent repeats in each experiment. Statistical significance was assessed using Student's *t*-test, where $*p \leq 0.0$ and $***p \leq 0.001$.

RESULTS

Dalbavancin Effect on Staphylococcal Biofilm Formation

Firstly, we evaluated dalbavancin's effect on staphylococcal biofilm formation by real-time impedance analysis when the antibiotic was added together with the bacterial inoculum. Most of the tested *S. aureus* and *S. epidermidis* strains had similar biofilm growth dynamics with comparable CI (correspondent to

biofilm mass) values. MRSA4 was the strain with the highest biofilm formation capacity (up to 26% higher CI than that of MRSA2 at 20 h), while the lowest CI values were observed for MRSA1 (Figure 1 and Supplementary Figure S1). The real-time dose-response experiments showed that dalbavancin is a highly effective antimicrobial and could prevent bacterial biofilm formation at low concentrations. The MBICs for the tested *S. aureus* strains were between 0.5–1 and 2 mg/L for *S. epidermidis* strain 43040 (Figure 1 and Supplementary Figure S2). Table 1 shows the values of MBIC and MIC (as measured by *E*-tests) of dalbavancin for *S. epidermidis* and *S. aureus* strains, indicating that the MBIC is up to 22 times higher compared to the growth of the same strains on agar plates.

Dalbavancin Effect on Biofilm Formation Compared to Other Antibiotics

To further evaluate the dalbavancin effect on biofilm formation in *S. aureus* and *S. epidermidis* strains, we compared the effect of dalbavancin on biofilm formation to four antibiotics with different mechanisms of action, all of them commonly used in clinical practice: vancomycin, linezolid, cloxacillin, and rifampicin. For these experiments, we selected the MRSA4 isolate, which showed the highest CI values compared to the other MRSA strains (Supplementary Figure S2), together with methicillin-susceptible *S. aureus* strain 240 and the clinical isolate of *S. epidermidis* 43040. Figures 2A–C show the percentage of biofilm formation inhibition/induction relative to the antibiotic-free control for each strain (corresponding to 100% in the graphs). Although the antibiotic effect appeared to be strain specific, dalbavancin and rifampicin prevented biofilm formation in a dose-dependent manner, showing higher biofilm inhibition rates than vancomycin, linezolid, and cloxacillin. Cloxacillin was only effective against *S. aureus* strain 240 and could partially inhibit biofilm formation at some of the tested concentrations in *S. epidermidis* 43040. However, none of the tested concentrations of this antibiotic could eliminate preformed biofilm completely in this strain or in MRSA4. In fact, the exposure of MRSA4 to low concentrations of cloxacillin (0.06–0.125 mg/L) was not only ineffective but in fact also promoted biofilm formation up to 20% compared to the untreated control (Figure 2B). Additionally, neither linezolid nor vancomycin appeared to be effective against *S. aureus* and *S. epidermidis* biofilm development at low concentrations, and both tested antibiotics induced biofilm growth at concentrations <4 mg/L in strain MRSA4. It is important to underline that the MBIC for all tested antibiotics is considerably higher than that estimated by the traditional *E*-test method (Supplementary Table S2).

Dalbavancin Effect on Established Biofilms

It is known that some antibiotics have a limited efficacy to penetrate in established bacterial biofilms (Jefferson et al., 2005). For this reason, we further tested the effect of dalbavancin on already-formed staphylococcal biofilms. In our experimental setting, we considered established biofilms those which were on exponential biofilm growth phase (Ferrer et al., 2017a), that

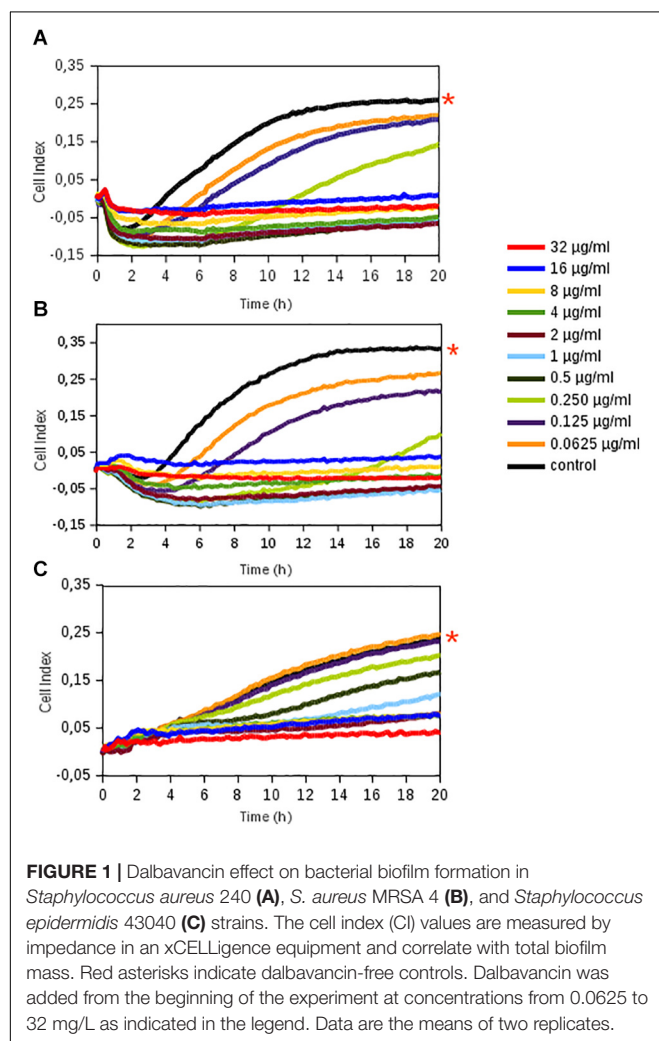


TABLE 1 | Comparison between dalbavancin MBICs at 20 h of growth, as determined by impedance measurements, and MICs measured by standard E-test.

Strain	MBIC (mg/L)	MIC (mg/L)
<i>Staphylococcus epidermidis</i> 43040	2	0.094
<i>Staphylococcus aureus</i> 240	0.5	0.064
MRSA1	1	0.125
MRSA2	0.5	0.094
MRSA3	0.5	0.023
MRSA4	0.5	0.125
MRSA5	0.5	0.125

is, between 6 and 9 h depending on the strain, as previous work has shown that an exopolymeric matrix is fully formed by that time (Ferrer et al., 2017b; Gutiérrez et al., 2017). **Figure 3** shows biofilm growth dynamics when different dalbavancin concentrations were added at the exponential biofilm growth phase. The data indicate that biofilm elimination was never achieved, but high concentrations of this antibiotic (8–32 mg/L) were able to reduce or fully prevent new biofilm formation

and its further development in all the tested strains. Moreover, dalbavancin at 32 mg/L concentration was able to decrease the CI values over 40% compared to antibiotic-free controls after 20 h of inoculation (**Figures 2D–F**). The potential effect of dalbavancin was evident in the methicillin-resistant isolate MRSA4, where all tested concentrations resulted in biofilm growth reduction and partial elimination. Additionally, a strain-dependent effect was observed at low concentrations: whereas a concentration of 0.50 mg/L prevented new biofilm growth in *S. epidermidis* 43040, concentrations lower than 4 mg/L in *S. aureus* 240 turned out to be ineffective (**Figures 2D–F, 3**).

Dalbavancin Effect on Established Biofilms Compared to Other Antibiotics

To evaluate the potential effect of dalbavancin in a comparative way, we performed dose-response experiments using conventional antibiotics on already-formed biofilms (**Figures 2D–F**). In contrast to dalbavancin, exposure of established MRSA4 biofilms to vancomycin, linezolid, cloxacillin, and rifampicin had no inhibitory effect at the maximum tested concentration of 32 mg/L. In addition, lower doses of these

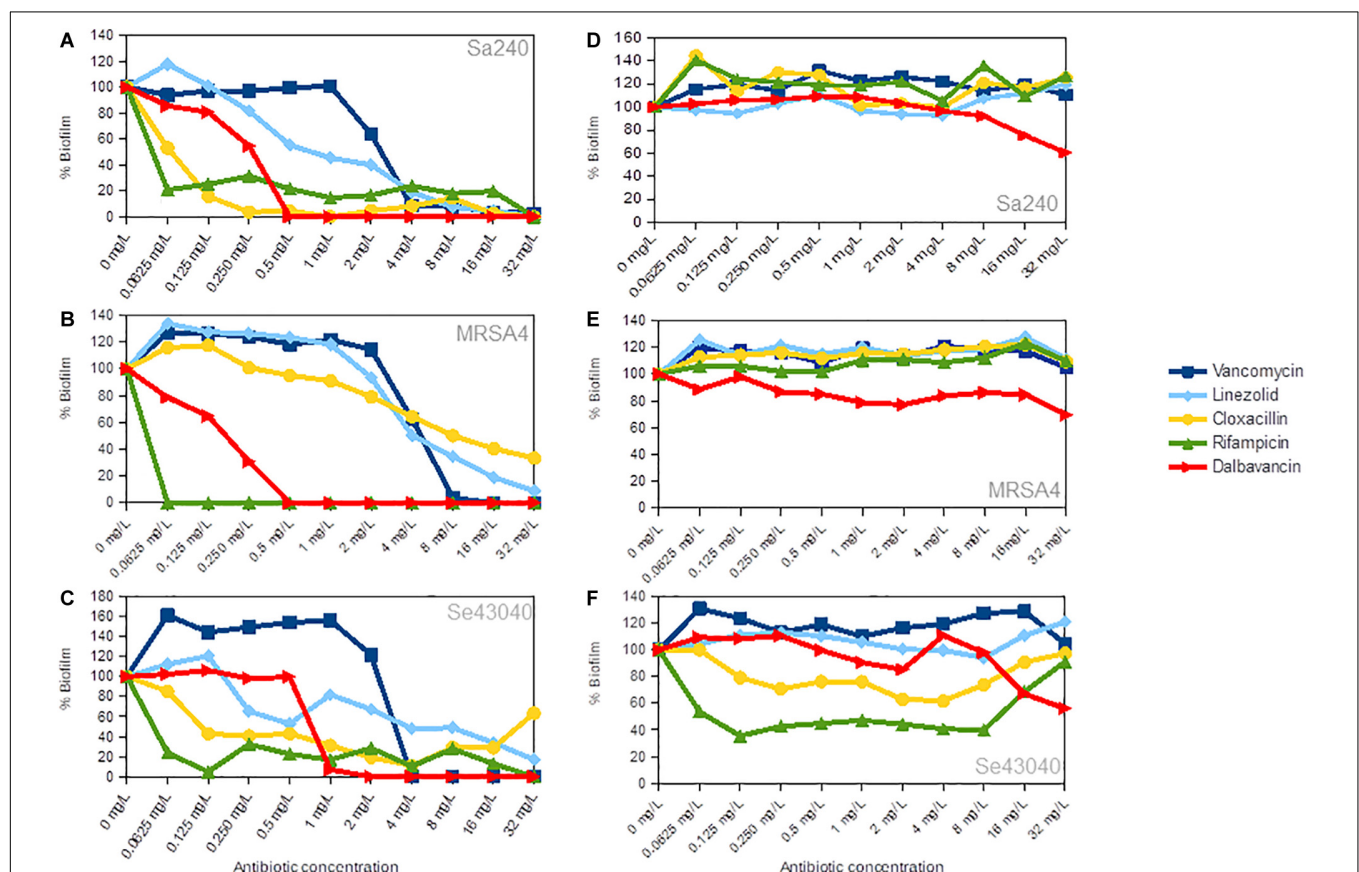
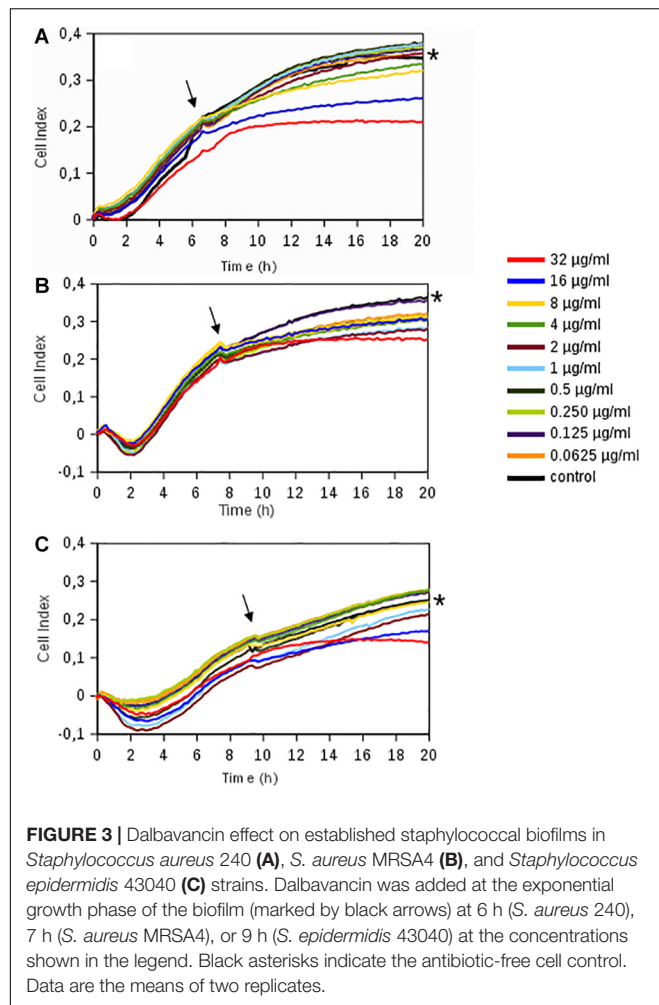


FIGURE 2 | Concentration-dependent effect of linezolid, vancomycin, cloxacillin, rifampicin, and dalbavancin on biofilms in *Staphylococcus aureus* 240, *S. aureus* MRSA4, and *Staphylococcus epidermidis* 43040 strains. **(A–C)** The antibiotics were added at the beginning of the experiment together with the bacterial inoculum. **(D–F)** The antibiotics were added when biofilms were already formed, at their exponential growth phase. All charts indicate biofilm formation at 20 h of growth expressed as the percentage of cell index (CI) compared with the control without antibiotic. Values below 100% indicate biofilm inhibition, whereas values over 100% indicate biofilm induction, in comparison with the biofilm mass achieved in the absence of each antibiotic.



antibiotics (<32 mg/L) increased biofilm formation in this strain. The data indicate that dalbavancin was the only effective antimicrobial showing a strong biofilm inhibition capacity for this strain. Dalbavancin also halted new biofilm formation at 8–32 mg/L in *S. aureus* 240, while the other tested antibiotics resulted in increased biofilm growth at these concentrations. In the case of *S. epidermidis* strain 43040, both rifampicin and cloxacillin were able to decrease biofilm growth at the concentrations ≤ 8 mg/L (Figure 2F). Surprisingly, higher concentrations of these antibiotics (8–32 mg/L) had a limited effect in *S. epidermidis* 43040. The least effective antibiotic on preformed biofilm growth inhibition was vancomycin. This antibiotic induced biofilm formation of all tested strains (>30% relative to the antibiotic-free controls) at 20 h of biofilm growth.

Combined Effect of Dalbavancin and Biofilm-Detaching Compounds

For this analysis, we selected an emerging therapeutic agent with mucolytic properties, NAC (Kundukad et al., 2017), and a natural plant protease, ficin, which has recently been described as an enzyme with unique properties to destroy the biofilm matrix (Baidamshina et al., 2017). **Supplementary Figure S3**

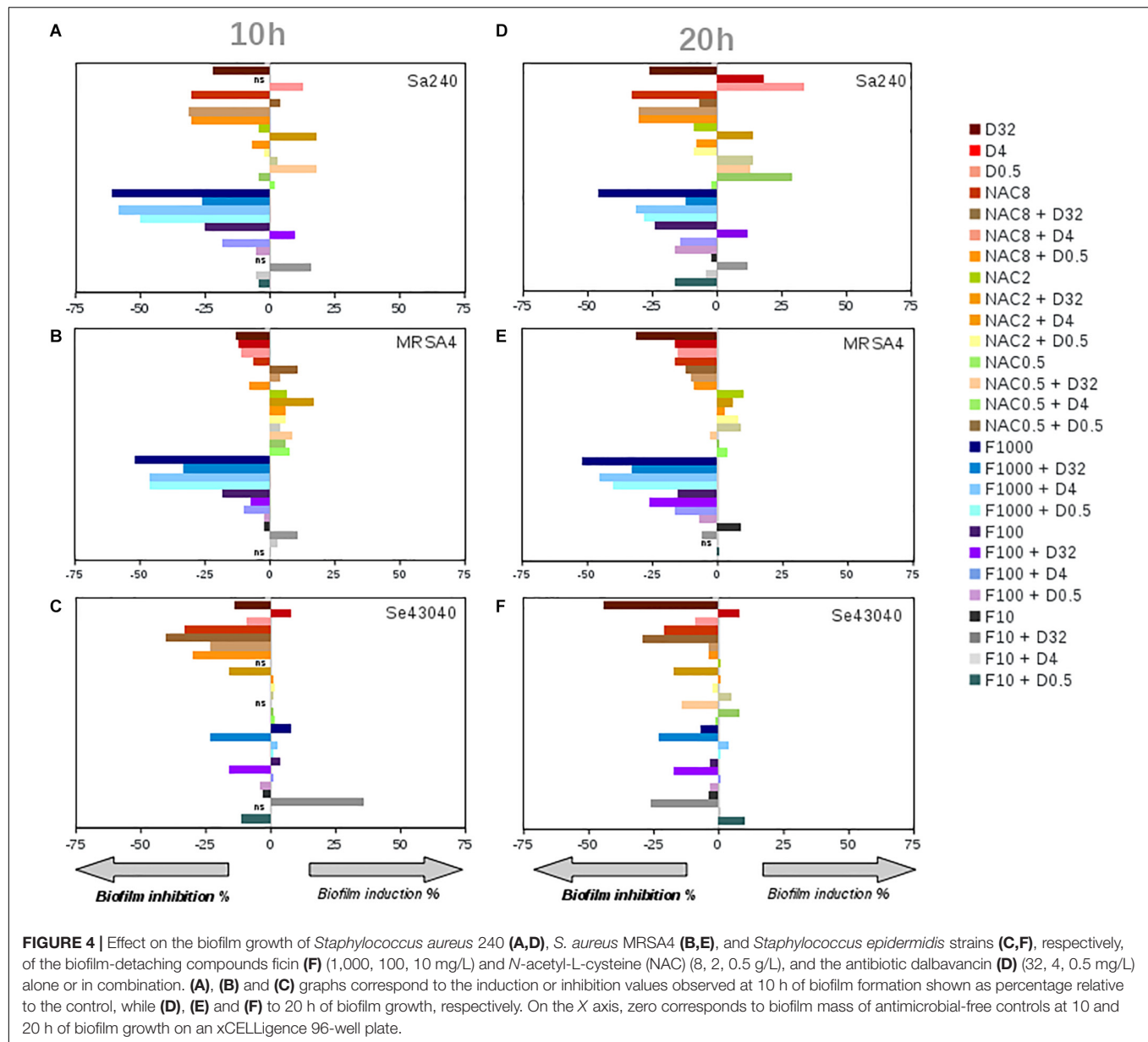
summarizes the effect of both anti-biofilm compounds on the biofilm formation of *S. aureus* 240, MRSA4, and *S. epidermidis* 43040 strains, when added at the moment of inoculation. Graphs show that all tested NAC concentrations induced biofilm formation in *S. epidermidis* 43040, while 8 g/L was able to slightly diminish biofilm formation in both Sa240 and MRSA4 strains. On the other hand, ficin (1,000, 100, or 10 mg/L) showed a notable effect on *S. aureus* biofilms, inhibiting their formation by 47% in Sa240 and 25% in MRSA4 strains, after 20 h of biofilm growth. On the contrary, this compound resulted in induction of *S. epidermidis* 43040 biofilm formation. Thus, the effect of this detaching compounds is species dependent.

Given that already-established biofilms are very difficult to eradicate, we next tested whether NAC or ficin alone or in combination with dalbavancin could have any effect on preformed staphylococcal biofilms. **Figure 4** sums up the effect of dalbavancin and biofilm-detaching compounds separately and in combination when they were added at the exponential biofilm growth phase. **Figures 4A–C** represent CI values taken at 10 h of biofilm development, while **Figures 4D–F** represent those taken at 20 h. Dalbavancin alone at the concentration of 32 mg/L (represented as D32) greatly diminished new biofilm formation for all the tested strains. NAC, when administered alone on already-formed biofilms, also had an inhibitory effect on all three tested strains (Figure 4). However, when dalbavancin and NAC were combined, the inhibitory effect was dramatically hampered, and in *S. aureus*, it even led to biofilm induction. This suggests that the combination of NAC and dalbavancin is antagonistic.

Ficin, when administered alone, had a significant effect in both *S. aureus* strains, preventing new biofilm formation up to 52% compared to an untreated control at both 10 and 20 h of biofilm growth (Figures 4A–E). However, ficin had no inhibitory effect on *S. epidermidis* 43040 biofilms. Interestingly, the combination of ficin with 32 mg/L of dalbavancin on this strain produces less inhibition than the antibiotic alone (Figure 4F), suggesting a potential counterproductive effect of both compounds. On the contrary, the combination of 32 mg/L dalbavancin and 1,000 mg/L ficin in *S. aureus* MRSA4 led to a significant improvement of biofilm inhibition relative to the antibiotic alone ($p < 0.05$) (Figure 5A), suggesting a potentiating effect. Although ficin alone produced higher biofilm reduction (Figure 5A), the detached cells were viable as they are not affected by this molecule (Figure 5B). This is confirmed by an increase in planktonic cells after ficin administration (Figure 6C). Thus, when using ficin, an effective antibiotic is needed in order to inactivate bacterial cells which are detached as a result of the enzyme's activity and to prevent further colonization.

Effect of Biofilm-Detaching Compounds on Planktonic Bacterial Growth

To investigate if NAC and ficin only hold biofilm-detaching properties or also have a direct antimicrobial effect on bacterial cell growth, we further assessed the effect of both compounds on planktonic bacterial growth. After the exposure of *S. aureus* 240, MRSA4, and *S. epidermidis* 4340 to different NAC concentrations (0.5–32 g/L), it was observed that 8 g/L reduced bacterial growth

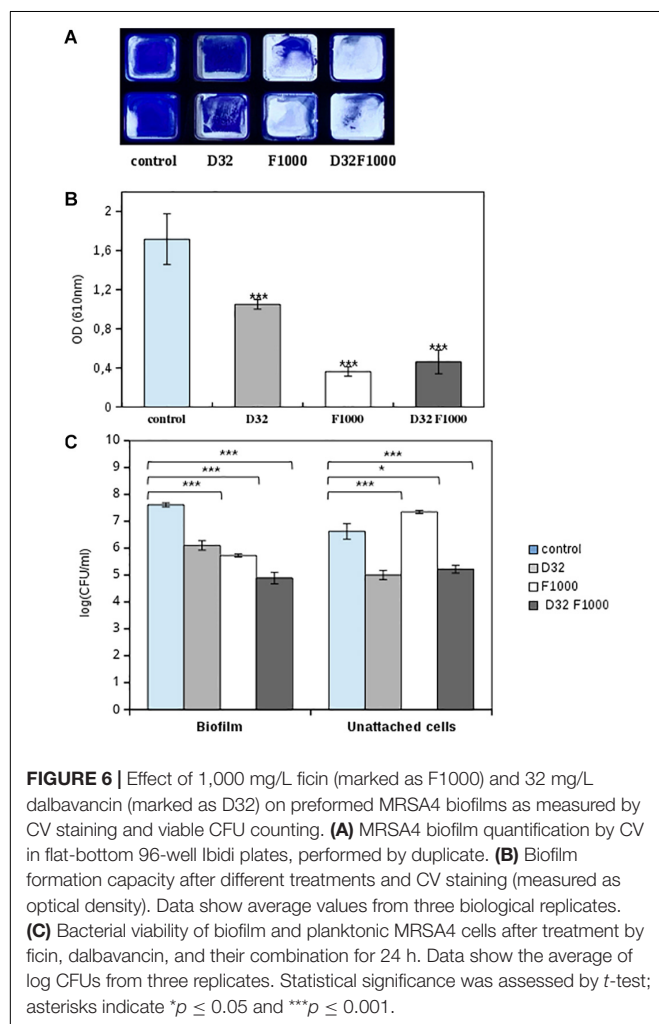
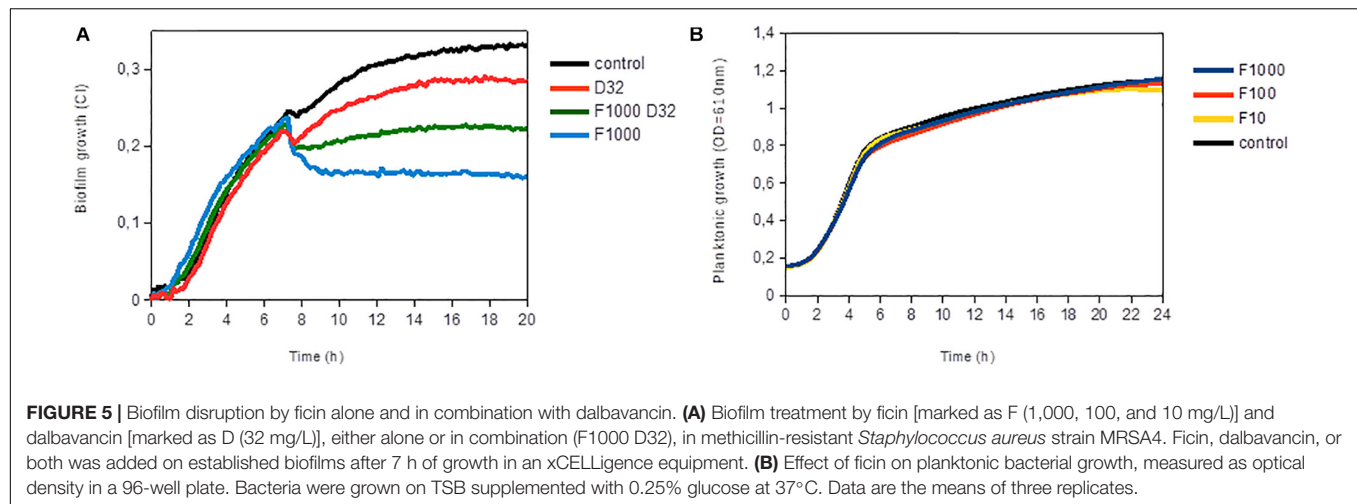


over 50%, indicating that this compound alone has a strong antimicrobial effect. Bacterial growth was fully eliminated when the NAC concentration reached 32 g/L (MIC for all tested strains) (data not shown). On the contrary, none of the tested ficin concentrations (1,000, 100, and 10 mg/L) affected planktonic bacterial growth, indicating that ficin has a proteolytic effect only on the biofilm exopolymetric matrix, resulting in an efficient biofilm-embedded cell dispersal (Figure 5B).

Comparison of Impedance Measurements With Classical Biofilm Quantification Methods

To verify that observed changes in CI are comparable to standard methodologies, we performed CV staining and CFUs of

MRSA4 biofilms untreated or treated with ficin and dalbavancin alone and their combination. Figures 6A,B represent optical density measurements at 24 h of biofilm growth when ficin and dalbavancin were added. The addition of dalbavancin alone significantly decreased the number of adhered bacterial cells on 96-well plates. Reduced staining in the wells was also observed in cases where ficin was added alone and in combination with dalbavancin, confirming our previous observations of the ability of ficin to detach bacterial cells from biofilms. We also performed viable cell counting in both biofilm and unadhered bacterial cells in supernatants (Figure 6C). CFU counts showed that the viability of biofilm-embedded cells and planktonic cells was significantly affected by dalbavancin alone. When ficin was added alone, cell viability was not affected and a lower number of bacterial cells were observed in biofilms, together with a higher



number of planktonic cells compared to the untreated control. These observations confirm the lack of antimicrobial properties of ficin and its biofilm-disaggregating activity. On the other hand,

when ficin was added together with dalbavancin, the viability of both biofilm and unadhered cells decreased almost three orders of magnitude in biofilm cells and two orders of magnitude in unattached cells, showing a potentiating effect and suggesting that ficin increases the susceptibility of biofilms to this antibiotic.

DISCUSSION

Biofilm-forming capacity of staphylococcal strains contributes enormously to the pathogenesis of implant-associated infections, protecting these opportunistic pathogens from both immune system attack and antibiotic treatment (Gries and Kielian, 2017). Dalbavancin has already been described as an antibiotic with a potent *in vitro* bactericidal activity against many gram-positive pathogens, including MRSA and MRSE, in a planktonic mode of growth (Chen et al., 2007). However, the effect of dalbavancin on bacterial biofilms remains unclear as it has only been tested in a few occasions by using standard methods such as CV staining or MIC determinations (Fernández et al., 2016; Knafl et al., 2017). The impedance-based method performed in the current manuscript allows studying of the dynamics of biofilm formation and therefore the extent of biofilm reduction at different time points, obviating the need to select for a specific endpoint (Ferrer et al., 2017b). In this study, we evaluate the dalbavancin effect on the pattern and dynamics of *in vitro* biofilm growth in one *S. epidermidis* and six *S. aureus* strains and compare its efficacy to four different conventional antibiotics used in clinical practice (vancomycin, cloxacillin, linezolid, and rifampicin). Our experiments prove that dalbavancin and rifampicin were the best therapeutic agents against *S. aureus* and *S. epidermidis* biofilm formation in a dose-dependent manner when added at the beginning of biofilm growth. Interestingly, the superior efficacy of these two antibiotics is not related to their mechanisms of action, as rifampicin inhibits RNA polymerase (Campbell et al., 2001) and dalbavancin interferes with bacterial cell wall synthesis (Chen et al., 2007). Although rifampicin has been used in clinical practice against staphylococcal biofilm-related infections for almost three decades (Zimmerli and Sendi, 2019),

this antibiotic should be administered carefully because of the danger of rapid emergence of rifampicin-resistant bacteria (Raad et al., 2007; Zhou et al., 2012). Thus, dalbavancin emerges as a promising solution in the fight against device-related infections, confirming the promising results obtained in animal models (Darouiche and Mansouri, 2005; Baldoni et al., 2013).

The impedance measurements performed in the current work show that, once the biofilm is formed, dalbavancin was the only tested antibiotic which could arrest new biofilm formation and prevent its further development in methicillin-resistant isolate MRSA4 and was effective in Sa240 and Se43040 at the concentrations of 8–32 mg/L. The other tested antimicrobials not only lacked an inhibitory effect on already-formed biofilms, but they also caused an induction of biofilm formation (Figures 2D–F). Given that some of these antibiotics have been shown to be able to penetrate through thick biofilms, their lack of inhibition could be due to a low metabolic activity of biofilm-embedded cells, which is known to decrease their susceptibility to antibiotics (Jefferson et al., 2005; Jacqueline and Caillon, 2014; Lopatkin et al., 2019). Thus, our data suggest that dalbavancin may act on established biofilms more efficiently than linezolid and vancomycin, which are among the most common antibiotics clinically administered for biofilm infections caused by *S. aureus* and *S. epidermidis* (Choo and Chambers, 2016). This may be facilitated by its mechanism of action, because this antibiotic not only inhibits bacterial cell wall synthesis but has also an ability to bind to bacterial membranes (Chen et al., 2013).

Given that even dalbavancin showed a limited efficacy to eradicate already-established biofilms, an effort was made to investigate its combined effect together with ficin and NAC, which have been reported to have biofilm-detaching properties. Unexpectedly, *in vitro* interactions between dalbavancin and biofilm-detaching compounds in preformed biofilms showed a dose and species-dependent effect (Figure 4). For example, the combination of NAC at concentrations of 8, 2, and 0.5 g/L with 32 mg/L of dalbavancin showed a decreased efficiency in inhibiting *S. epidermidis* 43040 biofilms compared to dalbavancin alone. This indicates that the combination of biofilm-detaching and antimicrobial compounds should be carefully tested in order to predict its combined effect.

We also observed that NAC had a direct antimicrobial effect on planktonic cells, while ficin did not inhibit bacterial growth at any of the tested concentrations (Figure 5B). This suggests that ficin is able to detach *S. aureus* biofilms by targeting only the biofilm matrix structure, in contrast to NAC. This should be considered when designing combined treatment strategies. For instance, our data demonstrate that ficin in combination with dalbavancin at final concentrations of 1,000 and 32 mg/L, respectively, showed an enhanced efficiency in the eradication of established MRSA4 biofilms compared to dalbavancin alone (Figure 5A). Although ficin alone provided an even greater biofilm reduction, its lack of antimicrobial activity implies that detached biofilm cells without the presence of an appropriate antibiotic could reach the bloodstream and result in serious medical complications. Therefore, we propose the combination

of both a biofilm-detaching compound and an efficient antibiotic for maximal efficiency.

Altogether, the observations from the current manuscript show that dalbavancin has a strong activity against staphylococcal biofilms *in vitro*, making this antibiotic a promising agent to combat biofilm-mediated infections. Although its effect on already-formed biofilms is limited, ficin appears to intensify its efficacy, and the combination of dalbavancin with this or other disaggregating compounds should be further studied in the future. The differences obtained between agar-grown and biofilm-grown cultures underline that the use of appropriate biofilm susceptibility tests, such as those provided by impedance measurements, may offer a more accurate alternative for the selection of fast and individualized antibiotic treatment. Whether the use of impedance-based biofilm susceptibility tests allow earlier discharge from the hospital and lower rates of treatment failure should be clinically evaluated in the future.

DATA AVAILABILITY STATEMENT

The raw data supporting the conclusions of this article will be made available by the authors, without undue reservation, to any qualified researcher.

AUTHOR CONTRIBUTIONS

AM, JR-D, and MF conceived and designed the study. MŽ performed the experiments and analyzed the data. AM provided reagents. MV performed *E*-tests. MV and JR-D provided bacterial strains. MŽ, AM, and MF drafted the manuscript. All authors revised and approved the final manuscript.

FUNDING

This work was supported by the Spanish Ministry of Science, Innovation and Universities (grant # RTI2018-102032-B-I00 to AM and scholarship #FPU17/01302 to MŽ).

ACKNOWLEDGMENTS

We thank ACEA Biosciences for providing *E*-plates and assessment for the use of the xCELLigence equipment.

SUPPLEMENTARY MATERIAL

The Supplementary Material for this article can be found online at: <https://www.frontiersin.org/articles/10.3389/fmicb.2020.00553/full#supplementary-material>

REFERENCES

- Baidamshina, D. R., Trizna, E. Y., Holyavka, M. G., Bogachev, M. I., Artyukhov, V. G., Akhatova, F. S., et al. (2017). Targeting microbial biofilms using Ficin, a nonspecific plant protease. *Sci. Rep.* 7:46068. doi: 10.1038/srep46068
- Baldoni, D., Furustrand Täfén, U., Aeppli, S., Angevaere, E., Oliva, A., Haschke, M., et al. (2013). Activity of dalbavancin, alone and in combination with rifampicin, against methicillin-resistant *Staphylococcus aureus* in a foreign-body infection model. *Int. J. Antimicrob. Agents* 42, 220–225. doi: 10.1016/j.ijantimicag.2013.05.019
- Bjarnsholt, T., Ciofu, O., Molin, S., Givskov, M., and Høiby, N. (2013). Applying insights from biofilm biology to drug development—can a new approach be developed? *Nat. Rev. Drug Discov.* 12, 791–808. doi: 10.1038/nrd4000
- Blasi, F., Page, C., Rossolini, G. M., Palleschi, L., Matera, M. G., Rogliani, P., et al. (2016). The effect of N-acetylcysteine on biofilms: implications for the treatment of respiratory tract infections. *Respir. Med.* 117, 190–197. doi: 10.1016/j.rmed.2016.06.015
- Brackman, G., and Coenye, T. (2015). Quorum sensing inhibitors as anti-biofilm agents. *Curr. Pharm. Des.* 21, 5–11. doi: 10.2174/1381612820666140905114627
- Calcagno, V. (2013). *glmulti: Model selection and multimodel inference made easy. R package version 1.0.7*. Available online at: <http://CRAN.R-project.org/package=glmulti> (accessed September, 2019).
- Campbell, E. A., Korzhova, N., Mustaev, A., Murakami, K., Nair, S., Goldfarb, A., et al. (2001). Structural mechanism for rifampicin inhibition of bacterial rna polymerase. *Cell* 104, 901–912. doi: 10.1016/S0092-8674(01)00286-0
- Chen, A. Y., Zervos, M. J., and Vazquez, J. A. (2007). Dalbavancin: a novel antimicrobial. *Int. J. Clin. Pract.* 61, 853–863. doi: 10.1111/j.1742-1241.2007.01318.x
- Chen, M., Yu, Q., and Sun, H. (2013). Novel strategies for the prevention and treatment of biofilm related infections. *Int. J. Mol. Sci.* 14, 18488–18501. doi: 10.3390/ijms140918488
- Choo, E. J., and Chambers, H. F. (2016). Treatment of methicillin-resistant *Staphylococcus aureus* bacteremia. *Infect. Chemother.* 48, 267–273. doi: 10.3947/ic.2016.48.4.267
- Chung, P. Y., and Toh, Y. S. (2014). Anti-biofilm agents: recent breakthrough against multi-drug resistant *Staphylococcus aureus*. *Pathog. Dis.* 70, 231–239. doi: 10.1111/2049-632X.12141
- Costa, F., Sousa, D. M., Parreira, P., Lamghari, M., Gomes, P., and Martins, M. C. L. (2017). N-acetylcysteine-functionalized coating avoids bacterial adhesion and biofilm formation. *Sci. Rep.* 7:17374. doi: 10.1038/s41598-017-17310-4
- Darouiche, R. O., and Mansouri, M. D. (2005). Dalbavancin compared with vancomycin for prevention of *Staphylococcus aureus* colonization of devices in vivo. *J. Infect.* 50, 206–209. doi: 10.1016/j.jinf.2004.05.006
- Di Pilato, V., Ceccherini, F., Sennati, S., D'Agostino, F., Arena, F., D'Atanasio, N., et al. (2020). In vitro time-kill kinetics of dalbavancin against *Staphylococcus* spp. biofilms over prolonged exposure times. *Diagn. Microbiol. Infect. Dis.* 96:114901. doi: 10.1016/j.diagmicrobio.2019.114901
- Dinicola, S., De Grazia, S., Carlomagno, G., and Pintucci, J. P. (2014). N-acetylcysteine as powerful molecule to destroy bacterial biofilms. A systematic review. *Eur. Rev. Med. Pharmacol. Sci.* 18, 2942–2948.
- EUCAST (2018). *Breakpoint Tables for Interpretation of MICs and Zone Diameters. Version 8.0*. Sweden: EUCAST.
- Fernández, J., Greenwood-Quaintance, K. E., and Patel, R. (2016). In vitro activity of dalbavancin against biofilms of staphylococci isolated from prosthetic joint infections. *Diagn. Microbiol. Infect. Dis.* 85, 449–451. doi: 10.1016/j.diagmicrobio.2016.05.009
- Ferrer, M. D., Lamarche, B., and Mira, A. (2017a). *App. Note N° 17. Studying Bacterial Biofilms Using Cellular Impedance. xCELLigence® Real-time cell analyzers*. San Diego, CA: ACEA Biosciences, Inc, 1–6.
- Ferrer, M. D., Rodriguez, J. C., Álvarez, L., Artacho, A., Royo, G., and Mira, A. (2017b). Effect of antibiotics on biofilm inhibition and induction measured by real-time cell analysis. *J. Appl. Microbiol.* 122, 640–650. doi: 10.1111/jam.13368
- Fleming, D., and Rumbaugh, K. (2017). Approaches to dispersing medical biofilms. *Microorganisms* 5:15. doi: 10.3390/microorganisms5020015
- Flemming, H. C., and Wingender, J. (2010). The biofilm matrix. *Nat. Rev. Microbiol.* 8, 623–633. doi: 10.1038/nrmicro2415
- Gries, C. M., and Kielian, T. (2017). Staphylococcal biofilms and immune polarization during prosthetic joint infection. *J. Am. Acad. Orthop. Surg.* 1, S20–S24. doi: 10.5435/JAAOS-D-16-00636
- Gutiérrez, D., Fernández, L., Martínez, B., Ruas-Madiedo, P., García, P., and Rodríguez, A. (2017). Real-time assessment of *Staphylococcus aureus* biofilm disruption by phage-derived proteins. *Front. Microbiol.* 8:1632. doi: 10.3389/fmicb.2017.01632
- Hall, C. W., and Mah, T. F. (2017). Molecular mechanisms of biofilm-based antibiotic resistance and tolerance in pathogenic bacteria. *FEMS Microbiol. Rev.* 41, 276–301. doi: 10.1093/femsre/fux010
- Jacqueline, C., and Caillon, J. (2014). Impact of bacterial biofilm on the treatment of prosthetic joint infections. *J. Antimicrob. Chemother.* 69, 37–40. doi: 10.1093/jac/dku254
- Jefferson, K. K., Goldmann, D. A., and Pier, G. B. (2005). Use of confocal microscopy to analyze the rate of vancomycin penetration through *Staphylococcus aureus* biofilms. *Antimicrob. Agents Chemother.* 49, 2467–2473. doi: 10.1128/AAC.49.6.2467-2473.2005
- Kaplan, J. B. (2010). Biofilm dispersal: mechanisms. clinical implications, and potential therapeutic uses. *J. Dent. Res.* 89, 205–218. doi: 10.1177/0022034509359403
- Knafl, D., Tobudic, S., Cheng, S. C., Bellamy, D. R., and Thalhhammer, F. (2017). Dalbavancin reduces biofilms of methicillin-resistant *Staphylococcus aureus* (MRSA) and methicillin-resistant *Staphylococcus epidermidis* (MRSE). *Eur. J. Clin. Microbiol. Infect. Dis.* 36, 677–680. doi: 10.1007/s10096-016-2845-z
- Kundukad, B., Schussman, M., Yang, K., Seviour, T., Yang, L., Rice, S. A., et al. (2017). Mechanistic action of weak acid drugs on biofilms. *Sci. Rep.* 7:4783. doi: 10.1038/s41598-017-05178-3
- Kussmann, M., Obermueller, M., Berndt, F., Reischer, V., Veletzky, L., Burgmann, H., et al. (2018). Dalbavancin for treatment of implant-related methicillin-resistant *Staphylococcus aureus* osteomyelitis in an experimental rat model. *Sci. Rep.* 8:9661. doi: 10.1038/s41598-018-28006-8
- Lopatkin, A. J., Stokes, J. M., Zheng, E. J., Yang, J. H., Takahashi, M. K., You, L., et al. (2019). Bacterial metabolic state more accurately predicts antibiotic lethality than growth rate. *Nat. Microbiol.* 4, 2109–2117. doi: 10.1038/s41564-019-0536-0
- Meeker, D. G., Beenken, K. E., Mills, W. B., Loughran, A. J., Spencer, H. J., Lynn, W. B., et al. (2016). Evaluation of antibiotics active against methicillin-resistant *Staphylococcus aureus* based on activity in an established biofilm. *Antimicrob. Agents Chemother.* 60, 5688–5694. doi: 10.1128/AAC.01251-16
- Moormeier, D. E., and Bayles, K. W. (2017). *Staphylococcus aureus* biofilm: a complex developmental organism. *Mol. Microbiol.* 104, 365–376. doi: 10.1111/mmi.13634
- Otto, M. (2013). Staphylococcal infections: mechanisms of biofilm maturation and detachment as critical determinants of pathogenicity. *Annu. Rev. Med.* 64, 175–188. doi: 10.1146/annurev-med-042711-140023
- Raad, I., Hanna, H., Jiang, Y., Dvorak, T., Reitzel, R., Chaiban, G., et al. (2007). Comparative activities of daptomycin, linezolid, and tigecycline against catheter-related methicillin-resistant *Staphylococcus bacteremic* isolates embedded in biofilm. *Antimicrob. Agents Chemother.* 51, 1656–1660. doi: 10.1128/AAC.00350-06
- Rodrigues, L. R. (2011). Inhibition of bacterial adhesion on medical devices. *Adv. Exp. Med. Biol.* 715, 351–367. doi: 10.1007/978-94-007-0940-9_22
- Roy, R., Tiwari, M., Donelli, G., and Tiwari, V. (2018). Strategies for combating bacterial biofilms: a focus on anti-biofilm agents and their mechanisms of action. *Virulence* 9, 522–554. doi: 10.1080/21505594.2017.1313372
- Seltzer, E., Dorr, M. B., Goldstein, B. P., Perry, M., Dowell, J. A., Henkel, T., et al. (2003). Once-Weekly Dalbavancin versus standard-of-care antimicrobial regimens for treatment of skin and soft-tissue infections. *Clin. Infect. Dis.* 37, 1298–1303. doi: 10.1086/379015
- Stepanovic, S., Vukovic, D., Dakic, I., Savic, B., and Svabic-Vlahovic, M. (2000). A modified microtiter-plate test for quantification of staphylococcal biofilm formation. 40, 175–179. doi: 10.03.248/s0167-7012(00)00122-6
- Stewart, P. S., and Costerton, J. W. (2001). Antibiotic resistance of bacteria in biofilms. *Lancet* 358, 135–138. doi: 10.4103/0974-8237.167866

- Zhou, W., Shan, W., Ma, X., Chang, W., Zhou, X., Lu, H., et al. (2012). Molecular characterization of rifampicin-resistant *Staphylococcus aureus* isolates in a Chinese teaching hospital from Anhui, China. *BMC Microbiol.* 12:240. doi: 10.1186/1471-2180-12-240
- Zhu, X., Rice, S. A., and Barraud, N. (2019). Nitric oxide and iron signaling cues have opposing effects on biofilm development in *Pseudomonas aeruginosa*. *Appl. Environ. Microbiol.* 85:e02175-18. doi: 10.1128/AEM.02175-18
- Zimmerli, W., and Sendi, P. (2019). Role of rifampin against staphylococcal biofilm infections in vitro, in animal models, and in orthopedic-device-related infections. *Antimicrob. Agents Chemother.* 63:e01746-18. doi: 10.1128/AAC.01746-18

Conflict of Interest: The authors declare that the research was conducted in the absence of any commercial or financial relationships that could be construed as a potential conflict of interest.

Copyright © 2020 Žiemytė, Rodríguez-Díaz, Ventero, Mira and Ferrer. This is an open-access article distributed under the terms of the Creative Commons Attribution License (CC BY). The use, distribution or reproduction in other forums is permitted, provided the original author(s) and the copyright owner(s) are credited and that the original publication in this journal is cited, in accordance with accepted academic practice. No use, distribution or reproduction is permitted which does not comply with these terms.



Cannabigerol Prevents Quorum Sensing and Biofilm Formation of *Vibrio harveyi*

Muna Aqawi^{1*}, Ruth Gallily², Ronit Vogt Sionov¹, Batya Zaks¹, Michael Friedman³ and Doron Steinberg¹

¹ The Biofilm Research Laboratory, The Faculty of Dental Medicine, The Institute of Dental Sciences, The Hebrew University of Jerusalem, Jerusalem, Israel, ² The Lautenberg Center for General and Tumor Immunology, The Hadassah Medical School, The Hebrew University of Jerusalem, Jerusalem, Israel, ³ The Department of Pharmaceutics, The Faculty of Medicine, The Institute of Drug Research, The Hebrew University of Jerusalem, Jerusalem, Israel

OPEN ACCESS

Edited by:

Bart Devreese,
Ghent University, Belgium

Reviewed by:

Alexandra Lianou,
Agricultural University of Athens,
Greece
Giordano Rampioni,
Roma Tre University, Italy

*Correspondence:

Muna Aqawi
muna.aqawi@mail.huji.ac.il

Specialty section:

This article was submitted to
Antimicrobials, Resistance
and Chemotherapy,
a section of the journal
Frontiers in Microbiology

Received: 17 January 2020

Accepted: 09 April 2020

Published: 07 May 2020

Citation:

Aqawi M, Gallily R, Sionov RV,
Zaks B, Friedman M and Steinberg D
(2020) Cannabigerol Prevents
Quorum Sensing and Biofilm
Formation of *Vibrio harveyi*.
Front. Microbiol. 11:858.
doi: 10.3389/fmicb.2020.00858

Cannabigerol (CBG) is a non-psychoactive cannabinoid naturally present in trace amounts in the Cannabis plant. So far, CBG has been shown to exert diverse activities in eukaryotes. However, much less is known about its effects on prokaryotes. In this study, we investigated the potential role of CBG as an anti-biofilm and anti-quorum sensing agent against *Vibrio harveyi*. Quorum sensing (QS) is a cell-to-cell communication system among bacteria that involves small signaling molecules called autoinducers, enabling bacteria to sense the surrounding environment. The autoinducers cause alterations in gene expression and induce bioluminescence, pigment production, motility and biofilm formation. The effect of CBG was tested on *V. harveyi* grown under planktonic and biofilm conditions. CBG reduced the QS-regulated bioluminescence and biofilm formation of *V. harveyi* at concentrations not affecting the planktonic bacterial growth. CBG also reduced the motility of *V. harveyi* in a dose-dependent manner. We further observed that CBG increased *LuxO* expression and activity, with a concomitant 80% downregulation of the *LuxR* gene. Exogenous addition of autoinducers could not overcome the QS-inhibitory effect of CBG, suggesting that CBG interferes with the transmission of the autoinducer signals. In conclusion, our study shows that CBG is a potential anti-biofilm agent via inhibition of the QS cascade.

Keywords: biofilm, bioluminescence, cannabinoids, motility, quorum sensing, *Vibrio harveyi*

INTRODUCTION

Bacteria can communicate by means of signaling molecules called autoinducers (AIs) in a process called quorum sensing (QS). Quorum sensing governs several processes which are critical for bacterial survival and allows them to respond to changes in cell density (Mukherjee and Bassler, 2019). These processes include biofilm formation, virulence factor secretion, bioluminescence, motility, antibiotic production, sporulation and development of genetic competence (Singh et al., 2009). Quorum sensing allows bacteria to switch between two distinct gene expression programs, one that is favored at low cell density (LCD) for individual, asocial behaviors, while the other is favored at high cell density (HCD) for social, group behaviors (Ng and Bassler, 2009).

The free living, marine quorum-sensing bacterium *Vibrio harveyi* produces at least three AIs, *harveyi* autoinducer 1 (HAI-1; acylated homoserine lactone; AHL), autoinducer 2 (AI-2; furanosyl borate diester), and cholera autoinducer 1 (CAI-1; a long-chain amino

ketone (Z)-3-aminoundec-2-en-4-one) that interact with their respective receptors LuxN, LuxP/Q and CqsS (Chen et al., 2002; Zhang et al., 2012; Soni et al., 2015). The autoinducers elicit signal transduction pathways in *V. harveyi* converging in the expression of bioluminescence and biofilm formation (Waters and Bassler, 2006). When no or low quantities of autoinducers are present (at low cell density), the receptors autophosphorylate and transfer phosphate to LuxO through LuxU. Phosphorylated LuxO in combination with the sigma factor σ^{54} activates the transcription of the genes encoding five regulatory small RNAs (qrr1-5) (Tu and Bassler, 2007). The qrr sRNAs together with the RNA-binding protein Hfq inhibit the translation of the mRNA of the master QS regulator LuxR. LuxO also reduces LuxR activity by inducing the expression of AphA (Rutherford et al., 2011). Therefore, at LCD, LuxR protein is not produced and there is no bioluminescence. In contrast, when the autoinducer concentrations are high (at high cell density), the receptors switch to phosphatases allowing for the dephosphorylation of LuxU and LuxO. This in turn results in LuxR-mediated induction of genes involved in bioluminescence and biofilm formation (Ng and Bassler, 2009; Zhang et al., 2012).

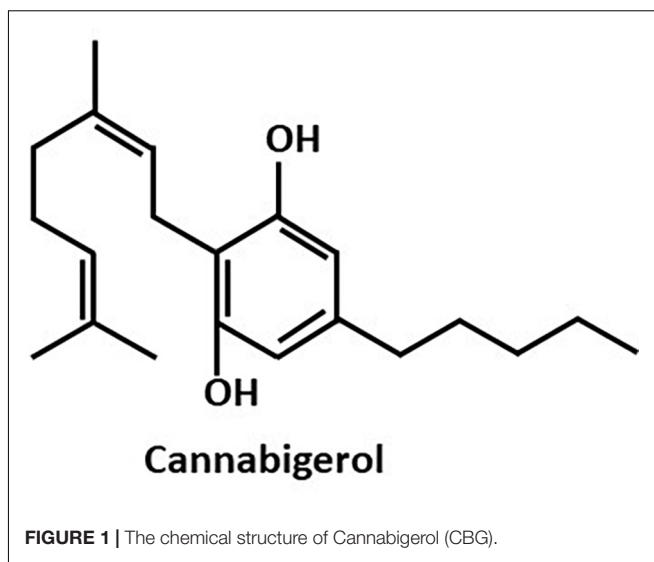
Since anti-QS compounds are known to have the ability to prohibit bacterial pathogenicity, research is currently directed toward disrupting QS as an attractive target for the development of novel anti-infective agents that do not rely on the use of antibiotics (Asfour, 2018). We have previously shown interference of the bacterial signal-transduction system by the synthetic cannabinoid receptor agonist HU-210 (Soni et al., 2015) and the endocannabinoid anandamide (Friedman et al., 2019). Here, we studied the anti-biofilm and anti-QS effects of the *Cannabis sativa* plant component cannabigerol (CBG) (Figure 1) using the marine biofilm-producing bacterial species *V. harveyi*. The phytocannabinoids of *C. sativa* have been shown to exert potential therapeutic activities in mammals (Turner et al., 2017). Specifically, CBG exerts anti-inflammatory, neuroprotective and anti-tumor properties (Eisohly et al., 1982), and has been shown to be effective in the treatment of glaucoma, psoriasis, dry-skin syndrome and pain (Olah et al., 2016). In addition, it elicited hyperphagia (Brierley et al., 2016) and attenuated colitis (Borrelli et al., 2013) in mice. On the contrary, much less is known about its effects on prokaryotes. A previous study showed that CBG displays antibacterial properties against methicillin-resistant *Staphylococcus aureus* strains (Appendino et al., 2008). Here we tested the anti-quorum sensing and anti-biofilm formation potential of CBG on *V. harveyi*.

MATERIALS AND METHODS

Materials

Cannabigerol (CBG) (hemp isolate, 98.5% purity) was purchased from NC Labs (Czech Republic) and dissolved in ethanol at a concentration of 18 mg/ml. As control, respective dilutions

Abbreviations: AB, Autoinducer bioassay; AI, Autoinducer; CBG, Cannabigerol; DPD, (S)-4,5-Dihydroxy-2,3-pentandione; LCD, low cell density; HCD, high cell density; QS, Quorum sensing.



of ethanol corresponding to the different CBG concentrations were used. (S)-4,5-Dihydroxy-2,3-pentandione (DPD, AI-2) was purchased from OMM Scientific Inc.

Bacterial Growth and Biofilm Formation

V. harveyi wild-type strain BB120 was obtained from ATCC (*Vibrio campbellii* BAA-1116™). The mutant bacterial strains were generously provided by Prof. B. Bassler (Princeton University) (Table 1; Bassler et al., 1993, 1994, 1997; Freeman and Bassler, 1999; Surette et al., 1999; Mok et al., 2003). For planktonic growth, the *V. harveyi* strains were incubated aerobically in complete autoinducer bioassay (AB) medium (300 mM NaCl, 50 mM MgSO₄, 2 mg/ml Casamino acids, 0.5 mM L-arginine, 20 µg/ml thiamine, 2 µg/ml riboflavin, 5 mM potassium phosphate and 0.5% glycerol; pH 7.5) at 30°C for 20–24 h. For biofilm formation, the bacteria were grown in complete AB medium supplemented with higher concentrations of thiamine (0.3 mg/ml) and riboflavin (0.3 µg/ml).

DNA Quantification by Quantitative (q) PCR

DNA extraction and quantification were performed as previously described (Periasamy and Kolenbrander, 2009; Assaf et al., 2014). Briefly, biofilm was allowed to form in the absence or presence of different concentrations of CBG and ethanol in polystyrene 48-well tissue culture plates (Nunc). At the end of incubation, the growth medium was removed, and the formed biofilms were washed twice with PBS. Then, 200 µl of NaOH (0.04 M) was added to each well and the plates were incubated in a hot water bath for 1 h at 60°C, followed by neutralization with 18.5 µl Tris:HCl pH 7.0. The amount of DNA in each sample was quantified by qPCR with specific primers for *V. harveyi* 16S rRNA (Table 2) using a Bio-Rad CFX Connect Real-time system and the Bio-Rad CFX Maestro program. The amount of DNA in each sample was calculated according to the standard curve obtained using known DNA concentrations of purified *V. harveyi*

TABLE 1 | *Vibrio harveyi* wild-type (wt) and mutant strains carrying genetic defects in the quorum sensing genes.

Strain	Sensor1 (LuxN)	Sensor2 (LuxP/LuxQ)	AI-1	AI-2	Gene	References
BB120 (wt)	+	+	+	+	Wild-type	Bassler et al., 1997
BB170	–	+	+	+	<i>luxN</i> [–]	Bassler et al., 1993
BB152	+	+	–	+	<i>luxM</i> [–]	Bassler et al., 1994
BB960	+	–	+	+	<i>luxQ</i> [–]	Bassler et al., 1994
BB886	+	–	+	+	<i>luxP</i> [–]	Bassler et al., 1994
MM77	+	+	–	–	<i>luxM</i> [–] , <i>luxS</i> [–]	Mok et al., 2003
MM30	+	+	+	–	<i>luxS</i> [–]	Surette et al., 1999
MM32	–	+	+	–	<i>luxS</i> [–] , <i>luxN</i> [–]	Surette et al., 1999
JAF 375	–	–	+	+	<i>luxQ</i> [–] , <i>luxN</i> [–]	Freeman and Bassler, 1999

TABLE 2 | Primers used for real-time PCR.

Gene	Forward primer	Reverse primer
16S rRNA	GAGTTGCGTTTCTTTCAA	TGTAGTTTTCGCTAATTC
LuxR	TCAATTGCAAGAGACCTCG	AGCAAACTTCAAGAGCGA
LuxU	ATGGACTCTACATTGGCACTT	AAGCTGGCAGCACTACTTTTC
LuxS	GGCGTACCAATCAAGCTCATGT	CGCAGGCTTTATGCGTAATCA
LuxM	ATTCTTGCCGACTCTGGTG	CAACACTTCGCAAAACGGCTT
LuxP	GTGGTTTACCCAGGACAGCA	GTTTGTCCTCACTCAGGACT
LuxN	AGGTATCGGCAAGCGTTCA	ATACGGCGATCCGCTTCAAT
LuxQ	GTCCAGCACTGATGACGAT	TGCCCATCGCGAGTAAACTT
LuxO	TCCTAATCAAACATGTGAAGC	GATGAAGCCTTGGTAATTTGG
aphA	ATCCATCAACTCTAGGTGATAACG	CGTCGCGAGTGCTAAGTACA
Hfq	CGTGAGCGTATCCCGTATCTAT	TTGCAGTTTGATACCGTTCACAAG
qrr1	CTCGGGTCACCTATCAACTGA	TGCGATCTATTGGCTCGTTCTG
qrr2	CTTAAGCCGAGGGTCACCTAGC	CAATTAGGGCGATTGGCTTATGT
qrr3	CTTAAGCCGAGGGTCACCTAGC	ACAAATTCGAGTCCACTAACAACGT
qrr4	CCTTATTAGCCGAGGGTCAC	GTTGATTGGCGGTATATCTTGTG
qrr5	GACGTTGTAGTGAACCAATTGTT	CACAAGGTTTGTGATTGGCTGTATA

DNA. Purified DNA was extracted from an overnight culture of *V. harveyi* BB120 using GenElute Bacterial Genomic DNA kit (Sigma Aldrich, St. Louis, MO, United States) as per the manufacturer's instructions.

Growth and Bioluminescence of Wild-Type and Mutant *V. harveyi* Strains

Overnight cultures (OD₅₉₅ ~0.7) of wild-type *V. harveyi* (BB120) and mutant *V. harveyi* strains were diluted 1:200 in complete AB medium, and 180 µl of the diluted bacterial cultures were transferred to each well of an optic flat-bottom white 96-well cell culture microplate (µCLEAR, Greiner Bio-One), together with 20 µl of CBG at different concentrations. The absorbance (OD₅₉₅) and luminescence were read in parallel every 30 min for 20 h using an infinite M200PRO TECAN plate reader. The plate reader was kept at a constant temperature of 30°C throughout the experiment. The luminescence values, representing quorum sensing, were normalized by dividing them with the respective absorbance values in order to correct for differences in growth rates. The area under the curve was calculated for each sample and compared with untreated control samples as previously described (Aharoni et al., 2008; Feldman et al., 2009).

RNA Extraction

The assay was performed similarly to the method used by Feldman et al. (2014) with slight modifications. An overnight culture of *V. harveyi* (OD₅₉₅ ~0.7) was diluted 1:10 in complete AB medium and incubated at 30°C under aerobic conditions

in the absence or presence of 2 µg/ml CBG for 10 h. Eight milliliter of bacterial culture were used for each sample. At the end of incubation, the supernatant was removed, and the cells were washed with 2 ml of PBS and incubated with 2 ml of RNA Protect (Qiagen, Hilden, Germany) for 5 min at room temperature. RNA was isolated using the RNeasy MINI kit (Qiagen) including on-column DNase digestion according to the manufacturer's instructions. RNA purity and quantity were determined using Nanodrop (Nanovue, GE Healthcare Life Sciences, Buckinghamshire, United Kingdom). Only samples with an OD₂₆₀/OD₂₈₀ ratio of 2 and an OD₂₆₀/OD₂₃₀ ratio above 2 were used for cDNA synthesis. The samples were stored at –80°C until use.

Reverse Transcription (RT) and Quantitative Real-Time PCR

The purified RNA was reverse transcribed into cDNA using the cDNA qScript cDNA synthesis kit (QuantaBio). The relative expression levels of target genes were analyzed by Bio-Rad CFX Connect Real-time system and the Bio-Rad CFX Maestro program. Power Sybr Green PCR Master mix (Applied Biosystems) was used to amplify the genes of 10 ng cDNA per well in combination with 300 nM of respective F/R primer set (Table 2). For each set of primers, a standard amplification curve (critical threshold cycle vs. exponential of concentration) was plotted, and only those with a slope around –3.2 were used for analysis. The PCR cycle involved initial heating at 50°C for 2 min, activation step at 95°C for 10 min, followed by 40 cycles of amplification (95°C for 15 s, 60°C for 1 min), and the dissociation curve was determined by initial heating at 95°C for 15 s, followed by 10 s at 60°C, and 0.5 temperature increment until reaching 95°C. The expression of 16S rRNA was used for normalization and to calculate the relative changes in target gene expression using the $2^{-\Delta\Delta Ct}$ method. Gene expression was expressed in relative values, setting the expression level of the untreated control to 1 for each gene (Assaf et al., 2014; Feldman et al., 2014).

Autoinducer Preparation

Supernatant from log-phase growing *V. harveyi* mutant strains in incomplete AB medium (300 mM NaCl, 50 mM MgSO₄, 2 mg/ml Casamino acids, 20 µg/ml thiamine, 2 µg/ml riboflavin; pH 7.5) was collected, filtrated (0.22 µm) and kept at –20°C. The BB152 (AI-1[–], AI-2⁺) was used for obtaining AI-2, while MM30

(AI-1⁺, AI-2⁻) was used for preparation of AI-1. Supernatant of MM77 (AI-1⁻, AI-2⁻) was used as a negative control.

Motility of *V. harveyi*

The motility assay was performed on soft agar plates as described previously (Yang and Defoirdt, 2015). Briefly, after cooling down autoclaved AB medium with 0.2% agar to 60°C, different concentrations of CBG along with riboflavin (0.02 µg/ml) and thiamine (0.02 mg/ml) were added and poured into small petri dishes. Agar plates without CBG served as controls. Following solidification, 3 µl of overnight *V. harveyi* culture (OD₅₉₅ ~ 0.5) were inoculated at the center of the agar plate and incubated at 30°C for 15h. The area of the motility halo was measured using Image J software (National Institute of Health) and compared with the control.

High Resolution Scanning Electron Microscopy (HR-SEM)

Biofilms were prepared as described above with different concentrations of CBG and corresponding ethanol dilutions. Biofilms without CBG served as additional controls. Biofilm was allowed to form on sterile circular glass pieces that were inserted into the wells of 96-well microtiter plates. After a 24 h incubation, the glass specimens were removed, rinsed with DDW and fixed in 4% glutaraldehyde for 40 min. The glass specimens were washed again with DDW and allowed to dry at room temperature. The specimens were then mounted on a metal stub and sputter coated with gold prior to SEM analysis. A high-resolution scanning electron microscope (Magellan XHR 400L, FEI Company, Holland) was used. Three specimens from each treatment group were prepared and examined under SEM to evaluate the effect of CBG on biofilm formation (Louwakul et al., 2017).

Statistical Analysis

Three independent experiments were conducted and triplicate samples were measured within each experiment. Statistical analysis of the collected data was performed using Student's *t*-test in Microsoft Excel. A *p* < 0.05 was considered significant.

RESULTS

CBG Prevents Quorum Sensing in *V. harveyi*

To explore the effect of CBG on quorum sensing of *V. harveyi* (wild-type strain BB120), the bacteria were exposed to different concentrations of CBG or the respective ethanol dilutions in complete AB growth medium and incubated for 20 h. Untreated *V. harveyi* served as an additional control. The planktonic growth was monitored by measuring the optical density (Figure 2A), and the induction of quorum sensing was monitored at the same time points by measuring bioluminescence (Figure 2B). We found that CBG at concentrations 1–20 µg/ml did not affect the bacterial growth (Figure 2A), but significantly reduced the bioluminescence (Figures 2B,C; 65 ± 4% inhibition; *p* < 0.05). Strong inhibition was already observed at 1 µg/ml CBG,

with only a slightly higher inhibition when increasing the concentration to 20 µg/ml (Figures 2B,C).

CBG Prevents Biofilm Formation by *V. harveyi*

Bacterial biofilm formation is associated with the quorum sensing process which can be critical for bacterial survival (Rutherford and Bassler, 2012). To test the effect of CBG on wild-type *V. harveyi* biofilm formation, the DNA content in biofilms was quantified in the absence or presence of different concentrations of CBG. The percentage reduction in biofilm formation was calculated in comparison to untreated samples and samples treated with respective dilutions of ethanol. According to the collected data, CBG at 20 and 50 µg/ml reduced the amount of bacteria in the biofilms to 58 ± 7 and 43 ± 8%, respectively (Figure 3A; *p* < 0.05). To further confirm the anti-biofilm activity, biofilms of *V. harveyi* formed in the absence or presence of 20 µg/ml CBG or respective ethanol dilutions were examined under a scanning electron microscope (SEM) at a magnification of x1000–5000. As can be seen from Figure 3B, the biofilm biomass in the CBG-treated group was strongly reduced in comparison to control samples. Moreover, the structure of CBG-treated biofilm was altered. The control biofilms appeared homogeneously and firmly aggregated, while biofilm exposed to CBG appeared as dispersed small aggregates and several single cells (Figure 3B).

CBG Reduces the Motility of *V. harveyi*

Motility is another potent virulence factor which has been shown to be associated with quorum sensing (Yang and Defoirdt, 2015). Therefore, the effect of CBG on the motility of wild-type *V. harveyi* was studied. The motility halos decreased with increasing concentrations of CBG in a dose-dependent manner (Figure 4A). Quantification of motility area showed a 74 ± 5 and 97 ± 1% reduction in motility in the presence of 20 and 50 µg/ml CBG, respectively (Figure 4B; *p* < 0.05). Ethanol as high as 2% had no effect on the motility (Figure 4B).

CBG Antagonizes the Quorum Sensing Signals Delivered by the Autoinducers

In order to study whether CBG interferes with the quorum sensing signals delivered by the autoinducers, we exogenously added autoinducers to autoinducer-deficient mutant strains and exposed them to CBG. The bioluminescence vs. planktonic growth was monitored each 30 min for a total period of 20 h. As expected, almost no bioluminescence was emitted by the double *luxM*, *luxS* null mutant MM77 lacking both AI-1 and AI-2 (Figure 5A, black line). Exogenously added AI-2 induced a strong bioluminescence response (Figure 5A, brown line), while AI-1 caused a more moderate increase (Figure 5A, green line). This is in line with the findings of Anetzberger et al. (Anetzberger et al., 2012). Importantly, the addition of CBG led to a 47.6 ± 5.3 and 63.2 ± 1.6% reduction of the AI-1 and AI-2-induced bioluminescence, respectively (Figures 5A,B, orange and red lines/columns). Similarly, CBG inhibited the AI-1-induced bioluminescence in the *luxM* null

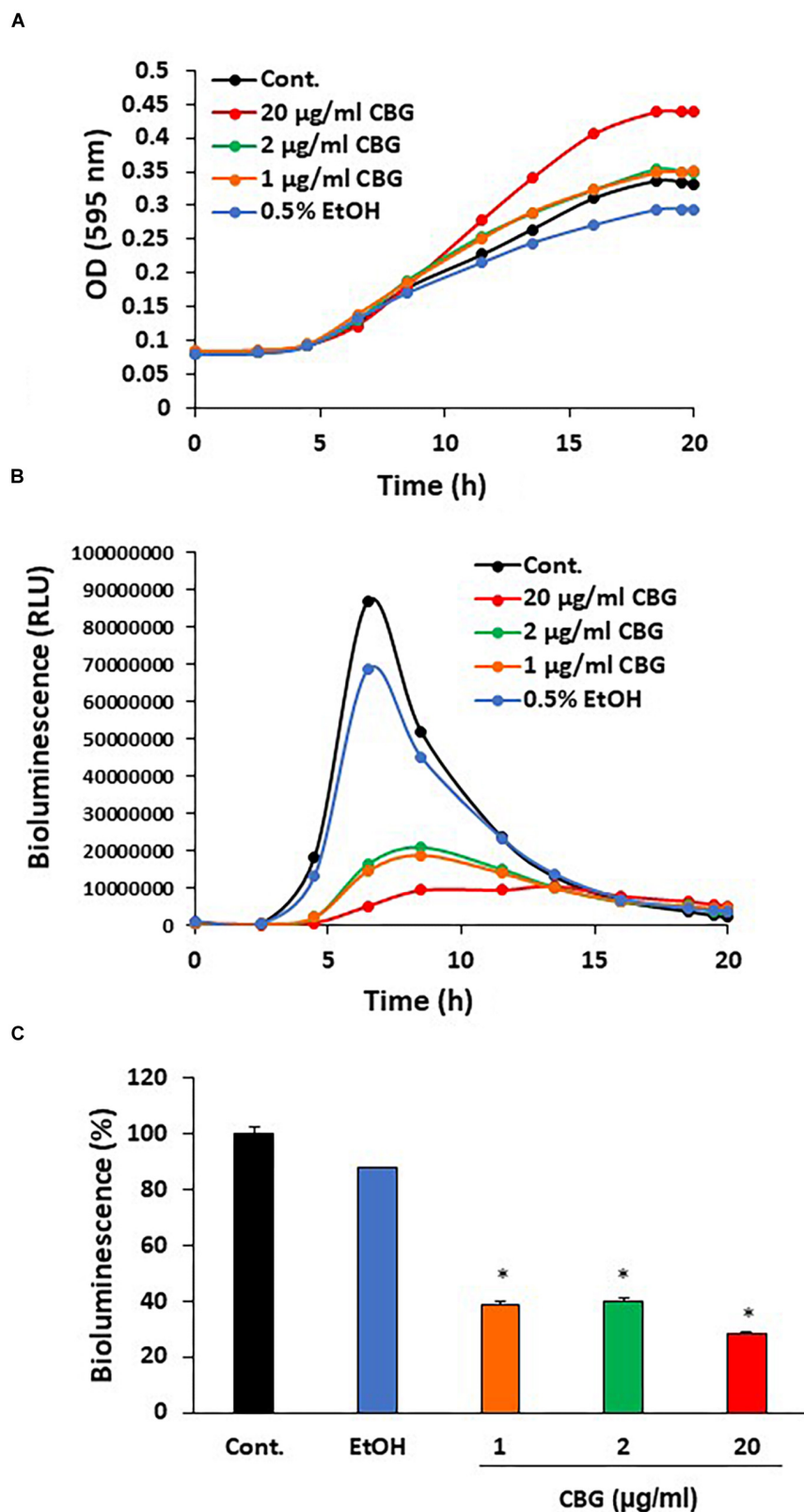


FIGURE 2 | Anti-quorum sensing activity of CBG on wild-type *V. harveyi* (BB120). **(A)** CBG did not affect the planktonic growth of *V. harveyi*. **(B)** CBD strongly prevented the bioluminescence of *V. harveyi*. The graphs represent the average of 3 samples. **(C)** The relative bioluminescence as determined by the area under the curve (AUC) of the graph presented in **(B)** $N = 3$, $*p < 0.05$.

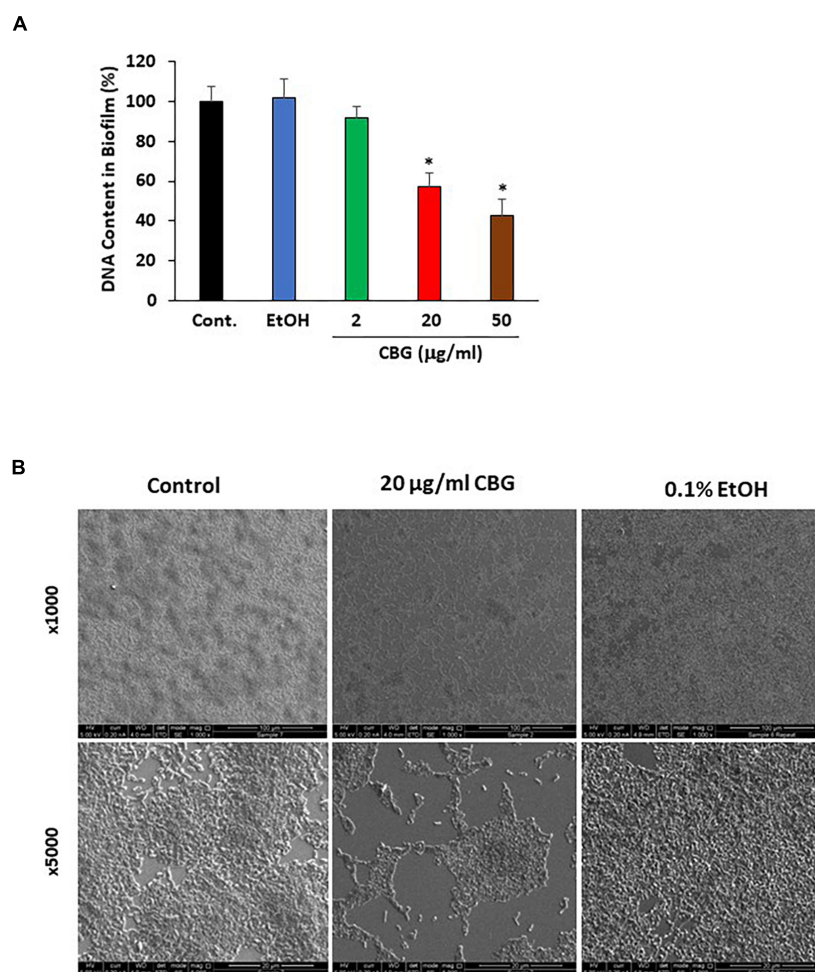


FIGURE 3 | Anti-biofilm activity of CBG on wild-type *V. harveyi* (BB120). **(A)** CBG reduced the amount of DNA in the biofilms formed by *V. harveyi*. *V. harveyi* were grown in complete AB medium for 24 h in the presence of various concentrations of CBG, and the amount of DNA in the biofilms were quantified by real-time PCR using primers for 16S rRNA. *N* = 3. **p* < 0.05. **(B)** Scanning electron microscopy of biofilms formed by wild-type *V. harveyi* in the presence or absence of 20 µg/ml CBG. 0.1% Ethanol (EtOH) served as vehicle control. Two different magnifications are shown (x1000 and x5000).

BB152 (AI-1⁻, AI-2⁺) strain (**Figure 5C**) and the DPD-induced bioluminescence in the *luxS* null MM30 (AI-1⁺, AI-2⁻) strain (**Figure 5D**). DPD is a precursor of AI-2 that spontaneously cyclizes into AI-2 (Papenfort and Bassler, 2016).

CBG Increases LuxO Expression and Activity

Since quorum sensing cascade is tightly regulated, where LuxO antagonizes the master regulator LuxR (Mukherjee and Bassler, 2019), it was querying to explore changes in the expression of quorum sensing-related genes following CBG treatment. To this end, wild-type *V. harveyi* was incubated in the absence or presence of 2 µg/ml CBG for 10 h, and the RNA was extracted for real-time PCR analysis. We observed that both the *luxU* and *luxO* gene expression were strongly induced (x3.5–4.5-fold induction) (**Figure 6A**). Also, the LuxO-regulated genes *aphA*, *hfg*, and *qrr1-5*, were strongly upregulated (x3–6-fold induction) (**Figure 6A**), indicating increased LuxO activity in the presence

of CBG. The strong increase in the regulatory small RNAs of the *qrr* family, explains the strong repression observed in *luxR* expression (80 ± 2% reduction; **Figure 6B**; *p* < 0.05). The simultaneous upregulation of AphA further antagonizes LuxR gene and protein expression (Mukherjee and Bassler, 2019). The expression of QS genes coding for autoinducer synthases (*luxM*, *luxS*) and receptors (*luxN*, *luxP*, *luxQ*) are shown in **Figure 6C**. The *luxQ* gene was highly induced, while *luxM*, *luxN*, and *luxP* were modestly induced. CBG had barely any effect on the *luxS* gene expression (**Figure 6C**).

The Use of Quorum Sensing Mutants of *V. harveyi* to Delineate the CBG Action Mechanism

In a further search for understanding the anti-quorum sensing activity of CBG, we used different mutants of *V. harveyi* deficient in autoinducer production and/or autoinducer receptors. The bioluminescence vs. planktonic growth was studied for each

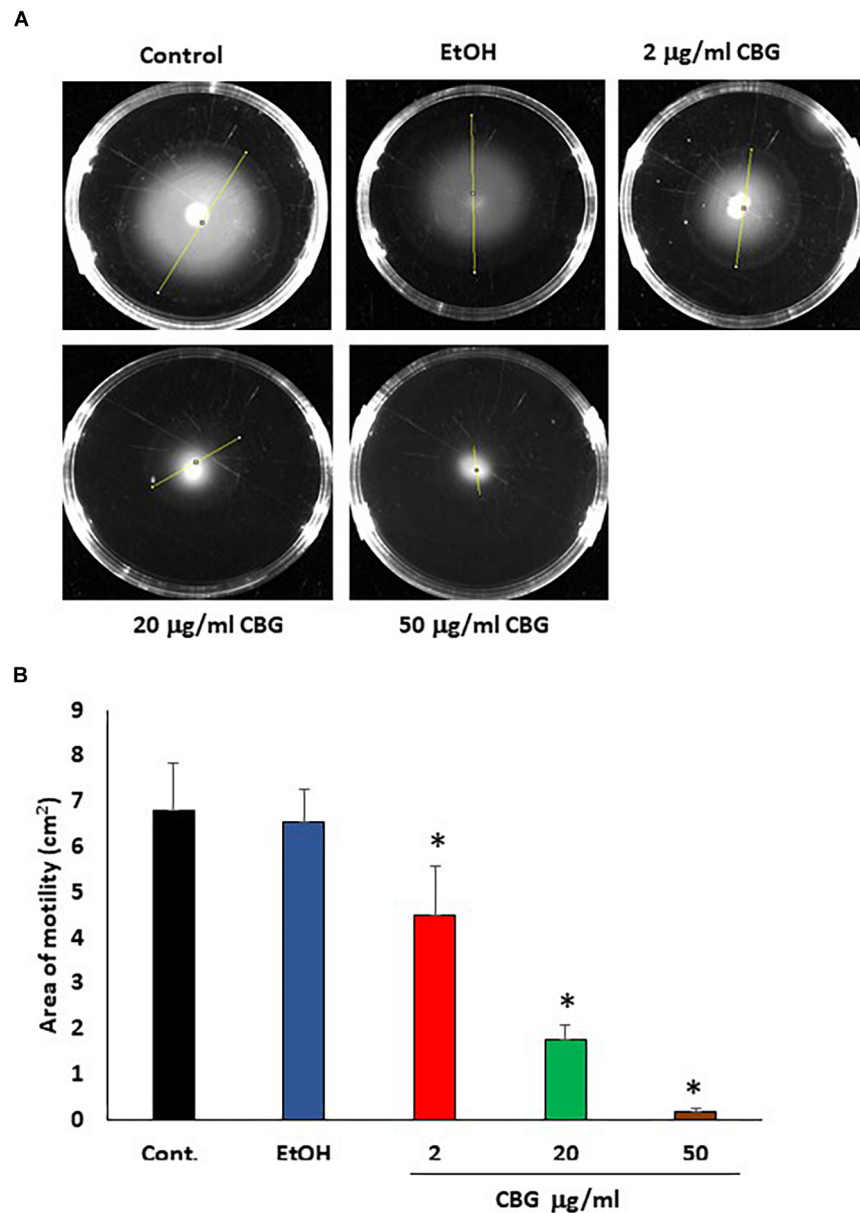


FIGURE 4 | CBG inhibits *V. harveyi* motility. **(A)** The motility of *V. harveyi* in soft agar containing the indicated concentrations of CBG. **(B)** The relative motility of *V. harveyi* in the presence of indicated concentrations of CBG as determined by the spreading area shown in **(A)** $N = 3$, * $p < 0.05$.

strain in the absence or presence of 1 or 2 µg/ml CBG (Figure 7). The *luxM* null strain lacking AI-1 showed a slightly reduced response to CBG in comparison to wild-type (Figure 7A vs. Figure 2B), whereas the *luxS* null strain lacking AI-2 showed almost no response to CBG (Figure 7B; $p < 0.05$). These findings suggest that CBG predominantly antagonizes AI-2, which is the major autoinducer during the exponential growth phase of *V. harveyi* (Anetzberger et al., 2012). Interestingly, mutants lacking either *luxP* or *luxQ*, which are the two components making up the AI-2 receptor, showed similar, and even stronger, reduction in bioluminescence in response to CBG in comparison to wild-type (Figures 7C,D), suggesting that CBG

acts downstream to this receptor. It should be noted that AI-2 acts only on the LuxP/Q receptor in *V. harveyi* (Pereira et al., 2013), and no bioluminescence induction was observed when AI-2 was exogenously added to the *luxP* or *luxQ* null mutants (data not shown). In contrast to the AI-2 receptor null mutants, the mutant lacking *luxN*, the receptor for AI-1, and the mutant lacking both *luxN* and *luxQ*, showed diminished response to CBG (Figures 7E,F; $p < 0.05$), suggesting that LuxN is a major receptor targeted by CBG.

To get a better understanding of the consequences of the elimination of one or more components of the autoinducers and/or their receptors, the relative bioluminescence of each

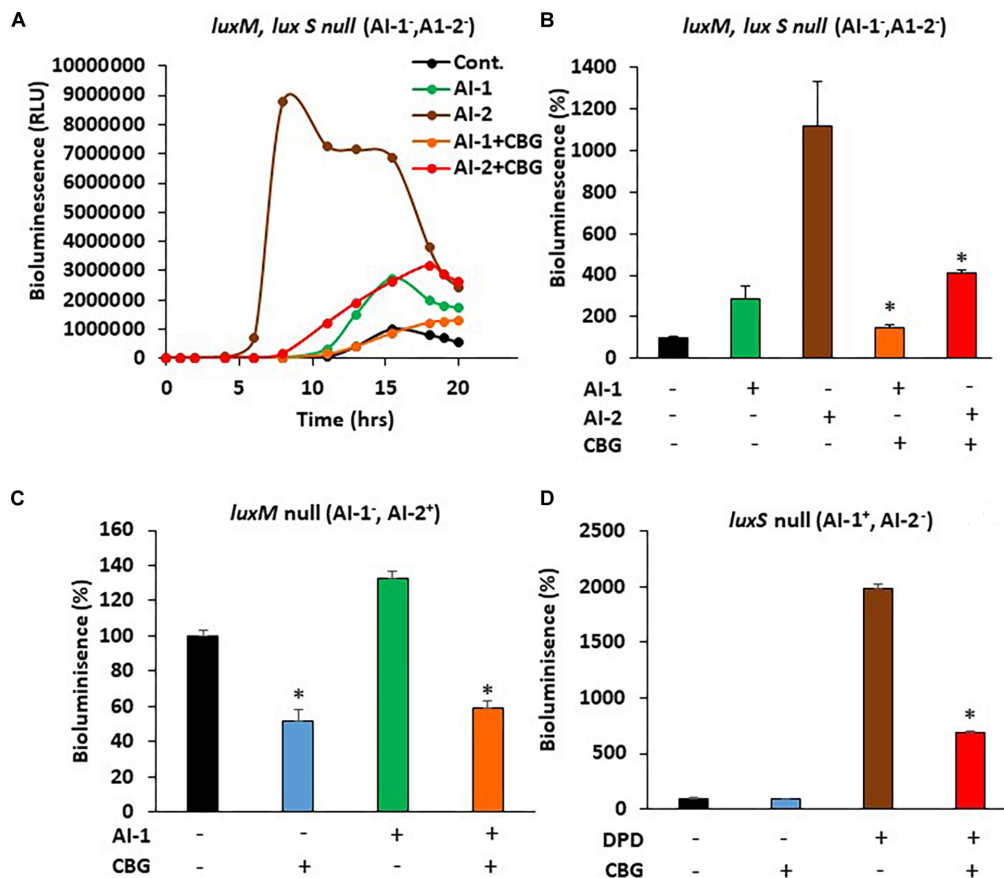


FIGURE 5 | CBG antagonizes the quorum sensing signals delivered by autoinducers. **(A)** The relative bioluminescence of *luxM, luxS* double mutant MM77 (AI-1⁻, AI-2⁻) strain was measured over time in the absence or presence of AI-1, AI-2 and/or 1 μ g/ml CBG. The bioluminescence was corrected for differences in bacterial growth by simultaneously measuring the optical density at 595 nm. **(B)** The relative bioluminescence as determined by the area under the curve (AUC) of the graph presented in **(A)** $N = 3$, $*p < 0.05$. **(C)** The relative bioluminescence as determined by the area under the curve (AUC) of *luxM* null mutant BB152 (AI-1⁻AI-2⁺) exposed to AI-1 and/or 1 μ g/ml CBG. $N = 3$, $*p < 0.05$. **(D)** The relative bioluminescence as determined by the area under the curve (AUC) of *luxS* null mutant MM30 (AI-1⁺AI-2⁻) exposed to the AI-2 precursor DPD (10 μ M) and/or 1 μ g/ml CBG. $N = 3$, $*p < 0.05$.

mutant strain was compared. The *luxM* null lacking AI-1 showed a 40% reduction in bioluminescence in comparison to wild-type, while the *luxS* null lacking AI-2, showed more than 98% reduction in bioluminescence (Supplementary Figure S1), again pointing to a major role of AI-2 vs. AI-1. The *luxS, luxN* double mutant that are deficient in both the AI-1 and AI-2 pathways showed almost no bioluminescence at all, as expected (Supplementary Figure S1). The *luxP* and *luxN* null mutants showed earlier and stronger bioluminescence (140% increase) than the wild-type (Supplementary Figure S1), a finding that suggests that even in the presence of autoinducers, these receptors still exert, to a certain extent, an agonistic action on LuxU/LuxO (Mukherjee and Bassler, 2019). LuxQ null, showed an earlier onset of bioluminescence, but similar total bioluminescence than the wild-type (Supplementary Figure S1). Of note, the *luxN, luxQ* double knockout mutant showed lower bioluminescence than the *luxN* single null mutant (Supplementary Figure S1), indicating that the two autoinducer receptors act in a mutual regulatory interplay. The latter may explain how can LuxN

indirectly affect AI-2 signaling and, in thus, demonstrate how the action of CBG can depend on both AI-2 and LuxN.

DISCUSSION

Since bacterial biofilm formation is a major virulence factor that impedes the control of pathogenic bacteria and the treatment of pertinent bacterial infections, much research has been conducted to find alternatives to current antibiotic therapy (Asfour, 2018). The quorum sensing system in *V. harveyi* has been extensively studied and quite well defined (Mukherjee and Bassler, 2019), making it a good model system for studying the anti-QS properties of the *Cannabis* compound CBG. The QS system regulates gene expression, including virulence determinants, in response to bacterial cell population density by means of signaling molecules called autoinducers (AIs) (Jiang et al., 2018). Medicinal plants have received recognition

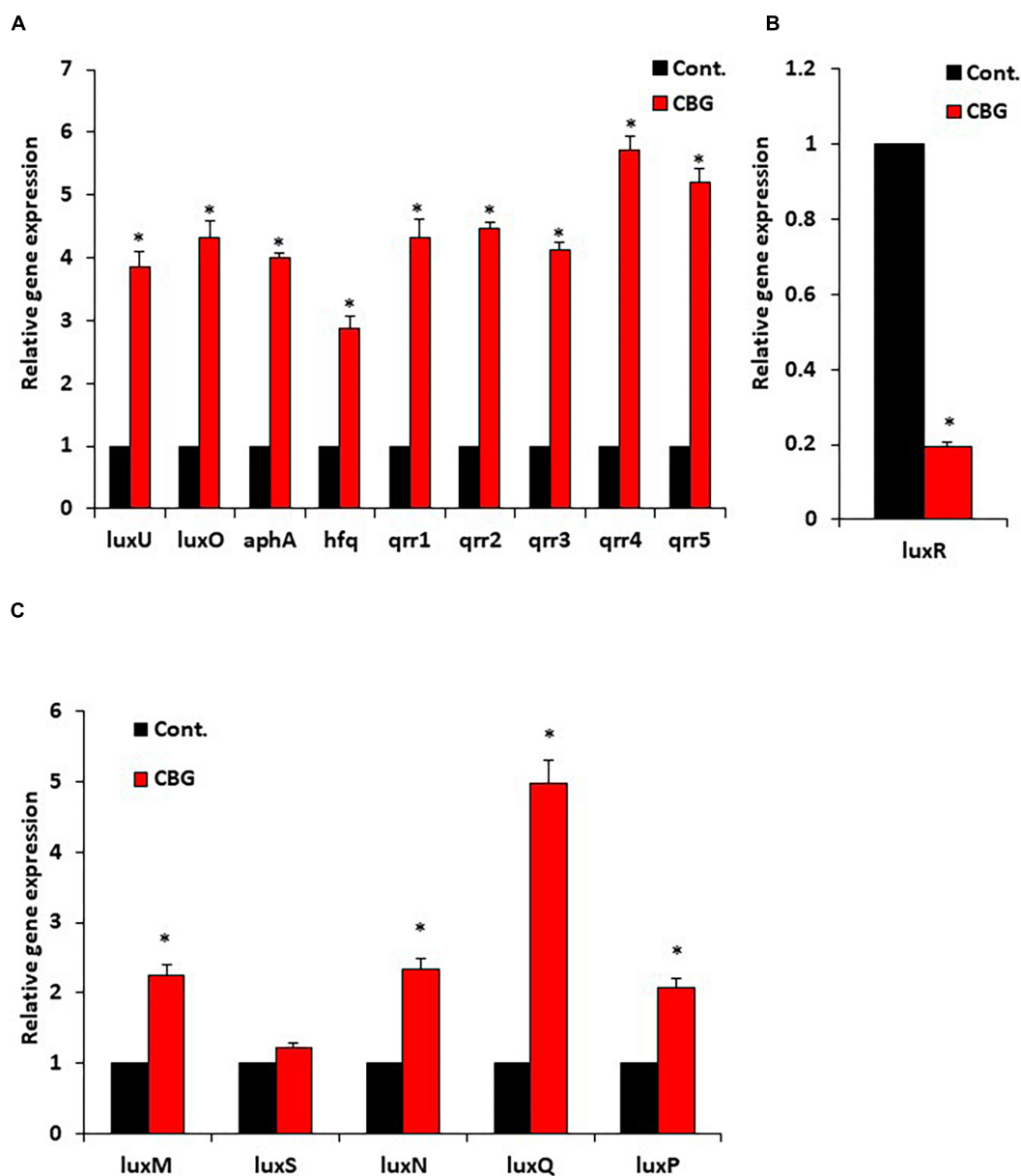


FIGURE 6 | CBG increases the LuxO expression and activity. **(A)** RNA from wild-type *V. harveyi* (BB120) that has been incubated with 2 $\mu\text{g/ml}$ CBG for 10 h were analyzed by real-time PCR for *luxU* and *luxO* gene expression as well as the expression of the LuxO-regulated genes *aphA*, *hfq*, and *qrr1-5*. The relative expression was compared to untreated bacteria incubated for the same time period using 16S rRNA as internal control. **(B)** The relative gene expression of *luxR* in the same samples described in **(A)**. **(C)** The relative gene expression of autoinducer synthases and autoinducer receptors, $N = 3$, $*p < 0.05$.

as a new source for effective QS inhibitory substances. Several phytochemicals and plant by-products have been acknowledged as QS quenching agents in *V. harveyi* including curcumin, flavonoids and components of cranberry (Feldman et al., 2009; Vikram et al., 2010; Packiavathy et al., 2013; Asfour, 2018).

In the present study, we investigated the effect of CBG on QS-regulated bioluminescence, biofilm formation and motility of *V. harveyi*. We demonstrated that CBG shows strong anti-quorum sensing and anti-biofilm activities on *V. harveyi* at

concentrations that do not affect their viability. In addition, CBG caused strong reduction in their motility. So far, the activities of CBG have mainly been studied in eukaryotes where it has been found to be neuroprotective, acting as an anti-oxidant (Giacoppo et al., 2017) and exert anti-inflammatory activities (Eisohly et al., 1982). CBG has previously been found to display anti-bacterial properties toward clinical isolates of methicillin-resistant *Staphylococcus aureus* (Appendino et al., 2008). However, its effect on the bacterial QS pathway has remained unknown.

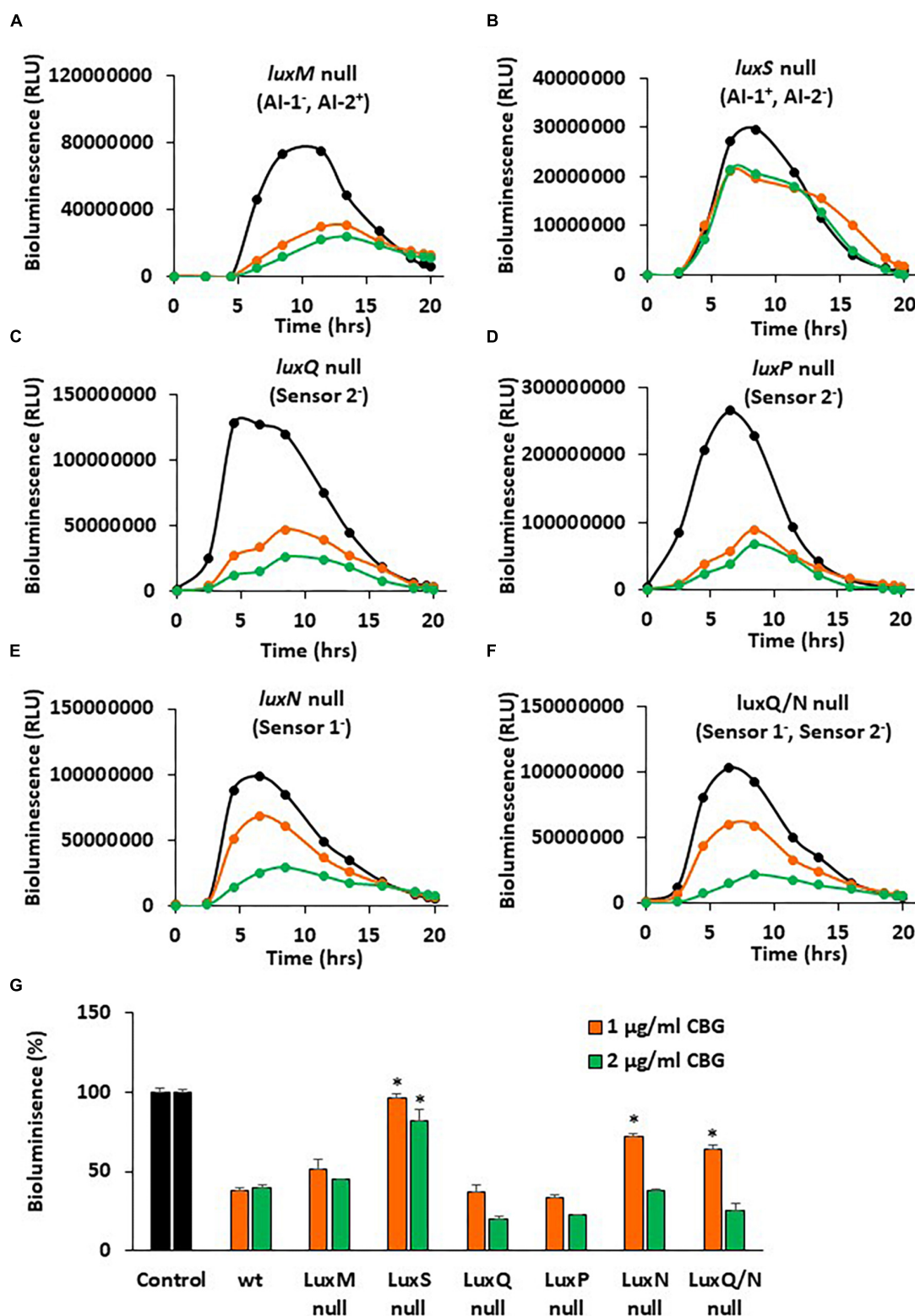


FIGURE 7 | *luxS* null and *luxN* null mutants showed diminished response to CBG. (A–F) The bioluminescence of the indicated mutant strains grown in the absence or presence of CBG. The black lines represent control samples of no CBG, the orange lines bacteria treated with 1 μ g/ml CBG, and the green lines bacteria treated with 2 μ g/ml CBG. Each line is the average of three samples. (G) The relative bioluminescence as determined by the area under the curve (AUC) of the graphs presented in (A–F), $N = 3$, $*p < 0.05$ in comparison to CBG-treated wild-type bacteria.

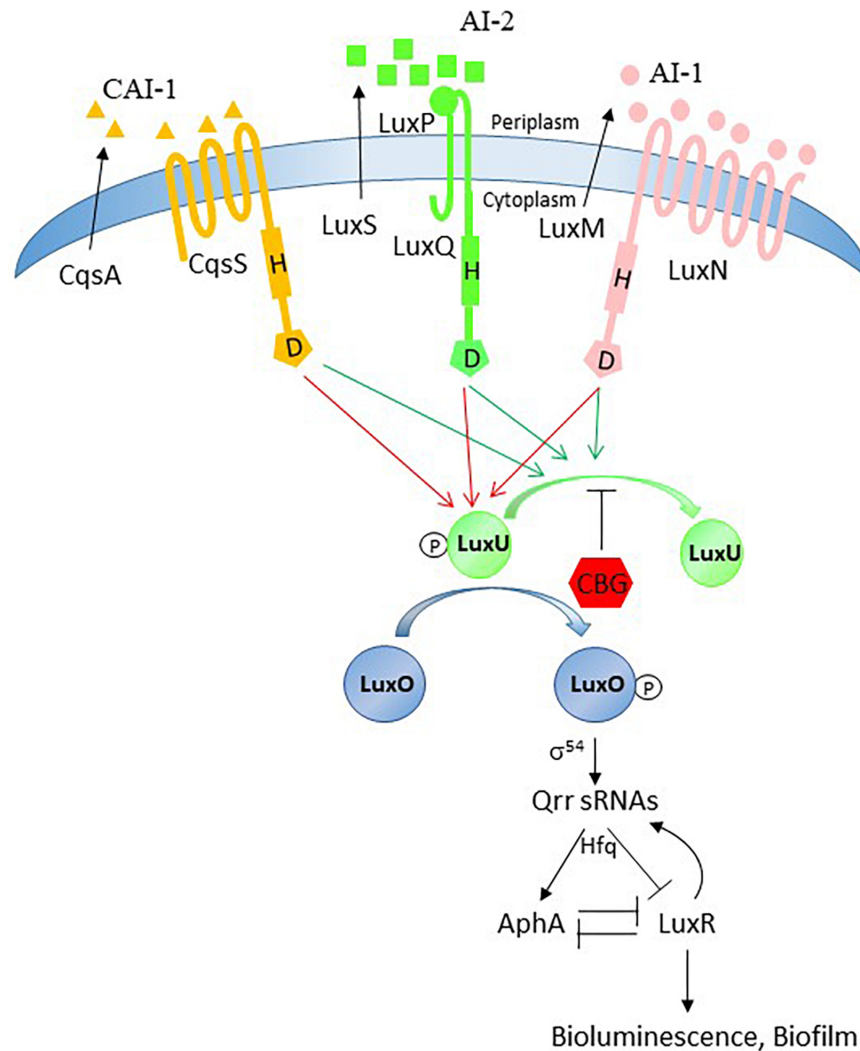


FIGURE 8 | Possible action mechanism of CBG. The quorum sensing system is tightly regulated and has many feedback loops. Our data provide evidence that the anti-quorum sensing activity of CBG is caused by antagonizing the signals delivered by AI-1 and AI-2. Based on our observation that LuxN is required for the anti-QS activity of CBG and CBG augments the LuxO activity, we propose that CBG prevents the dephosphorylation of LuxU.

The QS system in *V. harveyi* activates bioluminescence, and therefore this parameter served to monitor the QS status of the bacteria (Ng and Bassler, 2009; Soni et al., 2015). We conducted kinetic studies that simultaneously monitored bioluminescence and optical densities, allowing for study of the anti-QS effects of CBG. We observed that CBG already at 1 $\mu\text{g/ml}$ exhibited more than 60% inhibition of the bioluminescence of *V. harveyi*. Increasing the concentrations to 20 $\mu\text{g/ml}$ did not significantly augment the anti-quorum sensing effect, suggesting that a plateau effect is reached with 1 $\mu\text{g/ml}$ CBG. The growth of wild-type *V. harveyi* was unaffected by all tested concentrations of CBG, indicating that the effect is specifically directed against the quorum sensing system and not against bacterial viability in the terms of planktonic growth.

Biofilm formation is a major virulence factor that provides the microorganisms with a survival advantage. Therefore, it

was important to study the anti-biofilm activity of CBG. We observed that CBG indeed at its sub-MIC concentrations reduced the amount of bacteria in the biofilms and altered the biofilm structure. This indicates a specific anti-biofilm effect of CBG which is unrelated to its anti-bacterial activity.

Quorum sensing has been shown to enhance the flagellar-dependent motility of *V. harveyi* (Yang and Defoirdt, 2015), and the enhanced motility plays a key role in biofilm formation (O'Toole, 2011). Therefore, the effect of CBG on the motility of wild-type *V. harveyi* was investigated. We indeed observed that the motility of *V. harveyi* decreased with increasing concentrations of CBG in a dose-dependent manner. This finding further supports the anti-QS activity of CBG. Next, we were interested in the molecular mechanisms involved in the anti-QS activity of CBG. We first studied whether CBG could antagonize the quorum sensing signals delivered by the autoinducers AI-1

and AI-2. In the first series of experiments, the autoinducers were added exogenously to autoinducer-deficient strains in the absence or presence of CBG. The data obtained from these studies, clearly indicate that CBG can antagonize the QS signals delivered by both AI-1 and AI-2. When using autoinducer mutant strains, we observed that AI-2 had a much stronger impact on bioluminescence than AI-1 under physiological conditions, an observation that accords with previous studies showing that AI-2 is the major autoinducer during the early exponential phase of *V. harveyi* growth, while AI-1 and CAI-1 only appears at later stages (Anetzberger et al., 2012). The *luxS* null (AI-2⁻) mutant showed 98% less basal bioluminescence in comparison to wild-type, although it still emits bioluminescence. The *luxM* null (AI-1⁻) mutant showed a 40% reduction in basal bioluminescence in comparison to wild-type. Interestingly, CBG did not reduce the bioluminescence of the *luxS* null mutant, while still had a significant effect on the *luxM* null mutant. This means that the major anti-quorum sensing effect of CBG acts on interfering with the AI-2-dependent signals.

A surprising result was the observation that the *luxP* and *luxQ* null mutants deficient in the AI-2 receptor still responded well to the anti-QS activity of CBG. These mutants differed from the *luxS* mutant in still showing high bioluminescence, which might be due to the lack of agonism of the AI-2 receptor on LuxU/LuxO. The *luxP* and *luxQ* mutants rely mainly on the AI-1/LuxN for the induction of bioluminescence suggesting that it is this pathway that is targeted by CBG. We observed that the *luxN* null mutant responded less well to CBG than wild-type, providing further support that LuxN is a target of CBG. It is worth noting that the LuxN has nine transmembrane regions (Swem et al., 2008) and CBG is a hydrophobic molecule (Figure 1). It could be presumed that this structure of LuxN may facilitate the transport of the CBG molecules into the bacteria. Another possibility is that CBG increases the agonistic effect of LuxN on LuxU, by either increasing the LuxN kinase activity, or preventing the LuxN-mediated dephosphorylation of LuxU. In both cases, the response regulator LuxO will be kept active and antagonizes the master regulator LuxR involved in biofilm formation and bioluminescence. Indeed, gene expression studies showed that CBG induced the gene expression of *luxU* and *luxO* as well as the LuxO-regulated genes *aphA*, *hfq* and the small regulatory RNAs *qrr1-5*, demonstrating that CBG does increase the LuxO activity in *V. harveyi*. Concomitant with the increased LuxO activity, the *LuxR* gene expression was strongly reduced by CBG, which explains the anti-quorum and anti-biofilm activity of CBG (Figure 8).

In summary, the present study demonstrates the antagonistic effects of the *Cannabis* component CBG on QS-mediated processes in *V. harveyi*, including bioluminescence, biofilm formation and motility, at concentrations that do not affect planktonic growth. CBG antagonizes both the AI-1 and AI-2 pathways, through acting, among others, on LuxN with resulting increase in LuxO activity. The interference of CBG with the bacterial signal-transduction system provides a novel innovative way to combat bacterial biofilm formation.

DATA AVAILABILITY STATEMENT

The datasets generated for this study are available on request to the corresponding author.

AUTHOR CONTRIBUTIONS

MA, RG, RS, BZ, MF, and DS conceived the idea. MA designed and performed the experiments and analyzed the data. MA wrote the paper with RS and DS.

FUNDING

This study was partially supported by STEP-GTP sisters fellowship (2019–2020) and The Israeli Ministry of Agriculture (2017–2020, 0394928).

ACKNOWLEDGMENTS

We are grateful to Dr. Vitaly Gutkin at the Hebrew University Center for Nanoscience and Nanotechnology, for his assistance with the SEM analysis. We would like to thank Dr. Danielle Duanis Assaf and Dr. Mark Feldman for their scientific support. MA would also like to thank Dr. Mustafa Abu Dalu for his support for this study.

SUPPLEMENTARY MATERIAL

The Supplementary Material for this article can be found online at: <https://www.frontiersin.org/articles/10.3389/fmicb.2020.00858/full#supplementary-material>

REFERENCES

- Aharoni, R., Bronstheyn, M., Jabbour, A., Zaks, B., Srebnik, M., and Steinberg, D. (2008). Oxazaborolidine derivatives inducing autoinducer-2 signal transduction in *Vibrio harveyi*. *Bioorg. Med. Chem.* 16, 1596–1604. doi: 10.1016/j.bmc.2007.11.032
- Anetzberger, C., Reiger, M., Fekete, A., Schell, U., Stambrau, N., Plener, L., et al. (2012). Autoinducers act as biological timers in *Vibrio harveyi*. *PLoS One* 7:e48310. doi: 10.1371/journal.pone.0048310
- Appendino, G., Gibbons, S., Giana, A., Pagani, A., Grassi, G., Stavri, M., et al. (2008). Antibacterial cannabinoids from *Cannabis sativa*: a structure-activity study. *J. Nat. Prod.* 71, 1427–1430. doi: 10.1021/np8002673
- Asfour, H. Z. (2018). Anti-quorum sensing natural compounds. *J. Microsc. Ultrastruct.* 6, 1–10. doi: 10.4103/JMAU.JMAU_10_18
- Assaf, D., Steinberg, D., and Shemesh, M. (2014). Lactose triggers biofilm formation by *Streptococcus mutans*. *Int. Dairy J.* 42, 51–57.
- Bassler, B. L., Greenberg, E. P., and Stevens, A. M. (1997). Cross-species induction of luminescence in the quorum-sensing bacterium *Vibrio harveyi*. *J. Bacteriol.* 179, 4043–4045. doi: 10.1128/jb.179.12.4043-4045.1997

- Bassler, B. L., Wright, M., Showalter, R. E., and Silverman, M. R. (1993). Intercellular signalling in *Vibrio harveyi*: sequence and function of genes regulating expression of luminescence. *Mol. Microbiol.* 9, 773–786. doi: 10.1111/j.1365-2958.1993.tb01737.x
- Bassler, B. L., Wright, M., and Silverman, M. R. (1994). Multiple signalling systems controlling expression of luminescence in *Vibrio harveyi*: sequence and function of genes encoding a second sensory pathway. *Mol. Microbiol.* 13, 273–286. doi: 10.1111/j.1365-2958.1994.tb00422.x
- Borrelli, F., Fasolino, I., Romano, B., Capasso, R., Maiello, F., Coppola, D., et al. (2013). Beneficial effect of the non-psychotropic plant cannabinoid cannabigerol on experimental inflammatory bowel disease. *Biochem. Pharmacol.* 85, 1306–1316. doi: 10.1016/j.bcp.2013.01.017
- Brierley, D. I., Samuels, J., Duncan, M., Whalley, B. J., and Williams, C. M. (2016). Cannabigerol is a novel, well-tolerated appetite stimulant in pre-satiated rats. *Psychopharmacology* 233, 3603–3613. doi: 10.1007/s00213-016-4397-4
- Chen, X., Schauder, S., Potier, N., Van Dorsselaer, A., Pelczer, I., Bassler, B. L., et al. (2002). Structural identification of a bacterial quorum-sensing signal containing boron. *Nature* 415, 545–549. doi: 10.1038/415545a
- Eisohly, H. N., Turner, C. E., Clark, A. M., and Eisohly, M. A. (1982). Synthesis and antimicrobial activities of certain cannabichromene and cannabigerol related compounds. *J. Pharm. Sci.* 71, 1319–1323. doi: 10.1002/jps.2600711204
- Feldman, M., Al-Quntar, A., Polachek, I., Friedman, M., and Steinberg, D. (2014). Therapeutic potential of thiazolidinedione-8 as an antibiofilm agent against *Candida albicans*. *PLoS One* 9:e93225. doi: 10.1371/journal.pone.0093225
- Feldman, M., Weiss, E. I., Ofek, I., and Steinberg, D. (2009). Interference of cranberry constituents in cell-cell signaling system of *Vibrio harveyi*. *Curr. Microbiol.* 59, 469–474. doi: 10.1007/s00284-009-9462-3
- Freeman, J. A., and Bassler, B. L. (1999). A genetic analysis of the function of LuxO, a two-component response regulator involved in quorum sensing in *Vibrio harveyi*. *Mol. Microbiol.* 31, 665–677. doi: 10.1016/j.gene.2005.10.031
- Friedman, L., Smoum, R., Feldman, M., Mechoulam, R., and Steinberg, D. (2019). Does the endocannabinoid anandamide affect bacterial quorum sensing, vitality, and motility? *Cannabis Cannabinoid Res.* 4, 102–109.
- Giacoppo, S., Gugliandolo, A., Trubiani, O., Pollastro, F., Grassi, G., Bramanti, P., et al. (2017). Cannabinoid CB2 receptors are involved in the protection of RAW264.7 macrophages against the oxidative stress: an in vitro study. *Eur. J. Histochem.* 61:2749. doi: 10.4081/ejh.2017.2749
- Jiang, T., Zhu, P., Du, L., and Li, M. (2018). Identification of AI-2 quorum sensing inhibitors in *Vibrio harveyi* through structure-based virtual screening. *Methods Mol. Biol.* 1673, 353–362. doi: 10.1007/978-1-4939-7309-5_26
- Louwakul, P., Saelo, A., and Khemleelakul, S. (2017). Efficacy of calcium oxide and calcium hydroxide nanoparticles on the elimination of *Enterococcus faecalis* in human root dentin. *Clin. Oral Investig.* 21, 865–871. doi: 10.1007/s00784-016-1836-x
- Mok, K. C., Wingreen, N. S., and Bassler, B. L. (2003). *Vibrio harveyi* quorum sensing: a coincidence detector for two autoinducers controls gene expression. *EMBO J.* 22, 870–881. doi: 10.1093/emboj/cdg085
- Mukherjee, S., and Bassler, B. L. (2019). Bacterial quorum sensing in complex and dynamically changing environments. *Nat. Rev. Microbiol.* 17, 371–382. doi: 10.1038/s41579-019-0186-5
- Ng, W. L., and Bassler, B. L. (2009). Bacterial quorum-sensing network architectures. *Annu. Rev. Genet.* 43, 197–222. doi: 10.1146/annurev-genet-102108-134304
- Olah, A., Markovics, A., Szabo-Papp, J., Szabo, P. T., Stott, C., Zouboulis, C. C., et al. (2016). Differential effectiveness of selected non-psychotropic phytocannabinoids on human sebocyte functions implicates their introduction in dry/seborrheic skin and acne treatment. *Exp. Dermatol.* 25, 701–707. doi: 10.1111/exd.13042
- O'Toole, G. A. (2011). Microtiter dish biofilm formation assay. *J. Vis. Exp.* 30:2437. doi: 10.3791/2437
- Packiavathy, I. A., Sasikumar, P., Pandian, S. K., and Veera Ravi, A. (2013). Prevention of quorum-sensing-mediated biofilm development and virulence factors production in *Vibrio* spp. by curcumin. *Appl. Microbiol. Biotechnol.* 97, 10177–10187. doi: 10.1007/s00253-013-4704-5
- Papenfort, K., and Bassler, B. L. (2016). Quorum sensing signal-response systems in Gram-negative bacteria. *Nat. Rev. Microbiol.* 14, 576–588. doi: 10.1038/nrmicro.2016.89
- Pereira, C. S., Thompson, J. A., and Xavier, K. B. (2013). AI-2-mediated signalling in bacteria. *FEMS Microbiol. Rev.* 37, 156–181.
- Periasamy, S., and Kolenbrander, P. E. (2009). Mutualistic biofilm communities develop with *Porphyromonas gingivalis* and initial, early, and late colonizers of enamel. *J. Bacteriol.* 191, 6804–6811. doi: 10.1128/JB.01006-09
- Rutherford, S. T., and Bassler, B. L. (2012). Bacterial quorum sensing: its role in virulence and possibilities for its control. *Cold Spring Harb. Perspect. Med.* 2:a012427. doi: 10.1101/cshperspect.a012427
- Rutherford, S. T., van Kessel, J. C., Shao, Y., and Bassler, B. L. (2011). AphA and LuxR/HapR reciprocally control quorum sensing in *vibrios*. *Genes Dev.* 25, 397–408. doi: 10.1101/gad.2015011
- Singh, B. N., Singh, B. R., Singh, R. L., Prakash, D., Sarma, B. K., and Singh, H. B. (2009). Antioxidant and anti-quorum sensing activities of green pod of *Acacia nilotica* L. *Food Chem. Toxicol.* 47, 778–786. doi: 10.1016/j.fct.2009.01.009
- Soni, D., Smoum, R., Breuer, A., Mechoulam, R., and Steinberg, D. (2015). Effect of the synthetic cannabinoid HU-210 on quorum sensing and on the production of quorum sensing-mediated virulence factors by *Vibrio harveyi*. *BMC Microbiol.* 15:159. doi: 10.1186/s12866-015-0499-0
- Surette, M. G., Miller, M. B., and Bassler, B. L. (1999). Quorum sensing in *Escherichia coli*, *Salmonella typhimurium*, and *Vibrio harveyi*: a new family of genes responsible for autoinducer production. *Proc. Natl. Acad. Sci. U.S.A.* 96, 1639–1644. doi: 10.1073/pnas.96.4.1639
- Swem, L. R., Swem, D. L., Wingreen, N. S., and Bassler, B. L. (2008). Deducing receptor signaling parameters from *in vivo* analysis: LuxN/AI-1 quorum sensing in *Vibrio harveyi*. *Cell* 134, 461–473. doi: 10.1016/j.cell.2008.06.023
- Tu, K. C., and Bassler, B. L. (2007). Multiple small RNAs act additively to integrate sensory information and control quorum sensing in *Vibrio harveyi*. *Genes Dev.* 21, 221–233. doi: 10.1101/gad.1502407
- Turner, S. E., Williams, C. M., Iversen, L., and Whalley, B. J. (2017). Molecular pharmacology of phytocannabinoids. *Prog. Chem. Org. Nat. Prod.* 103, 61–101.
- Vikram, A., Jayaprakash, G. K., Jesudhasan, P. R., Pillai, S. D., and Patil, B. S. (2010). Suppression of bacterial cell-cell signalling, biofilm formation and type III secretion system by citrus flavonoids. *J. Appl. Microbiol.* 109, 515–527. doi: 10.1111/j.1365-2672.2010.04677.x
- Waters, C. M., and Bassler, B. L. (2006). The *Vibrio harveyi* quorum-sensing system uses shared regulatory components to discriminate between multiple autoinducers. *Genes Dev.* 20, 2754–2767. doi: 10.1101/gad.1466506
- Yang, Q., and Defoirdt, T. (2015). Quorum sensing positively regulates flagellar motility in pathogenic *Vibrio harveyi*. *Environ. Microbiol.* 17, 960–968. doi: 10.1111/1462-2920.12420
- Zhang, Y., Qiu, Y., Tan, Y., Guo, Z., Yang, R., and Zhou, D. (2012). Transcriptional regulation of opaR, qrr2-4 and aphA by the master quorum-sensing regulator OpaR in *Vibrio parahaemolyticus*. *PLoS One* 7:e34622. doi: 10.1371/journal.pone.0034622

Conflict of Interest: The authors declare that the research was conducted in the absence of any commercial or financial relationships that could be construed as a potential conflict of interest.

Copyright © 2020 Aqawi, Gallily, Sionov, Zaks, Friedman and Steinberg. This is an open-access article distributed under the terms of the Creative Commons Attribution License (CC BY). The use, distribution or reproduction in other forums is permitted, provided the original author(s) and the copyright owner(s) are credited and that the original publication in this journal is cited, in accordance with accepted academic practice. No use, distribution or reproduction is permitted which does not comply with these terms.



Hyperosmotic Infusion and Oxidized Surfaces Are Essential for Biofilm Formation of *Staphylococcus capitis* From the Neonatal Intensive Care Unit

Yue Qu^{1,2,3*}, Yali Li^{4,5}, David R. Cameron², Christopher D. Easton⁴, Xuebo Zhu¹, Minli Zhu¹, Mario Salwiczek^{2,4}, Benjamin W. Muir⁴, Helmut Thissen⁴, Andrew Daley^{6,7}, John S. Forsythe⁵, Anton Y. Peleg^{2,3*} and Trevor Lithgow^{2*}

OPEN ACCESS

Edited by:

Silvia Buroni,
University of Pavia, Italy

Reviewed by:

Walter Zingg,
Geneva University Hospitals (HUG),
Switzerland

Ewa Szczuka,
Adam Mickiewicz University
in Poznań, Poland

Marine Butin,
Hopices Civils de Lyon, France

*Correspondence:

Yue Qu
yue.qu@monash.edu
Anton Y. Peleg
anton.peleg@monash.edu
Trevor Lithgow
trevor.lithgow@monash.edu

Specialty section:

This article was submitted to
Antimicrobials, Resistance
and Chemotherapy,
a section of the journal
Frontiers in Microbiology

Received: 10 December 2019

Accepted: 17 April 2020

Published: 13 May 2020

Citation:

Qu Y, Li Y, Cameron DR, Easton CD, Zhu X, Zhu M, Salwiczek M, Muir BW, Thissen H, Daley A, Forsythe JS, Peleg AY and Lithgow T (2020) Hyperosmotic Infusion and Oxidized Surfaces Are Essential for Biofilm Formation of *Staphylococcus capitis* From the Neonatal Intensive Care Unit. *Front. Microbiol.* 11:920. doi: 10.3389/fmicb.2020.00920

¹ The Neonatal Intensive Care Unit, The Second Affiliated Hospital and Yuying Children's Hospital of Wenzhou Medical University, Wenzhou, China, ² Infection and Immunity Theme, Department of Microbiology, Biomedicine Discovery Institute, Monash University, Clayton, VIC, Australia, ³ Department of Infectious Diseases, The Alfred Hospital and Central Clinical School, Monash University, Melbourne, VIC, Australia, ⁴ The Commonwealth Scientific and Industrial Research Organisation (CSIRO) Manufacturing, Clayton, VIC, Australia, ⁵ Department of Materials Science and Engineering, Monash Institute of Medical Engineering, Monash University, Clayton, VIC, Australia, ⁶ Department of Microbiology, The Royal Children's Hospital, Parkville, VIC, Australia, ⁷ Department of Paediatrics, University of Melbourne, Parkville, VIC, Australia

Staphylococcus capitis is an opportunistic pathogen often implicated in bloodstream infections in the neonatal intensive care unit (NICU). This is assisted by its ability to form biofilms on indwelling central venous catheters (CVC), which are highly resistant to antibiotics and the immune system. We sought to understand the fundamentals of biofilm formation by *S. capitis* in the NICU, using seventeen clinical isolates including the endemic NRCS-A clone and assessing nine commercial and two modified polystyrene surfaces. *S. capitis* clinical isolates from the NICU initiated biofilm formation only in response to hyperosmotic conditions, followed by a developmental progression driven by *icaADBC* expression to establish mature biofilms, with polysaccharide being their major extracellular polymer substance (EPS) matrix component. Physicochemical features of the biomaterial surface, and in particular the level of the element oxygen present on the surface, significantly influenced biofilm development of *S. capitis*. A lack of highly oxidized carbon species on the surface prevented the immobilization of *S. capitis* EPS and the formation of mature biofilms. This information provides guidance in regard to the preparation of hyperosmolar total parenteral nutrition and the engineering of CVC surfaces that can minimize the risk of catheter-related bloodstream infections caused by *S. capitis* in the NICU.

Keywords: *Staphylococcus capitis*, biofilms, bloodstream infections, NICU, central venous catheters, surface chemistry, oxidized surfaces

INTRODUCTION

Premature newborns given intensive care and prolonged hospitalization in the neonatal intensive care unit (NICU) are peculiarly prone to infections, due to their immature immune system and invasive medical procedures such as catheterization (Beck-Sague et al., 1994). Catheter-related bloodstream infections (CRBSI) are common and occur at a rate of 1–18 infections per 1,000 central

line days (Blanchard et al., 2013; Yumani et al., 2013; Dubbink-Verheij et al., 2017). These infections are often associated with significant mortality and morbidity and contribute to high healthcare costs (Payne et al., 2004).

Staphylococcus capitis is an emerging opportunistic pathogen causing bloodstream infections in the NICU (Wang et al., 1999; Rasigade et al., 2012; Cui et al., 2013; Cheong et al., 2016). Neonatal patients infected with *S. capitis* often experience more severe morbidity relative to that of non-*S. capitis* coagulase-negative staphylococci (CoNS) (Ben Said et al., 2016). One specific clone of *S. capitis*, NRCS-A, was found to be highly endemic in the NICU and may have caused most *S. capitis* sepsis in neonatal patients worldwide (Butin et al., 2017a,b; Stenmark et al., 2019). In the NICU, *S. capitis* has been frequently isolated from central venous catheters (CVCs) explanted from CRBSI patients, supporting an important role of CVCs as the reservoir of invading bacteria (Ory et al., 2019). Past studies suggested that biofilm formation by *S. capitis* on medical devices such as CVCs correlates with its potential to establish infections (De Silva et al., 2002; Bradford et al., 2006). A direct link between neonatal sepsis caused by *S. capitis* and CVC implantation, however, has been questioned (Wang et al., 1999; Butin et al., 2019). Regardless, the importance of medical device surfaces as a host for bacterial colonization and biofilm formation has been well-established (Salwiczek et al., 2014). Direct contamination of implanted CVCs by bacteria from the NICU environment, patients' skin or microbial translocation from the gut, throat or nostrils of patients, and subsequently bacterial adherence and biofilm formation are considered the key initiating steps of CRBSI (Hitzenbichler et al., 2017).

Antibiotic treatments of *S. capitis* infections in the NICU are often suboptimal due to their intrinsic and emerging resistance to many first-line antibiotics, and their capacity to form biofilms on implanted medical devices (Butin et al., 2015, 2019; Zhou et al., 2015). Biofilm formation is a self-defensive strategy of many microorganisms to survive adverse environments including long-term antibiotic exposure (Otto, 2008, 2013). For members of the genus *Staphylococcus*, including *Staphylococcus aureus*, *Staphylococcus epidermidis* and *S. capitis*, a characteristic feature of their biofilm formation is the inter-cellular adhesion associated with the production of polysaccharide intercellular adhesin (PIA), a linear β -glucosaminoglycan (Poly- β -1,6-GlcNAc) attached to the cell surface (Mack et al., 1994; Heilmann et al., 1996; Cui et al., 2013). The synthesis and secretion of PIA in staphylococci depends on the gene cluster *icaADBC*; disruption of *icaADBC* prevents cellular aggregation and biofilm formation (Gerke et al., 1998; Vermont et al., 1998; Frebourg et al., 2000; Galdbart et al., 2000; Arciola et al., 2001; Cui et al., 2013).

New antibiofilm strategies such as ethanol lock therapy and impregnating catheter surfaces with antibiotics have been recently examined in large-scale clinical trials targeting pediatric and neonatal patients (Wolf et al., 2018; Gilbert et al., 2019). Failure of these strategies in preventing CRBSI in young populations highlights an urgent need for more effective prophylaxis. This study sought to establish a comprehensive understanding of the interactions between *S. capitis* and biomaterials at the pathogen-medical device interface, and

to provide valuable insights into more effective preventative strategies against CRBSI caused by *S. capitis* in the NICU.

MATERIALS AND METHODS

Strains and Growth Conditions

Seventeen *S. capitis* clinical isolates (isolates 6, 8, 11, 17, 18, 19, 21, 25, 44, 52, 57, 61, 70, 76, 77, 80, 91) from blood cultures of infants at the Royal Women's Hospital NICU (Parkville, Victoria, Australia) with confirmed bloodstream infections were used in this study for biofilm formation under different conditions. All isolates except isolates 44 and 77 belong to *S. capitis* subsp. *urealyticus*; isolates 44 and 77 belong to *S. capitis* subsp. *capitis* (Cui et al., 2013). These isolates typify a large collection of strains responsible for 55 episodes of sepsis in the NICU over the period 2000–2005 (Bradford et al., 2006; Cui et al., 2013). Eight isolates belonging to the unique NRCS-A clone (isolates 6, 8, 11, 17, 18, 19, 21, and 25), based on *smal* pulsed-field gel electrophoresis (PFGE) analysis were further selected to study interactions between *S. capitis* and biomaterials with different surface characteristics (D'mello et al., 2008; Butin et al., 2017b). Biofilm-positive *S. epidermidis* strain RP62A (ATCC 35984) and biofilm-negative *S. hominis* strain SP2 (ATCC 35982) were included as controls for biofilm production.

Biofilm Cultivation and Imaging

Bacterial biofilms were cultured in 96-well microplates and quantitatively assessed using an established method (Deighton et al., 2001). Tryptic soya broth (TSB, Oxoid), TSB with 4% NaCl, TSB with 1% glucose, and TSB with 4% ethanol were selected as biofilm growth media representing different environmental cues encountered in the NICU. Nine commercially available polystyrene microplates with different surface characteristics were tested, including DNA-BIND (Corning), Carbo-BIND (Corning), Universal-BIND (Corning), Not Treated (Corning), CellBIND (Corning), Ultra-Low-Attachment (Corning), Immobilizer (Corning), Tissue Culture Polystyrene (TCPS) from NUNC, and TCPS from BD Falcon. Biofilms were also established on 96-well microplate cutouts (BD Falcon) using TSB with 4% NaCl and qualitatively examined with confocal laser scanning microscopy (CLSI) as described previously (Qu et al., 2009). CLSI images were obtained on a Leica SP5 microscope. SYTO-9 (3.35 μ M, 15 min, 22°C) and Alexa Fluor 555 conjugated wheat germ agglutinin (WGA, 10 μ g/mL, 1 h, 22°C) were used to stain the biofilms sequentially. All biofilm experiments for quantitative analysis were repeated at least three times in triplicate, and qualitative assays were repeated at least three times.

Structural Analysis of *S. capitis* Biofilms

The composition of *S. capitis* biofilms was analyzed by treating mature biofilms with extracellular polymer substance (EPS) matrix-disrupting chemicals/enzymes respectively, including DNase I at 5 mg/mL, proteinase K at 100 μ g/mL, and sodium metaperiodate (NaIO₄) at 10 mM, for 2 h at 37°C with shaking (75 rpm) (Qin et al., 2007). Different buffers were used to prepare

chemical/enzymatic solutions (5 mM MgCl₂ and 5 mM CaCl₂ for DNase I, 20 mM Tris-HCl and 5 mM CaCl for proteinase K, and 50 mM sodium acetate, pH = 4.5 for NaIO₄). This was to ensure the maximum efficacy and stability of these reagents. Control wells were treated with buffer alone. The biofilm composition analysis assays were repeated at least three times in triplicate.

qPCR Analysis

Quantitative real-time (qRT)-PCR was used to assess expression of *icaADBC* and *icaR* by *S. capitis* after growth in TSB or TSB with 4% NaCl at 37°C for 5.5 h (Chaffin et al., 2012). Primers were designed based upon the *ica* sequence of *S. capitis* isolate 6 (Genbank JF930147.1; **Table 1**). As an internal control, 16S rRNA levels were quantified. Relative gene expression was determined using the $2^{-\Delta\Delta C_T}$ method (Schmittgen and Livak, 2008). These experiments were repeated on three different occasions in technical triplicate.

Atomic Force Microscopy (AFM)

An Asylum Research MFP-3D atomic force microscope (Santa Barbara, CA) was used to assess the surface topography of the bottom of microwells in different polystyrene microplates. Tapping mode was used for imaging in air with ultrasharp silicon nitride tips (NSC15 non-contact silicon cantilevers, Mikro-Masch, Spain). The tips had a typical force constant of 40 N/m and a resonant frequency of 320 kHz. Typical scan settings involved the use of an applied piezo deflection voltage of 0.6–0.7 V at a scan rate of 0.8 Hz. All images were processed (1st order flattening algorithm) using Igor Pro software and arithmetic mean roughness (Ra) values were extracted. The experiments were repeated three times.

X-Ray Photoelectron Spectroscopy (XPS) Analysis

XPS analysis was performed on the bottom of microwells originating from 96-well microplates using an AXIS HSi spectrometer (Kratos Analytical Ltd., United Kingdom) equipped with a monochromated Al-K α X-ray source at a power of 144 W

(12 mA, 12 kV). Instrument settings can be found elsewhere (Li et al., 2014). XPS analysis was performed using a method similar to that previously reported (Telford et al., 2012). Data processing was performed using CasaXPS processing software version 2.3.15 (Casa Software Ltd., Teignmouth, United Kingdom). Binding energies were referenced to the C 1s peak at 284.8 eV (aromatic hydrocarbon). These experiments were repeated on three different occasions in duplicate.

Surface Modification of Untreated Polystyrene Microplates

Ozone treatment and diethylene glycol dimethyl ether plasma polymer (DGpp) deposition were carried out on untreated polystyrene surfaces (Corning Not Treated microplates) to provide an oxidized surface chemistry. For ozone treatment, the microplate was placed in a UV/Ozone ProCleaner™ (BioForce) and exposed for 5 min. For DGpp deposition, plasma polymerization was carried out in a custom-built plasma reactor described previously (Li et al., 2014). The plasma deposition of films was performed using a frequency of 125 kHz, load power of 50 W and initial monomer pressure of 20 Pa with a treatment time of 120 s (final pressure 61 Pa).

Immobilization of Biofilm EPS Matrix on Microplate Surfaces

EPS matrix was isolated from staphylococcal biofilms following the method described by Taff et al. (2012). Biofilm matrix supernatants (100 μ L) were added into microwells in TCPS microplates (BD Falcon) and Not Treated microplates (Corning) and incubated for 3 or 20 h, at 37°C with gentle shaking (75 rpm). After washing with distilled water, the biofilm matrices immobilized on the surfaces were stained with Alexa Fluor 488 conjugated WGA (10 μ g/mL, 1 h in the dark) before imaging with an Olympus IX81 fluorescence microscope. Three biological repeats were carried out for this experiment.

Biofilm Formation and Surface Chemistry of Pediatric Central Venous Catheters

Pediatric double-lumen central venous catheters with blue FlexTip® (CVCs, Arrow, Teleflex Medical, North Carolina, United States) were pre-treated with fetal bovine serum (Sigma-Aldrich, Sydney, Australia) overnight before biofilm growth or surface chemistry analysis. This was to mimic the pre-exposure of implanted CVCs to human serum in late-onset catheter related bloodstream infections. CVCs were washed twice with PBS and cut to sections of 5 mm for biofilm analysis or 15 mm for surface chemistry analysis. For qualitative biofilm analysis, catheter sections were cultivated with *S. capitis* isolate 6 in TSB with 4% NaCl at 1×10^7 CFU/mL for 24 h, cut open in the middle, and prepared for scanning electron microscopy (Uwamahoro et al., 2012). For catheter surface chemistry analysis, all samples were suspended over the sample bar using a mask. To analyze the interior surface of the catheter, the double-lumen tube was cut open in the middle, and carefully

TABLE 1 | Oligonucleotide primers used in this study.

<i>icaR</i> F	CCATAGATATATTGGAGGGATCA
<i>icaR</i> R	GTCCAATTATCCAGTGCACC
<i>icaA</i> F	TATGAACACGTGCCATGTG
<i>icaA</i> R	CTTCATGTCCACCTTGAGCC
<i>icaD</i> F	AGGGAGAGCTTATTCATTGCG
<i>icaD</i> R	CTCCACGTTAAGAGCGATACG
<i>icaB</i> F	GGATATGATCAGCAGCCTC
<i>icaB</i> R	GCAGACACATTAGACGCCTC
<i>icaC</i> F	CACGGTTCAAATGATAAGCGC
<i>icaC</i> R	GAAACCGCTAAGAAGACGACC
16S rRNA F ^a	AGCAACGCGAAGAACCTTAC
16S rRNA R ^b	CAACATCTCACGACACGAGC

^aF, forward. ^bR, reverse.

spread flat. XPS analysis and data analysis were performed as described before. Untreated CVCs were also tested to make comparisons. Surface chemistry analysis of the CVC was repeated three times in duplicate, and biofilm scanning electron microscopy was repeated three times.

Statistical Analyses

To analyze differences in biofilm formation under different environmental conditions and on different surfaces, one-way ANOVA tests were performed with Minitab 19 for Windows using a significance level of 0.05 (p -value). Spearman correlation test was performed to determine the strength of a monotonic relationship between biofilm formation of *S. capitis* and biomaterial surface properties.

Ethics Review and Approval

This study used strains obtained from RMIT University, Australia. Monash University did not require the study to be reviewed or approved by an ethics committee because these strains were provided to the research team in isolation from any references to individual patients. The Australian National Statement on Ethical Conduct in Human Research covers the use of human participants, their data, or tissues or body fluids. Using these microorganisms was not considered subject to ethical review by the Human Research Ethics Committee.

RESULTS

Hyperosmotic Conditions Are Essential for *S. capitis* Biofilm Formation in the NICU

BD falcon TCPS 96-well microplates were utilized for quantitative analysis of biofilm formation by 17 *S. capitis* isolates under different environmental conditions. All these 17 *S. capitis* isolates carry *ica* locus (Cui et al., 2013). Twelve out of 15 *S. capitis* subsp. *urealyticus* clinical isolates formed biofilms. Among them, 10 isolates only produced biofilms in response to hyperosmotic conditions (4% (w/v) NaCl) but not under other environmental influences, such as TSB only, TSB with 1% glucose or 4% ethanol (Figure 1A). Two *S. capitis* subsp. *capitis* (clinical isolates 44 and 77) failed to form biofilms under any of the studied conditions. As controls, *S. epidermidis* RP62A formed biofilms under all environmental conditions studied, while *S. hominis* SP2 did not form biofilms under any of the conditions (Figure 1A). Other hyperosmotic conditions such as the presence of NaCl at 2% (w/v), KCl or MgCl₂ at 2–4% (w/v) were also able to induce biofilm formation of *S. capitis* (data not shown).

Quantitative RT-PCR showed that hyperosmotic treatment stimulated expression of *icaADBC* in representative clinical isolates of *S. capitis*, isolates 6, 80 and 91, with the mRNA levels for the *icaA*, *icaD*, *icaB*, *icaC* genes increased by 10–60-fold (Figure 1B).

Structural Analysis of Biofilms Formed by *S. capitis* Under Hyperosmotic Conditions

We quantitatively analyzed the composition of biofilms of isolates 6 and 19, by challenging established biofilms with component-disrupting chemicals or enzymes. Isolates 6 and 19 were selected as they represented two PFGE clusters after digestion with restriction enzyme *SacII* (Cui et al., 2013). These two clusters were responsible for 34 out of 55 episodes of *S. capitis* bloodstream infections at the Royal Women's Hospital NICU between 2000 and 2005 (Cui et al., 2013). The addition of sodium metaperiodate, not DNase I or proteinase K, to established biofilms caused detachment of ~90% of the *S. capitis* biomass, suggesting a major role for PIA in the integrity of mature biofilms (Figure 2A). In order to visualize the relative mass of PIA in *S. capitis* biofilms, mature biofilms were formed on TCPS cutouts and stained with SYTO-9 and WGA. WGA is a lectin that specifically recognizes PIA in *S. epidermidis* biofilms (Sanford et al., 1995). Three-dimensional reconstruction of CLSM images revealed similar data from both isolates: the mass of PIA stained with WGA (Figure 2B, red) is equivalent to the cellular mass stained with SYTO-9 (Figure 2B, green) in biofilm structures and the PIA forms a surface cap across the top of the cellular layer.

Features of Biomaterial Surfaces Dictate the Formation of Biofilms by *S. capitis*

In the initial screening, no biofilm was formed by any of the 17 *S. capitis* isolates under any of the tested environmental conditions if TCPS was replaced by polystyrene microplates without surface treatment (Not Treated, Corning). This observation provided an opportunity to address the features of biomaterial surfaces that stimulates biofilm formation by *S. capitis* isolates from the NICU. We tested biofilm formation of eight *S. capitis* isolates of the NRCS-A clone in nine commercial microplates from different companies (see Methods). Only the CellBIND and TCPS microplates supported *S. capitis* biofilm formation (Table 2). Contact angle measurements reflect hydrophobicity of biomaterial surfaces, but these measurements only weakly correlate with biofilm formation of *S. capitis*, as found in this study [correlation coefficient $r = -0.030$, CI $(-0.810, 0.469)$]. AFM traces the topography of a surface and allows calculation of a mean surface roughness, but again only very weak correlation was found between biofilm formation and surface roughness (Figure 3A) as measured by AFM (Figure 3B) [correlation coefficient $r = 0.083$, CI $(-0.616, 0.709)$]. XPS is a surface-sensitive technique used to quantify the elemental composition including oxygen, nitrogen and carbon content in the outer layer of biomaterials (Table 2). Here, Spearman's correlation tests demonstrated a moderate correlation between biofilm formation and surface %O [correlation coefficient $r = 0.567$, CI $(-0.216, 0.906)$] or a strong correlation between biofilm formation and O/C ratio [correlation coefficient $r = 0.611$, CI $(-0.160, 0.919)$]. No such correlations were found for other elements (nitrogen or carbon species detected by XPS). Information regarding functional groups can be obtained from interpreting high-resolution spectra; as carbon is typically

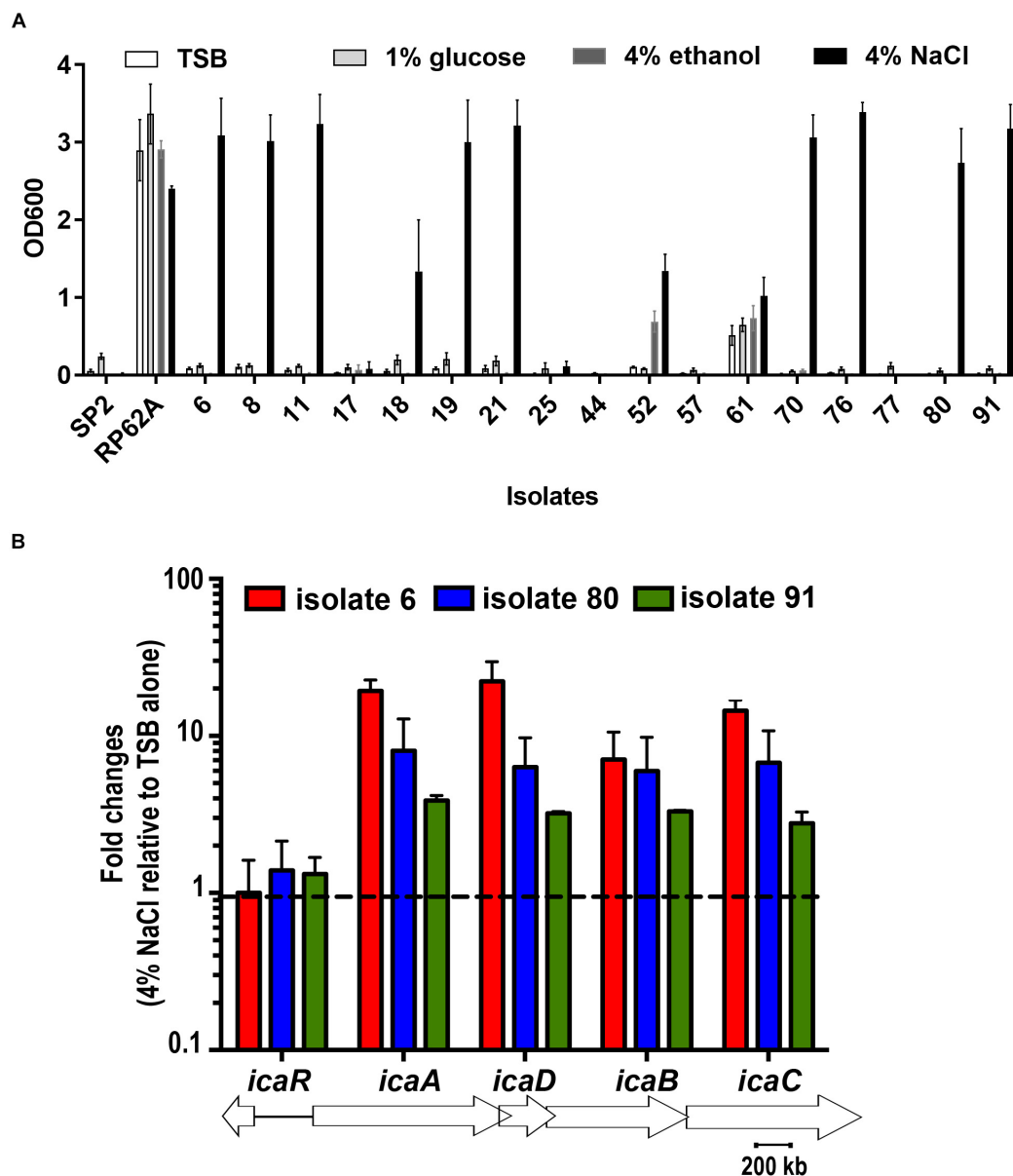


FIGURE 1 | (A) Biofilm formation of 17 clinical *S. capitis* isolates on tissue culture polystyrene (TCPS) surfaces under different environmental conditions. Microplates were seeded with bacteria in the indicated media, including Tryptic soya broth (TSB) only, TSB + 1% glucose, TSB + 4% ethanol, and TSB + 4% NaCl. Biofilm formation was monitored using crystal violet staining. Error bars represent standard errors of the means (SEM). **(B)** The indicated isolates were grown in TSB or in TSB + 4% NaCl for 5.5 h and the expression of *icaADBC* and *icaR* at these two conditions were analyzed and compared by quantitative reverse transcription polymerase chain reaction (RT-PCR). Isolates 8, 11, 18, 19, and 21 were also examined and showed similar results as isolates 6. Error bars represent SEM.

the most abundant element that can be detected by XPS in a polymer, it is often the most informative high-resolution spectrum (Figure 3C).

Highly Oxidized Surfaces Enable *S. capitis* EPS Immobilization and Promote Biofilm Maturation

When biofilm formation was monitored in distinct untreated polystyrene microplates two representative strains of *S. capitis*

(isolates 6 and 19) completed the early adherence phase of development, but failed to network the cell clusters even after 6 h incubation (Figure 4A). As polysaccharide was found to be the major component of *S. capitis* biofilm EPS matrix, a hypothesis was raised: a productive interaction between *S. capitis* EPS and highly oxidized surface might facilitate the networking needed for the subsequent phases of biofilm formation by *S. capitis*. Matrix materials extracted from mature biofilms of *S. capitis* could be immobilized on TCPS surfaces after a short exposure of 3 h, but not on untreated

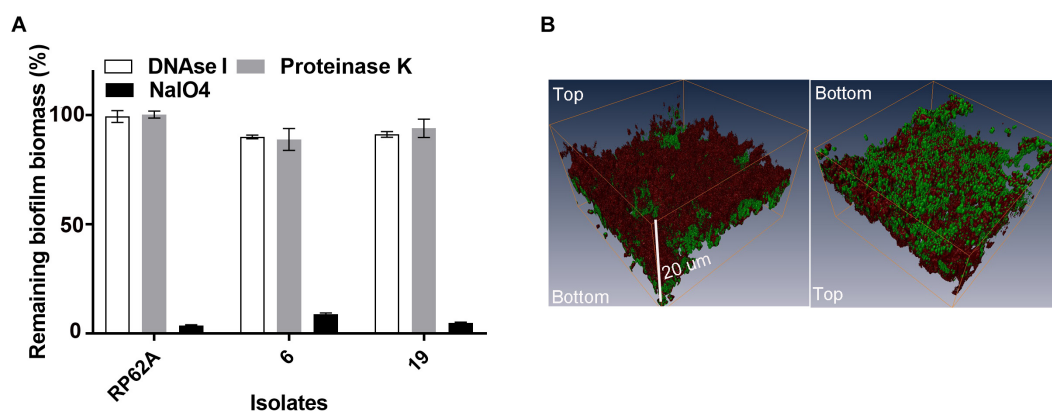


FIGURE 2 | (A) Analysis of the matrix composition of mature biofilms formed by *S. capitis*. **(A)** Mature biofilms (20 h old) were treated with 5 mg/mL of deoxyribonuclease I (DNase I), 10 mM of sodium periodate (NaIO₄), and 100 μg/mL of proteinase K for 2 h at 37°C, and the remaining biomass was assessed by crystal violet staining. **(B)** Confocal Laser Scanning Microscopy (CLSM) of *S. capitis* biofilms (isolate 6). Three-dimensional reconstructions show the staining pattern for polysaccharide intercellular adhesion [PIA, wheat germ agglutinin (WGA, red)] and cell mass (SYTO-9, green). The scale bar indicates the biofilm was ~20 μm thick.

TABLE 2 | Biofilm formation of *S. capitis* on different surfaces and their elemental composition [atomic% and atomic ratios (X/C)] derived from XPS survey spectra.

96-well microplates		Biofilm formation of isolates*									% Composition			Atomic ratios	
Maker	Surface treatment	RP62A	6	8	11	18	19	21	17	25	O 1s	N 1s	C 1s	O/C	N/C
Corning	DNA Bind	+	-	-	-	-	-	-	-	-	5.7 ± 0.3**	0.8 ± 0.1	93.5 ± 0.2	0.061 ± 0.003	0.008 ± 0.001
	Carbo-BIND	+	-	-	-	-	-	-	-	-	8.1 ± 1.6	4.7 ± 1.2	87.3 ± 2.7	0.093 ± 0.002	0.054 ± 0.015
	Universal-BIND	+	-	-	-	-	-	-	-	-	6.2 ± 0.5	NA	93.8 ± 0.5	0.066 ± 0.005	NA
	Not Treated	+	-	-	-	-	-	-	-	-	6.2 ± 0.3	NA	93.8 ± 0.3	0.066 ± 0.004	NA
	CellBIND	+	+	+	+	+	+	+	-	-	20.9 ± 0.5	1.2 ± 0.3	77.9 ± 0.6	0.269 ± 0.009	0.015 ± 0.004
	Ultra-Low Attachment	+	-	-	-	-	-	-	-	-	13.9 ± 1.0	11.0 ± 0.8	75.1 ± 1.7	0.185 ± 0.018	0.147 ± 0.014
NUNC	Immobilizer	+	-	-	-	-	-	-	-	-	12.2 ± 0.4	NA	87.8 ± 0.4	0.139 ± 0.005	NA
	TCPS	+	+	+	+	+	+	+	-	-	15.9 ± 0.2	NA	84.1 ± 0.2	0.190 ± 0.002	NA
Falcon	TCPS	+	+	+	+	+	+	+	-	-	16.4 ± 0.3	NA	83.6 ± 0.3	0.196 ± 0.004	NA
MODIFIED SURFACES															
	Ozone treated	+	+	+	+	+	+	+	-	-	11.9 ± 0.4	NA	88.1 ± 0.4	0.135 ± 0.005	NA
	DGpp treated	+	+	+	+	+	+	+	-	-	19.3 ± 0.2	NA	80.7 ± 0.2	0.239 ± 0.003	NA

*Only “+” and “-” are presented here to increase the readability of the table. +: biofilm-positive, with an OD600 > 0.24, -: biofilm-negative, with an OD600 < 0.12. Average biofilm biomass (OD600) of six biofilm-positive *S. capitis* strains on different surfaces were used for correlation analysis. **Presented in mean ± standard deviation. NA means there is no signal. XPS, X-ray photoelectron spectroscopy; O, oxygen; N, nitrogen; C, carbon; DGpp, diethylene glycol dimethyl ether plasma polymer.

polystyrene surface even when the exposure was extended to 20 h (Figure 4B).

Surface Chemistry of Pediatric Central Venous Catheters and *S. capitis* Biofilm Formation

To determine whether the model polystyrene surfaces are reflective of the surface of vascular access devices, sections of pediatric CVCs were subjected to biofilm formation and XPS analysis (Figure 5 and Table 3). Surfaces of untreated CVCs were found to have typical polyurethane surface chemistry (as per manufacturer’s information), but additional properties also, and partially supported biofilm formation of *S. capitis* under hyperosmotic conditions (Table 3 and Figure 5). Both exterior and interior surfaces of the untreated CVC contain oxygen

(10.7 ± 0.0% and 8.6 ± 0.2%, respectively) (Table 3). Exposure of CVCs to serum increased the oxygen level of exterior and interior surfaces to 16.9 ± 0.4% and 13.2 ± 0.8%, respectively, similar to that of biofilm-positive polystyrene surfaces, and supported more robust biofilm growth (Figure 5).

DISCUSSION

S. capitis has been only occasionally linked to several infections in adult patients, including infective endarteritis, prosthetic joint infections, catheter-related peritonitis, skin and soft-tissue infections, prosthetic valve endocarditis and meningitis (Oud, 2011; Takano et al., 2011; Basic-Jukic, 2017; Tevell et al., 2017; Lourtet-Hascoet et al., 2018; Natsis and Cohen, 2018; Yamamoto and Ohmagari, 2018). This opportunistic pathogen seems to have

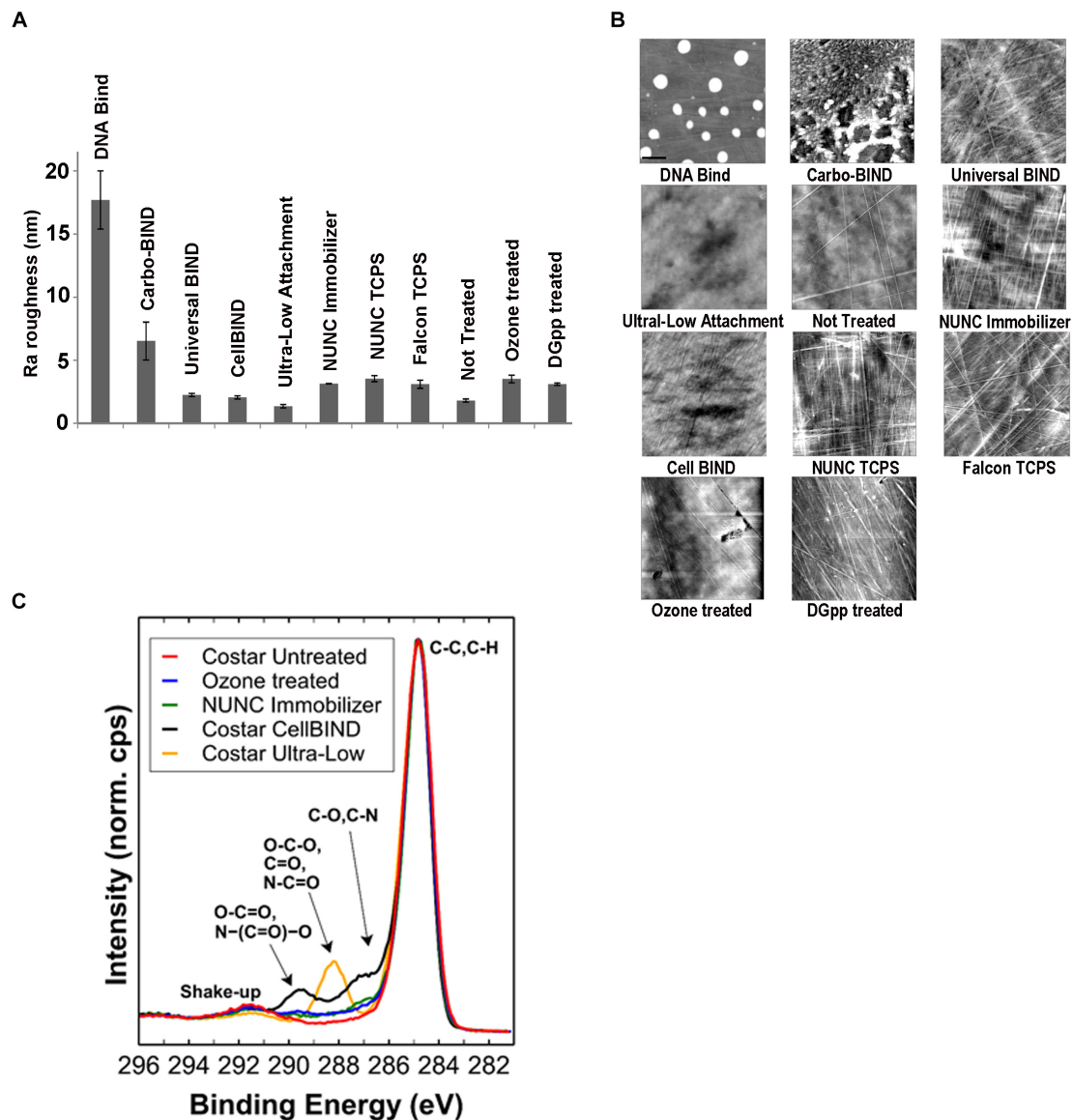


FIGURE 3 | Physicochemical characterization of biomaterial surfaces. **(A)** Roughness (Ra) values of different surfaces used in this study calculated from atomic force microscopy (AFM) scanning. Error bars represent SEM. **(B)** AFM tapping mode images of surface topographies. Images were collected over $10 \times 10 \mu\text{m}$ areas on microplates. For the DNA-Bind surface, the height trace image is displayed at 100 nm scale; all other images are displayed at 20 nm scale. **(C)** High-resolution C 1s spectral overlay including selected polystyrene samples. Spectra are normalized to maximum peak intensity of “Corning Not Treated” sample.

a greater clinical significance in the NICU, with a unique NRCS-A clone having caused many cases of severe sepsis in hospitalized neonates worldwide (Butin et al., 2016, 2017b). The current study examined biofilm formation of *S. capitis* isolated from the NICU and identified two key determinants that can be encountered in this specific clinical setting, including hyperosmotic conditions that activate the expression of biofilm operon *icaADBC* in *S. capitis* and highly oxidized surfaces that enable *S. capitis* EPS immobilization and biofilm maturation.

Biofilm formation of *S. capitis* has been found to be distinct from that of other coagulase-negative staphylococci that also cause CRBSI in the NICU (Cui et al., 2013). Using an evolutionary

model proposed by Qin et al. (2007) and data from Cui et al. (2013), we determined that biofilm formation of *S. capitis* isolated from the NICU was still at an early-mid stage in evolution: the majority of isolates are biofilm-positive through their ability to secrete sufficient PIA (*ica+*, PIA+); several isolates are able to express *ica* gene in response to hyperosmotic stimuli, but fail to produce PIA or form biofilms (*ica+*, PIA−). This is not surprising as the NICU was first introduced in 1960s and the evolutionary driving forces arising from the selection pressure of antibiotics for *S. capitis* are relatively contemporary. The (*ica+*, PIA−) phenotype has been previously characterized: isolate 17, for example, has a small deletion that removes three hydrophobic amino acids from

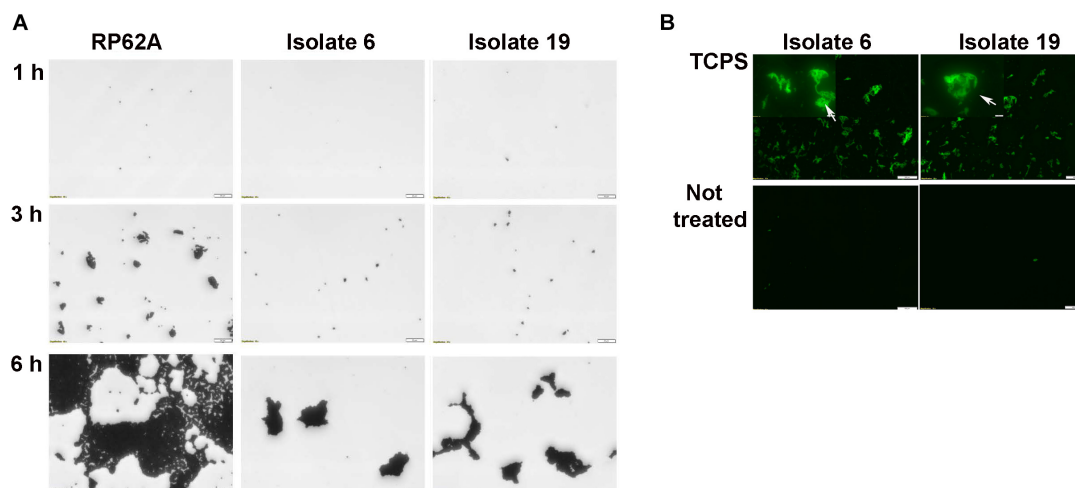


FIGURE 4 | Characterization of biofilm development of *S. capitis* isolates 6 and 19 on tissue culture polystyrene (TCPS) and Not Treated surfaces. **(A)** Biofilm development on the Not Treat surface in the first 6 h monitored by crystal violet staining and light microscopy. *S. capitis* isolates 6 and 19 failed to network their microcolony structures and form biofilms on Not Treated surfaces. *S. epidermidis* RP62a, used as a control, formed typical macrocolonies on the Not Treated surface at 6 h. Scale bar = 20 μ m. **(B)** Biofilm matrix of *S. capitis* isolates 6 and 9 was extracted, and the soluble extract was incubated with either TCPS or Not Treated surfaces, followed by wheat germ agglutinin (WGA) staining and fluorescence microscopy. Scale bar = 100 μ m.

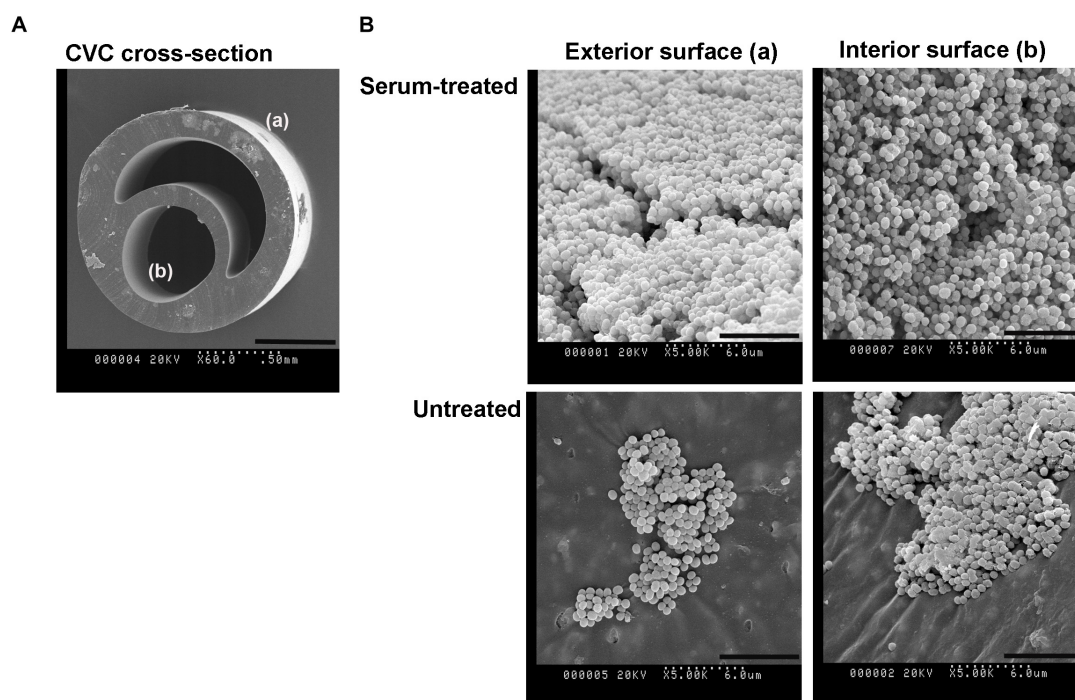


FIGURE 5 | *S. capitis* biofilm growth on pediatric central venous catheters (CVCs). **(A)** A cross-section of the double-lumen central venous catheter is shown, denoting the exterior surface (a), and interior surfaces (b). **(B)** CVCs were pre-treated with or without fetal bovine serum (FBS) overnight. After cultivation with *S. capitis* isolate 6, catheter sections were prepared for scanning electron microscopy; representative micrographs show robust biofilms on surfaces of serum-treated CVCs that contain high percentages of oxygen element. Scale bar = 0.5 mm (cross sections images) or 6 μ m (other images).

one of the critical transmembrane segments in IcaA, which would prevent IcaA assembly in the membrane and thereby prevent PIA production and biofilm formation (Cui et al., 2013). It is also possible that other *ica*-independent molecular mechanisms

might have been involved. Carter et al. (2018) recently reported that in contrast to the majority of NICU-associated *S. capitis* isolates that harbor *embp*, 2 out of 29 neonatal *S. capitis* clinical isolates lack this gene. *Embp* encodes a multifunctional cell

TABLE 3 | Elemental composition [atomic% and atomic ratios (X/C)] of pediatric CVCs derived from XPS survey spectra.

CVCs	Surfaces	% composition							Atomic ratios	
		Si 2p	S 2p	C 1s	N 1s	O 1s	Ba 3d	Na 1s	O/C	N/C
Untreated	Exterior	5.2 ± 0.0*	NA	80.7 ± 0.2	3.5 ± 0.2	10.7 ± 0.0	NA	NA	0.132 ± 0.000	0.043 ± 0.003
	Interior	1.3 ± 0.1	0.2 ± 0.0	85.8 ± 0.3	4.0 ± 0.1	8.6 ± 0.2	0.2 ± 0.0	NA	0.100 ± 0.002	0.046 ± 0.001
Serum-treated	Exterior	9.4 ± 1.1*	NA	69.7 ± 1.1	3.8 ± 0.5	16.9 ± 0.4	NA	0.1 ± 0.0	0.243 ± 0.010	0.055 ± 0.006
	Interior	2.1 ± 0.0	NA	77.4 ± 1.4	6.9 ± 0.7	13.2 ± 0.8	NA	0.4 ± 0.0	0.170 ± 0.013	0.089 ± 0.010

*Presented in mean ± standard deviation. NA means there is no signal. CVC, central venous catheter; XPS, X-ray photoelectron spectroscopy; Si, silicon; S, sulfur; C, carbon; N, nitrogen; O, oxygen; Ba, Barium; Na, sodium.

surface fibronectin binding protein and is critical for biofilm formation of *S. capitis* (Carter et al., 2018).

Unlike its close relative *S. epidermidis* that forms biofilms under many environmental conditions, *S. capitis* from the NICU appears to produce biofilms only under specific conditions. Most *S. capitis* isolates from the NICU require hyperosmotic condition for the activation of *icaADBC* and biofilm formation. Total parental nutrient (TPN) is frequently used in the NICU and might be the major source of hyperosmolarity. TPN has an osmolality up to 900 mOsm/L, ~3 times that of physiological saline (Boullata et al., 2014). Previous studies have listed infusion of TPN as an independent risk factor for biofilm-related CRBSI in the NICU (Beck-Sague et al., 1994; Boullata et al., 2014). Other infusates that might confer hyperosmolarity in the NICU include 3% NaCl solution that are occasionally used for the management of hyponatremia. Our study has also found that an osmolality as low as twice that of physiological saline readily induced biofilm formation of *S. capitis*. Preventing *S. capitis* infections by manipulating the osmolality of infusates in the NICU is thus less feasible.

A more practical strategy to prevent CRBSI in the NICU is to use non-permissive biomaterials for CVCs. We focused on the interaction between *S. capitis* and biomaterial surfaces. Although silicone and polyurethane are often preferred biomaterials for implantable medical devices including CVCs, we used polystyrene microplates to establish screening conditions to understand the formation of biofilms by *S. capitis*. The uniform sized and flat surfaces of these polystyrene microplates provided an ideal platform for quantitative and physicochemical analysis of biofilm formation. The available knowledge of how these commercially available surfaces are fabricated from the manufactures allows us to comparatively analyze surfaces that have different biological responses.

Analysis of the surface hydrophobicity and topography did not reveal differences in the surfaces examined that would explain the success or failure of biofilm formation. These findings are consistent with studies by others that found no significant correlation between biofilm formation of *S. epidermidis* and *S. aureus* and the contact angle, free energy, or roughness of biomaterial surfaces (Tidwell et al., 1997; Gottenbos et al., 2001; Hook et al., 2012). Surface chemistry however seems to play a critical role in the biofilm formation of *Staphylococcus* spp. (Hook et al., 2012; Mikulskis et al., 2018). We show that oxygen species present in the surface layer are essential for

biofilm formation of *S. capitis*: deliberate derivatization with oxygen species was necessary and sufficient to convert a surface that was non-permissive for biofilm formation into one which supported biofilm growth.

It has been proposed that surface cell growth correlates better to specific oxygen-containing functionalities than total oxygen content of a substratum (Tidwell et al., 1997; Hook et al., 2012). With the knowledge of how these surfaces are fabricated, and comparing O/C values presented in Table 2 and the high-resolution C 1s spectra (Figure 3C), it is expected that biofilm formation is also dependent on how the oxygen is presented at the surface, i.e., the functional groups. For example, surfaces of NUNC Immobilizer (O/C = 0.14) and Ozone treated (O/C = 0.14) microplates have almost identical concentrations of O, but biofilm formation occurs only in the Ozone treated microplate. A significant difference between these two microplates is the local environment of the O species on the surface which is influenced by how the oxygen was introduced to the surface. Ozone treatment of polystyrene surfaces is a non-specific modification that introduces a range of O species such as C-O, C = O, O-C-O, and O-C = O. This observation applies to all the surfaces that tested positive for biofilm formation in this study, as alternative discharge-based strategies employed herein such as Corona-gas treatment used for the CellBIND surface (as per manufacture's specification) are non-specific. In contrast, biofilm-negative NUNC Immobilizer is described by the manufacturer as presenting an ethylene glycol spacer and a stable electrophilic group, i.e., the surface chemistry is well-defined. The surface of Corning Ultra-Low Attachment microplate, which presents one of the highest values for O/C (0.19) is another well-defined biofilm-negative surface, described as having a covalently bound hydrogel layer (as per manufacture's specification), with the elemental quantification and C 1s spectrum suggesting a significant amount of amide groups present on the surface. All these suggest that surface treatments that introduce sufficient oxygen species in a non-specific manner result in biofilm formation. Findings derived from model polystyrene surfaces are further supported by experimental results from pediatric CVCs. Exposure of CVCs to serum significantly increased the oxygen composition of the surfaces, possibly due to the deposition of a conditioning film of host serum components, including proteins and electrolytes on the CVC surfaces. Such a conditioning film facilitates biofilm formation of *S. capitis*.

To address the detailed role of surface oxygen species in the biofilm formation of *S. capitis*, we further assessed the interaction between *S. capitis* biofilm EPS and biomaterial surfaces. It is well-known that EPS matrix plays an important role in the stability and antimicrobial resistance of mature biofilms (Flemming and Wingender, 2010). By biochemically dissecting the composition of *S. capitis* biofilms, we found PIA to be the predominant component of EPS matrix. This was further confirmed by high-resolution imaging using CLSM and PIA-specific staining. A specific binding between oxygen species and PIA was found: only on highly oxidized surfaces does PIA function as a crucial surface-binding adhesin, networking microcolonies and enabling the maturation stages of biofilm formation; otherwise similar surfaces were non-permissive to biofilm development.

Given the importance of biofilm formation in hospital-acquired infections, a deep understanding of the role that surface chemistry plays in this microbial developmental process offers opportunities for novel interventions. Based on our findings, we conclude that reducing the level of oxygen species on the biomaterial surface, for examples, using low-fouling surfaces for CVCs against protein adsorption (Salwiczek et al., 2014), as well as avoiding hyperosmotic treatments wherever possible would be a strategy to minimize infusion- and catheter-related *S. capitis* infections in the NICU. An evident limitation of this study is that it still suffers from an inability to comprehensively reflect the complexity of *in vivo* conditions in the NICU. Future studies that closely mimic the NICU environment and use CVCs with different surface oxygen levels should be conducted to verify the *in vitro* findings from this study.

REFERENCES

- Arciola, C. R., Baldassarri, L., and Montanaro, L. (2001). Presence of *icaA* and *icaD* genes and slime production in a collection of staphylococcal strains from catheter-associated infections. *J. Clin. Microbiol.* 39, 2151–2156. doi: 10.1128/JCM.39.6.2151-2156.2001
- Basic-Jukic, N. (2017). Acute peritonitis caused by *Staphylococcus capitis* in a peritoneal dialysis patient. *Perit. Dial. Int.* 37, 115–116. doi: 10.3747/pdi.2016.00083
- Beck-Sague, C. M., Azimi, P., Fonseca, S. N., Baltimore, R. S., Powell, D. A., Bland, L. A., et al. (1994). Bloodstream infections in neonatal intensive care unit patients: results of a multicenter study. *Pediatr. Infect. Dis. J.* 13, 1110–1116.
- Ben Said, M., Hays, S., Bonfils, M., Jourdes, E., Rasigade, J. P., Laurent, F., et al. (2016). Late-onset sepsis due to *Staphylococcus capitis* 'neonatalis' in low-birthweight infants: a new entity? *J. Hosp. Infect.* 94, 95–98. doi: 10.1016/j.jhin.2016.06.008
- Blanchard, A. C., Fortin, E., Rocher, I., Moore, D. L., Frenette, C., Tremblay, C., et al. (2013). Central line-associated bloodstream infection in neonatal intensive care units. *Infect. Control Hosp. Epidemiol.* 34, 1167–1173. doi: 10.1086/673464
- Boullata, J. I., Gilbert, K., Sacks, G., Labossiere, R. J., Crill, C., Goday, P., et al. (2014). A.S.P.E.N. clinical guidelines: parenteral nutrition ordering, order review, compounding, labeling, and dispensing. *JPEN J. Parenter Enteral. Nutr.* 38, 334–377. doi: 10.1177/0148607114521833
- Bradford, R., Abdul Manan, R., Daley, A. J., Pearce, C., Ramalingam, A., D'mello, D., et al. (2006). Coagulase-negative staphylococci in very-low-birth-weight infants: inability of genetic markers to distinguish invasive strains from blood culture contaminants. *Eur. J. Clin. Microbiol. Infect. Dis.* 25, 283–290. doi: 10.1007/s10096-006-0130-2
- Butin, M., Claris, O., and Laurent, F. (2019). Clinical impact of vancomycin heteroresistance in staphylococcal strains involved in neonatal sepsis: Discussion of a case report. *Arch. Pediatr.* 26, 236–237. doi: 10.1016/j.arcped.2019.03.002
- Butin, M., Martins-Simoes, P., Picaud, J. C., Kearns, A., Claris, O., Vandenesch, F., et al. (2015). Adaptation to vancomycin pressure of multiresistant *Staphylococcus capitis* NRCS-A involved in neonatal sepsis. *J. Antimicrob. Chemother.* 70, 3027–3031. doi: 10.1093/jac/dkv217
- Butin, M., Martins-Simoes, P., Pichon, B., Leyssene, D., Bordes-Couecou, S., Meugnier, H., et al. (2017a). Emergence and dissemination of a linezolid-resistant *Staphylococcus capitis* clone in Europe. *J. Antimicrob. Chemother.* 72, 1014–1020. doi: 10.1093/jac/dkw516
- Butin, M., Martins-Simoes, P., Rasigade, J. P., Picaud, J. C., and Laurent, F. (2017b). Worldwide endemicity of a multidrug-resistant *Staphylococcus capitis* clone involved in neonatal sepsis. *Emerg. Infect. Dis.* 23, 538–539. doi: 10.3201/eid2303.160833
- Butin, M., Rasigade, J. P., Martins-Simões, P., Meugnier, H., Lemriss, H., Goering, R. V., et al. (2016). Wide geographical dissemination of the multiresistant *Staphylococcus capitis* NRCS-A clone in neonatal intensive-care units. *Clin. Microbiol. Infect.* 22, 46–52. doi: 10.1016/j.cmi.2015.09.008
- Carter, G. P., Ussher, J. E., Da Silva, A. G., Baines, S. L., Heffernan, H., Riley, T. V., et al. (2018). Genomic analysis of multiresistant *Staphylococcus capitis* associated with neonatal sepsis. *Antimicrob. Agents Chemother.* 62, e898–e818. doi: 10.1128/AAC.00898-18
- Chaffin, D. O., Taylor, D., Skerrett, S. J., and Rubens, C. E. (2012). Changes in the *Staphylococcus aureus* transcriptome during early adaptation to the lung. *PLoS One* 7:e41329. doi: 10.1371/journal.pone.0041329
- Cheong, S. M., Totsu, S., Nakanishi, H., Uchiyama, A., and Kusuda, S. (2016). Outcomes of peripherally inserted double lumen central catheter in very low birth weight infants. *J. Neonatal. Perinatal. Med.* 9, 99–105. doi: 10.3233/NPM-16915054
- Cui, B., Smooker, P. M., Rouch, D. A., Daley, A. J., and Deighton, M. A. (2013). Differences between two clinical *Staphylococcus capitis* subspecies as revealed

DATA AVAILABILITY STATEMENT

The datasets generated for this study are available on request to the corresponding author.

AUTHOR CONTRIBUTIONS

YQ, TL, YL, and AP conceived and designed the experiments. YQ, YL, DC, and CE performed the experiments. YQ, TL, XZ, MZ, YL, DC, CE, HT, MS, HT, AD, JF, and BM analyzed the data. TL, HT, AD, JF, BM, AP, and YQ contributed reagents, materials, and analysis tools. YQ, TL, YL, and CE wrote the manuscript.

FUNDING

This work was supported by the National Natural Science Foundation of China (Grant No. 81772241 to YQ) and Micro@Monash seeding Grant to YQ and YL. TL was an ARC Australian Laureate Fellow.

ACKNOWLEDGMENTS

We thank Dr. Albert Parker from the Department of Mathematical Sciences of Montana State University for advices in statistical analysis and Mrs. Joan Clark from Monash Micro Imaging for her assistance in scanning electron microscopy.

- by biofilm, antibiotic resistance, and pulsed-field gel electrophoresis profiling. *J. Clin. Microbiol.* 51, 9–14. doi: 10.1128/JCM.05124-11
- De Silva, G. D. I., Kantzanou, M., Justice, A., Massey, R. C., Wilkinson, A. R., Day, N. P. J., et al. (2002). The *ica* operon and biofilm production in coagulase-negative staphylococci associated with carriage and disease in a neonatal intensive care unit. *J. Clin. Microbiol.* 40, 382–388. doi: 10.1128/jcm.40.02.382-388.2002
- Deighton, M. A., Capstick, J., Domalewski, E., and Van Nguyen, T. (2001). Methods for studying biofilms produced by *Staphylococcus epidermidis*. *Methods Enzymol.* 336, 177–195. doi: 10.1016/s0076-6879(01)36589-8
- D'mello, D., Daley, A. J., Rahman, M. S., Qu, Y., Garland, S., Pearce, C., et al. (2008). Vancomycin heteroresistance in bloodstream isolates of *Staphylococcus capitis*. *J. Clin. Microbiol.* 46, 3124–3126. doi: 10.1128/JCM.00592-08
- Dubbink-Verheij, G. H., Bekker, V., Pelsma, I. C. M., Van Zwet, E. W., Smits-Wintjens, V., Steggerda, S. J., et al. (2017). Bloodstream infection incidence of different central venous catheters in neonates: A descriptive cohort study. *Front. Pediatr.* 5:142. doi: 10.3389/fped.2017.00142
- Flemming, H. C., and Wingender, J. (2010). The biofilm matrix. *Nat. Rev. Microbiol.* 8, 623–633.
- Frebourg, N. B., Lefebvre, S., Baert, S., and Lemeland, J. F. (2000). PCR-Based assay for discrimination between invasive and contaminating *Staphylococcus epidermidis* strains. *J. Clin. Microbiol.* 38, 877–880.
- Galdabart, J. O., Allignet, J., Tung, H. S., Ryden, C., and El Solh, N. (2000). Screening for *Staphylococcus epidermidis* markers discriminating between skin-flora strains and those responsible for infections of joint prostheses. *J. Infect. Dis.* 182, 351–355. doi: 10.1086/315660
- Gerke, C., Kraft, A., Sussmuth, R., Schweitzer, O., and Gotz, F. (1998). Characterization of the N-acetylglucosaminyltransferase activity involved in the biosynthesis of the *Staphylococcus epidermidis* polysaccharide intercellular adhesin. *J. Biol. Chem.* 273, 18586–18593. doi: 10.1074/jbc.273.29.18586
- Gilbert, R., Brown, M., Rainford, N., Donohue, C., Fraser, C., Sinha, A., et al. (2019). Antimicrobial-impregnated central venous catheters for prevention of neonatal bloodstream infection (PREVAIL): an open-label, parallel-group, pragmatic, randomised controlled trial. *Lancet Child Adolesc. Health* 3, 381–390. doi: 10.1016/S2352-4642(19)30114-2
- Gottenbos, B., Grijpma, D. W., Van Der Mei, H. C., Feijen, J., and Busscher, H. J. (2001). Antimicrobial effects of positively charged surfaces on adhering Gram-positive and Gram-negative bacteria. *J. Antimicrob. Chemother.* 48, 7–13. doi: 10.1093/jac/48.1.7
- Heilmann, C., Schweitzer, O., Gerke, C., Vanittanakom, N., Mack, D., and Gotz, F. (1996). Molecular basis of intercellular adhesion in the biofilm-forming *Staphylococcus epidermidis*. *Mol. Microbiol.* 20, 1083–1091. doi: 10.1111/j.1365-2958.1996.tb02548.x
- Hitzenbichler, F., Simon, M., Salzberger, B., and Hanses, F. (2017). Clinical significance of coagulase-negative staphylococci other than *S. epidermidis* blood stream isolates at a tertiary care hospital. *Infection* 45, 179–186. doi: 10.1007/s15010-016-0945-4
- Hook, A. L., Chang, C. Y., Yang, J., Luckett, J., Cockayne, A., Atkinson, S., et al. (2012). Combinatorial discovery of polymers resistant to bacterial attachment. *Nat. Biotechnol.* 30, 868–875. doi: 10.1038/nbt.2316
- Li, Y., Muir, B. W., Easton, C. D., Thomsen, L., Nisbet, D. R., and Forsythe, J. S. (2014). A study of the initial film growth of PEG-like plasma polymer films via XPS and NEXAFS. *Appl. Surf. Sci.* 288, 288–294.
- Lourdet-Hascoet, J., Felice, M. P., Bicart-See, A., Bouige, A., Giordano, G., and Bonnet, E. (2018). Species and antimicrobial susceptibility testing of coagulase-negative staphylococci in periprosthetic joint infections. *Epidemiol Infect.* 146, 1771–1776. doi: 10.1017/S0950268818001437
- Mack, D., Nedelmann, M., Krokotsch, A., Schwarzkopf, A., Heesemann, J., and Laufs, R. (1994). Characterization of transposon mutants of biofilm-producing *Staphylococcus epidermidis* impaired in the accumulative phase of biofilm production: genetic identification of a hexosamine-containing polysaccharide intercellular adhesin. *Infect. Immun.* 62, 3244–3253.
- Mikulska, P., Hook, A., Dundas, A. A., Irvine, D., Sanni, O., Anderson, D., et al. (2018). Prediction of broad-spectrum pathogen attachment to coating materials for biomedical devices. *ACS Appl. Mater. Interfaces* 10, 139–149. doi: 10.1021/acsami.7b14197
- Natsis, N. E., and Cohen, P. R. (2018). Coagulase-negative staphylococcus skin and soft tissue infections. *Am. J. Clin. Dermatol.* 19, 671–677. doi: 10.1007/s40257-018-0362-9
- Ory, J., Cazaban, M., Richaud-Morel, B., Di Maio, M., Dunyach-Remy, C., Pantel, A., et al. (2019). Successful implementation of infection control measure in a neonatal intensive care unit to combat the spread of pathogenic multidrug resistant *Staphylococcus capitis*. *Antimicrob. Resist. Infect. Control.* 8:57. doi: 10.1186/s13756-019-0512-8
- Otto, M. (2008). Staphylococcal biofilms. *Curr. Top. Microbiol. Immunol.* 322, 207–228.
- Otto, M. (2013). Staphylococcal infections: mechanisms of biofilm maturation and detachment as critical determinants of pathogenicity. *Annu. Rev. Med.* 64, 175–188. doi: 10.1146/annurev-med-042711-140023
- Oud, L. (2011). Community-acquired meningitis due to *Staphylococcus capitis* in the absence of neurologic trauma, surgery, or implants. *Heart Lung.* 40, 467–471. doi: 10.1016/j.hrtlng.2010.09.002
- Payne, N. R., Carpenter, J. H., Badger, G. J., Horbar, J. D., and Rogowski, J. (2004). Marginal increase in cost and excess length of stay associated with nosocomial bloodstream infections in surviving very low birth weight infants. *Pediatrics* 114, 348–355. doi: 10.1542/peds.114.2.348
- Qin, Z., Yang, X., Yang, L., Jiang, J., Ou, Y., Molin, S., et al. (2007). Formation and properties of in vitro biofilms of *ica*-negative *Staphylococcus epidermidis* clinical isolates. *J. Med. Microbiol.* 56, 83–93. doi: 10.1099/jmm.0.46799-0
- Qu, Y., Istivan, T. S., Daley, A. J., Rouch, D. A., and Deighton, M. A. (2009). Comparison of various antimicrobial agents as catheter lock solutions: preference for ethanol in eradication of coagulase-negative staphylococcal biofilms. *J. Med. Microbiol.* 58, 442–450. doi: 10.1099/jmm.0.006387-0
- Rasigade, J. P., Raulin, O., Picaud, J. C., Tellini, C., Bes, M., Grando, J., et al. (2012). Methicillin-resistant *Staphylococcus capitis* with reduced vancomycin susceptibility causes late-onset sepsis in intensive care neonates. *PLoS One* 7:e31548. doi: 10.1371/journal.pone.0031548
- Salwiczek, M., Qu, Y., Gardiner, J., Strugnelli, R. A., Lithgow, T., Mclean, K. M., et al. (2014). Emerging rules for effective antimicrobial coatings. *Trends Biotechnol.* 32, 82–90. doi: 10.1016/j.tibtech.2013.09.008
- Sanford, B. A., Thomas, V. L., Mattingly, S. J., Ramsay, M. A., and Miller, M. M. (1995). Lectin-biotin assay for slime present in situ biofilm produced by *Staphylococcus epidermidis* using transmission electron microscopy (TEM). *J. Ind. Microbiol.* 15, 156–161. doi: 10.1007/bf01569820
- Schmittgen, T. D., and Livak, K. J. (2008). Analyzing real-time PCR data by the comparative C(T) method. *Nat. Protoc.* 3, 1101–1108. doi: 10.1038/nprot.2008.73
- Stenmark, B., Hellmark, B., and Soderquist, B. (2019). Genomic analysis of *Staphylococcus capitis* isolated from blood cultures in neonates at a neonatal intensive care unit in Sweden. *Eur. J. Clin. Microbiol. Infect. Dis.* 38, 2069–2075. doi: 10.1007/s10096-019-03647-3
- Taff, H. T., Nett, J. E., Zarnowski, R., Ross, K. M., Sanchez, H., Cain, M. T., et al. (2012). A *Candida* biofilm-induced pathway for matrix glucan delivery: implications for drug resistance. *PLoS Pathog.* 8:e1002848. doi: 10.1371/journal.ppat.1002848
- Takano, T., Ohtsu, Y., Terasaki, T., Wada, Y., and Amano, J. (2011). Prosthetic valve endocarditis caused by *Staphylococcus capitis*: report of 4 cases. *J. Cardiothorac. Surg.* 6:131. doi: 10.1186/1749-8090-6-131
- Telford, A. M., Meagher, L., Glattau, V., Gengenbach, T. R., Easton, C. D., and Neto, C. (2012). Micropatterning of polymer brushes: grafting from dewetting polymer films for biological applications. *Biomacromolecules* 13, 2989–2996. doi: 10.1021/bm3010534
- Tevell, S., Hellmark, B., Nilsson-Augustinsson, A., and Soderquist, B. (2017). *Staphylococcus capitis* isolated from prosthetic joint infections. *Eur. J. Clin. Microbiol. Infect. Dis.* 36, 115–122.
- Tidwell, C. D., Ertel, S. I., Ratner, B. D., Tarasevich, B. J., Atre, S., and Allara, D. L. (1997). Endothelial cell growth and protein adsorption on terminally functionalized, self-assembled monolayers of alkanethiolates on gold. *Langmuir* 13, 3404–3413.
- Uwamahoro, N., Qu, Y., Jelacic, B., Lo, T. L., Beaurepaire, C., Bantun, F., et al. (2012). The functions of Mediator in *Candida albicans* support a role in shaping species-specific gene expression. *PLoS Genet.* 8:e1002613. doi: 10.1371/journal.pgen.1002613

- Vermont, C. L., Hartwig, N. G., Fleer, A., De Man, P., Verbrugh, H., Van Den Anker, J., et al. (1998). Persistence of clones of coagulase-negative staphylococci among premature neonates in neonatal intensive care units: two-center study of bacterial genotyping and patient risk factors. *J. Clin. Microbiol.* 36, 2485–2490.
- Wang, S. M., Liu, C. C., Tseng, H. W., Yang, Y. J., Lin, C. H., Huang, A. H., et al. (1999). *Staphylococcus capitis* bacteremia of very low birth weight premature infants at neonatal intensive care units: clinical significance and antimicrobial susceptibility. *J. Microbiol. Immunol. Infect.* 32, 26–32.
- Wolf, J., Connell, T. G., Allison, K. J., Tang, L., Richardson, J., Branum, K., et al. (2018). Treatment and secondary prophylaxis with ethanol lock therapy for central line-associated bloodstream infection in paediatric cancer: a randomised, double-blind, controlled trial. *Lancet Infect. Dis.* 18, 854–863. doi: 10.1016/S1473-3099(18)30224-X
- Yamamoto, K., and Ohmagari, N. (2018). Infective endarteritis due to *Staphylococcus capitis*. *Intern. Med.* 57:1185. doi: 10.2169/internalmedicine.0070-17
- Yumani, D. F., Van Den Dungen, F. A., and Van Weissenbruch, M. M. (2013). Incidence and risk factors for catheter-associated bloodstream infections in neonatal intensive care. *Acta Paediatr.* 102, e293–e298. doi: 10.1111/apa.12256
- Zhou, W., Niu, D., Cao, X., Ning, M., Zhang, Z., Shen, H., et al. (2015). Clonal dissemination of linezolid-resistant *Staphylococcus capitis* with G2603T mutation in domain V of the 23S rRNA and the *cfr* gene at a tertiary care hospital in China. *BMC Infect. Dis.* 15:97. doi: 10.1186/s12879-015-0841-z

Conflict of Interest: The authors declare that the research was conducted in the absence of any commercial or financial relationships that could be construed as a potential conflict of interest.

Copyright © 2020 Qu, Li, Cameron, Easton, Zhu, Zhu, Salwiczek, Muir, Thissen, Daley, Forsythe, Peleg and Lithgow. This is an open-access article distributed under the terms of the Creative Commons Attribution License (CC BY). The use, distribution or reproduction in other forums is permitted, provided the original author(s) and the copyright owner(s) are credited and that the original publication in this journal is cited, in accordance with accepted academic practice. No use, distribution or reproduction is permitted which does not comply with these terms.



A Rational Designed PslG With Normal Biofilm Hydrolysis and Enhanced Resistance to Trypsin-Like Protease Digestion

Tiantian Su, Jing He, Ningna Li, Shiheng Liu, Sujuan Xu and Lichuan Gu*

State Key Laboratory of Microbial Technology, Shandong University, Qingdao, China

OPEN ACCESS

Edited by:

Silvia Buroni,
University of Pavia, Italy

Reviewed by:

Maria Ligia Rodrigues Macedo,
Federal University of Mato Grosso do
Sul, Brazil
Jerica Sabotič,
Institut Jožef Stefan (IJS), Slovenia

*Correspondence:

Lichuan Gu
lcgu@sdu.edu.cn

Specialty section:

This article was submitted to
Antimicrobials, Resistance
and Chemotherapy,
a section of the journal
Frontiers in Microbiology

Received: 03 December 2019

Accepted: 30 March 2020

Published: 13 May 2020

Citation:

Su T, He J, Li N, Liu S, Xu S and
Gu L (2020) A Rational Designed PslG
With Normal Biofilm Hydrolysis
and Enhanced Resistance
to Trypsin-Like Protease Digestion.
Front. Microbiol. 11:760.
doi: 10.3389/fmicb.2020.00760

A glycosyl hydrolase produced by *Pseudomonas aeruginosa*, PslG, has become a promising candidate for biofilm treatment because of its ability to inhibit and disperse biofilms by disrupting exopolysaccharide matrix at nanomolar concentrations. However, as a protein, PslG used for treatment may be degraded by the ubiquitous proteases (of which trypsin-like serine proteases are a major group) secreted by human cells. This would lead to an insufficient effective concentration of PslG. Here, based on the result of liquid chromatography–tandem mass spectrometry (LC-MS/MS) and structural analysis, we generate a PslG mutant (K286A/K433S) with greatly enhanced trypsin resistance. This measure raises IC_{50} (the concentration of trypsin that can degrade 50% of protein in 30 min at 37°C) from 0.028 mg mL⁻¹ of the wild-type PslG to 0.283 mg mL⁻¹ of PslG^{K286A/K433S}. In addition, biofilm inhibition assay shows that PslG^{K286A/K433S} is much more efficient than wild-type PslG in the presence of trypsin. This indicates that PslG^{K286A/K433S} is a better biofilm inhibitor than wild-type PslG in clinical use where trypsin-like proteases widely exist.

Keywords: *Pseudomonas aeruginosa*, biofilm, PslG, trypsin, protease

INTRODUCTION

Biofilms are highly structured matrix-enclosed bacterial communities adherent to surfaces (Costerton et al., 1995; Stoodley et al., 2002). Biofilm bacteria have extremely enhanced resistance to antibiotic treatments and host immune responses compared with their planktonic living states (Stewart and Costerton, 2001; Stewart and Franklin, 2008).

Pseudomonas aeruginosa is the most common opportunistic pathogen that causes 10–20% of infections in most hospitals and is associated with a high mortality rate up to 61% (Bodey et al., 1983; Kang et al., 2003). *P. aeruginosa* can cause both acute and chronic infections, which could be life-threatening. Chronic infection is more difficult to eradicate because of the formation of biofilms and elevated antibiotic resistance. *P. aeruginosa* has the ability to form biofilms on various surfaces, including biotic and abiotic surfaces (O'Toole et al., 2000). For example, *P. aeruginosa* can colonize on many medical implants such as catheters, ventilator tubes, and contact lenses, which is the major cause of hospital infections (Ahiwale et al., 2011). *P. aeruginosa* is also the leading cause of chronic respiratory infection and lung infections in patients with cystic fibrosis (Waters and Goldberg, 2019). Furthermore, amounting to 60–70% contact lens-related keratitis is caused by *P. aeruginosa*, which causes global blindness and visual impairment (Choy et al., 2008).

To date, the treatment of biofilm infection in clinic is either through mechanical debridement or use of antibiotics, which is arduous and inefficient because biofilm bacteria exhibit extremely high drug tolerance. Because of the critical role of extracellular matrix in biofilm formation and development, enzymes targeting the matrix molecules (proteins, extracellular DNA, and exopolysaccharides) have been gaining more and more attention for novel therapeutics (Mah and O'Toole, 2001; Kiedrowski et al., 2011; Newell et al., 2011; Moormeier et al., 2014; Fleming et al., 2017; Zhao et al., 2018). DNase I and its derivative DNase1L2 have been reported to prevent biofilm formation of *P. aeruginosa* and *Staphylococcus aureus* at early stage (Whitchurch, 2002; Eckhart et al., 2007). A purified β -N-acetylglucosaminidase, dispersin B, is able to disperse biofilms formed by *Aggregatibacter actinomycetemcomitans*, *Staphylococcus epidermidis*, and other species when supplied alone or in synergy with cefamandole nafate (Donelli et al., 2007; Darouiche et al., 2009). Other biofilm-degrading enzymes, including α -amylase, lysostaphin, and alginate lyase, also show antibiofilm activities against various pathogenic bacteria (Alkawash et al., 2006; Kokai-Kun et al., 2009; Kalpana et al., 2012; Singh et al., 2015; Algburi et al., 2017).

Our previous work revealed that a self-produced glycoside hydrolase PslG efficiently prevents biofilm formation and disassembles existing biofilms of a wide range of *Pseudomonas* strains by mainly disrupting the Psl matrix, which makes PslG an important candidate for biofilm treatment (Baker et al., 2015; Yu et al., 2015). Subsequently, Zhang et al. (2018) reported that PslG can affect the surface movement of *P. aeruginosa*. After adding PslG to the medium, bacteria move significantly faster and in a more random way with no clear preferred direction. Besides PslG, other glycoside hydrolases such as PelA have also been reported to exhibit biofilm-disrupting ability. However, compared to PelA, PslG has more advantages. Experimental data showed that PslG at a much lower half maximal effective concentration was more effective than PelA (Baker et al., 2016). Also, PslG does not inhibit bacteria growth and is non-toxic to human epithelial cells and immune cells. Furthermore, PslG treatment sensitized biofilm bacteria to antibiotics and thus can be used together with antibiotics (Yu et al., 2015). Finally, to our experience, the production of PslG is very easy because when expressed in *Escherichia coli* the yield is high.

As the most potent factor for biofilm disassembly and inhibition by far, PslG is gaining increasing attention. Recently, a clinic study using murine and porcine wound models showed that PslG can be used to treat *P. aeruginosa*-infected wounds by improving antibiotic efficacy and host innate immune activity (Pesttrak et al., 2019). Taken together, these results showed that PslG has promising potential to be used in clinic to combat biofilm-related infections, such as in burned patients, bacterial keratitis, and respiratory system and gastrointestinal tract infections. However, PslG has intrinsic disadvantages as a protein, because it could be digested by the ubiquitous proteases secreted by human cells. This may severely reduce the lifetime of PslG, thus restricting the enzyme activity. It has been reported that ~2% of the genes in human genome encode proteases, of which trypsin-like serine proteases are a major group (Overall

and Blobel, 2007; Wang et al., 2018). In addition, *P. aeruginosa* itself secretes several extracellular proteases such as protease IV and Ps-1, which are important virulence factors and have been characterized as trypsin-like proteases (Elliott and Cohen, 1986; Engel et al., 1998). Thus, development of trypsin-resistant variant may significantly improve PslG activity in clinical usage. In this study, we generate a liquid chromatography–tandem mass spectrometry (LC-MS/MS) and three-dimensional (3D) structure-based rational design of PslG to enhance its resistance to trypsin. By introducing double mutations K286A and K433S, the resistance of PslG to trypsin was significantly increased, and so was the biofilm inhibition activity in the presence of trypsin.

MATERIALS AND METHODS

Strains and Growth Conditions

Pseudomonas aeruginosa PAO1 was grown at 37°C in Luria–Bertani (LB) broth (Becton Dickinson, Franklin Lakes, NJ, United States) without sodium chloride (LBNS). Biofilms of *P. aeruginosa* were grown at 30°C in Jensen's medium, a chemically defined medium (Jensen et al., 1980). *E. coli* BL21 (DE3) was grown in LB broth at 37°C. All the safety procedures of institution biosafety level 2 standard were adhered to while working with *P. aeruginosa* PAO1.

Plasmid Construction and Protein Purification

Sequence encoding PslG (residues 31–442) was amplified from *P. aeruginosa* PAO1 genome DNA and cloned into PGL01, a vector modified from pET15b with a PreScission Protease (PPase) cleavage site for the removal of the His-tag. Plasmids expressing PslG with single or double mutations were constructed by using QuickChange with wild-type PGL01-PslG as the template (Xia et al., 2015). The primers used for QuickChange are listed in **Supplementary Table S1**.

Escherichia coli BL21 (DE3) cells expressing wild-type or mutant PslG were cultured in LB medium supplemented with 100 μ g mL⁻¹ ampicillin at 37°C until OD₆₀₀ reached 0.8 and were induced overnight with 0.12 mM isopropyl β -D-thiogalactopyranoside at 22°C. For protein purification, bacterial cells were harvested and resuspended in binding buffer (25 mM Tris pH 8.0, 200 mM NaCl) and lysed by sonication. After centrifugation at 4°C for 45 min, the supernatants were loaded onto a nickel affinity column (Chelating Sepharose Fast Flow; GE Healthcare, Chicago, IL, United States) and washed with binding buffer to remove the non-specific bindings. Then, the resins were resuspended in binding buffer and incubated with 0.12 mg mL⁻¹ PPase overnight at 4°C to remove the His tag. After elution with binding buffer, the protein samples were further purified by ion-exchange chromatography (Source 15Q HR 16/10; GE Healthcare) using gradient elution with 0–1 M NaCl, 25 mM Tris pH 8.0. Finally, the protein sample was purified by size-exclusion chromatography (Superdex 200 10/300 GL; GE Healthcare) in buffer containing 100 mM NaCl, 10 mM Tris pH 8.0.

Protein Digestion and LC-MS/MS Analysis

The sodium dodecyl sulfate (SDS) gel band of PslG was collected, washed with water, and destained in destaining buffer containing 50% acetonitrile (ACN) and 25 mM ammonium bicarbonate. The disulfide bonds from cysteinyl residues were reduced with 10 mM DTT for 1 h at 56°C, and then the thiol groups were alkylated with 55 mM iodoacetamide for 45 min at room temperature in darkness. The gel band was washed in turn with 25 mM ammonium bicarbonate and destaining buffer. All the liquids were removed, and the gel piece was dried in a SpeedVac, Eppendorf, Hamburg, Germany. The dried gel band was reswollen and covered with 25 mM ammonium bicarbonate containing 67 ng μL^{-1} trypsin and was incubated overnight at 37°C. The digestion was stopped by the addition of 0.1% formic acid (FA). Ten microliters of the resulting sample was loaded onto a C18 column using a gradient buffer containing 5–80% ACN and 0.1% FA. The peptides were then subjected to MS/MS analysis using MicrOTOF-QII (Bruker Daltonics, Billerica, MA, United States). The MS data were analyzed and matched to the protein sequence of PslG by Mascot search engine version 2.3.01.

Trypsin Proteolysis Analysis

Wild-type and mutant PslG proteins were either concentrated or diluted to 2.7 mg mL^{-1} with 10 mM Tris-HCl pH 8.0 and 100 mM NaCl. Trypsin from bovine pancreas powder was bought from Sigma-Aldrich, St. Louis, MI, United States and was made into stock solution at the concentration of 80 mg mL^{-1} with buffer containing 10 mM Tris-HCl pH 8.0 and 100 mM NaCl. Working solutions of trypsin were obtained through serial dilution using the same buffer. Equal volumes of PslG and trypsin solutions were mixed and incubated at 37°C for 30 min. $2 \times$ SDS loading buffer was added to the mixture to stop the reaction. The resulting samples were then loaded onto SDS-polyacrylamide gel electrophoresis (PAGE), stained with Coomassie brilliant blue, and quantified by densitometric scanning using ImageJ software¹. The experiments were repeated for at least three times with similar results, and representative images are shown.

Biofilm Inhibition and Disassembly Assay

For biofilm inhibition assay, an overnight culture of PAO1 was diluted 100 times and inoculated into Jensen's medium containing 50 nM wild-type or mutant PslG in a microtiter dish (Falcon 3911). After 24 h of static growth at 30°C, the medium and planktonic cells were discarded, and the wells were washed three times with water. The biofilms were stained with 0.1% crystal violet (CV) and washed three times with water. Then, the CV bound to biofilms was solubilized with 30% acetic acid and measured for absorbance at 560 nm. For disassembly assay, the culture was replaced by fresh medium containing 50 nM PslG after 24-h growth in Jensen's medium without PslG. After 30-min treatment at 30°C, the biofilm abundance was measured in the same way. For trypsin treatment experiments, trypsin was added

to PslG at indicated concentrations. The sample without PslG was used as an untreated control. For these experiments, data of three independent repeats are shown in the figures as means \pm SD.

Structural Modeling

The structural modeling of PslG^{K286A/K433S} was constructed using online server ITASSER (Zhang, 2008; Roy et al., 2010; Yang et al., 2015). The final model with the highest C score was selected from the top five models predicted. Structural alignment and figures were made using PyMOL.

RESULTS

LC-MS/MS and Structure-Based Selection of Proper Trypsin Cleavage Sites

PslG is predicted to be a periplasmic protein, resembling β -D-xylosidases from the CAZy glycosyl hydrolase family 39 (Friedman and Kolter, 2004; Franklin et al., 2011). The full-length protein of PslG contains 442 amino acids. The first 30 amino acids are predicted to be the signal peptide by SignalP 5.0. In our previous work, the crystal structure of PslG (amino acids 31–442) was solved at 2.0 Å, which consists of an N-terminal catalytic domain and a C-terminal carbohydrate-binding domain. Glu165 and Glu276 are the key catalytic residues (Yu et al., 2015). In this study, through combination of structural analysis and LC-MS/MS, we are able to design a trypsin-resistant mutant of PslG.

As known, trypsin cleaves peptides on the C-terminal side of lysine or arginine, except that there is a proline residue on the carboxyl side of the cleavage site. For initial screening of potential trypsin cleavage sites, PslG protein was digested with trypsin and subjected to LC-MS/MS analysis. Mascot search engine was used to match detected peptides to PslG amino acid sequences. Through this method, we found 34 potential cleavage sites in PslG, which are listed in **Figure 1**. According to our structure, 11 (R39, R120, R138, K175, R216, K283, K286, K361, K405, K407, and K433) of the 34 residues reside in the loop region other than in α -helices and β -strands, which contribute more to protein folding (**Figure 2**). Because PslG is a monomer in solution (Baker et al., 2015; Yu et al., 2015), residues located on the surface are exposed to solvent, thus making them more favorable for trypsin digestion. Together, we chose the residues that are most external, flexible, and far away from the catalytic site for mutation analysis. These mutants include single mutations R39Q, R120S, K175S, K283A, K361S, K405N, K433S, and one double mutation K286A/K433S. We also include K36A fully based on the structural analysis. Among these residues, K361, K405, and K433 are located in the C terminal carbohydrate-binding domain of PslG, and the others are located in the catalytic domain.

Trypsin-Proteolysis Analysis of Wild-Type and Mutant PslG

Recombinant proteins of wild-type and mutant PslG (31–442 residues) were purified from *E. coli* BL21 (DE3). All the mutant proteins showed similar expression level and good solubility

¹<http://rsbweb.nih.gov/ij/>

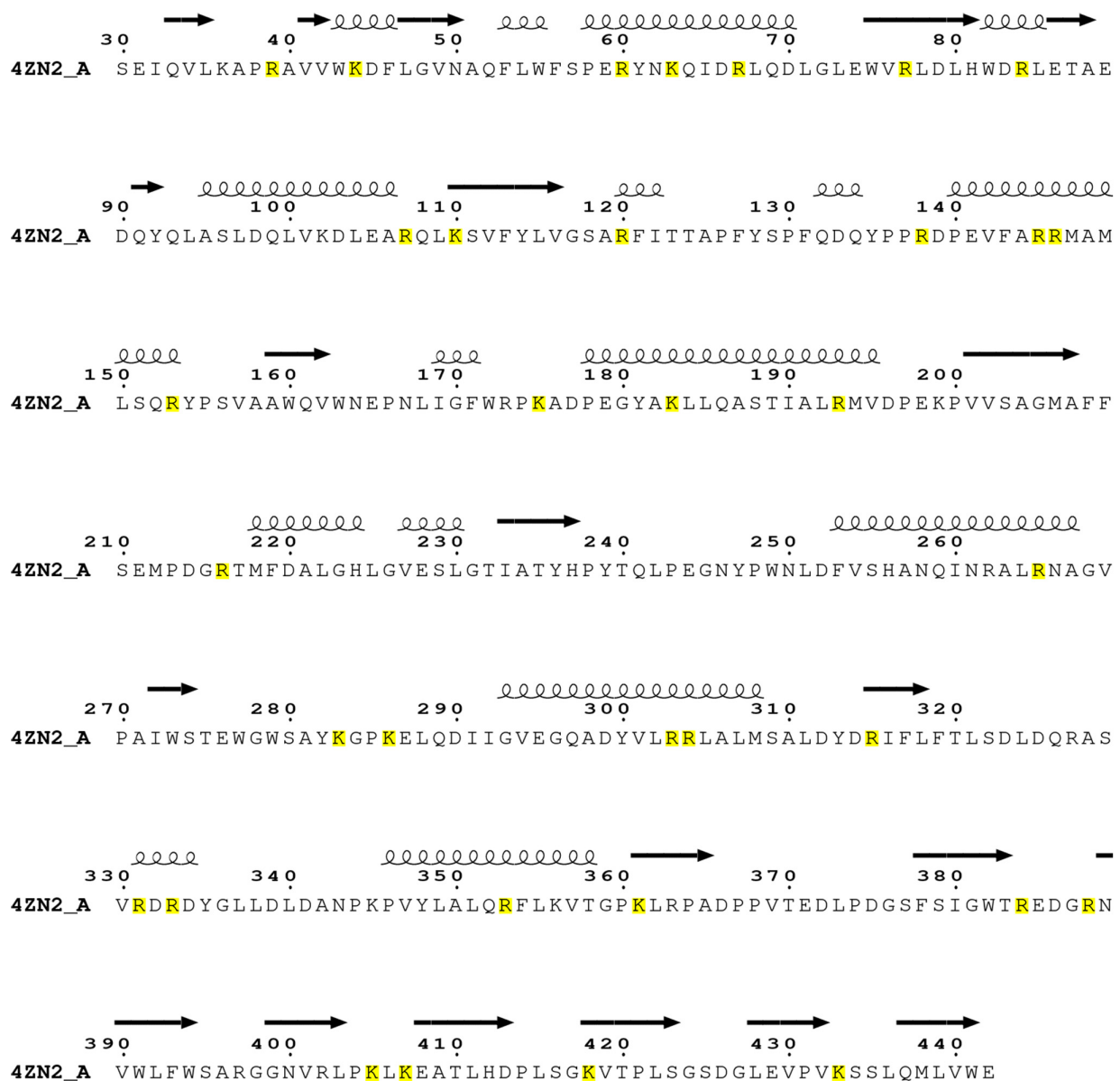
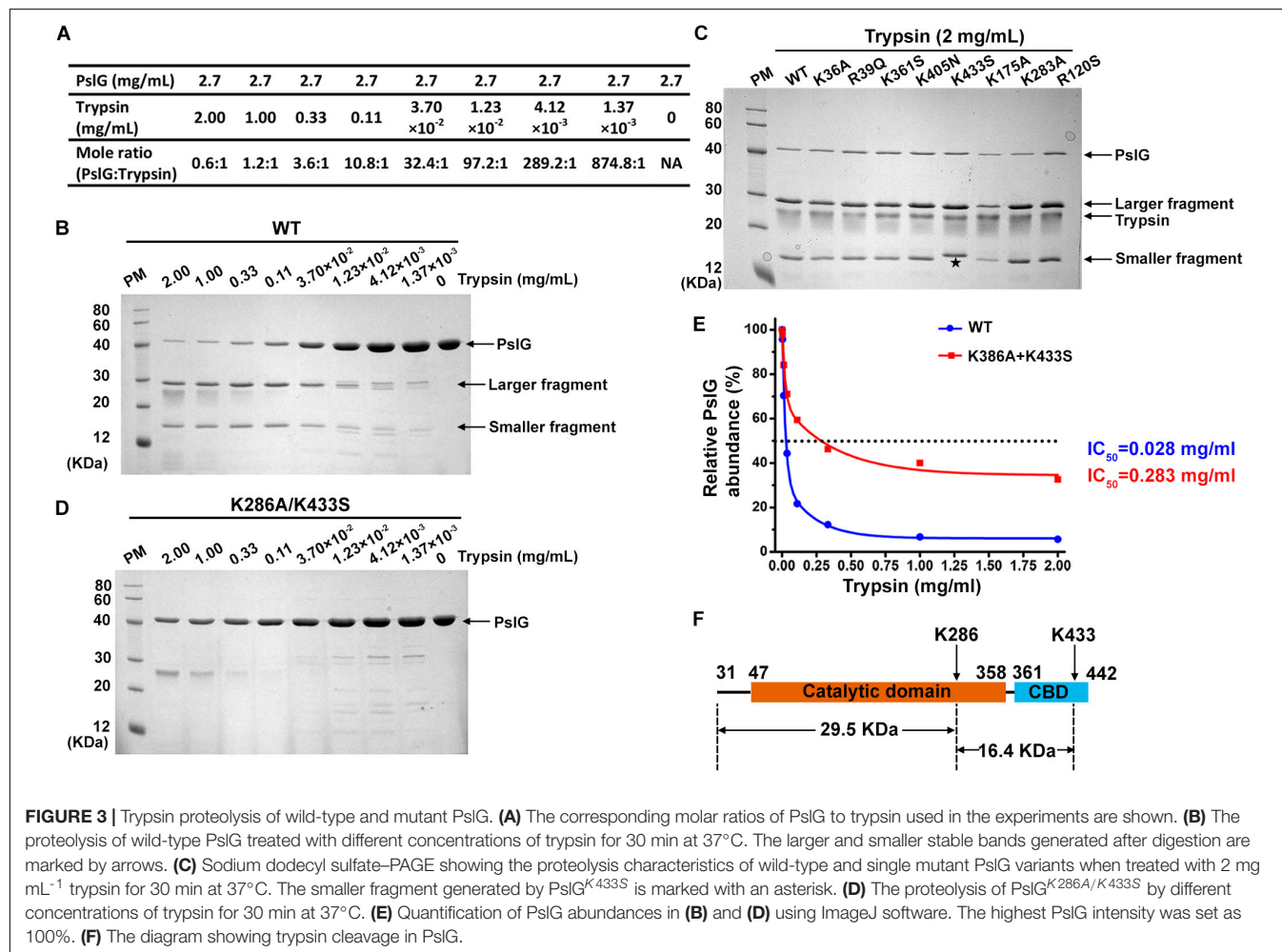
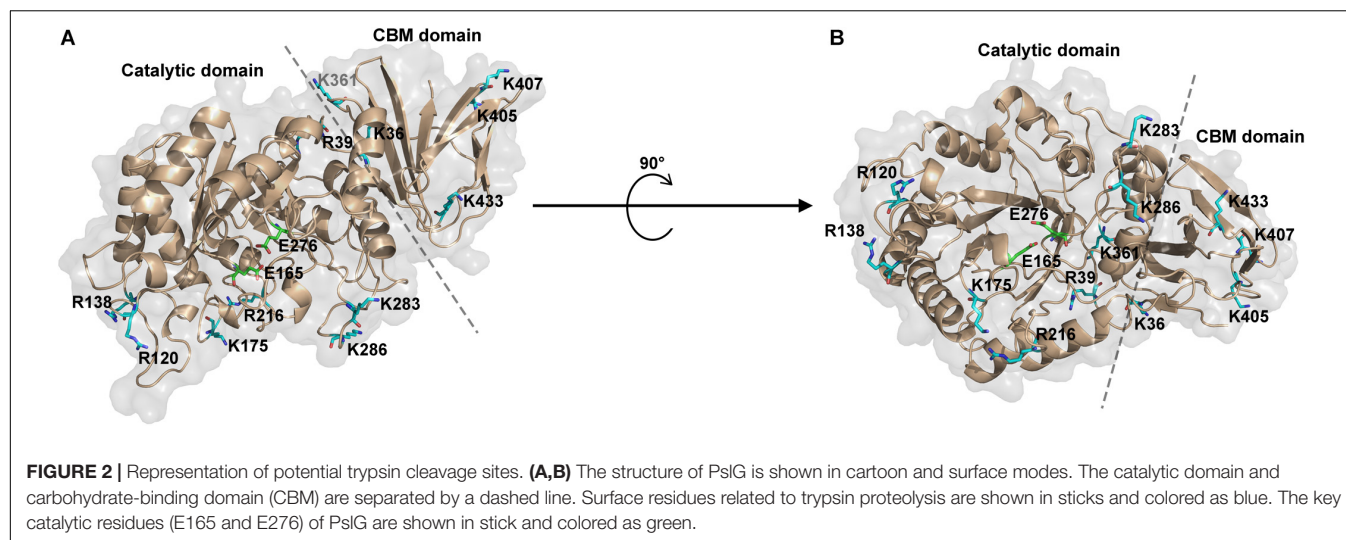


FIGURE 1 | Sequence analysis on the trypsin cleavage residues (highlighted with yellow color) in PsIG (PDB: 4ZN2) identified through LC-MS/MS. The catalytic domain of PsIG includes residues 47–358, whereas the carbohydrate-binding domain (CBM) of PsIG consists of residues 31–42 and 361–442.

comparable to wild-type PslG (**Figure 3C**). In order to determine the resistance of PslG mutations against trypsin, we evaluated the proteolysis of wild-type and mutant PslG with a serial dilution of trypsin (**Figure 3A**). After digestion, the protein samples were analyzed by SDS-PAGE. Our results revealed that wild-type PslG was sensitive to trypsin even at a very low trypsin concentration (3.70×10^{-2} mg/mL) (**Figure 3B**). The abundance of wild-type PslG was significantly decreased by approximately 85% when treated with 0.33 mg/mL trypsin. As shown, PslG was gradually hydrolyzed into two stable fragments, the molecular weights of which were approximately 30 and 16 kD, respectively.

The proteolysis characteristics of mutant proteins were then examined under the same condition. Except K433S, all the other single mutants showed no obvious difference compared with wild-type PslG when treated with indicated concentrations of trypsin (**Figure 3C** and **Supplementary Figure S1**). Interestingly, molecular weight of the smaller fragment was slightly increased in K433S (**Figure 3C**), which revealed that this mutation has an effect on the proteolysis of PslG. Because PslG was hydrolyzed into two fragments with molecular weights of 30 and 16 kD, we speculated that the related cleavage site may be located near residue 300. According to our previous LC-MS/MS analysis, this site will be either K283 or K286. Because single-mutation



K283A did not affect the proteolysis of PslG (Figure 3C), a double-mutant K286A/K433S was constructed and subjected to trypsin digestion assay. Further evaluation showed that the double-mutant (K286A/K433S) had significantly increased

resistance against trypsin (Figure 3D). IC₅₀ (the concentration of trypsin that can degrade 50% of protein) of wild-type PslG and PslG^{K286A/K433S} were approximately 0.028 and 0.283 mg mL⁻¹, respectively (Figure 3E), indicating an increase of an order

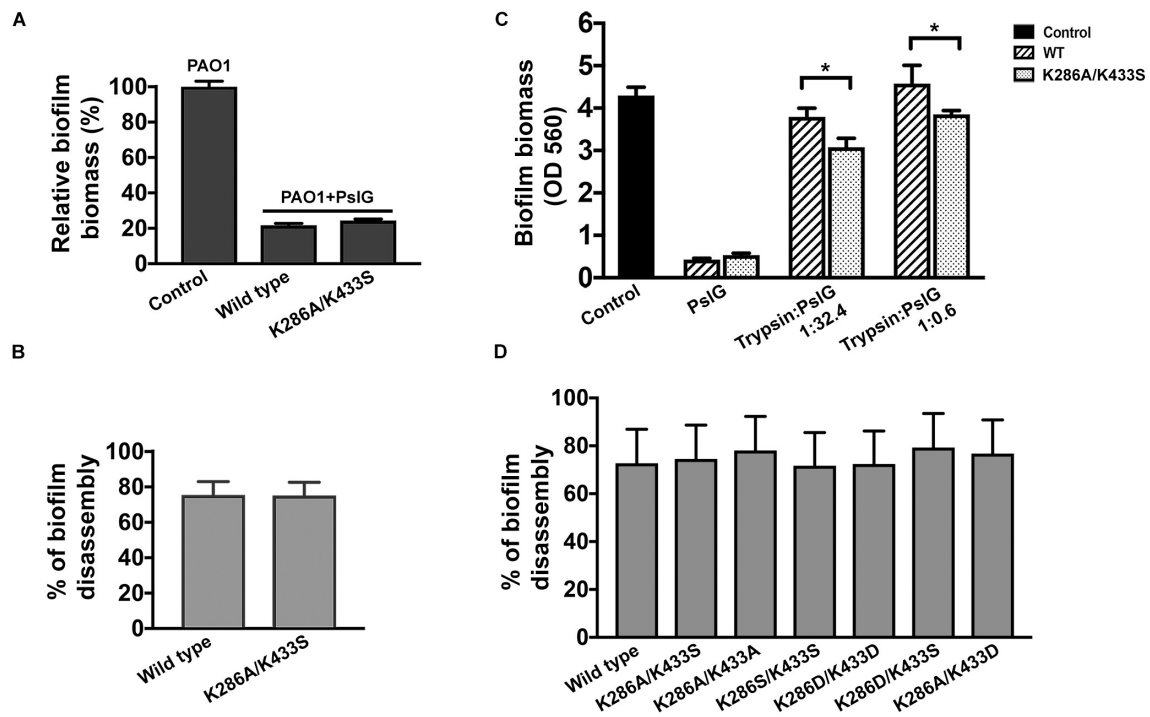


FIGURE 4 | Biofilm inhibition and disperse by wild-type and mutant PslG. **(A)** Biofilm inhibition by wild-type PslG and PslG^{K286A/K433S} in the absence of trypsin. The sample without PslG treatment was used as control and set as 100%. **(B)** Biofilm disassembly by wild-type PslG and PslG^{K286A/K433S}. The disassembly rates were calculated using the formula = [(A560 of untreated control - A560 of PslG-treated sample)/A560 of untreated control] × 100%. **(C)** Biofilm inhibition in the presence of different concentrations of trypsin. *T*-test was performed for testing differences between groups. **P* < 0.05. **(D)** Biofilm disassembly by PslG K286/K433 mutants. The disassembly rates were calculated as described in **(B)**.

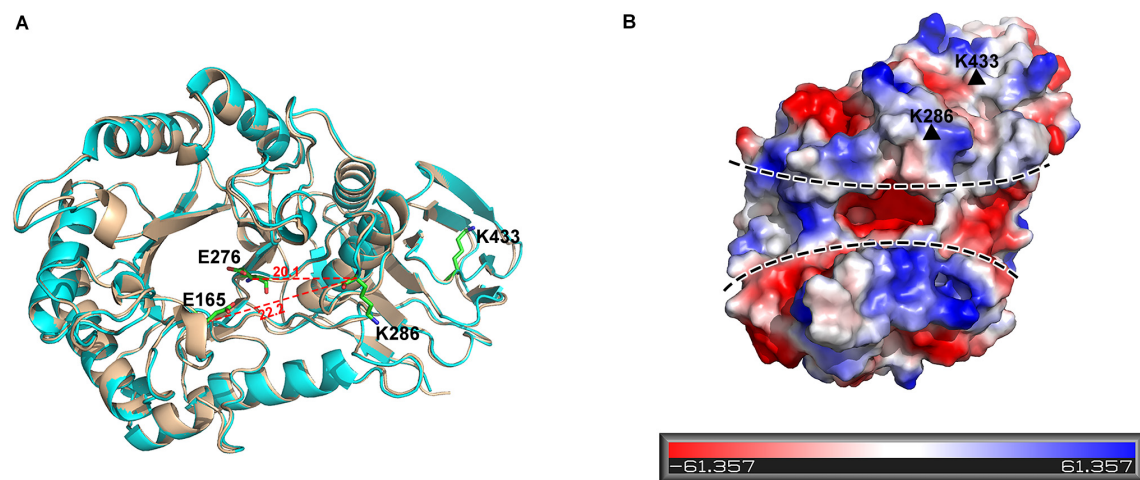


FIGURE 5 | K286 and K433 are spatially far away from the active sites, and their mutants do not affect structure folding. **(A)** Structural alignment of wild-type PslG and PslG^{K286A/K433S}. The crystal structure of PslG is shown in wheat. The structure of PslG^{K286A/K433S} was obtained through homologous modeling using ITASSER, and is shown in cyan. The key catalytic residues (E165 and E276) and trypsin hydrolysis sites (K286 and K433) are shown as sticks. **(B)** Electrostatic potential of PslG with negatively and positively charged regions colored in red and blue, respectively. The substrate-binding groove is marked by dashed lines, and residues K286 and K433 are marked by black triangles.

of magnitude in resistance resulting from the double mutation. The abundance of wild-type PslG was reduced to below 10% when treated with 1 or 2 mg mL⁻¹ trypsin. However, the

protein abundance of PslG^{K286A/K433S} remained approximately 40 and 30% after treatment with 1 and 2 mg mL⁻¹ trypsin, respectively. As expected, we found that the molecular weights

of fragments 31–286 and 287–433 precisely match those of the stable bands found in the proteolysis of the wild-type PslG. These two bands were not observed in the proteolysis of PslG^{K286A/K433S}. In accordance with this, the single-mutant K286A also showed greatly increased resistance to trypsin (Supplementary Figure S2). And the stable bands generated by trypsin digestion were also missing in the proteolysis of K286A. Taken together, these results indicated that residues K286 and K433 are essential trypsin cleavage sites of PslG, which cut PslG into three fragments: 31–286, 287–433, and 434–442 (Figure 3F). And this also explained why the smaller bands detected in K433S showed a slightly increased molecular weight.

PslG^{K286A/K433S} Showed Increased Activity in Biofilm Inhibition When Supplied With Trypsin

PslG was previously reported to be able to prevent biofilm formation and disassemble existing biofilms while supplied exogenously (Yu et al., 2015). To evaluate the biofilm-inhibiting activity, purified PslG^{K286A/K433S} or wild-type PslG was added into the culture media to a final concentration of 50 nM for inoculation. The biofilm biomass was measured after 24 h of growth. As shown in Figure 4A, the addition of PslG^{K286A/K433S} significantly reduced the biofilm formation of PAO1 by 80%, which was comparable to that of wild-type PslG. The biofilm disassembly activity was examined by incubating preformed biofilms with PslG^{K286A/K433S} or wild-type PslG. After 30-min treatment, both PslG^{K286A/K433S} and wild-type PslG disrupted approximately 75% of biofilms (Figure 4B), which is consistent with our previous results (Yu et al., 2015). Other mutants of these two residues also showed similar biofilm disassembly rate, which indicated that the mutation of K286 and K433 does not affect the enzymatic activity of PslG (Figure 4D).

To determine whether PslG^{K286A/K433S} possesses higher trypsin resistance during biofilm inhibition, two different concentrations of trypsin were inoculated together with PslG (Figure 4C). Although both the wild-type PslG and PslG^{K286A/K433S} showed decreased activities when subjected to trypsin treatment, the remaining activity of PslG^{K286A/K433S} was much higher than the wild-type PslG. When using low concentration of trypsin (trypsin:PslG was 1:32.4), wild-type PslG and PslG^{K286A/K433S} decreased biofilm formation by 10 and 30%, respectively (Figure 4C). When using high concentration of trypsin (trypsin:PslG was 1:0.6), wild-type PslG completely lost biofilm inhibiting activity, whereas PslG^{K286A/K433S} was still able to reduce biofilms by 10% (Figure 4C). These results revealed that PslG^{K286A/K433S} is much more stable and efficient in inhibiting biofilms than wild-type PslG in the presence of trypsin.

DISCUSSION

PslG was previously reported as a potent factor that can inhibit biofilm formation or disperse existing biofilms of *Pseudomonas* at nanomolar concentrations (Yu et al., 2015). Owing to the

potential use of PslG in chronic infection and biofilm treatment, we set out to develop a more stable and active form of this protein. In this study, we found that the double-residue mutant PslG^{K286A/K433S} selected from 35 mutants showed greatly increased resistance to one of the most widespread proteases—trypsin, compared with the wild-type PslG.

K286 resides in the upper edge of the active cleft of PslG catalytic domain, with its side chain pointing outward, whereas K433 is positioned in the loop area of the carbohydrate-binding domain (Figure 5A). Both of the lysine residues are distal to the active site (e.g., the nearest distance between C-alpha atoms of K286 and the key catalytic residue E276 is 20.1 Å). Additionally, surface potential analysis showed that both K286 and K433 are spatially apart from the negatively charged substrate-binding groove of PslG (Figure 5B). Thus, mutations of these two residues are supposed to have no effect on either catalytic activity or substrate binding of PslG. This is confirmed by the biofilm inhibition and disassembly experiments, indicating that enzymatic activity of PslG^{K286A/K433S} has no difference with the wild-type PslG in the absence of trypsin (Figures 4A,B). While subjected to trypsin treatment, the activity of PslG^{K286A/K433S} is significantly higher than that of wild-type PslG, which revealed that PslG^{K286A/K433S} has higher trypsin resistance (Figure 4C). Single mutants other than K286A and K433S, even though exposed to solvent as well, showed no significant difference compared with wild-type PslG when treated with trypsin. To validate the effect of Ca²⁺ on trypsin activity, we measured the PslG proteolysis with or without Ca²⁺ (Supplementary Figure S3). Our result indicated that calcium ions had no significant effect on the trypsin digestion of PslG. We also constructed a 3D structural model of PslG^{K286A/K433S} through homology modeling using I-TASSER (25–27). This homology model is nearly identical to the structure of wild-type PslG with a Z score of 66.7 and root-mean-square deviation (RMSD) of 0.4 (Figure 5A).

CONCLUSION

In summary, through a combined experimental and computational approach, we have developed a trypsin-resistant variant of PslG, which is a promising candidate for clinical and environmental biofilm treatment, although the immune response to PslG in clinical usage still needs more research. The enhanced trypsin resistance will lead to increased enzymatic activity of PslG when protease is present, thus promoting lower costs by reducing the dosage of PslG used. It is worth noting that other types of proteases could also affect the biofilm treatment using PslG, such as matrix metalloproteinases, cysteine cathepsins, and pepsin. These proteases may have different cleavage sites compared to trypsin. Future work of PslG mutants with specific resistance to these proteases is desirable by following similar procedure as this article. Our work may also shed light on the structural-based rational design of other enzymes related to biofilm inhibition, such as PelA.

DATA AVAILABILITY STATEMENT

The datasets generated for this study are available on request to the corresponding author.

AUTHOR CONTRIBUTIONS

LG and TS conceived the project. TS, JH, NL, SL, and SX performed the experiments and processed the data. TS analyzed the results and wrote the manuscript. All authors contributed to the editing of the manuscript.

REFERENCES

- Ahiwale, S., Tamboli, N., Thorat, K., Kulkarni, R., Ackermann, H., and Kapadnis, B. (2011). In vitro management of hospital *Pseudomonas aeruginosa* biofilm using indigenous T7-like lytic phage. *Curr. Microbiol.* 62, 335–340. doi: 10.1007/s00284-010-9710-6
- Algburi, A., Comito, N., Kashtanov, D., Dicks, L. M. T., and Chikindas, M. L. (2017). Control of biofilm formation: antibiotics and beyond. *Appl. Environ. Microbiol.* 83:e02508-16. doi: 10.1128/AEM.00165-17
- Alkawash, M. A., Soothill, J. S., and Schiller, N. L. (2006). Alginate lyase enhances antibiotic killing of mucoid *Pseudomonas aeruginosa* in biofilms. *APMIS* 114, 131–138. doi: 10.1111/j.1600-0463.2006.apm_356.x
- Baker, P., Hill, P. J., Snarr, B. D., Alnabseya, N., Pestrak, M. J., Lee, M. J., et al. (2016). Exopolysaccharide biosynthetic glycoside hydrolases can be utilized to disrupt and prevent *Pseudomonas aeruginosa* biofilms. *Sci. Adv.* 2:1501632. doi: 10.1126/sciadv.1501632
- Baker, P., Whitfield, G. B., Hill, P. J., Little, D. J., Pestrak, M. J., Robinson, H., et al. (2015). Characterization of the *Pseudomonas aeruginosa* glycoside hydrolase PslG reveals that its levels are critical for psl polysaccharide biosynthesis and biofilm formation. *J. Biol. Chem.* 290, 28374–28387. doi: 10.1074/jbc.M115.674929
- Bodey, G. P., Bolivar, R., Fainstein, V., and Jadeja, L. (1983). Infections caused by *Pseudomonas aeruginosa*. *Rev. Infect. Dis.* 5, 279–313.
- Choy, M. H., Stapleton, F., Willcox, M. D., and Zhu, H. (2008). Comparison of virulence factors in *Pseudomonas aeruginosa* strains isolated from contact lens- and non-contact lens-related keratitis. *J. Med. Microbiol.* 57, 1539–1546. doi: 10.1099/jmm.0.2008/003723-0
- Costerton, J. W., Lewandowski, Z., Caldwell, D. E., Korber, D. R., and Lappin-Scott, H. M. (1995). Microbial biofilms. *Annu. Rev. Microbiol.* 49, 711–745.
- Darouiche, R. O., Mansouri, M. D., Gawande, P. V., and Madhyastha, S. (2009). Antimicrobial and antibiofilm efficacy of triclosan and DispersinB combination. *J. Antimicrob. Chemother.* 64, 88–93. doi: 10.1093/jac/dk158
- Donelli, G., Francolini, I., Romoli, D., Guaglianone, E., Piozzi, A., Ragnunath, C., et al. (2007). Synergistic activity of dispersin B and cefamandole nafate in inhibition of staphylococcal biofilm growth on polyurethanes. *Antimicrob. Agents Chemother.* 51, 2733–2740. doi: 10.1128/AAC.01249-06
- Eckhart, L., Fischer, H., Barken, K. B., Tolker-Nielsen, T., and Tschachler, E. (2007). DNase1L2 suppresses biofilm formation by *Pseudomonas aeruginosa* and *Staphylococcus aureus*. *Br. J. Dermatol.* 156, 1342–1345. doi: 10.1111/j.1365-2133.2007.07886.x
- Elliott, B. W. Jr., and Cohen, C. (1986). Isolation and characterization of a lysine-specific protease from *Pseudomonas aeruginosa*. *J. Biol. Chem.* 261, 11259–11265.
- Engel, L. S., Hill, J. M., Caballero, A. R., Green, L. C., and O'Callaghan, R. J. (1998). Protease IV, a unique extracellular protease and virulence factor from *Pseudomonas aeruginosa*. *J. Biol. Chem.* 273, 16792–16797. doi: 10.1074/jbc.273.27.16792
- Fleming, D., Chahin, L., and Rumbaugh, K. (2017). Glycoside hydrolases degrade polymicrobial bacterial biofilms in wounds. *Antimicrob. Agents Chemother.* 61:e01998-16. doi: 10.1128/AAC.01998-16

FUNDING

This work was supported by the National Natural Science Foundation of China (31470732).

SUPPLEMENTARY MATERIAL

The Supplementary Material for this article can be found online at: <https://www.frontiersin.org/articles/10.3389/fmicb.2020.00760/full#supplementary-material>

- Franklin, M. J., Nivens, D. E., Weadge, J. T., and Howell, P. L. (2011). Biosynthesis of the *Pseudomonas aeruginosa* extracellular polysaccharides, alginate, Pel, and Psl. *Front. Microbiol.* 2:167. doi: 10.3389/fmicb.2011.00167
- Friedman, L., and Kolter, R. (2004). Genes involved in matrix formation in *Pseudomonas aeruginosa* PA14 biofilms. *Mol. Microbiol.* 51, 675–690. doi: 10.1046/j.1365-2958.2003.03877.x
- Jensen, S. E., Fecycz, I. T., and Campbell, J. N. (1980). Nutritional factors controlling exocellular protease production by *Pseudomonas aeruginosa*. *J. Bacteriol.* 144, 844–847.
- Kalpana, B. J., Aarthy, S., and Pandian, S. K. (2012). Antibiofilm activity of alpha-amylase from *Bacillus subtilis* S8-18 against biofilm forming human bacterial pathogens. *Appl. Biochem. Biotechnol.* 167, 1778–1794. doi: 10.1007/s12010-011-9526-2
- Kang, C. I., Kim, S. H., Kim, H. B., Park, S. W., Choe, Y. J., Oh, M. D., et al. (2003). *Pseudomonas aeruginosa* bacteremia: risk factors for mortality and influence of delayed receipt of effective antimicrobial therapy on clinical outcome. *Clin. Infect. Dis.* 37, 745–751. doi: 10.1086/377200
- Kiedrowski, M. R., Kavanaugh, J. S., Malone, C. L., Mootz, J. M., Voyich, J. M., Smeltzer, M. S., et al. (2011). Nuclease modulates biofilm formation in community-associated methicillin-resistant *Staphylococcus aureus*. *PLoS One* 6:e26714. doi: 10.1371/journal.pone.0026714
- Kokai-Kun, J. F., Chanturiya, T., and Mond, J. J. (2009). Lysostaphin eradicates established *Staphylococcus aureus* biofilms in jugular vein catheterized mice. *J. Antimicrob. Chemother.* 64, 94–100. doi: 10.1093/jac/dkp145
- Mah, T. F., and O'Toole, G. A. (2001). Mechanisms of biofilm resistance to antimicrobial agents. *Trends Microbiol.* 9, 34–39. doi: 10.1016/s0966-842x(00)01913-2
- Moormeier, D. E., Bose, J. L., Horswill, A. R., and Bayles, K. W. (2014). Temporal and stochastic control of *Staphylococcus aureus* biofilm development. *mBio* 5:e01341-14. doi: 10.1128/mBio.01341-14
- Newell, P. D., Boyd, C. D., Sondermann, H., and O'Toole, G. A. (2011). A c-di-GMP effector system controls cell adhesion by inside-out signaling and surface protein cleavage. *PLoS Biol.* 9:e1000587. doi: 10.1371/journal.pbio.1000587
- O'Toole, G., Kaplan, H. B., and Kolter, R. (2000). Biofilm formation as microbial development. *Annu. Rev. Microbiol.* 54, 49–79. doi: 10.1146/annurev.micro.54.1.49
- Overall, C. M., and Blobel, C. P. (2007). In search of partners: linking extracellular proteases to substrates. *Nat. Rev. Mol. Cell Biol.* 8, 245–257. doi: 10.1038/nrm2120
- Pestrak, M. J., Baker, P., Dellos-Nolan, S., Hill, P. J., Passos da Silva, D., Silver, H., et al. (2019). Treatment with the *Pseudomonas aeruginosa* Glycoside Hydrolase PslG Combats wound infection by improving antibiotic efficacy and host innate immune activity. *Antimicrob. Agents Chemother.* 63:e00234-19. doi: 10.1128/AAC.00234-19
- Roy, A., Kucukural, A., and Zhang, Y. (2010). I-TASSER: a unified platform for automated protein structure and function prediction. *Nat. Protoc.* 5, 725–738. doi: 10.1038/nprot.2010.5
- Singh, V., Verma, N., Banerjee, B., Vibha, K., Haque, S., Tripathi, C. K. M., et al. (2015). Enzymatic degradation of bacterial biofilms using *Aspergillus clavatus* MTCC 1323. *Microbiology* 84, 59–64.
- Stewart, P. S., and Costerton, J. W. (2001). Antibiotic resistance of bacteria in biofilms. *Lancet* 358, 135–138.

- Stewart, P. S., and Franklin, M. J. (2008). Physiological heterogeneity in biofilms. *Nat. Rev. Microbiol.* 6, 199–210. doi: 10.1038/nrmicro1838
- Stoodley, P., Sauer, K., Davies, D. G., and Costerton, J. W. (2002). Biofilms as complex differentiated communities. *Annu. Rev. Microbiol.* 56, 187–209. doi: 10.1146/annurev.micro.56.012302.160705
- Wang, H., Li, S., Wang, J., Chen, S., Sun, X. L., and Wu, Q. (2018). N-glycosylation in the protease domain of trypsin-like serine proteases mediates calnexin-assisted protein folding. *eLife* 7:e35672. doi: 10.7554/eLife.35672
- Waters, C. M., and Goldberg, J. B. (2019). *Pseudomonas aeruginosa* in cystic fibrosis: a chronic cheater. *Proc. Natl. Acad. Sci. U.S.A.* 116, 6525–6527. doi: 10.1073/pnas.1902734116
- Whitchurch, C. B. (2002). Extracellular DNA required for bacterial biofilm formation. *Science* 295, 1487–1487. doi: 10.1126/science.295.5559.1487
- Xia, Y., Chu, W., Qi, Q., and Xun, L. (2015). New insights into the QuikChange process guide the use of Phusion DNA polymerase for site-directed mutagenesis. *Nucleic Acids Res.* 43:e12. doi: 10.1093/nar/gku1189
- Yang, J., Yan, R., Roy, A., Xu, D., Poisson, J., and Zhang, Y. (2015). The I-TASSER Suite: protein structure and function prediction. *Nat. Methods* 12, 7–8.
- Yu, S., Su, T., Wu, H., Liu, S., Wang, D., Zhao, T., et al. (2015). PslG, a self-produced glycosyl hydrolase, triggers biofilm disassembly by disrupting exopolysaccharide matrix. *Cell Res.* 25, 1352–1367. doi: 10.1038/cr.2015.129
- Zhang, J., He, J., Zhai, C., Ma, L. Z., Gu, L., and Zhao, K. (2018). Effects of PslG on the surface Movement of *Pseudomonas aeruginosa*. *Appl. Environ. Microbiol.* 84:e00219. doi: 10.1128/AEM.00219-18
- Zhang, Y. (2008). I-TASSER server for protein 3D structure prediction. *BMC Bioinformatics* 9:40. doi: 10.1186/1471-2105-9-40
- Zhao, T., Zhang, Y., Wu, H., Wang, D., Chen, Y., Zhu, M. J., et al. (2018). Extracellular aminopeptidase modulates biofilm development of *Pseudomonas aeruginosa* by affecting matrix exopolysaccharide and bacterial cell death. *Environ. Microbiol. Rep.* 10, 583–593. doi: 10.1111/1758-2229.12682

Conflict of Interest: The authors have filed a patent application on the use of PslG^{K286A/K433S}.

The authors declare that the research was conducted in the absence of any commercial or financial relationships that could be construed as a potential conflict of interest.

Copyright © 2020 Su, He, Li, Liu, Xu and Gu. This is an open-access article distributed under the terms of the Creative Commons Attribution License (CC BY). The use, distribution or reproduction in other forums is permitted, provided the original author(s) and the copyright owner(s) are credited and that the original publication in this journal is cited, in accordance with accepted academic practice. No use, distribution or reproduction is permitted which does not comply with these terms.



Piperine Impedes Biofilm Formation and Hyphal Morphogenesis of *Candida albicans*

Arumugam Priya and Shunmugiah Karutha Pandian*

Department of Biotechnology, Alagappa University, Karaikudi, India

OPEN ACCESS

Edited by:

Sujogya Kumar Panda,
KU, Leuven, Belgium

Reviewed by:

Ranjith Kumar Manoharan,
Yeungnam University, South Korea
Jintae Lee,
Yeungnam University, South Korea
Rodnei Dennis Rossoni,
São Paulo State University, Brazil

*Correspondence:

Shunmugiah Karutha Pandian
sk_pandian@rediffmail.com

Specialty section:

This article was submitted to
Antimicrobials, Resistance
and Chemotherapy,
a section of the journal
Frontiers in Microbiology

Received: 20 January 2020

Accepted: 30 March 2020

Published: 13 May 2020

Citation:

Priya A and Pandian SK (2020)
Piperine Impedes Biofilm Formation
and Hyphal Morphogenesis
of *Candida albicans*.
Front. Microbiol. 11:756.
doi: 10.3389/fmicb.2020.00756

Candida albicans is the primary etiological agent associated with the pathogenesis of candidiasis. Unrestricted growth of *C. albicans* in the oral cavity may lead to oral candidiasis, which can progress to systemic infections in worst scenarios. Biofilm of *C. albicans* encompasses yeast and hyphal forms, where hyphal formation and yeast to hyphal morphological transitions are contemplated as the key virulence elements. Current clinical repercussions necessitate the identification of therapeutic agent that can limit the biofilm formation and escalating the susceptibility of *C. albicans* to immune system and conventional antifungals. In the present study, a plant-derived alkaloid molecule, piperine, was investigated for the antibiofilm and antihyphal activities against *C. albicans*. Piperine demonstrated a concentration-dependent antibiofilm activity without exerting negative impact on growth and metabolic activity. Inhibition in the hyphal development was witnessed through confocal laser-scanning microscopy and scanning electron microscopy. Interestingly, piperine displayed a tremendous potential to inhibit the virulence-associated colony morphologies, such as filamentation and wrinkling. Furthermore, piperine regulated morphological transitions between yeast and hyphal forms by inhibiting hyphal extension and swapping hyphal phase to yeast forms yet under filamentation-inducing circumstances. Remarkably, piperine-challenged *C. albicans* exhibited low potential for spontaneous antibiofilm resistance development. In addition, piperine effectively reduced *in vivo* colonization and prolonged survival of *C. albicans*-infected *Caenorhabditis elegans*, thereby expounding the distinct antivirulent potential. Transcriptomic analysis revealed piperine significantly downregulating the expression of several biofilm related and hyphal-specific genes (*ALS3*, *HWP1*, *EFG1*, *CPH1*, etc.). Furthermore, no acute toxicity was observed in the HBECs and nematodes exposed to piperine. Altogether, results from this study reveals the potential of piperine to inhibit biofilm and hyphal morphogenesis, and its *in vivo* efficacy and innocuous nature to HBECs suggests that piperine may be considered as a potential candidate for the treatment of biofilm-associated *C. albicans* infection, especially for oral candidiasis.

Keywords: piperine, oral candidiasis, antibiofilm, spontaneous resistance, yeast to hyphal transition, hyphal to yeast transition, wrinkle morphology, HBECs

INTRODUCTION

Members of *Candida* spp. are commensal inhabitants in human microbiota, which expedite their encounter with host surfaces, such as mucosal linings and abiotic prosthetic biomaterials (Ramage et al., 2005). Undesirable predisposing circumstances such as extremes in age, diminished immune system, diabetes mellitus, HIV/AIDS, and exploitation of broad-spectrum antibiotics pave way for *Candida* spp. to mount pathogenicity that consequently trails to candidiasis progressively (Akpan and Morgan, 2002; Millsop and Fazel, 2016). Among various forms of candidiasis, oral candidiasis is depicted to be the most common human fungal infection, specifically in the early and later life (Abu-Elteen and Abu-Alteen, 1998; Meira et al., 2017; Rath, 2017). *C. albicans* is the predominantly encountered species in oral candidiasis patients, irrespective of the denture status (Muadcheingka and Tantivitayakul, 2015). Commensal *C. albicans* in oral cavity generally causes no harm in the healthy individuals, as its growth is restrained by the immune barriers and other commensal microorganisms in the niche (Kaur et al., 2017). However, when any of these barriers are subsided, overgrowth of *C. albicans* can lead to mild local discomfort and altered taste sensation to severe systemic infections with significant morbidity and mortality (Rajendran et al., 2016).

Pathogenicity of opportunistic *C. albicans* infection is contingent on the virulence attributes, which are provoked for its ability to survive under specific environmental stress. The most-emphasized virulent traits of *C. albicans* include morphological transitions between yeast and filamentous forms, phenotypic switching of white to opaque cells, secretion of proteolytic and lipolytic enzymes, biofilm formation, and expression of host-recognizing proteins (Calderone and Fonzi, 2001; Kumamoto and Vines, 2005; Schaller et al., 2005).

Among the several virulent features, biofilm formation is imperious for *C. albicans* (Ramage et al., 2001; Lopez-Ribot, 2005). Also, *C. albicans* is the predominant fungal species associated with biofilm formation (Douglas, 2002). Biofilms of *C. albicans* are highly heterogeneous encompassing both cellular (matrix enclosed with microcolonies of yeast and hyphal cells) and noncellular (e.g., cell wall like polysaccharides) components. A well-structured *C. albicans* biofilm can be established on both biotic and abiotic surfaces, and resistance to antifungals by sessile-phase cells are ascertained to escalate with increase in biofilm formation (Chandra et al., 2001; Ganguly and Mitchell, 2011; Tobudic et al., 2012). Consequently, the high degree of biofilm-associated resistance hinders the efficacy of currently available therapies (Mathe and Van Dijck, 2013). Thus, in order to conquer the inabilities of current antifungal therapies for curing candidiasis, alternative therapeutic regimens targeting only the virulence attributes of pathogen will be advantageous (Anibal et al., 2010; Mehra et al., 2012).

From ancient times, medicinal plants have been expended to cure a vast range of human ailments. In last two decades, numerous plant-derived molecules have been explored for the antibiofilm activity as a prophylaxis against the biofilm formation (Abraham et al., 2012; Slobodnikova et al., 2016). Hampering the adherence of organism and allowing it to survive in a

planktonic state will eventually increase its susceptibility toward the host immune system and the antibiotic treatment (Nogueira et al., 2017). For oral biofilm infections, some of the antibiofilm agents derived from plant essential oils are systemically being evaluated in clinical trials (Lu et al., 2019). These studies provide a promising perspective regarding the use of plant based antibiofilm compounds for the oral care.

With this milieu, the present study was aimed at evaluating the antibiofilm potential of a plant alkaloid piperine against the sessile state of *C. albicans*, a notorious fungal species in the pathogenesis of oral candidiasis. Piperine is a major alkaloid bioactive component found in the seeds of pepper, which is renowned for imparting pungency to it. In ancient medicine, black pepper was used to treat an array of discomforts and diseases including influenza, rheumatism, migraine, etc. (Chavarria et al., 2016; Gorgani et al., 2017). Piperine was also reported for its numerous therapeutic activities such as antimicrobial, antioxidant, chemoprotective, antiinflammatory, neuroprotective activity, etc. (Mittal and Gupta, 2000; Pradeep and Kuttan, 2002). Thus, in the present study unexplored antibiofilm potential of piperine against *C. albicans* was investigated and found to exhibit a spectacular antibiofilm and antihyphal activity.

MATERIALS AND METHODS

Ethics Statement

In the present study, Human Buccal Epithelial Cells (HBECs) were collected from the healthy individuals by a gentle oral swab in the mucosal surface of cheeks, after obtaining a written informed consent. The experimental protocol and the use of HBECs were assessed and approved by the Institutional Ethical Committee, Alagappa University, Karaikudi (IEC Ref No: IEC/AU/2018/5). All methods were carried out in accordance with relevant guidelines and regulations.

Fungal Strain, Culture Media and Conditions

In this study, a reference fungal strain *C. albicans* obtained from American Type Culture Collection (ATCC 90028) was used. For maintenance, thawed suspension from glycerol stock (30%) stored at ultra-low deep-freezing condition (-80°C) was streaked on yeast extract peptone dextrose (YEPD) agar plates (1.8%) and incubated at 37°C for 24 h and stored at 4°C for further use. Routine culturing for *in vitro* assays was performed with YEPD broth. *In vitro* assays allied with biofilm formation, and hyphal development was carried out with Spider medium comprising 1% of mannitol, 0.2% of dipotassium hydrogen phosphate, and 1% of nutrient broth. To investigate the effect of piperine on the preformed hyphae of *C. albicans*, RPMI medium (HiMedia, India) was used.

Phytochemicals

Following phytochemicals were used for screening of potential antibiofilm molecule against *C. albicans*: cineole, 4-isopropyl

benzaldehyde, α -pinene, chlorogenic acid, α -terpinene, borneol, octadecene, lupenol, eicosene, ellagic acid, catechin, gallic acid, ferulic acid, limonene, piperine, carvacrol, α -methyl benzylamine, stearic acid, naringin, hesperidin, indole-3-acetic acid, eladic acid, caffeine, methyl palmitate, and 2,4-D-palmitoyl L-ascorbic acid. Piperine (PubChem CID: 638024) was procured from HiMedia, India. Stock solution of piperine was prepared as 50 mg mL⁻¹ with methanol and stored at room temperature for further use. To inspect the effect of methanol on viability and biofilm formation, medium containing inoculum and devoid of compound alone was added with methanol during initial screening assays as a vehicle control.

Screening of Phytochemicals With Potential Antibiofilm Activity Against *C. albicans*

A total of 25 different aforementioned phytochemicals was used for screening of potential antibiofilm molecule against *C. albicans* in a 24-well microtiter plate (MTP) assay using two different growth media, viz. YEPD and Spider broth for evaluation of growth and biofilm, respectively. Each well was loaded with 1 mL of respective medium, 1% of overnight *C. albicans* culture as inoculum, and phytochemicals at 500 μ g mL⁻¹ concentration. The plates were incubated at 37°C for 24 and 48 h for YEPD and Spider medium, respectively. After incubation period, the plates were read at 600 nm to assess the change in cell density. For assessment of biofilm, planktonic cells from Spider-grown cells were decanted and washed with PBS to remove loosely bound cells. Surface attached cells were then stained with 0.4% crystal violet for 10 min. Biofilm cells were finally quantified by addition of 15% glacial acetic acid followed by spectroscopic observation at 570 nm.

Effect of Piperine on Growth and Biofilm of *C. albicans*

Determination of Minimum Inhibitory Concentration (MIC)

Impact of piperine on the survival of *C. albicans* was assessed using microbroth dilution method according to the guidelines of Clinical and Laboratory Standards Institute (Clinical and Laboratory Standards Institute [CLSI], 2008). Briefly, 1% of overnight *C. albicans* culture was used to inoculate 1 mL of YEPD broth. Test groups were supplemented with varying concentrations of piperine, ranging from 2 to 1,024 μ g mL⁻¹. YEPD medium alone served as negative control. The plate was incubated for 24 h at 37°C. Following incubation, cell density was evaluated by measuring absorbance at 600 nm in multifunctional spectrophotometer (Spectra Max 3, Molecular Devices, United States). For visible assessment of the growth effects, 5 μ L of cells from each well was spotted on YEPD agar plate and incubated at 37°C for 24 h, and the image was photographed.

Metabolic Viability Assay

Metabolic viability of *C. albicans* control and piperine-treated cells was ascertained through a dye-based assay (Repp et al.,

2007). Stock solution of 10 mg mL⁻¹ of Alamar blue [Resazurin (7-Hydroxy-3H-phenoxazin-3-one 10-oxide)] was prepared in 1 \times phosphate buffered saline (PBS) and stored at 4°C until use. Control and piperine-treated *C. albicans* cells were cultured as previously mentioned. Post incubation, cells were harvested by centrifugation at 8,000 rpm for 10 min and washed twice with PBS. Cell pellets resuspended with 1 mL of 1 \times PBS were added with 100 μ g of Alamar blue and incubated in dark at 37°C for 18–24 h. Alamar blue added to PBS alone served as negative control. Subsequently, samples were centrifuged, and fluorescent intensity of the supernatant was observed at 560 and 590 nm of excitation and emission wavelengths, respectively.

Determination of Minimum Biofilm Inhibitory Concentration (MBIC)

The effect of piperine on the biofilm formation of *C. albicans* was performed in 24-well MTP (Muthamil et al., 2018). Briefly, overnight culture of *C. albicans* (1%) was used to inoculate 1 mL of Spider broth in the absence (untreated control) and presence (treated) of test phytochemical piperine with the increasing concentrations, from 2 to 1,024 μ g mL⁻¹. Appropriate vehicle and negative controls were maintained parallelly. The plates were incubated statically for 48 h at 37°C. Planktonic cells were aspirated and the biofilm cells that are adhered to the surface of wells were rinsed with sterile distilled water to detach loosely bound cells and allowed to air dry. Successively, the wells were stained with 0.4% crystal violet stain for 10 min at room temperature. Surplus stain that are not bound were removed and washed with sterile distilled water. Stain bound to the biofilm cells was resuspended with 1 mL of 15% glacial acetic acid. Absorbance was read at 570 nm using multifunctional spectrophotometer. A minimum of 80% inhibition in biofilm formation was considered as MBIC (Subramenium et al., 2018). The percentage of biofilm inhibition was determined by means of the following formula:

$$\text{Percentage of biofilm inhibition} = \left[\frac{(\text{Control OD}_{570 \text{ nm}} - \text{Treated OD}_{570 \text{ nm}})}{\text{Control OD}_{570 \text{ nm}}} \right] \times 100$$

Effect of BIC on Growth of *C. albicans*

To assess the effect of piperine (at BIC-32 μ g mL⁻¹) on growth of *C. albicans*, growth curve analysis was performed in the absence and presence of piperine and amphotericin B (antifungal, positive control for growth inhibition) over a 24-hour period with 1-hour time interval, spectroscopically. Growth curve was plotted as absorbance at 600 nm against time interval.

In situ Visualization of Biofilm Inhibition

For microscopic visualization, *C. albicans* cells in the absence and presence of piperine at BIC and sub-BIC concentrations were allowed to form biofilm for 48 h at 37°C on a 1- \times 1-cm glass surface immersed in 1 mL of Spider medium. The glass slide pieces were then washed twice with PBS and air-dried. Based on the microscopic analysis to be performed, slides were further processed accordingly (Prasath et al., 2019).

Light Microscopic Analysis

For light microscopic visualization, glass sides were stained with 0.4% crystal violet and incubated for 10 min. Excess stain was removed by washing in distilled water and air dried. Crystal violet stained biofilm cells were visualized under light microscope (Nikon Eclipse 80i, United States) at a magnification of $\times 400$, and the images were documented with the accompanied digital camera.

Confocal Laser Scanning Microscopic (CLSM) Analysis

For CLSM, glass slides were stained with 0.1% acridine orange and incubated in dark for 5 min. Slides were washed with distilled water to remove excess stain. Subsequently, the slides were air-dried and viewed under CLSM (LSM 710, Carl Zeiss, Germany).

Scanning Electron Microscopic (SEM) Analysis

For SEM analysis, the biofilm cells formed on the glass slides were fixed with 2.5% glutaraldehyde for 1.5 h, followed by dehydration for 5 min with increasing concentrations of ethanol (20, 40, 60, 80, and 100%). Eventually, the slides were air-dried completely and visualized under SEM (Quanta FEG 250, United States).

Effect of Piperine on Virulence Attributes of *C. albicans*

Effect of Piperine on Filamentous Morphology

Effect of piperine on filamentous morphology of *C. albicans* was appraised by the use of Spider medium supplemented with fetal bovine serum (FBS), as described by Muthamil et al. (2018), with minor modifications. Initially, the Spider agar was autoclaved and, when the temperature dampened to 55°C, 5% of FBS and piperine at sub-BICs and BIC were added. Solid agar devoid of compound alone served as control. After proper solidification, 5 μ L of 24 h old *C. albicans* culture was spotted on the center of agar surface and the plates were kept for incubation at 37°C for 5 days. The observed filamentous morphology was documented using Gel documentation system (Bio-Rad Laboratories, XR+, United States).

Impact on Wrinkle Morphology

Effect of piperine on colony morphology of *C. albicans* was appraised using solid agar medium. Autoclaved YEPD agar medium was added with sub-BICs and BIC of piperine once the temperature dampened below 55°C. YEPD agar plate without piperine was deliberated as control. Later, 5 μ L of overnight *C. albicans* culture was spotted at the midpoint of agar surface and incubated at 37°C for 72 h. At the end of incubation period, the colony morphologies were documented using gel documentation system.

Effect on Yeast-to-Hyphal Transition

Influence of piperine on the yeast-to-hyphal phase transition of *C. albicans* was reckoned by the method described by Messier et al. (2011), with presumed alterations. Briefly, 1% of overnight culture of *C. albicans* was inoculated in YEPD liquid medium comprising 10% FBS and incubated at 37°C under aerobic conditions with constant shaking at

160 rpm. Piperine in BIC/sub-BIC was added in the treatment groups whereas the similar constitution without piperine was deliberated as control. Yeast cells and hyphal forms were figured and documented by light microscopic observation after 4 h of incubation.

Effect on Hyphal-to-Yeast Transition

Efficacy of piperine to switch hyphal form to yeast cells was scrutinized by the procedure illustrated by Vedyappan et al. (2013). *C. albicans* was allowed to form hyphae by incubating in RPMI medium for 4 h at 37°C with gentle shaking. Consequently, after 4 h, piperine at sub-BICs and BIC was added and observed under light microscopy after 2, 4, and 6 h of incubation.

Assessment of Spontaneous Resistance Development by *C. albicans* Biofilm Against Piperine

Development of spontaneous resistance to piperine by *C. albicans* biofilm was determined based on the concept described by Min et al. (2017), which was further expounded according to this study. Overnight culture of *C. albicans* was adjusted to 1×10^8 cells and then challenged with varying concentrations of piperine ($1 \times$ and $10 \times$ of the sub-BICs and BIC) on YEPD agar plates and incubated at 37°C for 48 h. Prior to documentation, a single colony from each plate (control and piperine challenged) was used to inoculate YEPD liquid medium, which was further streaked on YEPD agar plates and maintained at 4°C for subsequent biofilm assays. Thereafter, MBIC was assessed for all the piperine-challenged *C. albicans* cells, similar to the protocol stated for determination of MBIC.

In addition to this, subsequent passage assay was performed from lowest ($8 \mu\text{g mL}^{-1}$) to highest concentration of piperine ($128 \mu\text{g mL}^{-1}$). Initial passage was commenced with $8 \mu\text{g mL}^{-1}$ concentration, and for subsequent passages, *C. albicans* was challenged twice with each concentration (8, 16, 32, 64 and $128 \mu\text{g mL}^{-1}$). A total of 10 passages was performed, and control and treated *C. albicans* from each passage were subjected to following analysis to assess the effect of continuous exposure of piperine on spontaneous resistance development. Initially, control and treated *C. albicans* from each passage were allowed to form biofilm on 24 well-MTP, followed by assessment of biofilm biomass through the crystal violet staining method, as described earlier.

To evaluate the hyphal extension, cells were incubated in hyphal inducing RPMI medium for 4 h and induction of hyphae was assessed microscopically after 1 and 4 h of incubation using Fluorescent microscope (Nikon Eclipse Ts2R, Japan).

In addition to surface attached biofilm and hyphal extension, air-liquid interface biofilm formation was evaluated through flor formation assay. Briefly, control and treated *C. albicans* from each passage was introduced as inoculum in 2 ml YEPD broth and incubated for 24 h. After incubation, the cells were pelleted by centrifugation and washed twice with PBS. Then, 2 mL of flor medium containing yeast nitrate broth with 4% ethanol was added and statically incubated at 30°C for 3 days. The biofilm formation on air-liquid interface was documented after incubation period (Prasath et al., 2019).

Disintegration off Mature Biofilm

Biofilm disruptive potential of piperine was evaluated using CLSM, with Live/Dead staining (BacLight, Molecular Probes, United States) (Kiran et al., 2015). *C. albicans* was allowed to form biofilm on 1 × 1-cm glass slide surface for 48 h at 37°C. Spent medium from the wells was decanted and piperine at 2 × BIC was supplemented to the wells added with fresh Spider broth. After 3 h of incubation at 37°C, glass slides were washed twice with PBS and stained with propidium iodide (PI) and SYTO9 (1 μM concentration of each) for 5 min. Unbound stains were excluded by a gentle rinse in PBS, and eventually, biofilm cells were visualized under CLSM.

Gene Expression Profiling by Real-Time PCR

Total RNA was extracted from *C. albicans* culture grown for 24 h at 37°C with a constant shaking at 160 rpm in the absence and presence of piperine at its BIC (32 μg mL⁻¹) by Trizol method of RNA isolation according to the manufacturers' protocol. Isolated RNA was dissolved in 20 μL of 0.1% diethylpyrocarbonate (DEPC)-treated water and the quality check was performed by agarose gel electrophoresis. Subsequently, RNA samples were reverse-transcribed into cDNA using high-capacity cDNA Reverse Transcription Kit (Applied Biosystems, United States) in the thermal cycler (Eppendorf, Germany).

qPCR reactions were performed in a total volume of 10 μL. The primers for the individual genes were added discretely with SYBR Green Master Mix (Applied Biosystems, United States) reagents at a predefined ratio. Expression profile

of candidate genes (list of genes, primer details, and function are provided in **Table 1**) were analyzed using the thermal cycler (7500 Sequence Detection System). The expression pattern of candidate genes was normalized against β-actin expression (housekeeping gene) and quantified using the $\Delta\Delta$ CT method (Livak and Schmittgen, 2001).

Effect of Piperine on *C. elegans* Survival and *in vivo* Biofilm of *C. albicans*

Toxicity of piperine and its impact on the biofilm formation of *C. albicans* *in vivo* condition was reviewed using a simple eukaryotic model organism *C. elegans*, which is often expended in toxicological investigation. Wild-type nematode (N₂) procured from *C. elegans* Genome Center (CGC) was used in this study. For all the evaluation, a synchronized population of nematodes (young adult) was obtained through bleaching. For assessment of toxicity and rescue, approximately 10 worms were transferred to 24-well MTP containing M9 buffer. *E. coli* OP50 (1 × 10³ cells) was used as a food source for the worms. Worms were segregated into four groups: (i) control group (*E. coli* OP50 alone); (ii) vehicle control containing methanol in addition to food source; (iii) piperine at various concentrations (16, 32, 64, 128, and 256 μg mL⁻¹); and (iv) *C. albicans* cells in the absence and presence of piperine at 16, 32, and 64 μg mL⁻¹, respectively. Survival rate of worms were monitored for every 24 h for 9 days using a stereo microscope (Nikon SZ-1000, Japan). For *in vivo* colonization assessment, worms were crushed in saline and plated on candida differential agar. Internal colonization was also observed under CLSM (Swetha et al., 2019; Valliammai et al., 2019).

TABLE 1 | List of genes, their function in pathogenicity of *C. albicans*, and primer sequences used in the study.

S.No	Gene	Function	Primer sequence (5'-3')		Candida Genome Database Reference number
			Forward	Reverse	
1	<i>CPH1</i>	Transcription factor involved in pseudohyphal and hypha formation	TATGACGCTTCTGGGTTTCC	ATCCCATGGCAATTTGTTGT	<i>C. albicans</i> CPH1/C1_07370C
2	<i>CDR2</i>	ATP-binding cassette (ABC) superfamily, Multidrug transporter	ATGGCTATTGTTGAACTGTCATTG	CCCTTTACCGAAAAGTGGAGTAG	<i>C. albicans</i> CDR2/C3_04890W
3	<i>EFG1</i>	Transcriptional regulator for switch between white and opaque cells. Required for biofilm formation	GCCTCGAGCACTTCCACTGT	TTTTTTCATCTTCCCACATGGTAGT	<i>C. albicans</i> EFG1/CR_07890W
4	<i>HST7</i>	Required for opaque mating or white biofilm formation	TCATCAGCTTCTCTATAC	TATTGAGGAAATGACAGTT	<i>C. albicans</i> HST7/CR_03900W
5	<i>UME6</i>	Transcriptional regulator of filamentous growth	ACCACCACTACCAACCAC	TATCCCCATTTCOAAGTCCA	<i>C. albicans</i> UME6/C1_06280C
6	<i>EAP1</i>	Cell adhesion, filamentation and invasion	TGTGATGGCGTTCTTGTTTC	GGTAGTGACGGTGATGATAGTGACA	<i>C. albicans</i> EAP1/C2_09530W
7	<i>HWP1</i>	Hyphal development, biofilm formation	GCTCCTGCTCCTGAAATGAC	CTGGAGCAATTGGTGAGGTT	<i>C. albicans</i> HWP1/C4_03570W
8	<i>RAS1</i>	Cell adhesion, filamentous growth, hyphal induction	CCCAACTATTGAGGATTCTTATCGTAAA	TCTCATGGCCAGATATTCTTCTTG	<i>C. albicans</i> RAS1/C2_10210C
9	<i>ALS3</i>	Adhesion, Agglutinin like protein	CAACTTGGGTTATTGAAACAAAAACA	AGAAACAGAAACCAAGAACAACC	<i>C. albicans</i> ALS3/CR_07070C
10	<i>TUP1</i>	Transcriptional repressor, represses filamentation, regulates switching	CTTGAGATTGGCCCATAGAA	TGGTGCCACAATCTGTTGTT	<i>C. albicans</i> TUP1/C1_00060W
11	<i>ALS1</i>	Cell surface adhesin	CCTATCTGACTAAGACTGCACC	ACAGTTGGATTTGGCAGTGGA	<i>C. albicans</i> ALS1/C6_03700W
12	<i>CDR4</i>	Putative ABC transporter superfamily	TACGGTGCTCCAAAATGTCC	TGGGCAGCAATAATGTAATCC	<i>C. albicans</i> CDR4/C1_08070W
13	<i>ECE1</i>	Hyphal specific protein, Candidalysin	CCAGAAATTGTTGCTCGTGTGCCA	TCCAGGACGCCATCAAAACGTTAG	<i>C. albicans</i> ECE1/C4_03470C

Effect of Piperine on Human Buccal Epithelial Cell (HBEC)

As this study is intended to evaluate the therapeutic potential of *C. albicans* for its application in oral candidiasis, safety evaluation was further evaluated with the HBEC. HBECs were collected from the healthy individuals with suitable oral hygiene by gently rubbing a sterile swab on the mucosal surface of the cheeks. Subsequently, the sterile swabs were suspended in sterile PBS and used immediately. The suspended HBECs were further centrifuged, and the pellets were washed thrice with sterile PBS (Souza et al., 2018). A suspension with 5.0×10^5 cells ml^{-1} was prepared by counting the cell suspension through Automatic cell counter (Countess II FL, Invitrogen, United States). HBECs were then incubated with different concentrations of piperine (8, 16, 32, 64, and 128 $\mu\text{g ml}^{-1}$) and incubated for 20 min at 37°C. Hydrogen peroxide was used as positive control. After 20 min of incubation, the cells were stained with crystal violet and visualized under microscope (Nikon Eclipse Ts2R, Japan) to assess morphological variations due to effect of the compound.

Statistical Analysis

All the experiments were carried out in three biological replicates with at least two technical replicates and values are presented as mean \pm standard deviation (SD). To analyze the significant difference between the values of control and treated samples, one-way analysis of variance (ANOVA) and Duncan's *post hoc* test was performed with the significant *p*-value of <0.05 by the SPSS statistical software package version 17.0 (Chicago, IL, United States).

RESULTS

Screening of Phytochemicals With Potential Antibiofilm Activity Against *C. albicans*

Growth and biofilm inhibitory potential of 25 different phytochemicals were evaluated against *C. albicans*. From **Figure 1A**, in comparison with the effect of phytochemicals on growth and biofilm, piperine was found to be the potential antibiofilm agent against *C. albicans*, as it inhibited $>90\%$ of biofilm formation without affecting the growth. All other phytochemicals were found to be either growth inhibitory with increased antibiofilm activity (if growth was found to be inhibited, apparently biofilm will not be formed) (e.g., α -terpinene, borneol) or non-growth inhibitory with no antibiofilm activity (e.g., naringin, hesperidin). Thus, from screening 25 different phytochemicals, piperine was found to be the only compound that had biofilm inhibitory potential without exerting negative impact on growth. Henceforth, piperine was chosen to study its antibiofilm efficacy and influence on other virulence attributes of *C. albicans*.

Antibiofilm Potential of Piperine With No Significant Impact on Growth and Metabolic Viability of *C. albicans*

Initially, the impact of piperine on growth of *C. albicans* was investigated by determination of MIC. Primarily, result revealed that the growth of *C. albicans* was not significantly influenced by piperine, even at the highest tested concentration (1,024 $\mu\text{g ml}^{-1}$). For substantiation of non-antifungal effect of piperine, the metabolic viability of *C. albicans* in the absence and presence of piperine was appraised by Alamar Blue assay. On visual observation, the resazurin dye (purple color) was found to be reduced to resorufin, a pink-colored fluorescent dye that evidenced the active cellular metabolism. Furthermore, the fluorescent intensity was found to be unchanged between control and piperine-treated *C. albicans*. For further validation, spot assay confirmed that piperine treatment did not affect the cell growth in comparison with the control. Distinctly, these results depicted that piperine does not exert negative impact on the growth and metabolic viability of *C. albicans* (**Figures 2A,B**).

Subsequently, evaluation of antibiofilm potential of piperine divulged the dose-dependent decrease in biofilm biomass of *C. albicans*. At 32 $\mu\text{g ml}^{-1}$ concentration, a maximum of 93% of biofilm was found to be inhibited by piperine. Successive concentrations above 32 $\mu\text{g ml}^{-1}$ did not display any significant increase in antibiofilm activity. Hence, 32 $\mu\text{g ml}^{-1}$ was considered as BIC, and further assays were carried out with BIC and sub BICs (**Figure 2C**).

Further, no significant change in the growth was observed between the growth of *C. albicans* in the absence and presence of 32 $\mu\text{g ml}^{-1}$ of piperine when compared to Amphotericin B, which completely inhibited the growth of *C. albicans* at 10 $\mu\text{g mL}^{-1}$ (**Figure 2D**).

Piperine Deteriorates Surface Adherence and Hyphal Development in *C. albicans*

Effect of piperine on biofilm architecture of *C. albicans* was perceived through microscopic observations. Light and CLSM micrographs disclosed the well-structured biofilm matrix with yeast and hyphal cells in control, whereas tremendously inhibited microcolony formation and hyphal network in a dose-dependent manner was seen in piperine treatment. In sub-BICs of piperine (16 and 8 $\mu\text{g mL}^{-1}$), shorter hyphal protrusions with scattered yeast cells were observed (**Figures 3A,B**).

Furthermore, SEM micrographs revealed similar discrepancy in the biofilm architecture of control and piperine-treated *C. albicans*. At BIC, hyphal protrusions and yeast to hyphal transitions were completely suppressed, and few yeast cells were found to be scarcely dispersed, whereas control *C. albicans* displayed a structurally complex and dynamic biofilm network encompassing cells with yeast and hyphal morphologies (**Figure 3C**).

Piperine Diminishes the Virulence Traits of *C. albicans*

Various virulence attributes of *C. albicans* was found to be impaired by the ability of piperine.

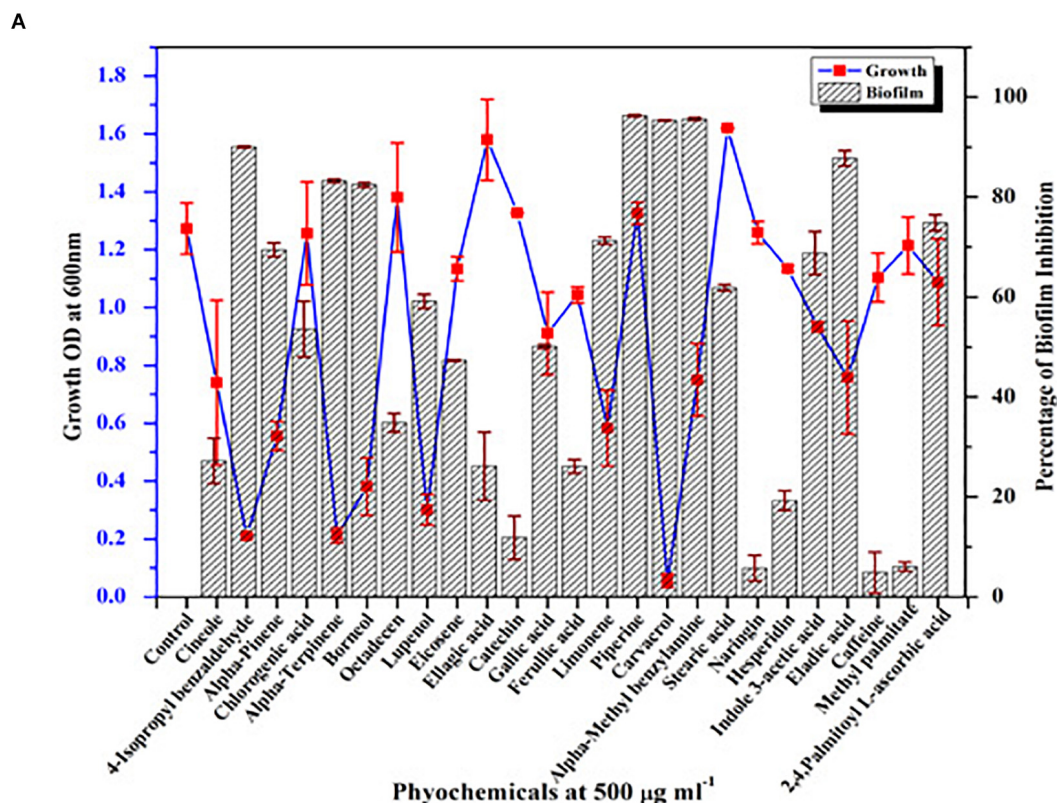


FIGURE 1 | Screening of phytochemical with potential antibiofilm activity against *C. albicans*. **(A)** Screening of various phytochemicals for antibiofilm activity against *C. albicans* through assessment of growth and biofilm inhibitory efficiency. Error bars represent standard deviations from the mean ($n = 3$). **(B)** Chemical structure of piperine, the potential antibiofilm molecule found through screening of various phytochemicals. The three major components in the chemical structure of piperine were boxed within red colored square viz. piperidine ring, conjugated double bonds, and methylenedioxyphenyl ring.

Filamentous Morphology

Filamentous morphology, especially in hyphal forms of *C. albicans*, contributes to the augmented virulence and pathogenicity, owing to its potential to breach and invade the host cells and confront immune attack. *C. albicans* treated with piperine at BIC was found to be devoid of filamentous growth. Complete suppression of filament development in *C. albicans* indicates the attenuated pathogenicity. Reduction in

filamentation was observed in sub-BIC's of piperine (16 and $8 \mu\text{g mL}^{-1}$) (Figure 4A).

Wrinkled Colony Morphology

Different from the smooth and flat colonies, wrinkled colonies of *C. albicans* facilitate improved access to oxygen, which in turn augments the hyphal development. Supplementing piperine to *C. albicans* culture resulted in the disappearance of wrinkle

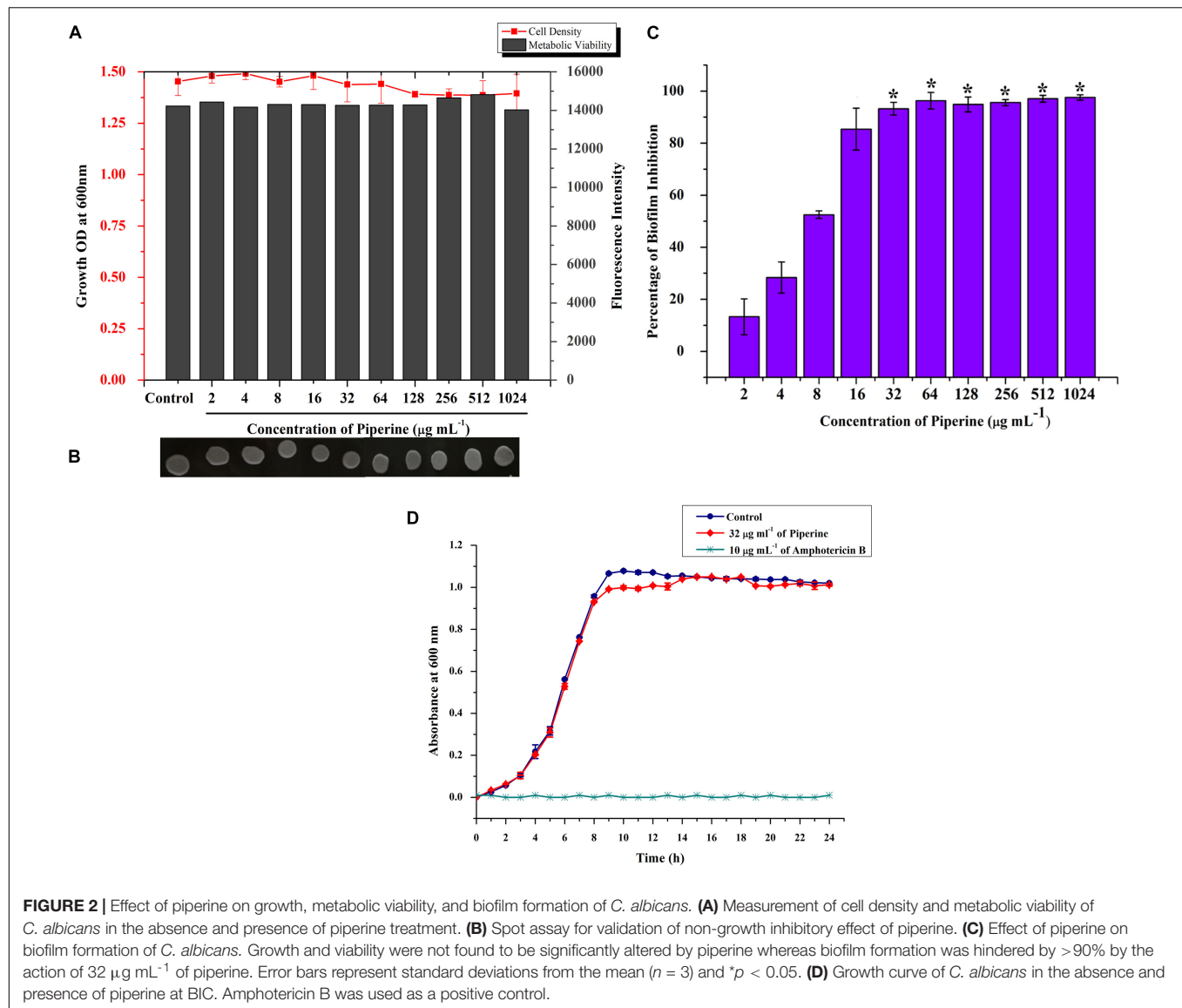


FIGURE 2 | Effect of piperine on growth, metabolic viability, and biofilm formation of *C. albicans*. **(A)** Measurement of cell density and metabolic viability of *C. albicans* in the absence and presence of piperine treatment. **(B)** Spot assay for validation of non-growth inhibitory effect of piperine. **(C)** Effect of piperine on biofilm formation of *C. albicans*. Growth and viability were not found to be significantly altered by piperine whereas biofilm formation was hindered by >90% by the action of 32 $\mu\text{g mL}^{-1}$ of piperine. Error bars represent standard deviations from the mean ($n = 3$) and $*p < 0.05$. **(D)** Growth curve of *C. albicans* in the absence and presence of piperine at BIC. Amphotericin B was used as a positive control.

phenotype, compared to the undulating filaments in untreated control. Even at the lowest sub-BIC (8 $\mu\text{g mL}^{-1}$), no wrinkling was observed which describes the potential antivirulent efficacy of piperine (Figure 4B).

Yeast to Hyphal Transition

It is postulated that yeast to hyphal transition is one of the prerequisites for the biofilm formation by *C. albicans*. Under hyphal inducing condition (supplemented with FBS), yeast to hyphal transition in piperine-treated and untreated *C. albicans* was microscopically observed. A highly entangled hyphal network with intruded yeast cell aggregates was witnessed in the control, whereas dispersed yeast cells with much-reduced aggregates were spotted in the piperine-treated *C. albicans* culture at its BIC. Dose-dependent response in yeast to hyphal transition was also evidenced. Furthermore, these results were in line with the antibiofilm and hyphal inhibition activities (Figure 5A).

Hyphal to Yeast Transition

In addition to restricting yeast to hyphal transition, competency of piperine to switch preformed hyphal cells to yeast state was evaluated under hyphal inducing condition (supplementation of RPMI medium). Preformed hyphal cells incubated with different concentrations of piperine were routinely monitored under light microscope and figured that after 6 h, over 90% of cells were swapped to yeast forms in BIC of piperine. Hyphal to yeast transition was observed in a dose- and time-dependent fashion (Figure 5B).

Diminished Potential for Spontaneous Resistance Development Against Piperine by *C. albicans*

Resistance development contributes to the recalcitrant and recurrent biofilm formation. Henceforth, the spontaneous antibiofilm resistance to piperine by *C. albicans* was evaluated.

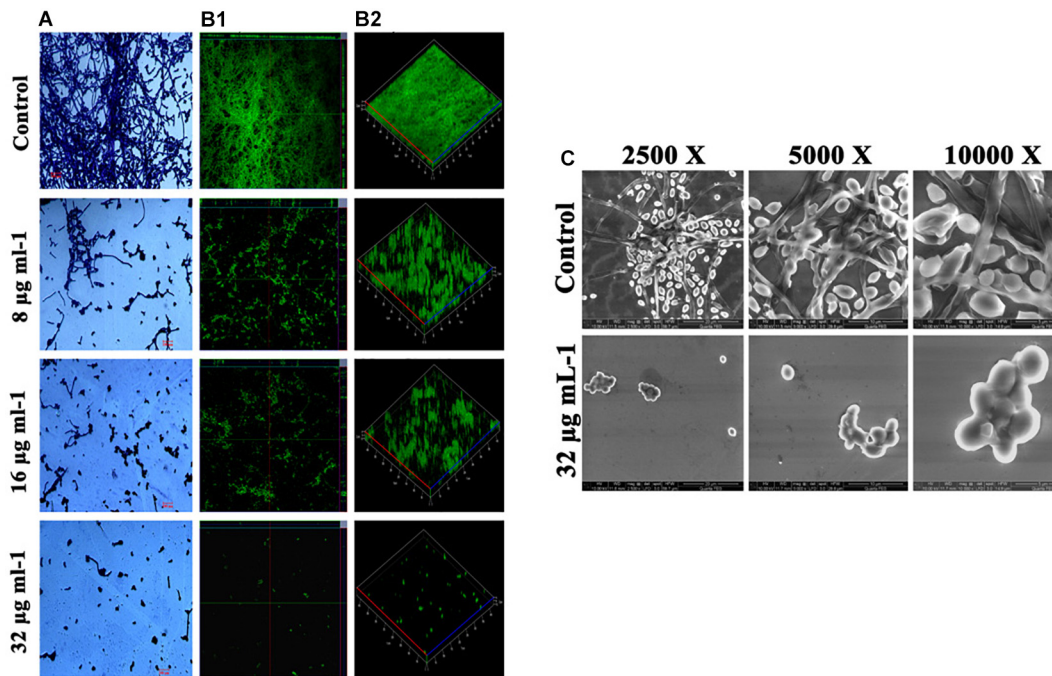


FIGURE 3 | Deterioration in the *C. albicans* surface adherence and hyphal development by piperine. **(A)** Light microscopic micrographs depicting decrease in the biofilm formation and hyphal development. **(B-1,B-2)** Biofilm architecture of *C. albicans* in ortho and 3D view, respectively. **(C)** SEM micrographs displaying the biofilm network of control and piperine-treated *C. albicans* under different magnifications.

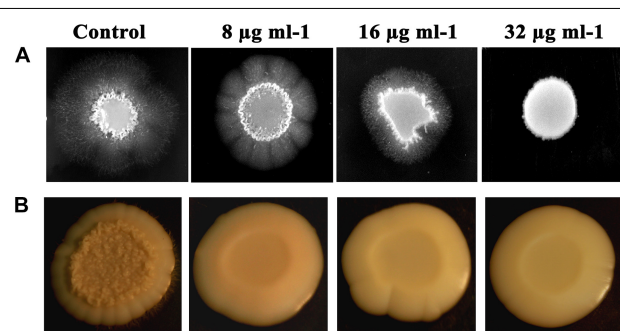


FIGURE 4 | Piperine impeding the primary virulence attributes of *C. albicans*. **(A)** Filamentous development of *C. albicans* under the impact of piperine. **(B)** Wrinkle colony morphology.

C. albicans cultured in piperine-challenged ($1\times$ and $10\times$ concentrations of 0.25, 0.5, 1, and 2 BIC) environment was assessed for the biofilm forming potential. Primarily, no reduction in number of colonies was observed in control and piperine-challenged plates. Wrinkled morphology was observed in all the colonies of control plates, whereas smooth and flat colonies were observed in the piperine-challenged plates (Figure 6A). This result was in line with the potential to suppress wrinkled colony morphology. In addition, this result also demonstrates the consistent antivirulent potential of piperine. Piperine-challenged *C. albicans* was found to form slightly diminished biofilm which makes it more vulnerable

to piperine in consequential supplement. Thus, for piperine challenged *C. albicans*, MBIC in subsequent treatment dropped below $32\ \mu\text{g mL}^{-1}$ (Figure 6B).

A resistance assay carried out by passaging *C. albicans* cells from a lower ($8\ \mu\text{g mL}^{-1}$) to a higher concentration ($128\ \mu\text{g mL}^{-1}$) of piperine was evaluated for resistance development if any by various assays. Biofilm biomass of *C. albicans* grown in the presence of $32\ \mu\text{g/mL}$ and greater concentration of piperine was found to be reduced (Figure 6D). In addition to this, the habituated cells were grown under hyphal inducing condition (RPMI medium) and found that piperine controlled the extensive hyphal network formation even in the successive passages (Figure 6C).

In addition to the biofilm forming ability and hyphal extension activity, biofilm formed in the air liquid interface was also found to be reduced in the passages continuously exposed to lower to higher concentration of piperine (Figure 6E).

All these results substantiate that piperine does not induce spontaneous or adaptive antibiofilm resistance development in *C. albicans*.

Dispersal of Mature *C. albicans* Biofilm by Piperine

In addition to the antibiofilm potential, the ability of piperine to disrupt the preformed biofilm was perceived through CLSM. Piperine at $2\times$ BIC effectively dislodged a massive part of the biofilm architecture with few hyphal protrusions left behind. Among them, a scarce

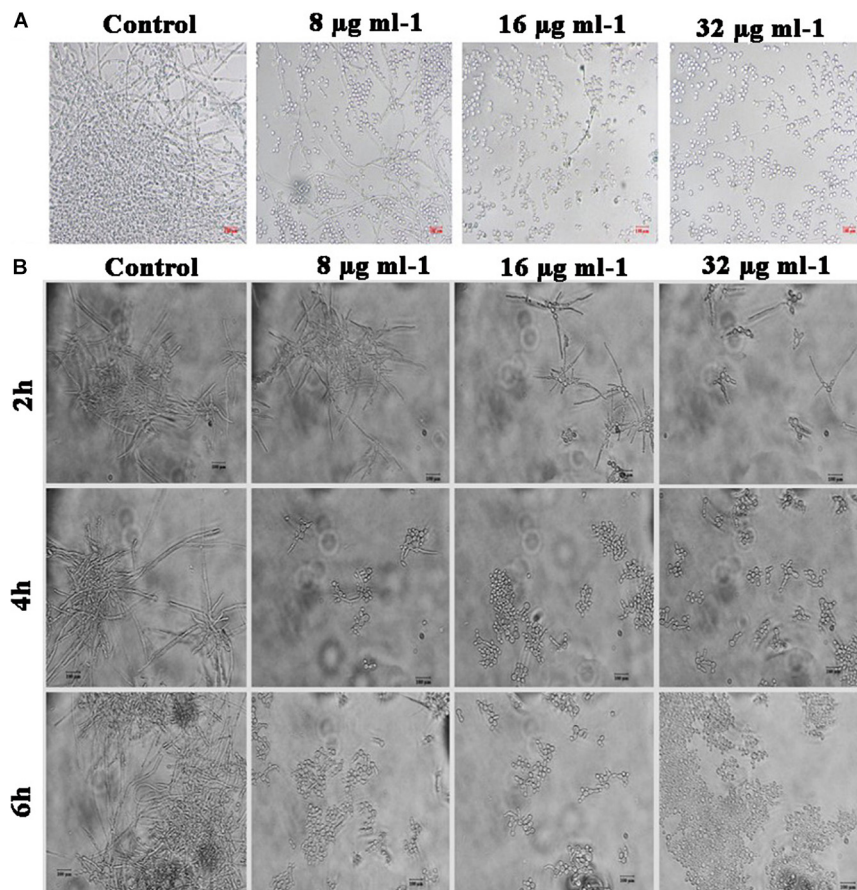


FIGURE 5 | Effect of piperine on phenotypic switching. **(A)** Control in the morphological transition from yeast to hyphal form. **(B)** Transition of preformed hyphal cells to yeast forms in time course (2, 4, and 6 h).

population was found to be deceased. This result expounded the mature biofilm-disruptive potential of piperine, which makes it more appropriate for not only the prevention but also for the treatment of established biofilm infection (Figure 7).

Differential Gene Expressions by Piperine

Transcriptional level of hyphal-specific and biofilm-related genes in *C. albicans* in the absence and presence of piperine was quantified by real time PCR. Piperine at BIC significantly downregulated the expression of transcriptional regulators of filamentous growth, such as *CPH1*, *UME6*, and *EFG1*, and hyphal specific genes, such as *EAP1*, *HWP1*, *HST7*, *RAS1*, *ECE1*, and biofilm-related genes such as *ALS3* and *ALS1*. In addition to this, candida drug resistance gene *CDR4* and *CDR2* was found to be significantly downregulated. Furthermore, a transcriptional repressor *TUP1*, which represses the genes responsible for initiating filamentous growth, was found to be upregulated. Altogether, the real-time PCR results substantiated the antibiofilm and antihyphal potential of piperine through significant alteration in the expression of hyphae and biofilm

specific genes (Figure 8). Interestingly, the drug resistance was also found to notably downregulated, which could also be correlated with decreased spontaneous resistance development.

Piperine With No Lethal Effect Diminished *in vivo* Colonization of *C. albicans* in *C. elegans*

In vivo toxic effect, rescuing potential from *C. albicans* infection and effect on *in vivo* antibiofilm potential of piperine was appraised using the *in vivo* model organism *C. elegans*. Toxic effect and potential anti-infective efficacy of piperine against *C. albicans* infection was evaluated by performing *C. albicans*–*C. elegans* liquid infection assay and assessed through survival assay, which revealed that piperine at sub-BIC, BIC, and $2 \times$ BIC does not hold any *in vivo* toxicity. Whereas $4 \times$ and $8 \times$ BIC was found to slightly inhibit the survival of *C. elegans*. The survival of worms exposed to the vehicle control–methanol was also found to be decreased similar to the range of $4 \times$ and $8 \times$ BIC-treated worms. Hence, at $4 \times$ and $8 \times$ BIC, it is not predictable to assess where the decreased survival was due to the compound or the vehicle control (Figure 9A). From the *C. albicans*–*C. elegans* liquid infection assay, it is evident that

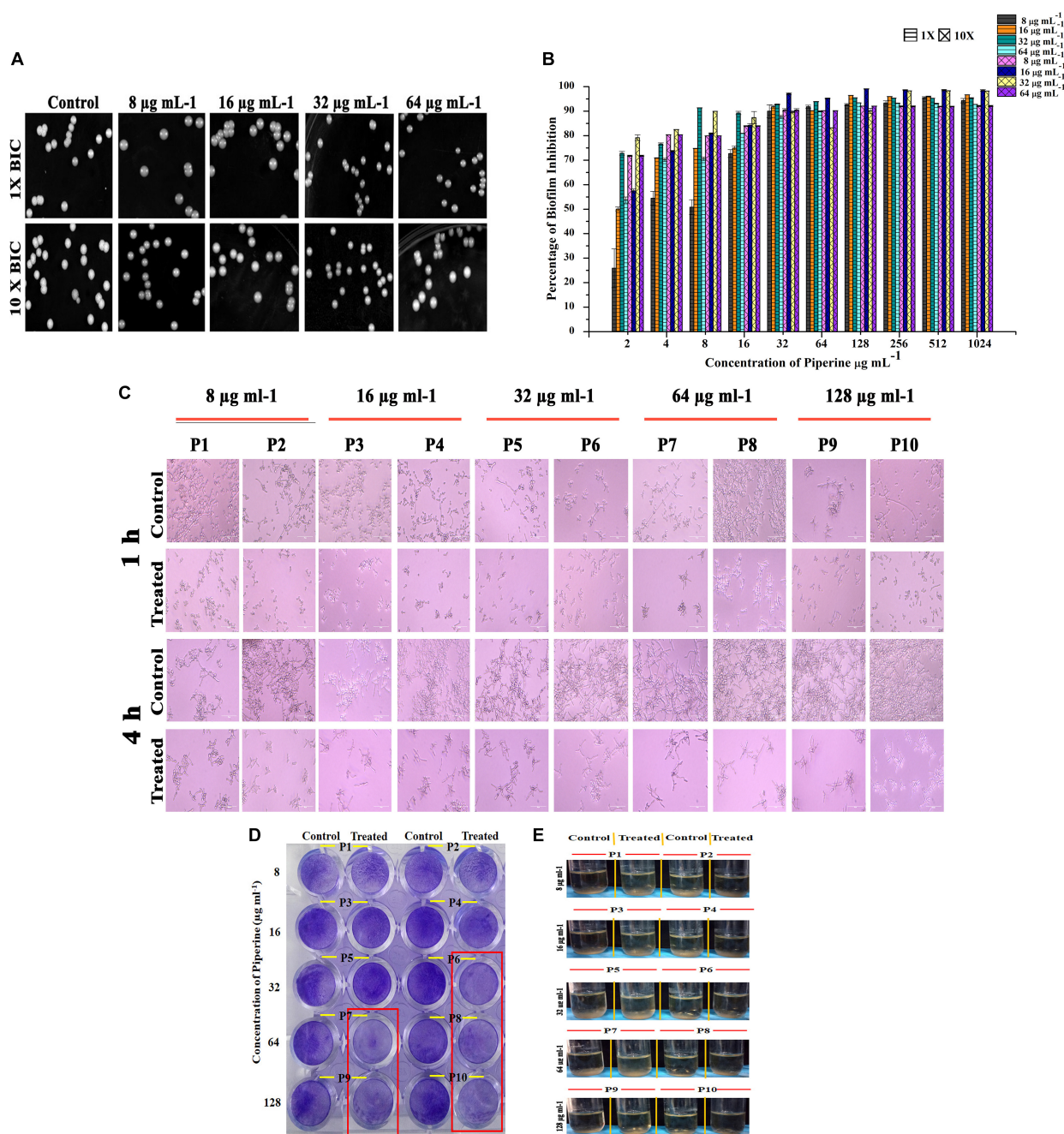


FIGURE 6 | Effect of piperine on spontaneous antibiofilm resistance development **(A)** Growth of *C. albicans* in piperine challenged plates. Top panel displays the *C. albicans* cells grown in the presence of 1 \times of 0.25, 0.5, 1, and 2 \times BIC. Bottom panel shows *C. albicans* grown under 10 \times concentration of 0.25, 0.5, 1, and 2 \times BIC. **(B)** Impairment in biofilm formation of piperine challenged *C. albicans* evidencing low potential for spontaneous antibiofilm resistance development. Error bars represent standard deviations from the mean ($n = 3$). **(C–E)** Effect of subsequent passage of *C. albicans* with piperine from lower to higher concentration on **(C)** hyphal extension, **(D)** biofilm formation, and **(E)** floor formation (air-liquid interface biofilm formation).

piperine rescued *C. elegans* from *C. albicans* infection. Decreased survival was observed in the *C. albicans*-infected worms, whereas piperine supplementation helped *C. elegans* to combat *C. albicans* infections in a concentration-dependent manner (**Figure 9A**). This was further reflected in the diminished internal colonization of *C. albicans*. The control worms had about 3.8×10^6 cells

whereas piperine treatment reduced the colonization and only 1.13×10^5 *C. albicans* cells were observed (**Figure 9B**). This was further substantiated through CLSM, wherein the colonization was measured through fluorescent intensity. Interestingly, CLSM micrographs showcased the internal abnormalities in *C. albicans*-infected worms. Deformities in eggs and internal hatching were

Control

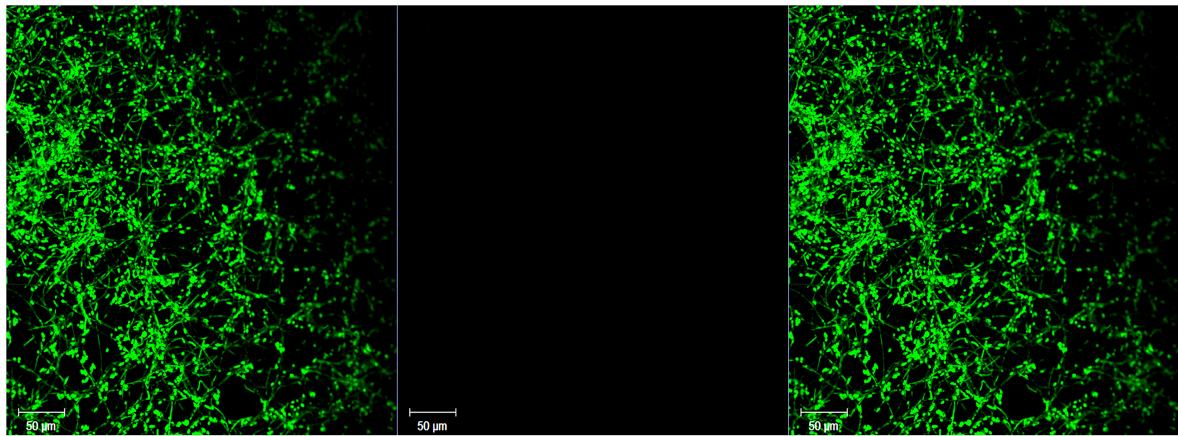
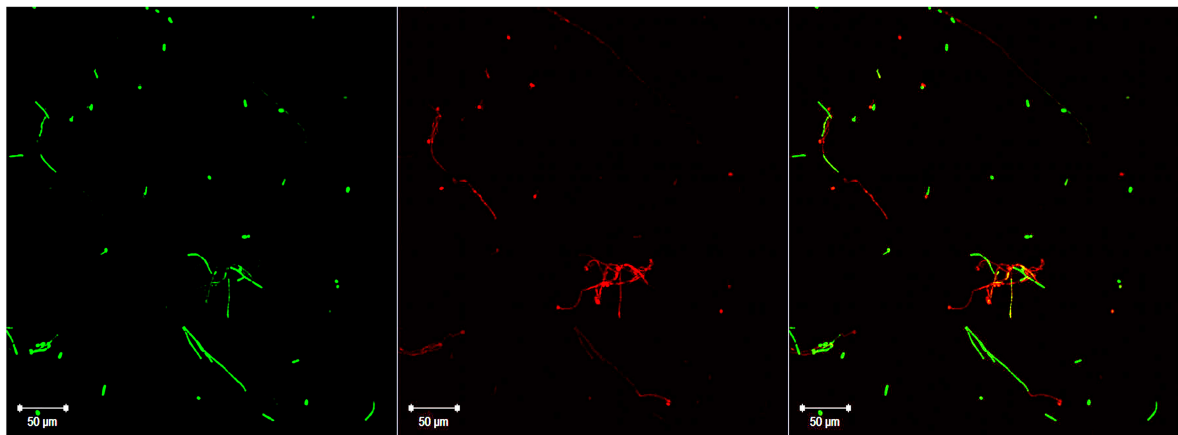
64 µg ml⁻¹

FIGURE 7 | Influence of piperine on disruption of preformed mature biofilm of *C. albicans*. Piperine effectively dislodged biofilm architecture of *C. albicans* at 64 µg mL⁻¹ concentration (2 × BIC), leaving behind few hyphal protrusions.

observed in the infected worms while piperine prevented all these abnormalities in treated group (**Figure 9C**). Concomitantly, the result pronounces piperine to be an ideal antibiofilm and anti-infective agent as it hinders not only the *in vitro* but also the *in vivo* colonization of *C. albicans*.

Piperine Does Not Affect the HBECs

In addition to the effect of piperine on *in vivo* toxicity and colonization on *C. elegans* animal model, HBECs were used to assess the safety of using piperine for treatment of oral candidiasis. From the microscopic analysis, HBECs were found to be healthy and normal in piperine treatment at 8 to 128 µg mL⁻¹ concentration, in comparison to the control cells. The positive control treated with H₂O₂ cells were found to be completely distorted. From this result, it can be concluded that piperine treatment is not lethal to the HBECs and found to be safe (**Figure 10**).

DISCUSSION

Amid the diverse fungal species, *C. albicans* stands as the predominant organism associated with the biofilm formation,

which is one of the major virulence traits devoted to its versatile pathogenicity. The sessile state of *C. albicans* embraces important clinical repercussions, owing to the increased drug resistance and recalcitrant nature and besides more significant morphological diversification and phenotype switching (Ramage et al., 2005). The proficiency of *C. albicans* to establish biofilm on both biotic (epithelial and mucosal membranes) and abiotic surfaces (prosthetics) often leads to candidiasis (Trindade et al., 2015). Since biofilm cells are more resistant to antibiotic therapy, preventing or disintegrating the biofilm formation is postulated to be an effectual therapeutic regimen. Based on this milieu, in order to attenuate the biofilm formation and virulence traits of *C. albicans*, with decreased avenue for resistance development, this study demonstrated the use of a plant alkaloid, piperine, as an effective antibiofilm and antihyphal molecule against *C. albicans* biofilm infection.

Antibiofilm molecule does not affect the survival of an organism and is thus contemplated to have trivial probability for resistance development (Rabin et al., 2015). Piperine markedly reduced the biofilm formation of *C. albicans* at the concentration of 32 µg mL⁻¹, without influencing the normal cellular and metabolic viability. Thus, piperine is considered as an ideal antibiofilm agent. Further, microscopic analysis demonstrated

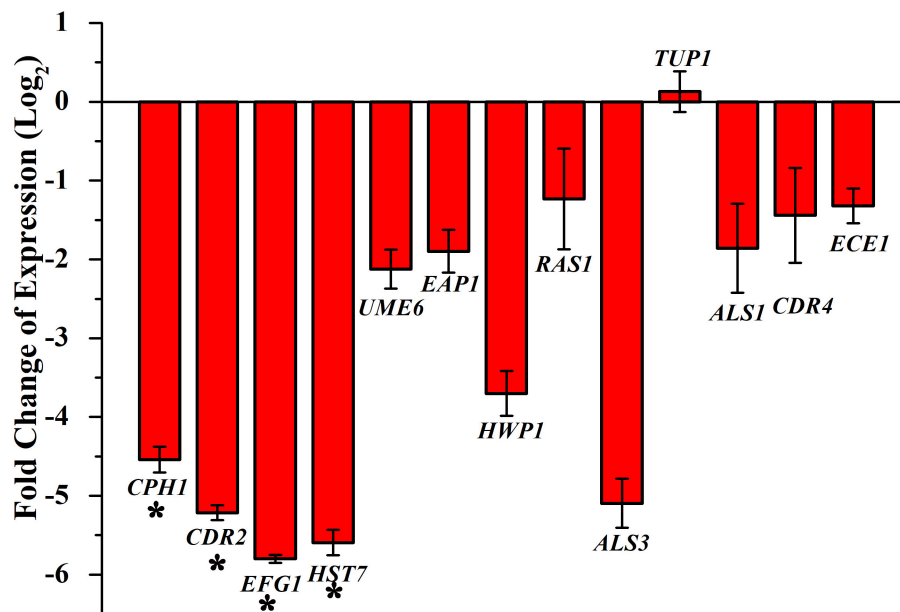


FIGURE 8 | Differential regulation of genes involved in biofilm and hyphal development of *C. albicans* by piperine at BIC (32 $\mu\text{g mL}^{-1}$). Filamentation-promoting genes, such as *CPH1*, *UME6*, and *EFG1*; hyphal growth-extending genes, such as *EAP1*, *HWP1*, *HST7*, *RAS1*, and *ECE1*; adhesion-supporting *ALS3* and *ALS1*; and drug resistance genes *CDR4* and *CDR2* are significantly downregulated by piperine. *tup1*, transcriptional repressor for the filamentation and hyphae-inducing genes, is upregulated. Error bars represent standard deviations from the mean ($n = 3$). * $p < 0.05$.

that piperine was effective in inhibiting adherence of *C. albicans* to surface and restricted the hyphal development in a dose-dependent manner. Morphological transition of *C. albicans* between yeast and filamentation forms contributes greatly to the pathogenicity. Both the morphological forms are critical to the virulent characteristics of *C. albicans* and exhibit distinct functions at different stages of disease progression, which includes adhesion, invasion and damage to the host tissue, dissemination of the infection, and circumvention from immune evasion and host response (Jacobsen et al., 2012). Notably, invasion and host tissue damage are dependent on the filamentous morphology (Vila et al., 2017). Thus, targeting the dimorphism and morphological transition of *C. albicans* can potentiate the therapy. The hyphal and filamentous morphologies are completely repressed by piperine which affirm its antivirulent potential. Similar to filamentous morphology, wrinkling in *C. albicans* is contemplated to be more virulent, as wrinkled colonies necessitate hyphal development and adhesins production (Lindsay et al., 2014). Piperine, even at the lowest concentration (8 $\mu\text{g mL}^{-1}$) restricted wrinkling of cells. Preventing the virulent morphologies associated with invasion and biofilm formation substantiates that piperine could possibly thwart invasive candidiasis. Besides preventing virulent morphologies and yeast to hyphal transition, piperine was shown to be proficient in transiting hyphal to yeast cells. Hyphal cells contribute more in the pathogenicity of *C. albicans* infection as mutants that are unable to form hyphae under *in vitro* conditions are generally found to be less virulent (Lo et al., 1997). Transmuting the pathogenic hyphal form to less-virulent yeast state will increase the susceptibility of *C. albicans* cells to host

immune response, as well as to therapeutics. Thus, piperine can not only be used for prevention of *C. albicans* infection, but also can act as an effective therapeutic regimen for established biofilm infections.

A common concern for any agent with therapeutic potential against microbes is the development of resistance. Due to widespread drug resistance to commonly used antibiotics, it is discreet to identify bioactive therapeutics that exhibit low resistance development. Also, *Candida* spp., develops several molecular mechanisms to resist attack by antifungal drugs (Krishnasamy et al., 2018). Though potential antibiofilm agents do not induce Darwinian selection pressure on microbes, the ability of the microbes to survive under selective-stressful environmental conditions can result in resistance development. The results of spontaneous resistance assay showed that *C. albicans* did not develop spontaneous resistance to piperine even at the concentrations 10-fold higher than the $2 \times$ BIC. Moreover, this is the first report to study the spontaneous antibiofilm resistance development.

Further, the gene expression analysis revealed that piperine significantly downregulated the expression of biofilm-, hyphal-, and filamentation-specific genes that are in line with the phenotypic assays. *EFG1* (gene encoding for enhanced filamentous growth protein 1) and *CPH1* (gene encoding for transcription factor CPH1) are two major transcription factors that are characterized as morphological regulators and are known to be involved in promoting filamentous growth and regulation of the expression of several genes with crucial function in invasion and/or biofilm formation (Dieterich et al., 2002; Staniszewska et al., 2015). Piperine treatment to

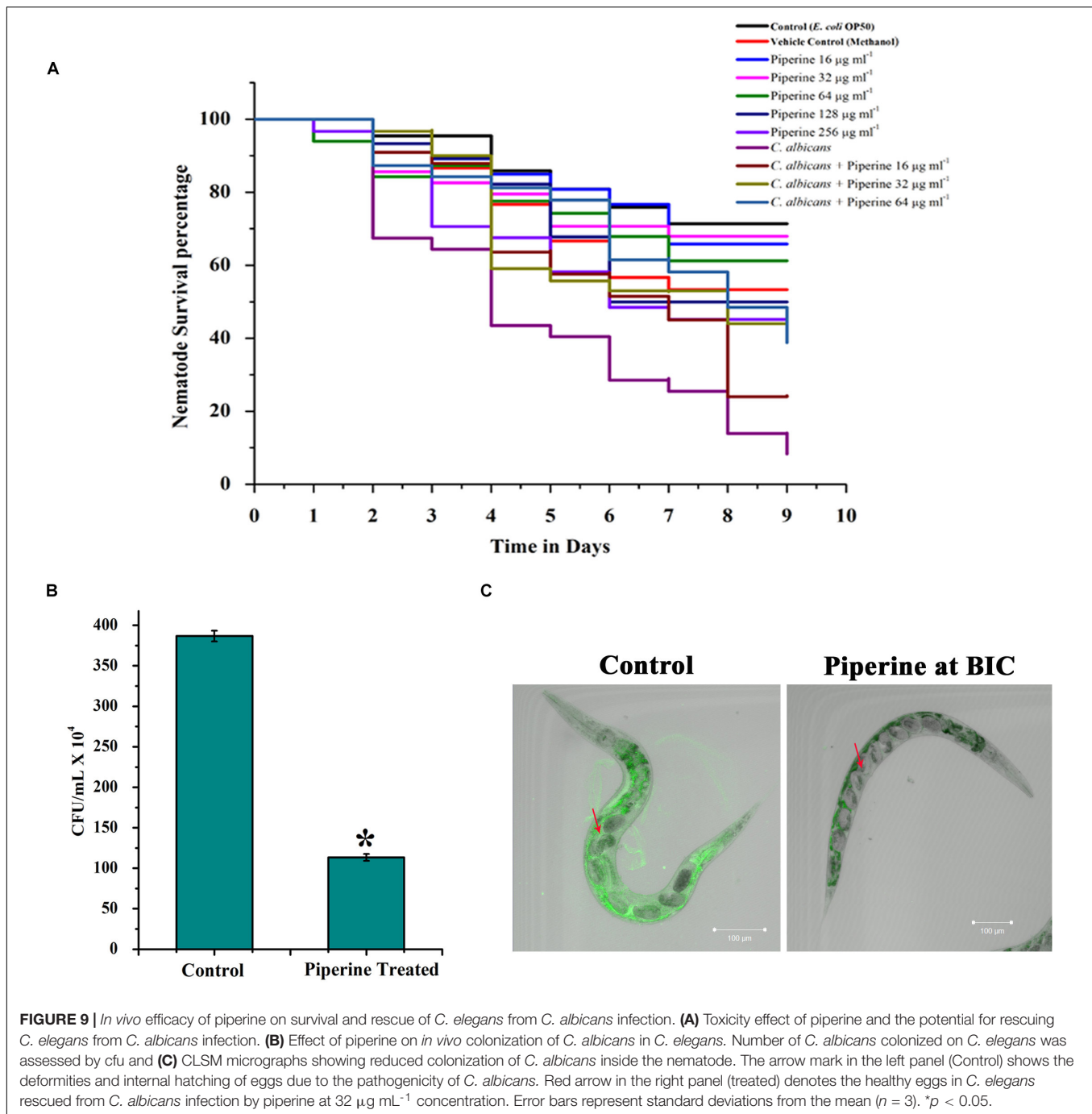


FIGURE 9 | *In vivo* efficacy of piperine on survival and rescue of *C. elegans* from *C. albicans* infection. **(A)** Toxicity effect of piperine and the potential for rescuing *C. elegans* from *C. albicans* infection. **(B)** Effect of piperine on *in vivo* colonization of *C. albicans* in *C. elegans*. Number of *C. albicans* colonized on *C. elegans* was assessed by cfu and **(C)** CLSM micrographs showing reduced colonization of *C. albicans* inside the nematode. The arrow mark in the left panel (Control) shows the deformities and internal hatching of eggs due to the pathogenicity of *C. albicans*. Red arrow in the right panel (treated) denotes the healthy eggs in *C. elegans* rescued from *C. albicans* infection by piperine at 32 $\mu\text{g mL}^{-1}$ concentration. Error bars represent standard deviations from the mean ($n = 3$). * $p < 0.05$.

C. albicans significantly downregulated the expression of both the transcription factors *EFG1* and *CPH1* by 5.7- and 4.5-fold, respectively. Another key filament-specific transcriptional regulator, *UME6*, which also regulates the transition of yeast to hyphae form (Banerjee et al., 2013), was found to be 2.1-fold downregulated by piperine treatment. *ECE1*, a hyphal specific gene, was found to be downregulated by 1.5-fold. *HWPI*, a gene that encodes for hyphal wall protein 1, is a major hyphal cell wall protein that plays a role of adhesin and is also required for hyphal development, mating, maintenance of biofilm integrity,

attachment to host, etc. Moreover, *hwp1* mutant *C. albicans* was shown to be defective in germination, hyphal development, and reduced interaction with the host system *in vivo* system (Tsuchimori et al., 2000). Piperine treatment resulted in 3.7-fold downregulation of *hwp1* which is well correlated with its potential in inhibition of hyphal formation as observed in phenotypic assays. Adhesin protein-encoding genes *EAP1* (cell wall adhesin) and *ALS3* and *ALS1* (agglutinin-like proteins) are involved in the process of adhesion to host surfaces and biofilm formation both *in vitro* and *in vivo* conditions (Hoyer, 2001; Li

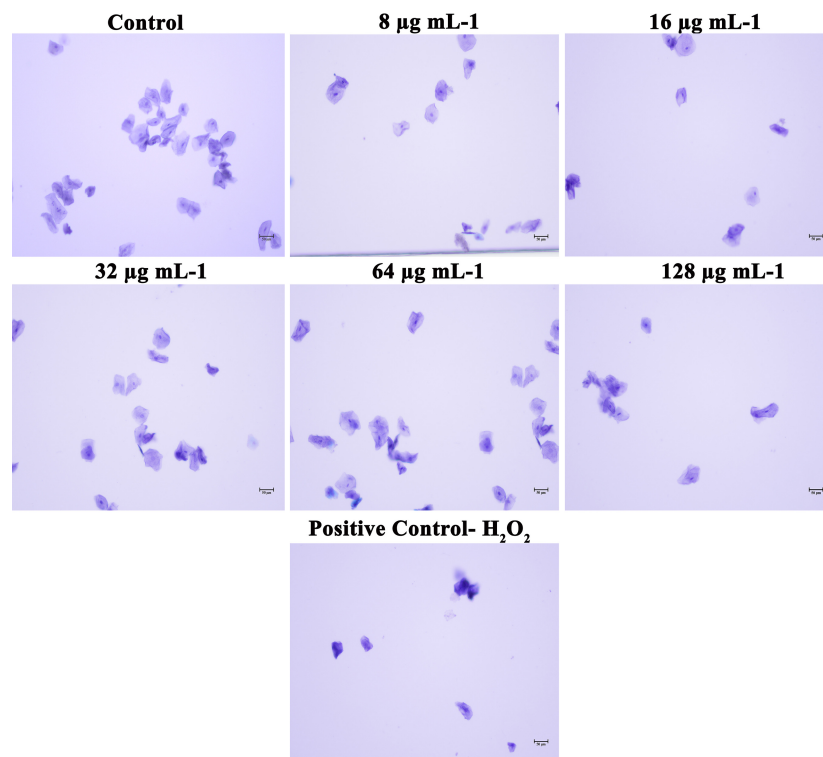


FIGURE 10 | Effect of piperine on HBECs. HBECs treated with 8, 16, 32, 64 and 128 $\mu\text{g mL}^{-1}$ of piperine were found to be healthy and normal, as the control cells, whereas HBECs treated with H_2O_2 were found to be completely distorted.

and Palecek, 2003). Piperine treatment significantly diminished the expression of both the adhesin genes *EAP1* and *ALS3* and *ALS1* by 1.8-, 5-, and 1.8-fold, respectively, which is directly corroborated with the decreased biofilm formation *in vitro* and reduced colonization in the *in vivo* *C. elegans* infection model. Furthermore, *RAS1*, which is involved in morphogenetic switching of *C. albicans* from yeast to polarized filamentous form (Martin et al., 2005) was found to be downregulated by 1.2-fold, due to the activity of piperine. This result further substantiates the potential of piperine to inhibit yeast to hyphal transition. *HST7*, which encodes for a serine/threonine-protein kinase STE7 homolog protein that plays a crucial role in mating (Chen et al., 2002), was found to be 5.5-fold less expressed in piperine-treated *C. albicans*. In addition, downregulation of *CDR2* and *CDR4*, a multidrug transporter gene (Mukherjee et al., 2003), signifies that piperine-treated *C. albicans* cells are less probable to develop antibiotic resistance. *TUP1*, a negative regulator of hyphal and filamentation related genes is found to be upregulated which further substantiates the antihyphal potential of piperine (Goffena et al., 2018).

For a bioactive compound to be taken for clinical applications, it should be non-toxic and must be effective *in vivo* conditions. The *in vivo* toxicity and antibiofilm potential of piperine was evaluated by using a simple eukaryotic model organism, *C. elegans*, which is the widely accepted model organism for toxicological analysis, as it shares homology with 83% of human genes (Dengg and van Meel, 2004; Henricson et al., 2004). The

fact that fundamental biological processes are highly conserved between *C. elegans* and humans, application of *C. elegans* in biomedical research and drug discovery process is constantly expanding. Furthermore, *C. elegans* was considered in the drug discovery process at the preclinical stage due to numerous advantages including morphology, lifestyle, growth, brood size, molecular and genetic amenabilities, etc. Due to these several advantages, it has been suggested that *C. elegans* could be incorporated in the preliminary drug discovery and target identification process, as well as in the secondary level, for toxicity screening and preclinical validation of drugs (Arya et al., 2010; Manoharan et al., 2017; Lee et al., 2018). *C. elegans* toxicity data can provide information about the drug effect on digestive, reproductive, endocrine, sensory, and neuromuscular systems. Moreover, research intended to rank toxicity in *C. elegans* have consistently shown a good correlation with rodent oral LD50 ranking (Hunt, 2017). Apart from involvement in toxicological analysis, *C. elegans* is being used as a model host system to review mammalian virulence and pathogenesis of bacterial and fungal organisms including *C. albicans* (Breger et al., 2007; Okoli et al., 2009). The *in vivo* study revealed that piperine does not display a lethal effect to *C. elegans*. Moreover, better survival was observed in piperine-treated *C. albicans* infection group than the infection control which clearly depicts that piperine assisted *C. elegans* to combat *C. albicans* infection. Better survival in *C. albicans*-infected worms was observed in a concentration-dependent manner.

Piperine, the bioactive natural molecule that belongs to the *Piperaceae* family, can be detected as the major component in piper species such as *Piper nigrum* L. (black pepper), *Piper longum* L. (long pepper). Additionally, piperine can also be found in the leaves of *Rhododendron fauriei*, seeds of *Anethum sowa*, *Fructus piperis* Long, and bark of *Careya arborea*. Piperine belongs to the largest class of secondary metabolites, alkaloids, and it imparts the pungent taste to pepper that is responsible for its application in human dietary utilization and as a food ingredient for centuries. In addition to dietetic application, piperine has been used in various traditional systems of medicine for curing array of disorders such as rheumatism, flu, muscular disorder, cold, fever, etc., and for increasing circulation of blood, flow of saliva, and stimulation of appetite and peristalsis. Equal proportion of black pepper, long pepper, and rhizomes of ginger are used for the formulation of Trikatu, an important ancient formulation that is still in use as an aid for digestive ailment. It has been reported that the effect of both black and long pepper is primarily caused by the presence of piperine (but not exclusively) (Meghwal and Goswami, 2013). A composition comprising a minimum of 98% of pure alkaloid piperine has been patented for its application as a bioavailability enhancer and augmentation of gastrointestinal absorption and systemic utilization of nutrients and nutritional supplements (patent no. US5536506A). Numerous reports are available on the potential of piperine to enhance the serum levels of drugs and nutrients in animals and human beings which includes drugs such as vasicine, rifampicin, theophylline, phenytoin, pyrazinamide, isoniazid, and propranolol and nutrients such as fat-soluble beta-carotene, water soluble vitamin B6, and minerals. Selvendiran et al. (2003) have reported that there is either no significant change in the health status nor toxicity in the Swiss albino mice treated with piperine when compared to control animals. Similarly, several other animal studies through oral administration have evaluated the various potentials of piperine (Lee et al., 1984; Suresh and Srinivasan, 2010; Johnson et al., 2011). In a human clinical study, oral administration of piperine has been shown to increase the swallow response of patients with oropharyngeal dysphagia (Rofes et al., 2014). Randomized clinical trials involving humans subjected to oral administration of piperine have been reported for the treatment of diverse diseases, and none of them have stated that piperine is toxic to neither animals nor humans (Badmaev et al., 2000; Volak et al., 2013; Panahi et al., 2017). Piperine has been evaluated for its immunomodulatory effect and reported to increase the total WBC count, bone marrow cellularity, etc. (Sunila and Kuttan, 2004; Pathak and Khandelwal, 2009). Owing to its numerous health benefits, traditional usage, generous clinical records, innocuous nature, and being expended as a therapeutic molecule for treatment of certain diseases, piperine could be considered as a risk-free candidate molecule for dentifrice application. Moreover, one potent nature of piperine that makes it as a desirable drug candidate for treating oral infectious diseases lies in its ability to increase the salivary flow rate. One of the predisposing host factors associated with oral candidiasis includes the reduced salivary flow rate (Radfar et al., 2003; Williams et al., 2011; Al-Kebsi et al., 2018). Along with the antibiofilm and antihyphal activity, increasing the salivary flow

rate is an added value to the therapeutic potential of piperine for oral candidiasis.

Piperine treatment was also found to be safe to the HBECs. Hence, together with these results and reports, piperine can be considered as safe for clinical purpose in human system for treating biofilm-associated *C. albicans* infections.

Altogether, the results have demonstrated the antibiofilm and antihyphal potential of a plant alkaloid molecule, piperine. The proficiency of piperine to inhibit morphological transitions and phenotype switching, with low potential for resistance development, exemplifies its therapeutic potential. Additionally, its non-toxic nature with respect to HBECs and *in vivo* anti-infective efficacy marks piperine as a promising drug molecule for preventing as well as treating the biofilm-associated *C. albicans* infection, specifically oral candidiasis.

DATA AVAILABILITY STATEMENT

All datasets generated for this study are included in the manuscript.

ETHICS STATEMENT

The studies involving human participants were reviewed and approved by Institutional Ethics Committee, Alagappa University (IEC Ref No: IEC/AU/2018/5). The patients or participants provided their written informed consent to participate in this study.

AUTHOR CONTRIBUTIONS

Both authors designed the study, read and approved the final version of the manuscript. AP performed the experiments, analyzed the data, prepared the figures and tables, and wrote the manuscript. SP revised the manuscript.

ACKNOWLEDGMENTS

The authors sincerely acknowledge the computational and bioinformatics facility provided by the Bioinformatics Infrastructure Facility (funded by DBT, GOI; File No. BT/BI/25/012/2012, BIF). The authors also thankfully acknowledge DST-FIST [Grant No. SR/FST/LSI-639/2015 (C)], UGC-SAP [Grant No. F.5-1/2018/DRS-II (SAP-II)], and DST PURSE [Grant No. SR/PURSE Phase 2/38 (G)] for providing instrumentation facilities. SP was thankful to UGC for Mid-Career Award [F.19-225/2018 (BSR)] and RUSA 2.0 [F.24-51/2014-U, Policy (TN Multi-Gen), Department of Education, Government of India]. The authors are grateful to Dr. K. Balamurugan, Professor, and M. Pooranachithra, Research Scholar, Department of Biotechnology, Alagappa University, for the support extended during *in vivo* analysis. Financial support provided to AP in the form of Research Assistant from DBT-BIF was gratefully acknowledged.

REFERENCES

- Abraham, K. P., Sreenivas, J. A., Venkateswarulu, T. C., Indira, M. I., Babu, D. J., Diwakar, T. E., et al. (2012). Investigation of the potential antibiofilm activities of plant extracts. *Int. J. Pharm. Pharm. Sci.* 4, 282–285.
- Abu-Elteen, K. H., and Abu-Alteen, R. M. (1998). The prevalence of *Candida albicans* populations in the mouths of complete denture wearers. *New Microbiol.* 21, 41–48.
- Akpan, A., and Morgan, R. (2002). Oral candidiasis. *Postgrad. Med. J.* 78, 455–459. doi: 10.1136/pmj.78.922.455
- Al-Kebisi, A. M., Al-Motareb, F. L., Al-Hamzy, M., Al-Shamahy, H. A., and Al-Sanabani, N. F. (2018). Multiple risk factors of *Candida albicans* associated denture stomatitis. *On. J. Dent. & Oral Health.* 1, 1–15. doi: 10.33552/OJDOH.2018.01.000511
- Anibal, P. C., Sardi, J. D. C. O., Peixoto, I. T. A., Moraes, J. J. D. C., and Hofling, J. F. (2010). Conventional and alternative antifungal therapies to oral candidiasis. *Braz. J. Microbiol.* 41, 824–831. doi: 10.1590/S1517-83822010000400001
- Arya, U., Das, C. K., and Subramaniam, J. R. (2010). *Caenorhabditis elegans* for preclinical drug discovery. *Curr. Sci.* 99, 1669–1680. doi: 10.1080/17460441.2017.1319358
- Badmaev, V., Majeed, M., and Prakash, L. (2000). Piperine derived from black pepper increases the plasma levels of coenzyme Q10 following oral supplementation. *J. Nutr. Biochem.* 11, 109–113. doi: 10.1016/S0955-2863(99)00074-1
- Banerjee, M., Uppuluri, P., Zhao, X. R., Carlisle, P. L., Vipulanandan, G., Villar, C. C., et al. (2013). Expression of UME6, a key regulator of *Candida albicans* hyphal development, enhances biofilm formation via Hgc1-and Sun41-dependent mechanisms. *Eukaryot. Cell* 12, 224–232. doi: 10.1128/EC.00163-12
- Breger, J., Fuchs, B. B., Aperis, G., Moy, T. I., Ausubel, F. M., and Mylonakis, E. (2007). Antifungal chemical compounds identified using a *C. elegans* pathogenicity assay. *PLoS Pathog.* 3:e18. doi: 10.1371/journal.ppat.0030018
- Calderone, R. A., and Fonzi, W. A. (2001). Virulence factors of *Candida albicans*. *Trends Microbiol.* 9, 327–335.
- Chandra, J., Kuhn, D. M., Mukherjee, P. K., Hoyer, L. L., McCormick, T., and Ghannoum, M. A. (2001). Biofilm formation by the fungal pathogen *Candida albicans*: development, architecture, and drug resistance. *J. Bacteriol.* 183, 5385–5394. doi: 10.1128/JB.183.18.5385-5394.2001
- Chavarria, D., Silva, T., Magalhaes e Silva, D., Remiao, F., and Borges, F. (2016). Lessons from black pepper: piperine and derivatives thereof. *Expert Opin. Ther. Pat.* 26, 245–264. doi: 10.1517/13543776.2016.1118057
- Chen, J., Chen, J., Lane, S., and Liu, H. (2002). A conserved mitogen-activated protein kinase pathway is required for mating in *Candida albicans*. *Mol. Microbiol.* 46, 1335–1344. doi: 10.1046/j.1365-2958.2002.03249.x
- Dengg, M., and van Meel, J. C. (2004). *Caenorhabditis elegans* as model system for rapid toxicity assessment of pharmaceutical compounds. *J. Pharmacol. Toxicol. Methods* 50, 209–214. doi: 10.1016/j.vascn.2004.04.002
- Dieterich, C., Schandar, M., Noll, M., Johannes, F. J., Brunner, H., Graeve, T., et al. (2002). *In vitro* reconstructed human epithelia reveal contributions of *Candida albicans* EFG1 and CPH1 to adhesion and invasion. *Microbiology* 148, 497–506. doi: 10.1099/00221287-148-2-497
- Douglas, L. J. (2002). Medical importance of biofilms in *Candida* infections. *Rev. Iberoam. Micol.* 19, 139–143.
- Ganguly, S., and Mitchell, A. P. (2011). Mucosal biofilms of *Candida albicans*. *Curr. Opin. Microbiol.* 14, 380–385. doi: 10.1016/j.mib.2011.06.001
- Goffena, J., Toenjes, K. A., and Butler, D. K. (2018). Inhibition of yeast-to-filamentous growth transitions in *Candida albicans* by a small molecule inducer of mammalian apoptosis. *Yeast* 35, 291–298. doi: 10.1002/yea.3287
- Gorgani, L., Mohammadi, M., Najafpour, G. D., and Nikzad, M. (2017). Piperine—the bioactive compound of black pepper: from isolation to medicinal formulations. *Compr. Rev. Food. Sci. Food Saf.* 16, 124–140. doi: 10.1111/1541-4337.12246
- Henricson, A., Sonnhammer, E. L., Baillie, D. L., and Gomes, A. V. (2004). Functional characterization in *Caenorhabditis elegans* of transmembrane worm-human orthologs. *BMC Genomics* 5:85. doi: 10.1186/1471-2164-5-85
- Hoyer, L. L. (2001). The ALS gene family of *Candida albicans*. *Trends Microbiol.* 9, 176–180. doi: 10.1016/S0966-842X(01)01984-9
- Hunt, P. R. (2017). The *C. elegans* model in toxicity testing. *J. Appl. Toxicol.* 37, 50–59. doi: 10.1002/jat.3357
- Jacobsen, I. D., Wilson, D., Wächter, B., Brunke, S., Naglik, J. R., and Hube, B. (2012). *Candida albicans* dimorphism as a therapeutic target. *Expert Rev. Anti Infect. Ther.* 10, 85–93. doi: 10.1586/eri.11.152
- Johnson, J. J., Nihal, M., Siddiqui, I. A., Scarlett, C. O., Bailey, H. H., Mukhtar, H., et al. (2011). Enhancing the bioavailability of resveratrol by combining it with piperine. *Mol. Nutr. Food. Res.* 55, 1169–1176. doi: 10.1002/mnfr.201100117
- Kaur, S., Soni, S., and Singh, R. (2017). Commensal and pathogen: *Candida albicans*. *AGEMS* 4, 18–21. doi: 10.18231/2348-7240.2017.0005
- Kiran, G. S., Priyadarshini, S., Anitha, K., Gnanamani, E., and Selvin, J. (2015). Characterization of an exopolysaccharide from probiont *Enterobacter faecalis* MS12 and its effect on the disruption of *Candida albicans* biofilm. *RSC Adv.* 5, 71573–71585. doi: 10.1039/C5RA10302A
- Krishnasamy, L., Krishnakumar, S., Kumaramanickavel, G., and Saikumar, C. (2018). Molecular mechanisms of antifungal drug resistance in *Candida* species. *J. Clin. Diagn. Res.* 12, DE01–DE06. doi: 10.2217/fmb.10.51
- Kumamoto, C. A., and Vines, M. D. (2005). Contributions of hyphae and hypha-co-regulated genes to *Candida albicans* virulence. *Cell. Microbiol.* 7, 1546–1554. doi: 10.1111/j.1462-5822.2005.00616.x
- Lee, E. B., Shin, K. H., and Woo, W. S. (1984). Pharmacological study on piperine. *Arch. Pharm. Res.* 7, 127–132. doi: 10.1007/BF02856625
- Lee, J. H., Kim, Y. G., Choi, P., Ham, J., Park, J. G., and Lee, J. (2018). Antibiofilm and antivirulence activities of 6-gingerol and 6-shogaol against *Candida albicans* due to hyphal inhibition. *Front. Cell Infect. Microbiol.* 8:299. doi: 10.3389/fcimb.2018.00299
- Li, F., and Palecek, S. P. (2003). EAP1, a *Candida albicans* gene involved in binding human epithelial cells. *Eukaryot. Cell* 2, 1266–1273. doi: 10.1128/EC.2.6.1266-1273.2003
- Lindsay, A. K., Morales, D. K., Liu, Z., Grahl, N., Zhang, A., Willger, S. D., et al. (2014). Analysis of *Candida albicans* mutants defective in the Cdk8 module of mediator reveal links between metabolism and biofilm formation. *PLoS Genet.* 10:e1004567. doi: 10.1371/journal.pgen.1004567
- Livak, K. J., and Schmittgen, T. D. (2001). Analysis of relative gene expression data using real-time quantitative PCR and the 2- $\Delta\Delta$ CT method. *Methods* 25, 402–408. doi: 10.1006/meth.2001.1262
- Lo, H. J., Kohler, J. R., DiDomenico, B., Loebenberg, D., Cacciapuoti, A., and Fink, G. R. (1997). Nonfilamentous *C. albicans* mutants are avirulent. *Cell* 90, 939–949. doi: 10.1016/S0092-8674(00)80358-X
- Lopez-Ribot, J. L. (2005). *Candida albicans* biofilms: more than filamentation. *Curr. Biol.* 15, R453–R455. doi: 10.1016/j.cub.2005.06.020
- Lu, L., Hu, W., Tian, Z., Yuan, D., Yi, G., Zhou, Y., et al. (2019). Developing natural products as potential anti-biofilm agents. *Chin. Med.* 14:11. doi: 10.1186/s13020-019-0232-2
- Manoharan, R. K., Lee, J. H., Kim, Y. G., and Lee, J. (2017). Alizarin and chrysazin inhibit biofilm and hyphal formation by *Candida albicans*. *Front. Cell Infect. Microbiol.* 7:447. doi: 10.3389/fcimb.2017.00447
- Martin, R., Walther, A., and Wendland, J. (2005). Ras1-induced hyphal development in *Candida albicans* requires the formin Bni1. *Eukaryot. Cell* 4, 1712–1724. doi: 10.1128/EC.4.10.1712-1724.2005
- Mathe, L., and Van Dijck, P. (2013). Recent insights into *Candida albicans* biofilm resistance mechanisms. *Curr. Genet.* 59, 251–264. doi: 10.1007/s00294-013-0400-3
- Meghwal, M., and Goswami, T. K. (2013). *Piper nigrum* and piperine: an update. *Phytother. Res.* 27, 1121–1130. doi: 10.1002/ptr.4972
- Mehra, T., Koberle, M., Braunsdorf, C., Mailander-Sanchez, D., Borelli, C., and Schaller, M. (2012). Alternative approaches to antifungal therapies. *Exp. Dermatol.* 21, 778–782. doi: 10.1111/exd.12004
- Meira, H. C., De Oliveira, B. M., Pereira, I. F., Naves, M. D., Mesquita, R. A., and Santos, V. R. (2017). Oral candidiasis: a retrospective study of 276 Brazilian patients. *J. Oral Maxillofac. Surg. Med. Pathol.* 21, 351–355. doi: 10.4103/jomfp.JOMFP_77_16
- Messier, C., Epifano, F., Genovese, S., and Grenier, D. (2011). Inhibition of *Candida albicans* biofilm formation and yeast-hyphal transition by 4-hydroxycordoin. *Phytomedicine* 18, 380–383. doi: 10.1016/j.phymed.2011.01.013
- Millson, J. W., and Fazel, N. (2016). Oral candidiasis. *Clin. Dermatol.* 34, 487–494. doi: 10.1016/j.clindermatol.2016.02.022
- Min, K. R., Galvis, A., Williams, B., Rayala, R., Cudic, P., and Ajdic, D. (2017). Antibacterial and antibiofilm activities of a novel synthetic cyclic lipopeptide against cariogenic *Streptococcus mutans* UA159. *Antimicrob. Agents Chemother.* 61:e00776. doi: 10.1128/AAC.00776-17

- Mittal, R., and Gupta, R. L. (2000). *In vitro* antioxidant activity of piperine. *Method Find Exp. Clin.* 22, 271–274. doi: 10.1358/mf.2000.22.5.796644
- Muadcheingka, T., and Tantivitayakul, P. (2015). Distribution of *Candida albicans* and non-*albicans* *Candida* species in oral candidiasis patients: correlation between cell surface hydrophobicity and biofilm forming activities. *Arch. Oral Biol.* 60, 894–901. doi: 10.1016/j.archoralbio.2015.03.002
- Mukherjee, P. K., Chandra, J., Kuhn, D. M., and Ghannoum, M. A. (2003). Mechanism of fluconazole resistance in *Candida albicans* biofilms: phase-specific role of efflux pumps and membrane sterols. *Infect. Immun.* 71, 4333–4340. doi: 10.1128/IAI.71.8.4333-4340.2003
- Muthamil, S., Balasubramaniam, B., Balamurugan, K., and Pandian, S. K. (2018). Synergistic effect of quinic acid derived from *Syzygium cumini* and undecanoic acid against *Candida* spp. biofilm and virulence. *Front. Microbiol.* 9:2835. doi: 10.3389/fmicb.2018.02835
- Nogueira, J. W., Costa, R. A., da Cunha, M. T., and Cavalcante, T. T. (2017). Antibiofilm activity of natural substances derived from plants. *Afr. J. Microbiol. Res.* 11, 1051–1060. doi: 10.5897/AJMR2016.8180
- Okoli, I., Coleman, J. J., Tempakakis, E., An, W. F., Holson, E., Wagner, F., et al. (2009). Identification of antifungal compounds active against *Candida albicans* using an improved high-throughput *Caenorhabditis elegans* assay. *PLoS One* 4:e7025. doi: 10.1371/journal.pone.0007025
- Panahi, Y., Khalili, N., Sahebi, E., Namazi, S., Atkin, S. L., Majeed, M., et al. (2017). Curcuminoids plus piperine modulate adipokines in type 2 diabetes mellitus. *Curr. Clin. Pharmacol.* 12, 253–258. doi: 10.2174/1574884713666180104095641
- Pathak, N., and Khandelwal, S. (2009). Immunomodulatory role of piperine in cadmium induced thymic atrophy and splenomegaly in mice. *Environ. Toxicol. Pharmacol.* 28, 52–60. doi: 10.1016/j.etap.2009.02.003
- Pradeep, C. R., and Kuttan, G. (2002). Effect of piperine on the inhibition of lung metastasis induced B16F-10 melanoma cells in mice. *Clin. Exp. Metastasis* 19, 703–708. doi: 10.1023/A:1021398601388
- Prasath, K. G., Sethupathy, S., and Pandian, S. K. (2019). Proteomic analysis uncovers the modulation of ergosterol, sphingolipid and oxidative stress pathway by myristic acid impeding biofilm and virulence in *Candida albicans*. *J. Proteomics* 208:103503. doi: 10.1016/j.jprot.2019.103503
- Rabin, N., Zheng, Y., Opoku-Temeng, C., Du, Y., Bonsu, E., and Sintim, H. O. (2015). Agents that inhibit bacterial biofilm formation. *Future Med. Chem.* 7, 647–671. doi: 10.4155/fmc.15.7
- Radfar, L., Shea, Y., Fischer, S. H., Sankar, V., Leakan, R. A., Baum, B. J., et al. (2003). Fungal load and candidiasis in Sjögren's syndrome. *Oral Surg. Oral Med. Oral Pathol. Oral Radiol.* 96, 283–287. doi: 10.1016/S1079-2104(03)00224-5
- Rajendran, R., Sherry, L., Nile, C. J., Sherriff, A., Johnson, E. M., Hanson, M. F., et al. (2016). Biofilm formation is a risk factor for mortality in patients with *Candida albicans* bloodstream infection—Scotland, 2012–2013. *Clin. Microbiol. Infect.* 22, 87–93. doi: 10.1016/j.cmi.2015.09.018
- Ramage, G., Saville, S. P., Thomas, D. P., and Lopez-Ribot, J. L. (2005). *Candida* biofilms: an update. *Eukaryot. Cell* 4, 633–638. doi: 10.1128/EC.4.4.633-638.2005
- Ramage, G., Walle, K. V., Wickes, B. L., and Lopez-Ribot, J. L. (2001). Characteristics of biofilm formation by *Candida albicans*. *Rev. Iberoam. Micol.* 18, 163–170.
- Rath, A. A. (2017). Clinical concerns of oral health in old age: an Indian perspective. *J. Geriatr. Care Res.* 4, 17–21.
- Repp, K. K., Menor, S. A., and Pettit, R. K. (2007). Microplae Alamar blue assay for susceptibility testing of *Candida albicans* biofilms. *Med. Mycol.* 45, 603–607. doi: 10.1080/13693780701581458
- Rofes, L., Arreola, V., Martin, A., and Clave, P. (2014). Effect of oral piperine on the swallow response of patients with oropharyngeal dysphagia. *J. Gastroenterol.* 49, 1517–1523. doi: 10.1007/s00535-013-0920-0
- Schaller, M., Borelli, C., Korting, H. C., and Hube, B. (2005). Hydrolytic enzymes as virulence factors of *Candida albicans*. *Mycoses* 48, 365–377. doi: 10.1111/j.1439-0507.2005.01165.x
- Selvendiran, K., Singh, J. P. V., Krishnan, K. B., and Sakthisekaran, D. (2003). Cytoprotective effect of piperine against benzo [a] pyrene induced lung cancer with reference to lipid peroxidation and antioxidant system in Swiss albino mice. *Fitoterapia* 74, 109–115. doi: 10.1016/S0367-326X(02)00304-0
- Slobodnikova, L., Fialova, S., Rendekova, K., Kovac, J., and Mucaji, P. (2016). Antibiofilm activity of plant polyphenols. *Molecules* 21:1717. doi: 10.3390/molecules21121717
- Souza, L. B., Silva-Rocha, W. P., Ferreira, M. R., Soares, L. A. L., Svidzinski, T. I., Milan, E. P., et al. (2018). Influence of *Eugenia uniflora* extract on adhesion to human buccal epithelial cells, biofilm formation, and cell surface hydrophobicity of *Candida* spp. from the oral cavity of kidney transplant recipients. *Molecules* 23:2418. doi: 10.3390/molecules231402418
- Staniszewska, M., Bondaryk, M., Zukowski, K., and Chudy, M. (2015). Role of SAP7-10 and morphological regulators (EFG1, CPH1) in *Candida albicans*' hypha formation and adhesion to colorectal carcinoma Caco-2. *Pol. J. Microbiol.* 64, 203–210.
- Subramenium, G. A., Swetha, T. K., Iyer, P. M., Balamurugan, K., and Pandian, S. K. (2018). 5-hydroxymethyl-2-furaldehyde from marine bacterium *Bacillus subtilis* inhibits biofilm and virulence of *Candida albicans*. *Microbiol. Res.* 207, 19–32. doi: 10.1016/j.micres.2017.11.002
- Sunila, E. S., and Kuttan, G. (2004). Immunomodulatory and antitumor activity of *Piper longum* Linn. and piperine. *J. Ethnopharmacol.* 90, 339–346. doi: 10.1016/j.jep.2003.10.016
- Suresh, D., and Srinivasan, K. (2010). Tissue distribution & elimination of capsaicin, piperine & curcumin following oral intake in rats. *Indian J. Med. Res.* 131, 682–691.
- Swetha, T. K., Pooranachithra, M., Subramenium, G. A., Divya, V., Krishnaswamy, B., and Pandian, S. K. (2019). Umbelliferone impedes biofilm formation and virulence of methicillin-resistant *Staphylococcus epidermidis* via impairment of initial attachment and intercellular adhesion. *Front. Cell Infect. Microbiol.* 9:357. doi: 10.3389/fcimb.2019.00357
- Tobudic, S., Kratzer, C., Lassnigg, A., and Presterl, E. (2012). Antifungal susceptibility of *Candida albicans* in biofilms. *Mycoses* 55, 199–204. doi: 10.1111/j.1439-0507.2011.02076.x
- Trindade, L. A., de Araújo Oliveira, J., de Castro, R. D., and de Oliveira Lima, E. (2015). Inhibition of adherence of *C. albicans* to dental implants and cover screws by *Cymbopogon nardus* essential oil and citronellal. *Clin. Oral. Investig.* 19, 2223–2231. doi: 10.1007/s00784-015-1450-3
- Tsuchimori, N., Sharkey, L. L., Fonzi, W. A., French, S. W., Edwards, J. E., and Filler, S. G. (2000). Reduced virulence of HWP1-deficient mutants of *Candida albicans* and their interactions with host cells. *Infect. Immun.* 68, 1997–2002. doi: 10.1128/IAI.68.4.1997-2002.2000
- Valliammai, A., Sethupathy, S., Priya, A., Selvaraj, A., Bhaskar, J. P., Krishnan, V., et al. (2019). 5-Dodecanolide interferes with biofilm formation and reduces the virulence of Methicillin-resistant *Staphylococcus aureus* (MRSA) through up regulation of agr system. *Sci. Rep.* 9:13744. doi: 10.1038/s41598-019-50207-y
- Vediappan, G., Dumontet, V., Pellissier, F., and d'Enfert, C. (2013). Gymnemic acids inhibit hyphal growth and virulence in *Candida albicans*. *PLoS One* 8:e74189. doi: 10.1371/journal.pone.0074189
- Vila, T., Romo, J. A., Pierce, C. G., McHardy, S. F., Saville, S. P., and Lopez-Ribot, J. L. (2017). Targeting *Candida albicans* filamentation for antifungal drug development. *Virulence* 8, 150–158. doi: 10.1080/21505594.2016.1197444
- Volak, L. P., Hanley, M. J., Masse, G., Hazarika, S., Harmatz, J. S., Badmaev, V., et al. (2013). Effect of a herbal extract containing curcumin and piperine on midazolam, flurbiprofen and paracetamol (acetaminophen) pharmacokinetics in healthy volunteers. *Br. J. Clin. Pharmacol.* 75, 450–462. doi: 10.1111/j.1365-2125.2012.04364.x
- Clinical and Laboratory Standards Institute [CLSI] (2008). *Reference Method for Broth Dilution Antifungal Susceptibility Testing of Filamentous Fungi; Approved Standard: Document M38-A2*, 2nd Edn. Wayne, PA: Clinical and Laboratory Standards Institute.
- Williams, D. W., Kuriyama, T., Silva, S., Malic, S., and Lewis, M. A. (2011). *Candida* biofilms and oral candidosis: treatment and prevention. *Periodontol.* 2000 55, 250–265. doi: 10.1111/j.1600-0757.2009.00338.x

Conflict of Interest: The authors declare that the research was conducted in the absence of any commercial or financial relationships that could be construed as a potential conflict of interest.

Copyright © 2020 Priya and Pandian. This is an open-access article distributed under the terms of the Creative Commons Attribution License (CC BY). The use, distribution or reproduction in other forums is permitted, provided the original author(s) and the copyright owner(s) are credited and that the original publication in this journal is cited, in accordance with accepted academic practice. No use, distribution or reproduction is permitted which does not comply with these terms.



Fighting Mixed-Species Microbial Biofilms With Cold Atmospheric Plasma

Yifan Rao¹, Weilong Shang¹, Yi Yang¹, Renjie Zhou^{2*} and Xiancai Rao^{1*}

¹ Department of Microbiology, College of Basic Medical Sciences, Key Laboratory of Microbial Engineering Under the Educational Committee in Chongqing, Army Medical University, Chongqing, China, ² Department of Emergency, Xinqiao Hospital, Army Medical University, Chongqing, China

OPEN ACCESS

Edited by:

Luis Cláudio Nascimento da Silva,
Universidade Ceuma, Brazil

Reviewed by:

Lucía Fernández,
Institute of Dairy Products of Asturias
(IPLA), Spain
Nuno F. Azevedo,
University of Porto, Portugal
Sang-Do Ha,
Chung-Ang University, South Korea

*Correspondence:

Renjie Zhou
zhou_rj@aliyun.com
Xiancai Rao
raoxiancai@126.com

Specialty section:

This article was submitted to
Antimicrobials, Resistance
and Chemotherapy,
a section of the journal
Frontiers in Microbiology

Received: 01 February 2020

Accepted: 24 April 2020

Published: 20 May 2020

Citation:

Rao Y, Shang W, Yang Y, Zhou R
and Rao X (2020) Fighting
Mixed-Species Microbial Biofilms
With Cold Atmospheric Plasma.
Front. Microbiol. 11:1000.
doi: 10.3389/fmicb.2020.01000

Most biofilms in nature are formed by multiple microbial species, and such mixed-species biofilms represent the actual lifestyles of microbes, including bacteria, fungi, viruses (phages), and/or protozoa. Microorganisms cooperate and compete in mixed-species biofilms. Mixed-species biofilm formation and environmental resistance are major threats to water supply, food industry, and human health. The methods commonly used for microbial eradication, such as antibiotic or disinfectant treatments, are often ineffective for mixed-species biofilm consortia due to their physical matrix barrier and physiological interactions. For the last decade, an increasing number of investigations have been devoted to the usage of cold atmospheric plasma (CAP), which is produced by dielectric barrier discharges or plasma jets to prevent or eliminate microbial biofilms. Here, we summarized the production of CAP, the inactivation of microorganisms upon CAP treatment, and the microbial factors affecting the efficacy of CAP procedure. The applications of CAP as antibiotic alternative strategies for fighting mixed-species biofilms were also addressed.

Keywords: mixed-species biofilms, cold atmospheric plasma, biofilm resistance, biofilm infection, biofilm eradication

INTRODUCTION

A biofilm represents a syntrophic microbial community in which microbes adhere to each other and to a biotic or abiotic surface (Scholtz et al., 2015). Biofilms are usually formed by a variety of microorganisms, and mixed-species biofilms can cause persistent infections in medicine, drinking water pollution in water reservoirs, and food spoilage in the industry (Sun et al., 2018; Fan et al., 2020; Tan et al., 2020). Approximately 60–80% of microbial infections are associated with mixed-species biofilms (Tytgat et al., 2019). In some disease situations, multispecies biofilm infections lead to worse outcomes than monospecies infections (Trifilio et al., 2015; Jorge et al., 2018). For example, patients with cystic fibrosis present a more rapid decline of lung function when co-infected with *Pseudomonas aeruginosa* and *Staphylococcus aureus* than those who are infected by only one species (Limoli et al., 2016; Limoli and Hoffman, 2019). Therefore, controlling mixed-species biofilms has been one of the hot research areas in recent years.

Microbial cells within a mixed-species biofilm present increased resistance to environmental conditions, such as antibiotic treatment, oxidative stress, and nutrient starvation, in comparison with planktonic cells (Bridier et al., 2015). For the last decade, most investigations have been

aimed at controlling biofilms by using different strategies (Ermolaeva et al., 2015), including bacteriophage therapy, biofilm matrix-active enzyme treatment, bacteriocin management, and using new antibiofilm compounds (such as essential oils, phenolic acids, curcumin, and polyphenolic components) (Simmons et al., 2018; Yuan et al., 2019). However, these techniques are not considered as perfect biofilm eradication strategies because of their potential to eventually contaminate the treated surface or lead to environmental pollution (Gupta and Ayan, 2019). Furthermore, many studies have warned that the complete elimination of mixed-species biofilms may not be achieved by using one treatment method only, and comprehensive measures are often required (Duske et al., 2015).

Plasma is one of the four fundamental states of matter in nature (Šimončicová et al., 2019). The “cocktail” constituents of plasma, including molecules and neutral atoms, charged particles, metastable radicals, and photons, play synergistic functions in microbial inactivation (Guo et al., 2018). In recent years, cold atmospheric plasma (CAP) has been extensively investigated for its potential as an alternative treatment in wound healing, dental cure, oncological therapy, and food decontamination (Scholtz et al., 2015; Jiao et al., 2019; Eggers et al., 2020). Significant progress has been made in controlling mixed-species biofilms with CAP, which is considered a rapid, environmentally friendly, energy saving, and versatile antimicrobial technology (Šimončicová et al., 2019). The present review focuses on the potential of CAP treatment to combat biofilms especially mixed-species biofilms, which are the dominant form of microorganisms existing in nature.

RESISTANCE OF MIXED-SPECIES BIOFILMS

The high resistance and physiological change in microorganisms due to external treatments from hostile environments are nerve-racking issues in biofilm control (Gupta and Ayan, 2019). Microbial cells in biofilms are embedded in extracellular polymeric substance (EPS), which makes up approximately 90% of the biofilm volume. Microorganisms cooperate and compete with each other to achieve the overall fitness in the consortia. EPS protects microbial cells from inactivation through host immunity and environment factors, such as antimicrobial agents, chemical disinfectants, and UV radiation (Rice et al., 2016).

Microbial Interactions in Mixed-Species Biofilms

The physiological events during the cell proliferation and the biofilm maturation of mixed-species communities are complex (Fan et al., 2020). One common interaction among microorganisms in mixed-species biofilms is the competition for nutrient acquisition and space occupation. Pang et al. (2019) showed that indigenous microbial cells in the runoff fluids of fresh salmon compete with *Listeria monocytogenes* for nutrients in mixed-species biofilms, resulting in a remarkable reduction in the number of *L. monocytogenes* cells compared with that in monospecies biofilms. Toxic substances, such as

bacteriocins, hydrogen peroxide, organic acids, and enzymes, which are secreted by some microbial species provide competitive advantages over other species within mixed-species biofilms (Rendueles and Ghigo, 2012). The biofilm formation of *Candida albicans* can be inhibited when co-cultured with *P. aeruginosa* through the secretion of virulence factors (Bandara et al., 2010). *Lactobacillus* metabolites can kill *L. monocytogenes* in mixed-species biofilms by using hydrogen peroxide, lactic acid, and bacteriocin (Winkelstroter et al., 2015).

The cooperative interactions are widely existent when all members in the consortia benefit each other during biofilm formation (Ren et al., 2014; Liu et al., 2016). The cooperative microbial interactions in mixed-species biofilms may be based on the enhancement of the adhesion of the secreted matrix produced by partners or through metabolic cross-feeding by the products that promote the growth of other members. The dual-species biofilms formed by *Lactococcus lactis* and *Pseudomonas fluorescens* result in increased bacterial adhesion by up to 20,000- and 100-fold, respectively (Yuan et al., 2019). The authors proposed that the poor biofilm former *L. lactis* may benefit from the enhanced adhesion ability supported by the quick matrix-producing *P. fluorescens*. By contrast, some metabolites that originated from *L. lactis* may be utilized as nutrient sources by *P. fluorescens*. Liu et al. (2016) showed that the mixed-species biofilm formed by *Escherichia coli*, *Salmonella enterica*, and *L. monocytogenes* are facilitated by *Ralstonia insidiosa*, which provides a microenvironment for microbial accumulation and growth in nutrient-limited environments through its highly efficient nutrient utilization and cell proliferation. Given the complex microbial interactions, a mixed-species biofilm often achieves substantially more biomass than a monospecies biofilm without the need to input more nutrients (Ren et al., 2015).

Enhanced Resistance Presented by Mixed-Species Biofilms

The resistance of microbial biofilms is reinforced in a synergistic manner after the formation of mixed-species communities (Burmolle et al., 2014). EPS plays a critical role in biofilm resistance enhancement (Rice et al., 2016). The production of EPS, such as exopolysaccharide, is increased in biofilm cells compared with their planktonic counterparts. The constitution of EPS also varies markedly depending on the environmental elements and the bacterial species involved (Flemming and Wingender, 2010). The EPS of *S. aureus* possesses proteins, eDNA, and polysaccharides (Rice et al., 2016), whereas the biofilm matrix of *P. aeruginosa* can produce at least three polysaccharides, namely, alginate, Psl, and Pel (Flemming and Wingender, 2010). Studies have proven that EPS can act as cement to enhance initial adhesion and promote bacterial accumulation on a surface (Souza et al., 2020). Components of the biofilm matrix may also act as a reserve source of energy facilitating the nutrient accumulation in the microenvironment (Ermolaeva et al., 2015). Therefore, methods that destroy the EPS are effective for biofilm prevention. For instance, eDNA is widely present in biofilms and DNase treatment is

currently considered effective in curing biofilm infections (Jiao et al., 2019). A study reported that a SigB(Q225P) mutation can enhance the *S. aureus* biofilm by downregulating the expression of the *nuc* gene, and the biofilm is evidently reduced after DNase I treatment compared with the untreated strain (Liu et al., 2018).

Besides the protection role of EPS, microbial interactions in mixed-species biofilms also may contribute to resistance enhancement. The organization of microorganisms within mixed-species biofilms is finely controlled for the fitness contribution of the whole consortium (Liu et al., 2016). Single-species biofilms lack commensal interactions between species, whereas mixed-species biofilms can form an intermixing structure (Yuan et al., 2019). The bacterial species may be present promiscuously throughout the community or as a layered structure, in which one species is in the bottom layers and the other one grows in the top layers. These spatial structures may be attributed to the survival rate of individual species within the mixed-species biofilms as a result of cooperative or competitive interactions (Nadell et al., 2016). In a dual-species biofilm infection, *P. aeruginosa* exhibits excellent colonizing capacity and often forms the basic biofilm structure, while *K. pneumoniae* usually takes shape as a tower-like structure at the biofilm top due to its higher growth rate (Chhibber et al., 2015). The interaction between *P. aeruginosa* and *K. pneumoniae* in the biofilms can enhance their resistance to the treatment of antimicrobial agents.

Mechanisms Underpinning the Enhanced Resistance of Mixed-Species Biofilms

The primary mechanisms of enhanced resistance within mixed-species biofilms are not entirely clear due to the change in the composition of the biofilm matrix and the enhanced microbial interactions in the consortia. Several speculations regarding the enhanced resistance in mixed-species biofilms have been proposed. First, some species may protect others by their aggregation with other strains within the three-dimensional structure spatially arranged by certain species (Lee et al., 2014). *Vibrio parahaemolyticus* is often located on the top layers of multispecies biofilms because of its competitive advantage, and its minimum inhibitory concentration against antibiotics is remarkably decreased when co-cultured with *L. monocytogenes* (Chen et al., 2019). The second mechanism involves the matrix of a mixed-species biofilm. The chemical interactions between the EPS produced by distinct species may result in a thick matrix, which varies in accordance with the microbial species involved and the changes in environmental condition (Flemming and Wingender, 2010). The thickness of the matrix is suggested to play functions in mixed-species biofilm resistance by blocking the reach of the risk factors to the lower layers of active microbes (Guillonneau et al., 2018). EPS has also been experimentally proven to bind to antibiotics with positive charges, such as aminoglycosides, blocking their antimicrobial effects on microbes (Ermolaeva et al., 2015). In the mixed-species biofilms formed by *Staphylococcus epidermidis* and *C. albicans*, the EPS derived from *S. epidermidis* can protect *C. albicans* by arresting the penetration of antifungal drugs, such as fluconazole (Delben et al., 2016).

In addition, the temporary alterations in microbial neighbors contribute to enhanced mixed-species biofilm recalcitrance. A species settling down in a mixed-species biofilm can alter the physiology of neighboring species by interspecies interactions (Herschend et al., 2017), such as antibiotic resistance gene exchange, antibiotic-inactivated enzyme transfer, quorum-sensing signal-induced gene expression changes, and metabolite-mediated electron transport chain inhibition (Hansen et al., 2017; Orazi and O'Toole, 2019). For example, carbapenemase resistance gene-carried plasmid can be transferred from *E. coli* to either *Acinetobacter baumannii* or *P. aeruginosa* in mixed-species biofilms but is not observed in the planktonic state of these organisms (Tanner et al., 2017; Potron et al., 2011). The 2-heptyl-4-hydroxyquinolone N-oxide secreted by *P. aeruginosa* can alter the susceptibility of *S. aureus* strains within mixed-species biofilms to several antibacterial agents, such as vancomycin, aminoglycosides, and chloroxylonol (Orazi and O'Toole, 2019). The fungus *C. albicans* can induce vancomycin resistance of *S. aureus* during mixed-species biofilm formation (Harriott and Noverr, 2010). These possible mechanisms can result in a 100- to 1000-fold more resistance for mixed-species biofilms to antibiotics than their planktonic cells and therapeutic challenge of persistent biofilm infections in the host (Høiby et al., 2010). Therefore, interfering with the aforementioned mechanisms may be a promising strategy for the control of biofilms in nature and diseases.

COLD ATMOSPHERIC PLASMA

Cold atmospheric plasma is an emerging antimicrobial strategy that could improve biofilm eradication (Julák et al., 2018; Gupta and Ayan, 2019). The word “plasma” was first used by Irving Langmuir in 1928 to describe quasineutral ionized or partially ionized gas generated by heating or through the application of a strong electromagnetic field (Šimončicová et al., 2019). Plasma is divided into thermal (at least 15,000 K) and non-thermal (less than 340 K) plasmas in accordance with the temperature of ionized gas. Non-thermal plasma, which is called CAP, is a partially ionized gas with a temperature generally close to room temperature (Gherardi et al., 2018). The systems of CAP can produce numerous species of active ingredients, such as positive and negative ions, neutral atoms (e.g., atomic oxygen and ozone), reactive molecules (e.g., superoxide and oxides of nitrogen), metastable radicals (e.g., OH and NO), and photons (e.g., UV). These components can work synergistically to kill microorganisms and also destroy the matrix of biofilms (Jiao et al., 2019).

Application-Oriented CAP Devices

The effectiveness of plasma may be dose-dependent, which depends on plasma source allocation, working gas supply, and biological target composition (Šimončicová et al., 2019). Currently, there is no single prototype that can be used for all applications. The most widely used plasma devices for biological applications are dielectric barrier discharges (DBDs)

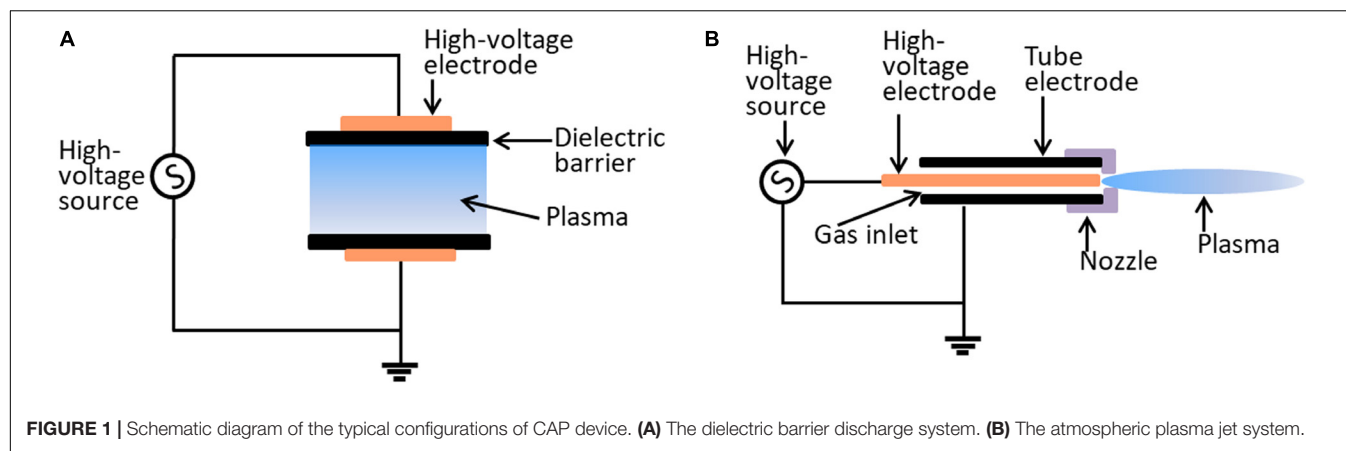


FIGURE 1 | Schematic diagram of the typical configurations of CAP device. **(A)** The dielectric barrier discharge system. **(B)** The atmospheric plasma jet system.

and atmospheric pressure plasma jets (APPJs) (Figure 1). The characteristics of DBD and APPJ are listed in Table 1. The defining features of DBDs and APPJs are the designs of dielectric material between the electrodes. DBD devices generally have electrode gaps ranging from tens of micrometers to a few centimeters and operate at frequencies of 50–500 kHz and voltage of tens of kilovolts. DBD devices, which are more suitable in the treatment of massive surfaces and large quantity of samples of varied shapes and sizes, are used in several fields, such as food industry (Šimončicová et al., 2019). In contrast with DBDs, APPJs are beneficial to use for the direct treatment of target objects (Gupta and Ayan, 2019). As such, the application of APPJ is advantageous in medicine, wherein APPJ may be used in localized decontamination, wound healing, and cancer therapy.

Inactivation of Microorganisms Upon CAP Treatment

Cold atmospheric plasma is a versatile strategy for microbial inactivation. The application of CAP for the prevention and eradication of mixed-species biofilms includes two aspects: the direct and indirect applications of CAP for biofilm destruction (Frias et al., 2020). The indirect way is done by first applying CAP on biotic or abiotic surfaces, which are then used to control biofilm formation, or by first activating water with CAP and treating the biofilm by using plasma-activated water (Patange et al., 2019; Zhou et al., 2019). The first investigation of bacterial inactivation by CAP was performed by imposing a voltage of 300 V to produce plasma by ionization of air (Krueger et al., 1957). In a further study, a high voltage (20 kV/cm) was imposed on four electrodes to treat *Saccharomyces cerevisiae* or *Bacillus subtilis* (formerly *Bacillus natto*), and cell destruction was observed (Mizuno and Hori, 1988). A set of plasma species can coordinate to inactivate microorganisms. Some species, such as molecules and neutral atoms, can break the bonds in the peptidoglycan structure of Gram-positive bacteria (Yusupov et al., 2012, 2013), whereas others may lead to the lipid peroxidation of the Gram-negative bacterial membrane (Joshi et al., 2011). After the disruption of the bacterial cell wall, reactive oxygen (ROS) or reactive nitrogen (RNS) species penetrates the bacteria to

damage further the intracellular protein and genomic DNA (Mai-Prochnow et al., 2014).

Several common observations have been achieved in the bacterial inactivation with CAP. First, Gram-positive bacteria are less sensitive to CAP treatment than Gram-negative bacteria, which is probably due to the thick and tough peptidoglycan layers of Gram-positive bacteria (Mai-Prochnow et al., 2016; Nishime et al., 2017). Pompl et al. (2009) reported that the cell disruption of *E. coli* under low-temperature plasma treatment is more serious than that of *S. aureus*. The antimicrobial effect of CAP was also stronger in *A. baumannii* and *Salmonella* Typhimurium (Gram-negative strains) than in *S. aureus* (Gram-positive isolate) (Hafner et al., 2018; Huang et al., 2020). However, Gram-positive *Enterococcus faecalis* presented higher overall susceptibility to CAP treatment compared with *P. aeruginosa*, and the mechanism underlying *E. faecalis*' high sensitivity to CAP processing is interesting and is worth further investigation. Second, vegetative bacterial cells are more susceptible to plasma sterilization than

TABLE 1 | Summary of comparable characteristics of DBD and APPJ plasmas.

Compared items	DBD plasma	APPJ plasma	References
Flowing working gas	Minimum or not required	Required	Šimončicová et al. (2019)
Plasma volume	Large	Small	Šimončicová et al. (2019)
Plasma production	Burns between flat electrodes with imposed AC, separated by a dielectric insulator	Ionizes the carrier gas (Ar, He, Air) by high-frequency electric voltage	Laroussi and Akan (2007)
Applied range	Usually an enclosed device for <i>ex vivo</i> or <i>in vitro</i> applications	A versatile jet configuration used for <i>in vivo</i> and <i>in vitro</i> modifications	Fridman et al. (2008)
Applied to surfaces	The surface is required to be a part of the high-voltage electrical circuit.	Not required	O'Connor et al. (2014)
Applied area	Expose large area	Strike only a small target area	Šimončicová et al. (2019)

their spore counterparts (O'Connor et al., 2014). Lastly, the complete eradication of bacterial biofilm requires a much longer treatment duration than killing its planktonic counterparts (Mai-Prochnow et al., 2014).

The mechanisms participating in CAP inactivation are considered complicated due to the numerous species in plasma. CAP may have numerous targets in bacterial cells, including cell wall, cell membrane, genomic DNA, and intracellular proteins (Vatansever et al., 2013; Mai-Prochnow et al., 2014). Several plasma–cell interactions have been involved in the bactericidal effect of CAP. One of these interactions is the mechanical etching role performed by the atomic and molecular radicals of CAP, resulting in pore formation and cell erosion on the polymeric surface of microorganisms (Handorf et al., 2018; Huang et al., 2020). Another interaction is the photodesorption implemented by UV radiation, which results in the subsequent chemical bond breakage of bacterial organic macromolecules (Van Der Paal et al., 2016; Brun et al., 2018). The third interaction is the DNA damage triggered by reactive species (Delben et al., 2016; Sakudo et al., 2018), and the last interaction is the oxidative damage of bacterial proteins, polysaccharides, and lipids caused by ROS and RNS (Edengeiser et al., 2015; Ji et al., 2018). As a result, Gram-negative bacteria, such as *P. aeruginosa*, often exhibit visible morphological changes in cell shape, whereas minor or inconspicuous morphological deformities are observed in Gram-positive bacteria, such as *S. aureus* and *E. faecalis*, after the CAP procedure (Nishime et al., 2017; Yang et al., 2020).

Microbial Factors Influencing the Efficacy of CAP Treatment

The efficacy of CAP treatment against biofilms formed by certain microorganisms varies depending on microbial type, growth phase, produced matrix, biofilm thickness, and process factors (Šimončicová et al., 2019). The bacterial envelope structure plays important roles in microbial defense for CAP processing (Mai-Prochnow et al., 2016). Gram-positive bacteria have a relatively thick cell wall (20–80 nm) composed of peptidoglycan, whereas Gram-negative bacteria have a thin cell wall (3–5 nm) but possess an additional outer membrane embedded by lipopolysaccharide and several pores. These differences in the microbial envelope can confer the different sensitivities of bacterial cells to CAP treatment. Mai-Prochnow et al. (2016) revealed that the bacterial cell wall thickness is correlated with the log₁₀ colony forming unit (CFU) reduction after different durations (1, 3, or 10 min) of CAP treatment. Moreover, *P. aeruginosa* exhibits more resistance to CAP when co-cultured with *S. epidermidis* as dual-species biofilms than that as a monospecies biofilm. Modic et al. (2017) reported the biphasic bacterial effect of ROS-dominated CAP, generated ROS-dominated gas-phase regimen with a low power discharge (8 W), and revealed that mixed-species biofilms containing *P. aeruginosa*, *S. aureus*, *E. faecalis*, and *K. pneumoniae* present a biphasic bacterial killing under ROS exposure. In the four-species biofilms, *P. aeruginosa* was much less susceptible to ROS-dominated plasma and presented a more gradual reduction in viable count across the 240 s of exposure (less than 3 log₁₀

CFU), whereas the three other species were more susceptible to ROS plasma with more than 3 log reduction in viable cell count, showing a quicker reduction between 60 and 120 s of plasma treatment.

Formation of the viable but non-culturable (VBNC) state of microorganisms also contributes to CAP resistance. Alessandria et al. (2019) showed the presence of inactivated bacterial cells or their VBNC state after CAP treatment through quantitative polymerase chain reaction amplification targeting the 16S rRNA. Liao et al. (2020) reported that a level of 7.4 to 7.6 log₁₀ CFU/ml of *S. aureus* VBNC cells can be induced after 8.1 to 24.3 kJ CAP treatment. The authors also found that most energy-dependent physiological activities are arrested, while the oxidative stress response-related pathways are obviously upregulated in *S. aureus* VBNC state. In addition, genome comparison between control cells and survivors in transposon-mutated *S. aureus* biofilms has shown that the genes involved in the synthesis of the pigment staphyloxanthin are associated with resistance to CAP treatment (Mai-Prochnow et al., 2015). A recent study showed that CAP-processed *S. aureus* cells present decreased pigment phenotype, and the deletion of the staphyloxanthin biosynthetic genes *crtM* and *crtN* confers Newman-Δ*crtM* and Newman-Δ*crtN*, but not Newman-Δ*crtO*, with increased sensitivity to CAP treatment (Yang et al., 2020). These data suggest that the yellow intermediates of *S. aureus* pigment's biosynthetic pathway are important factors for the resistance of *S. aureus* against CAP inactivation. The reason may be the antioxidant property of the golden carotenoid pigment for deactivating ROS and helping bacteria evade ROS killing (Chen et al., 2016). Other antioxidant molecules produced by microorganisms, such as pyocyanin of *P. aeruginosa*, may also protect bacteria from CAP treatment. The anti-CAP roles of antioxidant molecules need further investigation.

APPLICATION OF CAP ON MIXED-SPECIES BIOFILM CONTROL

The pioneering work regarding the possible inactivation of mixed-species biofilms through CAP has been conducted by Denes et al. (2001), who showed that the CAP deposition on mixed-species biofilms formed by *S. epidermidis*, *P. fluorescens*, and *S. Typhimurium* results in the decrease of 56.5% bacterial attachment and 72.2% biofilm formation. The authors concluded that the CAP deposition of polyethylene glycol-like structures may be useful for food processing and medical practice to reduce bacterial contamination. Mai-Prochnow et al. (2014) reviewed the advances in the decontamination of biofilm-associated bacteria by using CAP. Scholtz et al. (2015) recently reviewed the use of CAP as a tool for decontamination and disinfection, such as in microorganism inactivation, pollutant removal, surface modification, food preparation, biofilm degradation, wound therapy, nosocomial infection prevention, cancer treatment, prion inactivation, and apoptosis initiation. Gupta and Ayan (2019) presented an overview of plasma instrumentation and

summarized the studies of plasma on biofilms by mostly using monospecies biofilms.

Medical Applications

Mixed-species biofilms represent the primary environment of most pathogens in the clinical setting. The normal ecological environment of microbial consortia that often coexist with its dwelling host may be easily disrupted by invading pathogens, which can outcompete healthy normal flora during their growth and transform the commensal consortia into pathogenic biofilms (Tytgat et al., 2019). Many pathogens often colonize joint replacements, heart valves, and metal or plastic implants to form mixed-species biofilms, which cause life-threatening diseases (Julák et al., 2018). Gomila et al. (2019) conducted a multicenter retrospective cohort study on patients with complicated urinary tract infections from 20 hospitals in eight countries and found that 42.2% (341/807) of the patients have catheter-associated urinary tract infections. Another study conducted in Singapore reported that about 14.7% (69/470) of the patients who underwent peritoneal dialysis have been subjected to catheter removal due to infection (Kwan et al., 2019). Indwelling medical device-related and catheter-associated infections can be caused by mixed-species biofilms, and many pathogens involved in biofilm formation can be cultured (Figure 2). Mixed-species biofilm infections have raised great concerns and are difficult to cure (Azeredo et al., 2017).

As a novel antimicrobial strategy, applications of CAP in fighting mixed-species biofilms have been investigated (Table 2). In an early work, Koban et al. (2011) demonstrated the role of CAP in killing multispecies human saliva biofilms grown on titanium disks *in vitro* and found a 5.67 reduction in log₁₀ CFU after 10 min of DBD argon plasma treatment. The authors concluded that the treatment of mixed-species dental biofilms on titanium disks by using CAP resulted in a reduction of 1.50 log₁₀ CFU for saliva biofilm and that CAP is more efficient than chlorhexidine digluconate rinse. Koban's group also evaluated the synergistic effects of CAP and disinfectants against multispecies dental biofilms and reported that the combination of disinfecting agent NaOCl or hydrogen peroxide with CAP achieves a higher level of CFU reduction than each agent alone (Koban et al., 2013). Du et al. (2013) confirmed the synergistic effect of CAP with 2% chlorhexidine digluconate on mixed-species biofilms by incubating polyspecies bacteria from human dental root canal infections on sterile bovine dentin disks. Delben et al. (2016) reported the role of CAP on pathogenic oral biofilms constituted by *C. albicans* and *S. aureus*. In their study, the dual-species biofilms presented a considerable log₁₀ CFU/ml reduction (1.52 for *C. albicans* and 1.23 for *S. aureus*) after 60 s of CAP treatment. Colony counting, confocal laser scanning microscopy, and scanning electron microscopy revealed reduced viability and the alteration of the morphology of the microorganism/biofilm in plasma group in comparison with those in the negative control. Importantly, low cytotoxicity and high viability in the oral epithelium were observed after treatment with CAP. Further study showed no sign of necrosis in the plasma-treated epithelium, and cell proliferation was well maintained, indicating that CAP is a safe approach to eliminate pathogenic oral biofilms (Delben et al., 2016).

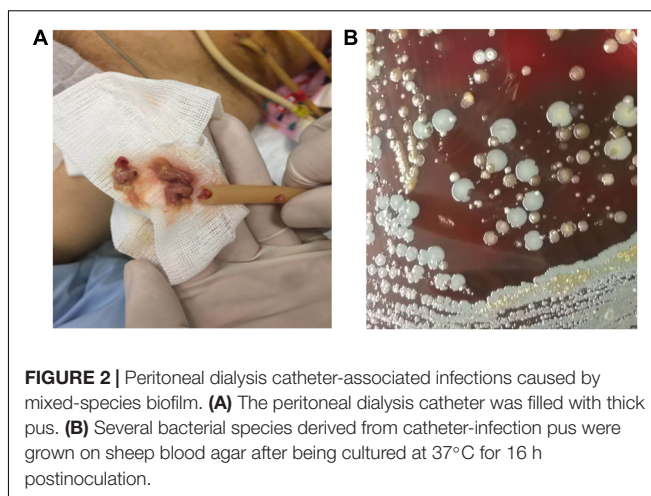


FIGURE 2 | Peritoneal dialysis catheter-associated infections caused by mixed-species biofilm. **(A)** The peritoneal dialysis catheter was filled with thick pus. **(B)** Several bacterial species derived from catheter-infection pus were grown on sheep blood agar after being cultured at 37°C for 16 h postinoculation.

Food Industrial Applications

Cold atmospheric plasma has also been proven to be a promising strategy for the control of multispecies biofilms formed by foodborne pathogens (Govaert et al., 2020; Huang et al., 2020). The cultures of *S. Typhimurium* mixed with cultivable indigenous microorganisms exhibited greater resistance to cold oxygen plasma (COP) compared with monoculture biofilms on fresh iceberg lettuce (Jahid et al., 2015). However, a reduction in log₁₀ CFU/cm² by approximately 4.6 was achieved in mixed cultures after COP treatment, and a notable shift in the colony type of *S. Typhimurium* from smooth to rugose was observed for biofilms on stainless-steel coupons even after 10 s of processing procedure with COP. By contrast, 5 min of COP treatment did not achieve any morphological shift in *S. Typhimurium* mixed biofilms on lettuce coupons. This difference may be ascribed to the penetration of COP to biotic and abiotic surfaces because COP does not penetrate the lettuce. Patange et al. (2019) showed that the bacterial biofilm populations of *L. monocytogenes* and *P. fluorescens* on abiotic surfaces treated with autologous conditioned plasma of high voltage (80 kV) has yielded non-detectable levels after 120 s of treatment. The inoculation on lettuce required an extended time to complete the eradication of mixed-species biofilms, and *L. monocytogenes* and *P. fluorescens* reduced by 2.2 and 4.2 log₁₀ CFU/ml, respectively, after 120 s of contained treatment. Govaert et al. (2020) reported the air-based CAP treatment of dual-species biofilms formed by *L. monocytogenes* and *S. Typhimurium*, and a result of log₁₀ CFU/cm²-reductions ranging between 1.5 and 2.5 was observed. The inactivation efficacy of CAP treatment may depend on the biofilm population type, but not the working gas supplied (Table 2).

Water-Treatment Applications

Mixed-species biofilms also grow and thrive in drinking water systems and usually result in human health concerns. Sun et al. (2018) treated the simulated polymicrobial drinking water biofilms with a 9 × 9 array of plasma jet, and results showed that all biofilms tested vanished in 20 min of CAP exposure. Confocal laser scanning microscopy revealed that the number

TABLE 2 | Direct CAP activity against mixed-species biofilms.

Microorganisms/biofilms	Plasma source	Working gas	Antimicrobial effect (processing duration)	References
Saliva mixed-species biofilms	Plasma jet (27 MHz) DBD plasma (40 kHz, 10 kV)	Argon Argon	1.42 reduction in log10 CFU (10 min) 5.67 reduction in log10 CFU (10 min)	Koban et al. (2011)
Dental root canal biofilms	Plasma jet (8 kV, 8 kHz)	Helium/oxygen + 2% chlorhexidine digluconate	76% dead of biofilm volume (5 min)	Du et al. (2013)
Multispecies subgingival biofilms	Plasma jet + H ₂ O ₂ (kNPen 09, 27 MHz)	Argon	3.41 ± 0.86 reduction in log10 CFU (10 min)	Koban et al. (2013)
<i>Salmonella</i> Typhimurium mixed with cultivable indigenous microorganisms	Plasma jet (1200~1250 mWs/cm ²)	Air	~4.6 reduction in log10 CFU/cm ² (60 s)	Jahid et al. (2015)
<i>Candida albicans</i> and <i>Staphylococcus aureus</i>	Plasma jet (220 V, 8 W)	Argon	Log10 CFU reduction for <i>C. albicans</i> (1.52 ± 0.18) and <i>S. aureus</i> (1.23 ± 0.21) (60 s)	Delben et al. (2016)
<i>Pseudomonas aeruginosa</i> and <i>Staphylococcus epidermidis</i>	Plasma jet	Argon	Log10 CFU reduction for <i>P. aeruginosa</i> (2.6 ± 0.4) and <i>S. epidermidis</i> (1.4 ± 0.5) (10 min)	Mai-Prochnow et al. (2016)
<i>Pseudomonas aeruginosa</i> , <i>Staphylococcus aureus</i> , <i>Klebsiella pneumoniae</i> , and <i>Enterococcus faecalis</i>	DBD plasma 8 W (ROS-dominated)	Air	Log10 CFU reduction for <i>P. aeruginosa</i> (2.3), <i>S. aureus</i> (2.8), <i>K. pneumoniae</i> (3.8), and <i>E. faecalis</i> (2.9) (120 s)	Modic et al. (2017)
	34.5 W (RNS-dominated)	Air	Log10 CFU reduction for <i>P. aeruginosa</i> (4.2), <i>S. aureus</i> (3.3), <i>K. pneumoniae</i> (4.2), and <i>E. faecalis</i> (3.3) (60 s)	
Complex multi-species biofilms of municipal water systems	Plasma jet (58 W/cm ²)	Helium	Fall from 122 ± 17 μm to 55 ± 13 μm in biofilm thickness (15 min)	Sun et al. (2018)
<i>Listeria monocytogenes</i> and <i>Salmonella</i> Typhimurium	DBD plasma (6.5 kV, 15 kHz)	Helium	2.8 reduction in log10 CFU/cm ² (15 min)	Govaert et al. (2019)
<i>Listeria monocytogenes</i> and <i>Pseudomonas fluorescens</i>	DBD plasma (80 kV)	Air	4.2 ± 0.2 reduction in log10 CFU (60 s)	Patange et al. (2019)
Mixed-species water biofilms	Underwater DBD microplasma bubbles (4.0 kV, 40 W)	Air	83% reduction in the existing biofilm load (15 min)	Zhou et al. (2019)
<i>Listeria monocytogenes</i> and <i>Salmonella</i> Typhimurium	DBD plasma (4 kV, 12 kHz)	Air	2.40 ± 0.31 reduction in log10 CFU (30 min)	Govaert et al. (2020)
		Helium	2.95 ± 0.23 reduction in log10 CFU (30 min)	

of active cells in mixed-species biofilms was reduced by more than 93% after 15 min of CAP treatment. Zhou et al. (2019) emphasized the importance of biochemically reactive species from plasma in the eradication of multispecies water biofilms and created a microplasma-bubble reactor to generate underwater microplasma bubbles that served as transport vehicles for delivering plasma reactive species to the water biofilm sites. The underwater microplasma bubbles generated in an artificial fish tank could enhance the mass transfer of ROS and RNS (mostly nitric oxide) into water for applications, such as initiating biofilm dispersal and treating bacterial biofilms on the skin of infected fish.

The microplasma bubbles are considered to be effective for underwater biofilm eradication. When reaching the close vicinity of a water biofilm, the self-burst of microbubbles may produce pressure waves that can break up the EPS matrix of the biofilms. Such pressure waves can further induce the bursting of other yet-to-burst microbubbles like a chain reaction to keep on disrupting the biofilm matrix until the whole biofilm structure is collapsed (Zhou et al., 2019). While the biofilm is dispersing, the resident microbial cells are

exposed to bactericidal plasma-activated water carrying ROS and RNS. However, the fundamental features of plasma-liquid physics and chemistry are largely unknown and are worth further investigation.

Limitation of CAP on Mixed-Species Biofilm Control

Most advantages of CAP process on multispecies biofilms have been accompanied by numerous limitations. The first obvious limitation is the weak penetrating capacity of plasma species into the deeper layers of mixed-species biofilms (Jiao et al., 2019). The increased production of EPS in biofilms may impede CAP penetration and prevent the antimicrobial effect of CAP on microbial cells at the bottom of the biofilms. The resistance of microbial cells and mixed-species biofilms to CAP varies depending on the microbial species involved, the changes in environmental condition, and the composition of active species generated by CAP systems (Jiao et al., 2019). The second limitation involves the nature and quantity of mixed-species biofilms to be sterilized. CAP sterilization in the food industry,

for example, the treatment of bulky and irregularly shaped food, limited volume of the investigated material should be considered (Scholtz et al., 2015). The rough biofilm surfaces often protect microbial cells from CAP exposure, and result in CAP treatment failure (Šimončicová et al., 2019). The third limitation involves the formation of VBNC microbial state. CAP treatment has been proven to induce the VBNC state of microbial cells, although the mechanisms underlying VBNC formation are obscure (Alessandria et al., 2019; Liao et al., 2020). The fourth limitation involves the servicing costs. Although the opening expenses and maintenance costs have been considerably decreased in CAP generated in ambient air, a CAP system that operates at low pressure usually requires high investment costs (Šimončicová et al., 2019). Possible solutions should be investigated to counter these limitations before the translation of CAP into real-life applications.

CONCLUSION

Naturally existing biofilms are composed of varied microbial species. The biological characteristics of microbes were explored as part of mixed-species biofilms rather than in strain isolation. The resident microorganisms in a mixed-species biofilm cooperate and/or compete to access available spaces and nutrients. The current information on microbial interactions among mixed-species biofilms are mainly derived from cultural investigations of polymicrobial biofilms *in vitro*, and information on actual interactions in mixed-species biofilms formed *in vivo* are scarce. Most common diseases, such as indwelling medical device-related and catheter-associated infections, are caused by mixed-species biofilms rather than by isolated pathogens.

Mixed-species biofilms display greater resistance to external stressors, including antibiotics and disinfectants.

REFERENCES

- Alessandria, V., Rantsiou, K., Cavallero, M. C., and Coccolin, L. S. (2019). Effect of atmospheric pressure plasma on *Listeria monocytogenes* attached to abiotic surfaces. *J. Food Protec.* 82, 233–237. doi: 10.4315/0362-028X.JFP-18-228
- Azeredo, J., Azevedo, N. F., Briandet, B., Cerca, N., Coenye, T., Costa, A. R., et al. (2017). Critical review on biofilm methods. *Crit. Rev. Microbiol.* 43, 313–351. doi: 10.1080/1040841X.2016.1208146
- Bandara, H. M., Yau, J. Y., Watt, R. M., Jin, L. J., and Samaranyake, L. P. (2010). *Pseudomonas aeruginosa* inhibits in-vitro *Candida* biofilm development. *BMC Microbiol.* 10:125. doi: 10.1186/1471-2180-10-125
- Bridier, A., Sanchez-Vizuet, P., Guilbaud, M., Piard, J., and Naïtali, M. (2015). Biofilm-associated persistence of food-borne pathogens. *Food Microbiol.* 45, 167–178. doi: 10.1016/j.fm.2014.04.015
- Brun, P., Bernabè, G., Marchiori, C., Scarpa, M., Zuin, M., Cavazzana, R., et al. (2018). Antibacterial efficacy and mechanisms of action of low power atmospheric pressure cold plasma: membrane permeability, biofilm penetration and antimicrobial sensitization. *J. Appl. Microbiol.* 125, 398–408. doi: 10.1111/jam.13780
- Burmole, M., Ren, D., Bjarnsholt, T., and Sørensen, S. J. (2014). Interactions in multispecies biofilms: do they actually matter? *Trends Microbiol.* 22, 84–91. doi: 10.1016/j.tim.2013.12.004
- Chen, F., Di, H., Wang, Y., Cao, Q., Xu, B., Zhang, X., et al. (2016). Small-molecule targeting of a diaphytoene desaturase inhibits *S. aureus* virulence. *Nat. Chem. Biol.* 12, 174–179. doi: 10.1038/nchembio.2003
- Chen, P., Wang, J. J., Hong, B., Tan, L., Yan, J., Zhang, Z., et al. (2019). Characterization of mixed-species biofilm formed by *Vibrio parahaemolyticus* and *Listeria monocytogenes*. *Front. Microbiol.* 10:2543. doi: 10.3389/fmicb.2019.02543
- Chhibber, S., Bansal, S., and Kaur, S. (2015). Disrupting the mixed-species biofilm of *Klebsiella pneumoniae* B5055 and *Pseudomonas aeruginosa* PAO using bacteriophages alone or in combination with xylitol. *Microbiology* 161, 1369–1377. doi: 10.1099/mic.0.000104
- Delben, J. A., Zago, C. E., Tyhovich, N., Duarte, S., and Vergani, C. E. (2016). Effect of atmospheric-pressure cold plasma on pathogenic oral bBiofilms and *in vitro* reconstituted oral epithelium. *PLoS One* 11:e0155427. doi: 10.1371/journal.pone.0155427
- Denes, A., Somers, E., Wong, A., and Denes, F. (2001). 12-Crown-4-ether and tri(ethylene glycol) dimethyl-ether plasma-coated stainless steel surfaces and their ability to reduce bacterial biofilm deposition. *J. Appl. Polym. Sci.* 81, 3425–3438. doi: 10.1002/app.1799
- Du, T., Shi, Q., Shen, Y., Cao, Y., Ma, J., Lu, X., et al. (2013). Effect of modified nonequilibrium plasma with chlorhexidine digluconate against endodontic biofilms *in vitro*. *J. Endod.* 39, 1438–1443. doi: 10.1016/j.joen.2013.06.027
- Duske, K., Jablonowski, L., Koban, I., Matthes, R., Holtfreter, B., Sckell, A., et al. (2015). Cold atmospheric plasma in combination with mechanical treatment improves osteoblast growth on biofilm covered titanium discs. *Biomaterials* 52, 327–334. doi: 10.1016/j.biomaterials.2015.02.035

AUTHOR CONTRIBUTIONS

YR, RZ, and XR contributed to the conception and design of the review. YR wrote the first draft of the manuscript. XR designed the figures. WS and YY contributed to various sections of the manuscript, including figures. All authors contributed to manuscript revision, editing, and approved the submitted version.

FUNDING

This work was supported by the National Key Biosafety Technology Research and Development Program of China (2017YFC1200404-4), the Biosafety Research Program of PLA (17SAZ08), and the National Natural Science Foundation of China (81672071).

- Edengeiser, E., Lackmann, J., Bründermann, E., Schneider, S., Benedikt, J., Bandow, J. E., et al. (2015). Synergistic effects of atmospheric pressure plasma-emitted components on DNA oligomers: a Raman spectroscopic study. *J. Biophotonics* 8, 918–924. doi: 10.1002/jbio.201400123
- Eggers, B., Marcinia, J., Memmert, S., Kramer, F. J., Deschner, J., and Nokhbehsaim, M. (2020). The beneficial effect of cold atmospheric plasma on parameters of molecules and cell function involved in wound healing in human osteoblast-like cells *in vitro*. *Odontology* 6:487. doi: 10.1007/s10266-020-00487-y
- Ermolaeva, S. A., Sysolyatina, E. V., and Gintsburg, A. L. (2015). Atmospheric pressure nonthermal plasmas for bacterial biofilm prevention and eradication. *Biointerphases* 10:29404. doi: 10.1116/1.4914382
- Fan, Y., Huang, X., Chen, J., and Han, B. (2020). Formation of a mixed-species biofilm is a survival strategy for unculturable lactic acid bacteria and *Saccharomyces cerevisiae* in *Daqu*, a Chinese traditional fermentation starter. *Front. Microbiol.* 11:138. doi: 10.3389/fmicb.2020.00138
- Flemming, H. C., and Wingender, J. (2010). The biofilm matrix. *Nat. Rev. Microbiol.* 8, 623–633. doi: 10.1038/nrmicro2415
- Frias, E., Iglesias, Y., Alvarez-Ordóñez, A., Prieto, M., González-Raurich, M., and López, M. (2020). Evaluation of cold atmospheric pressure plasma (CAPP) and plasma-activated water (PAW) as alternative non-thermal decontamination technologies for tofu: impact on microbiological, sensorial and functional quality attributes. *Food Res. Int.* 129:108859. doi: 10.1016/j.foodres.2019.108859
- Fridman, G., Friedman, G., Gutsol, A., Shekhter, A. B., Vasilets, V. N., and Fridman, A. (2008). Applied plasma medicine. *Plasma Process Polym.* 5, 503–533. doi: 10.1002/ppap.200700154
- Gherardi, M., Tonini, R., and Colombo, V. (2018). Plasma in dentistry: brief history and current status. *Trends Biotechnol.* 36, 583–585. doi: 10.1016/j.tibtech.2017.06.009
- Gomila, A., Carratalà, J., Eliakim-Raz, N., Shaw, E., Tebé, C., Wolkewitz, M., et al. (2019). Clinical outcomes of hospitalised patients with catheter-associated urinary tract infection in countries with a high rate of multidrug-resistance: the COMBACTE-MAGNET RESCUING study. *Antimicrob. Resist. Infect. Control.* 8:198. doi: 10.1186/s13756-019-0656-6
- Govaert, M., Smet, C., Graeffe, A., Walsh, J. L., and Van Impe, J. F. M. (2020). Inactivation of *L. monocytogenes* and *S. typhimurium* biofilms by means of an air-based cold atmospheric plasma (CAP) system. *Foods* 9:e157. doi: 10.3390/foods9020157
- Govaert, M., Smet, C., Walsh, J. L., and Van Impe, J. F. M. (2019). Dual-species model biofilm consisting of *Listeria monocytogenes* and *Salmonella Typhimurium*: development and inactivation with cold atmospheric plasma (CAP). *Front. Microbiol.* 10:2524. doi: 10.3389/fmicb.2019.02524
- Guillonnet, R., Baraquet, C., Bazire, A., and Molmeret, M. (2018). Multispecies biofilm development of marine bacteria implies complex relationships through competition and synergy and modification of matrix components. *Front. Microbiol.* 9:1960. doi: 10.3389/fmicb.2018.01960
- Guo, L., Xu, R., Zhao, Y., Liu, D., Liu, Z., Wang, X., et al. (2018). Gas plasma pre-treatment increases antibiotic sensitivity and persister eradication in methicillin-resistant *Staphylococcus aureus*. *Front. Microbiol.* 9:537. doi: 10.3389/fmicb.2018.00537
- Gupta, T. T., and Ayan, H. (2019). Application of non-thermal plasma on biofilm: a review. *Appl. Sci.* 9:3548. doi: 10.3390/app9173548
- Hafner, S., Ehrenfeld, M., Neumann, A. C., and Wieser, A. (2018). Comparison of the bactericidal effect of cold atmospheric pressure plasma (CAPP), antimicrobial photodynamic therapy (aPDT), and polihexanide (PHX) in a novel wet surface model to mimic oral cavity application. *J. CranioMaxilloFac. Surg.* 46, 2197–2202. doi: 10.1016/j.jcms.2018.09.006
- Handorf, O., Weihe, T., Bekeschus, S., Graf, A. C., Schnabel, U., Riedel, K., et al. (2018). Nonthermal plasma jet treatment negatively affects viability and structure of *Candida albicans* SC5314 biofilms. *Appl. Environ. Microbiol.* 84:e01163-18. doi: 10.1128/AEM.01163-18
- Hansen, L. B. S., Ren, D., Burmølle, M., and Sørensen, S. J. (2017). Distinct gene expression profile of *Xanthomonas retroflexus* engaged in synergistic multispecies biofilm formation. *ISME J.* 11, 300–303. doi: 10.1038/ismej.2016.107
- Harriott, M. M., and Noverr, M. C. (2010). Ability of *Candida albicans* mutants to induce *Staphylococcus aureus* vancomycin resistance during polymicrobial biofilm formation. *Antimicrob. Agents Chemother.* 54, 3746–3755. doi: 10.1128/AAC.00573-10
- Herschend, J., Damholt, Z. B. V., Marquard, A. M., Svensson, B., and Sørensen, S. J. (2017). A meta-proteomics approach to study the interspecies interactions affecting microbial biofilm development in a model community. *Sci. Rep.* 7:16483. doi: 10.1038/s41598-017-16633-6
- Hoiby, N., Bjarnsholt, T., Givskov, M., Molin, S., and Ciofu, O. (2010). Antibiotic resistance of bacterial biofilms. *Int. J. Antimicrob. Agents* 35, 322–332. doi: 10.1016/j.ijantimicag.2009.12.011
- Huang, M., Zhuang, H., Zhao, J., Wang, J., Yan, W., and Zhang, J. (2020). Differences in cellular damage induced by dielectric barrier discharge plasma between *Salmonella Typhimurium* and *Staphylococcus aureus*. *Bioelectrochemistry* 132:107445. doi: 10.1016/j.bioelechem.2019.107445
- Jahid, I. K., Han, N., Zhang, C. Y., and Ha, S. D. (2015). Mixed culture biofilms of *Salmonella Typhimurium* and cultivable indigenous microorganisms on lettuce show enhanced resistance of their sessile cells to cold oxygen plasma. *Food Microbiol.* 46, 383–394. doi: 10.1016/j.fm.2014.08.003
- Ji, S. H., Ki, S. H., Ahn, J. H., Shin, J. H., Hong, E. J., Kim, Y. J., et al. (2018). Inactivation of *Escherichia coli* and *Staphylococcus aureus* on contaminated perilla leaves by dielectric barrier discharge (DBD) plasma treatment. *Arch. Biochem. Biophys.* 643, 32–41. doi: 10.1016/j.abb.2018.02.010
- Jiao, Y., Tay, F. R., Niu, L., and Chen, J. (2019). Advancing antimicrobial strategies for managing oral biofilm infections. *Int. J. Oral Sci.* 11:28. doi: 10.1038/s41368-019-0062-1
- Jorge, L. S., Fucuta, P. S., Oliveira, M. G. L., Nakazone, M. A., de Matos, J. A., Chueire, A. G., et al. (2018). Outcomes and risk factors for polymicrobial posttraumatic osteomyelitis. *J. Bone Jt. Infect.* 3, 20–26. doi: 10.7150/jbji.22566
- Joshi, S. G., Cooper, M., Yost, A., Paff, M., Ercan, U. K., Fridman, G., et al. (2011). Nonthermal dielectric-barrier discharge plasma-induced inactivation involves oxidative DNA damage and membrane lipid peroxidation in *Escherichia coli*. *Antimicrob. Agents Chemother.* 55, 1053–1062. doi: 10.1128/AAC.01002-10
- Julák, J., Scholtz, V., and Vaňková, E. (2018). Medically important biofilms and non-thermal plasma. *World J. Microbiol. Biotechnol.* 34:178. doi: 10.1007/s11274-018-2560-2
- Koban, I., Geisel, M. H., Holtfreter, B., Jablonowski, L., Hübner, N. O., Matthes, R., et al. (2013). Synergistic effects of nonthermal plasma and disinfecting agents against dental biofilms *in vitro*. *ISRN Dent.* 2013:573262. doi: 10.1155/2013/573262
- Koban, I., Holtfreter, B., Hubner, N. O., Matthes, R., Sietmann, R., Kindel, E., et al. (2011). Antimicrobial efficacy of non-thermal plasma in comparison to chlorhexidine against dental biofilms on titanium discs *in vitro* – proof of principle experiment. *J. Clin. Periodontol.* 38, 956–965. doi: 10.1111/j.1600-051X.2011.01740.x
- Krueger, A. P., Smith, R. F., and Go, I. G. (1957). The action of air ions on bacteria. I. Protective and lethal effect on suspensions of staphylococci in droplets. *J. Gen. Physiol.* 41, 359–381. doi: 10.1085/jgp.41.2.359
- Kwan, J. R., Chong, T. T., Low, G. Z., Low, G. W., Htay, H., Foo, M. W., et al. (2019). Outcomes following peritoneal dialysis catheter removal with reinsertion or permanent transfer to haemodialysis. *J. Vasc. Access.* 20, 60–64. doi: 10.1177/1129729818773984
- Laroussi, M., and Akan, T. (2007). Arc-free atmospheric pressure cold plasma jets: a review. *Plasma Process Polym.* 4, 777–788. doi: 10.1002/ppap.200700006
- Lee, K. W. K., Periasamy, S., Mukherjee, M., Xie, C., Kjelleberg, S., and Rice, S. A. (2014). Biofilm development and enhanced stress resistance of a model, mixed-species community biofilm. *ISME J.* 8, 894–907. doi: 10.1038/ismej.2013.194
- Liao, X., Liu, D., and Ding, T. (2020). Nonthermal plasma induces the viable-but-nonculturable state in *Staphylococcus aureus* via metabolic suppression and the oxidative stress response. *Appl. Environ. Microbiol.* 86, e2216–e2219. doi: 10.1128/AEM.02216-19
- Limoli, D. H., and Hoffman, L. R. (2019). Help, hinder, hide and harm: what can we learn from the interactions between *Pseudomonas aeruginosa* and *Staphylococcus aureus* during respiratory infections? *Thorax* 74, 684–692. doi: 10.1136/thoraxjnl-2018-212616

- Limoli, D. H., Yang, J., Khansaheb, M. K., Helfman, B., Peng, L., Stecenko, A. A., et al. (2016). *Staphylococcus aureus* and *Pseudomonas aeruginosa* co-infection is associated with cystic fibrosis-related diabetes and poor clinical outcomes. *Eur. J. Clin. Microbiol. Infect. Dis.* 35, 947–953. doi: 10.1007/s10096-016-2621-0
- Liu, H., Shang, W., Hu, Z., Zheng, Y., Yuan, J., Hu, Q., et al. (2018). A novel SigB(Q225P) mutation in *Staphylococcus aureus* retains virulence but promotes biofilm formation. *Emerg. Microbes Infect.* 7:72. doi: 10.1038/s41426-018-0078-1
- Liu, W., Røder, H. L., Madsen, J. S., Bjarnsholt, T., Sørensen, S. J., and Burmølle, M. (2016). Interspecific bacterial interactions are reflected in multispecies biofilm spatial organization. *Front. Microbiol.* 7:1366. doi: 10.3389/fmicb.2016.01366
- Liu, N. T., Bauman, G. R., Francoeur, C. B., Shelton, D. R., Lo, Y. M., and Nou, X. (2016). *Ralstonia insidiosa* serves as bridges in biofilm formation by foodborne pathogens *Listeria monocytogenes*, *Salmonella enterica*, and *Enterohemorrhagic Escherichia coli*. *Food Control* 65, 14–20. doi: 10.1016/j.foodcont.2016.01.004
- Mai-Prochnow, A., Bradbury, M., Ostrikov, K., and Murphy, A. B. (2015). *Pseudomonas aeruginosa* biofilm response and resistance to cold atmospheric pressure plasma is linked to the redox-active molecule phenazine. *PLoS One* 10:e0130373. doi: 10.1371/journal.pone.0130373
- Mai-Prochnow, A., Clauson, M., Hong, J., and Murphy, A. B. (2016). Gram positive and Gram negative bacteria differ in their sensitivity to cold plasma. *Sci. Rep.* 6:38610. doi: 10.1038/srep38610
- Mai-Prochnow, A., Murphy, A. B., McLean, K. M., Kong, M. G., and Ostrikov, K. (2014). Atmospheric pressure plasmas: infection control and bacterial responses. *Int. J. Antimicrob. Agents* 43, 508–517. doi: 10.1016/j.ijantimicag.2014.01.025
- Mizuno, A., and Hori, Y. (1988). Destruction of living cells by pulsed high voltage application. *IEEE Trans. Ind. Appl.* 24, 387–394. doi: 10.1109/28.2886
- Modic, M., McLeod, N. P., Sutton, J. M., and Walsh, J. L. (2017). Cold atmospheric pressure plasma elimination of clinically important single- and mixed-species biofilms. *Int. J. Antimicrob. Agents* 49, 375–378. doi: 10.1016/j.ijantimicag.2016.11.022
- Nadell, C. D., Drescher, K., and Foster, K. R. (2016). Spatial structure, cooperation and competition in biofilms. *Nat. Rev. Microbiol.* 14, 589–600. doi: 10.1038/nrmicro.2016.84
- Nishime, T. M. C. C., Borges, A. C., Koga-ito, C. Y., Machida, M., Hein, L. R. O. O., and Kostov, K. G. (2017). Non-thermal atmospheric pressure plasma jet applied to inactivation of different microorganisms. *Surf. Coat. Technol.* 312, 19–24. doi: 10.1016/j.surfcoat.2016.07.076
- O'Connor, N., Cahill, O., Daniels, S., Galvin, S., and Humphreys, H. (2014). Cold atmospheric pressure plasma and decontamination. Can it contribute to preventing hospital-acquired infections? *J. Hosp. Infect.* 88, 59–65. doi: 10.1016/j.jhin.2014.06.015
- Orazi, G., and O'Toole, G. A. (2019). It takes a village: mechanisms underlying antimicrobial recalcitrance of polymicrobial biofilms. *J. Bacteriol.* 202:e0530-19. doi: 10.1128/JB.00530-19
- Pang, X., Wong, C., Chung, H. J., and Yuk, H. G. (2019). Biofilm formation of *Listeria monocytogenes* and its resistance to quaternary ammonium compounds in a simulated salmon processing environment. *Food Control* 98, 200–208. doi: 10.1016/j.foodcont.2018.11.029
- Patange, A., Boehm, D., Zuziana, D., Cullen, P. J., Gilmore, B., and Bourke, P. (2019). High voltage atmospheric cold air plasma control of bacterial biofilms on fresh produce. *Int. J. Food Microbiol.* 293, 137–145. doi: 10.1016/j.jifoodmicro.2019.01.005
- Pompl, P., Jamitzky, F., Shimizu, T., Steffes, B., Bunk, W., Schmidt, H. U., et al. (2009). The effect of low temperature plasma on bacteria as observed by repeated AFM imaging. *New J. Phys.* 11:115023. doi: 10.1088/1367-2630/11/11/115023
- Potron, A., Poirel, L., and Nordmann, P. (2011). Plasmid-mediated transfer of the bla(NDM-1) gene in Gram-negative rods. *FEMS Microbiol. Lett.* 324, 111–116. doi: 10.1111/j.1574-6968.2011.02392.x
- Ren, D., Madsen, J. S., de la Cruz-Perera, C. I., Bergmark, L., Sørensen, S. J., and Burmølle, M. (2014). High-throughput screening of multispecies biofilm formation and quantitative PCR-based assessment of individual species proportions, useful for exploring interspecific bacterial interactions. *Microb. Ecol.* 68, 146–154. doi: 10.1007/s00248-013-0315-z
- Ren, D., Madsen, J. S., Sørensen, S. J., and Burmølle, M. (2015). High prevalence of biofilm synergy among bacterial soil isolates in cocultures indicates bacterial interspecific cooperation. *ISME J.* 9, 81–89. doi: 10.1038/ismej.2014.96
- Rendueles, O., and Ghigo, J. M. (2012). Multi-species biofilms: how to avoid unfriendly neighbors. *FEMS Microbiol. Rev.* 36, 972–989. doi: 10.1111/j.1574-6976.2012.00328.x
- Rice, S. A., Wuertz, S., and Kjelleberg, S. (2016). Next-generation studies of microbial biofilm communities. *Microb. Biotechnol.* 9, 677–680. doi: 10.1111/1751-7915.12390
- Sakudo, A., Miyagi, H., Horikawa, T., Yamashiro, R., and Misawa, T. (2018). Treatment of *Helicobacter pylori* with dielectric barrier discharge plasma causes UV-induced damage to genomic DNA leading to cell death. *Chemosphere* 200, 366–372. doi: 10.1016/j.chemosphere.2018.02.115
- Scholtz, V., Pazlarova, J., Souskova, H., Khun, J., and Julak, J. (2015). Nonthermal plasma — A tool for decontamination and disinfection. *Biotechnol. Adv.* 33, 1108–1119. doi: 10.1016/j.biotechadv.2015.01.002
- Simmons, M., Drescher, K., Nadell, C. D., and Bucci, V. (2018). Phage mobility is a core determinant of phage-bacteria coexistence in biofilms. *ISME J.* 12, 531–543. doi: 10.1038/ismej.2017.190
- Šimončicová, J., Kryštofová, S., Medvecká, V., Ďurišová, K., and Kaliňáková, B. (2019). Technical applications of plasma treatments: current state and perspectives. *Appl. Microbiol. Biotechnol.* 103, 5117–5129. doi: 10.1007/s00253-019-09877-x
- Souza, J. G. S., Bertolini, M., Thompson, A., Mansfield, J. M., Grassmann, A. A., Maas, K., et al. (2020). Role of glucosyltransferase R in biofilm interactions between *Streptococcus oralis* and *Candida albicans*. *ISME J.* 10:608. doi: 10.1038/s41396-020-0608-4
- Sun, P. P., Araud, E. M., Huang, C., Shen, Y., Monroy, G. L., Zhong, S., et al. (2018). Disintegration of simulated drinking water biofilms with arrays of microchannel plasma jets. *NPJ Biofilms Microb.* 4:24. doi: 10.1038/s41522-018-0063-4
- Tan, C. A. Z., Antypas, H., and Kline, K. A. (2020). Overcoming the challenge of establishing biofilms in vivo: a roadmap for *Enterococci*. *Curr. Opin. Microbiol.* 53, 9–18. doi: 10.1016/j.mib.2020.01.013
- Tanner, W. D., Atkinson, R. M., Goel, R. K., Toleman, M. A., Benson, L. S., Porucznik, C. A., et al. (2017). Horizontal transfer of the blaNDM-1 gene to *Pseudomonas aeruginosa* and *Acinetobacter baumannii* in biofilms. *FEMS Microbiol. Lett.* 364:fnx048. doi: 10.1093/femsle/fnx048
- Trifilio, S., Zhou, Z., Fong, J. L., Zomas, A., Liu, D., Zhao, C., et al. (2015). Polymicrobial bacterial or fungal infections: incidence, spectrum of infection, risk factors, and clinical outcomes from a large hematopoietic stem cell transplant center. *Transpl. Infect. Dis.* 17, 267–274. doi: 10.1111/tid.12363
- Tytgat, H. L. P., Nobrega, F. L., van der Oost, J., and de Vos, W. M. (2019). Bowel biofilms: tipping points between a healthy and compromised gut? *Trends Microbiol.* 27, 17–25. doi: 10.1016/j.tim.2018.08.009
- Van Der Paal, J., Neyts, E. C., Verlact, C. C. W., and Bogaerts, A. (2016). Effect of lipid peroxidation on membrane permeability of cancer and normal cells subjected to oxidative stress. *Chem. Sci.* 7, 489–498. doi: 10.1039/c5sc02311d
- Vatansever, F., de Melo, W. C., Avci, P., Vecchio, D., Sadasivam, M., Gupta, A., et al. (2013). Antimicrobial strategies centered around reactive oxygen species - bactericidal antibiotics, photodynamic therapy, and beyond. *FEMS Microbiol. Rev.* 37, 955–989. doi: 10.1111/1574-6976.12026
- Winkelstroter, L. K., Tulini, F. L., and De Martinis, E. C. P. (2015). Identification of the bacteriocin produced by cheese isolate *Lactobacillus paraplantarum* FT259 and its potential influence on *Listeria monocytogenes* biofilm formation. *LWT Food Sci. Tech.* 64, 586–592. doi: 10.1016/j.lwt.2015.06.014
- Yang, Y., Wang, H., Zhou, H., Hu, Z., Shang, W., Rao, Y., et al. (2020). Protective effect of the golden staphyloxanthin biosynthesis pathway on *Staphylococcus aureus* under cold atmospheric plasma treatment. *Appl. Environ. Microbiol.* 86:e01998-19. doi: 10.1128/AEM.01998-19
- Yuan, L., Hansen, M. F., Røder, H. L., Wang, N., Burmølle, M., and He, G. (2019). Mixed-species biofilms in the food industry: current knowledge and novel control strategies. *Crit. Rev. Food Sci. Nutr.* 2019, 1–7. doi: 10.1080/10408398.2019.1632790
- Yusupov, M., Bogaerts, A., Huygh, S., Snoeckx, R., van Duin, A. C. T., and Neyts, E. C. (2013). Plasma-induced destruction of bacterial cell wall components:

- a reactive molecular dynamics simulation. *J. Phys. Chem. C* 117, 5993–5998. doi: 10.1021/jp3128516
- Yusupov, M., Neyts, E. C., Khalilov, U., Snoeckx, R., van Duin, A. C. T., and Bogaerts, A. (2012). Atomic-scale simulations of reactive oxygen plasma species interacting with bacterial cell walls. *New J. Phys.* 14:093043. doi: 10.1088/1367-2630/14/9/093043
- Zhou, R., Zhou, R., Wang, P., Luan, B., Zhang, X., Fang, Z., et al. (2019). Microplasma bubbles: reactive vehicles for biofilm dispersal. *ACS Appl. Mater. Interf.* 11, 20660–20669. doi: 10.1021/acsami.9b03961

Conflict of Interest: The authors declare that the research was conducted in the absence of any commercial or financial relationships that could be construed as a potential conflict of interest.

Copyright © 2020 Rao, Shang, Yang, Zhou and Rao. This is an open-access article distributed under the terms of the Creative Commons Attribution License (CC BY). The use, distribution or reproduction in other forums is permitted, provided the original author(s) and the copyright owner(s) are credited and that the original publication in this journal is cited, in accordance with accepted academic practice. No use, distribution or reproduction is permitted which does not comply with these terms.



Innovative Strategies Toward the Disassembly of the EPS Matrix in Bacterial Biofilms

Rita M. Pinto^{1,2,3}, Filipa A. Soares¹, Salette Reis¹, Cláudia Nunes¹ and Patrick Van Dijck^{2,3*}

¹ LAQV, REQUIMTE, Departamento de Ciências Químicas, Faculdade de Farmácia, Universidade Do Porto, Porto, Portugal,

² Laboratory of Molecular Cell Biology, Institute of Botany and Microbiology, KU Leuven, Leuven, Belgium, ³ Center for Microbiology, VIB-KU Leuven, Leuven, Belgium

OPEN ACCESS

Edited by:

Luis Cláudio Nascimento da Silva,
Universidade Ceuma, Brazil

Reviewed by:

Rosalía Cavaliere,
University of Technology
Sydney, Australia
Maria José Saavedra,
Universidade de Trás os Montes e Alto
Douro, Portugal

*Correspondence:

Patrick Van Dijck
patrick.vandijck@kuleuven.vib.be

Specialty section:

This article was submitted to
Antimicrobials, Resistance and
Chemotherapy,
a section of the journal
Frontiers in Microbiology

Received: 15 February 2020

Accepted: 21 April 2020

Published: 26 May 2020

Citation:

Pinto RM, Soares FA, Reis S, Nunes C
and Van Dijck P (2020) Innovative
Strategies Toward the Disassembly of
the EPS Matrix in Bacterial Biofilms.
Front. Microbiol. 11:952.
doi: 10.3389/fmicb.2020.00952

Bacterial biofilms represent a major concern at a worldwide level due to the high demand for implantable medical devices and the rising numbers of bacterial resistance. The complex structure of the extracellular polymeric substances (EPS) matrix plays a major role in this phenomenon, since it protects bacteria from antibiotics, avoiding drug penetration at bactericidal concentrations. Besides, this structure promotes bacterial cells to adopt a dormant lifestyle, becoming less susceptible to antibacterial agents. Currently, the available treatment for biofilm-related infections consists in the administration of conventional antibiotics at high doses for a long-term period. However, this treatment lacks efficiency against mature biofilms and for implant-associated biofilms it may be necessary to remove the medical device. Thus, biofilm-related infections represent an economical burden for the healthcare systems. New strategies focusing on the matrix are being highlighted as alternative therapies to eradicate biofilms. Here, we outline reported matrix disruptive agents, nanocarriers, and technologies, such as application of magnetic fields, photodynamic therapy, and ultrasounds, that have been under investigation to disrupt the EPS matrix of clinically relevant bacterial biofilms. In an ideal therapy, a synergistic effect between antibiotics and the explored innovated strategies is aimed to completely eradicate biofilms and avoid antimicrobial resistance phenomena.

Keywords: bacterial resistance, matrix disruptive agents, nanocarriers, photodynamic therapy, ultrasounds, magnetic nanoparticles

INTRODUCTION

A post-antibiotic era is now emerging due to the increasing figures of antimicrobial resistance cases at a worldwide level. This phenomenon occurs naturally, however the use and misuse of antimicrobial agents in humans and animals promoted its acceleration in the last decades (WHO, 2014).

Bacterial biofilms are key players in the development of antimicrobial resistance. Biofilms are formed when bacterial cells attach to a substratum or to other cells embedded in a protective polymeric extracellular matrix (Pinto et al., 2019). The biofilm formation process can be divided in three main stages: attachment, maturation, and detachment. As soon as a medical device is implanted in the human body, host matrix proteins immediately adhere to the implant surface. Bacterial cells are able to recognize and attach to these proteins, promoting bacterial colonization.

From this point, the biofilm grows by formation of a matrix of extracellular polymeric substances (EPS) around bacterial cells until it reaches a phase of maturation, adopting a three-dimension structure (Pinto et al., 2019). Eventually, environmental stimuli may lead to the detachment of single cells or cell clusters from the biofilm, promoting dissemination and colonization on other sites of the host (Beitelshees et al., 2018; Pinto et al., 2019).

In biofilm communities, the EPS matrix is responsible for intercellular interactions and protection of bacterial cells from hostile environment. Thus, this matrix mainly contributes to the increased antibiotic tolerance and resistance of biofilms compared with planktonic cells (Flemming et al., 2016; Fulaz et al., 2019). This review provides an overview of the characteristics of the EPS matrix and its role in antibiotic resistance. Besides, biofilm-associated diseases and innovative therapeutic strategies to disrupt the biofilm matrix are also outlined.

THE BIOFILM MATRIX AND ANTIMICROBIAL RESISTANCE

The formation of the biofilm matrix is a dynamic process with high energetic cost for bacteria since it requires production and secretion of extracellular material. In exchange, the EPS matrix provides mechanical stability to the biofilms and mediates interactions between cells (Flemming et al., 2016). In most cases, the biofilm matrix represents around 90% of the total biofilm biomass and is mainly composed by polysaccharides, lipids, proteins and extracellular DNA (eDNA) (Fulaz et al., 2019) (**Figure 1**). Extensive reviews regarding biofilm matrix and antimicrobial resistance can be found elsewhere (Donlan and Costerton, 2002; Flemming and Wingender, 2010).

Polysaccharides are one of the main constituents of the EPS matrix and they attach to cell surfaces forming a complex network. Most of these molecules are heteropolysaccharides composed by a mixture of neutral and charged sugar residues. Additionally, they can contain organic and inorganic substituents, which contributes to their polyanionic or polycationic nature. The exopolysaccharides composition

may differ between species and even between strains from the same species (Flemming and Wingender, 2010). Despite the heterogeneity among biofilms, exopolysaccharides are indispensable to biofilm formation and constitute the protective barrier of the EPS matrix (Flemming and Wingender, 2010; Fulaz et al., 2019). Besides, they are also responsible for water retention within the biofilm (Fulaz et al., 2019). Due to the high amount of water, the biofilm provides a highly hydrated environment that protects cells from fluctuations in water potential. In addition, the presence of water confers the biofilm a non-rigid structure with different viscosities that allow movement of the cells in the matrix (Flemming et al., 2016). As a result, a biofilm is a porous structure with macrocolonies surrounded by water-filled voids (Donlan, 2001a).

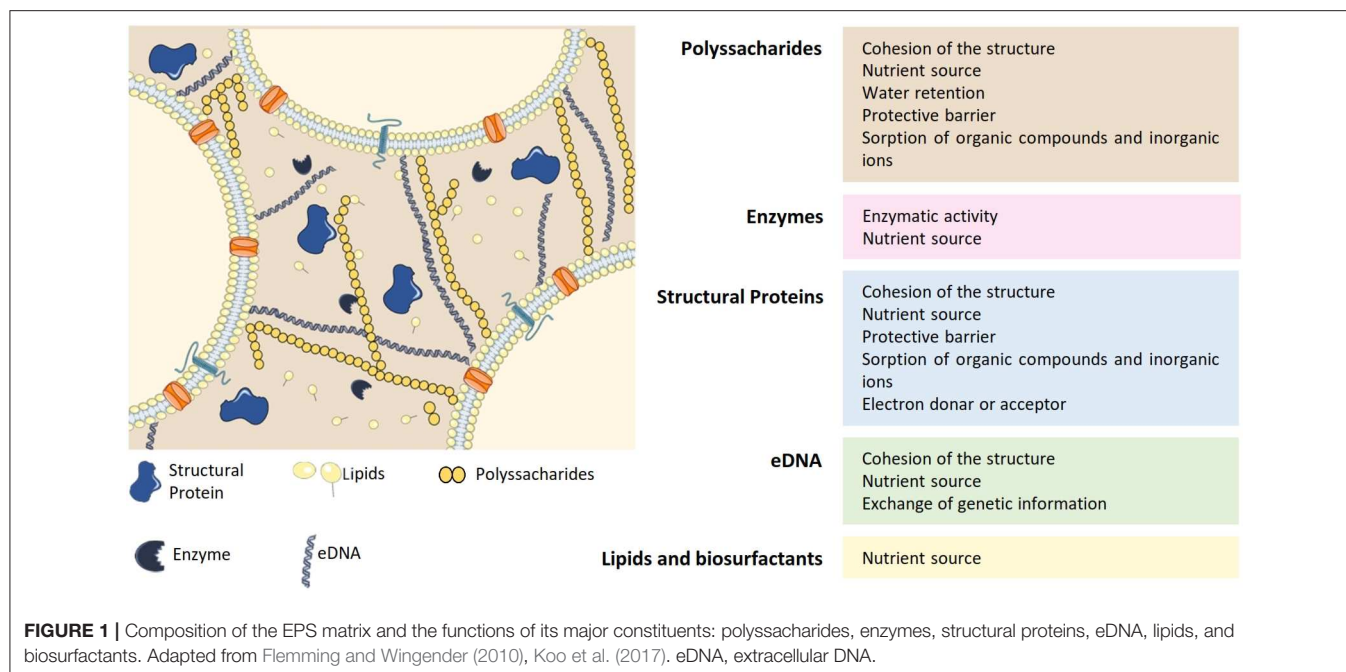
Extracellular proteins, such as structural proteins and enzymes, are also critical components of the matrix and can even be present in a higher amount than polysaccharides. Structural proteins are mainly involved in stabilization of the biofilm architecture, by connecting cells to the EPS (Fong and Yildiz, 2015). Enzymes are essentially involved in the degradation of other matrix components such as polysaccharides (e.g., dispersin B), matrix proteins (e.g., proteases), and eDNA (e.g., DNases). Thus, enzymatic activity within the biofilm provides nutrients to bacterial cells and promotes biofilm reorganization and dispersal (Fong and Yildiz, 2015).

Besides polysaccharides and proteins, eDNA also contributes for the structural integrity of the matrix (Fulaz et al., 2019). The contribution of this component for the three-dimensional structure of the biofilm differs greatly among species (Beitelshees et al., 2018). For instance, eDNA is a major component of *Pseudomonas aeruginosa* (*P. aeruginosa*) biofilms, while it is found in very low amounts in *Staphylococcus epidermidis* (*S. epidermidis*) biofilms (Beitelshees et al., 2018). Besides supporting the biofilm structure, eDNA facilitates exchange of genetic information between bacterial cells within the biofilm (Flemming and Wingender, 2010).

The complex nature of the matrix represents a diffusion barrier for antimicrobial agents, since it limits their penetration into deeper layers of the biofilm (Donlan and Costerton, 2002; Srivastava and Bhargava, 2016). Besides, within the matrix, antibiotics can interact with EPS components, leading to a decrease of their activity due to enzymatic degradation, complex formation owing to chelation, among other reactions (Flemming et al., 2016). The existence of various biofilm microenvironments, with different physical features such as low oxygen and pH, also influence the efficiency of antibacterial agents (Srivastava and Bhargava, 2016). Therefore, antimicrobial agents usually reach bacteria at sublethal concentrations, which boosts selection of antimicrobial resistance in the biofilm cells (Flemming et al., 2016).

In addition, bacterial cells embedded in the biofilm structure behave differently than in the planktonic state (Donlan and Costerton, 2002). In the lower regions of the biofilm, bacteria adopt a dormant lifestyle, since they have reduced access to nutrients and gaseous exchange (Flemming et al., 2016). These cells are metabolically less active than planktonic cells, leading to their reduced susceptibility to antibiotics (Anderson and

Abbreviations: AC, altering current; AgNPs, silver nanoparticles; ALA, 5-aminolevulinic acid; APTES, 3-aminopropyltriethoxysilane; C₂DA, *Cis*-2-decenoic acid; CES, carboxyethylsilanetriol; CLSM, confocal laser scanning microscopy; CS, chitosan; DC, direct current; DNase I, deoxyribonuclease I; *E. coli*, *Escherichia coli*; eDNA, extracellular DNA; EDTA, ethylenediaminetetraacetic acid; *E. faecalis*, *Enterococcus faecalis*; *E. faecium*, *Enterococcus faecium*; EOs, essential oils; EPS, extracellular polymeric substances; MBEC, minimum biofilm eliminating concentration; MIC, minimum inhibitory concentration; MNPs, magnetic nanoparticles; MOFs, metal organic frameworks; MRPA, multidrug-resistant *Pseudomonas aeruginosa*; MRSA, methicillin-resistant *Staphylococcus aureus*; NAC, *N*-acetyl cysteine; NPs, nanoparticles; PAE, poly(β -amino ester); *P. aeruginosa*, *Pseudomonas aeruginosa*; PAOI, *Pseudomonas aeruginosa* O1; PDT, photodynamic therapy; PEG, polyethylene glycol; PNAG, poly-*N*-acetylglucosamine; PS, photosensitizer; PTT, photothermal therapy; ROS, reactive oxygen species; SEM, scanning electron microscopy; SPIONs, superparamagnetic iron oxide nanoparticles; *S. epidermidis*, *Staphylococcus epidermidis*; *S. aureus*, *Staphylococcus aureus*; TMP, tetra-substituted *N*-methyl-pyridyl-porphine; USMB, ultrasound-targeted microbubble.



O'Toole, 2008). This resistance may lead to gene modification that can be transferred to other bacteria, through the facilitated intercellular communication promoted by the EPS matrix (Flemming et al., 2016). Thus, this phenomenon also contributes to the enhanced antibacterial resistance of biofilms.

Due to its complex composition and structure, the EPS matrix has a major role in the biofilm formation, development and survival. It is not only a protective barrier against external factors, but also a source of nutrients and enzymes, and an intercellular connector. Ultimately, the unique characteristics of the matrix contributes to the high antimicrobial tolerance and/or resistance of biofilms.

BIOFILMS IN MEDICAL DEVICES AND IN DISEASE

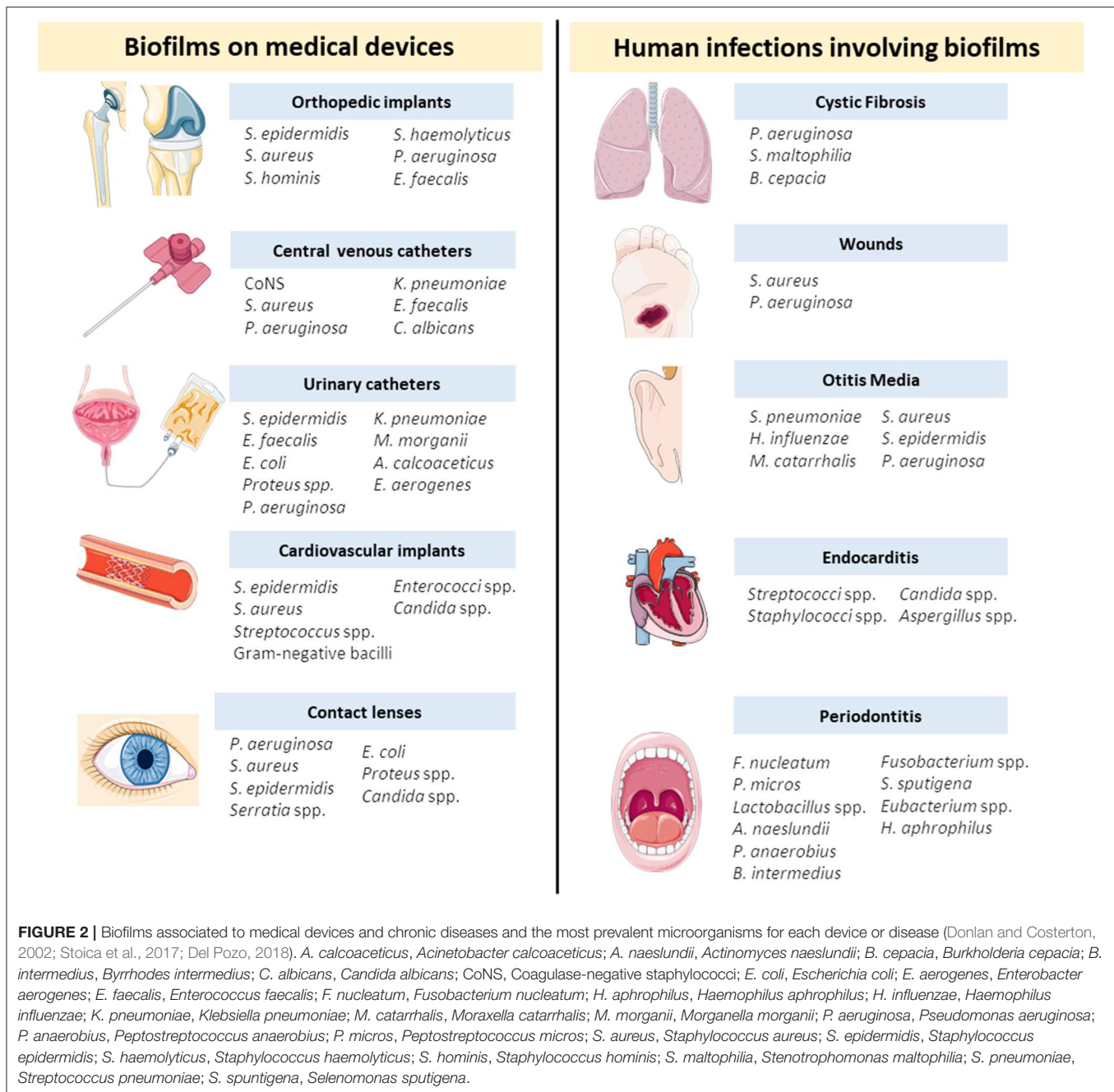
Nowadays, biofilms represent an enormous concern for healthcare systems due to the escalating figures of antimicrobial resistance events and the high demand for implantable medical devices (Archer et al., 2011). Several biofilm forming organisms are commonly associated to medical devices or to chronic infections such as cystic fibrosis, otitis media, and wounds. In **Figure 2** there is a detailed list of the most common medical devices and chronic infections and a list of the most prevalent microorganisms for each medical case.

Medical devices are known to increase the life quality of patients at a world level, but they are frequently associated to infections. When a medical device is implanted in the human body, colonization by bacteria occurs and a biofilm community may be established (Del Pozo, 2018). Several devices currently in medical use are prone to biofilm development by single or multiple microorganisms (Del Pozo, 2018). Some of the concerning examples will be further explored.

The number of orthopedic implants for bone fixation and joint replacement have been increasing in the last decades (Zimmerli, 2014). These implants are crucial to improve the life quality of patients, however, they are frequently associated to infections with devastating consequences, such as chronic pain and immobility (Ribeiro et al., 2012). According to Trampuz and Widmer, nearly 5% of orthopedic implants are infected and the susceptibility for infection increases by 5–40% in the case of a further surgery (Trampuz and Widmer, 2006). The infection may be caused by direct contamination of the device or from the contaminated wound and is frequently associated to opportunistic microorganisms (Stoica et al., 2017). For instance, studies show that periprosthetic joint infections are mainly associated to *Staphylococcus aureus* (*S. aureus*) and coagulase-negative staphylococci, such as *S. epidermidis* (Ribeiro et al., 2012; Zimmerli and Sendi, 2017). Most of these infections are caused by a single species, with only 16% of the cases being prompted by a mixed community (Stoica et al., 2017). Unfortunately, infections related to orthopedic implants are difficult to treat and usually require debridement and eventually removal of the device (Pinto et al., 2019). Extensive reviews addressing orthopedic implant-associated infections can be found in the literature (Ribeiro et al., 2012; Zimmerli, 2014; Zimmerli and Sendi, 2017).

Catheters are also extensively used in medical practice. Among these, urinary catheters-associated infections are the most common to occur and are predominantly caused by *Escherichia coli* (*E. coli*) and species of the genera *Pseudomonas*, *Klebsiella*, *Enterobacter*, and *Candida* (Stoica et al., 2017). On the other hand, coagulase-negative staphylococci (e.g., *S. epidermidis*) and *S. aureus* are the bacterial species mainly found in central venous catheters (Donlan, 2001b).

Less common medical devices-associated infections are verified in cardiovascular implants, such as cardiac prosthetic

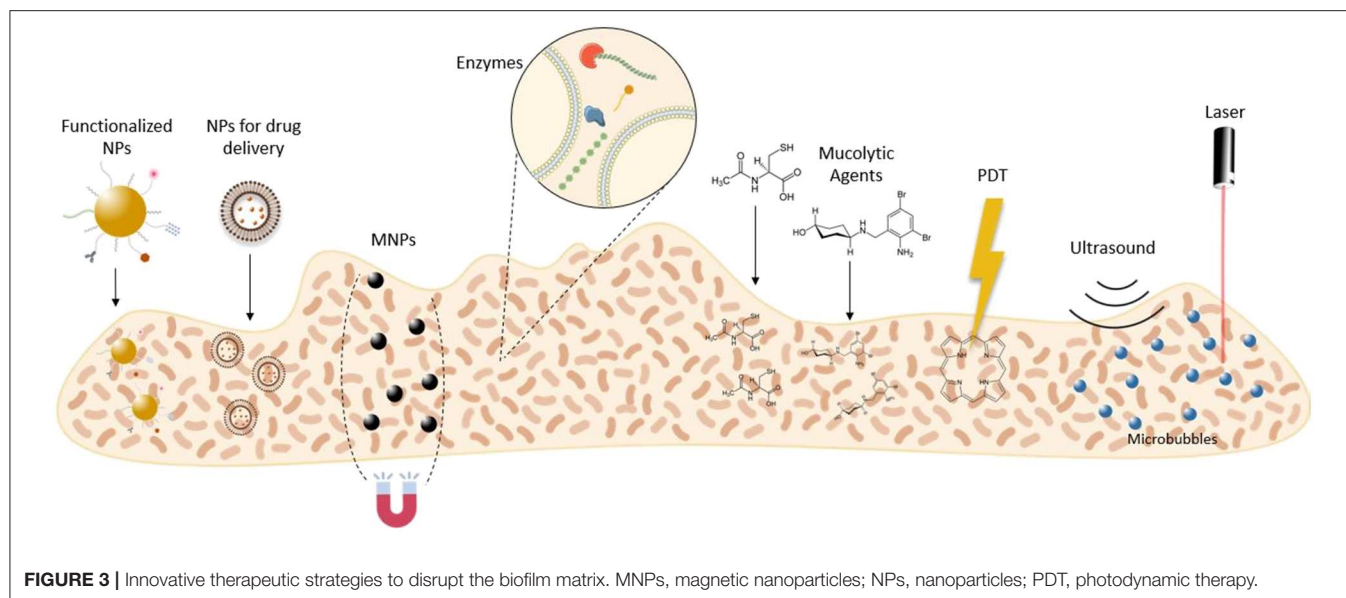


valves and stents (Stoica et al., 2017). Despite less frequent, these infections are a huge concern due to the high mortality rate that can reach 30% of the patients (Darouiche, 2004).

Besides implant-related infections, biofilms also play a role in chronic diseases in the oral cavity, ear, gastrointestinal, and urinary tracts, wounds and airways, among others (Del Pozo, 2018). For instance, the colonization of the lower respiratory tract by *P. aeruginosa* may lead to a chronic disease, cystic fibrosis, which is characterized by the accumulation of pulmonary secretions. Biofilms associated to chronic wounds, such as diabetic foot ulcers, are currently a clinical burden to patients since it delays the healing process (Del Pozo, 2018).

Infections in the middle ear are also very common, especially in childhood (Donlan and Costerton, 2002). Otitis media involves inflammation of the mucoperiosteal lining and the associated biofilms are difficult to treat due to the low penetration of antibiotics into the middle ear fluid. Another frequent condition involving biofilms is endocarditis, which develops when damaged endothelium interacts with bacteria or fungi in the bloodstream (Donlan and Costerton, 2002).

When a biofilm is established, cells or cell clusters may detach from the structure and colonize other sites, leading to new infections (Donlan and Costerton, 2002). Moreover, bacteria within biofilms produce endotoxins and are more resistant to



the host immune system (Donlan and Costerton, 2002). Despite the high complexity of biofilm-associated infections, current therapies still consist in the administration of conventional antimicrobial agents at high doses for a long-term period (Koo et al., 2017; Pinto et al., 2019). Ultimately, these therapies lack efficiency since they fail to approach combinatory strategies that target more than one component of the biofilm microenvironment (Koo et al., 2017).

NEW STRATEGIES TO ERADICATE BACTERIAL BIOFILMS

The EPS matrix remains a critical challenge for bacterial biofilm eradicating strategies, due to its complexity and variability (Fulaz et al., 2019). Nevertheless, many research works are emerging in this field. Thus, this review is focused on innovative strategies to disrupt the EPS matrix of mature biofilms. Here, we outline reported disruptive agents, nanocarriers, and technologies for matrix disassembly (Figure 3).

Matrix Disruptive Agents

The increasing resistance to antibiotics in combination with their lack of efficiency on biofilms are leading researchers to focus on the EPS matrix as a barrier to overcome. Thus, many studies in the literature highlight several antibiofilm agents capable of disrupting the EPS matrix in mature biofilms (Table 1).

Enzymes

In a biofilm community, enzymes are naturally secreted by bacterial cells and retained within the matrix. Among other functions, enzymes are essential for the remodeling process of the biofilm. During this process, specific enzymes degrade components of the EPS matrix, leading to active dispersal of the biofilm. Consequently, the dispersed cells are able to recolonize other sites of the host (Flemming et al., 2016).

Despite being considered a biofilm virulence factor, these enzymes may be engineered to be used in strategies for biofilm disassembly. For instance, recombinant dispersin B was produced by cloning in *E. coli* a synthetic gene encoding the protein from *Aggregatibacter actinomycetemcomitans* (Dobrynina et al., 2015). After purification, the enzyme was tested against biofilms of *S. epidermidis*, *Burkholderia cenocepacia*, and *Achromobacter xylosoxidans*. Dispersin B actively disrupted mature *S. epidermidis* biofilms at low concentrations (lower than 0.3 µg per sample). However, for the other two strains, a dispersin B concentration above 5 µg per sample was required to reduce the biofilm biomass (Dobrynina et al., 2015). Dispersin B is a glycosyl hydrolase able to specifically disrupt poly-*N*-acetylglucosamine (PNAG), which is the main exopolysaccharide of *S. epidermidis* biofilms (Chaignon et al., 2007). Contrarily, PNAG is not a predominant component of *Burkholderia cenocepacia* and *Achromobacter xylosoxidans* biofilms, which may explain their higher resistance to the recombinant enzyme (Yakandawala et al., 2011; Dobrynina et al., 2015). In a more complex approach, Chen et al. conjugated recombinant dispersin B with a silver-binding peptide, which promotes *in situ* formation of silver nanoparticles (AgNPs) in the presence of silver ions (Lee et al., 2008; Chen and Lee, 2018). In this combinatory strategy, the recombinant enzyme disrupts the matrix and the AgNPs kills the dispersed cells (Chen and Lee, 2018). Comparing to dispersin B alone, the enzyme-peptide conjugate showed at least a 2-fold higher activity against 48 h-old *S. epidermidis* biofilms (Chen and Lee, 2018).

Besides dispersin B, deoxyribonuclease I (DNase I) has also been highlighted for antibiofilm purposes. The effects of DNase I in combination with several antibiotics were evaluated on 24 h-old biofilms (Tetz et al., 2009). The enzyme alone showed a 40% reduction in biofilm biomass for all tested strains. However, it did not compromise the number of viable cells. Antibiotics in combination with DNase I showed a decrease of 2- to 15-fold in the number of colony forming units (CFUs) in comparison

TABLE 1 | Biofilm disruptive strategies based on matrix disruptive agents.

Strategy	Agent	Associated compound	Mechanism of action	Bacterial strains	Disease model	References
Enzymes	Dispersin B (0–20 µg/sample)	-	Disrupt PNAG	<i>S. epidermidis</i> (strain 210) <i>B. cenocepacia</i> (SCCH2:Bcn33-1220 ST709) <i>A. xylosoxidans</i> (SCCH3:Ach 33-1365 glt allele 2)	-	Dobrynina et al., 2015
	Dispersin B (0.03 U ml ⁻¹)	Ag-BP2 peptide	Disrupt PNAG	<i>S. epidermidis</i> (ATCC 35984)	-	Chen and Lee, 2018
	DNase I (5.0 µg ml ⁻¹)	Ampicillin Cefotaxime Rifampin Levofloxacin Azithromycin (50 × MIC)	Disrupt eDNA Antibacterial activity	<i>E. coli</i> (ATCC 25922) <i>H. influenzae</i> (VT 450-2006) <i>K. pneumoniae</i> (VT 1367) <i>P. aeruginosa</i> (ATCC 27853) <i>S. aureus</i> (ATCC 29213) <i>S. pyogenes</i> (VT 59) <i>A. baumannii</i> (VT 126)	-	Tetz et al., 2009
	Alginate lyase (15 U) DNase I (100 mg l ⁻¹)	Vancomycin (0.25 g l ⁻¹)	Disrupt EPS Antibacterial activity	<i>E. faecalis</i> (clinical isolates) <i>E. faecium</i> (clinical isolates)	Urinary tract infections	Torelli et al., 2017
	DNase I (0.5 µg ml ⁻¹) Marine bacterial DNase (0.5 µg ml ⁻¹)	Essential oils from: <i>Pogostemon heyneanus</i> <i>Cinnamomum tamala</i> 1 and 1.5% (v/v)	Target eDNA Antibacterial activity	MRSA (ATCC 33591)	-	Rubini et al., 2018
	Esperase® (8.3 × 10 ⁻⁴ U ml ⁻¹)	Prontosan® (10%) EDTA (10 mM)	Proteins cleavage Matrix disruption Antibacterial activity	<i>P. aeruginosa</i> (CIP 103.467) <i>S. aureus</i> (CIP 4.83)	Chronic wounds	Lefebvre et al., 2016
Mucolytic agent	Ambroxol (1.07 mg ml ⁻¹)	Ciprofloxacin (4.0 mg l ⁻¹)	Disrupt alginate Antibacterial activity	<i>P. aeruginosa</i> (PAO1)	Acute lung infection	Cheng et al., 2015
	Ambroxol (1.875 mg ml ⁻¹)	Vancomycin (2.0 and 5.0 mg ml ⁻¹)	Reduce EPS Antibacterial activity	<i>S. epidermidis</i> (ATCC 35984)	Catheter-related bloodstream infections	Zhang et al., 2015
	<i>N</i> -acetyl cysteine (12.5 mg ml ⁻¹)	-	Disrupt EPS	<i>S. epidermidis</i> (ATCC 12228) <i>P. acnes</i> (ATCC 6919) <i>M. smegmatis</i> (mc ² 155)	-	Eroshenko et al., 2017
	<i>N</i> -acetyl cysteine (0 – 100 mg ml ⁻¹)	-	Disrupt EPS	MRSA (clinical isolates) QRPA (clinical isolates)	Post-tympanostomy tube otorrhea	Jun et al., 2019
	<i>N</i> -acetyl cysteine (40 mg ml ⁻¹)	Linezolid (1.0 µg ml ⁻¹)	Disrupt EPS	<i>S. epidermidis</i> (clinical isolates: 9142 and 1457)	-	Leite et al., 2013

A. baumannii, *Acinetobacter baumannii*; *A. xylosoxidans*, *Achromobacter xylosoxidans*; *B. cenocepacia*, *Burkholderia cenocepacia*; *DNase I*, deoxyribonuclease I; *E. coli*, *Escherichia coli*; eDNA, extracellular DNA; EDTA, Ethylenediamine tetraacetic acid; *E. faecalis*, *Enterococcus faecalis*; *E. faecium*, *Enterococcus faecium*; EPS, extracellular polymeric substances; *H. influenzae*, *Haemophilus influenzae*; *K. pneumoniae*, *Klebsiella pneumoniae*; MIC, minimum inhibitory concentration; MRSA, Methicillin-resistant *Staphylococcus aureus*; *M. smegmatis*, *Mycobacterium smegmatis*; *P. acnes*, *Propionibacterium acnes*; *P. aeruginosa*, *Pseudomonas aeruginosa*; PNAG, poly-β(1-6)-*N*-acetylglucosamine; QRPA, quinolone-resistant *Pseudomonas aeruginosa*; *S. aureus*, *Staphylococcus aureus*; *S. epidermidis*, *Staphylococcus epidermidis*; *S. pyogenes*, *Streptococcus pyogenes*; U, unit.

with antibiotics alone. According to the authors, the disruption of eDNA by DNase I leads to a decrease of matrix material and, consequently, increases the efficiency of antibiotics (Tetz et al., 2009). Torelli et al. also reported the synergistic effect of matrix degrading enzymes and antibiotics. In this study,

the efficacy of vancomycin in combination with DNase I or alginate lyase against 48 h-old biofilms was assessed (Torelli et al., 2017). For this purpose, three clinical isolates of *Enterococcus faecalis* (*E. faecalis*) and *Enterococcus faecium* (*E. faecium*) derived from catheter-associated urinary tract infections were

used. In planktonic cells, both enzymes did not change the minimum inhibitory concentration (MIC) values of vancomycin. In *E. faecalis* biofilms, vancomycin alone, and vancomycin in combination with DNase I showed minimum biofilm eliminating concentration (MBEC) values of ~ 16 and 4 mg l^{-1} , respectively. On the other hand, alginate lyase showed more potential than DNase I against *E. faecium* biofilms, with a MBEC reduction from $\sim 16 \text{ mg l}^{-1}$ (antibiotic alone) to 2 mg l^{-1} (vancomycin and alginate lyase).

In alternative to antibiotics, essential oils (EOs) derived from plants were also combined with DNases to promote the eradication of established biofilms (Rubini et al., 2018). EOs from *Pogostemon heyneanus* and *Cinnamomum tamala* were tested against mature methicillin-resistant *Staphylococcus aureus* (MRSA) biofilms alone and in combination with DNase I or marine bacterial DNase extracted from marine bacterium *Vibrio alginolyticus*. In *in vitro* efficacy studies, both DNase I and marine bacterial DNase in combination with EOs showed a percentage of inhibition around 85%. Through scanning electron microscopy (SEM) and an EPS quantification assay it was possible to verify a great reduction of EPS matrix after treatment with the EOs (Rubini et al., 2018). Hence, the combination of EOs with enzymes seems a promising strategy for biofilm eradication.

In a more complex approach, proteases were combined with antiseptics and ethylenediamine tetra-acetic acid (EDTA) for eradication of *S. aureus* and *P. aeruginosa* biofilms in chronic wounds (Lefebvre et al., 2016). EDTA is reported to destabilize the biofilm through cation chelation and inhibition of matrix metalloprotease activity (Raad et al., 2002; Percival et al., 2005). EDTA and enzymes can potentiate antiseptics activity, allowing the administration of lower doses (Lefebvre et al., 2016). Unlike the previous mentioned studies, Lefebvre et al. tested non-specific enzymes, with a broad-spectrum effect for several bacterial strains. The combinatory treatment revealed synergistic effects for both strains, with a significant reduction on bacterial viability. Nevertheless, the authors highlighted the need to develop a system able to efficiently deliver these molecules to the biofilm (Lefebvre et al., 2016).

Other enzymes, such as proteinase K (Kumar Shukla and Rao, 2013), glycoside hydrolases P_{ELA}_h, and P_{SL}G_h (Baker et al., 2016), α -amylase (Kalpana et al., 2012; Watters et al., 2016), bromelain (Watters et al., 2016), lysostaphin (Watters et al., 2016), papain (Watters et al., 2016), and NucB (Shields et al., 2013) were investigated in a lesser extent for their ability to disrupt matrix components. Despite the promising *in vitro* efficacy of these enzymes, further studies in animal models are still required for validation purposes.

Compounds

Contrarily to enzymes, only few compounds have been reported to have active matrix disruptive properties. Among these, mucolytic agents, such as ambroxol and *N*-acetyl cysteine (NAC), are being highlighted for antibiofilm purposes.

Ambroxol is a frequently used mucolytic agent with antioxidant and anti-inflammatory effects in patients with pulmonary infections (Beeh et al., 2008; Paleari et al., 2011). Cheng et al. studied the combined effect of ambroxol with

ciprofloxacin in a rat model of acute lung infection. With this aim, 3-days old biofilms of the mucoid strain *Pseudomonas aeruginosa* O1 (PAO1) were grown in the inner surface of inoculation tubes and further intubated in rats by intratracheal placement (Cheng et al., 2015). The rats were then treated once a day by inhalatory administration of antibiotic and ambroxol, for a total period of 7 days. The combination of ambroxol with ciprofloxacin showed lower bacterial counts compared to treatments with the antibiotic or the mucolytic agent alone. The biofilm morphology was assessed by SEM, where it was possible to observe thinner and less fibrous biofilms after treatment with the combination of ambroxol and the antibiotic. These results indicate that ambroxol has a synergistic effect with ciprofloxacin on mucoid biofilms. The authors speculate that this effect is a consequence of ambroxol enzymatic activity against alginate, which is the main component of these biofilms (Cheng et al., 2015). Ambroxol antibiofilm activity was also assessed against *S. epidermidis* biofilms in catheter-related bloodstream infections (Zhang et al., 2015). *In vitro* efficacy studies showed that ambroxol in combination with vancomycin significantly reduced bacterial viability and biofilm thickness, when compared with ambroxol or the antibiotic alone. By confocal laser scanning microscopy (CLSM) analysis, it was observable larger pore channels in the biofilm structure after treatment with ambroxol. Hence, these changes in the EPS matrix facilitates antibiotics penetration. Further *in vivo* studies in a rabbit infection model confirmed a synergistic effect between ambroxol and vancomycin, with disruption of mature biofilms and reduced inflammatory response (Zhang et al., 2015).

NAC is also a mucolytic agent with potential to eradicate bacterial biofilms. This synthetic agent is an antioxidant that disrupts disulfide bonds in mucus and inhibits cysteine use, by competition. Regarding to biofilms, NAC reduces production of EPS matrix and promotes disruption of mature structures (Romano et al., 2013). Several studies of NAC alone or in combination with antibiotics have been reported in the literature. For instance, Eroshenko et al. studied the effect of NAC on *S. epidermidis*, *Propionibacterium acnes*, and *Mycobacterium smegmatis* biofilms. The results showed that NAC has a high disruptive effect on a mixed biofilm of *S. epidermidis* and *Propionibacterium acnes*, with a 61% biomass reduction compared to the control. However, an insignificant reduction of biofilm biomass was verified when both strains were cultured alone, after a 4 h treatment with NAC (Eroshenko et al., 2017). More recently, the efficacy of NAC alone as an antibiofilm agent was evaluated in MRSA and quinolone-resistant *P. aeruginosa* biofilms, which are common in tympanostomy-tube infections (Jun et al., 2019). For both biofilm types, NAC showed a decrease of biofilm biomass comparing to the control group. The antibiofilm activity of NAC was further confirmed by a decrease in bacterial colonies and by a decrease in observable biofilm structure in SEM images (Jun et al., 2019). Some other studies also shown the synergy between NAC and antibiotics, such as fosfomycin and linezolid (Marchese et al., 2003; Leite et al., 2013).

Some compounds able to inhibit the production of EPS components, have also been reported. For instance, Siala et al.

outlined the activity of the antifungal caspofungin acetate against MRSA biofilms. This lipopeptide acts in bacterial biofilms by inhibiting the PNAG synthesis. In combination with antibiotics, caspofungin acetate showed potential synergistic effects, both *in vitro* and in an animal model system for catheter-based infections (Siala et al., 2016). Besides this compound, other non-disruptive agents such as chitosan, *Cis*-2-decenoic acid (C₂DA), nitric oxide, and rhamnolipids, may also trigger cell dispersion in bacterial biofilm (Chung and Toh, 2014; Fleming and Rumbaugh, 2017).

Although the promising results of the reported matrix disruptive agents, their therapeutic use still presents several limitations such as low bioavailability and non-specific biodistribution, which leads to adverse side effects and low concentrations at the target site (Poznansky, 1984). Hence, innovative vehicles for efficient delivery of enzymes and drugs to the target biofilms are a step forward in the design of new antibiofilm therapies.

Nanocarriers

Nanosystems may play a critical role in both targeting and disruption of the EPS matrix. In the past few years, many researchers engineered sophisticated nanocarriers to increase penetration within the biofilm matrix and release their contents, such as antibiotics, closer to bacterial cells. This non-specific targeting is based on electrostatic interactions between the nanoparticles (NPs) and the matrix components (Fulaz et al., 2019).

The surface charge of NPs has an important role in the destruction of biofilms. The EPS matrix is mainly composed by substances with a negative charge, including the bacterial cell wall. Thus, the EPS matrix is more likely to interact with positively charged NPs, which may lead to increased diffusion within the matrix comparing to neutral or negatively charged NPs (Fulaz et al., 2019). Several studies reported that lipid and polymer-based NPs showed increased efficacy against biofilms when positively charged (Lin et al., 2017; Thomsen et al., 2017; Wang et al., 2019). For instance, positively charged polymeric NPs were designed to bind and efficiently deliver nitric oxide to MRSA biofilms, for the treatment of diabetic wounds (Hasan et al., 2019). Gold NPs and nanotubes were also engineered to promote electrostatic interactions with the biofilm, by immobilizing the cationic polymer chitosan at the particles surface (Laskar et al., 2017; Lu et al., 2018; Khan et al., 2019). However, cationic NPs are considered more cytotoxic than neutral and negatively charged particles, which is a consequence of an enhanced cellular uptake (Frohlich, 2012; Hühn et al., 2013). Thus, Su et al. developed polymeric micelles containing polyurethanes with surface charge switchable properties due to protonation and deprotonation of tertiary amine groups in acidic and basic environments, respectively. Consequently, at the acidic pH of the biofilm, the micelles were able to switch to a positively charged surface, increasing their interaction with the matrix (Su et al., 2018). Mixed-shell polymeric micelles composed of the polyethylene glycol (PEG) and poly(β -amino ester) (PAE) were also developed for a pH-triggered switch of the surface charge (Liu et al., 2016). Electrostatic interactions may also be manipulated through the

co-administration of negatively charged NPs with a penetration enhancer. Harper et al. observed that the co-administration of anionic α -tocopherol phosphate liposomes with a cationic electrolyte, Tris((hydroxymethyl)aminomethane), increased their penetration into the EPS matrix and interaction with bacteria. This phenomenon occurred due to ability of the cationic electrolyte to decrease the electrostatic interactions between the negatively charged liposomes and the biofilm components (Harper et al., 2019).

Targeting bacterial biofilms through electrostatic interactions and pH-triggered release, may offer appealing results for delivery of antimicrobial agents in higher concentrations to deeper layers of the biofilm. However, a complete physical removal of the biofilm is difficult to occur in biofilms of limited access (e.g., implant-related biofilms) (Flemming, 2011). Consequently, the remaining biofilm structures may provide an ideal site for colonization of other microbial cells. Additionally, mature biofilms contain dormant cells with higher resistance to antimicrobials, that may survive and recolonize the matrix (Flemming et al., 2016). Thus, a promising innovative approach consists in the addition of matrix disruptive enzymes and/or compounds, to the design of nanocarriers, in order to promote EPS disruption and dispersal of dormant cells (Table 2).

With the purpose to combine antibacterial and antibiofilm agents in a nanocarrier, Tan et al. developed positively charged chitosan NPs co-encapsulating oxacillin and DNase I to eradicate 24 h-old *S. aureus* mature biofilms. A repeated treatment during 48 h revealed that NPs loading both the DNase I and oxacillin exhibited higher antibiofilm activity than oxacillin-loaded NPs, with a 98.4% biofilm reduction. In addition, their positively charged surface facilitated penetration within the biofilm, without observable cytotoxicity effects against a human immortalized keratinocytes (HaCaT) cell line (Tan et al., 2018a). In a similar study, ciprofloxacin-loaded polymeric NPs were coated with DNase I covalently grafted to the cationic poly-L-lysine (Baelo et al., 2015). The results after a repeated treatment of 48 h-old *P. aeruginosa* biofilms for 3 days showed an eradication higher than 99.8%. The NPs safety profile was confirmed *in vitro* against J774 murine macrophages (Baelo et al., 2015). More recently, Tan et al. co-immobilized DNase I and cellobiose dehydrogenase in chitosan NPs to treat monomicrobial and polymicrobial biofilms of *Candida albicans* and *S. aureus*. Cellobiose dehydrogenase was selected as an antimicrobial agent since it uses cello-oligomers as a substrate to produce hydrogen peroxidase, which generates free radicals that promote oxidation of biofilm matrix components and has bactericidal effects (Henriksson et al., 2000; Gao et al., 2014; Tan et al., 2020). The efficiency of the developed NPs was tested in 24 h-old biofilms. The NPs revealed a high activity by reducing biofilm percentage more than 80% on both mono- and polymicrobial biofilms (Tan et al., 2020). NPs immobilizing only DNase I were also tested and showed no significant effect on the biofilms. According to the authors, this result is a consequence of the absence of a bactericidal agent, which allows dispersed bacterial cells to form a new biofilm. However, the co-immobilization with cellobiose dehydrogenase indicates a synergistic effect with DNase I (Tan et al., 2020).

TABLE 2 | Biofilm disruptive strategies based on nanodelivery systems.

Strategy	Composition of the material	Physicochemical characteristics	Mechanism of action	Bacterial strains	Disease model	References
Polymeric NPs	Chitosan TPP Encapsulated compound: Oxacillin Functionalization: DNase	Size: 166.7 nm PDI: 0.179 Z. Potential: +8.3 mV LC: 6.65%	Disrupt eDNA Electrostatic interactions Antibiotic controlled release	<i>S. aureus</i> (ATCC 6538)	-	Tan et al., 2018a
	PLGA PVA poly-L-lysine Encapsulated compound: Ciprofloxacin Functionalization: DNase I	Size: 251.9 nm PDI: 0.122 Z. Potential: + 28.9 ± 1.43 mV Ciprofloxacin content: 0.17 (w/w) (%)	Disrupt eDNA Antibiotic controlled release	<i>P. aeruginosa</i> (ATCC 15692) <i>S. aureus</i> (ATCC 12600)	Cystic fibrosis	Baelo et al., 2015
	Chitosan TPP Functionalization: DNase Cellobiose dehydrogenase	Size: 164.73 nm Z. Potential: + 13.07 mV	Disrupt eDNA Electrostatic interactions Antibacterial activity	<i>S. aureus</i> (ATCC 6538) <i>C. albicans</i> (DAY185)	-	Tan et al., 2020
	Chitosan TPP Encapsulated compound: Ciprofloxacin Functionalization: Alginate lyase	Size: 205.5 ± 9.0 nm PDI: 0.302 ± 0.031 Z. Potential: 12.2 ± 2.1 mV EE: 51.8 ± 2.1%	Disrupt extracellular alginate Antibacterial activity	<i>P. aeruginosa</i> (clinical isolate)	Cystic fibrosis	Patel et al., 2019
	Carboxymethyl chitosan Linolenic acid Functionalization: Dispersin B	LE: 51.14 ± 0.93% LC: 767.08 ± 13.90 mg g ⁻¹	Disrupt PNAG Electrostatic interactions	<i>S. aureus</i> (RN6390;15981; 8325; Col) <i>S. epidermidis</i> (QY301; RP62A; M187; 1457) <i>A. actinomycetemcomitans</i> (HK1651)	-	Tan et al., 2015
Gold NPs	Citrate-capped gold NPs Functionalization: Proteinase-K	Size: 27.17 ± 0.61 nm PDI: 0.238 ± 0.022 Z. Potential: -3.79 ± 0.21 mV	Disrupt extracellular proteins Antibacterial activity	<i>P. fluorescens</i> (PCL 1701)	-	Habimana et al., 2018
MOFs	gold MIL-88B (Fe) Cerium (IV) complexes	LC: 11.14 μ mol g ⁻¹	Target eDNA Peroxidase-like activity	<i>S. aureus</i> (ATCC 25923)	Topical wound	Liu et al., 2019

A. actinomycetemcomitans, *Actinobacillus actinomycetemcomitans*; *C. albicans*, *Candida albicans*; *DNase I*, deoxyribonuclease I; eDNA, extracellular DNA; EE, encapsulation efficiency; LC, loading capacity; LE, loading efficiency; MOFs, Metal-organic frameworks; NPs, nanoparticles; *P. aeruginosa*, *Pseudomonas aeruginosa*; PDI, polydispersity index; *P. fluorescens*, *Pseudomonas fluorescens*; PLGA, poly(lactic-co-glycolic acid); PNAG, poly-β(1-6)-N-acetylglucosamine; PVA, poly(vinyl alcohol); *S. aureus*, *Staphylococcus aureus*; *S. epidermidis*, *Staphylococcus epidermidis*; TPP, Tri-poly phosphate; Z. Potential, Zeta Potential.

The enzyme alginate lyase was also immobilized in polymeric NPs for matrix disruption purposes. Patel et al. designed ciprofloxacin-loaded NPs functionalized with alginate lyase for the treatment of biofilm-associated *P. aeruginosa* infection in cystic fibrosis. The *in vitro* efficacy assay against 48 h-old biofilms showed a complete disruption of the EPS matrix and no viable bacteria after repeated treatment for 72 h (Patel et al., 2019). This effect was not verified with antibiotic alone or in combination with alginate lyase and with non-functionalized NPs. Further, microscopy assessment of the biofilm confirmed the low biomass

and biofilm thickness after treatment with the functionalized NPs. Additionally, *in vitro* and *in vivo* toxicity studies indicated a good biocompatibility of the developed nanosystem (Patel et al., 2019). In another study, Tan et al. designed chitosan NPs for immobilization of dispersin B from *Aggregatibacter actinomycetemcomitans* HK1651. The *in vitro* antibiofilm efficacy of this formulation was evaluated on *S. aureus*, *S. epidermidis*, and *Aggregatibacter actinomycetemcomitans* 24 h-old biofilms (Tan et al., 2015). For all tested strains, free and immobilized dispersin B showed a similar disruptive effect on the biofilms. Thus, the

immobilization of the enzyme into polymeric NPs did not seem to compromise its activity (Tan et al., 2015).

Besides polymeric-based NPs, gold NPs were also functionalized with enzymes. Habimana et al. reported the synthesis of gold NPs functionalized with proteinase-K, combining bactericidal and matrix-degrading activities. The particles were tested against *Pseudomonas fluorescens* mature biofilms, showing a 78% thickness decrease comparing to the control (Habimana et al., 2018). However, this effect was similar to the non-functionalized particles (72% biofilm reduction).

Although the previous studies show a high potential of enzymes as antibiofilm therapies, their use is limited by high cost and poor stability (Wu et al., 2019). To overcome these issues, Liu et al. designed nanoenzymes based on metal organic frameworks (MOFs) and cerium (IV) complexes. In this system, MOFs have a peroxidase-like activity, which leads to bacterial cell death. On the other hand, cerium (IV) complexes mimic the DNase activity by hydrolyzing eDNA from 12 h-old *S. aureus* biofilms (Liu et al., 2019). *In vitro* efficacy studies showed the dispersal potential of the nanoenzyme. Nevertheless, the nanoenzyme alone was not able to have bactericidal activity. Hence, nanoenzymes were assessed in combination with free hydrogen peroxidase. In this condition, bacteria dispersed from the biofilm were efficiently killed. This result was further confirmed in *in vivo* studies using a subcutaneous model. Besides the antibiofilm effects, the treatment with the nanoenzyme and free hydrogen peroxidase revealed a significantly reduction of inflammation and negligible toxicity (Liu et al., 2019).

Technologies for Biofilm Physical Removal

In the past few years, several technologies have been optimized to disrupt bacterial biofilms. These technologies are mainly based on magnetic field in association with NPs, phototherapy and ultrasounds.

Magnetic Field

Early studies based on the success of using magnetic and electric fields to affect other physiological processes triggered the hypothesis that this strategy could be effective in bacterial biofilm control, when in combination with appropriate antibiotics (Grosman et al., 1992; Khoury et al., 1992; Sinisterra, 1992; Benson et al., 1994). Therefore, in the last decades, association of magnetic fields with magnetic nanoparticles (MNPs), namely superparamagnetic iron-oxide nanoparticles (SPIONs) began to emerge. Among these, various magnetic field-based strategies to disrupt bacterial biofilms were reported (Table 3).

Several studies showed that, besides the good biocompatibility and low cytotoxicity, MNPs can be controlled and concentrated close to a target, through the application of an external magnetic field. This allows a deeper penetration into the biofilm and interferes in the organization of the matrix (Subbiahdoss et al., 2012; Bandara et al., 2015; Li J. et al., 2019; Quan et al., 2019). Consequently, possible elimination of the target biofilm is achieved through its breakup, along with cell detachment. Bandara et al. aimed to investigate the efficacy of different application modes of magnetic fields (static one-sided, static switched, oscillating, static + oscillating) in eliminating *in vitro*

mature *P. aeruginosa* biofilms. These biofilms were treated with an aerosolized formulation containing different combinations of MNPs, ciprofloxacin and spray dried lactose (Bandara et al., 2015). Magnetic fields alone were able to disrupt the biofilms, negatively affecting the EPS matrix, either by interfering in its production or by direct disruption. Also, it was observed that the highest suppression of viability and biomass was achieved in biofilms exposed to a static switched field. The combination of static switched magnetic field with MNP/ciprofloxacin/MNP + ciprofloxacin showed the most promising results regarding the biofilm matrix disruption, which enables an easier penetration of the antibiotic to deeper layers of the biofilm (Bandara et al., 2015).

Besides magnetic targeting, MNPs also allow the increase in temperature by magnetic hyperthermia induction, through the application of alternating magnetic fields. Considering this additional effect, Li J. et al. compared the eradication efficiency of MNPs, with different sizes and concentrations, under AC and DC applied magnetic fields against MRSA biofilms. Greater cell detachment and matrix damage were observed for both 8 and 11 nm MNPs, exposed either to AC or DC magnetic fields. Considering all three tested sizes (8, 11, and 70 nm), although the application of AC fields allowed a local heating of the biofilms, DC fields showed to be the most effective strategy to break the EPS matrix and kill the bacteria. A 4.71 log₁₀ reduction was achieved in biofilm bacteria after the treatment with 30 mg ml⁻¹ of 11 nm NPs, under DC magnetic field (Li J. et al., 2019).

Although the type of the applied magnetic field and the size of MNPs are relevant, surface functionalities have also been suggested to be crucial in the interaction process with the EPS matrix and bacteria. Considering this, Subbiahdoss et al. showed that no differences in the antibiofilm efficacy were found between bare, carboxyethylsilanetriol(CES)-grafted and 3-aminopropyltriethoxysilane(APTED)-grafted SPIONs, against 24 h-old *S. epidermidis* biofilms. However, PEGylated SPIONs showed to be ineffective against staphylococcal biofilms. Optical cross-sections obtained using CLSM in the presence of magnetically concentrated CES-grafted SPIONs showed not only dead bacteria in the biofilm but also the formation of some channels across all the biofilm thickness (Subbiahdoss et al., 2012). In line with the previous findings, Quan et al. explored the mechanism behind the physical disruption of the biofilm matrix, responsible for the enhancement of the antimicrobial penetration. Similar to the results obtained by Subbiahdoss et al. (2012), formation of artificial channels, with around 1.4 μm of width, were observed in treated 24 h-old *S. aureus* biofilms. In addition, incubation of these biofilms with gentamicin caused a significant enhancement (4–6-fold) in staphylococcal killing, due to the improved penetration allowed by the non-biotical channels (Quan et al., 2019).

Other NPs have been added to this strategy in order to improve the antibiofilm effects of the magnetic field associated to MNPs. For instance, Wang et al. produced highly efficient nanoplateforms, consisting of gentamicin, tannic acid and AgNPs coated on MNPs, to test against established biofilms of *S. aureus*. Additionally to the MNPs expected effect, the presence of AgNPs caused the production of reactive oxygen species (ROS), which enhanced decomposition of polysaccharides and

TABLE 3 | Biofilm disruptive strategies based on magnetic field.

Strategy	Method of exposure	NPs	Additional compound	Physicochemical characteristics	Bacterial strains	Mechanism of action	References
External magnetic field	Static one-sided, Static switched, Oscillating, Static +oscillating	SPIONs (FluidMAGC-MX)	Ciprofloxacin loaded in spray-dried lactose particles	Size: 150 nm	<i>P. aeruginosa</i> (PAO1)	Disruption of the EPS matrix	Bandara et al., 2015
	AC and DC	Fe-oxide NPs coated with SiO ₂	–	Sizes: 8 nm, 11 nm, 70 nm	MRSA (ATCC 33592)	Damage and detachment of the matrix Magnetic hyperthermia	Li J. et al., 2019
	Static one-sided	Surface-modified SPIONs (CES, APTES, PEG functionalities)	-	<i>Bare:</i> Size: 13.7 ± 2.1 nm -Zeta potential: +43.7 ± 1.7 mV <i>CES-grafted:</i> Size: 13.8 ± 2.1 nm Zeta potential: –15.4 ± 0.5 mV <i>PEGylated:</i> Size: 14.9 ± 1.8 nm Zeta potential: –7.71 ± 0.9 mV <i>APTES-grafted:</i> Size: 17.8 ± 2.6 nm Zeta potential: +32.6 ± 0.3 mV	<i>S. aureus</i> (ATCC 12600) <i>S. epidermidis</i> (ATCC 35984)	Enhanced biofilm penetration Improved antibiotic efficacy	Subbiahdoss et al., 2012
	Static one-sided	SPIONs (Fe ₃ O ₄)	Free Gentamicin	Size: 278 ± 61 nm	<i>S. aureus</i> (ATCC 12600; ATCC 5298)	Creation of Artificial Channels in the matrix	Quan et al., 2019
	Static one-sided	Fe ₃ O ₄ @Ag@HA	Gentamicin	Zeta potential: –19.4 mV Saturation magnetization value: 45.3 emu g ^{–1}	<i>S. aureus</i> (ATCC 25922)	ROS production Disruption and decomposition of the matrix Enhanced antimicrobial efficiency	Wang et al., 2018a
	Static one-sided	IOPs (Encapsulated SPIONs)	Encapsulated methicillin	<i>SPIONs</i> Size: 5 ± 2.5 nm <i>IOPs</i> Size: 83 ± 6 nm Zeta Potential: –1 ± 3 mV	<i>S. epidermidis</i> (RP62a)	Enhanced biofilm penetration Targeted delivery	Geilich et al., 2017
	Static one-sided	Fe ₃ O ₄ @CS-PEG-Gent NPs	Gentamicin (loaded on the surface)	Size: ~40 nm Zeta potential: 8.7 mV	<i>S. aureus</i> (ATCC 5922)	Enhanced biofilm penetration Improved antibiotic efficacy	Wang et al., 2018b
	AC	SPIONs (Fe ₃ O ₄)	Vancomycin	Size: 16 nm	<i>S. aureus</i> (BCRC10451)	Hyperthermia Improve antibiotic efficacy	Fang et al., 2017

AC, alternative current; APTES, 3-aminopropyltriethoxysilane; CES, carboxyethylsilanetriol; CS, chitosan; DC, direct current; EPS, extracellular polymeric substances; Gent, gentamicin; HA, hyaluronic acid; IOPs, iron oxide polymersomes; MRSA, methicillin-resistant *Staphylococcus aureus*; NPs, nanoparticles; *P. aeruginosa*, *Pseudomonas aeruginosa*; PEG, polyethylene glycol; ROS, reactive oxygen species; *S. aureus*, *Staphylococcus aureus*; *S. epidermidis*, *Staphylococcus epidermidis*; SPIONs, superparamagnetic iron oxide nanoparticles.

proteins of the EPS matrix (Wang et al., 2018a). Iron oxide-encapsulating polymersomes, containing both hydrophobic SPIONs and the hydrophilic antibiotic methicillin, were also developed to eradicate antibiotic-resistant infections associated with 24 h-old *S. epidermidis* biofilms (Geilich et al., 2017). It was proved that this formulation was able to completely eradicate all

bacteria throughout the biofilm thickness, while not being toxic toward mammalian cells. Extensive bacterial death was observed within the boundaries of the magnetic field and SEM images of the biofilm ultrastructure showed both bacterial death and decoherence of the EPS matrix (Geilich et al., 2017). Wang et al. designed biocompatible Fe₃O₄/chitosan/PEG/Gentamicin MNPs

aiming to eradicate mature *S. aureus* biofilms. This strategy combined the inner magnetic core and the loaded antibiotic, allowing the improvement of the effectiveness and bioavailability of gentamicin at acidic media, through the application of an external magnetic field. CLSM images showed that, just by applying the NPs to the biofilms, the biofilm structure starts to disrupt, and the number of dead bacteria significantly increases (Wang et al., 2018b). The proposed explanation for this phenomenon is the existence of electrostatic interactions between the positively charged MNPs and the negatively charged EPS matrix. Adding the external magnetic field, the biofilm matrix was found to be completely compromised, with an extensive bacterial death observed (Wang et al., 2018b). Also, dual-catalytic iron oxide MNPs have recently demonstrated to controllably kill, degrade, and remove biofilms. These NPs generate free radicals with bactericidal activity and promote EPS matrix degradation. Besides, a subsequent removal of the fragmented biofilm debris is achieved via magnetically forced nanoparticle movement (Hwang et al., 2019).

To evaluate the effect of MNPs-induced hyperthermia associated with antibiotics to treat osteomyelitis, Fang et al. mimicked a clinical situation of a chronic infection in an animal model. A metallic needle was implanted into the bone marrow cavity of distal femur of male Wistar rats, after the injection of *S. aureus*. The temperature increase, achieved through magnetic hyperthermia, led to biofilm destruction, without any significant damage on the surrounding tissues (Fang et al., 2017). The subsequent local administration of vancomycin into the femoral canal allowed biofilm eradication. Consistently with *in vitro* results, *in vivo* efficacy studies showed that MNPs under AC fields were able to compromise the protection barrier of biofilms through MNPs-induced hyperthermia, affecting their structure and enhancing the therapeutic effect of antibiotics (Fang et al., 2017).

Photodynamic Therapy and Ultrasounds

Photodynamic therapy (PDT) and ultrasound mediated therapies are also examples of technologies with growing interest due to their noninvasiveness, relatively low cost, flexibility, and minimal risk of inducing microbial resistance (Briggs et al., 2018). Both strategies, while being effective carried out separately, have already been combined, as further explored. PDT involves the use of nontoxic dyes, called photosensitizers (PS), which in the presence of molecular oxygen and visible light of appropriate wavelength can be excited, leading to the production of ROS (Hu et al., 2018). As a multiple target strategy, the generated ROS can not only oxidize several cellular components (e.g., lipids and DNA), leading to cell inactivation, but can also attack EPS molecules, causing the degradation of matrix structure (de Melo et al., 2013; Hu et al., 2018). Usually, highly conjugated, unsaturated organic molecules with large absorption coefficient in the visible spectrum can behave as PS (Hu et al., 2018). Considering these properties, a wide range of compounds of remarkably different structures have already been used as PS to target different types of biofilms (Table 4).

Di Poto et al. demonstrated the efficiency of tetra-substituted (N-methyl-pyridyl) porphine (TMP) as a PS on *S. aureus* mature

biofilms. A TMP concentration of 10 μM and light doses of 150–200 J cm^{-2} allowed a significant decrease in survival of the biofilms (up to 2 log), with evident dispersion of the matrix and significant reduction in the number of adherent bacteria. Combining PDT with vancomycin resulted in 10^3 – 10^4 times lower counts than biofilm inhibitory concentrations used to kill untreated biofilms, showing that the detached and dispersed bacteria became more susceptible to antibiotics (Di Poto et al., 2009). Later, Li et al. revealed that 5-aminolevulinic acid (ALA) had potential to eliminate 24 h-old biofilms of MRSA and methicillin-resistant *S. epidermidis*. An increase of light dosage led to a gradual decrease in the survival as well as a decrease in the number of adherent bacteria in the biofilms of both strains (Li et al., 2013). After the highest dosage irradiation (300 J cm^{-2}), SEM images showed a greater disruption of both biofilms, only with few aggregated colonies remaining. The mechanism of action could be associated with the loss of cell-to-cell and cell-to-matrix interactions, which led to dispersion of the bacterial cells, comprising the biofilm structure (Li et al., 2013). The same mechanism can also be used to explain the morphological damages observed in *S. aureus* and multidrug-resistant *S. aureus* biofilms, after a treatment with porphyrin sodium (Jia et al., 2019). For both strains, when a light dose of 15 J cm^{-2} was applied, a typical biofilm structure was no longer observed, being the adhesion between bacteria completely compromised (Jia et al., 2019).

Tan et al. also reported the effect of ALA-PDT but on 48 h-old *P. aeruginosa* biofilms. Regarding the biofilm structure, SEM images showed that, for 20 mM ALA complemented with a 108 J cm^{-2} light source treatment, the biofilm was visibly sparse, with bacteria presenting cracks, breaks, and different sizes (Tan et al., 2018b). In another study, phenothiazinium dyes (Toluidine blue O, Azure A, and New methylene blue) were tested against 24 h-old *E. faecalis* and *Klebsiella pneumoniae* preformed biofilms (Misba et al., 2017). A clear disruption of the EPS matrix was observed, comparing to the control groups, with 8log₁₀ and 3log₁₀ reductions in bacterial count achieved for *E. faecalis* and *Klebsiella pneumoniae*, respectively. Besides the disruptive effect on preformed biofilms, the results also showed an inhibition of EPS production in both species (Misba et al., 2017).

As previously referred, EPS matrix and specifically polysaccharides represent a huge portion of a biofilm. Thus, considering the reported effects of PDT on the matrix, Beirão et al. investigated the influence of a Tetra-Py⁺-Me-induced PDT on the extracellular polysaccharides of 24 h-old *P. aeruginosa* biofilms. In fact, a reduction of 81% on the polysaccharides was observed, which shows that these EPS components may be a primary target of photodynamic damage (Beirão et al., 2014).

Nevertheless, like other compounds, PS are also limited in their effectiveness due to the difficulty to penetrate the biofilm matrix as well as possible rapid degradation. Additionally, it is reported that some PS tend to aggregate in water, which also limits an effective therapy (Huang et al., 2010). To overcome these issues, different types of nanocarriers and nanostructures, such as chitosan NPs, gold NPs, carbon nanotubes, and silica NPs, have been developed to deliver and protect PS (Darabpour et al., 2016, 2017; Anju et al., 2019a; Paramanathan et al., 2019;

TABLE 4 | Biofilm disruptive strategies based on photodynamic therapy.

Strategy	PS and associated compounds	Light Parameters	Time of exposure	Bacterial strains	Mechanism of action	References
PDT	TMP (10 μ M) Vancomycin	<i>Tungsten lamp</i> WL: 400–800 nm (white light) Power density: 166 mW cm ⁻² Fluence: 150–200 J cm ⁻²	~15–20 min	<i>S. aureus</i> (SA113, V329) MRSA (BH1C)	Bacteria dispersion Increased susceptibility to antibiotic	Di Poto et al., 2009
	ALA (40 mM)	<i>HPG5000 semiconductor laser</i> WL: 635 nm (red light) Fluence: 0–300 J cm ⁻²	-	MRSA (ATCC 43300) MRSE (287)	Dose-dependent phototoxicity Interference in cell-to-cell and cell-to-matrix interactions	Li et al., 2013
	S-PS (0.5, 1, and 2 μ g ml ⁻¹) EPIs	WL: 650 nm Fluences: 5, 10, 15 J cm ⁻²	1 h	<i>S. aureus</i> (CMCC 260003) MDR <i>S. aureus</i> (ATCC 29213)	Morphological damage caused by ROS Enhanced antimicrobial efficiency	Jia et al., 2019
	ALA (10 or 20 mM)	<i>LED</i> WL: 630 nm (red light) Power density: 90 mW cm ⁻² Fluence: 108 J cm ⁻²	20 min	<i>P. aeruginosa</i> (PAO1)	Dose-dependent growth inhibition and bacterial death Dispersion of the matrix	Tan et al., 2018b
	TBO, Azure A, and New MetB (10 μ M)	WL: 630 nm Power: 100 mW Power density: 0.130 W cm ⁻² Fluence: 100 J cm ⁻²	Maximum time exposure 13 min	<i>Enterococcus faecalis</i> (MTCC 2729) <i>Klebsiella pneumonia</i> (ATCC700603)	EPS disruption Reduction of EPS production	Misba et al., 2017
	Tetra-Py ⁺ -Me (20 μ g)	<i>13 parallel OSRAM 2' 18 W/840 lamps</i> WL: 380–700 nm (white light) Fluence: Maximum of 64.8 J cm ⁻² Power density: 4.0 mW cm ⁻²	Maximum time exposure 270 min	<i>S. aureus</i> (ATCC 700699) <i>P. aeruginosa</i> (57) <i>Candida albicans</i> (ATCC 10231)	Matrix decomposition (decrease of polysaccharides content)	Beirao et al., 2014
	TBO encapsulated in microemulsion (50 – 100 ppm) EDTA (100–500 ppm)	<i>LED lamps</i> WL: 610 – 630 nm (Red light) Fluence: 0.607 J cm ⁻²	15 min	<i>S. aureus</i> (ATCC 35556) <i>S. epidermidis</i> (ATCC 35984)	EPS disruption by EDTA chelating effect Enhanced penetration of the PS	Rout et al., 2018
	ICG and EDTA (2 mM or 5 mM) Vancomycin for MRSA Amikacin for MRPA	<i>Diode laser</i> WL: 808 nm Power density: 1.5 W cm ⁻² Fluence: 135 J cm ⁻²	90s	<i>S. aureus</i> (ATCC 25923) MRSA (10485) <i>P. aeruginosa</i> (ATCC 27853) MRPA (10911)	Formation of bacteria-free voids Bacterial death	Li X. et al., 2019
	Malachite green conjugated to carboxyl-functionalized multi-walled carbon nanotubes (50 μ g ml ⁻¹)	<i>Red Laser</i> WL: 660 nm Fluence: 58.49 J cm ⁻²	3 min	<i>P. aeruginosa</i> (PAO1) <i>S. aureus</i> (MCC 2408)	Improved biofilm inhibition EPS inhibition Reduced cell viability	Anju et al., 2019b
	Surface Coating: IR780 (0.02 mg ml ⁻¹) MoS2 and arginine-glycine-aspartic acid-cysteine	WL: 808 nm Power density: 0.5 W cm ⁻²	30 s intervals for 10 min	<i>S. aureus</i> (ATCC 29213)	Synergistic PDT/PTT effect (ROS generation/ local hyperthermia)	Li M. et al., 2019

(Continued)

TABLE 4 | Continued

Strategy	PS and associated compounds	Light Parameters	Time of exposure	Bacterial strains	Mechanism of action	References
	ICG loaded into mesoporous polydopamine NPs	Laser WL: 808 nm Power density: 0.75 W cm ⁻² Diameter: 15.6 mm	600 s	<i>S. aureus</i> (ATCC 29213)	Synergistic PDT/PTT effect (ROS generation/local hyperthermia)	Yuan et al., 2019
	RLP068/Cl (50 μM)	Diode laser WL: 689 nm Power density: 120 mW cm ⁻² Fluence: 60 J cm ⁻²	~8 min	MRSA (SAUMRBP2) <i>P. aeruginosa</i> (PAE2)	Decrease in biomass Decrease in the number of viable cells	Vassena et al., 2014
	MetB (0.3 mM)	Laser WL: 665 nm Fluence: 35 J cm ⁻² Power density: 35 mW cm ⁻²	16 min	<i>S. aureus</i> MRSA <i>S. epidermidis</i> <i>P. aeruginosa</i> <i>A. baumannii</i> (sourced from NCTC and ATCC)	Bactericidal effect Total (or partial) eradication of formed biofilms	Briggs et al., 2018

A. baumannii, *Acinetobacter baumannii*; ALA, 5-aminolevulinic acid; EDTA, ethylenediaminetetraacetic acid; EPIs, efflux pump inhibitors; EPS, extracellular polymeric substances; ICG, indocyanine green; LED, light-emitting diode; MDR *S. aureus*, multidrug-resistant *Staphylococcus aureus*; MetB, methylene blue; MRPA, multidrug-resistant *Pseudomonas aeruginosa*; MRSA, methicillin-resistant *Staphylococcus aureus*; MRSE, methicillin-resistant *Staphylococcus epidermidis*; NPs, nanoparticles; *P. aeruginosa*, *Pseudomonas aeruginosa*; PDT, photodynamic therapy; PS, photosensitizer; PTT, photothermal therapy; ROS, reactive oxygen species; *S. aureus*, *Staphylococcus aureus*; *S. epidermidis*, *Staphylococcus epidermidis*; S-PS, S-porphin sodium; TBO, toluidine blue O; TMP, tetra-substituted N-methyl-pyridyl-porphine; WL, wavelength.

Parasuraman et al., 2019; Mirzahosseini-pour et al., 2020). Rout et al. studied the potential of Toluidine blue O in solution and in microemulsion, as well as Toluidine blue O in microemulsion with EDTA, in 16 h-old *S. aureus* and *S. epidermidis* biofilms. SEM and fluorescence microscopy results showed that the most effective treatment was the one done with encapsulated Toluidine blue O, with higher biofilm damaged, regarding its EPS matrix as well as bacteria viability (Rout et al., 2018). The combination of this formulation with EDTA resulted in an enhanced inhibition of bacterial biofilms, being ~100% for *S. aureus* biofilms and 80% for *S. epidermidis* biofilms. Surfactants and EDTA combined were able to penetrate deeper into the biofilms, due to the smaller microemulsion size achieved with the encapsulation of Toluidine blue O. Additionally, the chelating effect of EDTA allowed EPS matrix disruption, through sequestration of Ca²⁺ and Mg²⁺ ions, leading to an easier penetration (Rout et al., 2018). Considering this effect, recent studies also proposed a combination of PDT, EDTA, and antibiotics as an efficient approach to disrupt the matrix of 24 h-old MRSA and multidrug-resistant *Pseudomonas aeruginosa* (MRPA) biofilms (Li X. et al., 2019). Consistently with the previous study, Li X. et al. showed that PDT mediated by EDTA promoted the formation of bacteria-free voids. In combination with antibiotics, a higher evidence of biofilm destruction was observed, with dead cells present throughout the entire thickness of the treated biofilms and decreased metabolic activities of 8.29% and 7.75% for MRSA and MRPA, respectively (Li X. et al., 2019). Applying a nanotechnological perspective, Darabpour et al. investigated the potentiality of a mixture of polycationic chitosan NPs and methylene blue on the PDT antibiofilm efficiency against 24 h-old *S. aureus* and *P. aeruginosa*. The high affinity of the polycationic chitosan NPs to the negatively charged EPS compromised the adhesion,

leading to the disruption of the biofilm (Darabpour et al., 2016). Using carbon nanotubes as a support nanostructure for cationic dye malachite green, Anju et al. proved that exopolysaccharide inhibition (57.84% for *S. aureus* and 37.25% for *P. aeruginosa*) and considerable biofilm reduction can also be achieved in *P. aeruginosa* and *S. aureus* biofilms (Anju et al., 2019b).

As known, bacteria tend to colonize and adhere to several medical devices, such as implants, which represents a huge concern. Considering this, great efforts have been made to design biocompatible and non-invasive phototherapeutic strategies, for instance, based on the coating of titanium implants and near-infrared light (Li M. et al., 2019; Yuan et al., 2019). Promising eradication results have been achieved for *S. aureus* biofilms by taking advantage of the synergistic effect of the ROS produced by PDT and the thermal effect of the photothermal therapy (PTT), without showing noticeable toxicity (Li M. et al., 2019; Yuan et al., 2019). PDT was also studied for prosthetic joint infections, as a mean to target the biofilms that cause these infections (Vassena et al., 2014; Briggs et al., 2018). Vassena et al. studied the application of RLP068/Cl as a PS in biofilms of mature MRSA and *P. aeruginosa*. This study revealed that besides the antimicrobial activity, the tested PS also promoted some biofilm disruption along with an estimated decrease of 45% and 38% in *S. aureus* and *P. aeruginosa* biomass, respectively (Vassena et al., 2014). Briggs et al. explored the effectiveness of methylene blue as a PS, growing bacteria on both polished titanium alloy and hydroxyapatite-coated disk for 3 days. *S. aureus*, MRSA, *S. epidermidis*, and *P. aeruginosa* biofilms were investigated on the polished surface, while only *P. aeruginosa* was tested in the hydroxyapatite-coated disk. PDT treatment presented significant effect on MRSA and *P. aeruginosa* biofilms and completely eradicated *S. aureus* and *S. epidermidis* biofilms.

They also showed that PDT was less effective when eradicating mature bacterial biofilms grown on hydroxyapatite-coated disk. However, with higher laser power, light intensity and exposure time, greater antibiofilm activity can be achieved (Briggs et al., 2018).

As an alternative to PDT, the use of ultrasounds to induce mechanical disruption of the biofilm structure has been also investigated (Table 5). Since the 90's, therapeutic ultrasounds combined with antibiotics have been showing promising results, both *in vitro* and *in vivo*, using low intensity (up to 3 W cm^{-2}) and low-frequency (a few 100 kHz–1 MHz) (Qian et al., 1997, 1999; Johnson et al., 1998; Carmen et al., 2004, 2005; Ensing et al., 2005). Even recently, the effect of low-intensity and low-frequency ultrasounds is still under investigation, for instance in combination with tobramycin, against beta-lactamases *E. coli* biofilms. It was found that the morphology of the biofilms subjected to the treatment was seriously affected, presenting reduced thickness and a loosened structure. As a consequence, the penetration of the antibiotic increased, which led to an increased antibacterial effect (Hou et al., 2019).

With the aim to achieve greater effects, gas-filled particles, called microbubbles have been associated with ultrasounds. Microbubbles provide nuclei for inertial cavitation and lower the threshold for ultrasounds-induced cavitation, resulting in a substantial effect with a reduced exposure time (He et al., 2011; Dong et al., 2017). He et al. showed that the application of ultrasound-targeted microbubbles (USMB) destruction could significantly improve vancomycin activity against 12 h-old *S. epidermidis* biofilms. Ultrasounds-activated sulfur hexafluoride microbubbles and vancomycin created micropores within the biofilm architecture, which facilitated the vancomycin penetration (He et al., 2011). Besides, a significant decrease in the number of viable cells ($7.17 \log_{10} \text{ CFU ml}^{-1}$) was observed, compared to an untreated control ($10.51 \log_{10} \text{ CFU ml}^{-1}$). *In vivo* *S. epidermidis* biofilms were grown on polyethylene disks and further subcutaneously implanted in rabbit models. The results revealed a significant decrease of the \log_{10} numbers of viable CFU cm^{-2} in biofilms treated with vancomycin and ultrasounds, alone or in combination with microbubbles. It is worth to note that the lowest number of viable cells was observed when microbubbles were added to the treatment (He et al., 2011).

The effect of USMB was also investigated by Dong et al. In this study, low-frequency ultrasounds (300 kHz) combined with vancomycin and microbubbles were evaluated in 24 h-old *S. epidermidis* biofilms. Once more, a reduction of the biofilm thickness was observed, which allowed vancomycin to reach inner layers (Dong et al., 2013). Although the biophysical effect of acoustically activated microbubbles is evident, the underlying mechanisms of interaction between the bubbles and the biofilm has not been elucidated yet (Dong et al., 2017). Therefore, besides the mechanical effects of the USMB treatment in combination with vancomycin, Dong et al. showed that ultrasonic energy could also present biochemical effects on extracellular matrix of *S. epidermidis* biofilms. An ultrasounds treatment (1 MHz, 0.5 W cm^{-2} , 50% duty cycle, for 5 min) combined with microbubbles interfered with *quorum sensing* regulator genes and reduced the

expression level of *icaA*, which is one of the encoding genes to polysaccharide intercellular adhesin, a major component of *S. epidermidis* EPS matrix. Although biochemical effects could not be completely distinguished from the mechanical effects of ultrasounds, the combination of all mechanisms resulted in a reduction of the biomass and an enhanced antibiotic activity, through fragilization of the matrix (Dong et al., 2017). As a continuum of the previous studies and with the aim of facilitate the translation of this technology, Dong et al. further explored this same synergistic effect in an *in vivo* rabbit model (Dong et al., 2018). Consistently, SEM images showed that when treated with USMB in combination with vancomycin, biofilms presented the greatest reduction in terms of thickness as well as bacterial density, compared to the other treatment groups. The susceptibility to the antibiotic significantly increased, since the reduction of bacterial counts with USMB + vancomycin treatment was close to three orders of magnitude compared with the control. Also, histopathologic examinations showed no damage to the skin and organs, as a consequence of ultrasounds alone or USMB, which indicates that these technologies may be well tolerated by the body and have the potential to be safely applied (Dong et al., 2018).

Other conventional antibiotics, such as gentamicin and streptomycin, have also been tested in association with USMB (Ronan et al., 2016). It was found that exposing 72 h-old *P. aeruginosa* biofilms to USMB alone caused significant structural damage to the biofilm, through the formation of voids and 5–20 μm diameter craters. The ultrasonic disruption of the microbubbles enables the resulting shockwaves and microjets to act nearby the biofilm, affecting not only the permeability of the cells but also the EPS matrix integrity. The additional action with the antibiotics led to a significant reduction in overall biomass and thickness of the treated biofilms as well as a reduction in the metabolic activity of the bacteria, detected by CO_2 production rate quantification (Ronan et al., 2016).

Besides ultrasounds, laser light can also be used to induce the vaporization of nanobubbles, producing similar damage on the matrix and potentiating antibiotic effects (Teirlinck et al., 2019). Teirlinck et al. tested this approach against *P. aeruginosa* and *S. aureus* biofilms, in conjugation with small gold NPs. When short laser pulses were applied to the biofilms, these NPs could absorb the energy of high intensity, heating the water surrounding of the particles that quickly evaporated, resulting in expanding and imploding water vapor nanobubbles (Teirlinck et al., 2019). The organized structure of the biofilm was compromised by the generated pressure waves, enabling a better diffusion of the drug molecules deep into the biofilm. In fact, the treatment with vapor nanobubbles enhanced the antibacterial effects of the tested compounds, achieving results comparable with the ones obtained for forced disrupted biofilms, by sonication and vortexing (Teirlinck et al., 2019).

Throughout this section, it was shown that both PDT and ultrasounds are efficient technologies for the eradication of biofilms. Niavarzi et al. recently considered the hypothesis of combining these two strategies, by using ultrasounds to activate a PS (methylene blue), followed by PDT. In fact, ultrasonic activation of PS in conjugation with the PDT increased the

TABLE 5 | Biofilm disruptive strategies based on ultrasounds and laser-induced microbubbles.

Strategy	MB/NB characteristics	Additional compounds	Parameters	Bacterial strains	Mechanism of action	References
Low-intensity and low-frequency ultrasound	-	Vancomycin (50 mg kg ⁻¹)	Frequency: 28.5 kHz Duty cycle: 1:3 Power density: 500 mW cm ⁻² Time of exposure: 24 or 48 h	<i>S. epidermidis</i> (ATCC 35984)	<i>In vivo</i> enhancement of antibiotic action	Carmen et al., 2004
	-	Gentamicin (8 mg kg ⁻¹)	Frequency: 28.5 kHz Duty cycle: 1:3 Power density: 500 mW cm ⁻² Time of exposure: 24 or 48 h	<i>E. coli</i> (ATCC 10798) <i>P. aeruginosa</i> (ATCC 27853)	<i>In vivo</i> enhancement of antibiotic action	Carmen et al., 2005
	-	Gentamicin (8 mg kg ⁻¹)	Frequency: 28.48 kHz Power density: 500 mW cm ⁻² Time of exposure: 24 to 72 h	<i>E. coli</i> (ATCC 10798)	<i>In vivo</i> enhancement of antibiotic action (applied locally or systemically)	Ensing et al., 2005
	-	Tobramycin (8 and 80 µg ml ⁻¹)	Frequency: 42 kHz Power density: 0.66 W cm ⁻² Time of exposure: 30 min	ESBLs <i>E. coli</i> (Clinic isolates)	Reduction of the biofilm thickness Loss of structure Enhanced of antibiotic penetration	Hou et al., 2019
USMB	SonoVue 30% (v/v)	Vancomycin (100 µg ml ⁻¹)	Frequency: 0.08 MHz Power density: 1.0 W cm ⁻² Duty cycle: 50% Time of exposure: 10 min	<i>S. epidermidis</i> (ATCC 35984)	Formation of micropores Reduction of the biofilm density Increased antibiotic penetration	He et al., 2011
	1% and 4% (v/v)	Vancomycin (32 mg l ⁻¹)	Frequency: 300 kHz Power density: 0.5 W cm ⁻² Duty cycle: 50% Time of exposure: 5 min	<i>S. epidermidis</i> (ATCC 35984)	Formation of micropores Reduction of biofilm thickness Enhancement of susceptibility	Dong et al., 2013
	1% and 4% (v/v)	Vancomycin (32 mg l ⁻¹)	Frequency: 1 MHz pulsed US waves Power density: 0.5 W cm ⁻² Duty cycle: 50% Time of exposure: 5 min	<i>S. epidermidis</i> (ATCC 35984)	Downregulation of the expression of <i>icaA</i> Interference with <i>quorum sensing</i> regulator genes	Dong et al., 2017
	1% (v/v) 4–6 µm	Vancomycin (25 mg kg ⁻¹)	Frequency: 300 kHz Power density: 0.5 W cm ⁻² Duty cycle: 50% Time of exposure: 24 to 72 h after surgery; 5 min, 2 times a day	<i>S. epidermidis</i> (ATCC 35984)	<i>In vivo:</i> Reduction of biofilm thickness Enhancement of susceptibility	Dong et al., 2018
	Perflutren lipid-coated microspheres filled with octafluoropropane gas (mean diameter: 1.1–3.3 µm)	Gentamicin sulfate (50 mg l ⁻¹); Streptomycin sulfate (50 mg l ⁻¹)	500 kHz at a peak negative pressure of 1.1 MPa; 16 cycle tone burst; Frequency: 1 kHz pulse repetition Time of exposure: 5 min	<i>P. aeruginosa</i> (PAO1)	Formation of craters Synergistic effect with the antibiotics	Ronan et al., 2016
Laser-induced vapor nanobubbles	NB produced by the laser thermal effect on 70 nm AuNP (1.4 × 10 ¹⁰ AuNP ml ⁻¹)	Pvp-I (0.01%) Chx (0.04%), BzCl (0.06%); Cetr (0.15%), Mupi (0.01%)	WL: 561 nm Fluence: 1.7 J cm ⁻² Laser beam diameter: ~150 µm Time of exposure: 1 or 2 laser pulses for 7 ns	<i>P. aeruginosa</i> (LMG 27622) <i>S. aureus</i> (Mu50)	Enhanced penetration of antibiotics Biofilm disruption	Teirlinck et al., 2019

AuNP, silver nanoparticles; BzCl, benzalkonium chloride; Cetr, cetrimeronium bromide; Chx, chlorhexidine; *E. coli*, *Escherichia coli*; ESBLs, extended-spectrum beta-lactamases; MB, microbubbles; Mupi, mupirocin; NB, nanobubbles; *P. aeruginosa*, *Pseudomonas aeruginosa*; Pvp-I, povidone-iodine; *S. aureus*, *Staphylococcus aureus*; *S. epidermidis*, *Staphylococcus epidermidis*; US, ultrasound; USMB, ultrasound and microbubbles; WL, wavelength.

penetration depth into *E. faecalis* biofilms, leading to greater antibiofilm activity of the PS compared to the use of PDT alone, with reduction bacterial counts of ~98%, comparing to the control group (Niavarzi et al., 2019).

FUTURE PERSPECTIVES

Biofilm-associated infections are nowadays a major concern for the healthcare systems. At a clinical level, the current therapies available are mainly focused only on a biocidal approach. Strategies focusing on targeting and disruption of the EPS matrix may be a promising approach to increase cell susceptibility to antibacterial agents (Fulaz et al., 2019). Antibiofilm agents have been reported in the literature to potentiate the activity of antibiotics due to their ability to disassemble the matrix. In a more complex strategy, NPs as carriers of antibiofilm agents have been developed. However, these nanocarriers are mostly focused on the immobilization of matrix disruptive enzymes, such as DNase I, dispersin B, and alginate lyase. To the best of our knowledge, nanocarriers for delivery of mucolytic agents with antibiofilm potential have not been developed.

Regarding the explored innovative technologies, it was shown that physical disturbance of the EPS matrix is also achieved, through generation of ROS, interference with matrix polysaccharides or creation of voids and craters in the biofilm structure. Although these mechanisms can efficiently disrupt biofilms without development of bacterial resistance, cell detachment can increase the risk of reinfection. Thus, a synergistic effect between the antibacterial effect of antibiotics and the mechanical disruption caused by these technologies is aimed in most reported studies.

In conclusion, the ideal strategy for biofilm eradication would consider the combination of antibacterial agents with strategies

for EPS disassembly. In this scenario, the EPS would be disrupted, and the dispersed bacterial cells would be further killed by a bactericidal agent. Hence, this innovative therapy would decrease bacterial resistance and prevent biofilm recurrence.

AUTHOR CONTRIBUTIONS

RP and FS drafted the manuscript. SR, CN, and PV reviewed and edited the manuscript. All authors read and approved the final version.

FUNDING

This work was supported by the project PTDC/NAN-MAT/31444/2017, financed by FCT/MCTES e FEDER through Programa Operacional Competitividade e Internacionalização - COMPETE 2020.

ACKNOWLEDGMENTS

RP and CN are thankful to Fundação para a Ciência e Tecnologia (FCT) for the Ph.D. Grant [SFRH/BD/130319/2017] and the investigator Grant [IF/00293/2015], respectively. PV is thankful to the Fund for Scientific Research Flanders (FWO grant WO.009.16N). FS is thankful for the grant [ICETA 2019-81]. The authors RP, FS, CN, and SR acknowledge to the institution LAQV - Laboratório Associado para a Química Verde (UIDB/50006/2020). RP also acknowledges the Programa Operacional Capital Humano (POCH), specifically the BiotechHealth Programme (Doctoral Programme on Cellular and Molecular Biotechnology Applied to Health Sciences). The authors acknowledge Servier Laboratories for permission for adaptation of figures.

REFERENCES

- Anderson, G. G., and O'Toole, G. A. (2008). Innate and induced resistance mechanisms of bacterial biofilms. *Curr. Top Microbiol. Immunol.* 322, 85–105. doi: 10.1007/978-3-540-75418-3_5
- Anju, V. T., Paramanathan, P., S. B.S., Sharan, A., Syed, A., Bahkali, N. A., et al. (2019a). Antimicrobial photodynamic activity of toluidine blue-carbon nanotube conjugate against *Pseudomonas aeruginosa* and *Staphylococcus aureus* - understanding the mechanism of action. *Photodiagnosis Photodyn. Ther.* 27, 305–316. doi: 10.1016/j.pdpdt.2019.06.014
- Anju, V. T., Paramanathan, P., Siddhardha, B., Sruthil Lal, S. B., Sharan, A., Alyousef, A. A., et al. (2019b). Malachite green-conjugated multi-walled carbon nanotubes potentiate antimicrobial photodynamic inactivation of planktonic cells and biofilms of *Pseudomonas aeruginosa* and *Staphylococcus aureus*. *Int. J. Nanomed.* 14, 3861–3874. doi: 10.2147/ijn.S202734
- Archer, N. K., Mazaitis, M. J., Costerton, J. W., Leid, J. G., Powers, M. E., and Shirliff, M. E. (2011). *Staphylococcus aureus* biofilms: properties, regulation, and roles in human disease. *Virulence* 2, 445–459. doi: 10.4161/viru.2.5.17724
- Baelo, A., Levato, R., Julian, E., Crespo, A., Astola, J., Gavalda, J., et al. (2015). Disassembling bacterial extracellular matrix with DNase-coated nanoparticles to enhance antibiotic delivery in biofilm infections. *J. Control Release* 209, 150–158. doi: 10.1016/j.jconrel.2015.04.028
- Baker, P., Hill, P. J., Snarr, B. D., Alnabehseya, N., Pestrak, M. J., Lee, M. J., et al. (2016). Exopolysaccharide biosynthetic glycoside hydrolases can be utilized to disrupt and prevent *Pseudomonas aeruginosa* biofilms. *Sci. Adv.* 2:e1501632. doi: 10.1126/sciadv.1501632
- Bandara, H. M., Nguyen, D., Mugarala, S., Osinski, M., and Smyth, H. D. (2015). Magnetic fields suppress *Pseudomonas aeruginosa* biofilms and enhance ciprofloxacin activity. *Biofouling* 31, 443–457. doi: 10.1080/08927014.2015.1055326
- Beeh, K. M., Beier, J., Esperester, A., and Paul, L. D. (2008). Antiinflammatory properties of ambroxol. *Eur. J. Med. Res.* 13, 557–562.
- Beirao, S., Fernandes, S., Coelho, J., Faustino, M. A., Tome, J. P., Neves, M. G., et al. (2014). Photodynamic inactivation of bacterial and yeast biofilms with a cationic porphyrin. *Photochem. Photobiol.* 90, 1387–1396. doi: 10.1111/php.12331
- Beitelshes, M., Hill, A., Jones, C. H., and Pfeifer, B. A. (2018). Phenotypic variation during biofilm formation: implications for anti-biofilm therapeutic design. *Materials* 11:1086. doi: 10.3390/ma11071086
- Benson, D. E., Grissom, C. B., Burns, G. L., and Mohammad, S. F. (1994). Magnetic field enhancement of antibiotic activity in biofilm forming *Pseudomonas aeruginosa*. *Asaio J.* 40, M371–M376. doi: 10.1097/00002480-199407000-00025
- Briggs, T., Blunn, G., Hislop, S., Ramalhet, R., Bagley, C., McKenna, D., et al. (2018). Antimicrobial photodynamic therapy - a promising treatment for prosthetic joint infections. *Lasers Med. Sci.* 33, 523–532. doi: 10.1007/s10103-017-2394-4
- Carmen, J. C., Roeder, B. L., Nelson, J. L., Beckstead, B. L., Runyan, C. M., Schaalje, G. B., et al. (2004). Ultrasonically enhanced vancomycin activity against *Staphylococcus epidermidis* biofilms *in vivo*. *J. Biomater. Appl.* 18, 237–245. doi: 10.1177/0885328204040540
- Carmen, J. C., Roeder, B. L., Nelson, J. L., Ogilvie, R. L., Robison, R. A., Schaalje, G. B., et al. (2005). Treatment of biofilm infections on implants with

- low-frequency ultrasound and antibiotics. *Am. J. Infect. Control.* 33, 78–82. doi: 10.1016/j.ajic.2004.08.002
- Chaignon, P., Sadvokaya, I., Ragunah, C., Ramasubbu, N., Kaplan, J. B., and Jabbouri, S. (2007). Susceptibility of staphylococcal biofilms to enzymatic treatments depends on their chemical composition. *Appl. Microbiol. Biotechnol.* 75, 125–132. doi: 10.1007/s00253-006-0790-y
- Chen, K. J., and Lee, C. K. (2018). Twofold enhanced dispersin B activity by N-terminal fusion to silver-binding peptide for biofilm eradication. *Int. J. Biol. Macromol.* 118, 419–426. doi: 10.1016/j.ijbiomac.2018.06.066
- Cheng, C., Du, L., Yu, J., Lu, Q., He, Y., and Ran, T. (2015). Ciprofloxacin plus erythromycin or ambroxol ameliorates endotracheal tube-associated *Pseudomonas aeruginosa* biofilms in a rat model. *Pathol. Res. Pract.* 211, 982–988. doi: 10.1016/j.prp.2015.10.003
- Chung, P. Y., and Toh, Y. S. (2014). Anti-biofilm agents: recent breakthrough against multi-drug resistant *Staphylococcus aureus*. *Pathog. Dis.* 70, 231–239. doi: 10.1111/2049-632x.12141
- Darabpour, E., Kashef, N., Amini, S. M., Kharrazi, S., and Djavid, G. E. (2017). Fast and effective photodynamic inactivation of 4-day-old biofilm of methicillin-resistant *Staphylococcus aureus* using methylene blue-conjugated gold nanoparticles. *J. Drug Deliv. Sci. Technol.* 37, 134–140. doi: 10.1016/j.jddst.2016.12.007
- Darabpour, E., Kashef, N., and Mashayekhan, S. (2016). Chitosan nanoparticles enhance the efficiency of methylene blue-mediated antimicrobial photodynamic inactivation of bacterial biofilms: an *in vitro* study. *Photodiagnosis Photodyn. Ther.* 14, 211–217. doi: 10.1016/j.pdpdt.2016.04.009
- Darouiche, R. O. (2004). Treatment of infections associated with surgical implants. *N. Engl. J. Med.* 350, 1422–1429. doi: 10.1056/NEJMra035415
- de Melo, W. C., Avci, P., de Oliveira, M. N., Gupta, A., Vecchio, D., Sadasivam, M., et al. (2013). Photodynamic inactivation of biofilm: taking a lightly colored approach to stubborn infection. *Expert Rev. Anti. Infect. Ther.* 11, 669–693. doi: 10.1586/14787210.2013.811861
- Del Pozo, J. L. (2018). Biofilm-related disease. *Expert Rev. Anti Infect. Ther.* 16, 51–65. doi: 10.1080/14787210.2018.1417036
- Di Poto, A., Sbarra, M. S., Provenza, G., Visai, L., and Speziale, P. (2009). The effect of photodynamic treatment combined with antibiotic action or host defence mechanisms on *Staphylococcus aureus* biofilms. *Biomaterials* 30, 3158–3166. doi: 10.1016/j.biomaterials.2009.02.038
- Dobrynina, O. Y., Bolshakova, T. N., Umyarov, A. M., Boksha, I. S., Lavrova, N. V., Grishin, A. V., et al. (2015). Disruption of bacterial biofilms using recombinant dispersin B. *Microbiology* 84, 498–501. doi: 10.1134/S0026261715040062
- Dong, Y., Chen, S., Wang, Z., Peng, N., and Yu, J. (2013). Synergy of ultrasound microbubbles and vancomycin against *Staphylococcus epidermidis* biofilm. *J. Antimicrob. Chemother.* 68, 816–826. doi: 10.1093/jac/dks490
- Dong, Y., Li, J., Li, P., and Yu, J. (2018). Ultrasound microbubbles enhance the activity of vancomycin against *Staphylococcus epidermidis* biofilms *in vivo*. *J. Ultrasound Med.* 37, 1379–1387. doi: 10.1002/jum.14475
- Dong, Y., Xu, Y., Li, P., Wang, C., Cao, Y., and Yu, J. (2017). Antibiofilm effect of ultrasound combined with microbubbles against *Staphylococcus epidermidis* biofilm. *Int. J. Med. Microbiol.* 307, 321–328. doi: 10.1016/j.ijmm.2017.06.001
- Donlan, R. M. (2001a). Biofilm formation: a clinically relevant microbiological process. *Clin. Infect. Dis.* 33, 1387–1392. doi: 10.1086/322972
- Donlan, R. M. (2001b). Biofilms and device-associated infections. *Emerging Infect. Dis.* 7, 277–281. doi: 10.3201/eid0702.010226
- Donlan, R. M., and Costerton, J. W. (2002). Biofilms: survival mechanisms of clinically relevant microorganisms. *Clin. Microbiol. Rev.* 15, 167–193. doi: 10.1128/CMR.15.2.167-193.2002
- Ensing, G. T., Roeder, B. L., Nelson, J. L., van Horn, J. R., van der Mei, H. C., Busscher, H. J., et al. (2005). Effect of pulsed ultrasound in combination with gentamicin on bacterial viability in biofilms on bone cements *in vivo*. *J. Appl. Microbiol.* 99, 443–448. doi: 10.1111/j.1365-2672.2005.02643.x
- Eroshenko, D., Polyudova, T., and Korobov, V. (2017). N-acetylcysteine inhibits growth, adhesion and biofilm formation of Gram-positive skin pathogens. *Microb. Pathog.* 105, 145–152. doi: 10.1016/j.micpath.2017.02.030
- Fang, C. H., Tsai, P. I., Huang, S. W., Sun, J. S., Chang, J. Z., Shen, H. H., et al. (2017). Magnetic hyperthermia enhance the treatment efficacy of peri-implant osteomyelitis. *BMC Infect. Dis.* 17, 516. doi: 10.1186/s12879-017-2621-4
- Fleming, D., and Rumbaugh, K. P. (2017). Approaches to dispersing medical biofilms. *Microorganisms* 5:15. doi: 10.3390/microorganisms5020015
- Flemming, H.-C. (2011). “Microbial biofouling: unsolved problems, insufficient approaches, and possible solutions,” in *Biofilm highlights*, eds F. Hans-Curt, W. Jost, and S. Ulrich (Berlin; Heidelberg: Springer), 81–109.
- Flemming, H. C., and Wingender, J. (2010). The biofilm matrix. *Nat. Rev. Microbiol.* 8, 623–633. doi: 10.1038/nrmicro2415
- Flemming, H. C., Wingender, J., Szewzyk, U., Steinberg, P., Rice, S. A., and Kjelleberg, S. (2016). Biofilms: an emergent form of bacterial life. *Nat. Rev. Microbiol.* 14, 563–575. doi: 10.1038/nrmicro.2016.94
- Fong, J. N. C., and Yildiz, F. H. (2015). Biofilm matrix proteins. *Microbiol. Spectr.* 3, 1–16. doi: 10.1128/microbiolspec.MB-0004-2014
- Frohlich, E. (2012). The role of surface charge in cellular uptake and cytotoxicity of medical nanoparticles. *Int. J. Nanomedicine*. 7, 5577–5591. doi: 10.2147/ijn.S36111
- Fulaz, S., Vitale, S., Quinn, L., and Casey, E. (2019). Nanoparticle-biofilm interactions: the role of the EPS matrix. *Trends Microbiol.* 27, 915–926. doi: 10.1016/j.tim.2019.07.004
- Gao, L., Giglio, K. M., Nelson, J. L., Sondermann, H., and Travis, A. J. (2014). Ferromagnetic nanoparticles with peroxidase-like activity enhance the cleavage of biological macromolecules for biofilm elimination. *Nanoscale* 6, 2588–2593. doi: 10.1039/c3nr05422e
- Geilich, B. M., Gelfat, I., Sridhar, S., van de Ven, A. L., and Webster, T. J. (2017). Superparamagnetic iron oxide-encapsulating polymersome nanocarriers for biofilm eradication. *Biomaterials* 119, 78–85. doi: 10.1016/j.biomaterials.2016.12.011
- Grosman, Z., Kolar, M., and Tesarikova, E. (1992). Effects of static magnetic field on some pathogenic microorganisms. *Acta Univ. Palacki. Olomuc. Fac. Med.* 134, 7–9.
- Habimana, O., Zaroni, M., Vitale, S., O'Neill, T., Scholz, D., Xu, B., et al. (2018). One particle, two targets: a combined action of functionalised gold nanoparticles, against *Pseudomonas fluorescens* biofilms. *J. Colloid Interface Sci.* 526, 419–428. doi: 10.1016/j.jcis.2018.05.014
- Harper, R. A., Carpenter, G. H., Proctor, G. B., Harvey, R. D., Gambogi, R. J., Geonnoti, A. R., et al. (2019). Diminishing biofilm resistance to antimicrobial nanomaterials through electrolyte screening of electrostatic interactions. *Colloids Surf. B* 173, 392–399. doi: 10.1016/j.colsurfb.2018.09.018
- Hasan, N., Cao, J., Lee, J., Naeem, M., Hlaing, S. P., Kim, J., et al. (2019). PEI/NONOates-doped PLGA nanoparticles for eradicating methicillin-resistant *Staphylococcus aureus* biofilm in diabetic wounds via binding to the biofilm matrix. *Mater. Sci. Eng. C* 103:109741. doi: 10.1016/j.msec.2019.109741
- He, N., Hu, J., Liu, H., Zhu, T., Huang, B., Wang, X., et al. (2011). Enhancement of vancomycin activity against biofilms by using ultrasound-targeted microbubble destruction. *Antimicrob. Agents Chemother.* 55, 5331–5337. doi: 10.1128/aac.00542-11
- Henriksson, G., Johansson, G., and Pettersson, G. (2000). A critical review of cellobiose dehydrogenases. *J. Biotechnol.* 78, 93–113. doi: 10.1016/S0168-1656(00)00206-6
- Hou, Y., Yang, M., Jiang, H., Li, D., and Du, Y. (2019). Effects of low-intensity and low-frequency ultrasound combined with tobramycin on biofilms of extended-spectrum beta-lactamases (ESBLs) *Escherichia coli*. *FEMS Microbiol. Lett.* 366:fnz026. doi: 10.1093/femsle/fnz026
- Hu, X., Huang, Y. Y., Wang, Y., Wang, X., and Hamblin, M. R. (2018). Antimicrobial photodynamic therapy to control clinically relevant biofilm infections. *Front. Microbiol.* 9:1299. doi: 10.3389/fmicb.2018.01299
- Huang, L., Dai, T., and Hamblin, M. R. (2010). Antimicrobial photodynamic inactivation and photodynamic therapy for infections. *Methods Mol. Biol.* 635, 155–173. doi: 10.1007/978-1-60761-697-9_12
- Hühn, D., Kantner, K., Geidel, C., Brandholt, S., De Cock, I., Soenen, S. J. H., et al. (2013). Polymer-coated nanoparticles interacting with proteins and cells: focusing on the sign of the net charge. *ACS Nano* 7, 3253–3263. doi: 10.1021/nn3059295
- Hwang, G., Paula, A. J., Hunter, E. E., Liu, Y., Baber, A., Karabucak, B., et al. (2019). Catalytic antimicrobial robots for biofilm eradication. *Sci. Robot.* 4:aaw2388. doi: 10.1126/scirobotics.aaw2388
- Jia, M., Mai, B., Liu, S., Li, Z., Liu, Q., and Wang, P. (2019). Antibacterial effect of S-Porphin sodium photodynamic therapy on *Staphylococcus aureus* and

- multiple drug resistance *Staphylococcus aureus*. *Photodiagnosis Photodyn. Ther.* 28, 80–87. doi: 10.1016/j.pdpdt.2019.08.031
- Johnson, L. L., Peterson, R. V., and Pitt, W. G. (1998). Treatment of bacterial biofilms on polymeric biomaterials using antibiotics and ultrasound. *J. Biomater. Sci. Polym. Ed.* 9, 1177–1185. doi: 10.1163/156856298x00712
- Jun, Y., Youn, C. K., Jo, E. R., and Cho, S. I. (2019). *In vitro* inhibitory activity of N-acetylcysteine on tympanostomy tube biofilms from methicillin-resistant *Staphylococcus aureus* and quinolone-resistant *Pseudomonas aeruginosa*. *Int. J. Pediatr. Otorhinolaryngol.* 126:109622. doi: 10.1016/j.ijporl.2019.109622
- Kalpana, B. J., Aarthi, S., and Pandian, S. K. (2012). Antibiofilm activity of alpha-amylase from *Bacillus subtilis* S8-18 against biofilm forming human bacterial pathogens. *Appl. Biochem. Biotechnol.* 167, 1778–1794. doi: 10.1007/s12010-011-9526-2
- Khan, F., Lee, J. W., Manivasagan, P., Pham, D. T. N., Oh, J., and Kim, Y. M. (2019). Synthesis and characterization of chitosan oligosaccharide-capped gold nanoparticles as an effective antibiofilm drug against the *Pseudomonas aeruginosa* PAO1. *Microb. Pathog.* 135:103623. doi: 10.1016/j.micpath.2019.103623
- Khoury, A. E., Lam, K., Ellis, B., and Costerton, J. W. (1992). Prevention and control of bacterial infections associated with medical devices. *ASAIO J.* 38, M174–M178. doi: 10.1097/00002480-199207000-00013
- Koo, H., Allan, R. N., Howlin, R. P., Stoodley, P., and Hall-Stoodley, L. (2017). Targeting microbial biofilms: current and prospective therapeutic strategies. *Nat. Rev. Microbiol.* 15, 740–755. doi: 10.1038/nrmicro.2017.99
- Kumar Shukla, S., and Rao, T. S. (2013). Dispersal of Bap-mediated *Staphylococcus aureus* biofilm by proteinase K. *J. Antibiot.* 66, 55–60. doi: 10.1038/ja.2012.98
- Laskar, K., Faisal, S. M., Rauf, A., Ahmed, A., and Owais, M. (2017). Undec-10-enoic acid functionalized chitosan based novel nano-conjugate: an enhanced anti-bacterial/biofilm and anti-cancer potential. *Carbohydr. Polym.* 166, 14–23. doi: 10.1016/j.carbpol.2017.02.082
- Lee, E., Kim, D. H., Woo, Y., Hur, H. G., and Lim, Y. (2008). Solution structure of peptide AG4 used to form silver nanoparticles. *Biochem. Biophys. Res. Commun.* 376, 595–598. doi: 10.1016/j.bbrc.2008.09.042
- Lefebvre, E., Vighetto, C., Di Martino, P., Larreta Garde, V., and Seyer, D. (2016). Synergistic antibiofilm efficacy of various commercial antiseptics, enzymes and EDTA: a study of *Pseudomonas aeruginosa* and *Staphylococcus aureus* biofilms. *Int. J. Antimicrob. Agents.* 48, 181–188. doi: 10.1016/j.ijantimicag.2016.05.008
- Leite, B., Gomes, F., Teixeira, P., Souza, C., Pizzolitto, E., and Oliveira, R. (2013). Combined effect of linezolid and N-acetylcysteine against *Staphylococcus epidermidis* biofilms. *Enferm. Infect. Microbiol. Clin.* 31, 655–659. doi: 10.1016/j.eimc.2012.11.011
- Li, J., Nickel, R., Wu, J., Lin, F., van Lierop, J., and Liu, S. (2019). A new tool to attack biofilms: driving magnetic iron-oxide nanoparticles to disrupt the matrix. *Nanoscale* 11, 6905–6915. doi: 10.1039/c8nr09802f
- Li, M., Li, L., Su, K., Liu, X., Zhang, T., Liang, Y., et al. (2019). Highly effective and noninvasive near-infrared eradication of a *Staphylococcus aureus* biofilm on implants by a photoresponsive coating within 20 min. *Adv. Sci.* 6:1900599. doi: 10.1002/advs.201900599
- Li, X., Guo, H., Tian, Q., Zheng, G., Hu, Y., Fu, Y., et al. (2013). Effects of 5-aminolevulinic acid-mediated photodynamic therapy on antibiotic-resistant staphylococcal biofilm: an *in vitro* study. *J. Surg. Res.* 184, 1013–1021. doi: 10.1016/j.jss.2013.03.094
- Li, X., Huang, W., Zheng, X., Chang, S., Liu, C., Cheng, Q., et al. (2019). Synergistic *in vitro* effects of indocyanine green and ethylenediamine tetraacetate-mediated antimicrobial photodynamic therapy combined with antibiotics for resistant bacterial biofilms in diabetic foot infection. *Photodiagnosis Photodyn. Ther.* 25, 300–308. doi: 10.1016/j.pdpdt.2019.01.010
- Lin, M. H., Hung, C. F., Aljuffali, I. A., Sung, C. T., Huang, C. T., and Fang, J. Y. (2017). Cationic amphiphile in phospholipid bilayer or oil-water interface of nanocarriers affects planktonic and biofilm bacteria killing. *Nanomedicine* 13, 353–361. doi: 10.1016/j.nano.2016.08.011
- Liu, Y., Busscher, H. J., Zhao, B., Li, Y., Zhang, Z., van der Mei, H. C., et al. (2016). Surface-adaptive, antimicrobially loaded, micellar nanocarriers with enhanced penetration and killing efficiency in staphylococcal biofilms. *ACS Nano* 10, 4779–4789. doi: 10.1021/acsnano.6b01370
- Liu, Z., Wang, F., Ren, J., and Qu, X. (2019). A series of MOF/Ce-based nanozymes with dual enzyme-like activity disrupting biofilms and hindering recolonization of bacteria. *Biomaterials* 208, 21–31. doi: 10.1016/j.biomaterials.2019.04.007
- Lu, B., Lu, F., Ran, L., Yu, K., Xiao, Y., Li, Z., et al. (2018). Imidazole-molecule-capped chitosan-gold nanocomposites with enhanced antimicrobial activity for treating biofilm-related infections. *J. Colloid Interface Sci.* 531, 269–281. doi: 10.1016/j.jcis.2018.07.058
- Marchese, A., Bozzolascio, M., Gualco, L., Debbia, E. A., Schito, G. C., and Schito, A. M. (2003). Effect of fosfomycin alone and in combination with N-acetylcysteine on *E. coli* biofilms. *Int. J. Antimicrob. Agents* 22(Suppl.2), 95–100. doi: 10.1016/s0924-8579(03)00232-2
- Mirzahasseinipour, M., Khorsandi, K., Hosseinzadeh, R., Ghazaeian, M., and Shahidi, F. K. (2020). Antimicrobial photodynamic and wound healing activity of curcumin encapsulated in silica nanoparticles. *Photodiagnosis Photodyn. Ther.* 29:101639. doi: 10.1016/j.pdpdt.2019.101639
- Misba, L., Zaidi, S., and Khan, A. U. (2017). A comparison of antibacterial and antibiofilm efficacy of phenothiazinium dyes between Gram positive and Gram negative bacterial biofilm. *Photodiagnosis Photodyn. Ther.* 18, 24–33. doi: 10.1016/j.pdpdt.2017.01.177
- Niavarzi, S., Pourhajibagher, M., Khedmat, S., Ghabraei, S., Chiniforush, N., and Bahador, A. (2019). Effect of ultrasonic activation on the efficacy of antimicrobial photodynamic therapy: evaluation of penetration depth of photosensitizer and elimination of *Enterococcus faecalis* biofilms. *Photodiagnosis Photodyn. Ther.* 27, 362–366. doi: 10.1016/j.pdpdt.2019.06.001
- Paleari, D., Rossi, G. A., Nicolini, G., and Olivieri, D. (2011). Ambroxol: a multifaceted molecule with additional therapeutic potentials in respiratory disorders of childhood. *Expert Opin. Drug Discov.* 6, 1203–1214. doi: 10.1517/17460441.2011.629646
- Paramanatham, P., Siddhardha, B., Lal Sb, S., Sharan, A., Alyousef, A. A., Al Dosary, M. S., et al. (2019). Antimicrobial photodynamic therapy on *Staphylococcus aureus* and *Escherichia coli* using malachite green encapsulated mesoporous silica nanoparticles: an *in vitro* study. *PeerJ* 7:e7454. doi: 10.7717/peerj.7454
- Parasuraman, P., Antony, A. P., Sharan, A., Siddhardha, B., Kasinathan, K., Bahkali, N. A., et al. (2019). Antimicrobial photodynamic activity of toluidine blue encapsulated in mesoporous silica nanoparticles against *Pseudomonas aeruginosa* and *Staphylococcus aureus*. *Biofouling* 35, 89–103. doi: 10.1080/08927014.2019.1570501
- Patel, K. K., Tripathi, M., Pandey, N., Agrawal, A. K., Gade, S., Anjum, M. M., et al. (2019). Alginate lyase immobilized chitosan nanoparticles of ciprofloxacin for the improved antimicrobial activity against the biofilm associated mucoid *P. aeruginosa* infection in cystic fibrosis. *Int. J. Pharm.* 563, 30–42. doi: 10.1016/j.ijpharm.2019.03.051
- Percival, S. L., Kite, P., Eastwood, K., Murga, R., Carr, J., Arduino, M. J., et al. (2005). Tetrasodium EDTA as a novel central venous catheter lock solution against biofilm. *Infect. Control Hosp. Epidemiol.* 26, 515–519. doi: 10.1086/502577
- Pinto, R. M., Lopes-de-Campos, D., Martins, M. C. L., Van Dijk, P., Nunes, C., and Reis, S. (2019). Impact of nanosystems in *Staphylococcus aureus* biofilms treatment. *FEMS Microbiol. Rev.* 43, 622–641. doi: 10.1093/femsre/fuz021
- Poznansky, M. J. (1984). Enzyme-albumin polymers. new approaches to the use of enzymes in medicine. *Appl. Biochem. Biotechnol.* 10, 41–56. doi: 10.1007/bf02783734
- Qian, Z., Sagers, R. D., and Pitt, W. G. (1997). The effect of ultrasonic frequency upon enhanced killing of *P. aeruginosa* biofilms. *Ann. Biomed. Eng.* 25, 69–76. doi: 10.1007/bf02738539
- Qian, Z., Sagers, R. D., and Pitt, W. G. (1999). Investigation of the mechanism of the bioacoustic effect. *J. Biomed. Mater. Res.* 44, 198–205. doi: 10.1002/(sici)1097-4636(199902)44:2<198::aid-jbm10>3.0.co;2-p
- Quan, K., Zhang, Z., Chen, H., Ren, X., Ren, Y., Peterson, B. W., et al. (2019). Artificial channels in an infectious biofilm created by magnetic nanoparticles enhanced bacterial killing by antibiotics. *Small* 15:e1902313. doi: 10.1002/smll.201902313
- Raad, I., Hachem, R., Tcholakian, R. K., and Sherertz, R. (2002). Efficacy of minocycline and EDTA lock solution in preventing catheter-related bacteremia, septic phlebitis, and endocarditis in rabbits. *Antimicrob. Agents Chemother.* 46, 327–332. doi: 10.1128/aac.46.2.327-332.2002
- Ribeiro, M., Monteiro, F. J., and Ferraz, M. P. (2012). Infection of orthopedic implants with emphasis on bacterial adhesion process and techniques used in studying bacterial-material interactions. *Biomater* 2, 176–194. doi: 10.4161/biom.22905

- Romano, C. L., Toscano, M., Romano, D., and Drago, L. (2013). Antibiofilm agents and implant-related infections in orthopaedics: where are we? *J. Chemother.* 25, 67–80. doi: 10.1179/1973947812y.0000000045
- Ronan, E., Edjiu, N., Kroukamp, O., Wolfaardt, G., and Karshafian, R. (2016). USMB-induced synergistic enhancement of aminoglycoside antibiotics in biofilms. *Ultrasonics* 69, 182–190. doi: 10.1016/j.ultras.2016.03.017
- Rout, B., Liu, C. H., and Wu, W. C. (2018). Increased anti-biofilm efficacy of toluidine blue on *Staphylococcus* species after nano-encapsulation. *Photodiagnosis Photodyn. Ther.* 21, 190–200. doi: 10.1016/j.pdpdt.2017.12.007
- Rubini, D., Banu, S. F., Nisha, P., Murugan, R., Thamotharan, S., Percino, M. J., et al. (2018). Essential oils from unexplored aromatic plants quench biofilm formation and virulence of Methicillin resistant *Staphylococcus aureus*. *Microb. Pathog.* 122, 162–173. doi: 10.1016/j.micpath.2018.06.028
- Shields, R. C., Mokhtar, N., Ford, M., Hall, M. J., Burgess, J. G., ElBadawey, M. R., et al. (2013). Efficacy of a marine bacterial nuclease against biofilm forming microorganisms isolated from chronic rhinosinusitis. *PLoS ONE* 8:e55339. doi: 10.1371/journal.pone.0055339
- Siala, W., Kucharikova, S., Braem, A., Vleugels, J., Tulkens, P. M., Mingeot-Leclercq, M. P., et al. (2016). The antifungal caspofungin increases fluoroquinolone activity against *Staphylococcus aureus* biofilms by inhibiting N-acetylglucosamine transferase. *Nat. Commun.* 7, 1–15. doi: 10.1038/ncomms13286
- Sinisterra, J. V. (1992). Application of ultrasound to biotechnology: an overview. *Ultrasonics* 30, 180–185. doi: 10.1016/0041-624X(92)90070-3
- Srivastava, S., and Bhargava, A. (2016). Biofilms and human health. *Biotechnol. Lett.* 38, 1–22. doi: 10.1007/s10529-015-1960-8
- Stoica, P., Chifiriuc, M. C., Rapa, M., and Lazăr, V. (2017). “Overview of biofilm-related problems in medical devices,” in *Biofilms and Implantable Medical Devices*, eds Y. Deng, and W. Lv (Cambridge, UK: Woodhead Publishing), 3–23.
- Su, Y., Zhao, L., Meng, F., Qiao, Z., Yao, Y., and Luo, J. (2018). Triclosan loaded polyurethane micelles with pH and lipase sensitive properties for antibacterial applications and treatment of biofilms. *Mater. Sci. Eng. C Mater. Biol. Appl.* 93, 921–930. doi: 10.1016/j.msec.2018.08.063
- Subbiahdoss, G., Sharifi, S., Grijpma, D. W., Laurent, S., van der Mei, H. C., Mahmoudi, M., et al. (2012). Magnetic targeting of surface-modified superparamagnetic iron oxide nanoparticles yields antibacterial efficacy against biofilms of gentamicin-resistant staphylococci. *Acta Biomater.* 8, 2047–2055. doi: 10.1016/j.actbio.2012.03.002
- Tan, Y., Cheng, Q., Yang, H., Li, H., Gong, N., Liu, D., et al. (2018b). Effects of ALA-PDT on biofilm structure, virulence factor secretion, and QS in *Pseudomonas aeruginosa*. *Photodiagnosis Photodyn. Ther.* 24, 88–94. doi: 10.1016/j.pdpdt.2018.07.005
- Tan, Y., Ma, S., Leonhard, M., Moser, D., Haselmann, G. M., Wang, J., et al. (2018a). Enhancing antibiofilm activity with functional chitosan nanoparticles targeting biofilm cells and biofilm matrix. *Carbohydr. Polym.* 200, 35–42. doi: 10.1016/j.carbpol.2018.07.072
- Tan, Y., Ma, S., Leonhard, M., Moser, D., Ludwig, R., and Schneider-Stickler, B. (2020). Co-immobilization of cellobiose dehydrogenase and deoxyribonuclease I on chitosan nanoparticles against fungal/bacterial polymicrobial biofilms targeting both biofilm matrix and microorganisms. *Mater. Sci. Eng. C Mater. Biol. Appl.* 108:110499. doi: 10.1016/j.msec.2019.110499
- Tan, Y., Ma, S., Liu, C., Yu, W., and Han, F. (2015). Enhancing the stability and antibiofilm activity of DspB by immobilization on carboxymethyl chitosan nanoparticles. *Microbiol. Res.* 178, 35–41. doi: 10.1016/j.micres.2015.06.001
- Teirlinck, E., Fraire, J. C., Van Acker, H., Wille, J., Swimberghe, R., Brans, T., et al. (2019). Laser-induced vapor nanobubbles improve diffusion in biofilms of antimicrobial agents for wound care. *Biofilm* 1:100004. doi: 10.1016/j.biofilm.2019.100004
- Tetz, G. V., Artemenko, N. K., and Tetz, V. V. (2009). Effect of DNase and antibiotics on biofilm characteristics. *Antimicrob. Agents Chemother.* 53, 1204–1209. doi: 10.1128/aac.00471-08
- Thomsen, H., Benkovics, G., Fenyvesi, E., Farewell, A., Malanga, M., and Ericson, M. B. (2017). Delivery of cyclodextrin polymers to bacterial biofilms - an exploratory study using rhodamine labelled cyclodextrins and multiphoton microscopy. *Int. J. Pharm.* 531, 650–657. doi: 10.1016/j.ijpharm.2017.06.011
- Torelli, R., Cacaci, M., Papi, M., Paroni Sterbini, F., Martini, C., Posteraro, B., et al. (2017). Different effects of matrix degrading enzymes towards biofilms formed by *E. faecalis* and *E. faecium* clinical isolates. *Colloids Surf. B* 158, 349–355. doi: 10.1016/j.colsurfb.2017.07.010
- Trampuz, A., and Widmer, A. F. (2006). Infections associated with orthopedic implants. *Curr. Opin. Infect. Dis.* 19, 349–356. doi: 10.1097/01.qco.0000235161.85925.e8
- Vassena, C., Fenu, S., Giuliani, F., Fantetti, L., Roncucci, G., Simonutti, G., et al. (2014). Photodynamic antibacterial and antibiofilm activity of RLP068/Cl against *Staphylococcus aureus* and *Pseudomonas aeruginosa* forming biofilms on prosthetic material. *Int. J. Antimicrob. Agents.* 44, 47–55. doi: 10.1016/j.ijantimicag.2014.03.012
- Wang, X., Deng, A., Cao, W., Li, Q., Wang, L., Zhou, J., et al. (2018b). Synthesis of chitosan/poly (ethylene glycol)-modified magnetic nanoparticles for antibiotic delivery and their enhanced anti-biofilm activity in the presence of magnetic field. *J. Mater. Sci.* 53, 6433–6449. doi: 10.1007/s10853-018-1998-9
- Wang, X., Wu, J., Li, P., Wang, L., Zhou, J., Zhang, G., et al. (2018a). Microenvironment-responsive magnetic nanocomposites based on silver nanoparticles/gentamicin for enhanced biofilm disruption by magnetic field. *ACS Appl. Mater. Interfaces* 10, 34905–34915. doi: 10.1021/acsami.8b10972
- Wang, Z., Bai, H., Lu, C., Hou, C., Qiu, Y., Zhang, P., et al. (2019). Light controllable chitosan micelles with ROS generation and essential oil release for the treatment of bacterial biofilm. *Carbohydr. Polym.* 205, 533–539. doi: 10.1016/j.carbpol.2018.10.095
- Watters, C. M., Burton, T., Kirui, D. K., and Millenbaugh, N. J. (2016). Enzymatic degradation of *in vitro* *Staphylococcus aureus* biofilms supplemented with human plasma. *Infect. Drug Resist.* 9, 71–78. doi: 10.2147/idr.S103101
- WHO (2014). *Antimicrobial Resistance: Global Report on Surveillance*. France: World Health Organization.
- Wu, J., Wang, X., Wang, Q., Lou, Z., Li, S., Zhu, Y., et al. (2019). Nanomaterials with enzyme-like characteristics (nanozymes): next-generation artificial enzymes (II). *Chem. Soc. Rev.* 48, 1004–1076. doi: 10.1039/C8CS00457A
- Yakandawala, N., Gawande, P. V., LoVetri, K., Cardona, S. T., Romeo, T., Nitz, M., et al. (2011). Characterization of the poly-beta-1,6-N-acetylglucosamine polysaccharide component of *Burkholderia* biofilms. *Appl. Environ. Microbiol.* 77, 8303–8309. doi: 10.1128/aem.05814-11
- Yuan, Z., Tao, B., He, Y., Mu, C., Liu, G., Zhang, J., et al. (2019). Remote eradication of biofilm on titanium implant via near-infrared light triggered photothermal/photodynamic therapy strategy. *Biomaterials* 223:119479. doi: 10.1016/j.biomaterials.2019.119479
- Zhang, Y., Fu, Y., Yu, J., Ai, Q., Li, J., Peng, N., et al. (2015). Synergy of ambrinol with vancomycin in elimination of catheter-related *Staphylococcus epidermidis* biofilm *in vitro* and *in vivo*. *J. Infect. Chemother.* 21, 808–815. doi: 10.1016/j.jiac.2015.08.017
- Zimmerli, W. (2014). Clinical presentation and treatment of orthopaedic implant-associated infection. *J. Intern. Med.* 276, 111–119. doi: 10.1111/joim.12233
- Zimmerli, W., and Sendi, P. (2017). Orthopaedic biofilm infections. *APMIS* 125, 353–364. doi: 10.1111/apm.12687

Conflict of Interest: The authors declare that the research was conducted in the absence of any commercial or financial relationships that could be construed as a potential conflict of interest.

Copyright © 2020 Pinto, Soares, Reis, Nunes and Van Dijck. This is an open-access article distributed under the terms of the Creative Commons Attribution License (CC BY). The use, distribution or reproduction in other forums is permitted, provided the original author(s) and the copyright owner(s) are credited and that the original publication in this journal is cited, in accordance with accepted academic practice. No use, distribution or reproduction is permitted which does not comply with these terms.



Anti-biofilm and Antibacterial Activities of Silver Nanoparticles Synthesized by the Reducing Activity of Phytoconstituents Present in the Indian Medicinal Plants

OPEN ACCESS

Edited by:

Luis Cláudio Nascimento da Silva,
Universidade Ceuma, Brazil

Reviewed by:

Palanivel Velmurugan,
Alagappa University, India
Atte Von Wright,
University of Eastern Finland, Finland
Clovis Macêdo Bezerra Filho,
Federal University of São Paulo, Brazil

*Correspondence:

Yugal Kishore Mohanta
ykmohanta@gmail.com
Tapan Kumar Mohanta
nostoc.tapan@gmail.com;
tapan.mohanta@unizwa.edu.om

†ORCID:

Abeer Hashem
orcid.org/0000-0001-6541-347X
Elsayed Fathi Abd_Allah
orcid.org/0000-0002-8509-8953

Specialty section:

This article was submitted to
Antimicrobials, Resistance
and Chemotherapy,
a section of the journal
Frontiers in Microbiology

Received: 22 September 2019

Accepted: 05 May 2020

Published: 23 June 2020

Citation:

Mohanta YK, Biswas K, Jena SK,
Hashem A, Abd_Allah EF and
Mohanta TK (2020) Anti-biofilm
and Antibacterial Activities of Silver
Nanoparticles Synthesized by
the Reducing Activity
of Phytoconstituents Present
in the Indian Medicinal Plants.
Front. Microbiol. 11:1143.
doi: 10.3389/fmicb.2020.01143

Yugal Kishore Mohanta^{1*}, Kunal Biswas², Santosh Kumar Jena³, Abeer Hashem^{4,5†},
Elsayed Fathi Abd_Allah^{6†} and Tapan Kumar Mohanta^{7*}

¹ Department of Botany, North Orissa University, Baripada, India, ² Department of Biotechnology, Maulana Abul Kalam Azad University of Technology, Haringhata, India, ³ Department of Biotechnology, North Orissa University, Baripada, India, ⁴ Botany and Microbiology Department, College of Science, King Saud University, Riyadh, Saudi Arabia, ⁵ Mycology and Plant Disease Survey Department, Plant Pathology Research Institute, Agriculture Research Center, Giza, Egypt, ⁶ Plant Production Department, College of Food & Agricultural Sciences, King Saud University, Riyadh, Saudi Arabia, ⁷ Natural and Medical Sciences Research Center, University of Nizwa, Nizwa, Oman

Biofilm forming from a variety of microbial pathogens can pose a serious health hazard that is difficult to combat. Nanotechnology, however, represents a new approach to fighting and eradicating biofilm-forming microorganisms. In the present study, the sustainable synthesis and characterization of biocompatible silver nanoparticles (AgNPs) from leaf extracts of *Semecarpus anacardium*, *Glochidion lanceolarium*, and *Bridelia retusa* was explored. Continuous synthesis was observed in a UV-vis spectroscopic analysis and the participating phytoconstituents, flavonoids, phenolic compounds, phytosterols, and glycosides, were characterized by Attenuated total reflectance-Fourier transform infrared spectroscopy. The size and surface charge of the particles were also measured by dynamic light scattering spectroscopy. Scanning electron microscopy study was employed to examine the morphology of the nanoparticles. The spectroscopic and microscopic study confirmed the successful synthesis of AgNPs by plant extracts acting as strong reducing agents. The synthesized AgNPs were screened for antibacterial and anti-biofilm activity against human pathogens *Pseudomonas aeruginosa*, *Escherichia coli*, and *Staphylococcus aureus*. Results of the study demonstrate the potential of phyto-synthesized AgNPs to act as anti-biofilm agents and for other biomedical applications.

Keywords: phyto-synthesis, silver nanoparticles, medicinal plants, anti-bacterial activity, anti-biofilm activity

INTRODUCTION

Nanotechnology is a multidisciplinary science focused on the wide-ranging properties of nanoparticles. Nanoparticles exhibit a broad range of physicochemical properties that greatly contrast their bulk analogs. Nanoparticles in the size range of 1-100 nm display unique and novel properties (Jeevanandam et al., 2018; Zia-ur-Rehman et al., 2018; Teulon et al., 2019). Nanoscale

materials exhibit their unique properties due to their high surface energy, large proportion of surface atoms, low level of imperfection, and spatial confinement (Bai et al., 2009). Nanoparticles have distinct advantages over bulk materials due to their surface plasmon light scattering, surface plasmon resonance (SPR), surface-enhanced Rayleigh scattering, and surface-enhanced Raman scattering (SERS) properties (Jain et al., 2007). Due to their unique features, nanoscale materials can be used as building blocks for various optoelectronics, electronics, chemical sensing, and biological applications (Ramanavicius et al., 2005).

Silver is recognized for its anti-microbial activity against a broad spectrum of pathogenic microorganisms (Mohanta et al., 2016b). Silver (Ag) has been used since ancient times for its medicinal properties and now the activity and application of silver nanoparticles (AgNPs) is being explored in medical research. Topical antimicrobial ointments and creams contain silver to prevent microbial infection of burns and open wounds. Silver is also commonly used in medical devices and implants that are manufactured with silver-impregnated polymers. In addition, several silver-containing consumer products, such as colloidal silver gel and silver-embedded fabrics, are now used in sporting equipment (Kim et al., 2007; Song and Kim, 2009).

The easiest and most convenient approach for the rapid synthesis of AgNPs, which has been used for decades, is by a chemical synthesis process. The chemical approach to AgNP synthesis, however, involves the use of several toxic reagents. As several metal nanoparticles, such as gold, platinum, and silver, are frequently used in ointments, creams, cosmetics, etc., that interface with human skin, methods of nanoparticle synthesis that have low toxicity and are eco-friendly need to be explored and developed (Nayak et al., 2015). Several biological approaches for the synthesis of metal nanoparticles have been proposed, including the use of microorganisms (Narayanan and Sakthivel, 2010) and plants (Mittal et al., 2013). Plant-mediated synthesis of nanoparticles is highly attractive as it requires less effort than maintaining and culturing microorganisms. Plants' biomolecules are natural and typically exhibit low toxicity to living cells which makes the use of plant metabolites in the synthesis of AgNPs favorable (Mittal et al., 2013).

Several reports pertaining to the plant-mediated synthesis of AgNPs have been published. These reports have demonstrated the efficiency of plant metabolites in the synthesis of bioactive AgNPs. Although plant-mediated synthesis of AgNPs has been demonstrated, it is important to note that each plant species has its unique composition of bioactive constituents. These plant secondary metabolites include flavonoids, phenolic compounds, glycosides, and sterols, which have been reported to be responsible for the reduction of silver ions to the elemental silver (Dauthal and Mukhopadhyay, 2016). Since plant species vary in the composition and quantity of secondary metabolites, a broad range of plant species should be examined for their ability and efficiency to biosynthesize metal nanoparticles. This exploration can be used to overcome biomedical constraints and other production-related problems. Synthesis of AgNPs using phyto-molecules may help to overcome the problems associated with toxic chemical reagents. The plant *Semecarpus anacardium* (family Anacardiaceae) is a well-known medicinal

plant in India. In the Ayurvedic system of medical treatment, different plant parts are commonly used as a medicine for alimentary tract impairments and certain dermatological problems. *S. anacardium* has a positive effect on blood pressure, cancer, and heart disease, as well as respiration and neurological disorders (Mohanta et al., 2007). *Glochidion lanceolarium* (family Phyllanthaceae) is an important ethnomedical plant used for the treatment of gastrointestinal complaints (Chanda et al., 2007) and *Bridelia retusa* (family Phyllanthaceae) exhibits pharmacologically potent antiviral, hypoglycemic, and immunomodulatory activity (Ghawate et al., 2015). The latter plant has also been reported to be effective in wound healing (Deore et al., 2014). The anticancer properties of these plants, however, have not been fully explored. Since many cancer drugs exhibit debilitating side effects and have a questionable impact on cancer cells, the use of natural medicines derived from natural sources should be urgently explored.

The management of public health is a major issue in the modern, industrial world, due to the rising pervasiveness of microbial resistance. Although numerous new antibiotics have been discovered and developed, multidrug-resistant bacteria are still becoming more prevalent and are creating a serious public health risk (Mohanty et al., 2017). Thus, there is a critical need to develop a new, powerful therapeutic approach to treat and kill Gram-negative, as well as Gram-positive, human pathogens. The biosynthesis and application of metal nanoparticles is now receiving great interest as a viable option due to its moderate success in being used to facilitate drug delivery (Zhang et al., 2008), treat chronic disease (Hong et al., 2008), and for its ability to treat bacterial infections in wounded tissues (Rai et al., 2009).

Comprehensive studies of antimicrobial resistance have revealed that bacterial infections that resist antibiotics are not due to free bacteria but rather to bacteria existing within a biofilm (Liu et al., 2019). Biofilm-forming bacteria are resistant to conventional antimicrobials due to: (1) the inability of the antimicrobial to penetrate the biofilm, (2) evolution complex drug resistance properties, and (3) biofilm mediated inactivation or modification of antimicrobial enzymes (Elbourne et al., 2019). Fortunately, nanoparticle-based antimicrobials have been developed and marketed to eradicate both planktonic and biofilm-forming antibiotic-resistant bacteria. Continuous research is being conducted to develop eco-friendly nanotechnologies utilizing natural phytochemicals to produce metal nanoparticle-based antimicrobials for the control of biofilm-forming pathogens.

In this regard, the objective of the current study was to explore the use of ethno-medicinally important plants, *S. anacardium*, *G. lanceolarium*, and *B. retusa* (Panda et al., 2016), for the synthesis of AgNPs utilizing secondary metabolites present in leaf extracts. The formation of AgNPs were monitored by microscopy and spectroscopy to evaluate the synthesis process, and the phytoconstituents most likely responsible for the synthesis of the AgNPs compounds were characterized using different qualitative tests. The phyto-mediated synthesized AgNPs were also screened for antibacterial and anti-biofilm activity against the human pathogens, *Pseudomonas aeruginosa*, *Escherichia coli* (Gram -ve),

and *Staphylococcus aureus* (Gram +ve) in order to assess their potential use in antimicrobial therapy.

MATERIALS AND METHODS

Chemicals and Reagents

The chemicals used during the experiments, such as Mueller Hinton medium and silver nitrate (AgNO_3), were purchased from Hi-media (India) and Sigma-Aldrich (India), respectively.

Microbial Strains and Plant Specimens

The bacterial strains of *P. aeruginosa* (MTCC 741), *E. coli* (MTCC 739), and *S. aureus* (MTCC 96) were used in the present study. The species were obtained from microbial type culture collection, IMTECH, Chandigarh, India and stored in the culture collection located in the Department of Botany, North Orissa University, India. The plants used for the phyto-assisted synthesis of AgNPs were collected from the Simlipal Biosphere Reserve, India. Before beginning the experiments, proper identification and deposition of plants were conducted in the Department of Botany, North Orissa University with allocation of voucher specimen numbers *S. anacardium* (NOU KL 024/2014), *G. lanceolarium* (NOU KL 085/2014), and *B. retusa* (NOU KL 080/2014).

Qualitative Phytochemical Analysis

The qualitative phytochemical analysis of *S. anacardium*, *G. lanceolarium*, and *B. retusa* extract was performed by following the standard method as reported by Arunachalam et al. (2012), with slight modifications. The obtained results were qualitatively expressed as positive (+) or negative (−) (Guruvaiah et al., 2012). The chemicals and reagents used in the study were purchased from Sigma-Aldrich (India).

Quantitative Phytochemical Analysis and *in vitro* Antioxidant Properties

Total Phenolic Content Determination

The total phenolic quantity, in the leaf extracts of *S. anacardium*, *G. lanceolarium*, and *B. retusa* were measured using the standard Folin–Ciocalteu method with required modifications (McDonald et al., 2001). All the experiments were performed in triplicate and the total phenolic content was expressed as gallic acid equivalent (GAE) in mg/g sample.

Total Flavonoids Content Determination

The total amount of flavonoids in the leaf extracts of *S. anacardium*, *G. lanceolarium*, and *B. retusa* was estimated by the standard aluminum chloride method with required modifications (Chang et al., 2002). All the estimations were carried out in triplicate and total flavonoid content was expressed as GAE in mg/g sample.

1,1-Diphenyl-2-Picryl-Hydrazil Radical Scavenging Activity

Potential antioxidant activity of leaf extracts of *S. anacardium*, *G. lanceolarium*, and *B. retusa* was determined using 1,1-diphenyl-2-picryl-hydrazil (DPPH) assay with required modifications

(McDonald et al., 2001). Various concentrations, such as 10, 20, 30, 40, and 50 mg/ml extracts, were taken for the study of DPPH scavenging activities. The results were expressed as percentage (%) radical scavenging activity. The minimum inhibitory concentration (MIC) was calculated and results were presented IC_{50} value. The equivalent concentrations of ascorbic acid were taken as a positive control.

Sample Preparation and Synthesis of Silver Nanoparticles

Fresh leaves were collected from healthy plants of *S. anacardium*, *G. lanceolarium*, and *B. retusa* growing in a hilly area of the Simlipal Biosphere Reserve, India. The plant leaves were thoroughly washed and then dried in a hot air oven. The dried leaves were then pulverized and passed through a 20-mesh sieve. Five gram of leaf powder were added to 50 ml of sterilized deionized water and sonicated for 15–20 min. The resulting mixture was filtered through Whatman's filter paper and maintained at 4°C until further use. Extracts were prepared from each of the species separately. The filtered leaf extracts were used to synthesize the AgNPs by adding 10 ml of extract to 90 ml of 1 mM AgNO_3 in an aqueous solution and incubating the resulting solution overnight at 60°C. A similar protocol was used for each of the plant extracts. The synthesis of AgNPs was monitored by UV–Vis spectrophotometry (Perkin Elmer-λ35) in the range of 350–600 nm.

Characterization of Silver Nanoparticles

The synthesized AgNPs were characterized using methods that have been previously described (Mohanta et al., 2016a). The size range and surface charge (Zeta) of dispersed NPs were determined using a Zeta sizer (Nano ZS90, Malvern Instruments Ltd, Malvern, United Kingdom). Attenuated total reflectance-Fourier transform infrared spectroscopy (ATR-FTIR, Bruker) analysis of spectra within the range of 500–4,000 cm^{-1} was conducted to determine the role of the phytoconstituents in NPs synthesis. Surface morphology was confirmed by observation of the synthesized AgNPs with a Field emission scanning electron microscope (FE-SEM; Jeol 6480LV JSM microscope, United States) operating at an acceleration voltage of 15 KV.

Antibacterial Activity and Minimum Inhibitory Concentration Evaluation of AgNPs

The different species of pathogenic bacteria were cultured in Mueller Hinton Broth (MHB) to determine the MIC of the synthesized AgNPs. Cell suspensions of each organism were adjusted to attain the required cell numbers per ml by measuring the turbidity of cell suspensions in a spectrophotometer (Perkin Elmer, Lambda35, Germany). The antimicrobial assay was conducted in 96-well microtiter plate using a two-fold serial dilution of AgNPs to determine 50% inhibition of microbial growth. Standard broth (MHB) was used according to the Clinical and Laboratory Standards Institute (CLSI) guidelines (Clinical, and Laboratory Standards Institute, 2005). In addition

to the synthesized AgNPs, the extracts from the respective plants were also assayed for antimicrobial activity. A standardized concentration of each test organism was obtained by adjusting the turbidity of each suspension culture to an OD = 0.003 at 600 nm (~100-fold dilution of parent culture). For the assay, 190 μ l of the test-adjusted cell suspension of an organism and 10 μ l of different concentrations (μ g/ml) of the AgNPs were added to wells of a microtiter plate. The same protocol was used to assay the plant extracts and the antibiotic Gentamycin, the latter of which was used as a positive control. To correct for the absorbance of the AgNPs or plant extracts, control wells were used containing 190 μ l MH broth (devoid of organisms) and 10 μ l of AgNPs or plant extract. The plates were wrapped with parafilm and incubated after a thorough mixing of the components. The MICs of AgNPs were expressed as an IC₅₀ value. All experiments were carried out in triplicate and the mean \pm standard deviation was calculated.

Anti-biofilm Activity and Minimum Inhibitory Concentration Determination for the AgNPs

A 96-well microtiter plate (flat bottom, polystyrene) was used to determine the anti-biofilm activity of the AgNPs as described by Gurunathan et al. (2014) and Barapatre et al. (2016). Individual wells of the plates were filled with 180 μ l of Muller Hinton Broth and 10 μ l of the test pathogens (OD = 1.0, 600 nm) were added. Subsequently, 10 μ l of AgNPs were added and the preparation was thoroughly mixed. A two-fold dilution series of the AgNPs was used to determine the MIC of AgNPs against biofilm formation. The same was used to test the anti-biofilm activity of the plant extracts and to determine their MIC. After completing the preparation of the test plates, they were incubated in a static condition for 24 h at 37°C. Mixtures without bacteria were used to adjust the OD for absorbance by the extract components. After incubation, the contents of the wells of the microtiter plates were discarded and gently washed with phosphate buffered saline (PBS, pH 7.2) to remove free-floating non-adherent bacterial cells from the walls and bottom of the wells. The wells of the microtiter plates were then air dried for 45 min. After drying, adherent “sessile” bacteria in the wells were fixed with 2% w/v sodium acetate and the wells were then flooded with crystal violet stain (0.1%, w/v) and incubated in the dark for 30 min. Afterward, the wells were thoroughly washed with sterile deionized water until all excess dye was removed. The plates were then air dried again. After complete drying, 200 μ l of ethanol (95%, v/v) was added to each well and absorbance at 620 nm was measured (Multi-scan plate reader, Thermo Fisher scientific). The percentage of inhibition of biofilm formation was calculated using following equation:

$$\% \text{ biofilm inhibition} = [1 - (\text{OD}_{620} \text{ of cells treated with Ag NPs or plant extracts} / \text{OD}_{620} \text{ of the non - treated control}) \times 100]. \quad (1)$$

All assays were conducted in triplicate and mean \pm standard deviation was calculated. The MIC for anti-biofilm potential was expressed as an IC₅₀.

Synergistic Antibacterial and Antibiofilm Activity

The synergistic antibacterial and antibiofilm activity was studied by taking different combinations of pure leaf extract and as-synthesized AgNPs from *S. anacardium*, *G. lanceolarium*, and *B. retusa* following the microbroth dilution method and microtiter plate anti-biofilm assay, respectively.

RESULTS AND DISCUSSION

Qualitative and Quantitative Phytochemicals Assessment and Their Antioxidant Activities

The qualitative and quantitative phytochemical examinations of the aqueous leaf extracts are summarized in Tables 1, 2. The qualitative phytochemical analysis revealed the existence of alkaloids, flavonoids, tannins, phenolic, proteins, and saponins in all three plants (*S. anacardium*, *G. lanceolarium*, and *B. retusa*) but resin, steroids, and sterols were not detected. Glycoside

TABLE 1 | Qualitative phytochemical screening of aqueous extract.

Name of the phytoconstituents	Observation		
	<i>S. anacardium</i>	<i>G. lanceolarium</i>	<i>B. retusa</i>
Alkaloids	+	+	+
Tannins and phenolic compounds	+	+	+
Glycoside	+	–	–
Flavonoids	+	+	+
Steroids and sterols	–	–	–
Triterpenoids	+	+	+
Sugars	–	–	+
Resins	–	–	–
Proteins	+	+	+
Saponins	+	+	+

+, present; –, absent.

TABLE 2 | Quantitative phytochemical constituents of aqueous extract.

Phytochemical constituent	mg/100 g dry weight (Mean \pm SD)		
	<i>S. anacardium</i>	<i>G. lanceolarium</i>	<i>B. retusa</i>
Total phenol content	545.57 \pm 25.00	330.57 \pm 26.00	410.25 \pm 22.15
Total flavonoid content	840.76 \pm 24.10	510.76 \pm 25.10	714.76 \pm 25.10

was present only in *S. anacardium* extract, whereas sugar was found in *B. retusa*. The phytochemical study of the leaf extract of these three plants showed that flavonoids, tannins, phenolic compounds, proteins, and saponins were present in the extract, which may be the principal chemical constituents responsible for the synthesis of AgNPs. Shankar et al. (2003) reported the possible role of terpenoids from *Geranium* leaf in the synthesis of nano-sized Ag particles. Polyols such as terpenoids, flavones, and polysaccharides in the *C. camphora* leaf were reported to be the main cause of the bio-reduction of silver and chloraurate ions (Huang et al., 2007). The quantitative phytochemical results supported the possibility of a greater potential for antioxidant activity (Table 2). The plant extract possesses huge potential for providing natural chemicals for the reduction of complex metals to derive respective nanoparticles for diverse important applications.

The antioxidant potential in terms of DPPH radical scavenging activity of *S. anacardium*, *G. lanceolarium*, and *B. retusa* positively responded toward the possible involvement of the antioxidant molecules from the leaf extract during the synthesis of AgNPs. It is well known that plants have a large repository of phenolics and flavonoids molecules which have super antioxidant capacity and are considered to be strong free radical scavengers. The DPPH radical scavenging result (Figure 1) revealed the antioxidant potentials of aqueous leaf extracts of three ethnomedicinally important plants. The percentage (%) DPPH scavenging activity (IC₅₀) was found to be 16.98 ± 0.12 μ g/ml, 30.71 ± 0.22 μ g/ml, and 22.66 ± 0.25 μ g/ml for *S. anacardium*, *G. lanceolarium*, and *B. retusa*, respectively. The presence of a significant concentration of total phenolics and flavonoids in *S. anacardium*, *G. lanceolarium*, and *B. retusa* leaves indicated a notable antioxidant activity. Previous research revealed that the high molecular weight and the adjacency aromatic rings and hydroxyl groups are more focused in the

free radical scavenging activity of bioactive phyto-compounds (Hagerman et al., 1998; Luximon-Ramma et al., 2002; Pratap Chandran et al., 2013). The antioxidant activities were highly correlated with the total phenolic and flavonoids levels. It is also essential to evaluate the antioxidant potential as some of the plant molecules still remain with AgNPs post-purification as a capping and stabilizing agent, which should not be harmful to normal cells during the cellular application of the nanoparticles. Thus, the antioxidant potential of *S. anacardium*, *G. lanceolarium*, and *B. retusa* established that the green synthesis process of AgNPs is highly safe for biomedical applications.

Synthesis and Characterization of AgNPs

The growing increase in microbial resistance to both currently available and newly developed antibiotics is a worldwide problem. Therefore, it is imperative that researchers identify and develop new methods to deal with antibiotic-resistant microbial pathogens, as well as the ever-growing appearance of new, virulent pathogens (Veerasamy et al., 2011). Currently, there is significant interest in the development of nanoparticles-based antibacterial agents to address the critical health problems brought about by the rapid evolution of drug-resistant microorganisms.

Silver has been recognized as an anti-infection agent since ancient times. Extensive research has been conducted on silver ions and silver conjugated salts as potential antimicrobial and anti-biofilm agents. Although silver has been used as a therapeutic agent, silver ions exhibit a level of toxicity and have low efficacy due to their inactivation caused by easily complexing with other molecules and their precipitation with other interfering salts (Mohanty et al., 2017). New strategies to address these problems are being explored, such as the use of leaf extracts of ethnomedicinal plants to synthesize AgNPs in a cost effective, bio-compatible, and eco-friendly manner.

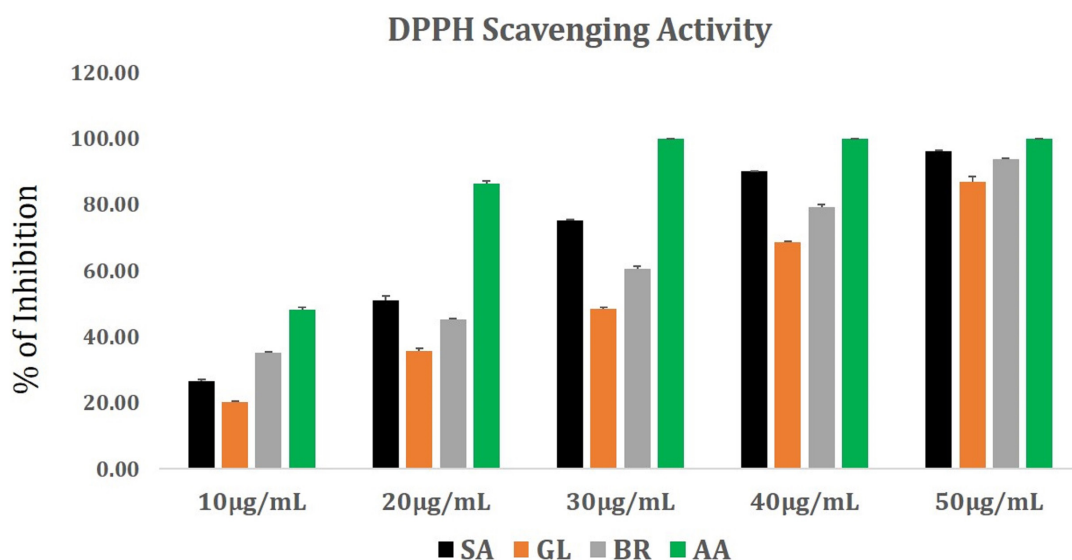


FIGURE 1 | DPPH radical scavenging activity of plant extracts from *G. lanceolarium* (GL), *S. anacardium* (SA), *B. retusa* (BR). Ascorbic acid (AA) is taken as standard.

The primary objective of the current study was to synthesize small-sized AgNPs using leaf extracts of the medicinal plants, *S. anacardium*, *G. lanceolarium*, and *B. retusa*, as a reducing, stabilizing, and capping agent. Silver nitrate (1 mM) was added to leaf extracts obtained from these plants and incubated overnight (60°C, pH 7.5) to regulate the size of particles. Successful synthesis of AgNPs was confirmed by visual observation of a color change of the solution, in which the pale-yellow color of the mixture of leaf extract and AgNO₃ turned to a deep brown color. No color change was observed in control mixtures consisting of just leaf extracts and sterile, deionized water. The appearance of a deep brown color indicates the formation of AgNPs (Gurunathan et al., 2014).

Prior to determining the antimicrobial activity of the AgNPs, a detailed characterization of the synthesized AgNPs was conducted using methods described in our previous publications (Mohanta and Behera, 2014; Mohanta et al., 2017a,b). UV-visible spectroscopy is an established method for the study of metal nanoparticles. We used UV-Vis spectrophotometric analysis to monitor the continuous synthesis of AgNPs. A strong and broad peak within the 420–430 nm range was frequently observed, which is the peak range characteristic for AgNPs (Figure 2). This unambiguous and characteristic peak is created due to the SPR of the particles, a characteristic that has been widely established and recognized for different metal nanoparticles in the 2–100 nm size range (Nayak et al., 2015). Notably, the nanoparticles were synthesized by the addition of 10 ml of leaf extract to 90 ml of a solution of AgNO₃.

The color of the reaction mixture turned from a pale yellow to a deep brown after an appropriate length of incubation, indicating the formation of AgNPs. It is believed that the change in color of the reaction mixture is due to the presence of specific phytochemicals in the leaf extract, suggesting that the reducing power of the phytoconstituents is responsible for the synthesis of the AgNPs. If so, this represents a novel, eco-friendly approach to the synthesis of metal nanoparticles. The absorption peak

characteristic of AgNPs was clearly detected due to the combined vibration of the electrons of AgNPs being in resonance with the specific wavelengths of light. The distinct and single SPR band at 420–430 nm confirms the reduction of Ag⁺ to Ag⁰. Similar observations have been made in studies on the synthesis of AgNPs (Krishnaraj et al., 2010; Gopinath et al., 2012; Iravani and Zolfaghari, 2013).

Particle Size Distribution and Surface Charge Analysis of AgNPs

It was important to determine the particle size and charge of the synthesized AgNPs in aqueous solution prior to assessing their antimicrobial and anti-biofilm activity. Particle size, surface charge, morphology, and particle composition are the major factors that determine the *in vitro* toxicity of AgNPs (Bhanumathi et al., 2017). A dynamic light scattering spectroscopy (DLS) analysis was conducted to measure particle size and charge in an aqueous solution. This technique allows for the rapid determination of particle size distribution and surface charge of nanoparticles in solution (Lim et al., 2013). Results of the DLS analysis revealed that the average particle sizes of the AgNPs synthesized from the three plant extracts were 62.72, 93.23, and 74.56 nm for *S. anacardium* (SA-AgNPs), *G. lanceolarium* (GL-AgNPs), and *B. retusa* (BR-AgNPs), respectively (Figures 3A–C). Particle sizes <100 nm have greater potential in biomedical applications, as the type of interaction that occurs between nanoparticles and cells is highly dependent on the size of the nanoparticle. Surface charge is another crucial aspect of nanoparticles that affects their ability to associate with or complex with macromolecules present on the surface or inside cells. Thus, the charge or Zeta potential of the AgNPs synthesized using the three different plant extracts was assessed to determine their potential to interact with biological macromolecules. Results indicated a charge of -19.9, -24.6, and -21.3 mV for the AgNPs synthesized using extracts of *S. anacardium*, *G. lanceolarium*, and *B. retusa*, respectively (Figures 2A–C). Several studies have been previously reported on the particle size and charge of AgNPs that support our results (Guruvaiah et al., 2012; Gurunathan et al., 2014; Chung et al., 2016).

Scanning Electronic Microscopic Analysis

Scanning Electronic Microscope (SEM) is an invaluable tool for obtaining structural information about nanoparticles and was therefore used to characterize the size and morphology of the AgNPs synthesized in the present study. Results obtained from the analysis of SEM micrographs of the synthesized AgNPs indicated that the synthesized nanoparticles were distinct, uniform in shape, spherical, and well-separated. The average size of the particles ranged between 52 and 96 nm (Figures 4a–c).

ATR-FTIR Analysis

The spectra obtained with Attenuated total reflectance Fourier transform infrared spectroscopy (ATR-FTIR) was used to classify the functional groups of the phytoconstituents present in the leaf extracts, which were potentially involved in the synthesis

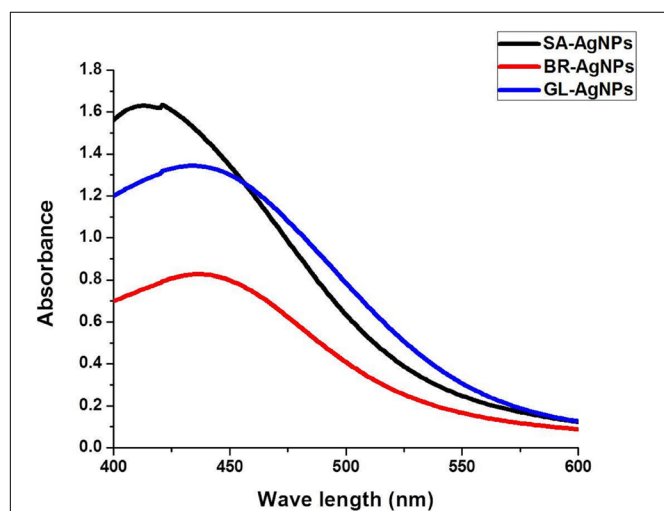
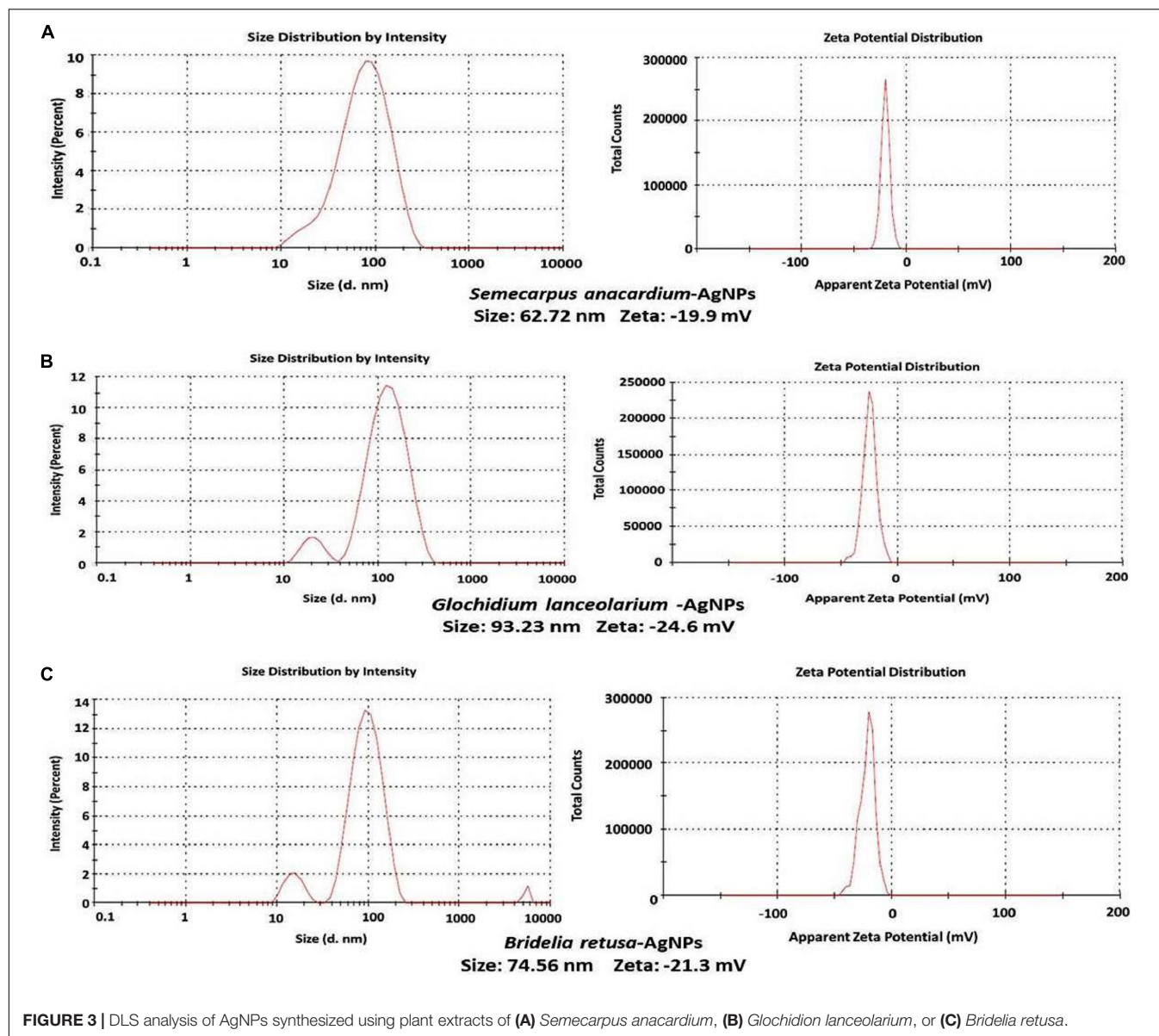


FIGURE 2 | UV-Vis spectrophotometric analysis of silver nanoparticles.

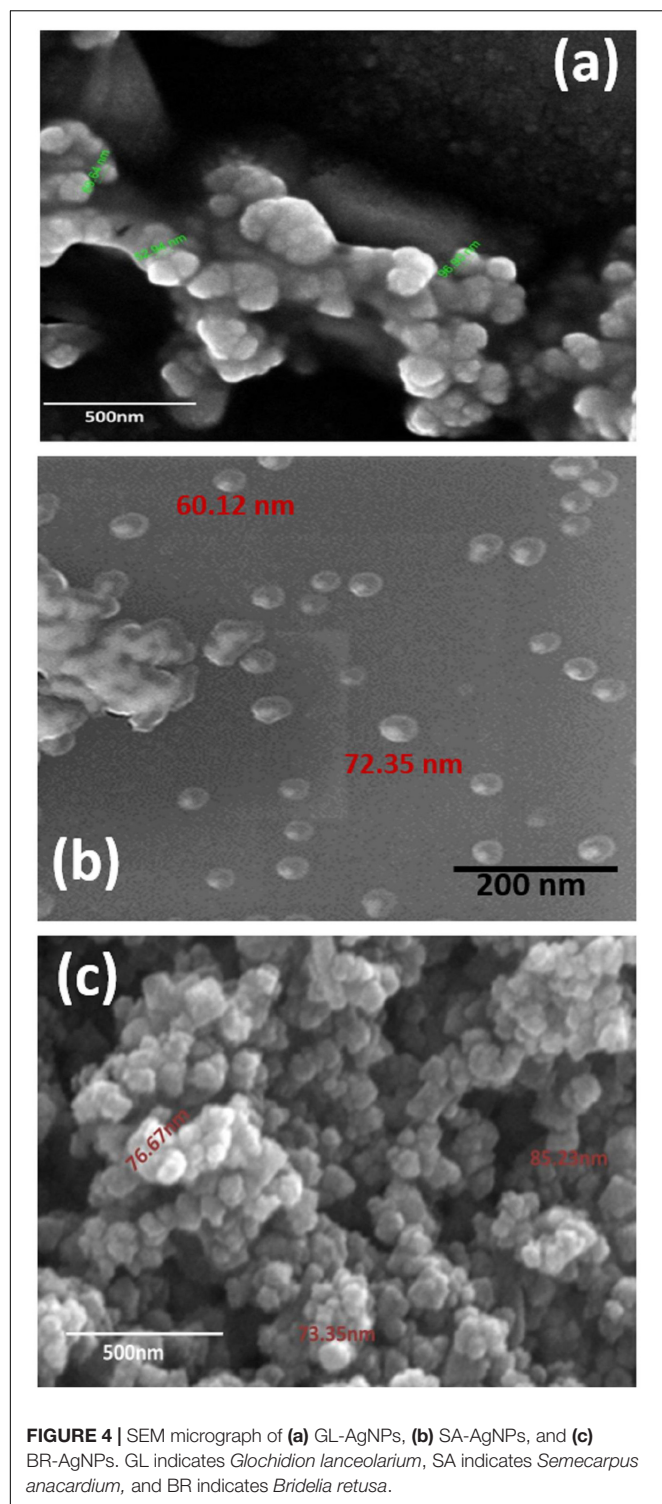


and stabilization of the synthesized silver nano-particles. The interaction of AgNPs with the phytoconstituents present in the leaf extracts of all three plant species exhibited intense peaks at 3735.93, 2247.27, 1537.60, 1717.06, and 570.99 cm^{-1} (Figure 5). A strong absorption peak at 3735.93 cm^{-1} strongly suggests the binding of silver ions with the hydroxyl ($-\text{OH}$) group stretching from water and the broad spectrum at 2247.27 cm^{-1} indicates a strong stretching of $-\text{C}\equiv\text{N}$ (nitrile) group. The other three bands (~ 1717.06 , 1537.60, and ~ 570.99 cm^{-1}) were due to stretching vibrations of $\text{C}=\text{O}$ (ketone), $\text{C}=\text{O}$ (amide), and $\text{C}-\text{I}$ functional groups. $\text{C}=\text{O}$ (ketone) and $\text{C}=\text{O}$ (amide) are generally present in proteins involved in the reduction of metal ions. These data suggest that hydroxyl and carbonyl groups may be responsible for the synthesis and stabilization of AgNPs. The IR data revealed that the compounds present in the leaf extract were present as a layer over the phyto-synthesized AgNPs and act as a stabilizing

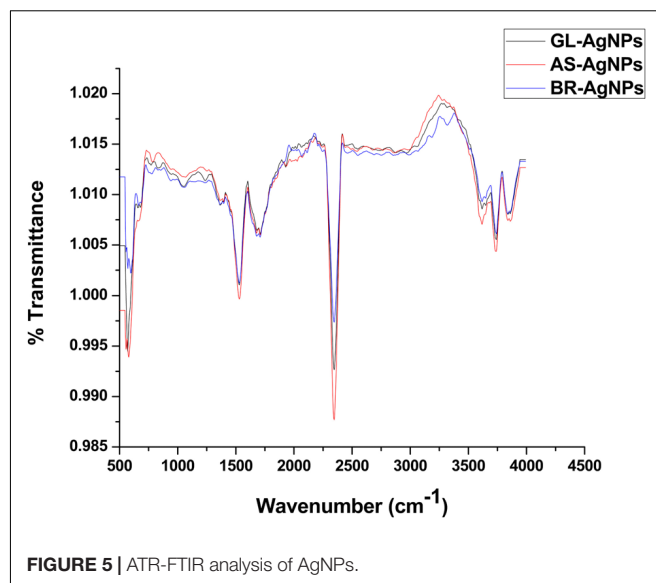
agent. Structural mechanism reveals that via Free amine groups or cysteine residues in the saponins, phenolics and quinones present in the leaf extracts have the ability to bind to the AgNPs and stabilize them through the surface-binding of a variety of plant compounds (Pant et al., 2012; Saranyaadevi et al., 2014).

Antibacterial Activity of AgNPs

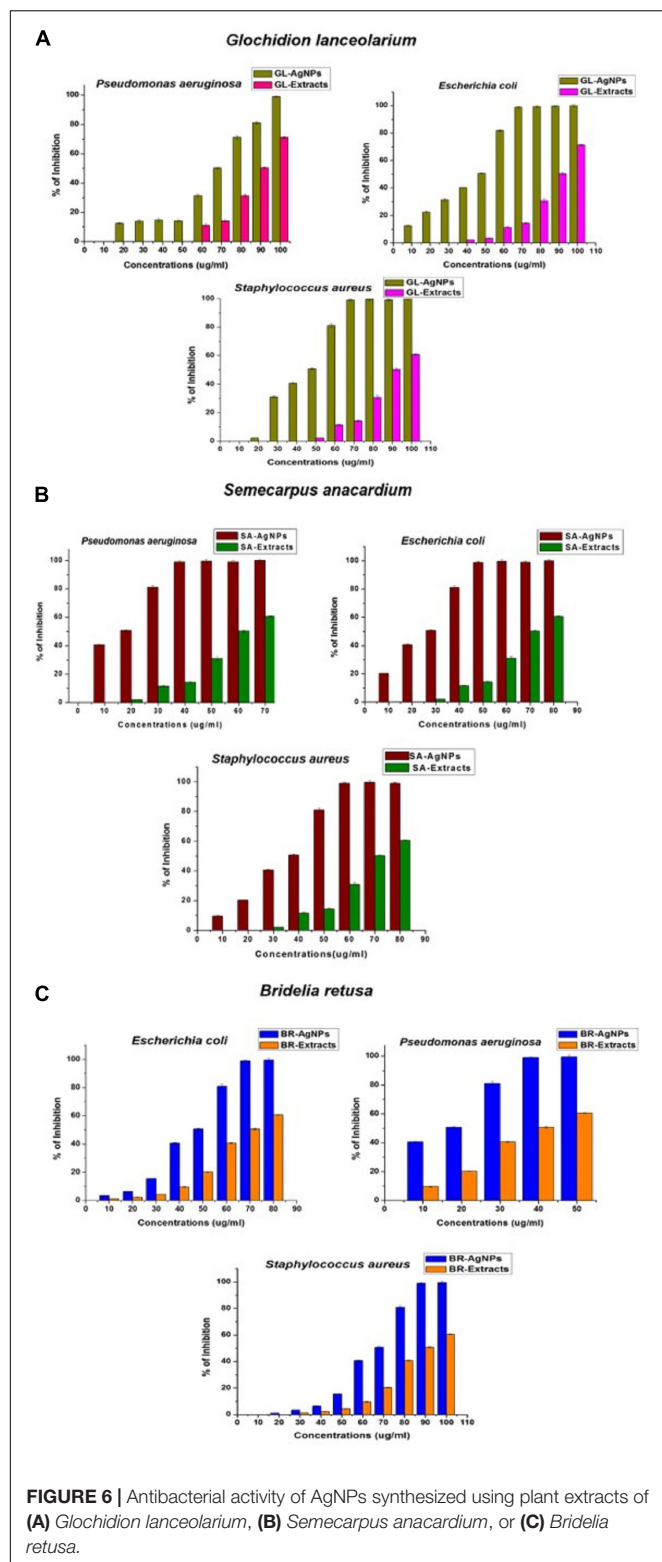
The bactericidal activity of AgNPs synthesized using the three different plant extracts was determined against Gram-positive and Gram-negative bacteria and revealed a dose-dependent relationship. Figure 6 illustrates the toxic activity of the plant synthesized AgNPs <100 nm at different concentrations (10–100 $\mu\text{g/ml}$) against the Gram-positive bacterium, *S. aureus*, and the Gram-negative bacteria *P. aeruginosa* and *E. coli*. Results indicate that the plant synthesized AgNPs can inhibit bacterial growth *in vitro*, relative to the growth of non-treated



bacteria or the negative control. These data further indicate that the inhibition of bacterial growth increases with increasing concentrations of the AgNPs. Each species of bacteria was inhibited in their growth at their respective MIC value. The MIC values of the AgNPs synthesized from the three different plant extracts were calculated for each bacterial species. AgNPs



exhibited excellent MIC (IC_{50}) values against the different species irrespective of the source plant that was used in their synthesis. The MICs (IC_{50}) of AgNPs synthesized using the leaf extract of *G. lanceolarium* was $43.94 \pm 0.2 \mu\text{g/ml}$, $68.6 \pm 0.5 \mu\text{g/ml}$, and $44.02 \pm 0.3 \mu\text{g/ml}$ against *S. aureus*, *P. aeruginosa*, and *E. coli*, respectively. Concentrations of $70 \mu\text{g/ml}$ (*S. aureus*), $100 \mu\text{g/ml}$ (*P. aeruginosa*), and $80 \mu\text{g/ml}$ (*E. coli*) resulted in $>99\%$ inhibition (Figure 6A). Similar results were observed with AgNPs synthesized with *S. anacardium* plant extract. The MICs (IC_{50}) of these AgNPs were $33.77 \pm 0.2 \mu\text{g/ml}$, $12.9 \pm 0.2 \mu\text{g/ml}$, and $23.49 \pm 0.2 \mu\text{g/ml}$ for *S. aureus*, *P. aeruginosa*, and *E. coli*, respectively. *S. anacardium* derived AgNPs exhibited $>99\%$ inhibition at concentrations of $60 \mu\text{g/ml}$ (*S. aureus*), $40 \mu\text{g/ml}$ (*P. aeruginosa*), and $50 \mu\text{g/ml}$ (*E. coli*) (Figure 6B). AgNPs synthesized using *B. retusa* plant extract also exhibited strong antibacterial activity against the test pathogens exhibiting MICs of $64.13 \pm 0.3 \mu\text{g/ml}$ (*S. aureus*), $12.90 \pm 0.2 \mu\text{g/ml}$ (*P. aeruginosa*), and $43.94 \pm 0.2 \mu\text{g/ml}$ (*E. coli*). AgNPs synthesized with *B. retusa* plant extract exhibited $>99\%$ inhibition at 90, 50, and $70 \mu\text{g/ml}$, against *S. aureus*, *P. aeruginosa*, and *E. coli*, respectively (Figure 6C). A comparison of the obtained inhibitory activity indicated that AgNPs synthesized using *G. lanceolarium* plant extract were more active against the Gram-positive bacterium (*S. aureus*) while the AgNPs synthesized using *S. anacardium* or *B. retusa* plant extracts exhibited stronger antibacterial activity against the Gram-negative bacteria, *P. aeruginosa* and *E. coli*. Although, AgNPs derived from plant extracts of all three plant species inhibited both Gram positive and Gram-negative bacteria. AgNPs derived from *S. anacardium* plant extract had the strongest antibacterial activity and was active against both types of bacteria. Therefore, we suggest that *S. anacardium* plant extracts have the potential to be commercially used to synthesize AgNPs $<100 \text{ nm}$. Apart from the antibacterial activity of the derived AgNPs, *S. anacardium* is also an important medicinal plant, containing alkaloids and polyphenols with high medicinal value, which



further strengthens its value in the production of bioactive nanoparticles. The individual plant extracts were also separately analyzed for bactericidal activity to compare their activity with the activity of AgNPs synthesized from their respective plant

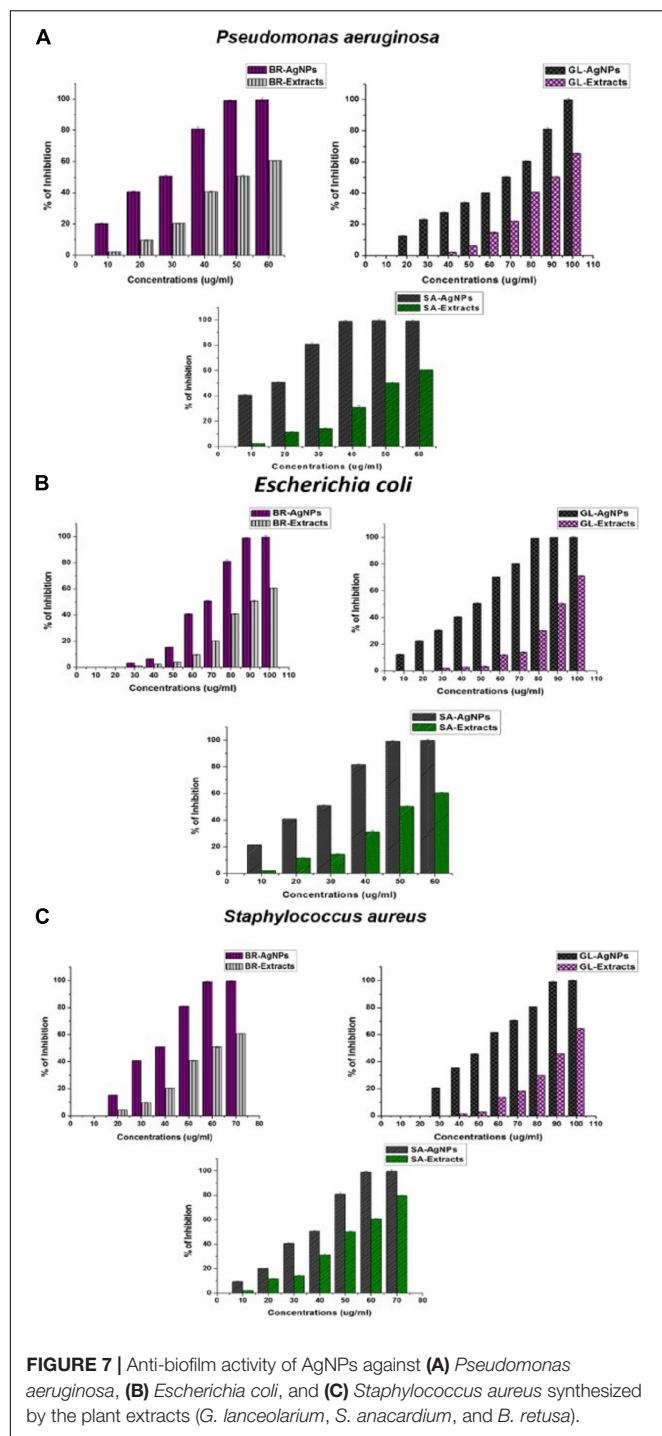
extracts. Results indicated that all of the plant-extract-derived AgNPs have greater antibacterial activity than the use of their respective plant extracts alone, further confirming the values of using plant-derived AgNPs as antibiotic compounds against human bacterial pathogens.

The AgNPs synthesized using plant extracts exhibited significantly greater antibacterial activity than AgNPs synthesized from other sources, such as bacteria, fungi, algae, etc. Multiple reports support the use of AgNPs as antibacterial agents (Rai et al., 2009; Ahmad et al., 2015; Kotakadi et al., 2015; Abbasi et al., 2016; Nayak et al., 2016) and several mechanisms have been proposed regarding the antibacterial activity of AgNPs. Earlier studies by Sondi and Salopek-Sondi (2004) focused on the interaction of AgNPs with *E. coli* and confirmed that at the first stage of interaction, AgNPs attach to the bacterial cell wall. After stable adherence, AgNPs penetrate the bacterium and induce cell death by rupturing the cell membrane. AgNPs acting as oxidizing agents on the surface of proteins present on the plasma membrane and cellular homeostasis have also been suggested as the mechanism underlying AgNP antibacterial activity. Another suggestion is that AgNPs attach to the cell membrane surface and decrease its permeability and respiration. The current study, although supportive of all the proposed mechanisms, confirms that the bactericidal activity involves the uptake of AgNPs. Notably, plant-synthesized AgNPs have an added advantage over chemically synthesized AgNPs due to the ability of plant metabolites to function as capping and stabilizing agents, as well as exhibiting their own antibacterial activity, which collectively enhances the antibacterial activity of AgNPs.

Anti-biofilm Activity of AgNPs

Silver nanoparticles have also been assayed for anti-biofilm activity against biofilm-forming bacteria. In the present study, the *in vitro* anti-biofilm activity of AgNPs was evaluated in a dose-dependent manner against the biofilm-forming bacteria *P. aeruginosa*, *E. coli*, and *S. aureus*. The individual species of bacteria were grown in 96-well microtiter plates for 24 h and then treatments of 10–100 µg/ml of the individually synthesized AgNPs were added to each well. Results of the assay revealed that the biosynthesized AgNPs inhibited biofilm formation by the bacterial species, relative to the negative control used in the experiment (Figures 7A–C). The MICs of anti-biofilm activity was expressed in terms of IC₅₀ and all AgNPs, irrespective of which extract was used in their synthesis, exhibited an excellent MIC value against bio-film formation.

Treatment of *P. aeruginosa* for 24 h with AgNPs (100 µg/ml) synthesized using *G. lanceolarium* plant extract, reduced biofilm formation by >99%. Similarly, AgNPs derived from *S. anacardium* and *B. retusa* at a concentration of 50 and 60 µg/ml, respectively, reduced biofilm formation by >99%. The MIC (IC₅₀) of AgNPs needed to inhibit biofilm formation were 68.94 ± 0.2 µg/ml, 12.9 ± 0.2 µg/ml, and 23.48 ± 0.2 µg/ml for AgNPs derived from *G. lanceolarium*, *S. anacardium*, and *B. retusa*, respectively. AgNPs derived from *S. anacardium* plant extract exhibited potent inhibition of biofilm formation at a very low IC₅₀ value. AgNPs derived from *B. retusa* also exhibited high levels of inhibition of biofilm formation against *P. aeruginosa*.



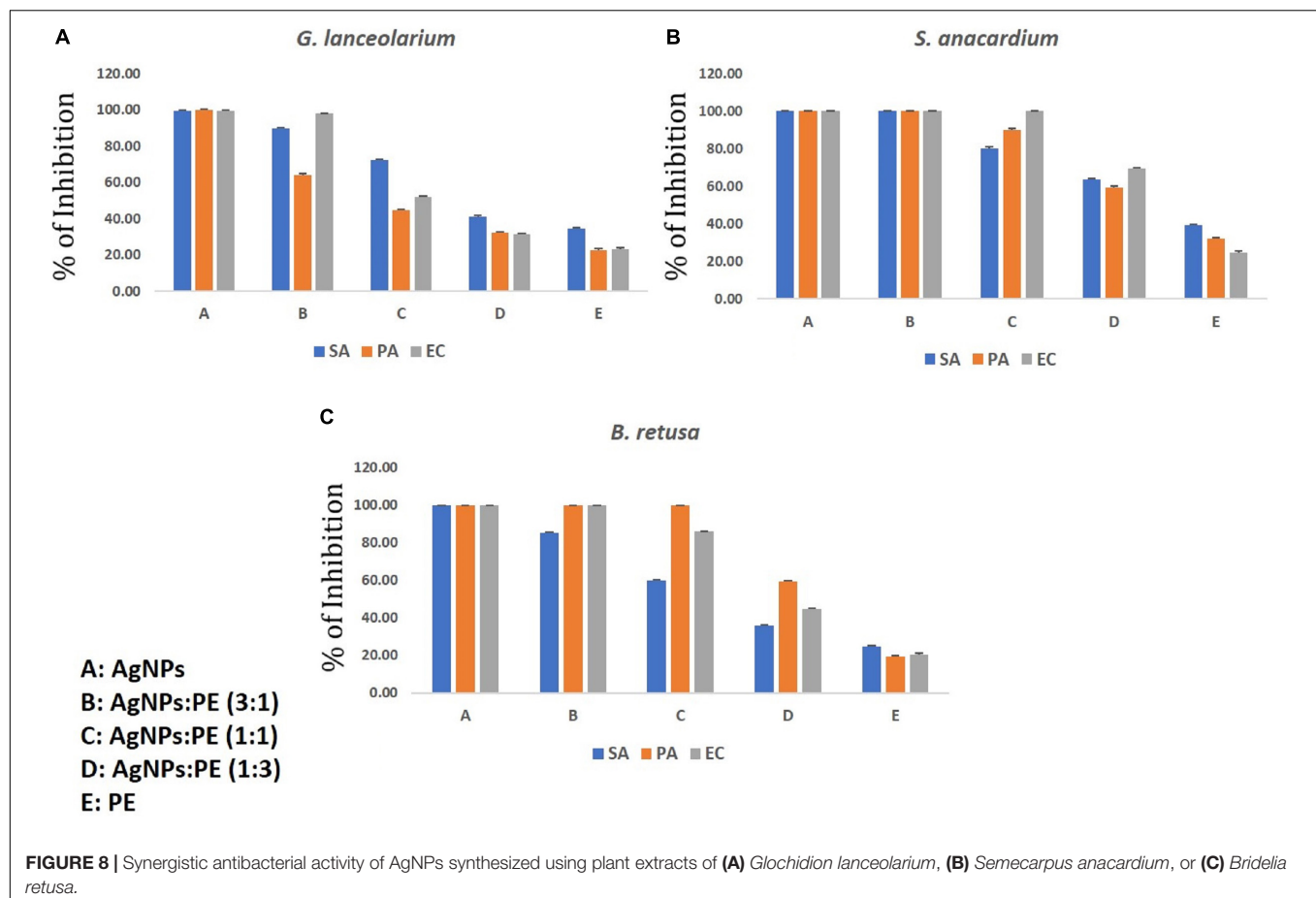
Notably, the AgNPs derived from all three plant sources exhibited anti-biofilm activity against *E. coli*. concentrations of 80, 50, and 100 µg/ml. AgNPs derived from *G. lanceolarium*, *S. anacardium*, and *B. retusa*, respectively, exhibited >99% inhibition against biofilm formation by *E. coli*, a Gram-negative bacterium. MIC (IC_{50}) values of 45.5 ± 0.2 µg/ml, 23.42 ± 0.15 µg/ml, and 64.14 ± 0.3 µg/ml were calculated for the AgNPs derived from *G. lanceolarium*, *S. anacardium*, and *B. retusa*, respectively.

In the case of the Gram-positive bacterium, *S. aureus*, >99% inhibition was evident at 90 µg/ml (*G. lanceolarium*), 60 µg/ml (*S. anacardium*), and 60 µg/ml (*B. retusa*). The AgNPs derived from both *S. anacardium* and *B. retusa* greatly inhibited biofilm formation by *S. aureus*. The AgNPs also exhibited potent antibiofilm activity against *S. aureus* with a calculated MIC (IC_{50}) of 52.54 ± 0.1 µg/ml (*G. lanceolarium*), 33.77 ± 0.2 µg/ml (*S. anacardium*), and 32.67 ± 0.15 µg/ml (*B. retusa*). The AgNPs derived from *S. anacardium* and *B. retusa* exhibited the best anti-biofilm activity against *S. aureus*.

Limited research has been conducted on the anti-biofilm activity of AgNPs. The formation of bacterial biofilms is the result of the synthesis and secretion of exopolysaccharides (EPSs) by bacterial cells, a prerequisite for biofilm formation (Landini et al., 2010). The bacteria respond to environmental cues that induce the synthesis of EPS. As a result, if the formation of EPS can be inhibited or prevented, then biofilm formation will also be restricted. This premise was the basis of our assay on the anti-biofilm activity of AgNPs. Kalishwaralal et al. (2010) previously reported the anti-biofilm activity of biosynthesized AgNPs against *P. aeruginosa* and *S. epidermidis*. In that study, AgNPs of 100 nm in size exhibited inhibited biofilm formation by 95–98%. Gurunathan et al. (2014) also studied anti-biofilm capacity of AgNPs against four human pathogens: *P. aeruginosa*, *Shigella flexneri*, *S. aureus*, and *Streptococcus pneumoniae*. They reported high levels of anti-biofilm activity by AgNPs of a particle size < 100nm. Ansari et al. (2013) also investigated the anti-biofilm activity of AgNPs and clearly demonstrated that the inhibition of EPS synthesis was directly proportional to anti-biofilm activity. Park et al. (2010) studied the antibiofilm activity of AgNPs against *P. aeruginosa* and proposed that biosorption may be the major factor responsible for the inactivation of biofilm formation. Goswami et al. (2015) also reported on biofilm eradication by AgNPs and found that the use of 15 mg/ml of AgNPs resulted in an 89% inhibition of biofilm formation in *S. aureus* and 75% in *E. coli*. Results of the present research confirm the efficacy of AgNPs against biofilms produced by the Gram-negative bacteria, *P. aeruginosa* and *E. coli*, and the Gram-positive bacterium, *S. aureus*, at reasonably low concentrations. The current results also revealed that the tested bacteria are highly sensitive to GL-AgNPs, BR-AgNPs, and SA-AgNPs, suggesting that the complex biofilm signaling mechanism could also be associated with cell survival. Recently, research has been conducted on conjugating the antibiotic, rifampicin, with chemically synthesized AgNPs for use in combatting biofilm formation by methicillin resistant *S. aureus* and *Klebsiella pneumoniae* (Farooq et al., 2019).

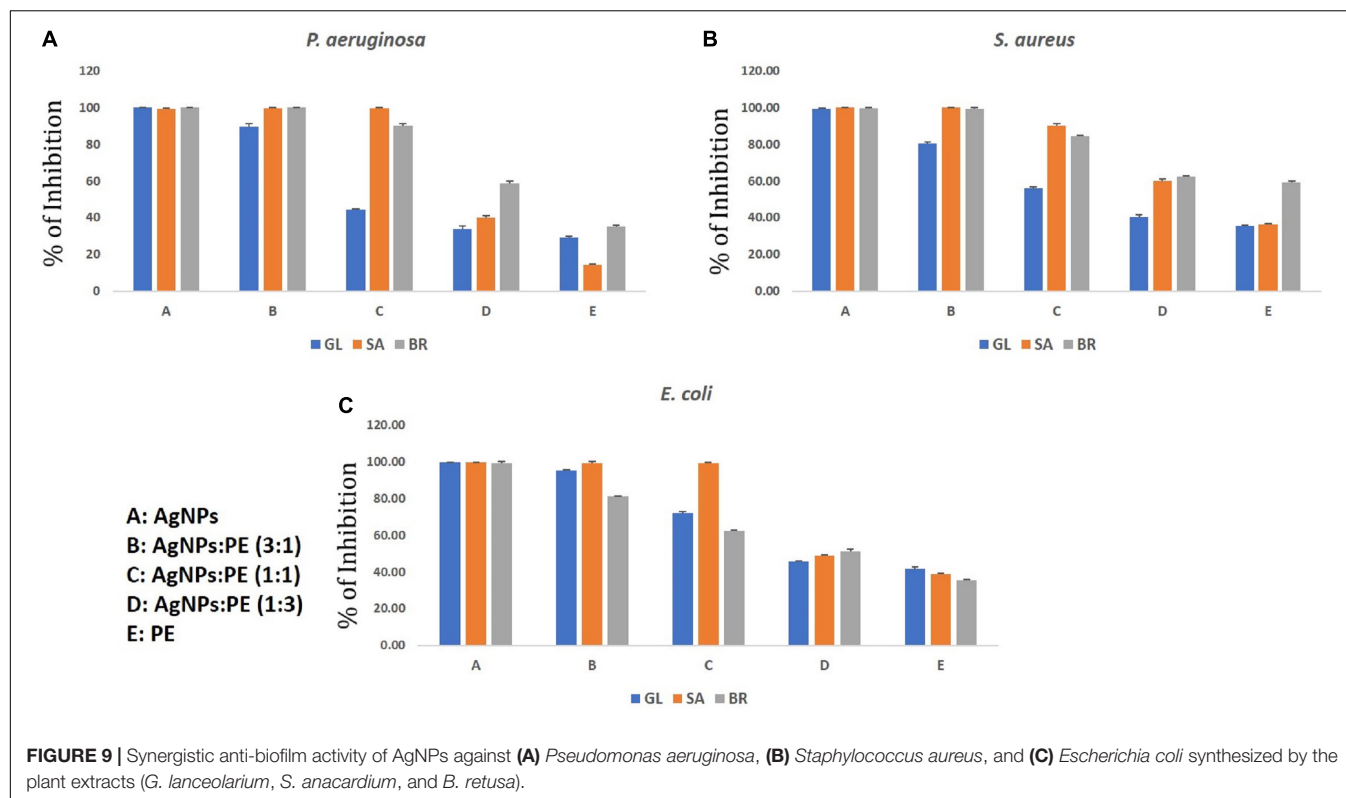
Synergistic Potential of Antibacterial and Antibiofilm Activity

The individual studies of antibacterial and antibiofilm activities on plant extract and synthesized AgNPs from the respective plant extracts have shown they have the reducing capacity to form respective bioactive AgNPs. The main aim of the synergistic activity study was to understand the possible



combinatorial potentiality of the AgNPs and plant extract to control the biofilm formation by the pathogenic organisms. As discussed, the plant constituents having a reducing capacity if silver metallic salts are involved and attached to the AgNPs to stabilize the particles. During the synergistic study, the different ratios of synthesized AgNPs and plant extracts were mixed and applied for the antibacterial and antibiofilm activities and measured in terms of the percentage (%) of inhibition against the microorganisms taken for the study. The synergistic results are quite relevant to the results of the individual results, but overall synergistic potentiality was not that accountable what the individual activities were shown by AgNPs. Hence the current results of the synergistic activity are not recommended for practical applications. The results of both AgNPs and respective plant extracts synergistically are depicted in Figures 8, 9. The total concentration of the test samples were kept at 100 µg/ml and made the same with AgNPs and plant extracts with different ratios and tested against the test strains. Overall, the synthesized AgNPs alone have greater potential than the addition of respective plant extracts for controlling bacterial growth and biofilm formations. It can be assumed that when the concentration of the raw plant extract was increased, the antibacterial and antibiofilm activity was reduced due to the presence of some microbial growth promoting plant constituents in the extract. On the

contrary, when the plant-synthesized AgNPs were applied, the results were highly significant for the purpose of the current study which revealed that the limited bioactive phytoconstituents with silver was highly active for the real world application in controlling the bacterial contaminations. In the antibacterial activity of GL-AgNPs (Figure 8A), it showed a greater potential effect against *S. aureus*, *P. aeruginosa*, and *E. coli*, while AgNPs showed reduced activities. When increasing concentrations of plant extract were added, the activity was lowered compared to the AgNPs. Therefore, the GL-AgNPs were shown to be highly promising for antibacterial activity rather than for synergistic applications. Likewise, in the case of SA-AgNPs (Figure 8B) and BR-AgNPs (Figure 8C), the individual AgNPs possessed greater potential compared to the synergetic activity. The antibacterial activity was reduced when the concentration of GL-AgNPs was low compared to GL-extracts against all *S. aureus*, *P. aeruginosa*, and *E. coli*. At a concentration of 100 µg/ml of GL-AgNPs, >99% inhibition was observed against all the pathogens, but when the concentration was reduced to a 1:3 ratio, the inhibition was 41, 32.10, and 31.4% against *S. aureus*, *P. aeruginosa*, and *E. coli*, respectively. Here it is clearly indicated that the GL-extract contains some nutritional factors for the microbes. In the case of SA-AgNPs, the 100% inhibition was found at a ratio of 3: 1 (AgNPs:SA-extracts) against all *S. aureus*, *P. aeruginosa*, and *E. coli*,



but the percentage of the inhibition was gradually reduced when the concentration of SA-AgNPs was decreased. Likewise, BR-AgNPs possess the potential to act against test strains with 99.8% inhibition against *S. aureus* by SA-AgNPs solely. A more interesting result was found against *P. aeruginosa* where 100% inhibition was observed at the concentration of 1: 1 (BR-AgNPs: BR-extracts). At a 3:1 ratio of BR-AgNPs and BR-extracts, 100% inhibition was found against *E. coli*. From the results, the AgNPs are shown to have a better effect than mixing with respective plant extracts. For all the microorganisms used in the study, the phyto-synthesized AgNPs alone had better results compared with adding respective plant extracts for an antibacterial purpose. As the study was targeted to promote the natural plant product-based synthesis and applications of nanoparticles, the synergetic combination was focused by using plant extracts rather than any commercial antibiotics used against the organisms. Many synergetic applications of the AgNPs, along with current commercial antibiotics with different concentrations, show more antibacterial activities (Martinez-Gutierrez et al., 2013; Hussain et al., 2019; Rolim et al., 2019).

Similar results were observed in the case of the synergistic antibiofilm activity where as-synthesized AgNPs were more potentially active than the results found when the respective plant extracts was added in different concentrations. The reduced activity with the addition of plant extracts reveals the presence of microbial growth promoting factors in the natural plant extracts, as well as little antagonistic activity. Hence, the phyto-synthesized AgNPs are more promising than the synergistic

application for controlling biofilm formations. Against all the three bacteria (*S. aureus*, *P. aeruginosa*, and *E. coli*), the respective AgNPs are more effective than the addition of respective plant extracts. The pure plant extracts were least active compared to the respective synthesized AgNPs. The lowest potential inhibition by the plant extracts reflects the presence of biofilm promoting entities. In the current study, *P. aeruginosa* was least inhibited by the SA-extracts (14%) which implies the extracts were supporting the biofilm formations. In other extracts, like GL-extracts and BR-extracts, the inhibition rate was 29.06 and 35.23%, respectively. In the case of *S. aureus* and *E. coli*, the inhibition was >95% in the ratio of 3(AgNPs: plant extracts) whereas <45% inhibition was observed in a 1:3 (AgNPs:plant extracts) ratio, which clearly showed least role of pure plant extracts in eradicating biofilm formation. The antibiofilm activity of AgNPs against *Acinetobacter baumannii*, *P. aeruginosa*, *S. aureus* (MRSA), *Streptococcus mutans*, and *Candida albicans* was studied extensively and reported the potentiality of AgNPs (Martinez-Gutierrez et al., 2013). Rolim et al. (2019) reported the antibiofilm activity of AgNPs against *P. aeruginosa* which supports our current results. However, the plant extract also has some potential of antimicrobial activity; these contain some microbial growth factors which help in growing, rather than inhibiting, the microbes. Hence, the AgNPs synthesized by the plant extracts were more promising than the sole plant extract and combination of plant extracts. The upcoming application of nanoparticles is highly promising as the uncontrolled spread of microbial contaminations is now a great threat worldwide.

CONCLUSION

In the present study, plant extracts, derived from three different medicinal plant species, were used to synthesize AgNPs. The use of the plant extracts has an advantage over chemical or physical synthesis of AgNPs due to their ability to stabilize AgNPs, their own antibacterial properties, their high level of efficacy, and their low toxicity. Their use represents an eco-friendly approach to the synthesis of AgNPs. The extracts of three new plant resources (*S. anacardium*, *G. lanceolarium*, and *B. retusa*) were found to have excellent potential for the commercial production of AgNPs. The plant-derived AgNPs exhibited strong antibacterial and anti-biofilm activity against different clinically important human pathogens. It is safer and more advantageous to biosynthesize metal nanoparticles using the natural reducing agents present in plants and microbes along with the conjugation of AgNPs to natural, antimicrobial molecules produced by microbes or plants. This line of research should be more greatly explored in the biomedical sciences. There is a high level of recently developed, drug-resistant microbes appearing in semi-tropical environments due to climate change, and this represents a significant health issue. Current antibiotics, and the antibiotic concept of fighting pathogens, is rapidly becoming insufficient for combatting new strains of existing pathogens and new disease-causing organisms. High throughput nanobiotechnology curated antimicrobials offer a new approach to treat microbial pathogens that are resistant to current treatment practices and for the treatment of biofilms. The present study demonstrates the potential of using plant-derived

AgNPs to inhibit biofilm formation for therapeutic treatments that represent a new method of effectively treating a variety of infectious diseases caused by pathogenic microbes.

DATA AVAILABILITY STATEMENT

The datasets generated for this study are available on request to the corresponding author.

AUTHOR CONTRIBUTIONS

YM was involved in the collection of plant materials, synthesis of Ag-NPs, antimicrobial and antibiofilm assays, and the preparation of the manuscript. KB and SJ helped in the characterization of Ag-NPs and drafting the manuscript. AH, EA_A, and TM were involved in editing and revising the manuscript. All the authors read and approved the final manuscript.

ACKNOWLEDGMENTS

The authors are very thankful to their respective institutes for providing research facilities. The authors would like to extend their sincere appreciation to the researchers supporting project number (RSP-2020/134), King Saud University, Riyadh, Saudi Arabia.

REFERENCES

- Abbasi, E., Milani, M., Aval, S. F., Kouhi, M., Akbarzadeh, A., Nasrabadi, H. T., et al. (2016). Silver nanoparticles: synthesis methods, bio-applications and properties. *Crit. Rev. Microbiol.* 42, 173–180. doi: 10.3109/1040841X.2014.912200
- Ahmad, N., Bhatnagar, S., Ali, S. S., and Dutta, R. (2015). Phytofabrication of bioinduced silver nanoparticles for biomedical applications. *Int. J. Nanomed.* 10, 7019–7030. doi: 10.2147/IJN.S94479
- Ansari, M., Maayah, Z., Bakheet, S., El-Kadi, A., and Korashy, H. (2013). The role of aryl hydrocarbon receptor signaling pathway in cardiotoxicity of acute lead intoxication in vivo and in vitro rat model. *Toxicology* 306, 40–49. doi: 10.1016/j.tox.2013.01.024
- Arunachalam, K. D., Suhashani, S., and Sathesh, K. A. (2012). Wound healing and Antigenotoxic activities of Aegle marmelos with relation to its antioxidant properties. *J. Pharm. Res.* 5, 1492–1502.
- Bai, X., Gao, Y., Liu, H., and Zheng, L. (2009). Synthesis of amphiphilic ionic liquids terminated gold nanorods and their superior catalytic activity for the reduction of nitro compounds. *J. Phys. Chem. C* 113, 17730–17736. doi: 10.1021/jp906378d
- Barapatre, A., Aadil, K. R., and Jha, H. (2016). Synergistic antibacterial and antibiofilm activity of silver nanoparticles biosynthesized by lignin-degrading fungus. *Bioresour. Bioprocess.* 3:8. doi: 10.1186/s40643-016-0083-y
- Bhanumathi, R., Vimala, K., Shanthi, K., Thangaraj, R., and Kannan, S. (2017). Bioformulation of Silver Nanoparticles as Berberine Carrier cum Anticancer Agent against Breast Cancer. *New J. Chem.* 41, 14466–14477. doi: 10.1039/C7NJ02531A
- Chanda, R., Mohanty, J. P., Bhuyan, N. R., Kar, P. K., and Nath, L. K. (2007). Medicinal plants used against gastrointestinal tract disorders by the traditional healers of Sikkim Himalayas. *Indian J. Tradit. Knowl.* 6, 606–610.
- Chang, C.-C., Yang, M.-H., Wen, H.-M., and Chern, J.-C. (2002). Estimation of total flavonoid content in propolis by two complementary colorimetric methods. *J. Food Drug Anal.* 10, 178–182.
- Chung, I.-M., Park, I., Seung-Hyun, K., Thiruvengadam, M., and Rajakumar, G. (2016). Plant-mediated synthesis of silver nanoparticles: their characteristic properties and therapeutic applications. *Nanoscale Res. Lett.* 11:40. doi: 10.1186/s11671-016-1257-1254
- Clinical, and Laboratory Standards Institute (2005).
- Dauthal, P., and Mukhopadhyay, M. (2016). Noble metal nanoparticles: plant-mediated synthesis, mechanistic aspects of synthesis, and applications. *Indus. Eng. Chem. Res.* 55, 9557–9577. doi: 10.1021/acs.iecr.6b00861
- Deore, U. V., Tatiya, A. U., and Surana, S. J. (2014). Wound healing activity of *Bridelia retusa* bark in experimental animals. *Int. J. Pharm. Pharm. Sci.* 6, 102–105.
- Elbourne, A., Truong, V. K., Cheeseman, S., Rajapaksha, P., Gangadoo, S., Chapman, J., et al. (2019). *The Use of Nanomaterials for the Mitigation of Pathogenic Biofilm Formation*. 1st Edn. Amsterdam: Elsevier Ltd, doi: 10.1016/bs.mim.2019.04.002
- Farooq, U., Ahmad, T., Khan, A., Sarwar, R., Shafiq, J., Raza, Y., et al. (2019). Rifampicin conjugated silver nanoparticles: a new arena for development of antibiotic film potential against methicillin resistant *Staphylococcus aureus* and *Klebsiella pneumoniae*. *Int. J. Nanomedicine* 14, 3983–3993. doi: 10.2147/ijn.s198194
- Ghawate, V. B., Jadhav, V. S., and Bhambar, R. S. (2015). Pharmacological activities of *Bridelia retusa*: a review. *Pharmacology* 9, 415–418.
- Gopinath, V., MubarakAli, D., Priyadarshini, S., Priyadarshini, N. M., Thajuddin, N., and Velusamy, P. (2012). Biosynthesis of silver nanoparticles from *Tribulus terrestris* and its antimicrobial activity: a novel biological

- approach. *Colloids Surf. B Biointerfaces* 96, 69–74. doi: 10.1016/j.colsurfb.2012.03.023
- Goswami, S., Sahareen, T., Singh, M., and Kumar, S. (2015). Role of biogenic silver nanoparticles in disruption of cell-cell adhesion in *Staphylococcus aureus* and *Escherichia coli* biofilm. *J. Ind. Eng. Chem.* 26, 73–80. doi: 10.1016/j.jiec.2014.11.017
- Gurunathan, S., Han, J. W., Kwon, D.-N., and Kim, J.-H. (2014). Enhanced antibacterial and anti-biofilm activities of silver nanoparticles against Gram-negative and Gram-positive bacteria. *Nanoscale Res. Lett.* 9:373. doi: 10.1186/1556-276X-9-373
- Guruvaiah, P., Arunachalam, A., and Velan, L. P. T. (2012). Evaluation of phytochemical constituents and antioxidant activities of successive solvent extracts of leaves of *Indigofera caerulea* Roxb using various in vitro antioxidant assay systems. *Asian Pacific J. Trop. Dis.* 2, S118–S123. doi: 10.1016/S2222-1808(12)60136-4
- Hagerman, A. E., Riedl, K. M., Jones, G. A., Sovik, K. N., Ritchard, N. T., Hartzfeld, P. W., et al. (1998). High Molecular Weight Plant Polyphenolics (Tannins) as Biological Antioxidants. *J. Agric. Food Chem.* 46, 1887–1892. doi: 10.1021/jf970975b
- Hong, B., Kai, J., Ren, Y., Han, J., Zou, Z., Ahn, C. H., et al. (2008). “Highly Sensitive Rapid, Reliable, and Automatic Cardiovascular Disease Diagnosis with Nanoparticle Fluorescence Enhancer and Mems,” in *Oxygen Transport to Tissue XXIX*, eds K. A. Kang, D. K. Harrison, and D. F. Bruley (Boston, MA: Springer), 265–273. doi: 10.1007/978-0-387-74911-2_30
- Huang, J., Li, Q., Sun, D., Lu, Y., Su, Y., Yang, X., et al. (2007). Biosynthesis of silver and gold nanoparticles by novel sundried *Cinnamomum camphora* leaf. *Nanotechnology* 18:105104.
- Hussain, A., Alajmi, M. F., Khan, M. A., Pervez, S. A., Hassan, I., Khan, R. A., et al. (2019). Biosynthesized Silver Nanoparticle (AgNP) From *Pandanus odorifer* Leaf Extract Exhibits Anti-metastasis and Anti-biofilm Potentials. *Front Microbiol.* 10:8. doi: 10.3389/fmicb.2019.00008
- Iravani, S., and Zolfaghari, B. (2013). Green Synthesis of Silver Nanoparticles Using *Pinus edularica* Bark Extract. *Biomed. Res. Int.* 2013:639725. doi: 10.1155/2013/639725
- Jain, P., Huang, X., El-Sayed, I. H., and El-Sayed, M. (2007). Review of some interesting surface Plasmon resonance-enhanced properties of noble metal nanoparticles and their applications to biosystems. *Plasmonics* 2, 107–118. doi: 10.1007/s11468-007-9031-1
- Jeevanandam, J., Barhoum, A., Chan, Y. S., Dufresne, A., and Danquah, M. K. (2018). Review on nanoparticles and nanostructured materials: history, sources, toxicity and regulations. *Beilstein J. Nanotechnol.* 9, 1050–1074. doi: 10.3762/bjnano.9.98
- Kalishwaralal, K., BarathManiKanth, S., Pandian, S., Deepak, V., and Gurunathan, S. (2010). Silver nanoparticles impede the biofilm formation by *Pseudomonas aeruginosa* and *Staphylococcus epidermidis*. *Colloids Surf. B Biointerfaces* 79, 340–344. doi: 10.1016/j.colsurfb.2010.04.014
- Kim, J. S., Kuk, E., Yu, K. N., Kim, J.-H., Park, S. J., Lee, H. J., et al. (2007). Antimicrobial effects of silver nanoparticles. *Nanomed. Nanotechnol. Biol. Med.* 3, 95–101. doi: 10.1016/j.nano.2006.12.001
- Kotakadi, V. S., Gaddam, S. A., Venkata, S. K., and Sai Gopal, D. V. R. (2015). New generation of bactericidal silver nanoparticles against different antibiotic resistant *Escherichia coli* strains. *Appl. Nanosci.* 5, 847–855. doi: 10.1007/s13204-014-0381-387
- Krishnaraj, C., Jagan, E. G., Rajasekar, S., Selvakumar, P., Kalaichelvan, P. T., and Mohan, N. (2010). Synthesis of silver nanoparticles using *Acalypha indica* leaf extracts and its antibacterial activity against water borne pathogens. *Colloids Surf. B Biointerfaces* 76, 50–56. doi: 10.1016/j.colsurfb.2009.10.008
- Landini, P., Antoniani, D., Burgess, J. G., and Nijland, R. (2010). Molecular mechanisms of compounds affecting bacterial biofilm formation and dispersal. *Appl. Microbiol. Biotechnol.* 86, 813–823. doi: 10.1007/s00253-010-2468-2468
- Lim, J., Yeap, S. P., Che, H. X., and Low, S. C. (2013). Characterization of magnetic nanoparticle by dynamic light scattering. *Nanoscale Res. Lett.* 8:1. doi: 10.1186/1556-276X-8-381
- Liu, Y., Shi, L., Su, L., Mei, H. C., Van Der, J. P. C., Ren, Y., et al. (2019). Nanotechnology-based antimicrobials and delivery systems for biofilm-infection control. *Yong. Chem. Soc. Rev.* 428–446. doi: 10.1039/c7cs00807d
- Luximon-Ramma, A., Bahorun, T., Soobrattee, M., and Aruoma, O. (2002). Antioxidant activities of phenolic, proanthocyanidins, and flavonoid components in extracts of *Cassia fistula*. *J. Agri. Food Chem.* 50, 5042–5047. doi: 10.1021/jf0201172
- Martinez-Gutierrez, F., Boegli, L., Agostinho, A., Sánchez, E. M., Bach, H., Ruiz, F., et al. (2013). Anti-biofilm activity of silver nanoparticles against different microorganisms. *Biofouling* 29, 651–660. doi: 10.1080/08927014.2013.794225
- McDonald, S., Prenzler, P. D., Antolovich, M., and Robards, K. (2001). Phenolic content and antioxidant activity of olive extracts. *Food Chem.* 73, 73–84. doi: 10.1016/S0308-8146(00)00288-0
- Mittal, A. K., Chisti, Y., and Banerjee, U. C. (2013). Synthesis of metallic nanoparticles using plant extracts. *Biotechnol. Adv.* 31, 346–356. doi: 10.1016/j.biotechadv.2013.01.003
- Mohanta, T., Patra, J., and Rath, S. (2007). Evaluation of antimicrobial activity and phytochemical screening of oils and nuts of *Semecarpus anacardium*. *Sci. Res. Essay* 2, 486–490.
- Mohanta, Y., Panda, S., Biswas, K., Tamang, A., Bandyopadhyay, J., De, D., et al. (2016a). Biogenic synthesis of silver nanoparticles from *Cassia fistula* (Linn.): in vitro assessment of their antioxidant, antimicrobial and cytotoxic activities. *IET Nanobiotechnol.* 10, 438–444. doi: 10.1049/iet-nbt.2015.0104
- Mohanta, Y., Singdevsachan, S., Parida, U., Panda, S., Mohanta, T., and Bae, H. (2016b). Green synthesis and antimicrobial activity of silver nanoparticles using wild medicinal mushroom *Ganoderma applanatum* (Pers.) Pat. from Similipal Biosphere Reserve, Odisha, India. *IET Nanobiotechnol.* 10, 184–189. doi: 10.1049/iet-nbt.2015.0059
- Mohanta, Y. K., and Behera, S. K. (2014). Biosynthesis, characterization and antimicrobial activity of silver nanoparticles by *Streptomyces* sp. SS2. *Bioprocess Biosyst. Eng.* 37, 2263–2269. doi: 10.1007/s00449-014-1205-1206
- Mohanta, Y. K., Panda, S. K., Bastia, A. K., and Mohanta, T. K. (2017a). Biosynthesis of silver nanoparticles from *Protium serratum* and investigation of their potential impacts on food safety and control. *Front. Microbiol.* 8:626. doi: 10.3389/fmicb.2017.00626
- Mohanta, Y. K., Panda, S. K., Jayabalan, R., Sharma, N., Bastia, A. K., and Mohanta, T. K. (2017b). Antimicrobial, antioxidant and cytotoxic activity of silver nanoparticles synthesized by leaf extract of *Erythrina suberosa* (Roxb.). *Front. Mol. Biosci.* 4:14. doi: 10.3389/fmolb.2017.00014
- Mohanty, S., Mishra, S., Jena, P., Jacob, B., Sarkar, B., and Sonawane, A. (2017). An investigation on the antibacterial, cytotoxic, and antibiofilm efficacy of starch-stabilized silver nanoparticles. *Nanomed. Nanotechnol. Biol. Med.* 8, 916–924. doi: 10.1016/j.nano.2011.11.007
- Narayanan, K., and Sakthivel, N. (2010). Biological synthesis of metal nanoparticles by microbes. *Adv. Colloid Interface Sci.* 156, 1–13. doi: 10.1016/j.cis.2010.02.001
- Nayak, D., Minz, A. P., Ashe, S., Rauta, P. R., Kumari, M., Chopra, P., et al. (2016). Synergistic combination of antioxidants, silver nanoparticles and chitosan in a nanoparticle based formulation: characterization and cytotoxic effect on MCF-7 breast cancer cell lines. *J. Colloid Interface Sci.* 470, 142–152. doi: 10.1016/j.cis.2016.02.043
- Nayak, D., Pradhan, S., Ashe, S., Rauta, P. R., and Nayak, B. (2015). Biologically synthesised silver nanoparticles from three diverse family of plant extracts and their anticancer activity against epidermoid A431 carcinoma Biologically synthesised silver nanoparticles from three diverse family of plant extracts and their a. *J. Colloid Interface Sci.* 457, 329–338. doi: 10.1016/j.cis.2015.07.012
- Panda, S. K., Mohanta, Y. K., Padhi, L., Park, Y. H., Mohanta, T. K., and Bae, H. (2016). Large scale screening of ethnomedicinal plants for identification of potential antibacterial compounds. *Molecules* 21, 1–20. doi: 10.3390/molecules21030293
- Pant, G., Nayak, N., and Prasuna, G. (2012). Enhancement of antidandruff activity of shampoo by biosynthesized silver nanoparticles from *Solanum trilobatum* plant leaf. *Appl. Nanosci.* 3, 431–439. doi: 10.1007/s13204-012-0164-y
- Park, E., Yi, J., Kim, Y., Choi, K., and Park, K. (2010). Silver nanoparticles induce cytotoxicity by a Trojan-horse type mechanism. *Toxicol. Vitro* 24, 872–878. doi: 10.1016/j.tiv.2009.12.001
- Pratap Chandran, R., Manju, S., Vysakhi, M. V., Shaji, P. K., and Achuthan Nair, G. (2013). In vitro antioxidant potential of methanolic and aqueous extracts of *Ardisia solanacea* Roxb. leaf. *J. Pharm. Res.* 6, 555–558. doi: 10.1016/j.jopr.2013.04.038

- Rai, M., Yadav, A., and Gade, A. (2009). Silver nanoparticles as a new generation of antimicrobials. *Biotechnol. Adv.* 27, 76–83. doi: 10.1016/j.biotechadv.2008.09.002
- Ramanavicius, A., Kausaite, A., and Ramanaviciene, A. (2005). Biofuel cell based on direct bioelectrocatalysis. *Biosens. Bioelectron.* 20, 1962–1967. doi: 10.1016/j.bios.2004.08.032
- Rolim, W. R., Lamilla, C., Pieretti, J. C., Dr, M., Tortella, G. R., Diez, M. C., et al. (2019). Comparison of antibacterial and antibiofilm activities of biologically synthesized silver nanoparticles against several bacterial strains of medical interest. 4, 143–159. doi: 10.1007/s40974-019-00123-128
- Saranyaadevi, K., Subha, V., Ravindran, R., and Renganathan, S. (2014). Green synthesis and characterization of silver nanoparticle using leaf extract of *Capparis zeylanica*. *Asian J. Pharm. Clin. Res.* 7, 44–48.
- Shankar, S., Ahmad, A., and Sastry, M. (2003). Geranium leaf assisted biosynthesis of silver nanoparticles. *Biotechnol. Prog.* 19, 1627–1631. doi: 10.1021/bp034070
- Sondi, I., and Salopek-Sondi, B. (2004). Silver nanoparticles as antimicrobial agent: a case study on *E. coli* as a model for Gram-negative bacteria. *J. Colloid Interface Sci.* 275, 177–182. doi: 10.1016/j.jcis.2004.02.012
- Song, J. Y., and Kim, B. S. (2009). Rapid biological synthesis of silver nanoparticles using plant leaf extracts. *Bioprocess Biosyst. Eng.* 32, 79–84. doi: 10.1007/s00449-008-0224-226
- Teulon, J.-M., Godon, C., Chantalat, L., Moriscot, C., Cambedouzou, J., Odorico, M., et al. (2019). On the Operational Aspects of Measuring Nanoparticle Sizes. *Nanomater* 9:18. doi: 10.3390/nano9010018
- Veerasamy, R., Xin, T., Gunasagaran, S., Xiang, T., Yang, E., and Jeyakumar, N. (2011). Biosynthesis of silver nanoparticles using mangosteen leaf extract and evaluation of their antimicrobial activities. *J. Saudi Chem. Soc.* 15, 113–120. doi: 10.1016/j.jscs.2010.06.004
- Zhang, L., Gu, F. X., Chan, J. M., Wang, A. Z., Langer, R. S., and Farokhzad, O. C. (2008). Nanoparticles in medicine: therapeutic applications and developments. *Clin. Pharmacol. Ther.* 83, 761–769. doi: 10.1038/sj.clpt.6100400
- Zia-ur-Rehman, M., Naeem, A., Khalid, H., Rizwan, M., Ali, S., and Azhar, M. (2018). “Responses of Plants to Iron Oxide Nanoparticles,” in *Nanomaterials in Plants, Algae, and Microorganisms*, eds D. K. Tripathi, P. Ahmad, S. Sharma, and D. K. Chauhan (Cambridge, MA: Academic Press), 221–238. doi: 10.1016/B978-0-12-811487-2.00010-4

Conflict of Interest: The authors declare that the research was conducted in the absence of any commercial or financial relationships that could be construed as a potential conflict of interest.

Copyright © 2020 Mohanta, Biswas, Jena, Hashem, Abd_Allah and Mohanta. This is an open-access article distributed under the terms of the Creative Commons Attribution License (CC BY). The use, distribution or reproduction in other forums is permitted, provided the original author(s) and the copyright owner(s) are credited and that the original publication in this journal is cited, in accordance with accepted academic practice. No use, distribution or reproduction is permitted which does not comply with these terms.



Corrigendum: Anti-biofilm and Antibacterial Activities of Silver Nanoparticles Synthesized by the Reducing Activity of Phytoconstituents Present in the Indian Medicinal Plants

OPEN ACCESS

Approved by:
Frontiers Editorial Office,
Frontiers Media SA, Switzerland

***Correspondence:**
Yugal Kishore Mohanta
ykmohanta@gmail.com
Tapan Kumar Mohanta
nostoc.tapan@gmail.com;
tapan.mohanta@unizwa.edu.om

†ORCID:
Abeer Hashem
orcid.org/0000-0001-6541-347X
Elsayed Fathi Abd_Allah
orcid.org/0000-0002-8509-8953

Specialty section:
This article was submitted to
Antimicrobials, Resistance and
Chemotherapy,
a section of the journal
Frontiers in Microbiology

Received: 30 June 2020

Accepted: 08 July 2020

Published: 11 September 2020

Citation:
Mohanta YK, Biswas K, Jena SK,
Hashem A, Abd_Allah EF and
Mohanta TK (2020) Corrigendum:
Anti-biofilm and Antibacterial Activities
of Silver Nanoparticles Synthesized by
the Reducing Activity of
Phytoconstituents Present in the
Indian Medicinal Plants.
Front. Microbiol. 11:1784.
doi: 10.3389/fmicb.2020.01784

Yugal Kishore Mohanta^{1*}, Kunal Biswas², Santosh Kumar Jena³, Abeer Hashem^{4,5†},
Elsayed Fathi Abd_Allah^{6†} and Tapan Kumar Mohanta^{7*}

¹ Department of Botany, North Orissa University, Baripada, India, ² Department of Biotechnology, Maulana Abul Kalam Azad University of Technology, Haringhata, India, ³ Department of Biotechnology, North Orissa University, Baripada, India, ⁴ Botany and Microbiology Department, College of Science, King Saud University, Riyadh, Saudi Arabia, ⁵ Mycology and Plant Disease Survey Department, Plant Pathology Research Institute, Agriculture Research Center, Giza, Egypt, ⁶ Plant Production Department, College of Food & Agricultural Sciences, King Saud University, Riyadh, Saudi Arabia, ⁷ Natural and Medical Sciences Research Center, University of Nizwa, Nizwa, Oman

Keywords: phyto-synthesis, silver nanoparticles, medicinal plants, anti-bacterial activity, anti-biofilm activity

A Corrigendum on

Anti-biofilm and Antibacterial Activities of Silver Nanoparticles Synthesized by the Reducing Activity of Phytoconstituents Present in the Indian Medicinal Plants

by Mohanta, Y. K., Biswas, K., Jena, S. K., Hashem, A., Abd_Allah, E. F., and Mohanta, T. K. (2020). Front. Microbiol. 11:1143. doi: 10.3389/fmicb.2020.01143

In the original article, there was an error in one of the grants numbers in the Acknowledgments section. The correct number for the Researchers Supporting Project, King Saud University is (RSP-2020/134). Furthermore, the authors would like to remove the grant number NO (RGP-271). The revised Acknowledgments section appears below.

The authors are very thankful to their respective institutes for providing research facilities. The authors would like to extend their sincere appreciation to the researchers supporting project number (RSP-2020/134), King Saud University, Riyadh, Saudi Arabia.

The authors would like to state that this does not change the scientific conclusions of the article in any way. The original article has been updated.

Copyright © 2020 Mohanta, Biswas, Jena, Hashem, Abd_Allah and Mohanta. This is an open-access article distributed under the terms of the Creative Commons Attribution License (CC BY). The use, distribution or reproduction in other forums is permitted, provided the original author(s) and the copyright owner(s) are credited and that the original publication in this journal is cited, in accordance with accepted academic practice. No use, distribution or reproduction is permitted which does not comply with these terms.



Monoclonal Antibodies Specific to the Extracellular Domain of Histidine Kinase YycG of *Staphylococcus epidermidis* Inhibit Biofilm Formation

Zhihui Lyu¹, Yongpeng Shang¹, Xiaofei Wang¹, Yang Wu¹, Jinxin Zheng², Huayong Liu¹, Ting Gong¹, Lina Ye¹ and Di Qu^{1*}

¹ Key Laboratory of Medical Molecular Virology of MOE and MOH, Department of Medical Microbiology and Parasitology, School of Basic Medical Sciences, Fudan University, Shanghai, China, ² Department of Infectious Diseases and Shenzhen Key Lab for Endogenous Infection, Shenzhen Nanshan Hospital, Shenzhen University, Shenzhen, China

OPEN ACCESS

Edited by:

Luis Cláudio Nascimento da Silva,
Universidade Ceuma, Brazil

Reviewed by:

Rodolfo Garcia-Contreras,
National Autonomous University
of Mexico, Mexico
Mario Eugenio Cancino-Diaz,
Escuela Nacional de Ciencias
Biológicas (IPN), Mexico

*Correspondence:

Di Qu
dqu@shmu.edu.cn

Specialty section:

This article was submitted to
Antimicrobials, Resistance
and Chemotherapy,
a section of the journal
Frontiers in Microbiology

Received: 30 April 2020

Accepted: 14 July 2020

Published: 07 August 2020

Citation:

Lyu Z, Shang Y, Wang X, Wu Y,
Zheng J, Liu H, Gong T, Ye L and
Qu D (2020) Monoclonal Antibodies
Specific to the Extracellular Domain
of Histidine Kinase YycG
of *Staphylococcus epidermidis* Inhibit
Biofilm Formation.
Front. Microbiol. 11:1839.
doi: 10.3389/fmicb.2020.01839

Staphylococcus epidermidis is frequently associated with biofilm-related infections. Biofilms drastically reduce the efficacy of conventional antibiotics and the host immune system. In *S. epidermidis* biofilm formation, a major role is played by the YycG/YycF two-component system, and previous findings have indicated that inhibitors targeting the cytoplasmic HATPase_c domain of YycG kinase in *S. epidermidis* exhibit bactericidal and biofilm-killing activities. Therefore, we hypothesized that monoclonal antibodies (mAbs) against YycG extracellular (YycG_{ex}) domain would block the signal transduction and influence the biofilm formation of *S. epidermidis*. In this study, we screened out two YycG_{ex}-specific mAbs showing the highest affinity for the target, mAbs 2F3 and 1H1. These mAbs inhibited *S. epidermidis* biofilm formation in a dose-dependent manner, and at a concentration of 160 µg/mL, mAbs 2F3 and 1H1 caused 78.3 and 93.1% biofilm reduction, respectively, relative to normal mouse IgG control. When co-cultivated with YycG_{ex} mAbs, *S. epidermidis* cells showed diminished initial-adherence capacity, and the antibody treatment further led to a marked decrease in the synthesis of polysaccharide intercellular adhesin and in the transcriptional level of genes encoding proteins involved in biofilm formation. Lastly, we determined that the epitopes recognized by the two YycG_{ex} mAbs are located within aa 59–70 of the YycG_{ex} domain. It indicates that the YycG_{ex} domain may be a potential candidate as a vaccine for the prevention of *S. epidermidis* biofilm infections.

Keywords: *Staphylococcus epidermidis*, biofilm, YycG histidine kinase, two-component system, epitope mapping

INTRODUCTION

Staphylococcus epidermidis is part of the normal bacterial flora colonizing the skin and mucous membranes of the human body (Yao et al., 2006; Fey and Olson, 2010). The main pathogenicity associated with *S. epidermidis* is the formation of thick, multilayered, highly structured biofilms on artificial surfaces (Vuong and Otto, 2002; McCann et al., 2008). Biofilm formation is a highly complex process that involves multiple regulatory factors, such as two-component systems (TCSs) (Sauer, 2003; Mikkelsen et al., 2011; Rasamiravaka et al., 2015; Wolska et al., 2016). The YycG/YycF

TCS is conserved in low-G + C gram-positive bacteria (Fabret and Hoch, 1998; Fukuchi et al., 2000), and the TCS regulates bacterial growth, cell-wall metabolism, cell division, virulence-factor expression, and biofilm formation (Ng et al., 2005; Senadheera et al., 2005; Bisicchia et al., 2007; Fukushima et al., 2008). Because YycG/YycF TCS plays an essential role in bacterial biological functions and because no YycG/YycF homologs or structurally similar proteins are expressed in humans, the YycG/YycF TCS represents a potential antibacterial target (Winkler and Hoch, 2008; Gotoh et al., 2010).

The YycG histidine kinase of *S. epidermidis* prototypically contains two transmembrane sections, an extracytoplasmic loop (YycG_{ex} domain), cytoplasmic HAMP and Per-Arnt-Sim (PAS) domains, and a catalytic core of HisKA and HATPase_c domains (Ng and Winkler, 2004; Dubrac et al., 2008). Our previous work demonstrated that inhibitors targeting the HATPase_c domain exhibit not only bactericidal activity but also potent activity against staphylococcal biofilms (Qin et al., 2006; Huang et al., 2012; Liu et al., 2014; Lv et al., 2017). Thus, we hypothesized that monoclonal antibodies (mAbs) against the YycG_{ex} domain would block the signal transduction and thereby influence the phenotypic properties of *S. epidermidis* RP62A. Analysis of the YycG sequence revealed that the YycG_{ex} domain contains aa 142–154 flanked by two transmembrane domains that adopt a PAS or PhoQ-DcuS-CitA fold (Santelli et al., 2007; Chang et al., 2010; Shah et al., 2013). The folding motif is regarded as a sensor that receives environmental signals and modulates YycG kinase activity (Ng and Winkler, 2004; Szurmant et al., 2008). Accordingly, we generated mAbs against the YycG_{ex} domain and investigated their effects on bacterial functions.

Out of nine YycG_{ex}-specific mAbs (2A9, 2B3, 2B4, 2F1, 2F3, 2E3, 2G9, 1H1, and 1H3) generated using hybridoma technology, two YycG_{ex} mAbs exhibiting the highest affinity for YycG_{ex} protein, mAbs 2F3 and 1H1, were selected for further experiments. Here, we investigated the anti-biofilm activities of these YycG_{ex} mAbs and identified the epitope recognized by the antibodies. Our results showed that YycG_{ex} mAbs inhibit *S. epidermidis* biofilm formation and that their target epitope is located within aa 59–70 of YycG_{ex} domain. We report, for the first time, that mAbs against the extracellular domain of a TCS can affect biofilm formation. Our findings indicate that the use of YycG_{ex} mAbs represents a potential treatment strategy against biofilm infection and, further, that the epitope recognized by YycG_{ex} mAbs could serve as a vaccine candidate for preventing *S. epidermidis* biofilm infections.

MATERIALS AND METHODS

Bacterial Strains, Culture Media, and Antibiotics

Staphylococcus epidermidis RP62A was obtained from American Type Culture Collection (ATCC 35984), and *S. epidermidis* clinical isolates were collected from the Department of Laboratory Medicine, Affiliated Gulou Hospital, Medical

College of Nanjing University. Staphylococcal strains were cultured in tryptic soy broth (TSB; Oxoid Ltd., Basingstoke, United Kingdom), and *Escherichia coli* strains DH5 α and BL21(DE3) were cultured in Luria-Bertani (LB) broth (1% tryptone, 0.5% yeast extract, 1% NaCl). Kanamycin sulfate was obtained from Sigma Aldrich (St. Louis, MO, United States).

Generation of mAbs Against the YycG_{ex} Domain

As noted in the introduction section, the *S. epidermidis* essential histidine kinase YycG contains these domains: two transmembrane sections, an extracytoplasmic domain, cytoplasmic HAMP and PAS domains, and the catalytic core of HisKA and HATPase_c domains. Our previous work showed that inhibitors targeting the HATPase_c domain, developed using a structure-based virtual-screening approach, exhibit both bactericidal activity and potent anti-biofilm activity in the case of staphylococci. Because the extracytoplasmic domain of the protein (YycG_{ex} domain) is considered to play roles in sensing external stimuli, we hypothesized that mAbs targeting the YycG_{ex} domain might block signal transduction by binding to this domain and thus influence bacterial biofilm formation. A 453-bp *NcoI/XhoI* DNA fragment encoding the YycG_{ex} domain (aa 34–184 of YycG) was amplified from the chromosomal DNA of *S. epidermidis* RP62A (GenBank accession number NC_002976) by using the primers *yycG_{ex}-F* and *yycG_{ex}-R* (Table 1). The *yycG_{ex}* DNA fragment was ligated into the pET28a (+) expression vector, and the resulting plasmid was transformed into *E. coli* DH5 α competent cells. The YycG_{ex} protein was expressed in *E. coli* BL21(DE3) cells and induced (for 14 h at 25°C) by adding isopropyl β -D-1-thiogalactopyranoside (IPTG; Thermo Fisher Scientific, Waltham, MA, United States) to a final concentration of 0.8 mM. The bacterial cells were lysed by sonication and centrifuged, and the supernatant was used for protein purification by using Ni-NTA agarose (Qiagen, Los Angeles, CA, United States) according to the manufacturer's instructions. Purified YycG_{ex} protein was dialyzed against Tris buffer-15% glycerol and then sterilized by passage through a 0.22- μ m-pore-size filter (Millipore, Bedford, MA, United States). The recombinant YycG_{ex} protein was used for immunizing BALB/c mice, and YycG_{ex}-specific mAbs were generated using the hybridoma technology by Abmart Inc. (Shanghai, China)¹.

Bacterial Dynamic Growth Curve

Overnight cultures of *S. epidermidis* RP62A were subcultured (1:200) in fresh TSB supplemented with 160 μ g/mL YycG_{ex} mAbs and incubated at 37°C for 12 h with shaking. The effect of mAbs on bacterial growth was automatically monitored every 0.5 h by measuring the optical density at 600 nm (OD₆₀₀) by using a BioScreen Growth Curve machine (Growth Curves USA, Piscataway, NJ, United States); normal mouse IgG (mIgG) served as the negative control. The experiments were performed in triplicate and the means and standard error of the mean (SEM) were calculated.

¹<http://www.ab-mart.com>

TABLE 1 | Primers used in this study^a.

Primers	Sequences (5'-3')
Primers used for expression of YycG_{ex} protein	
^b yycG _{ex} -F	<u>CATGCCATGG</u> TCACGAATAGTTAGAAAAGGAATT
^b yycG _{ex} -R	<u>CCGCTCGAG</u> CTGATTAATGTTGTTTCAGCTGATT
Primers used for qRT-PCR	
<i>gyrB</i> -F	AGAAGAGGAAGTTAGAGAAGA
<i>gyrB</i> -R	GCATATCCACTGTTATATTGAAG
<i>icaA</i> -F	ATCAAGCGAAGTCAATCTC
<i>icaA</i> -R	CAGCAATATCCTCAGTAATCA
<i>icaD</i> -F	CCAGACAGAGGCAATATCC
<i>icaD</i> -R	CAATCATCACAAACGATACAATACA
<i>icaB</i> -F	CATATTCCAGCAACAGGTT
<i>icaB</i> -R	GCAACAGATTGAGACGAAT
<i>icaC</i> -F	AGGCGTCGGAATGATGTTA
<i>icaC</i> -R	AGTTAGGCTGGTATTGGTCAA
<i>aap</i> -F	AACAACAACAACACCAACT
<i>aap</i> -R	GCCACCATAATGAACGATT
<i>bhp</i> -F	GTCTACTTGGCTCTTATGC
<i>bhp</i> -R	AGGTGCTTCAGTTGTAATAC
<i>fbe</i> -F	AAGCACATTACCGTTGAT
<i>fbe</i> -R	CCTACTAATATCGTATCTCCAT
<i>sarA</i> -F	GTAATGAACACGATGAAAGAACT
<i>sarA</i> -R	GCTTCTGTGATACGGTTGT
<i>altE</i> -F	AACGTGTCTGCTAATCG
<i>altE</i> -R	TTACCGCTATTGTAGTCTTC
<i>yycG</i> -F	ATAGTGATTCCCTTCTTGTTAG
<i>yycG</i> -R	GACTTGTTGTTGTTCTGT
<i>yycF</i> -F	GATGGTATGGAAGTATGT
<i>yycF</i> -R	CTGGTTGTGAATAATGAC
Primers used for truncation of the SUMO-tagged YycG_{ex}	
TF ₃₄₋₁₈₄ -F	ACGAATAGTTTAGAAAAGGAATTAC
TF ₃₄₋₁₈₄ -R	CTACTGATTAATGTTGTTTCAGCTGATT
TF ₃₄₋₈₃ -F	ACGAATAGTTTAGAAAAGGAATTAC
TF ₃₄₋₈₃ -R	CTAATTCAAAAGGTCCTGGATATCCTT
TF ₈₄₋₁₃₃ -F	GAATATGCGAATCGTCAAGAAATAG
TF ₈₄₋₁₃₃ -R	CTACGTTTGCCCTAAGGAGAGCGCC
TF ₁₃₄₋₁₈₄ -F	AATGATCATATGGTTCTTAAGGATT
TF ₁₃₄₋₁₈₄ -R	CTACTGATTAATGTTGTTTCAGCTGATTG
TF ₃₄₋₅₈ -F	ACGAATAGTTTAGAAAAGGAATTAC
TF ₃₄₋₅₈ -R	CTAGACGTCTAATTGCTTCGCATATTG
TF ₄₇₋₇₁ -F	AAGAACATAACACAATATGCGAAGC
TF ₄₇₋₇₁ -R	CTAGACTGAACCTTTATCTTATCCTTA
TF ₅₉₋₈₃ -F	AATATTGAAAAGGTTTATAAGG
TF ₅₉₋₈₃ -R	CTAATTCAAAAGGTCCTGGATATCC
TF ₄₇₋₅₈ -F	AAGAACATAACACAATAT
TF ₄₇₋₅₈ -R	CTAGACGTCTAATTGCTTC
TF ₅₉₋₇₀ -F	AATATTGAAAAGGTTTAT
TF ₅₉₋₇₀ -R	CTAACCTTTATCTTTATCC
TF ₇₁₋₈₃ -F	TCAGTCAACGCTCAAAAG
TF ₇₁₋₈₃ -R	CTAATTCAAAAGGTCCTGGAT
Primers used for site-directed mutagenesis of the SUMO-tagged T₃₄₋₈₃	
K47V/N48V/I49V-F	GCTGCTGCTACACAATATGCGAAGCAA
K47V/N48V/I49V-R	CTTGAAGTTATCGAGTAATTCCTTTTC
T50V/Q51V/Y52V-F	GCTGCTGCTGCGAAGCAATTAGACGTC

(Continued)

TABLE 1 | Continued

Primers	Sequences (5'-3')
T50V/Q51V/Y52V-R	ACGAATAGTTTAGAAAAGGAATTACTC
A53V/K54V/Q55V-F	GCTGCTGCTTTAGACGTCAATATTGAA
A53V/K54V/Q55V-R	ATATTGTGTTATGTTCTTCTTGAAAGTT
L56V/D57V/V58L-F	GCTGCTTGTGCTAATATTGAAAAGGTTT
L56V/D57V/V58L-R	CTTCGCATATTGTGTTATGTTCTTCTTG
N59V/I60V/E61V-F	GCTGCTGCTAAGGTTTATAAGGATAAAG
N59V/I60V/E61V-R	GACGTCTAATTGCTTCGCATATTGTGTT
K62V/V63L/Y64V-F	GCTGCTGCTAAGGATAAAGATAAAGG
K62V/V63L/Y64V-R	TTCAATATTGACGTCTAATTGCTTCG
K65V/D66V/K67V-F	GCTGCTGCTGATAAAGGTTTCAGTCAAC
K65V/D66V/K67V-R	ATAAACCTTTTCAATATTGACGTCTAA
D68V/K69V/G70V-F	GCTGCTGCTTCAGTCAACGCTCAAAAGG
D68V/K69V/G70V-R	TTTATCCTTATAAACCTTTTCAATATTG
K62V-F	GCTGTTTATAAGGATAAAGATAAAGGT
K62V-R	TTCAATATTGACGTCTAATTGCTTCGC
V63L-F	TTGTATAAGGATAAAGATAAAGGTTCA
V63L-R	CTTTTCAATATTGACGTCTAATTGCTT
Y64V-F	GCTAAGGATAAAGATAAAGGTTTCAGTC
Y64V-R	AACCTTTTCAATATTGACGTCTAATTG
K65V-F	GCTGATAAAGATAAAGGTTTCAGTCAAC
K65V-R	ATAAACCTTTTCAATATTGACGTCTAA
D66V-F	GCTAAAGATAAAGGTTTCAGTCAACGCT
D66V-R	CTTATAAACCTTTTCAATATTGACGTC
K67V-F	GCTGATAAAGGTTTCAGTCAACGCTCAA
K67V-R	ATCCTTATAAACCTTTTCAATATTGAC
D68V-F	GCTAAAGGTTTCAGTCAACGCTCAAAAG
D68V-R	TTTATCCTTATAAACCTTTTCAATATT
K69V-F	GCTGGTTTCAGTCAACGCTCAAAAGGAT
K69V-R	ATCTTTATCCTTATAAACCTTTTCAAT
G70V-F	GCTTCAGTCAACGCTCAAAAGGATATC
G70V-R	TTTATCTTTATCCTTATAAACCTTTTTC

Primers used for site-directed mutagenesis of YycG_{ex} in the *S. epidermidis* chromosome

^c yycG-attB1	<u>GGGGACAAGTTTGTACAAAAAAGCAGGCT</u> ATGAAGTGGCTTAAACAACTAC
^c yycG-attB2	<u>GGGGACCACCTTTGTACAAAGAAAGCTGGGT</u> ACAAGAAGGAATCACTATTTTCT

^aPrimers were designed according to the genomic sequence of *S. epidermidis* RP62A (GenBank accession number NC_002976). F, forward primer; R, reverse primer. ^bUnderlined sequences represent NcoI and XhoI restriction sites.

^cUnderlined sequences represent the Gateway BP reaction sites.

Determination of Viable Bacterial Cell Counts

The viable cell counts of bacteria incubated with YycG_{ex} mAbs were determined through plate counts on nutrient agar. Overnight cultures of *S. epidermidis* RP62A were diluted 1:200 into TSB containing 160 μg/mL YycG_{ex} mAbs and incubated at 37°C with shaking for 6 or 24 h; subsequently, 1-mL aliquots of bacterial cells were washed twice with ice-cold 0.9% NaCl solution and pelleted by centrifugation for 3 min at 4000 rpm. The pellets were resuspended in 1 mL of ice-cold 0.9% NaCl solution and serially diluted (10-fold), and then 5-μL aliquots from each dilution were spotted onto tryptic soy agar plates

and the CFU/mL values were calculated. Three independent experiments were performed for this assay.

Microtiter Plate Biofilm Assays

Inhibition of biofilm formation by YycG_{ex} mAbs was detected using a semiquantitative microtiter plate assay. Overnight planktonic cultures of *S. epidermidis* RP62A were diluted 1:200 in fresh TSB containing twofold serial dilutions of mAbs (20, 40, 80, and 160 µg/mL), and then microtiter plates containing the samples were initially incubated at 4°C for 2 h and later placed in a 37°C incubator for 24 h. After the incubation and the removal of non-adherent cells by washing thrice with phosphate-buffered saline (PBS), adherent biofilms were fixed with 95% methanol and stained with 2% (w/v) crystal violet, and then excess stain was removed by washing in distilled water. To quantify biofilm formation, OD₅₇₀ was determined using an xMark™ Microplate Absorbance Spectrophotometer (Bio-Rad Laboratories, Hercules, CA, United States). Bacteria treated with mIgG served as the control. The experiments were performed using three replicates and repeated thrice independently.

Structural Analysis of Biofilms Through Confocal Laser-Scanning Microscopy (CLSM)

Overnight cultures of *S. epidermidis* RP62A (1:200 dilution) were inoculated into 1 mL of TSB containing 80 µg/mL YycG_{ex} mAbs in FluoroDishes (FD35-100; WPI, Sarasota, FL, United States) and incubated statically at 37°C for 24 h. Planktonic cells were removed by washing with 0.9% NaCl solution, and biofilms were stained using a Live/Dead BacLight Viability kit (Thermo Fisher Scientific, Waltham, MA, United States) for 20 min at room temperature, protected from light exposure. We obtained a series of Z-section images by using a Leica confocal microscope (TCS-SP5, Leica, Wetzlar, Germany) with a 63 × oil-immersion objective and then generated three-dimensional images by using IMARIS 7.0.0 software package (Bitplane, Zurich, Switzerland). Three independent experiments were performed.

Bacterial Initial-Attachment Assays

Overnight-grown *S. epidermidis* RP62A cells were diluted 1:200 in TSB containing 160 µg/mL YycG_{ex} mAbs and incubated at 37°C with shaking at 220 rpm for 6 h. The bacteria were harvested by centrifugation and resuspended in PBS to an OD₆₀₀ of 0.1 or 1.0 and then loaded in triplicate into either 6-well or 96-well polystyrene microtiter plates, respectively (Nunc GmbH, Wiesbaden, Germany). After incubation for 2 h at 37°C, the plates were washed thrice with PBS to remove non-adherent bacteria, and the adherent bacteria were stained with 0.5% crystal violet as described previously (Lei et al., 2011) and visualized microscopically using an Axiovert 200 inverted microscope (Carl Zeiss, Thornwood, NY, United States) or stained with 2% crystal violet and used for OD₅₇₀ measurement. The experiments were performed using three replicates and repeated thrice independently.

Detection of Polysaccharide Intercellular Adhesin (PIA)

Polysaccharide intercellular adhesin was detected by performing a lectin dot-blot assay with horseradish peroxidase (HRP)-conjugated wheat germ agglutinin (WGA-HRP, Biotium, Inc. Hayward, CA, United States) as previously described (Wu et al., 2015). Briefly, overnight cultures of *S. epidermidis* RP62A were diluted 1:200 in TSB containing 160 µg/mL YycG_{ex} mAbs and incubated at 37°C with shaking at 220 rpm for 6 h. The bacteria were harvested and resuspended in 50 µL of 0.5 M EDTA (pH 8.0) and then incubated for 5 min at 100°C. After centrifugation (13,000 × g, 5 min), the supernatant was treated with proteinase K (20 mg/mL; Roche) at 37°C for 2 h, after which the enzyme was inactivated at 100°C for 10 min. Next, 1-µL aliquots of serially diluted PIA extracts were spotted onto nitrocellulose membranes (Millipore) by using a 96-well dot-blot vacuum manifold (Biometra GmbH, Niedersachsen, Germany), and after air-drying, the membranes were blocked for 2 h with 3% (w/v) skim milk in Tris-buffered saline containing 0.1% Tween-20 (TBST). Subsequently, the membranes were incubated with WGA-HRP (2 µg/mL) for 1 h at room temperature, and after washing thrice with TBST, the PIA signal was visualized using an enhanced chemiluminescence (ECL) Western blotting detection kit (Thermo Fisher Scientific, Waltham, MA, United States).

Detection of Extracellular DNA (eDNA)

Overnight cultures of *S. epidermidis* RP62A were diluted 1:200 into fresh TSB containing 160 µg/mL YycG_{ex} mAbs and incubated at 37°C with shaking for 24 h. Bacterial cells were harvested by centrifugation at 13,000 rpm for 10 min, and the resulting supernatants were filtered through 0.22-µm-pore-size filters (Millipore, Bedford, MA, United States) to obtain cell-free supernatants. The eDNA from the supernatants was isolated using an equal volume of phenol-chloroform-isoamyl alcohol (25:24:1, v/v/v) and then ethanol-precipitated. The precipitated eDNA was washed in 70% ethanol, air-dried, resuspended in TE buffer (10 mM Tris-Cl, 1 mM EDTA, pH 8.0), and visualized on gel-red-stained 1% agarose gels.

Bacterial Autolysis Assay

To measure autolysis, overnight-grown *S. epidermidis* RP62A was diluted 1:200 into TSB containing 1 M NaCl plus 160 µg/mL YycG_{ex} mAbs and incubated at 37°C for 6 h. Next, the bacterial cells were pelleted by centrifugation, and the pellets were washed thrice with ice-cold water and resuspended to an OD₆₀₀ of 1.0 in 50 mM glycine buffer, pH 8.0, containing 0.05% Triton X-100. Lastly, the bacterial cells were incubated at 37°C with shaking and the OD₆₀₀ was measured at 0.5-h intervals for 3 h. All experiments were repeated thrice.

RNA Isolation and qRT-PCR

Overnight cultures of *S. epidermidis* RP62A were diluted 1:200 into TSB containing 160 µg/mL YycG_{ex} mAbs and incubated at 37°C with shaking at 220 rpm for 6 h. The bacteria were collected by centrifugation at 4000 rpm for 10 min and

then washed twice with ice-cold 0.9% NaCl solution. The cell pellets were homogenized by using 0.1-mm zirconia-silica beads in a Mini-BeadBeater (Biospec Products, Bartlesville, OK, United States), operated at a speed of 4800 rpm for 60 s; 5 cycles of homogenization were performed with 1-min intervals on ice. Total RNA was extracted using a RNeasy kit (Qiagen, Los Angeles, CA, United States) according to the manufacturer's instruction. After RNA extraction, residual DNA was removed from the total RNA samples, and cDNA was synthesized by using a PrimeScript RT Reagent Kit with gDNA Eraser (Perfect Real Time) (Takara Bio Inc., Otsu, Japan) for manual description. qRT-PCR was performed on an Applied Biosystems 7500 Real Time PCR system (Applied Biosystems, Foster City, CA, United States) by using SYBR Premix Ex Taq (Takara Bio Inc., Otsu, Japan) and these cycling conditions: 95°C for 30 s, followed by 40 cycles of 95°C for 5 s and 60°C for 34 s. Melting curves were recorded after 40 cycles to confirm primer specificity by heating from 60°C to 95°C. All sample reactions were performed in triplicate with housekeeping gyrase B subunit gene (*gyrB*) used as an internal standard. Real-time PCR primers for each tested gene are listed in **Table 1**.

Epitope Mapping by Using Recombinant Truncated YycG_{ex} Proteins

To locate the epitopes recognized by YycG_{ex} mAbs, YycG_{ex} protein was truncated using the following method. DNA fragments encoding truncated YycG_{ex} proteins were subcloned into the *Bam*HI and *Xho*I sites of a pET SUMO vector, and nine plasmids containing inserts of the desired length were verified through sequencing. All primers used in this study are listed in **Table 1**. *E. coli* strain BL21(DE3) carrying the aforementioned recombinant plasmids were incubated in LB medium at 37°C with shaking (at 220 rpm) until an OD₆₀₀ of 0.6, and then 0.8 mM IPTG was added to induce expression at 25°C for 14 h; subsequently, cells were harvested by centrifugation and boiled in 400 µL of 1 × SDS sample buffer and stored at −20°C.

Identification of Key Residues Within the Epitope by Using Site-Directed Mutagenesis

A KOD -Plus- Mutagenesis Kit (Toyobo, Osaka, Japan) was used to introduce alanine substitutions into the YycG_{ex} domain according to the manufacturer's instructions. The plasmid pET SUMO expressing the truncated YycG_{ex} fragment TF_{34–83} was used as a template. The amplification conditions included an initial denaturation step of 2 min at 94°C, followed by 10 cycles of 10 s at 98°C, 30 s at 55°C, and 6 min at 68°C. The mutant plasmids were verified using DNA sequencing before use in transformation of *E. coli* strain BL21(DE3). The mutagenesis primers used in the assay are listed in **Table 1**.

Analysis of Binding of Truncated YycG_{ex} Proteins and YycG_{ex} mAbs by Using SDS-PAGE and Western Blotting

Cell pellets obtained from 5 mL of LB medium were boiled in 400 µL of 1 × SDS sample buffer for 10 min, and total proteins

were separated using 10% (w/v) SDS-PAGE. Gels were either stained with Coomassie Brilliant Blue R-250 or the proteins were electrophoretically transferred onto 0.45-µm PVDF membranes (Millipore, Bedford, MA, United States). After blocking for 2 h with 5% skim milk in PBST (PBS containing 0.05% Tween-20), the membranes were incubated with YycG_{ex} mAbs (1:1000 in PBST) at room temperature for 3 h. Binding was probed using HRP-conjugated anti-mouse IgG, and after washing for 60 min with PBST, band intensity was measured by staining with an ECL detection reagent (Thermo Fisher Scientific, Waltham, MA, United States), according to the manufacturer's instructions, and exposing the membranes to X-OMAT film (Kodak, Rochester, NY, United States).

Construction of YycG Mutated in Key Residue Involved in Binding YycG_{ex} mAbs

To identify the function of a key amino acid residue recognized by YycG_{ex} mAbs in *S. epidermidis* RP62A, we next constructed a *yycG* (K65V) mutant in the bacterial chromosome by means of allelic replacement, performed using the temperature-sensitive plasmid pKOR1 as described previously (Bae and Schneewind, 2006). Briefly, a 1.0-kb DNA fragment (1~1000 bp of *yycG*) was PCR-amplified from *S. epidermidis* RP62A genomic DNA (GenBank accession number NC_002976) by using the primers *yycG*-attB1/2 and then cloned into pKOR1 by using the Gateway BP cloning method, which yielded the plasmid pKOR1-*yycG*₁₀₀₀. We next used primers K65V-F (5'-GCTGATAAAGATAAAGGTTTCAGTCAAC-3') and K65V-R (5'-ATAAACCTTTTCAATATTGACGTCTAA-3') harboring the K65V mutation together with the plasmid pKOR1-*yycG*₁₀₀₀ as the template and used a KOD -Plus- Mutagenesis Kit (Toyobo, Osaka, Japan) according to the manufacturer's instructions. The mutated plasmid was first transformed into *E. coli* DC10B and then into *S. epidermidis* RP62A, and this was followed by allelic replacement as described previously (Zhu et al., 2010; Lou et al., 2011). The presence of the mutation (K65V) in the *S. epidermidis* genome was verified by sequencing the PCR product of YycG_{ex} amplified from the mutant genome.

Statistical Analysis

Experiments were performed using three replicates and repeated thrice independently. Results are expressed as means ± standard deviation (SD) or SEM. For statistical comparisons, Student's *t*-tests were performed using GraphPad Prism version 7 (GraphPad Software Inc., San Diego, CA, United States). *P* < 0.05 was considered statistically significant.

RESULTS

Effect of YycG_{ex} mAbs on the Phenotypic Properties of *S. epidermidis* RP62A

YycG/YycF TCS regulates *S. epidermidis* biofilm formation (Xu et al., 2017). Because inhibitors targeting the cytoplasmic HATPase_c domain of YycG exhibit anti-biofilm activity

(Qin et al., 2006; Huang et al., 2012; Liu et al., 2014; Lv et al., 2017), we generated mAbs against the extracellular domain of YycG (YycG_{ex}, aa 34–184) of *S. epidermidis* RP62A, and from nine hybridoma lines, we selected for further investigation the two mAbs (2F3 and 1H1) that exhibited the highest affinity for the protein.

Effect of YycG_{ex} mAbs on Biofilm Formation

To test the effect of YycG_{ex} mAbs on the biofilm formation of *S. epidermidis* RP62A, 20–160 µg/mL YycG_{ex} mAbs were incubated with the bacteria for 24 h at 37°C, and then biofilm formation was evaluated using a microtiter plate assay; here, mIgG-treated and untreated groups were used as controls.

YycG_{ex} mAbs inhibited *S. epidermidis* biofilm formation in a dose-dependent manner (**Figure 1A**), and mAbs 2F3 and 1H1 at 20 µg/mL reduced biofilm formation by 27.3 and 49.2%, respectively, relative to the control groups. At 160 µg/mL, mAbs 2F3 and 1H1 caused 78.3 and 93.1% biofilm reduction, respectively, whereas the mIgG-treated group only showed 5.9% inhibition. After incubation with YycG_{ex} mAbs (80 µg/mL) for 24 h at 37°C, *S. epidermidis* RP62A formed rough and loose biofilms, as observed by means of Live/Dead staining and CLSM, whereas the biofilms in the mIgG-treated and untreated groups were smooth and evenly distributed. However, the proportions of dead bacteria in the biofilm were similar in all groups (**Figure 1B**). YycG_{ex} mAbs 2F3 and 1H1 did not affect the growth

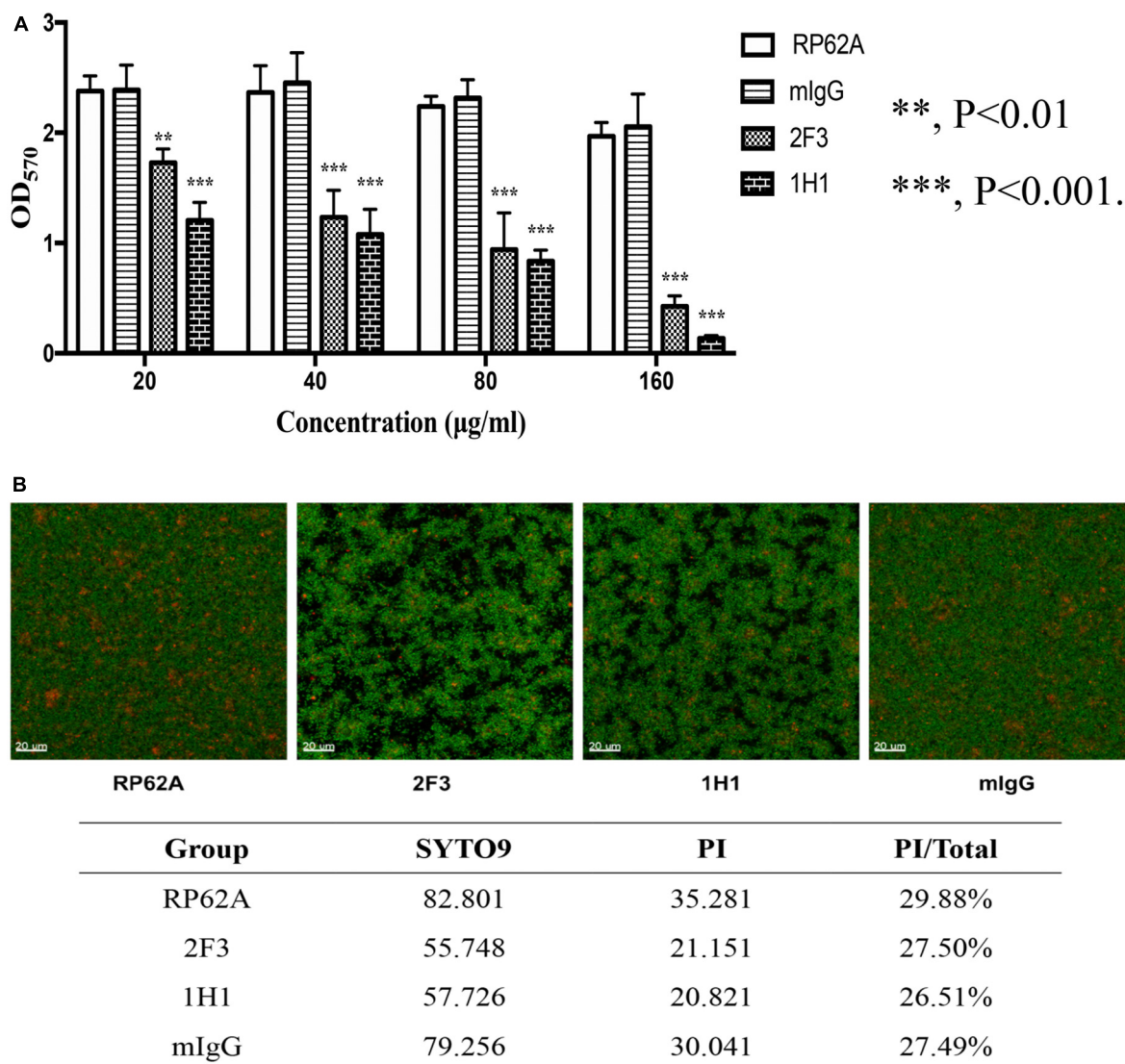


FIGURE 1 | Effects of YycG_{ex} mAbs on the biofilm formation of *S. epidermidis* RP62A. **(A)** Inhibition of biofilm formation by YycG_{ex} mAbs was detected using a microtiter plate assay. *S. epidermidis* RP62A was incubated with twofold serial dilutions of YycG_{ex} mAbs (160–20 µg/mL) at 37°C for 24 h. Biofilms were stained with 2% (w/v) crystal violet and the OD₅₇₀ was read. Statistical analyses were performed using Student's *t*-test. **(B)** Effect of YycG_{ex} mAbs on biofilm morphology of *S. epidermidis* RP62A, examined using CLSM. *S. epidermidis* RP62A was incubated with 80 µg/mL YycG_{ex} mAbs at 37°C for 24 h. Viable and dead cells fluoresced green and red, respectively. PI/Total values indicated the proportion of dead cells within the biofilms. RP62A, untreated; mIgG, normal mouse IgG treated.

and survival of *S. epidermidis* RP62A at the highest concentration tested (160 μ g/mL) (Supplementary Figure 1).

YycG_{ex} mAbs Influence Bacterial Initial Attachment

The first step in biofilm formation is bacterial adherence to a surface; thus, we determined how this initial attachment of *S. epidermidis* is affected by YycG_{ex} mAbs, and we used a semiquantitative microtiter plate assay to assess cell attachment. Under the microscope, no cell clusters were detected when *S. epidermidis* RP62A was cultured in the presence of YycG_{ex} mAbs for 6 h at 37°C, whereas clusters were observed in the mIgG-treated and untreated groups (Figure 2A). The adherent bacteria were quantitated by staining with crystal violet and measuring the OD₅₇₀: Both mAb 2F3 and mAb 1H1 significantly reduced the number of attached cells in the wells (OD₅₇₀ = 0.118 \pm 0.012 and 0.115 \pm 0.005, respectively) as compared to that in the untreated control group (OD₅₇₀ = 0.302 \pm 0.013) (P < 0.001) (Figure 2B).

Effect of YycG_{ex} mAbs on Extracellular Polysaccharide Substance (EPS)

To investigate the effect of YycG_{ex} mAbs on EPS production, PIA biosynthesis and eDNA release were determined in the case of *S. epidermidis* RP62A cultured with 160 μ g/mL YycG_{ex} mAbs at 37°C for 6 h. Almost no PIA was detected in the presence of 160 μ g/mL YycG_{ex} mAbs at dilutions up to 1:50 by using WGA-HRP in a lectin dot-blot assay, whereas a considerably stronger signal was detected in the mIgG-treated and untreated groups at dilutions up to 1:200 (Figure 3A). The release of eDNA into the supernatant of cells treated with YycG_{ex} mAbs was similar to that in the untreated *S. epidermidis* RP62A cells, as visualized on gel-red-stained 1% agarose gels (Figure 3B).

We next assessed the transcriptional levels of the biofilm-related genes *icaADBC*, *aap*, *bhp*, *fbe*, and *sarA* by performing qRT-PCR with RNA samples extracted from *S. epidermidis* RP62A incubated with 160 μ g/mL mAbs 2F3 and 1H1 at 37°C for 6 h. All of these genes were downregulated in the presence of YycG_{ex} mAbs, with a marked (8–13-fold) reduction in transcript levels being measured for *icaA*, *icaD*, and *icaB*, which encode PIA; by contrast, the expression of *altE*, *ycyG*, and *ycyF* did not differ between the mAb-treated and untreated groups (Figure 3C).

Epitope Mapping and Identification of Key Amino Acid Residues in the YycG_{ex} Domain

Localization of the B-cell epitopes recognized by YycG_{ex}-specific mAbs can help in identifying the main antigenic determinants of the YycG_{ex} domain and developing peptide vaccines for *S. epidermidis* biofilm infections. Thus, we mapped the epitopes within YycG_{ex} domain by using protein truncation combined with Western blotting analysis. Moreover, by performing alanine-scanning mutagenesis of YycG_{ex} proteins, we identified multiple residues that are essential for YycG_{ex} mAb binding.

Identification of Epitopes Recognized by YycG_{ex} mAbs

To locate the epitopes recognized by YycG_{ex} mAbs, we generated YycG_{ex} truncation fragments (TFs) of distinct sizes that were N-terminally fused to a SUMO-tag, and we used Western blotting to examine the binding of YycG_{ex} mAbs to these fragments. First, YycG_{ex} domain was truncated into three fragments: TF_{34–83}, TF_{84–133}, and TF_{134–184}. Both mAb 2F3 and mAb 1H1 recognized TF_{34–83} (Figure 4A). Next, TF_{34–83}

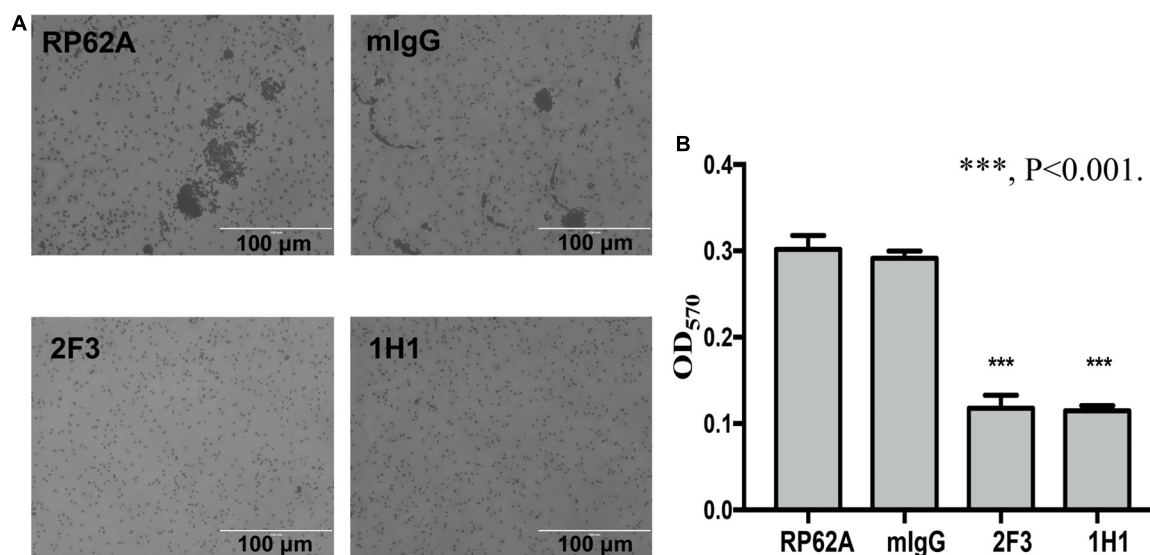


FIGURE 2 | Effect of YycG_{ex} mAbs on initial attachment of *S. epidermidis* RP62A. Bacterial cells were diluted in TSB containing 160 μ g/mL YycG_{ex} mAbs and incubated at 37°C with shaking at 220 rpm for 6 h. (A) Adherence ability visualized microscopically. (B) Cell attachment measured as OD₅₇₀ after crystal violet staining. Experiments were performed using three replicates and repeated thrice independently. RP62A: untreated; mIgG: normal mouse IgG treated. Statistical analyses were performed using Student's *t*-test. *** P < 0.001.

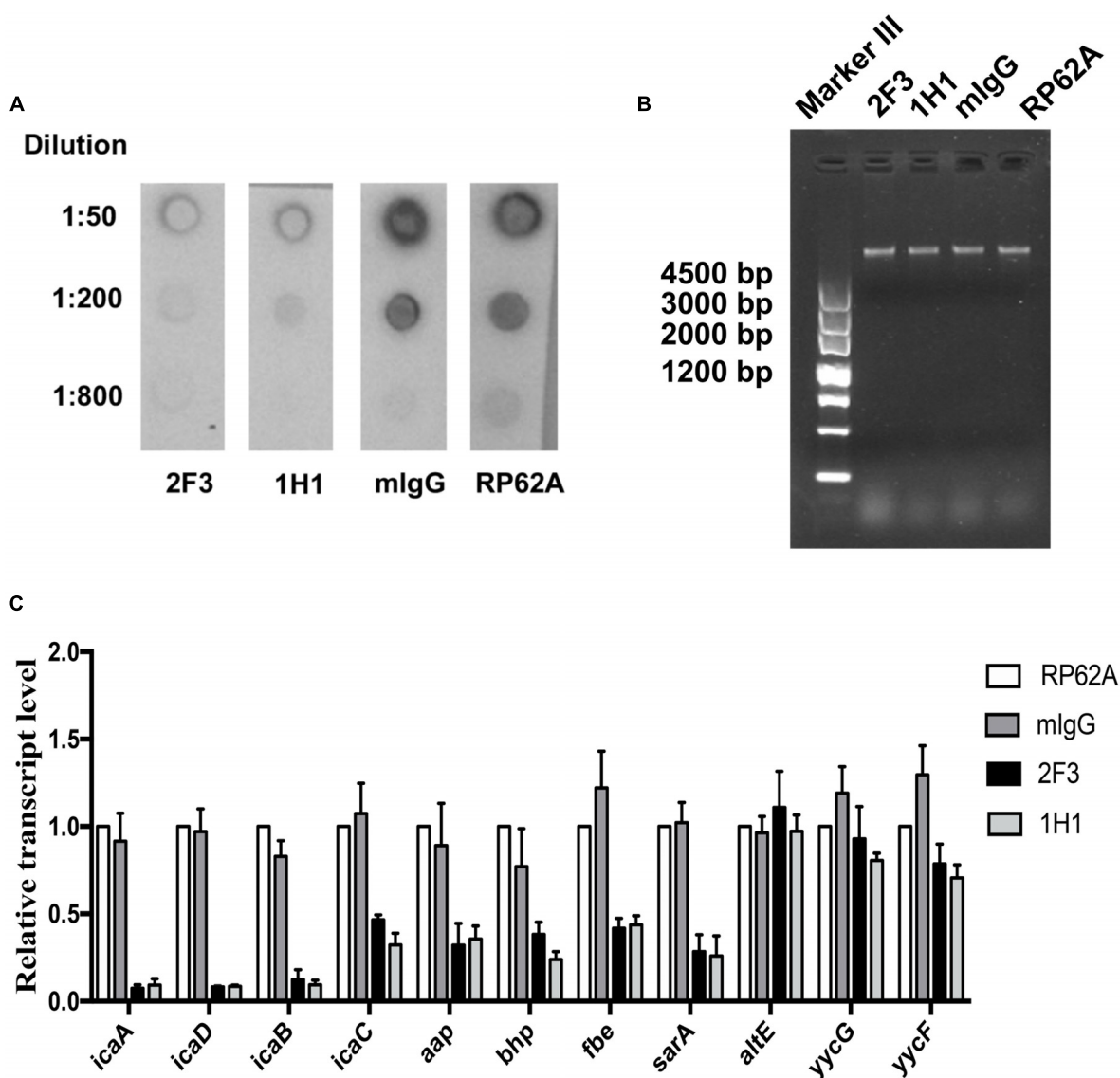


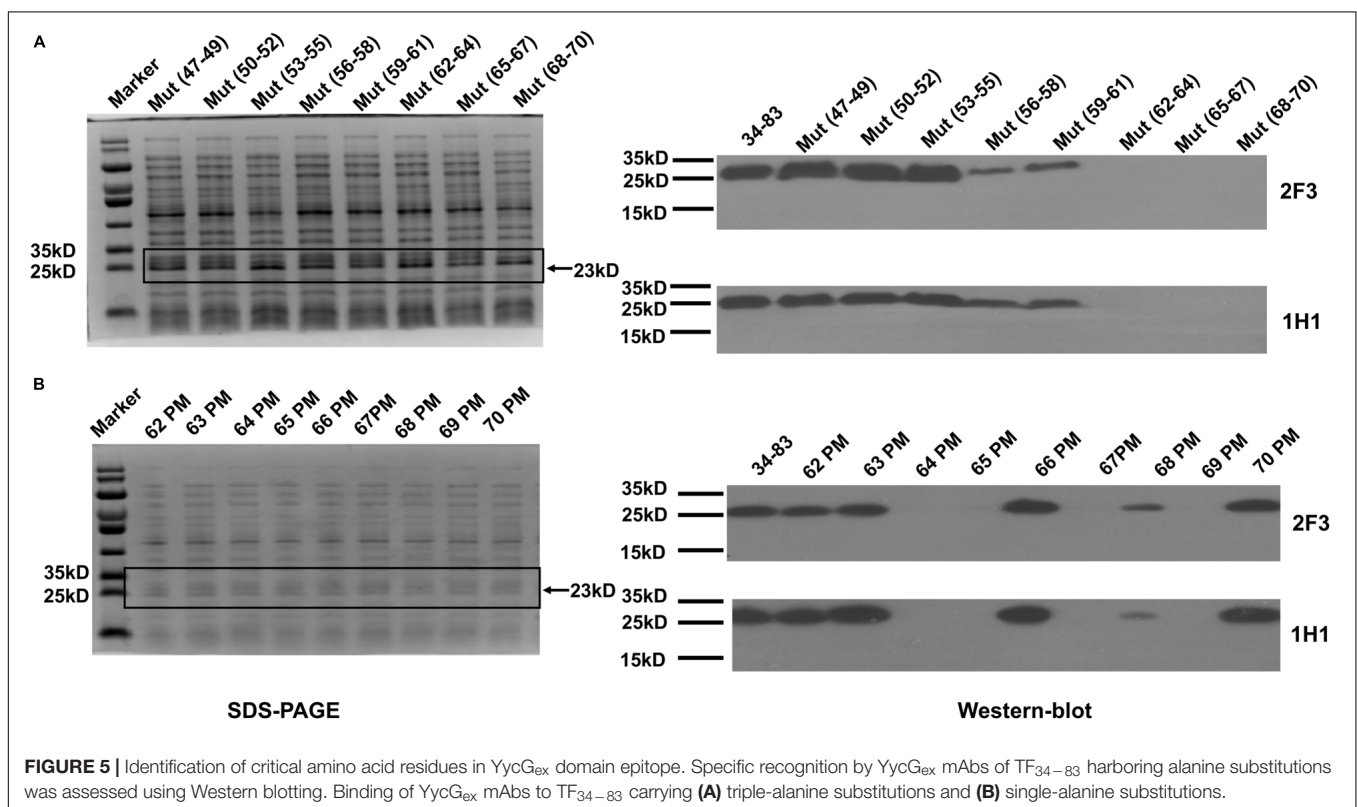
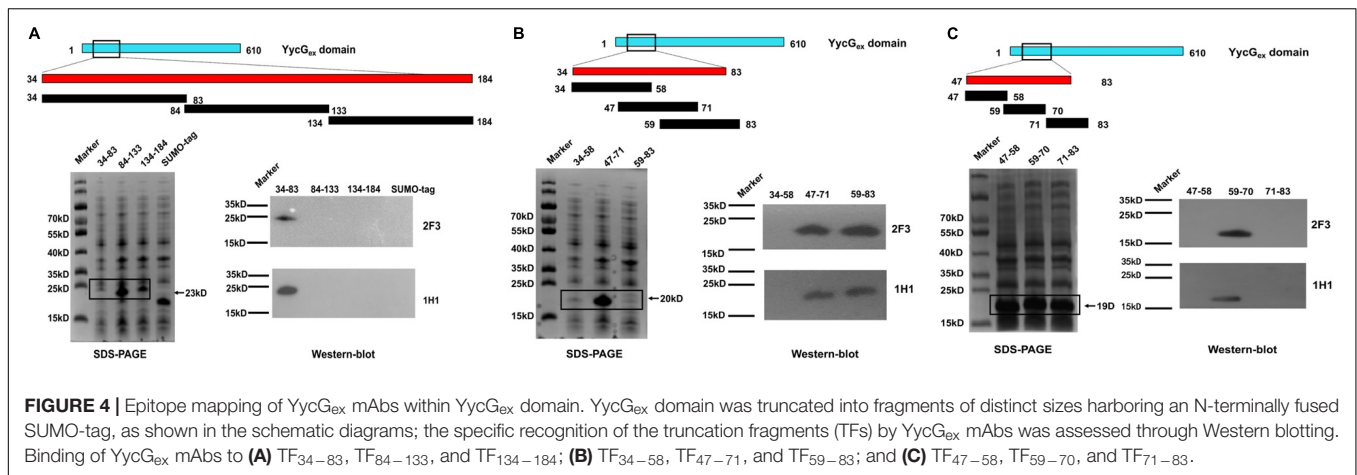
FIGURE 3 | Effect of YycG_{ex} mAbs on EPS synthesis and transcription of biofilm-related genes of *S. epidermidis* RP62A. Overnight cultures of *S. epidermidis* RP62A were diluted in TSB containing 160 μ g/mL YycG_{ex} mAbs and incubated at 37°C for 6 h. **(A)** Effect of YycG_{ex} mAbs on PIA synthesis. **(B)** Effect of YycG_{ex} mAbs on eDNA release. eDNA was isolated and analyzed on 1% agarose gels. **(C)** Effect of YycG_{ex} mAbs on transcriptional levels of biofilm-related genes. All reactions were performed in triplicate, with housekeeping gyrase B subunit gene (*gyrB*) used as an internal standard. RP62A, untreated; mIgG, normal mouse IgG treated.

was further truncated into TF_{34–58}, TF_{47–71}, and TF_{59–83}; mAbs 2F3 and 1H1 both reacted with TF_{47–71} and TF_{59–83}, which indicated that the YycG_{ex} mAbs recognize the region containing aa 47–83 (Figure 4B). Lastly, the fragment containing aa 47–83 of the YycG_{ex} domain was truncated into TF_{47–58}, TF_{59–70}, and TF_{71–83}, and YycG_{ex} mAbs were found to bind TF_{59–70} (Figure 4C).

Identification of Key Amino Acid Residues Within the mAb Epitope

To identify the amino acid residues in the epitope that are essential for binding by YycG_{ex} mAbs, we substituted every three amino acid residues with alanine individually within aa

47–70 by using site-directed mutagenesis; we constructed eight mutants and used Western blotting to examine their binding by YycG_{ex} mAbs. Binding of the epitope by both mAb 2F3 and mAb 1H1 was abolished by the mutations K62V/V63L/Y64V, K65V/D66V/K67V, and D68V/K69V/G70V, which indicated that the key amino acid residues in the epitope recognized by YycG_{ex} mAbs are located within aa 62–70: KVKDKDKG (Figure 5A). Consequently, we mutated these nine amino acid residues individually to alanine and then examined antibody binding; the binding of mAbs 2F3 and 1H1 to the epitope was abolished by four single mutations, Y64V, K65V, K67V, and K69V, which suggested that the key amino acid residues in the YycG_{ex} mAb epitope were Tyr64, Lys65, Lys67, and Lys69 (Figure 5B).

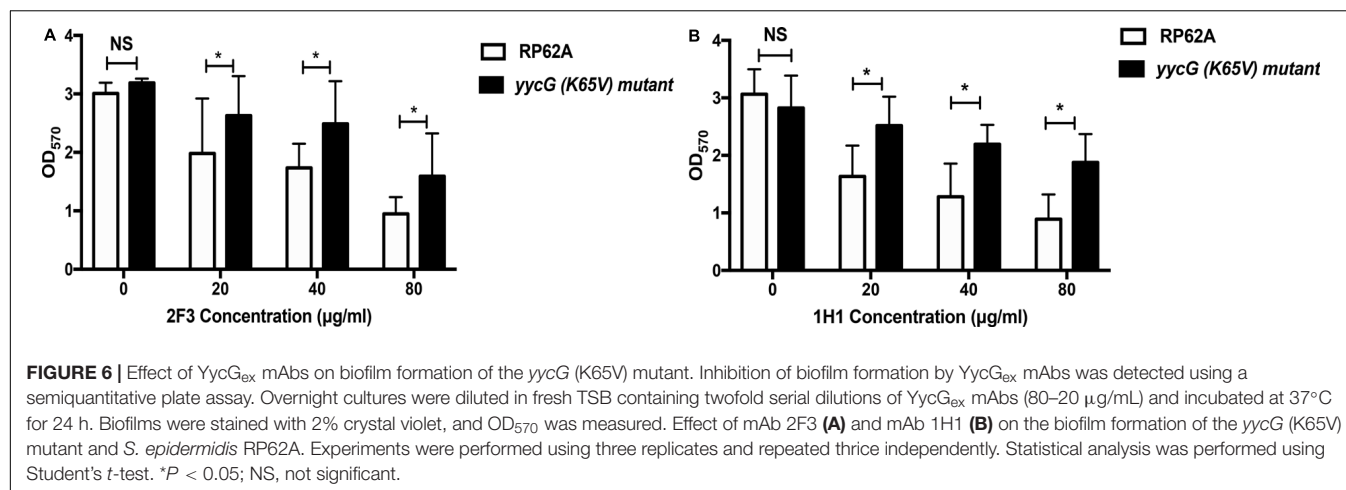


YycG K65V Mutation in *S. epidermidis* Decreases Biofilm Inhibition by YycG_{ex} mAbs

Lastly, to evaluate how the key amino acids in the mAb epitope (Tyr64, Lys65, Lys67, and Lys69) affect biofilm inhibition by YycG_{ex} mAbs, we generated *yycG* mutations in *S. epidermidis* RP62A (Y64V/K65V/K67V/K69V, Y64V, and K65V) through allelic replacement by using the temperature-sensitive plasmid pKOR1, but only the *yycG* (K65V)-mutant strain was screened out; viable mutant strains were not obtained in the case of the other mutations mentioned. The *yycG* (K65V) mutant was verified by sequencing the PCR product of YycG_{ex} amplified from the mutant genome, and pKOR1 plasmid loss from mutant

strains was confirmed through PCR amplification and agarose-gel analysis (Supplementary Figure 2A).

Growth curves and biofilm formation were no different between the *yycG* (K65V) mutant strain and the parental strain (Supplementary Figures 2B,C). However, the inhibitory effect of YycG_{ex} mAbs on biofilm formation of the *yycG* (K65V) mutant was significantly decreased with increasing concentrations of the antibodies (20, 40, and 80 μg/mL) as compared with the inhibition in the parental RP62A strain ($P < 0.05$) (Figure 6). At 80 μg/mL, mAbs 2F3 and 1H1 reduced the biofilm formation of RP62A strain by 68.5 and 70.9%, respectively, but caused only 50.0 and 33.5% reduction in the *yycG* (K65V) mutant.



DISCUSSION

Staphylococcus epidermidis has emerged as one of the most critical opportunistic pathogens of nosocomial infections in recent years because of the increase in frequency of invasive procedures (Vuong et al., 2003; Chessa et al., 2015). The main pathogenicity associated with *S. epidermidis* involves the formation of biofilms on implanted medical devices (Rupp, 2014; Hamad et al., 2015). The presence of the bacteria in biofilms drastically reduces the efficacy of conventional antibiotics and the host immune system, and this leads to persistent or recurrent infections (Wolcott et al., 2010; Romling and Balsalobre, 2012). The YycG/YycF TCS is essential for bacterial growth and plays a major role in biofilm formation (Fukuchi et al., 2000; Howell et al., 2003; Mohedano et al., 2005; Ahn and Burne, 2007; Bisicchia et al., 2007). YycG histidine kinase is a transmembrane protein, and we have shown that inhibitors that target the cytoplasmic HATPase_c domain of *S. epidermidis* exhibit bactericidal and biofilm-killing activities (Qin et al., 2006; Huang et al., 2012; Liu et al., 2014; Lv et al., 2017). Previous studies have found that the extracellular domain of the protein (YycG_{ex} domain) adopts a PAS fold predicted as a sensor of YycG by sensing environmental signals such as oxygen, light, redox potential, or the presence of specific ligands (Taylor and Zhulin, 1999; Santelli et al., 2007; Chang et al., 2010; Shah et al., 2013; Kim et al., 2016), but little is known of the nature of the signals and factors sensed by YycG. However, whether the blockade of YycG_{ex} domain would influence the signal transduction and biofilm formation of the bacterium has remained unclear. Therefore, in this study, we investigated the effect of mAbs against the YycG_{ex} domain on the biological functions of *S. epidermidis* RP62A.

We selected two mAbs showing the highest affinity for YycG_{ex} protein, mAbs 2F3 and 1H1, and we found that both mAbs reduced the biofilm formation of *S. epidermidis* RP62A in a dose-dependent manner under static conditions without affecting bacterial growth. Furthermore, both mAb 2F3 and mAb 1H1 reduced the biofilm formation of five *S. epidermidis* clinical isolates by 54.1–74.7% at the concentration of 160 µg/mL (Supplementary Table 1), which suggests that

YycG_{ex} mAbs represent potential candidates for use in clinical treatments to prevent biofilm formation. However, the cell wall of *S. epidermidis* is formed by a thick layer (20–80 nm) composed mainly of glycine-rich peptidoglycan that might impede the binding of YycG_{ex} mAbs to the YycG_{ex} domain, and this could be responsible for the high concentration of YycG_{ex} mAbs (160 µg/mL) required for producing their effect. Thus, further investigation is necessary to develop methods to reduce the treatment concentration of YycG_{ex} mAbs while retaining their strong biofilm-inhibition activity.

We found that YycG_{ex} mAbs diminished the capacity of *S. epidermidis* for initial attachment, which is the first step in biofilm formation. Biofilm formation is commonly divided into three steps: initial adhesion, accumulation, and maturation (Sauer, 2003; Wolska et al., 2016). After attaching to a surface, bacteria produce the EPS, a complex mixture of biopolymers primarily consisting of polysaccharides (PIA), proteins, and nucleic acids (eDNA) (Costerton et al., 1987; Vu et al., 2009). We detected the expression of genes (*aap*, *bhp*, *fbe*, and *sarA*) encoding proteins related to the initial attachment and accumulation of the *S. epidermidis* biofilm (Mack et al., 1994; Cho et al., 2002; Bowden et al., 2005; Vuong et al., 2005; Schaeffer et al., 2015), and all of these genes were downregulated after treatment with YycG_{ex} mAbs. The downregulation of *icaADB* expression was in accord with the decrease in PIA synthesis: The *ica* operon encodes PIA-synthesis enzymes, and PIA is a poly-β (1–6)-*N*-acetylglucosamine that plays critical roles in intercellular adhesion and in the structural integrity of biofilms (Heilmann et al., 1996; Gerke et al., 1998; Lister and Horswill, 2014; Arciola et al., 2015). Another key EPS component of biofilms is the eDNA released after bacterial autolysis, and this eDNA is related to initial cell adhesion and subsequent intracellular accumulation (Mann et al., 2009; Tang et al., 2013; Regina et al., 2014; Ibanez de Aldecoa et al., 2017). The release of eDNA into the supernatant and the Triton X-100-induced autolysis of the cells that were treated with YycG_{ex} mAbs were similar to those of untreated *S. epidermidis* RP62A cells (Supplementary Figure 3). The signals in the environment induce auto-phosphorylation of the cytoplasmic domain HATPase_c of YycG, and the

phosphoryl group is then transferred from histidine residue to an aspartate residue in the receiver domain of the YycF response regulator, which further results in the conformation change of YycF (Mohedano et al., 2005; Cronan and Thomas, 2009). Phosphorylated YycF is usually involved in the DNA-binding and transcription activation of the target genes. The previous study in our lab showed that in *S. epidermidis*, YycF not only regulates biofilm-associated regulators such as *arlRS*, *sarA*, and *sarX* but also binds to the promoters of *icaADBC* to directly modulate PIA production, which related with bacterial biofilm formation (Xu et al., 2017). Thus, YycG_{ex} mAbs might inhibit biofilm formation by affecting the signal transduction from YycG to YycF, which led to the downregulated expression level of *icaADBC* and diminished initial-adherence capacity and, thus, likely influenced the subsequent accumulation step.

Next, we determined that the epitope recognized by YycG_{ex} mAbs is located within aa 59–70, and by analyzing the antibody-binding region harboring alanine substitutions, we identified four critical amino acids in the epitope: Tyr64, Lys65, Lys67, and Lys69. To further evaluate how these key amino acids affect biofilm inhibition by YycG_{ex} mAbs, we generated *yycG* mutations in the *S. epidermidis* chromosome (Y64V/K65V/K67V/K69V, Y64V, and K65V). Ultimately, we screened out the *yycG* (K65V) mutant, and we found that YycG_{ex} mAbs more weakly affected the biofilm formation of the *yycG* (K65V) mutant as compared with that of the parental RP62A strain. This finding indicated that the residue K65 might be directly involved in the binding of YycG_{ex} mAbs to YycG_{ex} domain. However, we failed to obtain the mutants *yycG* (Y64V/K65V/K67V/K69V) and *yycG* (Y64V) in *S. epidermidis* RP62A, which indicates that some of these residues likely play a crucial role in maintaining bacterial growth and survival.

In summary, YycG_{ex} mAbs showed anti-biofilm activity in the case of *S. epidermidis* and the epitope recognized by the mAbs was located in aa 59–70 of the YycG_{ex} domain. The key amino acids within the epitope were identified as Tyr64, Lys65, Lys67, and Lys69, and the importance of Lys65 was confirmed in *S. epidermidis* RP62A through single-point chromosome mutagenesis. Our findings suggest that mAbs against the YycG_{ex} domain could be used in new treatment strategies targeting biofilm-associated infections caused by *S. epidermidis*. Moreover, the epitope recognized by YycG_{ex} mAbs could be used to further study the structure of the YycG_{ex} domain and might represent a vaccine candidate for the prevention of *S. epidermidis* biofilm infections. However, further investigation is necessary to elucidate the mechanism by which YycG_{ex} mAbs block *S. epidermidis* signal transduction. Moreover, the effect of YycG_{ex} mAbs against biofilm-associated

infections of *S. epidermidis* needs to be further investigated in a stable animal model.

DATA AVAILABILITY STATEMENT

The raw data supporting the conclusions of this article will be made available by the authors, without undue reservation.

ETHICS STATEMENT

All mice experimental procedures were approved by the Institutional Animal Care and Use Committee (IACUC) of School of Basic Medical Sciences, Fudan University (IACUC Animal Project Number 20150119-081) according to Regulations for the Administration of Affairs Concerning Experimental Animals, China.

AUTHOR CONTRIBUTIONS

ZL and DQ conceived and designed the experiments. ZL, YS, XW, YW, JZ, HL, TG, LY, and DQ performed the experiments. ZL, YS, and DQ created the figures, analyzed the data, and wrote the manuscript. All the authors contributed to the article and approved the submitted version.

FUNDING

This work was supported by the National Mega-project for Innovative Drugs (2019ZX09721001), the National Natural Science Foundation of China (81871622 and 81571955), and the National Mega-project for Infectious Diseases (2018ZX10734401).

ACKNOWLEDGMENTS

We would like to thank Dr. Li Chen, Fudan University, for kindly providing the pET SUMO vector.

SUPPLEMENTARY MATERIAL

The Supplementary Material for this article can be found online at: <https://www.frontiersin.org/articles/10.3389/fmicb.2020.01839/full#supplementary-material>

REFERENCES

- Ahn, S. J., and Burne, R. A. (2007). Effects of oxygen on biofilm formation and the AtlA autolysin of *Streptococcus mutans*. *J. Bacteriol.* 189, 6293–6302. doi: 10.1128/jb.00546-07
- Arciola, C. R., Campoccia, D., Ravaioli, S., and Montanaro, L. (2015). Polysaccharide intercellular adhesin in biofilm: structural and regulatory aspects. *Front. Cell. Infect. Microbiol.* 5:7. doi: 10.3389/fcimb.2015.00007
- Bae, T., and Schneewind, O. (2006). Allelic replacement in *Staphylococcus aureus* with inducible counter-selection. *Plasmid* 55, 58–63. doi: 10.1016/j.plasmid.2005.05.005
- Bisicchia, P., Noone, D., Lioliou, E., Howell, A., Quigley, S., Jensen, T., et al. (2007). The essential YycFG two-component system controls cell wall metabolism in

- Bacillus subtilis*. *Mol. Microbiol.* 65, 180–200. doi: 10.1111/j.1365-2958.2007.05782.x
- Bowden, M. G., Chen, W., Singvall, J., Xu, Y., Peacock, S. J., Valtulina, V., et al. (2005). Identification and preliminary characterization of cell-wall-anchored proteins of *Staphylococcus epidermidis*. *Microbiology* 151(Pt 5), 1453–1464. doi: 10.1099/mic.0.27534-0
- Chang, C., Tesar, C., Gu, M., Babnigg, G., Joachimiak, A., Pokkuluri, P. R., et al. (2010). Extracytoplasmic PAS-like domains are common in signal transduction proteins. *J. Bacteriol.* 192:1156. doi: 10.1128/JB.01508-09
- Chessa, D., Ganau, G., and Mazzarello, V. (2015). An overview of *Staphylococcus epidermidis* and *Staphylococcus aureus* with a focus on developing countries. *J. Infect. Dev. Ctries* 9, 547–550. doi: 10.3855/jidc.6923
- Cho, S. H., Naber, K., Hacker, J., and Ziebuhr, W. (2002). Detection of the icaADBC gene cluster and biofilm formation in *Staphylococcus epidermidis* isolates from catheter-related urinary tract infections. *Int. J. Antimicrob. Agents* 19, 570–575. doi: 10.1016/S0924-8579(02)00101-2
- Costerton, J. W., Cheng, K. J., Geesey, G. G., Ladd, T. I., Nickel, J. C., Dasgupta, M., et al. (1987). Bacterial biofilms in nature and disease. *Annu. Rev. Microbiol.* 41, 435–464. doi: 10.1146/annurev.mi.41.100187.002251
- Cronan, J. E., and Thomas, J. (2009). Bacterial fatty acid synthesis and its relationships with polyketide synthetic pathways. *Methods Enzymol.* 459, 395–433. doi: 10.1016/S0076-6879(09)04617-5
- Dubrac, S., Bisicchia, P., Devine, K. M., and Msadek, T. (2008). A matter of life and death: cell wall homeostasis and the WalKR (YycGF) essential signal transduction pathway. *Mol. Microbiol.* 70, 1307–1322. doi: 10.1111/j.1365-2958.2008.06483.x
- Fabret, C., and Hoch, J. A. (1998). A two-component signal transduction system essential for growth of *Bacillus subtilis*: implications for anti-infective therapy. *J. Bacteriol.* 180, 6375–6383. doi: 10.1128/180.23.6375-6383.1998
- Fey, P. D., and Olson, M. E. (2010). Current concepts in biofilm formation of *Staphylococcus epidermidis*. *Future Microbiol.* 5, 917–933. doi: 10.2217/fmb.10.56
- Fukuchi, K., Kasahara, Y., Asai, K., Kobayashi, K., Moriya, S., and Ogasawara, N. (2000). The essential two-component regulatory system encoded by *ycfF* and *ycfG* modulates expression of the *ftsAZ* operon in *Bacillus subtilis*. *Microbiology* 146(Pt 7), 1573–1583. doi: 10.1099/00221287-146-7-1573
- Fukushima, T., Szurmant, H., Kim, E. J., Perego, M., and Hoch, J. A. (2008). A sensor histidine kinase co-ordinates cell wall architecture with cell division in *Bacillus subtilis*. *Mol. Microbiol.* 69, 621–632. doi: 10.1111/j.1365-2958.2008.06308.x
- Gerke, C., Kraft, A., Sussmuth, R., Schweitzer, O., and Gotz, F. (1998). Characterization of the N-acetylglucosaminyltransferase activity involved in the biosynthesis of the *Staphylococcus epidermidis* polysaccharide intercellular adhesin. *J. Biol. Chem.* 273, 18586–18593. doi: 10.1074/jbc.273.29.18586
- Gotoh, Y., Eguchi, Y., Watanabe, T., Okamoto, S., Doi, A., and Utsumi, R. (2010). Two-component signal transduction as potential drug targets in pathogenic bacteria. *Curr. Opin. Microbiol.* 13, 232–239. doi: 10.1016/j.mib.2010.01.008
- Hamad, T., Hellmark, B., Nilsdotter-Augustinsson, A., and Soderquist, B. (2015). Antibiotic susceptibility among *Staphylococcus epidermidis* isolated from prosthetic joint infections, with focus on doxycycline. *Apmis* 123, 1055–1060. doi: 10.1111/apm.12465
- Heilmann, C., Schweitzer, O., Gerke, C., Vanittanakom, N., Mack, D., and Gotz, F. (1996). Molecular basis of intercellular adhesion in the biofilm-forming *Staphylococcus epidermidis*. *Mol. Microbiol.* 20, 1083–1091. doi: 10.1111/j.1365-2958.1996.tb02548.x
- Howell, A., Dubrac, S., Andersen, K. K., Noone, D., Fert, J., Msadek, T., et al. (2003). Genes controlled by the essential YycG/YycF two-component system of *Bacillus subtilis* revealed through a novel hybrid regulator approach. *Mol. Microbiol.* 49, 1639–1655. doi: 10.1046/j.1365-2958.2003.03661.x
- Huang, R. Z., Zheng, L. K., Liu, H. Y., Pan, B., Hu, J., Zhu, T., et al. (2012). Thiazolidine derivatives targeting the histidine kinase YycG are effective against both planktonic and biofilm-associated *Staphylococcus epidermidis*. *Acta Pharmacol. Sin.* 33, 418–425. doi: 10.1038/aps.2011.166
- Ibanez de Aldecoa, A. L., Zafra, O., and Gonzalez-Pastor, J. E. (2017). Mechanisms and regulation of extracellular DNA release and its biological roles in microbial communities. *Front. Microbiol.* 8:1390. doi: 10.3389/fmicb.2017.01390
- Kim, T., Choi, J., Lee, S., Yeo, K. J., Cheong, H. K., and Kim, K. K. (2016). Structural studies on the extracellular domain of sensor histidine kinase YycG from *Staphylococcus aureus* and its functional implications. *J. Mol. Biol.* 428, 3074–3089. doi: 10.1016/j.jmb.2016.06.019
- Lei, M. G., Cue, D., Roux, C. M., Dunman, P. M., and Lee, C. Y. (2011). Rsp inhibits attachment and biofilm formation by repressing *fmbA* in *Staphylococcus aureus* MW2. *J. Bacteriol.* 193, 5231–5241. doi: 10.1128/jb.05454-11
- Lister, J. L., and Horswill, A. R. (2014). *Staphylococcus aureus* biofilms: recent developments in biofilm dispersal. *Front. Cell. Infect. Microbiol.* 4:178. doi: 10.3389/fcimb.2014.00178
- Liu, H., Zhao, D., Chang, J., Yan, L., Zhao, F., Wu, Y., et al. (2014). Efficacy of novel antibacterial compounds targeting histidine kinase YycG protein. *Appl. Microbiol. Biotechnol.* 98, 6003–6013. doi: 10.1007/s00253-014-5685-8
- Lou, Q., Zhu, T., Hu, J., Ben, H., Yang, J., Yu, F., et al. (2011). Role of the SaeRS two-component regulatory system in *Staphylococcus epidermidis* autolysis and biofilm formation. *BMC Microbiol.* 11:146. doi: 10.1186/1471-2180-11-146
- Lv, Z., Zhao, D., Chang, J., Liu, H., Wang, X., Zheng, J., et al. (2017). Anti-bacterial and anti-biofilm evaluation of thiazolopyrimidinone derivatives targeting the histidine kinase YycG protein of *Staphylococcus epidermidis*. *Front. Microbiol.* 8:549. doi: 10.3389/fmicb.2017.00549
- Mack, D., Nedelmann, M., Krokotsch, A., Schwarzkopf, A., Heesemann, J., and Laufs, R. (1994). Characterization of transposon mutants of biofilm-producing *Staphylococcus epidermidis* impaired in the accumulative phase of biofilm production: genetic identification of a hexosamine-containing polysaccharide intercellular adhesin. *Infect. Immun.* 62, 3244–3253. doi: 10.1128/iai.62.8.3244-3253.1994
- Mann, E. E., Rice, K. C., Boles, B. R., Endres, J. L., Ranjit, D., Chandramohan, L., et al. (2009). Modulation of eDNA release and degradation affects *Staphylococcus aureus* biofilm maturation. *PLoS One* 4:e5822. doi: 10.1371/journal.pone.0005822
- McCann, M. T., Gilmore, B. F., and Gorman, S. P. (2008). *Staphylococcus epidermidis* device-related infections: pathogenesis and clinical management. *J. Pharm. Pharmacol.* 60, 1551–1571. doi: 10.1211/jpp/60.12.0001
- Mikkelsen, H., Sivaneson, M., and Filloux, A. (2011). Key two-component regulatory systems that control biofilm formation in *Pseudomonas aeruginosa*. *Environ. Microbiol.* 13, 1666–1681. doi: 10.1111/j.1462-2920.2011.02495.x
- Mohedano, M. L., Overweg, K., de la Fuente, A., Reuter, M., Altabe, S., Mulholland, F., et al. (2005). Evidence that the essential response regulator YycF in *Streptococcus pneumoniae* modulates expression of fatty acid biosynthesis genes and alters membrane composition. *J. Bacteriol.* 187, 2357–2367. doi: 10.1128/jb.187.7.2357-2367.2005
- Ng, W. L., Tsui, H. C., and Winkler, M. E. (2005). Regulation of the *pspA* virulence factor and essential *pcsB* murein biosynthetic genes by the phosphorylated VicR (YycF) response regulator in *Streptococcus pneumoniae*. *J. Bacteriol.* 187, 7444–7459. doi: 10.1128/jb.187.21.7444-7459.2005
- Ng, W. L., and Winkler, M. E. (2004). Singular structures and operon organizations of essential two-component systems in species of *Streptococcus*. *Microbiology* 150(Pt 10), 3096–3098. doi: 10.1099/mic.0.27550-0
- Qin, Z., Zhang, J., Xu, B., Chen, L., Wu, Y., Yang, X., et al. (2006). Structure-based discovery of inhibitors of the YycG histidine kinase: new chemical leads to combat *Staphylococcus epidermidis* infections. *BMC Microbiol.* 6:96. doi: 10.1186/1471-2180-6-96
- Rasamiravaka, T., Labtani, Q., Duez, P., and El Jaziri, M. (2015). The formation of biofilms by *Pseudomonas aeruginosa*: a review of the natural and synthetic compounds interfering with control mechanisms. *Biomed. Res. Int.* 2015:759348. doi: 10.1155/2015/759348
- Regina, V. R., Lokanathan, A. R., Modrzynski, J. J., Sutherland, D. S., and Meyer, R. L. (2014). Surface physicochemistry and ionic strength affects eDNA's role in bacterial adhesion to abiotic surfaces. *PLoS One* 9:e105033. doi: 10.1371/journal.pone.0105033
- Romling, U., and Balsalobre, C. (2012). Biofilm infections, their resilience to therapy and innovative treatment strategies. *J. Intern. Med.* 272, 541–561. doi: 10.1111/joim.12004
- Rupp, M. E. (2014). Clinical characteristics of infections in humans due to *Staphylococcus epidermidis*. *Methods Mol. Biol.* 1106, 1–16. doi: 10.1007/978-1-62703-736-5_1
- Santelli, E., Liddington, R. C., Mohan, M. A., Hoch, J. A., and Szurmant, H. (2007). The crystal structure of *Bacillus subtilis* YycI reveals a common fold for two members of an unusual class of sensor histidine kinase regulatory proteins. *J. Bacteriol.* 189, 3290–3295. doi: 10.1128/jb.01937-06

- Sauer, K. (2003). The genomics and proteomics of biofilm formation. *Genome Biol.* 4:219. doi: 10.1186/gb-2003-4-6-219
- Schaeffer, C. R., Woods, K. M., Longo, G. M., Kiedrowski, M. R., Paharik, A. E., Buttner, H., et al. (2015). Accumulation-associated protein enhances *Staphylococcus epidermidis* biofilm formation under dynamic conditions and is required for infection in a rat catheter model. *Infect. Immun.* 83, 214–226. doi: 10.1128/iai.02177-14
- Senadheera, M. D., Guggenheim, B., Spatafora, G. A., Huang, Y. C., Choi, J., Hung, D. C., et al. (2005). A VicRK signal transduction system in *Streptococcus mutans* affects gtfBCD, gbpB, and ftf expression, biofilm formation, and genetic competence development. *J. Bacteriol.* 187, 4064–4076. doi: 10.1128/jb.187.12.4064-4076.2005
- Shah, N., Gaupp, R., Moriyama, H., Eskridge, K. M., Moriyama, E. N., and Somerville, G. A. (2013). Reductive evolution and the loss of PDC/PAS domains from the genus *Staphylococcus*. *BMC Genomics* 14:524. doi: 10.1186/1471-2164-14-524
- Szurmant, H., Bu, L., Brooks, C. L., and Hoch, J. A. (2008). An essential sensor histidine kinase controlled by transmembrane helix interactions with its auxiliary proteins. *Proc. Natl. Acad. Sci. U.S.A.* 105, 5891–5896. doi: 10.1073/pnas.0800247105
- Tang, L., Schramm, A., Neu, T. R., Revsbech, N. P., and Meyer, R. L. (2013). Extracellular DNA in adhesion and biofilm formation of four environmental isolates: a quantitative study. *FEMS Microbiol. Ecol.* 86, 394–403. doi: 10.1111/1574-6941.12168
- Taylor, B. L., and Zhulin, I. B. (1999). PAS domains: internal sensors of oxygen, redox potential, and light. *Microbiol. Mol. Biol. Rev. MMBR* 63, 479–506. doi: 10.1128/mmbr.63.2.479-506.1999
- Vu, B., Chen, M., Crawford, R. J., and Ivanova, E. P. (2009). Bacterial extracellular polysaccharides involved in biofilm formation. *Molecules* 14, 2535–2554. doi: 10.3390/molecules14072535
- Vuong, C., Gerke, C., Somerville, G. A., Fischer, E. R., and Otto, M. (2003). Quorum-sensing control of biofilm factors in *Staphylococcus epidermidis*. *J. Infect. Dis.* 188, 706–718. doi: 10.1086/377239
- Vuong, C., Kidder, J. B., Jacobson, E. R., Otto, M., Proctor, R. A., and Somerville, G. A. (2005). *Staphylococcus epidermidis* polysaccharide intercellular adhesin production significantly increases during tricarboxylic acid cycle stress. *J. Bacteriol.* 187, 2967–2973. doi: 10.1128/jb.187.9.2967-2973.2005
- Vuong, C., and Otto, M. (2002). *Staphylococcus epidermidis* infections. *Microbes Infect* 4, 481–489.
- Winkler, M. E., and Hoch, J. A. (2008). Essentiality, bypass, and targeting of the YycFG (VicRK) two-component regulatory system in gram-positive bacteria. *J. Bacteriol.* 190, 2645–2648. doi: 10.1128/jb.01682-1687
- Wolcott, R. D., Rhoads, D. D., Bennett, M. E., Wolcott, B. M., Gogokhia, L., Costerton, J. W., et al. (2010). Chronic wounds and the medical biofilm paradigm. *J. Wound Care* 19, 45–52. doi: 10.12968/jowc.2010.19.2.46966
- Wolska, K. I., Grudniak, A. M., Rudnicka, Z., and Markowska, K. (2016). Genetic control of bacterial biofilms. *J. Appl. Genet.* 57, 225–238. doi: 10.1007/s13353-015-0309-2
- Wu, Y., Wu, Y., Zhu, T., Han, H., Liu, H., Xu, T., et al. (2015). *Staphylococcus epidermidis* SrrAB regulates bacterial growth and biofilm formation differently under oxic and microaerobic conditions. *J. Bacteriol.* 197, 459–476. doi: 10.1128/jb.02231-14
- Xu, T., Wu, Y., Lin, Z., Bertram, R., Gotz, F., Zhang, Y., et al. (2017). Identification of genes controlled by the essential YycFG two-component system reveals a role for biofilm modulation in *Staphylococcus epidermidis*. *Front. Microbiol.* 8:724. doi: 10.3389/fmicb.2017.00724
- Yao, Y., Vuong, C., Kocianova, S., Villaruz, A. E., Lai, Y., Sturdevant, D. E., et al. (2006). Characterization of the *Staphylococcus epidermidis* accessory-gene regulator response: quorum-sensing regulation of resistance to human innate host defense. *J. Infect. Dis.* 193, 841–848. doi: 10.1086/500246
- Zhu, T., Lou, Q., Wu, Y., Hu, J., Yu, F., and Qu, D. (2010). Impact of the *Staphylococcus epidermidis* LytSR two-component regulatory system on murein hydrolase activity, pyruvate utilization and global transcriptional profile. *BMC Microbiol.* 10:287. doi: 10.1186/1471-2180-10-287

Conflict of Interest: The authors declare that the research was conducted in the absence of any commercial or financial relationships that could be construed as a potential conflict of interest.

Copyright © 2020 Lyu, Shang, Wang, Wu, Zheng, Liu, Gong, Ye and Qu. This is an open-access article distributed under the terms of the Creative Commons Attribution License (CC BY). The use, distribution or reproduction in other forums is permitted, provided the original author(s) and the copyright owner(s) are credited and that the original publication in this journal is cited, in accordance with accepted academic practice. No use, distribution or reproduction is permitted which does not comply with these terms.



Antimicrobial Peptide Cec4 Eradicates the Bacteria of Clinical Carbapenem-Resistant *Acinetobacter baumannii* Biofilm

Weiwei Liu^{1,2,3†}, Zhaoying Wu^{1,2,3†}, Chengju Mao^{2,3}, Guo Guo³, Zhu Zeng^{1,3}, Ying Fei⁴, Shan Wan⁴, Jian Peng^{1,2,3*} and Jianwei Wu^{3*}

OPEN ACCESS

Edited by:

Luis Cláudio Nascimento da Silva,
Universidade Ceuma, Brazil

Reviewed by:

Cesar de la Fuente-Nunez,
University of Pennsylvania,
United States
Maria Bagattini,
University of Naples Federico II, Italy
Lucas Pinheiro Dias,
Federal University of Ceará, Brazil

*Correspondence:

Jian Peng
jianpeng@gmc.edu.cn
Jianwei Wu
wjw@gmc.edu.cn

[†] These authors have contributed
equally to this work

Specialty section:

This article was submitted to
Antimicrobials, Resistance
and Chemotherapy,
a section of the journal
Frontiers in Microbiology

Received: 16 February 2020

Accepted: 12 June 2020

Published: 11 August 2020

Citation:

Liu W, Wu Z, Mao C, Guo G,
Zeng Z, Fei Y, Wan S, Peng J and
Wu J (2020) Antimicrobial Peptide
Cec4 Eradicates the Bacteria
of Clinical Carbapenem-Resistant
Acinetobacter baumannii Biofilm.
Front. Microbiol. 11:1532.
doi: 10.3389/fmicb.2020.01532

¹ Immune Cells and Antibody Engineering Research Center of Guizhou Province, Guizhou Medical University, Guiyang, China, ² Key Laboratory of Environmental Pollution Monitoring and Disease Control, Ministry of Education, Guizhou Medical University, Guiyang, China, ³ The Key and Characteristic Laboratory of Modern Pathogen Biology, Basic Medical College, Guizhou Medical University, Guiyang, China, ⁴ The Center for Clinical Laboratories, The Affiliated Hospital of Guizhou Medical University, Guiyang, China

The drug resistance rate of *Acinetobacter baumannii* increases year on year, and the drugs available for the treatment of carbapenem-resistant *A. baumannii* (CRAB) infection are extremely limited. *A. baumannii*, which forms biofilms, protects itself by secreting substrates such as exopolysaccharides, allowing it to survive under adverse conditions and increasing drug resistance. Antimicrobial peptides are small molecular peptides with broad-spectrum antibacterial activity and immunomodulatory function. Previous studies have shown that the antimicrobial peptide Cec4 has a strong effect on *A. baumannii*, but the antibacterial and biofilm inhibition of this antimicrobial peptide on clinical carbapenem resistance *A. baumannii* is not thoroughly understood. In this study, it was indicated that most of the 200 strains of CRAB were susceptible to Cec4 with a MIC of 4 μ g/ml. Cec4 has a strong inhibitory and eradication effect on the CRAB biofilm; the minimum biofilm inhibition concentration (MBIC) was 64–128 μ g/ml, and the minimum biofilm eradication concentration (MBEC) was 256–512 μ g/ml. It was observed that Cec4 disrupted the structure of the biofilm using scanning electron microscopy (SEM) and confocal laser scanning microscopy (CLSM). A comparative transcriptome analysis of the effects of the antimicrobial peptide Cec4 on CRAB biofilm, identified 185 differentially expressed genes, including membrane proteins, bacterial resistance genes, and pilus-related genes. The results show that multiple metabolic pathways, two-component regulation systems, quorum sensing, and antibiotic synthesis-related pathways in *A. baumannii* biofilms were affected after Cec4 treatment. In conclusion, Cec4 may represent a new choice for the prevention and treatment of clinical infections, and may also provide a theoretical basis for the development of antimicrobial peptide drugs.

Keywords: antimicrobial peptide, Cec4, CRAB, biofilm, transcriptome

INTRODUCTION

Acinetobacter baumannii is a non-fermenting Gram-negative bacterium, and infections often occur in patients with poor immunity, especially in patients in intensive care units or in patients undergoing invasive surgery (Handal et al., 2017). It can cause hospital-acquired pneumonia, especially ventilator-associated pneumonia, bacteremia, urinary tract infection, secondary meningitis, etc., with a high mortality rate (Bentancor et al., 2012). At the same time, *A. baumannii* is prone to drug resistance and is even resistant to carbapenem antibiotics, including imipenem and meropenem (Maragakis and Perl, 2008). At present, most antibiotics, except tigecycline and polymyxin, do not affect it (Dafopoulou et al., 2019). Although tigecycline has a broad antibacterial spectrum and good antibacterial activity, the blood concentration is low, only 0.7–0.8 mg/L (Cai and Wang, 2011). Therefore, it remains controversial to use tigecycline to treat blood-related infections (Akalay et al., 2020); moreover, polymyxin has greater renal and neurotoxicity, limiting its use (Spapen et al., 2011). By organism, the highest overall rates of multidrug resistance reported in a study were among *A. baumannii* isolates, for which 44% of isolates collected globally were multidrug-resistant bacteria. Additionally, the treatment options for infections caused by such organisms are limited, which deserves attention (Giammanco et al., 2017). Recently, the World Health Organization (WHO) classified carbapenem-resistant *A. baumannii* (CRAB) as the first in the list of key pathogens for the development of new antibiotics (O'Shea, 2012).

When *A. baumannii* forms biofilms, its resistance increases rapidly (Eze et al., 2018). Biofilms are composed of bacteria that irreversibly adhere to the surface of living or non-living organisms and are surrounded by a secreted matrix of extracellular polysaccharide, protein, and DNA. Once the special structure forms, the bacteria express completely different genes from planktonic bacteria, with significant differences in morphology, physical and chemical properties, and antibiotic susceptibility (Jamal et al., 2018). The ability to form biofilms on abiotic surfaces under adverse conditions makes the biofilm phenotype an important virulence factor for *A. baumannii* infection (Eze et al., 2018). At the same time, it is beneficial for bacteria to survive on nutritionally limited abiotic surfaces and stressful environmental conditions (Alvarez-Fraga et al., 2016). Bacterial biofilms cause at least 65% of human infections, particularly implantable device-related infections and chronic disease infections (Williams and Costerton, 2012). Therefore, there is an urgent need for drugs that effectively treat biofilm-associated infections. At present, it has been reported that some natural product extracts and compounds can treat bacterial biofilms. Water extract of *Galla chinensis* suppressed biofilm and extracellular matrix formation of *Staphylococcus aureus* (Wu et al., 2019). Qin et al. (2014) reported the effects of two natural compounds on methicillin-resistant *Staphylococcus aureus* (MRSA). Ursolic acid can inhibit the formation of biofilms, while resveratrol combined with vancomycin can inhibit pre-formed mature biofilms. Silver nanoparticles do not affect the growth of planktonic *Staphylococcus aureus* but can reduce the production of biofilms at a concentration of 50 µg/ml

(Singh et al., 2019). However, in many cases, these anti-biofilm active ingredients are not sufficient enough to completely inhibit or eliminate bacterial biofilms and lack broad-spectrum anti-biofilm efficacy.

Antimicrobial peptides (AMPs) have a broad antibacterial spectrum and a wide range of sources, and have unique antibacterial mechanisms, making them less prone to drug resistance. It is generally believed that AMPs exert their microbicidal activity mainly through targeting the cell membrane by penetration and cell lysis activities (Aisenbrey et al., 2019). The MIC of human-derived cationic peptide LL-37 and its truncated fragments against drug-resistant *A. baumannii* is 16–32 µg/ml, and it inhibits the formation of biofilms (Feng et al., 2013). The peptide IDR-1018 exhibits broad-spectrum anti-biofilm activity against a variety of hospital pathogens, including *Pseudomonas aeruginosa* and *Klebsiella pneumonia* (de la Fuente-Nunez et al., 2014). Therefore, antimicrobial peptides are expected to become new drugs for the treatment of bacterial biofilm and associated infections (Kim et al., 2020; Neshani et al., 2020). Our previous study found that the peptide Cec4 had a minimum inhibitory concentration (MIC) of 4 µg/ml against an *A. baumannii* reference strain (ATCC19606), which is superior to the reported similar cecropin antimicrobial peptides Cec1, cecropin A and fusion peptide CA. (1–8) M (1–18) (Saugar et al., 2002; Batoni et al., 2011; Long et al., 2017). It was confirmed in the previous report that the semi-inhibitory concentration of Cec4 on the formation of standard *A. baumannii* biofilms (to inhibit the formation of biofilm by 50%) is about 4 µg/ml; this peptide is non-hemolytic on human red blood cells at high concentrations (100 × MIC) (Peng et al., 2019). However, whether the antimicrobial peptide Cec4 can inhibit CRAB and its biofilm to the same extent as with the *A. baumannii* (ATCC19606), remains elusive. Therefore, 200 strains of clinical CRAB were collected, and their ability to form biofilms was tested. Furthermore, the susceptibility and biofilm formation of *A. baumannii* isolates to the antimicrobial peptide Cec4 were evaluated, and the molecular mechanism of Cec4 on bacterial biofilm was analyzed by transcriptome analysis. In conclusion, this study is expected to provide new ideas for the treatment of clinical infections and presents a theoretical basis for research and development into new antibiotics.

MATERIALS AND METHODS

Synthesis and Preparation of Peptides

Antimicrobial peptide Cec4 (GWLKKIGKKIERVGNTRD ATIQAIQVAQAANVAATLKGK) was synthesized by Gil Biochemical Co., Ltd., Shanghai. Using solid-phase chemical synthesis, the purity (HPLC) > 97% and the mass of the peptide determined by spectrometry. It was dissolved to 10 mg/ml with distilled deionized H₂O (ddH₂O) and stored at –80°C for further analysis.

Bacterial Isolates and Growth Conditions

From October 2017 to December 2018, 200 isolates of CRAB from clinical samples of patients from the affiliated hospital

of Guizhou Medical University were collected and duplicate samples from the same patient were excluded. All of them come from sputum, blood, urine and so on. The collection and use of clinically isolated strains were approved by the Institutional review board (IRB) of Guizhou Medical University, China. The studies involving human participants were reviewed and approved by Guizhou Medical University and the affiliation of the ethics committee. The patients provided written informed consent to participate in this study. Minimum inhibitory concentrations (MICs) of these strains to nine antibiotics including amikacin, ertapenem, imipenem, meropenem, ceftazidime, ciprofloxacin, ceftriaxone, levofloxacin, and cefepime were assessed on MicroScan WalkAway 40-SI Analyzer (SIEMENS, Germany), according to the manufacturer's instructions. Resistance to cefotaxime was assessed using the standard disc diffusion method (Oxoid, Hampshire, United Kingdom). Interpretive breakpoints for susceptible, intermediate, and resistant were consistent with Clinical and Laboratory Standards Institute guidelines (Humphries et al., 2018). In order to ensure the accuracy of bacterial identification, the *16SrRNA* and *rpoB* genes of all strains were amplified, and PCR products were sequenced and analyzed. *A. baumannii* (ATCC19606) is a biofilm-forming positive strain. *Escherichia coli* ATCC25922 and *Pseudomonas aeruginosa* ATCC27853 were used as quality control bacteria. The above strains are stored in the Pathogen Biology Laboratory of Guizhou Medical University. Strains were grown on Mueller-Hinton Broth (MHB), Typic Soy Broth (TSB) or Luria-Bertani (LB) agar plates and incubated at 37°C.

Detecting the Minimum Inhibitory Concentration (MIC) Value

According to a previous study (Wiegand et al., 2008), the MIC of Cec4 peptide against 200 strains of CRAB was assessed using the broth microdilution assay in MHB. After adding different concentrations of antimicrobial peptide Cec4, the 96-well plate was placed in a constant temperature incubator at 37°C. After incubation for 24 h, it was observed. The MIC was defined as the lowest drug concentration that can inhibit bacterial growth by visual evaluation.

Quantitative Biofilm Formation Assay

According to the crystal violet staining method of a previous study (O'Toole, 2011), the 96-well tissue culture plate method was utilized for a quantitative evaluation of biofilm formation by 200 strains of CRAB. *A. baumannii* ATCC19606 was used as the positive control, and TSB medium without bacteria was used as the negative control. Absorbance at 570 nm (OD₅₇₀) was measured for each well to obtain quantitative data on biofilm formation as described previously (Badmasti et al., 2015). The mean ± standard deviation of the OD value of the negative control was defined as OD_c. Based on the OD value, the strains were divided into the following four groups: the OD value of the test strain was compared with OD_c, and OD₅₇₀ ≤ OD_c was negative for biofilm formation (−); OD_c < OD₅₇₀ ≤ 2 × OD_c indicates weak biofilm formation

(+); 2 × OD_c < OD₅₇₀ ≤ 4 × OD_c indicates moderate biofilm formation (++); 4 × OD_c < OD₅₇₀ indicates strong biofilm formation (+++).

Detection of the Minimum Biofilm Inhibition Concentration (MBIC) and Minimum Biofilm Eradication Concentration (MBEC)

In order to detect the inhibitory effect of Cec4 peptide on the growth of biofilms, a method described in the literature was used with modifications (Abouelhassan et al., 2017). Briefly, 200 μl of bacterial cells (1 × 10⁶ CFU/ml) of 10 strains (CRAB 3, 4, 53, 55, 78, 117, 120, 128, 130, 136) with the strongest biofilm formation ability was inoculated in a polyethylene 96-well plate; TSB culture medium containing no bacteria was used as the blank control, and the plate was incubated at 37°C for 24 h. The culture medium was subsequently removed, and wells were carefully washed with PBS three times to remove planktonic bacteria. And then, 200 μl of TSB culture medium containing Cec4 in serial doubling dilutions was added to each well. TSB medium without an antimicrobial peptide was used as a negative control, and plates were incubated at 37°C for 24 h. If OD₆₀₀ < 0.1, there was no bacterial growth, and the lowest concentration without bacterial growth at this time point was recorded; this is the MBIC. Then, cells and peptide in the 96-well cell culture plate were washed with PBS, and 200 μl of TSB culture medium was added to each well. The plate was incubated at 37°C for 24 h to re-grow the surviving biofilm bacteria. An OD₆₀₀ < 0.1 indicated that there was no bacterial growth. The lowest concentration at which no bacterial growth was recorded is the MBEC. In order to evaluate the eradication efficiency of Cec4 on the biofilm, the culture in the wells was removed and washed with PBS to remove non-adherent cells. The biofilm was quantified by the aforementioned method, and calculated using the equation

$$\left(1 - \frac{\text{OD}_{570} \text{ of the test}}{\text{OD}_{570} \text{ of non-treated control}}\right) \times 100.$$

Scanning Electron Microscopy (SEM)

According to a previous report (Ramalingam and Lee, 2018), the biofilm of CRAB 55 was cultured *in vitro* in a 6-well plate, and a sterile polylysine-treated cover glass and a sterile medical catheter cut at a length of 1 cm were added in advance as a biofilm growth carrier. Samples were processed by gradient dehydration with 20, 50, 70, 90, and 100% ethanol/tert-butanol mixture. The samples were dried in a critical point dryer and placed in a high vacuum evaporator, then sprayed gold with an ion sprayer and observed using a scanning electron microscope (Hitachi S-3400).

Confocal Laser Scanning Microscope Analysis

Confocal laser scanning microscopy analysis was carried out according to a previous study (Bortolin et al., 2016). A sterile polylysine-treated cover glass was used as the carrier, and the biofilm of CRAB 55 was cultivated according to the method of the previous step. Then, 1 mM SYTO9 and 10 mM propidium iodide (PI) were added and incubated for 15 min in the dark.

An Olympus Fluoview FV1000 confocal microscope (Olympus, Markham, ON, Canada) was used to obtain a fluorescence image. The bottom of the biofilm to the surface was scanned layer by layer along the Z-axis to record the earliest and last disappearance of fluorescence, and the corresponding biofilm thickness was calculated accordingly; each layer was 1 μm . The resulting stacks of images were quantified using an image processing package (ImageJ, United States) and subsequently rendered into three-dimensional mode using image analysis software (Imaris 7.2.3, Bitplane, Switzerland).

Motility Assays

As described by a previous study (McQueary and Actis, 2011), twitching plates were made with 10 g/l tryptone, 5 g/l yeast extract and 5 g/l NaCl and 1% Eiken agar, with different concentrations of Cec4 (or none). A single colony of CRAB 55 was picked from a normal LB agar (1.5%, wt/vol) plate and inoculated vertically to the bottom of the plate, so that it could grow at the intersection of the bottom of the agar layer and the culture dish. The plate was incubated at 37°C for 24 h, and motility was evaluated by observing the formation of a transparent halo around the growing colonies and measuring the diameter. Twitching motility assays were conducted on at least three separate occasions. As described in a previous study (Harding et al., 2013), surface motility plates are comprised of 5 g/l tryptone, 2.5 g/l NaCl and 0.35% Eiken agar, with different concentrations of Cec4 or not. The bacteria were cultured to the logarithmic phase, then a 2 μl of aliquot of an overnight culture was stabbed into the surface of the center of the plate, and motility was measured after incubating the plate at 37°C for 24 h. Surface-associated motility assays were conducted on at least three separate occasions.

Quantitative RT-PCR

According to a previous study (He et al., 2015), biofilm formation of CRAB 55 was conducted as described above, and after the biofilm had been treated with Cec4 or not, it was scraped from the plate with a cell spatula. Total RNA was extracted using Trizol. RNA was quantified and quality was assessed using a NanoDrop spectrophotometer (ND-2000, Thermo Scientific, Loughborough, United Kingdom), and the final RNA concentration was adjusted to 1 ng/ μl . cDNA was synthesized in a 20 μl reaction mixture using a PrimeScript RT reagent Kit with gDNA Eraser. According to the SYBR Premix Ex Taq TM Kit (Takara, Dalian, China) protocol, the reactions were run on an ABI7300 real-time PCR system using a 20 μl reaction volume. Gene expression levels were normalized to the abundance of *A. baumannii* 16S rRNA. Target genes included *CsuE*, *BfmR*, *BfmS*, *AbaI*, and *Bap*. The primers were designed with reference to the GenBank sequences. The primer sequences are shown in the **Supplementary Table S1**.

RNA-Seq

RNA Isolation, Library Construction and Sequencing

The four strains CRAB 4, 55, 78, and 117 with the strong biofilm-forming ability and similar characteristics were selected as four biological replicates. The logarithmic growth culture was washed

twice in sterile PBS and diluted to 10^6 cells/ml in TSB. Then, 4 ml of the culture was added to a flat-bottomed 6-well plate (Corning, United States) and incubated at 37°C for 24 h to form a biofilm. Samples were collected as a control group (Control 1, Control 2, Control 3 and Control 4). For the Cec4 treatment group (ABF1, ABF2, ABF3, and ABF4), after forming mature biofilms, non-adherent cells were removed, and TSB culture solution containing $4 \times \text{MIC}$ (16 $\mu\text{g/ml}$) of Cec4 was added. Biofilm samples were collected 24 h later.

The total RNA of these samples was extracted using Trizol reagent (Sigma-Aldrich, United States) according to the previously described method. The quality and quantity were determined by a NanoPhotometer spectrophotometer (IMPLEN, CA, United States) and an Agilent 2100 bioanalyzer (Agilent Technologies, CA, United States). RNA-seq library construction and RNA sequencing were performed by the Novogene Corporation (Beijing, China). Sequence reads were deposited at the National Center for Biotechnology Information under BioProject PRJNA607078 as SAMN14120700, SAMN14120701, SAMN14120702, SAMN14120703, SAMN14120704, SAMN14120705, SAMN14120706, SAMN14120707¹.

Identification of Differentially Expressed Genes and Annotation

Raw reads were generated from the image data and stored as FASTQ format. Raw data were filtered to remove adaptor contaminated and low-quality sequences and to obtain clean reads. Genomic mapping of the filtered sequence was performed using Bowtie2-2.2.3 (Langmead and Salzberg, 2012). The reference genome and gene model annotation file of *A. baumannii* AB030 was downloaded from GenBank (NZ_CP009257.1). HTSeq v0.6.1 was used to count the read numbers mapped to each gene. The expected number of fragments per kilobase of transcript sequence per million base pairs sequenced (FPKM) of each gene was calculated based on the length of the gene and reads count mapped to this gene (Trapnell et al., 2012). Differential expression analysis of two groups (four biological replicates per group) was performed using the DEGSeq R package (??) (Anders and Huber, 2012). The resulting *p*-values were adjusted using the Benjamini and Hochberg approach for controlling the false discovery rate. Genes with a corrected *p*-value < 0.05 and $\log_2(\text{Fold change}) > 1$ found by DEGSeq were assigned as differentially expressed. Gene ontology (GO) enrichment analysis of differentially expressed genes was implemented by the Goseq R package. The GO enrichment analysis of differentially expressed genes was achieved by Goseq software, and KOBAS software was used to test the statistical enrichment of differentially expressed genes in KEGG pathways (Kanehisa et al., 2008; Young et al., 2010). Significantly enriched KEGG pathways and GO terms were identified by a *p*-value < 0.05 using Fisher's exact test and a *p*-value < 0.01 in the hypergeometric distribution, respectively, and adjusted by false discovery rates (FDR) (Rivals et al., 2007; Boca and Leek, 2018).

¹<https://www.ncbi.nlm.nih.gov/sra/PRJNA607078>

Statistical Analysis

Statistical analysis was performed using GraphPad Prism software version 6.0 (Graph Pad Software, San Diego, CA, United States) and Student's *t*-test. Data are expressed as mean \pm standard deviation (SD). All experiments were performed in triplicate. A *p*-value < 0.05 was considered statistically significant.

RESULTS

Cec4 Inhibits Clinical Resistant Bacteria

It was reported that large differences have been shown between *A. baumannii* strains. In previous studies, Cec4 showed outstanding antibacterial activity against *A. baumannii*. Its MIC against standard *A. baumannii*(ATCC19606) was 4 $\mu\text{g/ml}$. In order to study its antibacterial effect on clinical CRAB, the susceptibility of CRAB to Cec4 was tested. As shown in **Figure 1A**, 98.5% of the 200 isolates of CRAB were susceptible to the peptide Cec4 with a MIC $\leq 4 \mu\text{g/ml}$. Only 1.5% of the strains had MIC $> 4 \mu\text{g/ml}$, which were 8 and 16 $\mu\text{g/ml}$, respectively (**Supplementary Table S2**). Therefore, the peptide Cec4 has great antibacterial effects on the majority of clinical carbapenem resistant bacteria.

The Biofilm Formation Ability of CRAB Strains

Bacteria in the form of biofilms have increased resistance to antibacterial drugs, external environmental pressures, and the host's immune system, which has brought great challenges to clinical treatment. Based on crystal violet staining, the ability of 200 isolates of CRAB to form biofilms was studied. As shown in **Figure 1B**, the OD570 value of the positive control strain ATCC19606 in the experimental plate was 1.191 ± 0.012 , and the negative control was 0.111 ± 0.005 . The OD570 value of the 200 resistant bacteria was between 0.1 and 1.9 (**Supplementary Table S2**). All 200 strains of CRAB were able to form biofilms. Among them, 53 strains (26.5%) had strong biofilm formation ability, 120 strains (60%) were moderate and 27 strains (13.5%) were weak.

Cec4 Inhibits and Eradicates Biofilm of CRAB Strains

After bacteria formed the biofilm, their resistance to drugs was greatly enhanced. Our previous studies have demonstrated that antimicrobial peptide Cec4 at 0.5 $\mu\text{g} / \text{mL}$ can inhibit the formation of *A. baumannii* biofilm (Peng et al., 2019). Regarding biofilm formation ability, the 10 strongest strains were selected to evaluate the ability of Cec4 to inhibit and eradicate their biofilm. As shown in **Supplementary Table S2**, the antimicrobial peptide Cec4 can inhibit the biofilm of the strains with the strongest CRAB biofilm formation ability at 64–128 $\mu\text{g/ml}$, and can eradicate the biofilm at 256–512 $\mu\text{g/ml}$. In order to determine the effect of Cec4 on the removal of biofilms, after the formation of mature biofilms, different concentrations of Cec4 were added to the culture for 24 h. The crystal violet staining method

was used to measure the absorbance at 570 nm to calculate the clearance rate of different concentrations of the peptide on mature biofilms. The results showed that $1 \times \text{MIC}$ (4 $\mu\text{g/ml}$) could clear more than 20% of mature biofilms, with MBEC₅₀ of 16 $\mu\text{g/ml}$ and MBEC₈₀ of 128 $\mu\text{g/ml}$ (**Figure 1C**).

Cec4 Destroys the Structure of Biofilms

Acinetobacter baumannii colonizes the surface of medical equipment and indwelling medical devices (including urinary catheters) to form biofilms, leading to long-term and recurrent infections in patients (Lin et al., 2019). Coverslips and urinary catheters were used as carriers to evaluate the ability of Cec4 to remove the biofilms formed on them. Clinical CRAB forms biofilm on coverslips and catheters, and the effects of Cec4 on the biofilm are shown in **Figure 2**. After 24 h in culture, for the untreated group, the *A. baumannii* that adhered to the coverslip mostly was bacilliform; the biofilm was dense and the cell membrane was intact, forming a typical “mushroom cloud” three-dimensional structure. After treatment with Cec4 at a concentration of $1 \times \text{MIC}$ (4 $\mu\text{g/ml}$), the biofilm structure was destroyed, and the cells were loosely distributed, and some cell surfaces appeared to be attacked. *A. baumannii* adhered to the catheter was mostly spherical and formed a thick biofilm, covered with extracellular substrates. After treatment with Cec4 (4 $\mu\text{g/ml}$), the biofilm structure was destroyed. Moreover, small vesicles appeared on the surface of the cell membrane, and even the collapse and disintegration of cells were observed.

To better understand the destructive effect of Cec4 on the biofilm, the fluorescent dyes SYTO®9 and propidium iodide were used to characterize bacteria in different states. Under the laser confocal scanning microscope, a large number of biofilm bacteria were aggregated into the control group, mainly living bacteria with green fluorescence (**Figure 3**). The total biomass was about $9 \times 10^6 \mu\text{m}^3$ and the average biofilm thickness was $> 16 \mu\text{m}$. The number of dead bacteria increased gradually after treated with Cec4 (4 $\mu\text{g/ml}$) for 2 h. It was found that many bacteria in the visual field emitted red fluorescence. The total biomass was about $4 \times 10^6 \mu\text{m}^3$, and the thickness of the biofilm was reduced to 7 μm . Therefore, the CLSM results are consistent with the SEM observations, showing that Cec4 has a strong damaging effect on CRAB strain biofilm.

Cec4 Decreases Twitching Motility and Surface-Associated Motility in CRAB

Acinetobacter baumannii adheres to the surface of the object through pili, which is the initial stage of biofilm formation. Twitching motility is a unique form of movement mediated by type IV pili. *A. baumannii* relies on the contraction and extension of type IV pili on the surface of the Petri dish, with the inoculation point as the center, and spreads around and forms interstitial colony expansion halo. We observed that, after incubation at 37°C overnight, two types of the colony grew on the Petri plate. There were colonies on the surface of the agar around the inoculation point (top colony) and a visible halo of bacteria that had twitched across the plate between the bottom of the agar and the plate (interstitial colony) (**Supplementary Figure S1**).

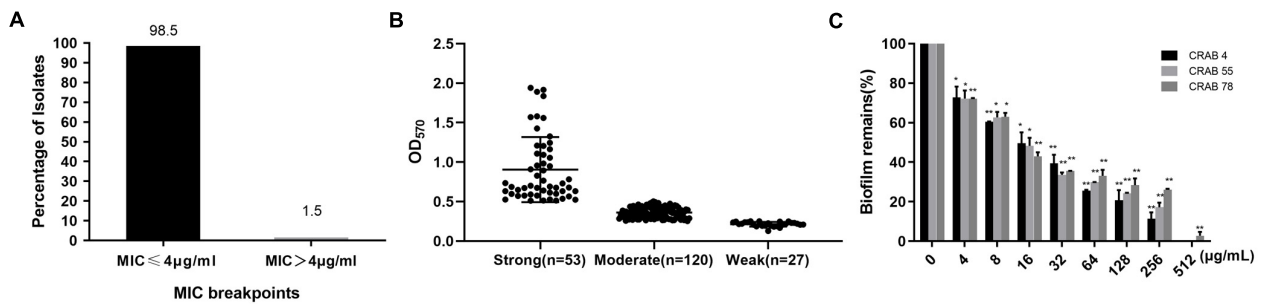


FIGURE 1 | Cec4 inhibits clinical resistant bacteria and biofilms. **(A)** Distribution of MIC value of Cec4 against 200 CRAB clinical isolates (μg/mL). **(B)** Quantification of biofilm formation in 200 CRAB clinical isolates. *A. baumannii* ATCC19606 was used as a positive control. Experiments were performed in triplicate and each bar represents the mean ± standard deviation. **(C)** The effects of Cec4 on mature biofilms of CRAB. The adherent biofilm was stained by crystal violet, and then the dye was extracted with ethanol, measured at a 570-nm absorbance, and presented as percentage of biofilm remains compared to untreated wells (0 μg/mL). All experiments were done in triplicate for statistical significance. **p* < 0.05; ***p* < 0.01.

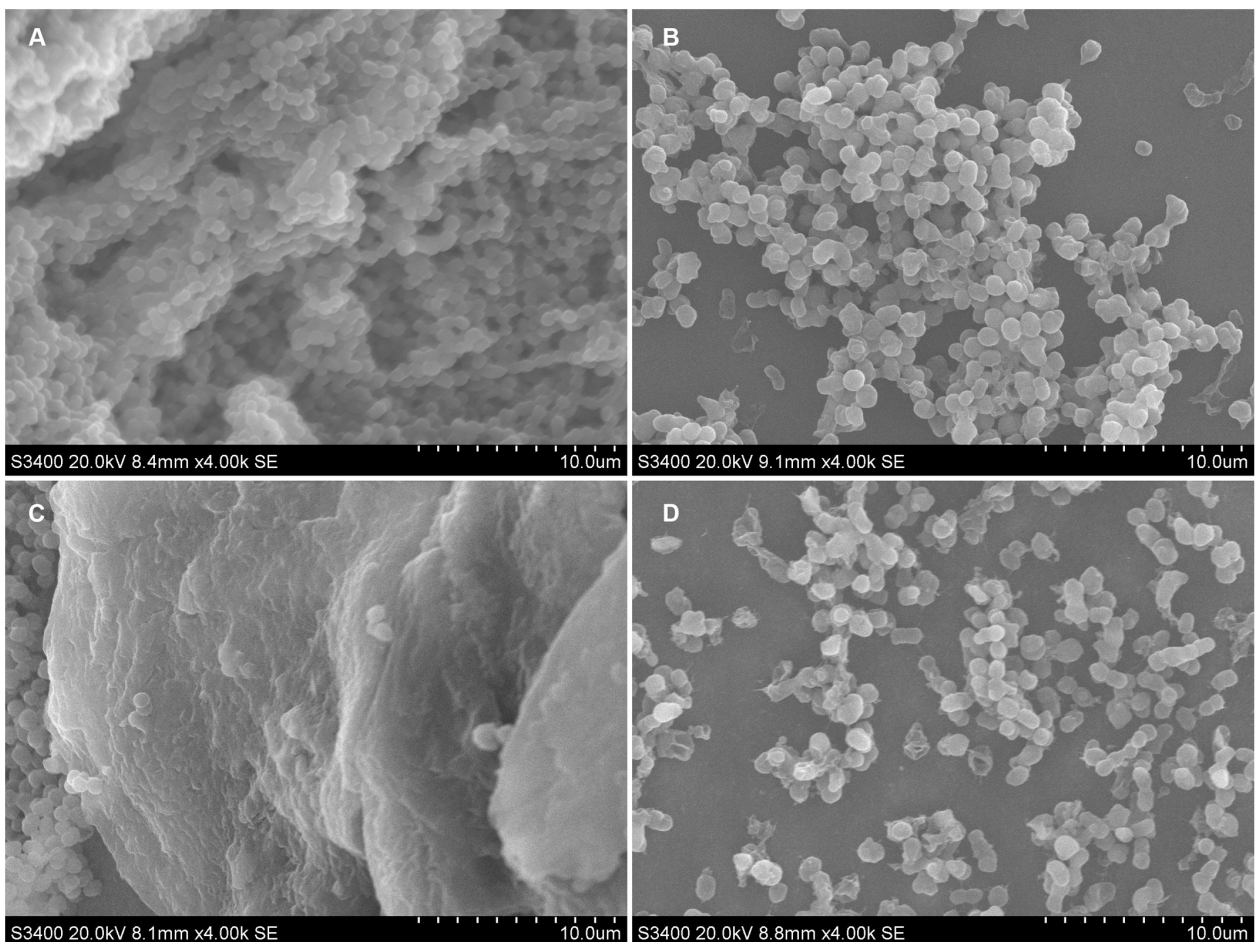


FIGURE 2 | Ultrastructural images of CRAB biofilm on sterile coverslip and catheters after treated with Cec4. **(A)** Coverslip without treatment, **(B)** Coverslip after Cec4 treatment, **(C)** catheter without treatment, and **(D)** catheter after Cec4 treatment. The selected images are the best representation of biofilms on coverslips and catheters.

Adding different concentrations of Cec4 decreased twitching motility. As the concentration of Cec4 increased, the twitching motility of bacteria decreased (**Figure 4A**). *A. baumannii* can

also move on the surface of a semi-solid medium, forming round colonies at the inoculation site of the moving plate (**Supplementary Figure S2**). The average colony diameter of

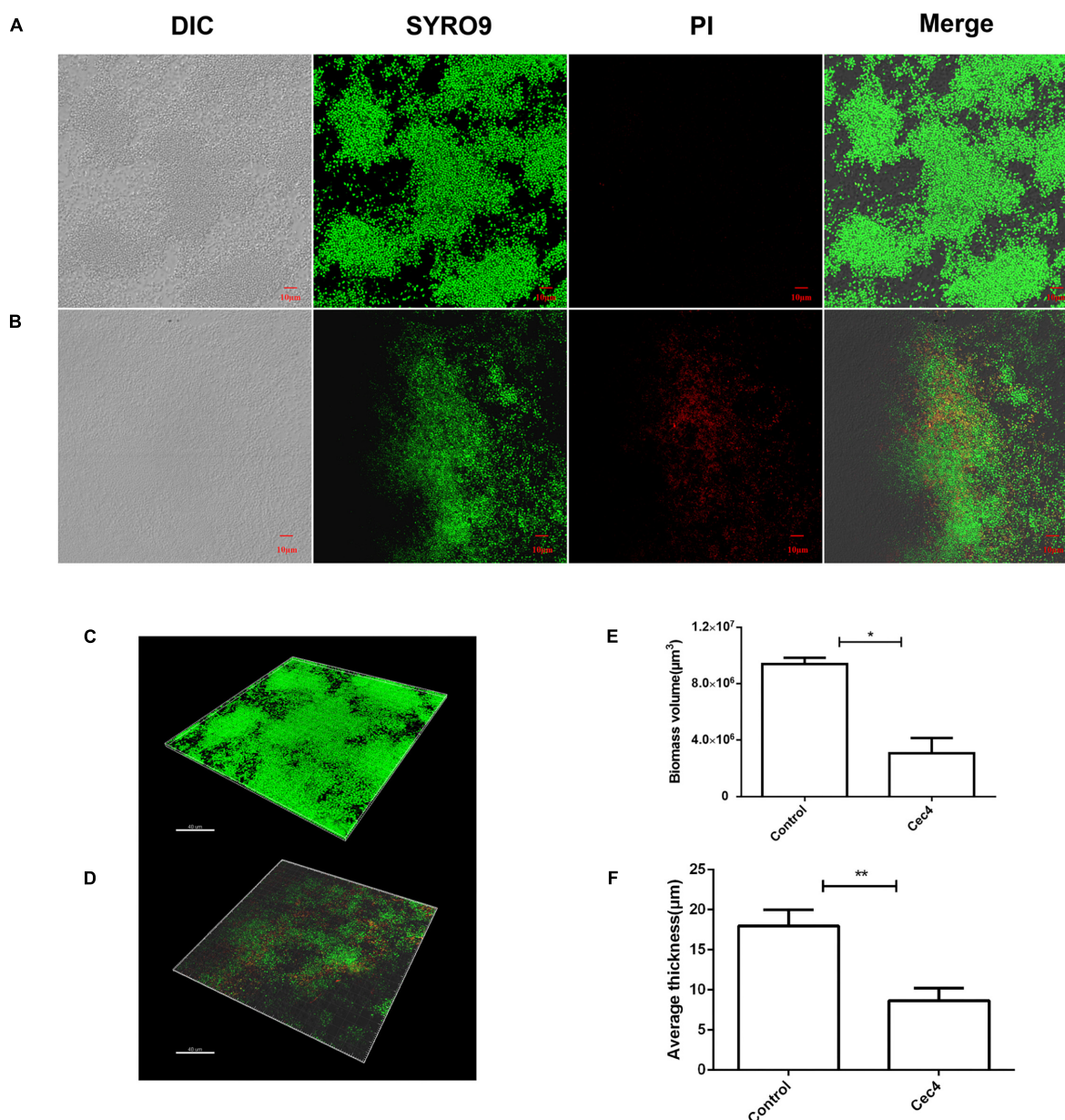


FIGURE 3 | The CRAB biofilm was removed effectively with Cec4. Confocal microscopy of CRAB biofilm without treatment (A) and after treatment with Cec4 (B). The three-dimensional reconstruction of CRAB biofilm without treatment (C) and after treatment with Cec4 (D). The total biomass volume (E) and thickness (F) of biofilm were calculated based on the fluorescence intensity. The results were averaged from three randomly selected positions of each sample. Data are expressed as mean \pm standard deviation (SD). * $p < 0.05$; ** $p < 0.01$.

the group with Cec4 was lower than that of the control group, which was consistent with the experimental results on twitching motility (Figure 4B).

Cec4 Alters the Expression of Biofilm-Related Genes

Many studies have shown that several genes of *A. baumannii* are involved in the formation of biofilms and adhesion to abiotic surfaces. In order to understand the effect of

Cec4 on these genes, the RNA of biofilm bacteria under different conditions was extracted. Next, the effect of Cec4 on the expression of *CsuE*, *BfmR*, *BfmS*, *AbaI*, and *Bap* related to biofilm formation was evaluated using qRT-PCR (Figure 4C). The results show that, compared with the control group, the pilus-related gene *CsuE* was down-regulated 1.8-fold; the two-component regulatory system genes *BfmR* and *BfmS* were down-regulated 3.6-fold and 3.9-fold, respectively; the quorum-sensing regulatory gene *AbaI* was down-regulated 6.3-fold, and the biofilm-related

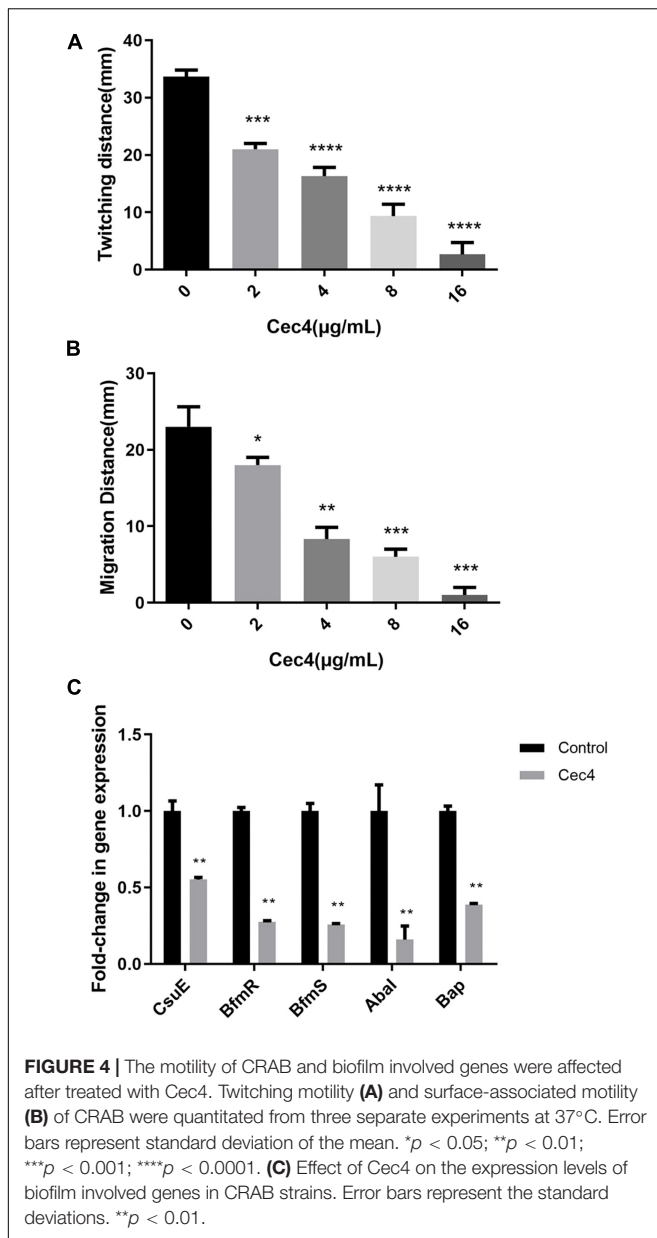


FIGURE 4 | The motility of CRAB and biofilm involved genes were affected after treated with Cec4. Twitching motility (A) and surface-associated motility (B) of CRAB were quantitated from three separate experiments at 37°C. Error bars represent standard deviation of the mean. * $p < 0.05$; ** $p < 0.01$; *** $p < 0.001$; **** $p < 0.0001$. (C) Effect of Cec4 on the expression levels of biofilm involved genes in CRAB strains. Error bars represent the standard deviations. ** $p < 0.01$.

gene *Bap* was down-regulated 2.6-fold. These results suggest that Cec4 inhibited the expression of these genes involved in biofilm formation.

Transcriptional Stress Response of CRAB Biofilm to Cec4

The RNA sequencing results revealed the differences in gene expression between ABF and control. There were 3403 genes co-expressed in these two samples; 40 genes were specificity expressed in ABF, and 6 genes were specificity expressed in control (Figure 5A). The volcano plots of the differentially expressed genes (DEGs) show that 185 genes were differentially expressed after Cec4 treatment, including 132 genes that were up-regulated (red) and 53 down-regulated genes (green) (Figure 5B).

Analysis of Differential Gene Expression

Transcriptome analysis revealed that the differential genes mainly included membrane protein-related genes, drug-resistant genes and pilus-related genes (Table 1). The expression of the amino acid ABC transporter permease, ATP-binding proteins (IX87_RS02655, IX87_RS02660, and artP) in the ABC transport system was down-regulated 1.68-fold, 1.61-fold, and 1.66-fold; the MFS transporter (IX87_RS20020) was down-regulated 2.96-fold, and the EamA family transporter (IX87_RS12100) expression was down-regulated 2.29-fold (Table 1). The expression of MBL fold metallo-hydrolase (IX87_RS19070) was down-regulated about 3-fold, ADC family cephalosporin-hydrolyzing class C beta-lactamase (IX87_RS08365) was down-regulated 1.27-fold; adeC/adeK/oprM family multidrug efflux complex outer membrane factor (IX87_RS16845) expression was up-regulated 1.37-fold (Table 1). The protein CsuA (IX87_RS06910) was down-regulated 1.51-fold, while the expression of pili assembly chaperone (IX87_RS02530) and type 4 fimbria biogenesis proteins FimT (IX87_RS10830) was up-regulated 1.8 and 1.42-fold (Table 1).

Enrichment Analysis of GO and KEGG Pathways

To further understand the function of the DEGs underlying the effect of low concentrations of Cec4 on CRAB biofilms, GO enrichment analysis was performed with the DEGs (Figure 6A). Based on sequence homology, DEGs were assigned to one or more GO terms and categorized into three main categories of GO function (biological process, molecular function, and cellular component). It is noteworthy that in the category of biological process, protein folding, extracellular polysaccharide biosynthetic process, cellular polysaccharide metabolic process, secondary metabolite biosynthetic process, protein catabolic process, dsRNA transport and regulation of DNA-templated transcription are significantly enriched. Outer membrane-bounded periplasmic space and pilus are significantly enriched in the cellular component category. Enzyme activity and nucleic acid transmembrane transporter activity are enriched in the molecular function category.

By enrichment analysis, the main KEGG metabolic pathways involved in DEGs are carbon metabolism, oxidative phosphorylation, the two-component system, ABC transporters, nucleotide excision repair, biosynthesis of antibiotics, quorum sensing, microbial metabolism in diverse environments, and β -lactam resistance (Figure 6B). It is indicated that Cec4 affected the energy metabolism of biofilm bacteria and the bacteria two-component system. By interfering with the expression of type IV pili assembly protein in the two-component system, bacterial motility function was affected. In addition, the β -lactam antibiotics are the most widely used group of antibiotics, which exert their effect by interfering with the structural cross-linking of peptidoglycans in bacterial cell walls. Bacterial resistance to β -lactam antibiotics can be achieved by producing inactivating enzymes called β -lactamases, altering the β -lactam targets of penicillin-binding proteins (PBPs), and so on. After Cec4 treatment, genes in the β -lactam resistance pathway were

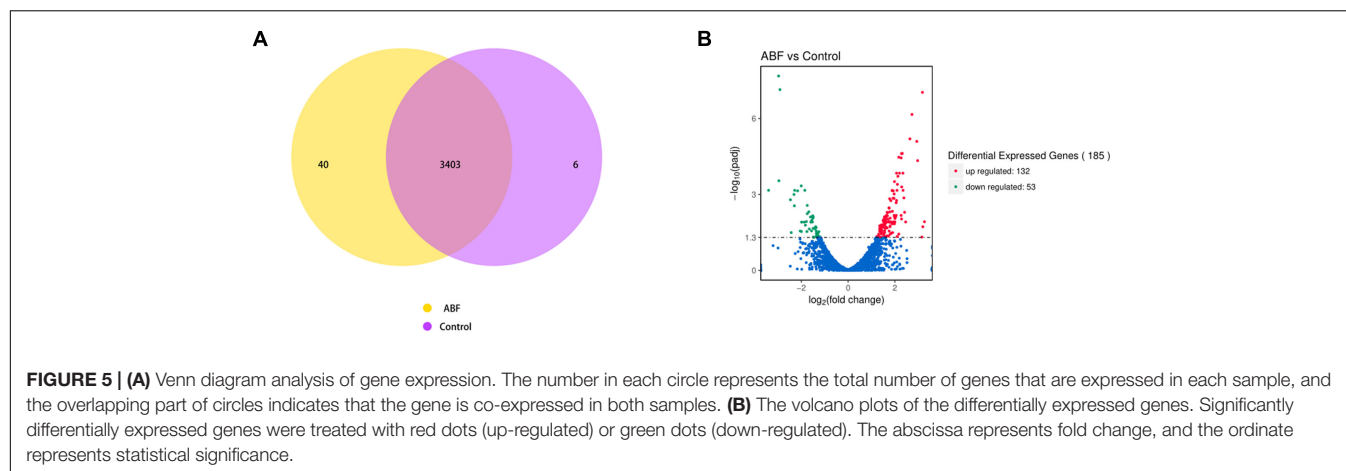


TABLE 1 | The genes up-regulated or down-regulated response to Cec4.

Gene name	Description	log ² Fold_change	Corrected p-value
Membrane protein			
IX87_RS20020	MFS transporter	-2.96	2.87×10^{-4}
IX87_RS02655	amino acid ABC transporter permease	-1.68	4.86×10^{-3}
artP	amino acid ABC transporter ATP-binding protein	-1.66	2.30×10^{-2}
IX87_RS02660	amino acid ABC transporter permease	-1.61	7.77×10^{-3}
IX87_RS12100	EamA family transporter	-2.29	6.85×10^{-4}
Bacterial resistance			
IX87_RS19070	MBL fold metallo-hydrolase	-2.97	2.11×10^{-8}
IX87_RS08365	ADC family cephalosporin-hydrolyzing class C beta-lactamase	-1.27	4.86×10^{-2}
IX87_RS16845	adeC/adeK/oprM family multidrug efflux complex outer membrane factor	1.37	2.90×10^{-2}
Pili			
IX87_RS06910	protein CsuA	-1.51	8.64×10^{-3}
IX87_RS02530	pili assembly chaperone	1.8	1.23×10^{-2}
IX87_RS10830	type 4 fimbrial biogenesis protein FimT	1.42	3.63×10^{-2}

down-regulated. More importantly, quorum sensing (QS) allows bacteria to share information about cell density and adjust gene expression accordingly, and controls including virulence, motility, sporulation and biofilm formation. Therefore, the transcriptome results indicate that Cec4 mainly affected the expression of energy metabolism and quorum sensing signaling pathway genes.

DISCUSSION

It has been reported that after bacteria form a biofilm, the MIC value for antibiotics can be increased by 1000 times or more (Alhede et al., 2011). The antimicrobial peptide can down-regulate quorum sensing, prevent the initial adhesion of bacteria to the surface, target bacteria before they form a biofilm, kill bacteria embedded in biofilms, or destroy mature biofilms to achieve the effect of inhibiting or eradicating biofilms (Batoni et al., 2016). Previous experiments have shown that Cec4 has the best antibacterial effect on *A. baumannii*, and it has very low hemolysis to human red blood cells even in high concentrations (600 µg/mL) (Peng et al., 2019). Our experiment results also

indicated that Cec4 had little cytotoxic effect on the two human cell lines HepG2 and Hela (data not shown). In this study, 200 isolates of CRAB from different clinical patients were collected to detect their biofilm formation ability and to evaluate the inhibitory effect of Cec4 on biofilms. Screening at a concentration of 4 µg/mL revealed that 98.5% of the strains were susceptible to Cec4. Thus, Cec4 has a strong inhibitory activity against standard *A. baumannii* and can also inhibit clinical CRAB. The crystal violet staining method showed that the collected clinical CRAB could form biofilms, and 26.5% of the strains could strongly form a biofilm. Cec4 eradicated more than 20% of mature biofilms at a concentration of 4 µg/mL, and the MBEC₅₀ was 16 µg/mL. When treated with Cec4 with a concentration of 256–512 µg/mL, the biofilm was completely eradicated. The SEM results indicated that the biofilm formed on the medical silicone catheter was thick, with extracellular polysaccharides and other substrates that completely covered the cells. After Cec4 was treated for 2 h, the biofilm was easily detached, and the cells were damaged or collapsed. The CLSM results further quantified the thickness and volume of the biofilms. The results show that, after 24 h, the biofilm that formed on the coverslips was thick and dense, and mainly composed of live bacteria with a thickness

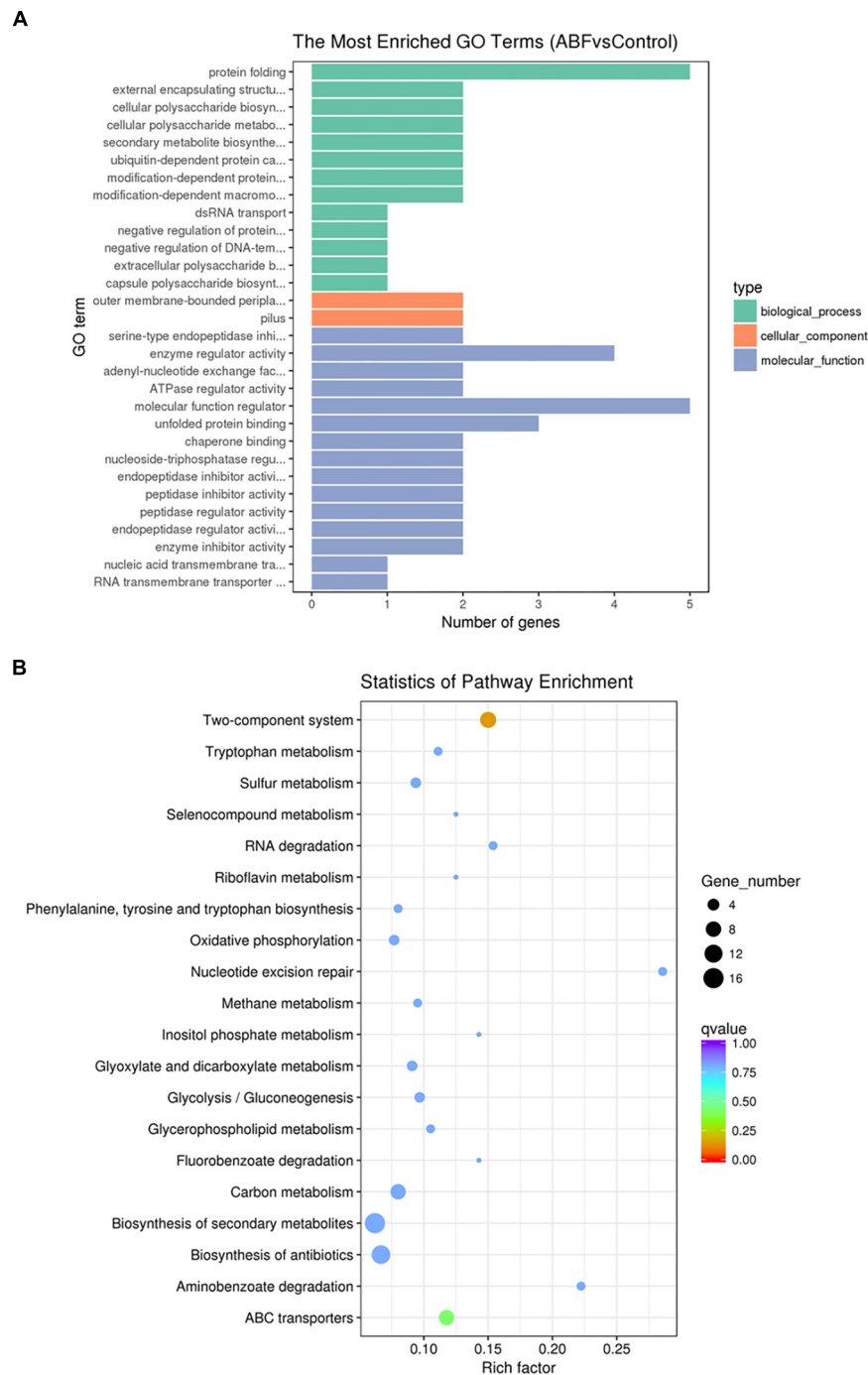


FIGURE 6 | (A) Gene Ontology (GO) analysis of differentially expressed genes. **(B)** Statistical enrichment of differentially expressed genes in KEGG pathways.

of 10–20 μm . After treatment with Cec4, the number of dead bacteria gradually increased, and the biofilm became significantly thinner. Therefore, these results indicate that Cec4 has a good eradication ability on biofilm forming of clinical CRAB.

It has been reported that *A. baumannii* adheres to the surface of living or non-living organisms by pili participating in the initial stage of biofilm formation, and thereby forming

a biofilm. The results show that Cec4 decreased pili-mediated motility in a concentration dependent manner. Under the action of Cec4 with a sub-inhibitory concentration (2 $\mu\text{g/ml}$), motility was also suppressed, and no transparent halo was formed. It has been reported that peptide 1037 inhibited the swimming of *P. aeruginosa* PA14, but stimulated twitching motility (de la Fuente-Nunez et al., 2012). The expression

of the CsuA/BABCDE chaperone complex is necessary for the assembly and production of pili associated with abiotic surface adhesion, while the Csu operon is controlled by a two-component system consisting of a BfmS-encoded sensor kinase and a BfmR-encoded response regulator. Insertion inactivation of BfmR results in the loss of expression of the CsuA/BABCDE operon, and impaired pilus production and biofilm formation (Tomaras et al., 2008). The qRT-PCR results show that Cec4 reduced the expression of *CsuE*, *BfmR* and *BfmS* genes. Clinical isolates of *A. baumannii* M2 can produce N-acyl-homoserine lactone (3-OH-C12-HSL), a product of the *abaI* autoinducer synthetase gene, which is very important for the formation of complete biofilms on abiotic surfaces (Niu et al., 2008). Our research shows that Cec4 significantly reduced the expression of *AbaI*. Therefore, we speculate that Cec4 may affect quorum sensing in bacteria. In addition, *A. baumannii* encodes for a protein associated with the biofilm, Bap. *A. baumannii* strain 307-0294, mutations in large outer membrane proteins that are highly similar to *Staphylococcus* biofilm-associated protein (Bap) were lost, resulting in a reduction in the volume and thickness of the biofilm formed by the strain (Loehfelm et al., 2008). Cec4 reduced the expression of the *Bap* gene, which was consistent with its effect on the biofilm. In conclusion, Cec4 affects the expression of genes involved in the formation of *A. baumannii* biofilms, such as quorum-sensing and motility genes.

Through the neutralization or decomposition of LPS and the interference of gene expression, abnormal regulation of the genes for biofilm survival, thus inhibiting the formation of biofilm (Li et al., 2004). It has been reported that peptide 1018 can inhibit bacterial stress response via the (p)ppGpp signaling molecule (Reffuveille et al., 2014); however, there are few reports on the mechanism of inhibition and eradication of biofilm by antimicrobial peptides. To further investigate the mechanism of action of Cec4, we used RNA-Seq to study the transcriptomic profile of CRAB biofilms treated with Cec4. The RNA-Seq results show that gene expression of CRAB biofilms was extensively altered after Cec4 treatment. Compared with the control group, membrane proteins, bacterial resistance and pilus-related genes were differentially expressed. Iron ion as an important signal regulator mediates the expression of adhesion, and then affects the formation of biofilms (Gentile et al., 2014). Our results show that bacterial ferritin was down-regulated, iron ion uptake and storage-related gene expression were increased. Besides, drug efflux-related genes and ABC transporter-related genes expressions in iron-containing cells were up-regulated. GO terms were abundant in biological process categories, indicating that bacterial biological processes were significantly affected, including the synthesis and metabolism of polysaccharides and proteins. In addition, KEGG analysis showed that multiple metabolic pathways, two-component regulation systems, quorum sensing and antibiotic synthesis-related pathways in *A. baumannii* biofilms were affected after Cec4 treatment. Most importantly, the two-component signal transduction system regulates ABC transporters and type IV pili assembly proteins and participates in the growth and formation of

biofilm bacteria (Xue et al., 2020). Whiteley et al. (2017) mentioned that quorum sensing is involved in the formation of biofilms. Cec4 may inhibit the growth of biofilms by affecting the quorum sensing signaling pathway. Therefore, the results show that Cec4 regulates the CRAB biofilm through multiple targets, and further experiments such as gene knockout verification are required to determine the key anti-biofilm mechanisms.

In summary, this study showed that Cec4 has good antibacterial activity against planktonic clinical CRAB and its biofilm. However, the biofilm formation of clinical strains has great differences. It is reported that resistant strains achieve high levels of biofilm-specific resistance despite producing weak biofilms (Qi et al., 2016). So, the epidemiological analysis of the 200 clinic CRAB strains is very important in understanding their genetic relationship. For example, it was shown that, of the cases of *A. baumannii* acquisition, at least 17% were cases of patient-to-patient transmission in the Intensive Care Unit (Harris et al., 2019). Furthermore, deeper explorations of epidemiologic studies, such as bacterial molecular typing, drug resistance, and virulence factors detecting clinical strains, would improve our understanding of their relationship. In conclusion, these results provide a new strategy for the treatment of clinical biofilm-related infections, and also lay the foundation for the development of antimicrobial peptides as new antibacterial drugs.

DATA AVAILABILITY STATEMENT

The sequencing data in the article have been deposited at the National Center for Biotechnology Information under BioProject PRJNA607078 as SAMN14120700, SAMN14120701, SAMN14120702, SAMN14120703, SAMN14120704, SAMN14120705, SAMN14120706, and SAMN14120707 (<https://www.ncbi.nlm.nih.gov/sra/PRJNA607078>).

AUTHOR CONTRIBUTIONS

ZW and WL conceived and designed the experiments. ZW, WL, and CM performed the experiments. WL, ZW, ZZ, and GG analyzed the data. YF, SW, and ZZ contributed materials and analysis tools. JP and JW wrote the manuscript. All authors analyzed the data and contributed to the manuscript, gave final approval of the version to be published, and agreed to be accountable for all aspects of the work.

FUNDING

This research was funded by the National Natural Science Foundation of China (No. 81660347), the Guizhou Provincial Science and Technology Plan Project ([2017]1154), and the Key Technologies R&D Program for Science and Technology Department of Guizhou Province ([2019]2823) is co-financed. Funders had no role in study design, data collection or analysis, preparation of the manuscript or the decision to publish

it. We also thank proof-reading-service for proofreading the manuscript (www.proof-reading-service.com).

SUPPLEMENTARY MATERIAL

The Supplementary Material for this article can be found online at: <https://www.frontiersin.org/articles/10.3389/fmicb.2020.01532/full#supplementary-material>

REFERENCES

- Abouelhassan, Y., Yang, Q., Yousaf, H., Nguyen, M. T., Rolfe, M., Schultz, G. S., et al. (2017). Nitroxoline: a broad-spectrum biofilm-eradicating agent against pathogenic bacteria. *Int. J. Antimicrob. Agents* 49, 247–251. doi: 10.1016/j.ijantimicag.2016.10.017
- Aisenbrey, C., Marquette, A., and Bechinger, B. (2019). The mechanisms of action of cationic antimicrobial peptides refined by novel concepts from biophysical investigations. *Adv. Exp. Med. Biol.* 1117, 33–64. doi: 10.1007/978-981-13-3588-4_4
- Akalay, S., Vanassche, T., and De Munter, P. (2020). Tigecycline-induced life-threatening coagulopathy in a patient with a *Mycobacterium abscess*: a case report and step-by-step diagnostic approach. *Acta Clin. Belg.* 1–5. doi: 10.1080/17443286.2020.1747197 [Epub ahead of print].
- Alhede, M., Kragh, K. N., Qvortrup, K., Allesen-Holm, M., Van Gennip, M., Christensen, L. D., et al. (2011). Phenotypes of non-attached *Pseudomonas aeruginosa* aggregates resemble surface attached biofilm. *PLoS One* 6:e27943. doi: 10.1371/journal.pone.0027943
- Alvarez-Fraga, L., Perez, A., Rumbo-Feal, S., Merino, M., Vallejo, J. A., Ohneck, E. J., et al. (2016). Analysis of the role of the LH92_11085 gene of a biofilm hyper-producing *Acinetobacter baumannii* strain on biofilm formation and attachment to eukaryotic cells. *Virulence* 7, 443–455. doi: 10.1080/21505594.2016.1145335
- Anders, S., and Huber, W. (2012). *Differential Expression of RNA-Seq Data at the Gene Level*. The DESeq Package. Heidelberg: EMBL.
- Badmasti, F., Siadat, S. D., Bouzari, S., Ajdari, S., and Shahcheraghi, F. (2015). Molecular detection of genes related to biofilm formation in multidrug-resistant *Acinetobacter baumannii* isolated from clinical settings. *J. Med. Microbiol.* 64, 559–564. doi: 10.1099/jmm.0.000058
- Batoni, G., Maisetta, G., Brancatisano, F. L., Esin, S., and Campa, M. (2011). Use of antimicrobial peptides against microbial biofilms: advantages and limits. *Curr. Med. Chem.* 18, 256–279. doi: 10.2174/092986711794088399
- Batoni, G., Maisetta, G., and Esin, S. (2016). Antimicrobial peptides and their interaction with biofilms of medically relevant bacteria. *Biochim. Biophys. Acta* 1858, 1044–1060. doi: 10.1016/j.bbame.2015.10.013
- Bentancor, L. V., Camacho-Peiro, A., Bozkurt-Guzel, C., Pier, G. B., and Maira-Litran, T. (2012). Identification of Ata, a multifunctional trimeric autotransporter of *Acinetobacter baumannii*. *J. Bacteriol.* 194, 3950–3960. doi: 10.1128/JB.06769-11
- Boca, S. M., and Leek, J. T. (2018). A direct approach to estimating false discovery rates conditional on covariates. *PeerJ* 6:e6035. doi: 10.7717/peerj.6035
- Bortolin, M., De Vecchi, E., Romano, C. L., Toscano, M., Mattina, R., and Drago, L. (2016). Antibiofilm agents against MDR bacterial strains: is bioactive glass BAG-S53P4 also effective? *J. Antimicrob. Chemother.* 71, 123–127. doi: 10.1093/jac/dkv327
- Cai, Y., and Wang, R. (2011). Tigecycline: benefits and risks. *Lancet Infect. Dis.* 11, 804–805. doi: 10.1016/s1473-3099(11)70183-9
- Dafopoulou, K., Vourli, S., Tsakris, A., and Pournaras, S. (2019). An update on polymyxin susceptibility testing methods for *Acinetobacter baumannii*. *Expert Rev. Anti Infect. Ther.* 17, 699–713. doi: 10.1080/14787210.2019.1667230
- de la Fuente-Nunez, C., Korolik, V., Bains, M., Nguyen, U., Breidenstein, E. B., Horsman, S., et al. (2012). Inhibition of bacterial biofilm formation and swarming motility by a small synthetic cationic peptide. *Antimicrob. Agents Chemother.* 56, 2696–2704. doi: 10.1128/AAC.00064-12
- de la Fuente-Nunez, C., Reffuveille, F., Haney, E. F., Straus, S. K., and Hancock, R. E. (2014). Broad-spectrum anti-biofilm peptide that targets a cellular stress response. *PLoS Pathog.* 10:e1004152. doi: 10.1371/journal.ppat.1004152
- Eze, E. C., Chenia, H. Y., and El Zowalaty, M. E. (2018). *Acinetobacter baumannii* biofilms: effects of physicochemical factors, virulence, antibiotic resistance determinants, gene regulation, and future antimicrobial treatments. *Infect. Drug Resist.* 11, 2277–2299. doi: 10.2147/idr.s169894
- Feng, X., Sambanthamoorthy, K., Palys, T., and Paranavitana, C. (2013). The human antimicrobial peptide LL-37 and its fragments possess both antimicrobial and antibiofilm activities against multidrug-resistant *Acinetobacter baumannii*. *Peptides* 49, 131–137. doi: 10.1016/j.peptides.2013.09.007
- Gentile, V., Frangipani, E., Bonchi, C., Minandri, F., Runci, F., and Visca, P. (2014). Iron and *Acinetobacter baumannii* biofilm formation. *Pathogens* 3, 704–719. doi: 10.3390/pathogens3030704
- Giammanco, A., Cala, C., Fasciana, T., and Dowzicky, M. J. (2017). Global assessment of the activity of tigecycline against multidrug-resistant gram-negative pathogens between 2004 and 2014 as part of the tigecycline evaluation and surveillance trial. *mSphere* 2:e00310-16. doi: 10.1128/mSphere.00310-16
- Handal, R., Handal, R., Qunibi, L., Sahouri, I., Juhari, M., Dawodi, R., et al. (2017). Characterization of carbapenem-resistant *Acinetobacter baumannii* strains isolated from hospitalized patients in palestine. *Int. J. Microbiol.* 2017:8012104. doi: 10.1155/2017/8012104
- Harding, C. M., Tracy, E. N., Carruthers, M. D., Rather, P. N., Actis, L. A., and Munson, R. S. Jr. (2013). *Acinetobacter baumannii* strain M2 produces type IV pili which play a role in natural transformation and twitching motility but not surface-associated motility. *mBio* 4:e00360-13. doi: 10.1128/mBio.00360-13
- Harris, A. D., Johnson, J. K., Pineles, L., O'Hara, L. M., Bonomo, R. A., and Thom, K. A. (2019). Patient-to-patient transmission of *Acinetobacter baumannii* gastrointestinal colonization in the intensive care unit. *Antimicrob. Agents Chemother.* 63:e00392-19.
- He, X., Lu, F., Yuan, F., Jiang, D., Zhao, P., Zhu, J., et al. (2015). Biofilm formation caused by clinical *Acinetobacter baumannii* isolates is associated with overexpression of the AdeFGH efflux pump. *Antimicrob. Agents Chemother.* 59, 4817–4825. doi: 10.1128/AAC.00877-15
- Humphries, R. M., Ambler, J., Mitchell, S. L., Castanheira, M., Dingle, T., Hindler, J. A., et al. (2018). CLSI methods development and standardization working group best practices for evaluation of antimicrobial susceptibility tests. *J. Clin. Microbiol.* 56:e01934-17. doi: 10.1128/JCM.01934-17
- Jamal, M., Ahmad, W., Andleeb, S., Jalil, F., Imran, M., Nawaz, M. A., et al. (2018). Bacterial biofilm and associated infections. *J. Chin. Med. Assoc.* 81, 7–11. doi: 10.1016/j.jcma.2017.07.012
- Kanehisa, M., Araki, M., Goto, S., Hattori, M., Hirakawa, M., Itoh, M., et al. (2008). KEGG for linking genomes to life and the environment. *Nucl. Acids Res.* 36, D480–D484. doi: 10.1093/nar/gkm882
- Kim, S., Lee, D.-W., Jin, J.-S., and Kim, J. (2020). Antimicrobial activity of LysSS, a novel phage endolysin, against *Acinetobacter baumannii* and *Pseudomonas aeruginosa*. *J. Glob. Antimicrob. Resist.* 22, 32–39. doi: 10.1016/j.jgar.2020.01.005
- Langmead, B., and Salzberg, S. L. (2012). Fast gapped-read alignment with Bowtie 2. *Nat. Methods* 9, 357–359. doi: 10.1038/nmeth.1923
- Li, P., Wohland, T., Ho, B., and Ding, J. L. (2004). Perturbation of Lipopolysaccharide (LPS) Micelles by Sushi 3 (S3) antimicrobial peptide. The importance of an intermolecular disulfide bond in S3 dimer for binding,

FIGURE S1 | Images of twitching motility after treated with Cec4. From left to right (A–E), the concentration of Cec4 is 0, 2, 4, 8, 16 µg/ml.

FIGURE S2 | Images of surface-associated motility after treated with Cec4. From left to right (A–E), the concentration of Cec4 is 0, 2, 4, 8, 16 µg/ml.

TABLE S1 | Oligonucleotide primers used in this study.

TABLE S2 | The MICs, MBIC, MBEC, sample source and drug susceptibility of 200 CRAB strains.

- disruption, and neutralization of LPS. *J. Biol. Chem.* 279, 50150–50156. doi: 10.1074/jbc.M405606200
- Lin, M. F., Lin, Y. Y., and Lan, C. Y. (2019). A method to assess influence of different medical tubing on biofilm formation by *Acinetobacter baumannii*. *J. Microbiol. Methods* 160, 84–86. doi: 10.1016/j.mimet.2019.03.023
- Loehfelm, T. W., Luke, N. R., and Campagnari, A. A. (2008). Identification and characterization of an *Acinetobacter baumannii* biofilm-associated protein. *J. Bacteriol.* 190, 1036–1044. doi: 10.1128/JB.01416-07
- Long, H., Yang, J., Peng, J., and Wu, J. W. (2017). Antimicrobial activity of *Musca domestica* cecropin - 4 (mdCec 4) against *Acinetobacter baumannii*. *Chin. J. Microbiol. Immunol.* 37, 891–896. doi: 10.3760/cma.j.issn.0254-5101.2017.12.002
- Maragakis, L. L., and Perl, T. M. (2008). *Acinetobacter baumannii*: epidemiology, antimicrobial resistance, and treatment options. *Clin. Infect. Dis.* 46, 1254–1263. doi: 10.1086/529198
- McQueary, C. N., and Actis, L. A. (2011). *Acinetobacter baumannii* biofilms: variations among strains and correlations with other cell properties. *J. Microbiol.* 49, 243–250. doi: 10.1007/s12275-011-0343-7
- Neshani, A., Sedighian, H., Mirhosseini, S. A., Ghazvini, K., Zare, H., and Jahangiri, A. (2020). Antimicrobial peptides as a promising treatment option against *Acinetobacter baumannii* infections. *Microb. Pathog.* 146:104238. doi: 10.1016/j.micpath.2020.104238
- Niu, C., Clemmer, K. M., Bonomo, R. A., and Rather, P. N. (2008). Isolation and characterization of an autoinducer synthase from *Acinetobacter baumannii*. *J. Bacteriol.* 190, 3386–3392. doi: 10.1128/JB.01929-07
- O'Shea, M. K. (2012). *Acinetobacter* in modern warfare. *Int. J. Antimicrob. Agents* 39, 363–375. doi: 10.1016/j.ijantimicag.2012.01.018
- O'Toole, G. A. (2011). Microtiter dish biofilm formation assay. *J. Vis. Exp.* 2437. doi: 10.3791/2437
- Peng, J., Long, H., Liu, W., Wu, Z., Wang, T., Zeng, Z., et al. (2019). Antibacterial mechanism of peptide Cec4 against *Acinetobacter baumannii*. *Infect. Drug Resist.* 12, 2417–2428. doi: 10.2147/idr.s214057
- Qi, L., Li, H., Zhang, C., Liang, B., Li, J., Wang, L., et al. (2016). Relationship between antibiotic resistance, biofilm formation, and biofilm-specific resistance in *Acinetobacter baumannii*. *Front. Microbiol.* 7:483. doi: 10.3389/fmicb.2016.00483
- Qin, N., Tan, X., Jiao, Y., Liu, L., Zhao, W., Yang, S., et al. (2014). RNA-Seq-based transcriptome analysis of methicillin-resistant *Staphylococcus aureus* biofilm inhibition by ursolic acid and resveratrol. *Sci. Rep.* 4:5467. doi: 10.1038/srep05467
- Ramalingam, K., and Lee, V. A. (2018). Antibiofilm activity of an EDTA-containing nanoemulsion on multidrug-resistant *Acinetobacter baumannii*. *Artif. Cells Nanomed. Biotechnol.* 46, 737–743. doi: 10.1080/21691401.2018.1468771
- Reffuveille, F., De La Fuente-Nunez, C., Mansour, S., and Hancock, R. E. (2014). A broad-spectrum antibiofilm peptide enhances antibiotic action against bacterial biofilms. *Antimicrob. Agents Chemother.* 58, 5363–5371. doi: 10.1128/AAC.03163-14
- Rivals, I., Personnaz, L., Taing, L., and Potier, M. C. (2007). Enrichment or depletion of a go category within a class of genes: which test? *Bioinformatics* 23, 401–407. doi: 10.1093/bioinformatics/btl633
- Saugar, J. M., Alarcon, T., Lopez-Hernandez, S., Lopez-Brea, M., Andreu, D., and Rivas, L. (2002). Activities of Polymyxin B and Cecropin A-Melittin Peptide CA(1-8)M(1-18) against a multiresistant strain of *Acinetobacter baumannii*. *Antimicrob. Agents Chemother.* 46, 875–878. doi: 10.1128/aac.46.3.875-878.2002
- Singh, N., Rajwade, J., and Paknikar, K. M. (2019). Transcriptome analysis of silver nanoparticles treated *Staphylococcus aureus* reveals potential targets for biofilm inhibition. *Colloids Surf. B Biointerf.* 175, 487–497. doi: 10.1016/j.colsurfb.2018.12.032
- Spapen, H., Jacobs, R., Van Gorp, V., Troubleyn, J., and Honore, P. M. (2011). Renal and neurological side effects of colistin in critically ill patients. *Ann. Intensive Care* 1:14. doi: 10.1186/2110-5820-1-14
- Tomaras, A. P., Flagler, M. J., Dorsey, C. W., Gaddy, J. A., and Actis, L. A. (2008). Characterization of a two-component regulatory system from *Acinetobacter baumannii* that controls biofilm formation and cellular morphology. *Microbiology* 154, 3398–3409. doi: 10.1099/mic.0.2008/019471-0
- Trapnell, C., Roberts, A., Goff, L., Pertea, G., Kim, D., Kelley, D. R., et al. (2012). Differential gene and transcript expression analysis of RNA-seq experiments with TopHat and Cufflinks. *Nat. Protoc.* 7, 562–578. doi: 10.1038/nprot.2012.016
- Whiteley, M., Diggle, S. P., and Greenberg, E. P. (2017). Bacterial quorum sensing: the progress and promise of an emerging research area. *Nature* 551, 313–320. doi: 10.1038/nature24624
- Wiegand, I., Hilpert, K., and Hancock, R. E. W. (2008). Agar and broth dilution methods to determine the minimal inhibitory concentration (MIC) of antimicrobial substances. *Nature Protoc.* 3, 163–175. doi: 10.1038/nprot.2007.521
- Williams, D. L., and Costerton, J. W. (2012). Using biofilms as initial inocula in animal models of biofilm-related infections. *J. Biomed. Mater. Res. B Appl. Biomater.* 100, 1163–1169. doi: 10.1002/jbm.b.31979
- Wu, S., Liu, Y., Zhang, H., and Lei, L. (2019). The pathogenicity and transcriptome analysis of methicillin-resistant *Staphylococcus aureus* in response to water extract of *Galla chinensis*. *Evid. Based Complement. Alternat. Med.* 2019:3276156. doi: 10.1155/2019/3276156
- Xue, M., Raheem, M. A., Gu, Y., Lu, H., Song, X., Tu, J., et al. (2020). The KdpD/KdpE two-component system contributes to the motility and virulence of avian pathogenic *Escherichia coli*. *Res. Vet. Sci.* 131, 24–30. doi: 10.1016/j.rvsc.2020.03.024
- Young, M. D., Wakefield, M. J., Smyth, G. K., and Oshlack, A. (2010). Gene ontology analysis for RNA-seq: accounting for selection bias. *Genome Biol.* 11:R14. doi: 10.1186/gb-2010-11-2-r14

Conflict of Interest: The authors declare that the research was conducted in the absence of any commercial or financial relationships that could be construed as a potential conflict of interest.

Copyright © 2020 Liu, Wu, Mao, Guo, Zeng, Fei, Wan, Peng and Wu. This is an open-access article distributed under the terms of the Creative Commons Attribution License (CC BY). The use, distribution or reproduction in other forums is permitted, provided the original author(s) and the copyright owner(s) are credited and that the original publication in this journal is cited, in accordance with accepted academic practice. No use, distribution or reproduction is permitted which does not comply with these terms.



Sodium New Houttuynia Inhibits *Candida albicans* Biofilm Formation by Inhibiting the Ras1-cAMP-Efg1 Pathway Revealed by RNA-seq

Jiadi Wu^{1†}, Daqiang Wu^{1,2,3*†}, Yeye Zhao¹, Yuanqing Si¹, Longfei Mei¹, Jing Shao^{1,2,3}, Tianming Wang³, Guiming Yan^{3*} and Changzhong Wang^{1,2,3*}

¹ Department of Pathogenic Biology and Immunology, College of Integrated Chinese and Western Medicine, Anhui University of Chinese Medicine, Hefei, China, ² Research Institute of Integrated Traditional Chinese and Western Medicine, Anhui University of Chinese Medicine, Hefei, China, ³ Key Laboratory of Chinese Herbal Compound Formula in Anhui Province, Hefei, China

OPEN ACCESS

Edited by:

Sujogya Kumar Panda,
KU Leuven, Belgium

Reviewed by:

Shunmugiah Karutha Pandian,
Alagappa University, India
Sudhanshu Shukla,
Amity University, India
Rodnei Dennis Rossoni,
São Paulo State University, Brazil

*Correspondence:

Daqiang Wu
daqwu@126.com
Guiming Yan
922-119@163.com
Changzhong Wang
ahwcz63@sina.com

[†]These authors have contributed
equally to this work

Specialty section:

This article was submitted to
Antimicrobials, Resistance
and Chemotherapy,
a section of the journal
Frontiers in Microbiology

Received: 24 April 2020

Accepted: 06 August 2020

Published: 25 August 2020

Citation:

Wu J, Wu D, Zhao Y, Si Y, Mei L,
Shao J, Wang T, Yan G and Wang C
(2020) Sodium New Houttuynia
Inhibits *Candida albicans* Biofilm
Formation by Inhibiting
the Ras1-cAMP-Efg1 Pathway
Revealed by RNA-seq.
Front. Microbiol. 11:2075.
doi: 10.3389/fmicb.2020.02075

Here, we aim to investigate the antifungal effect and mechanism of action of sodium new houttuynia (SNH) against *Candida albicans*. Microdilution analysis results showed that SNH possesses potent inhibitory activity against *C. albicans* SC5314, with a MIC₈₀ of 256 μ g/mL. Furthermore, we found that SNH can effectively inhibit the initial adhesion of *C. albicans*. Inverted microscopy, crystal violet staining, scanning electron microscopy and confocal laser scanning microscopy results showed that morphological changes during the transition from yeast to hypha and the biofilm formation of *C. albicans* are repressed by SNH treatment. We also found that SNH can effectively inhibit the biofilm formation of clinical *C. albicans* strains (Z103, Z3044, Z1402, and Z1407) and SNH in combination with fluconazole, berberine chloride, caspofungin and itraconazole antifungal agents can synergistically inhibit the biofilm formation of *C. albicans*. Eukaryotic transcriptome sequencing and qRT-PCR results showed that SNH treatment resulted in significantly down-regulated expression in several biofilm formation related genes in the Ras1-cAMP-Efg1 pathway (*ALS1*, *ALA1*, *ALS3*, *EAP1*, *RAS1*, *EFG1*, *HWP1*, and *TEC1*) and significantly up-regulated expression in yeast form-associated genes (*YWP1* and *RHD1*). We also found that SNH can effectively reduce the production of key messenger cAMP in the Ras1-cAMP-Efg1 pathway. Furthermore, using *Galleria mellonella* as an *in vivo* model we found that SNH can effectively treat *C. albicans* infection *in vivo*. Our presented results suggest that SNH exhibits potential antibiofilm effects related to inhibiting the Ras1-cAMP-Efg1 pathway in the biofilm formation of *C. albicans*.

Keywords: *Candida albicans*, sodium new houttuynia, anti-adhesive, anti-biofilm, Ras1-cAMP-Efg1 pathway

Abbreviations: AOD, average optical density; BBR, berberine chloride; cAMP, cyclic adenosine monophosphate; CAS, caspofungin; cDNA, complementary deoxyribonucleic acid; CFU, colony-forming unit; CLSM, confocal laser scanning microscopy; DEPC, diethylpyrocarbonate; FIC, fractional inhibitory concentration; FICI, fractional inhibitory concentration index; FLZ, fluconazole; GO, gene ontology; ITZ, itraconazole; LD₅₀, lethal dose 50%; MFC, minimum fungicidal concentrations; MIC₈₀, minimum inhibitory concentrations of 80%; PBS, phosphate-buffered saline; PC, principal component; PCA, principle component analysis; PCR, polymerase chain reaction; qRT-PCR, quantitative reverse transcription polymerase chain reaction; RNA, ribonucleic acid; SEM, scanning electron microscopy; SNH, sodium new houttuynia; TTT, 2,3-Bis-(2-methoxy-4-nitro-5-sulphophenyl)-2H-tetrazolium-5-carboxanilide.

INTRODUCTION

Fungal infections caused by *Candida albicans*, an opportunistic fungal pathogen (Naglik et al., 2006), are a growing threat in the immune deficient population (Wang et al., 2018), and *C. albicans* is the species most frequently implicated in different forms of invasive candidiasis (Rodriguezcerdeira et al., 2019). *C. albicans* is a dimorphic yeast that can interconvert from a yeast state to a hyphal state, commonly existing in mucosae and the digestive tract (Pizarrocerda and Cossart, 2006; Martin et al., 2018). Adherence of *C. albicans* to host cells, a prerequisite for infection, plays a significant role in pathogenesis, as it allows the establishment of a strong link to host cell surfaces and provides a focal point for infection by enabling persistence in harsh conditions (Pizarrocerda and Cossart, 2006; Martin et al., 2018). This high adherence is the main cause of fungal infection in human hosts, indicating that the highly infectious nature of this fungus may be related to its strong adherence capacity (Albrecht et al., 2006).

Numerous human infections are caused by biofilms of pathogenic microorganisms, especially fungi (Oshiro et al., 2019). Biofilm formation is initiated through adherence (Simon et al., 2018). Biofilms are complex microbial communities organized in an extracellular polymeric matrix comprising proteins, polysaccharides and DNA (Simon et al., 2018). Biofilm formation is a major concern in the clinic, as biofilms allow microorganisms to become significantly more resistant to antifungal agents and host immune clearance (Holm et al., 2015). The adhesion and biofilm formation of *C. albicans* significantly increases the risk of fungal infections with possible lethal complications (Tan et al., 2019). Therefore, new anti-adherence and anti-biofilm agents and strategies for *C. albicans* are urgently needed.

Natural products have been used as traditional medicines since ancient times (Boufridi and Quinn, 2018). *Houttuynia cordata* is an edible vegetable with a fishy taste which is widely consumed in southwest China, and also a traditional Chinese herb for treating lung and skin infections caused by pathogenic bacteria and fungi (Lu et al., 2013). Recent studies have indicated that *Houttuynia cordata* and its active ingredients demonstrate cogent antibacterial, anti-inflammatory, antiviral and anti-lung cancer activities (Jiang et al., 2019). The main effective component of *Houttuynia cordata* is sodium houttuyfonate (SH) which has a fishy odor, and has been widely used for the treatment of purulent skin infections and respiratory tract infections in China (Jiang et al., 2019). SH is not only effective against gram positive bacteria (Ye et al., 2007), but is also effective against fungi, and can be used as a synergistic companion with FLZ against *C. albicans* (Huang et al., 2015; Shao et al., 2017). Because of the instability of the chemical structure of SH, its derivative, SNH, has been synthesized with improved stability, and it also has a fishy odor (Lu et al., 2013). SNH has been widely used in pharmaceutical and medical applications in China and demonstrates extensive biological and antimicrobial properties (Yang et al., 2016). Previous studies have shown that SNH can significantly inhibit a variety of bacteria through H₂O₂ stress (Wu et al., 2015; Yang et al., 2016). However, the antifungal mechanism of SNH remains unclear. Therefore, we performed an RNA-seq

assay to investigate the transcriptome changes in *C. albicans* treated using SNH. The transcription of genes involved in H₂O₂ stress was not significantly changed by SNH in *C. albicans*, implying that the antifungal mechanism of SNH may not be similar to its antibacterial mechanisms.

Therefore, in the current study, we aim to investigate the effects of SNH on the adherence and biofilm formation of *C. albicans* both *in vitro* and *in vivo*, and the possible antifungal mechanisms of SNH.

MATERIALS AND METHODS

Strain and Cultivation

Candida albicans SC5314 was a gift from Prof. Yuanying Jiang, School of Pharmacy, Second Military Medical University (Shanghai, China). *C. albicans* Z103, Z3044, Z1402, and Z1407 were purchased from the Clinical Laboratory of Anhui Provincial Hospital (Hefei, China). *C. albicans* was streaked from -80°C glycerol stocks onto Sabouraud's agar (Hope Biotech Co., Qingdao, China) plates. The strain was routinely inoculated for three generations in Sabouraud's agar plates, a single colony was chosen for each inoculation, and then this was activated and propagated in liquid Sabouraud medium (Hope Biotech Co., Qingdao, China) at 37°C for 12–16 h until the strain reached the exponential growth phase. The revived *Candida* cells were pooled through centrifugation at 3000 g. After washing twice using sterile PBS (Leagene, Beijing, China), the *Candida* cells were resuspended in RPMI-1640 medium (Invitrogen, Carlsbad, CA, United States) and adjusted to a defined cell density using a hemocytometer prior to subsequent tests.

Determination of Minimum Inhibitory Concentrations of 80% (MIC₈₀)

Sodium new houttuyfonate, (HPLC $\geq 98\%$) was purchased from Shanghai Yuanye Bio-Technology Co., Ltd., and the production batch number was A23A9E59436. The *C. albicans* was diluted to 2×10^3 CFU/mL. The minimum inhibitory concentration of 80% (MIC₈₀) of SNH was determined in a 96-well flat-bottomed microplate (Corning, NA, United States) using the microdilution method. The SNH was serially two-fold diluted in a range of 1024–32 $\mu\text{g/mL}$. The fungal cells were incubated with the drugs used at 37°C for 24 h, and the OD value of each well was measured at 620 nm using a microplate reader. The value of the control well was controlled at approximately 0.2, and compared with the control well, the drug concentration in the lowest concentration well where the OD value decreased by more than 80% represented the MIC₈₀ (the drug concentration when fungal growth was inhibited by 80%). The above experiment was repeated three times in parallel. It is accepted that when the MIC₈₀ value can be accurately repeated or with only one concentration difference, then the higher concentration is used as the MIC₈₀ value; when the MIC₈₀ value differs by more than two concentrations, a re-test is needed until the requirements are met (Barchiesi et al., 1994; Pfaller and Barry, 1994).

Determination of Minimum Fungicidal Concentrations (MFC)

To determine the minimum fungicidal concentration (MFC), 20 μ L of medium was removed from the 96-well plate for MIC detection and diluted 100-fold in PBS, and added to a solid sand agar plate, spread evenly, and then placed in a 37°C incubator for 24 h, before counting the number of colonies (Silva et al., 2019). The MFC was determined as the lowest drug concentration such that fewer than three fungal colonies were observed after a 24 h incubation at 35°C. The MFC determinations were repeated three times.

Initial Adhesive Growth Curve

The *C. albicans* solution was diluted to 2×10^6 CFU/mL. After 0, 2 and 4 h of incubation, the fungal solution for each group in each time period was placed on a mixing shaker to fully shake it, until the cells adhering to the bottom of the tube were completely resuspended in the culture medium. Immediately, 100 μ L of the suspension containing *Candida* for each group was serially diluted 1000-fold in PBS. The diluted suspension containing *Candida* was placed on the mixing shaker again, and fully shaken and mixed at the same time and frequency. A total of 100 μ L of the 1000-fold diluted suspension was then evenly plated on Sabouraud's agar in triplicate for a 24 h incubation at 37°C for yeast cell counting.

XTT Reduction Assays

Candida albicans cell culture medium (100 μ L; 2×10^6 CFU/mL) was co-incubated with the same volumes of SNH or FLZ in a 96-well flat-bottomed microplate at 37°C for 2 h and 4 h (for adherence) or 24 h (for biofilms). The XTT salt [2,3-bis(2-methoxy-4-nitro-5-sulfophenyl)2H-tetrazolium-5-carboxanilide sodium salt] (Shanghai Yuanye Bio-Technology Co., Ltd., Shanghai, China) was dissolved in Ringer's solution at a final concentration of 0.5 mg/mL. Immediately before each assay, a menadione (Shanghai Dibai Biotechnology Co., Ltd., Shanghai, China) solution was prepared at a final concentration of 0.4 mM and filter-sterilized. The XTT solution was mixed with the menadione solution at a ratio of 20:1 (v/v). Each well was washed twice with 200 μ L of sterile PBS to remove planktonic cells, and finally 50 μ L of newly prepared XTT solution was added to each well (Manoharan et al., 2017a; Rossoni et al., 2019). All well plates were incubated for 30 min in the dark, and colorimetric changes in the solutions were measured using a microplate reader (Thermo Labserv K3, Beijing, China) at 492 nm.

Inverted Microscope

Candida albicans cell culture medium (1 mL; 2×10^6 CFU/mL) was co-incubated with the same volumes of SNH or FLZ in a 6-well flat-bottomed microplate at 37°C for 4 h (for yeast) and 6 h (for hyphae). After that, all plates were observed using a high-power lens ($\times 400$) and photographed using the OLYMPUS IX51 (Tokyo, Japan).

Quantitative Determination of Biofilms Using Crystal Violet

As previously reported (Manoharan et al., 2017b), *C. albicans* was inoculated into 96-well plates for a static biofilm formation assay. Overnight cultures of *C. albicans* strains were inoculated into Potato Dextrose Broth (PDB, Hangwei, Hangzhou, China) at a 600 nm initial turbidity of 0.05 (total volume of 200 μ L), with or without essential oils or different concentrations of its main components (0.0005 to 0.05%, incubate under v/v or w/v) for 24 h, without shaking, at 37°C. The samples were washed twice using sterile PBS to remove all non-adherent planktonic cells, and then stained with crystal violet (Macklin, Shanghai, China) for 20 min, washed gently with sterile PBS twice and stained with crystal violet with 95% ethanol to quantify biofilm formation. The absorbance of each well was measured at a wavelength of 570 nm, and the results were calculated by averaging the data.

Crystal Violet Staining

As previously reported (Manoharan et al., 2017c), slides with an area of 1 cm² were soaked in a 75% ethanol solution for 24 h, washed with sterile PBS, and placed in a 6-well plate. *C. albicans* cell culture medium (1 mL; 2×10^6 CFU/mL) was co-incubated with the same volumes of SNH or FLZ in a 6-well flat-bottomed microplate at 37°C for 24 h (for biofilms). After that, the upper layer medium was discarded and rinsed with sterile PBS three times, stained with crystal violet solution, observed using a high-power lens ($\times 400$) and photographed using an OLYMPUS BX51 (Tokyo, Japan).

Confocal Laser Scanning Microscopy (CLSM)

Candida albicans cell culture medium (500 μ L; 2×10^6 CFU/mL) was co-incubated with the same volumes of SNH or FLZ in a 15mm glass-bottom confocal dish (Biosharp, Hefei, China) at 37°C for 24 h. After that, the upper layer medium was discarded and the dish was rinsed gently with PBS twice to remove planktonic fungi. Acridine orange dye solution (1 mg/mL, Yanye, Shanghai, China) was diluted to a final concentration of 0.01% in PBS, and then 200 μ L of 0.01% acridine orange dye solution was added into the confocal dish and incubated for 30 min in the dark. Finally, a photograph was obtained using a camera mounted on a laser scanning confocal microscope at an excitation wavelength of 488 nm, and the AOD of the fluorescence in the photo was analyzed using Image J.

Scanning Electron Microscopy (SEM)

Slides with an area of 1 cm² were soaked in a 75% ethanol solution for 24 h, washed with sterile PBS, and placed in a 6-well plate. *C. albicans* cell culture medium (1 mL; 2×10^6 CFU/mL) was co-incubated with the same volumes of SNH or FLZ in a 6-well flat-bottomed microplate at 37°C for 24 h (for biofilm). The slides were rinsed gently with PBS twice to remove planktonic fungi, and then placed in pre-chilled 2.5% glutaraldehyde solution and fixed for 2 h in the dark. The slides were then placed in an ethanol solution for gradient dehydration (30%, 10 min; 70%, 10 min; 90%, 10 min; 100%,

10 min), taken out and place in a ventilated and dry place to dry overnight. The glass slides were stuck in a metal plate using carbon tape and placed in a vacuum gold-plating machine for vacuum and gold plating. After the sample was prepared, it was placed into a Schottky Field Emission Scanning Electron Microscope (GeminiSEM 500, Germany) for observation ($\times 500$) and to acquire images.

An Assessment of Synergy Between SNH and Several Antifungal Agents

Four antifungal agents were investigated: FLZ (HPLC $\geq 98\%$), BBR (HPLC $\geq 98\%$), CAS (HPLC $\geq 98\%$), and ITZ (HPLC $\geq 98\%$), which were purchased from Shanghai Yuanye Bio-Technology Co., Ltd. First, we tested the MIC₈₀ concentration of these four antifungal agents alone against *Candida albicans* SC5314 through 96 well microplate experiments. After that, we combined these four antifungal agents with SNH separately, and conducted synergistic MIC₈₀ experiments through a checkerboard microdilution method; that is, the two drugs were used in combination on a 96-well plate in a two-dimensional checkerboard longitudinal (A to H) and horizontal (2 to 11) two-fold dilution in two directions, respectively. For example, for the combined use of SNH and FLZ, the final concentration of SNH was controlled at 2–256 $\mu\text{g/mL}$, and the final concentration of FLZ was controlled at 0.005–4 $\mu\text{g/mL}$. The final concentration ranges of the other antifungal agents used in combination with SNH were as follows: the final concentration of BBR was controlled at 0.125–64 $\mu\text{g/mL}$, the final concentration of CAS was controlled at 0.005–4 $\mu\text{g/mL}$, and the final concentration of ITZ was controlled at 0.01–8 $\mu\text{g/mL}$.

Evaluation of the effect of combination medicine: The FICI is the main parameter for evaluating the interaction mode of two drugs. The FIC is the ratio of the MIC required for each drug when combined for antimicrobial activity and the MIC when used alone. FICI is equal to the sum of the FIC of the two drugs. This experiment used the latest standards of international journals: the interaction between the two drugs is determined to be synergistic when $\text{FICI} \leq 0.5$, it is an irrelevant effect when $0.5 < \text{FICI} \leq 4$, and when $\text{FICI} > 4$, the two drugs produce an antagonistic effect.

We also used CLSM to observe the effect of SNH combined with several antifungal agents on a *Candida albicans* SC5314 biofilm, and set up a Control group, a MIC FLZ group, a MIC BBR group, a MIC CAS group, a MIC ITZ group and the above four drugs combined with MIC SNH group. The analysis method is consistent with the CLSM method described previously, and the AOD of the fluorescence in the photo was analyzed using Image J.

Eukaryotic Transcriptome Sequencing

Candida albicans cells were harvested by centrifugation and the pellet was flash-frozen in liquid nitrogen. (1) Total RNA was extracted from the tissue using TRIzol[®] Reagent (Plant RNA Purification Reagent for plant tissue) according the manufacturer's instructions (Invitrogen) and genomic DNA

was removed using DNase I (TaKara). Then RNA quality was determined by 2100 Bioanalyser (Agilent) and quantified using the ND-2000 (NanoDrop Technologies). Only high-quality RNA sample ($\text{OD}_{260/280} = 1.8\sim 2.2$, $\text{OD}_{260/230} \geq 2.0$, $\text{RIN} \geq 6.5$, $28\text{S}:18\text{S} \geq 1.0$, $> 2 \mu\text{g}$) was used to construct sequencing library. (2) RNA-seq transcriptome library was prepared following TruSeq[™] RNA sample preparation Kit from Illumina (San Diego, CA, United States) using 1 μg of total RNA. Shortly, messenger RNA was isolated according to polyA selection method by oligo(dT) beads and then fragmented by fragmentation buffer firstly. Secondly double-stranded cDNA was synthesized using a SuperScript double-stranded cDNA synthesis kit (Invitrogen, CA, United States) with random hexamer primers (Illumina). Then the synthesized cDNA was subjected to end-repair, phosphorylation and "A" base addition according to Illumina's library construction protocol. Libraries were size selected for cDNA target fragments of 200–300 bp on 2% Low Range Ultra Agarose followed by PCR amplified using Phusion DNA polymerase (NEB) for 15 PCR cycles. After quantified by TBS380, paired-end RNA-seq sequencing library was sequenced with the Illumina HiSeq xten/NovaSeq 6000 sequencer (2×150 bp read length). The Illumina platform converts the sequenced image signals into textual signals via CASAVA Base Calling and stores them in raw data in fastq format, and performs sequencing-related quality assessments on the raw sequencing data for each sample. (3) The raw paired end reads were trimmed and quality controlled by SeqPrep¹ and Sickle² with default parameters. Then clean reads were separately aligned to reference genome with orientation mode using TopHat³ (Trapnell et al., 2009) software. The mapping criteria of bowtie was as follows: sequencing reads should be uniquely matched to the genome allowing up to 2 mismatches, without insertions or deletions. Then the region of gene were expanded following depths of sites and the operon was obtained. In addition, the whole genome was split into multiple 15kbp windows that share 5kbp. New transcribed regions were defined as more than 2 consecutive windows without overlapped region of gene, where at least 2 reads mapped per window in the same orientation. (4) To identify DEGs (differential expression genes) between two different samples, the expression level of each transcript was calculated according to the fragments per kilobase of exon per million mapped reads (FRKM) method. RSEM⁴ (Li and Dewey, 2011) was used to quantify gene abundances. R statistical package software EdgeR (Empirical analysis of Digital Gene Expression in R⁵, Robinson et al., 2010) was utilized for differential expression analysis. In addition, functional-enrichment analysis including GO and Kyoto Encyclopedia of Genes and Genomes (KEGG) were performed to identify which DEGs were significantly enriched in GO terms and metabolic pathways at Bonferroni-corrected P -value ≤ 0.05 compared with

¹<https://github.com/jstjohn/SeqPrep>

²<https://github.com/najoshi/sickle>

³<http://tophat.cbcb.umd.edu/>, version 2.0.0

⁴<http://deweylab.biostat.wisc.edu/rsem/>

⁵<http://www.bioconductor.org/packages/2.12/bioc/html/edgeR.html>

the whole-transcriptome background. GO functional enrichment and KEGG pathway analysis were carried out by Goatools⁶ and KOBAS⁷ (Xie et al., 2011). (5) The TopHat-Cufflinks pipeline was used to predict gene isoforms from our RNA-seq data. In TopHat⁸ (Trapnell et al., 2009), the option “min-isoform-fraction” was disabled, instead “coverage-search,” “butterfly search,” and “microexon-search” were used. The expected fragment length was set to 200 bp and the “small-anchor-fraction” was set to 0.08, which requires at least 8 bp on each side of an exon junction for our 100-bp RNA-seq data. Cuffcompare was used to compare and merge the reference annotation and the isoform predictions. (6) All the alternative splice events that occurred in our sample were identified by using recently releases program Multivariate Analysis of Transcript Splicing (MATS⁹) (Shen et al., 2012). Only the isoforms that were similar to the reference or comprised novel splice junctions were considered, and the splicing differences were detected as exon inclusion, exclusion, alternative 5' AGATCGGAAGAGCACACGTC, 3' AGATCGGAAGAGCGTCGTGT, and intron retention events. The high-quality sequencing data were analyzed on the free online platform of Majorbio I-Sanger Cloud Platform¹⁰. The transcriptomic data have been deposited into the SRA database under the accession numbers of PRJNA544616 (<https://www.ncbi.nlm.nih.gov/sra/PRJNA544616>).

Quantitative RT-PCR

Firstly, a 1×10^6 CFU/mL fungal culture was incubated for 4 h (for adherence) or 24 h (for biofilms) at 37°C. The fungal cells were collected through centrifugation for 3 min at 12700 g, and then total RNA samples were extracted in accordance with the manufacturer's instructions for the MagExtractor-RNA kit (Toyobo, Tokyo, Japan). Extracted total RNA (6 µL) was mixed with 2 µL of 4 × DNA Master I (containing gDNA remover) and 2 µL 5RT-Master Mix II through instant centrifugation at 3000 g, and reverse-transcribed into cDNA as recommended by the instructions of the ReverTra Ace qPCR RT Master Mix with gDNA Remover kit (Toyobo, Tokyo, Japan), with procedures as follows: pre-denature RNA in GeneTest series gene amplifier (BIO-GENER, Hangzhou, China) at 65°C for 5 min, 4°C for 1 min, and then at 37°C for 15 min, 50°C for 5 min, 98°C for 5 min, and 4°C for 1 min to finally generate cDNA. The prepared cDNA was diluted 10-fold prior to use for semi-quantitative PCR and qRT-PCR. Primers for *C. albicans* (Table 1) were designed using Primer Premier 5.0 and synthesized by Sangon Biotech. The qRT-PCR mixture (25 µL) was freshly prepared containing 12.5 µL of SYBR green fluorescent dyes, 1 µL of PCR forward primer, 1 µL of PCR reverse primer, 0.5 µL of cDNA, and 10 µL of DEPC treated water. The qRT-PCR process was performed using an ABI7000 fluorescence quantitative PCR system with the following cycles: 95°C for 60 s for pre-denaturation alone with 95°C for 15 s, 50°C for 15 s, and 72°C for 45 s for a total of 40

cycles. All data were normalized to the housekeeping gene β -actin as the internal reference gene. The relative target-gene expression was calculated as a fold change of the $2^{-\Delta\Delta C_t}$ value, in which $\Delta C_t = C_t \text{ target gene} - C_t \text{ internal reference genes}$, as previously described (Livak and Schmittgen, 2001).

Semi-Quantitative PCR

The preparation steps for the cDNA are the same as those described previously. The primer sequences used in the semi-quantitative PCR are shown in Table 1. The PCR mixture (25 µL) was freshly prepared containing 12.5 µL of 2 × EasyTaq® PCR SuperMix, 0.5 µL of PCR forward primer, 0.5 µL of PCR reverse primer, 0.5 µL of cDNA, and 11 µL of DEPC treated water. PCR conditions were as follows: 94°C for 5 min, 35 cycles at 94°C for 30 s, 50°C for 30 s, 72°C for 30 s, with a final extension at 72°C for 5 min. The PCR process was performed using a GeneTest series gene amplifier (BIO-GENER, Hangzhou, China). PCR products were analyzed using a 1.5% agarose gel and compared with a D2000 plus DNA Ladder (Solarbio, Beijing, China). The horizontal electrophoresis conditions were 110 v, 80 mA, 20 min, and the agarose gel was placed into a JY04S-3E imaging analysis system (Junyi, Beijing, China) for gel imaging. The brightness of the PCR products was observed, and it was proportional to the target gene expression.

Detection of cAMP Levels

Candida albicans cell culture medium (1 mL; 2×10^6 CFU/mL) was co-incubated with the same volumes of SNH or FLZ in a 6-well flat-bottomed microplate at 37°C for 2 h and 4 h (for adherence) or 24 h (for biofilms). The *Candida*

TABLE 1 | Primers for qRT-PCR.

Oligo Name	Sequence (5' to 3')	Length (bp)
β -actin-Forward	ACC GAA GCT CCA ATG AAT CC	20
β -actin-Reverse	CCG GTG GTT CTA CCA GAA GAG	21
ALS1-Forward	GGA TCT GTT ACT GGT GGA GCT GTT G	25
ALS1-Reverse	ATG TGT TGG TTG AAG GTG AGG ATG AG	26
ALA1-Forward	GGC TAC GTG TTA CAC ACT GGT	21
ALA1-Reverse	TCA ACG CCA TCT CCA AGG AC	20
ALS3-Forward	CAA CTT GGG TTA TTG AAA CAA AAA CA	26
ALS3-Reverse	AGA AAC AGA AAC CCA AGA ACA ACC T	25
EAP1-Forward	ATC TAC CTC CTA CAC GAC TGA CAC TG	26
EAP1-Reverse	TGT ATG AGA ACA AGA ACC GCC ATC AC	26
RAS1-Forward	GAG GTG GTG GTG TTG GTA	18
RAS1-Reverse	TTC TTC TTG TCC AGC AGT ATC	21
EFG1-Forward	ATT GAG ATG TTG CGG CAG GAT AC	23
EFG1-Reverse	ACT GGA CAG ACA GCA GGA C	19
HWP1-Forward	ACA GGT AGA CGG TCA AGG	18
HWP1-Reverse	GGG TAA TCA TCA CAT GGT TC	20
TEC1-Forward	AGG TTC CCT GGT TTA AGT G	19
TEC1-Reverse	ACT GGT ATG TGT GGG TGA T	19
YWP1-Forward	CTG ATA TTC GTA ATG CTG GTA AAG TG	26
YWP1-Reverse	GGA GTT TCA CCC ATT AAT CTT CTT C	25
RHD1-Forward	TTA GAG AAA TGT GGC TGT GGT G	22
RHD1-Reverse	TCA CAT AAC CCT TTA TCA GGC C	22

⁶<https://github.com/tanghaibao/Goatools>

⁷<http://kobas.cbi.pku.edu.cn/home.do>

⁸<http://tophat.cbcb.umd.edu/>, version2.0.0

⁹<http://rnaseq-mats.sourceforge.net/>

¹⁰www.i-sanger.com

cells were scraped using a cell scraper, suspended in medium, and centrifuged for 3 min at 12700 g. The supernatant was analyzed for cAMP in accordance with the manufacturer's protocol, and the cAMP concentration of each group was examined using a microplate reader (Thermo Labserv K3, Beijing, China) and ELISA kits purchased from RUIXIN Biotech (Quanzhou, China).

In vivo Evaluation of Antifungal Efficacy of SNH Against *C. albicans*

Old *Galleria mellonella* larvae were purchased from Tianjin Huiyude Biological Technology Co., Ltd., each weighing 0.2–0.3 g, and they were approximately 2–3 cm in length. They were stored in a refrigerator at 4°C until use. The larvae were placed on an ultra-clean bench, activated at room temperature for 30 min, and then the *in vivo* injection experiment was performed.

Preparation of *Candida* injection: a single colony was chosen on the Sabouraud's agar plate and inoculated into liquid Sabouraud medium, which was placed on a shaker at 220 rpm, at 37°C, for 12 h, and then the cells were collected, the upper medium was removed, and the cells were resuspend in PBS. The cell concentration was adjusted to 8×10^6 CFU/mL, 10 μ L of *Candida* solution was injected into the right anterior side of the second section of the stomach and foot. Larvae were inoculated with 8×10^4 yeast cells per 10 μ L into the hemolymph, as described previously (Bergin et al., 2006; Harding et al., 2013; Manoharan et al., 2017b).

All drugs were dissolved in PBS without any cosolvent to avoid the toxic effects of cosolvents for insects. The drugs were sonicated for a few seconds, and then placed in a 75°C water bath for 20 min. During this period, the drug solutions were shaken and mixed continuously until the drug was completely dissolved and diluted with PBS to 512 μ g/mL, 256 μ g/mL, and 128 μ g/mL (SNH), and 128 μ g/mL and 64 μ g/mL (FLZ).

Galleria mellonella larvae ($n = 20$ larvae per group) were grouped as follows: PBS group, infection (*C. albicans* 8×10^4 CFU/larvae) group, infection + SNH 512 μ g/mL group, infection + SNH 256 μ g/mL group, infection + SNH 128 μ g/mL group, infection + FLZ 128 μ g/mL group, infection + FLZ 64 μ g/mL group, uninfected + SNH 512 μ g/mL group, uninfected + SNH 256 μ g/mL group, uninfected + SNH 128 μ g/mL group, uninfected + FLZ 128 μ g/mL group and uninfected + FLZ 64 μ g/mL group. Larvae in the infected group were infected with PBS containing *C. albicans* SC5314 strains ($LD_{50} = 8 \times 10^4$ CFU/larvae); drugs groups were administered 1 h post-infection with 10 μ L of SNH or FLZ. The PBS group and uninfected group were injected with sterile PBS. The changes in the larvae body were observed every 12 h. If the larvae body was melanized and there was no turning movement, the larvae body was considered to be dead. The larvae were observed continuously for 84 h and the number of deaths was recorded to determine the survival rate of each group. In view of studies that show that the LD_{50} of SNH is 119.14 mg/kg (Jiang et al., 2006) and the LD_{100} of SNH is 200 mg/kg (Lou et al., 2012), our research group selected the dose range 1024–32 μ g/mL for SNH in previous experiments (Wang et al., 2019; Zhao et al., 2019).

Therefore, the safety range of SNH is large, and it has no obvious cytotoxicity.

Statistical Analysis

All experiments were repeated at least three times. Data represent biological replicates. Data meet the assumptions of the statistical tests described for each Figure. Results are expressed as the mean \pm SD. Differences between experimental groups were assessed for significance using a two-tailed unpaired Student's *t*-test with GraphPad Prism 5 software. The $*p < 0.05$, $**p < 0.01$, and $***p < 0.001$ levels were considered to indicate statistical significance.

RESULTS

Determination of MIC_{80} and MFC

Using a microplate reader, we found (Figure 1A) that the cell growth ratio of the 256 μ g/mL SNH group to the control group was 17.15%; that is, 82.85% of *Candida* growth was inhibited within 24 h. The value of the control well was controlled at approximately 0.2, and compared with the control well, the drug concentration in the lowest concentration well where the OD value decreased by more than 80% was the MIC_{80} (the drug concentration when fungal growth was inhibited by 80%). Therefore, the MIC_{80} of SNH in *C. albicans* SC5314 was determined to be 256 μ g/mL. The 64 μ g/mL (1/4 MIC_{80}) dose group had a poor fungal inhibitory effect and had no practical clinical significance, and the 1024 μ g/mL (4 MIC_{80}) dose group had fungal inhibitory effects that were too strong, which does not conform to the principle of using the lowest dose within the effective dose range. Therefore, the 64 μ g/mL and 1024 μ g/mL dose groups were not investigated further. We observed the effects of 128 μ g/mL (1/2 MIC_{80}), 256 μ g/mL (1 MIC_{80}), and 512 μ g/mL (2 MIC_{80}) SNH, and 128 μ g/mL FLZ on the adherence and biofilm formation of *C. albicans*. In addition, through MFC detection, it was found that with SNH at MIC, 2 MIC and 4 MIC for 24 h the number of colonies was greater than three (Figure 1B), indicating that SNH has no fungicidal effect on *C. albicans* SC5314, and only inhibits fungal action.

SNH Inhibits *C. albicans* Adhesion and Hypha Growth

Through a CFU plate count (Figure 1C), we found that SNH treatment for 0 h resulted in no significant difference compared with the control group. After 2 h of SNH treatment, the CFU counts in the SNH groups were less than those in the control group, but the difference was not statistically significant. After 4 h of SNH treatment, the CFU counts in the SNH groups were significantly less than those in the control group, and the difference was statistically significant. The *p*-Value for the SNH 512 μ g/mL group was <0.001 , the *p*-Value for the SNH 256 μ g/mL group was <0.01 , and the *p*-Value for the SNH 128 μ g/mL group was <0.05 . This shows that SNH exerts the best anti-fungal effect by 4 h of initial adhesion. In addition,

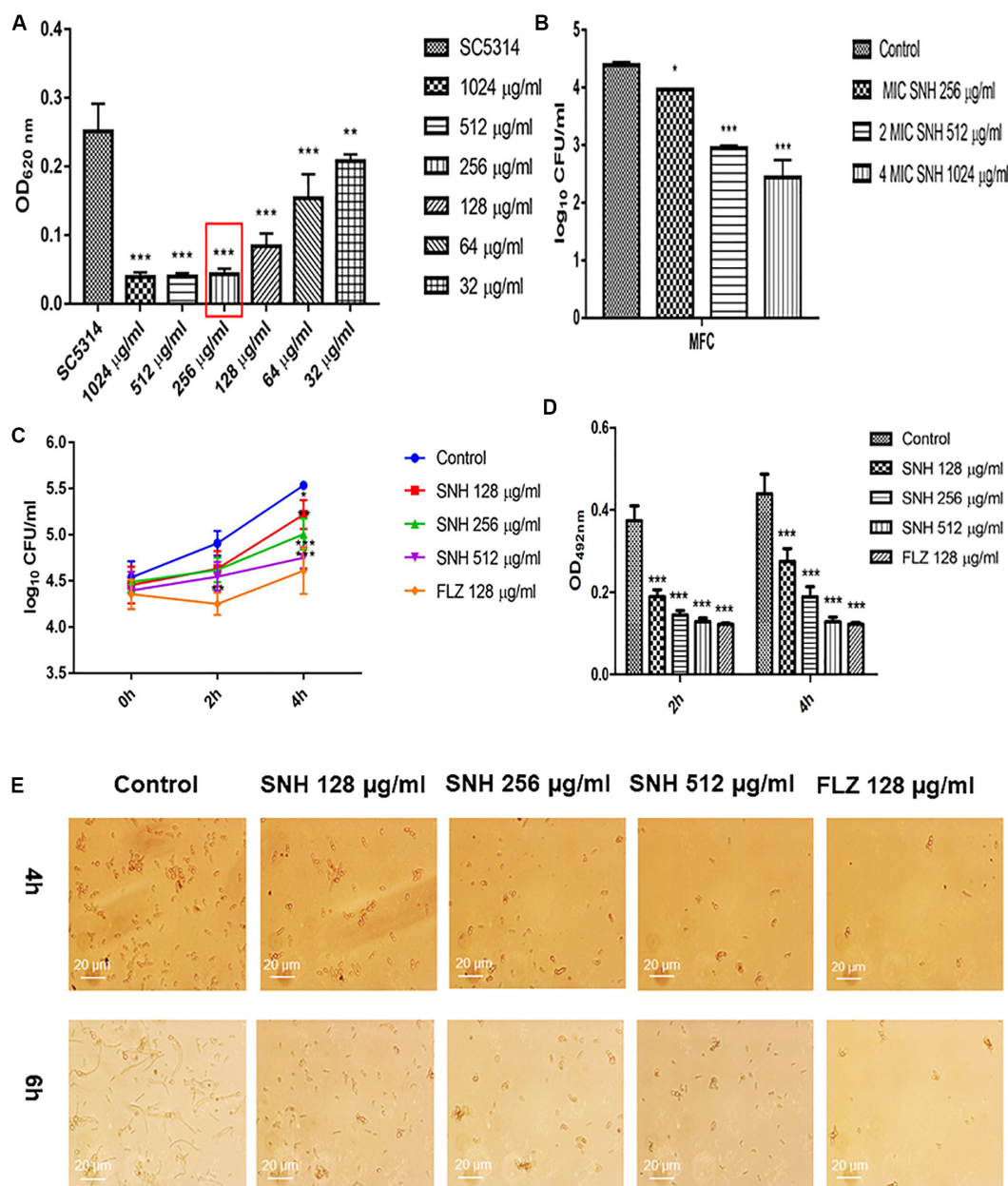


FIGURE 1 | (A) Determination of MIC₅₀ of SNH on *C. albicans* SC5314 by microdilution method. The drug-free strain-containing medium was set as the control. Data are shown as mean ± SD. ****p* < 0.001 and ***p* < 0.01, compared with the control. **(B)** Determination of MFC of SNH on *C. albicans* SC5314 by plate count. The drug-free strain-containing medium was set as the control. Data are shown as mean ± SD. ****p* < 0.001 and **p* < 0.05, compared with the control. **(C)** Effect of SNH on CFU of adhesive cells of *C. albicans* SC5314. The initial adhesive growth curve measurements were taken for the first 4h. The drug-free strain-containing medium was set as the control. Data are shown as mean ± SD. **p* < 0.05, compared with the control. **(D)** Effect of SNH on adherence metabolic activity in *C. albicans* SC5314 by the XTT reduction assay. The drug-free strain-containing medium was set as the control. Data are shown as mean ± SD. ****p* < 0.001, compared with the control. **(E)** Observation of morphological changes of *C. albicans* yeast (4 h) and hypha (6 h) by inverted microscope (×400). The initial inoculum was newly prepared at 2×10^6 CFU/mL. The drug-free strain-containing medium was set as the control.

through an XTT assay, we found that the addition of SNH to *C. albicans* after a 2 and 4 h incubation can significantly reduce adherence activity (Figure 1D) in a concentration-dependent manner. The *p*-Value of the SNH groups at 2 h and 4 h were <0.001. Therefore, the results show that SNH can effectively inhibit the initial adhesion activity of *C. albicans*. The inverted

microscope results (Figure 1E) indicate that SNH and FLZ treatment are similar and can effectively reduce cell adhesion in *C. albicans* when administered for 4 h. In addition, we also found that the control group demonstrated obvious slender hyphae at 6 h, while the hyphae of *C. albicans* were effectively inhibited after SNH treatment, whereby only a few yeast-like cells appeared,

and no obvious hyphae were observed (**Figure 1E**). This result suggests that SNH can effectively inhibit the transition of yeast to hyphae in *C. albicans*, thereby providing the possibility of biofilm inhibition.

SNH Affects the Biofilm Formation of *C. albicans*

Through an XTT assay (**Figure 2A**), we found that at 24 h, compared with the control group, SNH treatment of *C. albicans* significantly reduced the biofilm OD₄₉₂ value in a concentration-dependent manner. Each SNH group demonstrated effectively inhibited biofilm metabolic activity ($p < 0.05$). In addition, through the crystal violet quantitative biofilm experiment (**Figure 2B**), it was also found that SNH can effectively inhibit biofilm dispersion and biofilm volume ($p < 0.001$). Among the groups, the SNH 512 $\mu\text{g/mL}$ group inhibited biofilm growth by 74.91%, the SNH 256 $\mu\text{g/mL}$ group inhibited biofilm growth by 62.51%, and the SNH 128 $\mu\text{g/mL}$ group inhibited biofilm growth by 40.63%. We also observed the growth and morphological changes in *C. albicans* biofilms after SNH treatment through crystal violet staining, CLSM, and SEM (**Figures 2D–F**). The images showed that the control group demonstrated a large and thick biofilm at 24 h. SNH inhibited the formation of biofilms at 24 h, but single fungal bodies and a small biofilm structure was observed, and so it appears that SNH inhibits the formation of large biofilm structures. In addition, the CLSM analysis (**Figure 2C**) also showed that SNH can effectively inhibit biofilm formation ($p < 0.001$). In summary, SNH has the potential to inhibit *C. albicans* biofilms.

SNH Inhibits Biofilms of Several Clinical Strains of *C. albicans*

To further investigate the potential of SNH against *C. albicans* biofilms, we selected four clinical strains of *C. albicans*, Z1402, Z1407, Z103, and Z3044 for these experiments. First, the MIC₈₀ of SNH in clinical strains of *C. albicans* was detected through a 96-well microdilution method. Interestingly, the MIC₈₀ of SNH in clinical strains was better than that in standard strains, whereby the MIC₈₀ of SNH in clinical strains decreased 1–2-fold compared with that in standard strains. The MIC₈₀ of SNH in Z103 was 64 $\mu\text{g/mL}$ (**Figure 3C**) and the MIC₈₀ of SNH in Z3044 was 128 $\mu\text{g/mL}$ (**Figure 3D**). Moreover, the MIC₈₀ of SNH in both Z1402 and Z1407 was 256 $\mu\text{g/mL}$ (**Figures 3A,B**), which was the same as that in SC5314. We further tested the biofilm dispersion and biofilm quantity in four clinical strains treated using SNH through a crystal violet quantitative biofilm experiment. Each clinical strain was established in 2 MIC SNH, MIC SNH and 1/2 MIC SNH groups. It was found that the OD_{570nm} of each SNH group was significantly lower than that of the control group ($p < 0.01$). The SNH 512 $\mu\text{g/mL}$ group demonstrated 38.61% inhibition of biofilm growth of Z1402, the SNH 256 $\mu\text{g/mL}$ group demonstrated 37.24% inhibition of biofilm growth of Z1402, and the SNH 128 $\mu\text{g/mL}$ group demonstrated 25.06% inhibition of biofilm growth of Z1402 (**Figure 3E**). The SNH 512 $\mu\text{g/mL}$ group demonstrated 53.08% inhibition of biofilm growth of Z1407,

the SNH 256 $\mu\text{g/mL}$ group demonstrated 51.41% inhibition of biofilm growth of Z1407, and the SNH 128 $\mu\text{g/mL}$ group demonstrated 45.73% inhibition of biofilm growth of Z1407 (**Figure 3F**). The SNH 512 $\mu\text{g/mL}$ group demonstrated 51.38% inhibition of biofilm growth of Z103, the SNH 256 $\mu\text{g/mL}$ group demonstrated 49.52% inhibition of biofilm growth of Z103, and the SNH 128 $\mu\text{g/mL}$ group demonstrated 42.03% inhibition of biofilm growth of Z103 (**Figure 3G**). The SNH 512 $\mu\text{g/mL}$ group demonstrated 56.32% inhibition of biofilm growth of Z3044, the SNH 256 $\mu\text{g/mL}$ group demonstrated 46.51% inhibition of biofilm growth of Z3044, and the SNH 128 $\mu\text{g/mL}$ group demonstrated 33.49% inhibition of biofilm growth of Z3044 (**Figure 3H**). We also observed biofilm growth and morphological changes in four clinical *C. albicans* strains after SNH treatment through crystal violet staining (**Figure 3I**). The images show that the clinical strain control groups all demonstrated large and thick biofilms at 24 h. While SNH can inhibit biofilm formation at 24 h, small biofilm structures could be seen, and therefore it could be considered that SNH inhibits the formation of large biofilm structures of *C. albicans* clinical strains. In terms of the ability of 2 MIC SNH to inhibit biofilms, SNH at this concentration can reduce the biofilm quantities of Z3044, Z1407 and Z103 by more than 50%, but has a poor ability to inhibit the biofilms of Z1402. In terms of the ability of 1 MIC SNH to inhibit biofilms, SNH at this concentration can inhibit biofilms by more than 50% for Z1407. In terms of the ability of 1/2 MIC SNH to inhibit biofilms, SNH inhibition of the biofilms of clinical strains was weakened, and no group with more than 50% biofilm inhibition was observed. In general, the ability of SNH to inhibit the biofilms of *C. albicans* clinical strains was in the order: Z1407 > Z103 > Z3044 > Z1402.

SNH Combined With Various Categories of Antifungal Against *C. albicans* Biofilm

Here, we investigated four antifungals, FLZ, BBR, CAS, and ITZ, combined with SNH to observe their ability to inhibit *C. albicans* SC5314 biofilms. First, we tested the MIC₈₀ of the four antifungal drugs against *C. albicans* SC5314 through a microdilution method in 96-well plates, and then tested the MIC₈₀ of the four antifungal drugs combined with SNH using a checkerboard microdilution method. The results are shown in **Table 2**. It was found that the FICI of SNH combined with FLZ, BBR, CAS, or ITZ was 0.27, 0.50, 0.27, and 0.50, respectively. These FICI values were all ≤ 0.05 , which indicated that SNH had synergistic effects with these four antifungals. We further investigated the effect of SNH combined with the four antifungals against *C. albicans* biofilms through CLSM (**Figure 4F**), and analyzed the AOD value of the fluorescence images (**Figures 4A–E**). Here, we investigated the drugs alone and in combination with a 1 MIC dose for the experiments. The results showed that the four antifungals alone had anti-biofilm abilities, and minimal biofilm growth and yeast cells could be seen. However, when the four antifungals were combined with SNH, their anti-biofilm capabilities were strengthened, and compared with the control group, large-scale hyphal

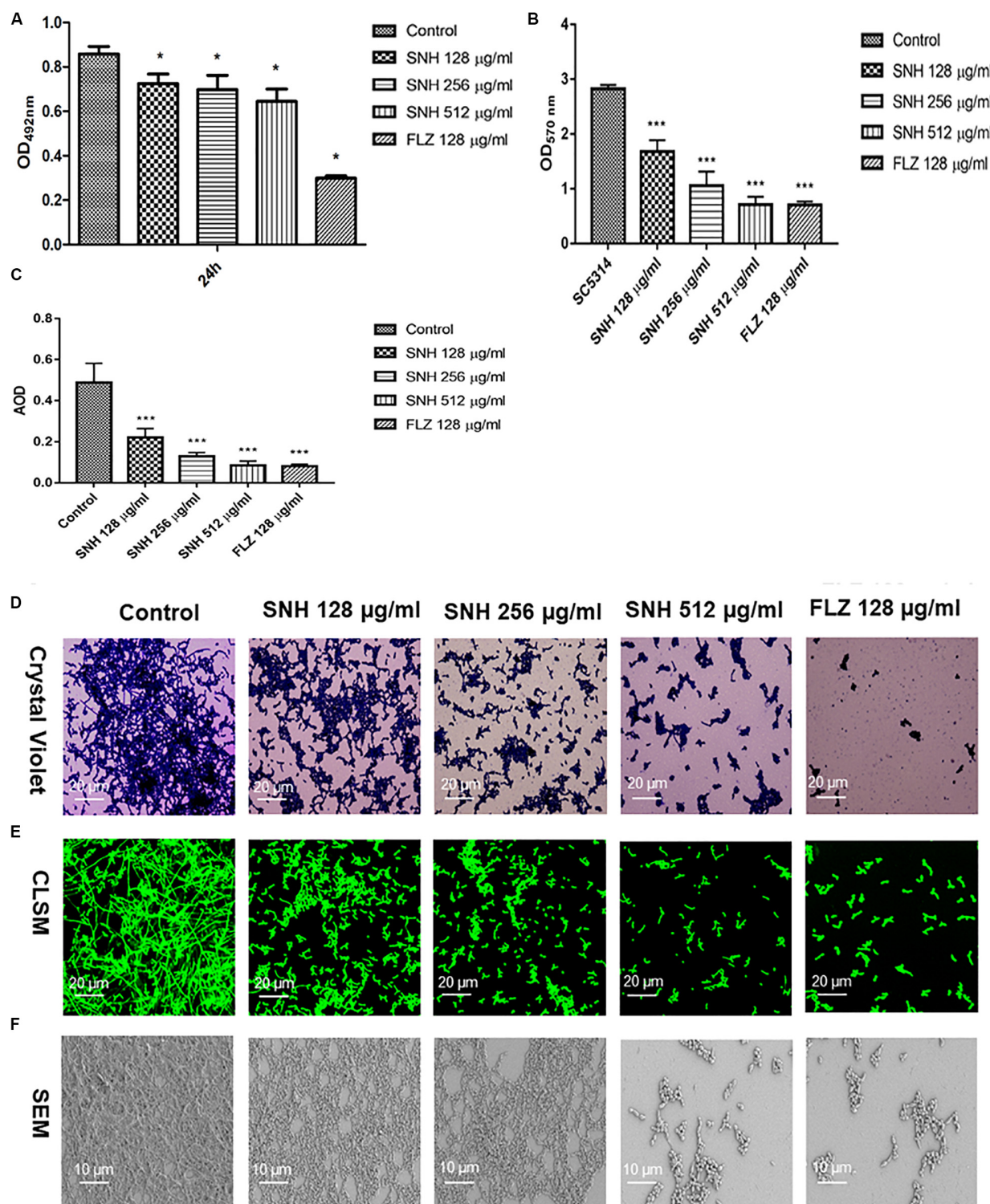


FIGURE 2 | (A) Effect of SNH on biofilm metabolic activity in *C. albicans* SC5314 by the XTT reduction assay. The drug-free strain-containing medium was set as the control. Data are shown as mean \pm SD. * $p < 0.05$, compared with the control. **(B)** Quantitative determination of *C. albicans* SC5314 biofilm by crystal violet. The drug-free strain-containing medium was set as the control. Data are shown as mean \pm SD. *** $p < 0.001$, compared with the control. **(C)** Analyze the AOD (AOD) of CLSM fluorescent *C. albicans* SC5314 biofilm by Image J. The drug-free strain-containing medium was set as the control. Data are shown as mean \pm SD. *** $p < 0.001$, compared with the control. **(D)** Crystal Violet Staining of *C. albicans* SC5314 biofilm by optical microscope ($\times 400$). **(E)** Observation of morphological changes of *C. albicans* SC5314 biofilm by CLSM ($\times 400$). **(F)** Observation of morphological changes of *C. albicans* SC5314 biofilm by SEM ($\times 500$). The initial inoculum was newly prepared at 2×10^6 CFU/mL. The drug-free strain-containing medium was set as the control.

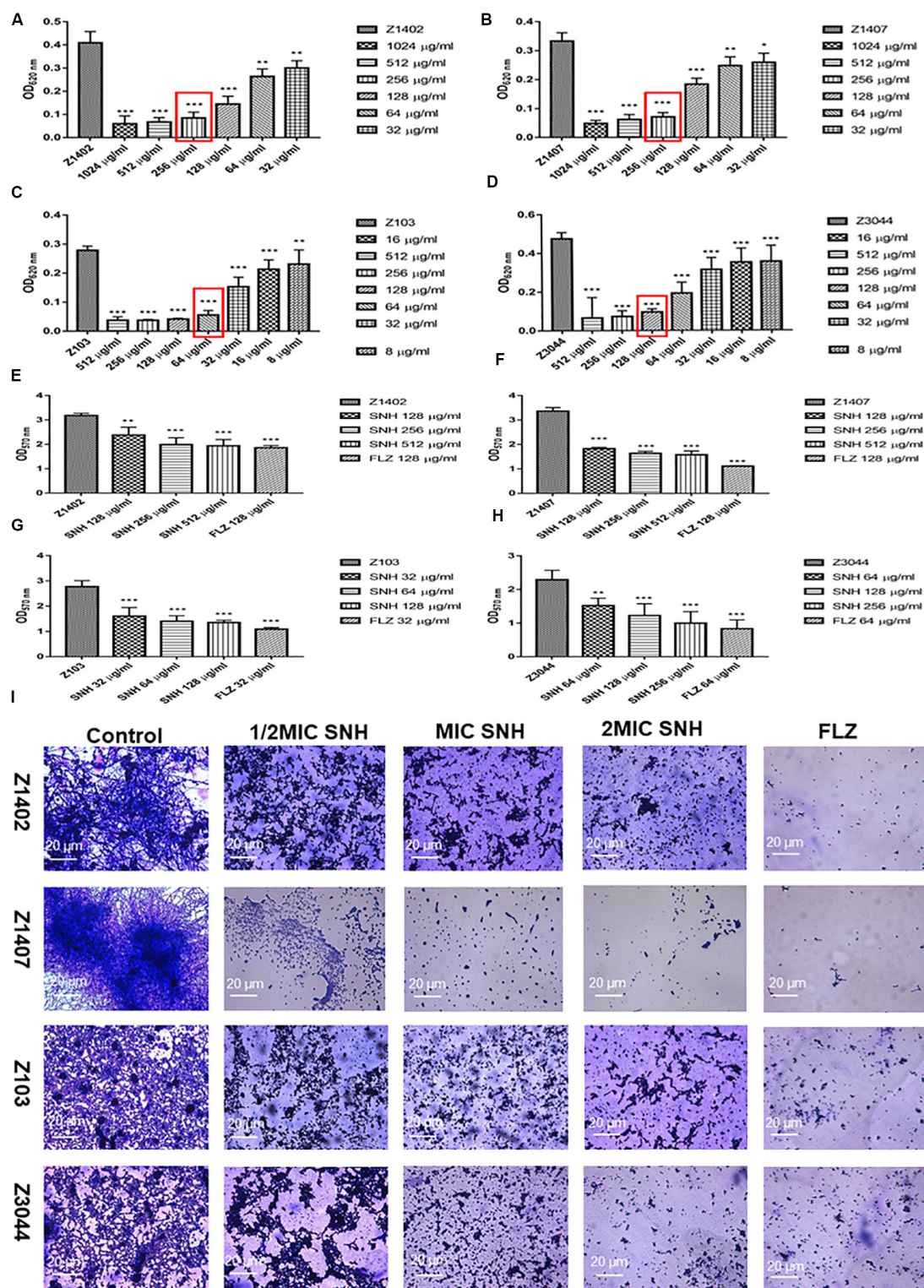


FIGURE 3 | (A–D) Determination of MIC₈₀ of SNH on *C. albicans* Z1402, Z1407, Z103, and Z3044 by microdilution method, respectively. The drug-free strain-containing medium was set as the control. Data are shown as mean ± SD. *** $p < 0.001$, ** $p < 0.01$, and * $p < 0.05$, compared with the control. **(E–H)** Quantitative determination of *C. albicans* Z1402, Z1407, Z103 and Z3044 biofilm by crystal violet, respectively. The drug-free strain-containing medium was set as the control. Data are shown as mean ± SD. *** $p < 0.001$ and ** $p < 0.01$, compared with the control. **(I)** Crystal Violet Staining of *C. albicans* Z1402, Z1407, Z103, and Z3044 biofilm by optical microscope (×400), respectively. The initial inoculum was newly prepared at 2×10^6 CFU/mL. The drug-free strain-containing medium was set as the control.

TABLE 2 | Interaction of SNH and antifungals against *C. albicans* SC5314 by MIC₈₀ of checkerboard microdilution assay.

	MIC ₈₀ (μg/ml) alone	MIC ₈₀ (μg/ml) in combination	FIC index for combination	Mode of interaction
SNH/FLZ	256/1	4/0.25	0.27	Syn
SNH/BBR	256/16	64/4	0.50	Syn
SNH/CAS	256/0.25	1/0.125	0.50	Syn
SNH/ITZ	256/8	4/2	0.27	Syn

SNH, Sodium new houttuynfonate; FLZ, Fluconazole; BBR, Berberine chloride; CAS, Caspofungin; ITZ, Itraconazole; Syn, Synergism.

structures were completely inhibited, and only single yeast-like cells were observed. Moreover, compared with the control group, the anti-biofilm activity observed following treatment with SNH combined with the four antifungals was significantly enhanced ($p < 0.01$).

SNH Affects the Transcriptome of *C. albicans*

The results described above indicate that SNH can effectively inhibit adhesion and biofilm formation in *C. albicans*. To elucidate the underlying mechanism, we examined the transcriptomic changes in *C. albicans* under SNH treatment. As shown in **Figure 5A**, the total transcriptomes of the blank control group and the 256 μg/mL SNH group are basically consistent. As shown in **Figure 5B**, 5711 genes overlap in the two groups, with 55 and 107 genes uniquely expressed in the Control and SNH treatment groups, respectively. As shown in **Figures 5C,D**, we found that the expression levels in the blank control group and the 256 μg/mL SNH group were significantly clustered in two groups, while the blank control group and the 256 μg/mL SNH group had high intra-group correlation. As shown in the volcano map in **Supplementary Figure S1**, a total of 5873 genes are assembled in the two groups. Compared with the control group, the expression of 611 genes, including 361 down-regulated and 250 up-regulated genes, changed significantly in the SNH group with fold changes > 2 and a p -Value < 0.05 (**Supplementary Figure S1**).

To gain insights into the biological pathways related to the 611 genes, hierarchical clustering (**Supplementary Figure S2**) of these genes was performed using Matlab to group the data into those genes increasing and decreasing in abundance following SNH treatment. GO enrichment results (**Figures 5E,F**) indicate that the genes generally down-regulated in SNH treatment are enriched in pathways associated with biological processes including regulation of biological process, growth, detoxification, response to stimulus, cellular processes, biological regulation, biological adhesion, cell aggregation, and cellular component biosynthesis including cell, cell part, membrane, membrane part and extracellular region, and molecular function including binding, catalytic activity and antioxidant activity. As shown in **Supplementary Table S1**, SNH can significantly down-regulate the expression of several genes, such as *RAS1*, *ALS3*, and *HWP1*, which are key to the pathogenesis of *C. albicans*. The three genes are involved in biological adhesion, cell aggregation and

positive regulation of biological processes and also members of the Ras1-cAMP-Efg1 pathway.

SNH Affects the Expression of Biofilm Related Genes and cAMP Production of the Ras1-cAMP-Efg1 Pathway

To verify the transcriptome results described above, we examined several genes related to adhesion and biofilms, especially those related to the Ras1-cAMP-Efg1 pathway through the semi-quantitative PCR and qRT-PCR methods. In accordance with the transcriptome data, the expression of *ALS1*, *ALA1*, *ALS3*, *EAP1*, *RAS1*, *EFG1*, *HWP1*, and *TEC1* in this pathway are down-regulated after SNH treatment in a dose dependent manner (**Figures 6A–D**) and the expression of *YWPI* and *RHD1* are up-regulated after SNH treatment in a dose dependent manner (**Figure 6E**), which could explain the defects in adhesion, transition from yeast to hyphae and biofilm formation of *C. albicans* under SNH treatment. Among these, *ALS1* and *ALA1* are involved in the initial adhesion of *C. albicans*, and *ALS3* and *EAP1* are involved in the formation of *C. albicans* biofilms. Compared with the control group, SNH treatment significantly reduced the expression levels of the adhesion-related genes, *ALA1* and *ALS1* (**Figure 6A**). The *ALA1* gene in the SNH 512, 256, and 128 μg/mL groups was down-regulated by 1.91-fold, 1.65-fold, and 1.39-fold, respectively, and the *ALS1* gene in the SNH 512, 256, and 128 μg/mL groups was down-regulated by 1.65-fold, 1.39-fold, and 1.16-fold, respectively. Moreover, SNH reduced the expression levels of the biofilm-related genes *ALS3* and *EAP1* (**Figure 6B**); specifically, the *ALS3* gene in the SNH 512, 256, and 128 μg/mL groups was down-regulated by 2.85-fold, 2.28-fold, and 1.37-fold, respectively, and the *EAP1* gene in the SNH 512, 256, and 128 μg/mL groups was down-regulated by 2.24-fold, 1.54-fold, and 1.18-fold, respectively. In addition, down-regulated the expression levels of the Ras1-cAMP-Efg1 pathway-related genes, *RAS1*, *EFG1*, *TEC1*, and *HWP1* (**Figures 6C,D**). Specifically, the *RAS1* gene in the SNH 512, 256, and 128 μg/mL groups was down-regulated by 5.36-fold, 2.64-fold, and 1.71-fold, respectively, and the *EFG1* gene in the SNH 512, 256, and 128 μg/mL groups was down-regulated by 1.83-fold, 1.38-fold, and 1.24-fold, respectively. The *TEC1* gene in the SNH 512, 256, and 128 μg/mL groups was down-regulated by 3.35-fold, 1.90-fold, and 1.52-fold, respectively, and the *HWP1* gene in the SNH 512, 256, and 128 μg/mL groups was down-regulated by 3.55-fold, 1.72-fold, and 1.39-fold, respectively. The *YWPI* and *RHD1* genes play a negative regulatory role in the adhesion of yeast-like cells, and the adhesion of biofilms formed by *YWPI*- or *RHD1*-deficient strains is enhanced (**Figure 6E**). The *YWPI* gene in the SNH 512, 256, and 128 μg/mL groups was up-regulated by 8.90-fold, 2.18-fold, and 1.93-fold, respectively, and the *RHD1* gene in the SNH 512, 256, and 128 μg/mL groups was up-regulated by 3.83-fold, 1.34-fold, and 1.10-fold, respectively.

To further explore the effects of SNH in the Ras1-cAMP-Efg1 pathway, we determined the production of cAMP in *C. albicans* treated with SNH at 4 h and 24 h after drug treatment. The results (**Figure 6F**) show that SNH can significantly

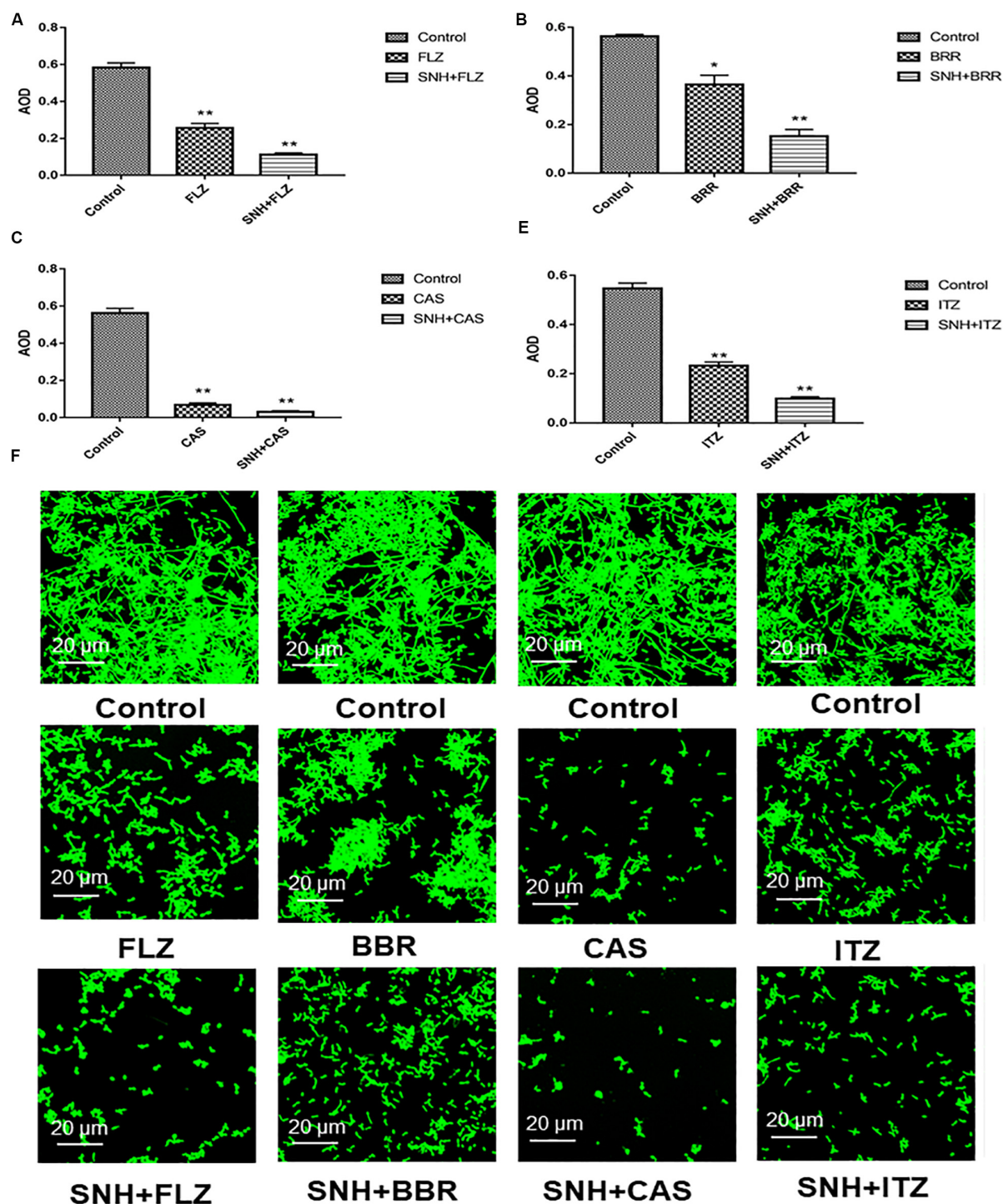


FIGURE 4 | (A–E) Analyze the average optical density (AOD) of SNH and FLZ, BBR, CAS, ITZ on *C. albicans* SC5314 biofilm by Image J, respectively. The drug-free strain-containing medium was set as the control. Data are shown as mean \pm SD. ** $p < 0.01$ and * $p < 0.05$, compared with the control. **(F)** Observation of morphological changes of SNH and FLZ, BBR, CAS, ITZ on *C. albicans* SC5314 biofilm by CLSM ($\times 400$), respectively. The initial inoculum was newly prepared at 2×10^6 CFU/mL. The drug-free strain-containing medium was set as the control.

reduce the production of cAMP both at 4 h and 24 h in a dose-dependent manner. The positive control, FLZ, also significantly inhibited the production of cAMP in *C. albicans*.

Therefore, our results indicate that SNH can significantly reduce the production of cAMP which is the key messenger molecule of the Ras1-cAMP-Efg1 pathway in *C. albicans*.

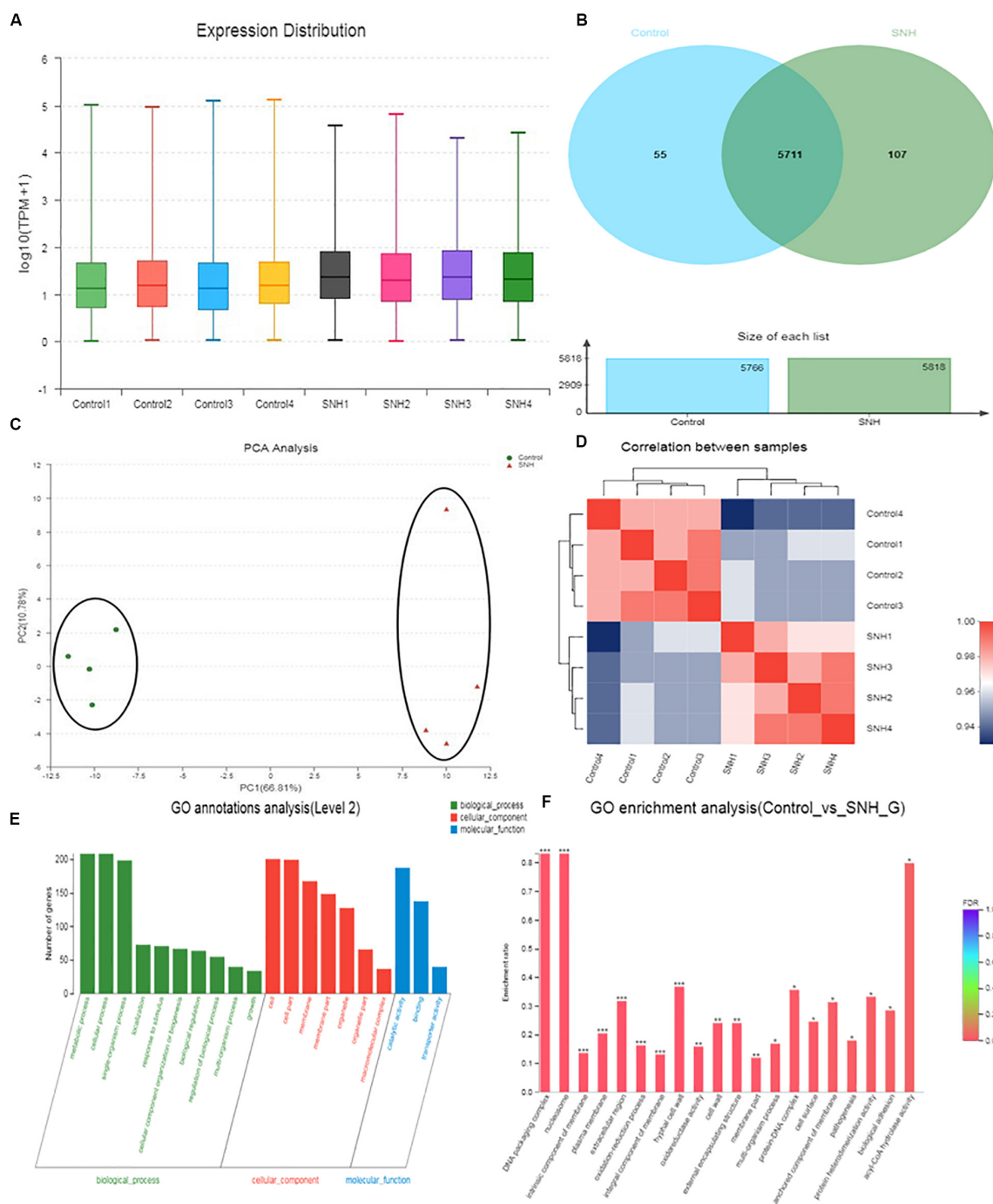


FIGURE 5 | Effect of SNH on the transcriptome of *C. albicans* SC5314. **(A)** The abscissa is the sample name and the ordinate is $\log_{10}(\text{TPM} + 1)$. Each color in the figure represents a sample, and the horizontal line in the figure indicates the median of gene expression in the sample. **(B)** Venn diagram of the number of genes in the Control and SNH treatments, respectively. **(C)** The right and lower sides of the figure are sample names, and the left and upper sides are sample clustering, and the squares of different colors represent the correlation between the two samples in the principle component analysis (PCA). **(D)** After the sample is analyzed by dimensionality reduction, there are relative coordinate points on the principal component. The distance between each sample point represents the distance of the sample. The closer the distance is, the higher the similarity between samples. The horizontal axis represents the contribution of principal component 1 (PC1) to the differentiated samples in the two-dimensional map, and the vertical axis represents the contribution of principal component 2 (PC2) to the differentiated samples in the two-dimensional map. **(E)** The abscissa in the figure represents the secondary classification term of GO, the left ordinate indicates the percentage of genes or transcripts contained in the secondary classification, and the right ordinate indicates the genetic/transcription of the secondary classification. **(F)** The abscissa indicates the GO term, and the ordinate indicates the enrichment rate refers to the ratio of the number of genes/samples enriched in the GO term to the number of the annotation gene/background number. The color indicates the significance of the enrichment, and the redder the default color indicates that the GO term is significantly more enriched, with the FDR < 0.001 mark being ***, the FDR < 0.01 mark being **, and the FDR < 0.05 mark being *.

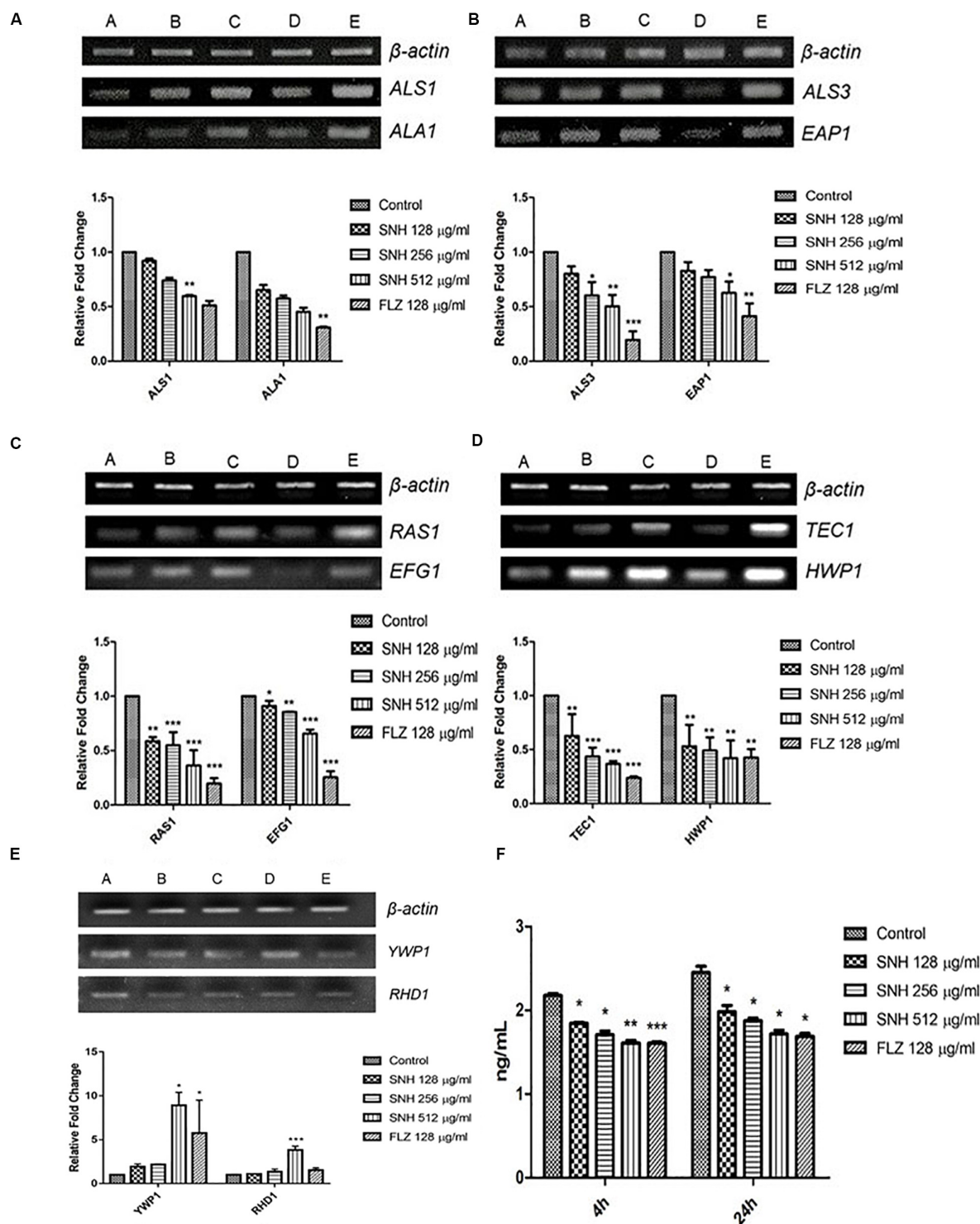


FIGURE 6 | Expression changes of biofilm related genes and protein of Ras1-cAMP-Efg1 pathway by SNH treatment in *C. albicans* SC5314. **(A)** The expression levels of adhesion-related genes *ALS1* and *ALA1*. **(B)** The expression levels of biofilm-related genes *ALS3* and *EAP1*. **(C–D)** The expression levels of Ras1-cAMP-Efg1 pathway-related genes *RAS1*, *EFG1*, *TEC1*, and *HWP1*. **(E)** The expression of yeasts-related genes *YWP1* and *RHD1*. Gene expression results were detected by RT-PCR nucleic acid electrophoresis bands and qRT-PCR quantitative analysis. The drug-free strain-containing medium was set as the control. Data are shown as mean \pm SD. (A,B,C,D,E) were respectively expressed as SNH 512 $\mu\text{g/mL}$ group, SNH 256 $\mu\text{g/mL}$ group, SNH 128 $\mu\text{g/mL}$ group, and FLZ 128 $\mu\text{g/mL}$ group, Control group. * $p < 0.05$, ** $p < 0.01$, and *** $p < 0.001$ are calculated by comparing with the control group. **(F)** Effects of SNH on the production of cAMP protein of *C. albicans* SC5314. The drug-free strain-containing medium was set as the control. Data are shown as mean \pm SD. * $p < 0.05$, ** $p < 0.01$, and *** $p < 0.001$ are calculated by comparing with the control group.

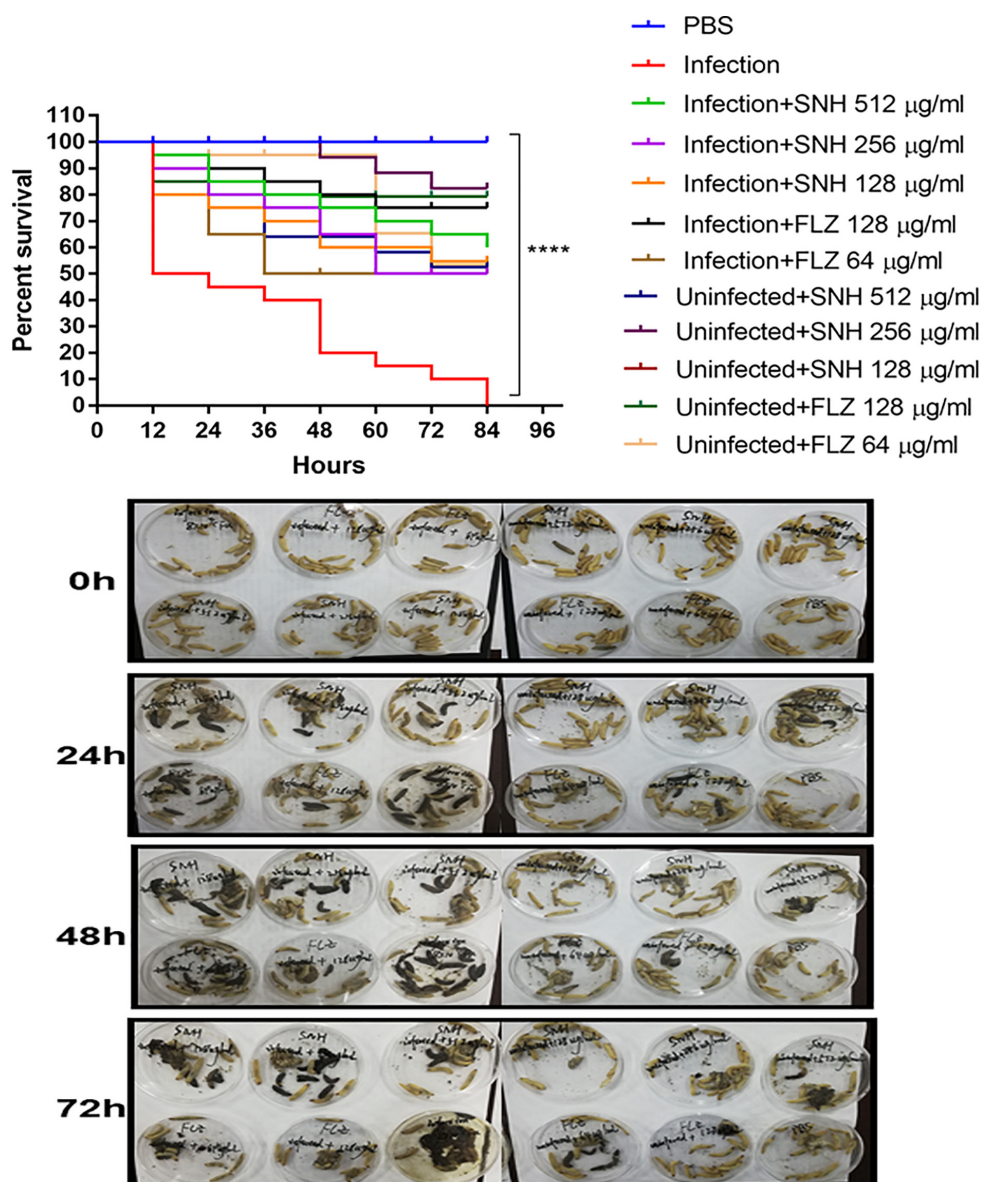


FIGURE 7 | *In vivo* evaluation of antifungal efficacy of SNH against *C. albicans*. Survival of *G. mellonella* larvae infected with LD₅₀ dose of *C. albicans* SC5314 strains (8×10^4 CFU/larvae) and treated with SNH 1 h post-infection. *C. albicans* SC5314 induced infection (10 μL) was treated with SNH (10 μL), keeping respective controls (infected, infected with FLZ-treatment, PBS). Data expressed as the mean of three independent experiments. Survival curves were plotted using the Kaplan-Meier method and statistical analysis were performed using the log-rank test for multiple comparisons. **** $p < 0.0001$.

We speculated that the mechanism of SNH in *C. albicans* biofilm inhibition may be related to blocking the Ras1-cAMP-Efg1 signaling pathway.

Determination of LD₅₀ of *C. albicans* SC5314 Strains in *G. mellonella* Larvae

Inoculation of *G. mellonella* with *C. albicans* SC5314 strains resulted larval killing in a fungal concentration-dependent manner (Supplementary Figure S3). Based on the survival study, 8×10^4 CFU/larvae was determined as the LD₅₀ in *G. mellonella* larvae.

SNH Effectively Treats *C. albicans* Infection *in vivo*

As shown in Figure 7, the survival rate in the PBS group was 100%. The survival rate in the infected group was only 50% after 12 h. In the next 72 h, larvae in the infected group continued to die, and the final survival rate of the infected group was 0% after 84 h. It can be seen that the 256 $\mu\text{g/mL}$ and 128 $\mu\text{g/mL}$ SNH control groups did not show obvious drug toxicity, and particularly in the uninfected + SNH 128 $\mu\text{g/mL}$ group, no larvae died after 84 h. The survival rate in the uninfected + SNH 256 $\mu\text{g/mL}$ group was 85% after 84 h, and the survival rate

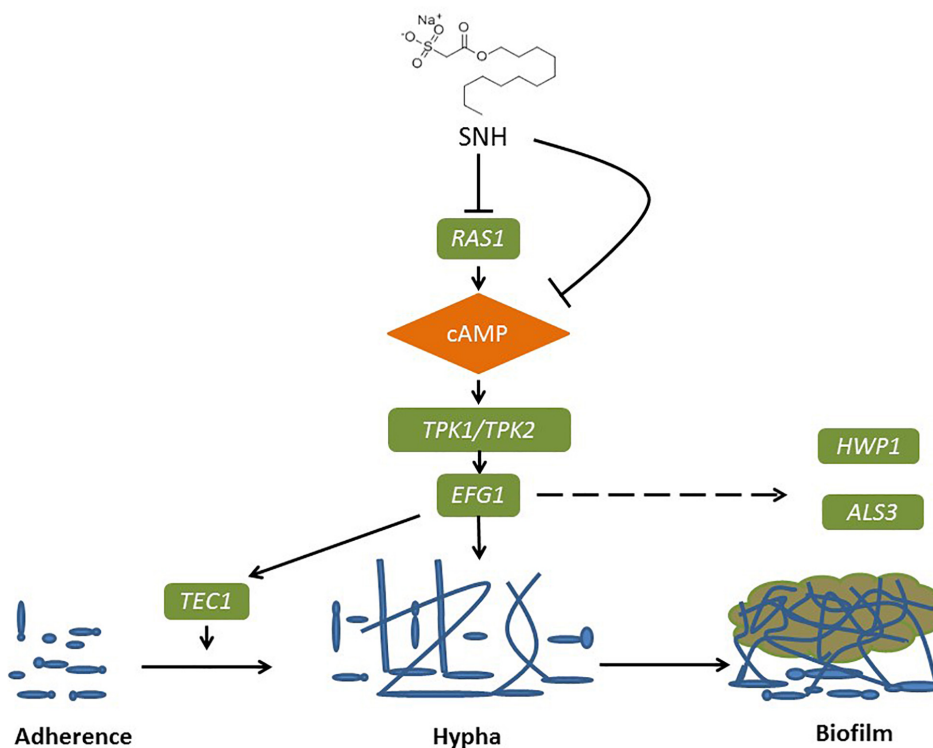


FIGURE 8 | Possible mechanism of SNH inhibits the biofilm formation of *C. albicans* by repression of Ras1-cAMP-Efg1 pathway.

of the uninfected + SNH 512 $\mu\text{g/mL}$ group was 55% after 84 h. These results indicate that SNH is slightly toxic at high concentrations, and SNH is not toxic at low concentrations. We further investigated the effects of SNH treatment at 1 h post-infection and found that the survival rate of the infection + SNH 512 $\mu\text{g/mL}$ group was 60% after 60 h, the survival rate of the infection + SNH 256 $\mu\text{g/mL}$ group was 50% after 84 h, and the survival rate of the infection + SNH 128 $\mu\text{g/mL}$ group was 55% after 84 h. These results show that compared with the survival rate of the infected group, the survival rate of all SNH dose groups remained at least above 50%, and the difference was statistically significant ($p < 0.0001$). This indicates that SNH plays an obvious antifungal role in the body, thereby improving the survival rate of larvae infected by *C. albicans*.

DISCUSSION

The medical impact of *Candida albicans* is usually attributed to its ability to form biofilms, which are tightly packed cell communities that tightly adhere to a surface and are embedded in a protective polymer extracellular matrix (Simonetti et al., 2019). Fungal pathogens form biofilms that are highly resistant to antibacterial treatment. When yeast cells adhere to a solid surface in approximately 1–2 h, the adherent cells proliferate and divide early, followed by biofilm formation, forming a complex three-dimensional structure, which is bound together by hyphae and an outer polymer matrix. After 24 h of cultivation,

a mature biofilm is formed, which is a network of yeast, hyphae, pseudohyphae and extracellular material (Ramage et al., 2005; Lohse et al., 2018). In the current study, we demonstrated that SNH is effective in inhibiting the adhesion and biofilm formation of *C. albicans*. Importantly, SNH not only suppresses adhesion but also inhibits the formation of a mature biofilm. Adhesion is the first stage of biofilm development (Douglas, 2003). The adhesion of *C. albicans* was significantly decreased after SNH treatment, indicating that SNH inhibits biofilm formation by suppressing adhesion (Li et al., 2017). Furthermore, to prevent the formation of biofilms, the transformation of yeast cells to hyphae should be prevented (Kavanaugh et al., 2014), and we found that SNH can significantly repress the yeast-to-hypha morphological transition, which is key to the biofilm maturation of *C. albicans*. The present results suggest that the anti-biofilm activity of SNH may be attributed to its anti-adhesion and anti-morphological transformation activities (Bachmann et al., 2002). Recently, Liu et al. (2020) revealed that sodium houctuyfonate, a derivative of SNH, in combination with berberine, palmatine, jatrorrhizine, and cinnamaldehyde can synergistically inhibit several *Candida* isolates, and induce cell wall remodeling of these isolates. In XTT reduction assays, we found that SNH had strong antifungal activity within 4 h of initial adhesion, which was significantly better than SNH antifungal activity during the 24-h biofilm formation phase. Through inverted microscope observations, we found that SNH can effectively inhibit *C. albicans* adhesion during the initial adhesion phase, and SNH can inhibit large thick biofilm formation during the

biofilm phase, but there were still many single fungal cells or small biofilms observable through CLSM and SEM. To further examine the effect of SNH on *C. albicans* biofilms *in vitro*, we also selected four clinical strains of *C. albicans*, and found that SNH can still effectively inhibit biofilm formation through quantification and crystal violet staining. We speculated whether these SNH anti-biofilm effects are related to fungicidal activity. A previous study found that the antimicrobial peptide VLL-28 can inhibit yeast cell growth in the suspended state, prevent cell adhesion and eliminate established biofilms *in vitro*, and also found that VLL-28 can reduce the quantity of *Candida* biofilms, but with no fungicidal effects (Roschetto et al., 2018). Our research also found that SNH inhibits the adhesion and growth of yeast cells and is effective against biofilms. SNH can reduce *C. albicans* biofilms, but cannot effectively kill fungi. This result can be interpreted by the ability of SNH to affect the structure and stability of the biofilm matrix by interacting with one or more components, thereby inducing the decomposition of the biofilm without killing the cells.

Oral infections caused by *Candida* are usually biofilms, and *Candida* is the most common fungal pathogens in humans (Millsop and Fazel, 2016; Vipulanandan et al., 2018). Biofilm resistance is an important factor in human disease. *Candida* biofilms represent an important virulence factor, and their reduction is particularly important in combating infection (Stringaro et al., 2018). Among the phenotypic changes observed in cells that form part of biofilms, the most clinically relevant feature is their increased resistance to antifungal therapy (Mukherjee and Chandra, 2004). Compared with plankton, biofilm cells can display an up to 1000-fold increased resistance (Rossoni et al., 2019). Before conducting clinical trials, *in vivo* studies should be conducted to assess the potential antifungal effect of SNH in *C. albicans*. In determining the potential toxicity of fungal pathogens, mature *Galleria mellonella* larvae have proven to be a promising substitute for mammals (Glavis-Bloom et al., 2012; Arvanitis et al., 2013). The current study is the first to investigate the anti-*C. albicans* properties of SNH using *G. mellonella*. The results show that SNH has a therapeutic effect on *C. albicans* infection *in vivo*, and this is maintained after 24 h of mature biofilm formation. In the following 60 h, compared with the infection group where larvae continued to die until the survival rate was 0%, the SNH groups maintained a survival rate of more than 50%. The present study shows that SNH has an antifungal biofilm effect both *in vitro* and *in vivo*.

Because of the increased abuse of traditional antifungal drugs and antibiotics, the resistance of *C. albicans*, especially to FLZ, is increasing. Antifungal treatment faces serious hurdles, and there is an urgent need to find new antifungal drugs. To date, most of the reported chemicals that claim to have potential antifungal functions have a high MIC. However, these antifungal agents usually have a strong resistance reversal potential in FLZ-resistant *C. albicans* (Letscher-Bru et al., 2013; Padmavathi et al., 2015). Therefore, it may be necessary to find a new drug that can increase the antifungal activity of FLZ as another method to expand the antifungal library (Guo et al., 2008). Studies have found that SH and FLZ have a synergistic effect in FLZ-resistant *C. albicans*, and SH has strong potential to enhance

FLZ treatment (Shao et al., 2017). Since higher MIC values may hinder the future development of pharmaceutical products, the combination of different forms of Chinese medicine monomers and traditional antifungal drugs is conducive to realizing the effectiveness of anti-fungal pathogens. Liu et al. reported a good antifungal effect through the combination of SH and various traditional Chinese medicine monomers (Liu et al., 2020). Here, we chose SNH and four antifungals and observed changes in the MIC and biofilm formation, and found that SNH combined with four antifungals has a significant antifungal biofilm effect. It is suggested that SH or SNH could have significant clinical potential in combination with different antifungals, in terms of reducing MIC, and producing significant anti-biofilm effects, providing treatment options for the clinical treatment of fungal infections.

With the development of genomics and the advent of whole genome sequencing platforms, metabolic pathways and related genes involved in fungal pathogenesis have been revealed (Chong et al., 2018). The current study found that the anti-adhesive effects of SNH are more significant than its anti-biofilm effects, and to verify that SNH may inhibit biofilm formation by inhibiting initial adhesion, we sequenced the transcriptome of *C. albicans* at an initial adhesion phase in 256 $\mu\text{g/mL}$ (1 MIC₈₀) SNH treatment and control groups through a high-throughput RNA sequencing method. Compared with the genomic data, the transcriptomic analysis provided more significant information about the relevant genes under different conditions (Grumaz et al., 2013; Giosa et al., 2017). To clarify the anti-adhesion and anti-biofilm mechanism of SNH, further PCR results were combined with GO enrichment analysis of the transcriptome sequencing results. Compared with the control group, the expression of 611 genes, including 361 down-regulated and 250 up-regulated genes, was significantly altered in the SNH group. Among these, several important adhesion- and biofilm-related genes were down-regulated after SNH treatment such as *RAS1*, *ALS3*, and *HWP1*, which are components of the Ras1-cAMP-Efg1 pathway. The down-regulation of these genes may contribute to the anti-adhesive and anti-biofilm activity of SNH. We found that the expression of *ALS1*, *ALA1*, *ALS3*, *EAP1*, *RAS1*, *EFG1*, *HWP1*, and *TEC1* in the Ras1-cAMP-Efg1 pathway of *C. albicans* was significantly down-regulated after SNH treatment in a dose-dependent manner and the expression of *YWPI* and *RHD1* of *C. albicans* was up-regulated after SNH treatment in a dose-dependent manner, as assessed through qRT-PCR and semi-qRT-PCR assays.

The Ras1-cAMP-Efg1 pathway is responsible for the adhesion, yeast-hyphal transition, biofilm formation and virulence of *C. albicans* (Davis-Hanna et al., 2008). Compounds of natural origin may represent a new strategy to prevent fungal adhesion and biofilm formation (De Vita et al., 2014). Certain natural products, such as magnolol and honokiol, can inhibit the adhesion, yeast-hyphal transition and biofilm formation of *C. albicans* through inactivation of the Ras1-cAMP-Efg1 pathway (Sun et al., 2015). More specifically, Ras plays a key role in controlling yeast/hyphal morphogenesis, cell adhesion and biofilm formation in *C. albicans* (Piispanen et al., 2011). Accordingly, *EFG1* is the central regulator of biofilm formation of *C. albicans* (Theberge et al., 2013). It is essential for Candidulin

growth, and is considered to be essential for the interaction between *C. albicans* and human host cells (Stoldt et al., 1997). The *TEC1* gene, encoding transcription factors, positively regulates the expression of hypha-specific genes such as *HWP1* and *ALS3* (Panariello et al., 2017). The *ALS* gene family plays an essential role in the adherence stage of *C. albicans*, and contributes to the invasion of cells and subsequently host cell damage (Sundstrom, 2002; Liu and Filler, 2011). *ALAI* and *ALS1* encode proteins that increase adherence, and produce germ tubes that exhibit thigmotropic behavior and seek solid surfaces, and grow within host tissues (Hoyer et al., 1995; Sundstrom, 2002). *HWP1* codes for a cell surface glycoprotein targeted by mammalian transglutaminase that is required for cell adhesive interactions during biofilm formation (Ene and Bennett, 2009). The involvement of *HWP1* in *C. albicans* adhesion is supported by the *EAP1* gene which encodes a glucan-crosslinked cell wall protein (Li and Palecek, 2003). Similar to many other genes, *HWP1* and *EAP1* are downstream effectors of *EFG1* and *NRG1* as transcription factors (Li and Palecek, 2003; Remmele et al., 2015). Furthermore, expressed cell wall adhesions, including *ALS* and *HWP*, are crucial for *C. albicans* attachment to host tissue and for multispecies biofilm formation (Theberge et al., 2013). Notably, *ALS1*, *ALS3*, and *HWP1* play complementary roles during biofilm formation suggesting that they might interact to promote adhesion between adjacent cellular surfaces (Lo et al., 1997). Both *ALS3* and *HWP1* are developmentally regulated and exclusively expressed in *C. albicans* hyphae (Hoyer et al., 1998), which falls under the domain of the cAMP-protein kinase-A signaling pathway that regulates yeast-hypha morphogenesis via the transcription factor *EFG1* (Lo et al., 1997; Hoyer et al., 1998; Bastidas et al., 2009; Zhang et al., 2017). Overall, *HWP1* is a downstream component of the cAMP-dependent PKA pathway and is positively regulated by *EFG1* (Lin et al., 2018). The results of PCR and eukaryotic transcriptome sequencing show that SNH can inhibit the gene expression of *ALS1*, *ALAI*, *ALS3*, *EAP1*, *RAS1*, *EFG1*, *HWP1*, and *TEC1* in the Ras1-cAMP-Efg1 pathway of *C. albicans*. In addition, we determined the effects of SNH on the production of cAMP which is the key messenger molecule in the Ras1-cAMP-Efg1 pathway of *C. albicans*. Previous studies have found that the yeast-to-mycelium transition of *C. albicans* is positively regulated by the Ras1-cAMP-Efg1 and MAPK signaling pathways, while cAMP is an intermediate regulator of morphogenesis (Chang et al., 2012). The results showed that SNH can also effectively repress the production of cAMP at two different time points (4 and 24 h) throughout the *C. albicans* growth cycle. Combined with the transcriptome and qRT-PCR results, these data suggest that SNH inhibits the activity of the Ras-cAMP-Efg1 pathway and leads to an alteration to mechanisms underlying *C. albicans* adherence growth, yeast-hyphal transition and biofilm formation (Figure 8). In addition, a previous study found that *YWPI*-deficient blastoconidia exhibited increased adhesiveness and biofilm formation, suggesting that *YWPI* may promote the dispersal of yeast forms of *C. albicans* (Granger et al., 2005). We also evaluated the expression of the yeast-specific gene *RHD1*, and previous studies have shown that expression patterns of *Candida* species-related genes are significantly increased

during hyphae-specific gene expression over the duration of biofilm formation. On the contrary, the expression of genes suppressing yeast-specific genes (*RHD1*) and filament formation was decreased (Park et al., 2014; Lee et al., 2017). Since *YWPI* and *RHD1* play a negative regulatory role in the adhesion of yeast-like cells, the adhesion of biofilms formed by *YWPI*- or *RHD1*-deficient strains is enhanced (Chandra et al., 2001; Znaidi et al., 2013). Therefore, we detected through PCR that the relative expression levels of *YWPI* and *RHD1* genes in the SNH treatment group were increased in the 24-h biofilm state compared with the control group.

It has been reported that FLZ can exert antifungal effects by regulating the Ras-cAMP-PKA signaling pathway (Liu et al., 2017; Sun et al., 2019). Coincidentally, our experimental results also found that FLZ can down-regulate the expression of genes related to the Ras1-cAMP-Efg1 signaling pathway and the secretion level of cAMP, which demonstrates that FLZ could exert antifungal effects by regulating the Ras1-cAMP-Efg1 signaling pathway. At present, there are no reports that SNH can exert antifungal effects through the Ras1-cAMP-Efg1 signaling pathway. However, we were surprised to find that SNH can down-regulate the expression of genes related to the Ras1-cAMP-Efg1 signaling pathway and the secretion level of cAMP. The mechanism of SNH against *C. albicans* may be related to the regulation of the Ras1-cAMP-Efg1 signaling pathway. In the future, studies are required to investigate the hyphae invasion/virulence of SNH-treated *C. albicans*, with relevant cell experiments to investigate possible mechanisms. In addition, by optimizing the chemical structure of SNH, its bioavailability was improved. Slow release drug delivery agents could also be used to prolong the release and action time of SNH.

CONCLUSION

In summary, through *in vivo* and *in vitro* experiments, it was found that SNH has an obvious anti-*C. albicans* biofilm and infection effect. In addition, SNH combined with other antifungals can have synergistic efficacy in terms of anti-*C. albicans* biofilm effects. The results of eukaryotic transcriptome sequencing and PCR indicated that the anti-*C. albicans* biofilm mechanism of SNH may be closely related to the Ras1-cAMP-Efg1 pathway. Further gene knockout studies are required to verify that SNH regulates this pathway to inhibit adhesion, yeast hypha transition and biofilm formation. Our results reveal potential new applications for existing natural products of *Houttuynia cordata* which is an edible vegetable and traditional Chinese herb that has potential as a treatment to inhibit opportunistic fungal pathogens.

DATA AVAILABILITY STATEMENT

The datasets presented in this study can be found in online repositories. The names of the repository/repositories and accession number(s) can be found below: <https://www.ncbi.nlm.nih.gov/sra/PRJNA544616>, PRJNA544616.

AUTHOR CONTRIBUTIONS

DW, GY, and CW conceived and designed the study. JW and DW wrote the manuscript. JS and TW critically reviewed the manuscript and provided general advice. JW, YS, YZ, and LM performed the experiments and analyzed the data. All authors have read and agreed to the published version of the manuscript.

FUNDING

The research was funded by the National Natural Science Foundation of China (Grant No. 81503115), China Postdoctoral Science Foundation (Grant No. 2019M662185), Outstanding Young Talents Key Project of Anhui Institution of Higher Education, Provincial first-class undergraduate program (Grant No. 2018ylzy057), and Natural Science Foundation of Anhui Province (Grant No. 2008085MH300). The Funding is used to cover laboratory expenses, sample preparation, and sequencing. These funding agencies have no role in research design, data collection, analysis of results, or manuscript writing.

REFERENCES

- Albrecht, A., Felk, A., Pichova, I., Naglik, J. R., Schaller, M., de Groot, P., et al. (2006). Glycosylphosphatidylinositol-anchored proteases of *Candida albicans* target proteins necessary for both cellular processes and host-pathogen interactions. *J. Biol. Chem.* 281, 688–694. doi: 10.1074/jbc.M509297200
- Arvanitis, M., Glavis-Bloom, J., and Mylonakis, E. (2013). Invertebrate models of fungal infection. *Biochim. Biophys. Acta* 1832, 1378–1383. doi: 10.1016/j.bbdis.2013.03.008
- Bachmann, S. P., Vandewalle, K., Ramage, G., Patterson, T. F., Wickes, B. L., Graybill, J. R., et al. (2002). In vitro activity of caspofungin against *Candida albicans* biofilms. *Antimicrob. Agents* 46, 3591–3596. doi: 10.1128/aac.46.11.3591-3596.2002
- Barchiesi, F., Colombo, A. L., McGough, D. A., and Rinaldi, M. G. (1994). Comparative study of broth macrodilution and microdilution techniques for in vitro antifungal susceptibility testing of yeasts by using the National Committee for Clinical Laboratory Standards' proposed standard. *J. Clin. Microbiol.* 32, 2494–2500. doi: 10.1128/jcm.32.10.2494-2500.1994
- Bastidas, R. J., Heitman, J., and Cardenas, M. E. (2009). The protein kinase Tor1 regulates adhesin gene expression in *Candida albicans*. *PLoS Pathog.* 5:e1000294. doi: 10.1371/journal.ppat.1000294
- Bergin, D., Murphy, L., Keenan, J., Clynes, M., and Kavanagh, K. (2006). Pre-exposure to yeast protects larvae of *Galleria mellonella* from a subsequent lethal infection by *Candida albicans* and is mediated by the increased expression of antimicrobial peptides. *Microbes Infect.* 8, 2105–2112. doi: 10.1016/j.micinf.2006.03.005
- Boufridi, A., and Quinn, R. J. (2018). Harnessing the properties of natural products. *Annu. Rev. Pharmacol.* 58, 451–470. doi: 10.1146/annurev-pharmtox-010716-105029
- Chandra, J., Mukherjee, P. K., Leidich, S. D., Faddoul, F. F., Hoyer, L. L., Douglas, L. J., et al. (2001). Antifungal resistance of *Candida* biofilms formed on denture acrylic in vitro. *J. Dent. Res.* 80, 903–908. doi: 10.1177/00220345010800031101
- Chang, W., Li, Y., Zhang, L., Cheng, A., and Lou, H. (2012). Retigeric acid B attenuates the virulence of *Candida albicans* via inhibiting adenylyl cyclase activity targeted by enhanced farnesol production. *PLoS One* 7:e41624. doi: 10.1371/journal.pone.0041624
- Chong, P. P., Chin, V. K., Wong, W. F., Madhavan, P., Yong, V. C., and Looi, C. Y. (2018). Transcriptomic and genomic approaches for unravelling *Candida*

ACKNOWLEDGMENTS

We thank the sequencing facilities of Majorbio Gene Cloud Platform for the preparation, sequencing, and bioinformatics analysis of the transcriptome data.

SUPPLEMENTARY MATERIAL

The Supplementary Material for this article can be found online at: <https://www.frontiersin.org/articles/10.3389/fmicb.2020.02075/full#supplementary-material>

FIGURE S1 | Volcano plot diagram of the extent of the gene differential expression between two groups.

FIGURE S2 | Hierarchical cluster analysis of the 611 significantly expression changing genes between two groups.

FIGURE S3 | Determination of LD₅₀ of *C. albicans* SC5314 strains in *G. mellonella* larvae.

TABLE S1 | Expression changes of several genes in Ras1-cAMP-Efg1 pathway determined by transcriptomic analysis.

TABLE S2 | Complete list of genes with significantly expression changes determined by transcriptomic analysis.

albicans biofilm formation and drug resistance—an update. *Genes* 9:540. doi: 10.3390/genes9110540

- Davis-Hanna, A., Piispanen, A. E., Stateva, L. I., and Hogan, D. A. (2008). Farnesol and dodecanol effects on the *Candida albicans* Ras1-cAMP signaling pathway and the regulation of morphogenesis. *Mol. Microbiol.* 67, 47–62. doi: 10.1111/j.1365-2958.2007.06013.x
- De Vita, D., Friggeri, L., D'Auria, F. D., Pandolfi, F., Piccoli, F., Panella, S., et al. (2014). Activity of caffeic acid derivatives against *Candida albicans* biofilm. *Bioorg. Med. Chem. Lett.* 24, 1502–1505. doi: 10.1016/j.bmcl.2014.02.005
- Douglas, L. J. (2003). *Candida* biofilms and their role in infection. *Trends Microbiol.* 11, 30–36. doi: 10.1016/s0966-842x(02)00002-1
- Ene, I. V., and Bennett, R. J. (2009). Hwp1 and related adhesins contribute to both mating and biofilm formation in *Candida albicans*. *Eukaryot. Cell.* 8, 1909–1913. doi: 10.1128/EC.00245-09
- Giosa, D., Felice, M. R., Lawrence, T. J., Gulati, M., Scordino, F., Giuffrè, L., et al. (2017). Whole RNA-sequencing and transcriptome assembly of *Candida albicans* and *Candida africana* under chlamydo-spore-inducing conditions. *Genome Biol. Evol.* 9, 1971–1977. doi: 10.1093/gbe/evx143
- Glavis-Bloom, J., Muhammed, M., and Mylonakis, E. (2012). Of model hosts and man: using *Caenorhabditis elegans*, *Drosophila melanogaster* and *Galleria mellonella* as model hosts for infectious disease research. *Adv. Exp. Med. Biol.* 710, 11–17. doi: 10.1007/978-1-4419-5638-5_2
- Granger, B. L., Flenniken, M. L., Davis, D. A., Mitchell, A. P., and Cutler, J. E. (2005). Yeast wall protein 1 of *Candida albicans*. *Microbiology* 151, 1631–1644. doi: 10.1099/mic.0.27663-0
- Grumaz, C., Lorenz, S., Stevens, P., Lindemann, E., Schöck, U., Retey, J., et al. (2013). Species and condition specific adaptation of the transcriptional landscapes in *Candida albicans* and *Candida dubliniensis*. *BMC Genomics* 14:212. doi: 10.1186/1471-2164-14-212
- Guo, X. L., Leng, P., Yang, Y., Yu, L. G., and Lou, H. X. (2008). Plagiochin E, a botanic-derived phenolic compound, reverses fungal resistance to fluconazole relating to the efflux pump. *J. Appl. Microbiol.* 104, 831–838. doi: 10.1111/j.1365-2672.2007.03617.x
- Harding, C. R., Schroeder, G. N., Collins, J. W., and Frankel, G. (2013). Use of *Galleria mellonella* as a model organism to study *Legionella pneumophila* infection. *J. Vis. Exp.* 81:e50964. doi: 10.3791/50964
- Holm, K., Svensson, P. J., and Rasmussen, M. (2015). Invasive *Fusobacterium necrophorum* infections and Lemièrre's syndrome: the role of thrombophilia

- and EBV. *Eur. J. Clin. Microbiol.* 34, 2199–2207. doi: 10.1007/s10096-015-2469-8
- Hoyer, L. L., Payne, T. L., Bell, M., Myers, A. M., and Scherer, S. (1998). *Candida albicans* ALS3 and insights into the nature of the ALS gene family. *Curr. Genet.* 33, 451–459. doi: 10.1007/s002940050359
- Hoyer, L. L., Scherer, S., Shatzman, A. R., and Livi, G. P. (1995). *Candida albicans* ALS1: Domains related to a *Saccharomyces cerevisiae* sexual agglutinin separated by a repeating motif. *Mol. Microbiol.* 15, 39–54. doi: 10.1111/j.1365-2958.1995.tb02219.x
- Huang, W., Duan, Q., Li, F., Shao, J., Cheng, H., and Wu, D. (2015). Sodium houttuynfonate and EDTA-Na2 in combination effectively inhibits *Pseudomonas aeruginosa*, *Staphylococcus aureus* and *Candida albicans* in vitro and in vivo. *Bioorg. Med. Chem. Lett.* 25, 142–147. doi: 10.1016/j.bmcl.2014.10.072
- Jiang, C., Yu, J., Qin, S., Zhao, J., and Yu, Z. (2006). Acute toxicity study of sodium new houttuynfonate. *J. Anim. Sci. Vet. Med.* 38, 54–55.
- Jiang, R., Hu, C., Li, Q., Cheng, Z., Gu, L., Li, H., et al. (2019). Sodium new houttuynfonate suppresses metastasis in NSCLC cells through the Linc00668/miR-147a/slug axis. *J. Exp. Clin. Cancer Res.* 38:155. doi: 10.1186/s13046-019-1152-9
- Kavanaugh, N. L., Zhang, A. Q., Nobile, C. J., Johnson, A. D., and Ribbeck, K. (2014). Mucins suppress virulence traits of *Candida albicans*. *mBio* 5:e01911. doi: 10.1128/mBio.01911-14
- Lee, K. H., Park, S. J., Choi, S. J., and Park, J. Y. (2017). *Proteus vulgaris* and *Proteus mirabilis* decrease *Candida albicans* biofilm formation by suppressing morphological transition to its hyphal form. *Yonsei Med. J.* 58, 1135–1143. doi: 10.3349/ymj.2017.58.6.1135
- Letscher-Bru, V., Obszynski, C., Samsoen, M., Sabou, M., Waller, J., and Candolfi, E. (2013). Antifungal activity of sodium bicarbonate against fungal agents causing superficial infections. *Mycopathologia* 175, 153–158. doi: 10.1007/s11046-012-9583-2
- Li, B., and Dewey, C. N. (2011). RSEM: accurate transcript quantification from RNA-Seq data with or without a reference genome. *BMC Bioinformatics* 12:323. doi: 10.1186/1471-2105-12-323
- Li, D. D., Chai, D., Huang, X. W., Guan, S. X., Du, J., Zhang, H. Y., et al. (2017). Potent in vitro synergism of flucanazole and osthole against fluconazole-resistant *Candida albicans*. *Antimicrob. Agents Chemother.* 61:e436–e417. doi: 10.1128/AAC.00436-17
- Li, F., and Palecek, S. P. (2003). EAP1, a *Candida albicans* gene involved in binding human epithelial cells. *Eukaryot Cell.* 2, 1266–1273. doi: 10.1128/ec.2.6.1266-1273.2003
- Lin, C. J., Wu, C. Y., Yu, S. J., and Chen, Y. L. (2018). Protein kinase A governs growth and virulence in *Candida tropicalis*. *Virulence* 9, 331–347. doi: 10.1080/21505594.2017.1414132
- Liu, J., Li, Q., Wang, C., Shao, J., Wang, T., Wu, D., et al. (2020). Antifungal evaluation of traditional herbal monomers and their potential for inducing cell wall remodeling in *Candida albicans* and *Candida auris*. *Biofouling* 36, 319–331. doi: 10.1080/08927014.2020.1759559
- Liu, X., Li, T., Wang, D., Yang, Y., Sun, W., Liu, J., et al. (2017). Synergistic antifungal effect of fluconazole combined with licofelone against resistant *Candida albicans*. *Front. Microbiol.* 8:2101. doi: 10.3389/fmicb.2017.02101
- Liu, Y., and Filler, S. G. (2011). *Candida albicans* Als3, a multifunctional adhesin and invasin. *Eukaryot. Cell.* 10, 168–173. doi: 10.1128/EC.00279-10
- Livak, K. J., and Schmittgen, T. D. (2001). Analysis of relative gene expression data using real-time quantitative PCR and the 2⁻(Delta Delta C (T)) Method. *Methods* 25, 402–408. doi: 10.1006/meth.2001.1262
- Lo, H. J., Köhler, J. R., Didomenico, B., Loebenberg, D., Cacciapuoti, A., and Fink, G. R. (1997). Nonfilamentous *C. albicans* mutants are avirulent. *Cell* 90, 939–949. doi: 10.1016/s0092-8674(00)80358-x
- Lohse, M. B., Gulati, M., Johnson, A. D., and Nobile, C. J. (2018). Development and regulation of single- and multi-species *Candida albicans* biofilms. *Nat. Rev. Microbiol.* 16, 19–31. doi: 10.1038/nrmicro.2017.107
- Lou, X., Luan, Y., Jiang, B., Chen, X., and Zhong, D. (2012). Acute toxicity of sodium houttuynfonate in BALB/c mice and its injury to cells. *Chin. J. Pharmacol. Toxicol.* 26, 653–657. doi: 10.3867/j.issn.1000-3002.2012.05.010
- Lu, X., Yang, X., Li, X., Lu, Y., Ren, Z., Zhao, L., et al. (2013). In vitro activity of sodium new houttuynfonate alone and in combination with oxacillin or netilmicin against methicillin-resistant *Staphylococcus aureus*. *PLoS One* 8:e68053. doi: 10.1371/journal.pone.0068053
- Manoharan, R. K., Lee, J. H., Kim, Y. G., Kim, S. I., and Lee, J. (2017a). Inhibitory effects of the essential oils α -longipinene and linalool on biofilm formation and hyphal growth of *Candida albicans*. *Biofouling* 33, 143–155. doi: 10.1080/08927014.2017.1280731
- Manoharan, R. K., Lee, J. H., Kim, Y. G., and Lee, J. (2017b). Alizarin and chrysazin inhibit biofilm and hyphal formation by *Candida albicans*. *Front. Cell. Infect. Microbiol.* 7:447. doi: 10.3389/fcimb.2017.00447
- Manoharan, R. K., Lee, J. H., and Lee, J. (2017c). Antibiofilm and antihyphal activities of cedar leaf essential oil, camphor, and fenchone derivatives against *Candida albicans*. *Front. Microbiol.* 8:1476. doi: 10.3389/fmicb.2017.01476
- Martin, H., Govern, M. M., Abbey, L., Gilroy, A., Mullins, S., Howell, S., et al. (2018). Inhibition of adherence of the yeast *Candida albicans* to buccal epithelial cells by synthetic aromatic glycoconjugates. *Eur. J. Med. Chem.* 160, 82–93. doi: 10.1016/j.ejmech.2018.10.011
- Millsop, J. W., and Fazel, N. (2016). Oral candidiasis. *Clin. Dermatol.* 34, 487–494. doi: 10.1016/j.clindermatol.2016.02.022
- Mukherjee, P. K., and Chandra, J. (2004). *Candida* biofilm resistance. *Drug Resist. Updat.* 7, 301–309. doi: 10.1016/j.drug.2004.09.002
- Naglik, J. R., Fostira, F., Ruprai, J., Staab, J. F., Challacombe, S. J., and Sundstrom, P. (2006). *Candida albicans* HWP1 gene expression and host antibody responses in colonization and disease. *J. Med. Microbiol.* 55, 1323–1327. doi: 10.1099/jmm.0.46737-0
- Oshiro, K. G. N., Rodrigues, G., Monges, B. E. D., Cardoso, M. H., and Franco, O. L. (2019). Bioactive peptides against fungal biofilms. *Front. Microbiol.* 10:2169. doi: 10.3389/fmicb.2019.02169
- Padmavathi, A. R., Bakkiyaraj, D., Thajuddin, N., and Pandian, S. K. (2015). Effect of 2, 4-di-tert-butylphenol on growth and biofilm formation by an opportunistic fungus *Candida albicans*. *Biofouling* 31, 565–574. doi: 10.1080/08927014.2015.1077383
- Panariello, B. H. D., Klein, M. I., Pavarina, A. C., and Duarte, S. (2017). Inactivation of genes TEC1 and EFG1 in *Candida albicans* influences extracellular matrix composition and biofilm morphology. *J. Oral Microbiol.* 9:1385372. doi: 10.1080/20002297.2017.1385372
- Park, S. J., Han, K. H., Park, J. Y., Choi, S. J., and Lee, K. H. (2014). Influence of bacterial presence on biofilm formation of *Candida albicans*. *Yonsei Med. J.* 55, 449–458. doi: 10.3349/ymj.2014.55.2.449
- Pfaller, M. A., and Barry, A. L. (1994). Evaluation of a novel colorimetric broth microdilution method for antifungal susceptibility testing of yeast isolates. *J. Clin. Microbiol.* 32, 1992–1996. doi: 10.1128/jcm.32.8.1992-1996.1994
- Piispanen, A. E., Bonnefoi, O., Carden, S., Deveau, A., Bassilana, M., and Hogan, D. A. (2011). Roles of Ras1 membrane localization during *Candida albicans* hyphal growth and farnesol response. *Eukaryot. Cell.* 10, 1473–1484. doi: 10.1128/EC.05153-11
- Pizarrocerda, J., and Cossart, P. (2006). Bacterial adhesion and entry into host cells. *Cell* 124, 715–727. doi: 10.1016/j.cell.2006.02.012
- Ramage, G., Saville, S. P., Thomas, D. P., and López-Ribot, J. L. (2005). *Candida* biofilms: an update. *Eukaryot Cell.* 4, 633–638. doi: 10.1128/EC.4.4.633-638.2005
- Remmele, C. W., Luther, C. H., Balkenhol, J., Dandekar, T., Müller, T., and Dittrich, M. T. (2015). Integrated inference and evaluation of host-fungi interaction networks. *Front. Microbiol.* 6:764. doi: 10.3389/fmicb.2015.00764
- Robinson, M. D., McCarthy, D. J., and Smyth, G. K. (2010). EdgeR: a Bioconductor package for differential expression analysis of digital gene expression data. *Bioinformatics* 26, 139–140. doi: 10.1093/bioinformatics/btp616
- Rodriguezdeira, C., Gregorio, M. C., Molares-Vila, A., López-Barcenas, A., Fabbrocini, G., Bardhi, B., et al. (2019). Biofilms and vulvovaginal candidiasis. *Colloids Surf. B Biointerfaces* 174, 110–125. doi: 10.1016/j.colsurfb.2018.11.011
- Roschetto, E., Contursi, P., Vollaro, A., Fusco, S., Notomista, E., and Catania, M. R. (2018). Antifungal and anti-biofilm activity of the first cryptic antimicrobial peptide from an archaeal protein against *Candida* spp. clinical isolates. *Sci. Rep.* 8:17570. doi: 10.1038/s41598-018-35530-0
- Rossoni, R. D., de Barros, P. P., Lopes, L., Ribeiro, F. C., Nakatsuka, T., Kasaba, H., et al. (2019). Effects of surface pre-reacted glass-ionomer (S-PRG) eluate on *Candida* spp.: antifungal activity, anti-biofilm properties, and protective effects on *Galleria mellonella* against *C. albicans* infection. *Biofouling* 35, 997–1006. doi: 10.1080/08927014.2019.1686485
- Shao, J., Cui, Y., Zhang, M., Wang, T., Wu, D., and Wang, C. (2017). Synergistic in vitro activity of sodium houttuynfonate with fluconazole against clinical

- Candida albicans* strains under planktonic growing conditions. *Pharm. Biol.* 55, 355–359. doi: 10.1080/13880209.2016.1237977
- Shen, S., Park, J. W., Huang, J., Dittmar, K. A., Lu, Z. X., Zhou, Q., et al. (2012). MATS: a Bayesian framework for flexible detection of differential alternative splicing from RNA-Seq data. *Nucleic Acids Res.* 40:e61. doi: 10.1093/nar/gkr1291
- Silva, D. R., Rosalen, P. L., Freires, I. A., Sardi, J., Lima, R. F., Lazarini, J. G., et al. (2019). Anadenanthera Colubrina vell Brenan: anti-*Candida* and antibiofilm activities, toxicity and therapeutical action. *Braz. Oral Res.* 33:e023. doi: 10.1590/1807-3107bor-2019.vol33.0023
- Simon, G., Berube, C., Voyer, N., and Grenier, D. (2018). Anti-biofilm and anti-adherence properties of novel cyclic dipeptides against oral pathogens. *Bioorg. Med. Chem.* 27, 2323–2331. doi: 10.1016/j.bmc.2018.11.042
- Simonetti, G., Palocci, C., Valletta, A., Kolesova, O., Chronopoulou, L., Donati, L., et al. (2019). Anti-*Candida* biofilm activity of pterostilbene or crude extract from non-fermented grape pomace entrapped in biopolymeric nanoparticles. *Molecules* 24:2070. doi: 10.3390/molecules24112070
- Stoldt, V. R., Sonneborn, A., Leuker, C. E., and Ernst, J. F. (1997). Efg1p, an essential regulator of morphogenesis of the human pathogen *Candida albicans*, is a member of a conserved class of bHLH proteins regulating morphogenetic processes in fungi. *EMBO J.* 16, 1982–1991. doi: 10.1093/emboj/16.8.1982
- Stringaro, A., Colone, M., and Angioletti, L. (2018). Antioxidant, antifungal, antibiofilm, and cytotoxic activities of mentha spp. essential oils. *Medicines* 5:112. doi: 10.3390/medicines5040112
- Sun, L., Liao, K., and Wang, D. (2015). Effects of magnolol and honokiol on adhesion, yeast-hyphal transition, and formation of biofilm by *Candida albicans*. *PLoS One* 10:e0117695. doi: 10.1371/journal.pone.0117695
- Sun, W., Zhang, L., Lu, X., Feng, L., and Sun, S. (2019). The synergistic antifungal effects of sodium phenylbutyrate combined with azoles against *Candida albicans* via the regulation of the Ras-cAMP-PKA signalling pathway and virulence. *Can. J. Microbiol.* 65, 105–115. doi: 10.1139/cjm-2018-0337
- Sundstrom, P. (2002). Adhesion in *Candida* spp. *Cell. Microbiol.* 4, 461–469. doi: 10.1046/j.1462-5822.2002.00206.x
- Tan, Y., Leonhard, M., Moser, D., Ma, S., and Schneider-Stickler, B. (2019). Antibiofilm efficacy of curcumin in combination with 2-aminobenzimidazole against single- and mixed-species biofilms of *Candida albicans* and *Staphylococcus aureus*. *Colloids Surf. B Biointerfaces* 174, 28–34. doi: 10.1016/j.colsurfb.2018.10.079
- Theberge, S., Semlali, A., Alamri, A., Leung, K. P., and Rouabhia, M. (2013). *C. albicans* growth, transition, biofilm formation, and gene expression modulation by antimicrobial decapeptide KSL-W. *BMC Microbiol.* 13:246. doi: 10.1186/1471-2180-13-246
- Trapnell, C., Pachter, L., and Salzberg, S. L. (2009). TopHat: discovering splice junctions with RNA-Seq. *Bioinformatics* 25, 1105–1111. doi: 10.1093/bioinformatics/btp120
- Vipulanandan, G., Herrera, M., Wiederhold, N. P., Li, X., Mintz, J., Wickes, B. L., et al. (2018). Dynamics of mixed *Candida* species biofilms in response to antifungals. *J. Dent. Res.* 97, 91–98. doi: 10.1177/0022034517729351
- Wang, T., Huang, W., Duan, Q., Wang, J., Cheng, H., Shao, J., et al. (2019). Sodium houttuynfonate in vitro inhibits biofilm dispersion and expression of bdlA in *Pseudomonas aeruginosa*. *Mol. Biol. Rep.* 46, 471–477. doi: 10.1007/s11033-018-4497-9
- Wang, T., Shao, J., Da, W., Li, Q., Shi, G., Wu, D., et al. (2018). Strong synergism of palmatine and fluconazole/Itraconazole against planktonic and biofilm cells of *Candida* species and efflux-associated antifungal mechanism. *Front. Microbiol.* 9:2892. doi: 10.3389/fmicb.2018.02892
- Wu, D. Q., Cheng, H., Duan, Q., and Huang, W. (2015). Sodium houttuynfonate inhibits biofilm formation and alginate biosynthesis-associated gene expression in a clinical strain of *Pseudomonas aeruginosa* in vitro. *Exp. Ther. Med.* 10, 753–758. doi: 10.3892/etm.2015.2562
- Xie, C., Mao, X., Huang, J., Ding, Y., Wu, J., Dong, S., et al. (2011). KOBAS 2.0: a web server for annotation and identification of enriched pathways and diseases. *Nucleic Acids Res.* 39, W316–W322. doi: 10.1093/nar/gkr483
- Yang, X. Y., Shi, T., Du, G., Liu, W., Yin, X. F., Sun, X., et al. (2016). ITRAQ-Based Proteomics revealed the bactericidal mechanism of sodium new houttuynfonate against *Streptococcus pneumoniae*. *J. Agric. Food Chem.* 64, 6375–6382. doi: 10.1021/acs.jafc.6b02147
- Ye, X., Li, X., Yuan, L., Ge, L., Zhang, B., and Zhou, S. (2007). Interaction of houttuynfonate homologues with the cell membrane of gram-positive and gram-negative bacteria. *Colloids Surf. A Physicochem. Eng. Asp.* 301, 412–418. doi: 10.1016/j.colsurfa.2007.01.012
- Zhang, M., Chang, W., Shi, H., Zhou, Y., Zheng, S., Li, Y., et al. (2017). Biatrisporin D displays anti-virulence activity through decreasing the intracellular cAMP levels. *Toxicol. Appl. Pharmacol.* 322, 104–112. doi: 10.1016/j.taap.2017.03.004
- Zhao, Y., Si, Y., Mei, L., Wu, J., Shao, J., Wang, C., et al. (2019). Effects of sodium houttuynfonate on transcriptome of *Pseudomonas aeruginosa*. *BMC Res. Notes* 12:685. doi: 10.1186/s13104-019-4721-2
- Znaldi, S., Nesseir, A., Chauvel, M., Rossignol, T., and d'Enfert, C. (2013). A comprehensive functional portrait of two heat shock factor-type transcriptional regulators involved in *Candida albicans* morphogenesis and virulence. *PLoS Pathog.* 9:e1003519. doi: 10.1371/journal.ppat.1003519

Conflict of Interest: The authors declare that the research was conducted in the absence of any commercial or financial relationships that could be construed as a potential conflict of interest.

Copyright © 2020 Wu, Wu, Zhao, Si, Mei, Shao, Wang, Yan and Wang. This is an open-access article distributed under the terms of the Creative Commons Attribution License (CC BY). The use, distribution or reproduction in other forums is permitted, provided the original author(s) and the copyright owner(s) are credited and that the original publication in this journal is cited, in accordance with accepted academic practice. No use, distribution or reproduction is permitted which does not comply with these terms.



Antifungal Photodynamic Activity of Hexyl-Aminolevulinate Ethosomes Against *Candida albicans* Biofilm

Yingzhe Wang, Jinru Song, Feiyin Zhang, Kang Zeng* and Xiaoliang Zhu*

Department of Dermatology, Nanfang Hospital, Southern Medical University, Guangzhou, China

OPEN ACCESS

Edited by:

Sujogya Kumar Panda,
KU Leuven, Belgium

Reviewed by:

Kelly Ishida,
University of São Paulo, Brazil
Ravikumar Bapurao Shinde,
Rajarshi Shahu College, India

*Correspondence:

Xiaoliang Zhu
nfnpfk@163.com
Kang Zeng
nfnpfkzk@126.com

Specialty section:

This article was submitted to
Antimicrobials, Resistance and
Chemotherapy,
a section of the journal
Frontiers in Microbiology

Received: 14 May 2020

Accepted: 05 August 2020

Published: 11 September 2020

Citation:

Wang Y, Song J, Zhang F,
Zeng K and Zhu X (2020) Antifungal
Photodynamic Activity of
Hexyl-Aminolevulinate Ethosomes
Against *Candida albicans* Biofilm.
Front. Microbiol. 11:2052.
doi: 10.3389/fmicb.2020.02052

Biofilm formation is responsible for the development of chronic and recurrent *Candida albicans* infections. The generation of biofilms is commonly accompanied by high resistance to conventional antifungal drugs, which can increase up to 1,000-fold. Fortunately, antimicrobial photodynamic therapy (aPDT) has shown excellent potential to treat biofilm infections. However, the current most commonly used photosensitizer (PS), aminolevulinic acid (ALA), is hydrophilic, unstable, and has low permeability, leading to unsatisfactory effects on biofilm eradication. To solve these problems, more stable lipophilic PSs and more effective permeability carriers could be considered as two effective solutions. Hexyl-aminolevulinate (HAL) has good bioavailability as a PS, and we proved in a previous study that ethosomes (ES), lipid-based nanocarriers, promote percutaneous drug penetration. In our previous study, a HAL-ES system presented superior photodynamic effects compared to those of ALA or HAL alone. Therefore, here, we aim to evaluate the biological effects of HAL-ES-mediated aPDT on *C. albicans* biofilm. An XTT sodium salt assay showed that aPDT using 0.5% HAL decreased *C. albicans* biofilm activity by $69.71 \pm 0.43\%$. Moreover, aPDT with 0.5% HAL-ES further decreased biofilm activity by $92.95 \pm 0.16\%$ and inhibited growth of $25.71 \pm 1.61\%$ within 48 h, mostly via its effect on the hyphae growth, which correlated with a three-fold increase in *C. albicans* plasma membrane permeabilization. Notably, HAL-ES-mediated aPDT significantly reduced the sessile minimum inhibitory concentration 50 (SMIC50) of fluconazole to $<2.0 \mu\text{g/ml}$, and the 21-day survival rate of *C. albicans* biofilm-infected mice increased from 6.7 to 73.3%. It also significantly reduced the drug resistance and *in vivo* pathogenicity of *C. albicans* biofilm. These results demonstrate that HAL-ES-mediated aPDT could be an effective therapy for *C. albicans* biofilm infections; while also serving as a particularly promising effective treatment for cutaneous or mucocutaneous candidiasis and the prevention of progression to systemic candidiasis.

Keywords: *Candida albicans*, biofilm, photodynamic therapy, hexyl-aminolevulinate, ethosomes

INTRODUCTION

Candida albicans is a fungus naturally present in the skin and mucosa of healthy people, which can be pathogenic in case of systemic or local decline of immunity. Cutaneous candidiasis is a common disease affecting people of all ages, accounting for approximately 7.1% of patients with dermatosis (Penate et al., 2009). With the widespread use of antifungal drugs, drug resistance in *C. albicans* has become increasingly severe, especially considering azoles, such as fluconazole, while biofilm formation has been identified as the leading cause underlying *C. albicans* drug resistance (Holmes et al., 2012). Biofilms are composed of spores, pseudohyphae, and hyphae surrounded by a self-produced extracellular matrix (Wall et al., 2019). Microbes embedded in a biofilm can tolerate 100–1,000 times higher antibiotic concentrations than their corresponding free-living counterparts (Ceri et al., 1999). Since approximately 80% of human infections are related to biofilm formation, reduction or even elimination of biofilm is a major challenge in the treatment of fungal infections (Römling and Balsalbre, 2012).

Antimicrobial photodynamic therapy (aPDT) reportedly showed valuable therapeutic potential against biofilms (Baltazar et al., 2015; Hu et al., 2018). aPDT employs a photosensitizer (PS) accumulated in cells to generate, *via* irradiation with visible light, reactive oxygen species (ROS) that attack adjacent targets, including microbial pathogens and the biofilm matrix (Hu et al., 2018). In comparison with traditional antibiotic therapies, aPDT presents the advantages of reduced side effects, increased safety, and its efficacy is not affected by common microbial resistance mechanisms (Al-Mutairi et al., 2018). However, the current most commonly used PS, aminolevulinic acid (ALA), is hydrophilic and unstable, resulting in unsatisfactory penetration of biological barriers, such as plasma membranes; it also has low bioavailability, which significantly affects aPDT efficiency.

Hexyl-aminolevulinic acid (HAL) is a lipophilic PS. Compared to ALA, HAL has an additional hexyl group that confers extra membrane permeability and higher bioavailability (Togsverd-Bo et al., 2012). HAL offers the advantages of low therapeutic concentrations, few side effects, and better economic value (Neittaanmäki-Perttu et al., 2016). Besides, HAL-mediated PDT has contributed to the diagnosis and treatment of tumors and skin diseases, such as bladder cancer (Helander et al., 2016) and solar keratosis (Neittaanmäki-Perttu et al., 2017). However, its efficacy in biofilm elimination, which is crucial to the treatment of cutaneous candidiasis, has not yet been studied.

Ethosomes (ES) are an innovative vesicular delivery system with lipid bilayers. This system is composed of alcohol, phospholipids, and water, and has high encapsulation efficiency, small particle size, excellent stability, and low irritation potential. In our previous studies, we proved that ES more effectively promotes the penetration of lipophilic drugs into the deep layer of the skin through hair follicles and cuticles compared to liposomes and a hydroethanolic solution (Zhu et al., 2013; Yang et al., 2017). It can, therefore, be speculated that if HAL is effective in biofilm elimination, ES may boost the therapeutic effect, possibly even at lower HAL concentrations.

In the present study, we studied the photodynamic effect and the mechanism of HAL-ES in *C. albicans* biofilm, as well as its effects on fluconazole susceptibility and the *in vivo* pathogenicity of *C. albicans* biofilm.

MATERIALS AND METHODS

Strains, Cultures, and Chemicals

C. albicans strain SC5314 was used in all experiments and was maintained on YPD agar (0.5% yeast extract, 1% bacto-peptone, 2% glucose, and 1.4% agar) plates at 37°C. HAL-ES at a 0.5% concentration was prepared by the injection-sonication-filtering method. Next, 0.12 g of soybean phospholipid (AVT, Shanghai, China) was mixed with 1.25 ml of ethanol to form an alcohol-based phase. In the aqueous phase, 20 mg of HAL (NMT Biotech, Suzhou, China) were dissolved in 2.75 ml of double-distilled water. The alcohol-based phase was slowly injected into the water phase (200 µl/min) under sealed conditions on a magnetic stirrer (700 rpm) for 5 min. The solution was then processed by an ultrasonic disruptor (JY92-IIN 650 W, Scientz, Ningbo, China) for 3 min at 97.5 W: the ultrasound was turned on for 5-s periods between 3-s intervals. The solution was then filter-sterilized and stored in the dark at 4°C for use within 30 min. The entire operation was performed in the dark. A blank solution of ES without HAL was prepared in the same way.

Solutions containing 0.5% HAL, 5% ALA, and 0.5% ALA were prepared in double-distilled water, filter-sterilized, and stored briefly in the dark at 4°C.

Biofilm Preparation

A single colony of *C. albicans* was picked from the YPD agar medium using an inoculating loop, inoculated into a shake tube containing 5 ml of YPD liquid medium, and cultured overnight at 37°C with shaking at 200 rpm. The fungal suspension was centrifuged for 10 min (3,000 rpm, 4°C) and washed twice with sterile phosphate-buffered saline (PBS). The final pellet was resuspended in Gibco RPMI 1640 medium (Thermo Fisher Scientific, Waltham, MA, United States) and diluted to a cell density of 1.0×10^6 cells/ml. Subsequently, 200 µl of the diluted fungal suspension was added to the selected wells of the 96-well plate, the plate was sealed with parafilm and incubated it at 37°C. After 24 h, samples were rinsed gently with PBS thrice to remove non-adherent planktonic cells. Finally, 200 µl of RPMI 1640 medium was added, and the incubation was continued for another 24 h.

aPDT of Biofilms

To observe the effects of HAL-ES-mediated aPDT, *C. albicans* biofilms were treated with 0.5% HAL-ES, 0.5% HAL, 5% ALA, 0.5% ALA, blank ES, or PBS. Each well received 100 µl of PS, and the biofilms were incubated at 37°C for 30 min in the dark. The liquid in biofilms was then discarded, and wells were carefully rinsed thrice with sterile PBS to remove the residual drug. Next, 100 µl of sterile PBS was added to each well, and the biofilms

were immediately irradiated with a light-emitting diode (LED) source (LED-IB PDT; Wuhan Yage Optic and Electronic Technique Co. Ltd., Wuhan, China) for 30 min (wavelength range: 633 ± 10 nm; power: 60 mW/cm²; irradiation distance: 10 cm). Finally, biofilms were incubated with RPMI 1640 medium in the dark for 0, 24, or 48 h before subsequent analysis.

Biofilm Activity Assay

The evaluation of *C. albicans* biofilm activity was based on XTT (a tetrazolium salt) reduction by metabolically active fungal cells (Pierce et al., 2010). In each well, 100 μ l of an XTT salt solution (Sigma-Aldrich, St. Louis, MO, United States; 0.5 mg/ml in PBS) and 1 μ l of a menadione solution (10 mM in acetone) was applied, and the plate was incubated at 37°C in the dark for 2 h. Using a multichannel pipette, 80 μ l of the resulting colored supernatant was removed from each well and transferred to the corresponding wells of a new 96-well plate. The plates were analyzed in a microplate reader (CLARIOstar Plus, BMG LABTECH, Ortenberg, Germany) at 490 nm.

Visualization of Biofilm Structure

The structure of the *C. albicans* biofilm was observed by crystal violet staining. After methanol fixation, biofilms were stained with 0.1% crystal violet and left to dry overnight at room temperature. The observation was performed under an inverted microscope (IX71, Olympus, Tokyo, Japan).

Fluorometric Estimation of Plasma Membrane Permeabilization

After aPDT and 0, 24, and 48 h of incubation, biofilms were carefully washed thrice with sterile physiological saline and were incubated in 0.2 ml of physiological saline containing 5 μ M SYTOX Green (Molecular Probes Inc., Eugene, OR, United States) for 1 h at 37°C. The fluorescence intensity of each well was measured by a microplate reader. The excitation wavelength was 488 nm, and the emission range was 508–538 nm.

Biofilm Testing for Fluconazole Susceptibility

Fluconazole (Sigma-Aldrich) was 2-fold serially diluted in RPMI 1640, from 1,024 to 2 μ g/ml. Wells containing biofilm received 100 μ l of each dilution, in addition to positive (no drug) and negative (empty wells) controls. After incubation at 37°C in the dark for 24–48 h, sessile minimum inhibitory concentration (SMIC) values in *C. albicans* biofilm were defined using the XTT assay as described above. SMIC50 and SMIC80 represent the antifungal concentrations at which we observed a 50 or 80% decrease in colorimetric readings in comparison to those in the positive control biofilms (Pierce et al., 2010).

In vivo Pathogenicity of *C. albicans* Biofilm

Six- to eight-week-old BALB/c female mice (18–22 g) were used in this study. The mice were obtained from the Laboratory Animal Center, Nanfang Hospital, Southern Medical University, Guangzhou, People's Republic of China. The animal use and care protocols were reviewed and approved by the Institutional

Animal Care and Use Committee of Nanfang Hospital, Southern Medical University (NFYY-2019-71). All procedures of animal experiments adhered to the Principles of Laboratory Animal Care guidelines of the Laboratory Animal Center of Southern Medical University, following the principles of the Declaration of Helsinki. We evaluated *C. albicans* biofilm pathogenicity *in vivo* using a mouse model of systemic infection. Biofilms were subjected to aPDT, further incubated for 48 h, and finally detached by scraping the microplate surface with a sterile spatula. The biofilm suspension was then collected in a 50-ml centrifuge tube. The microplate was carefully washed twice with sterile PBS, which was then transferred to the same centrifuge tube. The suspension was centrifuged for 15 min (3,000 rpm, 4°C) and washed three times with sterile PBS. Finally, the biofilm suspensions of the control group were diluted to achieve an OD₆₀₀ = 0.1, equivalent to 1×10^6 cells/ml. Biofilm suspensions of the 0.5% HAL-ES, 0.5% HAL, 0.5% ALA, and blank ES groups were partly diluted at the same dilution ratio as that of the control group, partly diluted to OD₆₀₀ = 0.1. Each group had 15 mice, which were injected with 0.1 ml of a thoroughly mixed biofilm suspension in their tail veins. The survival rates of mice were recorded every 24 h.

Statistical Analysis

All results were obtained from three independent experiments, and each value was expressed as the mean \pm standard deviation (SD). Statistical differences were evaluated by analysis of variance (ANOVA) and *post hoc* comparison with the Tukey-Kramer and Games-Howell tests. The survival data were analyzed by a log-rank (Mantel-Cox) test. $p < 0.05$ was considered significant.

RESULTS

HAL-ES-Mediated aPDT Decreased *C. albicans* Biofilm Activity and Growth

After performing HAL-ES-mediated aPDT, we observed a sharp reduction in the activity and growth of *C. albicans* biofilm (Figure 1). Immediately after aPDT, when compared to the control group ($100.00 \pm 0.63\%$), 0.5% HAL-ES-mediated aPDT significantly reduced *C. albicans* biofilm activity ($7.05 \pm 0.16\%$, $p < 0.001$). Biofilm activity was also inhibited in the 0.5% HAL and blank ES groups ($30.29 \pm 0.43\%$ and $30.10 \pm 0.59\%$, respectively; $p < 0.001$). After 24 h, 0.5% HAL-ES-mediated aPDT significantly inhibited the growth of *C. albicans* biofilm ($42.67 \pm 4.24\%$) compared to the control group ($100.00 \pm 2.25\%$, $p < 0.001$). The blank ES group also had slightly decreased biofilm growth ($83.15 \pm 4.12\%$, $p < 0.01$). Biofilm activity in the 0.5% HAL group was restored to the same level as that in the control group ($95.03 \pm 3.06\%$, $p > 0.05$). After 48 h, when compared to the control group ($100.00 \pm 4.74\%$), 0.5% HAL-ES-mediated aPDT still inhibited the growth of *C. albicans* biofilm ($74.29 \pm 1.61\%$, $p < 0.01$). The biofilm activity in the blank ES group was restored to control levels ($94.90 \pm 10.11\%$, $p > 0.05$). Moreover, the biofilm activity of the 0.5% HAL group was not statistically different from the control group ($102.58 \pm 4.97\%$, $p > 0.05$). Similarly, the biofilm activity of

the 5 and 0.5% ALA groups was not statistically different from the control group at 0 h ($98.65 \pm 0.09\%$ and $96.63 \pm 1.75\%$, respectively; $p > 0.05$), 24 h ($101.25 \pm 3.72\%$ and $101.74 \pm 3.23\%$, respectively; $p > 0.05$) and 48 h ($101.07 \pm 3.15\%$ and $100.38 \pm 1.41\%$, respectively; $p > 0.05$).

HAL-ES-Mediated aPDT Reduced *C. albicans* Biofilm Formation

At 24 h after aPDT, biofilm morphology was observed by an inverted microscope (Figure 2). The structure of biofilm formation was very different between the HAL-ES group and the other experimental groups. Biofilm formation in the HAL-ES group showed a few scattered larger microcolonies with rare hyphal connections (Figure 2A). The 5% ALA (Figure 2B), 0.5% ALA (Figure 2C), 0.5% HAL (Figure 2D), blank ES (Figure 2E), and control groups (Figure 2F) showed a large number of *C. albicans* microcolonies, and the hyphae between colonies were densely woven into an extensive network.

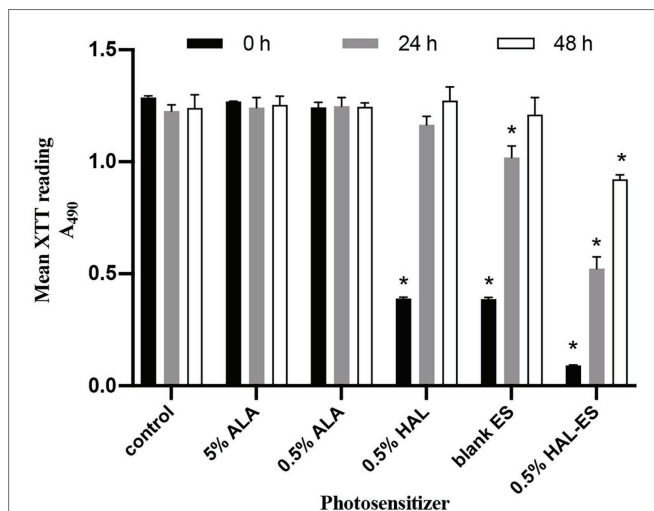


FIGURE 1 | *C. albicans* biofilm activity after aPDT with different photosensitizers (PS). Data are presented as means \pm SD ($n = 3$). * $p < 0.05$ when compared to control.

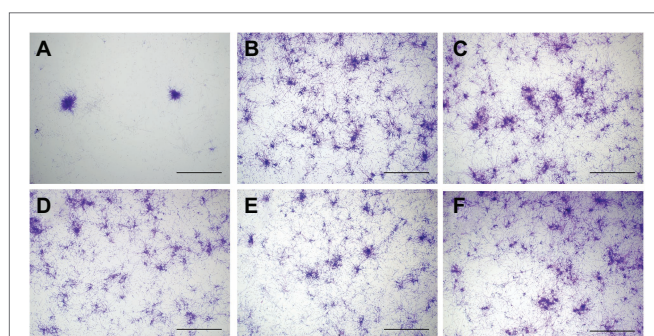


FIGURE 2 | *C. albicans* biofilm morphology at 24 h after aPDT ($\times 40$). (A) 0.5% HAL ES, (B) 5% ALA, (C) 0.5% ALA, (D) 0.5% HAL, (E) blank ES, and (F) control. Bars: 100 μ m.

HAL-ES-Mediated aPDT Increased Plasma Membrane Permeabilization in *C. albicans* Biofilms

To further investigate the mechanism of HAL-ES-mediated aPDT on *C. albicans* biofilms, we used SYTOX Green to study plasma membrane permeability (Figure 3). SYTOX Green is a high-affinity fluorescent nucleic acid stain that penetrates cells with compromised plasma membranes, but not those with intact membranes (Giroldo et al., 2009).

Immediately after aPDT, the 0.5% HAL-ES, 0.5% HAL, and blank ES groups showed increased fluorescence intensity (138.33 ± 3.055 , 130.67 ± 8.505 , and 155.67 ± 6.506 , respectively) compared to the control group (80.67 ± 5.508 , all $p < 0.001$). At 24 h after aPDT, the fluorescence intensity in the 0.5% HAL-ES and blank ES groups increased (209.00 ± 10.583 and 182.67 ± 10.263 , respectively) when compared to the control group (90.67 ± 7.234 , $p < 0.001$), but the fluorescence intensity of the 0.5% HAL group was restored to that of the control group (91.33 ± 2.517 , $p > 0.05$). After 48 h, the 0.5% HAL-ES group had the highest fluorescence intensity (408.67 ± 18.556 , $p < 0.001$) compared to the control group (131.67 ± 11.372), and the blank ES group presented a slightly increased fluorescence intensity (209.67 ± 6.429 , $p < 0.001$). At different incubation periods, the fluorescence intensities of the 5 and 0.5% ALA groups were almost the same as that of the control.

HAL-ES-Mediated aPDT Increased the Susceptibility of *C. albicans* Biofilms to Fluconazole

As shown in Table 1, in the 0.5% HAL-ES group, the SMIC50 values were less than 2.0 μ g/ml at 0, 24, and 48 h after aPDT, whereas the SMIC80 values were 4.0, 8.0, and $>1,024$ μ g/ml, respectively. The SMIC50 and SMIC80 values of the 0.5% HAL and blank ES groups were equal to those of the 0.5% HAL-ES group at 0 h after aPDT, but with evident biofilm formation,

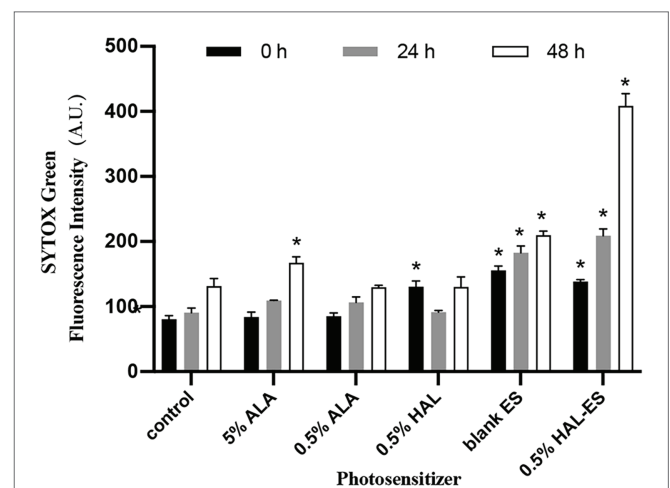
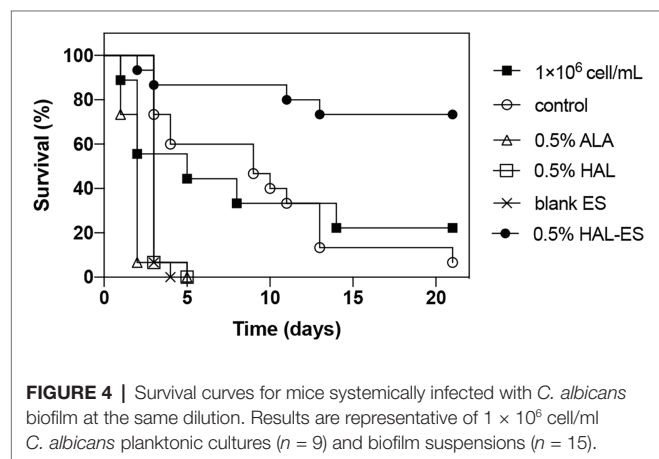


FIGURE 3 | Plasma membrane permeability in biofilms after aPDT. Data were presented as means \pm SD ($n = 3$). * $p < 0.05$ as compared to control.

TABLE 1 | Fluconazole antifungal susceptibility of *Candida albicans* biofilm after aPDT.

Time after aPDT	SMIC ($\mu\text{g}\cdot\text{ml}^{-1}$)	Control	0.5%ALA	0.5%HAL	Blank ES	0.5% HAL-ES
0 h	SMIC 50	>1,024	>1,024	<2	<2	<2
	SMIC 80	>1,024	>1,024	4	4	4
24 h	SMIC 50	>1,024	>1,024	32	16	<2
	SMIC 80	>1,024	>1,024	128	128	8
48 h	SMIC 50	>1,024	>1,024	>1,024	>1,024	<2
	SMIC 80	>1,024	>1,024	>1,024	>1,024	>1,024

SMIC50 and SMIC80 were read as the lowest concentrations that produced a 50 or 80% reduction in growth compared with that of the drug-free control. aPDT, antimicrobial photodynamic therapy; ALA, aminolevulinic acid; HAL, hexyl-aminolevulinic; ES, ethosomes.



the SMIC50 values were both greater than 1,024 $\mu\text{g}/\text{ml}$ at 48 h after aPDT. In the 0.5% ALA group, the SMIC50 values were >1,024 $\mu\text{g}/\text{ml}$ at 0, 24, and 48 h after aPDT.

HAL-ES-Mediated aPDT Weakened the *in vivo* Pathogenicity of *C. albicans* Biofilm

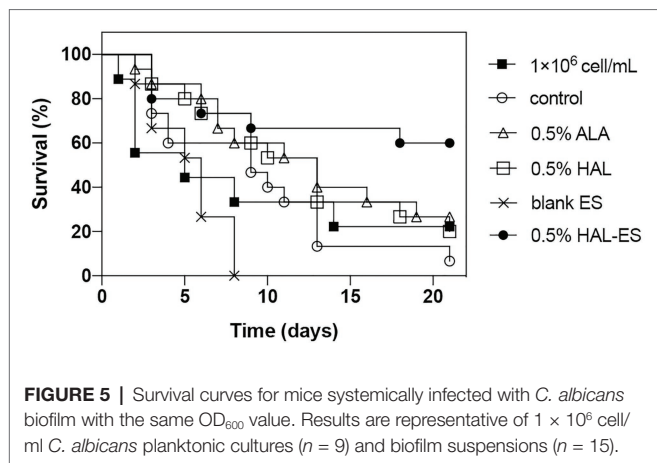
Compared with the control, the survival rate (Figures 4, 5) of the 0.5% HAL-ES group was significantly improved (21-day survival rate at the same biofilm dilution factor and the same biofilm OD_{600} value is 73.3 and 60%, respectively; $p = 0.0004$ and $p = 0.0055$). The survival rate of the control group when using *C. albicans* biofilm suspension was not significantly different from when using 1×10^6 cells/ml planktonic cultures (21-day survival of 6.7 and 22.2%, respectively; $p > 0.05$). Furthermore, when the biofilm was at the same dilution factor, all mice in the 0.5% ALA, 0.5% HAL, and blank ES groups died within 5 days. Meanwhile, when the biofilm was at the same OD_{600} value, the survival rates of the 0.5% ALA and 0.5% HAL groups were not significantly different from the control group (21-day survival of 26.7 and 20%, respectively; $p > 0.05$), and all mice in the blank ES groups died within 8 days.

DISCUSSION

aPDT has been proven to inactivate biofilm effectively and is considered a promising alternative to antifungal drugs. This treatment first employs a PS topically to a confined area and

then irradiates it with a specific light wavelength capable of exciting the PS to induce production of cytotoxic ROS in the presence of ambient molecular oxygen, which subsequently causes cell death by disruption of macromolecules (e.g., DNA, RNA, and proteins), and membranes. However, aPDT requires more effective PS and carriers to improve biofilm eradication efficiency (Hu et al., 2018). This study has shown that, compared to 5 and 0.5% ALA-mediated aPDT, 0.5% HAL-mediated aPDT inhibited *C. albicans* biofilm activity due to the higher bioavailability of HAL (Togsverd-Bo et al., 2012). Moreover, 0.5% HAL-ES-mediated aPDT further significantly inhibited the activity and growth of *C. albicans* biofilm within 48 h, mainly due to the effective reduction of biofilm hyphae. This can be because ES, as a nanocarrier, contains a high concentration of ethanol and is of reduced size, allowing the drug to effectively penetrate the structure of biofilm and cell membranes (Zhang et al., 2014; Niu et al., 2019). Hyphae play a pivotal role in the spatial structure and compressive strength of biofilms (Paramonova et al., 2009). Targeting hyphae formation can thus significantly weaken *C. albicans* biofilm drug resistance. Furthermore, aPDT can directly damage the biofilm through ROS, thereby physically disrupting the colony aggregation process (Fila et al., 2016). Finally, aPDT can trigger changes in genes related to the morphological transformation of the *C. albicans* yeast phase to its hyphal form (Paramonova et al., 2009), which are essential for biofilm formation (Mayer et al., 2013). In contrast, 5 and 0.5% ALA-mediated aPDT had no significant effects on *C. albicans* biofilm under our experimental conditions, which was consistent with previous studies (Monfrecola et al., 2004; Shi et al., 2016).

The mechanism underlying HAL-ES-mediated aPDT antimicrobial effect might be mediated by the physical destruction of microbial structures, such as plasma membranes (Hamblin, 2016). Our results showed that damage to the plasma membrane in viable *C. albicans* treated with HAL-ES-mediated aPDT was more significant than that observed in the 0.5% HAL and blank ES groups. With the growth of *C. albicans* biofilm, the SYTOX Green fluorescence intensity in the 0.5% HAL-ES group tripled at 48 h after aPDT, suggesting that plasma membrane damage gradually accumulated and eventually led to inhibition of *C. albicans* growth and biofilm formation (Girollo et al., 2009). On the other hand, 5 and 0.5% ALA had almost no effects on the plasma membrane, which could be that HAL is lipophilic, while ALA is hydrophilic, allowing easier penetration of HAL through the lipid bilayer, which ensures more prominent photodynamic effects that destabilize the plasma membrane.



Meanwhile, membrane permeability also increased in the blank ES group, which could be due to the ethanol and small particle sizes of ES. It shall be highlighted that the damage caused by HAL-ES-mediated aPDT to the plasma membrane exceeded the additive effects of HAL and ES treatments, which could be because, under the same conditions, ES permits the deeper penetration of HAL into the biofilm.

Increased plasma membrane permeability facilitates entry and accumulation of drugs into the cell and ultimately plays an antifungal role, which in this study was reflected by a reduction in *C. albicans* biofilm drug resistance (Holmes et al., 2012). Our results showed that aPDT mediated by 0.5% HAL-ES, 0.5% HAL, and blank ES enhanced fluconazole susceptibility in *C. albicans* biofilm, which is related to the reduced biofilm activity after aPDT, illustrating the effectiveness of combining aPDT and fluconazole, after all, the highest dose of fluconazole elicited negligible effects against the activity of the *C. albicans* biofilm. Moreover, 0.5% HAL-ES-mediated aPDT more effectively sensitizes biofilms to fluconazole than 0.5% HAL or blank ES even if the fluconazole susceptibility gradually weakened as the biofilm grew, suggesting that in clinical treatment, earlier administration of aPDT combined with fluconazole, will require lower doses of fluconazole to achieve satisfactory antifungal effects. The reduced fluconazole susceptibility may also be explained by other mechanisms, such as the promotion of phenotypic changes involving the drug resistance-related genes *MDR1*, *QDR1*, and *ERG* (Wall et al., 2019).

The *in vivo* pathogenicity of biofilms in the HAL-ES group was the lowest of all groups. This is due to the inhibition of biofilm growth and the increased permeability of the plasma membrane. Interestingly, the *in vivo* pathogenicity of biofilms in the 0.5% ALA, 0.5% HAL, and blank ES groups was increased when compared to that in the control group. This result could be due to increased biofilm formation and mutagenesis caused by the stress response (Jolivet-Gougeon and Bonnaure-Mallet, 2014). Previous studies have shown that sub-lethal photodynamic therapy and a low ethanol concentration can increase the biofilm formation ability (Kashef et al., 2013; Pourhajibagher et al., 2016; Tango et al., 2018), and an antimicrobial treatment can induce 105 times more biofilm variability than that observed in free-living cultures (Driffield et al., 2008). Notably, while the fluconazole susceptibility of *C. albicans* biofilm decreased

and pathogenicity increased in the 0.5% HAL and ES groups, biofilm pathogenicity was significantly weakened in the 0.5% HAL-ES group, suggesting that aPDT requires an efficient PS to reduce *C. albicans* biofilm pathogenicity.

In conclusion, this study proved that HAL-ES-mediated aPDT had more potent antifungal photodynamic activity than did HAL-mediated, and ALA-mediated aPDT. Its mechanism of action could be related to the inhibition of *C. albicans* growth and biofilm formation, as well as the reduction of drug resistance and *in vivo* pathogenicity. HAL-ES-mediated aPDT is, therefore, a promising novel treatment against *C. albicans* biofilms. Moreover, ES is a nanoparticle with excellent percutaneous penetration efficiency. In our previous studies, it was confirmed that its percutaneous flux is much higher than that of liposomes and hydroethanolic solution (Zhu et al., 2013; Yang et al., 2017). Therefore, HAL-ES-mediated aPDT can offer an alternative treatment for patients with cutaneous or mucosal *C. albicans* biofilm infections. It is particularly suitable for patients for whom topical antifungal agents have been proven ineffective, or who have contraindications to oral antifungal drugs. Lastly, HAL-ES-mediated aPDT can also function synergistically with fluconazole treatment to prevent local candidiasis from developing into a systemic infection.

DATA AVAILABILITY STATEMENT

All datasets presented in this study are included in the article/supplementary material.

ETHICS STATEMENT

The animal study was reviewed and approved by The Institutional Animal Care and Use Committee of Nanfang Hospital, Southern Medical University (NFYY-2019-71).

AUTHOR CONTRIBUTIONS

XZ and YW designed the experiments. YW performed most of the experiments. JS participated in the animal experiments. FZ participated in data analysis. XZ, KZ, and YW wrote the manuscript. All authors contributed to the article and approved the submitted version.

FUNDING

This work was supported by a grant from Natural Science Foundation of Guangdong Province, China (grant number 2018A030313216).

ACKNOWLEDGMENTS

We would like to acknowledge Dr. Xiaowen Huang for providing us SC5314.

REFERENCES

- Al-Mutairi, R., Tovmasyan, A., Batinic-Haberle, I., and Benov, L. (2018). Sublethal photodynamic treatment does not lead to development of resistance. *Front. Microbiol.* 9:1699. doi: 10.3389/fmicb.2018.01699
- Baltazar, L. M., Ray, A., Santos, D. A., Cisalpino, P. S., Friedman, A. J., and Nosanchuk, J. D. (2015). Antimicrobial photodynamic therapy: an effective alternative approach to control fungal infections. *Front. Microbiol.* 6:202. doi: 10.3389/fmicb.2015.00202
- Ceri, H., Olson, M. E., Stremick, C., Read, R. R., Morck, D., and Buret, A. (1999). The Calgary biofilm device: new technology for rapid determination of antibiotic susceptibilities of bacterial biofilms. *J. Clin. Microbiol.* 37, 1771–1776. doi: 10.1128/JCM.37.6.1771-1776.1999
- Driffield, K., Miller, K., Bostock, J. M., O'Neill, A. J., and Chopra, I. (2008). Increased mutability of *Pseudomonas aeruginosa* in biofilms. *J. Antimicrob. Chemother.* 61, 1053–1056. doi: 10.1093/jac/dkn044
- Fila, G., Kasimova, K., Arenas, Y., Nakonieczna, J., Grinholc, M., Bielawski, K. P., et al. (2016). Murine model imitating chronic wound infections for evaluation of antimicrobial photodynamic therapy efficacy. *Front. Microbiol.* 7:1258. doi: 10.3389/fmicb.2016.01258
- Giroldo, L. M., Felipe, M. P., de Oliveira, M. A., Munin, E., Alves, L. P., and Costa, M. S. (2009). Photodynamic antimicrobial chemotherapy (PACT) with methylene blue increases membrane permeability in *Candida albicans*. *Lasers Med. Sci.* 24, 109–112. doi: 10.1007/s10103-007-0530-2
- Hamblin, M. R. (2016). Antimicrobial photodynamic inactivation: a bright new technique to kill resistant microbes. *Curr. Opin. Microbiol.* 33, 67–73. doi: 10.1016/j.mib.2016.06.008
- Helander, L., Sharma, A., Krokan, H. E., Plaetzer, K., Krammer, B., Tortik, N., et al. (2016). Photodynamic treatment with hexyl-aminolevulinate mediates reversible thiol oxidation in core oxidative stress signaling proteins. *Mol. Biosyst.* 12, 796–805. doi: 10.1039/C5MB00744E
- Holmes, A. R., Keniya, M. V., Ivnitiski-Steele, I., Monk, B. C., Lamping, E., Sklar, L. A., et al. (2012). The monoamine oxidase A inhibitor clorgyline is a broad-spectrum inhibitor of fungal ABC and MFS transporter efflux pump activities which reverses the azole resistance of *Candida albicans* and *Candida glabrata* clinical isolates. *Antimicrob. Agents Chemother.* 56, 1508–1515. doi: 10.1128/AAC.05706-11
- Hu, X., Huang, Y. -Y., Wang, Y., Wang, X., and Hamblin, M. R. (2018). Antimicrobial photodynamic therapy to control clinically relevant biofilm infections. *Front. Microbiol.* 9:1299. doi: 10.3389/fmicb.2018.01299
- Jolivet-Gougeon, A., and Bonnaure-Mallet, M. (2014). Biofilms as a mechanism of bacterial resistance. *Drug Discov. Today Technol.* 11, 49–56. doi: 10.1016/j.ddtec.2014.02.003
- Kashef, N., Akbarizare, M., and Kamrava, S. K. (2013). Effect of sub-lethal photodynamic inactivation on the antibiotic susceptibility and biofilm formation of clinical *Staphylococcus aureus* isolates. *Photodiagn. Photodyn. Ther.* 10, 368–373. doi: 10.1016/j.pdpdt.2013.02.005
- Mayer, F. L., Wilson, D., and Hube, B. (2013). *Candida albicans* pathogenicity mechanisms. *Virulence* 4, 119–128. doi: 10.4161/viru.22913
- Monfrecola, G., Procaccini, E. M., Bevilacqua, M., Manco, A., Calabrò, G., and Santoianni, P. (2004). In vitro effect of 5-aminolevulinic acid plus visible light on *Candida albicans*. *Photochem. Photobiol. Sci.* 3, 419–422. doi: 10.1039/B315629J
- Neittaanmäki-Perttu, N., Karppinen, T., Tani, T., Snellman, E., and Grönroos, M. (2017). Long-term outcome of low-concentration hexyl-5-aminolevulinate daylight photodynamic therapy for treatment of actinic keratoses. *Acta Derm. Venereol.* 97, 120–121. doi: 10.2340/00015555-2484
- Neittaanmäki-Perttu, N., Neittaanmäki, E., Pölönen, I., Snellman, E., and Grönroos, M. (2016). Safety of novel amino-5-laevulinate photosensitizer precursors in photodynamic therapy for healthy human skin. *Acta Derm. Venereol.* 96, 108–110. doi: 10.2340/00015555-2131
- Niu, X. -Q., Zhang, D. -P., Bian, Q., Feng, X. -F., Li, H., Rao, Y. -F., et al. (2019). Mechanism investigation of ethosomes transdermal permeation. *Int. J. Pharm.* X 1:100027. doi: 10.1016/j.ijpx.2019.100027
- Paramonova, E., Krom, B. P., van der Mei, H. C., Busscher, H. J., and Sharma, P. K. (2009). Hyphal content determines the compression strength of *Candida albicans* biofilms. *Microbiology* 155, 1997–2003. doi: 10.1099/mic.0.021568-0
- Penate, Y., Guillermo, N., Melwani, P., Martel, R., and Borrego, L. (2009). Dermatologists in hospital wards: an 8-year study of dermatology consultations. *Dermatology* 219, 225–231. doi: 10.1159/000232390
- Pierce, C. G., Uppuluri, P., Tummala, S., and Lopez-Ribot, J. L. (2010). A 96 well microtiter plate-based method for monitoring formation and antifungal susceptibility testing of *Candida albicans* biofilms. *J. Vis. Exp.* 44:2287. doi: 10.3791/2287
- Pourhajibagher, M., Chiniforush, N., Shahabi, S., Ghorbanzadeh, R., and Bahador, A. (2016). Sub-lethal doses of photodynamic therapy affect biofilm formation ability and metabolic activity of *Enterococcus faecalis*. *Photodiagn. Photodyn. Ther.* 15, 159–166. doi: 10.1016/j.pdpdt.2016.06.003
- Römling, U., and Balsalobre, C. (2012). Biofilm infections, their resilience to therapy and innovative treatment strategies. *J. Intern. Med.* 272, 541–561. doi: 10.1111/joim.12004
- Shi, H., Li, J., Zhang, H., Zhang, J., and Sun, H. (2016). Effect of 5-aminolevulinic acid photodynamic therapy on *Candida albicans* biofilms: an in vitro study. *Photodiagn. Photodyn. Ther.* 15, 40–45. doi: 10.1016/j.pdpdt.2016.04.011
- Tango, C. N., Akkermans, S., Hussain, M. S., Khan, I., Van Impe, J., Jin, Y. -G., et al. (2018). Modeling the effect of pH, water activity, and ethanol concentration on biofilm formation of *Staphylococcus aureus*. *Food Microbiol.* 76, 287–295. doi: 10.1016/j.fm.2018.06.006
- Togsværd-Bo, K., Lerche, C. M., Philipsen, P. A., Poulsen, T., Wulf, H. C., and Haedersdal, M. (2012). Porphyrin biodistribution in UV-exposed murine skin after methyl- and hexyl-aminolevulinate incubation: PpIX distribution in UV-exposed skin: MAL & HAL. *Exp. Dermatol.* 21, 260–264. doi: 10.1111/j.1600-0625.2012.01442.x
- Wall, G., Montelongo-Jauregui, D., Vidal Bonifacio, B., Lopez-Ribot, J. L., and Uppuluri, P. (2019). *Candida albicans* biofilm growth and dispersal: contributions to pathogenesis. *Curr. Opin. Microbiol.* 52, 1–6. doi: 10.1016/j.mib.2019.04.001
- Yang, L., Wu, L., Wu, D., Shi, D., Wang, T., and Zhu, X. (2017). Mechanism of transdermal permeation promotion of lipophilic drugs by ethosomes. *Int. J. Nanomed.* 12, 3357–3364. doi: 10.2147/IJN.S134708
- Zhang, Y. -T., Shen, L. -N., Wu, Z. -H., Zhao, J. -H., and Feng, N. -P. (2014). Evaluation of skin viability effect on ethosome and liposome-mediated psoralen delivery via cell uptake. *J. Pharm. Sci.* 103, 3120–3126. doi: 10.1002/jps.24096
- Zhu, X., Li, F., Peng, X., and Zeng, K. (2013). Formulation and evaluation of lidocaine base ethosomes for transdermal delivery. *Anesth. Analg.* 117, 352–357. doi: 10.1213/ANE.0b013e3182937b74

Conflict of Interest: The authors declare that the research was conducted in the absence of any commercial or financial relationships that could be constructed as a potential conflict of interest.

Copyright © 2020 Wang, Song, Zhang, Zeng and Zhu. This is an open-access article distributed under the terms of the Creative Commons Attribution License (CC BY). The use, distribution or reproduction in other forums is permitted, provided the original author(s) and the copyright owner(s) are credited and that the original publication in this journal is cited, in accordance with accepted academic practice. No use, distribution or reproduction is permitted which does not comply with these terms.



Glabridin Averts Biofilms Formation in Methicillin-Resistant *Staphylococcus aureus* by Modulation of the Surfaceome

Bhavana Gangwar^{1†}, Santosh Kumar^{1,2†} and Mahendra P. Darokar^{1*}

¹ Molecular Bioprospection Department, CSIR-Central Institute of Medicinal and Aromatic Plants, Lucknow, India,

² Department of Biological Sciences, The University of Texas at Dallas, Richardson, TX, United States

OPEN ACCESS

Edited by:

Sujogya Kumar Panda,
KU Leuven, Belgium

Reviewed by:

Anabela Portela Borges,
University of Porto, Portugal
Jianfeng Wang,
Jilin University, China

*Correspondence:

Mahendra P. Darokar
mp.darokar@cimap.res.in;
mpdarokar@yahoo.com

[†] These authors have contributed
equally to this work

Specialty section:

This article was submitted to
Antimicrobials, Resistance
and Chemotherapy,
a section of the journal
Frontiers in Microbiology

Received: 27 April 2020

Accepted: 07 July 2020

Published: 17 September 2020

Citation:

Gangwar B, Kumar S and
Darokar MP (2020) Glabridin Averts
Biofilms Formation
in Methicillin-Resistant
Staphylococcus aureus by
Modulation of the Surfaceome.
Front. Microbiol. 11:1779.
doi: 10.3389/fmicb.2020.01779

Staphylococcus aureus is an opportunistic bacterium of the human body and a leading cause of nosocomial infections. Methicillin resistant *S. aureus* (MRSA) infections involving biofilm lead to higher mortality and morbidity in patients. Biofilm causes serious clinical issues, as it mitigates entry of antimicrobials to reach the etiological agents. It plays an important role in resilient chronic infections which place an unnecessary burden on antibiotics and the associated costs. To combat drug-resistant infection involving biofilm, there is a need to discover potential anti-biofilm agents. In this study, activity of polyphenolic flavonoid glabridin against biofilm formation of methicillin resistant clinical isolates of *S. aureus* is being reported for the first time. Crystal violet assay and scanning electron microscopy evidences shows that glabridin prevents formation of cells clusters and attachment of methicillin resistant clinical isolate (MRSA 4423) of *S. aureus* to the surface in a dose dependent manner. Gel free proteomic analysis of biofilm matrix by LC-ESI-QTOF confirmed the existence of several proteins known to be involved in cells adhesion. Furthermore, expression analysis of cell surface proteins revealed that glabridin significantly down regulates an abundance of several surface-associated adhesins including fibronectin binding proteins (FnbA, FnbB), serine-aspartate repeat-containing protein D (SdrD), immunoglobulin-binding protein G (Sbi), and other virulence factors which were induced by extracellular glucose in MRSA 4423. In addition, several moonlighting proteins (proteins with multiple functions) such as translation elongation factors (EF-Tu, EF-G), chaperone protein (DnaK), glyceraldehyde 3-phosphate dehydrogenase (GAPDH) and pyruvate kinase (PK) were detected on the cell surface wherein their abundance was inversely proportional to surface-associated adhesins. This study clearly suggests that glabridin prevents biofilm formation in *S. aureus* through modulation of the cell surface proteins.

Keywords: adhesins, biofilm, cell surface proteome, glabridin, moonlight proteins, MRSA

INTRODUCTION

Staphylococcus aureus is a common bacterium of the human body which can cause numerous diseases (Tong et al., 2015). *S. aureus* is considered one of the leading causes of nosocomial and community-acquired infections (Haque et al., 2018). Drug-resistance in *S. aureus* is achieved in several ways, including the acquisition of resistance genes, target alteration, efflux pumps and

biofilm (Appelbaum, 2006; Tiwari and Sen, 2006; Foster, 2017; Santajit and Indrawattana, 2016; Gebreyohannes et al., 2019). Like other bacteria, the formation of biofilms in *S. aureus* is an alternative type of microbial growth and a leading cause of resistance to antimicrobials (López et al., 2010; Mah, 2012). Around 80% of chronic and recurrent infections in the human body are associated with bacterial biofilm (Sharma et al., 2019). *S. aureus* cells within biofilms are more resistant to antibiotics than planktonic cells due to the altered environment, multilayered structure, and incomplete penetration of the antibiotics (Mah, 2012; Sharma et al., 2019). Reports suggest that bacteria in the biofilm can be 10–1,000 times more resistant to antimicrobials than their planktonic counterparts (Gebreyohannes et al., 2019). Biofilm growth can prevent entry of the antibiotics during treatment as well as protecting pathogens against host immune defenses. Biofilm formation by MRSA in medical devices, implants, chronic wounds, and host tissue reduces susceptibility to antimicrobial agents (Sharma et al., 2019; Neopane et al., 2018).

The biofilm life cycle of microbes contains four stages, the initial attachment of bacteria, microbial colonies formation, bacterial growth leading to extracellular matrix (ECM) generation and maturation, followed by the dispersal of the bacteria to find new niches (Kostakioti et al., 2013). The ECM components contain extracellular polymeric substances (EPS) including proteins that helps cell to adhere on biotic and abiotic surfaces (Donlan and Costerton, 2002; López et al., 2010; Karygianni et al., 2020). To date, many adhesive proteins have been identified as important components of the attachment process and biofilm matrix development in *S. aureus* (Foster et al., 2014; Jan-Roblero et al., 2016). *S. aureus* cell surface-associated proteins in biofilm are well characterized such as SdrC (BapA homologs), intercellular adhesions (IcaA,D,B,C), fibronectin-binding protein A (FnBA), fibronectin-binding protein B (FnBB), clumping factor B (ClfB), and *S. aureus* surface protein (SasG) (Donlan and Costerton, 2002; Speziale et al., 2014). These surface adhesins are regulated by complex network of transcriptional regulators AlrRS, SarA, Agr, SaeRS and AcrR under various environmental conditions (Paharik and Horswill, 2016). Therefore, study of biofilm formation and finding anti-biofilm agents against pathogens such as *S. aureus* is highly important as it can help choose the right treatment.

Plant derived medicines are gaining interest with regards to controlling antibiotic-resistant bacterial infections and biofilm. Plants are rich in a variety of secondary metabolites such as flavonoids, polyphenol, terpenoids, alkaloids etc. Many plants such as Licorice have been used to cure various bacterial infections in traditional practices by humans since ancient times all over the world (Cowan, 1999; Rohinishree and Negi, 2016; Mamedov and Egamberdieva, 2019). Plant derived phytomolecules have shown antimicrobial and antibiofilm activity against Gram-negative and Gram-positive pathogenic bacteria including *S. aureus* (Sánchez et al., 2016; Rubini et al., 2018). The ethanolic extract of licorice was shown to have antimicrobial and antibiofilm activity against *Porphyromonas gingivalis* (Suwannakul and Chaibenjawong, 2017). *Glycyrrhiza glabra* (Licorice) contains over 20 triterpenoids and nearly

300 flavonoids (Wang et al., 2015). Glabridin (Glb), is a polyphenolic flavonoid compound and one of the most active ingredients present in licorice roots. Glabridin is reported to have antioxidant, anti-inflammatory, anticancer, antiviral, antimicrobial and drug-resistance modifying activity in addition to immunomodulatory, hepatoprotective, and cardioprotective effects (Simmler et al., 2013; Singh et al., 2015). Glabridin has been shown to inhibit Gram-positive and Gram-negative bacteria including biofilm forming pathogens such as *Staphylococcus* sp., *Pseudomonas aeruginosa*, *Bacillus* sp., *Streptococcus* sp., *Escherichia coli*, *Mycobacterium tuberculosis*, and fungi (Gupta et al., 2013; Gupta et al., 2008; Singh et al., 2015; Irani et al., 2010; Fatima et al., 2009; Wang et al., 2015). Although, glabridin has been reported to possess antimicrobial activity against several pathogens, its detailed mechanism of action is not yet known. In an earlier report, it was found that glabridin in a dose-dependent manner produced reactive oxygen species (ROS) that damages cellular proteins ultimately leading to growth inhibition of *S. aureus* (Singh et al., 2015). This study reports for the first time an antibiofilm activity of glabridin against a glucose-induced biofilm of *S. aureus*. The mechanism of glabridin action has also been determined through the expression of genes/proteins that are involved in biofilm formation in the methicillin resistant clinical isolate MRSA 4423 of *S. aureus*.

MATERIALS AND METHODS

Bacterial Strains, Culture Conditions, Chemicals and Enzymes

The drug-sensitive strain MTCC 96 (ATCC9144) of *S. aureus* was procured from the Microbial Type Culture Collection, CSIR-Institute of Microbial Technology Chandigarh, India. Clinical isolates of *S. aureus* were obtained from Dr. K. N. Prasad (Laboratory of Clinical Microbiology, SGPGIMS, Lucknow, India) (Gupta et al., 2012). Standard Mueller-Hinton agar and cation-adjusted Mueller-Hinton broth media (MHA and MHB, Hi-Media, Mumbai, India) were used to culture bacteria. Tryptic soy broth (TSB, Hi-Media, Mumbai, India) medium was used for Biofilm assays. Glabridin, antibiotics, phosphate-buffered saline, DMSO, glucose and lysostaphin was procured from Sigma-Aldrich (St. Louis, MO, United States). Crystal Violet used in this study was used from Hi-Media (Mumbai, India). Trypsin Gold, Mass Spectrometry Grade was obtained from Promega (Madison, WI, United States). Taq DNA polymerase master mix, c-DNA synthesis kit and SYBR Green qPCR super mix was purchased from Genetix (Thermo, United States).

Detection of *mecA* Gene and Antimicrobial Susceptibility Testing of *S. aureus* Clinical Isolates

To identify MRSA strains, PCR amplification of the *mecA* gene was performed using the genomic DNA of clinical isolates as template, *mecA* specific primers (Supplementary Table S1) and Taq DNA polymerase master mix as per recommended method in a Mastercycler EP Gradient (Eppendorf, Germany)

(Pournajaf et al., 2014). The antibacterial activity of glabridin and antibiotics (belonging to different classes) against *S. aureus* clinical isolates was determined by the broth microdilution assay using 96 'U'-bottom micro-titer plates as per CLSI guidelines (CLSI, 2018). *S. aureus* was cultured in 5 mL broth in tubes and incubated overnight at 37 °C in a shaking incubator (Eppendorf, Germany). The initial bacterial inoculum size was standardized to obtain 10⁶ cfu/mL. A series of different concentrations of antibiotics (listed in **Supplementary Table S2**) was prepared by twofold serial dilution in a 96-well plate, except for the negative control, followed by inoculation with 10⁶ cfu/mL *S. aureus* and 24 h incubation at 37 °C. MIC was determined by finding the lowest concentration which inhibited the growth as per CLSI guidelines (CLSI, 2018).

Growth Curve Study

To measure the effect of glabridin on the survival of MRSA, three clinical isolates were selected that made strong (MRSA 4423), moderate (MRSA 4627), and weak (MRSA 2071) biofilm along with the sensitive strain MTCC 96. Overnight pre-grown cells were inoculated (10⁶ cfu/ml) in fresh MHB and TSB media and challenged with a range of glabridin (2 MIC to 1/16 MIC). The cultures were grown during shaking (180 rpm) at 37°C for 12 h and optical density was monitored every 1 h time intervals (OD_{600nm}) with Multiskan GO Microplate Spectrophotometer (Thermo Scientific, United States). Each test was performed in three culture replicates, averaged and graph were plotted with OD_{600nm} in Y-axis and time in X-axis.

Biofilm Formation Assay

The biofilm formation assay was conducted in TSB medium with 1% glucose in three replicates using a 96-well plate (Lade et al., 2019). Suspension of all clinical isolates of MRSA were precultured overnight and ~10⁶ cfu/mL cell suspension was used to inoculate into each well. For the dose-dependent anti-biofilm assay, glabridin was tested in sub-inhibitory concentrations ranging from 7.8 to 0.78 µg/ml. Control experiments were set with DMSO and without glucose wherever required, TSB medium without cultures was used as a negative control. The plates were incubated at 37 °C for 48 h under static conditions (without shaking). After incubation, the OD was measured at 600 nm then the media was decanted in biohazard collection and wells were carefully rinsed three times with 1X phosphate buffered saline (PBS) to remove non-adherent cells and wash off the media components. The attached biofilm cells in wells were stained with 0.1% crystal violet for 15 min at room temperature (Lade et al., 2019). The excess stain was removed by rinsing with water. The crystal violet bound to attached cells was solubilized with 95% ethanol and quantified by measuring absorbance at OD_{595nm} (Kumar and Spiro, 2017). Absorbance was recorded, and graphs were plotted with values averaged from three biological and three technical replicates in each condition. Effect of glabridin on biofilm formation was calculated by normalizing the absorbance of crystal violet with culture OD (OD_{595nm}/OD_{600nm}) of MRSA 4423. The following method

described by Stepanović et al. (2000) was used to calculate cut-off OD (OD_{cut}) value to classify MRSA isolates biofilm formation as weak (+), moderate (++) and strong (+++) based upon the OD_{595nm}.

Formula used for biofilm gradation:

$OD_{cut} = 3 \times \text{standard deviation (SD) of ODs above the } OD_{avg} \text{ of negative control.}$

$OD \leq OD_{cut} = \text{Non-biofilm former, } OD_{cut} < OD \leq 2 \times OD_{cut} = \text{Weak biofilm former, } 2 \times OD_{cut} < OD \leq 4 \times OD_{cut} = \text{Moderate biofilm former, } OD > 4 \times OD_{cut} = \text{Strong biofilm former.}$

Biofilm Dispersal Assay

The biofilm detachment assay was performed as described by Kaplan et al. (2004), Boles and Horswill (2008), and Shukla and Rao (2017). Briefly, after the establishment of MRSA 4423 biofilms in the polystyrene, 96-well microtiter plate, wells were rinsed with 1X PBS. Prior to staining, biofilms were incubated separately with trypsin and proteinase K (1.0 µg/ml each), DNase I and RNase E (10 µg/ml each) for 1 h at 37°C. Microtiter plate wells were washed thrice with deionized water to remove dispersed cells and stained using the 0.1% crystal violet as mentioned above in biofilm assay. The crystal violet dissolved in 95% ethanol was quantified by measuring absorbance at OD_{595nm} using a Multiskan GO Microplate Spectrophotometer (Thermo Scientific, United States). Biofilms with no enzyme treatment were used as a control and medium without bacteria and enzymes was used as a blank. The experiment was set in triplicates and a graph was plotted against averaged values (OD_{595nm}) from all sets.

Scanning Electron Microscopy (SEM) Analysis of MRSA Biofilm

An overnight culture of MRSA 4423 was diluted in TS broth to obtain 10⁶ cfu/ml. Glabridin was tested at 6.25 µg/ml (1/2 MIC), 3.125 µg/ml (1/4 MIC) and 1.56 µg/ml (1/8 MIC). For each concentration, 3 mL of bacterial suspension was supplemented with the desired amount of compound and added into individual wells in a 6-well plate. The plate was incubated at 37 °C for 48 h to allow the formation of biofilm. The bacterial cells were processed for SEM as described elsewhere (Kong et al., 2018). Briefly, the samples were fixed overnight at 4°C in 4% (v/v) glutaraldehyde, rinsed three times with 1X PBS and dehydrated through a graded ethanol series (35, 50, and 70%), followed by 100% propanol. The samples were platinum-coated using a platinum sputtering unit and observed using a scanning electron microscope (JSM-6490, JEOL, Japan).

ECM-Associated Protein Analysis

The biofilm ECM proteins were extracted using a method as described by Ythier et al. (2012). Briefly, the culture of MRSA 4423 was grown in the presence of glucose for 48 h in static conditions, and non-adherent cells were removed by decanting and rinsing with 1X PBS. To shave off proteins from biofilm ECM, 1 µg/ml trypsin enzyme was used. After 1 h of enzymatic treatment at 37°C, cells were separated by

centrifugation at 16,000g, 4°C for 15 min, and partially digested proteins in supernatant were transferred into a new tube and the peptide mix was processed for identification by Liquid Chromatography/High Resolution Mass Spectrometry (LC-ESI-QTOF) (Agilent, United States).

Collection of Differentially Expressed Proteins From the Cell-Surface of *S. aureus*

To identify changes in proteins present on the cell surface of MRSA 4423 due to glucose and glabridin, cultures were grown in presence of 1% glucose and supplemented with glabridin (1/4 MIC). Cells grown only with glucose were used as a biofilm positive control and cells grown without both glucose and glabridin were used as a biofilm negative control. After 48 h of growth under static conditions, 5 ml cells of equal OD were collected from each set grown in triplicates, centrifuged at 4,000g for 10 min and supernatant was discarded. Pellets were washed twice with 1X PBS and cells were resuspended in 1 ml of 1X PBS. To collect surface proteins, all cell suspensions were treated with 1 µg/ml trypsin enzyme for 1 h at 37°C (Ythier et al., 2012). Trypsin shaved proteins in supernatants fraction were collected by centrifugation at 16,000g for 10 min in 4°C and processed as above for identification by LC-ESI-QTOF (Agilent, United States).

Identification of Proteins by LC-ESI-QTOF

Trypsin digested proteins were identified by LC-ESI-QTOF as per the standard process described elsewhere (Kaplan et al., 2004; Brun et al., 2020). Briefly, trypsin shaved proteins obtained from cell surface or ECM were treated with DTT and iodoacetamide for 1 h and the samples were digested with trypsin (1 µg/ml) for another 12–16 h at 37°C. The trypsin enzyme was inactivated by adding 5% Tri-Fluoro acetic acid (TFA) to the peptide mixtures in tube. Peptide mixtures were pooled from three independent replicates, quantified and purified with C18 matrix column as per recommended protocol (Agilent, United States). Purified peptide mixtures were concentrated using a speed vacuum centrifugation unit at 4°C. Concentrated peptides were resuspended in 1% TFA and 5% acetonitrile (ACN) solution and submitted for identification by LC-ESI-QTOF. The MS/MS data was identified against *S. aureus* protein database (NCBI) using Spectrum Mill software (Agilent, United States) and spectral counts were used to calculate the fold change as described elsewhere (Liu et al., 2004).

Quantitative Real-Time PCR (qRT-PCR) Analysis

Quantitative real time PCR was performed to check gene expression levels of the differentially expressed proteins found on MRSA 4423 cell-surface under the biofilm condition and in presence of glabridin. Briefly, *S. aureus* cells grown for 48 h were collected by centrifugation at 4°C, 4,000g and supernatants were discarded. The cell pellets were washed with 1X PBS twice and stored overnight at –80°C. To extract RNA, pellets

were resuspended in a 150 µl lysis buffer containing 50 µg/ml lysostaphin, 10 mM Tris, and 1 mM EDTA in DEPC treated water and incubated for 15 min at 37°C. Total RNA was isolated through the Trizol method and quality was assessed as described previously (Kumar et al., 2012). The DNA free RNA (0.5 µg) was used in reverse transcription and the cDNA was synthesized in a final volume of 20 µl using random hexamer primers as per the manufacturer's instructions of GeneSure First-Strand cDNA Synthesis Kit for RT-PCR (Thermo, United States). Quantitative RT-PCR (qPCR) was carried out using gene specific primers (**Supplementary Table S1**) and SYBR Green in a Quantstudio5 real time PCR system (Applied Biosystems, Thermo, United States). The PCR cycling conditions were set according to manufacturer recommendations of the GeneSure™ SYBR Green/ROX Kit (Thermo, United States). Negative controls and genomic DNA contamination controls were included in the experiment. The *S. aureus* 16S rRNA was used as an endogenous control to normalize the expression of each gene. The relative expression (RQ) of target genes of interest were analyzed using $\Delta\Delta C_t$ values compared to the untreated control (Atshan et al., 2013; Kong et al., 2018).

Statistical Analysis

All experiments were performed in three replicates. Data are presented as means \pm standard deviation. Statistical analysis was performed using one-way Analysis of Variance (ANOVA) followed by Tukey tests and the difference $p \leq 0.05$ were considered significant.

RESULTS

Assessing Presence of *mecA* Gene and Antimicrobial Susceptibility Profiling of *S. aureus* Clinical Isolates

Clinical isolates of *S. aureus* were tested for the presence of the *mecA* gene known to be a marker for methicillin resistance. All *S. aureus* clinical isolates were verified for the existence of the *mecA* gene in PCR amplification (**Supplementary Figure S1**). As expected, no amplification of the *mecA* gene was observed in drug sensitive strain MTCC 96 of *S. aureus* (**Supplementary Figure S1**). All clinical isolates that harbored the *mecA* gene also showed a high level of resistance toward oxacillin and other antibiotics of beta lactam class (**Supplementary Table S2**). Compared to the sensitive strain MTCC 96, MRSA isolates showed a high level of resistance toward different antibiotics except for daptomycin, bacitracin, tetracycline, linezolid, and teicoplanin to which most of these isolates were found susceptible. In case of glycopeptides, only two clinical isolates (MRSA 2071 and MRSA 1745) showed vancomycin intermediate resistant *S. aureus* (VISA) (**Supplementary Table S2**).

Biofilm Formation Ability of MRSA Isolates

The biofilm formation ability of five MRSA clinical isolates was studied under static conditions. It was observed that MRSA

isolates, grown in TSB medium, could not adhere to polystyrene surface. However, the addition of 1% glucose into TSB medium significantly induced the formation of biofilm and cells were found to be adhered on the polystyrene surface as demonstrated by crystal violet staining (**Figure 1A**). Reference strain MTCC 96 did not form biofilm under either condition. Among all clinical isolates, MRSA 4423 was found to develop a strong biofilm followed by moderate levels of biofilm by MRSA 4627 and MRSA 10760. While the other remaining two MRSA clinical isolates MRSA 2071 and MRSA 1745 were found to form weak biofilm in the presence of 1% glucose (**Figure 1A**). Therefore, the strong biofilm forming isolate MRSA 4423 was considered for further study.

Enzymatic Detachment of MRSA Biofilm

The components of the biofilm matrix are usually nucleic acids (eDNA), exopolysaccharide and proteins. It was observed that trypsin and proteinase K treatments were able to remove the attached cells of MRSA 4423 completely from the polystyrene plate (**Figure 1B**). The selective detachment of biofilm within an hour by low concentration of proteases (trypsin and proteinase K), indicates the involvement of proteins in biofilm extracellular matrix (ECM) attached to polystyrene surfaces.

Effect of Glabridin on Growth and Biofilm Formation

A strong anti-staphylococcal activity of glabridin was observed with minimal inhibitory concentration (MIC) 12.5 $\mu\text{g/ml}$ against both the drug sensitive strain (MTCC 96) and the MRSA clinical isolate (MRSA 4423) (**Supplementary Table S2**). To assess the antibiofilm efficacy of glabridin against MRSA 4423 forming strong biofilm, sublethal concentrations of glabridin ranging from 0.78 $\mu\text{g/ml}$ (1/16 MIC) to 6.25 $\mu\text{g/ml}$ (1/2 MIC) were added at the beginning of the experiments in a 96-well plate. Reduced biofilm formation was observed in presence of glabridin at sublethal concentration ranging from 1/4 MIC to 1/16 MIC, while at 1/2 MIC, glabridin was observed to completely prevent the biofilm formation (**Figure 1C**). To confirm whether reduced biofilm formation in presence of glabridin is independent of its planktonic growth inhibition activity, change in growth under biofilm conditions in the presence and absence of Glabridin was recorded. Thus, a dose dependent effect of Glabridin on biofilm reduction was clearly observed (**Figure 1C**). Similar observation on biofilm in the presence of glabridin was found against moderate biofilm forming clinical isolate MRSA 4627 (data not shown).

Growth Curve Study

A growth kinetics study, in both TSB and MHB media, showed that glabridin completely inhibited the growth of strong biofilm formation in isolate MRSA 4423 at the concentration of 12.5 $\mu\text{g/ml}$ (MIC value) (**Figures 2A,B**). Glabridin, at 1/2 MIC concentration, partially inhibited the growth of *S. aureus* which was recovered at around 12 h

and reached the optical density close to the control cultures. Similarly, glabridin at 12.5 $\mu\text{g/ml}$ concentration was observed to completely inhibit the growth of other clinical isolates of MRSA (forming moderate and weak biofilm) as well as the drug sensitive strain MTCC 96 (**Figures 2A,B**). Thus, a dose dependent reduction in growth of MRSA was observed upon exposure to the glabridin and at 12.5 $\mu\text{g/ml}$ (MIC value) concentration.

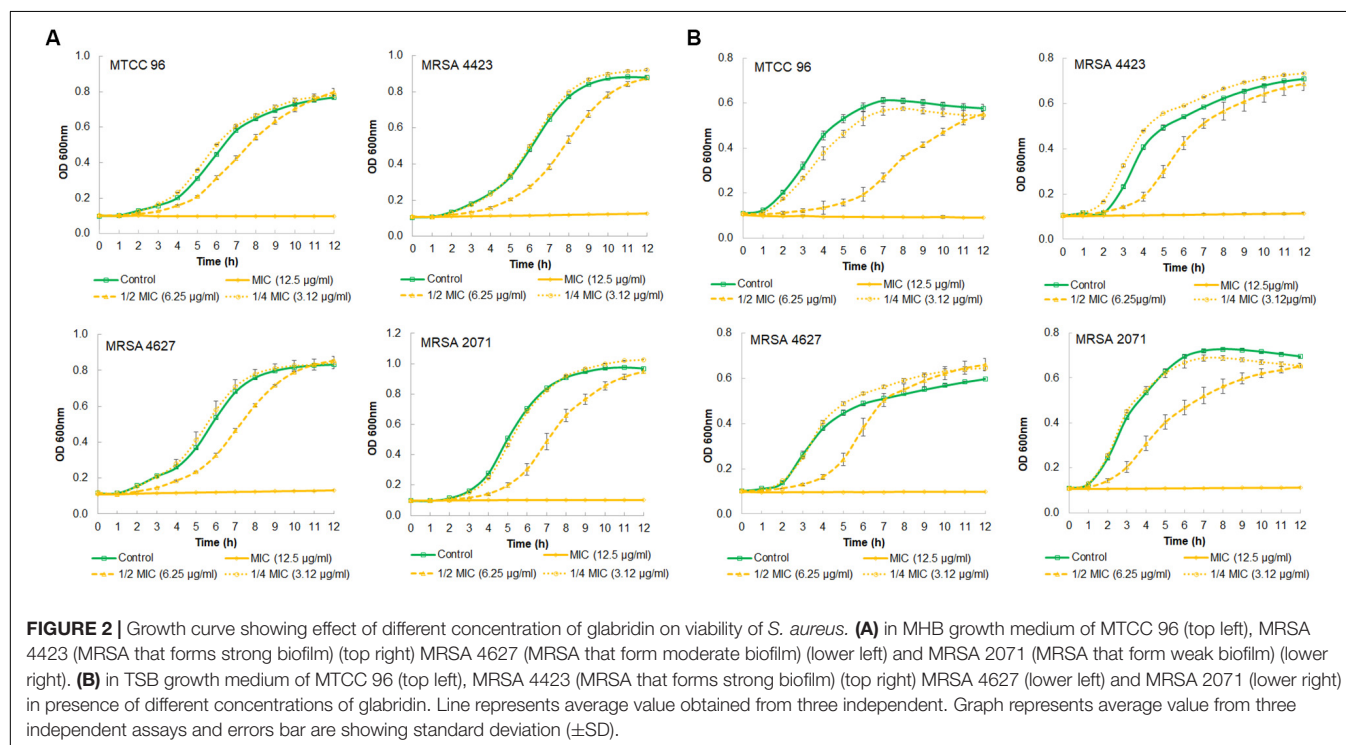
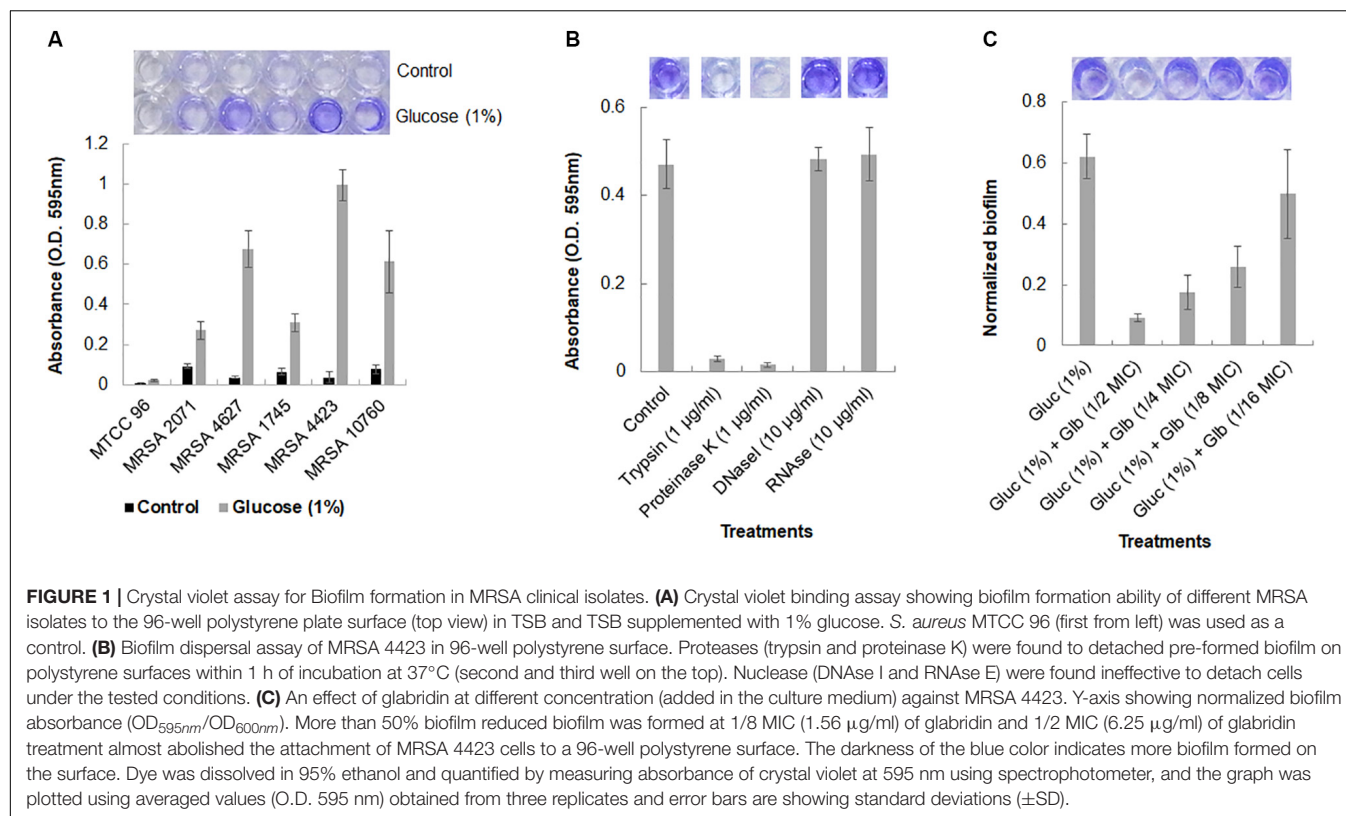
Scanning Electron Microscopy (SEM) Analysis of MRSA Biofilm

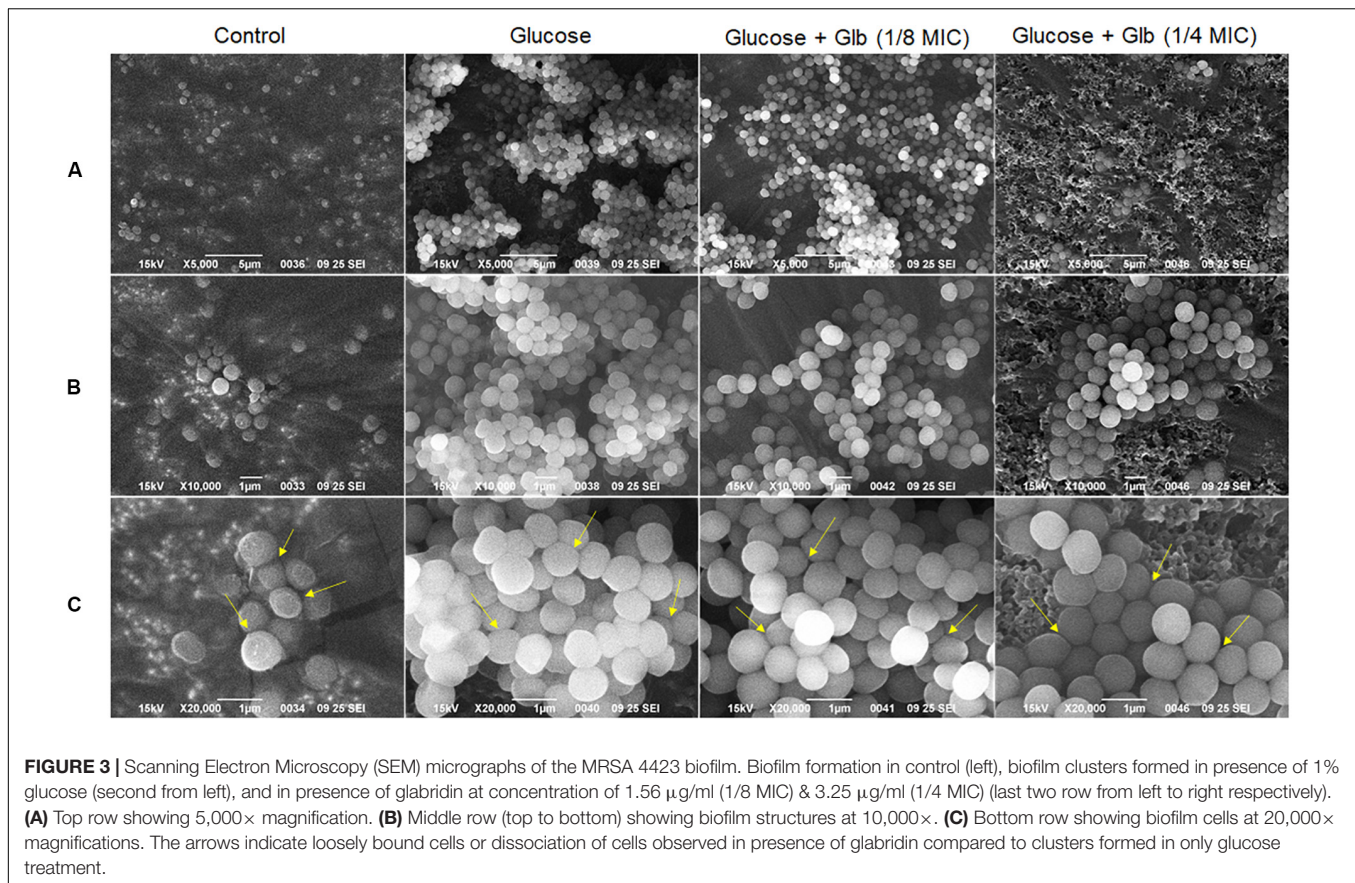
Further, the impact of glabridin on biofilm of MRSA 4423 was studied using a scanning electron microscope (SEM) upon the exposure of cells to two different concentrations of glabridin (1/8 and 1/4 MIC). Under the 5,000 \times magnification, in the control, very few cells were found attached to the surface, but in the presence of 1% glucose, highly organized cell clusters and tunnels were formed between these clusters (**Figure 3A**). These cell clusters were barely observed when supplemented with glabridin (1/8 MIC), and less tightly bound cells were observed. Furthermore, very less cell clusters compared to biofilm were observed on the surface of cells exposed to 1/4 MIC of glabridin when observed under the 10,000 \times and 20,000 \times magnifications (**Figures 3B,C**).

Proteomic Analysis of Biofilm Matrix (ECM)

The genome of biofilm forming methicillin-resistant *S. aureus* N315 published at the KEGG database¹ revealed the presence of surface proteins that are known to play a role in biofilm formation. Since different bacterial strains can express different sets of genes/proteins under similar conditions, therefore, the presence of proteins was checked in the ECM of MRSA 4423 that was formed upon glucose treatment. MS/MS analysis of proteins in ECM and cells imbedded in ECM by LC-ESI-QTOF identified several cell surface proteins involved in adhesions such as mannosyl-glycoprotein endo-beta-N-acetylglucosamidase or bifunctional autolysin (Atl), glycerol phosphate lipoteichoic acid synthase of LTA family (ItaS), CHAP domain-containing hypothetical protein (SsaA), immunoglobulin-binding protein (Sbi), N-acetylmuramoyl-L-alanine amidase (similar to autolysin), fibronectin-binding proteins (FnB A & FnB B), fibrinogen-binding proteins (Efb) and matrix-binding protein (Ebh). Other proteins including 5'-nucleotidase, gamma-hemolysin subunit B (HlgB), translation elongation factors (EF-Tu & EF-G), glyceraldehyde-3-phosphate dehydrogenase (GAPDH), Peptidase Pbp2a (MecA), and β -lactamase (BlaZ) were also identified in biofilm ECM of MRSA 4423 (**Supplementary Table S4**). The presence of surface-associated adhesins in ECM correlates well with the protease assay which detached the cells from the polystyrene surface. A lack of cell attachment in the absence of glucose and presence of glabridin suggested these proteins are possibly compromised under these conditions compared to the biofilm

¹https://www.genome.jp/dbget-bin/www_bget?gn:T00051





forming condition (1% glucose). Therefore, we decided to find differentially expressed proteins on the cell surface due to the presence of glucose and glabridin.

Analysis of Differentially Expressed Cell Surface Proteins in Presence of Glabridin

Differentially expressed proteins on the cell surface of MRSA 4423 in the biofilm condition were identified with and without the exposure to glabridin. As compared to the control, the supplement of glucose induces expression levels of cell surface-associated proteins such as Atl, FnbA, FnbB, SdrD, 5'-nucleotidase, Sbi, SsaA, N-acetylmuramoyl-L-alanine amidase, hypothetical protein with LPXTG-domain (similar to 5'-nucleotidase), and FKLRK-domain that are several-fold higher. Exposure of cells to glabridin downregulated the abundance of many glucose-induced proteins such as FnbAB, SdrD, Sbi, FKLRK-protein, LPXTG-protein, Efb, 5'-nucleotidase and N-acetylmuramoyl-L-alanine amidase. However, abundance of other cell surface proteins such as Atl and CHAP-domain proteins did not change significantly.

Interestingly, on the cell surface of MRSA 4423, several moonlight proteins (a single protein with multiple functions) such as EF-Tu, EF-G, GAPDH, molecular chaperone (DnaK) and pyruvate kinase (PK) were also identified (Table 1). The abundance of these moonlight proteins was reduced on the surface of cells supplemented with glucose (Table 1).

However, treatment of glabridin reversed the effect of glucose. Thus, the abundance of moonlighting proteins was found correlated oppositely to the surface-associated adhesins on the cell surface (Figure 4).

Gene Expression Analysis

To validate expression of proteins identified by LC-ESI-QTOF on the cell surface, qRT-PCR was performed for both categories of genes encoding surface-associated adhesins and moonlight proteins under the similar growth conditions used for surface protein identification. In comparison to the control, the culture grown under the biofilm inducing condition showed higher expression levels of genes for surface adhesins *fnbA* (9.9-fold), *fnbB* (10.6-fold), 5'-nucleotide (23-fold), FKLRK-domain (3.7-fold) and LPXTG-domain (3.1-fold) except gene *sbi* which remained unaffected (Figure 5A). However, glabridin (at 1/4 MIC) was found to significantly down regulate the expression of genes for these surface adhesins *fnbA* (−1.6-fold), *fnbB* (−1.6-fold), 5'-nucleotidase (−1.3-fold), FKLRK-domain (−2.8-fold) and LPXTG-domain (−1.7-fold) when compared to the biofilm inducing condition (Figure 5A).

Interestingly, up regulation in expression of genes for moonlight proteins such as *tufA* (3.4-fold), *fusA* (9.7-fold), *dnaK* (3.7-fold), *pykA* (3.7-fold) and *gapA* (14.8-fold) was also observed under the biofilm inducing conditions compared to the control. In the presence of glabridin, further enhancement

TABLE 1 | Protein list showing the top 25 hits identified by LC-ESI-QTOF analysis of MRSA 4423 cell surface proteome upon the exposure of glabridin.

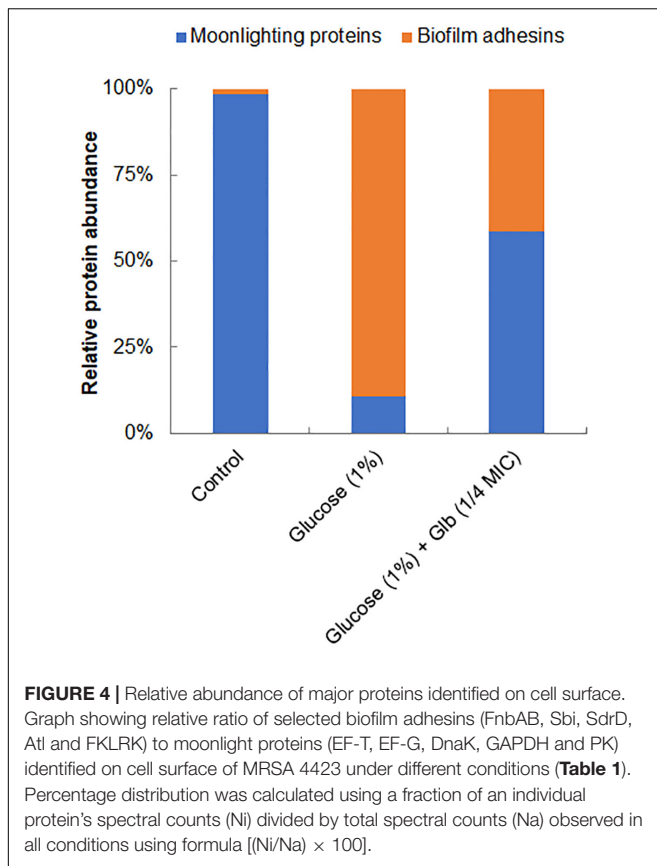
S.N.	Relative protein abundance* # (spectra, total intensity)			Proteins name	Protein MW (Da)	pI	Database Accession #	%AA Coverage	MS/MS Search Score	Fold change	
	Control	Glu	Glu + Glib							Glu/Control	Glu + Glib/Glu
1.	0 0.00E + 00	69 6.72E + 07	62 5.05E + 07	Mannosyl-glycoprotein endo-beta-N-acetylglucosamidase (AtI)	137390.6	9.62	ALK38880.1	47.6	484.65	up	−1.1
2.	128 1.62E + 09	33 8.02E + 07	55 2.96E + 08	Translational elongation factor Tu (TufA)	43159.9	4.74	AIA27105.1	73.6	317.16	−3.9	+1.7
2.	3 1.17E+07	0 0.00E + 00	3 1.66E + 06	Translational elongation factor Tu, partial	8757.6	4.96	KMR26954.1	38.2	21.88	nd	up
3.	1 9.59E + 04	62 7.30E + 07	7 1.14E + 06	Fibronectin-binding protein FnbA	111806.4	4.64	KMS18095.1	42.6	264.99	+62	−8.9
3.	1 9.59E + 04	3 1.99E + 06	1 1.17E + 05	Fibronectin-binding protein FnbB	104799.4	4.66	QBS27992.1	2.9	20.05	+3	−3
4.	42 2.57E + 08	9 6.21E + 06	23 1.99E + 07	Translational elongation factor G (FusA)	76926.4	4.8	OWU45296.1	53.1	240.98	−4.6	+2.6
5.	43 9.94E + 07	5 3.06E + 06	21 1.50E + 07	Pyruvate kinase (PykA)	63329.4	5.24	AIA28225.1	50.4	240.03	−8.6	+4.2
6.	7 1.55E + 06	28 4.78E + 07	67 2.12E + 08	Penicillin-hydrolyzing class A beta-lactamase BlaZ	31405.8	9.58	OWU47924.1	49.8	237.92	+4	+2.4
7.	8 1.34E + 06	37 2.44E + 07	38 3.13E + 07	PBP2a family beta-lactam-resistant transpeptidase MecA	76232.3	8.7	OWU35180.1	36.6	223.76	+4.625	+1.0
8.	6 1.02E + 06	34 2.28E + 07	36 2.90E + 07	Peptidase	76100.2	8.7	KMS44729.1	36.6	216.54	+5.67	+1.0
9.	39 1.18E + 08	0 0.00E + 00	2 1.30E + 06	Formate acetyltransferase	85316.8	5.31	AIA26805.1	45.2	214.94	nd	up
10.	19 2.39E + 07	16 1.29E + 07	40 6.07E + 07	Enolase	47173.1	4.55	AIA27354.1	56.4	194.35	−1.18	+2.5
11.	15 3.13E + 07	12 7.58E + 06	38 6.42E + 07	glyceraldehyde-3-phosphate dehydrogenase	36394.3	4.89	AIA27350.1	69.9	187.99	−1.25	+3.2
12.	0	15	10	Glycerol phosphate lipoteichoic acid	74398.7	9.04	AIA27296.1	34.9	173.88	up	−1.5

(Continued)

TABLE 1 | Continued

S.N.	Relative protein abundance* # (spectra, total intensity)			Proteins name	Protein MW (Da)	pI	Database Accession #	%AA Coverage	MS/MS Search Score	Fold change	
	Control	Glu	Glu + Glb							Glu/Control	Glu + Glb/Glu
13.	0.00E + 00	1.92E + 07	7.28E + 06	synthase	66472.3	4.67	KMS23456.1	32.4	160.86	nd	up
	25 5.77E + 07	0 0.00E + 00	10 5.08E + 06	Molecular chaperone DnaK							
14.	25 3.87E + 07	1 1.52E + 05	7 2.87E + 06	Cysteine synthase	33032.1	5.39	AIA27070.1	74.1	147.61	-25	+7
	18 3.49E + 07	0 0.00E + 00	0 0.00E + 00	Threonyl-tRNA synthase							
15.	1 5.88E + 05	16 3.64E + 06	7 2.01E + 06	Hydrolase, SdrD	149704.2	4.12	KMR76067.1	13.8	145.67	+16	-2.29
	21 1.40E + 07	0 0.00E + 00	2 1.09E + 05	Glucosamine-fructose-6-phosphate aminotransferase							
17.	12 3.69E + 06	0 0.00E + 00	10 2.69E + 06	Malate: quinone oxidoreductase	56183.1	6.12	KMS00114.1	40.5	140.79	nd	up
	17 2.21E + 07	4 6.00E + 05	10 6.23E + 06	Phosphoglycerate kinase							
18.	4 1.04E + 06	42 7.80E + 07	50 8.40E + 07	CHAP domain protein	30433.8	9.1	KMS46097.1	52.0	130.25	+10.5	+1.2
	24 2.86E + 07	1 3.10E + 04	0 0.00E + 00	ATP F0F1 synthase subunit beta							
19.	12 5.45E + 06	2 1.41E + 06	7 1.83E + 06	2-Oxoisovalerate dehydrogenase	35245.4	4.65	AIA27584.1	52.9	116.91	-6.0	+3.5
	20 3.09E + 07	0 0.00E + 00	1 7.47E + 04	6'-Aminoglycoside N-acetyltransferase (AAC(6'))							
20.	0 0.00E + 00	21 7.32E + 07	16 7.37E + 07	5'-Nucleotidase	33351.3	9.49	AIA26892.1	30.7	113.59	up	-1.3
	0 0.00E + 00	23 5.53E + 07	0 0.00E + 00	Immunoglobulin-binding protein Sbi							
21.	0 0.00E + 00	23 5.53E + 07	0 0.00E + 00	Immunoglobulin-binding protein Sbi	50117.5	9.4	KMR92723.1	23.1	111.45	up	nd
	0 0.00E + 00	23 5.53E + 07	0 0.00E + 00	Immunoglobulin-binding protein Sbi							

*Glu = Glucose, Glb = Glabridin. Glu/Control = shows fold change due to presence of glucose compared to control, and Glu + Glb/Glu = shows fold change due to glabridin treatment compared to glucose treatment (biofilm inducing condition). Color intensity shows relative abundance of protein under control and treatments conditions as observed in analysis by Spectrum mill software (Agilent, United States). The darkness of the color (from light yellow to dark red) represents a higher abundance of proteins in the samples. Full list of protein can be accessed in **Supplementary Table S5**. up = denotes uniquely present proteins, nd = denotes not detected/absence of protein. A probability score of $P < 0.05$ was used as the criterion for identification. Total protein was pooled from three replicates in each case, quantified, and an equal amount of protein was processed from each set for identification.



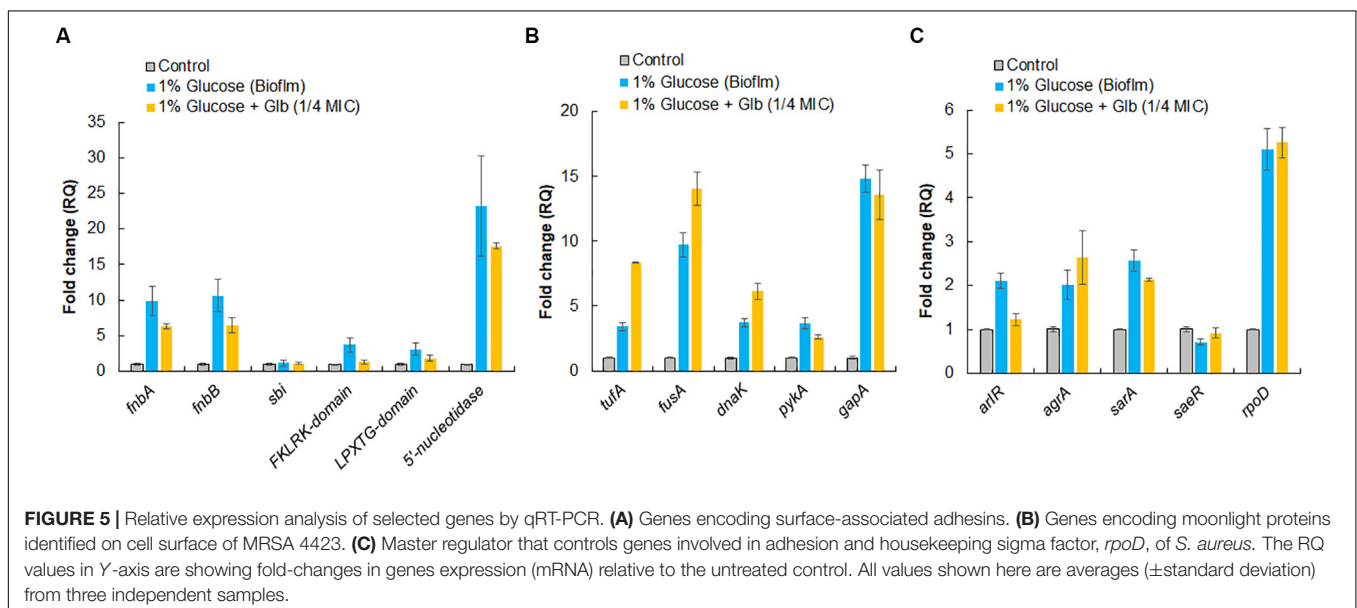
in expression of *tufA* (2.5-fold), *fusA* (~1.5-fold) and *dnaK* (1.7-fold) was detected (Figure 5B). It was also observed that genes master regulators of biofilm such as *arlR*, *sarA*, and *agrA* were upregulated more than 2 fold under the biofilm inducing conditions compared to the control and glabridin

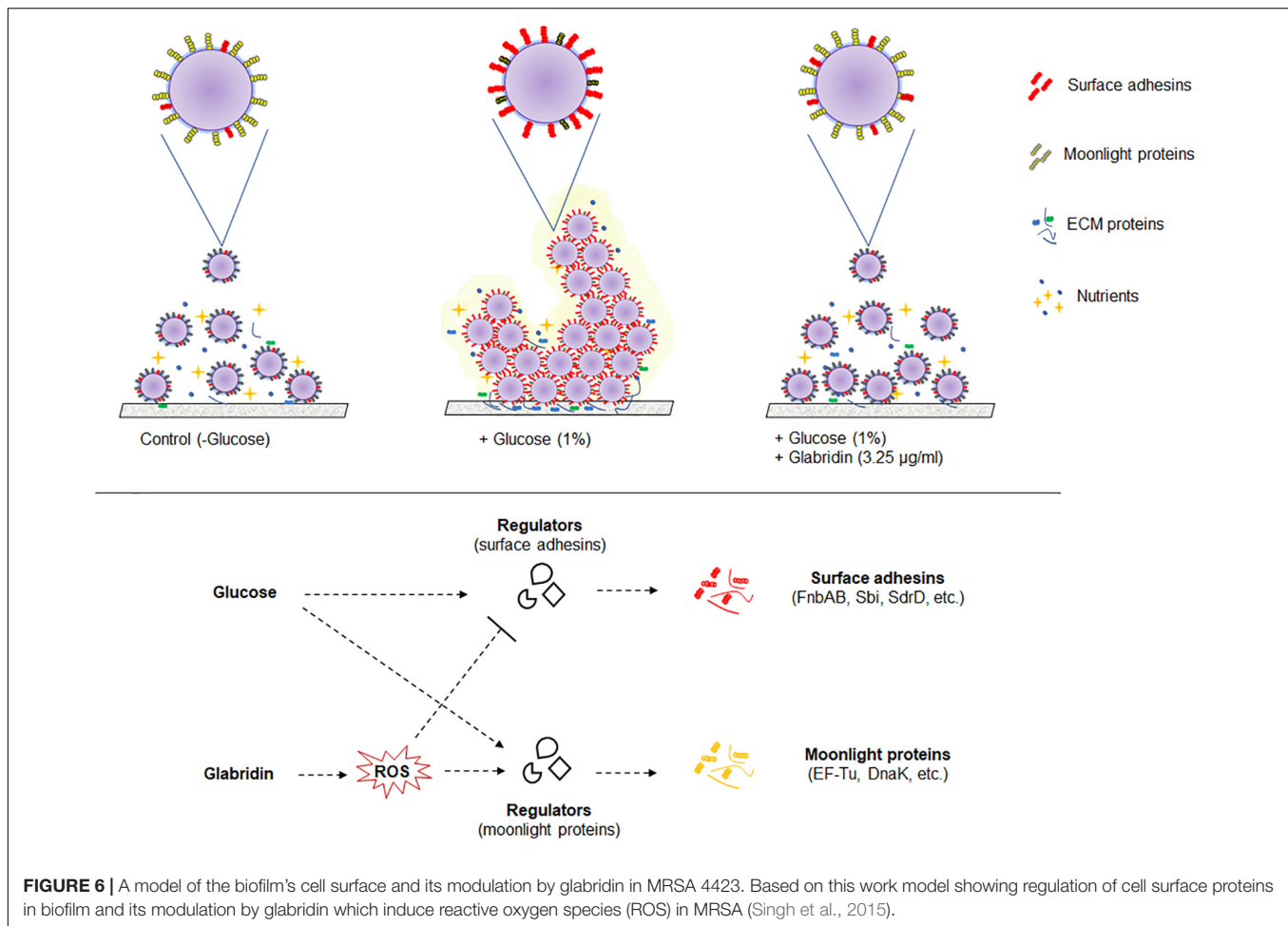
downregulated expression of *arlR* (−1.7-fold) and *sarA* to some extent (−1.2-fold), while expression of *agrA* was marginally upregulated (1.3-fold) compared to the biofilm inducing conditions. Expression of *saeR* was decreased (−1.4-fold) under the biofilm inducing condition compared to the control and glabridin was able to restore its expression to the level of control. Housekeeping sigma factor, *rpoD*, expression was found to increase about 5-fold under the biofilm inducing condition than control and its expression didn't change significantly in the presence of glabridin (Figure 5C).

DISCUSSION

Microorganisms including several pathogenic bacteria produce biofilms as a survival strategy under harsh environments and biofilm embedded bacteria are often a challenge to treat using drugs. Various reports correlate drug resistance with the biofilm formation ability of *S. aureus* and other microorganisms (Awoke et al., 2019; Reffuveille et al., 2017; Sharma et al., 2019). To date, several environmental factors such as glucose, salt (NaCl), ethanol, high temperature, antibiotics stress, and low oxygen have been described to support biofilm formation in *S. aureus* (Jefferson, 2004; Fitzpatrick et al., 2005). Recent studies have focused on the development of antimicrobial drugs to inhibit the formation of biofilm and/or other virulence factors which appear promising with regards to controlling bacterial infections without spreading resistance (Lee et al., 2013, 2014, 2016; Phuong et al., 2017; Kong et al., 2018; Selvaraj et al., 2019).

In crystal violet binding assay, clinical isolate MRSA 4423 was found forming robust biofilms when supplemented with 1% glucose in TSB culture media, which is in accordance with earlier reports (Croes et al., 2009; Lim et al., 2004). Biofilm formation in TSB culture media, supplemented with 1% glucose has been shown to promote the formation of biofilms





in *S. aureus* with greater reproducibility (Lade et al., 2019). Beside bactericidal activity, Glabridin was found to prevent the development of glucose-induced biofilm in MRSA 4423 in a concentration dependent manner. The growth curve study suggests that glabridin is capable of inhibiting planktonic growth of MRSA isolates independent of its ability to inhibit biofilm formation, most likely due to its adverse impact on biofilm formation and lack of resistance mechanism toward glabridin in clinical isolates of MRSA. Furthermore, SEM analysis showed that glabridin can effectively inhibit the formation of cell-clusters leading to a biofilm condition.

Exogenously added proteases such as proteinase K and trypsin have often been used as effective biofilm dispersal agents, likely by surface structure degradation (Boles and Horswill, 2008; Chaignon et al., 2007). Proteinase-K cleaves the peptide bonds of aliphatic, aromatic, or hydrophobic amino acids, while trypsin specifically cleaves peptide bonds of lysine and arginine (Chaignon et al., 2007). Identification of highly abundant proteins in the biofilm ECM indicates why the proteases, not nucleases, were capable of detaching the biofilm of MRSA 4423 from the surface presumably because either the DNA contributed insignificantly or was mounted by proteins. Comparative analysis revealed various highly abundant surface-associated adhesins

whose expression was enhanced in the presence of glucose as compared to the non-biofilm condition (culture grown without glucose). Upon the exposure of cells to glabridin, down-regulation in the expression of surface proteins like FnBA, FnBB, SdrD, 5'-nucleotidase, Sbi, a hypothetical protein with LPXTG-domain, FKLRK-domain protein, Hld and Efb homolog was observed. Expression of some other cell surface proteins such as Atl, peptidase and CHAP-domain did not change significantly, suggesting that under the tested conditions these are probably not regulated by the response elevated by glabridin in MRSA 4423 (Table 1). Interestingly, most of the proteins abundant in biofilm ECM were basic in nature and on averaged isoelectric point (PI) of most abundant proteins presents in top of the list showed $PI > 7$ (Supplementary Table S4). However, most of the proteins abundant on the cell surface were acidic in nature with an average $PI < 7$ (Supplementary Table S5). Since the bacterial cell surface is negative in nature, therefore it possibly favors acidic proteins to attach to. Importantly, down regulation of adhesion proteins in the presence of glabridin correlated well with biofilm formation preventing activity as observed in crystal violet binding assay (Figure 1C). The role of several surface-associated adhesins identified on the cell surface of *S. aureus* have been characterized in detail (Foster et al., 2014; Kwiecinski et al., 2014). The function

of some of the most abundant surface-associated proteins identified in this study are described in **Supplementary Table S3**.

Expression analysis of genes encoding surface proteins by qRT-PCR showed upregulation of adhesins which is in accordance with other studies where surface-associated genes are upregulated in biofilm of *S. aureus* (Speziale et al., 2014; Hiltunen et al., 2019). Glabridin was found to significantly downregulate the expression of surface-associated biofilm adhesins such as *fnbA*, *fnbB*, *sbi* etc. in qRT-PCR analysis which might be an appropriate reason for low abundance of these adhesins on the cell surface in response to glabridin in MRSA 4423. Transcriptional regulatory network of surface-associated adhesins is very complex where multiple gene regulators such as *agrA*, *sarA*, *saeR/S*, and *arlRS* inter-play to control expression of these proteins and fine-tune the formation of biofilm (Paharik and Horswill, 2016; Burgui et al., 2018; Toledo-Arana et al., 2005). Therefore, expression of transcriptional regulators was further confirmed at transcript level.

Indeed, qRT-PCR analysis showed change in expression level of key regulators that are involved in biofilm formation. The expression of *arlR* was found upregulated in the presence of glucose (biofilm inducing conditions) as compared to the control, while in the presence of glabridin, significant down regulation was observed suggesting that *arlR* plays positive role in biofilm formation of MRSA 4423. Activation of quorum sensing regulator, *agrA*, is known to trigger production of exo-proteases responsible for detachment of established biofilms in *S. aureus* (Boles and Horswill, 2008; Yarwood et al., 2004; Vuong et al., 2000). Thus, upregulation of *agrA* in presence of glabridin under biofilm conditions might be able to induce a response which is inhibiting biofilm formation in MRSA 4423.

Transcription regulator *sarA* is known to positively regulate biofilm proteins (FnBPs, PIA, BapA) and inhibits *agrA* activity in *S. aureus* (Wolz et al., 2000; Paharik and Horswill, 2016). Transcriptional regulator *sarA* expression in presence of glucose (biofilm inducing condition) was found to be upregulated, while it was down regulated in presence of glabridin, which is positively correlated to lower level of surface protein adhesins (FnAB) upon the exposure to glabridin in MRSA 4423. The *saeR* controls both of the factors that are known to promote the biofilm formation and dispersal, and therefore affects the biofilm formation either positively or negatively depending on growth conditions and strain backgrounds of *S. aureus* (Harraghy et al., 2005; Liu et al., 2016). There was no significant change observed in the expression level of *saeR* under the tested conditions. High expression of *rpoD* was found under the biofilm conditions in MRSA 4423 suggesting its requirement for the expression of housekeeping genes and metabolic factors to survive and persist in biofilm which is in accordance with other studies where *rpoD* expression was shown to increase during biofilm formation in *Helicobacter pylori*, and *Xylella fastidiosa* (De la Cruz et al., 2017; de Souza et al., 2004).

The study of cell surface proteins of MRSA 4423 led to identification of several other highly abundant proteins such as EF-Tu, EF-G, DnaK, PK and GAPDH etc. which are commonly known as moonlighting proteins. On the cell surface of MRSA 4423, the abundance of many moonlight proteins was found

inversely proportional to the biofilm related proteins in the presence of two different treatments, glucose and glabridin. Analysis of their gene expression in presence of glucose showed higher expression level. Similarly, other biofilm studies in bacteria have also showed higher expression of several cellular proteins that play moonlighting functions including EF-Tu, EF-G, and DnaK (Resch et al., 2005; Zimaro et al., 2013). Higher transcript level (mRNA) in the presence of glucose indicating cells are metabolically more active in biofilm conditions than in the control (planktonic culture). Interestingly, glabridin further increased expression of genes encoding EF-Tu, EF-G and DnaK proteins, probably because glabridin triggers ROS generation, leading to a damage response that enhances expression of these protein with chaperones properties (Singh et al., 2015; Caldas et al., 1998; Caldas et al., 2000; Singh et al., 2007). Thus, reduced expression of biofilm-adhesins in presence of glabridin possibly favors the attachment of moonlight proteins to the cell surface leading to alteration in the surfaceome architecture that ultimately influences adherence of MRSA 4423 (**Figure 6**).

Moonlighting proteins are reported to play important role, as a second function, in interaction with other proteins (**Supplementary Table S4**). To date, around four hundred moonlight proteins are listed in MoonProt database² which are hypothesized to contribute in bacterial virulence, adhesion and modulation of cell signaling processes (Wang et al., 2014). The moonlighting protein EF-Tu is recognized as pathogen-associated molecular pattern (PAMP) by the pattern recognition receptors (PRRs) present on the surface of host cells (Harvey et al., 2019; Furukawa et al., 2014). Thus, in biofilm conditions, downregulation of moonlighting proteins and upregulation of surface-associated adhesins could be a survival strategy of *S. aureus* to colonize within a host without eliciting an immune response (Zipfel, 2008). The mechanism identified in this study by which glabridin prevents biofilm formation could lead to the development of novel agents against *S. aureus* and other pathogenic bacteria. Reported literature suggests that glabridin is non-cytotoxic and a suitable candidate for drug development as it has been found safe when administered orally (Aoki et al., 2007; Cheema et al., 2014). Further studies may help to understand the association between moonlight and biofilm-related proteins, their role in virulence and to tackle drug resistance in bacteria.

CONCLUSION

In the present study, it has been experimentally demonstrated that glabridin, a polyphenolic flavonoid, as a possible agent preventing biofilm formation in methicillin-resistant clinical isolate of *S. aureus*. Proteomics and real-time qPCR expression analysis upon the exposure to glabridin resulted in alteration of surface proteins that are known to be involved in biofilm formation of *S. aureus*. Besides adhesins, proteins known as moonlighting proteins whose expression is inversely proportional to biofilm-associated adhesins were found to

²<http://www.moonlightingproteins.org/>

be affected in the presence of glabridin. To the best of our knowledge, this is the first experimental evidence demonstrating involvement of glabridin in controlling expression of cell surface proteins and preventing adherence of *S. aureus*. Therefore, glabridin is likely a good candidate to be developed as phytopharmaceutical agent against *S. aureus* preventing biofilm formation.

DATA AVAILABILITY STATEMENT

All datasets presented in this study are included in the article/**Supplementary Material**.

AUTHOR CONTRIBUTIONS

BG and SK performed the experiments and analyzed the data. BG, SK, and MD conceived the idea and wrote the manuscript. All authors read and approved the manuscript.

REFERENCES

- Aoki, F., Nakagawa, K., and Kitano, M. (2007). Clinical safety of licorice flavonoid oil (LFO) and pharmacokinetics of glabridin in healthy humans. *J. Am. Coll. Nutr.* 26, 209–218. doi: 10.1080/07315724.2007.10719603
- Appelbaum, P. C. (2006). The emergence of vancomycin-intermediate and vancomycin-resistant *Staphylococcus aureus*. *Clin. Microbiol. Infect.* 12, 16–23. doi: 10.1111/j.1469-0691.2006.01344.x
- Atshan, S. S., Shamsudin, M. N., Karunanidhi, A., van Belkum, A., Lung, L. T., Sekawi, Z., et al. (2013). Quantitative PCR analysis of genes expressed during biofilm development of methicillin resistant *Staphylococcus aureus* (MRSA). *Infect. Genet. Evol.* 18, 106–112. doi: 10.1016/j.meegid.2013.05.002
- Awoke, N., Kassa, T., and Teshager, L. (2019). Magnitude of biofilm formation and antimicrobial resistance pattern of bacteria isolated from urinary catheterized inpatients of jimma university medical center, Southwest Ethiopia. *Int. J. Microbiol.* 2019:5729568. doi: 10.1155/2019/5729568
- Boles, B. R., and Horswill, A. R. (2008). Agr-mediated dispersal of *Staphylococcus aureus* biofilms. *PLoS Pathog.* 4:e1000052. doi: 10.1371/journal.ppat.1000052
- Brun, A., Magallanes, M. E., Martínez del Río, C., Barrett-Wilt, G. A., Karasov, W. H., and Caviedes-Vidal, E. (2020). A Fast and Accurate Method to Identify and Quantify Enzymes in Brush-Border Membranes: In Situ Hydrolysis Followed by Nano LC-MS/MS. *Methods Protoc.* 3:15. doi: 10.3390/mps3010015
- Burgui, S., Gil, C., Solano, C., Lasa, I., and Valle, J. (2018). A systematic evaluation of the two-component systems network reveals that ArlRS is a key regulator of catheter colonization by *Staphylococcus aureus*. *Front. Microbiol.* 9:342. doi: 10.3389/fmicb.2018.00342
- Caldas, T., Laalami, S., and Richarme, G. (2000). Chaperone properties of bacterial elongation factor EF-G and initiation factor IF2. *J. Biol. Chem.* 275, 855–860. doi: 10.1074/jbc.275.2.855
- Caldas, T. D., El Yaagoubi, A., and Richarme, G. (1998). Chaperone properties of bacterial elongation factor EF-Tu. *J. Biol. Chem.* 273, 11478–11482. doi: 10.1074/jbc.273.19.11478
- Chaignon, P., Sadovskaya, I., Ragunah, Ch., Ramasubbu, N., Kaplan, J. B., and Jabbouri, S. (2007). Susceptibility of staphylococcal biofilms to enzymatic treatments depends on their chemical composition. *Appl. Microbiol. Biotechnol.* 75:125. doi: 10.1007/s00253-006-0790-y
- Cheema, H. S., Prakash, O., Pal, A., Khan, F., Bawankule, D. U., and Darokar, M. P. (2014). Glabridin induces oxidative stress mediated apoptosis like cell death of malaria parasite *Plasmodium falciparum*. *Parasitol. Int.* 63, 349–358. doi: 10.1016/j.parint.2013.12.005
- CLSI (2018). *Methods for Dilution Antimicrobial Susceptibility Tests for Bacteria That Grow Aerobically*. 11th ed. CLSI supplement M07. Wayne, PA: Clinical and Laboratory Standards Institute.
- Cowan, M. M. (1999). Plant products as antimicrobial agents. *Clin. Microbiol. Rev.* 12, 564–582.
- Croes, S., Deurenberg, R. H., Boumans, M. L., Beisser, P. S., Neef, C., and Stobberingh, E. E. (2009). *Staphylococcus aureus* biofilm formation at the physiologic glucose concentration depends on the *S. aureus* lineage. *BMC Microbiol.* 9:229. doi: 10.1186/1471-2180-9-229
- De la Cruz, M. A., Ares, M. A., von Bargen, K., Panunzi, L. G., Martínez-Cruz, J., and Valdez-Salazar, H. A. (2017). Gene expression profiling of transcription factors of *Helicobacter pylori* under different environmental conditions. *Front. Microbiol.* 8:615. doi: 10.3389/fmicb.2017.00615
- de Souza, A. A., Takita, M. A., Coletta-Filho, H. D., Caldana, C., Yanai, G. M., Muto, N. H., et al. (2004). Gene expression profile of the plant pathogen *Xylella fastidiosa* during biofilm formation in vitro. *FEMS Microbiol. Lett.* 237, 341–353. doi: 10.1016/j.femsle.2004.06.055
- Donlan, R. M., and Costerton, J. W. (2002). Biofilms: survival mechanisms of clinically relevant microorganisms. *Clin. Microbiol. Rev.* 15, 167–193. doi: 10.1128/cmr.15.2.167-193.2002
- Fatima, A., Gupta, V. K., Luqman, S., Negi, A. S., Kumar, J. K., Shanker, K., et al. (2009). Antifungal activity of *Glycyrrhiza glabra* extracts and its active constituent glabridin. *Phytother. Res.* 23, 1190–1193. doi: 10.1002/ptr.2726
- Fitzpatrick, F., Humphreys, H., and O'Gara, J. P. (2005). The genetics of staphylococcal biofilm formation—will a greater understanding of pathogenesis lead to better management of device-related infection. *Clin. Microbiol. Infect.* 11, 967–973. doi: 10.1111/j.1469-0691.2005.01274.x
- Foster, T. J. (2017). Antibiotic resistance in *Staphylococcus aureus*. Current status and future prospects. *FEMS Microbiol. Res.* 41, 430–449. doi: 10.1093/femsre/fux007
- Foster, T. J., Geoghegan, J. A., Ganesh, V. K., and Höök, M. (2014). Adhesion, invasion and evasion: the many functions of the surface proteins of *Staphylococcus aureus*. *Nat. Rev. Microbiol.* 12, 49–62. doi: 10.1038/nrmicro3161
- Furukawa, T., Inagaki, H., Takai, R., Hirai, H., and Che, F. S. (2014). Two distinct EF-Tu epitopes induce immune responses in rice and Arabidopsis. *Mol. Plant Microbe Interact.* 27, 113–124. doi: 10.1094/MPMI-10-13-0304-R
- Gebreyohannes, G., Nyerere, A., Bii, C., and Sbatu, D. B. (2019). Challenges of intervention, treatment, and antibiotic resistance of biofilm-forming microorganisms. *Heliyon* 5:e02192. doi: 10.1016/j.heliyon.2019.e02192

ACKNOWLEDGMENTS

The authors gratefully acknowledge the help of Prof. K. N. Prasad, Laboratory of Clinical Microbiology, Sanjay Gandhi Post Graduate Institute of Medical Sciences (SGPGIMS), Lucknow, India for providing methicillin-resistant clinical isolates of *S. aureus*. Indian Council of Medical Research (ICMR), New Delhi, India is gratefully acknowledged for providing Senior Research Fellowship to BG. This work was part of CSIR Network Project BSC-0203 and MLP-06 of CSIR-CIMAP, Lucknow, India. The Biological Central Facility and encouragement provided by Director, CSIR-CIMAP is gratefully acknowledged.

SUPPLEMENTARY MATERIAL

The Supplementary Material for this article can be found online at: <https://www.frontiersin.org/articles/10.3389/fmicb.2020.01779/full#supplementary-material>

- Gupta, A., Maheshwari, D. K., and Khandelwal, G. (2013). Antibacterial activity of *Glycyrrhiza glabra* roots against certain gram-positive and gram-negative bacterial strains. *J. Appl. Nat. Sci.* 5, 459–464. doi: 10.31018/jans.v5i2.354
- Gupta, V. K., Fatima, A., Faridi, U., Negi, A. S., Shanker, K., Kumar, J. K., et al. (2008). Antimicrobial potential of *Glycyrrhiza glabra* roots. *J. Ethnopharmacol.* 5, 377–380. doi: 10.1016/j.jep.2007.11.037
- Gupta, V. K., Verma, S., Gupta, S., Singh, A., Pal, A., Srivastava, S. K., et al. (2012). Membrane-damaging potential of natural L-(–)-usnic acid in *Staphylococcus aureus*. *Eur. J. Clin. Microb. Infect. Dis.* 31, 3375–3383. doi: 10.1007/s10096-012-1706-7
- Haque, M., Sartelli, M., McKimm, J., and Abu Bakar, M. (2018). Health care-associated infections - an overview. *Infect. and Drug Resist.* 11, 2321–2333. doi: 10.2147/IDR.S177247
- Harraghy, N., Kormanec, J., Wolz, C., Homerova, D., Goerke, C., Ohlsen, K., et al. (2005). *sae* is essential for expression of the staphylococcal adhesins Eap and Emp. *Microbiology* 151, 1789–1800. doi: 10.1099/mic.0.27902-0
- Harvey, K. L., Jarocki, V. M., Charles, I. G., and Djordjevic, S. P. (2019). The diverse functional roles of elongation factor Tu (EF-Tu) in microbial pathogenesis. *Front. Microbiol.* 10:2351. doi: 10.3389/fmicb.2019.02351
- Hiltunen, A. K., Savijoki, K., Nyman, T. A., Miettinen, I., Ihala, P., Peltonen, J., et al. (2019). Structural and functional dynamics of *Staphylococcus aureus* biofilms and biofilm matrix proteins on different clinical materials. *Microorganisms* 7:584. doi: 10.3390/microorganisms7120584
- Irani, M., Sarmadi, M., Bernard, F., Ebrahimi Pour, G. H., and Shaker Bazarnov, H. (2010). Leaves antimicrobial activity of *Glycyrrhiza glabra* L. *Iran. J. Pharm. Res.* 9, 425–428.
- Jan-Roblero, J., Rodriguez-Martinez, S., Cancino-Diaz, M. E., and Candino-Diaz, J. C. (2016). “Staphylococcus biofilms,” in *Microbial Biofilms-Importance and Applications*, eds D. Dhanasekaran and N. Thajuddin (Rijeka: InTech), doi: 10.5772/62943
- Jefferson, K. K. (2004). What drives bacteria to produce a biofilm? *FEMS Microbiol. Lett.* 236, 163–173. doi: 10.1016/j.femsle.2004.06.005
- Kaplan, J. B., Veliyagounder, K., Raganath, C., Rohde, H., Mack, D., Knobloch, J. K., et al. (2004). Genes involved in the synthesis and degradation of matrix polysaccharide in *Actinobacillus actinomycetemcomitans* and *Actinobacillus pleuropneumoniae* biofilms. *J. Bacteriol.* 186, 8213–8220. doi: 10.1128/JB.186.24.8213-8220.2004
- Karygianni, L., Ren, Z., Koo, H., and Thurnheer, T. (2020). Biofilm matrixome: extracellular components in structured microbial communities. *Trends Microbiol.* 28, 668–681. doi: 10.1016/j.tim.2020.03.016
- Kong, C., Chee, C. F., Richter, K., Thomas, N., Abd Rahman, N., and Nathan, S. (2018). Suppression of *Staphylococcus aureus* biofilm formation and virulence by a benzimidazole derivative. *UM-C162. Sci. Rep.* 8:2758. doi: 10.1038/s41598-018-21141-2
- Kostakioti, M., Hadjifrangiskou, M., and Hultgren, S. J. (2013). Bacterial biofilms: development, dispersal, and therapeutic strategies in the dawn of the post antibiotic era. *Cold Spring Harb. Perspect. Med.* 3:a010306. doi: 10.1101/cshperspect.a010306
- Kumar, S., Rai, A. K., Mishra, M. N., Shukla, M., Singh, P. K., and Tripathi, A. K. (2012). RpoH2 sigma factor controls the photooxidative stress response in a non-photosynthetic rhizobacterium. *Azospirillum brasilense* Sp7. *Microbiology* 158, 2891–2902. doi: 10.1099/mic.0.062380-0
- Kumar, S., and Spiro, S. (2017). Environmental and genetic determinants of biofilm formation in *Paracoccus denitrificans*. *mSphere* 2, e00350-17. doi: 10.1128/mSphereDirect.00350-17
- Kwiciński, J., Jin, T., and Josefsson, E. (2014). Surface proteins of *Staphylococcus aureus* play an important role in experimental skin infection. *APMIS* 122, 1240–1250. doi: 10.1111/apm.12295
- Lade, H., Park, J. H., Chung, S. H., Kim, I. H., Kim, J. M., Joo, H. S., et al. (2019). Biofilm Formation by *Staphylococcus aureus* clinical isolates is differentially affected by glucose and sodium chloride supplemented culture media. *J. Clin. Med.* 8:1853. doi: 10.3390/jcm8111853
- Lee, J. H., Kim, Y. G., Ryu, S. Y., and Lee, J. (2016). Calcium-chelating alizarin and other anthraquinones inhibit biofilm formation and the hemolytic activity of *Staphylococcus aureus*. *Sci. Rep.* 6:19267. doi: 10.1038/srep19267
- Lee, J. H., Park, J. H., Cho, H. S., Joo, S. W., Cho, M. H., and Lee, J. (2013). Antibiofilm activities of quercetin and tannic acid against *Staphylococcus aureus*. *Biofouling* 29, 491–499. doi: 10.1080/08927014.2013.788692
- Lee, K., Lee, J. H., Ryu, S. Y., Cho, M. H., and Lee, J. (2014). Stilbenes reduce *Staphylococcus aureus* hemolysis, biofilm formation, and virulence. *Foodborne Pathog. Dis.* 11, 710–717. doi: 10.1089/fpd.2014.1758
- Lim, Y., Jana, M., Luong, T. T., and Lee, C. Y. (2004). Control of glucose- and NaCl-induced biofilm formation by rbf in *Staphylococcus aureus*. *J. Bacteriol.* 186, 722–729. doi: 10.1128/jb.186.3.722-729.2004
- Liu, H., Sadygov, R. G., and Yates, J. R. I. I. (2004). A model for random sampling and estimation of relative protein abundance in shotgun proteomics. *Anal. Chem.* 76, 4193–4201. doi: 10.1021/ac0498563
- Liu, Q., Yeo, W. S., and Bae, T. (2016). The SaeRS Two-Component System of *Staphylococcus aureus*. *Genes* 7:81. doi: 10.3390/genes7100081
- López, D., Vlamakis, H., and Kolter, R. (2010). Biofilms. *Cold Spring Harb. Perspect. Biol.* 2:a000398. doi: 10.1101/cshperspect.a000398
- Mah, T.-F. (2012). Biofilm-specific antibiotic resistance. *Future Microbiol.* 7, 1061–1072. doi: 10.2217/fmb.12.76
- Mamedov, N. A., and Egamberdieva, D. (2019). “Phytochemical constituents and pharmacological effects of licorice: a review,” in *Plant and Human Health*, eds K. R. Hakeem, and M. Ozturk (Berlin: Springer), 1–21. doi: 10.1007/978-3-030-04408-4_1
- Neopane, P., Nepal, H. P., Shrestha, R., Uehara, O., and Abiko, Y. (2018). In vitro biofilm formation by *Staphylococcus aureus* isolated from wounds of hospital-admitted patients and their association with antimicrobial resistance. *Int. J. Gen. Med.* 11, 25–32. doi: 10.2147/IJGM.S153268
- Paharik, A. E., and Horswill, A. R. (2016). The Staphylococcal biofilm: adhesins, regulation, and host response. *Microbiol. Spectr.* 4:2. doi: 10.1128/microbiolspec.VMBF-0022-2015
- Phuong, N. T. M., Van Quang, N., Mai, T. T., Anh, N. V., Kuhakarn, C., Reutrakul, V., et al. (2017). Antibiofilm activity of α -mangostin extracted from *Garcinia mangostana* L. against *Staphylococcus aureus*. *Asian Pac. J. Trop. Med.* 10, 1154–1160. doi: 10.1016/j.apjtm.2017.10.022
- Pournajaf, A., Ardebili, A., Goudarzi, L., Khodabandeh, M., Narimani, T., and Abbaszadeh, H. (2014). PCR-based identification of methicillin-resistant *Staphylococcus aureus* strains and their antibiotic resistance profiles. *Asian Pac. J. Trop. Biomed.* 4, S293–S297. doi: 10.12980/APJTB.4.2014C423
- Reffuveille, F., Josse, J., Vallé, Q., Gangloff, C. M., and Gangloff, S. C. (2017). “*Staphylococcus aureus* biofilms and their impact on the medical field,” in *The Rise of Virulence and Antibiotic Resistance in Staphylococcus Aureus*, ed. S. Enany (London: IntechOpen), 187–214. doi: 10.5772/66380
- Resch, A., Rosenstein, R., Nerz, C., and Götz, F. (2005). Differential gene expression profiling of *Staphylococcus aureus* cultivated under biofilm and planktonic conditions. *Appl. Environ. Microbiol.* 71, 2663–2676. doi: 10.1128/AEM.71.5.2663-2676.2005
- Rohinishree, Y. S., and Negi, P. S. (2016). Effect of licorice extract on cell viability, biofilm formation and exotoxin production by *Staphylococcus aureus*. *J. Food Sci. Technol.* 53, 1092–1100. doi: 10.1007/s13197-015-2131-6
- Rubini, D., Banu, S. F., Nisha, P., Murugan, R., Thamotharan, S., Percino, M. J., et al. (2018). Essential oils from unexplored aromatic plants quench biofilm formation and virulence of Methicillin resistant *Staphylococcus aureus*. *Microb. Pathog.* 122, 162–173. doi: 10.1016/j.micpath.2018.06.028
- Sánchez, E., Rivas Morales, C., Castillo, S., Leos-Rivas, C., García-Becerra, L., and Mizael Ortiz Martínez, D. (2016). Antibacterial and Antibiofilm Activity of Methanolic Plant Extracts against Nosocomial Microorganisms. *Evid. Based Complement. Altern. Med.* 2016, 1–8. doi: 10.1155/2016/1572697
- Santajit, S., and Indrawattana, N. (2016). Mechanisms of Antimicrobial Resistance in ESKAPE Pathogens. *Biomed Res. Int.* 2016:2475067. doi: 10.1155/2016/2475067
- Selvaraj, A., Jayasree, T., Valliammai, A., and Pandian, S. K. (2019). Myrtenol Attenuates MRSA biofilm and virulence by suppressing *sarA* expression dynamism. *Front. Microbiol.* 10:2027. doi: 10.3389/fmicb.2019.02027
- Sharma, D., Misra, L., and Khan, A. U. (2019). Antibiotics versus biofilm: an emerging battleground in microbial communities. *Antimicrob. Resist. Infect. Control* 8:76. doi: 10.1186/s13756-019-0533-3
- Shukla, S. K., and Rao, T. S. (2017). *Staphylococcus aureus* biofilm removal by targeting biofilm-associated extracellular proteins. *Indian J. Med. Res.* 146, S1–S8. doi: 10.4103/ijmr.IJMR_410_15
- Simmler, C., Pauli, G. F., and Chen, S. N. (2013). Phytochemistry and biological properties of glabridin. *Fitoterapia* 90, 160–184. doi: 10.1016/j.fite.2013.07.003

- Singh, V., Pal, A., and Darokar, M. P. (2015). A polyphenolic flavonoid glabridin: oxidative stress response in multidrug-resistant *Staphylococcus aureus*. *Free Radic. Biol. Med.* 87, 48–57. doi: 10.1016/j.freeradbiomed.2015.06.016
- Singh, V. K., Utaida, S., Jackson, L. S., Jayaswal, R. K., Wilkinson, B. J., and Chamberlain, N. R. (2007). Role for dnaK locus in tolerance of multiple stresses in *Staphylococcus aureus*. *Microbiology* 153, 3162–3173. doi: 10.1099/mic.0.2007/009506-0
- Speziale, P., Pietrocola, G., Foster, T. J., and Geoghegan, J. A. (2014). Protein-Based biofilm matrices in staphylococci. *Front. Cell. Infect. Microbiol.* 4:171. doi: 10.3389/fcimb.2014.00171
- Stepanović, S., Vuković, D., Dakić, I., Savić, B., and Švabić-Vlahović, M. (2000). A modified microtiter-plate test for quantification of staphylococcal biofilm formation. *J. Microbiol. Methods* 40, 175–179. doi: 10.1016/s0167-7012(00)00122-6
- Suwannakul, S., and Chaibenjawong, P. (2017). Antibacterial Activities of *Glycyrrhiza gabra* Linn. (Licorice) Root Extract against *Porphyromonas gingivalis* and its inhibitory effects on cysteine proteases and biofilms. *J. Dent. Indones.* 24, 85–92. doi: 10.14693/jdi.v24i3.1075
- Tiwari, H. K., and Sen, M. R. (2006). Emergence of vancomycin resistant *Staphylococcus aureus* (VRSA) from a tertiary care hospital from northern part of India. *BMC Infect. Dis.* 6:156. doi: 10.1186/1471-2334-6-156
- Toledo-Arana, A., Merino, N., Vergara-Irigaray, M., Débarbouillé, M., Penadés, J. R., and Lasa, I. (2005). *Staphylococcus aureus* Develops an Alternative, ica-Independent Biofilm in the Absence of the arlRS Two-component system. *J. Bacteriol.* 15, 5318–5329. doi: 10.1128/JB.187.15.5318-5329.2005
- Tong, S. Y., Davis, J. S., Eichenberger, E., Holland, T. L., and Fowler, V. G. (2015). *Staphylococcus aureus* infections: epidemiology, pathophysiology, clinical manifestations, and management. *Clin. Microbiol. Rev.* 28, 603–661. doi: 10.1128/CMR.00134-14
- Vuong, C., Saenz, H. L., Gotz, F., and Otto, M. (2000). Impact of the agr quorum sensing system on adherence to polystyrene in *Staphylococcus aureus*. *J. Infect. Dis.* 182, 1688–1693. doi: 10.1086/317606
- Wang, L., Yang, R., Yuan, B., Liu, Y., and Liu, C. (2015). The antiviral and antimicrobial activities of licorice, a widely used Chinese herb. *Acta Pharm. Sin. B* 5, 310–315. doi: 10.1016/j.apsb.2015.05.005
- Wang, Y., Yi, L., Zhang, Z., Fan, H., Cheng, X., and Lu, C. (2014). Biofilm Formation, Host-Cell Adherence, and Virulence Genes Regulation of *Streptococcus suis* in Response to Autoinducer-2 Signaling. *Curr. Microbiol.* 68, 575–580. doi: 10.1007/s00284-013-0509-0
- Wolz, C., Pöhlmann-Dietze, P., Steinhuber, A., Chien, Y. T., Manna, A., van Wamel, W., et al. (2000). Agr-independent regulation of fibronectin binding protein(s) by the regulatory locus sar in *Staphylococcus aureus*. *Mol. Microbiol.* 36, 230–243. doi: 10.1046/j.1365-2958.2000.01853.x
- Yarwood, J. M., Bartels, D. J., Volper, E. M., and Greenberg, E. P. (2004). Quorum sensing in *Staphylococcus aureus* biofilms. *J. Bacteriol.* 186, 1838–1850. doi: 10.1128/jb.186.6.1838-1850.2004
- Ythier, M., Resch, G., Waridel, P., Panchaud, A., Gfeller, A., Majcherzyk, P., et al. (2012). Proteomic and transcriptomic profiling of *Staphylococcus aureus* surface LPXTG-proteins: correlation with agr genotypes and adherence phenotypes. *Mol. Cell Proteomics* 11, 1123–1139. doi: 10.1074/mcp.M111.014191
- Zimaro, T., Thomas, L., Marondedze, C., Garavaglia, B. S., Gehring, C., Ottado, J., et al. (2013). Insights into xanthomonas axonopodis pv. citri biofilm through proteomics. *BMC Microbiol.* 13:186. doi: 10.1186/1471-2180-13-186
- Zipfel, C. (2008). Pattern-recognition receptors in plant innate immunity. *Curr. Opin. Immunol.* 20, 10–16. doi: 10.1016/j.coi.2007.11.003

Conflict of Interest: The authors declare that the research was conducted in the absence of any commercial or financial relationships that could be construed as a potential conflict of interest.

Copyright © 2020 Gangwar, Kumar and Darokar. This is an open-access article distributed under the terms of the Creative Commons Attribution License (CC BY). The use, distribution or reproduction in other forums is permitted, provided the original author(s) and the copyright owner(s) are credited and that the original publication in this journal is cited, in accordance with accepted academic practice. No use, distribution or reproduction is permitted which does not comply with these terms.



Antimicrobial Hypochlorous Wound Irrigation Solutions Demonstrate Lower Anti-biofilm Efficacy Against Bacterial Biofilm in a Complex *in-vitro* Human Plasma Biofilm Model (hpBIOM) Than Common Wound Antimicrobials

Julian-Dario Rembe^{1*}, Lioba Huelsboemer^{2†}, Isabell Plattfaut², Manuela Besser² and Ewa K. Stuermer³

OPEN ACCESS

Edited by:

Sujogya Kumar Panda,
KU Leuven, Belgium

Reviewed by:

Idalina Machado,
University of Porto, Portugal
Tim Maisch,
University of Regensburg, Germany
Seok Hong,
Northwestern University,
United States

*Correspondence:

Julian-Dario Rembe
julian-dario.rembe@uni-wh.de

[†]These authors share first authorship

Specialty section:

This article was submitted to
Antimicrobials, Resistance and
Chemotherapy,
a section of the journal
Frontiers in Microbiology

Received: 21 May 2020

Accepted: 11 September 2020

Published: 09 October 2020

Citation:

Rembe JD, Huelsboemer L,
Plattfaut I, Besser M and
Stuermer EK (2020) Antimicrobial
Hypochlorous Wound Irrigation
Solutions Demonstrate Lower Anti-
biofilm Efficacy Against Bacterial
Biofilm in a Complex *in-vitro* Human
Plasma Biofilm Model (hpBIOM) Than
Common Wound Antimicrobials.
Front. Microbiol. 11:564513.
doi: 10.3389/fmicb.2020.564513

¹Department of Vascular and Endovascular Surgery, University Hospital Düsseldorf, Heinrich-Heine-University of Düsseldorf, Düsseldorf, Germany, ²Chair for Translational Wound Research, Centre for Biomedical Education and Research, Witten/Herdecke University, Witten, Germany, ³Department of Vascular Medicine, University Heart and Vascular Center Hamburg, Translational Wound Research, University Medical Centre Hamburg-Eppendorf, Hamburg, Germany

Biofilms pose a relevant factor for wound healing impairment in chronic wounds. With 78% of all chronic wounds being affected by biofilms, research in this area is of high priority, especially since data for evidence-based selection of appropriate antimicrobials and antiseptics is scarce. Therefore, the objective of this study was to evaluate the anti-biofilm efficacy of commercially available hypochlorous wound irrigation solutions compared to established antimicrobials. Using an innovative complex *in-vitro* human plasma biofilm model (hpBIOM), quantitative reduction of *Pseudomonas aeruginosa*, *Staphylococcus aureus*, and Methicillin-resistant *S. aureus* (MRSA) biofilms by three hypochlorous irrigation solutions [two <0.08% and one 0.2% sodium hypochlorite (NaClO)] was compared to a 0.04% polyhexanide (PHMB) irrigation solution and 0.1% octenidine-dihydrochloride/phenoxyethanol (OCT/PE). Efficacy was compared to a non-challenged planktonic approach, as well as with increased substance volume over a prolonged exposure (up to 72 h). Qualitative visualization of biofilms was performed by scanning electron microscopy (SEM). Both reference agents (OCT/PE and PHMB) induced significant biofilm reductions within 72 h, whereby high volume OCT/PE even managed complete eradication of *P. aeruginosa* and MRSA biofilms after 72 h. The tested hypochlorous wound irrigation solutions achieved no relevant penetration and eradication of biofilms despite increased volume and exposure. Only 0.2% NaClO managed a low reduction under prolonged exposure. The results demonstrate that low-dosed hypochlorous wound irrigation solutions are significantly less effective than PHMB-based irrigation solution and OCT/PE, thus unsuitable for biofilm eradication on their own. The used complex hpBIOM thereby mimics the highly challenging clinical wound micro-environment, providing a more profound base for future clinical translation.

Keywords: wound infection, biofilm, antimicrobial, antiseptic, hypochlorous acid, human plasma biofilm model, wound irrigation, chronic wound

INTRODUCTION

In wound management, controlling microbial bioburden is a key factor of prophylactic and therapeutic regimes. While wound contamination and colonization can mostly be handled with vigilance and mechanical cleansing, local infection with the potential threat of systemic spread requires antimicrobial intervention (IWII, 2016). Possible interventions range from preserved antimicrobials-containing wound irrigation solutions to antiseptics, debridement and systemic antibiotics in case of systemic spread. Biofilm formation thereby represents a specifically difficult to diagnose and manage complication in wound therapy. According to recent evaluations, over 78% of all chronic wounds are challenged by biofilm formation (Malone et al., 2017). Biofilms are structured communities of microorganisms attached to a surface (e.g., wound bed) encased within an extracellular matrix (ECM) referred to as the extracellular polymeric substance (EPS; Percival et al., 2015). Microorganisms embedded in the EPS demonstrate a significant tolerance and resilience to antimicrobial substances, biocides, and the host immunity due to a variety of factors such as polymicrobial heterogeneity, genetic diversity, and resistance transfer, dormant metabolism and the EPS itself functioning as a high-protein mechanical and diffusion barrier for antimicrobials (Hall-Stoodley and Stoodley, 2009; Hoiby et al., 2010; Percival et al., 2015; Salisbury et al., 2018). As a result, wound antimicrobials and antiseptics need to be thoroughly investigated regarding their anti-biofilm efficacy (Schultz et al., 2017).

Several *in-vitro* models have been applied for this purpose, growing wound biofilms on plastic or metal surfaces, in many cases without additional organic and/or human material (Brackman and Coenye, 2016; Schultz et al., 2017; Shukla et al., 2020). Such approaches are feasible for evaluating biocides and disinfectants for (surface) decontamination, but in case of wound antimicrobials, the more complex composition of the wound microenvironment (cytokines, proteases, fibrin, cells, etc.) with high-protein, organic challenge as well as the human immune system need to be considered. Therefore, our research group developed an innovative human plasma biofilm model (hpBIOM) for quantifiable testing of anti-biofilm activity of antimicrobial and antiseptic agents in a challenging wound biofilm environment, aiming to resemble the *in-vivo* situation (Besser et al., 2019, 2020).

Due to the recent renaissance of hypochlorous acid based antimicrobial wound irrigation solutions (Severing et al., 2019) with contrasting evidence regarding anti-biofilm efficacy, this study focused on the evaluation of these agents compared to

established antimicrobial and antiseptic agents. Prolonged exposure times, increased substance volumes, and varying agents (with differing substance concentrations) were investigated using the hpBIOM and compared to a planktonic test setup to provide a comprehensive analysis.

MATERIALS AND METHODS

Microbial Strains

Staphylococcus aureus (DSM-799) and *Pseudomonas aeruginosa* (DSM-939; both German Collection of Microorganisms and Cell Cultures (DSMZ), Braunschweig, Germany) as well as a clinical MRSA strain (provided by the Institute for Medical Laboratory Diagnostics, Helios University Hospital Wuppertal, Germany) were selected. All strains were previously tested for biofilm formation on plastic surfaces (data not shown). All strains were cultivated on casein/soy peptone agar plates (CSA) according to standard protocols and the second subculture was used for experiments.

Antimicrobials and Antiseptics

Five antimicrobial solutions in total (Table 1) were evaluated. Three chlorine-based and -releasing agents, used as antimicrobial wound irrigation solutions: ActiMaris® forte [0.2% sodium hypochlorite (NaClO)/3% sal maris; AMF], Lavanox® (<0.08% NaClO; LVX), and Kerrasol® (<0.08% NaClO; KSL).

As reference substances, a polyhexanide (PHMB)-based antimicrobial irrigation solution (Lavasorb®; 0.04% PHMB) and the antiseptic Octenidine-dihydrochloride/phenoxylethanol (Octenisept®; 0.1% OCT/PE) were used. All products were handled in a sterile manner and according to manufacturer instructions.

Neutralizing Agent and Dissolving Solution

To stop antimicrobial activity after specific designated exposure times, a neutralizing solution was used comprising of 40 g Tween 80, 30 g saponin, 4 g lecithin, 3 g sodium thiosulfate (all Carl Roth GmbH & Co. KG, Karlsruhe, Germany) and 10 g sodium dodecyl sulfate (SDS; Caesar & Loretz GmbH, Hilden, Germany), and 500 ml double distilled H₂O (ddH₂O). The neutralizing solution composition was based on specifications from the standards (DIN EN 13727; DIN, 2013). Concentration, volume, and efficacy of the neutralizing solution have been preliminarily validated internally and demonstrated a sufficient

TABLE 1 | Overview of the tested antiseptics and antimicrobial wound irrigation solutions, product specifications, manufacturer, and composition as specified by the manufacturer.

Test solution	Product	Manufacturer	Composition	Category
OCT/PE	Octenisept®	Schülke & Mayr GmbH	0.1 g octenidin-dihydrochlorid, 2.0 g 2-phenoxyethanol (per 100 ml)	Antiseptic
PHMB	Lavasorb®	Fresenius Kabi AG	0.4 g polyhexanide, 0.02 g macrogolum 4,000 (per 1,000 ml)	Antimicrobial irrigation solution
	AMF	ActiMaris® forte	ActiMaris AG	Antimicrobial irrigation solution
NaClO	LVX	Lavanox®	Serag Wiessner GmbH & Co KG	Antimicrobial irrigation solution
	KSL	KerraSol™	Crawford Healthcare GmbH	Antimicrobial irrigation solution

neutralizing efficacy for all tested antiseptics and antimicrobials, non-toxicity toward microbial strains used in a planktonic, as well as a biofilm setup and showed no interference with the integrity of the biofilm model.

For dissolving the model after successful conduction of experiments to recover and quantify surviving microorganisms, a 10% (w/v) bromelain solution was used, as bromelain exhibits a fibrinolytic activity and has been previously used for debridement and biofilm dispersal purposes (Maurer, 2001; Pavan et al., 2012; Besser et al., 2019, 2020). Therefore, 10 tablets of Bromelain-POS® (500 F.I.P. units per tablet; URSAPHARM Arzneimittel GmbH, Saarbrücken, Germany) were dissolved in 100 ml phosphate buffered saline (PBS) and the solution stored at 4°C until further use. Bromelain was later added to the model in a 1:1 (v/v) ratio to the model volume (1.5 ml per model). Before usage, bromelain was warmed to 37°C for improved enzyme performance. The bromelain solution has been preliminarily tested and validated and showed no antimicrobial effect of its own.

Human Plasma Biofilm Model Preparation

The development and use of the hpBIOM has been described in detail elsewhere (Besser et al., 2019, 2020) and was adapted to fit the specific agents and purpose pursued here. In brief, human plasma (citrate buffered) and buffy coat from anonymous donors were obtained from the DRK-Blutspendedienst West (Hagen, Germany). To remove as many residual erythrocytes as possible, the buffy coat was centrifuged at 3,000 rpm at room temperature (RT) for 30 min. Subsequently, plasma and buffy coat were merged, gently mixed in a sterile glass bottle, and continuously agitated at 22°C. A microbial test suspension was prepared by colony picking and adjusted to a 0.5 McFarland standard ($\sim 1.5 \times 10^8$ cfu/ml) using a spectrophotometer (EON™; BioTek Germany, Bad Friedrichshall, Germany). Finally, a “master mix” was prepared by adding the appropriate amount of microbial test solution to the plasma and buffy coat mixture, resulting in a final bacterial concentration of $\sim 1.5 \times 10^6$ cfu per individual hpBIOM. Next, 18.26 µl calcium chloride (CaCl₂; 500 mM) per ml plasma was added to the master mix, to induce fibrin polymerization, gently mixed, and immediately transferred into 12-well plates (1.5 ml per model/well containing plasma, buffy coat, and pathogenic bacteria). The plates were incubated for 12 h on a rotation shaker at 50 rpm and 37.0°C for the plasma solution to polymerize with pathogens rearranging and forming an ECM, finally yielding a stable biofilm disc/clot with integrated bacteria (\sim concentration of 1.5×10^7 cfu/ml), EPS as well as human plasma and immune cells.

Antimicrobial Treatment of the hpBIOM and Quantification of Bacterial Survival

After hpBIOM preparation, each clot was treated with 300 µl of antiseptic/antimicrobial test substance for 0.5, 2, 6, and 24 h. To additionally investigate the effect of prolonged exposure (in terms of remanence effect without reapplication) and/or increased substance volume (1 ml), experiments were additionally extended to 48 and 72 h with 300 µl or 1 ml of active substance

against the clinically isolated MRSA strain and *P. aeruginosa*. After the specified treatment periods, antimicrobial activity was neutralized by adding 1.2 ml of the specified neutralizing solution to each well, detaching the model from the well walls with a pipette tip (in order to fully distribute the neutralizing solution around the model) and placing the plates on a rotation shaker at RT for 5 min \pm 10 s. Subsequently, each hpBIOM was carefully transferred into a 15 ml falcon tube with 1 ml bromelain solution for dissolving the model. An additional 0.5 ml of bromelain solution was used to wash out the well to detach remaining microorganisms and added to the falcon tube.

In case of the 1 ml test setup, models were already detached and transferred into 15 ml falcon tubes for neutralization, due to the higher necessary amount of neutralizing solution (4 ml to keep a 1:8 ratio) and bromelain subsequently added to the tube after neutralization. After 2–3 h, the hpBIOM was completely dissolved. For quantification, the resulting solution was thoroughly vortexed, serially tenfold diluted, 50 µl of each dilution spread on agar plates and incubated overnight at 37°C under aerobic conditions. Remaining microbial counts after treatment were quantified by determining colony counts (in cfu/ml) using a Colony Counter Pen (eCount™, VWR Leicestershire, United Kingdom) and reduction rates calculated compared to an untreated control, as well as initial bacterial counts.

Quantitative Suspension Method

To compare the anti-biofilm efficacy of the tested antiseptics and antimicrobials to the efficacy on planktonic bacteria, all tested substances were additionally evaluated using a quantitative suspension method (QSM). The QSM is based on DIN EN 13727 (DIN, 2013) and has been modified for direct comparison to the hpBIOM. Thereby, a bacterial test suspension was prepared by colony picking, adjusted to 1.5×10^7 cfu/ml initial concentration (as for hpBIOM) and 1.5 ml of the prepared bacterial test suspension was treated with 300 µl of the respective antiseptic or antimicrobial for 0.5, 2, 6, or 24 h. To neutralize antimicrobial activity, 1.2 ml neutralizing solution was added and the samples subsequently incubated for 5 min \pm 10 s on a rotation shaker at RT. Reduction rates (in cfu/ml) were quantified in the same manner as described for hpBIOM.

Visualization of Biofilm Using Scanning Electron Microscopy

To visualize the morphology and structure of the bacterial biofilm with and without antiseptic/antimicrobial treatment, scanning electron microscopy (SEM) was performed for selected experimental setups (see Table 2). After neutralization of the antiseptic/antimicrobial agents, the models were fixed with a glutaraldehyde/PVP-solution containing 2.5% glutaraldehyde, 2% polyvinylpyrrolidone (PVP), and 0.5% sodium nitrite (NaNO₂) in 0.1 M cacodylate buffer for 1 h at 4°C. Samples were washed in 0.1 M cacodylate buffer and stored at 4°C until preparation of freeze fracture fragments with liquid nitrogen. For glycocalyx staining, the samples were subsequently incubated in a solution containing 2% arginine-hydrochloride (HCL), glycine, sucrose, and

TABLE 2 | Specification and overview of the experimental setups used for visualization of biofilm formation in the human plasma biofilm model (hpBIOM) using scanning electron microscopy (SEM).

Image	Setup/ substance	Pathogen	Maturation time*	Treatment period
4 (a)	CTRL	<i>P. aeruginosa</i>	12 h	-
4 (b)	CTRL	<i>P. aeruginosa</i>	18 h	-
4 (c)	CTRL	<i>P. aeruginosa</i>	36 h	-
5 (a)	CTRL	<i>P. aeruginosa</i>	12 h	0 h
5 (b)	OCT/PE	<i>P. aeruginosa</i>	12 h	6 h
5 (c)	OCT/PE	<i>P. aeruginosa</i>	12 h	24 h
5 (d)	NaOCl (<0.08%)	<i>P. aeruginosa</i>	12 h	24 h

Figures 4A–C demonstrate a representative biofilm development over time.

Figures 5A–D show the biofilm surface structure under treatment with antiseptics (OCT/PE) or antimicrobial wound irrigation solution (<0.08% NaOCl) over time compared to the initial structure. *Before application of test substance, if any (not in case of CTRL).

sodium glutamate for 18 h at RT. The samples were rinsed with ddH₂O and 0.1 M cacodylate buffer followed by immersion in a mixture of 2% tannic acid and guanidine-HCL for 5.5 h at RT. After another rinsing step with ddH₂O and 0.1 M cacodylate buffer samples were incubated over night at 4°C. For staining, the samples were placed in a 1% osmium tetroxide (OsO₄) solution for 30 min at RT. After three rinsing steps with 0.1 M cacodylate buffer, the samples were again stored over night at 4°C. Finally, samples were dehydrated using isopropyl alcohol and acetone and dried in liquid CO₂ using a critical point dryer (BAL-TEC AG, Balzers, Liechtenstein). Via the sputter coater (BAL-TEC AG, Balzers, Liechtenstein), samples were sputtered with gold palladium and finally examined with a Zeiss Sigma SEM (Zeiss, Oberkochen, Germany) using 2 kV acceleration voltage and an inlens detector.

Statistical Analysis

All experiments were performed in triplicates with three different anonymous donors. Microbial reduction rates (in $\Delta\log_{10}$ cfu/ml) were calculated for all tested antiseptic/antimicrobial solutions. High antimicrobial efficacy is defined as a reduction in initial microbial counts by at least 3 \log_{10} reduction steps, as defined for antiseptics tested under organic challenge by national and international standards (DIN, 2013). Data are expressed as means \pm standard error of the mean (*sem*) and were analyzed using the statistics program GraphPad PRISM (Version 8.2.1; GraphPad Software Inc., La Jolla, United States). Statistical analysis was performed using two-way ANOVA, followed by Holm-Sidak *posthoc* test for evaluation of multiple comparisons. A value of $p \leq 0.05$ was considered statistically significant (* $p \leq 0.05$; ** $p \leq 0.01$; *** $p \leq 0.001$; and **** $p \leq 0.0001$).

RESULTS

Antimicrobial Efficacy on Planktonic Bacteria (QSM) Within 24 h

On bacteria in a planktonic state, the three tested antimicrobial hypochlorous wound irrigation solutions containing NaClO/

hypochlorous acid (HClO) demonstrated no bacterial reduction against any tested pathogen within 24 h (Figure 1).

Both reference substances, OCT/PE and PHMB-based irrigation solution, achieved a highly significant reduction of *P. aeruginosa* (4.77 ± 1.41 and $5.25 \pm 0.93 \log_{10}$ steps, respectively; $p < 0.0001$), *S. aureus* (6.18 ± 0.00 and $4.82 \pm 1.36 \log_{10}$ steps; $p < 0.0001$), and MRSA (both $6.18 \pm 0.00 \log_{10}$ steps; $p < 0.0001$) within 30 min of exposure (Figures 2A–C). After 2 h of exposure, OCT/PE and PHMB both fully eradicated all three tested pathogens, except PHMB against *S. aureus*, needing 6 h for complete eradication (Figure 2C).

All reduction rates of the QSM are summarized in Supplementary Table 1.

Anti-biofilm Efficacy (hpBIOM) Within 24 h

As in the QSM, the tested hypochlorous wound irrigation solutions showed no antimicrobial/anti-biofilm activity in the complex biofilm model (hpBIOM). No bacterial reduction could be observed against any tested pathogen within 24 h (Figure 1).

The tested reference substances showed a reduced effect within 24 h: against a methicillin-resistant (MRSA) as well as a methicillin-susceptible (MSSA) *S. aureus* biofilm, PHMB showed no statistically significant reduction within 24 h compared to an untreated control (Figures 2B,C; $p = 0.90/0.93$), while OCT/PE managed a statistically significant low reduction of 0.83 ± 0.23 (Figure 2B; $p = 0.014$) and $1.28 \pm 0.32 \log_{10}$ steps (Figure 2C; $p = 0.0002$).

A higher efficacy could be observed against *P. aeruginosa* biofilms. Both antiseptics induced a statistically significant reduction within 24 h of treatment compared to the control, whereby OCT/PE achieved $2.68 \pm 0.46 \log_{10}$ steps ($p = 0.0008$) and PHMB $2.97 \pm 0.59 \log_{10}$ steps (Figure 2A; $p = 0.0002$).

Anti-biofilm Efficacy (hpBIOM) Under Prolonged Exposure (up to 72 h) and/or Increased Substance Volume (1 ml)

Prolonged exposure times of up to 72 h for 0.3 ml OCT/PE and PHMB increased bacterial reduction of all three pathogens with a continuous decrease in bacterial counts yielding highest reductions after 72 h of exposure compared to the untreated control (Figures 2A–C). For MRSA and MSSA, OCT/PE reached higher overall reduction rates than PHMB after 72 h (MRSA: 4.45 ± 1.73 vs. $0.96 \pm 0.79 \log_{10}$; MSSA: 2.19 ± 0.29 vs. $0.97 \pm 0.79 \log_{10}$; Figures 2B,C). Against *P. aeruginosa* biofilms, PHMB achieved higher reduction rates than OCT/PE after 72 h (4.23 ± 1.95 vs. $3.54 \pm 1.34 \log_{10}$; Figure 2A). In case of antimicrobial hypochlorous irrigation solutions, a prolonged exposure with 0.3 ml showed no improved effect (Figure 1).

When increasing the substance volume per treatment to 1.0 ml, both OCT/PE and PHMB demonstrated a significant increase of bacterial reduction within 24 h compared to 0.3 ml (Figure 3). OCT/PE achieved a nearly complete eradication of MRSA and *P. aeruginosa* after 24 h and especially against MRSA biofilms, it showed a significantly higher reduction than PHMB (5.64 ± 0.53 vs. $1.63 \pm 0.63 \log_{10}$; $p < 0.0001$; Figure 3B). For hypochlorous solutions, an increase in volume did not

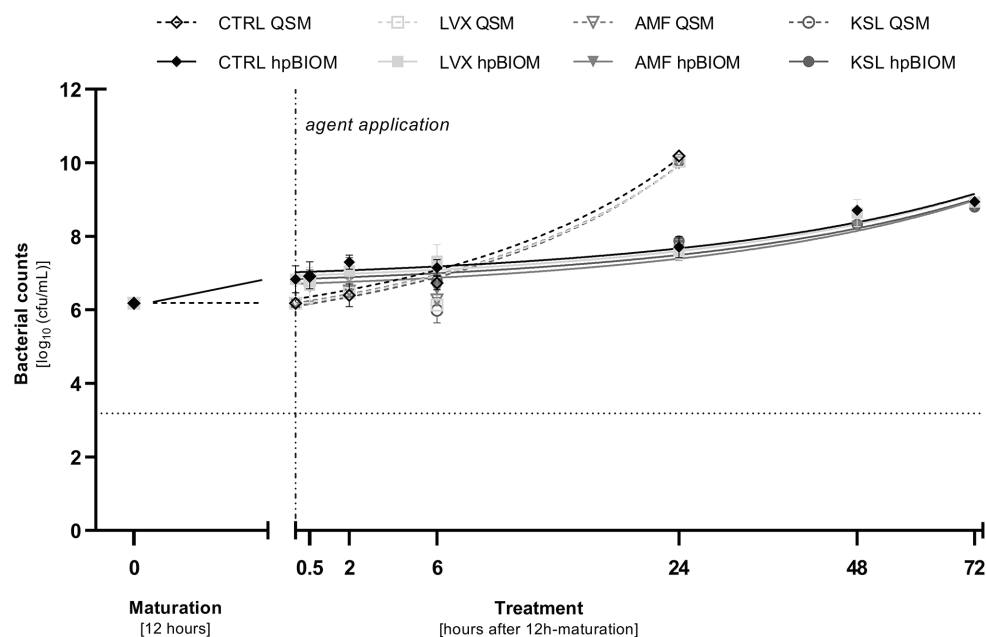


FIGURE 1 | Reduction rates of 0.3 ml of tested antimicrobial irrigation solutions Lavanox® (LVX; <0.08% NaClO), Kerrasol® (KSL; <0.08% NaClO), and Actimaris®forte (AMF; 0.2% NaClO, 3% sal maris) compared to an untreated control (CTRL) in planktonic (QSM) and biofilm (hpBIOM) form (here against *Pseudomonas aeruginosa*). Bacterial counts (in log₁₀ cfu/ml) are outlined over the course of 72 h of treatment after an initial biofilm maturation period of 12 h. Dotted horizontal line indicates the cut-off for a high antimicrobial efficacy (≥ 3 log₁₀ reduction steps). Dashed vertical line indicates onset of treatment with the different antimicrobial agents after 12 h of biofilm maturation. Values are expressed as means \pm standard error of the mean (*sem*) and time-kill-curves of bacteria in planktonic state (QSM) are only depicted for 24 h. All experiments were performed in triplicates.

result in an increase in antimicrobial efficacy within 24 h (Supplementary Table 2).

The highest anti-biofilm efficacy was observed under the combination of prolonged exposure and increased substance volume of 1 ml (Figures 3A,B). OCT/PE managed to completely eradicate both MRSA and *P. aeruginosa* biofilms after 72 h. In case of *P. aeruginosa* biofilms, PHMB achieved full eradication before OCT/PE, after only 48 h (Figure 3A), while against MRSA it proved significantly less effective (2.73 log₁₀ reduction steps less than OCT/PE after 72 h; $p = 0.0004$), not achieving complete eradication and even demonstrating a certain regrowth between 48 and 72 h (Figure 3B).

In terms of the antimicrobial hypochlorous solutions, the highest concentrated product (AMF; 0.2% sodium hypochlorite) demonstrated a low bacterial reduction against MRSA biofilm of 1.35 ± 0.58 log₁₀ steps ($p = 0.0016$) after 48 h. However, regrowth between 48 and 72 h could be observed (Figure 3B) as well.

Scanning Electron Microscopy of the hpBIOM

The monitoring and visualization of the hpBIOM using SEM (representative imaging provided from *P. aeruginosa* biofilms; Table 2) showed a good maturation and development of the biofilm with initial microcolony formation and subsequent development of EPS/glycocalyx, encapsulating bacteria (Figure 4) within 18 h. After 36 h of maturation, a densely formed surface

of interconnected, polymerized fibrins with encapsulated bacteria and densely distributed EPS can be observed.

Under treatment with hypochlorous solutions and antiseptics compared to no treatment, a loss in surface density of the biofilm model can be observed with increasing treatment time of the antiseptic OCT/PE (Figure 5). After 6 h of treatment, the biofilm surface shows an increased number of holes and less integrity compared to the initial untreated surface structure (Figure 5B). After 24 h of treatment, the surface is deranged and “broken-open” into a loosened structure with fine filaments, readily penetrable by OCT/PE (Figure 5C). After 24 h of treatment with <0.08% NaClO, the surface structure remained densely connected without visual loosening of surface structure or holes (Figure 5D). Additionally, newly build-up superficial EPS structures appeared, covering some area of the biofilm surface structure.

DISCUSSION

Biofilms pose a great challenge in chronic wound care and are a major factor for wound chronicity and impaired healing (James et al., 2008; Percival and Suleman, 2015; IWII, 2016; Percival, 2017; Schultz et al., 2017). Adequately addressing this challenge by improving knowledge and developing precise, comprehensive and new therapeutic strategies, including accurate agent efficacy profiles, is an important research goal in modern

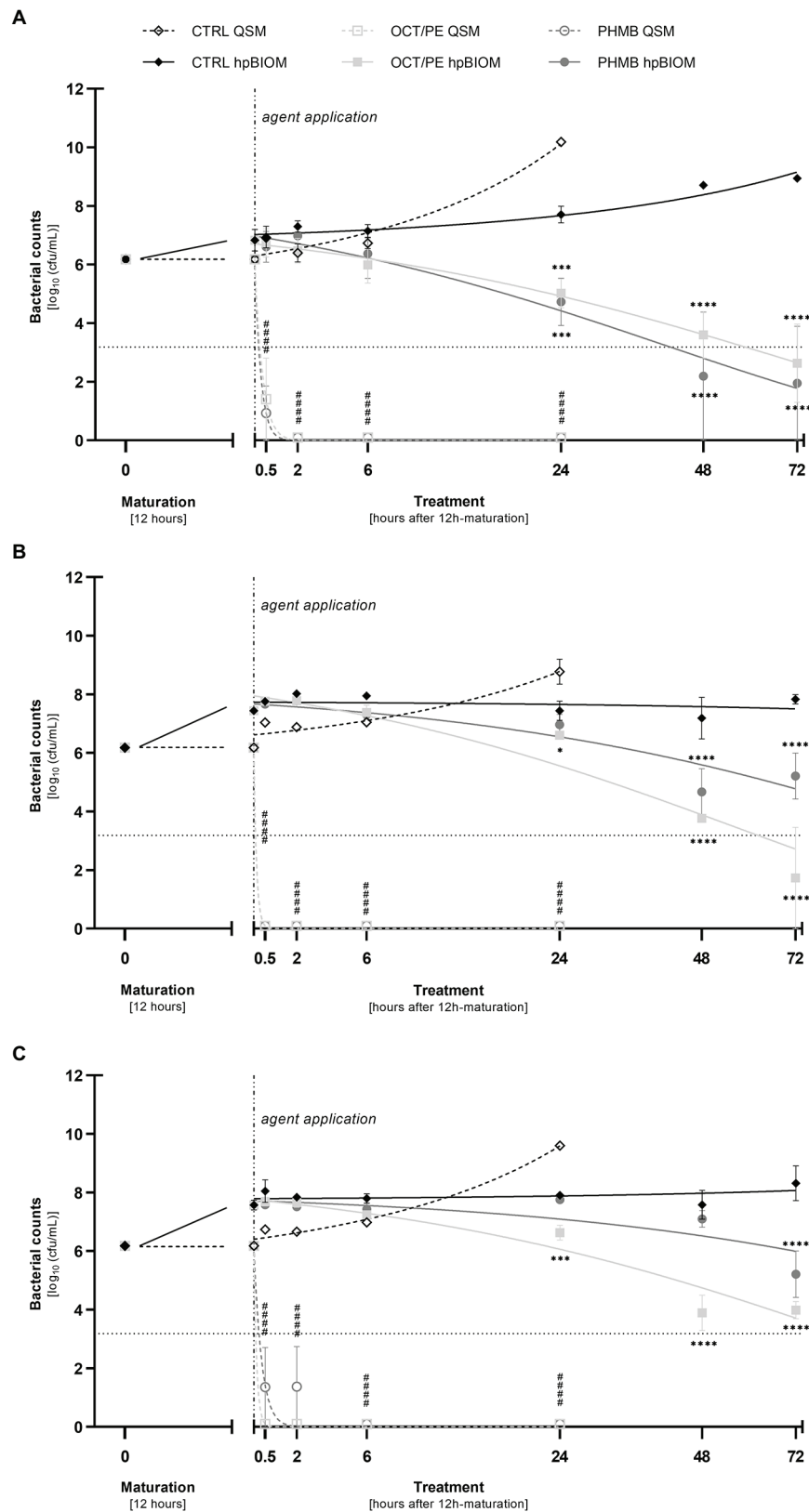


FIGURE 2 | (Continued)

FIGURE 2 | Reduction of *P. aeruginosa* (A), MRSA (B), and *S. aureus* (C) in planktonic (QSM) vs. biofilm (hpBIOM) form by 0.3 ml of tested antiseptics octenidine-dihydrochloride/phenoxylethanol (OCT/PE) and polyhexanide (PHMB) compared to an untreated control (CTRL). Remaining bacterial counts (in \log_{10} cfu/ml) are outlined over the course of 72 h of treatment after an initial biofilm maturation period of 12 h. Dotted horizontal line indicates the cut-off for a high antimicrobial efficacy ($\geq 3 \log_{10}$ reduction steps). Dashed vertical line indicates onset of treatment with the different antimicrobial agents after 12 h of biofilm maturation. Values are expressed as means \pm sem. Significant reductions compared to the untreated control are expressed as * $p \leq 0.05$, ** $p \leq 0.01$, *** $p \leq 0.001$, or **** $p \leq 0.0001$ (# in case of QSM). All experiments were performed in triplicates [Time-kill-curves of bacteria in planktonic state (QSM) are only depicted for 24 h].

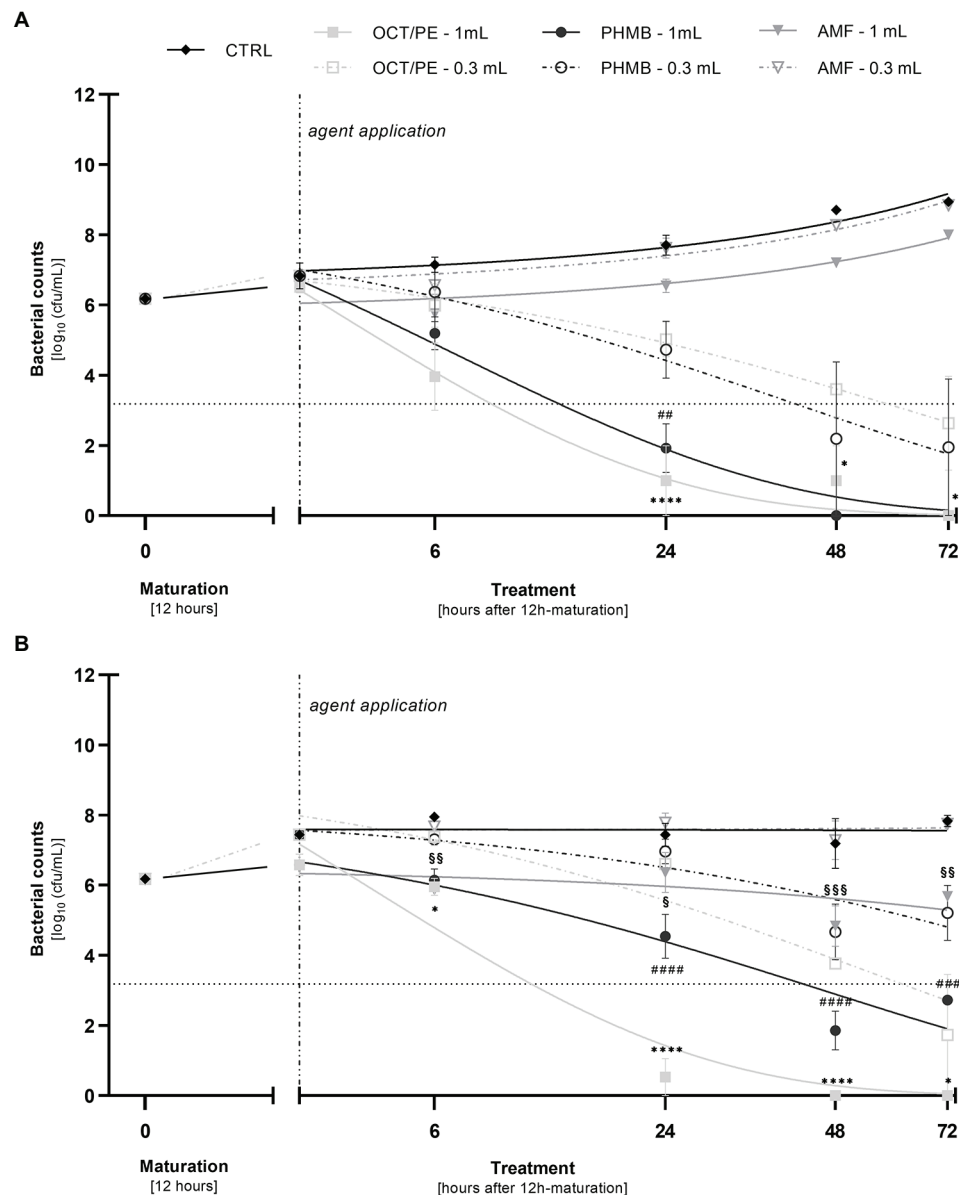


FIGURE 3 | Comparison of the reduction of *P. aeruginosa* (A) and MRSA (B) in the biofilm model (hpBIOM) between 0.3 and 1.0 ml of tested antimicrobial substances in a prolonged exposure of up to 72 h. Graphs depict bacterial counts (in \log_{10} cfu/ml) after treatment with octenidine-dihydrochloride/phenoxylethanol (OCT/PE), polyhexanide (PHMB), or 0.2% sodium hypochlorite (AMF) compared to an untreated control (CTRL). Values are expressed as means \pm sem and a significant increase in reduction under 1.0 ml substance volume is expressed as * $p \leq 0.05$, ** $p \leq 0.01$, *** $p \leq 0.001$, or **** $p \leq 0.0001$ (* for PHMB; # for OCT/PE, and \$ for AMF). Dotted horizontal line indicates the cut-off for a high antimicrobial efficacy ($\geq 3 \log_{10}$ reduction steps). Dashed vertical line indicates onset of treatment with the different antimicrobial agents after 12 h of biofilm maturation. All experiments were performed in triplicates.

wound management (Schultz et al., 2017; Schwarzer et al., 2019; Stoffel et al., 2020).

Due to the extensive resilience of microorganisms residing within polymicrobial communities protected by EPS, rigorous and highly efficient anti-biofilm regimens are necessary. A form of repetitive, effective debridement represents the fundamental base of current anti-biofilm strategies (Wolcott et al., 2010; IWII, 2016; Schultz et al., 2017). Debridement alone, however, is insufficient for complete biofilm eradication (Schwartz et al., 2014; Schultz et al., 2017), as is the lone application of (even highly efficient) antimicrobial and antiseptic agents, making a combination of both approaches the current gold standard (Hoiby et al., 2015; Koo et al., 2017; Schultz et al., 2017). However, reported data on efficacy of available antimicrobial and antiseptic agents varies greatly depending on various factors and to date no agent can be clearly favored as being best suited for the treatment of chronic wound biofilms (Schultz et al., 2017; Schwarzer et al., 2019). Foremost, heterogeneity in study design/experimental setup and lacking transferability from adequate *in-vitro* to *in-vivo* studies and the clinical reality have been identified as a main limitation in current research (Schwarzer et al., 2019; Stoffel et al., 2020).

Another major concern is the sometimes liberal extrapolation of results in basic “non-challenging” test scenarios (e.g., antimicrobial efficacy in planktonic assays or biofilms grown on plastic surfaces without introduction of organic load) to clinical “real-world” situations. The significant differences in efficacy between a standard planktonic (DIN EN 13727; DIN, 2013) and *in-vitro* biofilm assay as well as between different forms of biofilm assays have been demonstrated before (Brackman and Coenye, 2016; Johani et al., 2018; Shukla et al., 2020) and could be reproduced in this study (**Figures 2A–C**) when comparing reduction rates of QSM to hpBIOM. Where bacteria in a planktonic state are easily eradicated by the antiseptic OCT/PE and the PHMB-based antimicrobial irrigation solution within 30 min, reduction rates are significantly reduced in the more complex hpBIOM (**Figures 2A–C**) which introduces organic challenge faced by antimicrobial agents in human biofilm-burdened chronic wounds (higher protein load, hard-to-penetrate EPS structure, immune cells, dormant bacteria, etc.). These results emphasize the dependency of an agent’s performance based on the environment it acts in and are calling for more comprehensive testing of agents before recommendations can be declared.

Most static and liquid-flow-based *in-vitro* models are limited to factors such as growth on plastic surfaces and lack adequate organic conditions reflecting a wound environment, let alone the heterogenous, individual conditions in human chronic wound biofilms (Brackman and Coenye, 2016). The development of the hpBIOM (**Figures 4A–C**; Besser et al., 2019, 2020) aimed to narrow the gap between *in-vitro* and *in-vivo* biofilm research and provides a translational approach. The use of a complex biofilm model based on human material, including plasma and immune cells, addresses the interactions of microbial biofilms with the human wound micro-environment (James et al., 2008; Percival et al., 2015), as well as the relevant loss in efficacy

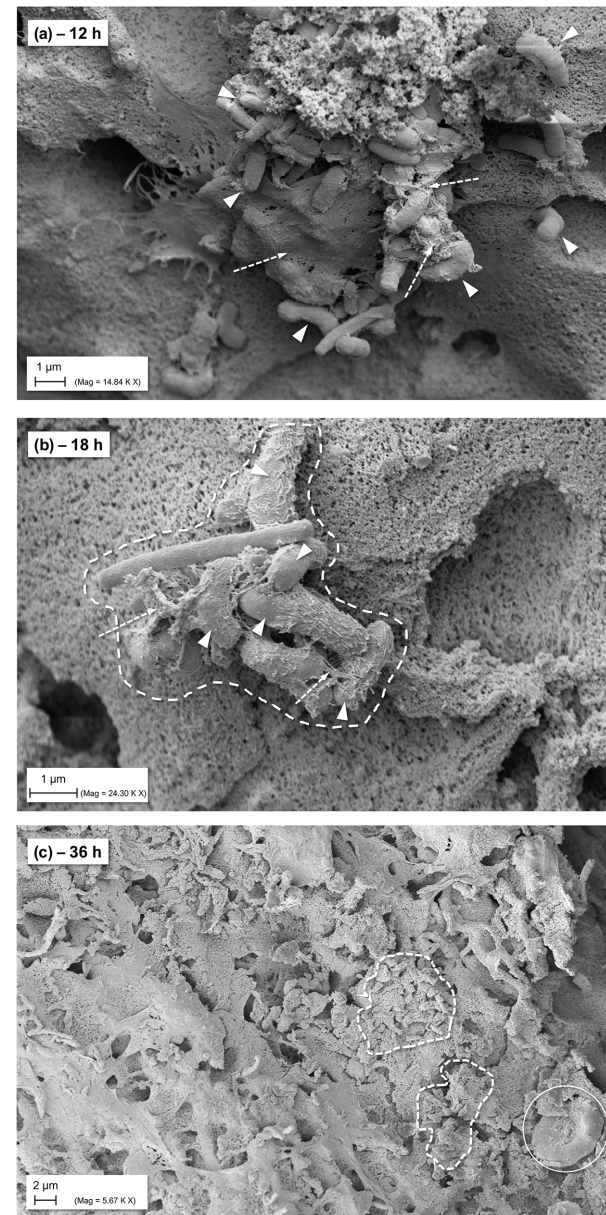


FIGURE 4 | SEM images of general biofilm maturation and development in the hpBIOM (here *P. aeruginosa*) without treatment (CTRL). **(A)** Formed microcolony in a 12 h matured biofilm with bacterial attachment and initially formed extracellular polymeric substance (EPS)/glycocalyx (arrows with dashed lines); arrowheads indicate bacteria. **(B)** Eighteen hours matured biofilm: dashed framing circles bacterial microcolony with single bacteria (arrowheads) connected by EPS/glycocalyx (arrows with dashed lines). **(C)** Surface view of 36 h matured biofilm with densely integrated and glycocalyx-surrounded bacteria (dashed framing) and human cells (white circle; erythrocyte).

of antiseptics and antimicrobials under challenging conditions (Rembe et al., 2018; Radischat et al., 2020).

This is especially true for newly introduced commercial agents, to provide comprehensive data on efficacy profiles in complex test scenarios and better estimate performance in *in-vivo* and in clinical situations. The presented work aimed

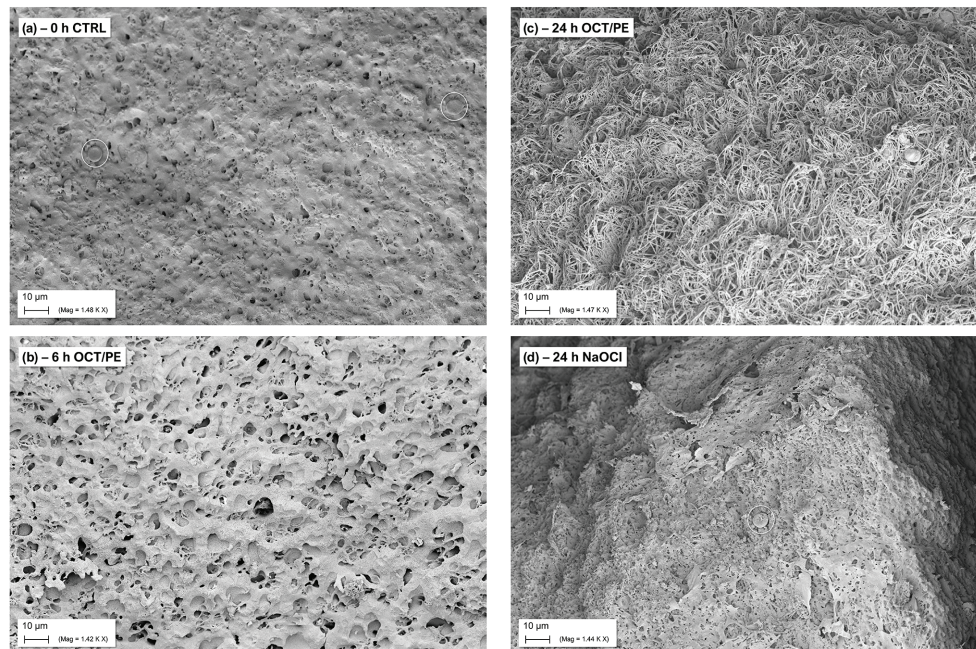


FIGURE 5 | SEM visualization of biofilm surface alteration in the hpBIOM (here *P. aeruginosa*) under treatment with antiseptics and antimicrobial wound irrigation solutions. **(A)** Densely connected surface structure of a 12 h-maturated biofilm before treatment, white circles depict human erythrocytes. **(B)** After 6 h of treatment with OCT/PE: surface structure appears less compact with several holes as potential entry points. **(C)** After 24 h of treatment with OCT/PE: surface is deranged and “broken-open” into a loosened structure with fine filaments, readily penetrable. **(D)** After 24 h of treatment with <0.08% NaClO: remaining densely connected surface structure, no visible penetration, additional build-up superficial EPS structures (white circle depicts human erythrocyte).

to provide such data for commercially available chlorine-based agents (HOCl, NaOCl) and included the current “best-practice” antiseptic/antimicrobial agents as base of reference (OCT/PE and PHMB-based irrigation solution).

The presented results on antimicrobial hypochlorous wound irrigation solutions thereby highlight the necessity for complex evaluation models, as well as the careful distinction between agent classes. Generally, differentiation between an antiseptic agent and an antimicrobial wound irrigation solution is important: an antiseptic agent is a highly effective, chemical agent designated to eliminate microorganisms *via* a direct, pharmacological mode of action. An antimicrobial irrigation solution, on the other hand, has a primarily mechanistic approach, reducing microorganisms by means of dilution, mechanical detachment *via* washing off microorganisms from surfaces such as wounds and additional effects, such as lowering surface tension, pH modulation, preservation, and antimicrobial efficacy depending on nature and concentration of added active ingredient. Differentiation between these kinds of solutions is key for therapeutic implications, indications, and correct application in clinical practice. Otherwise, misguided expectations of, for example, a sufficient antibacterial or anti-biofilm effect, lead to insufficient local treatment. While antiseptics mostly undergo a more rigorous evaluation process regarding antimicrobial efficacy before commercial introduction, irrigation solutions are often licensed as medical devices with certain additives but a primary mechanistic mode of action. That makes licensing legitimately easier, however, classification in the field

of anti-infective (antimicrobial, antiseptic, and anti-biofilm) agents reasonably more complicated since comprehensive efficacy evaluations are not provided. Oftentimes, antimicrobial modes of action are transferred from general concepts and similar agents or products without actually providing data, or only very basic, on the product itself in its specific formulation (considering concentration, pH, volume, etc.). In case of hypochlorous wound irrigation solutions, the generalized transferred concept is the “oxidative burst,” a defensive mechanism used by the human innate immune system, specifically neutrophils, *via* the conversion of H_2O_2 to HClO, a bactericidal agent, using the enzyme myeloperoxidase (Wang et al., 2007). While this effect might be highly efficient in endogenous pathogen defense, differences such as local concentrations, duration of exposure, endogenous production as needed, and other factors need to be accounted for if comparing endogenously produced HClO and externally administered HClO formulations. Such extrapolations often result in insufficient differentiation of antiseptics and antimicrobial irrigation solutions in wound care regarding their efficacy, with the potential risk of insufficient local anti-infective and anti-biofilm treatment. For these reasons, clearly and specific evaluated antimicrobial and anti-biofilm efficacy profiles for antiseptics as well as antimicrobial irrigation solutions in test setups “as-close-as-possible” to real life scenarios are necessary.

In a previous publication (Severing et al., 2019), we demonstrated and discussed the differences between commercially available hypochlorous wound irrigation solutions depending on agent

concentration, pH-value, and test setup against planktonic bacteria, whereby LVX, KSL, and especially AMF showed a high short-term efficacy on planktonic bacteria. The results of the now presented work are based on these preliminary evaluations and extend them in terms of potential anti-biofilm efficacy. Unfortunately, no efficacy of either agent could be detected in the human biofilm model (hpBIOM) over the course of 72 h (**Figure 1**). The antiseptic reference agent OCT/PE and the PHMB-based irrigation solution, on the contrary, achieved significantly higher reductions of microorganisms (**Figures 2A–C**) and visual breaking open of biofilm structures (**Figures 5A–C**). In contrast to our earlier publication (Severing et al., 2019), hypochlorous agents not only failed to reduce microbial counts in a biofilm setup but also in the planktonic method (QSM; **Figure 1**). This is however most likely attributed to the experimental setup with a deliberately chosen lower “agent to microbial test suspension”-ratio in the planktonic QSM (1:5 compared to 8:1 in standards), to unify the ratio in both models (QSM and hpBIOM). OCT/PE and PHMB, however, still achieved complete eradication of all tested planktonic microorganisms within 6 h in the QSM (**Figures 2A–C**) even in low ratio setups. In a planktonic setup with higher volumes of hypochlorous irrigation solutions, higher reduction rates were achieved (Severing et al., 2019). These results standing in contrast to earlier studies on the efficacy of chlorine-based and comparable agents, at the same time underline the necessity for careful distinction of agent and solution formulations, as well as test settings. The discrepancies in studies evaluating different forms of chlorine-based solutions, reporting higher efficacies than reported here, mainly derive from the vast heterogeneity of study designs. Many *in-vitro* studies used stationary biofilms on plastic surfaces without organic challenge (D’Atanasio et al., 2015; Day et al., 2017; Romanowski et al., 2018), even though the relevance of such challenge has been widely acknowledged (Brackman and Coenye, 2016; Sato et al., 2019). Especially the influence of high and differential protein loads have been described as a major influential factor of antimicrobial efficacy (Kapalschinski et al., 2017; Radischat et al., 2020) and a study by Johani et al. (2018) directly demonstrates the loss of efficacy of relevant antimicrobial substances in short term application on *in-vitro* vs. *in-vivo* models, also for hypochlorous agents.

Also, as outlined earlier, the exact composition of solutions needs to be considered, differentiating between solutions containing mainly sodium-hypochlorite, hypochlorous acid, or both, as well as the concentration and pH of solution. Our previous publication demonstrates the increased efficacy of higher vs. lower concentrated chlorine-based solutions (Severing et al., 2019) on planktonic bacteria. The same pattern can be observed against biofilms in the here presented results, where the higher concentrated AMF (0.2% NaClO) is the only tested chlorine-based agent exhibiting any anti-biofilm effect (**Figure 3B**). However, this effect only occurs under increased volume and extended exposure. Compared to the antiseptic OCT/PE or the PHMB solution, the effect is still negligible and even though significantly increased compared to lower volumes, probably irrelevant in clinical practice. An additional influential aspect to be considered is the pH of evaluated solutions: more extreme acidic or alkaline preparations prove

more effective (Percival et al., 2014; D’Atanasio et al., 2015; Wiegand et al., 2015; Day et al., 2017; Severing et al., 2019). Agents with acidic pH values in the work of D’Atanasio et al. (acidic solution with pH < 3) or Day et al. (acidic solution with pH of 5.5) or alkaline pH values (AMF with pH of 9.5), achieved effective microbial reductions compared to rather neutral pH ranges (pH of 6.5–8.7; e.g., LVX and KSL).

Further relevant aspects influencing the efficacy of especially antimicrobial wound irrigation solutions are substance volume and mechanical detachment under actual irrigation. To investigate whether an increase in substance volume would yield an improved anti-biofilm effect of hypochlorous solutions, the volume capabilities of the hpBIOM were exhausted to administer as much agent as possible (increasing the volume >3-fold to 1.0 ml). The reference substances OCT/PE and PHMB exhibited a significant increase in anti-biofilm efficacy, with OCT/PE and PHMB achieving complete eradication of *P. aeruginosa* (**Figure 3A**) and OCT/PE also eradicating MRSA biofilms within 72 h. The only hypochlorous solution, demonstrating an increase in efficacy compared to the lower volume was AMF (**Figures 3A,B**) with LVX and KSL showing no effect (**Supplementary Table 2**). Also, in case of AMF, the increased effect compared to the lower volume is rather irrelevant with at best $1.35 \pm 0.58 \log_{10}$ reduction compared to initial bacterial counts within 72 h (**Figure 3B**). For the reference substances on the contrary, the increase in administered volume as well as a prolonged exposure not only demonstrates a statistical significance regarding efficacy improvement but also proves clinically relevant by achieving the high reduction of bacterial counts ($\geq 3 \log_{10}$ reduction steps; **Figures 3A,B**) generally demanded from antiseptics under challenging conditions (DIN, 2013). This underlines the dose-dependency and differential approach antiseptics and antimicrobial irrigation solutions apply (“pharmacological” vs. “mechanical”) in terms of antimicrobial efficacy. The relevance of additional aspects such as dilution, mechanical detachment/debridement, and reduction in surface tension to the overall antimicrobial and cleansing effects of especially wound irrigation solutions reported in other studies (Kammerlander et al., 2011; Assadian et al., 2018) is indirectly highlighted here. On the other hand, this aspect needs to be accounted for as a limitation to this study and the here reported results: the intention of this work was to evaluate the anti-biofilm effect of the antimicrobial hypochlorous agents within antimicrobial wound irrigation solutions compared to a PHMB-based irrigation solution and the antiseptic OCT/PE. Additionally, the approach of simple increase in volume and duration of application to ameliorate antimicrobial efficacy of hypochlorous agents was to be evaluated, however, demonstrated no relevant improve in performance in contrast to PHMB-based solutions or OCT/PE (**Figures 3A,B**). Nevertheless, in clinical usage, the mechanical detachment effect and repetitive application, that cannot be adequately reproduced in the experimental approach used here, may result in an increased reduction of microbial and even biofilm burden. Naturally, concentration as well as applied volume cannot be infinitely increased due to potential limiting side-effects and toxicity, which needs to be acknowledged in the evaluation of antimicrobial

and antiseptic agents. Thereby, especially highly potent agents exert a higher cytotoxicity potential, whereby antimicrobial efficacy and cytotoxicity rise directly proportional to each other as demonstrated in several earlier studies (Hirsch et al., 2010; Severing et al., 2019). Herein lies another potential benefit of irrigation solutions with antimicrobial additives such as hypochlorous agents: while the sole antimicrobial efficacy is relevantly less compared to other agents, the likewise relevantly lower cytotoxicity allows for a far higher safely administrable substance volume, potentially making up for the lower direct antimicrobial effect *via* dilution and mechanical cleansing. This is most certainly the case for the decontamination and decolonization of chronic wounds, where the regenerating wound bed is to be protected from negative toxic influence and only a somewhat lower antimicrobial effect is desired.

The reported results highlight the necessity to apply antimicrobial irrigation solutions and antiseptics for a sufficient amount of time, to achieve biofilm penetration and effectively reduce bacterial counts (if used alone). The difficulty of biofilm penetration observed here indirectly confirms the current “state of the art” treatment approach of combining local antimicrobial treatment with debridement to mechanically break open dense biofilm structures and facilitate antimicrobial penetration. Generally, data on agent specific efficacy profiles need to be extended and investigated in more comprehensive and complex models to avoid confusion and misconception. Agent classification and situation-based therapeutic regimens are needed with distinguishing between highly potent antiseptics, more and less effective antimicrobial irrigation solutions and neutral irrigation solution in modern complex wound management.

Low-dosed, (near-)neutral pH hypochlorous wound irrigation solutions seem unsuitable for sole and first-line anti-biofilm treatment based on the inability to reduce bacterial counts in this complex hpBIOM. Naturally, these results should be translated to clinical practice with caution since above discussed limitations as well as further aspects such as the use of mono-species biofilms, short maturation times (12 h), and the unclear effect of repetitive extensive volume irrigation, still apply. However, more mature and multi-species biofilms would exhibit even higher bacterial resilience, as partly already demonstrated in another work of our research group (Besser et al., 2020) and, therefore, pose an even greater challenge for hypochlorous irrigation solutions. The anti-biofilm capacities in terms of eradication and antimicrobial effect of such wound irrigation solutions are, therefore, limited. The potential dilution and mechanical detachment of early,

loosely attached microorganisms combined with the additive effect of a low-ranging antimicrobial efficacy, rather support hypochlorous wound irrigation solutions as suited for decontamination and decolonisation of acute and chronic wounds and, therefore, prevention of (re-)contamination/infection, rather than primary treatment of mature biofilms.

DATA AVAILABILITY STATEMENT

The datasets used and/or analyzed during the current study are available from the corresponding author on reasonable request or are available as supplementary data files.

AUTHOR CONTRIBUTIONS

JDR, LH, and ES designed the study. JDR and LH performed experiments, data analysis, and drafted the figures. MB and IP helped with data analysis, interpretation, and experimental setup. IP and LH performed SEM imaging. JDR, LH, and ES drafted and finalized the manuscript. All authors contributed to the article and approved the submitted version.

FUNDING

The work was supported by the internal grant program of the Faculty of Health at Witten/Herdecke University, Germany (IFF2018-61) and the German “Initiative Chronische Wunde e.V.” (ICW e.V.).

ACKNOWLEDGMENTS

The authors would like to thank Martin Arnold, Susanne Haußmann, and Ella Naumova for their assistance in conducting the scanning electron microscopy.

This manuscript has been released as a pre-print at Research Square (Rembe et al., 2020).

SUPPLEMENTARY MATERIAL

The Supplementary Material for this article can be found online at: <https://www.frontiersin.org/articles/10.3389/fmicb.2020.564513/full#supplementary-material>

REFERENCES

- Assadian, O., Kammerlander, G., Geyrhofer, C., Luch, G., Doppler, S., Tuchmann, F., et al. (2018). Use of wet-to-moist cleansing with different irrigation solutions to reduce bacterial bioburden in chronic wounds. *J. Wound Care* 27 (Suppl. 10), S10–S16. doi: 10.12968/jowc.2018.27.Sup10.S10
- Besser, M., Dietrich, M., Weber, L., Rembe, J. D., and Stuermer, E. K. (2020). Efficacy of antiseptics in a novel 3-dimensional human plasma biofilm model (hpBIOM). *Sci. Rep.* 10:4792. doi: 10.1038/s41598-020-61728-2
- Besser, M., Terberger, J., Weber, L., Ghebremedhin, B., Naumova, E. A., Arnold, W. H., et al. (2019). Impact of probiotics on pathogen survival in an innovative human plasma biofilm model (hpBIOM). *J. Transl. Med.* 17:243. doi: 10.1186/s12967-019-1990-4
- Brackman, G., and Coenye, T. (2016). In vitro and in vivo biofilm wound models and their application. *Adv. Exp. Med. Biol.* 897, 15–32. doi: 10.1007/5584_2015_5002
- D’Atanasio, N., Capezone de Joannon, A., Mangano, G., Meloni, M., Giarratana, N., Milanese, C., et al. (2015). A new acid-oxidizing solution: assessment of its role on methicillin-resistant *Staphylococcus aureus* (MRSA) biofilm morphological changes. *Wounds* 27, 265–273.

- Day, A., Alkhalil, A., Carney, B. C., Hoffman, H. N., Moffatt, L. T., and Shupp, J. W. (2017). Disruption of biofilms and neutralization of bacteria using hypochlorous acid solution: an in vivo and in vitro evaluation. *Adv. Skin Wound Care* 30, 543–551. doi: 10.1097/01.ASW.0000526607.80113.66
- DIN (2013). EN 13727:2012+A1:2013. Chemical disinfectants and antiseptics—Quantitative suspension test for the evaluation of bactericidal activity in the medical area—Test method and requirements (phase 2, step 1); German version.
- Hall-Stoodley, L., and Stoodley, P. (2009). Evolving concepts in biofilm infections. *Cell. Microbiol.* 11, 1034–1043. doi: 10.1111/j.1462-5822.2009.01323.x
- Hirsch, T., Koerber, A., Jacobsen, F., Dissemmond, J., Steinau, H. U., Gatermann, S., et al. (2010). Evaluation of toxic side effects of clinically used skin antiseptics in vitro. *J. Surg. Res.* 164, 344–350. doi: 10.1016/j.jss.2009.04.029
- Hoiby, N., Bjarnsholt, T., Givskov, M., Molin, S., and Ciofu, O. (2010). Antibiotic resistance of bacterial biofilms. *Int. J. Antimicrob. Agents* 35, 322–332. doi: 10.1016/j.ijantimicag.2009.12.011
- Hoiby, N., Bjarnsholt, T., Moser, C., Bassi, G. L., Coenye, T., Donelli, G., et al. (2015). ESCMID guideline for the diagnosis and treatment of biofilm infections 2014. *Clin. Microbiol. Infect.* 21 (Suppl. 1), S1–S25. doi: 10.1016/j.cmi.2014.10.024
- IWII (2016). Wound infection in clinical practice. Wounds International.
- James, G. A., Swogger, E., Wolcott, R., Pulcini, E., Secor, P., Sestrich, J., et al. (2008). Biofilms in chronic wounds. *Wound Repair Regen.* 16, 37–44. doi: 10.1111/j.1524-475X.2007.00321.x
- Johani, K., Malone, M., Jensen, S. O., Dickson, H. G., Gosbell, I. B., Hu, H., et al. (2018). Evaluation of short exposure times of antimicrobial wound solutions against microbial biofilms: from in vitro to in vivo. *J. Antimicrob. Chemother.* 73, 494–502. doi: 10.1093/jac/dkx391
- Kammerlander, G., Assadian, O., Eberlein, T., Zweitmuller, P., Luchsinger, S., and Andriessen, A. (2011). A clinical evaluation of the efficacy and safety of singlet oxygen in cleansing and disinfecting stagnating wounds. *J. Wound Care* 20, 149–158. doi: 10.12968/jowc.2011.20.4.149
- Kapalschinski, N., Seipp, H. M., Kuckelhaus, M., Harati, K. K., Kolbenschlag, J. J., Daigeler, A., et al. (2017). Albumin reduces the antibacterial efficacy of wound antiseptics against *Staphylococcus aureus*. *J. Wound Care* 26, 184–187. doi: 10.12968/jowc.2017.26.4.184
- Koo, H., Allan, R. N., Howlin, R. P., Stoodley, P., and Hall-Stoodley, L. (2017). Targeting microbial biofilms: current and prospective therapeutic strategies. *Nat. Rev. Microbiol.* 15, 740–755. doi: 10.1038/nrmicro.2017.99
- Malone, M., Bjarnsholt, T., McBain, A. J., James, G. A., Stoodley, P., Leaper, D., et al. (2017). The prevalence of biofilms in chronic wounds: a systematic review and meta-analysis of published data. *J. Wound Care* 26, 20–25. doi: 10.12968/jowc.2017.26.1.20
- Maurer, H. R. (2001). Bromelain: biochemistry, pharmacology and medical use. *Cell. Mol. Life Sci.* 58, 1234–1245. doi: 10.1007/PL00000936
- Pavan, R., Jain, S., Shraddha, , and Kumar, A. (2012). Properties and therapeutic application of bromelain: a review. *Biotechnol. Res. Int.* 2012:976203. doi: 10.1155/2012/976203
- Percival, S. L. (2017). Importance of biofilm formation in surgical infection. *Br. J. Surg.* 104, e85–e94. doi: 10.1002/bjs.10433
- Percival, S. L., McCarty, S., Hunt, J. A., and Woods, E. J. (2014). The effects of pH on wound healing, biofilms, and antimicrobial efficacy. *Wound Repair Regen.* 22, 174–186. doi: 10.1111/wrr.12125
- Percival, S. L., McCarty, S. M., and Lipsky, B. (2015). Biofilms and wounds: an overview of the evidence. *Adv. Wound Care* 4, 373–381. doi: 10.1089/wound.2014.0557
- Percival, S. L., and Suleman, L. (2015). Slough and biofilm: removal of barriers to wound healing by desloughing. *J. Wound Care* 24, 498–510. doi: 10.12968/jowc.2015.24.11.498
- Radischat, N., Augustin, M., Herberger, K., Wille, A., and Goroncy-Bermes, P. (2020). Influence of human wound exudate on the bactericidal efficacy of antiseptic agents in quantitative suspension tests on the basis of European Standards (DIN EN 13727). *Int. Wound J.* 17, 781–789. doi: 10.1111/iwj.13336
- Rembe, J. D., Fromm-Dornieden, C., Bohm, J., and Stuermer, E. K. (2018). Influence of human acute wound fluid on the antibacterial efficacy of different antiseptic polyurethane foam dressings: an in vitro analysis. *Wound Repair Regen.* 26, 27–35. doi: 10.1111/wrr.12612
- Rembe, J. D., Huelsboemer, L. F., Besser, M., and Stuermer, E. K. (2020). Anti-biofilm activity of antimicrobial hypochlorous wound irrigation solutions compared to common wound antiseptics and bacterial resilience in an innovative in-vitro human plasma biofilm model (hpBIOM). Research Square [Preprint]. doi: 10.21203/rs.3.rs-22421/v1
- Romanowski, E. G., Stella, N. A., Yates, K. A., Brothers, K. M., Kowalski, R. P., and Shanks, R. M. Q. (2018). In vitro evaluation of a hypochlorous acid hygiene solution on established biofilms. *Eye Contact Lens* 44 (Suppl. 2), S187–S191. doi: 10.1097/ICL.0000000000000456
- Salisbury, A. M., Woo, K., Sarkar, S., Schultz, G., Malone, M., Mayer, D. O., et al. (2018). Tolerance of biofilms to antimicrobials and significance to antibiotic resistance in wounds. *Surg. Technol. Int.* 33, 59–66.
- Sato, A., Yamaguchi, T., Hamada, M., Ono, D., Sonoda, S., Oshiro, T., et al. (2019). Morphological and biological characteristics of *Staphylococcus aureus* biofilm formed in the presence of plasma. *Microb. Drug Resist.* 25, 668–676. doi: 10.1089/mdr.2019.0068
- Schultz, G., Bjarnsholt, T., James, G. A., Leaper, D. J., McBain, A. J., Malone, M., et al. (2017). Consensus guidelines for the identification and treatment of biofilms in chronic nonhealing wounds. *Wound Repair Regen.* 25, 744–757. doi: 10.1111/wrr.12590
- Schwartz, J. A., Goss, S. G., Facchin, F., Avdagic, E., and Lantis, J. C. (2014). Surgical debridement alone does not adequately reduce planktonic bioburden in chronic lower extremity wounds. *J. Wound Care* 23, S4–S13. doi: 10.12968/jowc.2014.23.Sup9.S4
- Schwarzer, S., James, G. A., Goeres, D., Bjarnsholt, T., Vickery, K., Percival, S. L., et al. (2019). The efficacy of topical agents used in wounds for managing chronic biofilm infections: a systematic review. *J. Infect.* 80, 261–270. doi: 10.1016/j.jinf.2019.12.017
- Severing, A. L., Rembe, J. D., Koester, V., and Stuermer, E. K. (2019). Safety and efficacy profiles of different commercial sodium hypochlorite/hypochlorous acid solutions (NaClO/HClO): antimicrobial efficacy, cytotoxic impact and physicochemical parameters in vitro. *J. Antimicrob. Chemother.* 74, 365–372. doi: 10.1093/jac/dky432
- Shukla, S. K., Sharma, A. K., Gupta, V., Kalonia, A., and Shaw, P. (2020). Challenges with wound infection models in drug development. *Curr. Drug Targets.* doi: 10.2174/1389450121666200302093312 [Epub ahead of print]
- Stoffel, J. J., Kohler Riedi, P., and Hadj Romdhane, B. (2020). A multi-model regime for evaluating effectiveness of antimicrobial wound care products in microbial biofilms. *Wound Repair Regen.* 28, 438–447. doi: 10.1111/wrr.12806
- Wang, L., Bassiri, M., Najafi, R., Najafi, K., Yang, J., Khosrovi, B., et al. (2007). Hypochlorous acid as a potential wound care agent: part I. stabilized hypochlorous acid: a component of the inorganic armamentarium of innate immunity. *J. Burns Wounds* 6:e5.
- Wiegand, C., Abel, M., Ruth, P., Elsner, P., and Hipler, U. C. (2015). pH influence on antibacterial efficacy of common antiseptic substances. *Skin Pharmacol. Physiol.* 28, 147–158. doi: 10.1159/000367632
- Wolcott, R. D., Rumbaugh, K. P., James, G., Schultz, G., Phillips, P., Yang, Q., et al. (2010). Biofilm maturity studies indicate sharp debridement opens a time-dependent therapeutic window. *J. Wound Care* 19, 320–328. doi: 10.12968/jowc.2010.19.8.77709

Conflict of Interest: The authors declare that the research was conducted in the absence of any commercial or financial relationships that could be construed as a potential conflict of interest.

Copyright © 2020 Rembe, Huelsboemer, Plattfaut, Besser and Stuermer. This is an open-access article distributed under the terms of the Creative Commons Attribution License (CC BY). The use, distribution or reproduction in other forums is permitted, provided the original author(s) and the copyright owner(s) are credited and that the original publication in this journal is cited, in accordance with accepted academic practice. No use, distribution or reproduction is permitted which does not comply with these terms.

GLOSSARY

Term	Definition
AMF	Actimaris® forte
CaCl ₂	Calcium chloride
CFU	Colony forming units
CSA	Casein/soy peptone agar
CTRL	Control
DIN	German institute for standardization
DRK	German red cross
DSMZ	German Collection of Microorganisms and Cell Cultures
ddH ₂ O	Double distilled water
ECM	Extracellular matrix
EPS	Extracellular polymeric substance
HCL	Hydrochloride
HClO	Hypochlorous acid
hpBIOM	Human plasma biofilm model
KSL	Kerrasol®
LVX	Lavanox®
MRSA	Methicillin-resistant <i>S. aureus</i>
MSSA	Methicillin-susceptible <i>S. aureus</i>
NaClO	Sodium hypochlorite
NaNO ₂	Sodium nitrite
OCT/PE	Octenidine dihydrochloride/phenoxyethanol
OsO ₄	Osmium tetroxide
PBS	Phosphate buffered saline
PHMB	Polyhexamethylene-biguanide
PVP	Polyvinylpyrrolidone
QSM	Quantitative suspension method
RT	Room temperature
SEM	Scanning electron microscopy
<i>sem</i>	Standard error of the mean
SDS	Sodium dodecyl sulfate



Antimicrobial Potential of *Streptomyces ansochromogenes* (PB₃) Isolated From a Plant Native to the Amazon Against *Pseudomonas aeruginosa*

OPEN ACCESS

Edited by:

Natalia V. Kirienko,
Rice University, United States

Reviewed by:

Koshy Philip,
University of Malaya, Malaysia
Devendra Dusane,
The Ohio State University,
United States

*Correspondence:

Rita de Cássia Mendonça de
Miranda
rita.miranda@ceuma.br;
ritamend30@gmail.com

Specialty section:

This article was submitted to
Antimicrobials, Resistance
and Chemotherapy,
a section of the journal
Frontiers in Microbiology

Received: 20 June 2020

Accepted: 09 September 2020

Published: 09 October 2020

Citation:

Amorim EAdF, Castro EJM,
Souza VdS, Alves MS, Dias LRL,
Melo MHF, da Silva IMA, Villis PCM,
Bonfim MRQ, Falcai A, Silva MRC,
Monteiro-Neto V, Aliança A, da
Silva LCN and de Miranda RdCM
(2020) Antimicrobial Potential
of *Streptomyces ansochromogenes*
(PB₃) Isolated From a Plant Native
to the Amazon Against *Pseudomonas*
aeruginosa.
Front. Microbiol. 11:574693.
doi: 10.3389/fmicb.2020.574693

Erika Alves da Fonseca Amorim¹, Erima Joussielly Mendonça Castro¹,
Viviane da Silva Souza², Mateus Silva Alves¹, Léo Ruben Lopes Dias¹,
Maycon Henrique Franzoi Melo¹, Ilana Mirian Almeida da Silva¹,
Paulo Cesar Mendes Villis¹, Maria Rosa Quaresma Bonfim¹, Angela Falcai¹,
Maria Raimunda Chagas Silva¹, Valério Monteiro-Neto^{1,2}, Amanda Aliança¹,
Luís Cláudio Nascimento da Silva¹ and Rita de Cássia Mendonça de Miranda^{1*}

¹ Programa de Pós Graduação, Universidade CEUMA, São Luís, Brazil, ² Programa de Pós Graduação, Universidade Federal do Maranhão, São Luís, Brazil

The objective of this study was to evaluate the antibacterial action of filamentous bacteria isolated from the *Byrsonima crassifolia* leaf. An endophytic bacterium has been identified by classical and molecular techniques as *Streptomyces ansochromogene*. Screening for antibacterial action against pathogens with medical relevance (*Klebsiella pneumoniae* ATCC 700603, *Pseudomonas aeruginosa* ATCC 15692, *Staphylococcus aureus* ATCC 6538, *Corynebacterium diphtheriae* ATCC 27012, *Mycobacterium abscessus*, *Cryptococcus gattii* ATCC 24065, and *Cryptococcus neoformans* ATCC 24067) demonstrated activity against the bacterium *P. aeruginosa* ATCC 0030 with inhibition diameter zones (IDZ) of 17.6 ± 0.25 mm in the preliminary screening in solid medium. After fermentation in liquid medium, an IDZ of 19.6 ± 0.46 mm and a minimum inhibitory concentration (MIC) of 0.5 mg/mL were detected. The antibiofilm action was observed with 100% inhibition of biofilm formation at a concentration of 0.250 mg/mL. When the infection curve was prepared, it was observed that the metabolite was effective in protecting the larvae of *Tenebrio molitor*. The metabolite does not show toxicity for eukaryotic cells. The leishmanicidal activity demonstrated that the metabolite presented a dose-dependent effect on the promastigotes forms of *Leishmania amazonensis* growth and the estimated IC₅₀/72 h was 71.65 ± 7.4 μg/mL. Therefore, it can be concluded that the metabolite produced by the endophytic bacterium *Streptomyces* sp. is promising for future use as an alternative strategy against bacterial resistance.

Keywords: endophytes, biotechnological potential, actinomycetes, metabolites, endophytic, resistance

INTRODUCTION

Antimicrobial resistance is a dangerous and constantly increasing problem, leading to an increase in health care costs, decreased treatment options, and a higher incidence of mortality due to bacterial and fungal infections worldwide. Global initiatives are calling for urgent action not only to develop new antimicrobial therapies but also decrease the contribution of humans to increasing antimicrobial resistance (World Health Organization, 2015).

The excessive and inappropriate use of antibiotics continues to be a major factor in the expansion of antimicrobial resistance, and the search for new drugs has been an alternative to minimize the damage caused by this phenomenon.

Among the resistant microorganisms, a bacterium of most concern is *Pseudomonas aeruginosa*. According to Pang et al. (2019), *P. aeruginosa* is an opportunistic pathogen and a major cause of morbidity and mortality in patients with cystic fibrosis and immunocompromised individuals. The authors emphasize that the eradication of *P. aeruginosa* has become increasingly difficult due to its remarkable ability to resist antibiotics by intrinsic and acquired methods. The exchange of genetic material, which occurs naturally within or between species Gram-negative bacilli, is considered to be a factor responsible for the acquisition of resistance. Thus, the ability of *P. aeruginosa* to become resistant during antibiotic treatment is inherent to the species and is often inevitable (Lincopan and Trabulsi, 2008). In intensive care units (ICUs) in Brazilian hospitals, antibiotic resistance is very worrying.

National epidemiological studies carried out, aimed at hospitalized patients, evaluated 3,728 isolates, including Gram-positive and Gram-negative bacteria, obtained from 12 hospital centers in four states, and *P. aeruginosa* was responsible for 496 (13.3%) cases and the third most frequent pathogen, with 30.2% resistance to Integrated Pest Management (IPM) (Sader et al., 2001; Pang et al., 2019).

It is necessary to search for alternatives for treating diseases caused by these resistant microorganisms. Brazil is the country with the greatest biodiversity on the planet (Laihonon et al., 2004), and the Amazon ecosystem is one of the richest and most important because of its plant diversity that can house compounds with antimicrobial action.

The use of plants as a medicine is a practice adopted by traditional people; however, large-scale production of medicines is difficult. Therefore, the use of microorganisms that live inside the plant (endophytic) can be an alternative for the production of biologically active compounds through biotechnological techniques (Jiang et al., 2013; Hussain et al., 2015; Rajamani et al., 2018).

Among the microorganisms that produce bioactive compounds, those of the *Actinomycetales* family stand out, especially *Streptomyces* spp., which is known for its ability to produce substances with several antimicrobial, antimalarial, and antitumor actions (Supong et al., 2016; Elkhayat and Goda, 2017; Bunbamrung et al., 2020; Mahmood and Kataoka, 2020).

Considering these facts, this work aims to assess the antimicrobial potential of *Streptomyces ansochromogene*,

isolated from *Byrsonima crassifolia* leaf, against pathogens of clinical interest.

MATERIALS AND METHODS

Microorganisms

The microorganism used in this work is an endophytic bacterium previously isolated from *Byrsonima crassifolia* leaf, a plant native to the region of the Legal Amazon (Brazil). The bacterium is deposited in the culture bank of Ceuma University under the code PB₃.

To test the antimicrobial potential of the isolated bacteria, the following microorganisms were used: *Klebsiella pneumoniae* ATCC 700603, *P. aeruginosa* ATCC 15692, *Staphylococcus aureus* ATCC 6538, *Corynebacterium diphtheriae* ATCC 27012, *Mycobacterium abscessus massiliense* Go01, *Cryptococcus gattii* ATCC 24065, and *Cryptococcus neoformans* ATCC 24067.

To assess the Leishmanicidal potential, *Leishmania amazonensis* (MHOM/BR/76/MA-76) was used.

Identification of the Microorganism

Classical Identification

For classic identification of the isolate, the microculture technique was performed. Previously isolated and purified microorganism was inoculated in a Petri dish containing the BDA medium that favors radial growth. A coverslip was partially inserted into the medium to facilitate the growth of hyphae on its surface. This was incubated in an oven at 28°C for 5 days (Shirling and Gottlieb, 1966; Matsuura, 2004). Structures such as conidiospores, hyphae, spore chains, and conidia were stained with cotton blue and observed under an optical microscope with 100x magnification lenses. Genera level identification was possible by observation of macroscopic characteristics and microscopic morphological structures. For the morphological description of the genera, the criteria adopted by Rapper and Fennell, 1965, Pitt, 1979, Pitt and Samson, 1990 and Klich and Pitt, 1988.

Molecular Identification: DNA Extraction, Amplification of the 16sR Region, and Sequencing

Molecular identification was used to confirm the bacterial species previously identified by classical techniques. Thus, the bacteria were grown in Petri dishes for five days and incubated in PBS for 2 h at 27°C. After centrifugation at 7500 rpm for 10 min, supernatant was discarded and pellet was suspended in 180 µL of lysozyme (200 µg/mL), incubated for 30 min at 37°C. To this solution, 20 µL of proteinase K and another 200 µL of Buffer AL buffer solution (QIAmp) were added. The solution was homogenized and incubated for 30 min at 56°C, then for another 15 min at 95°C. The material was centrifuged and 200 µL of absolute ethanol was added and centrifuged again. The samples were transferred to the Purification Kit (QIAmp DNA mini kit) and centrifuged for 1 min at 8000 rpm. The filtrate was discarded, and 500 µL of AW2 buffer solution (QIAmp) was added and centrifuged for 3 min at 1400 rpm. The filtrate was discarded again and centrifuged for 1 min at 1400 rpm, and then 50 µL

of Buffer AE buffer solution (QIAmp) was added and incubated for 1 min and centrifuged again for 1 min at 8000 rpm. This last step was repeated (1X). A small amount of the target DNA was added to a PCR buffer solution (10 mM Tris-HCl [pH 8.0], 50 mM KCl) containing DNA polymerase, universal primers P27F (5'-AGAGTTTGATCCTGGCTCA-3'), and P1492R (5'-GGTTACCTTGTTACGACTT-3') (Lee et al., 2007). In PCR tubes, 0.25 mL of the mixture was placed, which was subjected to approximately 40 replication cycles *in vitro* (Thermociclador) for 1 min at 95°C, 45 s at 57°C, and 30 s at 72°C. DNA was quantified using NanoDrop® ND-1000 UV-Vis. The samples were applied to an agarose gel immersed in a TBE buffer solution and electrophoresis was performed for 40 min. The gel was stained with UniSafedye (0.1 µL/mL) for 40 min, protected from light and read on an ultraviolet light transilluminator. The PCR product was sequenced and analyzed using MegaSoftware® and Blast (NCBI). The sequence of the 16S rRNA gene obtained by PCR was analyzed and manually aligned with strains of the genus found in the GenBank/NCBI database with Clustal-X. The phylogenetic tree was built using MEGA version 7.0. The sequence was submitted to GENBANK/PUBMED and deposited under code MT634691.

Preliminary Antimicrobial Screening

Solid Media Assay

Antimicrobial activity testing was performed on solid medium through the diffusion of the bioactive compound in agar using the method described by Ichikawa et al. (1971). This method is also known as the Gelose Block Method using the isolated endophytic microorganism. After ten days of incubation at 28°C, circular agar blocks of 6 mm in diameter were removed from the plates with colonies grown by clogging and transferred to the plates containing MH, previously seeded with the standard microorganisms at 5×10^5 UFC/mL. This test was performed in triplicates. After 24 h at a temperature of 37°C, the diameters (mm) of the inhibition halos of each block were measured, analyzing the longest distance between 2 rectilinear points that cross the block of glucose in half. A Matsuura scale (2004) was used to classify the results, so that the arithmetic mean and standard deviation of the results were obtained. The results were expressed as mean inhibition diameter zones (IDZ) in millimeters (mm).

Antimicrobial Activity

Submerged Fermentation

To obtain the active metabolite produced by the isolated microorganism, submerged fermentation was carried out in Erlenmeyer flasks (250 mL) containing 50 mL of useful volume of potato dextrose (PD) medium. The flasks were incubated in a rotary incubator at 30°C for 5 days. After this period, the sample was filtered to assess biological activities.

Secondary metabolites extraction

To obtain the metabolite(s) of interest, liquid-liquid extraction was performed according to the methodology described by Trisuwana et al. (2008). Therefore, after the incubation period, the fermented culture was filtered through a vacuum filter, and

the free extract of microbial cells was separated. The fermented filtrate was subjected to centrifugation and filtered again in a 22 µm filter, ensuring that the extract did not contain microbial cells.

To extract the compounds of interest, 25 mL of the filtrate and 25 mL of ethyl acetate were added to a separating funnel, shaken vigorously for 10 min, and placed at rest for 30 min. After the mentioned time, the organic phase containing the analytes of interest was collected. The solvent was then evaporated on a rotary evaporator, and the product yield was determined.

For the evaluation of biological activities, the extract was resuspended in dimethylsulfoxide (DMSO) to reach a known concentration of 1 mg/mL.

Agar diffusion assay

The liquid medium assay was performed using the plate diffusion test (Bauer et al., 1966) to determine whether the microorganisms selected in the previous assay secrete metabolites to the external environment. The plate diffusion test was established as a standard by the Clinical and Laboratory Standards Institute (CLSI) and consists of the application of 10 µL of the metabolite produced in 6 mm diameter wells, made in petri dishes with 20 mL of Mueller Hinton agar medium, seeded with gram-negative bacteria, incubated at 37°C for up to 72 h. After this period, IDZs were measured with the aid of a caliper. In the 6 mm wells, 10 µL of DMSO and 10 µL of chloramphenicol (30 µg) were used as negative and positive controls, respectively.

Determination of Minimum Inhibitory Concentration

For the determination of the minimum concentration capable of inhibiting bacterial growth, the microdilution test was performed, using a 96-well 6-mm multi-well plate, the metabolite was diluted in dimethyl sulfoxide (DMSO). The calculation to determine the concentration followed the CLSI protocol, which recommends 1000 µg/mL.

The technique described by Zgoda and Porter (2001) was adapted. Mueller Hinton broth (190 µL) and the metabolite (10 µL) diluted in DMSO at an initial concentration of 1000 µg/mL were dispensed in the first row of wells. In the other wells, 100 µL of medium Muller Hinton broth was added. A serial dilution was then performed in the nine consecutive wells, removing 100 µL from the well of the highest concentration, resulting in dilutions from 1000 µg/mL to 0.0625 µg/mL. In the penultimate well, the inoculum and extract were not added to have a negative control. In the last well, medium and inoculum were added as positive control. Microbial growth was determined by bacterial colony growth. The concentration of the bacterial suspension was determined according to the McFarland scale 5×10^5 CFU/mL. The plate was incubated at 37°C for 24–48 h.

Evaluation of Antibiofilm Activity

The inhibitory capacity of the metabolite in biofilm formation was assessed according to the method recommended by Stepanović et al. (2007). The method consists of adding 100 µL of Broth Muller Hinton medium to all 96 wells of a multi-well plate. The first and last rows are the negative and positive controls, respectively. In the second row, another 50 µL of culture

medium was added, totaling 150 μL of medium. Then, 50 μL of the metabolite in sub-MICs was added to this second row, totaling a volume of 200 μL in the second row. Serial dilution was performed up to the penultimate row before the positive control. After diluting 100 μL of the inoculum on a 0.3×10^8 scale, all wells were added, except for the negative control. The plate was incubated at 37°C for 24 h. After this period, the contents of the plate were removed, and the wells were washed with PBS buffer or saline solution. To fix the biofilm, 200 μL of methanol was placed in the wells for 15 min at room temperature. This was washed with PBS or saline again. The wells were stained with crystal violet and incubated for 15 min at 37°C . They were then washed in running water to remove excess dye. After drying, 250 μL of ethanol was used for suspension in the wells, and ethanol was transferred to a new plate that was taken to read the optical density in a 550 nm microplate reader. To determine the cell viability of bacterial biomass, the test was repeated and the crystal violet was replaced by resazurin indicator.

Action of Metabolite on Biofilm

Eradicating the action of preformed biofilm was assessed using the method of Klein et al. (2015), with modifications. It was divided into two stages: 1. For the previous formation of the biofilm and 2. Evaluating the eradication of the formed biofilm. The first step consisted of the formation of the biofilm in a 96-well plate, where 100 μL of Muller Hinton broth culture medium was added to all wells, and the first and last rows were the negative and positive controls, respectively. Then, 100 μL of the standardized microbial inoculum was added to 0.3×10^8 cells, except in the first row, which was the negative control. This plate was incubated at 37°C for 24 h. Later, the second stage began, where the contents of the plate were removed, and the wells were washed with PBS buffer or saline solution. Then, 100 μL of Muller Hinton broth medium was added to the washed wells. In the second row of the wells, the metabolite was placed in supra-MIC ($4 \times \text{MIC}$), followed by serial dilution. This plate was incubated again for 24 h at 37°C .

After this step, the contents of the wells were gently removed and washed with PBS buffer. Then, 200 μL of methanol was placed for 15 min at room temperature. The wells were again washed with PBS buffer, stained with crystal violet, and incubated at 37°C for 15 min. After that, the plate was washed under running water, and after drying, the wells received 250 μL of ethanol. This suspension was transferred to a new plate and was taken to read optical density in an Elisa reader at 550nm.

Infection and Survival Curve in an Alternative Model

To standardize the inoculum concentration scale in its pathogenic potential of *P. aeruginosa*, 5 standardized solutions were prepared of 0.1, 0.2, 0.3, 0.3 and 0.5×10^8 cells using Newbauer Chamber. Each concentration was inoculated into 10 larvae of *T. molitor* to observe mortality levels. The smallest scale that obtained the ability to kill *T. molitor*, in less days of observation, was the inoculum scale used for infection and survival curves (Figure 4A). Having the inoculum scale defined

previously, four groups composed of 10 *T. molitor* each were established. Of these, three groups were infected with the pathogen, after 2 h of infection, one group was treated with 10 μL of the test extract, another group received no treatment, and the fourth group was not infected, for quality control of *T. molitor*. They were observed for 10 days, where the survival time was observed.

Leishmanicidal Activity Against Promastigotes

To determine the IC₅₀ (a concentration that inhibits 50% of parasite growth) value, promastigote forms of *Leishmania amazonensis* (MHOM/BR/76/MA-76) were incubated in the presence of increasing concentrations of the secondary metabolite (7.8–500 $\mu\text{g/mL}$). The cells were diluted at a concentration of 1×10^6 parasites/mL. As a control, cells incubated with Schneider's medium were used. After 72 h of incubation the surviving parasites were counted in a Neubauer chamber (INCYTO CChip DHC-N01, Cheonan-Si, South Korea). The IC₅₀ value was determined by linear regression analysis using SPSS 8.0 software (IBM Co., New York, United States) for Windows. Each experiment was performed in biological duplicate and technical triplicate.

Cytotoxicity Assay

The MTT method is based on the determination of the ability of living cells to reduce 3-(4,5 Dimethyl Thiazol-2-IL)-2,5-Diphenyl Tetrazolium (MTT) bromide forming insoluble crystals of formazan violet. After treatment, the culture medium was removed and a 10% solution of MTT (5mg/mL) in PBS was added to each well. Then, the cultures were incubated at 37°C for 3 hours, protected from light. For solubilization of formazan crystals, 100 μL of dimethylsulfoxide (DMSO) was added to each well and the presence of violet formazan crystals was observed. The spectrophotometric reading of the absorbance was performed in an ELISA plate reader (Bio-Rad Microplate Reader Benchmark, Inc., United States) at a wavelength of 550 nm. The percentage of dead cells was calculated in relation to the positive toxicity control.

RESULTS

Microorganism Identification Classical Identification

The classical identification of microorganism was carried out through macro and microscopic observation of the colonies. Features such as colony color, pigment production in the culture medium, and microscopic structures were considered. Macroscopic observation of the colony in a Petri dish showed a grayish colony, with predominant aerial mycelium and dark pigment release (Figure 1A). On microscopic observation, it was possible to identify the gray spore chain structures, branched mycelia similar to filamentous fungus hyphae, characteristics compatible with actinobacteria of the genus *Streptomyces* (Figure 1B) (Olmos et al., 2013; Raju et al., 2014). Spores

similar to those of fungi, known as astropores and spiral-shaped sporophores, were also observed (Walkman & Henrici, 1943; Ensign, 1978).

Molecular Identification by PCR

Molecular identification demonstrated a 97.11% genetic similarity with *Streptomyces ansochromogene*. Then, macroscopic identification of the strain genus was confirmed. The evolutionary analysis was performed in MEGA X. A total of 1510 positions were present in the final dataset, involving 7 nucleotide sequences, and the codon positions included were 1st + 2nd + 3rd + uncoded. Evolutionary history took place using the maximum likelihood method and the Tamura and Nei (1993). The tree for heuristic research was automatically generated by Join-Join, BioNJ, and

distance matrix in estimated pairs using the maximum likelihood approach, selecting the topology most likely to log (2471.39) (**Figure 2**).

Screening of Antimicrobial Potential of Isolated Bacteria

The antimicrobial potential of the *S. ansochromogene* was evaluated using a solid test against seven microorganisms of clinical interest. *S. ansochromogene* was shown to be active for all microorganisms tested, except for *Cryptococcus neoformans* ATCC 24067 (**Table 1**). The higher activities were observed for *M. abscessus*, *C. diphtheriae* ATCC 27012, and *K. pneumoniae* ATCC 700603 with IDZs of 39.3 ± 0.11 mm, 38.3 ± 0.28 mm, and 30 ± 0 mm, respectively. In this test, the bacterium was also

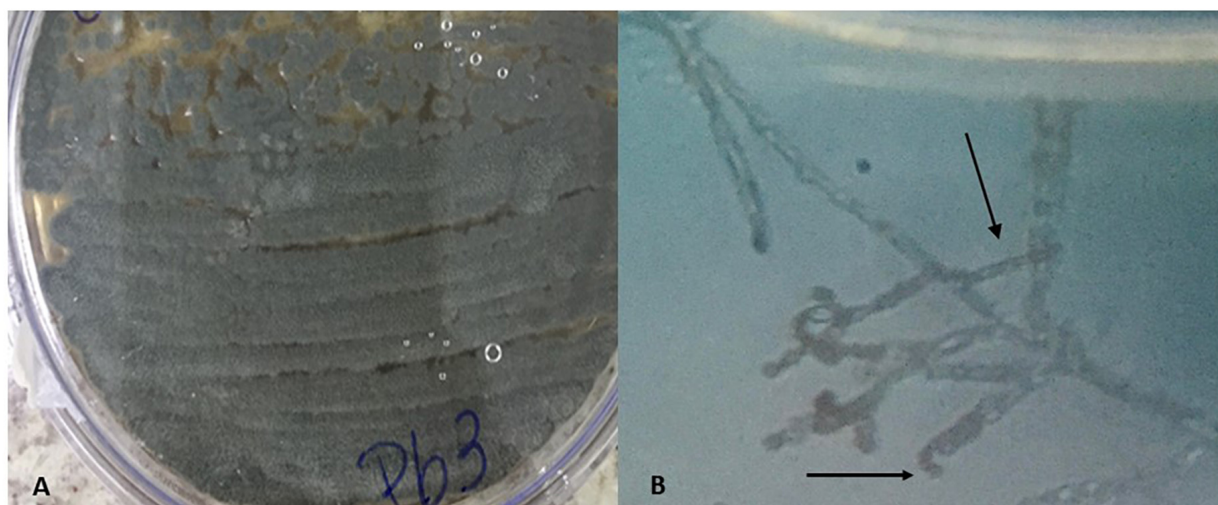


FIGURE 1 | Macroscopic characteristic with aerial mycelium of grayish color showing the production of pigment **(A)** and microscopic with spiral-shaped sporophores characteristic of bacteria of the genus *Streptomyces* **(B)**.



FIGURE 2 | Phylogenetic tree likelihood, based on the sequences of the 16S rRNA gene relating eight strains of bacteria of the genus *Streptomyces*. Branch nodes have an initialization value based on 1000 resampled datasets.

TABLE 1 | Diameters of inhibitions zones formed by *Streptomyces ansochromogene* against the pathogens tested in medium solid assays.

Microorganisms pathogens	PB3
<i>Klebsiella pneumoniae</i> (ATCC 700603)	30 ± 0
<i>Pseudomonas aeruginosa</i> (ATCC 15692)	17.6 ± 0.25
<i>Staphylococcus aureus</i> (ATCC 6538)	14.3 ± 0.11
<i>Corynebacterium diphtheriae</i> (27012)	38.3 ± 0.28
<i>Mycobacterium abscessus</i> (IC)	39.3 ± 0.11
<i>Cryptococcus neoformans</i> (24067)	0
<i>Cryptococcus gattii</i> (24065)	26 ± 0.1

active against the pathogenic yeast *C. gattii* 24065 and the bacteria *P. aeruginosa* ATCC 15692 and *S. aureus* ATCC 6538 with IDZs of 26 ± 0.1 , 14.3 ± 0.11 , and 17.6 ± 0.25 , respectively.

Agar Diffusion Assay

To investigate whether *S. ansochromogene* PB3 secreted the active metabolite (s), a liquid test was performed followed by liquid-liquid extraction with ethyl acetate. The crude extract was obtained with a yield of 0.16 g/L and tested against *K. pneumoniae* (ATCC 700603); *P. aeruginosa* (ATCC 15692); *C. diphtheriae* (ATCC 27012); *M. abscessus* and *C. gattii* (ATCC 24065). Showing inhibitory activity against *P. aeruginosa* ATCC 15692 (IDZ 19.6 ± 0.47 mm) (Table 2).

Determination of Minimum Inhibitory Concentration

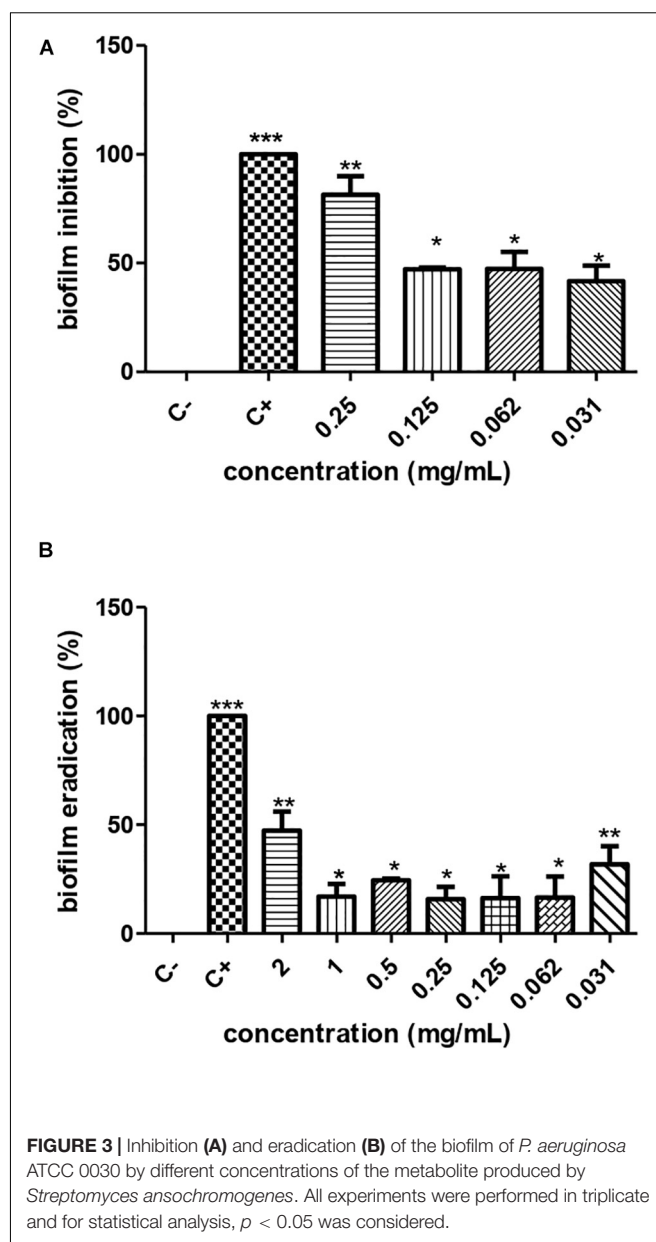
To evaluate the lowest concentration that inhibited the growth of *P. aeruginosa* (ATCC 15692) determined in the previous test, the minimum inhibitory concentration (MIC) was evaluated according to the CLSI protocol. The end point of the MIC was considered to be its lowest concentration, where there was no color change. All tests were performed in triplicates. The minimum inhibitory concentration was 0.5 mg/mL for the extracted metabolite.

Anti-biofilm Activity

According to the crystal violet technique, the metabolite produced by *S. ansochromogene* PB3 inhibited the biofilm formed by *P. aeruginosa*, at sub-MICs of 0.25 mg/mL, 0.125 mg/mL, 0.0625 mg/mL, and 0.0312 mg/mL, eradicating 82.54%, 46.53%, 33.44%, and 27.98%, respectively. This presented antimicrobial activity on *P. aeruginosa* biomass (ATCC 15692). The cellular

TABLE 2 | Diameters of inhibitions zones formed by *Streptomyces ansochromogene* against the pathogens tested in medium liquid assays.

Microorganisms pathogens	PB3
<i>Klebsiella pneumoniae</i> (ATCC 700603)	0
<i>Pseudomonas aeruginosa</i> (ATCC 15692)	19.6 ± 0.47
<i>Staphylococcus aureus</i> (ATCC 6538)	0
<i>Corynebacterium diphtheriae</i> (ATCC 27012)	0
<i>Mycobacterium abscessus</i> (IC)	0
<i>Cryptococcus gattii</i> (ATCC 24065)	0



infeasibility of biomass in the first inhibitory concentrations was confirmed by a test with resazurin (Figure 3A).

Action of Metabolite on Biofilm

The metabolite produced by *S. ansochromogene* PB3 reduced 50% of the biofilm formed, at a hyperinhibitory concentration of 2 mg/ml (Figure 3B). The resazurin test confirmed the cellular infeasibility of the biofilm bacterial biomass at this concentration.

Infection and Survival Curves in an Alternative Model

The metabolite produced by the strain of *S. ansochromogene* at a concentration of 1 mg/L showed the ability to increase the life span of *T. molitor* infected with the pathogen *P. aeruginosa*.

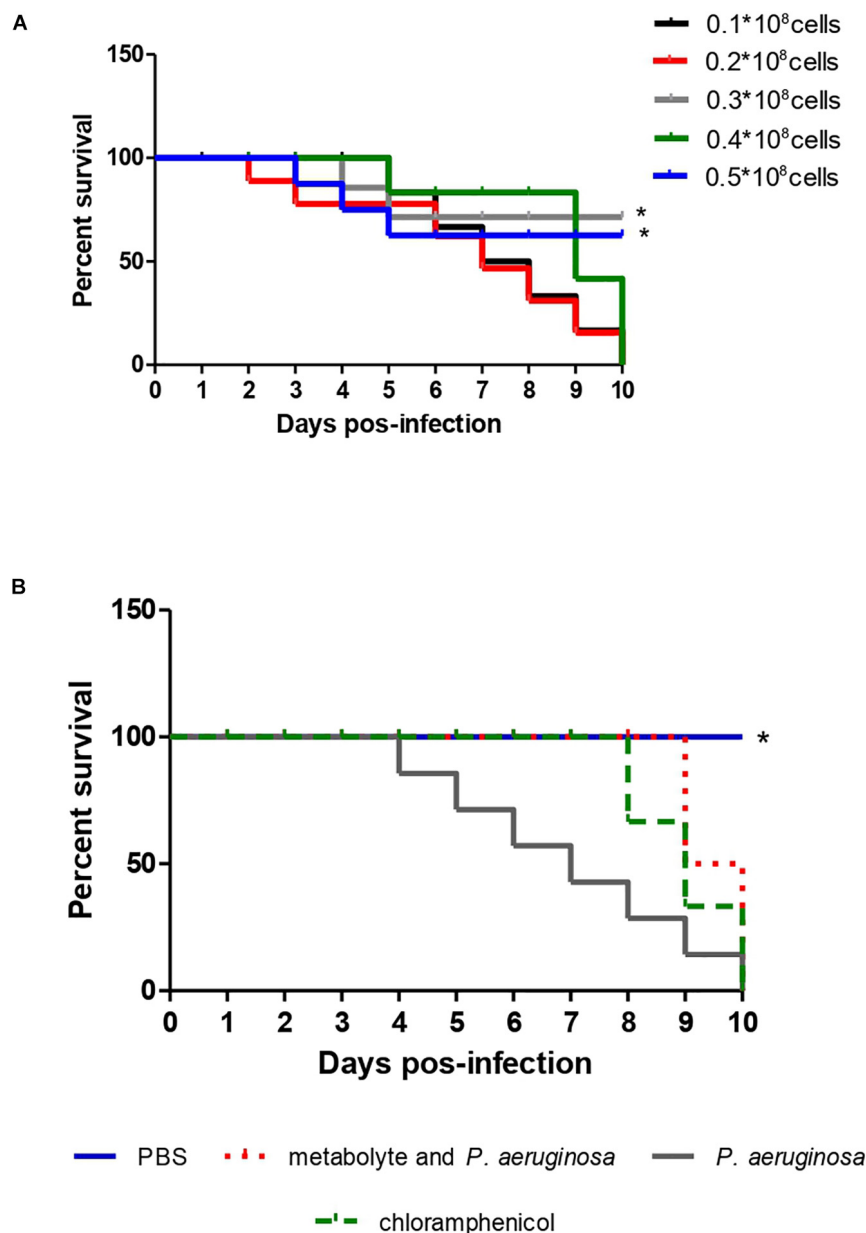


FIGURE 4 | Survival curve of 10 *T. molitor* larvae infected with different concentrations of *P. aeruginosa* cells ATCC 0030 for standardization of the inoculum **(A)** and for treatment with metabolite produced by *Streptomyces ansochromogenes* **(B)**. All experiments were carried out in triplicate for statistical analysis, $p < 0.05$ was considered.

The larvae infected with a standard solution of 0.3×10^8 of *P. aeruginosa* were all dead on the eighth day but those infected with the bacterium and inoculated with the metabolite survived until the eighth day; two larvae died on the ninth and tenth days, a behavior similar to the larvae infected with *P. aeruginosa* and treated with chloramphenicol (**Figure 4B**). When the statistical analysis was performed, a significant difference was observed between the treatment of the larva with the metabolite in relation to the larva infected with *P. aeruginosa* ($p = 0.0082$); however,

there was no difference when comparing the treatment of the larva with the metabolite and chloramphenicol.

Leishmanicidal Activity Against Promastigotes

The results demonstrated that the metabolite presented a dose-dependent effect on the promastigotes forms of *L. amazonensis* (MHOM/BR/76/MA-76) growth; it is possible to observe that in

the five highest concentrations the metabolite was able to reach more than 50% growth inhibition (Figure 5A). The estimated $IC_{50}/72\text{ h}$ was $71.65 \pm 7.4\text{ }\mu\text{g/mL}$.

Cytotoxicity Assay

The toxicity test was carried out to assess the potential of the metabolite to cause damage to cells of eukaryotic organisms. The result of the cytotoxicity test showed that the metabolite produced by the bacterium *S. ansochromogene* is not toxic to the cell at any concentration tested (Figure 5B).

DISCUSSION

The bacterium used in this work was isolated from a leaf of *Byrsonima crassifolia* and was shown to be promising against *P. aeruginosa*. Endophytic microorganisms have been

increasingly studied owing to their potential as excellent agents with diverse biological activities (Gos et al., 2017; Pinheiro et al., 2017; Rajamani et al., 2018; Singh et al., 2018). To identify the isolated bacterium, classical and molecular identification was performed, obtaining the bacterium *S. ansochromogene*. Molecular identification was used as the main tool for identifying these bacteria because in many cases, they can be confused with fungi. Van Nguyen et al. (2019) reported the genome sequence of an endophytic *Streptomyces* sp. that produced a bioactive compound of clinical interest. Bacteria of the genus *Streptomyces* are known to produce bioactive compounds with diverse biological activities. Its morphology and high metabolic potential favor the permanence of the bacteria inside the plant where there is a symbiotic relationship between the plant and the microorganism. Several authors have reported the isolation of bacteria of this genus associated with plants used by humans for various purposes. Lei et al. (2016) isolated a *Streptomyces* sp. from a medicinal plant (*Polygonum cuspidatum*) and observed its antimicrobial activity against Gram-negative bacteria *Escherichia coli*. Al-Ansari et al. (2019) reported the isolation of ten actinomycetes from the soil, of which five demonstrated activity against *Enterobacter aerogenes* and *Proteus mirabilis*. Kalyani et al. (2019) isolated 143 actinomycetes, including a *Streptomyces* sp. NLKPB-45 showed activity against Gram-positive bacteria, *S. aureus*, and Gram-negative *Escherichia coli* and *P. aeruginosa*.

In this study, the bacterium isolated from the leaf of *Byrsonima crassifolia* was identified as *S. ansochromogene* and showed activity against several pathogens of clinical interest, including the Gram-negative bacterium *P. aeruginosa*. This makes the study of the metabolite produced by the bacteria promising.

The prospecting of compounds with activity against *P. aeruginosa* has been increasingly intensified due to the phenomenon of resistance to antimicrobials that these bacteria have demonstrated. Neves et al. (2011) reported the phenomenon of resistance to antimicrobials by this bacterium as an endemic, affecting an important portion and with strains resistant to the main antibiotics for clinical use. Although the search for active compounds is reported in the literature, there are not many studies showing activity of bacteria of the genus *Streptomyces* sp. against *P. aeruginosa*. Kalyani et al. (2019) reported the activity of *Streptomyces* sp. NLKPB-45 against Gram-negative bacteria *Escherichia coli* and *P. aeruginosa*. Ashitha et al. (2019) isolated endophytic bacteria from the Chinese medicinal plant *Artemisia nilagirica* (Clarke) Pamp. Among the isolates, the bacterium *Burkholderia* sp. showed activity against several pathogens of clinical interest, including the bacterium *P. aeruginosa* MTCC 2453.

The concentration at which the metabolite shows activity is extremely important to assess its viability. In this work, extraction of the active fraction of the metabolite was performed using ethyl acetate solvent to determine the lowest concentration that showed activity (MIC). Lei et al. (2016) reported the activity of the metabolite acetate fraction produced by *Streptomyces* sp. A09916 against Gram-negative bacteria *Salmonella* sp. S11A235 at a concentration of 0.125 mg/L. Kumar et al. (2020) obtained the active fraction of the metabolite produced by *Streptomyces*

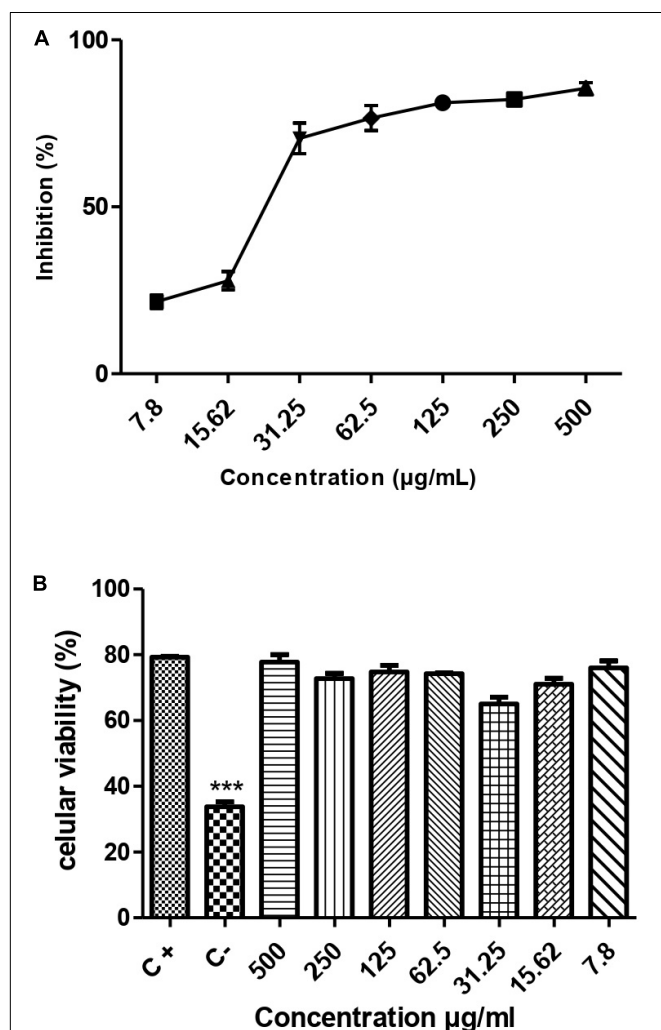


FIGURE 5 | Leishmanicidal activity (A) and cytotoxicity (B) of the metabolite produced by the endophytic bacteria *Streptomyces ansochromogenes* (PB3). All experiments were carried out in triplicate for statistical analysis, $p < 0.05$ was considered.

olivaceus LEP 7 with a Minimum Inhibitory Concentration of 50 µg/mL against the bacterium *P. aeruginosa*.

One of the main problems that make infections by the *P. aeruginosa* bacteria even more difficult to treat is that, in addition to the resistance phenomenon, these bacteria also have the ability to form biofilms due to the high capacity to carry out the quorum sense due to the glycidic nature of its cell wall (Satpathy et al., 2016). Given this characteristic, it is important to investigate the ability of the metabolite to prevent formation or eradicate the biofilm. In this study, the acetate fraction extracted from the metabolite of the endophytic bacteria *S. ansochromogene* showed the ability to inhibit and eradicate biofilms formed by *P. aeruginosa* at subinhibitory concentrations. The two phenomena (inhibition and eradication of biofilm) are related to the tested concentration of the metabolite, which can be explained by the selectivity of the membrane, which allows the metabolite to penetrate the cell at lower concentrations, making it more efficient. Antibiofilm activity has been investigated and reported by several authors. Æiríæ et al. (2019) reported the importance of the search for metabolites that inhibit the phenomenon of quorum sense, the first step in the formation of biofilms. The authors emphasize that many plants already have this known activity; however, the search for metabolites produced by microorganisms with this activity should be intensified. Younis et al. (2016) reported the metabolite antibiofilm activity produced by a species of *Streptomyces* sp. isolated from a marine environment. The authors emphasized the ability of the metabolite acetate fraction to inhibit the phenomenon of quorum sense, thus preventing the formation of biofilm. Pattnaik et al. (2018) reported the antibiofilm activity of the extract of the metabolite produced by the fungus *Diaporthe phaseolorum* SSP12 against a biofilm formed by *P. aeruginosa* PAO1. The authors also emphasized the ability of the extract to inhibit $79\% \pm 3.5\%$ quorum sensing formation in concentrations of 0.750 µg/mL, which is commonly performed by strains of these bacteria. The use of compounds with anti-biofilm activity has been reported as a possible alternative therapy for treating various infections as a solution to the phenomenon of microbial resistance (Santhakumari and Ravi, 2019).

Biofilm formation is a strategy used by *P. aeruginosa* to cause infections, so it is important to test the metabolite activity *in vivo*. In this study, the capacity of the *S. ansochromogene* metabolite was tested in an alternative model using *T. molitor* larvae. In this evaluation, it was observed that the metabolite at the concentration (0.5 mg/mL) established in the MIC had the capacity to inhibit the infection caused by *P. aeruginosa* bacteria in *T. molitor*. The larvae treated with the metabolite showed greater survival than those treated with the antibiotic chloramphenicol, emphasizing the protective effect of the metabolite. Because the use of animal models is decreasing for ethical reasons, alternative models have been reported in the literature as an excellent way to evaluate the effectiveness of compounds in living beings. Silva et al. (2019) assessed the ability of *S. aureus* to infect *Galleria mellonella* larvae. The authors observed the pathogen's ability to infect and form biofilms inside the animal.

Leishmaniasis is a treatable and curable disease, but drugs that used in treatment have several limitations because of serious side effect (World Health Organization (WHO), 2018; Araújo et al., 2019). The results showed that the secondary metabolite inhibited the growth of promastigote forms, a fact observed by Santiago et al. (2012) that isolated 564 endophytic fungi from plants of the Antarctic, these 19 sources leishmanicidal activity against a promastigote form of *L. amazonensis*. This activity is reinforced by the cytotoxicity test that shows that the metabolite is not toxic to the cell at any concentration tested, suggesting its specificity for the protozoan.

CONCLUSION

The endophytic bacterium *S. ansochromogene* has anti-microbial potential because it produces a metabolite that can be used for its antimicrobial and antibiofilm action against the bacterium *P. aeruginosa* and against *L. amazonensis* in promastigote form. In view of these results, studies will be carried out with the objective of identifying the compound and expanding its spectrum of action, evaluating whether it has activity against other protozoa and tumors.

DATA AVAILABILITY STATEMENT

The datasets presented in this study can be found in online repositories. The names of the repository/repositories and accession number(s) can be found below: <https://www.ncbi.nlm.nih.gov/genbank/>, MT634691.

AUTHOR CONTRIBUTIONS

This manuscript has as main objective to show the action of one or more compounds produced by a microorganism called *Streptomyces ansochromogenes* isolated from a plant in face of a common actia in contaminated wounds called *Pseudomonas aeruginosa*. This bacterium has the ability to form biofilms to be able to colonize contaminated wounds when an infection process begins, so it is important that compounds manage to prevent this mechanism. All authors contributed to the article and approved the submitted version.

FUNDING

This work was supported by the Fundação de Amparo a Pesquisa do Estado do Maranhão—FAPEMA (ECT-05756/18).

ACKNOWLEDGMENTS

The authors would like to thank Universidade Ceuma for supporting research.

REFERENCES

- Al-Ansari, M., Alkubaisi, N., Vijayaragavan, P., and Murugan, K. (2019). Antimicrobial potential of *Streptomyces* sp. to the Gram positive and Gram negative pathogens. *J. Infect. Public Health* 12, 861–866. doi: 10.1016/j.jiph.2019.05.016
- Araújo, I. A. C., de Paulo, R. C., Alves, C. L., Faria, K. F., de Oliveira, M. M., Mendes, G. G., et al. (2019). Efficacy of lapachol on treatment of cutaneous and visceral leishmaniasis. *Exp. Parasitol.* 199, 67–73. doi: 10.1016/j.exppara.2019.02.013
- Ashitha, A., Midhun, S. J., Sunil, M. A., Nithin, T. U., Radhakrishnan, E. K., et al. (2019). Bacterial endophytes from *Artemisia nilagirica* (Clarke) Pamp., with antibacterial efficacy against human pathogens. *Microb. Pathog.* 135:103624. doi: 10.1016/j.micpath.2019.103624
- Bauer, A. W., Kirby, W. M., Sherris, J. C., and Turck, M. (1966). Antibiotic susceptibility testing by a standardized single disk method. *Am. J. Clin. Pathol.* 45, 493–496. doi: 10.1093/ajcp/45.4_ts.493
- Bunbamrung, N., Intaraudom, C., Drama, A., Thawai, C., Tadtong, S., Auncharoen, P., et al. (2020). Antibacterial, antitubercular, antimalarial and cytotoxic substances from the endophytic *Streptomyces* sp. *Phytochemistry* 172:112275. doi: 10.1016/j.phytochem.2020.112275
- Eiríe, A. D., Petrović, J. D., Glamočlija, J. M., Smiljković, M. S., Nikolić, M. M., Stojković, D. S., et al. (2019). Natural products as biofilm formation antagonists and regulators of quorum sensing functions: a comprehensive review update and future trends. *S. Afr. J. Bot.* 120, 65–80. doi: 10.1016/j.sajb.2018.09.010
- Elkhatay, E. S., and Goda, A. M. (2017). Antifungal and cytotoxic constituents from the endophytic fungus *Penicillium* sp. *Bull. Fac. Pharm. Cairo Univ.* 55, 85–89. doi: 10.1016/j.bfopcu.2017.03.001
- Ensign, J. C. (1978). Formation, properties, and germination of actinomycete spores. *Annu. Rev. Microbiol.* 32, 185–219. doi: 10.1146/annurev.mi.32.100178.001153
- Gos, F. M. W. R., Savi, D. C., Shaaban, K. A., Thorson, J. S., Aluizio, R., Possiede, Y. M., et al. (2017). Antibacterial activity of endophytic actinomycetes isolated from the medicinal plant *Vochysia divergens* (Pantanal, Brazil). *Front. Microbiol.* 8:1642. doi: 10.3389/fmicb.2017.01642
- Hussain, H., John, M., Al-Harrasi, A., Shah, A., Hassan, Z., Abbas, G., et al. (2015). Phytochemical investigation and antimicrobial activity of an endophytic fungus *Phoma* sp. *J. King Saud Univ. Sci.* 27, 92–95.
- Ichikawa, T., Date, M., Ishikura, T., and Ozaki, A. (1971). Improvement of kasugamycin-producing strain by the agar piece method and the prototroph method. *Folia Microbiol.* 16, 218–224.
- Jiang, S., Qian, D., Yang, N., Tao, J., and Duan, J. (2013). Biodiversity and antimicrobial activity of endophytic fungi in *Angelica sinensis*. *Chin. Herb. Med.* 5, 264–271.
- Kalyani, B. S., Krishna, P. S., and Sreenivasulu, K. (2019). Screening and identification of novel isolate *Streptomyces* sp. NLKPB45 from Nellore coastal region for its biomedical applications. *Saudi J. Biol. Sci.* 26, 1655–1660. doi: 10.1016/j.sjbs.2018.08.027
- Klein, M. L., Hwang, G., Santos, P. H. S., Campanella, O. H., and Koo, H. (2015). *Streptococcus mutans*-derived extracellular matrix in cariogenic oral biofilms. *Front. Cell. Infect. Microbiol.* 5:10. doi: 10.3389/fcimb.2015.00010
- Klich, M. A., and Pitt, J. I. (1988). *Laboratory Guide to Common Aspergillus Species and their Teleomorphs*. Sydney, NSW: CSIRO, Division of Food Processing.
- Kumar, R. S., Ahmad, P., Keerthana, S. S., Cressida, P. J., Moorthy, I. G., and Raja, S. S. (2020). Extraction and purification of an antimicrobial bioactive element from lichen associated *Streptomyces olivaceus* LEP7 against wound inhabiting microbial pathogens. *J. King Saud Univ. Sci.* 32, 2009–2015. doi: 10.1016/j.jksus.2020.01.039
- Laihonon, P., Kalliola, R., and Salo, J. (2004). The biodiversity information clearing-house mechanism (CHM) as a global effort. *Environ. Sci. Policy* 7, 99–108. doi: 10.1016/j.envsci.2003.12.003
- Lee, S. W., Won, K., Lim, H. K., and Kim, J. C. (2007). Screening for novel lipolytic enzymes from uncultured soil microorganisms. *Appl. Microbiol. Biotechnol.* 65, 720–726. doi: 10.1007/s00253-004-1722-3
- Lei, W., Peng, Q., Long, X.-F., Zhang, S., Zhi-Gang, Z., and Yong-Qiang, T. (2016). Comparative analysis of chemical constituents, antimicrobial and antioxidant activities of ethylacetate extracts of *Polygonum cuspidatum* and its endophytic actinomycete, *Streptomyces* sp. A0916. *Chin. J. Nat. Med.* 14, 117–123. doi: 10.1016/S1875-5364(16)60004-3
- Lincopan, N., and Trabulsi, L. R. (2008). “*Pseudomonas Aeruginosa*,” in *Microbiologia*, 5th Edn, eds L. R. Trabulsi and F. Alterthum (São Paulo: Atheneu), 369–381.
- Mahmood, A., and Kataoka, R. (2020). Metabolite profiling reveals a complex response of plants to application of plant growth-promoting endophytic bacteria. *Microbiol. Res.* 234, 126421. doi: 10.1016/j.micres.2020.126421
- Matsuura, T. (2004). *Caracterização Taxonomica de Actinomicetos Endofíticos Produtores de Antibióticos Isolados de Cupuaçuzeiro (Theobroma grandiflorum Schum.)*. Takeshi Matsuura. Campinas: Universidade Estadual de Campinas.
- Neves, P. R., Mamizuka, E. M., Levy, C. E., and Lincopan, N. (2011). *Pseudomonas aeruginosa* multirresistente: um problema endêmico no Brasil. *J. Bras. Patol. Med. Lab.* 47, 409–420. doi: 10.1590/S1676-24442011000400004
- Olmos, E., Mehmood, N., Husein, L. H., Goergen, J.-L., Fick, M., and Delaunay, S. (2013). Effects of bioreactor hydrodynamics on the physiology of *Streptomyces*. *Bioprocess Biosyst. Eng.* 36, 259–272. doi: 10.1007/s00449-012-0794-1
- Pang, Z., Raudonis, R., Glick, B. R., Lin, T. J., and Cheng, Z. (2019). Antibiotic resistance in *Pseudomonas aeruginosa*: mechanisms and alternative therapeutic strategies. *Biotechnol. Adv.* 37, 177–192. doi: 10.1016/j.biotechadv.2018.11.013
- Pattanaik, S. S., Ranganathan, S., Ampasala, D. R., Syed, A., Ameen, F., and Busi, S. (2018). Attenuation of quorum sensing regulated virulence and biofilm development in *Pseudomonas aeruginosa* PAO1 by *Diaporthe phaseolorum* SSP12. *Microb. Pathog.* 118, 177–189. doi: 10.1016/j.micpath.2018.03.031
- Pinheiro, E. A. A., Pina, J. R. S., Feitosa, A. O., Carvalho, J. M., Borges, F. C., Marinho, P. S. B., et al. (2017). Bioprospecting of antimicrobial activity of extracts of endophytic fungi from *Bauhinia guianensis*. *Rev. Argent. Microbiol.* 49, 3–6. doi: 10.1016/j.ram.2016.08.005
- Pitt, I. (1979). *The Genus Penicillium and its Teleomorphic States Eupenicillium and Talaromyces*. New York, NY: Academic Press.
- Pitt, I., and Samson, R. A. (1990). Approaches to *Penicillium* and *Aspergillus* systematics. *Stud. Mycol.* 32, 77–90.
- Rajamani, T., Suryanarayanan, T. S., Murali, T. S., and Thirunavukkarasu, N. (2018). Distribution and diversity of foliar endophytic fungi in the mangroves of Andaman Islands, India. *Fungal Ecol.* 36, 109–116. doi: 10.1016/j.funeco.2018.09.007
- Raju, R., Gromyko, O., Fedorenko, V., Luzketskyy, A., and Müller, R. (2014). Albalflavonol B, a new sesquiterpene isolated from the terrestrial actinomycete, *Streptomyces* sp. *J. Antibiot.* 68, 286–288. doi: 10.1038/ja.2014.138
- Rapper, K. B., and Fennell, I. (1965). *The Genus Aspergillus*. Baltimore: Williams & Wilkins.
- Sader, H. S., Gales, A. C., Pfaller, M. A., Mendes, R. E., Zoccoli, C., Barth, A., et al. (2001). Pathogen frequency and resistance patterns in Brazilian hospitals: summary of results from three years of the SENTRY antimicrobial surveillance program. *Braz. J. Infect. Dis.* 5, 200–214. doi: 10.1590/S1413-86702001000400006
- Santhakumari, S., and Ravi, A. V. (2019). Targeting quorum sensing mechanism: an alternative anti-virulent strategy for the treatment of bacterial infections. *S. Afr. J. Bot.* 120, 81–86. doi: 10.1016/j.sajb.2018.09.028
- Santiago, I. F., Alves, T. M. A., Rabello, A., Sales Junior, P. A., Romanha, A. J., Zani, C. L., Rosa, C. A., and Rosa L. H. (2012). Leishmanicidal and antitumoral activities of endophytic fungi associated with the Antarctic angiosperms *Deschampsia Antarctica* Desv. and *Colobanthus quitensis* (Kunth) Bartl. *Extremophiles* 16, 95–103. doi: 10.1007/s00792-011-0409-9
- Santiago, I. F., Alves, T. M. A., Rabello, A., Sales Junior, P. A., Romanha, A. J., Zani, C. L., Rosa, C. A., and Rosa L. H. (2012). Leishmanicidal and antitumoral activities of endophytic fungi associated with the Antarctic angiosperms *Deschampsia Antarctica* Desv. and *Colobanthus quitensis* (Kunth) Bartl. *Extremophiles* 16, 95–103. doi: 10.1007/s00792-011-0409-9
- Satpathy, S., Sen, S. K., Pattanaik, S., and Raut, S. (2016). Review on bacterial biofilm: an universal cause of contamination. *Biocatal. Agric. Biotechnol.* 7, 56–66. doi: 10.1016/j.bcab.2016.05.002
- Shirling, E. B., and Gottlieb, D. (1966). Methods for characterization of *Streptomyces* species. *Int. J. Sys. Evol. Microbiol.* 16, 313–340. doi: 10.1099/00207713-16-3-313
- Silva, R., Roberta, B. F., Silva, T. D., and Macedo, A. J. (2019). Alternative method in *Galleria mellonella* larvae to study biofilm infection and treatment. *Microb. Pathog.* 137:103756. doi: 10.1016/j.micpath.2019.103756

- Singh, H., Naik, B., Kumar, V., and Bisht, G. S. (2018). Screening of endophytic actinomycetes for their herbicidal activity. *Ann. Agrar. Sci.* 16, 101–107. doi: 10.1016/j.aasci.2017.11.001
- Stepanoviæ, S., Vukovic, D., Hola, V., Bonaventura, G. D., Djukiæ, S., Cirkoviæ, I., et al. (2007). Quantification of biofilm in microtiter plates: overview of testing conditions and practical recommendations for assessment of biofilm production by *Staphylococci*. *APMIS* 115, 891–899. doi: 10.1111/j.1600-0463.2007.apm_630.x
- Supong, K., Thawai, C., Choowong, W., Kittiwongwattana, C., Thanaboripat, D., Laosinwattana, C., et al. (2016). Antimicrobial compounds from endophytic *Streptomyces* sp. BCC72023 isolated from rice (*Oryza sativa* L.). *Res. Microbiol.* 167, 290–298. doi: 10.1016/j.resmic.2016.01.004
- Tamura, K., and Nei, M. (1993). Estimation of the number of nucleotide substitutions in the control region of mitochondrial DNA in humans and chimpanzees. *Mol. Biol. Evol.* 10, 512–526.
- Trisuwan, K., Rukachaisirikul, V., Sukpondma, Y., Preedanon, S., Phongpaichit, S., Rungjindamai, N., et al. (2008). Epoxydons and a pyrone from the marine-derived fungus *Nigrospora* sp. PSU-F5. *J. Nat. Prod.* 71, 1323–1326. doi: 10.1021/np8002595
- Van Nguyen, H., Truong, P. M., Duong, H. T., Dinh, H. M., and Nguyen, C. H. (2019). Genome sequence data of *Streptomyces* sp. SS52, an endophytic strain for daidzein biosynthesis. *Data Brief* 27:104746. doi: 10.1016/j.dib.2019.104746
- Walkman & Henrici (1943). *Bergey's Manual of Systematic Bacteriology*. Baltimore: Williams and Wilkins, 2452–2492.
- World Health Organization (2015). *Global Action Plan on Antimicrobial Resistance*. Geneva: World Health Organization.
- World Health Organization (WHO) (2018). *Leishmaniasis Fact Sheet*. Available online at: <https://www.who.int/en/news-room/fact-sheets/detail/leishmaniasis> (accessed August 12, 2020).
- Younis, K. M., Usup, G., and Ahmad, A. (2016). Secondary metabolites produced by marine streptomyces as antibiofilm and quorum-sensing inhibitor of uropathogen *Proteus mirabilis*. *Environ. Sci. Poll. Res. Int.* 23, 4756–4767. doi: 10.1007/s11356-015-5687-9
- Zgoda, J. R., and Porter, J. R. (2001). A convenient microdilution method for screening natural products against bacteria and fungi. *Pharm. Biol.* 39, 221–225. doi: 10.1076/phbi.39.3.221.5934

Conflict of Interest: The authors declare that the research was conducted in the absence of any commercial or financial relationships that could be construed as a potential conflict of interest.

Copyright © 2020 Amorim, Castro, Souza, Alves, Dias, Melo, da Silva, Villis, Bonfim, Falcai, Silva, Monteiro-Neto, Aliança, da Silva and de Miranda. This is an open-access article distributed under the terms of the Creative Commons Attribution License (CC BY). The use, distribution or reproduction in other forums is permitted, provided the original author(s) and the copyright owner(s) are credited and that the original publication in this journal is cited, in accordance with accepted academic practice. No use, distribution or reproduction is permitted which does not comply with these terms.



Natural Anti-biofilm Agents: Strategies to Control Biofilm-Forming Pathogens

Rojita Mishra^{1†}, Amrita Kumari Panda^{2†}, Surajit De Mandal³, Muhammad Shakeel³, Satpal Singh Bisht⁴ and Junaid Khan⁵

¹ Department of Botany, Polasara Science College, Polasara, India, ² Department of Biotechnology, Sant Gahira Guru University, Ambikapur, India, ³ Key Laboratory of Bio-Pesticide Innovation and Application of Guangdong Province, College of Agriculture, South China Agricultural University, Guangzhou, China, ⁴ Department of Zoology, Kumaun University, Nainital, India, ⁵ Department of Pharmacy, Sant Gahira Guru University, Ambikapur, India

OPEN ACCESS

Edited by:

Sujogya Kumar Panda,
KU Leuven, Belgium

Reviewed by:

Murugan Kasi,
Manonmaniam Sundaranar University,
India
Fazlurrahman Khan,
Sharda University, India

*Correspondence:

Rojita Mishra
rojitamishra@gmail.com

[†] These authors have contributed
equally to this work and share first
authorship

Specialty section:

This article was submitted to
Antimicrobials, Resistance
and Chemotherapy,
a section of the journal
Frontiers in Microbiology

Received: 27 May 2020

Accepted: 30 September 2020

Published: 29 October 2020

Citation:

Mishra R, Panda AK,
De Mandal S, Shakeel M, Bisht SS
and Khan J (2020) Natural Anti-biofilm
Agents: Strategies to Control
Biofilm-Forming Pathogens.
Front. Microbiol. 11:566325.
doi: 10.3389/fmicb.2020.566325

Pathogenic microorganisms and their chronic pathogenicity are significant concerns in biomedical research. Biofilm-linked persistent infections are not easy to treat due to resident multidrug-resistant microbes. Low efficiency of various treatments and *in vivo* toxicity of available antibiotics drive the researchers toward the discovery of many effective natural anti-biofilm agents. Natural extracts and natural product-based anti-biofilm agents are more efficient than the chemically synthesized counterparts with lesser side effects. The present review primarily focuses on various natural anti-biofilm agents, i.e., phytochemicals, biosurfactants, antimicrobial peptides, and microbial enzymes along with their sources, mechanism of action via interfering in the quorum-sensing pathways, disruption of extracellular polymeric substance, adhesion mechanism, and their inhibitory concentrations existing in literature so far. This study provides a better understanding that a particular natural anti-biofilm molecule exhibits a different mode of actions and biofilm inhibitory activity against more than one pathogenic species. This information can be exploited further to improve the therapeutic strategy by a combination of more than one natural anti-biofilm compounds from diverse sources.

Keywords: microbial biofilm, therapeutic strategies, phytochemicals, multidrug resistance, antimicrobial peptides, biosurfactant

BACKGROUND

The antimicrobial tolerance of biofilms has emerged as a significant challenge to medical scientists across diverse healthcare sectors. Synthetic drugs, combinational therapy, and antibiotic hybrids could not achieve and deliver the desired results during the treatment. The hunt for novel antimicrobials in drug resistance emergency insists on the scientific society to search novel natural anti-biofilm agents. The focus of the present review is to revisit various natural products to overcome the biofilm-forming microorganisms and provide concise information on existing

Abbreviations: AHL, acyl-homoserine lactone; AMP, anti-microbial peptide; BFC, biofilm-forming capacity; CLSM, confocal laser scanning microscopy; CSH, cell surface hydrophobicity; eDNA, extracellular DNA; EPS, extracellular polymeric substances; GA, ginkgolic acid; HSL, homoserine lactone; MBIC, minimum biofilm inhibitory concentration; MFC, minimal fungicidal concentration; MIC, minimum inhibitory concentration; PMNs, polymorphonuclear leukocytes; QS, quorum sensing; SEM, scanning electron microscopy; TEM, transmission electron microscopy.

confines and recent developments in the modification of different natural anti-biofilm agents to make them effective drug candidates for clinical exploitation.

The Biofilms

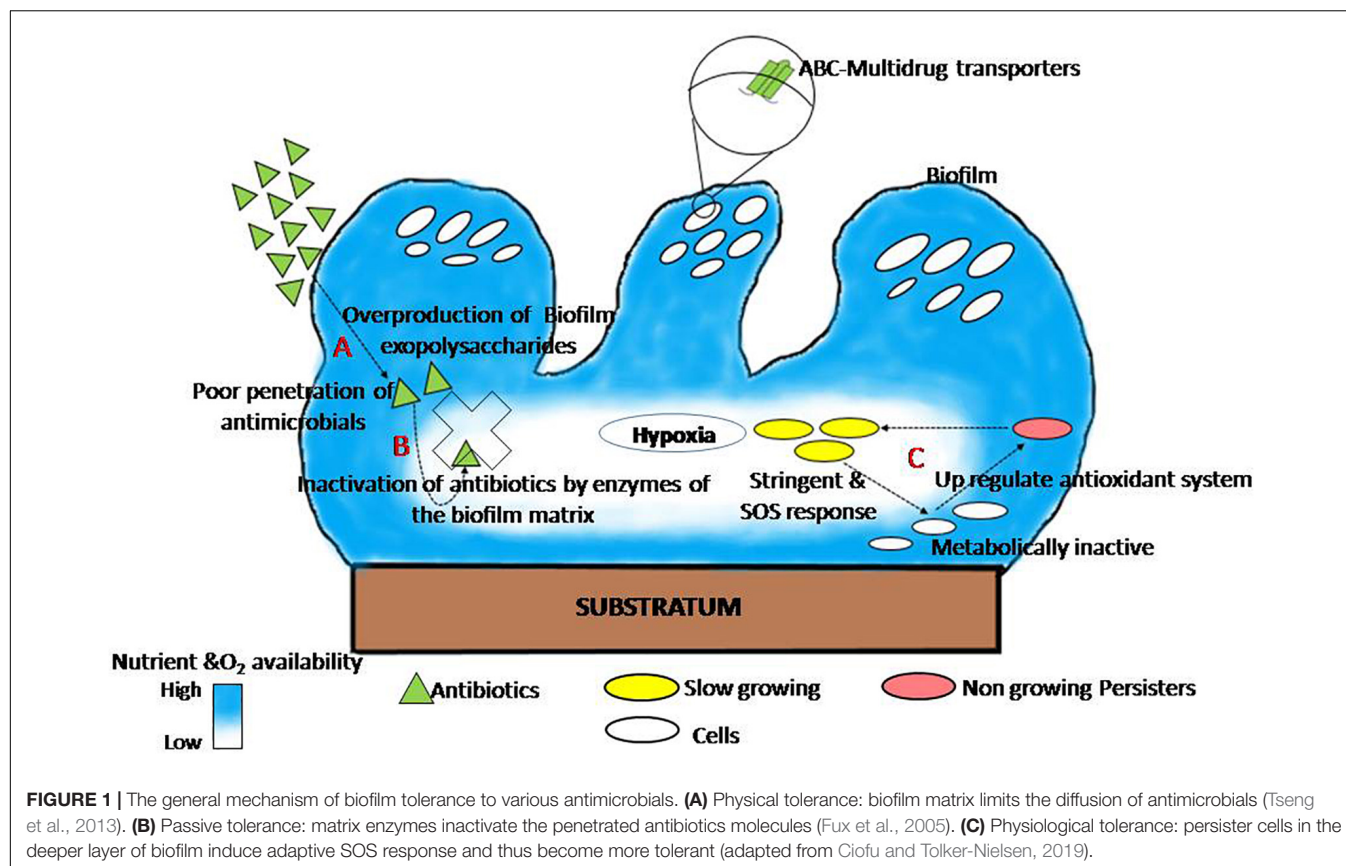
The concept of biofilm was first developed by Marshall et al. (1971) and further described by Fletcher, Characklis, and Costerton, "Biofilm is the unique pattern of growth in the life cycle of microbes that provides specific properties, advantages and higher level of organization to the free living bacterial cells during colonization" (Characklis, 1973; Fletcher and Floodgate, 1973; Geesey et al., 1978; Flemming and Wuertz, 2019). The description of biofilm is much more clarified by Flemming and Wuertz (2019) that biofilms are aggregates of microorganisms with distinct sessile cells followed by cell division to form small clusters, microcolonies, and larger sums. The film underneath the biofilm is only in direct contact with the substratum in a multilayered heterogeneous microbial mat. Biofilms are extensively used in various biotechnological applications, for example, biofuel production, degradation of wastewater, and filtration of drinking water (Flemming et al., 2016b). The negative impact of biofilm includes bio-fouling (Flemming, 2011), corrosion (Little and Lee, 2015), and deterioration of the drinking water quality (Wingender and Flemming, 2011). All higher eukaryotes, including humans, are populated by microorganisms that form biofilms (De Vos, 2015). Human dental plaque, skin, and gut represent one of the dominant biofilms in eukaryotic habitats. The widespread uses of medical devices create several new niches for bacterial biofilm formations (Qvortrup et al., 2019).

Cells in biofilm survive harsh growth conditions as biofilms are surrounded by high molecular weight extracellular polymeric substances (EPS) that attach cells (Branda et al., 2005; Flemming and Wingender, 2010). The EPS are composed of proteins, lipids, polysaccharides, and extracellular DNA and play an essential function in the pathogenesis of the numerous microbial infections (Ch'ng et al., 2019). It has also been reported that microbial cells inside the biofilms are found to be resistant against UV, metal toxicity, acid exposure, desiccation, pH gradients, etc. (Costerton et al., 1999; Hall-Stoodley et al., 2004). In accretion to various physical and chemical tolerances, EPS confers immune resistance to many resident pathogenic microbes within biofilms by inhibiting neutrophil-mediated phagocytosis (Gunn et al., 2016). Izano et al. (2009) reported that the eDNA and intercellular adhesins of EPS act as a barrier for the penetration of a variety of antimicrobials. The eDNA present within the EPS chelate human antimicrobial peptides (AMPs) and lessen the antimicrobial activity of these peptides (Jones et al., 2013). So far, many studies have been carried out to identify the method of biofilm formation and subsequent preventive strategies to strike the challenges, especially the drug resistance due to biofilm formation (Roy et al., 2018).

The presence of glycocalyx, outer membrane structure, and efflux pumps; and heterogeneity in growth rate, genetic adaptation, metabolic state, and metabolism of cells within a biofilm are the leading causes of biofilm that acquire resistance

against antimicrobials (Singh et al., 2017). The mode of biofilm establishment in several human pathogens, as well as its drug resistance mechanism, is well documented and reviewed by different researchers and plotted (Figure 1). This figure explains the shared mechanism of biofilm tolerance under three sections. (1) Physical tolerance: the excess production of EPS restricts the penetration and diffusion of antimicrobials; as a result, cells in the biofilm get more time to become tolerant. Similar observations found that EPS production augments antimicrobial tolerance; an isogenic $\Delta csgD$ mutant of *Salmonella Typhimurium* (EPS-deficient mutant) is much susceptible to hydrogen peroxide (MacKenzie et al., 2017) and ciprofloxacin (Tabak et al., 2009). Therefore, therapeutic strategies that destabilize and inhibit EPS are the best anti-biofilm approaches to inhibit biofilms and reduce significant problems of antimicrobial resistance. A similar observation has been recorded by Deokar and Kadam (2020) and Dieltjens et al. (2020) that EPS inhibition reduces cell adhesion as well as drug tolerance in biofilms. (2) Passive tolerance: enzymes present in the biofilm matrix inactivate the antimicrobial molecules. The mechanism for the neutralization of antimicrobials through the biofilm matrix components have also been reported (Fux et al., 2005), and there are reports that catalase enzymes present in the biofilm matrix are responsible for tolerance of *Staphylococcus epidermidis* biofilm against various physicochemical agents (Olwal et al., 2019). (3) Physiological tolerance: metabolically inactive cells in the deeper layers of biofilm exhibit adaptive stress responses that regulate the tolerance of biofilms to various antimicrobials. Persister cells become more tolerant of a variety of antibiotics after phenotypic and reversible changes induced by starvation, ecological factors, and several other adaptive responses such as SOS and stringent response (Harms et al., 2016; Ciofu and Tolker-Nielsen, 2019; Soares et al., 2019).

Persister cells are slow-dividing bacteria, less susceptible to antibiotics, and they have an essential role for biofilm re-establishment (Dawson et al., 2011). Persister cells upregulate the expression of various toxin-antitoxin genes that blocks translation which leads to lessen cellular metabolism and eventually guarantees their survival in the presence of antibiotics (Lewis, 2005). These cells revive to vegetative dividing cells to reoccur infection after the end of antibiotic action (Lewis, 2010). Persister cells have been confined from antibiotics because these cells express the toxin-antitoxin system where the antibiotic target is blocked by the toxin module (Lewis, 2005). Oxygen scarcity and little metabolic activity in biofilms provide *P. aeruginosa* greater tolerance to many antibiotics (Wilkins et al., 2014). Sudden changes in pH between layers in a biofilm play a role to accumulate organic acids, thus deactivating the penetrating compounds (Wilkins et al., 2014). The development of gradients of oxygen, pH, nutrients, and electron acceptors all over the biofilm makes microenvironments where cells respond by altering their gene expression (Spormann, 2008; Stewart and Franklin, 2008). Complex (polymicrobial) biofilm made up of many species is generally more resistant to antibiotics than biofilm made up of a single species (Van der Veen and Abee, 2011). Cell diversity and



metabolic conditions play the most important role in antibiotic tolerance of biofilms.

However, with the advance of sequencing technology, a ton of genomic data have been generated, which allows further illustration of the unknown molecular mechanism in the association of biofilm formation and drug resistance. The RNA-seq transcriptome analysis identified arsenic resistance operon genes (*arsR* and *arsD*), sporulation regulatory gene (*paiA*), ABC drug transporter classes, and penicillin-binding proteins associated with the *Enterococcus faecalis* biofilm formation and drug resistance (Seneviratne et al., 2017). They found higher-level expression of *arsD* in biofilm mode to avoid cell toxicity and suggested that *arsD* gene knockout could be a possible way of inhibiting biofilm formation. Similarly, they also observed the reduced level of expression of the *paiA* gene in biofilms. Padhi et al. (2016) reported that *Mtb* Rv0024 protein expression plays a significant role in the biofilm formation and subsequent resistance against anti-tuberculosis drugs in non-pathogenic *Mycobacterium smegmatis* strain.

The present tendency of antifungal tolerance is also a significant area of concern; therefore, direct research in a direction of novel antifungal compounds with targeted mechanisms of action are required (Sharma and Bisht, 2020). Many studies reported that the biofilm of *Candida albicans* is tolerant to many antifungal drugs as compared with the planktonic yeast cells. Moreover, the formation of mannan-glucan complex promoted by the extracellular vesicles (EVs)

is also linked to drug resistance and reported in *C. albicans*, *C. glabrata*, *C. tropicalis*, and *C. parapsilosis* (Mitchell et al., 2015; Dominguez et al., 2018; Zarnowski et al., 2018). It has also been reported that overexpression of efflux pumps, a mutation in the target site of the drug, persisted cells, the interaction between biofilm and host immunity system as well as proteins associated with the filamentation process were involved in the biofilm-associated resistance mechanism of fungi (Borghi et al., 2016). Analyzing the transcriptional network regulating biofilm growth of *C. albicans* illustrates six major transcription regulators such as *Efg1* and *Tec1* for cell morphology regulation; *Bcr1*, *Brg1*, and *Ndt80* for biofilm formation; and *Tec1* and *Rob1* which controls the normal process of biofilm formation (Fox and Nobile, 2012; Uppuluri et al., 2018). Thus, an in-depth understanding of the molecular pathway involved in the biofilm formation and subsequent antibiotic resistance is essential to formulate the preventive measures. This review aims to focus on the natural anti-biofilm agents effective against a broad range of microbial biofilms and strategies related to recent biofilm treatments.

Anti-biofilm Agents Based on Natural Products

The formation and development of biofilms is a complicated procedure involving different stages which can be the target of natural anti-biofilm agents for the prevention of biofilm

development. Some of the well-studied stages of biofilm development include (1) attachment of bacterial cells to a suitable biotic/abiotic surface, (2) development of biofilm structure, (3) maturation of biofilm, and (4) dispersion (Boles and Horswill, 2008). The first two stages are highly critical in the development of biofilms and targeting one or both of these stages seems to be the ideal strategy for inhibition of biofilm formation. The attachment stage involves cytoskeletal elements (predominantly flagella, fimbriae) and lipopolysaccharides as key players. Surface signaling/communication of a group of bacteria, also termed as Quorum Sensing is a key player in the formation of biofilm. The natural anti-biofilm agents either act solely or synergistically by diverse mechanisms, as illustrated in **Figure 2**.

Phytochemicals

There are broadly five classes of natural compounds that have high anti-biofilm properties. Those are phenolics, essential oils, terpenoids, lectins, alkaloids, polypeptides, and polyacetylenes (Yong et al., 2019). Phenolics are a group of compounds. It has seven subclasses which include phenolic acids, quinones, flavonoids, flavones, flavonols, tannins, and coumarins, out of which tannins, specifically condensed tannins, have anti-biofilm activity (Trentin et al., 2011). These entire compounds act on biofilm by six main mechanisms like substrate deprivation, membrane disruption, and binding to adhesin complex and cell wall; bind to proteins; interact with eukaryotic DNA; and block viral fusion (Cowan, 1999; Lu et al., 2019).

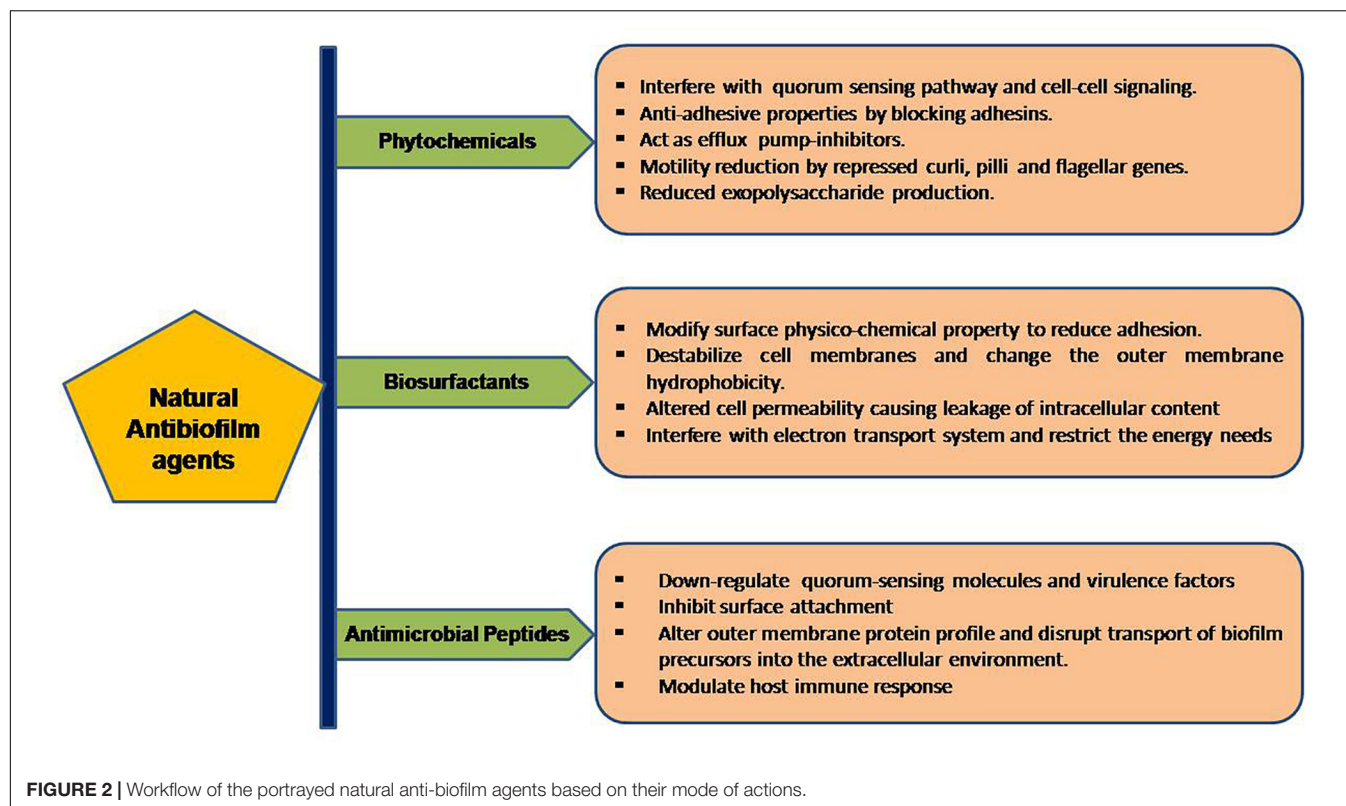
Several solvents, i.e., water, methanol, ethanol, chloroform, ether, dichloromethanol, and acetone, were used for the extraction of natural compounds from various sources for anti-biofilm activity. Various experiments carried out by researchers found that water extracts anthocyanins, sugars like tannins, saponins, terpenoids, polypeptides, and lectins. Ethanol extracts compounds, i.e., tannins, polyphenols, polyacetylenes, flavonol, terpenoids, sterols, alkaloids, and propolis whereas methanol extracts anthocyanins, terpenoids, saponins, tannins, xanthoxylines, quassinoids, totarol, flavones, lactones, phenones, and polyphenols (Cowan, 1999). Extraction with chloroform yields terpenoids and flavonoids; dichloromethanol yields only terpenoids (Cowan, 1999); ethers when used as solvent results in the extraction of terpenoids, alkaloids, fatty acids, and coumarins whereas acetone isolates flavonols. Hydroquinone and caffeic acid methyl ester, isolated from *Cnestis ferruginea* Vahl ex DC. aqueous extract, showed promising results against *S. aureus* (Kouakou et al., 2019). Many researchers worked on bioactive compounds from medicinal plants for the discovery of novel natural anti-biofilm compounds. The anti-biofilm properties of Indian medicinal plants have been exploited and found that *Cinnamomum glaucescens* (Nees) Hand.-Mazz, *Syzygium praecox* Roxb. Rathakr. & N. C. Nair, *Bischofia javanica* Blume, *Elaeocarpus serratus* L., *Smilax zeylanica* L., *Acacia pennata* (L.) Willd., *Trema orientalis* (L.) Blume, *Acacia pennata* (L.) Willd., *Holigarna caustica* (Dennst.) Oken, *Murraya paniculata* (L.) Jack, and *Pterygota alata* (Roxb.) R. Br. extracts have promising anti-biofilm activity against *S. aureus* (Panda et al., 2020). 12-Methoxy-trans-carnosic acid

and carnosol identified from the methanolic extract of *Salvia officinalis* L., an Algerian medicinal plant, have shown anti-biofilm activity against *Candida* biofilm in *in vitro* conditions (Kerkoub et al., 2018).

Phytochemicals inhibit the quorum sensing mechanism mainly by blocking the quorum sensing inducers like AHL, autoinducers, and autoinducers type 2 (Ciric et al., 2019). Garlic extracts play a vital role in the inhibition of quorum sensing signaling molecules of *Pseudomonas* and *Vibrio* spp. biofilms (Harjai et al., 2010; Lu et al., 2019). Emodin helps in the proteolysis of transcription factors associated with the quorum sensing and acts as its potent inhibitor (Ding et al., 2011). Quorum quenchers, along with antibiotics, are the best alternative anti-biofilm agents, as discussed by many researchers (Paluch et al., 2020). Phytochemicals also play a significant role in inhibiting bacterial adhesions and suppression of genes related to biofilm formation (Adnan et al., 2020). Biofilm development at the initial stages can be outlaid by interfering with the forces (Van der Waals force of attraction, electrostatic attraction, sedimentation and Brownian movements) which are responsible for the support of bacterial attachment to various surfaces (Roy et al., 2018). Phytocompounds have the potential to interfere with the extension along with the capability to stop the accessibility to nutrients essential for adhesion and bacterial growth (Sandasi et al., 2010).

There are reports on the anti-adhesive properties of ethanolic and acetone extract of *Psidium guajava* L. (Razak and Rahim, 2003) and extracts from various *Eugenia* spp. on *C. albicans* (Sardi et al., 2017). An alkaloid (norbougaine) has shown a significant effect on *P. aeruginosa* biofilm by preventing adhesion due to loss of cell motility (Majik et al., 2013). A very recent study on *Adiantum philippense* L. crude extract has shown a promising role in decreasing the content of biofilm exopolysaccharides (Adnan et al., 2020). They observed that *Adiantum philippense* L. crude extract restrains biofilm at the initial stages by targeting adhesin proteins, deforming the pre-formed biofilms, and obstructing EPS production. Various researchers identified a different group of phytocompounds especially polyphenols such as 7-epiclusianone, tannic acid, and casbane which prevent cell surface attachment (Murata et al., 2010; Carneiro et al., 2011; Payne et al., 2013; Adnan et al., 2020).

Members of Enterobacteriaceae express curli, an amyloid fiber on the cell surface that helps in the attachment to characters and cell aggregation and enhances biofilm formation as well as cellular invasion (Tursi et al., 2020). Cegelski et al. (2009) found that pyridones affect the expression of the CsgA curli subunit and hamper curli biogenesis. Phloretin, ginkgolic acid, and phytocompounds from Malaysian plants help in the regulation of curli and pilli genes (Lee et al., 2011, 2014a,b; Johari et al., 2020). Vikram et al. (2013) reported that a citrus sterol β -sitosterol glucoside inhibited *E. coli* O157:H7 biofilm formation and motility by suppressing flagellar operon *flhDC*. The phytocompounds of curlicide and pilicide nature can be exploited in therapeutic strategies of Enterobacteriaceae biofilm prevention (Johari et al., 2020). Phytocompounds having fewer side effects can be a better therapeutic agent for biofilm-related



infections, but recent reports suggest a combined approach which is always better than the individualistic approach. Few plant-based antimicrobials with the potential of anti-biofilm activity are summarized in **Table 1**.

Biosurfactants

Biosurfactants (BS) hinder biofilm formation by varying the cell adhesion ability through less cell surface hydrophobicity, membrane disruption, and inhibited electron transport chain, thus restricting cellular energy demand (Satpute et al., 2016). Biosurfactants of different classes are produced by various microorganisms that exhibit antibacterial, antifungal, and anti-biofilm activities (Paraszkiewicz et al., 2019). The effect of biosurfactants from *Lactobacillus plantarum* and *Pediococcus acidilactici* on quorum sensing signaling molecules and expressions of biofilm-linked genes in *Staphylococcus aureus* was evaluated (Yan et al., 2019). They reported that biosurfactants reduce the growth of *S. aureus* biofilm by regulating the expression of biofilm-related genes *dltB*, *icaA*, *cidA*, etc. BS from *Lactobacillus plantarum* significantly reduced *cidA* gene expression at 12.5 mg/ml (Yan et al., 2019). Biosurfactant from *Pediococcus acidilactici* downregulates the gene expression of autoinducer-2 (AI-2) signaling molecules, accessory gene regulator (*agr A*), and staphylococcal accessory regulatory (*sar A*) at 50 mg/ml (Yan et al., 2019). Previous studies reported that the anti-biofilm activity of *Lactobacillus*-derived BS loaded liposomes had greater ability than free BS to inhibit *S. aureus* (MRSA) biofilm formation and elimination (Giordani et al., 2019). Few biosurfactants along with their consequence on

biofilm growth, development, and dispersal are summarized in **Table 2**.

Ohadi et al. (2020) identified an anionic lipopeptide from *Acinetobacter junii* which self-aggregates to form β sheet-rich biosurfactant vesicles. This biosurfactant is thermostable and less toxic, so it can be used as an anti-biofilm agent. Biofilms that are developed by dermatophytes are very difficult to eradicate. A lipopeptide biosurfactant obtained from *Beauveria bassiana*, which is an insect-attacking fungus, plays an important role as an anti-biofilm agent in *ex vivo* conditions for *M. canis* (Abdel-Aziz et al., 2020). It acts by disrupting cell membrane integrity and interfering with cell membrane permeability. The biosurfactant from *B. bassiana* overcome the disadvantage of expensive production as it was produced from steep corn liquor. This can be a promising biosurfactant for recalcitrant dermatophytosis. Surfactin, a cyclic lipopeptide, was found to be very effective along with its metal complex against *C. albicans* biofilm-related infections. This biosurfactant also controls the expression of hyphal specific genes and mainly act by decreasing cellular surface hydrophobicity (Janek et al., 2020).

Rhamnolipids produced from *Pseudomonas aeruginosa* MN1 have higher anti-adhesive and anti-biofilm activity than that of surfactin (Abdollahi et al., 2020). Glycolipid isolated from *Burkholderia* sp. WYAT7, an endophyte of *Artemisia nilagirica* (Clarke) Pamp, has anti-biofilm activity against *S. aureus* (Ashitha et al., 2020). A broad-range glycolipoprotein, rich in Leu-His-Trp amino acids identified from *Acinetobacter indicus* M6 has low toxicity and removed 82.5% of biofilm at a

TABLE 1 | Anti-biofilm activity of phytochemicals with their mechanism of action.

Compound	Source	Experimental details	Pathogenic species	Molecular mechanism	Inhibitory concentration	References
Ajoene	<i>Allium sativum</i> L.	<i>In vitro</i> (PMNs killing assays) and <i>in vivo</i> (pulmonary infection mice model)	<i>Pseudomonas aeruginosa</i> <i>P. aeruginosa</i> <i>Staphylococcus aureus</i>	Downregulates rhamnolipid production Inhibits small regulatory RNA molecules (<i>rsmY</i> , <i>rsmZ</i> , and <i>malI</i>) that operate in the later phase of QS signaling	20 µg/ml ajoene reduces rhamnolipid production by 1/3 IC ₅₀ for <i>rsmY</i> = 2.5 µg/ml <i>rsmZ</i> = 2.3 µg/ml	Jakobsen et al., 2012 Jakobsen et al., 2017
Allicin	<i>Allium sativum</i> L.	<i>In vitro</i> (Δ <i>pqsABCD</i> knockout strain)	<i>Pseudomonas aeruginosa</i>	Decreases the bacterial adhesion in the initial stages of biofilm formation as it reduces EPS formation It controls the expression of virulence factors hence interfere with the QS system	250 µM inhibit production of virulence factors such as pyocyanin, elastase, and pyoverdine and rhamnolipids	Xu et al., 2019
Carvacrol (monoterpenoid)	<i>Origanum vulgare</i> L.	<i>In vitro</i> (qPCR for relative expression of <i>lasI/lasR</i> genes) and docking modeling of proteins LasI and LasR	<i>Pseudomonas aeruginosa</i>	Post-translational inhibition against <i>lasI</i> , which effects AHL production. It mainly acts on QS machinery	C6-AHL production reduced up to 80% with 1.9 mM of carvacrol	Tapia-Rodriguez et al., 2019
Emodin (anthraquinone)	<i>Polygonum cuspidatum</i> Siebold & Zucc. and <i>Rheum palmatum</i> L.	<i>In vitro</i> (crystal violet biofilm assay and SEM analysis)	<i>Staphylococcus aureus</i>	Decreases the release of eDNA and downregulates the expression of biofilm-forming related genes like <i>cidA</i> , <i>icaA</i> , <i>dlbA</i> , <i>agrA</i> , <i>sortaseA</i> , and <i>sarA</i>	MIC = 8 µg/ml	Yan et al., 2017
Emodin (anthroquinone)	<i>Rheum palmatum</i> L.	<i>In vitro</i> (microdilution assay, kinase assay) and molecular docking for emodin in CK2 (Autodock Vina)	<i>Candida albicans</i> <i>Candida krusei</i> <i>Candida parapsilosis</i> <i>Candida tropicalis</i>	Biofilm formation is inhibited by targeting cellular kinase signaling It acts on planktonic cells by reducing hyphal formation. It acts as a competitive inhibitor of CK2	MIC = 12.5 µg/ml MFC = 25 µg/ml MIC and MFC = 25 µg/ml	Janeczko et al., 2017
Aloe-emodin	<i>Rheum officinale</i> Baill.	<i>In vitro</i> (CLSM assays and Congo red assay)	<i>Staphylococcus aureus</i>	Reduce the production of extracellular proteins and polysaccharide intercellular adhesin	MIC and MFC = 50 µg/ml Inhibited biofilm formation on polyvinyl chloride surfaces at 32 µg/ml	Xiang et al., 2017
Hordenine	<i>Hordeum vulgare</i> L. (sprouting)	<i>In vitro</i> (SEM and CLSM assays, qPCR for QS-related genes)	<i>Pseudomonas aeruginosa</i>	Decreases AHL production Virulence factors (proteases, elastase, pyocyanin, rhamnolipid, alginate, and pyroverdine) production decreased significantly. Inhibit swimming and swarming activity Down-regulates the expression of <i>lasI</i> , <i>lasR</i> , <i>rhlI</i> and <i>rhlR</i> genes.	1 mg/ml of hordenine along with 0.4 µg/ml of netilmicin reduced biofilms by 88% C4-HSL production decreased up to 69% at 0.5 mg/ml	Zhou et al., 2018
Pulverulentone A	<i>Callistemon citrinus</i> (Curtis) skeels leaves	<i>In vitro</i> (broth microdilution assay, CLSM, TEM analysis)	Methicillin-resistant <i>Staphylococcus aureus</i>	Reduces styphyloxanthin production, thus inhibiting biofilm formation Disrupts the cell membrane	MIC = 125 µg/ml Production of the virulence factor decreased by 65.9%	Shehabeldine et al., 2020

(Continued)

TABLE 1 | Continued

Compound	Source	Experimental details	Pathogenic species	Molecular mechanism	Inhibitory concentration	References
Vitexin (flavon)	<i>Vitex species</i>	<i>In vitro</i> (safranin staining, microscopy methods, EPS quantification) <i>In vivo</i> murine model (catheter-associated infection), molecular docking	<i>Pseudomonas aeruginosa</i>	Attenuates formation of EPS, QS-associated factors (swarming motility, production of protease, pyoverdine and pyocyanin) Molecular docking studies confirmed it attenuates <i>Las A</i> , <i>Las B</i> , and <i>Lux R</i>	MIC = 260 µg/ml 39.04% decrease in <i>Las A</i> protease and 37.54% <i>Las B</i> elastase	Das et al., 2016
5-Hydroxymethylfurfural	<i>Musa acuminata</i> Colla.	<i>In vitro</i> (biofilm, <i>Las B</i> elastase, protease, and rhamnolipid quantification assays)	<i>Pseudomonas aeruginosa</i>	Inhibits the production of biofilm proteins, EPS, and cell surface hydrophobicity productions Downregulates the expression of QS-regulated virulence genes	MBIC = 400 µg/ml Reduces production of biofilm proteins, biofilm adherence, EPS and CSH to the level of 79, 82, and 77%, respectively Inhibits the production of <i>LasA</i> protease, <i>LasB</i> elastase, pyocyanin, alginate, and rhamnolipid 77, 75, 68, 80, 78, and 69%, respectively	Vijayakumar and Ramanathan, 2020
Phytol	<i>Piper betle</i> L.	<i>In vitro</i> (microscopic analysis, transcriptional analysis of QS-regulated genes)	<i>Serratia marcescens</i>	Inhibits the swarming motility and hydrophobicity Downregulates QS genes	Significantly inhibits the production of biofilm and EPS to the level of 65 and 43%	Srinivasan et al., 2016
Isolimononic acid and ichangin	<i>Citrus species</i>	<i>In vitro</i> (Caco-2 cell adhesion and survival assay, AI-3 reporter assay)	Enterohaemorrhagic <i>Escherichia coli</i> <i>Vibrio harveyi</i>	Decreases the adherence Downregulates flagellar genes, <i>ler</i> (transcriptional regulator of LEE) Represses the expression of the flagellar master regulator (<i>flhC</i> and <i>flhD</i>) Regulates <i>luxO</i> expression, thus acting as potent modulators of bacterial cell-cell signaling	IC ₂₅ (isolimononic acid) = 19.7 µM IC ₂₅ (ichangin) = 28.3 µM <i>ler</i> repressed by 5-fold, <i>flhC</i> and <i>flhD</i> repressed by 4.6 and 6.9, respectively IC ₅₀ (isolimononic acid) = 94.18 µM	Vikram et al., 2012 Vikram et al., 2011
(R)-Bgugaine	<i>Arisarum vulgare</i> O. Targ. Tozz.	<i>In vitro</i> (static biofilm inhibition assay)	<i>Pseudomonas aeruginosa</i>	Affects flagella related functions, inhibits pyocyanin pigmentation, <i>LasA</i> protease, rhamnolipid production.	Reduces biofilm density by 83% at 1.8 mM	Majik et al., 2013

(Continued)

TABLE 1 | Continued

Compound	Source	Experimental details	Pathogenic species	Molecular mechanism	Inhibitory concentration	References
Zingerone	<i>Zingiber officinale</i> Roscoe	<i>In vitro</i> (microtiter plate assay, motility assay, quorum sensing signal molecules quantitative assay) and molecular docking of TraR, LasR, and PqsR proteins	<i>Pseudomonas aeruginosa</i> PAO1	Reduces swimming, swarming, and twitching motility. Suppresses pyocyanin, hemolysin, rhamnolipid, protease and elastase Molecular docking analysis proved that it could bind with all the quorum sensing receptors and stops receptor–ligand interaction, suppresses QS-dependent gene expression	Sub MIC = 10 mg/ml Reduces the BFC of <i>P. aeruginosa</i> PAO1 as A ₅₇₀ from 1.1 to 0.5	Kumar et al., 2015
Baicalin	<i>Scutellaria baicalensis</i> Georgi	<i>In vivo</i> (mouse peritoneal implant infection model)	<i>Pseudomonas aeruginosa</i>	Inhibits LasA protease, LasB elastase, pyocyanin, rhamnolipid, motilities and exotoxin A virulence factors Decreases the expression of <i>lasI</i> , <i>lasR</i> , <i>rhlI</i> , <i>rhlR</i> , <i>pqsR</i> , and <i>pqsA</i> genes and reduces the QS signaling molecule 3-oxo-C12-HSL and C4-HSL	MIC > 1024 µg/ml C4-HSL levels decreased 77.2% at 64 µg/ml baicalin	Luo et al., 2017
Curcumin	<i>Curcuma longa</i> L.	<i>In vitro</i> (crystal violet biofilm assay, pellicle formation assay, surface motility assay, mixed culture biofilm assay) <i>In vivo</i> (<i>Caenorhabditis elegans</i> model organism, <i>C. elegans</i> killing assay)	<i>Acinetobacter baumannii</i> , <i>C. albicans</i>	Inhibits pellicle formation, Pili motility, and ring biofilm formation Molecular docking analysis proved that curcumin interacts with the biofilm response regulator BfmR	MIC > 500 µg/ml for <i>A. baumannii</i> ATCC 17978 planktonic cell Reduces <i>A. baumannii</i> ATCC 17978 biofilm production by 93% at 100 µg/ml	Raorane et al., 2019
Epigallocatechin-3-gallate (EGCG)	<i>Camellia sinensis</i> (L.) Kuntze (green tea)	<i>In vitro</i> (growth assay, CR-binding assay, TEM analysis)	<i>Escherichia coli</i> BW25113	Suppresses curli production and expression of curli-related proteins <i>csgA</i> , <i>csgB</i> , and <i>csgD</i> Enhances the degradation of sigma factor (RpoS) by ClpXP protease	IC ₅₀ = 5.9 ± 0.8 µM	Arita-Morioka et al., 2018
Ginkgolic acid (GA) and hydroginkgolic acid	<i>Pistacia lentiscus</i> L. (fruit)	<i>In vitro</i> , <i>in vivo</i> (human lung A549 infection model, <i>C. elegans</i> infection model)	<i>Pseudomonas aeruginosa</i> H103	Decreases virulence factor production Modifies the membrane fluidity Regulates virulence through the ECFσSigX	IC ₅₀ of pyocyanin inhibition = 6.3 µg/ml 100 µg/ml GA reduces pyocyanin production by 82%	Tahrioui et al., 2020

(Continued)

TABLE 1 | Continued

Compound	Source	Experimental details	Pathogenic species	Molecular mechanism	Inhibitory concentration	References
7-Epiclusianone	<i>Rheedia brasiliensis</i> (Mart.) Planch. & Triana	<i>In vivo</i> A rodent model of dental caries	<i>Streptococcus mutans</i>	Increases cariostatic activity by disrupting insoluble exopolysaccharides and intracellular polysaccharides	70–80% less severe smooth-surface lesions and 50–70% less severe sulcal-surface lesions than the vehicle control treatment 50–70% reduction of exopolysaccharides	Murata et al., 2010 Branco-de-Almeida et al., 2011
Tannic acid	Not specified	<i>In vitro</i> (crystal violet microplate biofilm assay, Congo red binding assay)	<i>E. coli</i> BW25113	Efficiently killed bacteria in <i>pgaA</i> mutant biofilms by inhibiting the formation of polysaccharide in the matrix Affects intracellular SOS response and decreases the expression of genes involved in this pathway	MIC = 1 mg/ml	Samoilova et al., 2019a Samoilova et al., 2019b
Diterpene derivative (C ₃₁ H ₅₀ O ₃)	<i>Myrmecodia pendens</i> Merr. & L.M. Perry	<i>In vitro</i> (broth microdilution assay, MBIC analysis by Perumal method)	<i>Streptococcus mutans</i> ATCC 25175	Not specified	MBIC = 50 ppm and MIC = 40 ppm	Gartika et al., 2018
Chelerythrine	<i>Bocconia cordata</i> Willd.	<i>In vitro</i> (broth microdilution assay, crystal violet assay) and <i>in vivo</i> (mono- and dual species culture models)	<i>Candida albicans</i> and <i>Staphylococcus aureus</i>	Inhibits hyphae formation Reduces biofilm formation by decreasing eDNA, polysaccharide, and protein levels	The MICs (monospecies) = 4 µg/ml and MBIC _{90S} (monospecies) = 2 µg/ml MICs (dual species) = 6 µg/ml and MBIC _{90S} (dual species) = 3 µg/ml	Qian et al., 2020
Hyperforin	<i>Hypericum perforatum</i> L.	<i>In vitro</i> (quorum sensing inhibition assay, human plasma protein-coated assay, static microtiter plate crystal violet assay)	<i>Staphylococcus aureus</i> AH1872	Exhibits anti-biofilm activity and a moderate amount of quorum quenching activity, but a detailed mechanism is not specified	MIC ₅₀ (flowering aerial part) = 0.512% v/v Exhibit moderate inhibition of quorum sensing (QSIC ₅₀ = 0.064–0.512% v/v)	Lyles et al., 2017
Warburganal, polygodial, alpha-linolenic acid (ALA)	<i>Warburgia ugandensis</i> Sprague subsp. <i>ugandensis</i>	<i>In vitro</i> (tetrazolium reduction assay, checkerboard assay)	<i>Candida albicans</i> <i>Candida glabrata</i> <i>S. epidermidis</i> <i>S. aureus</i>	α,β-unsaturated 1,4-dialdehyde in polygodial and warburganal is responsible for the potent antifungal activity on developing biofilms Polygodial affects mitochondrial ATPase and leads to reduced ergosterol levels	BIC ₅₀ (warburganal) = 4.5 ± 1 µg/ml and BIC ₅₀ (polygodial) = 10.8 ± 5 µg/ml BIC ₅₀ (warburganal) = 37.9 ± 8 µg/ml BIC ₅₀ (ALA) = 25 µg/ml	Kipanga et al., 2020

NS, not specified.

TABLE 2 | Biosurfactants reported recently with anti-biofilm activities.

Class	Source microorganism	Pathogen strains	Effect on biofilm	Dose	References
Lipopeptide biosurfactants (LPBs)	<i>Acinetobacter junii</i>	Biofilm of <i>Staphylococcus aureus</i> , <i>Proteus mirabilis</i> , and <i>Pseudomonas aeruginosa</i>	Biofilm disruption 35, 10, and 32%, respectively Biofilm disruption 52, 31, and 70%, respectively	1250 µg/ml 2500 µg/ml	Ohadi et al., 2020
Lipopeptide	<i>Beauveria bassiana</i>	<i>Microsporum canis</i>	25.76% biofilm eradication	1.95 µg/ml	Abdel-Aziz et al., 2020
Lipopeptide surfactin-C15	<i>B. subtilis</i> #309	<i>Candida albicans</i>	85% inhibition to biofilm formation	960 µg/ml	Janek et al., 2020
Lipopeptide surfactin	<i>Bacillus safensis</i> F4	<i>Staphylococcus epidermidis</i>	80% anti-adhesive activity	6.25 mg/ml	Abdelli et al., 2019
Lipopeptide pontifacin	<i>Pontibacter korlensis</i> strain SBK-47	<i>Bacillus subtilis</i> , <i>Staphylococcus aureus</i> , <i>Salmonella typhi</i> , and <i>Vibrio cholerae</i>	99% anti-adhesive activity	2 mg/ml	Balan et al., 2016
Lipopeptide	<i>Bacillus subtilis</i> AC7	<i>Candida albicans</i>	Reduced adhesion up to 67–69% and biofilm formation up to 56–57%	2 mg/ml	Ceresa et al., 2016
Glycolipoprotein	<i>Acinetobacter indicus</i> M6	Methicillin-resistant <i>Staphylococcus aureus</i>	82.5% removal of biofilm	500 µg/ml	Karlapudi et al., 2020
Glycolipid	<i>Burkholderia</i> sp. WYAT7	<i>Staphylococcus aureus</i>	41% inhibition to biofilm formation 79% inhibition to biofilm formation	1 mg/ml 2 mg/ml	Ashitha et al., 2020
Rhamnolipids	<i>Pseudomonas aeruginosa</i> MN1	<i>Streptococcus mutans</i>	Dissociation of 67% of the preformed biofilm	12.5 mg/ml	Abdollahi et al., 2020
Rhamnolipids	<i>Burkholderia thailandensis</i> E264	<i>Streptococcus oralis</i> , <i>Actinomyces naeslundii</i> , <i>Neisseria mucosa</i> , and <i>Streptococcus sanguinis</i>	90% inhibition of <i>S. sanguinis</i> biofilm 70% inhibition of <i>S. oralis</i> biofilm 70% inhibition of <i>N. mucosa</i> biofilm 50% inhibition of <i>A. naeslundii</i> biofilm	0.39 mg/ml 0.78 mg/ml 6.25 mg/ml 12.5 mg/ml	Elishikh et al., 2017
Exopolysaccharides	<i>Pandorea pnomenus</i> MS5	<i>Burkholderia cepacia</i>	Inhibit <i>Burkholderia cepacia</i> biofilm formation	0.25 mg/ml	Sacco et al., 2019

concentration of 500 µg/ml (Karlupudi et al., 2020). The EPS from *Pandoraea pnomenusa* MS5 serves as an anti-biofilm agent against *Burkholderia cepacia* (Sacco et al., 2019). This surfactant is a heteropolysaccharide, with two functional carbonyls and hydroxyl groups, and has oil-emulsifying capacity.

Biosurfactants are appropriate coating agents for medical implants such as urinal catheters, bone implants, etc. to inhibit biofilms originated from pathogenic organisms without using synthetic drugs. Rhamnolipids and spherolipids are reported to be potential agents for the inhibition of biofilms formed by Gram-negative and Gram-positive microbes (Sharahi et al., 2019). Few studies reported that cell-associated biosurfactant from *Lactobacillus acidophilus* inhibits biofilm formation of *Proteus vulgaris* and *S. aureus* on polydimethylsiloxane (PDMS)-based implants (Satpute et al., 2019). *L. rhamnosus*-derived biosurfactants cause cell lysis by disrupting the membrane structure, thus can be used as an anti-biofilm agent for multispecies biofilms on silicone devices, i.e., voice prostheses in case of laryngectomy (Tan et al., 2017). The anti-biofilm activity of biosurfactants can augment extensively in combination with caprylic acid that inhibits biofilm formation of *P. aeruginosa*, *E. coli*, and *B. subtilis* (Diaz De Rienzo et al., 2016); amphotericin B (AmB) or fluconazole synergistically acts against biofilm formation and preformed biofilm of *C. albicans* (Haque et al., 2016); and surfactants such as SDS led to the destruction of *P. aeruginosa* PAO1 biofilms (Nguyen et al., 2020).

Antimicrobial Peptides

AMPs are broad-acting antimicrobial agents widely used in the treatment of both fungal and bacterial biofilms (Pletzer et al., 2016). These peptides disrupt biofilms developed on medical devices such as catheters, artificial valves, stents, dentures, etc. occupied in hospital-acquired infections by *S. aureus*, *Klebsiella pneumoniae*, *P. aeruginosa*, *Enterococcus faecium*, *Acinetobacter*, and *Enterobacter* spp. (ESKAPE), and non-ESKAPE pathogens (Rajput and Kumar, 2018). AMPs are substitute to traditional antibiotics that are less vulnerable to bacterial resistance by attacking the bacterial cell membrane (Hirt et al., 2018). AMPs occur naturally in humans, animals, plants, and microbes and act on bacterial cell membranes by interacting with membrane phospholipids electrostatically, followed by insertion into membrane, thus killing bacteria. There are reports of synergizing AMPs with antimicrobial compounds to suppress various molecular pathways of biofilm formation (Shahrour et al., 2019).

Amphibian skin is a source for many AMPs effective against various biofilm-causing microorganisms. Yuan et al. (2019) isolated an AMP Japonicin-2LF from Fujian large-headed frog skin secretion (*Limnonectes fujianensis*) that inhibits MRSA biofilms by membrane permeabilization. Japonicin-2LF behaves like a detergent and eradicates both planktonic and sessile pathogens in biofilms. This property can be exploited to use this peptide as a promising drug candidate in cystic fibrosis patients for the cure of MRSA infection. The main drawback of using AMPs to treat biofilm-based infections is that they are very much prone to degradation by various bacterial proteases.

An AMP from frog skin named esculentin-1a, i.e., Esc (1-21), and its D-amino acid-containing diastereomer Esc (1-21)-1c inhibited *P. aeruginosa* biofilm formation by its membrane-perturbing activity. Previous studies reported that Esc (1-21)-1c showed potential activity against chronic lung *Pseudomonas* infections of cystic fibrosis patients (Casciaro et al., 2019). The introduction of D-amino acids at Leu¹⁴ and Ser¹⁷ into the AMP (esculentin-1a) sequence increases the AMP stability (Casciaro et al., 2019); decreases *P. aeruginosa* swimming, swarming, and twitching motility; and finally inhibits biofilm formation. The peptide inhibits the *P. aeruginosa* biofilm formation by three mechanisms. First, it downregulates the *fleN* gene that controls the number of flagella in *P. aeruginosa* inhibiting flagella-mediated swimming. Second, it decreases the mRNA level of type IV pili biosynthesis genes at very low concentration, i.e., 1/8 MIC, and inhibits the twitching motility of *P. aeruginosa* that is very much essential for micro-colony formation and colonization during biofilm development. Third, it downregulates *lasI* gene encoding for the quorum-sensing molecule acyl-homoserine lactone (AHL) synthase as well as *lasB* gene encoding the virulence factors elastase *LasB*.

In summary, Esc (1-21)-1c lowers the expression of virulence genes and bacterial motility genes, and ultimately prevents biofilm formation. These two anti-pseudomonal peptides esculentin-1a (1-21) and its diastereomer Esc (1-21)-1c have shown promising results in bronchial epithelium repair of cystic fibrosis patients. Cappiello et al. (2019) observed that esculentin repairs bronchial epithelium in cystic fibrosis patients by promoting bronchial cell migration, activating epidermal growth factor receptors, and also increases the secretion of IL-8 for the re-epithelialization process. Besides, the peptide esculentin-1a lowers the expression of mRNA encoding rhamnosyltransferase subunits, i.e., *RhlA* and *RhlB*, key enzymes in the biosynthesis of bacterial surfactant rhamnolipids. A recent study by Parducho et al. (2020) reported a specific mode of action of the AMP human Beta-Defensin 2 that increases the roughness of the bacterial surface, alters outer membrane protein profile, and interferes with the transfer of biofilm precursors into the extracellular space (Figure 2).

The melittin peptide of bee venom exhibit antibacterial activity, prevents MRSA systemic infections and initiates the wound healing process in MRSA-infected mice model (Choi et al., 2015). Khozani et al. (2019) studied the efficiency of melittin and found that it degraded about 90–95% of *P. aeruginosa* biofilm biomass at 50 µg concentrations during 24 h. Human cathelicidin LL-37 inhibits bacterial adhesion and biofilm mass of *S. epidermidis* ATCC 35984 at a very low concentration (Hell et al., 2010). In addition to anti-biofilm activity, LL-37 exhibits immunomodulatory activity such as cellular recruitment (Tjabringa et al., 2006), enhances host adaptive immune responses (Diamond et al., 2009), and modulates inflammatory responses (Mookherjee et al., 2006). The dual property of AMPs to counter bacterial biofilms as well as modulating the host immune system can be exploited to design a novel strategy to combat drug-resistant microbial biofilms.

Parducho et al. (2020) reported the inhibitory property of human Beta-Defensin 2 in *P. aeruginosa* biofilm by inducing

structural changes, altering outer membrane protein profile and interfering with the transfer of biofilm precursors into the extracellular space. Few natural peptides with anti-biofilm activity and their disadvantages are listed in **Table 3**. A peptide DRAMP ID: DRAMP18417 derived from the venom of scorpion (*Tityus obscurus*) has shown promising anti-biofilm activity against *Candida* spp. and *Cryptococcus neoformans* strains (Guilhelmelli et al., 2016). These peptides inhibit fungal biofilms at initial adhesion and mature stages, and exhibit minimal hemolytic and cytotoxic activity on erythrocytes and murine peritoneal macrophages.

Pathogens which form the biofilms on the implanted medical devices, human skin, gut, and oral cavities generally communicate through quorum sensing (QS) signals. The quorum sensing inhibiting potential of AMPs from natural sources offers an alternative antibiotic-free approach to overcome biofilm-associated infections. To date, more than 3000 AMPs have been discovered, but only seven of them have been approved by the FDA (Chen and Lu, 2020). There is a severe scarcity of clinical studies on natural AMPs due to their poor performance, cytotoxic and hemolytic activities, unpredicted side effects such as kidney injuries, damage to central nervous systems, etc. The futility of natural AMPs in pre-clinical stages may be due to variations between the clinical setting and their resident conditions. So, clinical research needs to be exaggerated and optimized for the use of these natural anti-biofilm agents against various drug-tolerant biofilms. It is essential to exploit the structure of different naturally occurring AMPs to develop novel therapeutic peptides with improved stability and activity in comparison with their natural counterparts.

Efforts have been made to design novel specifically targeted multi-domain AMPs composed of a species-targeting peptide linked to a broad-spectrum antimicrobial killing peptide domain (Sztukowska et al., 2019). C16G2 is one of the first functional specifically targeted AMPs designed by fusion of a 16-mer region of the *Streptococcus mutans* competence-stimulating peptide (CSP) as the targeting domain, flexible triglycine linker and G2 AMP, a 16-residue fragment of novispirin G10 (Steinstraesser et al., 2002), and a derivative of ovipirin-1 (N-terminal 18 residues of the sheep cathelicidin SMAP29). C16G2 inhibits the biofilm growth of *S. mutans* effectively both in pure culture and in a multispecies community (Guo et al., 2015). This peptide not only kills *S. mutans* but also reduces other species that are metabolically dependent on *S. mutans* and mediates the re-establishment of oral microbiome. This specifically targeted AMP avoids the loss of natural microflora by selectively targeting the pathogens and leaving commensal *Streptococci* undamaged. C16G2 has completed a single-blind, open-label phase II clinical trial in various varnish and strip formulations (ClinicalTrials.gov Identifier: NCT03196219) among female and male dental subjects.

Similarly, attempts have been made to target only the pathogenic organisms of the biofilm without influencing the normal microflora (Xu et al., 2020). They designed peptides by fusing species-specific enterococcal pheromone cCF10 with a broad-spectrum AMP C6. They proved that incorporation of cCF10 at the N terminus of C6 drastically increased antimicrobial

activity against *E. faecalis* comparative with C6 alone. They also reported that the hybrid peptides stimulated negligible hemolysis against human RBCs at antimicrobial levels, demonstrating that these fusion peptides could be exploited as potential anti-biofilm agents for clinical implementation.

Therapeutic Strategies Using Natural Products

The failure of conventional antibiotic therapies indicates that biofilm treatments need auxiliary upgradation (Zhang et al., 2020). Natural anti-biofilm agents selectively exterminate the persistent biofilms and allow the diffusion of antimicrobials into the biofilm matrix. These natural products target various phases of biofilm cycle to degrade the biofilm matrix and finally kills the released cells (**Figure 3**). A better understanding of the disruption and dispersal mechanism of biofilms will help researchers to design improved anti-biofilm strategies.

A recent study reported that elasnin (an anti-biofilm compound from an actinobacteria *Streptomyces mobaraensis* DSM 40847) destroyed the matrix in a multispecies biofilm and making them more vulnerable to antibiotics (Long et al., 2020). To improve the current strategies of biofilm inhibition, the concern of the present review is to exploit natural agents for the development of an effective and safe strategy. This review aims to cover some current systems that are being put into practice to disintegrate EPS, quench QS networks, inhibit adhesion, and interrupt biofilm formation (**Figure 4**).

Extracellular Polymeric Substance (EPS)–Targeting Strategies

Microbial EPSs secreted by a large variety of microorganisms mainly composed of polysaccharides, structural proteins, and extracellular DNA. The EPS matrix supports microbial adhesion to a surface, aggregation in multilayered biofilms, and functions as a three-dimensional scaffold that provides hydration, digestive capacity, and protection against antimicrobial compounds, antibiotics, and host effector molecules (Flemming et al., 2016a). The EPS matrix can actively alter nutrient gradients and portray pathogenic environments that contribute to tolerance and virulence traits. So, many therapeutic strategies are designed to target the EPS matrix to eliminate biofilms, disaggregate bacteria, and interrupt the pathogenic environment. Many bacterial enzymes and secondary metabolites interfere with the quorum sensing mechanisms of pathogenic bacteria, thus disrupting the biofilm formation (Khan et al., 2019). Biofilm matrix-degrading enzymes such as beta-N-acetylglucosaminidase and dispersin B secreted by the Gram-negative periodontal pathogen *Actinobacillus actinomycetemcomitans* disintegrate mature biofilms of *Staphylococcus epidermidis*. Cocktail of two EPS-degrading enzymes, DNase I and dispersin B, has been found to inhibit staphylococcal skin colonization and remove pre-attached *S. aureus* cells from the skin and enhance their povidone-iodine susceptibility in an *in vivo* pig skin colonization model (Kaplan et al., 2018). Hogan et al. (2017) reported that lysostaphin was an effective anti-staphylococcal agent and its therapeutic efficacy can be improved

TABLE 3 | Sources and effects of AMPs.

Name of AMPs	Amino acid sequence	Net charge	3D structure	Source	Effects on biofilm	Disadvantages	References
Japonicin-2LF	FIVPSIFLLK KAFCIALKKC	4	Helix	Frog skin secretion	Eradicates the methicillin-resistant <i>S. aureus</i> biofilm matrix as well as kills all the sessile bacteria	Futile against <i>P. aeruginosa</i> biofilms. The anti-biofilm activity concealed by the changes in LPS contents and cell wall structure of microorganisms	Yuan et al., 2019
Dermaseptin-PT9	GLWSKIKDAAKT AGKAALGFVNEMV	2	Helix	Frog skin secretion	Inhibits the biofilm formation of <i>S. aureus</i> , MRSA, and <i>E. coli</i>	More potent activity against Gram-negative bacteria	Li et al., 2019
Phylloseptin-PTa	FLSLIPAA ISAVSALANHF	2	Helix	Frog skin secretion	More potent against <i>S. aureus</i> biofilm	Anti-biofilm activity changed by the hydrophobicity, charges and α -helicity of the peptides	Liu et al., 2017
Moronecidin-like	FFRNLWKGA AAFRAGHAAWRA	6	Unknown	Seahorse	Inhibits surface attachment of <i>S. aureus</i> biofilm	More effectual against Gram-positive bacteria than Gram-negative bacteria. The outer membrane proteins of Gram-negative bacteria may hinder translocation of AMPs through the outer membrane	Mohammadi et al., 2018
Mastoporan	LNLKALL AVAKKIL	4	Helix	European hornet venom	Suppresses biofilm formation by <i>S. aureus</i> and <i>P. aeruginosa</i>	Release histamine from mammalian mast cells may lead to an immune response	Chen et al., 2018
Melittin	GIGAVLKVLTG LPALISWIKRQ	6	Helix	Honeybee venom	Induce disintegration of the MDR <i>P. aeruginosa</i> and degrades the biofilm	The toxicity of melittin on normal cells is a disadvantage for clinical applications (in case of third-degree burn patients, all three layers of skin are destroyed, so cytotoxicity of melittin hardly limits its applications)	Khazani et al., 2019
NA-CATH	KRFKFFKKLKNSV KKRAKFFKKPKVIGVTFPF	15	Helix	Chinese cobra (<i>Naja atra</i>)	Prevent biofilm formation of <i>Burkholderia thailandensis</i>	The small size of the peptide restricts its large-scale synthesis	Blower et al., 2015 de Barros et al., 2019
Defensin ZmD32	RTCQSQSHRFGRGCLRRS NCANVCRTGEGFPGG RCRGFRRCFCCTTHC	12	Combine Helix and Beta structure	Corn, <i>Zea mays</i>	Active against <i>Candida albicans</i> biofilms	Anti-biofilm activity of many defensins lost in the presence of salt	Kerenga et al., 2019
Capsicumicine	RSCQQQIQ AQLSSCQQYLKQ	–	Unknown	Red pepper, <i>Capsicum bacattum</i>	Prevents the establishment of <i>S. epidermidis</i> biofilm by matrix anti-assembly (MAA) mechanism	NS	Von Borowski et al., 2020
Rhesus theta defensin-1	GFCRCLRRGVCRCICTR	5	Beta	Monkey leukocytes	Active against established <i>C. albicans</i> biofilms	Most of the host defense peptides exhibit undesirable pro-inflammatory properties and low bioavailability	Basso et al., 2019

NS, not specified.

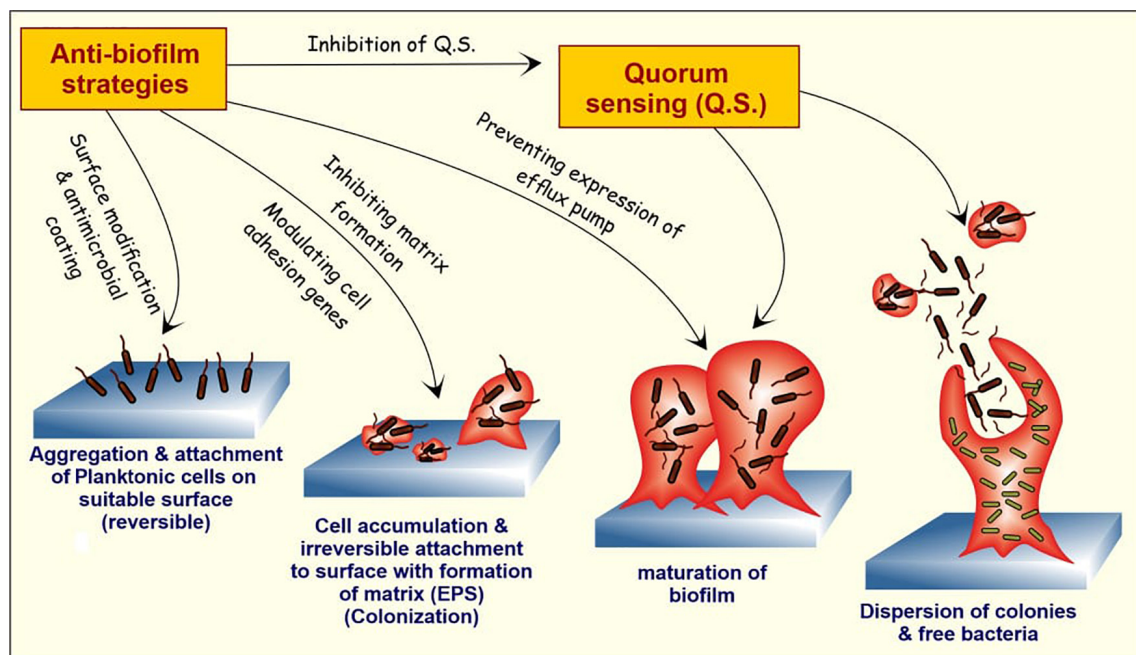


FIGURE 3 | The stages of biofilm formation and potential targets for anti-biofilm agents. The bacterial cells in humans attach to the matrix-forming proteins by forming a covalent linkage with peptidoglycan structure or by non-covalent attachment. With attachment and aggregation of a sufficient number of cells, the formation of EPS matrix takes place, and the attachment now becomes resistant to external repulsive forces. With the maturation of biofilm, the cells within the bulk structure start further communication with each other and start secreting specialized proteins and DNA, and some of them are involved in the formation of the efflux pump. At last, the dispersion of free planktonic cells from the formed biofilm further promotes the formation of new biofilms in the periphery. The natural anti-biofilm compounds can attack at one or different stages of biofilm formation and development, thus inhibiting it.

in combination with antibiotics. Few biofilm-degrading enzymes with their mechanism of biofilm inhibition are summarized in **Table 4**.

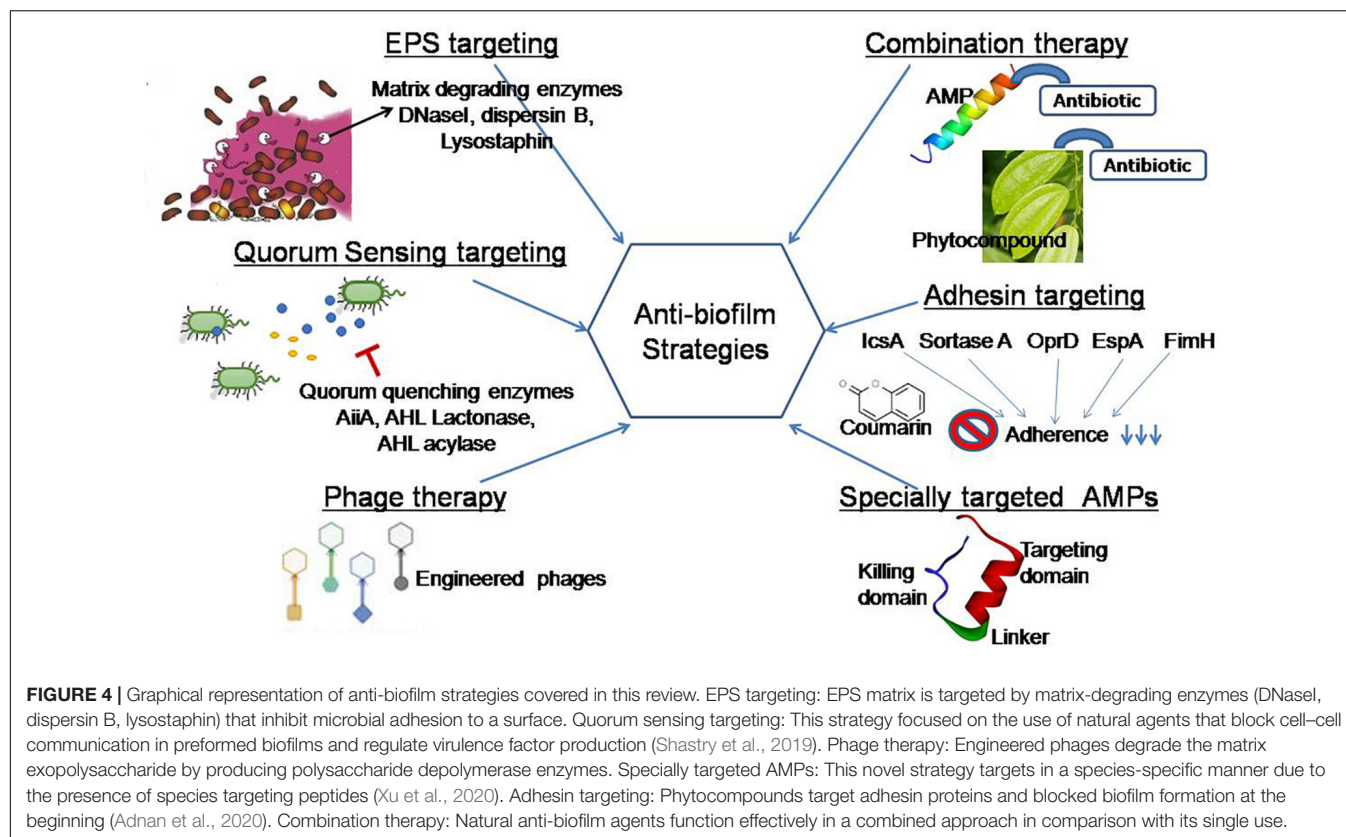
The existing enzymes which have less catalytic activity can enhance their catalytic properties against the biofilms by modeling and engineering approach. The site-directed mutational analysis is considered as another approach to modulate the biofilm-inhibiting properties of the enzymes. Thus, broad-spectrum enzymes/peptides, as well as secondary compounds, must be isolated from bacteria for bioprospection, which can target a broad range of QS signaling molecules and structural part of the biofilms. The complete elimination of heterogeneous biofilms needs amalgamation of hydrolytic enzymes that can degrade proteins, polysaccharides, eDNA, and QS molecules (Yuan et al., 2020). The application of matrix-degrading enzymes in biofilm control is presently limited due to cost, handling procedures, and low industrial accessibility (Nahar et al., 2018).

Quorum Sensing Targeting Strategies

Prevention of cell-to-cell communication (quorum sensing) is an efficient strategy to restrain biofilm formation (Sharahi et al., 2019). It is reported that metalloprotein AHL-lactonase from the cell-free extract of endophytic *Enterobacter* species causes degradation of *N*-AHL, thus significantly inhibiting biofilm formation by *Aeromonas hydrophila* (Shastry et al., 2019). The result of a recent study reported that *Lactobacillus crustorum*

ZHG 2-1 as novel quorum-quenching bacteria degrade *N*-3-oxododecanoyl-*dl*-homoserine lactone (3-oxo-C12-HSL) and *N*-butyryl-*dl*-homoserine lactone (C4-HSL) and functions as an anti-biofilm agent against *P. aeruginosa* (Cui et al., 2020). Several quorum quenching (QQ) enzymes and compounds have been reported. The majority of these QQ molecules have been isolated from natural sources (LaSarre and Federle, 2013). The result of a recent study revealed QS inhibitory potentials of ethyl acetate extracts from cell-free supernatants and cells of *Natrinemaversi forme* against *P. aeruginosa* biofilm (Başaran et al., 2020). Many QS inhibitors from plant-based natural products have been identified (Caceres et al., 2020; Zhong et al., 2020) and proposed to be effective in future biofilm targeting strategies. The role of natural anti-biofilm agents in the inhibition of quorum sensing molecules is mentioned in the first part of the review. Here, we attempted to explain their effect on the disruption of QS mechanism. These anti-biofilm agents disrupt quorum-sensing systems mainly in two ways: (1) inhibition and degradation of signal molecules, and (2) mimicking the signal molecules for inhibition of their binding to corresponding receptors (Kalia, 2013).

On the other hand, quorum quenchers are usually species specific; therefore, a combination of quenchers is required to eliminate mixed-species biofilms. Ajoene, a sulfur-rich molecule from garlic, decreases the expression of small regulatory RNAs (sRNAs) in both Gram-negative (*P. aeruginosa*) and Gram-positive (*S. aureus*) bacteria. Ajoene is the first compound to



be identified to target broad-spectrum range quorum sensing inhibitors, i.e., lowers the RNAIII expressions in *S. aureus* (Scoffone et al., 2019) and RsmY and RsmZ in *P. aeruginosa* (Jakobsen et al., 2017). Ajoene lowered expression of small regulatory RNAs (*rsmY* and *rsmZ*) in *P. aeruginosa* as a result of which it represses translation of biofilm matrix polysaccharides Pel and Psl and the type VI secretion system (T6SS). The T6SS in *P. aeruginosa* plays an essential role in the expression of various virulence factors and greatly concerned with the biofilm formation, pyocyanin production, and pathogenicity of the organism (Li et al., 2020). These findings suggest that T6SS may be a prospective therapeutic target against *P. aeruginosa* infections. Jakobsen et al. (2017) also found that ajoene lowers the expression of regulatory RNA and RNAIII, and inhibits the expression of RNAIII-dependent virulence factors such as lipase, protease, and α -hemolysin in *S. aureus*. Emodin (1, 2, 8-trihydroxy-6-methyl anthraquinone), an anthraquinone derivative identified from *Rheum palmatum* (Chinese rhubarb) and *Polygonum cuspidatum* (Asian knotweed), effectively downregulated *luxS* gene in *Streptococcus suis* (Yang et al., 2015) and *icaA*, *sarA*, and *agrA* genes in *S. aureus* (Yan et al., 2017).

The anti-biofilm peptide Human Cathelicidin LL-37 affects the bacterial cell signaling system and inhibits *P. aeruginosa* biofilm formation at 0.5 $\mu\text{g/ml}$ by downregulating genes of the QS system (Di Somma et al., 2020). AMPs interact with membranes of bacteria and, in turn, activate genes that are regulated through QS. These QS autoinducers passed through

the plasma membrane with the help of membrane vesicles. This process, in turn, activates the expression of virulence genes associated with QS. Autoinducers help in interspecies signal transduction; one interesting autoinducer is small autoinducing peptide molecule (AIP) from *Lactobacilli* that inhibits the viability of microbes and acts as a suppressor of bacteriotxin production. During the process of suppression of exotoxin production, they interfere with the agr QS system (Vasilchenko and Rogozhin, 2019). However, quorum quenchers can be rinsed away during biofilm formation that makes limited uses of these inhibitors confined to small areas of biofilm only (Koo et al., 2017). Thus, combination approach of these inhibitors along with other strategies leads to a novel therapeutic approach.

Phage Therapy

Lytic bacteriophages have been used as an effective therapeutic strategy to remove biofilm cells. A recently published study proved that two lytic phages vB_SauM_ME18 and vB_SauM_ME126 are potential natural antimicrobials for inhibiting biofilm of MDR *S. aureus* (Gharieb et al., 2020). Recent investigations have shown that (engineered) phage-derived enzymes—polysaccharide depolymerase or peptidoglycan-degrading enzymes—are promising therapeutic anti-biofilm candidates (Reuter and Kruger, 2020). Phage therapy got its first FDA approval in the year 2019 in which patients received phage treatment at the School of Medicine, University of California San Diego (UCSD) phage therapy center (Pires et al., 2020). The administration of phage therapy is active only in a few

TABLE 4 | Biofilm-degrading enzymes against various human pathogens.

Enzymes	Source	Pathogenic bacteria	Molecular mechanism of biofilm inhibition	References
Serine protease, Esp	<i>Staphylococcus epidermidis</i>	<i>Staphylococcus aureus</i>	Esp degrades <i>S. aureus</i> surface proteins and host receptors	Sugimoto et al., 2013
Lysostaphin	<i>Staphylococcus simulans</i>	Methicillin-resistant <i>Staphylococcus aureus</i> (MRSA)	Cleaves the pentaglycine cross-bridges of peptidoglycan and destroyed EPS matrix	Algburi et al., 2017 Hogan et al., 2017
α -Amylase	<i>Bacillus subtilis</i> S8-18	Methicillin-resistant <i>Staphylococcus aureus</i> (MRSA)	Degrades the preform mature biofilm by disrupting EPS matrix	Kalpana et al., 2012
Cellulase	<i>Penicillium funiculosum</i> <i>Trichoderma reesei</i>	<i>Pseudomonas aeruginosa</i>	Decreases the adhesion of cells to the surface and polysaccharide matrix	Loiselle and Anderson, 2003
Cellulase	<i>Aspergillus niger</i> <i>Bacillus</i> sp. DGV19	<i>Burkholderia cepacia</i>	Degrades the exopolysaccharide	Rajasekharan and Ramesh, 2013
Alginate lyase	<i>Bacillus circulans</i> ATCC 15518	<i>Pseudomonas aeruginosa</i>	Degrades the exopolysaccharide	Alkawash et al., 2006
Hyaluronan	<i>Streptococcus equi</i>	<i>Staphylococcus aureus</i>	NS	Ibberson et al., 2016
Cysteine, histidine dependent amidohydrolase/peptidase CHAP _K	Myoviridae staphylococcal Phage K	<i>Staphylococcus aureus</i>	Cleaves the peptide bond involving D-alanine and the first glycine in the pentaglycine cross-bridge of <i>Staphylococcal</i> cell wall peptidoglycan	Fenton et al., 2013
Endolysin LysH5	Phage vB_SauS-philPLA88	<i>Staphylococcus aureus</i> , <i>Staphylococcus epidermidis</i>	Anti-persister agents	Gutierrez et al., 2014
DNase I	Human stratum corneum	<i>Pseudomonas aeruginosa</i> , <i>Staphylococcus aureus</i>	Degradation of extracellular DNA prevents the formation of biofilm	Eckhart et al., 2007
DNase I and Proteinase K	NS	<i>Actinomyces oris</i> , <i>Fusobacterium nucleatum</i> , <i>Streptococcus mutans</i> , <i>Streptococcus oralis</i> , and <i>Candida albicans</i>	Affected the structural integrity of the biofilms by removal of eDNA and extracellular proteins	Karygianni et al., 2020
Trypsin	Pancreatic serine endoprotease	<i>Pseudomonas aeruginosa</i>	Destroy the protein contents of the biofilm matrix	Banar et al., 2016

NS, not specified.

countries, and its clinical use faces many challenges such as the establishment of phage banks with characterized phages; safety, stability, and quality of phage preparations during production; and the evolution of bacterial resistance to phages.

Combination Therapy

Natural anti-biofilm agents sensitize antibiotics and established to be more effective when used in amalgamation (Zhang et al., 2020). They also reported that the combined application of sodium houthuyfonate and levofloxacin act in a better manner to inhibit biofilm formation. Sodium houthuyfonate, a plant-derived anti-neuropeptide, effectively disrupts biofilm dispersion in *P. aeruginosa* (Wang et al., 2019). Naringin, a flavanone glycoside extracted from citrus and grapefruits, was found to be more effective against *P. aeruginosa* biofilms in comparison with individual treatment of marketed antibiotics ciprofloxacin and tetracycline (Dey et al., 2020). Naringin depletes biofilm EPS and facilitates the diffusion of antimicrobials, reduces pellicle formation, and decreases the flagellar movement of bacteria on catheter surfaces.

Zhou et al. (2018) tested the effect of hordenine, a polyphenolic compound from barley, on biofilm formation individually as well as in combination with an aminoglycoside antibiotic, netilmicin. The results were promising, showing up to 88% reduction in *P. aeruginosa* PAO1 biofilms by a combination of hordenine and netilmicin, which was significantly better than the effect of any of the individual treatments. It indicates that the drug-herb combination therapy may be explored for effective anti-biofilm formulation opportunities. The SEM study showed a reduction in the thickness of the biofilm layer and the disruption of its architecture. The results of the study also revealed downregulation in the expression of quorum-sensing regulatory genes, especially *lasR*, by hordenine as the possible mechanism against biofilm development. Actinobacterial compounds from different microbial species have also shown potential anti-biofilm activity against different pathogenic bacteria by interrupting the cell surface and interaction between cells (Azman et al., 2019). Studies focusing on a combination of more than one natural anti-biofilm compound/s from different sources or acting on different stages of biofilm development will further help in developing more effective agents targeting biofilms. Moreover, the selection of a more effective compound is also necessary as the efficacy of natural compounds against biofilm development is different against different strains of bacteria.

Anti-biofilm Biomaterial Therapy

The adhesion of biofilm-associated pathogenic organisms on implant surfaces restricts their clinical applications, so many attempts have been made by various researchers to coat biomaterial as a preventive strategy. Natural polymer-based surface coatings, such as anti-adhesive coatings of algal polysaccharide ulvan, dextran, and dermatan sulfate, and antimicrobial-releasing polysaccharide coatings etc. have been popularized during the last decade (Junter et al., 2016). A recent report on anti-adhesive CyanoCoating (a coating from marine cyanobacterium *Cyanothece* sp. CCY 0110) was exploited as a defensive strategy against a broader range of microbes

(especially *Proteus mirabilis*, *E. coli*, and *C. albicans* biofilms) in catheter-linked urinary tract infections (Costa et al., 2020). The molecular mechanism to prevent the cell adhesion is that the hydrophilic polysaccharides form a hydration layer on the surface which acts as a physical barrier (Damodaran and Murthy, 2016) and prevents cell adhesion to the surface. Calcium phosphate cement and hydroxyapatite are the calcium phosphate materials that are used as a bone coating to avoid infections of biofilm, but they have various limitations in clinical trials (Pan et al., 2018). Implant-related infections can be avoided by chitosan hydrogel coatings which prevent bacterial adhesion and biofilm formation due to membrane leaching (Pan et al., 2018). A group of natural polymers were used as drug transporters in various forms like fibers, strips, gels (Badam gum, Karaya gum, chitosan), films (chitosan), nanoparticles, and microparticles which help in delivering antibiotics to the targeted site mainly for periodontal biofilm-forming pathogens (Chi et al., 2019). Nisin, an FDA-approved AMP, acts as anti-biofilm agent synergistically with conventional antibiotics against methicillin-resistant *Staphylococcus aureus*, *Streptococcus pneumoniae*, *Enterococci*, and *Clostridium difficile* (Shin et al., 2016). A recent report stated that nisin in conjugation with gellan gum, a biocompatible polysaccharide, shows promising results in biomaterial research (Peng et al., 2020).

CONCLUSION AND FUTURE DIRECTIONS

The occurrence of many biofilm-based human infections and their multiple antimicrobial resistance is a major concern in medicine and human health. The elevated rate of resistance to antibiotics in biofilm leads to the discovery and characterization of novel natural anti-biofilm agents. This review describes different types of phytocompounds, antimicrobial peptides, and biosurfactants that exhibit promising biofilm-inhibiting ability. Natural anti-biofilm agents could be effectively used to deal with certain surgeries and diseases where there is a possibility of untraceable infection sites like bone, dental, eye lenses, and breast implants. These agents of natural origin are structurally and functionally more diverse in comparison with conventional antibiotics. The structure and function of natural anti-biofilm agents from various sources have been exploited to develop numerous advanced therapeutic strategies showing increased activity, stability, and reliability. Here, we continue to analyze the efficacy of specially targeted AMPs against drug-tolerant pathogenic biofilms without disturbing the natural microflora.

Natural products, mainly phytochemicals, as anti-biofilm agents have been studied more in *in vitro* and *in vivo* conditions, but not a single FDA-approved drug was developed despite huge efforts. Most of them failed in phase II and phase III clinical trials (Lu et al., 2019). The possible reason for this failure may be the availability of the compound in humans after administration which decreases the efficacy of the compounds. One possible solution to this problem is a combination of strategies like antibiotics, along with natural anti-biofilm agents for better results. Combination therapy of natural agents with commercial

antibiotics needs urgent exploitation in the future to advance anti-biofilm activity. Quorum quenchers of natural origin along with antibiotics can be a novel lead for species-specific biofilm destruction, and it has a promising utilization aspect in biomedical industries. More studies should be directed in this regard for converting the novel anti-biofilm phytochemicals into drugs. Most of the clinical studies on natural anti-biofilm compounds as reported in <http://clinicaltrials.gov> are focused on oral biofilms, and very few are related to urinary tract infections (Lu et al., 2019). Further studies in *in vivo* models and clinical trials are needed to test the efficiency of natural anti-biofilm agents in the future.

The review also explains the quorum quenching molecules and EPS-degrading enzymes of natural origin along with their mode of action on various biofilms. The mechanism of action of various natural agents against biofilm remains unknown. More studies on the mode of action may help to identify novel anti-biofilm agents. Anti-adhesion strategy can be a novel strategy for biofilm treatments on a broad range of bacteria as it targets and prevents attachment of bacteria to the cell surface. Very few studies have been made in this area, so future research in targeting biofilm in the direction of adhesin proteins may lead to the discovery of unique natural anti-biofilm agents. Pili and curli gene expression regulating phytochemicals can control biofilm formation. More work in these directions or a combination of phytochemical which has anti-adhesion properties may be a better therapeutic strategy for biofilm-related ailments.

The failure of natural medicines in clinical trials can be checked by rigorous quality control. The discovery of accurate markers that are sensitive and stable can resolve the problem and

help in better quality control of natural anti-biofilm agents. It is a significant challenge faced by natural product research for the discovery of useful QC markers as natural compounds have a very complex structural lattice (Zhang et al., 2020). Drug efficacy of natural compounds is mainly based on network pharmacology methods. As a result, more research in this direction can enhance success rate in clinical trials at the final stage. Novel natural anti-biofilm agents in therapeutics may be possible if rigorous studies will be done in quality control, pharmacokinetic and pharmacodynamic co-relationships (PK-PD), and PK-PD interactions with metabolomics of host for evaluation of safety and efficacy of the drug.

AUTHOR CONTRIBUTIONS

AP, RM, SD, MS, and SS drafted the manuscript. AP, RM, and JK were responsible for preparing the tables and figures in the manuscript. AP and RM equally contributed to the development of this manuscript. SS assisted to revise the manuscript. All the authors read and approved the final manuscript.

ACKNOWLEDGMENTS

The authors gratefully acknowledge Prof. Hans-Curt Flemming, Biofilm Centre, Faculty of Chemistry, University of Duisburg-Essen, Essen, Germany, and Visiting Professor, Singapore Centre for Environmental Life Sciences Engineering (SCELSE), Singapore for his invaluable conceptual and technical advice to this work.

REFERENCES

- Abdel-Aziz, M. M., Al-Omar, M. S., Mohammed, H. A., and Emam, T. M. (2020). In-vitro and Ex-vivo anti-biofilm activity of a lipopeptide biosurfactant produced by the Entomopathogenic *Beauveria bassiana* strain against *Microsporum canis*. *Microorganisms* 8:232. doi: 10.3390/microorganisms8020232
- Abdelli, F., Jardak, M., Elloumi, J., Stien, D., Cherif, S., Mnif, S., et al. (2019). Antibacterial, anti-adherent and cytotoxic activities of surfactin (s) from a lipolytic strain *Bacillus safensis* F4. *Biodegradation* 30, 287–300. doi: 10.1007/s10532-018-09865-4
- Abdollahi, S., Tofghi, Z., Babae, T., Shamsi, M., Rahimzadeh, G., Rezvanifar, H., et al. (2020). Evaluation of anti-oxidant and anti-biofilm activities of biogenic surfactants derived from *Bacillus amyloliquefaciens* and *Pseudomonas aeruginosa*. *Ira. J. Pharm. Res.* 19, 115–126. doi: 10.22037/ijpr.2020.1101033
- Adnan, M., Patel, M., Deshpande, S., Alreshidi, M., Siddiqui, A. J., Reddy, M. N., et al. (2020). Effect of *Adiantum philippense* extract on biofilm formation, adhesion with its antibacterial activities against foodborne pathogens, and characterization of bioactive metabolites: an *in vitro-silico* approach. *Front. Microbiol.* 11:823. doi: 10.3389/fmicb.2020.00823
- Algburi, A., Comito, N., Kashtanov, D., Dicks, L. M., and Chikindas, M. L. (2017). Control of biofilm formation: antibiotics and beyond. *Appl. Environ. Microbiol.* 83, e2508–e2516. doi: 10.1128/AEM.02508-16
- Alkawash, M. A., Sothill, J. S., and Schiller, N. L. (2006). Alginate lyase enhances the antibiotic killing of mucoid *Pseudomonas aeruginosa* in biofilms. *Apmis* 114, 131–138. doi: 10.1111/j.1600-0463.2006.apm_356.x
- Arita-Morioka, K. I., Yamanaka, K., Mizunoe, Y., Tanaka, Y., Ogura, T., and Sugimoto, S. (2018). Inhibitory effects of Myricetin derivatives on curli-dependent biofilm formation in *Escherichia coli*. *Sci. Rep.* 8:8452. doi: 10.1038/s41598-018-26748-z
- Asitha, A., Radhakrishnan, E. K., and Jyothis, M. (2020). Characterization of biosurfactant produced by the endophyte *Burkholderia* sp. WYAT7 and evaluation of its antibacterial and anti-biofilm potentials. *J. Biotechnol.* 313, 1–10. doi: 10.1016/j.jbiotec.2020.03.005
- Azman, A. S., Mawang, C. I., Khairat, J. E., and AbuBakar, S. (2019). Actinobacteria—a promising natural source of anti-biofilm agents. *Int. Microbiol.* 22, 403–409. doi: 10.1007/s10123-019-00066-4
- Balan, S. S., Kumar, C. G., and Jayalakshmi, S. (2016). Pontifactin, a new lipopeptide biosurfactant produced by a marine *Pontibacter korlensis* strain SBK-47: purification, characterization and its biological evaluation. *Process Biochem.* 51, 2198–2207. doi: 10.1016/j.procbio.2016.09.009
- Banar, M., Emameini, M., Satarzadeh, M., Abdollahi, N., Beigverdi, R., van Leeuwen, W. B., et al. (2016). Evaluation of mannosidase and trypsin enzymes effects on biofilm production of *Pseudomonas aeruginosa* isolated from burn wound infections. *PLoS One* 11:e0164622. doi: 10.1371/journal.pone.0164622
- Başaran, T. I., Berber, D., Gökalsın, B., Tramice, A., Tommonaro, G., Abbamondi, G. R., et al. (2020). Extremophilic *Natrinema versiforme* against *Pseudomonas aeruginosa* quorum sensing and biofilm. *Front. Microbiol.* 11:79. doi: 10.3389/fmicb.2020.00079
- Basso, V., Tran, D. Q., Schaal, J. B., Tran, P., Eriguchi, Y., Ngole, D., et al. (2019). *Rhesus Theta* Defensin 1 promotes long term survival in Systemic Candidiasis by host directed mechanisms. *Sci. Rep.* 9:16905. doi: 10.1038/s41598-019-53402-z

- Blower, R. J., Barksdale, S. M., and Van Hoek, M. L. (2015). Snake cathelicidin NA-CATH and smaller helical antimicrobial peptides are effective against *Burkholderia thailandensis*. *PLoS Negl. Trop. Dis.* 9:e0003862. doi: 10.1371/journal.pntd.0003862
- Boles, B. R., and Horswill, A. R. (2008). Agr-mediated dispersal of *Staphylococcus aureus* biofilms. *PLoS Pathog.* 4:e1000052. doi: 10.1371/journal.ppat.1000052
- Borghi, E., Borgo, F., and Morace, G. (2016). Fungal biofilms: Update on resistance. *Adv. Exp. Med. Biol.* 931, 37–47. doi: 10.1007/5584_2016_7
- Branco-de-Almeida, L. S., Murata, R. M., Franco, E. M., dos Santos, M. H., de Alencar, S. M., and Koo, H. (2011). Effects of 7-epiclusianone on *Streptococcus mutans* and caries development in rats. *Planta Med.* 77, 40–45. doi: 10.1055/s-0030-1250121
- Branda, S. S., Vik, S., Friedman, L., and Kolter, R. (2005). Biofilms: the matrix revisited. *Trends Microbiol.* 13, 20–26. doi: 10.1016/j.tim.2004.11.006
- Caceres, M., Hidalgo, W., Stashenko, E., Torres, R., and Ortiz, C. (2020). Essential oils of aromatic plants with antibacterial, anti-biofilm and anti-quorum sensing activities against pathogenic bacteria. *Antibiotics* 9:147. doi: 10.3390/antibiotics9040147
- Carneiro, V. A., dos Santos, H. S., Arruda, F. V. S., Bandeira, P. N., Albuquerque, M., Pereira, M. O., et al. (2011). Casbane diterpene as a promising natural antimicrobial agent against biofilm-associated infections. *Molecules* 16, 190–201. doi: 10.3390/molecules16010190
- Cappiello, F., Ranieri, D., Carnicelli, V., Casciaro, B., Chen, H. T., Ferrera, L., et al. (2019). Bronchial epithelium repair by Esculentin-1a-derived antimicrobial peptides: involvement of metalloproteinase-9 and interleukin-8, and evaluation of peptides' immunogenicity. *Sci Rep.* 9:18988. doi: 10.1038/s41598-019-55426-x
- Casciaro, B., Cappiello, F., Loffredo, M. R., Ghirg, F., and Mangoni, M. L. (2019). The Potential of frog skin peptides for anti-Infective therapies: the Case of Esculentin-1a (1-21) NH₂. *Curr. Med. Chem.* 27, 1405–1419. doi: 10.2174/0929867326666190722095408
- Cegelski, L., Pinkner, J. S., Hammer, N. D., Cusumano, C. K., Hung, C. S., Chorell, E., et al. (2009). Small-molecule inhibitors target *Escherichia coli* amyloid biogenesis and biofilm formation. *Nat. Chem. Biol.* 5, 913–919. doi: 10.1038/nchembio.242
- Ceresa, C., Rinaldi, M., Chiono, V., Carmagnola, I., Allegrone, G., and Fracchia, L. (2016). Lipopeptides from *Bacillus subtilis* AC7 inhibit adhesion and biofilm formation of *Candida albicans* on silicone. *Anton. Van Leeuw.* 109, 1375–1388. doi: 10.1007/s10482-016-0736-z
- Characklis, W. G. (1973). Attached microbial growths – I. Attachment and growth. *Water Res.* 7, 1113–1127. doi: 10.1016/0043-1354(73)90066-3
- Chen, C. H., and Lu, T. K. (2020). Development and challenges of antimicrobial peptides for therapeutic applications. *Antibiotics* 9:24. doi: 10.3390/antibiotics9010024
- Chen, X., Zhang, L., Wu, Y., Wang, L., Ma, C., Xi, X., et al. (2018). Evaluation of the bioactivity of a mastoparan peptide from wasp venom and of its analogs designed through targeted engineering. *Int. J. Biol. Sci.* 14, 599–607. doi: 10.7150/ijbs.23419
- Chi, M., Qi, M. A. L., Wang, P., Weir, M. D., Melo, M. A., Sun, X., et al. (2019). Novel bioactive and therapeutic dental polymeric materials to inhibit periodontal pathogens and biofilms. *Int. J. Mol. Sci.* 20:278. doi: 10.3390/ijms20020278
- Ch'ng, J.-H., Chong, K. K., Lam, L. N., Wong, J. J., and Kline, K. A. (2019). Biofilm-associated infection by *Enterococci*. *Nat. Rev. Microbiol.* 17, 82–94. doi: 10.1038/s41579-018-0107-z
- Choi, J. H., Jang, A. Y., Lin, S., Lim, S., Kim, D., Park, K., et al. (2015). Melittin, a honeybee venom-derived antimicrobial peptide, may target methicillin-resistant *Staphylococcus aureus*. *Mol. Med. Rep.* 12, 6483–6490. doi: 10.3892/mmr.2015.4275
- Ciofiu, O., and Tolker-Nielsen, T. (2019). Tolerance and resistance of *Pseudomonas aeruginosa* biofilms to antimicrobial agents-how *P. aeruginosa* can escape antibiotics. *Front. Microbiol.* 10:913. doi: 10.3389/fmicb.2019.00913
- Ciric, A. D., Petrovic, J. D., Glamoclija, J. M., Smiljkovic, M. S., Nikolic, M. M., Stojkovic, D. S., et al. (2019). Natural products as biofilm formation antagonists and regulators of quorum sensing functions: a comprehensive review update and future trends. *South Afr J Bot* 120, 65–80. doi: 10.1016/j.sajb.2018.09.010
- Costa, B., Mota, R., Tamagnini, P., Martins, M. C. L., and Costa, F. (2020). Natural cyanobacterial polymer-based coating as a preventive strategy to avoid catheter-associated urinary tract infections. *Mar. Drugs* 18:279. doi: 10.3390/md18060279
- Costerton, J. W., Stewart, P. S., and Greenberg, E. P. (1999). Bacterial biofilms: a common cause of persistent infections. *Science* 284, 1318–1322. doi: 10.1126/science.284.5418.1318
- Cowan, M. M. (1999). Plant products as antimicrobial agents. *Clin. Microbiol. Rev.* 12, 564–582. doi: 10.1128/CMR.12.4.564
- Cui, T., Bai, F., Sun, M., Lv, X., Li, X., Zhang, D., et al. (2020). Lactobacillus crustorum ZHG 2-1 as novel quorum-quenching bacteria reducing virulence factors and biofilms formation of *Pseudomonas aeruginosa*. *LWT* 117:108696. doi: 10.1016/j.lwt.2019.108696
- Damodaran, V. B., and Murthy, N. S. (2016). Bio-inspired strategies for designing antifouling biomaterials. *Biomater. Res.* 20:18. doi: 10.1186/s40824-016-0064-4
- Das, M. C., Sandhu, P., Gupta, P., Rudrapaul, P., De, U. C., Tribedi, P., et al. (2016). Attenuation of *Pseudomonas aeruginosa* biofilm formation by Vitexin: a combinatorial study with azithromycin and gentamicin. *Sci Rep.* 6, 23347. doi: 10.1038/srep23347
- Dawson, C. C., Intapa, C., and Jabra-Rizk, M. A. (2011). "Persisters": survival at the cellular level. *PLoS Pathog.* 7:e1002121. doi: 10.1371/journal.ppat.1002121
- de Barros, E., Gonçalves, R. M., Cardoso, M. H., Santos, N. C., Franco, O. L., and Candido, E. D. S. (2019). Snake venom cathelicidins as natural antimicrobial peptides. *Front. Pharmacol.* 10:1415. doi: 10.3389/fphar.2019.01415
- De Vos, W. M. (2015). Microbial biofilms and the human intestinal microbiome. *NPJ Biofilms Microb.* 1:15005. doi: 10.1038/npjbiofilms.2015.5
- Deokar, S., and Kadam, D. (2020). *An Update on the Management of Urinary Tract Infections in An Era of Drug Resistance: Anti-Biofilm Strategy*. Available at SSRN: <https://ssrn.com/abstract=3533744> (accessed February 7, 2020).
- Dey, P., Parai, D., Banerjee, M., Hossain, S. T., and Mukherjee, S. K. (2020). Naringin sensitizes the anti-biofilm effect of ciprofloxacin and tetracycline against *Pseudomonas aeruginosa* biofilm. *Int. J. Med. Microbiol.* 310:151410. doi: 10.1016/j.ijmm.2020.151410
- Di Somma, A., Moretta, A., Cane, C., Cirillo, A., and Duilio, A. (2020). Antimicrobial and Antibiofilm Peptides. *Biomolecules* 10:652. doi: 10.3390/biom10040652
- Diamond, G., Beckloff, N., Weinberg, A., and Kisich, K. O. (2009). The roles of antimicrobial peptides in innate host defense. *Curr. Pharm. Des.* 15, 2377–2392. doi: 10.2174/138161209788682325
- Diaz De Rienzo, M. A., Stevenson, P. S., Marchant, R., and Banat, I. M. (2016). Effect of biosurfactants on *Pseudomonas aeruginosa* and *Staphylococcus aureus* biofilms in a bioFlux channel. *Appl. Microbiol. Biotechnol.* 100, 5773–5779. doi: 10.1007/s00253-016-7310-5
- Dijlts, L., Appermans, K., Lissens, M., Lories, B., Kim, W., Van der Eycken, E. V., et al. (2020). Inhibiting bacterial cooperation is an evolutionarily robust anti-biofilm strategy. *Nat. Commun.* 11:107. doi: 10.1038/s41467-019-13660-x
- Ding, X., Yin, B., Qian, L., Zeng, Z., Yang, Z., Li, H., et al. (2011). Screening for novel quorum-sensing inhibitors to interfere with the formation of *Pseudomonas aeruginosa* biofilm. *J. Med. Microbiol.* 60, 1827–1834. doi: 10.1099/jmm.0.024166-0
- Dominguez, E., Zarnowski, R., Sanchez, H., Covelli, A. S., Westler, W. M., Azadi, P., et al. (2018). Conservation and divergence in the *Candida* species biofilm matrix mannan-glucan complex structure, function, and genetic control. *mBio.* 9:e00451-18. doi: 10.1128/mBio.00451-18
- Eckhart, L., Fischer, H., Barken, K. B., Tolker-Nielsen, T., and Tschachler, E. (2007). DNase1L2 suppresses biofilm formation by *Pseudomonas aeruginosa* and *Staphylococcus aureus*. *Br. J. Dermatol.* 156, 1342–1345. doi: 10.1111/j.1365-2133.2007.07886.x
- Elshikh, M., Fustun, S., Chebbi, A., Ahmed, S., Marchant, R., and Banat, I. M. (2017). Rhamnolipids from non-pathogenic *Burkholderia thailandensis* E264: physicochemical characterization, antimicrobial and anti-biofilm efficacy against oral hygiene related pathogens. *New Biotechnol.* 36, 26–36. doi: 10.1016/j.nbt.2016.12.009
- Fenton, M., Keary, R., McAuliffe, O., O'Mahony, J., and Coffey, A. (2013). Bacteriophage-Derived Peptidase CHAPK eliminates and prevents *Staphylococcal* Biofilms. *Int. J. Microbiol.* 2013:625341. doi: 10.1155/2013/625341
- Flemming, H.-C. (2011). *Biofilm Highlights*. Hoboken, NJ: Springer, 81–109.
- Flemming, H.-C., Neu, T. R., and Wingender, J. (eds) (2016a). *The Perfect Slime: Microbial Extracellular Polymeric Substances (EPS)*. London: IWA publishing.

- Flemming, H. C., and Wingender, J. (2010). The biofilm matrix. *Nat. Rev. Microbiol.* 8, 623–633. doi: 10.1038/nrmicro2415
- Flemming, H. C., Wingender, J., Szewzyk, U., Steinberg, P., Rice, S. A., and Kjelleberg, S. (2016b). Biofilms: an emergent form of bacterial life. *Nat. Rev. Microbiol.* 14, 563–575. doi: 10.1038/nrmicro.2016.94
- Flemming, H. C., and Wurtz, S. (2019). Bacteria and archaea on Earth and their abundance in biofilms. *Nat. Rev. Microbiol.* 17, 247–260. doi: 10.1038/s41579-019-0158-9
- Fletcher, M. M., and Floodgate, G. D. (1973). An electron microscopic demonstration of an acidic polysaccharide involved in the adhesion of a marine bacterium to solid surfaces. *J. Gen. Microbiol.* 74, 325–334. doi: 10.1099/00221287-74-2-325
- Fox, E. P., and Nobile, C. J. (2012). A sticky situation: untangling the transcriptional network controlling biofilm development in *Candida albicans*. *Transcription* 3, 315–322. doi: 10.4161/trns.22281
- Fux, A., Costerton, W., Stewart, P., and Stoodley, P. (2005). Survival strategies of infectious biofilms. *Trends Microbiol.* 13, 34–40. doi: 10.1016/j.tim.2004.11.010
- Gartika, M., Pramesti, H. T., Kurnia, D., and Satari, M. H. (2018). A terpenoid isolated from sarang semut (*Myrmecodia pendans*) bulb and its potential for the inhibition and eradication of *Streptococcus mutans* biofilm. *BMC Compl. Alt. Med.* 18:151. doi: 10.1186/s12906-018-2213-x
- Geesey, G. G., Mutch, R., and Costerton, J. W. (1978). Sessile bacteria: an important component of the microbial population in small mountain streams. *Limnol. Oceanogr.* 23, 1214–1224. doi: 10.4319/lo.1978.23.6.1214
- Gharieb, R. M. A., Saad, M. F., Mohamed, A. S., and Tartor, Y. H. (2020). Characterization of two novel lytic bacteriophages for reducing biofilms of zoonotic multidrug-resistant *Staphylococcus aureus* and controlling their growth in milk. *LWT* 124:109145. doi: 10.1016/j.lwt.2020.109145
- Giordani, B., Costantini, P. E., Fedi, S., Cappelletti, M., Abruzzo, A., Parolin, C., et al. (2019). Liposomes containing biosurfactants isolated from *Lactobacillus gasseri* exert anti-biofilm activity against methicillin-resistant *Staphylococcus aureus* strains. *Eur. J. Pharm. Biopharm.* 139, 246–252. doi: 10.1016/j.ejpb.2019.04.011
- Guilhelmelli, F., Vilela, N., Smidt, K. S., de Oliveira, M. A., da Cunha Moraes, A., Rigonato, M. C., et al. (2016). Activity of scorpion venom-derived antifungal peptides against planktonic cells of *Candida* spp. and *Cryptococcus neoformans* and *Candida albicans* biofilms. *Front. Microbiol.* 7:1844. doi: 10.3389/fmicb.2016.01844
- Gunn, J. S., Bakaletz, L. O., and Wozniak, D. J. (2016). What's on the outside matters: the role of the extracellular polymeric substance of gram-negative biofilms in evading host immunity and as a target for therapeutic intervention. *J. Biol. Chem.* 291, 12538–12546. doi: 10.1074/jbc.R115.707547
- Guo, L., Mclean, J. S., Yang, Y., Eckert, R., Kaplan, C. W., Kyme, P., et al. (2015). Precision-guided antimicrobial peptide as a targeted modulator of human microbial ecology. *Proc. Natl. Acad. Sci. U.S.A.* 112, 7569–7574. doi: 10.1073/pnas.1506207112
- Gutierrez, D., Ruas-Madiedo, P., Martínez, B., Rodríguez, A., and García, P. (2014). Effective removal of staphylococcal biofilms by the endolysin LysH5. *PLoS One* 9:e107307. doi: 10.1371/journal.pone.0107307
- Hall-Stoodley, L., Costerton, J. W., and Stoodley, P. (2004). Bacterial biofilms: from the natural environment to infectious diseases. *Nat. Rev. Microbiol.* 2, 95–108. doi: 10.1038/nrmicro821
- Haque, F., Alfatah, M., Ganesan, K., and Bhattacharyya, M. S. (2016). Inhibitory effect of sophorolipid on *Candida albicans* biofilm formation and hyphal growth. *Sci. Rep.* 6:23575. doi: 10.1038/srep23575
- Harjai, K., Kumar, R., and Singh, S. (2010). Garlic blocks quorum sensing and attenuates the virulence of *Pseudomonas aeruginosa*. *FEMS Immunol. Med. Microbiol.* 58, 161–168. doi: 10.1111/j.1574-695X.2009.00614.x
- Harms, A., Maisonneuve, E., and Gerdes, K. (2016). Mechanisms of bacterial persistence during stress and antibiotic exposure. *Science* 354, 42–68. doi: 10.1126/science.aaf4268
- Hell, E., Giske, C. G., Nelson, A., Römling, U., and Marchini, G. (2010). Human cathelicidin peptide LL37 inhibits both attachment capability and biofilm formation of *Staphylococcus epidermidis*. *Lett. Appl. Microbiol.* 50, 211–215. doi: 10.1111/j.1472-765X.2009.02778.x
- Hirt, H., Hall, J. W., Larson, E., and Gorr, S. U. (2018). A D-enantiomer of the antimicrobial peptide GL13K evades antimicrobial resistance in the gram-positive bacteria *Enterococcus faecalis* and *Streptococcus gordonii*. *PLoS One* 13:e0194900. doi: 10.1371/journal.pone.0194900
- Hogan, S., Zapotoczna, M., Stevens, N. T., Humphreys, H., O'Gara, J. P., and O'Neill, E. (2017). Potential use of targeted enzymatic agents in the treatment of *Staphylococcus aureus* biofilm-related infections. *J. Hosp. Infect.* 96, 177–182. doi: 10.1016/j.jhin.2017.02.008
- Ibberson, C. B., Parlet, C. P., Kwiecinski, J., Crosby, H. A., Meyerholz, D. K., and Horswill, A. R. (2016). Hyaluronan modulation impacts *Staphylococcus aureus* biofilm infection. *Inf. Immun.* 84, 1917–1929. doi: 10.1128/IAI.01418-15
- Izano, E. A., Shah, S. M., and Kaplan, J. B. (2009). Intercellular adhesion and biocide resistance in nontypeable *Haemophilus influenzae* biofilms. *Microb. Pathog.* 46, 207–213. doi: 10.1016/j.micpath.2009.01.004
- Jakobsen, T. H., van Gennip, M., Phipps, R. K., Shanmugham, M. S., Christensen, L. D., Alhede, M., et al. (2012). Ajoene, a sulfur-rich molecule from garlic, inhibits genes controlled by quorum sensing. *Antimicrob. Agents Chemother.* 56, 2314–2325. doi: 10.1128/AAC.05919-11
- Jakobsen, T. H., Warming, A. N., Vejborg, R. M., Moscoso, J. A., Stegger, M., Lorenzen, F., et al. (2017). A broad range of quorum sensing inhibitor working through sRNA inhibition. *Sci. Rep.* 7:9857. doi: 10.1038/s41598-017-09886-8
- Janeczko, M., Maslyk, M., Kubiński, K., and Golczyk, H. (2017). Emodin, a natural inhibitor of protein kinase CK2, suppresses growth, hyphal development, and biofilm formation of *Candida albicans*. *Yeast* 34, 253–265. doi: 10.1002/yea.3230
- Janek, T., Drzymala, K., and Dobrowolski, A. (2020). In vitro efficacy of the lipopeptide biosurfactant surfactin-C15 and its complexes with divalent counterions to inhibit *Candida albicans* biofilm and hyphal formation. *Biofouling* 36, 210–221. doi: 10.1080/08927014.2020.1752370
- Johari, N. A., Amran, S. S. D., Kamaruzzaman, A. N. A., Man, C. A. I. C., and Yahya, M. F. Z. R. (2020). Anti-biofilm potential and mode of action of Malaysian plant species: a review. *Sci. Lett.* 14, 34–46.
- Jones, E. A., McGillivray, G., and Bakaletz, L. O. (2013). Extracellular DNA within a nontypeable *Haemophilus influenzae*-induced biofilm binds human defensin-3 and reduces its antimicrobial activity. *J. Innate Immun.* 5, 24–38. doi: 10.1159/000339961
- Junter, G. A., Thebault, P., and Lebrun, L. (2016). Polysaccharide-based antibiofilm surfaces. *Acta Biomater.* 30, 13–25. doi: 10.1016/j.actbio.2015.11.010
- Kalia, V. C. (2013). Quorum sensing inhibitors: an overview. *Biotechnol. Adv.* 31, 224–245. doi: 10.1016/j.biotechadv.2012.10.004
- Kalpna, B. J., Aarthi, S., and Pandian, S. K. (2012). Anti-biofilm activity of α -amylase from *Bacillus subtilis* S8-18 against biofilm-forming human bacterial pathogens. *Appl. Biochem. Biotechnol.* 167, 1778–1794. doi: 10.1007/s12010-011-9526-2
- Kaplan, J. B., Mlynek, K. D., Hettiarachchi, H., Alamneh, Y. A., Biggemann, L., Zurawski, D. V., et al. (2018). Extracellular polymeric substance (EPS)-degrading enzymes reduce staphylococcal surface attachment and biocide resistance on pig skin *in vivo*. *PLoS One* 13:e025526. doi: 10.1371/journal.pone.0205526
- Karlapudi, A. P., Venkateswarulu, T. C., Krupanidhi, S., Rohini, K. K., Indira, M., and Vidya, P. K. (2020). Evaluation of anti-cancer, anti-microbial and anti-biofilm potential of biosurfactant extracted from an *Acinetobacter* M6 strain. *J. King Saud. Univ. Sci.* 32, 223–227. doi: 10.1016/j.jksus.2018.04.007
- Karygianni, L., Attin, T., and Thurnheer, T. (2020). Combined DNase and proteinase treatment interferes with composition and structural integrity of multispecies oral biofilms. *J. Clin. Med.* 9:983. doi: 10.3390/jcm9040983
- Kerenga, B. K., McKenna, J. A., Harvey, P. J., Quimbar, P., Garcia, D., Lay, F. T., et al. (2019). Salt-tolerant antifungal and antibacterial activities of the corn defensin ZmD32. *Front. Microbiol.* 10:795. doi: 10.3389/fmicb.2019.00795
- Kerkoub, N., Panda, S. K., Yang, M.-R., Lu, J.-G., Jiang, Z.-H., Nasri, H., et al. (2018). Bioassay-Guided isolation of anti-*Candida* biofilm compounds from methanol extracts of the aerial parts of *Salvia officinalis* (Annaba, Algeria). *Front. Pharmacol.* 9:1418. doi: 10.3389/fphar.2018.00141
- Khan, F., Oloketuyi, S. F., and Kim, Y. M. (2019). Diversity of bacteria and bacterial products as anti-biofilm and anti-quorum sensing drugs against pathogenic bacteria. *Curr. Drug Targets* 20, 1156–1179. doi: 10.2174/1389450120666190423161249
- Khozani, R. S., Shabbazzadeh, D., Harzandi, N., Feizabadi, M. M., and Bagheri, K. P. (2019). Kinetics study of an antimicrobial peptide, melittin, in

- simultaneous biofilm degradation and eradication of potent biofilm-producing MDR *Pseudomonas aeruginosa* isolates. *Int. J. Pept. Res. Ther.* 25, 329–338. doi: 10.1007/s10989-018-9675-z
- Kipanga, P. N., Liu, M., Panda, S. K., Mai, A. H., Veryser, C., Van Puyvelde, L., et al. (2020). Biofilm inhibiting properties of compounds from the leaves of *Warburgia ugandensis* Sprague subsp. *ugandensis* against *Candida* and staphylococcal biofilms. *J. Ethnopharmacol.* 248:112352. doi: 10.1016/j.jep.2019.112352
- Koo, H., Allan, R. N., Howlin, R. P., Stoodley, P., and Hall-Stoodley, L. (2017). Targeting microbial biofilms: current and prospective therapeutic strategies. *Nat. Rev. Microbiol.* 15, 740–755. doi: 10.1038/nrmicro.2017.99
- Kouakou, K., Panda, S. K., Yang, M.-R., Lu, J.-G., Jiang, Z.-H., Van Puyvelde, L., et al. (2019). Isolation of antimicrobial compounds from *Cnestis ferruginea* Vahl ex. DC (Connaraceae) leaves through bioassay-guided fractionation. *Front. Microbiol.* 10:705. doi: 10.3389/fmicb.2019.00705
- Kumar, L., Chhibber, S., Kumar, R., Kumar, M., and Harjai, K. (2015). Zingerone silences quorum sensing and attenuates virulence of *Pseudomonas aeruginosa*. *Fitoterapia* 102, 84–95. doi: 10.1016/j.fitote.2015.02.002
- LaSarre, B., and Federle, M. J. (2013). Exploiting quorum sensing to confuse bacterial pathogens. *Microbiol. Mol. Biol. Rev.* 77, 73–111. doi: 10.1128/MMBR.00046-12
- Lee, J.-H., Kim, Y.-G., Ryu, S. Y., Cho, M. H., and Lee, J. (2014a). Ginkgolic acids and *Ginkgo biloba* extract inhibit *Escherichia coli* O157: H7 and *Staphylococcus aureus* biofilm formation. *Int. J. Food Microbiol.* 174, 47–55. doi: 10.1016/j.ijfoodmicro.2013.12.030
- Lee, J.-H., Kim, Y.-G., Ryu, S. Y., Cho, M. H., and Lee, J. (2014b). Resveratrol oligomers inhibit biofilm formation of *Escherichia coli* O157: H7 and *Pseudomonas aeruginosa*. *J. Nat. Prod.* 77, 168–172. doi: 10.1021/np400756g
- Lee, J.-H., Regmi, S. C., Kim, J.-A., Cho, M. H., Yun, H., Lee, C.-S., et al. (2011). Apple flavonoid phloretin inhibits *Escherichia coli* O157: H7 biofilm formation and ameliorates colon inflammation in rats. *Infect. Immun.* 79, 4819–4827. doi: 10.1128/IAI.05580-11
- Lewis, K. (2005). Persister cells and the riddle of biofilm survival. *Biochemistry* 70, 267–274. doi: 10.1007/s10541-005-0111-6
- Lewis, K. (2010). Persister cells. *Annu. Rev. Microbiol.* 64, 357–372.
- Li, M., Xi, X., Ma, C., Chen, X., Zhou, M., Burrows, J. F., et al. (2019). A Novel Dermaseptin isolated from the skin secretion of *Phyllomedusa tarsius* and its cationicity-enhanced analogue exhibiting effective antimicrobial and anti-proliferative activities. *Biomolecules* 9:628. doi: 10.3390/biom9100628
- Li, Y., Chen, L., Zhang, P., Bhagirath, A. Y., and Duan, K. (2020). ClpV3 of the H3-Type VI Secretion System (H3-T6SS) affects multiple virulence factors in *Pseudomonas aeruginosa*. *Front. Microbiol.* 11:1096. doi: 10.3389/fmicb.2020.01096
- Little, B. J., and Lee, J. S. (2015). Microbiologically influenced corrosion: an update. *Int. Mat. Rev.* 59, 384–393. doi: 10.1179/1743280414Y.3840000000035
- Liu, J., Wu, Q., Li, L., Xi, X., Wu, D., Zhou, M., et al. (2017). Discovery of phyloleptins that defense against gram-positive bacteria and inhibit the proliferation of the non-small cell lung cancer cell line, from the skin secretions of *Phyllomedusa* frogs. *Molecules* 22:1428. doi: 10.3390/molecules22091428
- Loiselle, M., and Anderson, K. W. (2003). The use of cellulase in inhibiting biofilm formation from organisms commonly found on medical implants. *Biofouling* 19, 77–85. doi: 10.1080/0892701021000030142
- Long, L., Chiang, H. Y., and Qian, P. Y. (2020). A potent anti-biofilm agent inhibits and eradicates mono-and multi-species biofilms. *bioRxiv[Preprint]*. doi: 10.1101/2020.03.25.009126
- Lu, L., Hu, W., Tian, Z., Yuan, D., Yi, G., Zhou, Y., et al. (2019). Developing natural products as potential anti-biofilm agents. *Chin. Med.* 14:11. doi: 10.1186/s13020-019-0232-2
- Luo, J., Dong, B., Wang, K., Cai, S., Liu, T., Cheng, X., et al. (2017). Baicalin inhibits biofilm formation, attenuates the quorum sensing-controlled virulence and enhances *Pseudomonas aeruginosa* clearance in a mouse peritoneal implant infection model. *PLoS One* 12:e0176883. doi: 10.1371/journal.pone.0176883
- Lyles, J. T., Kim, A., Nelson, K., Bullard-Roberts, A. L., Hajdari, A., Mustafa, B., et al. (2017). The chemical and antibacterial Evaluation of St. John's Wort Oil Macerates Used in Kosovar Traditional Medicine. *Front. Microbiol.* 8:1639. doi: 10.3389/fmicb.2017.01639
- MacKenzie, K. D., Palmer, M. B., Köster, W. L., and White, A. P. (2017). Examining the link between biofilm formation and the ability of pathogenic *Salmonella* strains to colonize multiple host species. *Front. Vet. Sci.* 25:138. doi: 10.3389/fvets.2017.00138
- Majik, M. S., Naik, D., Bhat, C., Tilve, S., Tilvi, S., and D'Souza, L. (2013). Synthesis of (R)-norbgugaine and its potential as quorum sensing inhibitor against *Pseudomonas aeruginosa*. *Bioorg. Med. Chem. Lett.* 23, 2353–2356. doi: 10.1016/j.bmcl.2013.02.051
- Marshall, K. C., Stout, R., and Mitchell, R. (1971). Mechanisms of the initial events in the sorption of marine bacteria to surfaces. *J. Gen. Microbiol.* 68, 337–348. doi: 10.1099/00221287-68-3-337
- Mitchell, K. F., Zarnowski, R., Sanchez, H., Edward, J. A., Reinicke, E. L., Nett, J. E., et al. (2015). Community participation in biofilm matrix assembly and function. *Proc. Natl. Acad. Sci. U.S.A.* 112, 4092–4097. doi: 10.1073/pnas.1421437112
- Mohammadi, M., Taheri, B., Momenzadeh, N., Salarinia, R., Nabipour, I., Farshadzadeh, Z., et al. (2018). Identification and characterization of novel antimicrobial peptide from hippocampus comes by In Silico and experimental studies. *Mar. Biotechnol.* 20, 718–728. doi: 10.1007/s10126-018-9843-3
- Mookherjee, N., Brown, K. L., Bowdish, D. M., Doria, S., Falsafi, R., Hokamp, K., et al. (2006). Modulation of the TLR-mediated inflammatory response by the endogenous human host defense peptide LL-37. *J. Immunol.* 176, 2455–2464. doi: 10.4049/jimmunol.176.4.2455
- Murata, R. M., Branco-de-Almeida, L. S., Franco, E. M., Yatsuda, R., dos Santos, M. H., de Alencar, S. M., et al. (2010). Inhibition of *Streptococcus mutans* biofilm accumulation and development of dental caries in vivo by 7-epiclusianone and fluoride. *Biofouling* 26, 865–872. doi: 10.1080/08927014.2010.527435
- Nahar, S., Mizan, M. F. R., Ha, A. J. W., and Ha, S. D. (2018). Advances and future prospects of enzyme-based biofilm prevention approaches in the food industry. *Compr. Rev. Food Sci. Food Saf.* 17, 1484–1502. doi: 10.1111/1541-4337.12382
- Nguyen, B. V., Nagakubo, T., Toyofuku, M., Nomura, N., and Utada, A. S. (2020). Synergy between Sophorolipid biosurfactant and SDS increases the efficiency of *P. aeruginosa* biofilm disruption. *Langmuir* 36, 6411–6420. doi: 10.1021/acs.langmuir.0c00643
- Ohadi, M., Forootanfar, H., Dehghannoudeh, G., Eslaminejad, T., Ameri, A., Shakibaie, M., et al. (2020). Antimicrobial, anti-biofilm, and anti-proliferative activities of lipopeptide biosurfactant produced by *Acinetobacter junii* B6. *Microb. Pathog.* 138:103806. doi: 10.1016/j.micpath.2019.103806
- Olwal, C. O., Ang'ienda, P. O., and Ochiol, D. O. (2019). Alternative sigma factor B (σ^B) and catalase enzyme contribute to *Staphylococcus epidermidis* biofilm's tolerance against physico-chemical disinfection. *Sci. Rep.* 9:5355. doi: 10.1038/s41598-019-41797-8
- Padhi, A., Naik, S. K., Sengupta, S., Ganguli, G., and Sonawane, A. (2016). Expression of *Mycobacterium tuberculosis* NLPc/p60 family protein Rv0024 induce biofilm formation and resistance against cell wall acting anti-tuberculosis drugs in *Mycobacterium smegmatis*. *Microbe Infect.* 18, 224–236. doi: 10.1016/j.micinf.2015.11.007
- Paluch, E., Rewak-Soroczynska, J., Jędrusik, I., Mazurkiewicz, E., and Jermakow, K. (2020). Prevention of biofilm formation by quorum quenching. *Appl. Microbiol. Biotechnol.* 104, 1871–1881. doi: 10.1007/s00253-020-10349-w
- Pan, C., Zubin, Z., and Xiaowei, Y. (2018). Coatings as the useful drug delivery system for the prevention of implant-related infections. *J. Orthop. Sur. Res.* 13:220. doi: 10.1186/s13018-018-0930-y
- Panda, S. K., Das, R., Lavigne, R., and Luyten, W. (2020). Indian medicinal plant extracts to control multidrug-resistant *S. aureus*, including in biofilms. *South Afr. J. Bot.* 128, 283–291. doi: 10.1016/j.sajb.2019.11.019
- Paraszkiewicz, K., Moryl, M., Plaza, G., Bhagat, D. K., Satpute, S., and Bernat, P. (2019). Surfactants of microbial origin as anti-biofilm agents. *Int. J. Environ. Health Res.* 11, 1–20. doi: 10.1080/09603123.2019.1664729
- Parducho, K. R., Beadell, B., Ybarra, T., Bush, M., Escalera, E., Mendez, M., et al. (2020). The antimicrobial peptide human beta-defensin 2 inhibits biofilm production of *Pseudomonas aeruginosa* without compromising metabolic activity. *Front. Immunol.* 11:805. doi: 10.3389/fimmu.2020.00805
- Payne, D. E., Martin, N. R., Parzych, K. R., Rickard, A. H., Underwood, A., and Boles, B. R. (2013). Tannic acid inhibits *Staphylococcus aureus* surface colonization in an IsaA-dependent manner. *Infect. Immun.* 81, 496–504. doi: 10.1128/IAI.00877-12

- Peng, X., Zhu, L., Wang, Z., and Zhan, X. (2020). Enhanced stability of the bactericidal activity of nisin through conjugation with gellan gum. *Int. J. Biol. Macromol.* 148, 525–532. doi: 10.1016/j.ijbiomac.2020.01.164
- Pires, D. P., Costa, A. R., Pinto, G., Meneses, L., and Azeredo, J. (2020). Current challenges and future opportunities of phage therapy. *FEMS Microbiol. Rev.* fuaa017. doi: 10.1093/femsre/fuua017
- Pletzer, D., Coleman, S. R., and Hancock, R. E. (2016). Anti-biofilm peptides as a new weapon in antimicrobial warfare. *Curr. Opin. Microbiol.* 33, 35–40. doi: 10.1016/j.mib.2016.05.016
- Qian, W., Zhang, J., Wang, W., Liu, M., Fu, Y., Li, X., et al. (2020). Efficacy of chelerythrine against mono- and dual-species biofilms of *Candida albicans* and *Staphylococcus aureus* and its properties of inducing hypha-to-yeast transition of *C. albicans*. *J. Fungi* 6:45. doi: 10.3390/jof6020045
- Qvortrup, K., Hultqvist, L., Nilsson, M., Jakobsen, T. H., Jansen, C. U., Uhd, J., et al. (2019). Small molecule anti-biofilm agents developed on the basis of mechanistic understanding of biofilm formation. *Front. Chem.* 7:742. doi: 10.3389/fchem.2019.00742
- Rajasekharan, S. K., and Ramesh, S. (2013). Cellulase inhibits *Burkholderia cepacia* biofilms on diverse prosthetic materials. *Pol. J. Microbiol.* 62, 327–330.
- Rajput, A., and Kumar, M. (2018). *Anti-Biofilm Peptides: A New Class of Quorum Quenchers and Their Prospective Therapeutic Applications: Biotechnological Applications of Quorum Sensing Inhibitors*. Singapore: Springer, 87–110. doi: 10.1007/978-981-10-9026-4_5
- Raorane, C. J., Lee, J. H., Kim, Y. G., Rajasekharan, S. K., Garcia-Contreras, R., and Lee, J. (2019). Antibiofilm and Antivirulence Efficacies of Flavonoids and Curcumin Against *Acinetobacter baumannii*. *Front. Microbiol.* 10:990. doi: 10.3389/fmicb.2019.00990
- Razak, F. A., and Rahim, Z. H. (2003). The anti-adherence effect of *Piper betle* and *Psidium guajava* extracts on the adhesion of early settlers in dental plaque to saliva-coated glass surfaces. *J. Oral Sci.* 45, 201–206. doi: 10.2334/josnusd.45.201
- Reuter, M., and Kruger, D. H. (2020). Approaches to optimize therapeutic bacteriophage and bacteriophage-derived products to combat bacterial infections. *Virus Genes* 56, 136–149. doi: 10.1007/s11262-020-01735-7
- Roy, R., Tiwari, M., Donelli, G., and Tiwari, V. (2018). Strategies for combating bacterial biofilms: a focus on anti-biofilm agents and their mechanisms of action. *Virulence* 9, 522–554. doi: 10.1080/21505594.2017.1313372
- Sacco, L. P., Castellane, T. C. L., Polachini, T. C., de Macedo Lemos, E. G., and Alves, L. M. C. (2019). Exopolysaccharides produced by *Pandora* shows emulsifying and anti-biofilm activities. *J. Polym. Res.* 26, 91. doi: 10.1007/s10965-019-1737-1
- Samoilova, Z., Smirnova, G., and Oktyabrsky, O. (2019a). The effect of catechin, tannic and gallic acids on biofilm formation in *Escherichia coli* depends on medium composition. *Asian J. Microbiol. Biotechnol.* 4, 16–23.
- Samoilova, Z., Tyulenev, A., Muzyka, N., Smirnova, G., and Oktyabrsky, O. (2019b). Tannic and gallic acids alter redox-parameters of the medium and modulate biofilm formation. *AIMS Microbiol.* 5, 379–392. doi: 10.3934/microbiol.2019.4.379
- Sandasi, M., Leonard, C. M., and Viljoen, A. M. (2010). The in-vitro anti-biofilm activity of selected culinary herbs and medicinal plants against *Listeria monocytogenes*. *Lett. Appl. Microbiol.* 50, 30–35. doi: 10.1111/j.1472-765X.2009.02747.x.LAM2747
- Sardi, J. C., Freires, I. A., Lazarini, J. G., Infante, J., de Alencar, S. M., and Rosalen, P. L. (2017). Unexplored endemic fruit species from Brazil: anti-biofilm properties, insights into mode of action, and systemic toxicity of four *Eugenia* spp. *Microb. Pathog.* 105, 280–287. doi: 10.1016/j.micpath.2017.02.044
- Satpute, S. K., Banpurkar, A. G., Banat, I. M., Sangshetti, J. N., Patil, R. H., and Gade, W. N. (2016). Multiple roles of biosurfactants in biofilms. *Curr. Pharm. Des.* 22, 1429–1448. doi: 10.2174/1381612822666160120152704
- Satpute, S. K., Mone, N. S., Das, P., Banat, I. M., and Banpurkar, A. G. (2019). Inhibition of pathogenic bacterial biofilms on PDMS based implants by *L. acidophilus* derived biosurfactant. *BMC Microbiol.* 19:39. doi: 10.1186/s12866-019-1412-z
- Scoffone, V. C., Trespido, G., Chiarelli, L. R., Barbieri, G., and Buroni, S. (2019). Quorum sensing as antivirulence target in cystic fibrosis pathogens. *Int. J. Mol. Sci.* 20:1838. doi: 10.3390/ijms20081838
- Seneviratne, C. J., Suriyanarayanan, T., Swarup, S., Chia, K. H. B., Nagarajan, N., and Zhang, C. (2017). Transcriptomics analysis reveals putative genes involved in biofilm formation and biofilm-associated drug resistance of *Enterococcus faecalis*. *J. Endodont.* 43, 949–955. doi: 10.1016/j.joen.2017.01.020
- Shahrour, H., Ferrer-Espada, R., Dandache, I., Barcena-Varela, S., Sanchez-Gomez, S., Chokr, A., et al. (2019). AMPs as anti-biofilm agents for human therapy and prophylaxis. *Adv. Exp. Med. Biol.* 1117, 257–279. doi: 10.1007/978-981-13-3588-4_14
- Sharahi, J. Y., Azimi, T., Shariati, A., Safari, H., Tehrani, M. K., and Hashemi, A. (2019). Advanced strategies for combating bacterial biofilms. *J. Cell Physiol.* 234, 14689–14708. doi: 10.1002/jcp.28225
- Sharma, D., and Bisht, G. S. (2020). Recent updates on antifungal peptides. *Mini Rev. Med. Chem.* 20, 260–268. doi: 10.2174/1389557519666190926112423
- Shastri, R. P., Rekha, P. D., and Rai, V. R. (2019). Biofilm inhibitory activity of metalloprotein AHL-lactonase from the cell-free lysate of endophytic *Enterobacter* species isolated from *Coscinium fenestratum* Gaertn. *Biocat. Agri. Biotechnol.* 18:101009. doi: 10.1016/j.bcab.2019.01.047
- Shehabeldine, A. M., Ashour, R. M., Okba, M. M., and Saber, F. R. (2020). *Callistemon citrinus* bioactive metabolites as new inhibitors of methicillin-resistant *Staphylococcus aureus* biofilm formation. *J. Ethnopharmacol.* 254, 112669. doi: 10.1016/j.jep.2020.112669
- Shin, J. M., Gwak, J. W., Kamarajan, P., Fenno, J. C., Rickard, A. H., and Kapila, Y. L. (2016). Biomedical applications of Nisin. *J. Appl. Microbiol.* 120, 1449–1465. doi: 10.1111/jam.13033
- Singh, S., Singh, S. K., Chowdhury, I., and Singh, R. (2017). Understanding the mechanism of bacterial biofilms resistance to antimicrobial agents. *Open Microbiol. J.* 11, 53–62. doi: 10.2174/1874285801711010053
- Soares, A., Roussel, V., Pestel-Caron, M., Barreau, M., Caron, F., Bouffartigues, E., et al. (2019). Understanding ciprofloxacin failure in *Pseudomonas aeruginosa* biofilm: persister cells survive matrix disruption. *Front. Microbiol.* 10:2603. doi: 10.3389/fmicb.2019.02603
- Spormann, A. M. (2008). Physiology of microbes in biofilms. *Curr. Top. Microbiol. Immunol.* 322, 17–36. doi: 10.1007/978-3-540-75418-3_2
- Srinivasan, R., Devi, K. R., Kannappan, A., Pandian, S. K., and Ravi, A. V. (2016). *Piper betle* and its bioactive metabolite phytol mitigates quorum sensing mediated virulence factors and biofilm of nosocomial pathogen *Serratia marcescens* in vitro. *J. Ethnopharmacol.* 193, 592–603. doi: 10.1016/j.jep.2016.10.017
- Steintraesser, L., Tack, B. F., Waring, A. J., Hong, T., Boo, L. M., Fan, M. H., et al. (2002). Activity of novispirin G10 against *Pseudomonas aeruginosa* in vitro and infected burns. *Antimicrob. Agents Chemother.* 46, 1837–1844. doi: 10.1128/AAC.46.6.1837-1844.2002
- Stewart, P. S., and Franklin, M. J. (2008). Physiological heterogeneity in biofilms. *Nat. Rev. Microbiol.* 6, 199–210. doi: 10.1038/nrmicro1838
- Sugimoto, S., Iwamoto, T., Takada, K., Okuda, K. I., Tajima, A., Iwase, T., et al. (2013). *Staphylococcus epidermidis* Esp degrades specific proteins associated with *Staphylococcus aureus* biofilm formation and host-pathogen interaction. *J. Bacteriol.* 195, 1645–1655. doi: 10.1128/JB.01672-12
- Sztukowska, M. N., Roky, M., and Demuth, D. R. (2019). Peptide and non-peptide mimetics as potential therapeutics targeting oral bacteria and oral biofilms. *Mol. Oral Microbiol.* 34, 169–182. doi: 10.1111/omi.12267
- Tabak, M., Scher, K., Chikindas, M. L., and Yaron, S. (2009). The synergistic activity of triclosan and ciprofloxacin on biofilms of *Salmonella Typhimurium*. *FEMS Microbiol. Lett.* 301, 69–76. doi: 10.1111/j.1574-6968.2009.01804.x
- Tahrioui, A., Ortiz, S., Azuama, O. C., Bouffartigues, E., Benalia, N., Tortuel, D., et al. (2020). Membrane-Interactive Compounds From *Pistacia lentiscus* L. Thwart *Pseudomonas aeruginosa* Virulence. *Front. Microbiol.* 11:1068. doi: 10.3389/fmicb.2020.01068
- Tan, Y., Leonhard, M., Moser, D., and Schneider-Stickler, B. (2017). Inhibition activity of *Lactobacilli* supernatant against fungal-bacterial multispecies biofilms on silicone. *Microb. Pathog.* 113, 197–201. doi: 10.1016/j.micpath.2017.10.051
- Tapia-Rodriguez, M. R., Bernal-Mercado, A. T., Gutierrez-Pacheco, M. M., Vazquez-Armenta, F. J., Hernandez-Mendoza, A., Gonzalez-Aguilar, G. A., et al. (2019). Virulence of *Pseudomonas aeruginosa* exposed to carvacrol: alterations of the Quorum sensing at enzymatic and gene levels. *J. Cell Commun. Signal.* 13, 531–537. doi: 10.1007/s12079-019-00516-8
- Tjabringa, G. S., Ninaber, D. K., Drijfhout, J. W., Rabe, K. F., and Hiemstra, P. S. (2006). Human cathelicidin LL-37 is a chemoattractant for eosinophils and

- neutrophils that acts via formyl-peptide receptors. *Int. Arch. Allergy Immunol.* 140, 103–112. doi: 10.1159/000092305
- Trentin, D. S., Giordani, R. B., Zimmer, K. R., da Silva, A. G., da Silva, M. V., dos Santos, et al. (2011). Potential of medicinal plants from the Brazilian semi-arid region Caatinga) against *Staphylococcus epidermidis* planktonic and biofilm lifestyles. *J. Ethnopharmacol.* 137, 327–335. doi: 10.1016/j.jep.2011.05.030
- Tseng, B. S., Zhang, W., Harrison, J. J., Quach, T. P., Song, J. L., Penterman, J., et al. (2013). The extracellular matrix protects *Pseudomonas aeruginosa* biofilms by limiting the penetration of tobramycin. *Environ. Microbiol.* 15, 2865–2878. doi: 10.1111/1462-2920.12155
- Tursi, S. A., Puligedda, R. D., Szabo, P., Nicastro, L. K., Miller, A. L., Qiu, C., et al. (2020). *Salmonella Typhimurium* biofilm disruption by a human antibody that binds a pan-amyloid epitope on curli. *Nat. Commun.* 11, 1–13. doi: 10.1038/s41467-020-14685-3
- Uppuluri, P., Zaldivar, M. A., Anderson, M. Z., Dunn, M. J., Berman, J., Ribot, J. L. L., et al. (2018). *Candida albicans* dispersed cells are developmentally distinct from the biofilm and planktonic cells. *mBio* 9:e001338-18. doi: 10.1128/mBio.01338-18
- Van der Veen, S., and Abee, T. (2011). Mixed species biofilms of *Listeria monocytogenes* and *Lactobacillus plantarum* show enhanced resistance to benzalkonium chloride and peracetic acid. *Int. J. Food Microbiol.* 144, 421–431. doi: 10.1016/j.ijfoodmicro.2010.10.029
- Vasilchenko, A. S., and Rogozhin, E. A. (2019). Sub-Inhibitory effects of antimicrobial peptides. *Front. Microbiol.* 10:1160. doi: 10.3389/fmicb.2019.01160
- Vijayakumar, K., and Ramanathan, T. (2020). *Musa acuminata* and its bioactive metabolite 5-Hydroxymethylfurfural mitigates quorum sensing (*las* and *rhl*) mediated biofilm and virulence production of nosocomial pathogen *Pseudomonas aeruginosa* in vitro. *J. Ethnopharmacol.* 246:112242. doi: 10.1016/j.jep.2019.112242
- Vikram, A., Jayaprakasha, G. K., Uckoo, R. M., and Patil, B. S. (2013). Inhibition of *Escherichia coli* O157: H7 motility and biofilm by β -sitosterol glucoside. *Biochim. Biophys. Acta Gen. Subj.* 1830, 5219–5228. doi: 10.1016/j.bbagen.2013.07.022
- Vikram, A., Jesudhasan, P., Pillai, S., and Patil, B. (2012). Isolimononic acid interferes with *Escherichia coli* O157: H7 biofilm and TTSS in QseBC and QseA dependent fashion. *BMC Microbiol.* 12:261. doi: 10.1186/1471-2180-12-261
- Vikram, A., Jesudhasan, P. R., Jayaprakasha, G. K., Pillai, S. D., and Patil, B. S. (2011). Citrus limonoids interfere with *Vibrio harveyi* cell-cell signalling and biofilm formation by modulating the response regulator *LuxO*. *Microbiol.* 157(Pt. 1), 99–110. doi: 10.1099/mic.0.041228-0
- Von Borsowski, R. G., Sophie, C. H. A. T., Schneider, R., Giudice, E., Zimmer, A. R., Gnoatto, S. C. B., et al. (2020). Capsicumine: a new peptide from red peppers turns out to be a powerful anti-biofilm agent and displays a new mechanism of action, matrix anti-assembly. *bioRxiv[Preprint]* doi: 10.1101/2020.04.03.022020
- Wang, T., Huang, W., Duan, Q., Wang, J., Cheng, H., Shao, J., et al. (2019). Sodium houttuyfonate in vitro inhibits biofilm dispersion and expression of *bdIA* in *Pseudomonas aeruginosa*. *Mol. Biol. Rep.* 46, 471–477. doi: 10.1007/s11033-018-4497-9
- Wilkins, M., Hall-Stoodley, L., Allan, R. N., and Faust, S. N. (2014). New approaches to the treatment of biofilm-related infections. *J. Infect.* 69, S47–S52. doi: 10.1016/j.jinf.2014.07.014
- Wingender, J., and Flemming, H.-C. (2011). Biofilms in drinking water and their role as a reservoir for pathogens. *Int. J. Hyg. Environ. Health* 214, 417–423. doi: 10.1016/j.ijheh.2011.05.009
- Xiang, H., Cao, F., Ming, D., Zheng, Y., Dong, X., Zhong, X., et al. (2017). Aloe-emodin inhibits *Staphylococcus aureus* biofilms and extracellular protein production at the initial adhesion stage of biofilm development. *Appl. Microbiol. Biotechnol.* 101, 6671–6681. doi: 10.1007/s00253-017-8403-5
- Xu, L., Shao, C., Li, G., Shan, A., Chou, S., Wang, J., et al. (2020). Conversion of broad-spectrum antimicrobial peptides into species-specific antimicrobials capable of precisely targeting pathogenic bacteria. *Sci. Rep.* 10:944. doi: 10.1038/s41598-020-58014-6
- Xu, Z., Zhang, H., Yu, H., Dai, Q., Xiong, J., Sheng, H., et al. (2019). Allicin inhibits *Pseudomonas aeruginosa* virulence by suppressing the *rhl* and *pqs* quorum-sensing systems. *Can. J. Microbiol.* 65, 563–574.
- Yan, X., Gu, S., Cui, X., Shi, Y., Wen, S., Chen, H., et al. (2019). Antimicrobial, anti-adhesive and anti-biofilm potential of biosurfactants isolated from *Pediococcus acidilactici* and *Lactobacillus plantarum* against *Staphylococcus aureus* CMCC26003. *Microb. Pathog.* 127, 12–20. doi: 10.1016/j.micpath.2018.11.039
- Yan, X., Gu, S., Shi, Y., Cui, X., Wen, S., and Ge, J. (2017). The effect of emodin on *Staphylococcus aureus* strains in planktonic form and biofilm formation in vitro. *Arch. Microbiol.* 199, 1267–1275. doi: 10.1007/s00203-017-1396-8
- Yang, Y. B., Wang, S., Wang, C., Huang, Q. Y., Bai, J. W., Chen, J. Q., et al. (2015). Emodin affects biofilm formation and expression of virulence factors in *Streptococcus suis* ATCC700794. *Arch. Microbiol.* 197, 1173–1180. doi: 10.1007/s00203-015-1158-4
- Yong, Y. Y., Dykes, G. A., and Choo, W. S. (2019). Biofilm formation by staphylococci in health-related environments and recent reports on their control using natural compounds. *Crit. Rev. Microbiol.* 45, 201–222. doi: 10.1080/1040841X.2019.1573802
- Yuan, L., Hansen, M. F., Roder, H. L., Wang, N., Burmolle, M., and He, G. (2020). Mixed-species biofilms in the food industry: current knowledge and novel control strategies. *Crit. Rev. Food Sci. Nutr.* 60, 2277–2293. doi: 10.1080/10408398.2019.1632790
- Yuan, Y., Zai, Y., Xi, X., Ma, C., Wang, L., Zhou, M., et al. (2019). A novel membrane-disruptive antimicrobial peptide from frog skin secretion against cystic fibrosis isolates and evaluation of anti-MRSA effect using *Galleria mellonella* model. *Biochim. Biophys. Acta Gen. Subj.* 1863, 849–856. doi: 10.1016/j.bbagen.2019.02.013
- Zarnowski, R., Sanchez, H., Covelli, A. S., Dominguez, E., Jaromin, A., Berhardt, J., et al. (2018). *Candida albicans* biofilm-induced vesicles confer drug resistance through matrix biogenesis. *PLoS Biol.* 16:e2006872. doi: 10.1371/journal.pbio.2006872
- Zhang, L., Liang, E., Cheng, Y., Mahmood, T., Ge, F., Zhou, K., et al. (2020). Is combined medication with natural medicine a promising therapy for bacterial biofilm infection? *Biomed. Pharmacother.* 128:110184. doi: 10.1016/j.biopha.2020.110184
- Zhong, L., Ravichandran, V., Zhang, N., Wang, H., Bian, X., Zhang, Y., et al. (2020). Attenuation of *Pseudomonas aeruginosa* quorum sensing by natural products: virtual screening, evaluation and biomolecular interactions. *Int. J. Mol. Sci.* 21:2190. doi: 10.3390/ijms21062190
- Zhou, J. W., Luo, H. Z., Jiang, H., Jian, T. K., Chen, Z. Q., and Jia, A. Q. (2018). Hordenine: a novel quorum sensing inhibitor and antibiofilm agent against *Pseudomonas aeruginosa*. *J. Agri. Food Chem.* 66, 1620–1628. doi: 10.1021/acs.jafc.7b05035

Conflict of Interest: The authors declare that the research was conducted in the absence of any commercial or financial relationships that could be construed as a potential conflict of interest.

Copyright © 2020 Mishra, Panda, De Mandal, Shakeel, Bisht and Khan. This is an open-access article distributed under the terms of the Creative Commons Attribution License (CC BY). The use, distribution or reproduction in other forums is permitted, provided the original author(s) and the copyright owner(s) are credited and that the original publication in this journal is cited, in accordance with accepted academic practice. No use, distribution or reproduction is permitted which does not comply with these terms.



Antibacterial Activity of *Cinnamomum camphora* Essential Oil on *Escherichia coli* During Planktonic Growth and Biofilm Formation

Lei Wang, Kang Zhang, Kai Zhang, Jingyan Zhang, Jingjing Fu, Jie Li, Guibo Wang, Zhengying Qiu, Xuezhi Wang and Jianxi Li*

Key Lab of Veterinary Pharmaceutical Development, Ministry of Agriculture and Rural Affairs, Engineering and Technology Research Center of Traditional Chinese Veterinary Medicine, Gansu Province, Lanzhou Institute of Husbandry and Pharmaceutical Sciences of Chinese Academy of Agricultural Sciences, Lanzhou, China

OPEN ACCESS

Edited by:

Sanket J. Joshi,
Sultan Qaboos University, Oman

Reviewed by:

Srinandan Chakravarthy,
SASTRA University, India
Maria Aparecida Scatamburlo
Moreira,
Universidade Federal de Viçosa, Brazil

*Correspondence:

Jianxi Li
ljianxil@163.com

Specialty section:

This article was submitted to
Antimicrobials, Resistance
and Chemotherapy,
a section of the journal
Frontiers in Microbiology

Received: 11 May 2020

Accepted: 21 October 2020

Published: 12 November 2020

Citation:

Wang L, Zhang K, Zhang K,
Zhang J, Fu J, Li J, Wang G, Qiu Z,
Wang X and Li J (2020) Antibacterial
Activity of *Cinnamomum camphora*
Essential Oil on *Escherichia coli*
During Planktonic Growth
and Biofilm Formation.
Front. Microbiol. 11:561002.
doi: 10.3389/fmicb.2020.561002

Bacterial biofilms are believed to be principal virulence factors for many localized chronic infectious diseases. *Escherichia coli* is one of the most common microbial pathogens and frequently causes biofilm-associated opportunistic infections, such as diarrhea, endometritis and mastitis. *Cinnamomum camphora* essential oil (CCEO) has shown potential in treating intractable chronic endometritis in dairy cows. There is little scientific evidence regarding the effect of CCEO on bacterial biofilms. The objective of this study was to investigate the effect of CCEO on *E. coli* biofilm formation and how CCEO affects *E. coli* in suspension and in a biofilm. CCEO killed all clinical *E. coli* strains in either planktonic or biofilm state isolated from dairy cows with clinical endometritis. The minimum inhibitory concentration (MIC) for 90% of the organisms was 4.297 $\mu\text{L/mL}$, the minimum bactericidal concentration for 90% of the organisms was 6.378 $\mu\text{L/mL}$, the minimum biofilm inhibitory concentration for 90% of the organisms was 6.850 $\mu\text{L/mL}$, and the minimum biofilm eradication concentration (MBEC) for 90% of the organisms was 8.467 $\mu\text{L/mL}$. The MBECs were generally two times higher than the MICs. Flow cytometry analysis confirmed that significant bacterial killing occurred during the first 1 h after exposure to subinhibitory concentrations of CCEO. In addition, CCEO exerted a significant inhibitory effect on *E. coli* biofilm formation, and bacterial killing occurred during the first 30 min of exposure to subinhibitory biofilm concentrations of CCEO. The biofilm yield of *E. coli* was significantly reduced after CCEO treatment, along with an increased dead/live microbial ratio in biofilms compared with that in the non-treated control, as confirmed by scanning electron microscopy images and confocal laser scanning microscopy images. These data revealed that CCEO efficiently kills *E. coli* during planktonic growth and biofilm formation.

Keywords: *Cinnamomum camphora* essential oil, bactericidal effect, *Escherichia coli*, planktonic growth, biofilm

INTRODUCTION

Bacterial biofilms, an emergent form of bacterial life, are “aggregates of microorganisms in which cells are frequently embedded in a self-produced matrix of extracellular polymeric substances that are adherent to each other and/or a surface” (Vert et al., 2012; Flemming et al., 2016). The National Institutes of Health revealed that 65% of all microbial infections and 80% of all chronic infections are associated with biofilm formation. Microorganisms in biofilms develop elevated resistance to antimicrobial agents and host defense systems through the physical barrier of the extracellular matrix, metabolic dormancy or molecular persistence programs (Van Acker et al., 2014). During the dispersion of a biofilm, the microbial cells within the biofilm quickly proliferate and disperse to switch from a sessile to a motile form. Detachment then occurs in a natural pattern (Costerton et al., 1999). The formation of bacterial biofilms increases the hardness of the bacteria and contributes to their persistence during infection, posing great challenges in the use of conventional antimicrobials. Nonetheless, the control of biofilm formation and treatment of existing biofilms remains tenuous, with few new therapeutic options currently available for clinical use. Targeting microbial biofilms is a current and prospective therapeutic strategy (Koo et al., 2017).

The essential oil of *Cinnamomum camphora* (L.) Presl (CCEO) has a broad range of antimicrobial, insecticidal, anti-inflammatory and antioxidant activities. CCEO contains 330 different compounds, including linalool and camphor, which are the main antibacterial components (Zhang et al., 2019). Many studies have been carried out on the antibacterial activity of CCEO, revealing, for example, activities against *Escherichia coli*, *Staphylococcus aureus*, and *Choanephora cucurbitarum* (Pragadheesh et al., 2013; Zhang et al., 2014; Wu et al., 2019). Preliminary clinical trials have shown that the cure rate of dairy cows suffering from resistant endometritis or chronic endometritis treated with chloramphenicol and furacilin oil increases significantly when 20% camphor oil has been added (Meng et al., 1984). Our previous studies in the lab of traditional Chinese veterinary medicine in Lanzhou Institute of Husbandry and Pharmaceutical Sciences of Chinese Academy of Agricultural Sciences also showed that 35 of 48 cows recovered from endometritis following treatment with 4% CCEO (sweet almond oil as solvent) under field conditions (data not published). However, there is little scientific evidence indicating that this bioactivity is associated with the inhibition of bacterial biofilm formation by CCEO. *E. coli* is one of the most common microbial pathogens and frequently causes biofilm-associated opportunistic infections, such as endometritis (Ferris et al., 2016). We speculated that CCEO inhibits *E. coli* in biofilms, which contributes to the cure of refractory endometritis. Therefore, we studied the effect of CCEO on planktonic growth and biofilm formation by *E. coli* isolated from dairy cows suffering from clinical endometritis and how CCEO affects *E. coli* in suspension and in a biofilm.

MATERIALS AND METHODS

Materials

Cinnamomum camphora essential oil was purchased from Jiangxi Huitong Pharmaceutical Fragrance Oil Co., Ltd., and analyzed via gas chromatography-mass spectrometry. Thirty-one compounds were identified, constituting 70.04% (v/v) of the oil. The major compound was linalool (17.98%, v/v), followed by camphor (17.15%, v/v), eucalyptol (12.71%, v/v), and alpha-terpineol (3.43%, v/v).

Bacterial Strains

Forty-four clinical strains of *E. coli* were isolated from the intrauterine mucus of Holstein cows affected with clinical endometritis 21–50 days after calving, and the cows were collected from five farms located in Gansu Province, Shaanxi Province, and Qinghai Province in Northwest China. Then, these clinical strains were identified as *E. coli* using colony morphology analysis on blood agar, Gram staining, biochemical identification and 16S rDNA sequencing. Accession numbers of their 16S rRNA sequences in GenBank are KJ57728-KJ5772872 and MW025989-MW026027. *E. coli* ATCC 25922 was purchased from the American Type Culture Collection. Biofilm formation of *E. coli* was determined by the crystal violet method. All the strains were stored at -80°C in a microbiology laboratory located in the Lanzhou Institute of Husbandry and Pharmaceutical Sciences of Chinese Academy of Agricultural Sciences, Lanzhou, China.

Determination of the Minimum Inhibitory Concentration (MIC) and Minimum Bactericidal Concentration (MBC)

The minimum inhibitory concentration (MIC) and minimum bactericidal concentration (MBC) of CCEO against forty-four *E. coli* isolates and *E. coli* ATCC25922 were determined using the broth microdilution method according to Kwieciński et al. (2009) with minor modifications. *E. coli* was incubated (37°C , shaking) in Mueller-Hinton (MH) broth until the exponential growth phase was reached. A diluted bacterial suspension was added to a 96-well microtiter plate at a final concentration of 1×10^5 CFU/mL based on a turbidity comparator (DensiCHEK plus, BioMerieux SA, France). Serial twofold dilutions of CCEO were prepared and added to each well to obtain a final concentration range from 0.25 to 128 $\mu\text{L/mL}$. All wells contained 1% DMSO (v/v) to enhance the solubility of CCEO. In addition, there were solvent control (test bacteria and MH broth containing 1% DMSO), bacterial control (test bacteria and MH broth), blank control (MH broth containing 1% DMSO and corresponding concentrations of CCEO), blank solvent control (MH broth containing 1% DMSO) and blank medium (MH broth). All plates were incubated at 37°C for 24 h, and growth was evaluated by the turbidimetric method. The MIC was defined as the lowest CCEO concentration at which no visible growth was detected (optical density at 600 nm ($\text{OD}_{600\text{ nm}}$) ≤ 0.05).

From the wells representing the MIC and the three next highest concentrations, 10 μL of the test solutions was removed

and plated on MH agar, and the plates were incubated at 37°C for 24 h. Finally, the number of colonies on the agar was counted. The MBC was defined as the lowest concentration at which no colonies were observed. The MIC and MBC were determined for all 44 clinical *E. coli* strains and *E. coli* ATCC 25922. For each strain, at least three replicates were analyzed, and the modal value was determined.

Determination of the Minimum Biofilm Inhibitory Concentration (MBIC) and Minimum Biofilm Eradication Concentration (MBEC)

The minimum biofilm inhibitory concentration (MBIC) of CCEO against 39 *E. coli* isolates and *E. coli* ATCC25922 was determined using the microdilution method with minor modifications (Al-Shabib et al., 2017). A bacterial suspension (2×10^7 CFU/mL) in Luria-Bertani (LB) broth was added to a 96-well microtiter plate (100 μ L per well) with serial twofold dilutions of CCEO (0.5 to 256 μ L/mL, 100 μ L per well). All wells contained a final DMSO concentration of 1% (v/v). In addition, there were solvent control (test bacteria and LB broth containing 1% DMSO), bacterial control (test bacteria and LB broth), blank control (LB broth containing 1% DMSO and corresponding concentrations of CCEO), blank solvent control (LB broth containing 1% DMSO) and blank medium (LB broth). All plates were incubated at 37°C for 24 h, and then, the medium was aspirated. Each well was washed three times with PBS, dried, fixed with 200 μ L of methanol for 15 min, stained with 0.3% (w/v) crystal violet for 5 min, and rinsed with deionized water. Subsequently, 200 μ L of 33% (v/v) glacial acetic acid was added to the wells. Finally, the plates were shaken at room temperature for 5 min, and the OD_{600 nm} was measured using a microplate reader (SpectraMax M2^e, Molecular Devices, United States). The MBIC was defined as the lowest concentration of CCEO that resulted in at least 90% inhibition of biofilm formation compared with that in the control without CCEO.

The minimum biofilm eradication concentration (MBEC) of CCEO against *E. coli* was determined by the microdilution method with minor modifications (Ramage et al., 2001). Two hundred microliters of bacterial suspension (1×10^7 CFU/mL) in LB broth was added to each well in a 96-well microtiter plate for biofilm formation. After incubation at 37°C for 24 h, the medium was aspirated, and each well was washed three times with PBS. Subsequently, serial twofold dilutions of CCEO (0.25 to 128 μ L/mL) were added to the wells containing biofilms. All wells contained a final DMSO concentration of 1% (v/v). In addition, solvent control (biofilm and LB broth containing 1% DMSO), biofilm control (biofilm and LB broth), blank control (LB broth containing 1% DMSO and corresponding concentrations of CCEO), blank solvent control (LB broth containing 1% DMSO) and blank medium (LB broth) were also performed. The plates were incubated at 37°C for 24 h, the medium was aspirated, and each well was washed three times with PBS. Subsequently, the biofilms were stained with 0.3% (w/v) crystal violet and rinsed with deionized water. Finally,

33% (v/v) glacial acetic acid was added, and measurements were made with the method described above. The MBEC was defined as the lowest CCEO concentration that resulted in at least 80% eradication of biofilms compared with that in the control without CCEO.

Planktonic Time-Dependent Killing Assay

In test tubes, *E. coli* ATCC 25922 suspensions (1×10^5 CFU/mL) were mixed with CCEO at a final concentration of 0 (control), 1, 2, 4, or 8 μ L/mL and with 1% DMSO (v/v) in all tubes. All tubes were incubated at 37°C with shaking. After 5, 15, and 30 min and 1, 2, 4, 8, 12, and 24 h, 100 μ L was removed from each tube, serially diluted, plated on MH agar and incubated at 37°C for 24 h. The number of viable *E. coli* cells was determined by counting the colonies formed. The detection limit was 10 CFU/mL. A sample from the 0 μ L/mL CCEO tube taken immediately after mixing was used as a “time 0” control. Measurements were performed in three independent experiments. Time-kill curves were constructed by plotting the mean colony counts (Log₁₀ CFU/mL) versus time.

Flow Cytometry (FCM) Assay

The effect of CCEO on *E. coli* ATCC 25922 cell viability during planktonic growth was analyzed by flow cytometry (FCM) with minor modifications (Kang et al., 2018). *E. coli* ATCC 25922 suspensions (1×10^6 CFU/mL) were treated with CCEO at 0 μ L/mL (control), 2, 4, and 8 μ L/mL for 0.5, 1, 4, and 24 h at 37°C. The samples were centrifuged at 10000 rpm for 5 min, the medium was removed, and the cells were resuspended in physiological saline. Then, the cells were stained with SYTO 9 and propidium iodide (PI) dyes from the LIVE/DEAD BacLight Bacterial Viability Kit (Molecular Probes, Invitrogen, France) in the dark for 15 min. The samples were centrifuged again at 10000 rpm for 5 min, the supernatant fluid was removed, and the cells were resuspended in physiological saline. FCM (Cytomics FC 500, Beckman Coulter, United States) was used to determine the viability of the *E. coli* cells. The acquisition time/events of the protocol were 300 s/100000 cells.

Biofilm Time-Dependent Killing Assay

A bacterial suspension of *E. coli* ATCC 25922 (2×10^7 CFU/mL) in LB broth was added to a 96-well microtiter plate (100 μ L per well). CCEO solutions (0, 2, 4, 8, and 16 μ L/mL) in 100 μ L of LB with 1% DMSO (v/v) were also added to the wells. The plates were incubated at 37°C for 5, 15, 30, 60, 120, 240, and 480 min. The medium was then aspirated, the wells were washed three times with PBS, and 200 μ L of LB was added to each well. Then, 40 μ L of CCK-8 solution from the Cell Counting Kit-8 assay (CCK-8, Beyotime Biotechnology, China) was added to the wells with the biofilms. Following incubation at 37°C for 2 h, the absorbance at 450 nm was recorded. All measurements were performed in three independent experiments.

Scanning Electron Microscopy (SEM) Analysis

The effects of CCEO on bacterial attachment and biofilm formation were examined using scanning electron microscopy (SEM) according to a previously described method with minor modifications (Kang et al., 2018). *E. coli* ATCC 25922 suspensions (1×10^7 CFU/mL) were prepared in LB broth with CCEO concentrations of 0, 2, and 4 $\mu\text{L/mL}$. The samples were incubated to form biofilms on a glass coverslip (8 mm) in a 24-well polystyrene plate for 24 h without shaking at 37°C. The samples were fixed for 4 h using 2.5% glutaraldehyde, washed with PBS and dehydrated using a graded ethanol series (30, 50, 70, 85, 90, 100, and 100%; 15 min each). After drying, the samples were sputter-coated with gold and then imaged with SEM (JSM-5600, JEOL, Japan).

Confocal Laser Scanning Microscopy (CLSM) Analysis

The effects of CCEO on viable bacteria during biofilm formation were examined using confocal laser scanning microscopy (CLSM). After the *E. coli* ATCC 25922 suspensions (1×10^7 CFU/mL) were incubated with CCEO concentrations of 0 and 2 $\mu\text{L/mL}$ for 24 h, the biofilms were stained with SYTO 9 and PI from the LIVE/DEAD BacLight Bacterial Viability Kit (Molecular Probes, Invitrogen, France). After staining in the dark for 15 min, the samples were washed with PBS and imaged with a CLSM (LSM 700, Zeiss, Germany) equipped with a 40 \times objective lens. The excitation/emission maxima were approximately 483/500 nm for the SYTO 9 stain and 305/617 nm for PI. Each sample took six fields, and three independent experiments were performed.

The images obtained from CLSM were quantified for biomass of dead cells and live cells with COMSTAT (Heydorn et al., 2000; Vorregaard, 2008)¹.

Statistical Analysis

Statistical analysis was performed with SPSS software, version 16.0 (SPSS, Inc., United States). One-way analysis of variance was performed to detect the significant effects of variables, followed by a Student–Newman–Keuls test. Differences were considered significant at $p < 0.05$.

RESULTS

CCEO Has a Strong Bactericidal Effect and Disrupts Biofilms

From 44 *E. coli* isolates from dairy cows with endometritis in China, 39 *E. coli* isolates could form biofilms. CCEO exhibited significant bactericidal activity against *E. coli* and strong activity against the *E. coli* biofilm. The cumulative MIC, MBC, MBIC, and MBEC values of CCEO against the clinical isolates of *E. coli* are summarized in Figure 1. For the clinical isolates, the MICs ranged from 2 to 8 $\mu\text{L/mL}$, the MBCs ranged from 2 to 16 $\mu\text{L/mL}$,

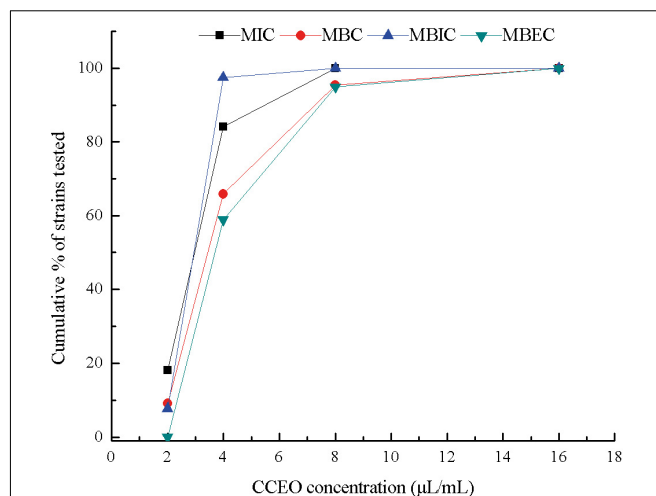


FIGURE 1 | Cumulative minimum inhibitory concentration (MIC), minimum bactericidal concentration (MBC), minimum biofilm inhibitory concentration (MBIC), and minimum biofilm eradication concentration (MBEC) of *C. camphora* essential oil (CCEO) against clinical strains of *E. coli* isolated from dairy cows affected with clinical endometritis in China, expressed as a percentage of the tested strains. MIC and MBC, $n = 44$; MBIC and MBEC, $n = 39$.

the MBICs ranged from 2 to 8 $\mu\text{L/mL}$, and the MBECs ranged from 4 to 16 $\mu\text{L/mL}$ (details in Supplementary Table S1). The MIC for 50% of the organisms (MIC_{50}) was 2.953 $\mu\text{L/mL}$, the MIC for 90% of the organisms (MIC_{90}) was 4.297 $\mu\text{L/mL}$, and the MBC_{50} and MBC_{90} were 3.870 and 6.378 $\mu\text{L/mL}$, respectively. The MBIC_{50} , MBIC_{90} , MBEC_{50} , and MBEC_{90} were 3.619, 6.850, 4.693, and 8.467 $\mu\text{L/mL}$, respectively. For *E. coli* ATCC 25922, the MIC, MBC, MBIC, and MBEC were 4, 8, 4, and 8 $\mu\text{L/mL}$, respectively.

Effect of CCEO on Planktonic Growth and Cell Viability of *E. coli*

When *E. coli* ATCC 25922 was exposed to 1 and 2 $\mu\text{L/mL}$ CCEO for 1 h, the number of viable cells was the lowest (Figure 2A). After exposure to 1 $\mu\text{L/mL}$ CCEO for 4 h, the inhibition of *E. coli* by CCEO was the strongest, and only 0.1% of the viable *E. coli* cells in the control without CCEO were observed in the exposed group. After treatment with 2 $\mu\text{L/mL}$ CCEO, the number of viable *E. coli* cells was reduced by two \log_{10} steps (99% killed) after 5 min (Figure 2B), and a reduction of three \log_{10} steps (99.9% killed) was observed after 1 to 4 h (Figure 2A). Treatment with 4 $\mu\text{L/mL}$ CCEO resulted in a reduction of five \log_{10} steps (99.999% killed) after 5 min, and viable *E. coli* cells were detected (approximately 16.7 CFU/mL) until the addition of 4 $\mu\text{L/mL}$ CCEO for 24 h. After treatment with 8 $\mu\text{L/mL}$ CCEO, no viable *E. coli* was detected during the observation period. The rate of killing was dosage-dependent over the range of CCEO concentrations tested. The bactericidal activity of CCEO was related to the *E. coli* growth phase, with the lowest level in viable counts observed at approximately 1 h.

Flow cytometry dual-parameter dot plots of *E. coli* ATCC25922 treated with CCEO at 0, 2, 4, and 8 $\mu\text{L/mL}$

¹ www.comstat.dk

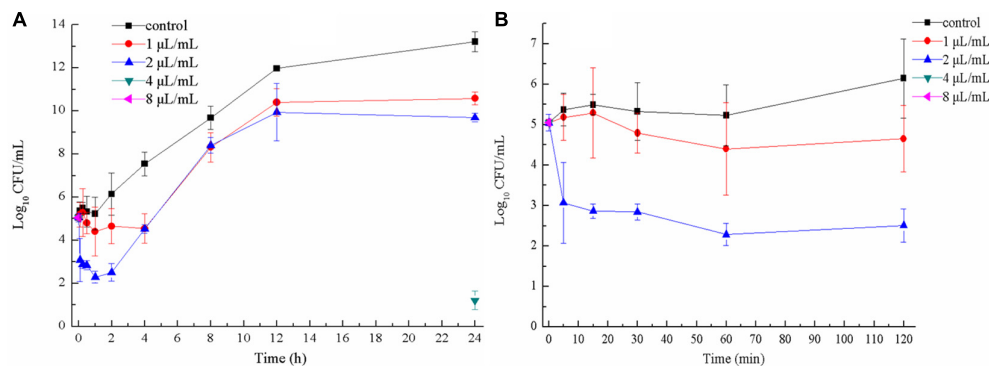


FIGURE 2 | Time-kill curves of *C. camphora* essential oil (CCEO) at 0, 1, 2, 4, or 8 $\mu\text{L/mL}$ against planktonic *E. coli* ATCC 25922 for 24 h (A) and for 2 h (B). A sample of 0 $\mu\text{L/mL}$ CCEO was used as a control. Data indicates confidence interval at 95% of three independent experiments.

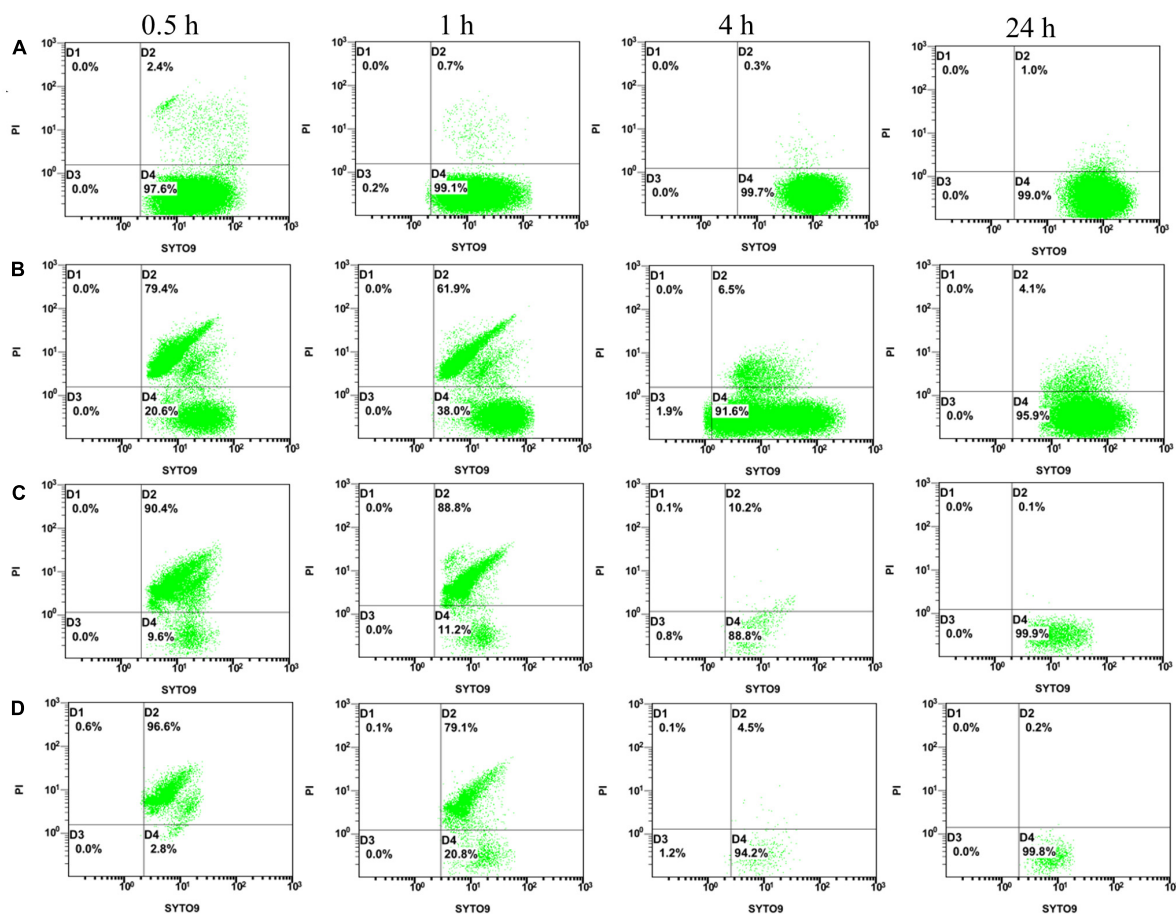
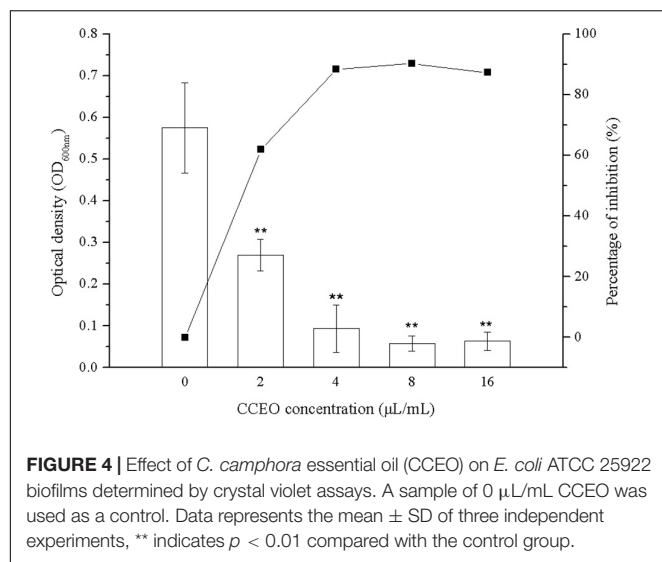


FIGURE 3 | Flow cytometry (FCM) dot plots for *E. coli* ATCC 25922: (A) control; (B) treated with *C. camphora* essential oil (CCEO) at 2 $\mu\text{L/mL}$ for 0.5, 1, 4, and 24 h; (C) treated with CCEO at 4 $\mu\text{L/mL}$ for 0.5, 1, 4, and 24 h; and (D) treated with CCEO at 8 $\mu\text{L/mL}$ for 0.5, 1, 4, and 24 h. A sample of 0 $\mu\text{L/mL}$ CCEO was used as a control.

and stained with SYTO 9 and PI are shown in **Figure 3**. More than 97% of the *E. coli* cells in the control group with 0 $\mu\text{L/mL}$ CCEO were located in the D4 quadrant (**Figure 3A**), indicating that the untreated *E. coli* cells had intact cell membranes and were almost all viable. After treatment with 2 $\mu\text{L/mL}$ CCEO,

the number of cells was lowest at 1 h; moreover, only 98633 cells were acquired in 300 s at 1 h, 100000 cells were acquired in 267.8 s at 0.5 h, 100000 cells were acquired in 26.9 s at 4 h and 100000 cells were acquired in 23.9 s at 24 h (**Figure 3B**). The cells shown in **Figures 3C,D** were all acquired in 300 s, and



the lowest values were observed at 4 h after treatment with 4 or 8 μL/mL CCEO. After exposure to CCEO, the number of cells dramatically decreased, and the number of viable cells decreased with increasing CCEO concentration. The proportion of viable cells increased over time.

Effect of CCEO on *E. coli* Biofilm Formation

Biofilm formation of *E. coli* ATCC 25922 was significantly inhibited after exposure to CCEO, as shown by quantitative crystal violet assays (Figure 4) and SEM analysis (Figure 5). CCEO at 2 μL/mL significantly inhibited biofilm formation ($p < 0.01$). Eighty-eight percent of *E. coli* biofilm formation was inhibited after treatment with 4 μL/mL CCEO, and an increase in the CCEO concentration did not further inhibit biofilm formation (Figure 4). SEM analysis also yielded interesting results. Compared with the control without CCEO, CCEO decreased the number of *E. coli* cells and disrupted biofilm formation (Figures 5A–C). After treatment with 4 μL/mL CCEO, the morphology of *E. coli* cells was destroyed and it was difficult to find intact *E. coli* cells in the microscopic field after exposure for 6 h (Figure 5C).

Effect of CCEO on the Viability of *E. coli* During Biofilm Formation

Viable cells in biofilms of *E. coli* ATCC 25922 were detected by CCK-8 assays (Figure 6) and CLSM analysis (Figure 7). After 30 min, the viability of the bacteria in biofilms exposed to 1 μL/mL CCEO was 42.33% of the control value and that after exposure to 2 μL/mL CCEO was 29.45% of the control value. However, as the exposure time increased, the inhibitory effect of CCEO gradually weakened. When 4 μL/mL CCEO was added, 82% of the biofilm formation was inhibited after exposure for 5 min, and that proportion reached 90% after exposure for 30 min. Increasing the CCEO concentration to 8 μL/mL had a similar effect as the exposure to 4 μL/mL CCEO on the kinetics of biofilm killing. These effects appeared to be dosage

dependent up to 4 μL/mL CCEO. Fast killing occurred during the first 30 min, and then, the rate of killing decreased in a time-dependent manner for 4 and 8 μL/mL CCEO (Figure 6). In the CLSM images, the morphology of the *E. coli* biofilms treated with 2 μL/mL CCEO was disrupted compared with that of the untreated group (control) (Figures 7A,B). The biomass of live cells was significantly reduced after CCEO treatment compared with the control at the same time ($p < 0.01$) (Figure 7C). The ratio of dead/live cells was significantly increased after treatment with CCEO at 24 h ($p < 0.01$) (Figure 7D).

DISCUSSION

Cinnamomum camphora essential oil has been shown to exhibit medicinal activities, such as antimicrobial, insecticidal, anti-inflammatory and antioxidant activities. The obtained MICs and MBCs confirmed the high susceptibility of clinical strains to CCEO. *E. coli* biofilm formation can cause antimicrobial resistance and is closely related to persistent *E. coli* infection (Venkatesan et al., 2015; Ferris et al., 2016). In recent years, studies have shown that natural products affect *E. coli* biofilm formation (Jagani et al., 2009; Serra et al., 2016; Kang et al., 2017). In this context, we showed that CCEO efficiently kills *E. coli* in both suspension and biofilms. The MIC of CCEO obtained in this study was similar to the MIC of CCEO against *E. coli* found by Zhou et al. (2016). However, this value was far lower than the concentration required for antifungal activity against *Colletotrichum gloeosporioides*, *Botrytis cinerea*, and *Fusarium graminearum* reported by Wang et al. (2017). This discrepancy might be partly explained by the fact that the chemical compositions of different CCEOs are not the same, and different CCEOs have different inhibitory effects on bacteria, with a stronger inhibitory effect on gram-negative bacteria than on gram-positive bacteria (Jantan and Goh, 1992; Pelissier et al., 1995; Shi et al., 2013; Zhou et al., 2016). Our data showed that the MBICs were similar to the MBCs and that the MBECs were almost twice as high as the MICs (details in Supplementary Table S1). Most antibiotics are up to 1000 times less efficient against bacteria in biofilms than against those in suspension (Melchior et al., 2006), which makes CCEO a very promising antibacterial agent. For the potential clinical use of CCEO, it is important to establish the kinetics of its action against bacteria in suspension and in biofilms.

Time-kill curves and FCM analysis were used to confirm the antibacterial mode of CCEO. In FCM analysis, the fluorescent stains SYTO 9 and PI were used to evaluate microbial viability. SYTO 9 can combine with nucleic acids in all bacterial cells to emit green fluorescence, while PI penetrates only damaged bacterial membranes and combines with DNA from dead bacteria to emit red fluorescence. When SYTO 9 and PI are both present, SYTO 9 fluorescence is reduced (Oliveira et al., 2015). Our results indicated that CCEO can effectively kill *E. coli* in a dose-dependent manner, with the fastest killing occurring during the first 5 min. The antibacterial mode of action is consistent with that of tea tree oil (Kwieciński et al., 2009). The lowest level in viable bacteria was observed at approximately 1 h after

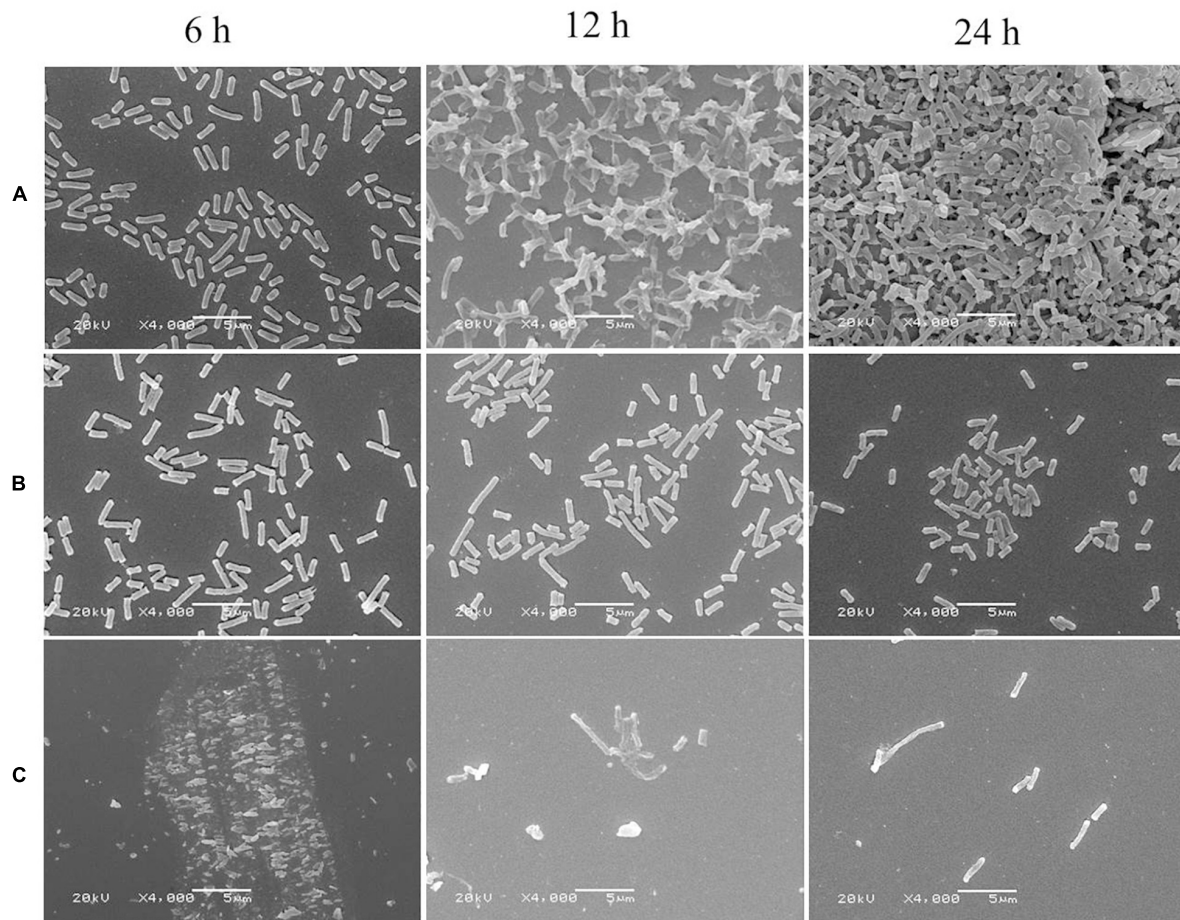


FIGURE 5 | Scanning electron microscopy (SEM) images of *E. coli* ATCC 25922 biofilms: (A) control; (B) treated with *C. camphora* essential oil (CCEO) at 2 $\mu\text{L/mL}$ for 6, 12, and 24 h; (C) treated with CCEO at 4 $\mu\text{L/mL}$ for 6, 12, and 24 h. A sample of 0 $\mu\text{L/mL}$ CCEO was used as a control.

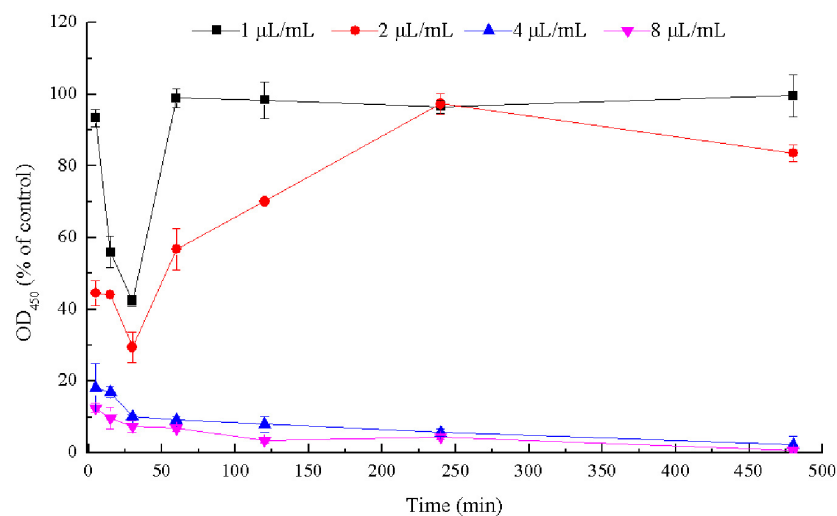


FIGURE 6 | Time-kill curves of *C. camphora* essential oil (CCEO) at 1, 2, 4, or 8 $\mu\text{L/mL}$ against *E. coli* ATCC 25922 biofilms. Data represents the mean \pm SD of three independent experiments.

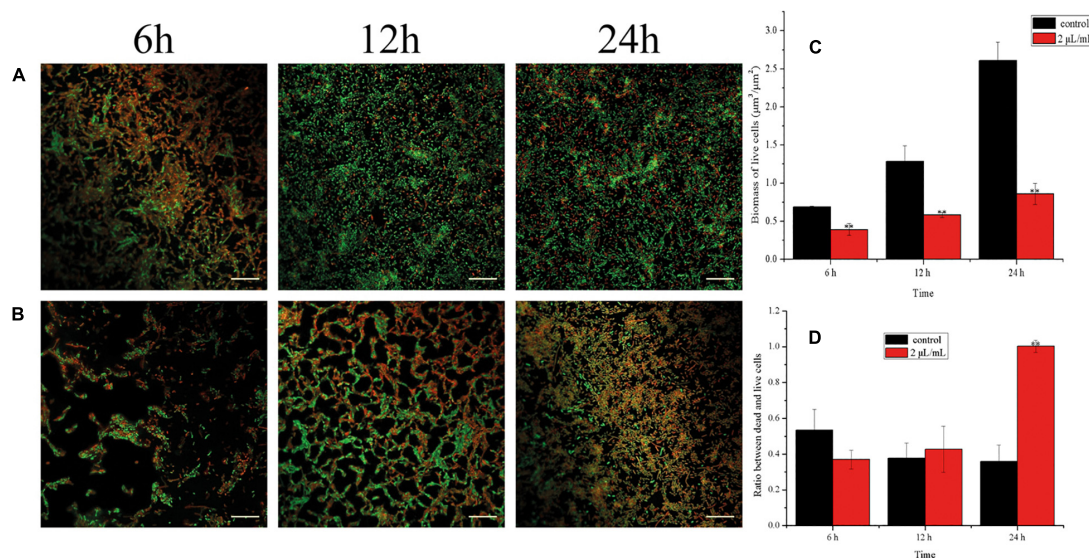


FIGURE 7 | Analyses of live/dead bacteria in *E. coli* ATCC 25922 biofilms: **(A)** Confocal laser scanning microscopy (CLSM) images of *C. camphora* essential oil (CCEO) at 0 μL/mL for 6, 12 and 24 h; **(B)** CLSM images of CCEO at 2 μL/mL for 6, 12 and 24 h; Green, live bacteria, red, dead bacteria; Images from three independent replicates with 20 μm bars are representative; **(C)** Biomass of live cells in biofilm; **(D)** Ratio between dead and live cells in biofilm. A sample of 0 μL/mL CCEO was used as a control. Data represents the mean ± SD of three independent experiments, ** indicates $p < 0.01$ compared with the control at the same time.

treatment with subinhibitory concentrations of CCEO in our study. This finding is consistent with an early study on the vapor-phase antibacterial action of essential oil from *C. camphora* var. *linaloofera* Fujita (Wu et al., 2019). These findings may be a result of the bacteria being in the lag phase in the first 1 h; the damage of most bacteria caused by subinhibitory concentrations of CCEO could be gradually recovered. After entering the logarithmic phase, bacteria grow rapidly with steady geometric progression. When the rate of bacterial growth exceeded the rate of CCEO-mediated killing, the number of viable bacteria increased. After exposure to 4 or 8 μL/mL CCEO, the number of bacterial cells sharply decreased, and mainly dead cells were detected by FCM. After treatment with 4 or 8 μL/mL CCEO for 4 h, the number of bacterial cells decreased to the lowest level, with mostly viable cells detected, and the number of bacterial cells increased after 24 h based on our FCM results. This finding indicated that the killing cells were disrupted at 4 h after treatment with CCEO, and the effectiveness of CCEO decreased over time. Therefore, we speculated that the pharmacodynamic time of CCEO was less than 24 h. After treatment with 4 or 8 μL/mL CCEO, viable bacterial cells were detected by FCM, but no cells were detected by the CFU assay. One reason may be that the number of viable bacteria was very low, approximately 1 CFU/mL or even lower, at this time point, while the detection limit of the CFU assay was 10 CFU/mL. In addition, a few *E. coli* cells might exhibit sublethal injury at this time point and may then begin to multiply after recovery when the effect of CCEO is reduced (Lewis, 2007; Spilimbergo et al., 2010). Treatment with plant essential oils, such as carvacrol and citral, for 4–6 h resulted in the maximum proportion of bacterial sublethal injury (Somolinos et al., 2008; Silva et al., 2015). Thus, it is necessary to administer CCEO twice in a 24 h period in clinical use.

Escherichia coli biofilms show five stages of development: initial adhesion/attachment to the substrate, irreversible attachment, early development, biofilm maturation, and biofilm dispersion. The early stages of biofilm formation play an important role in the establishment of biofilms on a contact surface because these stages represent the commitment of free-living planktonic bacterial cells to a coordinated biofilm mode of survival (Karunakaran and Biggs, 2011). CCEO degraded the cell membrane and led to the leakage of cytoplasmic materials. Bacterial killing occurred during the first 1 h after exposure to CCEO, and we speculated that the inhibitory effect of CCEO on biofilms also appeared in the early stage. Thus, we tested whether CCEO can inhibit *E. coli* biofilm formation in the present study. Crystal violet assays are commonly used to detect the formation of bacterial biofilms. In this study, the crystal violet assay results showed that CCEO significantly decreased biofilm formation by *E. coli* in a dose-dependent manner. Our SEM results were consistent with this finding, indicating that CCEO strongly inhibited *E. coli* biofilm formation. We also found that 4 μL/mL CCEO could disrupt the biofilm and inhibit *E. coli* cell growth. A similar finding was reported by Kwieciński et al. (2009), who found that tea tree oil (1%) disrupted the biofilm of *S. aureus* due not only to bacterial killing but also partly to extracellular matrix damage and subsequent removal of the biofilm from the surface. Cui et al. (2016) observed that clove oil effectively inhibited the biofilm of *E. coli* O157:H7; clove oil causes physiological and morphological changes in cells and leads to the loss of intracellular constituents and the death of bacterial cells. Wu et al. (2019) reported vapor-phase antibacterial action of the essential oil from *C. camphora* var. *linaloofera* Fujita against *E. coli*; this oil partly degraded the cell membrane and increased membrane permeability, resulting

in leakage of cytoplasmic materials and prominent distortion and shrinkage of the bacterial cells. Chen et al. (2020) reported that the essential oil from the leaves of *C. camphora* (Linn.) Presl inhibited Methicillin-resistant *S. aureus* via damaging cell membranes and disturbing the amino metabolism. We also found the cell membranes of *E. coli* were partially ruptured and the cytoplasmic materials leaked after the treatment with 2 $\mu\text{L/mL}$ CCEO (details in **Supplementary Figure S1**). Thus, we speculated that CCEO could penetrate the *E. coli* biofilm and inhibit bacterial proliferation to reduce the biofilm formation.

The biofilm yield depends on the number of bacteria residing in the biofilm. To quantify the viable count, researchers commonly use mechanical methods (e.g., ultrasonication or scraping) to separate biofilms from the solid surface to which they are adhered (Webber et al., 2015). However, these methods may damage *E. coli* cells. In this study, we performed quantitative analysis of live bacterial cells in biofilms by CCK-8 staining. This method determines the viability of bacterial biofilms based on the reduction of tetrazolium salts to formazan by viable metabolizing bacteria (Berk et al., 2012; Chen et al., 2019). Using this method, our study showed that 4 $\mu\text{L/mL}$ CCEO could inhibit the metabolism of *E. coli* in biofilms, and the rate of killing was concentration dependent up to 4 $\mu\text{L/mL}$ CCEO. Further increases in the CCEO concentration did not significantly accelerate bacterial killing in biofilms. A high respiratory rate of the biofilms was observed after treatment with 2 $\mu\text{L/mL}$ CCEO, particularly at 4 h. This finding is in contrast to the data of crystal violet assay suggesting that 2 $\mu\text{L/mL}$ CCEO significantly inhibited the biofilm. This might be explained by the different methods of viability testing and biofilm formation and the different objects to study. The crystal violet assay was used to detect the effect of CCEO on the biofilm formation of *E. coli*. Not only bacteria but also extracellular polymeric substances such as exopolysaccharides in biofilms were detected by the crystal violet assay. The CCK-8 method determines the respiratory rate of bacteria in the biofilms, including many already lethally injured cells that might still exhibit metabolism. Bacterial viability was inhibited before exposure to CCEO for 4 h, and it was difficult for the injured bacterial cells to secrete the same amount of extracellular polymeric substances like the untreated control. Thus, the inhibition effect of CCEO measured by the crystal violet assay was not consistent with the results of CCK-8. The number of live bacteria in the biofilm was lowest at 30 min, which was inconsistent with the findings at 1 h in suspension. This discrepancy is possibly due to the different growth curves of bacteria in suspension and in biofilms. Furthermore, CLSM and SYTO 9 and PI staining are commonly used to visualize cell viability in biofilms (Kulshrestha et al., 2016). CLSM images also indicated that the number of viable biofilm cells was significantly reduced and the ratio of dead/live cells was significantly increased following treatment with 2 $\mu\text{L/mL}$ CCEO. These results suggested that CCEO killed *E. coli* and inhibited bacterial proliferation to reduce the biofilm formation.

Overall, CCEO exhibited significant antibacterial activity against *E. coli* in suspension and biofilms, two states frequently encountered in living organisms. The MBECs of CCEO against clinical *E. coli* strains were generally two times higher than the

MICs. CCEO killed *E. coli* quickly and effectively at 4 $\mu\text{L/mL}$ and caused the destruction of *E. coli* biofilms. The effect of CCEO on *E. coli* *in vivo* and the mechanism of action of CCEO against *E. coli* biofilms need to be further studied.

DATA AVAILABILITY STATEMENT

The original contributions presented in the study are included in the article/supplementary material, further inquiries can be directed to the corresponding author.

ETHICS STATEMENT

The animal study was reviewed and approved by Animal Ethics Committee of Lanzhou Institute of Husbandry and Pharmaceutical Sciences of CAAS.

AUTHOR CONTRIBUTIONS

LW, KnZ, KiZ, JF, JZ, and JEL designed and performed the lab experiments and analyzed the data. LW, GW, and ZQ designed the figures and analyzed the image data. XW and JXL discussed the results and supervised the project. LW wrote the manuscript in consultation with KnZ, KiZ, JZ, GW, ZQ, XW, and JXL. All authors contributed to the article and approved the submitted version.

FUNDING

This work was supported by the National Natural Science Foundation of China (No. 31902316), the National Innovation Program of Agricultural Science and Technology in CAAS (No. CAAS-ZDXT2018008), the Science and Technology Innovation Project of CAAS Collaborative Innovation (No. CAAS-XTCX2016011-01-09), Chinese Central Government for Basic Scientific Research Operations in Commonwealth Research Institutes (No. 1610322020014), Innovation Project of Traditional Chinese Veterinary Medicine and Clinical Science (No. CAAS-ASTIP-2015-LIHPS), National Dairy Industry and Technology System (No. CARS36), and Gansu Province Science and Technology Foundation for Youths (No. 20JR5RA575).

ACKNOWLEDGMENTS

We thank Prof. Wanxia Pu for her help in identifying clinical isolates of *E. coli*.

SUPPLEMENTARY MATERIAL

The Supplementary Material for this article can be found online at: <https://www.frontiersin.org/articles/10.3389/fmicb.2020.561002/full#supplementary-material>

REFERENCES

- Al-Shabib, N. A., Husain, F., Ahmad, I., Khan, M. S., Khan, R. A., and Khan, J. M. (2017). Rutin inhibits mono-multi-species biofilm formation by food-borne drug resistant *Escherichia coli* and *Staphylococcus aureus*. *Food Control* 79, 325–332. doi: 10.1016/j.foodcont.2017.03.004
- Berk, V., Fong, J. C. N., Dempsey, G. T., Develiöglu, O. N., Zhuang, X. W., Liphardt, J., et al. (2012). Molecular architecture and assembly principles of *vibrio cholerae* biofilms. *Science* 337, 236–239. doi: 10.1126/science.1222981
- Chen, J. L., Tang, C. L., Zhang, R. F., Ye, S. X., Zhao, Z. M., Huang, Y. Q., et al. (2020). Metabolomics analysis to evaluate the antibacterial activity of the essential oil from the leaves of *Cinnamomum camphora* (Linn.) Presl. *J. Ethnopharmacol.* 253, 112652–112662. doi: 10.1016/j.jep.2020.112652
- Chen, L. M., Yang, D., Feng, J., Zhang, M., Qian, Q. P., and Zhou, Y. L. (2019). Switchable modulation of bacterial growth and biofilm formation based on supramolecular tripeptide amphiphiles. *J. Mater. Chem. B* 7, 6420–6427. doi: 10.1039/c9tb00973f
- Costerton, J. W., Stewart, P. S., and Greenberg, E. P. (1999). Bacterial biofilms: a common cause of persistent infections. *Science* 284, 1318–1322. doi: 10.1126/science.284.5418.1318
- Cui, H. Y., Zhou, H., Lin, L., Zhao, C. T., Zhang, X. J., Xiao, Z. H., et al. (2016). Antibacterial activity and mechanism of cinnamon essential oil and its application in milk. *J. Anim. Plant Sci.* 26, 533–541.
- Ferris, R. A., McCue, P. M., Borlee, G. I., Loncar, K. D., Henet, M. L., and Borlee, B. (2016). In vitro efficacy of non-antibiotic treatments on biofilm disruption of gram-negative pathogens and an in vivo model of infectious endometritis utilizing isolates from the equine uterus. *J. Clin. Microbiol.* 54, 631–639. doi: 10.1128/jcm.02861-15
- Flemming, H. C., Wingender, J., Szewzyk, U., Steinberg, P., Rice, S. A., and Kjelleberg, S. (2016). Biofilms: an emergent form of bacterial life. *Nat. Rev. Microbiol.* 14, 563–575. doi: 10.1038/nrmicro.2016.94
- Heydorn, A., Nielsen, A. T., Hentzer, M., Sternberg, C., Givskov, M., Ersbøll, B. K., et al. (2000). Quantification of biofilm structures by the novel computer program COMSTAT. *Microbiology* 146(Pt 10), 2395–2407. doi: 10.1099/0022287-146-10-2395
- Jagani, S., Chelikani, R., and Kim, D. S. (2009). Effects of phenol and natural phenolic compounds on biofilm formation by *Pseudomonas aeruginosa*. *Biofouling* 25, 321–324. doi: 10.1080/08927010802660854
- Jantan, I. B., and Goh, S. H. (1992). Essential oils of *Cinnamomum* species from Peninsular Malaysia. *J. Essent. Oils Res.* 4, 161–164.
- Kang, J. M., Li, Q. Q., Liu, L., Jin, W. Y., Wang, J. F., and Sun, Y. Y. (2017). The specific effect of gallic acid on *Escherichia coli* biofilm formation by regulating pgaABCD genes expression. *Appl. Microbiol. Biotechnol.* 102, 1837–1846. doi: 10.1007/s00253-017-8709-3
- Kang, J. M., Liu, L., Wu, X. X., Sun, Y. Y., and Liu, Z. F. (2018). Effect of thyme essential oil against *Bacillus cereus* planktonic growth and biofilm formation. *Appl. Microbiol. Biotechnol.* 102, 10209–10218. doi: 10.1007/s00253-018-9401-y
- Karunakaran, E., and Biggs, C. A. (2011). Mechanisms of *Bacillus cereus* biofilm formation: an investigation of the physicochemical characteristics of cell surfaces and extracellular proteins. *Appl. Microbiol. Biotechnol.* 89, 1161–1175. doi: 10.1007/s00253-010-2919-2
- Koo, H., Allan, R. N., Howlin, R. P., Stoodley, P., and Hall-Stoodley, L. (2017). Targeting microbial biofilms: current and prospective therapeutic strategies. *Nat. Rev. Microbiol.* 15, 740–755. doi: 10.1038/nrmicro.2017.99
- Kulshrestha, S., Khan, S., Hasan, S., Khan, M. E., Misba, L., and Khan, A. U. (2016). Calcium fluoride nanoparticles induced suppression of *Streptococcus mutans* biofilm: an in vitro and in vivo approach. *Appl. Microbiol. Biotechnol.* 100, 1901–1914. doi: 10.1007/s00253-015-7154-4
- Kwieciński, J., Eick, S., and Wójcik, K. (2009). Effects of tea tree (*Melaleuca alternifolia*) oil on *Staphylococcus aureus* in biofilms and stationary growth phase. *Int. J. Antimicrobial Agents* 33, 343–347. doi: 10.1016/j.ijantimicag.2008.08.028
- Lewis, K. (2007). Persister cells, dormancy and infectious disease. *Nat. Rev. Microbiol.* 5, 48–56. doi: 10.1038/nrmicro1557
- Melchior, M. B., Vaarkamp, H., and Fink-Gremmels, J. (2006). Biofilms: a role in recurrent mastitis infections? *Vet. J.* 171, 398–407. doi: 10.1016/j.tvjl.2005.01.006
- Meng, X. G., Pu, Y., Zhang, G. Q., Xu, F. T., Zheng, X. D., Zheng, L., et al. (1984). Camphor compound in the treatment of stubborn endometritis in dairy cattle. *J. Vet. Univ.* 3, 225–227.
- Oliveira, K. Á. R. D., Sousa, J. P. D., Medeiros, J. A. D. C., Magnani, M., Júnior, J. P. D. S., and Souza, E. L. D. (2015). Synergistic inhibition of bacteria associated with minimally processed vegetables in mixed culture by carvacrol and 1, 8-cineole. *Food Control* 47, 334–339. doi: 10.1016/j.foodcont.2014.07.014
- Pelissier, Y., Marion, C., and Prunac, S. (1995). Volatile components of leaves, stems and bark of *Cinnamomum camphora* Nees et Ebermaier. *J. Essent. Oil Res.* 7, 313–315. doi: 10.1080/10412905.1995.9698525
- Pragadeesh, V. S., Saroj, A., Yadav, A., Chanotiya, C. S., Alam, M., and Samad, A. (2013). Chemical characterization and antifungal activity of *Cinnamomum camphora* essential oil. *Ind. Crops Prod.* 49, 628–633. doi: 10.1016/j.indcrop.2013.06.023
- Ramage, G., Vande Walle, K., Wickes, B. L., and Lopez-Ribot, J. L. (2001). Standardized method for in vitro antifungal susceptibility testing of *Candida albicans* biofilms. *Antimicrob. Agents Chemother.* 45, 2475–2479. doi: 10.1128/aac.45.9.2475-2479.2001
- Serra, D. O., Mika, F., Richter, A. M., and Hengge, R. (2016). The green tea polyphenol EGCG inhibits *E. coli* biofilm formation by impairing amyloid curli fibre assembly and downregulating the biofilm regulator CsgD via the sigma(E)-dependent sRNA RybB. *Mol. Microbiol.* 101, 136–151. doi: 10.1111/mmi.13379
- Shi, S. J., Wu, Q. D., Su, J. Y., Li, C. W., Zhao, X. N., Xie, J. H., et al. (2013). Composition analysis of volatile oils from flowers, leaves and branches of *Cinnamomum camphora* cv. Borneol in China. *J. Essent. Oil Res.* 25, 394–400.
- Silva, A., Genoves, S., Martorell, P., Zanini, S. F., Rodrigo, D., and Martinez, A. (2015). Sublethal injury and virulence changes in *Listeria monocytogenes* and *Listeria innocua* treated with antimicrobials carvacrol and citral. *Food Microbiol.* 50, 5–11. doi: 10.1016/j.fm.2015.02.016
- Somolinos, M., Garcia, D., Pagan, R., and Mackey, B. (2008). Relationship between sublethal injury and microbial inactivation by the combination of high hydrostatic pressure and citral or tert-butyl hydroquinone. *Appl. Environ. Microbiol.* 74, 7570–7577. doi: 10.1128/aem.00936-08
- Spilimbergo, S., Foladori, P., Mantoan, D., Ziglio, G., and Mea, G. D. (2010). High-pressure CO₂ inactivation and induced damage on *Saccharomyces cerevisiae* evaluated by flow cytometry. *Process Biochem.* 45, 647–654. doi: 10.1016/j.procbio.2009.12.013
- Van Acker, H., Van Dijk, P., and Coenye, T. (2014). Molecular mechanisms of antimicrobial tolerance and resistance in bacterial and fungal biofilms. *Trends Microbiol.* 22, 326–333. doi: 10.1016/j.tim.2014.02.001
- Venkatesan, N., Perumal, G., and Doble, M. (2015). Bacterial resistance in biofilm-associated bacteria. *Future Microbiol.* 10, 1743–1750. doi: 10.2217/fmb.15.69
- Vert, M., Doi, Y., Hellwich, K. H., Hess, M., Hodge, P., Kubisa, P., et al. (2012). Terminology for biorelated polymers and applications (IUPAC Recommendations 2012). *Pure Appl. Chem.* 84, 377–410. doi: 10.1351/pac-rec-10-12-04
- Vorregaard, M. (2008). *Comstat2-a Modern 3D Image Analysis Environment for Biofilms, in Informatics and Mathematical Modelling*. Kongens Lyngby: Technical University of Denmark.
- Wang, J., Cao, X. S., Song, L., Ding, Z. Q., Tang, F., and Yue, Y. D. (2017). Comparative chemical composition and antifungal activity of the essential oils of *Cinnamomum camphora* L. Presl Leaves from three geographic origins. *Food Sci.* 38, 131–136.
- Webber, B., Canova, R., Esper, L. M., Perdoncini, G., Nascimento, V. P. D., Pilotto, F., et al. (2015). The use of vortex and ultra-sound techniques for the in vitro removal of *Salmonella* spp. biofilms. *Acta Sci. Vet.* 43, 1–5.
- Wu, K. G., Lin, Y. H., Chai, X. H., Duan, X. J., Zhao, X. X., and Chun, C. (2019). Mechanisms of vapor-phase antibacterial action of essential oil from *Cinnamomum camphora* var. *linaloofera* Fujita against *Escherichia coli*. *Food Sci. Nutr.* 7, 2546–2555. doi: 10.1002/fsn.3.1104

- Zhang, J. N., Li, Z. Y., Wang, X. Q., and Wu, D. F. (2014). The chemical components characterization of essential oil from *Cinnamomum camphora* leaves in Nanchang and its study on inhibitory and bactericidal activity towards *Staphylococcus aureus* and *Escherichia coli*. *Lishizhen Med. Mater. Med. Res.* 25, 2381–2384.
- Zhang, Z. H., Tong, Y. Q., Qian, X. Y., and Li, S. L. (2019). Research progress of chemical components and pharmacological activities of *Cinnamomum camphora* L. *Presl. Sci. Technol. Food Industry* 10, 320–333.
- Zhou, H. X., Li, Z. H., Fu, X. J., and Zhang, H. (2016). Study on subcritical fluid extraction of essential oil from *Cinnamomum camphora* and its antibacterial activity. *J. Chin. Med. Mater.* 39, 1357–1360.

Conflict of Interest: The authors declare that the research was conducted in the absence of any commercial or financial relationships that could be construed as a potential conflict of interest.

Copyright © 2020 Wang, Zhang, Zhang, Zhang, Fu, Li, Wang, Qiu, Wang and Li. This is an open-access article distributed under the terms of the Creative Commons Attribution License (CC BY). The use, distribution or reproduction in other forums is permitted, provided the original author(s) and the copyright owner(s) are credited and that the original publication in this journal is cited, in accordance with accepted academic practice. No use, distribution or reproduction is permitted which does not comply with these terms.



Maipomycin A, a Novel Natural Compound With Promising Anti-biofilm Activity Against Gram-Negative Pathogenic Bacteria

Junliang Zhang^{1,2}, Xiaoyan Liang^{3,4}, Shiling Zhang¹, Zhiman Song¹, Changyun Wang^{3,4,5} and Ying Xu^{1*}

¹ Shenzhen Key Laboratory of Marine Bioresource and Eco-Environmental Science, Shenzhen Engineering Laboratory for Marine Algal Biotechnology, College of Life Sciences and Oceanography, Shenzhen University, Shenzhen, China, ² Key Laboratory of Optoelectronic Devices and Systems of Ministry of Education and Guangdong Province, College of Physics and Optoelectronic Engineering, Shenzhen University, Shenzhen, China, ³ Key Laboratory of Marine Drugs, Ministry of Education of China, School of Medicine and Pharmacy, Ocean University of China, Qingdao, China, ⁴ Laboratory for Marine Drugs and Bioproducts, Qingdao National Laboratory for Marine Science and Technology, Qingdao, China, ⁵ Institute of Evolution and Marine Biodiversity, Ocean University of China, Qingdao, China

OPEN ACCESS

Edited by:

Luis Cláudio Nascimento da Silva,
Universidade Ceuma, Brazil

Reviewed by:

Maria José Saavedra,
Universidade de Trás-os-Montes e
Alto Douro, Portugal
Rodolfo García-Contreras,
National Autonomous University
of Mexico, Mexico

*Correspondence:

Ying Xu
boxuying@szu.edu.cn

Specialty section:

This article was submitted to
Antimicrobials, Resistance
and Chemotherapy,
a section of the journal
Frontiers in Microbiology

Received: 23 August 2020

Accepted: 15 December 2020

Published: 12 January 2021

Citation:

Zhang J, Liang X, Zhang S,
Song Z, Wang C and Xu Y (2021)
Maipomycin A, a Novel Natural
Compound With Promising
Anti-biofilm Activity Against
Gram-Negative Pathogenic Bacteria.
Front. Microbiol. 11:598024.
doi: 10.3389/fmicb.2020.598024

Pathogenic bacterial biofilms play an important role in recurrent nosocomial and medical device-related infections. Once occurred, the complex structure of the biofilm promotes the development of antibiotic resistance and becomes extremely difficult to eradicate. Here we describe a novel and effective anti-biofilm compound maipomycin A (MaiA), which was isolated from the metabolites of a rare actinomycete strain *Kibdelosporangium phytohabitans* XY-R10. Its structure was deduced from analyses of spectral data and confirmed by single-crystal X-ray crystallography. This natural product demonstrated a broad spectrum of anti-biofilm activities against Gram-negative bacteria. Interestingly, the addition of Fe(II) or Fe(III) ions could block the biofilm inhibition activity of MaiA because it is an iron chelator. However, not all iron chelators showed biofilm inhibition activity, suggesting that MaiA prevents biofilm formation through a specific yet currently undefined pathway. Furthermore, MaiA acts as a synergist to enhance colistin efficacy against *Acinetobacter baumannii*. Our results indicate that MaiA may potentially serve as an effective antibiofilm agent to prevent Gram-negative biofilm formation in future clinical applications.

Keywords: maipomycin A, biofilm inhibition, Gram-negative bacteria, iron chelator, antibiotics enhancer

INTRODUCTION

Bacterial resistance against antibiotics is now a global health problem of increasing importance, one of the major mechanisms of resistance is the formation of biofilms by pathogens. Biofilms are sessile microbial communities embedded in self-produced polymeric substances (polysaccharide, protein (polysaccharides, proteins, and DNA), which help microbes colonization of the surface of human organs or medical devices (Flemming and Wingender, 2010). The biofilms act as effective barriers to prevent drugs permeation and alter the physiological states of bacteria (Hall and Mah, 2017). Consequently, bacterial cells of biofilms possess more resistant (10–1,000 times) to antibiotics compared with planktonic forms (Stewart and Costerton, 2001).

It has been reported that biofilms contribute over 80% of human pathogen infections (Pandini et al., 2017). The biofilms of “ESKAPE” pathogens (*Enterococcus faecalis*, *Staphylococcus aureus*, *Klebsiella pneumoniae*, *Acinetobacter baumannii*, *Pseudomonas aeruginosa*, and *Enterobacter* spp.) commonly present the most acute threat (Ma et al., 2020). Of particular concerns are the emergence of Gram-negative bacteria (GNB) like *A. baumannii*, *P. aeruginosa*, *K. pneumoniae*, and *Enterobacter* spp., which are often recalcitrant to “the last line of antibiotics” such as carbapenems and colistin (Smith et al., 2018; Luther et al., 2019). In recent years, nosocomial infections caused by biofilm forming GNB such as pneumonia, urinary tract infections, endocarditis, wound infection, and bacteremia, are becoming increasingly deadly (Lyczak et al., 2000; Dijkshoorn et al., 2007; Prowle et al., 2011; Frykberg and Banks, 2015). In particular, ventilator-associated pneumonia with a mortality rate as high as 60% (Bertolini et al., 2018), and catheter-associated urinary tract infections with morbidity rate approximately to 70% (Shuman and Chenoweth, 2018) are resulted from biofilm-related infections mainly caused by *A. baumannii*, *P. aeruginosa*, and *Enterobacter* spp.

Currently, antibiotic treatment is the most important and effective way to control microbial infections and prevent biofilm formation (Bjarnsholt et al., 2018). However, it is almost impossible to eradicate biofilm infections with antibiotics *in vivo* (Wu et al., 2015). Therefore, the necessity to find effective drugs that could inhibit and eliminate biofilms is an important attention. Based on the advancements of biofilm formation mechanism, numerous anti-biofilm molecules are discovered with different action modes such as inhibit quorum sensing, hinder cell adhesion, disperse extracellular polymeric substance and interfere with c-di-GMP signaling pathways, and so on (Roy et al., 2018). The natural products have greater structural and biochemical diversity compared with synthetic compounds (Genilloud, 2017), thus it is useful in the development of anti-biofilm agents. Recently, there have been reports about a variety of bacterial products including small molecules, enzymes, exopolysaccharides, and peptides isolated possessing anti-biofilm activities against different pathogens (Khan et al., 2019). Most of these studies have only studied the biofilm inhibition effect against a single species or genus of bacteria, such as *P. aeruginosa*, *Escherichia coli*, or *Staphylococcus*. Yet only very few natural products like exopolysaccharides showed broad-spectrum anti-biofilm effects (Valle et al., 2006; Jiang et al., 2011; Sayem et al., 2011; Mahdhi et al., 2017).

In our continuing effort to screen microbial natural products against biofilms, we identified a non-toxic, effective and broad-spectrum anti-biofilm compound butanolide derived from a marine *Streptomyces* sp. in previous work (Yin et al., 2019). Here we report the isolation and characterization of a new compound maipomycin A (MaiA) derived from a mangrove rare actinomycete strain. We then evaluated its anti-biofilm efficiency against several pathogenic bacteria to inquire its broad-spectrum anti-biofilm ability. In addition, we investigated the possible mode of action of MaiA, and compared the biofilm inhibition activity with its two analogs to analyze their structure-activity

relationships. Finally, the synergistic antibacterial and anti-biofilm effect between MaiA with antibiotics was also examined.

MATERIALS AND METHODS

Strains and Chemicals

Gram-negative and Gram-positive bacterial strains including *A. baumannii* ATCC 19606, *P. aeruginosa* ATCC 27853, *E. coli* ATCC 25922, *K. pneumoniae* ATCC 13883, methicillin-sensitive *S. aureus* ATCC 25923 (MSSA), methicillin-resistant *S. aureus* ATCC 43300 (MRSA), and several clinical strains of multidrug-resistant were kindly provided by Prof. Dai-Jie Chen from the Shanghai Jiao Tong University. Chemicals, media, and antibiotics were purchased from Sigma-Aldrich (Poole, United Kingdom) unless otherwise stated. Collismycin A and other two analogs were obtained from Alfa Chemistry (New York, United States) and Shenzhen GenProMetab Biotechnology Company.

Bioassay-Guided Isolation and Structure Determination of the Anti-biofilm Compound

The strain *Kibdelosporangium phytohabitans* XY-R10 was isolated from the root sediments (3–5 cm) of a mangrove plant *Kandelia candel* (L.) Druce, collected from Mai Po Inner Deep Bay Ramsar Site (E 114.05°, N 22.49°; Hong Kong, China). The bacterium was cultivated in multiple 250 mL Erlenmeyer flasks each containing 80 mL of SGTPY medium (5 g starch, 5 g glucose, 1 g tryptone, 1 g peptone, 1 g yeast extract, and 17 g sea salts dissolved in 1 L of distilled water) at 28°C with agitation of 200 rpm for 6 days. The culture broth (10 L) was extracted with a double volume of ethyl acetate (EtOAc) three times. The combined EtOAc layers were dried by an evaporator to give a total crude extract (1.5 g), which was then applied to ODS column eluted with a step-gradient of water, (4:1) water/methanol (MeOH), (3:2) water/MeOH, (2:3) water/MeOH, (1:4) water/MeOH, and 100% MeOH, yielding six fractions. The fractions were tested in algicidal bioassays and the active fraction (4:1) water/MeOH was separated further using a Phenomenex Kinetex column (250 mm × 10.0 mm, 5 µm; ACN-H₂O, 25:75, 4 mL/min) on a semi-preparative HPLC (waters, 2495 series equipped with a photodiode array detector), which eventually afford the active compound 5 mg of MaiA.

To resolve the chemical structure of MaiA, NMR experiments were carried out on a Bruker Avance III 600 MHz spectrometer with DMSO-*d*₆ as the solvent and the data were analyzed with Bruker Topspin software. Accurate mass spectra of MaiA was recorded using an Agilent 6545 Q-TOF mass spectrometer coupled to a 1260 HPLC system. Single-crystal data were measured on an Agilent Xcalibur diffractometer with an Atlas (Gemini ultra Cu) detector.

Minimum Inhibitory Concentration and Drug Combination Studies

Minimum inhibitory concentration (MIC) was determined by broth microdilution according to the Clinical and Laboratory

Standards Institute guidelines. Bacteria were cultured in cation-adjusted Mueller Hinton broth at $35 \pm 2^\circ\text{C}$. The MIC was defined as the lowest concentration of antibiotics with no visible growth. In order to determine the effects of combinations of MaiA with antibiotics, combinations of various dilutions of MaiA and a second drug were tested for growth inhibition by microdilution. The synergistic effect was evaluated by the fractional inhibitory concentration (FIC) index (Odds, 2003).

Anti-biofilm Assays

An anti-biofilm formation assay was performed as previously described with minor modifications (Nair et al., 2016; Park et al., 2016). Briefly, an overnight culture of each strain was diluted in MH medium (for Gram-negative strains), or LB supplemented with 0.5% glucose (for Gram-positive strains) to achieve an OD_{595} value of 0.1. Then incubated statically in a 24-well flat-bottom polystyrene plate (Jet Bio-Filtration, Co., Ltd., China) with or without the varying concentrations of compounds at 37°C for 24 h. Subsequently, planktonic cells were discarded and the wells were rinsed twice with sterile PBS gently and then dried. Biofilms were stained with 0.1% crystal violet (CV) and dissolved in 30% acetic acid, and absorbance at 570 nm (OD_{570}) was measured to quantify biofilm biomass. The minimum biofilm inhibitory concentration (MBIC) was defined as the minimum concentration of compounds or antibiotics showing no color development (Nair et al., 2016). The effect of different concentrations of MaiA on the growth of bacteria was monitored by measuring absorbance at 595 nm using a spectrophotometer.

The metabolic activity of biofilm was examined by a metabolic dye reduction assay using MTT [3-(4,5-dimethyl-2-thiazolyl)-2,5-diphenyl-2H-tetrazolium bromide] according to the previous method (Yin et al., 2019). The activated succinate dehydrogenase in the viable cell of biofilm could reduce the yellow tetrazolium salt (MTT) to formazan, and the resulting product forms a blue solution when dissolved in DMSO. The metabolic activity was correlated to the optical density at 570 nm.

Synergistic activity of MaiA combined with antibiotics was measured following anti-biofilm assay.

Iron Chelating Activity of MaiA

Maipomycin A dissolved in Mili-Q water (Merck) mixed with aqueous FeSO_4 or FeCl_3 solution at the molar ratio of 0:1 and 2:1, respectively. The mixture was then subjected to HPLC and HPLC-Q-TOF MS analysis. Pure MaiA was injected as the standard.

Iron Rescue Experiment

Effect of addition of exogenous iron on the inhibition of *A. baumannii* ATCC 19606 biofilm formation by MaiA was investigated. *A. baumannii* was treated with 52 μM MaiA for 0, 3, 6, and 12 h, respectively, followed by addition of Fe(II) and Fe(III) ions. Biofilm biomass was quantified by CV stain after 24 h incubation in 24-well flat-bottom plate.

Confocal Laser Scanning Microscopy Analysis of Biofilm Structure

Anti-biofilm formation assay was established on glass coverslips placed in 24-well flat-bottom plates. After removal of supernatant and rinsed twice with sterile PBS, biofilm cells were stained using the BacLight Live/Dead Viability Kit (L7007, Invitrogen, Carlsbad, United States) at 37°C for 15 min in the dark and imaged with laser confocal microscope Leica TCS SP8 (excitation 488 nm, emission 588 nm) with a $20\times$ objective. Confocal images were processed using LAS X software to reconstruct 3D views of the biofilm. COMSTAT software was used to calculate biomass ($\mu\text{m}^3/\mu\text{m}^2$), mean thickness (μm), and other parameters (Heydorn et al., 2000).

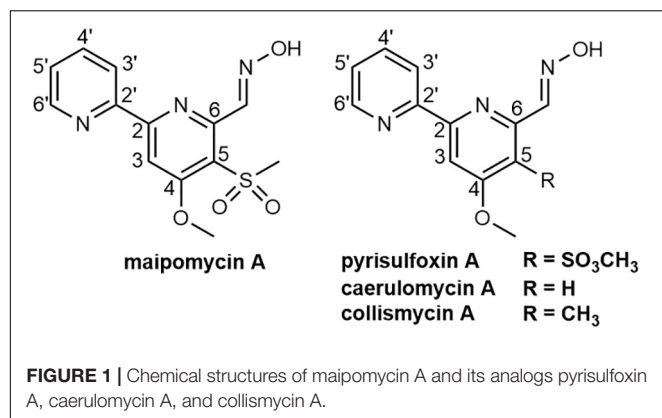
Data Analysis

Data were presented as the mean value \pm standard deviation of three replicates. Comparison of data between treatments and controls were carried out by one-way ANOVA followed by Tukey's HSD test using SPSS15.0 software. A *P* value less than 0.05 was considered statistically significant.

RESULTS

Identification of the Anti-biofilm Compound From *K. phytohabitans* XY-R10

In this study, we found the crude extract of *K. phytohabitans* XY-R10 was able to inhibit the biofilm formation of *A. baumannii* ATCC 19606. Following bioassay-guided fractionation, MaiA with strong anti-biofilm activities was obtained. To identify the chemical structure of MaiA, high-resolution mass, and high-field NMR spectral analyses were carried out (Supplementary Figures 1–7). The ^1H NMR spectrum of MaiA showed two singlet methyl signals at δ_{H} 3.41, 4.16, five doublet olefinic or aromatic signals at δ_{H} 7.57, 8.02, 8.20, 8.42, 8.77, 8.84, and one exchangeable proton signal at δ_{H} 11.73. The ^{13}C NMR and ^1H NMR data revealed that MaiA contained two methyl groups (δ_{C} 44.72, 57.25) and eleven olefinic or aromatic carbon atoms (Supplementary Table 1). These spectroscopic features suggested that MaiA belonged to the family of 2, 2'-bipyridyl, and was most similar to pyrisulfoxin A (PyrA), which was isolated as an antibiotic (Tsuge et al., 1999). The only significant differences in the NMR spectra between these two compounds were the chemical shifts of C-5 (δ_{C} 124.5 in 1 vs. δ_{C} 127.7 in PyrA) and C-9 (δ_{C} 44.72 in 1 vs. δ_{C} 39.4 in PyrA). Deduced from the positive ion $[\text{M} + \text{H}]^+$ observed at m/z 308.0698 by Q-TOF MS, the molecular formula of MaiA was then determined to be $\text{C}_{13}\text{H}_{13}\text{N}_3\text{O}_4\text{S}$, which has one more oxygen atom than that of PyrA ($\text{C}_{13}\text{H}_{13}\text{N}_3\text{O}_3\text{S}$). The increase of one oxygen atom, together with the downfield shifts of C-5 and the upfield shifts of C-9, indicated the presence of a sulfonyl group in MaiA, instead of the sulfoxide group in PyrA. HMBC analysis connected the methyl protons H-9 (δ_{H} 3.41) to the quaternary carbon C-5 (δ_{C} 124.5) of the aromatic ring (Figure 1 and Supplementary Figure 1), for which the methyl sulfonyl group was allocated



to the C-5 position. The planar configuration of MaiA was also confirmed by the analysis of the X-ray single-crystal diffraction data (Supplementary Tables 2–8 and Supplementary Figure 8). These data collectively suggested that the anti-biofilm compound isolated from *K. phytohabitans* XY-R10 was 4-methyloxyl-5-methylsulfonyl-2,2'-bipyridyl-6-carboxaldehyde oxime, a novel compound which we named maipomycin A, abbreviated as MaiA.

MaiA Showed a Weak Antibacterial Activity Against Pathogens

The antibacterial ability of MaiA was evaluated against a panel of Gram-positive and Gram-negative organisms. MIC values indicated that MaiA showed no antibacterial effect against most bacteria (MIC > 256 $\mu\text{g/mL}$), but had a weak antibacterial activity against *A. baumannii* (MIC = 128 $\mu\text{g/mL}$) including the reference strains and clinical isolates (Supplementary Table 9).

MaiA Effectively Inhibit a Variety of GNB Biofilms Formation

Maipomycin A was tested in preventing biofilm formation of pathogens using a CV staining method to quantify the production of biofilms biomass. It showed an effective inhibitory activity against the Gram-negative bacteria biofilm formation with a dose-dependent manner from 2 to 64 $\mu\text{g/mL}$ (Figure 2C). The MBIC value of MaiA for *A. baumannii* ATCC 19606 and *P. aeruginosa* ATCC 27853 was 8 and 32 $\mu\text{g/mL}$, respectively. The percentage of biofilm biomass at MBIC was reduced by 84.3% for *A. baumannii*, and 82.6% for *P. aeruginosa* compared with control. It was notable that MaiA only had a slight inhibition on the planktonic cell growth of these two strains at MBIC concentration (Figures 2A,B), but it could inhibit biofilm formation effectively (Figures 2E,F).

In order to investigate whether MaiA has a broad anti-biofilm formation ability, several strains were selected for further investigation. Results displayed that MaiA could inhibit most Gram-negative bacteria biofilm formation and MBICs ranging from 8 to 32 $\mu\text{g/mL}$ (Supplementary Figures 9A,D–I). However, MaiA had no anti-biofilm activity against *S. aureus* at concentrations up to 64 $\mu\text{g/mL}$ (Supplementary Figures 9B,C).

The metabolic activity of the biofilm cells was measured by MTT staining, which is commonly used for the quantitative analysis of biofilm. The cell metabolic activity of *A. baumannii* and *P. aeruginosa* biofilm decreased significantly and dose-dependently when treated with MaiA (Figure 2D). The MBIC value of MaiA was 8 $\mu\text{g/mL}$ for *A. baumannii*, and 32 $\mu\text{g/mL}$ for *P. aeruginosa* determined by MTT stain. The metabolic activity of both strains was reduced by more than 80% at MBIC.

Confocal Microscopy Analysis of Biofilm Matrix Upon MaiA Treatment

Confocal laser scanning microscopy (CLSM) was employed to analyze changes in biofilm formation. The reconstructed three-dimensional biofilm images revealed that MaiA at MBIC markedly inhibited biofilm formation compared to control (Figure 3A). The calculation results of COMSTAT software also confirmed the effect of biofilm inhibition. MaiA reduced the biomass ($\mu\text{m}^3/\mu\text{m}^2$) and mean thickness (μm) of *A. baumannii* ATCC 19606 biofilms by >90% and >80% for *P. aeruginosa* ATCC 27853 (Figure 3B). Furthermore, the increases in roughness coefficient and surface to biovolume ratio suggested the heterogeneity and incompleteness of biofilm development. These results also showed that MaiA was an effective agent to inhibit biofilm formation against both *A. baumannii* and *P. aeruginosa*.

MaiA Is an Iron Chelator and Its Activity Can Be Blocked by Both Fe(II) and Fe(III) Ions

2,2'-Bipyridine-containing compounds such as caerulomycin A (CaeA; Figure 1) exerts its immunosuppressive effect by depleting intracellular irons (Kaur et al., 2015), and ColA (Figure 1) acts as an iron chelator to inhibit tumor cell growth (Kawatani et al., 2016). We, therefore, hypothesized that MaiA might exert its antibiofilm activity through chelating irons, which were essential for both growth and biofilm formation for most bacteria (Schaible and Kaufmann, 2004). In order to prove this hypothesis, we carried out a series of experiments.

Firstly, we found that MaiA indeed chelated Fe(II) ions to form a purple complex (Figure 4A). HPLC-MS analysis further confirmed that this complex was formed by two molecules of MaiA and one molecule of Fe (Figures 4B,C). The isotope pattern of this complex in the mass spectrum was also very characteristic for compounds containing an iron atom. The confirmation of MaiA as an iron chelator suggests the bacterium might have originally produced this compound as a siderophore to acquire irons.

Secondly, the addition of exogenous iron together with MaiA could rescue *A. baumannii* ATCC 19606 biofilm formation in a dose-dependent manner (Figures 4D,E). MaiA significantly impaired biofilm formation without the addition of iron. The inhibition was attenuated when the mole ratio of MaiA and iron was 2:1 or 1:1 owing to MaiA completely chelated the additional iron. Moreover, the biofilm biomass did not decrease if Fe(II) was added 3 h or 6 h after treatment of MaiA (Figure 4F).

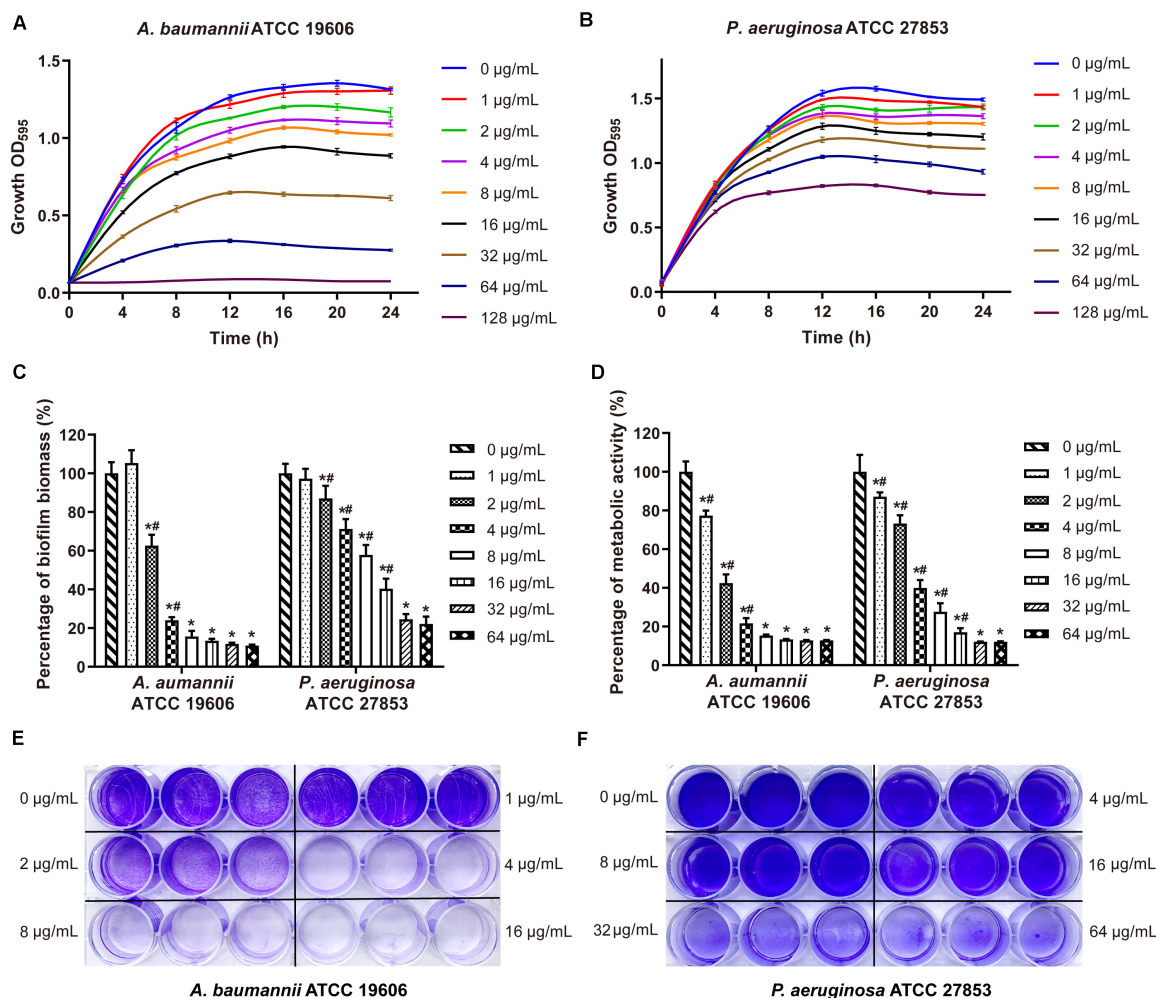


FIGURE 2 | Effects on bacteria growth and biofilm formation by maipomycin A (MaiA). Growth curves of *A. baumannii* (A) and *P. aeruginosa* (B) treated with various concentrations of MaiA. Effects of MaiA on biomass (C) and cell metabolic activity (D) in bacterial biofilms. CV stain assay of MaiA on *A. baumannii* (E) and *P. aeruginosa* (F) biofilm biomass formation in the 24-well flat bottom plate. *Indicates $P < 0.05$ compared with untreated controls. #Indicates $P < 0.05$ compared with the previous concentration.

The rescue experiment suggested iron was associated with the MaiA's anti-biofilm activity.

Maipomycin A could be deactivated regardless of Fe(II) or Fe(III) ions were added. We found that MaiA forms a complex with Fe(III) ions more slowly than Fe(II) ions (Supplementary Figures 10B,C). The color and ultraviolet-visible spectra between (MaiA)₂-Fe(II) and (MaiA)₂-Fe(III) are slightly different (Figure 4A and Supplementary Figure 10). Moreover, it seemed difficult to distinguish (MaiA)₂-Fe(II) from (MaiA)₂-Fe(III) using HPLC or mass spectrum analysis (Supplementary Figure 13).

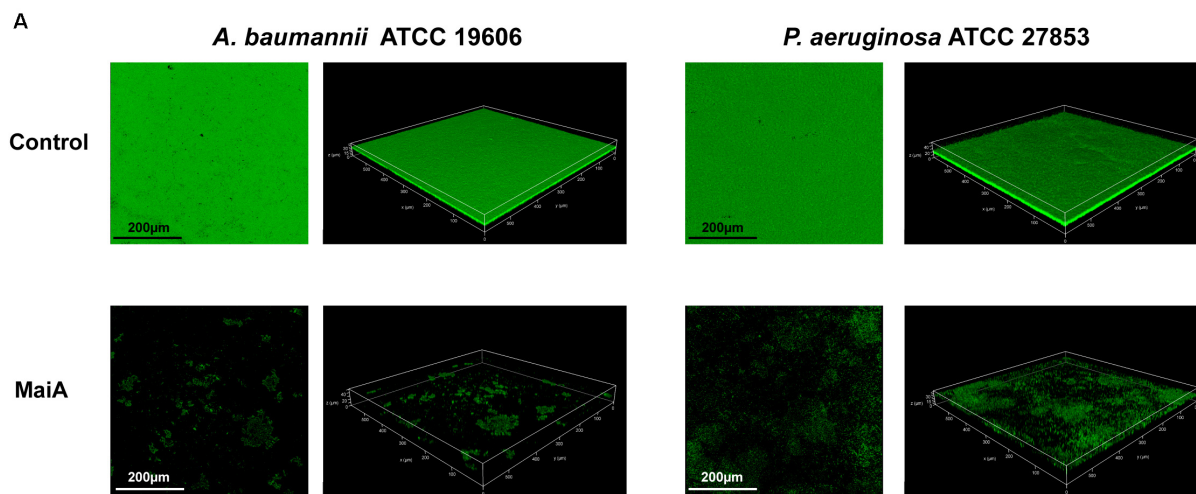
Activities of MaiA Analogs and Synthetic Iron Chelators

We also investigated the anti-biofilm activity of MaiA's analogs and other iron chelators. ColA showed strong anti-biofilm activity. The MBIC values of ColA for *A. baumannii* ATCC

19606 and *P. aeruginosa* ATCC 27853 were 8 and 16 µg/mL, respectively, (Figure 5 and Supplementary Figure 11). The activity of the other analogs maipomycin B (MaiB) and 4-Methoxy-5-methylsulfanyl-[2,2']bipyridinyl-6-carbaldehyde were much weaker than MaiA and ColA. MaiA and ColA both have a 6-carboxaldehyde oxime group, different from the 6-carbaldehyde group of MaiB and 4-Methoxy-5-methylsulfanyl-[2,2']bipyridinyl-6-carbaldehyde. Therefore, the activity may be related to 6-carboxaldehyde oxime. As two well-known iron chelators, the biofilm inhibition activity of ethylene diamine tetraacetic acid (EDTA) and 2,2'-dipyridyl (2DP) was weaker than MaiA or ColA.

MaiA Increases the Efficacy of Colistin Against *A. baumannii*

Different classes of antibiotics were combined with MaiA for screen drug interaction against a panel of Gram-positive and



B

Features	<i>A. baumannii</i> ATCC 19606		<i>P. aeruginosa</i> ATCC 27853	
	Control (Untreated)	Maipomycin A (8 μg/mL)	Control (Untreated)	Maipomycin A (32 μg/mL)
Biomass (μm ³ /μm ²)	15.67±0.67	0.67±0.63*	41.93±3.66	6.24±0.69*
Average thickness (μm)	22.05±0.81	1.23±1.08*	66.43±14.19	13.97±3.18*
Roughness coefficient	0.11±0.01	1.85±0.10*	0.06±0.01	0.27±0.10*
Surface to biovolume ratio	0.93±0.05	2.21±0.36*	0.89±0.16	2.41±0.03*

FIGURE 3 | CLSM analyses of biofilm inhibition by maipomycin A (MaiA). **(A)** 3D image of biofilm after 24 h of incubation in glass coverslips. Control was untreated, and MaiA was treated at MBIC concentrations. **(B)** Quantitative analyses of biofilm spatial characteristics using COMSTAT software. The values were expressed as mean ± SD. *Indicates $P < 0.05$ compared with untreated controls.

Gram-negative organisms. We found that MaiA itself only displayed a weak antibacterial activity but it could potentiate colistin against *A. baumannii* efficiently (**Supplementary Table 11**). A dose-response study with MaiA was performed against all four *A. baumannii* strains at concentrations of 32, 16, and 8 μg/mL. The MIC of colistin reduced 4–8 folds when used in combination with MaiA, and a synergistic effect between these two compounds could be observed ($\text{FICIs} \leq 0.5$; **Supplementary Table 12**). MaiA also enhanced the anti-biofilm activity of colistin yet with only an additive effect. Furthermore, a similar synergistic effect was also observed between colistin and the other two iron chelators ColA and 2DP (**Supplementary Table 13**).

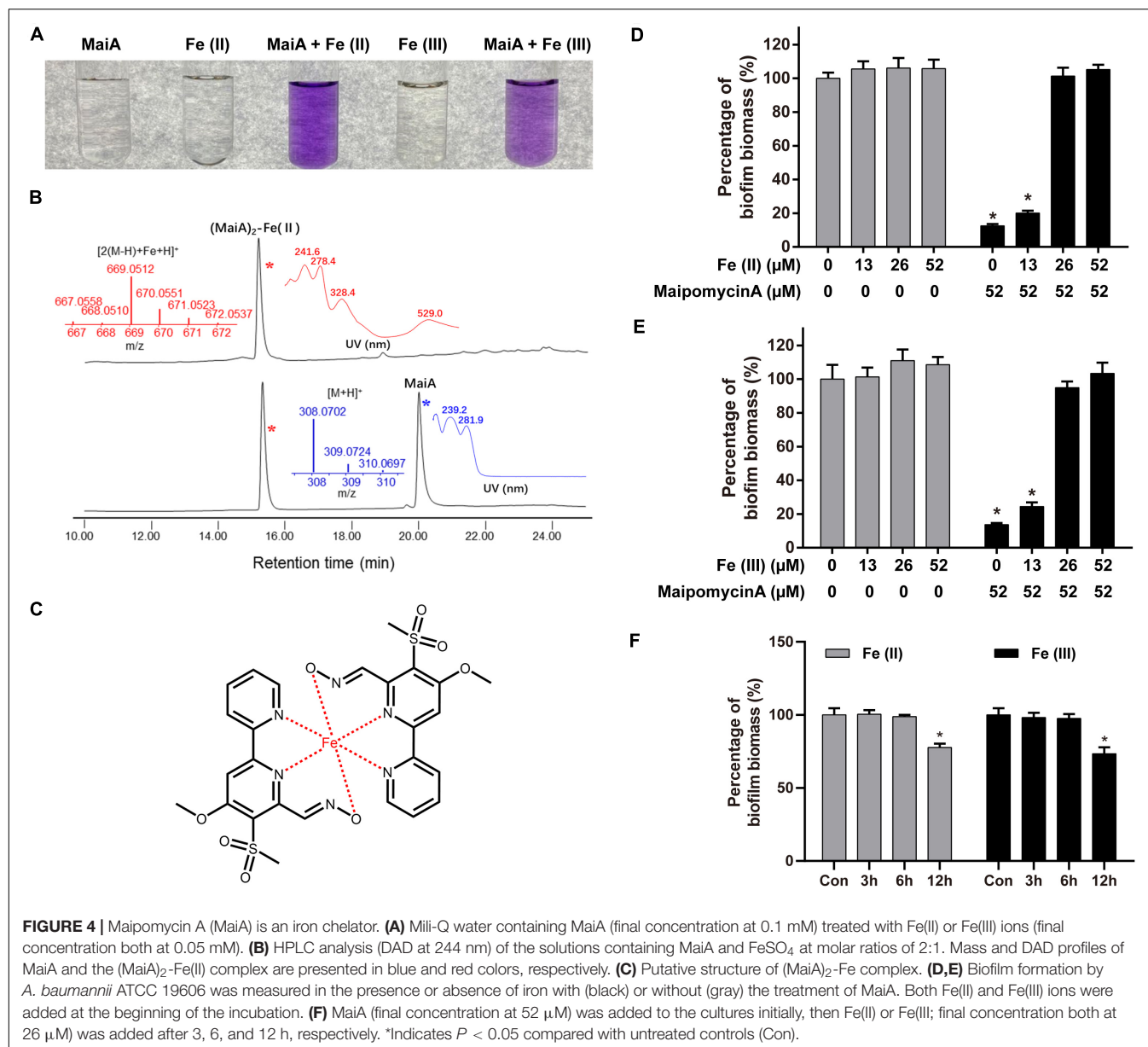
When MaiA and Fe were treated with a molar ratio of 2:1 after combined with colistin, the enhancement effect completely disappeared (data not shown), indicating that the iron ions might be an interrupter and the MaiA-Fe complex seems not to be the potentiator.

DISCUSSION

Biofilms are microbial communities of bacteria encased in a self-produced matrix that encrust biotic or abiotic surfaces

(Flemming and Wingender, 2010). Biofilm formation is an important virulence factor for a variety of bacteria that cause chronic and persistent infections. Within biofilms, the physiology of bacteria cells would change and become tolerant to antibiotics (Stewart and Costerton, 2001). This causes difficulties in clinical therapeutics and increases the mortality of severe patients. In previous studies, we have reported the butenolide, an antifouling compound derived from a marine *Streptomyces* sp., could effectively inhibit biofilm formation and eradicate preformed biofilm (Yin et al., 2019). In our continuing effort to discover anti-biofilm natural products from marine microbes, a novel secondary metabolite Maipomycin A (which was initially misnamed as Kibdelomycin A; Xu et al., 2017) was isolated from *K. phytohabitans* XY-R10, which showed a promising inhibition of GNB biofilm formation at low concentrations.

Maipomycin A bears a unique 2,2'-bipyridine structure and an unusual oxime functionality. Similar compounds include CaeA (Funk and Divekar, 1959), collismycin A (ColA; Gomi et al., 1994), and pyrisulfoxin A (PyrA; Tsuge et al., 1999). Interestingly, CaeA, ColA, and PyrA were all initially isolated from different *Streptomyces* strains, while MaiA was isolated from *K. phytohabitans*, a non-*Streptomyces* actinomycete.

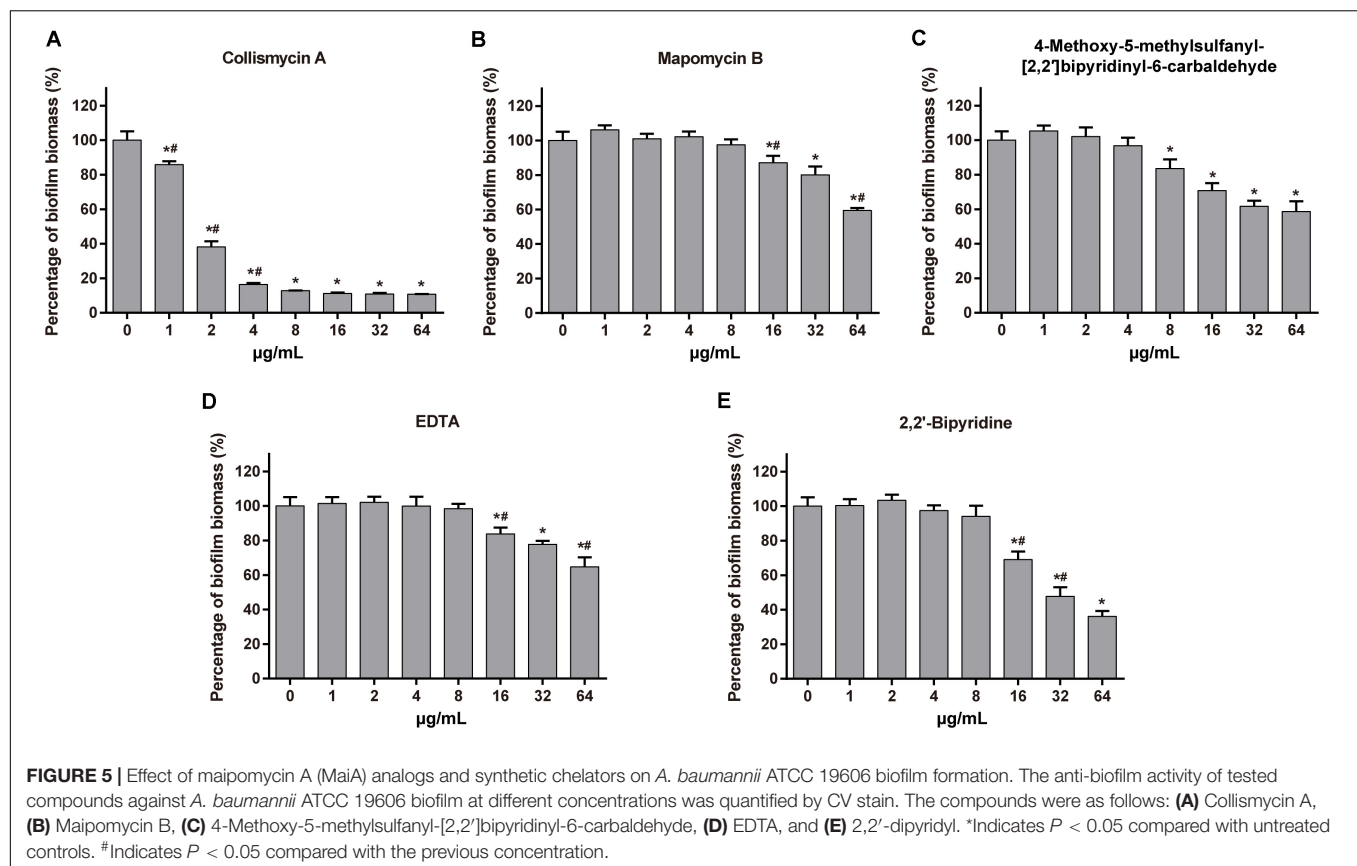


Furthermore, it is remarkable that MaiA contains a sulfone moiety which is extremely rare in natural products with only two known examples, echinosulfone A and sulfadixiamycins (Dunbar et al., 2017).

In this study, we found that MaiA was able to inhibit biofilm formation of GNB, but not effective for gram-positive bacteria (GPB). MaiA showed a limited impact on planktonic growth of the tested GNB strains at MBIC, indicating it did not prevent biofilm development through antibacterial activities. Concerning the rapid development of antibiotic resistance, MaiA could be a safer agent in which poses less selective pressure to bacteria compared to the antibiotics when used for preventing biofilm infections. Furthermore, we also found MaiA inhibits *A. baumannii* from forming biofilms

on medical materials *in vitro*, such as catheters (silicone) and endotracheal tubes (polyvinyl chloride; **Supplementary Figure 12**). These results showed that MaiA may have a good potential as a broad-spectrum anti-GNB biofilm agent in future applications.

Iron is known to play a significant role in bacterial growth and is relevant for biofilm formation (Schaible and Kaufmann, 2004; Banin et al., 2005). Many exogenous iron chelators have been discovered as anti-biofilm agents, such as lactoferrin (Singh et al., 2002), EDTA (Banin et al., 2006), 2,2'-dipyridyl (O'May et al., 2009), and cahuitamycins (Park et al., 2016). Two approved drugs, deferasirox, and deferoxamine as iron scavengers can reduce biofilm formation in cystic fibrosis cells (Moreau-Marquis et al., 2009). Recently, a 2,2'-bipyridine-containing compound



collismycin C is reported to inhibit biofilm formation of *S. aureus* (Lee et al., 2017). The anti-biofilm activity was blocked when Fe(III) ions were added together with collismycin C. Similar results were also obtained in our study as both Fe(II) and Fe(III) ions can interrupt the activity of MaiA. The compounds used in this study have different efficacies against biofilms. Among the compounds we tested, only MaiA and ColA showed good activity against biofilms of *A. baumannii* and *P. aeruginosa*. Once EDTA was incubated with MaiA as a competitor, the amount of complex formed by MaiA and iron was greatly reduced (**Supplementary Figures 14B,C**). The affinity of MaiA toward Fe(II) and Fe(III) ions seem to be weaker than EDTA, but MaiA was much better than EDTA in regard to the anti-biofilm activity. In our exploration of the metal selectivity of MaiA, it may not only chelate Fe(II) and Fe(III) ions. The chelation of MaiA and iron ions may be negatively affected by other metal as competitors (**Supplementary Figure 15**). Our findings suggested that the ability to chelate iron may not be the sole basis for MaiA activity. The connection among chelators, iron acquisition and biofilm formation in different pathogens requires further investigation.

Caerulomycin A (Funk and Divekar, 1959), ColA (Gomi et al., 1994), and 2DP (Thompson et al., 2012) have been reported to have antibacterial activity. In our results, MaiA or ColA could act as synergists to increase the efficacy of

colistin against *A. baumannii*. Colistin is the last-line agent to treat GNB infections, but it is easy to cause neurotoxicity and nephrotoxicity because of the narrow therapeutic indices (Falagas and Kasiakou, 2006). One promising strategy to overcome the toxicity of colistin is to combine its use with synergists to enhance the antibacterial effect without increasing the dose of drug (Lenhard et al., 2016). Therefore, MaiA and ColA may be able to provide potential solutions. Another iron chelator *N,N'*-bis (2-hydroxybenzyl) ethylenediamine-*N,N'*-diacetic acid combined with colistin is highly effective against biofilms of *P. aeruginosa* (Mettrick et al., 2020). Slight enhancements of anti-biofilm were observed when colistin coupled with MaiA, ColA, or 2DP. The mechanistic investigation of how iron chelators increase the antibacterial activity of colistin is currently underway.

In summary, we have discovered a novel compound Maipomycin A from *K. phytohabitans* XY-R10 and it could effectively inhibit biofilm formation of most Gram-negative bacteria with a minor antibacterial effect. MaiA turned out to be an iron chelator and its antibiofilm activity could be blocked by both Fe(II) and Fe(III) ions. In addition, MaiA showed the effect of enhancing colistin against *A. baumannii*. These combined results suggest MaiA might be a promising candidate for the development of a new anti-biofilm agent and colistin enhancer with great potential in the future application.

DATA AVAILABILITY STATEMENT

The raw data supporting the conclusions of this article will be made available by the authors, without undue reservation.

AUTHOR CONTRIBUTIONS

YX, CW, and JZ planned experiments. JZ, XL, SZ, and ZS conducted experiments. The manuscript was written by YX and JZ. All authors read and approved the manuscript prior to submission.

FUNDING

This work was supported by the Scientific and Technical Innovation Council of Shenzhen (KQJSCX20170727101743831), the National Natural Science Foundation of China (No. 41830535), the China National Key Research and

Development Project (No. 2018YFA0902500), and the Science and Technology Project (JCYJ20180305123659726) from Shenzhen Bureau of Science, Technology.

ACKNOWLEDGMENTS

We gratefully acknowledge Prof. Dai-Jie Chen (Shanghai Jiao Tong University, Shanghai, China) for kindly providing the Gram-negative and Gram-positive bacterial strains. We also gratefully acknowledge the supports from the Instrumental Analysis Center of Shenzhen University (Lihu Campus) and Mr. Jian-Cheng Li.

SUPPLEMENTARY MATERIAL

The Supplementary Material for this article can be found online at: <https://www.frontiersin.org/articles/10.3389/fmicb.2020.598024/full#supplementary-material>

REFERENCES

- Banin, E., Brady, K. M., and Greenberg, E. P. (2006). Chelator-induced dispersal and killing of *Pseudomonas aeruginosa* cells in a biofilm. *Appl. Environ. Microbiol.* 72, 2064–2069. doi: 10.1128/aem.72.3.2064-2069.2006
- Banin, E., Vasil, M. L., and Greenberg, E. P. (2005). Iron and *Pseudomonas aeruginosa* biofilm formation. *Proc. Natl. Acad. Sci. U.S.A.* 102, 11076–11081. doi: 10.1073/pnas.0504266102
- Bertolini, G., Nattino, G., Tascini, C., Poole, D., Viaggi, B., Carrara, G., et al. (2018). Mortality attributable to different *Klebsiella* susceptibility patterns and to the coverage of empirical antibiotic therapy: a cohort study on patients admitted to the ICU with infection. *Intensive Care Med.* 44, 1709–1719. doi: 10.1007/s00134-018-5360-0
- Bjarnsholt, T., Buhlin, K., Dufrêne, Y. F., Gomelsky, M., Moroni, A., Ramstedt, M., et al. (2018). Biofilm formation - what we can learn from recent developments. *J. Intern. Med.* 284, 332–345. doi: 10.1111/joim.12782
- Dijkshoorn, L., Nemec, A., and Seifert, H. (2007). An increasing threat in hospitals: multidrug-resistant *Acinetobacter baumannii*. *Nat. Rev. Microbiol.* 5, 939–951. doi: 10.1038/nrmicro1789
- Dunbar, K. L., Scharf, D. H., Litomska, A., and Hertweck, C. (2017). Enzymatic carbon-sulfur bond formation in natural product biosynthesis. *Chem. Rev.* 117, 5521–5577. doi: 10.1021/acs.chemrev.6b00697
- Falagas, M. E., and Kasiakou, S. K. (2006). Toxicity of polymyxins: a systematic review of the evidence from old and recent studies. *Crit. Care* 10:R27. doi: 10.1186/cc3995
- Flemming, H. C., and Wingender, J. (2010). The biofilm matrix. *Nat. Rev. Microbiol.* 8, 623–633. doi: 10.1038/nrmicro2415
- Frykberg, R. G., and Banks, J. (2015). Challenges in the treatment of chronic wounds. *Adv. Wound Care* 4, 560–582. doi: 10.1089/wound.2015.0635
- Funk, A., and Divekar, P. V. (1959). Caerulomycin, a new antibiotic from *Streptomyces caerulescens* Baldacci, I. Production, isolation, assay, and biological properties. *Can. J. Microbiol.* 5, 317–321. doi: 10.1139/m59-039
- Genilloud, O. (2017). Actinomycetes: still a source of novel antibiotics. *Nat. Prod. Rep.* 34, 1203–1232. doi: 10.1039/c7np00026j
- Gomi, S., Amano, S., Sato, E., Miyadoh, S., and Kodama, Y. (1994). Novel antibiotics SF2738A, B and C, and their analogs produced by *Streptomyces* sp. *J. Antibiot.* 47, 1385–1394. doi: 10.7164/antibiotics.47.1385
- Hall, C. W., and Mah, T. F. (2017). Molecular mechanisms of biofilm-based antibiotic resistance and tolerance in pathogenic bacteria. *FEMS Microbiol. Rev.* 41, 276–301. doi: 10.1093/femsre/fux010
- Heydorn, A., Nielsen, A. T., Hentzer, M., Sternberg, C., Givskov, M., Ersbøll, B. K., et al. (2000). Quantification of biofilm structures by the novel computer program COMSTAT. *Microbiology* 146(Pt 10), 2395–2407. doi: 10.1099/00221287-146-10-2395
- Jiang, P., Li, J., Han, F., Duan, G., Lu, X., Gu, Y., et al. (2011). Antibiofilm activity of an exopolysaccharide from marine bacterium *Vibrio* sp. QY101. *PLoS One* 6:e18514. doi: 10.1371/journal.pone.0018514
- Kaur, S., Srivastava, G., Sharma, A. N., and Jolly, R. S. (2015). Novel immunosuppressive agent caerulomycin A exerts its effect by depleting cellular iron content. *Br. J. Pharmacol.* 172, 2286–2299. doi: 10.1111/bph.13051
- Kawatani, M., Muroi, M., Wada, A., Inoue, G., Futamura, Y., Aono, H., et al. (2016). Proteomic profiling reveals that collismycin A is an iron chelator. *Sci. Rep.* 6:38385. doi: 10.1038/srep38385
- Khan, F., Oloketuyi, S. F., and Kim, Y. M. (2019). Diversity of bacteria and bacterial products as antibiofilm and antitumor sensing drugs against pathogenic bacteria. *Curr. Drug Targets* 20, 1156–1179. doi: 10.2174/1389450120666190423161249
- Lee, J. H., Kim, E., Choi, H., and Lee, J. (2017). Collismycin C from the micronesian marine bacterium *Streptomyces* sp. MC025 inhibits *Staphylococcus aureus* biofilm formation. *Mar. Drugs* 15:387. doi: 10.3390/md15120387
- Lenhard, J. R., Nation, R. L., and Tsuji, B. T. (2016). Synergistic combinations of polymyxins. *Int. J. Antimicrob. Agents* 48, 607–613. doi: 10.1016/j.ijantimicag.2016.09.014
- Luther, A., Urfer, M., Zahn, M., Müller, M., Wang, S. Y., Mondal, M., et al. (2019). Chimeric peptidomimetic antibiotics against Gram-negative bacteria. *Nature* 576, 452–458. doi: 10.1038/s41586-019-1665-6
- Lyczak, J. B., Cannon, C. L., and Pier, G. B. (2000). Establishment of *Pseudomonas aeruginosa* infection: lessons from a versatile opportunist. *Microbes Infect.* 2, 1051–1060. doi: 10.1016/s1286-4579(00)01259-4
- Ma, Y. X., Wang, C. Y., Li, Y. Y., Li, J., Wan, Q. Q., Chen, J. H., et al. (2020). Considerations and caveats in combating ESKAPE pathogens against nosocomial infections. *Adv. Sci.* 7:1901872. doi: 10.1002/advsc.201901872
- Mahdhi, A., Leban, N., Chakroun, I., Chaouch, M. A., Hafsa, J., Fdhila, K., et al. (2017). Extracellular polysaccharide derived from potential probiotic strain with antioxidant and antibacterial activities as a prebiotic agent to control pathogenic bacterial biofilm formation. *Microb. Pathog.* 109, 214–220. doi: 10.1016/j.micpath.2017.05.046
- Mettrick, K., Hassan, K., Lamont, I., and Reid, D. (2020). The iron-chelator, N,N'-bis (2-hydroxybenzyl) ethylenediamine-N,N'-diacetic acid is an effective colistin adjunct against clinical strains of biofilm-dwelling *Pseudomonas aeruginosa*. *Antibiotics* 9:114. doi: 10.3390/antibiotics9040144

- Moreau-Marquis, S., O'Toole, G. A., and Stanton, B. A. (2009). Tobramycin and FDA-approved iron chelators eliminate *Pseudomonas aeruginosa* biofilms on cystic fibrosis cells. *Am. J. Respir. Cell Mol. Biol.* 41, 305–313. doi: 10.1165/rcmb.2008-0299OC
- Nair, S., Desai, S., Poonacha, N., Vipra, A., and Sharma, U. (2016). Antibiofilm activity and synergistic inhibition of *Staphylococcus aureus* biofilms by bactericidal protein P128 in combination with antibiotics. *Antimicrob. Agents Chemother.* 60, 7280–7289. doi: 10.1128/aac.01118-16
- Odds, F. C. (2003). Synergy, antagonism, and what the checkerboard puts between them. *J. Antimicrob. Chemother.* 52:1. doi: 10.1093/jac/dkg301
- O'May, C. Y., Sanderson, K., Roddam, L. F., Kirov, S. M., and Reid, D. W. (2009). Iron-binding compounds impair *Pseudomonas aeruginosa* biofilm formation, especially under anaerobic conditions. *J. Med. Microbiol.* 58(Pt. 6), 765–773. doi: 10.1099/jmm.0.004416-0
- Pandin, C., Le Coq, D., Canette, A., Aymerich, S., and Briandet, R. (2017). Should the biofilm mode of life be taken into consideration for microbial biocontrol agents? *Microb. Biotechnol.* 10, 719–734. doi: 10.1111/1751-7915.12693
- Park, S. R., Tripathi, A., Wu, J., Schultz, P. J., Yim, I., McQuade, T. J., et al. (2016). Discovery of cahuitamycins as biofilm inhibitors derived from a convergent biosynthetic pathway. *Nat. Commun.* 7:10710. doi: 10.1038/ncomms10710
- Prowle, J. R., Echeverri, J. E., Ligabo, E. V., Sherry, N., Taori, G. C., Crozier, T. M., et al. (2011). Acquired bloodstream infection in the intensive care unit: incidence and attributable mortality. *Crit. Care* 15:R100. doi: 10.1186/cc10114
- Roy, R., Tiwari, M., Donelli, G., and Tiwari, V. (2018). Strategies for combating bacterial biofilms: a focus on anti-biofilm agents and their mechanisms of action. *Virulence* 9, 522–554. doi: 10.1080/21505594.2017.1313372
- Sayem, S. M., Manzo, E., Ciavatta, L., Tramice, A., Cordone, A., Zanfardino, A., et al. (2011). Anti-biofilm activity of an exopolysaccharide from a sponge-associated strain of *Bacillus licheniformis*. *Microb. Cell Fact.* 10:74. doi: 10.1186/1475-2859-10-74
- Schaible, U. E., and Kaufmann, S. H. (2004). Iron and microbial infection. *Nat. Rev. Microbiol.* 2, 946–953. doi: 10.1038/nrmicro1046
- Shuman, E. K., and Chenoweth, C. E. (2018). Urinary catheter-associated infections. *Infect. Dis. Clin. North Am.* 32, 885–897. doi: 10.1016/j.idc.2018.07.002
- Singh, P. K., Parsek, M. R., Greenberg, E. P., and Welsh, M. J. (2002). A component of innate immunity prevents bacterial biofilm development. *Nature* 417, 552–555. doi: 10.1038/417552a
- Smith, P. A., Koehler, M. F. T., Girgis, H. S., Yan, D., Chen, Y., Chen, Y., et al. (2018). Optimized arylomycins are a new class of Gram-negative antibiotics. *Nature* 561, 189–194. doi: 10.1038/s41586-018-0483-6
- Stewart, P. S., and Costerton, J. W. (2001). Antibiotic resistance of bacteria in biofilms. *Lancet* 358, 135–138. doi: 10.1016/s0140-6736(01)05321-1
- Thompson, M. G., Corey, B. W., Si, Y., Craft, D. W., and Zurawski, D. V. (2012). Antibacterial activities of iron chelators against common nosocomial pathogens. *Antimicrob. Agents Chemother.* 56, 5419–5421. doi: 10.1128/aac.01197-12
- Tsuge, N., Furihata, K., Shin-Ya, K., Hayakawa, Y., and Seto, H. (1999). Novel antibiotics pyrisulfoxin A and B produced by *Streptomyces californicus*. *J. Antibiot.* 52, 505–507. doi: 10.7164/antibiotics.52.505
- Valle, J., Da Re, S., Henry, N., Fontaine, T., Balestrino, D., Latour-Lambert, P., et al. (2006). Broad-spectrum biofilm inhibition by a secreted bacterial polysaccharide. *Proc. Natl. Acad. Sci. U.S.A.* 103, 12558–12563. doi: 10.1073/pnas.0605399103
- Wu, H., Moser, C., Wang, H. Z., Høiby, N., and Song, Z. J. (2015). Strategies for combating bacterial biofilm infections. *Int. J. Oral. Sci.* 7, 1–7. doi: 10.1038/ijos.2014.65
- Xu, Y., Hu, Z., Wang, C., Liang, X., and Li, S. (2017). *Novel Natural Algicide With Low Toxicity to Non-Target Organisms*. U.S. Patent No WO2018133114A1. Washington, DC: U.S. Patent and Trademark Office.
- Yin, Q., Liang, J., Zhang, W., Zhang, L., Hu, Z. L., Zhang, Y., et al. (2019). Butenolide, a marine-derived broad-spectrum antibiofilm agent against both Gram-positive and Gram-negative pathogenic bacteria. *Mar. Biotechnol.* 21, 88–98. doi: 10.1007/s10126-018-9861-1

Conflict of Interest: The authors declare that the research was conducted in the absence of any commercial or financial relationships that could be construed as a potential conflict of interest.

Copyright © 2021 Zhang, Liang, Zhang, Song, Wang and Xu. This is an open-access article distributed under the terms of the Creative Commons Attribution License (CC BY). The use, distribution or reproduction in other forums is permitted, provided the original author(s) and the copyright owner(s) are credited and that the original publication in this journal is cited, in accordance with accepted academic practice. No use, distribution or reproduction is permitted which does not comply with these terms.



Recent Advances in a Polydopamine-Mediated Antimicrobial Adhesion System

Indu Singh¹, Gagan Dhawan^{1*}, Seema Gupta^{1*} and Pradeep Kumar^{2*}

¹ Acharya Narendra Dev College, University of Delhi, Delhi, India, ² Nucleic Acids Research Laboratory, CSIR-Institute of Genomics and Integrative Biology, Delhi, India

OPEN ACCESS

Edited by:

Silvia Buroni,
University of Pavia, Italy

Reviewed by:

Qi Zhao,
University of Dundee, United Kingdom
Sylvia Natalie Kłodzinska,
University of Copenhagen, Denmark

*Correspondence:

Gagan Dhawan
gagandhawan@andc.du.ac.in
Seema Gupta
seemagupta@andc.du.ac.in
Pradeep Kumar
pkumar@igib.res.in

Specialty section:

This article was submitted to
Antimicrobials, Resistance
and Chemotherapy,
a section of the journal
Frontiers in Microbiology

Received: 16 September 2020

Accepted: 02 December 2020

Published: 12 January 2021

Citation:

Singh I, Dhawan G, Gupta S and
Kumar P (2021) Recent Advances in a
Polydopamine-Mediated Antimicrobial
Adhesion System.
Front. Microbiol. 11:607099.
doi: 10.3389/fmicb.2020.607099

The drug resistance developed by bacteria during antibiotic treatment has been a call to action for researchers and scientists across the globe, as bacteria and fungi develop ever increasing resistance to current drugs. Innovative antimicrobial/antibacterial materials and coatings to combat such infections have become a priority, as many infections are caused by indwelling implants (e.g., catheters) as well as improving postsurgical function and outcomes. Pathogenic microorganisms that can exist either in planktonic form or as biofilms in water-carrying pipelines are one of the sources responsible for causing water-borne infections. To combat this, researchers have developed nanotextured surfaces with bactericidal properties mirroring the topographical features of some natural antibacterial materials. Protein-based adhesives, secreted by marine mussels, contain a catecholic amino acid, 3,4-dihydroxyphenylalanine (DOPA), which, in the presence of lysine amino acid, empowers with the ability to anchor them to various surfaces in both wet and saline habitats. Inspired by these features, a novel coating material derived from a catechol derivative, dopamine, known as polydopamine (PDA), has been designed and developed with the ability to adhere to almost all kinds of substrates. Looking at the immense potential of PDA, this review article offers an overview of the recent growth in the field of PDA and its derivatives, especially focusing the promising applications as antibacterial nanocoatings and discussing various antimicrobial mechanisms including reactive oxygen species-mediated antimicrobial properties.

Keywords: biofilm, polymerization, ROS, polydopamine, antimicrobial, surface coating

INTRODUCTION

A considerable number of catecholic residues similar to those found in the mussel foot proteins (mytilus foot proteins, MFP-3 and 5) and melanin have attracted the attention of researchers around the globe. A plethora of articles/reviews has been presented on the structure, reaction mechanism, and biomedical and biotechnological applications of materials containing these functionalities (Solano, 2014, 2017; Ahn, 2017; Ball, 2017; Forooshani and Lee, 2017; Maier and Butler, 2017; Rahimnejad and Zhong, 2017; Moulay, 2018; Park et al., 2019). Polydopamine (PDA) is one such material and is an extremely interesting polymer, ennobled with unique features – such as adherence to all types of surfaces even under water, a characteristic attributed to the catechol moieties in its monomeric building blocks. The polymer, reaped by dopamine oxidation, contains

indole and dopamine units in various oxidation states and also, to a smaller extent, pyrroles. The oxidized o-quinone and o-hydroquinone groups in its chemical structure underlie the complex oxidation chemical characteristics of PDA (Lynge et al., 2011; Jia et al., 2019). Further, it has been shown that, during oxidation of dopamine, reactive oxygen species are generated, which act as bactericidal against both Gram-positive and Gram-negative bacteria (Lynge et al., 2011). Hence, the coating of such materials on the surfaces affects the growth and survival of microorganisms. Work has also indicated that PDA has the potential to reduce the *in vivo* toxicity of biomaterials, which come in contact with the tissues or blood and suggest it to be a versatile platform (Hong et al., 2011).

Since the method reported by Lee et al. (2007) for dopamine self-polymerization to form thin films, surface-adherent, multifunctional PDA coatings through simple dip-coating of a wide-range of inorganic and organic materials, many PDA-based nanomaterials have been generated. In a recent study, it has been shown that PDA nanoparticles synthesized by laccase catalysis were more stable in strongly alkaline and acidic solutions than those synthesized by more traditional chemical routes (Li et al., 2018), although chemical oxidation processes are more cost effective for mass production and reproducibility. Various additives incorporated during synthesis can tune material properties via covalent cross-linking or physical entrapment and through non-covalent interactions (Ang et al., 2016; Chen et al., 2018; Wang et al., 2018), such as cation- π interactions (Hong et al., 2018). In a similar vein, chemically reactive nanoparticles can act as core templates for multifunctional use, such as coatings on the surface of other template/core materials (Lin et al., 2015; Hong et al., 2017). A review article by Ball has described the synthesis methods that yield PDA nanoparticles in the absence/presence of templating agents along with the use of thin PDA layers on nanoparticles or nanotubes (Ball, 2017). The results of synthesis in the presence of templating agent indicate a strong correlation between the catecholamine and the templating molecules with awaited investigation on the nature and the strength of interactions (Ball, 2018).

ROLE OF COVALENT AND NON-COVALENT INTERACTIONS IN POLYDOPAMINE SURFACE CHEMISTRY

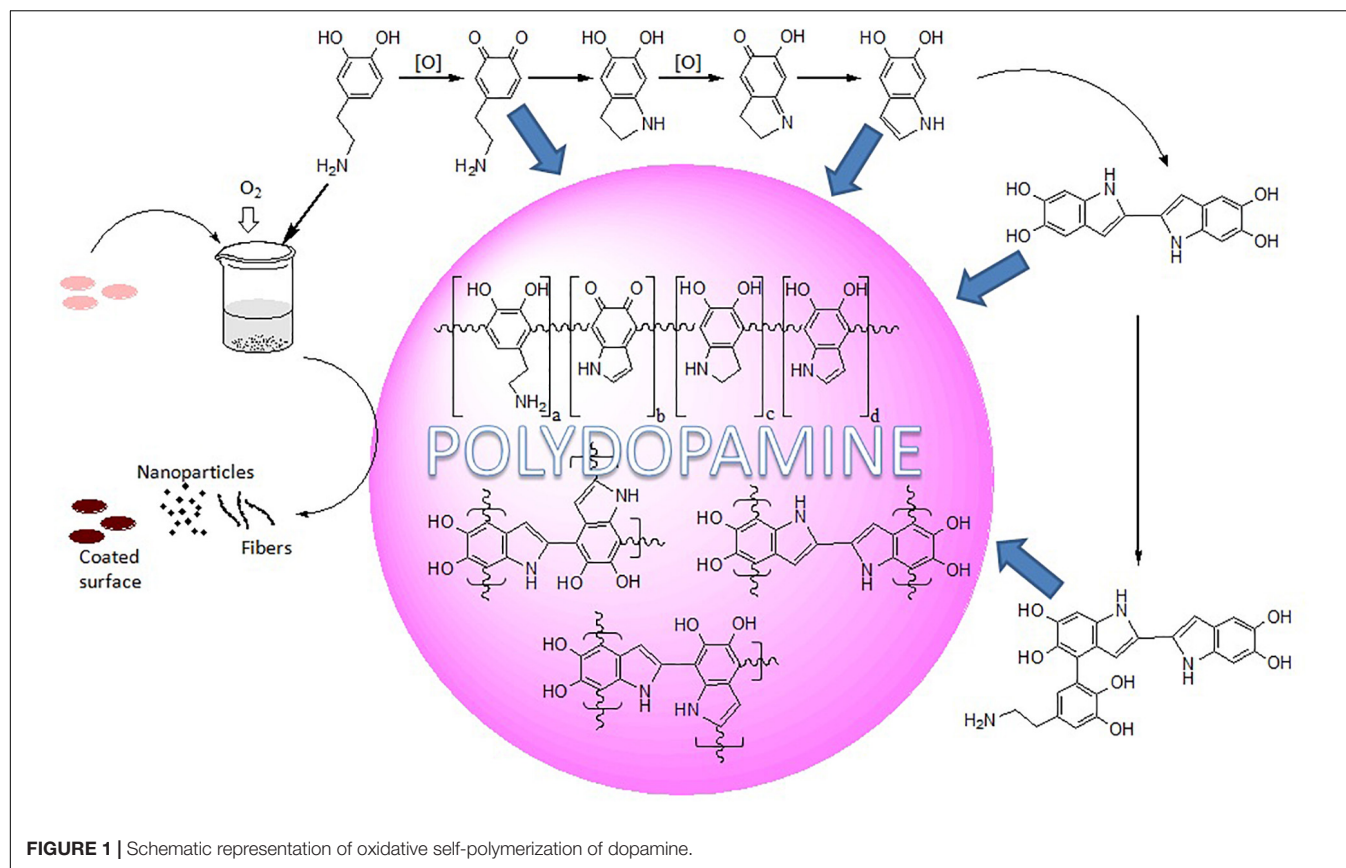
Despite the research being carried out, the chemical basis of the amazing underwater adhesion properties of PDA remains unclear. Mussel adhesiveness has persuaded scientists to explore the self-polymerization of dopamine under alkaline conditions. The solution to this puzzle could provide a universal type of coating for polymers, metals, and ceramics irrespective of their physical and chemical properties. The polymerized layer, enriched with catechol groups, can immobilize primary amine or thiol-based biomolecules through a simple dipping process. In one of the studies, Hong et al. (2012) have demonstrated that a small amount of free dopamine left physically entrapped in synthesized PDA does not exhibit cytotoxicity, as it is

rarely released due to strong non-covalent π - π interactions with aromatic rings.

Work to understand the PDA structure is still under deliberation and suggests that it is composed of dihydroxyindole, indole, and dopamine units, covalently linked (Figure 1). Further verification of the presence of covalently linked dihydroxyindole and indole units between their aromatic rings leading to different degrees of unsaturation has been suggested by Liebscher et al. (2013). The work by Alfieri et al. (2017) has concluded that PDA is different from 5,6-dihydroxyindole and melanin, and PDA film formation requires amine-containing structural components for adhesion and film-forming properties. Further, the group has noticed that PDA film formation involves competition/dynamic interactions among the intermolecular amine-quinone condensation processes, while film deposition accelerates with quinone-forming oxidants and depends on dopamine concentration and becomes practically negligible below 1 mM dopamine (Alfieri et al., 2018). The catechol groups of PDA have the ability to reduce noble metal salts (Ag^+ , Au^{3+}) to metal nanoparticles and immobilize the nanoparticles within the scaffolds, thereby preventing aggregation or leaching (Holten-Andersen et al., 2009). A review by Ho and Ding (Ho and Ding, 2014) has highlighted the probable adhesion mechanisms, chemical/physical properties, and applications of PDA. Liebscher has presented an overview on the chemistry and properties of PDA and its analogs (Liebscher, 2019). Among all the rationale for the overall mechanism for the polydopamine formation, two different pathways have also been suggested: self-assembled (dopamine)₂/5,6-dihydroxyindole (DHI) trimmers, assembled via quadrupole-quadrupole, hydrogen bonding, and π - π interactions, and dopamine-DHI-DHI conjugates, formed via covalent bond (Hong et al., 2012). However, all the views conclude that the insoluble biopolymer PDA system, formed by autooxidation of the catecholamine neurotransmitter dopamine, encompasses non-cyclized dopamine units, 5,6-dihydroxyindole (DHI), indole-5,6-quinone (IQ), and their oligomers as the main structural units (Barclay et al., 2017).

As PDA and eumelanins are found in various parts of the human body, they possess excellent physicochemical properties and provide good biocompatibility (d'Ischia et al., 2014). Hence, PDA holds considerable promise for integration with biological tissues. Polydopamine coatings are accepted as the foremost outfit for functionalization of practically any kind of material surface. The absence of strong π -conjugated system of catechol in DHI is caused by protonated uncyclized amines supporting the formation of polydopamine (Lee et al., 2019). Several factors, viz., initial dopamine concentration, pH, reaction temperature, and choice of buffer and oxidant, are reported to play important roles during the preparation of PDA coatings, and, subsequently, the physical properties of PDA coatings control the surface characteristics, which, in turn, might significantly alter the antibacterial activities (Ding et al., 2016).

Surface wettability is an important property based on surface energy and morphology of the material that addresses adhesion. The hydrophobic surface exhibits stronger adhesion with the PDA coatings compared to the hydrophilic surfaces, as a



“hydrophobic depletion layer” on the hydrophobic substrate is suggested to enhance the PDA adhesion by allowing an intimate contact between PDA and the substrate (Zhang et al., 2017). The hydrophilic behavior of PDA due to the presence of polar functional groups supports cell attachment and growth. Various co-deposition processes have been suggested to address the insufficient hydrophilicity in PDA (Qiu et al., 2018).

ROLE OF MICHAEL ADDITION/SCHIFF BASE REACTIONS

Polydopamine is moderately hydrophilic due to the large volumes of catechol, quinine, and amine groups. Reactants bearing functionalities such as amines and thiols can target the diketone or catechol groups exposed on the PDA surface via aza- or thio-Michael addition and Schiff base reactions, which can tune the surface properties of the polymer (Figure 2). Hence, PDA coatings can play the role as anchor to tether biopolymers consisting of thiols and amines (Lee et al., 2009; Huang et al., 2015; Liu and Huang, 2016; Tang et al., 2018; Yang et al., 2019). This has allowed immobilization of oligonucleotide-based aptamers and molecular probes and multifunctional nanoparticles for potential applications in nanomedicine and biosensors (Wang C. et al., 2016; Zheng et al., 2018; Jia et al., 2019). The phenolic groups of PDA have been reported to enhance the nucleation sites in the carbon dot formation

to fabricate fluorescent PDA-passivated N-doped carbon dots (Bai et al., 2018).

BROAD SPECTRUM OF POLYDOPAMINE NANOPARTICLES AS BIOMATERIALS/NANOCOATINGS

Polydopamine finds numerous applications even as stable suspension of nanoparticles (NPs), particularly as biomaterials. The use of PDA/hybrids in various fields, e.g., converting light to heat for cancer treatment by hyperthermia (Liu F. et al., 2015; Dong et al., 2016; Wang X. et al., 2016; Li Y. et al., 2017; Nieto et al., 2018; Tian and Lei, 2019), catalytic therapy for tumors (Zhu et al., 2019), and for sensing (Kong et al., 2016; Wang Z. et al., 2017; Zhao et al., 2017; Gu et al., 2018), as well as PDA NPs loaded scaffolds in the field of tissue engineering (Deng et al., 2019), are all worth mentioning. A review article that highlights the progress in fluorescent PDA nanomaterials has been published by Yang et al. (2020b). PDA nanoparticles as sensors (Jiao et al., 2017; Ma et al., 2017), theranostics (Dong et al., 2016), or for drug release (Li W.Q. et al., 2017; Wang X. et al., 2019)/gene delivery (Priyam et al., 2018) are exploited regularly; for example, the toxic nature of polyethylenimine could be suppressed during covalent conjugation with PDA for gene delivery (Priyam et al., 2018). A review by Xiong et al. (2019) has discussed in detail the developments of PDA nanocarriers to

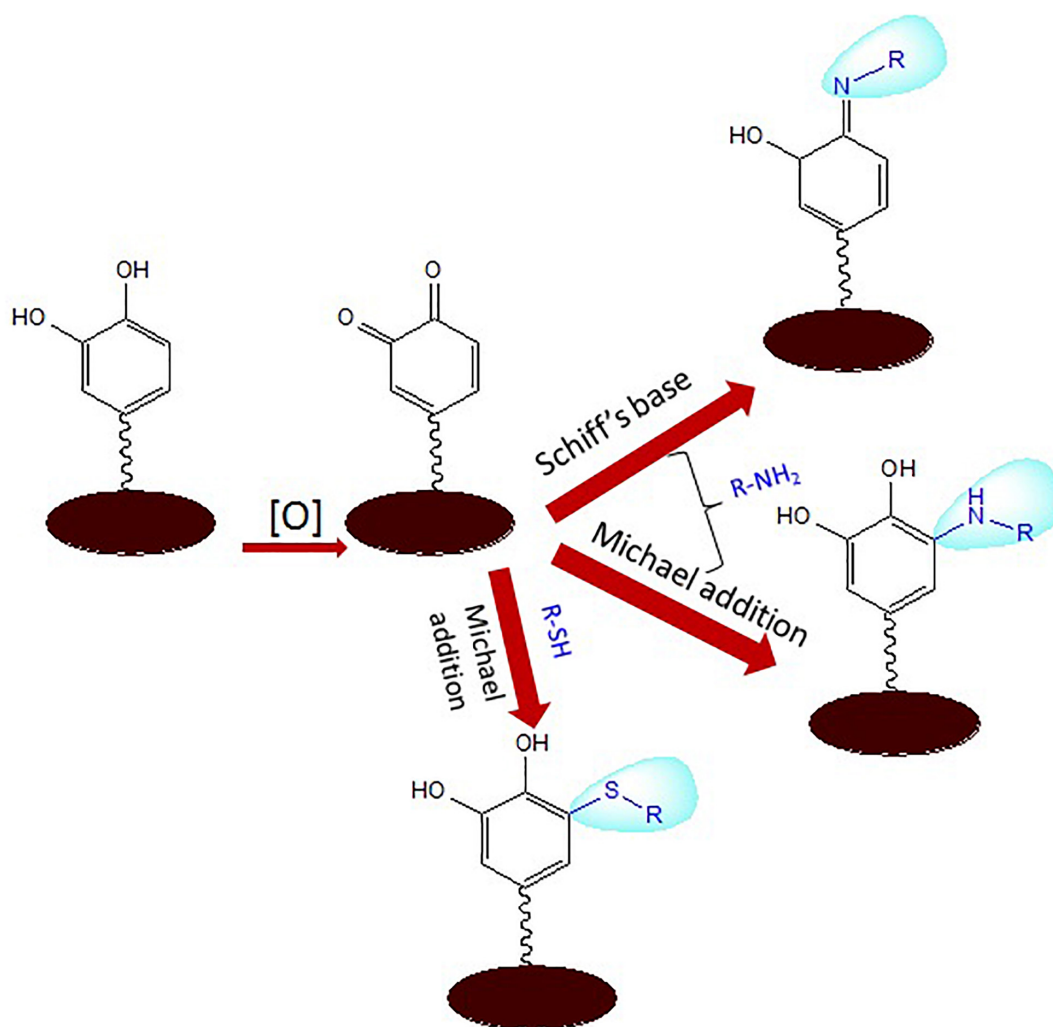


FIGURE 2 | Schiff base and Michael addition reactions of aminated and thiolated ligands with reactive functionalities of polydopamine (PDA).

deliver photosensitizers through chemical conjugation, physical absorption, and encapsulation strategies. A review by Batul et al. (2017) has discussed about the developments made in the area of drug delivery, photothermal therapy, and bone and tissue engineering using polydopamine nanostructures.

Polydopamine nanoparticles have been observed to display synergistic therapeutic effects for combined chemotherapy and photothermal therapy for cancer (Zhu and Su, 2017). PDA in association with photosensitizers conjugated to hyaluronic acid complexed nanoparticles has been reported to allow tumor-specific photodynamic therapy with degradation of the hyaluronic acid by the tumor-localized intracellular enzymes releasing the photosensitizer nanoparticles (Han et al., 2016).

Similarly, calcium carbonate–polydopamine ($CaCO_3$ –PDA) composite hollow nanoparticles have been reported to offer a multifunctional theranostic nanoplatform. The pH-dependent nanoparticles, quenched by PDA, could be photoactivated only in the acidic environment of a tumor whereby they released the photosensitizer and displayed multimodal imaging capability due

to strong affinity between metal ions and PDA and exhibit high antitumor PDT efficacy (Dong et al., 2018). Various metal ions have been loaded onto PDA nanoparticles for bioimaging and photothermal cancer therapy simultaneously (Miao et al., 2015; Ge et al., 2017; Feng et al., 2020; Liu et al., 2020). Photocatalytic organic nanoparticles composed of flavin-conjugated PDA NPs have been described to display xenobiotic-degrading enzyme analogous activity (Fruk and Crocker, 2019).

APPLICATIONS OF POLYDOPAMINE NANOCOATINGS

Polydopamine coatings have been designed to enhance mucopenetration as well as cell uptake of NPs for mucosal drug delivery applications (Poinard et al., 2019). Mallinson et al., with the help of atomic force microscopy, suggested that PDA could be a useful coating to reduce interaction with proteins, which would otherwise lead to fouling (Mallinson et al., 2018).

The hydrophilicity, aqueous durability under the physiological conditions, biocompatibility, as well as ease of functionalization make PDA nanocoatings apt candidates for numerous tissue engineering applications. PDA-assisted hydroxyapatite coating onto porous $\text{Ti}_6\text{Al}_4\text{V}$ scaffolds has been reported to promote osteointegration and osteogenesis *in vivo* and could be useful for bone defect repair (Li et al., 2015). Ku and Park (2010) introduced PDA coatings for potential vascular tissue engineering applications (Ku and Park, 2010). It has been shown that PDA offers simple, effective, and inexpensive alternative for bone tissue engineering compared to traditional surface modification and tissue regeneration (Huang S. et al., 2016; Lee et al., 2017; Zhou et al., 2019). Madhurakkat Perikamana et al. (2015) have discussed in detail various techniques for versatile surface modification for tissue engineering.

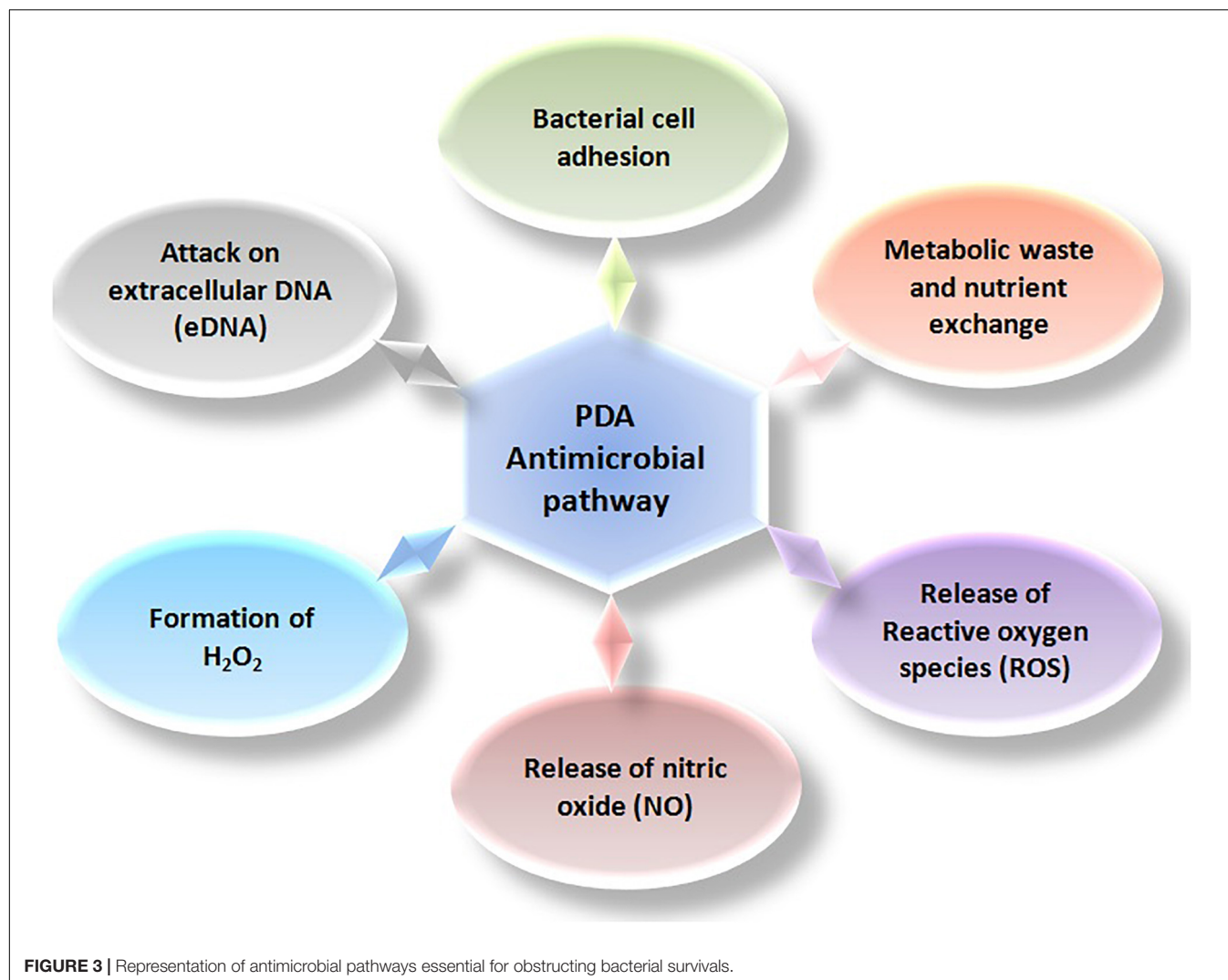
PDA AS A REACTIVE OXYGEN SPECIES SCAVENGER

The redox activities of catechol groups, pro- and antioxidant, in mussel adhesive proteins are a potential treasure for clinical applications. Catechol oxidation by air generates H_2O_2 and $\text{O}_2^{\cdot-}$ as reactive by-products. Forooshani et al. (2017) have reviewed the regulation of reactive oxygen species (ROS) and their effects in living system. The group further applied this redox chemistry of adhesive moiety to design microgels, which had the potential to generate H_2O_2 as and when needed for antimicrobial and antiviral applications (Meng et al., 2019). The antimicrobial property of PDA could also be accredited to the catechol moieties, which are released in a controlled manner and autoxidize in the presence of oxygen, forming semiquinone and quinone. The oxidation process generates ROS including two well-known disinfectants, superoxide anions ($\text{O}_2^{\cdot-}$) and H_2O_2 (Alfieri et al., 2017; Ryu et al., 2018). PDA is able to remove ROS that are generated during inflammatory responses. PDA nanoparticles have been shown to possess antioxidative properties to remove ROS and suppress ROS-induced inflammation in periodontal diseases without any side effects (Bao et al., 2018) and have been used effectively in the treatment of acute inflammation-induced injury (Zhao et al., 2018). PDA-coated hemoglobin nanoparticles showed oxidative protection of hemoglobin and antioxidative properties to remove ROS as well as reduce ROS generation besides exhibiting high oxygen affinity and low cytotoxicity (Wang Q. et al., 2017). Arginine-doped PDA has been shown to be a free-radical scavenger due to greater accessibility to free radicals and so has exhibited superior antioxidant performance than PDA-melanins (Yang et al., 2020a). A nanocomposite based on $\text{V}_2\text{O}_5/\text{PDA}/\text{MnO}_2$ has been reported to exhibit an ability to remove intracellular reactive oxygen species and mimic intracellular antioxidant enzyme-based defense system flaunting potential for inflammation therapy (Huang Y. et al., 2016). Cu-loaded PDA coatings are being seen as a favorable platform for blood contact materials, which have the capability to catalyze the decomposition of S-nitrosothiols and release NO for a longer period thus maintaining the anticoagulant effects (Zhou et al., 2020).

APPLICATIONS OF POLYDOPAMINE AS ANTIBACTERIAL AGENT

Polydopamine has been illustrious for antibacterial and antifungal effects against several microorganisms (Figure 3). Su et al. (2016) have raised the scope of PDA by developing a simple shaking-assisted method to produce roughened polydopamine (rPDA) coatings at a variety of substrates. In the absence of an external antibacterial agent, the projected rPDA coatings displayed significantly enhanced antibacterial activity against Gram-positive and Gram-negative bacteria. Patel et al. (2018) have revealed that PDA coatings using different buffers could help in manipulating antibacterial activities, since the selection of the buffer could control the percentage of a particular functional group present in that PDA coating. Tris and sodium hydroxide-mediated PDA coating exhibited higher antibacterial activity as compared to that obtained using sodium bicarbonate and phosphate-buffered saline (PBS), which might be due to the presence of abundant hydroxyl groups on the surface of the coating. The findings of the study outlined the effect of different chemistries on the morphology and physicochemical properties of the PDA coatings that ultimately affected the antibacterial or antifouling properties. Zhou et al. have also suggested an alternative route to expedite PDA coating on the surfaces. High temperature with rapid shaking for 30 min produced the coated surfaces similar to properties exhibited by the surfaces coated for 24 h (Zhou et al., 2014).

Polydopamine has been observed to possess redox-dependent properties, which make this material to perform as an antioxidant as well as a pro-oxidant. It can accept or donate electrons repeatedly to exhibit beneficial radical-scavenging properties as well as to generate ROS, which account for its antimicrobial properties (Liu and Huang, 2016; Lakshminarayanan et al., 2018; Liu et al., 2019). Its chemistry involves two electron transfer between quinone and hydroquinone structures. Catecholic moieties of PDA are responsible for donating electrons to oxygen molecule to generate hydrogen peroxide, which subsequently produces hydroxyl radical advocating the localized and instant antibacterial activity. These properties are greatly influenced by the presence of metal ions and near-infrared (NIR) irradiation. The series of reactions that occur during electron transfer (respiratory chain) is important for bacterial growths as well as PDA redox state, as respiratory chain inhibitors have been illustrated in Figure 4. Mechanistically, *in situ* formation of different forms of polydopamine acts as pro-oxidant/antioxidant owing to acceptance of electrons (e^-) from the environmental oxygen and vice versa. The oxidized form of PDA attained by metal binding (Ag^+ , Au^{3+} , Pt^{4+} , Cu^{2+}) inflates the generation of quinone moieties and affinity for binding other biomolecules to enhance microbial inhibitory effect (Liebscher, 2019). Electron-donating behavior of PDA produces detrimental pro-oxidant effects on bacterial survival via generation of reactive oxygen species (ROS) via conversion of environmental oxygen (O_2) to superoxide radical ($\text{O}_2^{\cdot-}$). Generated ROS expedite the activity of superoxide dismutase (SOD; metalloenzyme), thus forming H_2O_2 , which further produces OH. Combined effects



of hydroxyl ion and the presence of NADH on Fe-S cluster along with cofactor FMN enrich bacterial cellular membrane with quinones (Quinone pool) (Larosa and Remacle, 2018). Synthesized quinone facilitates the formation of heme b and heme o_3 for survival of prokaryotes. The transfer of electrons is an essential pathway for cellular respiration within microbes, especially bacteria. Herein, the pro-oxidant effect of PDA escalates ROS production and disrupts the chain of Fe-S cluster, thus leading to inhibition of formation of quinone and thus famine quinone pool. Irradiation and metal binding also alter the redox state behavior of PDA for exhibiting antimicrobial properties. PDA nanocoating exhibits a broad absorption range from visible to NIR, which can be tailored for various photothermal behaviors (Zou et al., 2020). The study by Lei et al. (2016) has reported that this PDA nanocoating possesses very high photothermal conversion properties upon NIR irradiation, which leads to the killing of all local microbes independently on genus. Medical-device-associated infections have been drastically increasing in the current scenario. Surface functionalization via altering surface topography (surface

roughness/wettability/surface energy), chemical modification (smart surfaces), and multifunctional surfaces (nanoform layer/antimicrobial coating using antibiotics, antimicrobial peptides: AMPs) help in combating microbial adhesion using different pathways, i.e., contact killing mechanism, electrostatic repulsion between surface and bacterial cell, rupturing cellular membrane by nanopillars, hydrophilicity block action of bacterial cell adhesins (proteins, flagella, pilli), cationic/zwitterionic moieties repel negative charge strains and bind to +ve charge strain, thus rupturing cell membrane leading to leakage of cellular matrix (Ghilini et al., 2019).

ENDOWING ANTIMICROBIAL POTENTIAL BY PDA FABRICATED HYDROPHILIC AND CHARGED SURFACES

Alteration in the topographic pattern of various substrates (glass, polycarbonate, implants, pristine, etc.) helps in mitigating

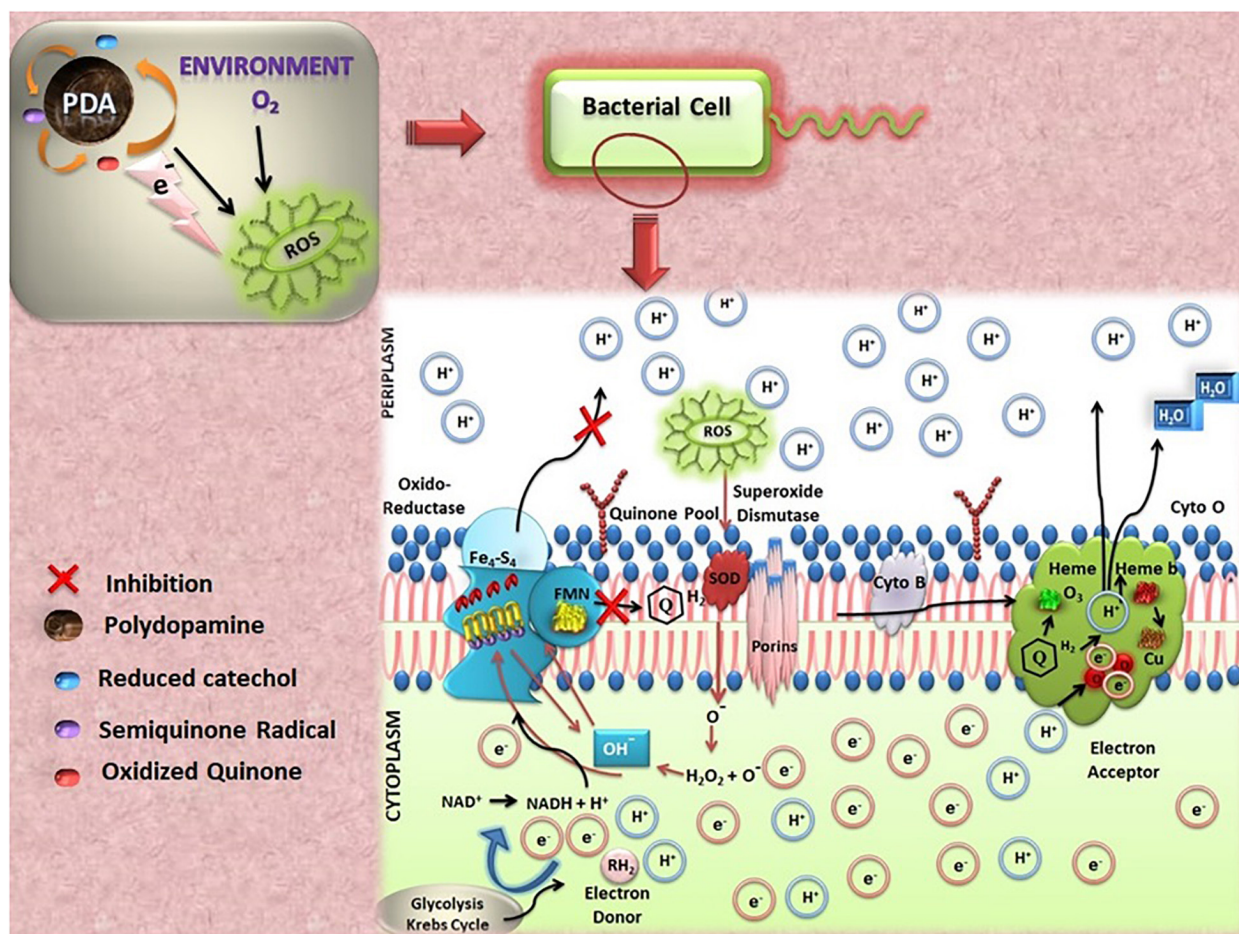


FIGURE 4 | Representation of reactions occurred during electron transfer from polydopamine (PDA).

microbial adhesion, i.e., biofilm formation. This approach is well suited for coating medical implants and biomedical devices to combat microbial-associated infections. Nowadays, compromised surface geometry allows wide range of microbes for the attachment. Adhered microbes attract other microbial community for biofilm formation, and fouling tendency also supports biofilm formation. A recent study by Khanzada et al. revealed that cross-linked PDA-GO functionalized RO membranes exhibited bactericidal and antifouling properties. They demonstrated that hydrophilic behavior and smooth edges of the surface hindered bacterial adhesion and long-term survival. The rationale behind this outcome was the negative charge on the surface due to the presence of COOH, leading to electrostatic repulsion between the surface and Gram-negative strain and PDA-GO imparted synergistic effects on bacterial cellular damage via ROS production (Khanzada et al., 2020). In another study, an increase in surface roughness and hydrophilicity during surface modification with PDA-functionalized adhesions have been shown as important factors that expedite the binding of bacteria onto surfaces (Su et al., 2016); however, positively charged functional moieties in PDA cause lysis. Likewise, cationic polymer (chitooligosaccharide)-conjugated PDA-polyurethane (PDA-PU)

membranes have shown significantly improved antibacterial activity as compared to PDA-PU membranes, which showed marginal enhancement in the properties over native PU membranes (Luo et al., 2017). In yet another report, Ahmed et al. have demonstrated the importance of hydrophilic behavior of PDA-functionalized polysulfone (PSF) substrate enriched with hydrophilic natural organic matter (NOM) for combating microbial adhesion. Herein, microbial adherence has been blocked by inhibiting interaction between cell surface adhesins, i.e., pilli and flagella and PDA-functionalized surface (Ahmed et al., 2018). A summary of the important PDA-based systems along with their mechanism of action on the microbes is depicted in Table 1.

CATIONIC CHARGE ENRICHED PDA-FABRICATED SURFACES: EFFECT ON ANTIMICROBIAL PROPERTIES

Chemical moieties used for surface modifications such as cationic polymers, antimicrobial peptides (AMPs), zwitterionic polymers, and quaternary ammonium compounds (QAC) have been employed to introduce antifouling, antimicrobial, and

TABLE 1 | Summary of some of the polydopamine (PDA)-associated nanostructures and their bacterial inhibitory mechanism.

S.No.	PDA conjugated ligands	Nanoform	Bacterial inhibition pathway	References
1	PEG or sulfobetain@PDA(Ag)@substrate Substrate: TiO ₂ , glass, Au, Nitinol alloy, PDMS, PS	Nanocoating	⊗ bacterial adsorption on substrate due to dense tightly bound water layer	Liu and Huang, 2016
2	PDA@substrate Substrate: glass, stainless steel, plastic, gauze	Nanocoating	⊙ bacterial cell surface	Su et al., 2016
3	NO@PDA hollow nanoparticles	Nanoparticles (Spherical)	NO release, ↑ nitrosative and oxidative stress within bacteria	Park et al., 2016
4	NO@PDA@substrate and NO@PEG@PDA@substrate	Nanocoating	Release NO and ⊗ bacterial adherence on surface	Sadrearhami et al., 2019
5	Ag@PDA@Ti	Nanocoating	ROS production, ⊙ membrane integrity	Zhou et al., 2020
6	Cu@Ag@PDA@PET fabric	Nanocoating	Interaction of Cu NPs with bacterial cell wall followed by rupturing	Wang K. et al., 2020
7	PDA@Ag-PVP NPs	Nanocoating	ROS mediated bacterial membrane damage	Niyonshuti et al., 2020
8	Ag@PDA@polyamide	Nanocoating	⊙ metabolic exchange through cell membrane thus cause cell death	Yang et al., 2016
9	Ag@PDA@PSU membrane	Nanocomposite layer	⊙ bacterial cell integrity	Tang et al., 2015
10	PLA-Au@PDA@Ag nanofibers	Nanofibers	⊙ DNA replication and bacterial intracellular processes and cell lysis	Zhang et al., 2019
11	Cu/Ag-PDA nanohybrids	Nanoparticles	↑ in ROS level, membrane damage, ⊗ nutrient intake and membrane enzymatic/protein activities, cell death	Yeroslavsky et al., 2016
12	Colistin(Ag)@PDA	Hybrid Nanospheres	Synergistic effects of Colistin and Ag ⁺ . Membrane-damaging bactericidal activity. Adherence to membrane followed by generation of pores	Ran et al., 2020
13	Ag@PDA@PEEK implant material	Nanocoating	Synergistic effect for Inhibiting bacterial membrane sulphur containing enzymes, thus ⊗ cellular respiration and cell death	Gao et al., 2017
14	Ag@PDA@sericin-PVA film	Nanocoating	Interaction with bacterial membrane followed by penetration by Ag ions	Cai et al., 2017
15	Ag@PDA@TPU porous membrane	Nanocoating	↑ DNA damage, ⊗ respiratory enzyme followed by cell death	Liu M. et al., 2018
16	Col@Ag@PDA@PP 3D scaffold	Nanofibrous scaffold	↓ nutrient reservoir for bacteria and ⊗ migration thus perform killing effect	Qian et al., 2019
17	Hydrophobic silica@PDA@fabric	Nanocomposite layer	Charge dependent cytoplasmic membrane disruption, surface roughness and hydrophobicity interfere bacterial cellular communication and causes cell death	Song et al., 2019
18	γ-MG@PDA@contact lenses and AMP@PDA@contact lenses	Nanofilm	Bacterial membranolytic action, ↑ surface roughness ⊗ bacterial adhesion	Dhand et al., 2020
19	Cefotaxime@PDA@Ti implants	Nanocoating	Prevent adhesion and proliferation of bacteria	He et al., 2014
20	CS@Ag@HA@PDA@Ti implants CS-chitosan; HA-hydroxyapatite	Hybrid nanocoating	⊗ DNA replication, electron transport chain (ETC), and ↑ membrane permeability and leak intercellular constituents.	Li et al., 2016
21	Ag@PDA@Ti implants	Nanocoating	Ag ions interfere with cell division, generating reactive Oxygen species, induce stress in microorganisms, DNA damage, and finally cell death	Choi et al., 2019
22	Ag@PDA-CS@Ti	Nanocoating	Anti-adhesion activity of PDA-CS surface and antibacterial activity of Ag NPs	Wang B.B. et al., 2020
23	Cu ²⁺ @PDA@Ti	Nanocoating	Copper ions generate ROS by redox activities, interruption in the protein assembling and metabolism process followed by cell death	He et al., 2015 Wang L. et al., 2017
24	Ag@PDA@TiO ₂ @Ti	Nanocoating	Ag ion mediated increase of intracellular stress and thus apoptosis	Jia et al., 2016

(Continued)

TABLE 1 | Continued

S.No.	PDA conjugated ligands	Nanoform	Bacterial inhibition pathway	References
25	Ag@PDA@TiO ₂	Nanocoating	Ag mediated bacterial cell membrane cracking, protein denaturation, DNA damage and killing	Gao et al., 2019
26	Ag@PDA@TiO ₂ @Ti substrate	Nanorods	⊗ bacterial cell wall synthesis and protein denaturation	Guan et al., 2019
27	RGD@PDA@MoS ₂ @TiO ₂ @Ti substrate	Nanocoating	↑ cellular GSH oxidation, contact killing mechanism and laser induced leakage of internal matrix due to hyperthermia in bacteria causes lysis effects	Yuan et al., 2019
28	Sulfobetain@PDA(Cu)@ Zirconia disk	Nanocoating	Radical-mediated impairing intracellular bacteria	Fan et al., 2018
29	Ag@PDA@g-C ₃ N ₄ scaffold	Nanosheets	Photogenerated electrons form ·OH, O ₂ ⁻ destruct biomolecules thus ↑ bacterial cell death	Wu Y. et al., 2018
30	Ag@PDA@Graphene oxide matrix	Nanocomposite	Interfere Cell permeability, ATP production, leak RNA thus kills bacteria	Liao et al., 2019
31	Ag@PDA@MoS ₂ sheet	Nanosheets	Photothermal induced cell membrane disruption and bactericidal effect.	Yuwen et al., 2018

↑: Increasing; ↓: Decreasing; ⊗: Inhibition; ⊕: Disruption/Interfere; ·OH: Hydroxyl radical; O₂⁻: Superoxide radical.

antibiofilm properties, and the resulting surfaces have been used for combating device-associated infections (Ghilini et al., 2019). Gram-negative bacterial strains specifically adhere to cationic surfaces for longer time period, leading to penetration of bioactive molecules into the cell membrane via different transporter and porins. These frontrunners advocate for hindering series of metabolic activities essential for bacterial survival. On the other hand, Gram-positive bacterial community repels surfaces due to electrostatic repulsion, thus unable to promote biofilm formation. PDA has been proven as a versatile biopolymer for surface functionalization in conjugation with various positively charge compounds, as shown by Yao et al. (2018) in the fabrication of zwitterionic polysulfone surface to mitigate biofouling process and microbial adhesion. The approach helped in designing and developing smart surfaces that could inhibit biofilm formation, thus decreasing biofilm-associated infections. A recent study by Zhou et al. scrutinized the activity of cocktail functional polymers, cationic monomer, and cross-linker deposited on the catheter surface. These combinations inflated surface hydrophilicity as well as cationic charge, expediting biofilm inhibition (Zhou et al., 2018).

A review by Jia et al. (2019) has mentioned about the role of PDA-based coatings to improve the antimicrobial and osseointegration of orthopedic implants. The adhesive character of PDA has been used to attach the antimicrobial enzyme lysozyme, covalently, to various surfaces to produce antibacterial and antibiofilm interfaces (Yeroslavsky et al., 2015). An easy, two-step, shaking-assisted PDA coating technique has been suggested to create antimicrobial polypropylene (PP) mesh having the capability to produce H₂O₂ (Forooshani et al., 2019). The coating was found to be more effective against Gram-negative bacteria, while Gram-positive bacteria showed a resistance. However, the generation of a higher amount of H₂O₂ as well as longer exposure time was found to be enough to destroy Gram-positive bacteria. Aminoglycoside conjugates of PDA have been evaluated for antimicrobial potency against

different bacterial strains (clinical as well as resistant ones) e.g., PDA-kanamycin, PDA-gentamicin, and PDA-neomycin nanoconjugates (Singh et al., 2020). PDA deposited onto the polydimethylsiloxane (PDMS) surface has been used to tether synthetic antimicrobial cysteinylated tryptophan-arginine-rich peptide (CWFWKWRRRRR-NH₂) (CWR11) that displayed antimicrobial functionality over 21 days on catheter-relevant surfaces to combat catheter-associated urinary tract infections (Lim et al., 2015). Similarly, immobilization of liposomal amphotericin B (LAmB) on a PDA-coated PDMS surface, a material commonly used in the manufacturing of urinary catheters, was shown to impart the ability to resist *Candida albicans* colonization (Alves et al., 2019).

Antifouling surfaces composed of a zwitterionic copolymer, made up of 2-methacryloyloxyethyl phosphorylcholine and dopamine methacrylamide followed by covalent codeposition on polyethylenimine (PEI)/PDA surfaces, showed antibacterial activity against Gram-negative and Gram-positive bacteria along with adsorption resistance to bovine serum albumin after *in situ* deposition of AgNPs (Asha et al., 2018).

A material surface, composed of PDA-coated Fe₃O₄ nanoparticles followed by covalent tethering of barbituric acid, has been developed. Postreaction with sodium hypochlorite generated N-halamine groups on the imide functions of the barbituric acid, and the resulting surface displayed excellent antimicrobial activity against both Gram-positive and Gram-negative bacteria. These bifunctional nanoparticles with excellent antibacterial as well as magnetic properties not only destroyed targeted bacterial colonies but could also be recovered by applying an external magnetic field (Akter et al., 2018). In a similar type of study, N-halamine functions have been generated on PDA surface, and the resulting surface has showed significantly higher antibacterial activity toward Gram-positive and Gram-negative bacteria within a brief contact time as compared to the activity displayed by the only PDA-coated substrate (Chien et al., 2020).

The contribution of PDA to provide stability as an adhesive and antibacterial activity has been validated during evaluation of PDA/alginate/Fe₃O₄ hydrogel beads. The coating of PDA on to Alg/Fe₃O₄ beads not only significantly increased the stability in different pH, hydrophilicity, and elasticity but also performed strongly against bacterial strains (Matai et al., 2019). These beads have been demonstrated to be used repeatedly as antibacterial agents.

Polydopamine coatings have been employed on the surface of satellite telemetry tags, with coating conditions tailored to generate varying amounts of hydrogen peroxide. The coating displayed the ability to diminish the adhesion of *E. coli* and *Psychrobacter cryohalolentis* and, therefore, has the potential to decrease the chances for tissue infection at the tag implant site (Tyo et al., 2019).

Nitric oxide at low concentration affects cellular signaling within biofilms. Park et al. (2016) and Adnan et al. (2018) have reported PDA nanoparticles with diazeniumdiolate groups that could deliver nitric oxide (NO) for antibacterial therapy with negligible toxicity. A technology, using catecholamine to coat surfaces of body-implantable materials having diazeniumdiolate groups that could supply NO *in vivo* and that could be used without triggering cytotoxicity, has been patented (Kim et al., 2017). Further, PDA films with low-fouling and NO-releasing capabilities containing both diazeniumdiolate and polyethylene glycol (PEG) functionalities with NO release capability to over 48 h have been reported and showed the ability to inhibit the attachment of a multidrug-resistant strain and efficiently destroy the biofilm (Sadrearhami et al., 2019). Since catechol groups in PDA provide the ability to coordinate metal ions, Cu²⁺-loaded PDA coatings were able to catalyze NO release (Zhou et al., 2020).

The mechanism suggested in the synthesis of PDA/copper-doped calcium silicate (Cu-CaSil) bioactive hydrogel validated the coordination between PDA and Cu²⁺ ions. The projected complex showed enhanced photothermal performance of the hydrogel as observed by mass extinction coefficient profile and improved bioactivity. Laser irradiation of this hydrogel showed an excellent antibacterial activity. Stronger NIR absorption has been attributed to the presence of PDA polymer and Cu-CaSil powder, two hydrogel components, both possessing photothermal property, and the right PDA/Cu ratio leads to a number of tetracoordinated structures in PDA-Cu complex responsible for enhancing absorption intensity. Since heat treatments are known to kill bacteria, the photothermal effect of the composite hydrogel PDA/Cu-CaSil with synergistic antibacterial function of Cu²⁺ ions created unique “hot ions effect” by heating Cu²⁺ ions through laser irradiation (Xu et al., 2020). Further, Cu/Ag/PDA/PET fabrics have been shown to possess good antibacterial property against *E. coli* (~99%) due to the adhesive ability of PDA and its strong binding to Cu NPs. The self-polymerization of dopamine under alkaline conditions forming PDA nanoparticles assisted a change in morphology of PET fabrics. The catechol moieties and amine functional groups in PDA reduced Ag⁺ to Ag NPs that were fastened on fiber surface via chelation between PDA and Ag⁺ ions. These Ag NPs, as catalytic seeds, facilitated deposition of Cu NPs on the surface of fabrics through chemical copper plating. Thus, PDA,

functioning as template, expedited Cu NPs deposition onto the surface of fabric that displayed killing of most of the adhered bacteria (Wang K. et al., 2020).

The antimicrobial activity of Ag implants is mainly attributed to binding of Ag⁺ to thiol groups present in bacterial enzymes. Its use has been exploited with many PDA-assisted coatings (Yun'an Qing et al., 2018). Ag-coated PDA microspheres have been used to kill *Staphylococcus aureus* cells due to the elevated ROS level (Guo et al., 2019). The abundance of catechol and amine groups on the surface of PDA particles are the active sites for *in situ* reduction in the silver precursors, and the formed AgNPs can be fixed there; Wu C. et al. (2015) used [Ag(NH₃)₂]⁺ ions as a precursor for polydopamine-assisted electroless Ag metallization, which showed an excellent antibacterial performance against *Escherichia coli* and *S. aureus*.

The PDA coatings incorporated with Ag ions illustrate an attractive approach, as the combination facilitates interactions with biological system without cytotoxicity and exhibits antibacterial capability as well. The synergistic effects between PDA coating and AgNPs have been highlighted in a study based on X-ray photoelectron spectroscopy (XPS) and Fourier-transform infrared spectroscopy (FTIR) analysis by Niyonshuti et al. (2020). The study indicated that the PDA coating becomes thicker as the PDA deposition time is increased. The coordination between Ag and catechol groups on the PDA coating was found to significantly increase the potency of AgNPs against *E. coli*. Thus, a PDA coating is observed to play a significant role in enhancing the antimicrobial properties of AgNPs. The result indicated that catechol-rich PDA coating resulted in an increased ROS generation and significant damage to the bacterial membrane. The reducing catechol groups of PDA have further been explored to form well-dispersed AgNPs on different substrates for controlling biofouling and as antimicrobial reverse osmosis membranes, which, in turn, expose the potential of PDA to modify surface chemistries and morphological features of the membranes (Tang et al., 2015; Yang et al., 2016). Since the catechol groups in the PDA films chelate with Ag, the *in situ* reduction in Ag⁺ to Ag⁰ and binding of Ag⁰ to N- and O-sites in PDA film produce seed precursor, which helps in building up of AgNPs on the central venous catheters (CVCs) surface, demonstrating significant antimicrobial potency and appropriate biological safety (Wu K. et al., 2015).

A bio-nanocomposite coating using the mycogenerated AgNPs and PDA has been reported to display antibiofilm activity on biofilms of multidrug-resistant *A. baumannii* used in central venous catheter (Neethu et al., 2020). AgNPs formed by reduction through catechol have been reported not to be sensitive to oxygen and so have a longer-lasting antimicrobial effect (Wu H. et al., 2018). Zhang et al. (2019) combined the antimicrobial effect of three materials to boost the potential of bio-coated PLA-Au@PDA@Ag nanofibers. The large surface area of the AuNPs in the fibers facilitated the enhancement of the cell penetration with simultaneous production of oxidative stress by the biological system, thereby exhibiting high antibacterial activity. PDA, with its antibacterial effects, too, acted as a binder for different interfaces with effective anchoring groups.

Metal-containing PDA-NPs are suggested to be highly microbicidal and display effective antibiofilm activity (Yeroslavsky et al., 2016). Besides this, sonochemically synthesized Ag-PDA NPs and Cu/Ag-PDA hybrid NPs with copper shell and Ag core have been demonstrated to convert the surface to antibacterial. The projected system also gets benefited from the partial contribution to the antimicrobial activity from the stable PDA-semiquinone and ROS generated by the metal-PDA NPs under physiological conditions as suggested by Yeroslavsky et al. (2016). The synergistic actions of two or more antibacterial drugs as nanohybrids have been established to be effective in the treatment of refractory bacterial infections. The colistin-loaded PDA nanospheres decorated with silver nanodots are reported by Ran et al. (2020) to exhibit powerful antibacterial and antibiofilm effects.

The metal-ion-reducing ability of catechol in PDA with consequently depositing the Ag nanoparticles has been utilized to support antibacterial coatings for poly(ether ether ketone) (PEEK) implants. The PEEK-PDA-Ag implant was reported to inhibit growth of *E. coli* and *S. aureus* on the surface and the surrounding bone tissue compared to PEEK without affecting osseointegration (Gao et al., 2017). Further, PDA and silk fibroin have been introduced to the porous PEEK surface to balance the biocompatibility and antibacterial ability of PEEK implant by Yan et al. (2018). The study reported a first time PDA-assisted *in situ* growth of AgNPs and immobilization of silk fibroin (SF)/gentamicin sulfate (GS) coating upon porous PEEK surface. The dual application of PDA, reducing Ag⁺ into AgNPs followed by firm fastening onto PEEK surface and biocompatibility serving osteogenesis, was presented as a synergistic bacteria killing ability in AgNP-incorporated SF/GS coating constructed upon porous PEEK surface (Yan et al., 2018). PDA synthesized in one step is reported by Cai et al. (2017) to act as both a metal ion chelating as well as reducing agent to synthesize, *in situ*, AgNPs on the sericin/poly(vinyl alcohol) (PVA) composite film, which displayed long-standing antibacterial activities. In another study, Liu M. et al. (2018) have demonstrated prominent antibacterial activity of a porous thermoplastic polyurethane (TPU) membrane coated with PDA NPs followed by a layering of nanosilver and its use as a profound antibacterial invasion dressing (i.e., wound dressing) with high biocompatibility for wounds caused by clinical and antibiotic-resistant bacteria. Using mussel-inspired PDA coating technology, a scaffold (PP-PDA-Ag-COL) was generated by Qian et al. in a multistep process. An electrospun poly (lactide-co-glycolide) (PLGA)/poly(epsilon-caprolactone) (PCL) matrix was first coated with PDA NPs followed by coating with AgNPs via *in situ* reduction to incorporate antibacterial and osteogenic properties. The resulting PP-PDA-Ag matrix was then coated with type I collagen (COL) to further improve the properties including biocompatibility of the scaffold. Collagen I coating not only enhanced the cytocompatibility but also resulted in the consistent release of silver ions over more extended periods. The tailored PP-PDA-Ag-COL structure maintained the three-dimensional interfiber architecture of the scaffold (Qian et al., 2019). The emergence of PDA thin layer on the AgNPs, which exhibit cytotoxicity, has been presented to be highly

biocompatible with almost no toxic effects on the cells and that too without compromising on the optical characteristics (Yilmaz, 2020). Various groups have also developed diversified types of PDA-coated surfaces; for instance, PDA-dyed hair prevented the scalp from bacterial infection. Likewise, PDA-coated cotton fabric, on treatment with quaternized nanosilica followed by hexadecyltrimethoxysilane, produced a superhydrophobic and excellent antibacterial material with good washable properties (Song et al., 2019). The design and development of antimicrobial contact lenses is another area where PDA-based coatings have been tested against bacterial adhesion and formation of biofilm. Dhand et al. examined the covalent and non-covalent interactions of antimicrobial agents with PDA coating on contact lenses. The results showed that surface properties of the lenses remained unaffected, and the coating displayed excellent antimicrobial activity to prevent biofilm formation for longer duration without any side effects on ocular cells (Dhand et al., 2020). The current state of the art for polydopamine research has revealed PDA as a smart adhesive biopolymer that has the potential to deal with diversified medical as well as environmental challenges.

The incorporation of antimicrobial agents on otherwise corrosion-resistant Ti surfaces is one of the effective modifications to enhance the biological properties of the implants, especially useful for orthopedic implant applications. The study on Ti-PDA-cefotaxime sodium (Ti-PDA-CS) substrates by He et al. indicated that the CS retained its biological activity even after immobilization onto the surface. The conjugated surface exhibited excellent *in vitro* antibacterial activity (He et al., 2014). The combination of PDA with hydroxyapatite (HA), a naturally occurring mineral form, with the formula Ca₁₀(PO₄)₆(OH)₂, calcium-phosphate (CaP)-based material, imparts good mechanical strength as well as corrosion resistance on the surface of implant materials. The formation of CaP biominerals onto the PDA-coated surface grown by layer-by-layer model brings morphological change emphasizing strong affinity between CaP and PDA moieties. The chemistry in PDA-HA coatings works well for antibacterial resistance. A review on functionalization of PDA-HA with applications toward bone-tissue engineering has highlighted the antimicrobial resistance (Kaushik et al., 2020). *In vitro* studies of a hybrid coating composed of bioactive species, hydroxyapatite (HA)/chitosan (CS)/Ag matrix, an organic-inorganic hybrid, onto the surface of a PDA-modified Ti implant could control the release of silver ion for good self-antibacterial execution as well as good osteoinductive ability. The catechol groups of PDA are supported to accelerate the formation of HA crystals and bridge the binding strength between HA and Ti substrate (Li et al., 2016). PDA-Ag coating on Ti surface has also been testified by Choi et al. (2019) to inhibit the formation of biofilm, microbial colonization, and pathogenesis of gum disease in the mouth, i.e., retardation of microbial growth. Furthermore, CS/AgNPs coating has been reinforced by employing PDA as an intermediate bridging layer on the urinary catheter and Ti surfaces, a simple immersion method in acid solution that is reported to exhibit phenomenal refinement in preventing bacterial adhesion. The availability of hydroxyl groups in chitosan (CS) molecules to reinforce

antimicrobial AgNPs and control the Ag ions release besides strong attachment by PDA worked for a durable and efficient antibacterial coating (Wang B.B. et al., 2020).

The PDA acts as bonding glue for coating metal ions on the substrates. Cu(II) ions immobilization through PDA chelation on Ti surface for implant materials is reported to display antibacterial property (He et al., 2015). Wang et al. evaluated the antibacterial activity and osseointegration performance of Cu-deposited Ti substrates with PDA coating in the presence of bacterial infection both *in vitro* and *in vivo*. The Cu^{2+} ions affixed through coordination interaction inside the PDA coating showed sustained release of the metal ions. It was proposed that the released Cu^{2+} ions could effectively inhibit the bacteria in contact with the Ti-PDA-Cu substrate surfaces (Wang L. et al., 2017). Besides metal ion-PDA chemistry, there is interest to validate the effect of concentration of various metal ions on the antibacterial effect of Ti implants induced as self-assembled layer of adhesive PDA. The bacterial viability has been found to be inversely correlated with the ion concentration gradient of divalent Cu^{2+} , Zn^{2+} , and Sr^{2+} metal ions on PDA-coated Ti implant surface. The coated Ti implants may leach these ions to produce positive antibacterial efficacy. The chemical binding of metal ions with PDA has been suggested to control the release rate of the ion coating. Even though a strong Zn-PDA coordination bond in Zn coating slowed the release rate compared to Sr coating at the same concentration, 2% Zn coating and 10% Sr coating could inhibit bacterial growth of bacteria without any toxic effect on cells. The controversial results regarding the antibacterial activities of the PDA coatings suggest that the mechanism of bactericidal properties is still obscure (Kao et al., 2019).

The covalent adhesion and chelating talent of PDA have been exploited with bioactive and biocompatible titania coatings, TiO_2 , on Ti substrate and AgNPs, respectively, by Jia et al. (2016) for orthopedic coatings. Gao et al. also presented *in vitro* and *in vivo* bactericidal and antibiofilm activities of TiO_2 -PDA-Ag coating. The comparison in Ag release kinetics between the TiO_2 -Ag (without PDA) coatings and TiO_2 -PDA-Ag coating on Ti implants by electrochemical anodization synthesis showed a burst release in the former and a controlled-release pattern in the latter. Larger reduction of bacterial growth with overproduction of ROS observed in TiO_2 -Ag coating was recommended for the burst release, but the balance of cytotoxicity and the antibacterial effects lied in TiO_2 -PDA-Ag coatings (Gao et al., 2019). On the other hand, Guan et al. (2019) reported more durable and efficient antibacterial property in Ag- TiO_2 @PDA nanorods (NRDs) by hydrothermal synthesis than that of Ag TiO_2 NRDs, based on the synergistic effect of selective physical punctual and controlled release of silver ions. The ability of PDA to effectively transfer photoinduced electrons and protons and improve the photocatalytic activity has been applied in a three-dimensional Ag/ TiO_2 /PDA nanofilm. PDA, as transformation interface, could support the photocatalytic mechanism to generate some ROS such as hydroxyl radical, hydrogen peroxide, and superoxides, which could cause bacterial inactivation. The study supported the future aspect of intermediate PDA layer as a favorable antibacterial coating on a wide variety of substrates such as plastic glass and metal alloy (Wen et al., 2020). Yuan et al. (2019)

designed a functional MoS_2 /PDA-Arg-Gly-Asp-OH coating on Ti implants to inhibit *in situ* bacterial infection and mend osseointegration.

The material surface analyses of PDA onto the zirconia surface showed significant increase in cell adhesion and proliferation as compared with pristine zirconia. The coating suggested as peri-implant soft-tissue integration influenced human gingival fibroblasts and decreased adherent bacteria (Liu M. et al., 2015).

Silver nanoparticles developed using PDA coatings on rod-like mesoporous silica (SBA-15) gave SBA-15/PDA/Ag nanocomposites, which exhibited prolonged inhibitory effect on the growth of *E. coli*, *S. aureus*, and *Aspergillus fumigatus* (Song et al., 2018). A bioinspired coating with dual functioning antimicrobial, due to PDA and Cu^{2+} ions with a coating of zwitterionic sulfobetaine, via aza-Michael addition reaction, has been tested on commercial silicone-based urinary catheters (Fan et al., 2018). The hydrophobic-hydrophilic character, due to presence of amino, hydroxyl, and phenyl functions, good degradability, and antimicrobial properties of PDA have been exploited by Liu C. et al. (2018) to develop PDA-coated amorphous silica nanoparticle for hemorrhage control. PDA/SiNP displayed promising character for aggregating cells and inducing clotting. Compared to the commercial formulation, Celox, these coated nanoparticles shortened the blood clotting time to 150 s. These particles were found to achieve adequate hemostasis by accelerating coagulation and reducing blood loss during femoral artery and vein injury. PDA/SiNPs exhibited antimicrobial activity even for a longer duration with high hemocompatibility.

A PDA layer coating, synthesized by the H_2O_2 /horseradish peroxidase method, has been found to reduce the cytotoxicity of carbon nanotubes (CNTs), enhance their dispersion, and endow better broad-spectrum photothermal antimicrobial activities in a gelatin-grafted dopamine/chitosan composite hydrogel (Liang et al., 2019). A PDA-based colloidal material synthesized through one-step dopamine polymerization by nitrogen-doped carbon dots has been reported to show an antibacterial effect against *S. aureus* through microorganism entrapment/ROS generation (Maruthapandi et al., 2019). The antibacterial activity of bio-photocatalyst on PDA-graphitic carbon nitride ($\text{g-C}_3\text{N}_4$) with uniformly dispersed AgNPs has been described (Wu Y. et al., 2018). Liao et al. used graphene oxide to form antibacterial Ag-PDA-RGO nanocomposites and evaluated their antimicrobial performance against Gram-positive and Gram-negative bacteria. The projected nanocomposites not only exhibited excellent antimicrobial activity but also opened newer avenues for a wide range of modern biomedical applications (Liao et al., 2019). Similarly, MoS_2 -PDA-Ag nanosheets demonstrated good antibacterial activity and eradicated *S. aureus* biofilms and wound infections (Yuwen et al., 2018).

CONCLUSION AND FUTURE PROSPECTIVE

This article makes a feature of the antibacterial role of PDA and the recent developments in the biomedical fields. The

proficiency in robust adhesion of this polymer inspired by a structure similar to DOPA present in the amino acid sequence of mussel foot protein appeals to the researchers to try various substrates for surface modification. The self-polymerization of dopamine (DA) is still a mystery, but it has not stopped work on its functionalization, reacting quickly with amine and thiol-containing moieties.

The strong metal-chelating, covalent cross-linking, and redox capabilities have made it an innovative coating. Various forms of PDA nanomaterials, viz., NPs, microcapsules, and PDA hybrid nanospheres, hydrogels, and nanocomposites applicable for cell interfacing, biosensing, drug delivery, and tissue engineering, have been synthesized. As discussed for antimicrobial activities, PDA quardaries the cell membrane and barricades the cell surface, preventing diffusion of nutrients and wastes inside/out of the cell cytosol, leading to cell lysis. The positive charge on the functional groups in PDA is also responsible for lysis by contacting the bacterial cell wall.

The antimicrobial activity of PDA could be attributed to the presence of catechol, which forms semiquinone and quinones

that get auto-oxidized in the presence of oxygen, generating ROS and subsequently preventing the growth of bacteria. However, the basis of different responses to different bacteria is still unclear. In some of the nanohybrid systems, the PDA role is restricted to stabilization of the adhesion of antimicrobial films or control the release of antimicrobial metal ions. PDA itself is being known for antibacterial activity due to regulated production of H_2O_2 during auto-oxidation; hence, optimization in its release is desired.

The versatile chemistry of biocompatible PDA warrants its study in medically relevant materials with or without passive and active agents, which prevent microbial biofilm formation and thus hold great potential for growth for diverse applications.

AUTHOR CONTRIBUTIONS

IS and SG compiled the manuscript. GD helped in editing and compilation. PK conceived the idea, edited, and supervised the task to completion. All authors contributed to the article and approved the submitted version.

REFERENCES

- Adnan, N. N. M., Sadrearhami, Z., Bagheri, A., Nguyen, T. K., Wong, E. H., Ho, K. K., et al. (2018). Exploiting the versatility of polydopamine-coated nanoparticles to deliver nitric oxide and combat bacterial biofilm. *Macromol. Rapid Commun.* 39:1800159. doi: 10.1002/marc.201800159
- Ahmed, S. B., Hasane, A., Wang, Z., Mansurov, A., and Castrilloin, S. R. V. (2018). Bacterial adhesion to ultrafiltration membranes: role of hydrophilicity, natural organic matter, and cell-surface macromolecules. *Environ. Sci. Technol.* 52, 162–172. doi: 10.1021/acs.est.7b03682
- Ahn, B. K. (2017). Perspectives on mussel-inspired wet adhesion. *J. Am. Chem. Soc.* 139, 10166–10171. doi: 10.1021/jacs.6b13149
- Akter, N., Chowdhury, L., Uddin, J., Ullah, A. A., Shariare, M. H., and Azam, M. S. (2018). N-halamine functionalization of polydopamine coated Fe_3O_4 nanoparticles for recyclable and magnetically separable antimicrobial materials. *Mater. Res. Exp.* 5:115007. doi: 10.1088/2053-1591/aadc56
- Alferi, M. L., Micillo, R., Panzella, L., Crescenzi, O., Oscurato, S. L., Maddalena, P., et al. (2017). Structural basis of polydopamine film formation: Probing 5, 6-dihydroxyindole-based eumelanin type units and the porphyrin issue. *ACS Appl. Mater. Inter.* 10, 7670–7680. doi: 10.1021/acsami.7b09662
- Alferi, M. L., Panzella, L., Oscurato, S. L., Salvatore, M., Avolio, R., Errico, M. E., et al. (2018). The chemistry of polydopamine film formation: The amine-quinone interplay. *Biomimetics* 3:26. doi: 10.3390/biomimetics3030026
- Alves, D. F., Vaz, A. T., Grainha, T., Rodrigues, C. F., and Pereira, M. O. (2019). Design of an antifungal surface embedding liposomal amphotericin B through a mussel adhesive-inspired coating strategy. *Front. Chem.* 7:431. doi: 10.3389/fchem.2019.00431
- Ang, J. M., Du, Y., Tay, B. Y., Zhao, C., Kong, J., Stubbs, L. P., et al. (2016). One-pot synthesis of Fe (III)-polydopamine complex nanospheres: Morphological evolution, mechanism, and application of the carbonized hybrid nanospheres in catalysis and Zn-air battery. *Langmuir* 32, 9265–9275. doi: 10.1021/acs.langmuir.6b02331
- Asha, A. B., Chen, Y., Zhang, H., Ghaemi, S., Ishihara, K., Liu, Y., et al. (2018). Rapid mussel-inspired surface zwitteration for enhanced antifouling and antibacterial properties. *Langmuir* 35, 1621–1630. doi: 10.1021/acs.langmuir.8b03810
- Bai, Y., Zhang, B., Chen, L., Lin, Z., Zhang, X., Ge, D., et al. (2018). Facile one-pot synthesis of polydopamine carbon dots for photothermal therapy. *Nanoscale Res. Lett.* 13, 1–9.
- Ball, V. (2017). Composite materials and films based on melanins, polydopamine, and other catecholamine-based materials. *Biomimetics* 2:12. doi: 10.3390/biomimetics2030012
- Ball, V. (2018). Polydopamine nanomaterials: Recent advances in synthesis methods and applications. *Front. Bioeng. Biotechnol.* 6:109. doi: 10.3389/fbioe.2018.00109
- Bao, X., Zhao, J., Sun, J., Hu, M., and Yang, X. (2018). Polydopamine nanoparticles as efficient scavengers for reactive oxygen species in periodontal disease. *ACS Nano* 12, 8882–8892. doi: 10.1021/acsnano.8b04022
- Barclay, T. G., Hegab, H. M., Clarke, S. R., and Ginic-Markovic, M. (2017). Versatile surface modification using polydopamine and related polycatecholamines: Chemistry, structure, and applications. *Adv. Mater. Interf.* 4:1601192. doi: 10.1002/admi.201601192
- Batul, R., Tamanna, T., Khaliq, A., and Yu, A. (2017). Recent progress in the biomedical applications of polydopamine nanostructures. *Biomater. Sci.* 5, 1204–1229. doi: 10.1039/c7bm00187h
- Cai, R., Tao, G., He, H., Song, K., Zuo, H., Jiang, W., et al. (2017). One-step synthesis of silver nanoparticles on polydopamine-coated sericin/polyvinyl alcohol composite films for potential antimicrobial applications. *Molecules* 22:721. doi: 10.3390/molecules22050721
- Chen, M., Wen, Q., Gu, F., Gao, J., Zhang, C. C., and Wang, Q. (2018). Mussel chemistry assembly of a novel biosensing nanoplatfrom based on polydopamine fluorescent dot and its photophysical features. *Chem. Eng. J.* 342, 331–338. doi: 10.1016/j.cej.2018.02.099
- Chien, H.-W., Chiu, T.-H., and Stable, N. - (2020). halamine on polydopamine coating for high antimicrobial efficiency. *Eur. Polym. J.* 130:109654. doi: 10.1016/j.eurpolymj.2020.109654
- Choi, S.-H., Jang, Y.-S., Jang, J.-H., Bae, T.-S., Lee, S.-J., and Lee, M.-H. (2019). Enhanced antibacterial activity of titanium by surface modification with polydopamine and silver for dental implant application. *J. Appl. Biomater. Funct. Mater.* 17:2280800019847067.
- d'Ischia, M., Napolitano, A., Ball, V., Chen, C. T., and Buehler, M. J. (2014). Polydopamine and eumelanin: From structure-property relationships to a unified tailoring strategy. *Acc. Chem. Res.* 47, 3541–3550. doi: 10.1021/ar500273y
- Deng, Y., Yang, W.-Z., Shi, D., Wu, M., Xiong, X.-L., Chen, Z.-G., et al. (2019). Bioinspired and osteopromotive polydopamine nanoparticle-incorporated fibrous membranes for robust bone regeneration. *NPG Asia Mater.* 11, 1–13.
- Dhand, C., Ong, C. Y., Dwivedi, N., Varadarajan, J., Halleluay Periyah, M., Jianyang Lim, E., et al. (2020). Mussel-inspired durable antimicrobial contact lenses: The role of covalent and noncovalent attachment of antimicrobials. *ACS Biomater. Sci. Eng.* 6, 3162–3173. doi: 10.1021/acsbmaterials.0c00229
- Ding, Y. H., Floren, M., and Tan, W. (2016). Mussel-inspired polydopamine for bio-surface functionalization. *Biosurf. Biotribol.* 2, 121–136. doi: 10.1016/j.bsbt.2016.11.001

- Dong, Z., Feng, L., Hao, Y., Chen, M., Gao, M., Chao, Y., et al. (2018). Synthesis of hollow biomimetic CaCO₃-polydopamine nanoparticles for multimodal imaging-guided cancer photodynamic therapy with reduced skin photosensitivity. *J. Am. Chem. Soc.* 140, 2165–2178. doi: 10.1021/jacs.7b11036
- Dong, Z., Gong, H., Gao, M., Zhu, W., Sun, X., Feng, L., et al. (2016). Polydopamine nanoparticles as a versatile molecular loading platform to enable imaging-guided cancer combination therapy. *Theranostics* 6:1031. doi: 10.7150/thno.14431
- Fan, Y.-J., Pham, M. T., and Huang, C.-J. (2018). Development of antimicrobial and antifouling universal coating via rapid deposition of polydopamine and zwitterionization. *Langmuir* 35, 1642–1651. doi: 10.1021/acs.langmuir.8b01730
- Feng, J., Xu, Z., Luo, D., and Liu, X. (2020). Multiplexed imaging with coordination nanoparticles for cancer diagnosis and therapy. *ACS Appl. Bio Mater.* 3, 713–720. doi: 10.1021/acsabm.9b01038
- Forooshani, P. K., and Lee, B. P. (2017). Recent approaches in designing bioadhesive materials inspired by mussel adhesive protein. *J. Polym. Sci.* 55, 9–33. doi: 10.1002/pola.28368
- Forooshani, P. K., Meng, H., and Lee, B. P. (2017). “Catechol redox reaction: reactive oxygen species generation, regulation, and biomedical applications,” in *Advances in Bioinspired and Biomedical Materials*, Vol. 1, eds Y. Ito, X. Chen, and Kang I-K (Washington, DC: ACS Symposium Series), 179–196. doi: 10.1021/bk-2017-1252.ch010
- Forooshani, P. K., Polega, E., Thomson, K., Akream, M. S., Pinnaratip, R., Trought, M., et al. (2019). Antibacterial properties of mussel-inspired polydopamine coatings prepared by simple two-step shaking-assisted method. *Front. Chem.* 7:631. doi: 10.3389/fchem.2019.00631
- Fruk, L., and Crocker, L. (2019). Flavin Conjugated polydopamine nanoparticles displaying light-driven monooxygenase activity. *Front. Chem.* 7:278. doi: 10.3389/fchem.2019.00278
- Gao, C., Cheng, H., Xu, N., Li, Y., Chen, Y., Wei, Y., et al. (2019). Poly (dopamine) and Ag nanoparticle-loaded TiO₂ nanotubes with optimized antibacterial and ROS-scavenging bioactivities. *Nanomedicine* 14, 803–818. doi: 10.2217/nmm-2018-0131
- Gao, C., Wang, Y., Han, F., Yuan, Z., Li, Q., Shi, C., et al. (2017). Antibacterial activity and osseointegration of silver-coated poly (ether ether ketone) prepared using the polydopamine-assisted deposition technique. *J. Mater. Chem. B* 5, 9326–9336. doi: 10.1039/c7tb02436c
- Ge, R., Lin, M., Li, X., Liu, S., Wang, W., Li, S., et al. (2017). Cu²⁺-loaded polydopamine nanoparticles for magnetic resonance imaging-guided pH- and near-infrared-light-stimulated thermochemotherapy. *ACS Appl. Mater. Inter.* 9, 19706–19716. doi: 10.1021/acsami.7b05583
- Ghilini, F., Pissinis, D. E., Miñán, A., Schilardi, P. L., and Diaz, C. (2019). How functionalized surfaces can inhibit bacterial adhesion and viability. *ACS Biomater. Sci. Eng.* 5, 4920–4936. doi: 10.1021/acsbiomaterials.9b00849
- Gu, G. E., Park, C. S., Cho, H.-J., Ha, T. H., Bae, J., Kwon, O. S., et al. (2018). Fluorescent polydopamine nanoparticles as a probe for zebrafish sensory hair cells targeted in vivo imaging. *Sci. Rep.* 8, 1–8.
- Guan, M., Chen, Y., Wei, Y., Song, H., Gao, C., Cheng, H., et al. (2019). Long-lasting bactericidal activity through selective physical puncture and controlled ions release of polydopamine and silver nanoparticles-loaded TiO₂ nanorods in vitro and in vivo. *Int. J. Nanomed.* 14:2903. doi: 10.2147/ijn.s202625
- Guo, A., Mu, Q., Cai, A., and Wang, X. (2019). Mussel-inspired green synthesis of Ag-coated polydopamine microspheres for selective antibacterial performance. *Micro Nano Lett.* 14, 394–398. doi: 10.1049/mnl.2018.5357
- Han, J., Park, W., Park, S.-J., and Na, K. (2016). Photosensitizer-conjugated hyaluronic acid-shielded polydopamine nanoparticles for targeted photomediated tumor therapy. *ACS Appl. Mater. Inter.* 8, 7739–7747. doi: 10.1021/acsami.6b01664
- He, S., Zhou, P., Wang, L., Xiong, X., Zhang, Y., Deng, Y., et al. (2014). Antibiotic-decorated titanium with enhanced antibacterial activity through adhesive polydopamine for dental/bone implant. *J. Royal Soc. Inter.* 11:20140169. doi: 10.1098/rsif.2014.0169
- He, T., Zhu, W., Wang, X., Yu, P., Wang, S., Tan, G., et al. (2015). Polydopamine assisted immobilization of copper (II) on titanium for antibacterial applications. *Mater. Technol.* 30(Suppl.6), B68–B72.
- Ho, C.-C., and Ding, S.-J. (2014). Structure, properties and applications of mussel-inspired polydopamine. *J. Biomed. Nanotechnol.* 10, 3063–3084. doi: 10.1166/jbn.2014.1888
- Holten-Andersen, N., Mates, T. E., Toprak, M. S., Stucky, G. D., Zok, F. W., and Waite, J. H. (2009). Metals and the integrity of a biological coating: The cuticle of mussel byssus. *Langmuir* 25, 3323–3326. doi: 10.1021/la8027012
- Hong, S. H., Sun, Y., Tang, C., Cheng, K., Zhang, R., Fan, Q., et al. (2017). Chelator-free and biocompatible melanin nanoplateform with facile-loading gadolinium and copper-64 for bioimaging. *Bioconjug. Chem.* 28, 1925–1930. doi: 10.1021/acs.bioconjchem.7b00245
- Hong, S., Kim, K. Y., Wook, H. J., Park, S. Y., Lee, K. D., Lee, D. Y., et al. (2011). Attenuation of the in vivo toxicity of biomaterials by polydopamine surface modification. *Nanomedicine* 6, 793–801.
- Hong, S., Na, Y. S., Choi, S., Song, I. T., Kim, W. Y., and Lee, H. (2012). Non-covalent self-assembly and covalent polymerization co-contribute to polydopamine formation. *Adv. Funct. Mater.* 22, 4711–4717. doi: 10.1002/adfm.201201156
- Hong, S., Wang, Y., Park, S. Y., and Lee, H. (2018). Progressive fuzzy cation- π assembly of biological catecholamines. *Sci. Adv.* 4:eart7457. doi: 10.1126/sciadv.aat7457
- Huang, N., Zhang, S., Yang, L., Liu, M., Li, H., Zhang, Y., et al. (2015). Multifunctional electrochemical platforms based on the Michael addition/Schiff base reaction of polydopamine modified reduced graphene oxide: Construction and application. *ACS Appl. Mater. Inter.* 7, 17935–17946. doi: 10.1021/acsami.5b04597
- Huang, S., Liang, N., Hu, Y., Zhou, X., and Abidi, N. (2016). Polydopamine-assisted surface modification for bone biosubstitutes. *BioMed. Res. Int.* 2016, 1–9. doi: 10.1155/2016/2389895
- Huang, Y., Liu, Z., Liu, C., Ju, E., Zhang, Y., Ren, J., et al. (2016). Self-assembly of multi-nanozymes to mimic an intracellular antioxidant defense system. *Angew. Chem. Int. Ed.* 55, 6646–6650. doi: 10.1002/anie.201600868
- Jia, L., Han, F., Wang, H., Zhu, C., Guo, Q., Li, J., et al. (2019). Polydopamine-assisted surface modification for orthopaedic implants. *J. Orthop. Translat.* 17, 82–95. doi: 10.1016/j.jot.2019.04.001
- Jia, Z., Xiu, P., Li, M., Xu, X., Shi, Y., Cheng, Y., et al. (2016). Bioinspired anchoring AgNPs onto micro-nanoporous TiO₂ orthopedic coatings: trap-killing of bacteria, surface-regulated osteoblast functions and host responses. *Biomaterials* 75, 203–222. doi: 10.1016/j.biomaterials.2015.10.035
- Jiao, L., Xu, Z., Du, W., Li, H., and Yin, M. (2017). Fast preparation of polydopamine nanoparticles catalyzed by Fe²⁺/H₂O₂ for visible sensitive smartphone-enabled cytosensing. *ACS Appl. Mater. Inter.* 9, 28339–28345. doi: 10.1021/acsami.7b10564
- Kao, H., Chen, C. C., Huang, Y. R., Chu, Y. H., Csík, A., and Ding, S. J. (2019). Metal ion-dependent tailored antibacterial activity and biological properties of polydopamine-coated titanium implants. *Surf. Coat. Technol.* 378:124998. doi: 10.1016/j.surfcoat.2019.124998
- Kaushik, N., Nguyen, L. N., Kim, J. H., Choi, E. H., and Kaushik, N. K. (2020). Strategies for using polydopamine to induce biomineralization of hydroxyapatite on implant materials for bone tissue engineering. *Int. J. Mol. Sci.* 21:6544. doi: 10.3390/ijms21186544
- Khanzada, N. K., Rehman, S., Leu, S. Y., and An, A. K. (2020). Evaluation of anti-bacterial adhesion performance of polydopamine cross-linked graphene oxide RO membrane via *in situ* optical coherence tomography. *Desalination* 479:114339. doi: 10.1016/j.desal.2020.114339
- Kim, W. J., Kim, J., Lee, H., and Hong, S. (2017). *Method of preparing coating film containing nitrogen monoxide on surface of material using catecholamine*. Google Patents:US20140127277A1. Pohang-city, KR: Postech Academy-Industry Foundation.
- Kong, X.-J., Wu, S., Chen, T.-T., Yu, R.-Q., and Chu, X. (2016). MnO₂-induced synthesis of fluorescent polydopamine nanoparticles for reduced glutathione sensing in human whole blood. *Nanoscale* 8, 15604–15610. doi: 10.1039/c6nr04777g
- Ku, S. H., and Park, C. B. (2010). Human endothelial cell growth on mussel-inspired nanofiber scaffold for vascular tissue engineering. *Biomaterials* 31, 9431–9437. doi: 10.1016/j.biomaterials.2010.08.071
- Lakshminarayanan, R., Madhavi, S., and Sim, C. P. C. (2018). *Oxidative polymerization of dopamine: A high-definition multifunctional coatings for electrospun nanofibers-an overview*. London, UK: Intechopen.
- Larosa, V., and Remacle, C. (2018). Insights into the respiratory chain and oxidative stress. *Biosci. Rep.* 38:BSR20171492.

- Lee, D. J., Lee, Y.-T., Zou, R., Daniel, R., and Ko, C.-C. (2017). Polydopamine-laced biomimetic material stimulation of bone marrow derived mesenchymal stem cells to promote osteogenic effects. *Sci. Rep.* 7, 1–14. doi: 10.1155/2016/4851081
- Lee, H. A., Ma, Y., Zhou, F., Hong, S., and Lee, H. (2019). Material-independent surface chemistry beyond polydopamine coating. *Acc. Chem. Res.* 52, 704–713. doi: 10.1021/acs.accounts.8b00583
- Lee, H., Dellatore, S. M., Miller, W. M., and Messersmith, P. B. (2007). Mussel-inspired surface chemistry for multifunctional coatings. *Science* 318, 426–430. doi: 10.1126/science.1147241
- Lee, H., Rho, J., and Messersmith, P. B. (2009). Facile conjugation of biomolecules onto surfaces via mussel adhesive protein inspired coatings. *Adv. Mater.* 21, 431–434. doi: 10.1002/adma.200801222
- Lei, W., Ren, K., Chen, T., Chen, X., Li, B., Chang, H., et al. (2016). Polydopamine nanocoating for effective photothermal killing of bacteria and fungus upon near-infrared irradiation. *Adv. Mater. Interfaces* 3:1600767. doi: 10.1002/admi.201600767
- Li, F., Yu, Y., Wang, Q., Yuan, J., Wang, P., and Fan, X. (2018). Polymerization of dopamine catalyzed by laccase: Comparison of enzymatic and conventional methods. *Enzyme Microb. Technol.* 119, 58–64. doi: 10.1016/j.enzmictec.2018.09.003
- Li, M., Liu, X., Xu, Z., Yeung, K., and Wu, S. (2016). Dopamine modified organic-inorganic hybrid coating for antimicrobial and osteogenesis. *ACS Appl. Mater. Inter.* 8, 33972–33981. doi: 10.1021/acsami.6b09457
- Li, W.-Q., Wang, Z., Hao, S., He, H., Wan, Y., Zhu, C., et al. (2017). Mitochondria-targeting polydopamine nanoparticles to deliver doxorubicin for overcoming drug resistance. *ACS Appl. Mater. Inter.* 9, 16793–16802. doi: 10.1021/acsami.7b01540
- Li, Y., Jiang, C., Zhang, D., Wang, Y., Ren, X., Ai, K., et al. (2017). Targeted polydopamine nanoparticles enable photoacoustic imaging guided chemophotothermal synergistic therapy of tumor. *Acta Biomater* 47, 124–134. doi: 10.1016/j.actbio.2016.10.010
- Li, Y., Yang, W., Li, X., Zhang, X., Wang, C., Meng, X., et al. (2015). Improving osteointegration and osteogenesis of three-dimensional porous $\text{Ti}_6\text{Al}_4\text{V}$ scaffolds by polydopamine-assisted biomimetic hydroxyapatite coating. *ACS Appl. Mater. Inter.* 7, 5715–5724. doi: 10.1021/acsami.5b00331
- Liang, Y., Zhao, X., Hu, T., Han, Y., and Guo, B. (2019). Mussel-inspired, antibacterial, conductive, antioxidant, injectable composite hydrogel wound dressing to promote the regeneration of infected skin. *J. Coll. Inter. Sci.* 556, 514–528. doi: 10.1016/j.jcis.2019.08.083
- Liao, J., He, S., Guo, S., Luan, P., Mo, L., and Li, J. (2019). Antibacterial performance of a mussel-inspired polydopamine-treated Ag/graphene nanocomposite material. *Materials* 12:3360. doi: 10.3390/ma12203360
- Liebscher, J. (2019). Chemistry of polydopamine—Scope, variation, and limitation. *Eur. J. Org. Chem.* 2019, 4976–4994. doi: 10.1002/ejoc.201900445
- Liebscher, J., Mroiczyński, R., Scheidt, H. A., Filip, C., Haßdane, N. D., Turcu, R., et al. (2013). Structure of polydopamine: A never-ending story? *Langmuir* 29, 10539–10548. doi: 10.1021/la4020288
- Lim, K., Chua, R. R. Y., Ho, B., Tambyah, P. A., Hadinoto, K., and Leong, S. S. J. (2015). Development of a catheter functionalized by a polydopamine peptide coating with antimicrobial and antibiofilm properties. *Acta Biomater.* 15, 127–138. doi: 10.1016/j.actbio.2014.12.015
- Lin, J.-H., Yu, C.-J., Yang, Y.-C., and Tseng, W.-L. (2015). Formation of fluorescent polydopamine dots from hydroxyl radical-induced degradation of polydopamine nanoparticles. *Phys. Chem. Chem. Phys.* 17, 15124–15130. doi: 10.1039/c5cp00932d
- Liu, C., Yao, W., Tian, M., Wei, J., Song, Q., and Qiao, W. (2018). Mussel-inspired degradable antibacterial polydopamine/silica nanoparticle for rapid hemostasis. *Biomaterials* 179, 83–95. doi: 10.1016/j.biomaterials.2018.06.037
- Liu, C.-Y., and Huang, C.-J. (2016). Functionalization of polydopamine via the aza-Michael reaction for antimicrobial interfaces. *Langmuir* 32, 5019–5028. doi: 10.1021/acs.langmuir.6b00990
- Liu, F., He, X., Zhang, J., Chen, H., Zhang, H., and Wang, Z. (2015). Controllable synthesis of polydopamine nanoparticles in microemulsions with pH-activatable properties for cancer detection and treatment. *J. Mater. Chem. B* 3, 6731–6739. doi: 10.1039/c5tb01159k
- Liu, H., Qu, X., Tan, H., Song, J., Lei, M., Kim, E., et al. (2019). Role of polydopamine's redox-activity on its pro-oxidant, radical-scavenging, and antimicrobial activities. *Acta Biomater.* 88, 181–196. doi: 10.1016/j.actbio.2019.02.032
- Liu, M., Liu, T., Chen, X., Yang, J., Deng, J., He, W., et al. (2018). Nano-silver-incorporated biomimetic polydopamine coating on a thermoplastic polyurethane porous nanocomposite as an efficient antibacterial wound dressing. *J. Nanobiotechnol.* 16, 1–19.
- Liu, M., Zhou, J., Yang, Y., Zheng, M., Yang, J., and Tan, J. (2015). Surface modification of zirconia with polydopamine to enhance fibroblast response and decrease bacterial activity in vitro: a potential technique for soft tissue engineering applications. *Coll. Surf. B* 136, 74–83. doi: 10.1016/j.colsurfb.2015.06.047
- Liu, Y., Li, Z., Yin, Z., Zhang, H., Gao, Y., Huo, G., et al. (2020). Amplified photoacoustic signal and enhanced photothermal conversion of polydopamine coated gold nanobipyramids for photo-theranostics and synergistic chemotherapy. *ACS Appl. Mater. Inter.* 12, 14866–14875. doi: 10.1021/acsami.9b22979
- Luo, C., Liu, W., Luo, B., Tian, J., Wen, W., Liu, M., et al. (2017). Antibacterial activity and cytocompatibility of chitooligosaccharide-modified polyurethane membrane via polydopamine adhesive layer. *Carbohydr. Polym.* 156, 235–243. doi: 10.1016/j.carbpol.2016.09.036
- Lynge, M. E., van der Westen, R., Postma, A., and Städler, B. (2011). Polydopamine—A nature-inspired polymer coating for biomedical science. *Nanoscale* 3, 4916–4928. doi: 10.1039/c1nr10969c
- Ma, L., Liu, F., Lei, Z., and Wang, Z. (2017). A novel upconversion@polydopamine core@shell nanoparticle based aptameric biosensor for biosensing and imaging of cytochrome c inside living cells. *Biosens. Bioelectron.* 87, 638–645. doi: 10.1016/j.bios.2016.09.017
- Madhurakkat Perikamana, S. K., Lee, J., Lee, Y. B., Shin, Y. M., Lee, E. J., Mikos, A. G., et al. (2015). Materials from mussel-inspired chemistry for cell and tissue engineering applications. *Biomacromolecules* 16, 2541–2555. doi: 10.1021/acs.biomac.5b00852
- Maier, G. P., and Butler, A. (2017). Siderophores and mussel foot proteins: the role of catechol, cations, and metal coordination in surface adhesion. *JBC J. Biol. Inorg. Chem.* 22, 739–749. doi: 10.1007/s00775-017-1451-6
- Mallinson, D., Mullen, A. B., and Lamprou, D. A. (2018). Probing polydopamine adhesion to protein and polymer films: microscopic and spectroscopic evaluation. *J. Mater. Sci.* 53, 3198–3209. doi: 10.1007/s10853-017-1806-y
- Maruthapandi, M., Natan, M., Jacobi, G., Banin, E., Luong, J. H., and Gedanken, A. (2019). Antibacterial activity against Methicillin-resistant *Staphylococcus aureus* of colloidal polydopamine prepared by carbon dot stimulated polymerization of dopamine. *Nanomaterials* 9:1731. doi: 10.3390/nano9121731
- Matai, I., Garg, M., Rana, K., and Singh, S. (2019). Polydopamine functionalized hydrogel beads as magnetically separable antibacterial materials. *RSC Adv.* 9, 13444–13457. doi: 10.1039/c9ra00623k
- Meng, H., Forooshani, P. K., Joshi, P. U., Osborne, J., Mi, X., Meingast, C., et al. (2019). Biomimetic recyclable microgels for on-demand generation of hydrogen peroxide and antipathogenic application. *Acta Biomater.* 83, 109–118. doi: 10.1016/j.actbio.2018.10.037
- Miao, Z.-H., Wang, H., Yang, H., Li, Z.-L., Zhen, L., and Xu, C.-Y. (2015). Intrinsically Mn^{2+} -chelated polydopamine nanoparticles for simultaneous magnetic resonance imaging and photothermal ablation of cancer cells. *ACS Appl. Mater. Inter.* 7, 16946–16952. doi: 10.1021/acsami.5b06265
- Moulay, S. (2018). Recent trends in mussel-inspired catechol-containing polymers (A Review). *Orient. J. Chem.* 34, 1153–1197. doi: 10.13005/ojc/340301
- Neethu, S., Midhun, S. J., Radhakrishnan, E., and Jyothis, M. (2020). Surface functionalization of central venous catheter with mycofabricated silver nanoparticles and its antibiofilm activity on multidrug resistant *Acinetobacter baumannii*. *Microb. Pathog.* 138:103832. doi: 10.1016/j.micpath.2019.103832
- Nieto, C., Vega, M. A., Marcelo, G., and del Valle, E. M. M. (2018). Polydopamine nanoparticles kill cancer cells. *RSC Adv.* 8, 36201–36208. doi: 10.1039/c8ra05586f
- Niyonshuti, I. I., Krishnamurthi, V. R., Okyere, D., Song, L., Benamara, M., Tong, X., et al. (2020). Polydopamine surface coating synergizes the antimicrobial activity of silver nanoparticles. *ACS Appl. Mater. Interfaces* 12, 40067–40077. doi: 10.1021/acsami.0c10517
- Park, D., Kim, J., Lee, Y. M., Park, J., and Kim, W. J. (2016). Polydopamine hollow nanoparticle functionalized with N-diazeniumdiolates as a nitric oxide

- delivery carrier for antibacterial therapy. *Adv. Healthc. Mater.* 5, 2019–2024. doi: 10.1002/adhm.201600150
- Park, J., Moon, H., and Hong, S. (2019). Recent advances in melanin-like nanomaterials in biomedical applications: A mini review. *Biomater. Res.* 23, 1–10.
- Patel, K., Singh, N., Yadav, J., Nayak, J. M., Sahoo, S. K., Lata, J., et al. (2018). Polydopamine films change their physicochemical and antimicrobial properties with a change in reaction conditions. *Phys. Chem. Chem. Phys.* 20, 5744–5755. doi: 10.1039/c7cp08406d
- Poinard, B., Kamaluddin, S., Tan, A. Q. Q., Neoh, K. G., and Kah, J. C. Y. (2019). Polydopamine coating enhances mucopenetration and cell uptake of nanoparticles. *ACS Appl. Mater. Inter.* 11, 4777–4789. doi: 10.1021/acsami.8b18107
- Priyam, A., Nagar, P., Sharma, A. K., and Kumar, P. (2018). Mussel-inspired polydopamine-polyethylenimine conjugated nanoparticles as efficient gene delivery vectors for mammalian cells. *Coll. Surf. B* 161, 403–412. doi: 10.1016/j.colsurfb.2017.10.063
- Qian, Y., Zhou, X., Zhang, F., Diekwisch, T. G., Luan, X., Yang, J., et al. (2019). PCL scaffold modification including silver impregnation, collagen coating, and electrospinning significantly improve biocompatibility, antimicrobial, and osteogenic properties for orofacial tissue regeneration. *ACS Appl. Mater. Inter.* 11, 37381–37396. doi: 10.1021/acsami.9b07053
- Qiu, W. Z., Yang, H. C., and Xu, Z. K. (2018). Dopamine-assisted co-deposition: An emerging and promising strategy for surface modification. *Adv. Coll. Interface Sci.* 256, 111–125. doi: 10.1016/j.cis.2018.04.011
- Rahimnejad, M., and Zhong, W. (2017). Mussel-inspired hydrogel tissue adhesives for wound closure. *RSC Adv.* 7, 47380–47396. doi: 10.1039/c7ra06743g
- Ran, H.-H., Cheng, X., Gao, G., Sun, W., Jiang, Y.-W., Zhang, X., et al. (2020). Colistin-loaded polydopamine nanospheres uniformly decorated with silver nanodots: A nanohybrid platform with improved antibacterial and antibiofilm performance. *ACS Appl. Bio Mater.* 3, 2438–2448. doi: 10.1021/acsabm.0c00163
- Ryu, J. H., Messersmith, P. B., and Lee, H. (2018). Polydopamine surface chemistry: A decade of discovery. *ACS Appl. Mater. Inter.* 10, 7523–7540. doi: 10.1021/acsami.7b19865
- Sadrearhami, Z., Shafiee, F. N., Ho, K. K., Kumar, N., Krasowska, M., Blencowe, A., et al. (2019). Antibiofilm nitric oxide-releasing polydopamine coatings. *ACS Appl. Mater. Inter.* 11, 7320–7329. doi: 10.1021/acsami.8b16853
- Singh, I., Priyam, A., Jha, D., Dhawan, G., Gautam, H. K., and Kumar, P. (2020). Polydopamine-aminoglycoside nanoconjugates: Synthesis, characterization, antimicrobial evaluation and cytocompatibility. *Mater. Sci. Eng. C* 107:110284. doi: 10.1016/j.msec.2019.110284
- Solano, F. (2014). Melanins: Skin pigments and much more—types, structural models, biological functions, and formation routes. *N. J. Sci.* 2014:498276.
- Solano, F. (2017). Melanin and melanin-related polymers as materials with biomedical and biotechnological applications—Cuttlefish ink and mussel foot proteins as inspired biomolecules. *Int. J. Mol. Sci.* 18:1561. doi: 10.3390/ijms18071561
- Song, J., Chen, P., and Liu, W. (2019). A superhydrophobic and antibacterial surface coated on cotton fabrics by polydopamine. *Fibers Polym.* 20, 1380–1386. doi: 10.1007/s12221-019-1183-z
- Song, Y., Jiang, H., Wang, B., Kong, Y., and Chen, J. (2018). Silver-incorporated mussel-inspired polydopamine coatings on mesoporous silica as an efficient nanocatalyst and antimicrobial agent. *ACS Appl. Mater. Inter.* 10, 1792–1801. doi: 10.1021/acsami.7b18136
- Su, L., Yu, Y., Zhao, Y., Liang, F., and Zhang, X. (2016). Strong antibacterial polydopamine coatings prepared by a shaking-assisted method. *Sci. Rep.* 6:24420.
- Tang, L., Livi, K. J., and Chen, K. L. (2015). Polysulfone membranes modified with bioinspired polydopamine and silver nanoparticles formed *in situ* to mitigate biofouling. *Environ. Sci. Technol. Lett.* 2, 59–65. doi: 10.1021/acs.estlett.5b00008
- Tang, L., Mo, S., Liu, S. G., Liao, L. L., Li, N. B., and Luo, H. Q. (2018). Synthesis of fluorescent polydopamine nanoparticles by Michael addition reaction as an analysis platform to detect iron ions and pyrophosphate efficiently and construction of an IMPLICATION logic gate. *Sensor Actuat B- Chem.* 255, 754–762. doi: 10.1016/j.snb.2017.08.069
- Tian, Y., and Lei, M. (2019). Polydopamine-based composite nanoparticles with redox-labile polymer shells for controlled drug release and enhanced chemo-photothermal therapy. *Nanoscale Res. Lett.* 14, 1–10.
- Tyo, A. G., Welch, S., Hennenfent, M., Forooshani, P. K., Lee, B. P., and Rajachar, R. M. (2019). Development and characterization of an antimicrobial polydopamine coating for conservation of Humpback Whales. *Front. Chem.* 7:618. doi: 10.3389/fchem.2019.00618
- Wang, B. B., Quan, Y. H., Xu, Z. M., and Zhao, Q. (2020). Preparation of highly effective antibacterial coating with polydopamine/chitosan/silver nanoparticles via simple immersion. *Prog. Org. Coat.* 149:105967. doi: 10.1016/j.porgcoat.2020.105967
- Wang, C., Zhou, J., Wang, P., He, W., and Duan, H. (2016). Robust nanoparticle–DNA conjugates based on mussel-inspired polydopamine coating for cell imaging and tailored self-assembly. *Bioconjug. Chem.* 27, 815–823. doi: 10.1021/acs.bioconjugchem.6b00021
- Wang, D., Wu, H., Zhou, J., Xu, P., Wang, C., Shi, R., et al. (2018). In situ one-pot synthesis of MOF–polydopamine hybrid nanogels with enhanced photothermal effect for targeted cancer therapy. *Adv. Sci.* 5:1800287. doi: 10.1002/adv.201800287
- Wang, K., Ma, Q., Zhang, Y., Wang, S., and Han, G. (2020). Ag NPs-assisted synthesis of stable Cu NPs on PET fabrics for antibacterial and electromagnetic shielding performance. *Polymers* 12:783. doi: 10.3390/polym12040783
- Wang, L., Yang, X., Cao, W., Shi, C., Zhou, P., Li, Q., et al. (2017). Mussel-inspired deposition of copper on titanium for bacterial inhibition and enhanced osseointegration in a periprosthetic infection model. *RSC Adv.* 7, 51593–51604. doi: 10.1039/c7ra10203h
- Wang, Q., Zhang, R., Lu, M., You, G., Wang, Y., Chen, G., et al. (2017). Bioinspired polydopamine-coated hemoglobin as potential oxygen carrier with antioxidant properties. *Biomacromolecules* 18, 1333–1341. doi: 10.1021/acs.biomac.7b00077
- Wang, X., Wang, N., Yang, Y., Wang, X., Liang, J., Tian, X., et al. (2019). Polydopamine nanoparticles carrying tumor cell lysate as a potential vaccine for colorectal cancer immunotherapy. *Biomater. Sci.* 7, 3062–3075. doi: 10.1039/c9bm00010k
- Wang, X., Zhang, J., Wang, Y., Wang, C., Xiao, J., Zhang, Q., et al. (2016). Multi-responsive photothermal-chemotherapy with drug-loaded melanin-like nanoparticles for synergetic tumor ablation. *Biomaterials* 81, 114–124. doi: 10.1016/j.biomaterials.2015.11.037
- Wang, Z., Zhang, J., Chen, F., and Cai, K. (2017). Fluorescent miRNA analysis enhanced by mesopore effects of polydopamine nanoquenchers. *Analyst* 142, 2796–2804. doi: 10.1039/c7an00528h
- Wen, L., Wanpei, H., Qian, L., Xu, L., Rongsheng, C., Hongwei, N., et al. (2020). Antibacterial properties of Ag/TiO₂/PDA nanofilm on anodized 316L stainless steel substrate under illumination by a normal flashlight. *J. Mater. Sci.* 2020, 1–13. doi: 10.1007/s10853-020-04610-w
- Wu, C., Zhang, G., Xia, T., Li, Z., Zhao, K., Deng, Z., et al. (2015). Bioinspired synthesis of polydopamine/Ag nanocomposite particles with antibacterial activities. *Mater. Sci. Eng. C* 55, 155–165. doi: 10.1016/j.msec.2015.05.032
- Wu, H., Liu, Y., Huang, J., Mao, L., Chen, J., and Li, M. (2018). Preparation and characterization of antifouling and antibacterial polysulfone ultrafiltration membranes incorporated with a silver–polydopamine nanohybrid. *J. Appl. Polym. Sci.* 135:46430. doi: 10.1002/app.46430
- Wu, K., Yang, Y., Zhang, Y., Deng, J., and Lin, C. (2015). Antimicrobial activity and cytocompatibility of silver nanoparticles coated catheters via a biomimetic surface functionalization strategy. *Int. J. Nanomed.* 10, 7241–7252. doi: 10.2147/ijn.s92307
- Wu, Y., Zhou, Y., Xu, H., Liu, Q., Li, Y., Zhang, L., et al. (2018). Highly active, superstable, and biocompatible Ag/polydopamine/g-C₃N₄ bactericidal photocatalyst: synthesis, characterization, and mechanism. *ACS Sust. Chem. Eng.* 6, 14082–14094. doi: 10.1021/acssuschemeng.8b02620
- Xiong, Y., Xu, Z., and Li, Z. (2019). Polydopamine-based nanocarriers for photosensitizer delivery. *Front. Chem.* 7:471. doi: 10.3389/fchem.2019.00471
- Xu, Q., Chang, M., Zhang, Y., Wang, E., Xing, M., Gao, L., et al. (2020). PDA/Cu bioactive hydrogel with "Hot Ions Effect" for inhibition of drug-resistant bacteria and enhancement of infectious skin wound healing. *ACS Appl. Mater. Interfaces* 12, 31255–31269. doi: 10.1021/acsami.0c08890
- Yan, J., Zhou, W., Jia, Z., Xiong, P., Li, Y., Wang, P., et al. (2018). Endowing polyetheretherketone with synergistic bactericidal effects and improved

- osteogenic ability. *Acta Biomater.* 79, 216–229. doi: 10.1016/j.actbio.2018.08.037
- Yang, P., Gu, Z., Zhu, F., and Li, Y. (2020a). Structural and functional tailoring of melanin-like polydopamine radical scavengers. *CCS Chemistry* 2, 128–138. doi: 10.31635/ccschem.020.201900077
- Yang, P., Zhang, S., Chen, X., Liu, X., Wang, Z., and Li, Y. (2020b). Recent developments in polydopamine fluorescent nanomaterials. *Mater. Horizons* 7, 746–761. doi: 10.1039/c9mh01197h
- Yang, X., Niu, X., Mo, Z., Guo, R., Liu, N., Zhao, P., et al. (2019). Electrochemical chiral interface based on the Michael addition/Schiff base reaction of polydopamine functionalized reduced graphene oxide. *Electrochim. Acta* 319, 705–715. doi: 10.1016/j.electacta.2019.07.040
- Yang, Z., Wu, Y., Wang, J., Cao, B., and Tang, C. Y. (2016). *In situ* reduction of silver by polydopamine: A novel antimicrobial modification of a thin-film composite polyamide membrane. *Environ. Sci. Technol.* 50, 9543–9550. doi: 10.1021/acs.est.6b01867
- Yao, L., He, C., Chen, S., Zhao, W., Xie, Y., and Sun, S. (2018). Co-deposition of polydopamine and zwitterionic polymer on membrane surface with enhanced stability and antibiofouling property. *Langmuir* 35, 1430–1439. doi: 10.1021/acs.langmuir.8b01621
- Yeroslavsky, G., Girshevitz, O., Foster-Frey, J., Donovan, D. M., and Rahimpour, S. (2015). Antibacterial and antibiofilm surfaces through polydopamine-assisted immobilization of lysostaphin as an antibacterial enzyme. *Langmuir* 31, 1064–1073. doi: 10.1021/la503911m
- Yeroslavsky, G., Lavi, R., Alishaev, A., and Rahimpour, S. (2016). Sonochemically-produced metal-containing polydopamine nanoparticles and their antibacterial and antibiofilm activity. *Langmuir* 32, 5201–5212. doi: 10.1021/acs.langmuir.6b00576
- Yilmaz, A. (2020). The employment of a conformal polydopamine thin layer reduces the cytotoxicity of silver nanoparticles. *Turk. J. Zool.* 44, 126–133. doi: 10.3906/zoo-1912-38
- Yuan, Z., Tao, B., He, Y., Liu, J., Lin, C., Shen, X., et al. (2019). Biocompatible MoS₂/PDOPA-RGD coating on titanium implant with antibacterial property via intrinsic ROS-independent oxidative stress and NIR irradiation. *Biomaterials* 217:119290. doi: 10.1016/j.biomaterials.2019.119290
- Yun'an Qing, L. C., Li, R., Liu, G., Zhang, Y., Tang, X., Wang, J., et al. (2018). Potential antibacterial mechanism of silver nanoparticles and the optimization of orthopedic implants by advanced modification technologies. *Int. J. Nanomed.* 13:3311. doi: 10.2147/ijn.s165125
- Yuwen, L., Sun, Y., Tan, G., Xiu, W., Zhang, Y., Weng, L., et al. (2018). MoS₂@polydopamine-Ag nanosheets with enhanced antibacterial activity for effective treatment of *Staphylococcus aureus* biofilms and wound infection. *Nanoscale* 10, 16711–16720. doi: 10.1039/c8nr04111c
- Zhang, C., Gong, I., Xiang, I., Du, Y., Hu, W., and Zeng, H. (2017). Deposition and adhesion of polydopamine on the surfaces of varying wettability. *ACS Appl. Mater. Interfaces* 9, 30943–30950. doi: 10.1021/acsami.7b09774
- Zhang, Q., Wang, Y., Zhang, W., Hickey, M. E., Lin, Z., Tu, Q., et al. (2019). *In situ* assembly of well-dispersed Ag nanoparticles on the surface of polylactic acid-Au@polydopamine nanofibers for antimicrobial applications. *Coll. Surf. B* 184:110506. doi: 10.1016/j.colsurfb.2019.110506
- Zhao, H., Zeng, Z., Liu, L., Chen, J., Zhou, H., Huang, L., et al. (2018). Polydopamine nanoparticles for the treatment of acute inflammation-induced injury. *Nanoscale* 10, 6981–6991. doi: 10.1039/c8nr00838h
- Zhao, Y.-Y., Li, L., Yu, R.-Q., Chen, T.-T., and Chu, X. (2017). CoOOH-induced synthesis of fluorescent polydopamine nanoparticles for the detection of ascorbic acid. *Anal. Methods* 9, 5518–5524. doi: 10.1039/c7ay01566f
- Zheng, A., Zhang, X., Huang, Y., Cai, Z., Liu, X., and Liu, J. (2018). Polydopamine-assisted versatile modification of a nucleic acid probe for intracellular microRNA imaging and enhanced photothermal therapy. *RSC Adv.* 8, 6781–6788. doi: 10.1039/c8ra00261d
- Zhou, C., Song, H., Loh, J. L. C., She, J., Deng, L., and Liu, B. (2018). Grafting antibiofilm polymer hydrogel film onto catheter by SARA SI-ATRP. *J. Biomater. Sci., Polym. Ed.* 29, 2106–2123. doi: 10.1080/09205063.2018.1507268
- Zhou, L., Li, X., Wang, K., Shen, F., Zhang, L., Li, P., et al. (2020). Cu||-loaded polydopamine coatings with *in situ* nitric oxide generation function for improved hemocompatibility. *Regen. Biomater.* 7, 153–160. doi: 10.1093/rb/rbz043
- Zhou, P., Deng, Y., Lyu, B., Zhang, R., Zhang, H., Ma, H., et al. (2014). Rapidly-deposited polydopamine coating via high temperature and vigorous stirring: Formation, characterization and biofunctional evaluation. *PLoS One* 9:e113087. doi: 10.1371/journal.pone.0113087
- Zhou, T., Yan, L., Xie, C., Li, P., Jiang, L., Fang, J., et al. (2019). A mussel-inspired persistent ROS-scavenging, electroactive, and osteoinductive scaffold based on electrochemical-driven *in situ* nanoassembly. *Small* 15:1805440. doi: 10.1002/smll.201805440
- Zhu, Y., Xin, N., Qiao, Z., Chen, S., Zeng, I., Zhang, Y., et al. (2019). Novel tumor-microenvironment-based sequential catalytic therapy by Fe (II)-engineered polydopamine nanoparticles. *ACS Appl. Mater. Inter.* 11, 43018–43030. doi: 10.1021/acsami.9b17951
- Zhu, Z., and Su, M. (2017). Polydopamine nanoparticles for combined chemo- and photothermal cancer therapy. *Nanomaterials* 7:160. doi: 10.3390/nano7070160
- Zou, Y., Chen, X., Yang, P., Liang, G., Yang, Y., Gu, Z., et al. (2020). Regulating the absorption spectrum of polydopamine. *Sci. Adv.* 6:eabb4696. doi: 10.1126/sciadv.abb4696

Conflict of Interest: The authors declare that the research was conducted in the absence of any commercial or financial relationships that could be construed as a potential conflict of interest.

Copyright © 2021 Singh, Dhawan, Gupta and Kumar. This is an open-access article distributed under the terms of the Creative Commons Attribution License (CC BY). The use, distribution or reproduction in other forums is permitted, provided the original author(s) and the copyright owner(s) are credited and that the original publication in this journal is cited, in accordance with accepted academic practice. No use, distribution or reproduction is permitted which does not comply with these terms.



A Study of the Disruptive Effect of the Acetate Fraction of *Punica granatum* Extract on *Cryptococcus* Biofilms

Paulo C. M. Villis^{1†}, Alessandra T. de Macedo^{2†}, Haryne L. A. Furtado^{2†}, Pedro H. C. Fontenelle², Ingrid S. Gonçalves¹, Thayariane L. Mendes², Brenda L. A. Motta², Pedro L. L. Marinho², Aruanã J. M. C. R. Pinheiro³, Lídio G. Lima-Neto³, Cristina A. Monteiro⁴, Luis C. N. da Silva⁵, Gabriella F. Ferreira⁶, Rodrigo A. Holanda⁷ and Julliana R. A. Santos^{2*}

OPEN ACCESS

Edited by:

Hemda Garelick,
Middlesex University, United Kingdom

Reviewed by:

Ashutosh Singh,
University of Lucknow, India
Janaina De Cássia Orlandi Sardi,
University of Campinas, Brazil

*Correspondence:

Julliana R. A. Santos
julliana.santos@ceuma.br

[†] These authors have contributed
equally to this work

Specialty section:

This article was submitted to
Antimicrobials, Resistance
and Chemotherapy,
a section of the journal
Frontiers in Microbiology

Received: 31 May 2020

Accepted: 18 December 2020

Published: 18 January 2021

Citation:

Villis PCM, de Macedo AT, Furtado HLA, Fontenelle PHC, Gonçalves IS, Mendes TL, Motta BLA, Marinho PLL, Pinheiro AJMCR, Lima-Neto LG, Monteiro CA, da Silva LCN, Ferreira GF, Holanda RA and Santos JRA (2021) A Study of the Disruptive Effect of the Acetate Fraction of *Punica granatum* Extract on *Cryptococcus* Biofilms. *Front. Microbiol.* 11:568258. doi: 10.3389/fmicb.2020.568258

¹ Laboratório de Eletroquímica e Biotecnologia, Universidade Ceuma, São Luís, Brazil, ² Laboratório de Microbiologia Ambiental, Universidade Ceuma, São Luís, Brazil, ³ Laboratório das Infecções do Trato Respiratório, Universidade Ceuma, São Luís, Brazil, ⁴ Laboratório de Microbiologia Aplicada, Universidade Ceuma, São Luís, Brazil, ⁵ Laboratório de Patogenicidade Microbiana, Universidade Ceuma, São Luís, Brazil, ⁶ Programa Multicêntrico de Pós-Graduação em Bioquímica e Biologia Molecular, Departamento de Farmácia, Universidade Federal de Juiz de Fora (Campus Avançado Governador Valadares), Governador Valadares, Brazil, ⁷ Laboratório de Biologia Molecular de Microrganismos Patogênicos, Universidade Ceuma, São Luís, Brazil

Cryptococcosis, caused by yeasts of the genus *Cryptococcus*, is an infectious disease with a worldwide distribution. *Cryptococcus neoformans* and *Cryptococcus gattii* are the species that commonly cause this disease in humans; however, infections caused by *Cryptococcus laurentii*, especially in immunocompromised patients, are increasingly being reported. Owing to the increase in the resistance of fungi to antifungals, and a lack of treatment options, it is important to seek new therapeutic alternatives such as natural products. Among these are plant species such as *Punica granatum*, which is used in folk medicine to treat various diseases. This study aimed to evaluate the activity of the acetate fraction of *P. granatum* leaf extract against environmental and clinical isolates of *Cryptococcus*. Three environmental isolates of *C. laurentii*, PMN, PMA, and PJJ II, isolated from soils of different municipalities in the state of Maranhão, a clinical isolate, *C. gattii*, from a patient with neurocryptococcosis, and a standard strain of *C. gattii* (ATCC 32068) were used. The minimum and fractional inhibitory concentrations (MIC and FIC, respectively) and time-kill curve of the extract and fluconazole were determined to assess the susceptibility profile of the fungal isolates. Larvae of *Tenebrio molitor* were infected with *Cryptococcus* strains, and the effects of acetate fraction of *P. granatum* extract and fluconazole on the survival and fungal burden were determined. The extract activity was tested against pre-formed biofilms. The acetate fraction of *P. granatum* extract showed promising antifungal activity against all the species of *Cryptococcus* evaluated in this study, with an MIC value lower than that of fluconazole. The indices obtained in the FIC test indicated that the antimicrobial effect of the combination of the extract and antifungal was indifferent for 80% of the isolates. The *P. granatum* acetate fraction reduced the pre-formed biofilm of some isolates, showing better activity than

fluconazole, which is consistent with results from fluorescence microscopy. This is the first study on the use of *P. granatum* and its ability to inhibit *Cryptococcus* biofilms; therefore, further studies and tests are needed to investigate the components and mechanism of action of *P. granatum* against cryptococcosis agents.

Keywords: *Cryptococcus gattii*, *Cryptococcus laurentii*, biofilm, *Punica granatum*, cryptococcosis

INTRODUCTION

Cryptococcosis is a globally distributed fungal infection caused by species of the genus *Cryptococcus* (May et al., 2016), which are encapsulated yeasts found in the environment. The two most clinically prevalent species in humans are *Cryptococcus neoformans* and *Cryptococcus gattii* (Maziarz and Perfect, 2016; Castro-Láinez et al., 2019); however, there has been an increase in cryptococcal infections caused by an unusual species, *Cryptococcus laurentii* (Santos et al., 2016).

Such infections occur through the inhalation of propagules present in the environment. These yeasts can cause lung infection and show tropism in the central nervous system (CNS), which can cause meningoencephalitis, the severe form of the disease. Cryptococcal species have several virulence factors which allow them to progress from latent infection to disease in immunocompetent individuals as well as in immunosuppressed patients, especially those with HIV/AIDS (Chen et al., 2017).

Cryptococcus laurentii is a rare human pathogen which was previously considered saprophytic and non-pathogenic. Infections caused by this fungus, especially in immunocompromised patients, have been reported (Gupta et al., 2018). *Cryptococcus laurentii* and *Cryptococcus albidus* are responsible for 80% of cases other than those of *C. neoformans* and *C. gattii*. They are capable of causing localized and systemic infections in humans, and their clinical manifestations vary from skin lesions to fungemia (Ajesh and Sreejith, 2012).

Cryptococcus spp. present several virulence factors that contribute to the spread and permanence of the fungus in the body. The main ones include the ability to grow at the temperature of the human body; a polysaccharide capsule which prevents phagocytosis; the production of enzymes such as laccase, superoxide dismutase, phospholipase, and urease; and biofilm formation (Tavares et al., 2019).

Biofilms, which are rich in extracellular polymeric matrices (EPMs), provide protection against phagocyte activity in tissues, and make cryptococcal cells resistant to standard antifungal therapy (Jabra-Rizk et al., 2004). The biofilm of *Cryptococcus* spp. is highly resistant to azole antifungals, whereas amphotericin B (AMB) and its lipid formulations show good efficacy; however, the effective concentrations are above the therapeutic range, and hence cause severe toxicity and renal dysfunction (Kumari et al., 2017).

For the clinical treatment of cryptococcosis, the combination of AMB and 5-fluorocytosine (5FC) is prescribed, although the latter is not available in underdeveloped countries such as Brazil, followed by a maintenance period with fluconazole (Worasilchai et al., 2017). The indiscriminate use of azoles and lack of patient adherence to the correct treatment have promoted an increase

in resistant clinical isolates (Rêgo et al., 2019). Therefore, it is necessary to search for new molecules with antifungal activity. To this end, extracts of natural products are suitable alternatives owing to their low toxicity and high antimicrobial activity. Several studies have shown that plants are rich in active molecules that exhibit medicinal properties (Akroum, 2017).

Punica granatum is a plant that originated in the Middle East but is currently grown across the Mediterranean, China, India, South Africa, and America. It is used in folk medicine to treat various diseases such as ulcers, fever, diarrhea, and microbial infections (Endo et al., 2010). In addition, different parts of *P. granatum*, such as the leaves, flowers, and seeds, have antimicrobial, antioxidant, and antifungal properties (Lavaee et al., 2018). The antifungal activity of *Punica granatum* extract has already been reported against some species of *Candida* (Anibal et al., 2013; Mansourian et al., 2014; Akroum, 2017; Paul et al., 2018) and against dermatophyte fungi (Foss et al., 2014).

The occurrence of infectious diseases is directly linked to the environmental conditions to which people are exposed. Hence, it is essential to design studies that consider the relationship between urban planning, the development of diseases and systemic infections, and above all, the environmental relevance of using plant extracts for the treatment of fungal diseases. Therefore, this study aimed to evaluate the activity of the acetate fraction of *P. granatum* leaf extract against clinical and reference isolates of *C. gattii* and environmental isolates of *C. laurentii*.

MATERIALS AND METHODS

Ethical Aspects

The studies involving human participants were reviewed and approved by the research ethics committee of the CEUMA University (approval number: 2.927.864), considering all ethical aspects that involve the use of human participants, according to Resolution 466/12 of the National Health Council. The participant provided their written informed consent to participate in this study.

Strains

The standard strain of *C. gattii* (ATCC 32068), three environmental isolates of *C. laurentii* from soils of different municipalities in the State of Maranhão (PMN, PMA, and PJJ II), and a clinical isolate of *C. gattii* from a patient with neurocryptococcosis (CEP n° 2.927.864) were obtained, and stored in the Culture collection of the Laboratory of Environmental Microbiology of UNICEUMA.

These samples were seeded and grown on Sabouraud Dextrose Agar (SDA), at a temperature of 28°C for the environmental samples and 37°C for the clinical samples, for a period of 48 h.

Preparation of Acetate Fraction and Antifungals

The leaves of *P. granatum* were obtained from the Herbarium of the Federal University of Maranhão (UFMA) in São Luís - Maranhão, Brazil. They were completely dried at 40°C in a greenhouse, and crushed to obtain a powder, which was mixed with 70% alcohol and occasionally shaken for 7 days at room temperature. The ethyl acetate fraction of pomegranate leaves were obtained as previously described (Marques et al., 2016). The acetate fraction of the lyophilized extract, which was obtained *via* evaporation and drying, was kindly provided by Prof. Dr. Lídio Gonçalves Lima Neto (UNICEUMA).

For the antifungal microdilution test, the acetate powder fraction was diluted in distilled water to a concentration of 1000 µg/mL.

TABLE 1 | Minimum inhibitory concentration (MIC) of acetate fraction of *P. granatum* and fluconazole against isolates of *Cryptococcus* spp.

Strain	MIC (µg/mL)	
	<i>P. granatum</i>	Fluconazole
PNM (<i>C. laurentii</i>)	1.95	32
PMA (<i>C. laurentii</i>)	1.95	32
PJL II (<i>C. laurentii</i>)	1.95	32
<i>Cryptococcus gattii</i> I.C.	15.62	32
ATCC 32068 (<i>C. gattii</i>)	31.25	32

P., Punica; *C.I.*, clinical isolate.

Minimum Inhibitory Concentration (MIC)

The minimum inhibitory concentration (MIC) was determined using a microdilution test in 96-well microplates (Clinical and Laboratory Standards Institute, 2008). The inoculants were prepared from the isolates grown on SDA, by suspending them in 4 mL of sterile saline and comparing them with a McFarland scale

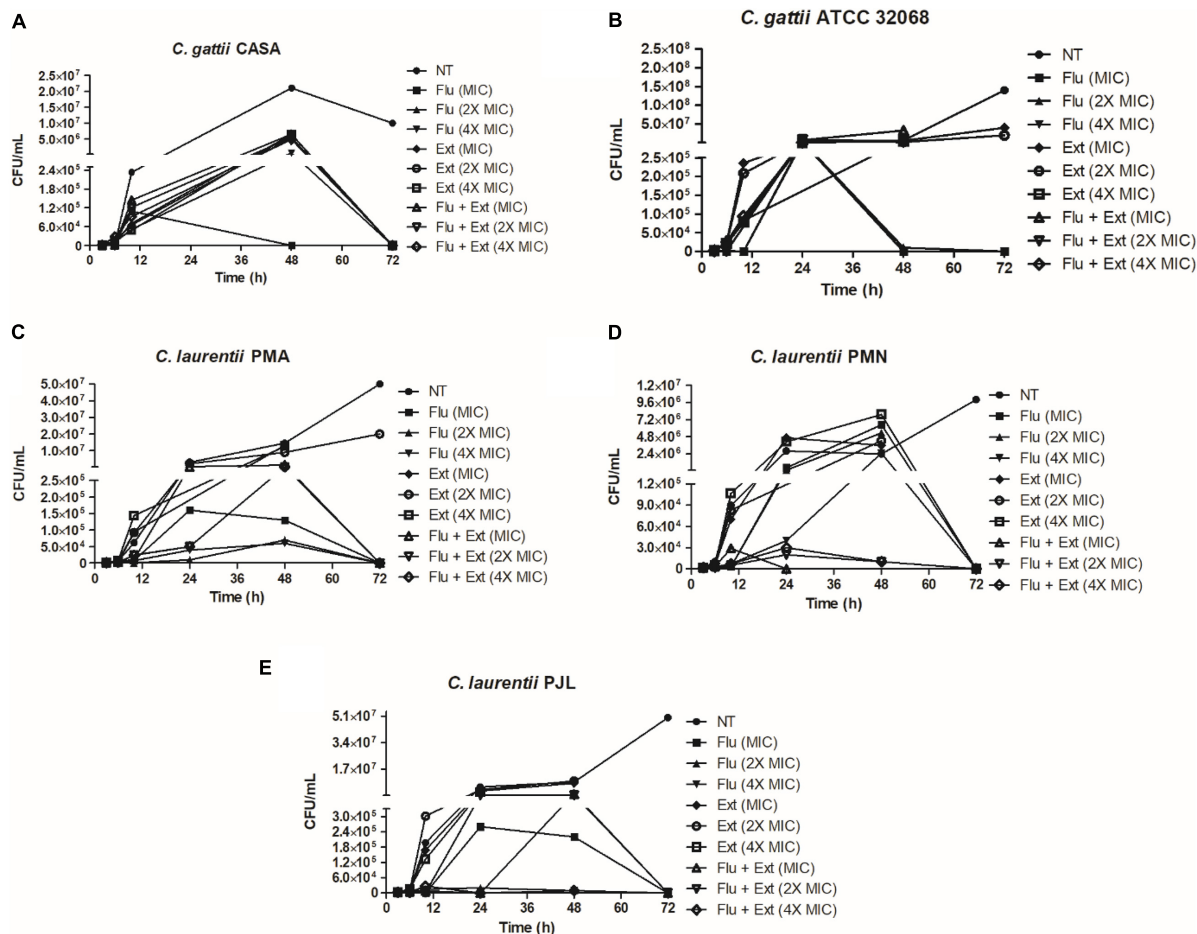


FIGURE 1 | Time-kill curves of fluconazole and acetate fraction of *P. granatum* extract alone or in combination against *Cryptococcus* strains. Time-kill curve were performed with fluconazole or acetate fraction of *P. granatum* extract at 1× MIC, 2× the MIC, and 4× the MIC. **(A)** Time-kill curve performed against *C. gattii* CASA. **(B)** Time-kill curve performed against *C. gattii* ATCC 36068. **(C)** Time-kill curve performed against *C. laurentii* PMA. **(D)** Time-kill curve performed against *C. laurentii* PMN. **(E)** Time-kill curve performed against *C. laurentii* PJL.

TABLE 2 | Fractional inhibitory concentration (FIC) of acetate fraction of *P. granatum* extract against *Cryptococcus* isolates.

Isolated	FIC average	Type of interaction
PMN (<i>C. laurentii</i>)	8.2	Antagonism
PMA (<i>C. laurentii</i>)	–	Indifferent
PJL II (<i>C. laurentii</i>)	3.23	Indifferent
<i>Cryptococcus gattii</i> I.C.	3.73	Indifferent
ATCC 32068 (<i>C. gattii</i>)	1.23	Indifferent

C.I., clinical isolate.

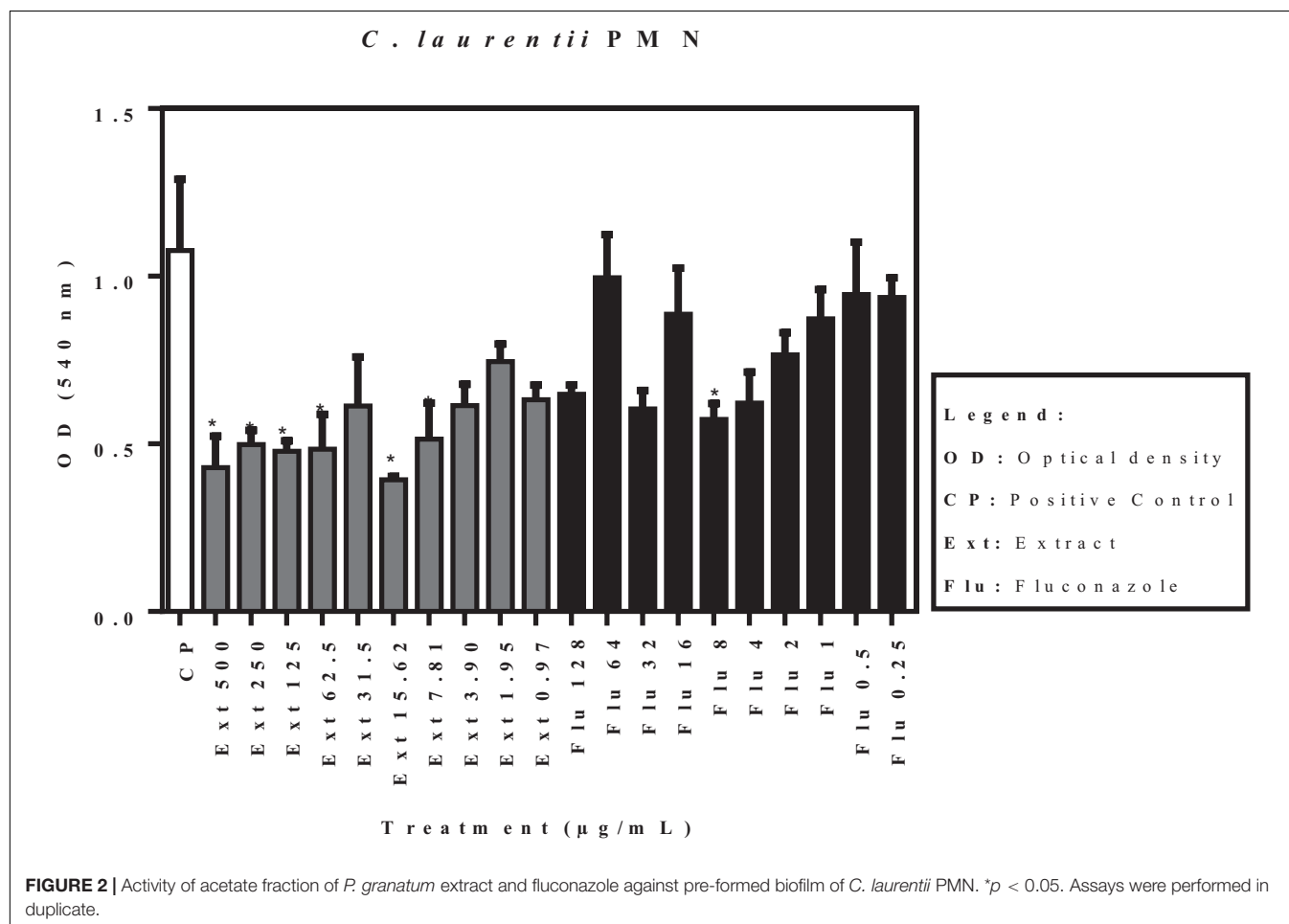
of 0.5×10^6 CFU/mL. Then, they were diluted in RPMI medium to a concentration of 0.5×10^3 CFU/mL. Initially, 100 μ L of RPMI medium was placed in each well; then, 100 μ L of extract was added in the 2nd column alone, whereas serial dilution was performed up to the 11th column, to prepare a concentration range of 500 to 0.97 μ g/mL. Thereafter, 100 μ L inoculum was added to each well, with the exception of the 12th column, which represented the sterility control. The microplates were incubated at 28 or 37°C for 72 h. After the incubation period, a visual reading was performed to determine the MIC. The viability dye, resazurin, was also added to confirm the results.

Time-Kill Curves

An assay was performed to evaluate the time-kill kinetics of the acetate fraction of *P. granatum* extract and fluconazole alone or in combination against *Cryptococcus*. For fluconazole (FLU) and the extract (EXT), the tested concentrations were equal to the MIC, twice the MIC (2 \times the MIC), and four times the MIC (4 \times the MIC) for each strain. In combination, EXT and FLU at MIC, twice the MIC (2 \times the MIC), and four times the MIC (4 \times the MIC) were tested. A 100- μ L inoculum of *Cryptococcus* strain was placed on microtiter plates containing antifungal agent alone or in combination. In sequence, the results were determined by plating an amount of 10 μ L from each well on SDA, followed by incubation at 37°C (clinical isolates) and 28°C (environmental isolates) at different intervals for 72 h prior to colony counting. After the incubation period, the CFU count was performed (Santos et al., 2012).

Fractional Inhibitory Concentration (FIC)

The fractional inhibitory concentration (FIC) values were determined using a checkerboard microdilution, in which fluconazole (FLU) and the extract (EXT) were tested in combination. Antifungal concentrations varied from 0.25 to 128 μ g/mL.



RPMI medium and RPMI medium + inoculum were added to the sterility and growth control wells, respectively. Fifty microliters of RPMI medium was placed in each well; then, the extract was added and dilution of the 2nd to 11th columns was started. In the 2nd column, an additional 37.5 μ L of RPMI medium, followed by 12.5 μ L of extract, made up to 100 μ L, was added. Finally, 10 μ L of fungal inoculum was added to each well, with the exception of the sterility control wells. The samples were incubated at 28°C or 37°C, in the range of 16 to 20 h.

Then, the FIC was determined using the formula:

$$FIC = \frac{MIC \text{ Fluconazole in combination}}{MIC \text{ Fluconazole}} + \frac{MIC \text{ Extract in combination}}{MIC \text{ Extract}}$$

The index was calculated for all combinations, and the results were expressed as the arithmetic means of the FIC. The interaction was classified as synergism for $FIC \leq 0.5$, indifferent for $0.5 > FIC \leq 4.0$, and antagonism for $FIC > 4.0$ (Odds, 2003).

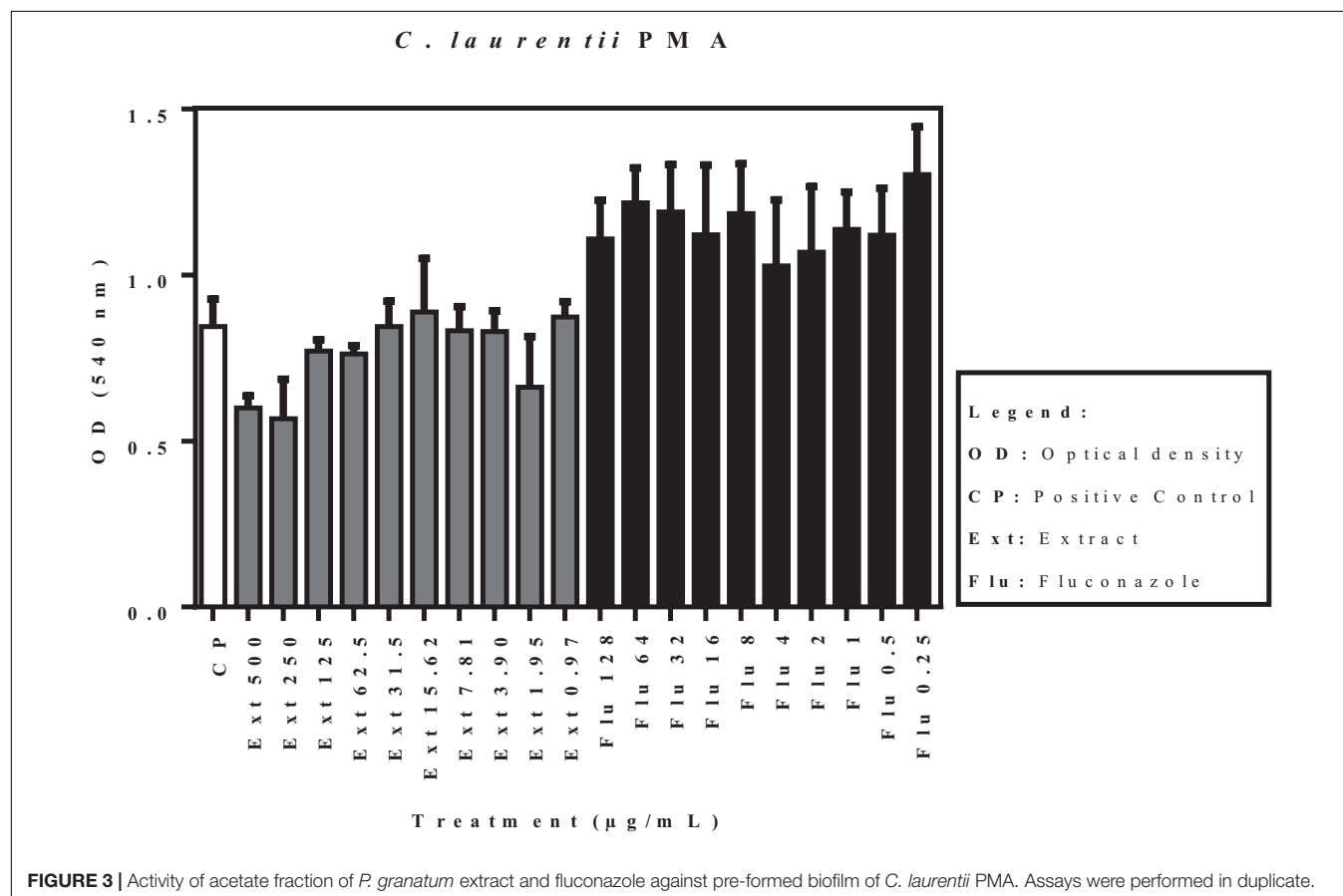
Activity of Acetate Fraction of *P. granatum* Extract Against Pre-formed Biofilm

Biofilms were prepared according to the methodology of Brillhante et al. (2015) and Kumari et al. (2017), with

modifications. Firstly, the samples were cultured on plates containing Sabouraud agar and incubated at 37°C for 48 h. After subculturing in Sabouraud broth, and incubation at 37°C for 24 h, the sample suspensions were centrifuged at 3000 rpm for 10 min; then, the supernatants were discarded, and the pellets were washed twice with PBS. Subsequently, the cells were re-suspended in RPMI medium to obtain a concentration of 1×10^6 cells/mL. Tests were performed in triplicate in 96-well plates, wherein, initially, 100 μ L of the fungal suspension was added to 100 μ L of RPMI medium and incubated at 37°C for 48 h; soon after, the samples were exposed to 100 μ L of the extract and 100 μ L of fluconazole and incubated at 37°C for 48 h. Then, the plates were washed twice with PBS to remove non-adhered cells. To evaluate the viability of the biofilm, 100 μ L of MTT was added, followed by incubation at 37°C for 4 h, and a reading was performed using a spectrophotometer at 492 nm.

Fluorescence Microscopy Assay

The fluorescence microscopy assay was performed in duplicate, according to the methodology of Jurcisek et al. (2011) with modifications. A 24-well plates containing coverslips were used. The samples *C. laurentii* PMA, *C. gattii* 32068 ATCC, and *C. gattii* CASA were previously grown on SDA for 72 h. Inocula were adjusted to 1 to 5×10^6 cells/mL. A 500 μ L of inoculum was added to each well, and 500 μ L of RPMI in the well corresponding to the negative control. The plates were incubated



for an hour and a half at 37°C (clinical strain and ATCC) and 28°C (environmental strain). Subsequently, the wells were washed twice with PBS and 500 µL of RPMI was added. The plates were incubated for 24 h. After the incubation period, 500 µL of the acetate fraction of *P. granatum* extract, fluconazole and combination at MIC, 2× MIC, 4× MIC concentrations were added. Then, the plates were incubated again for 24 h. They were washed twice with PBS, fixed with 500 µL of methanol for 10 min, and finally, the coverslips were stained with Acridine Orange (10 µg/mL) and mounted on slides. The reading was performed under a fluorescence microscope (Imager Z2, ZEISS, Germany). The sum of fluorescences was used to evaluate disturbances on biofilm. Assays were performed in triplicate.

Survival Curve and Quantification of Fungal Burden in Larvae of *Tenebrio molitor*

Larvae of *Tenebrio molitor* were used in all experiments. Larvae were inoculated with 10 µL of 10³ (*C. gattii* CASA) or 10⁵ CFU/larvae (*C. laurentii* PMA, PJI, PMN and ATCC) or PBS only (control). To verify efficacy of treatment, fluconazole and/or acetate fraction of *P. granatum* extract (MIC) was administered once from 1 day post infection (d.p.i.) Larvae were monitored twice daily for survival (de Souza et al., 2015).

Groups of larvae of *Tenebrio molitor* ($n = 10/\text{group}$) were inoculated with 10³ (*C. gattii* CASA) or 10⁵ CFU/larvae (*C. laurentii* PMA, PJI, PMN, and ATCC 32068) or PBS only (control) to obtain larvae homogenates in 1 mL of PBS at 3 days post inoculation. The larvae homogenates were plated onto SDA with chloramphenicol for the determination of colony forming units (CFU) as described (de Souza et al., 2015).

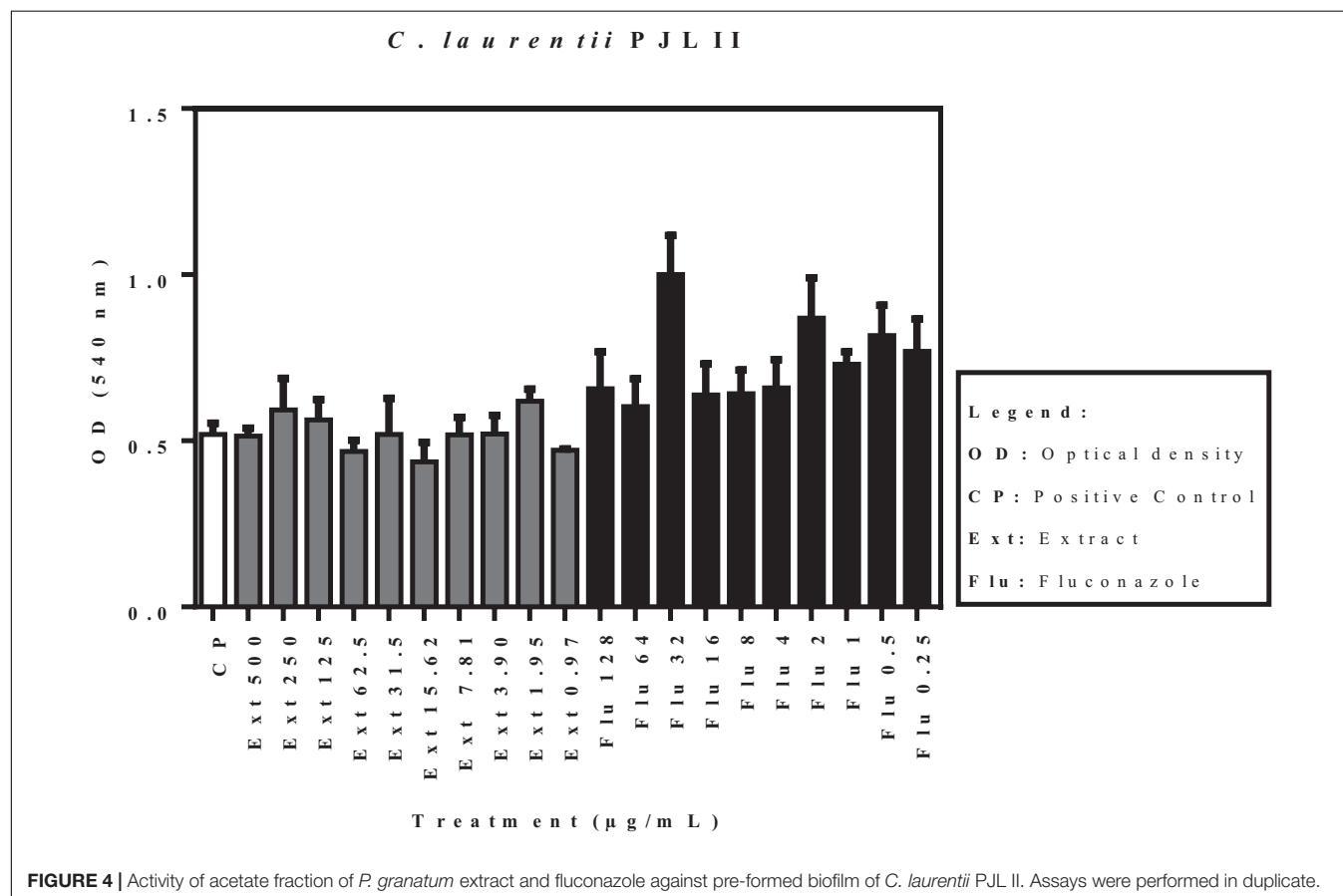
Statistical Analysis of Data

The results are presented as mean ± standard deviation. Statistical analyses were performed using version 5.0 of GraphPad Prism (GraphPad Software, San Diego, CA, United States). The Student's non-parametric *t*-test and analysis of variance (ANOVA) were used. Survival curve was plotted by Kaplan Meier analysis and results were analyzed using the log rank test. A significance level of 95% was considered to differentiate the measurements ($p < 0.05$).

RESULTS

Minimum Inhibitory Concentration and Time-Kill Curves

The acetate fraction of *P. granatum* showed antifungal activity against all the species of *Cryptococcus* tested in this study (Table 1).



For the *C. gattii* clinical isolate, the acetate fraction of *P. granatum* presented a MIC value of 15.62 $\mu\text{g/mL}$, whereas for samples of *C. laurentii* (PMA, PJJ II, and PNM) and *C. gattii* (ATCC 32068), it exhibited MIC values of 1.95 and 31.25 $\mu\text{g/mL}$, respectively. All the isolates had a MIC with respect to fluconazole (32 $\mu\text{g/mL}$).

To evaluate the kinetic of the action of the acetate fraction of *P. granatum* and the antifungal tested, the assays of time-kill curves were performed (Figure 1). For FLU and/or extract against *C. gattii* CASA (clinical strain, Figure 1A), reduction of CFU occurred only after 48 h. FLU and/or extract against *C. gattii* ATCC 32068, increased this period to 72 h (Figure 1B). When the tests were carried out with fluconazole and/or extract against *C. laurentii* strains, *C. laurentii* PMA (Figure 1C), *C. laurentii* PMN (Figure 1D), *C. laurentii* PJJ (Figure 1E), the profile of reduction of the CFU was slower for each strain. It was possible to observe a reduction after 72 h.

Fractional Inhibitory Concentration

A comparison of the test results showed that one sample exhibited growth at all concentrations tested, i.e., it was resistant to all the concentrations evaluated. The indices obtained indicated that the antimicrobial effect of the combination of the acetate fraction of *P. granatum* and antifungal (fluconazole) was indifferent for most

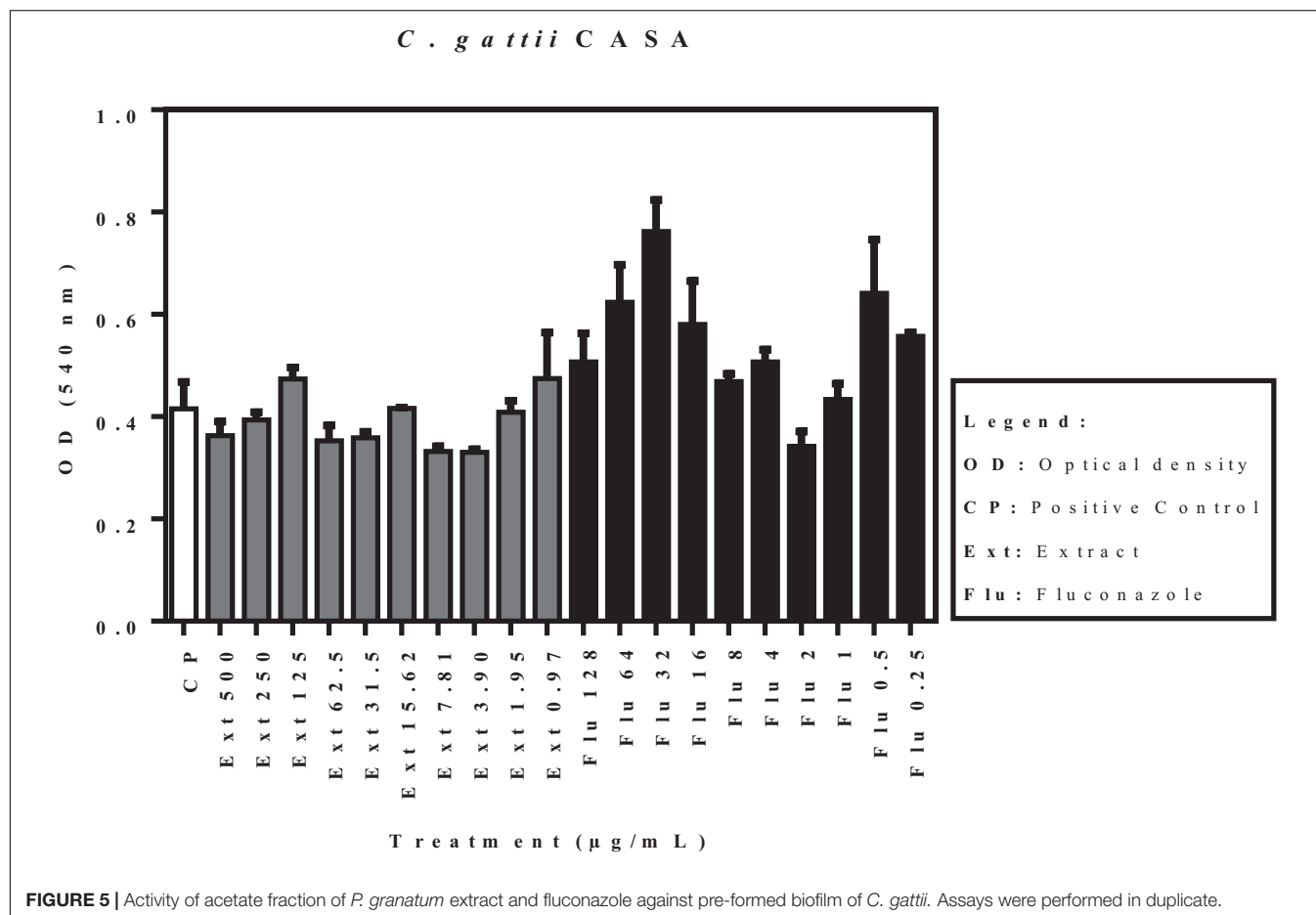
of the samples tested, with $1 > \text{FIC} < 4$, whereas the interaction was antagonistic against only one of the isolates of *C. laurentii* (PNM) (Table 2).

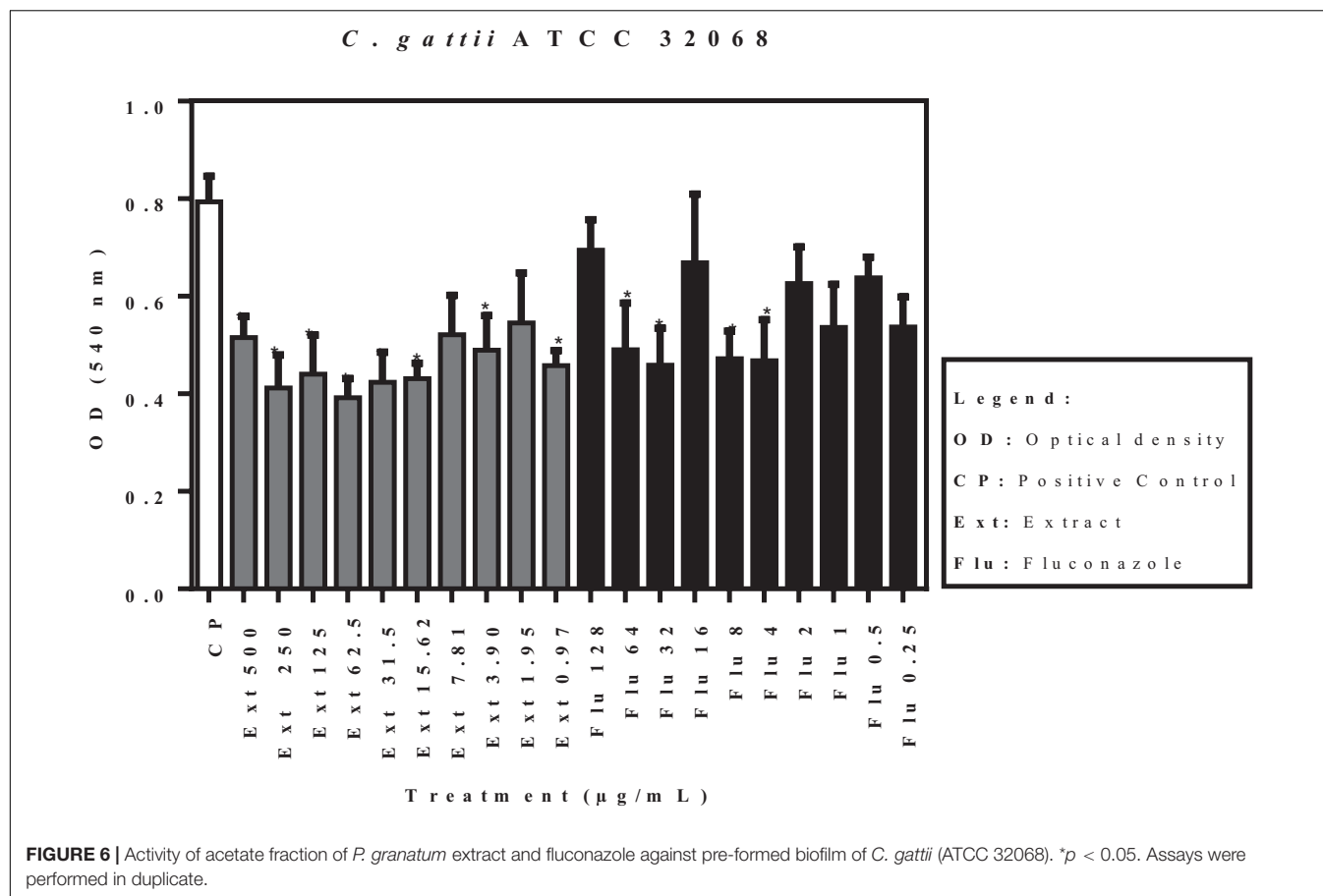
Activity of Acetate Fraction of *P. granatum* Extract Against Pre-formed Biofilm

Figure 2 shows the activity of the acetate fraction of *P. granatum* extract and fluconazole against a pre-formed biofilm of *C. laurentii* PMN. Six of the ten concentrations of the acetate fraction showed significant activity, whereas only one concentration of fluconazole (8 $\mu\text{g/mL}$) showed significant activity when compared to the positive control.

The effects of the acetate fraction of *P. granatum* extract and fluconazole on the isolates (*C. laurentii* PMA and PJJ II, and *C. gattii*), reflected by the optical density, are shown in Figures 3–5. According to the statistical analysis carried out on the pre-formed biofilms, none of the samples showed a significant difference ($p < 0.05$) when compared to the positive control.

Figure 6 shows the activity of the acetate fraction of *P. granatum* extract and fluconazole against a pre-formed biofilm of *C. gattii* (ATCC 32068). Of the ten concentrations of the acetate fraction that were tested, eight presented significant activity. Concentrations of 7.81 and 1.91 $\mu\text{g/mL}$ were not statistically





significant when compared to the control. On the contrary, only four concentrations of fluconazole showed significant activity compared to the positive control.

Fluorescence Microscope

Yeast cells were stained with 10 μg/mL acridine orange and visualized at 50× and 400× magnification (within red rectangles). Disturbances on biofilms occurred at equal or greater MIC and/or higher concentrations when compared with non-treated cells, as follow: *C. laurentii* PMA at 4× MIC for Ext or Flu, and 4× MIC for Flu + Ext; *C. gattii* ATCC 38068 at 1× MIC for Ext or Flu, and 1× MIC for Flu + Ext; and *C. gattii* CASA at 2× MIC for Ext or Flu (Figure 7).

Survival and CFU/g of Larvae

The median survival in the group infected and non-treated (NT) with the *C. gattii* CASA (clinical strain) was 4 days versus 7 days for the group infected with this strain and treated with fluconazole (Figure 8A). Acetate fraction of *P. granatum* extract alone or in combination with fluconazole increased survival of larvae infected with *C. gattii* CASA compared to the non-treated larvae (NT) or treated with fluconazole alone (Figure 8A). On the other hand, larvae infected with the *C. gattii* ATCC or *C. laurentii* strains and treated or not treated survived for 10 days post-inoculation (data not shown).

In addition, acetate fraction of *P. granatum* extract or fluconazole (MIC) reduced the fungal burden in the larvae infected with *C. gattii* CASA compared to non-treated larvae (Figure 8B). Acetate fraction of *P. granatum* extract and/or fluconazole (MIC) reduced the fungal burden in the larvae infected with *C. gattii* ATCC 32068 ($p < 0.05$) compared to non-treated larvae (Figure 8C). However, no reduction in CFU/g of larvae was observed when infected with *C. laurentii* PMA and treated with fluconazole or extract alone, but the combination showed a tendency to reduce the fungal burden in comparison to the non-treated group (Figure 8D).

DISCUSSION

The indiscriminate use of antimicrobial drugs has been growing steadily owing to a lack of knowledge about the damage that such use can cause. Therefore, the use of medicinal plants has been gaining ground due to their antimicrobial, anti-inflammatory, and antioxidant activity against fungi and bacteria (Dos Santos et al., 2017).

According to Brandão et al. (2014), several studies have been carried out on the use of plants with medicinal properties, as therapeutic alternatives, in view of the development of resistance by groups of microorganisms; however, there is no standard

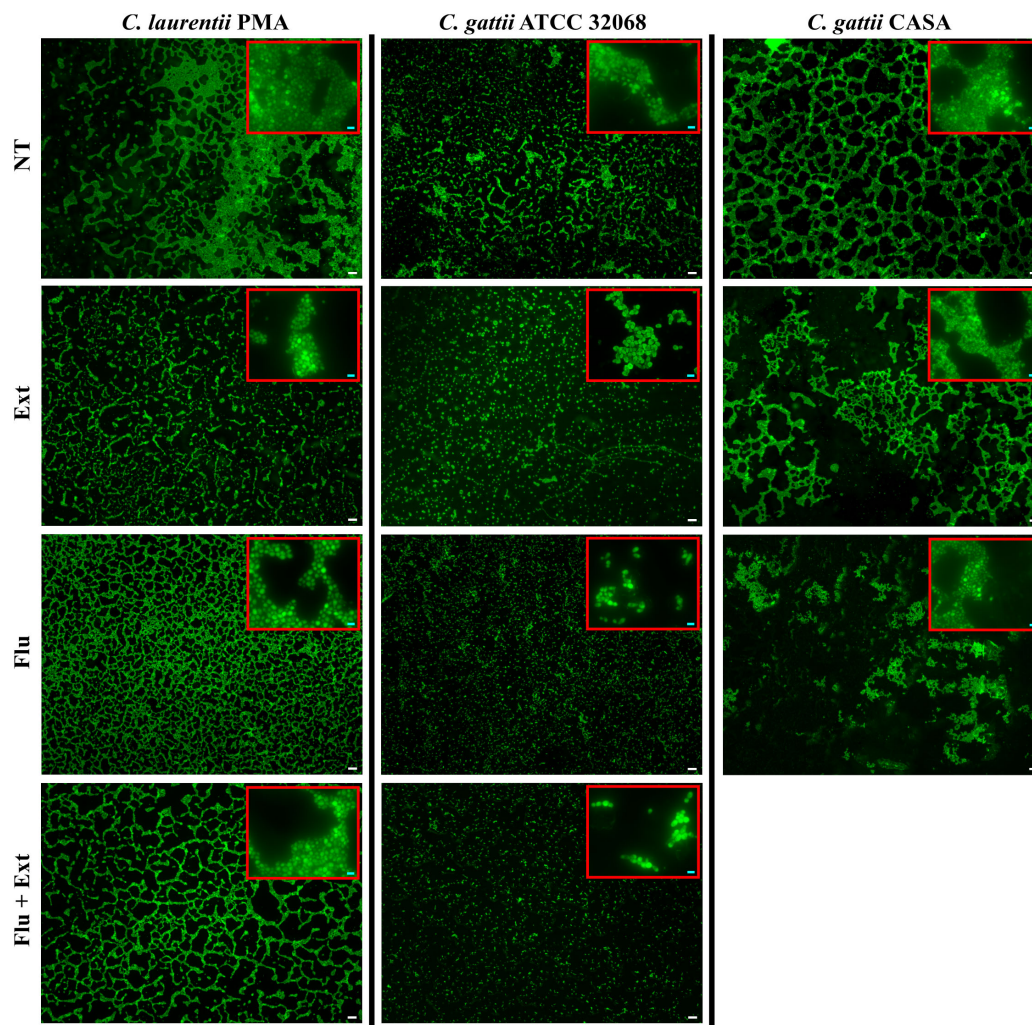


FIGURE 7 | Aspects of biofilms of *Cryptococcus* spp. after treatment with acetate fraction of *P. granatum* extract and/or fluconazole. Yeast cells were stained with 10 $\mu\text{g/mL}$ acridine orange and visualized at 50 \times and 400 \times magnification (within red rectangles). Disturbances on biofilms occurred at equal or greater MIC when compared with non-treated cells, as follow: *C. laurentii* PMA at 4 \times MIC for Ext or Flu, and 4 \times MIC for Flu + Ext; *C. gattii* ATCC 32068 at 1 \times MIC for Ext or Flu, and 1 \times MIC for Flu + Ext; and *C. gattii* CASA at 2 \times MIC for Ext or Flu. The sum of fluorescences was used to evaluate disturbances on biofilm. Assays were performed in triplicate. "NT," "Ext," "Flu," and "Flu + Ext" mean non-treated; acetate fraction of *P. granatum* extract, fluconazole and combination between them, respectively. MIC mean minimal inhibitory concentration. White (50 μm) and bright blue (5 μm) bars.

regarding the formulation of the concentrations or the type of technique to be used.

Owing to research in the area of phytopharmaceuticals, approximately 350 000 species of plants with antimicrobial characteristics have been identified in Brazilian Universities, showing that there is potential for natural products in medicinal therapy (Pinto et al., 2013).

According to Silva et al. (2013), the plant species *P. granatum*, popularly known as Romã, Romãzeira, or Romeira, is used by many, owing to its therapeutic properties as well as antimicrobial and anti-inflammatory activity. Frias and Kozusnyandeani (2010) verified these characteristics through phytochemical analysis of extracts linked to secondary metabolites such as tannins and flavonoids, which promote fungicidal or fungistatic capacity. In a study using animal models,

Pinheiro et al. (2018, 2019) found that the galoyl-HHDP-glucose molecule, which is present in *P. granatum* leaves, may have been one of the compounds associated with anti-inflammatory effects, which were previously investigated using treatments with hydro-alcoholic extracts and ethyl acetate fractions of *P. granatum*, wherein the fraction was effective in reducing lung inflammation.

According to Marques et al. (2016), and Pinheiro et al. (2018, 2019), the extract shows no toxicity either in an LPS-induced acute lung injury mouse model or in cellular cytotoxicity assays at the concentrations used in this study. These characteristics confirm that the studied compound can impart benefits to certain therapeutic approaches, considering that the use of antimicrobials has been increasing dramatically, and is causing the development of resistance in clinical isolates, i.e.,

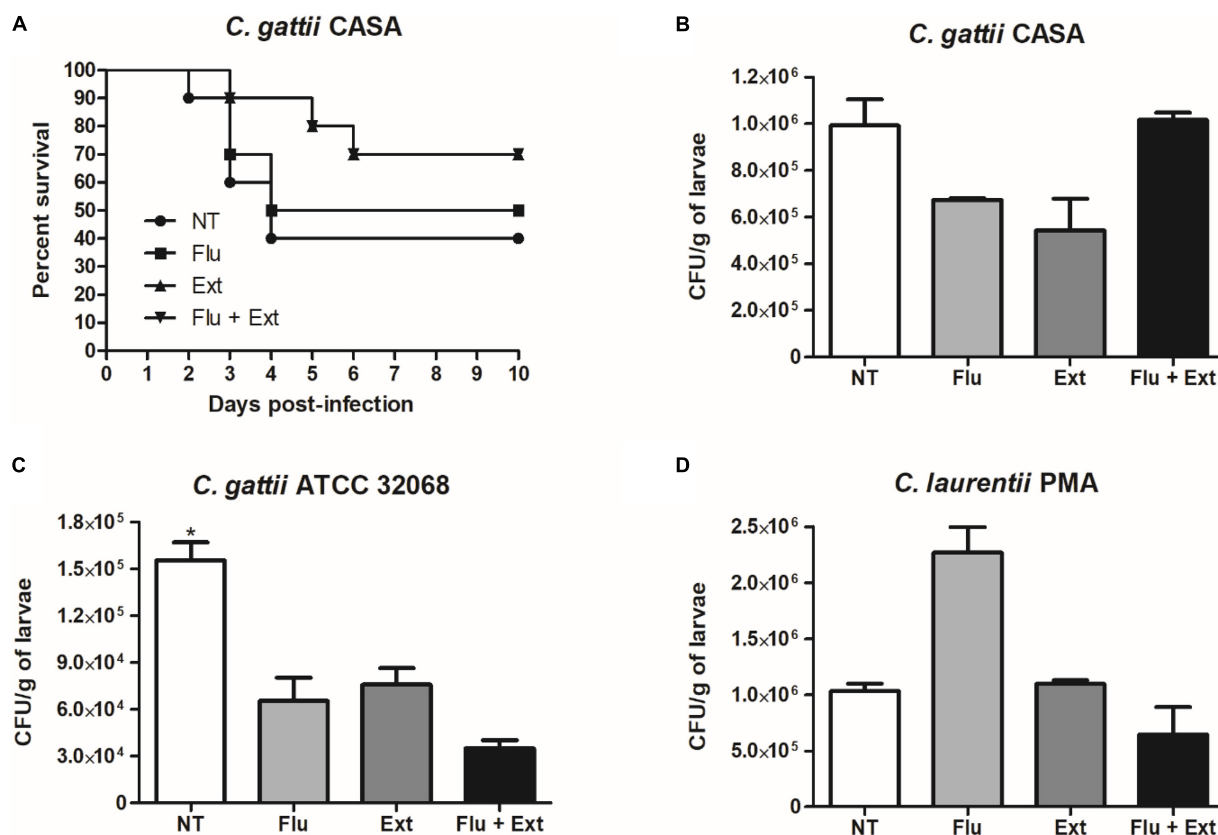


FIGURE 8 | Larvae ($n = 10$) were monitored daily for the survival curve (A). Fungal burden in larvae infected with the *C. gattii* CASA strain and treated with fluconazole, acetate fraction of *P. granatum* extract or combination (B). Fungal burden in larvae infected with the *C. gattii* ATCC 32068 strain and treated with fluconazole, acetate fraction of *P. granatum* extract or combination (C). Fungal burden in larvae infected with the *C. laurentii* PMA strain and treated with fluconazole, acetate fraction of *P. granatum* extract or combination (D). NT, non-treated group; Flu, fluconazole; Ext, extract. * $p < 0.05$.

environmental fungi of clinical interest. Therefore, studies on the activity of this extract are important, since there are no reports on the effect of *P. granatum* extracts on *Cryptococcus* spp., to evaluate the antifungal potential of *P. granatum* leaf extracts against these yeasts.

In our study, the indices obtained indicated that the antimicrobial effect of the combination of the acetate fraction and antifungal was indifferent for most of the tested isolates. It is important to note that the choice of fluconazole was based on its use in the treatment of diseases caused by yeasts, mainly in immunocompromised patients (Mukherjee et al., 2005).

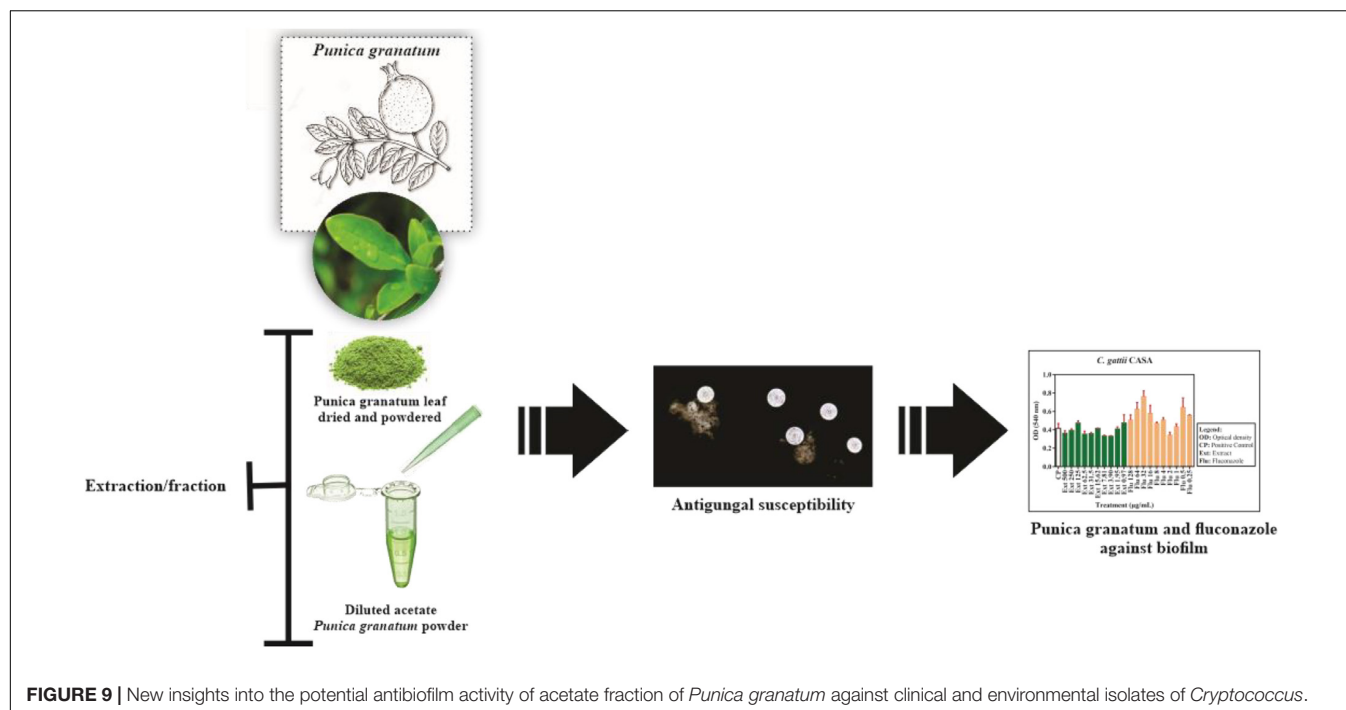
The susceptibility to acetate fraction of *P. granatum* extract and fluconazole alone or in combination were confirmed with lower fluorescence intensity for biofilms of *C. gattii* CASA (clinical strain) and *C. gattii* ATCC in comparison to non-treated cells, and in the *in vivo* tests in larvae of *Tenebrio molitor*. Also, the susceptibility to acetate fraction of *P. granatum* alone or in combination with fluconazole for *C. laurentii* PMA was confirmed by lower fluorescence intensity compared to non-treated cells. On the other hand, the reduced susceptibility to fluconazole was confirmed with higher fluorescence intensity for *C. laurentii* PMA in comparison to non-treated cells, and in the *in vivo* tests in larvae of *Tenebrio molitor*, as this drug was unable

to reduce the CFU in the larvae. Additionally, environmental isolates of fluconazole-resistant *Cryptococcus* have also been reported (Chowdhary et al., 2011).

In light of the scarcity of new classes of antimicrobial drugs or different targets of action, combinations of phyto-therapeutic and antimicrobial products are considered as accessible strategies for the treatment of patients affected by diseases caused by fungi; such combinations will increase the number of molecular targets against which current agents are effective (Kumari et al., 2017).

Although fluconazole in combination with the acetate fraction of *P. granatum* extracts had different effects on samples of *Cryptococcus* spp., the MIC values and suggested a potential for inhibiting antifungal growth. Also, the time-kill curves confirmed the kinetics of growth and the dynamism of the action of the acetate fraction of *P. granatum* extract and fluconazole either alone or in combination. In addition, our survival and CFU data confirmed the potential efficacy of acetate fraction of *P. granatum* extract in the outcome of antifungal therapy of cryptococcosis.

Due to the increasing number of cases of diseases caused by fungi in nosocomial environments, and the emergence of new strains resistant to antimicrobials, mainly associated with the ability to form biofilms, it has become essential to develop new classes of drugs with low phyto-therapeutic resistance



(Pessoa et al., 2012). The acetate fraction of *P. granatum* used in this study did not demonstrate anti-biofilm activity at some concentrations when compared to the results of Cavaleiro et al. (2015) and Cardoso et al. (2016) which indicated a strong antifungal activity of the extracts of *Ocimum basilicum* and *Angelica major* against samples of *C. neoformans* and potential anti-biofilm activity against *Candida* spp.

It is important to highlight that there are still controversies regarding the biofilm formation mechanism of *Cryptococcus* spp. The ability to form biofilms is evident in environmental isolates, and may be related to other virulence factors such as the yeast polysaccharide capsule, especially when they are subjected to environmental conditions, confirming that *in vitro* cryptococcal biofilms are less susceptible to antifungal agents in these circumstances (Ravi et al., 2009). In addition, some authors have mentioned that the development of biofilms from isolates of *C. neoformans* depends on other characteristics such as capsular production, the physical properties of the substrate, and the environmental conditions; therefore, such aspects of microbial biofilms may be important for the administration of therapies against diseases related to fungal biofilms (Martinez and Casadevall, 2007).

This is the first study on the anti-biofilm capacity of the acetate fraction of *P. granatum* against *Cryptococcus* isolates (Figure 9). However, further studies are needed to determine the active components of *P. granatum* and explain the mechanism of action against fungi that affect immunocompetent and immunocompromised individuals. These studies will complement the reduction in the use of antimicrobial drugs in the fight against fungal diseases, and highlight the importance of using herbal medicines in their treatment, particularly in a

country like Brazil, where the flora are abundant and can be harnessed to address the current scenario of antimicrobial use.

DATA AVAILABILITY STATEMENT

The raw data supporting the conclusions of this article will be made available by the authors, without undue reservation.

ETHICS STATEMENT

The studies involving human participants were reviewed and approved by the research ethics committee of the CEUMA University (approval number: 2.927.864), considering all ethical aspects that involve the use of human participants, according to Resolution 466/12 of the National Health Council. The participant provided their written informed consent to participate in this study.

AUTHOR CONTRIBUTIONS

PV and JS designed the study. AM, IG, PF, HF, TM, BM, PM, and AP developed the method. LN, CM, LS, GF, RH, and JS conducted the analysis and critically revised the manuscript. PV, AM, PF, HF, TM, and JS wrote the manuscript. All authors approved the final version of the manuscript.

ACKNOWLEDGMENTS

We would like to thank the Universidade CEUMA (UNICEUMA), São Luís, MA, Brazil.

REFERENCES

- Ajesh, K., and Sreejith, K. (2012). *Cryptococcus laurentii* biofilms: structure, development and antifungal drug resistance. *Mycopathologia* 174:409. doi: 10.1007/s11046-012-9575-2
- Akroum, S. (2017). Antifungal activity of acetone extracts from *Punica granatum* L., *Quercus suber* L. and *Vicia faba* L. *J. Mycol. Méd.* 27, 83–89. doi: 10.1016/j.mycmed.2016.10.004
- Anibal, P. C., Peixoto, I. T., Foglio, M. A., and Höfling, J. F. (2013). Antifungal activity of the ethanolic extracts of *Punica granatum* L. and evaluation of the morphological and structural modifications of its compounds upon the cells of *Candida* spp. *Braz. J. Microbiol.* 44, 839–848. doi: 10.1590/S1517-83822013005000060
- Brandão, D. O., Fernandes, F. H. A., Ramos Júnior, F. J. L., Silva, P. C. D., Santana, C. P., De Medeiros, F. D., et al. (2014). Validation of UPLC method for determination of gallic acid from *Ximenia americana* L. *Planta Med.* 80:P2060. doi: 10.1055/s-0034-1395050
- Brilhante, R. S. N., Caetano, E. P., Oliveira, J. S., Castelo-Branco, D. S. C. M., Souza, E. R. Y., and Alencar, L. P. (2015). Simvastatin inhibits planktonic cells and biofilms of *Candida* and *Cryptococcus* species. *Braz. J. Infect. Dis.* 19, 459–465. doi: 10.1016/j.bjid.2015.06.001
- Cardoso, N. R., Alviano, C. S., Blank, A. F., Romanos, M. T. V., Fonseca, B., Rozental, S., et al. (2016). Synergism effect of the essential oil from *Ocimum basilicum* var. Maria Bonita and its major components with fluconazole and its influence on ergosterol biosynthesis. *Evid. Based Complement. Altern. Med.* 69, 241–248. doi: 10.1155/2016/5647182
- Castro-Láinez, M. T., Deliz-Aguirre, R., Antunez, D., Marco Cruz-Codina, M., Cahuayme-Zuniga, L., Vitale, K., et al. (2019). *Cryptococcus laurentii* meningitis in a non-HIV patient. *IDCases* 18:e00612. doi: 10.1016/j.idcr.2019.e00612
- Cavaleiro, C., Salgueiro, L., Gonçalves, M. J., Hrimpeng, K., Pinto, J., and Pinto, E. (2015). Antifungal activity of the essential oil of *Angelica major* against *Candida*, *Cryptococcus*, *Aspergillus* and dermatophyte species. *J. Nat. Med.* 69, 241–248. doi: 10.1007/s11418-014-0884-2
- Chen, Y., Farrer, R. A., Giamberardino, C., Sakthikumar, S., Jones, A., Yang, T., et al. (2017). Microevolution of serial clinical isolates of *Cryptococcus neoformans* var. *grubii* and *C. gattii*. *mBio* 8:e00166-17.
- Chowdhary, A., Randhawa, H. S., Sundar, G., Kathuria, S., and Prakash, A. (2011). In vitro antifungal susceptibility profiles and genotypes of 308 clinical and environmental isolates of *Cryptococcus neoformans* var. *grubii* and *Cryptococcus gattii* serotype B from North-Western India. *J. Med. Microbiol.* 60, 961–967. doi: 10.1099/jmm.0.029025-0
- Clinical and Laboratory Standards Institute (2008). *Reference Method for Broth Dilution Antifungal Susceptibility Testing of Yeasts. Approved Standard M27-A3*, 3rd Edn, Wayne, PA: Clinical and Laboratory Standards Institute.
- de Souza, P. C., Morey, A. T., Castanheira, G. M., Bocate, K. P., Panagio, L. A., Nazareth, L., et al. (2015). *Tenebrio molitor* (Coleoptera: tenebrionidae) as an alternative host to study fungal infections. *J. Microbiol. Methods* 17, 365–375.
- Dos Santos, J. E. F., Junior, A. A. S., Barbosa, R. N., Santos, A. C. S., Lopes, D. H. G., De Oliveira, N. T., et al. (2017). In Vitro antifungal activity of medicinal plants against yeasts isolated from vaginal secretion. *Sabios Rev. Saúde Biol.* 11, 34–44.
- Endo, E. H., Cortez, D. A. G., Ueda-Nakamura, T., Nakamura, C. V., and Filho, B. P. D. (2010). Potent antifungal activity of extracts and pure compound isolated from pomegranate peels and synergism with fluconazole against *Candida albicans*. *Res. Microbiol.* 161, 534–540.
- Foss, S. R., Nakamura, C. V., Ueda-Nakamura, T., Cortez, D. A., Endo, E. H., and Dias Filho, B. P. (2014). Antifungal activity of pomegranate peel extract and isolated compound punicalagin against dermatophytes. *Ann. Clin. Microbiol. Antimicrob.* 13:32. doi: 10.1186/s12941-014-0032-6
- Frias, D. F. R., and Kozusnyandeani, D. I. (2010). Use of extracts of medicinal plants and *Eucalyptus* oil in the in vitro control of *Microsporium canis*. *Rev. Cubana Plant. Med.* 15, 119–125.
- Gupta, M., Mishra, A. K., and Singh, S. K. (2018). *Cryptococcus laurentii* fungemia in a low birth weight preterm neonate: India. *J. Infect. Public Health* 11, 896–897. doi: 10.1016/j.jiph.2018.04.012
- Jabra-Rizk, M. A., Falkler, W. A., and Meiller, T. F. (2004). Biofilmes de fungos e resistência a medicamentos. *Doenças Infecç. Emerg.* 10, 14–19. doi: 10.3201/eid1001.030119
- Jurcisek, J. A., Dickson, A. C., Bruggeman, M. E., and Bakaletz, L. O. (2011). In vitro biofilm formation in an 8-well chamber slide. *J. Vis. Exp.* 47:2481. doi: 10.3791/2481
- Kumari, P., Mishra, R., Arora, N., Chatrath, A., Gangwar, R., Roy, P., et al. (2017). Antifungal and anti-biofilm activity of essential oil active components against *Cryptococcus neoformans* and *Cryptococcus laurentii*. *Front. Microbiol.* 8:2161. doi: 10.3389/fmicb.2017.02161
- Lavaee, F., Motaghi, D., Jassbi, A. R., Jafarian, H., Ghasemi, F., and Badiee, P. (2018). Antifungal effect of bark and root extracts of *Punica granatum* on oral *Candida* isolates. *Curr. Med. Mycol.* 4, 20–24.
- Mansourian, A., Boojarpour, N., Ashnagar, S., Momen Beitollahi, J., and Shamshiri, A. R. (2014). The comparative study of antifungal activity of *Syzygium aromaticum*, *Punica granatum* and nystatin on *Candida albicans*; an in vitro study. *J. Mycol. Med.* 24, e163–e168. doi: 10.1016/j.mycmed.2014.07.001
- Marques, L., Pinheiro, A., Araujo, J., de Oliveira, R., Silva, S., Abreu, I., et al. (2016). Antiinflammatory effects of a pomegranate leaf extract in LPS-induced peritonitis. *Planta Med.* 82, 1463–1467. doi: 10.1055/s-0042-108856
- Martinez, L. R., and Casadevall, A. (2007). *Cryptococcus neoformans* biofilm formation depends on surface support and carbon source and reduces fungal cell susceptibility to heat, cold, and UV light. *Appl. Environ. Microbiol.* 73, 4592–4601. doi: 10.1128/AEM.02506-06
- May, R., Stone, N., Wiesner, D., Bicanic, T., and Nielsen, K. (2016). *Cryptococcus*: from environmental saprophyte to global pathogen. *Nat. Rev. Microbiol.* 14, 106–117. doi: 10.1038/nrmicro.2015.6
- Maziarz, E. K., and Perfect, J. R. (2016). Cryptococcosis. *Infect. Dis. Clin. North Am.* 30, 179–206. doi: 10.1016/j.idc.2015.10.006
- Mukherjee, P. K., Sheehan, D. J., Hitchcock, C. A., and Ghannoum, M. A. (2005). Combination treatment of invasive fungal infections. *Clin. Microbiol. Rev.* 18, 163–194. doi: 10.1128/CMR.18.1.163-194.2005
- Odds, F. C. (2003). Synergy, antagonism, and what the checkerboard puts between them. *J. Antimicrob. Chemother.* 2:1. doi: 10.1093/jac/dkg301
- Paul, S., Mohanram, K., and Kannan, I. (2018). Antifungal activity, gas chromatographic-mass spectrometric analysis and in silico study of *Punica Granatum* peel extracts against fluconazole resistant strains of *Candida* species. *Curr. Pharm. Biotechnol.* 19, 250–257. doi: 10.2174/1389201019666180515104800
- Pessoa, C. C. B., Silva, S. H. M., and Gomes, F. S. (2012). Produção de fatores de virulência in vitro por isolados de *Cryptococcus neoformans* e *Cryptococcus gattii* de origem clínica em Belém, Estado do Pará, Brasil. *Rev. Pan. Amazônia. Saúde* 3, 59–65. doi: 10.5123/s2176-62232012000200008
- Pinheiro, A. J. M. C. R., Gonçalves, J. S., Dourado, A. W. A., Sousa, E. M., Brito, N. M., and Silva, L. K. (2018). *Punica granatum* L. leaf extract attenuates lung inflammation in mice with acute lung injury. *J. Immunol. Res.* 2018:6879183. doi: 10.1155/2018/6879183
- Pinheiro, A. J. M. C. R., Mendes, A. R. S., Neves, M. D. F. J., Prado, C. M., Bittencourt-Mernak, M. I., Santana, F. P. R., et al. (2019). Galloyl-Hexahydroxydiphenol (HHDP)-glucose isolated from *Punica granatum* L. leaves protects against Lipopolysaccharide (LPS)-induced acute lung injury in BALB/c Mice. *Front. Immunol.* 10:1978. doi: 10.3389/fimmu.2019.01978
- Pinto, C. M. F., De Oliveira Pinto, C. L., and Donzeles, S. M. L. (2013). Pepper *Capsicum*: chemical, nutritional properties, pharmacological and medicinal products and their potential for agribusiness. *Rev. Bras. Agrop. Sustent.* 3, 108–120.
- Ravi, S., Pierce, C., Witt, C., and Wormley, F. L. Jr. (2009). Biofilm formation by *Cryptococcus neoformans* under distinct environmental conditions. *Mycopathologia* 167, 307–314. doi: 10.1007/s11046-008-9180-6
- Rêgo, M. F., Rodrigues, R. E. F., Do Nascimento, W. S., and Silva, H. M. (2019). Bibliographical analysis of main aspects of cryptococcosis. *Braz. J. Health Ver.* 2, 3797–3807. doi: 10.34119/bjhrv2n4-141
- Santos, J. R. A., César, I. C., Costa, M. C., Ribeiro, N. Q., Holanda, R. A., and Ramos, L. H. (2016). Pharmacokinetics/Pharmacodynamic correlations of fluconazole in murine model of cryptococcosis. *Eur. J. Pharm. Sci.* 92, 235–243. doi: 10.1016/j.ejps.2016.05.022
- Santos, J. R. A., Gouveia, L. F., Taylor, E. L. S., Resende-Stoianoff, M. A., Pianetti, G. A., César, I. C., et al. (2012). Dynamic interaction between fluconazole and amphotericin B AGAINST *Cryptococcus gattii*. *Antimicrob. Agents Chemother.* 56, 2553–2558. doi: 10.1128/AAC.06098-11

- Silva, B. T., Dos Anjos, C., Novo, S. M. F., Matsumoto, L. S., Peixoto, E. C., Silva, L. P., et al. (2013). In vitro antimicrobial activity of *Punica granatum* L. extract on *Staphylococcus aureus* isolated in bovine milk. *Biosci. J.* 29, 974–984.
- Tavares, E. R., Gionco, B., Morguette, A. E. B., Andriani, G. M., Morey, A. T., Do Carmo, A. O., et al. (2019). Phenotypic characteristics and transcriptome profile of *Cryptococcus gattii* biofilm. *Sci. Rep.* 9:6438. doi: 10.1038/s41598-019-42896-2
- Worasilchai, N., Tangwattachuleeporn, M., Meesilpavikkai, K., Folba, C., Kangogo, M., Groß, U., et al. (2017). Chindamporn, diversity and antifungal drug susceptibility of *Cryptococcus* isolates in Thailand. *Med. Mycol.* 55, 680–685. doi: 10.1093/mmy/myw130

Conflict of Interest: The authors declare that the research was conducted in the absence of any commercial or financial relationships that could be construed as a potential conflict of interest.

Copyright © 2021 Villis, de Macedo, Furtado, Fontenelle, Gonçalves, Mendes, Motta, Marinho, Pinheiro, Lima-Neto, Monteiro, da Silva, Ferreira, Holanda and Santos. This is an open-access article distributed under the terms of the Creative Commons Attribution License (CC BY). The use, distribution or reproduction in other forums is permitted, provided the original author(s) and the copyright owner(s) are credited and that the original publication in this journal is cited, in accordance with accepted academic practice. No use, distribution or reproduction is permitted which does not comply with these terms.



Antibiofilm Activity of Small-Molecule ZY-214-4 Against *Staphylococcus aureus*

Jingyi Yu¹, Lulin Rao¹, Lingling Zhan¹, Yan Zhou², Yinjuan Guo^{3,4}, Xiaocui Wu^{3,4}, Zengqiang Song^{2*} and Fangyou Yu^{3,4*}

¹ Department of Laboratory Medicine, The First Affiliated Hospital of Wenzhou Medical University, Wenzhou, China, ² School of Pharmaceutical Sciences, Wenzhou Medical University, Wenzhou, China, ³ Department of Clinical Laboratory, Shanghai Pulmonary Hospital, Tongji University School of Medicine, Shanghai, China, ⁴ Shanghai Key Laboratory of Tuberculosis, Shanghai Pulmonary Hospital, Tongji University School of Medicine, Shanghai, China

OPEN ACCESS

Edited by:

Luis Cláudio Nascimento da Silva,
Universidade Ceuma, Brazil

Reviewed by:

Adline Princy Solomon,
SASTRA University, India
Jintae Lee,
Yeungnam University, South Korea
Arumugam Veera Ravi,
Alagappa University, India

*Correspondence:

Zengqiang Song
songzengqiang09@163.com
Fangyou Yu
wzjyfy@163.com

Specialty section:

This article was submitted to
Antimicrobials, Resistance
and Chemotherapy,
a section of the journal
Frontiers in Microbiology

Received: 19 October 2020

Accepted: 11 January 2021

Published: 03 February 2021

Citation:

Yu J, Rao L, Zhan L, Zhou Y,
Guo Y, Wu X, Song Z and Yu F (2021)
Antibiofilm Activity of Small-Molecule
ZY-214-4 Against *Staphylococcus*
aureus. *Front. Microbiol.* 12:618922.
doi: 10.3389/fmicb.2021.618922

Staphylococcus aureus is the most important pathogenic bacteria in humans. As the resistance of *S. aureus* to existing antibiotics is increasing, there is an urgent need for new anti-infective drugs. *S. aureus* biofilms cause persistent infections and resist complete eradication with antibiotic therapy. The present study investigated the inhibitory effect of the novel small-molecule ZY-214-4 (C₁₉H₁₁BrNO₄) on *S. aureus* biofilm formation. At a subinhibitory concentration (4 μg/ml), ZY-214-4 had no effect on the growth of *S. aureus* strains and also showed no cytotoxicity in human normal bronchial epithelial cells (Bease-2B). The results of a semi-quantitative biofilm test showed that ZY-214-4 prevented *S. aureus* biofilm formation, which was confirmed by scanning electron microscopy and confocal laser scanning microscopy. ZY-214-4 significantly suppressed the production of polysaccharide intercellular adhesion and prevented cell aggregation, and also inhibited the mRNA expression of *icaA* and other biofilm-related genes (*eno*, *clfA/B*, *fnbB*, *fib*, *ebpS*, *psmα*, and *psmβ*) in clinical *S. aureus* isolates. Thus, at a subinhibitory concentration, ZY-214-4 inhibits biofilm formation by preventing cell aggregation, highlighting its clinical potential for preventing or treating *S. aureus* infections.

Keywords: *Staphylococcus aureus*, small-molecule compound, biofilm, *icaA*, cell aggregation

INTRODUCTION

“An antimicrobial agent” is defined as a chemical produced by microbes that can inhibit the growth of and even destroy bacteria and other microorganisms (Waksman, 1947). Most antimicrobial agents exert bacteriostatic or bactericidal effects (Gordon et al., 2013). *Staphylococcus aureus* can cause a range of infections from mild skin and soft tissue to serious life-threatening infections (Bauer and Sampathkumar, 2017) that place a significant burden on healthcare systems (Dayan et al., 2016). In recent years, virulence suppression strategies have emerged to combat *S. aureus* that prevent infection by inhibiting the action or production of virulence factors rather than targeting bacterial pathways (Cegelski et al., 2008; Escaich, 2008). However, *S. aureus* is resistant to almost all known antibiotics (Lowy, 2003). As such, there is a need for new compounds that can block the production of pathogenic factors and biofilm formation by *S. aureus* at sub-bacterial concentrations.

Biofilm formation presents a major challenge for the eradication of chronic *S. aureus* infections (Craft et al., 2019). The process of biofilm formation includes initial adhesion, proliferation, maturation, and diffusion (Boles and Horswill, 2011), with polysaccharide intercellular adhesin (PIA) providing a stable hydrated matrix that holds cells together in a three-dimensional (3D) structure (Atshan et al., 2012). PIA is also known as poly-N-acetyl glucosamine and is encoded by the intercellular adhesion gene (*ica*) (O'Gara, 2007). The recognition of Microbial Surface Components Recognize Adhesive Matrix Molecules (MSCRAMMs) determines the primary stage of *S. aureus* biofilm development, that is, the initial attachment to the host cell surface. These MSCRAMMs includes elastin binding protein (*ebpS*), laminin-(*eno*), fibronectin binding protein (*fnbA* and *fnbB*), fibrinogen binding protein (*fib*) and aggregation factor (*clfA* and *clfB*). But separation and diffusion also play important roles. Formylated phenol-soluble modulins (PSM-mec) isolated from hospital-acquired methicillin-resistant *S. aureus* was shown to promote the formation of biofilm on the surface of medical instruments that resisted penetration by antibiotics, resulting in an increased rate of nosocomial infection and chronic infections (Queck et al., 2009). PSMs are major facilitators of cell spreading (Tsompanidou et al., 2013); PSM deficiency was shown to negatively affect biofilm maturation and dissociation (Periasamy et al., 2012).

ZY-214-4 ($C_{19}H_{10}BrNO_4$) is a small molecule that contains a chromone ring and N-phenyl-substituted maleimide. Chromone and its derivatives are present in natural products and pharmaceuticals as key scaffolds; and chromone derivatives have demonstrated antimicrobial activities against *Penicillium*, *Escherichia coli*, and *Shigella flexneri* (Verma and Pratap, 2010; Gaspar et al., 2014; Reis et al., 2017). Maleimide motifs are found in many natural products and drug candidates and exhibit a broad spectrum of biological activities including anti-tumor and anti-bacterial activities (Martinez et al., 2005; Wagner et al., 2009; Thoma et al., 2011). However, there has been no research to date on the antibacterial activity of chromone-maleimide hybrids.

In this study, we investigated the effect of a subinhibitory concentration of the small-molecule ZY-214-4 on *S. aureus* biofilm formation in order to assess the clinical potential of ZY-214-4 for preventing and treating persistent *S. aureus* infection.

MATERIALS AND METHODS

Bacterial Strains

The *S. aureus* strains used in this study are listed in Table 1. Strains SA21, SA882, and SA923 were isolated from patients at The First Affiliated Hospital of Wenzhou Medical University. The

medical records of patients and *S. aureus* isolates were obtained for research purposes with the approval of the Ethics Committee of The First Affiliated Hospital of Wenzhou Medical University; and written, informed consent was obtained from patients.

Synthesis of ZY-214-4

ZY-214-4 was synthesized at the School of Pharmacy, Wenzhou Medical University (Figure 1). Chromone 1 (0.2 mmol, 1 equiv) and maleimide 2 (0.5 mmol, 2.5 equiv) were dissolved in a 12 ml screwcapped tube with 2 ml of 1,2-dichloroethane (0.1 M). (Ru[p-cymene] Cl_2) $_2$ (0.01 mmol, 0.05 equiv), AgNTf $_2$ (0.04 mmol, 0.2 equiv), and AgOAc (0.6 mmol, 3 equiv) were added to the reaction mixture at room temperature in air, which was then heated to 120°C in a heating mantle with stirring for 0.5 h. After terminating the reaction, the reaction mixture was loaded onto a silica gel column and purified with a petroleum ether/EtOAc mixture to obtain product 3 at a yield of 75% (Supplementary Figure 2). All reagents used were of analytical grade (Zhou et al., 2020).

Determination of Minimum Inhibitory Concentration (MIC)

ZY-214-4 was dissolved in dimethyl sulfoxide (DMSO) (Boyun, Shanghai, China) at a concentration of 20 µg/ml. The MIC of ZY-214-4 was determined with the microbroth dilution method, and was defined as the lowest concentration at which there was no visible cell growth. In order to exclude the influence of the solvent on biofilm formation, we used a DMSO control in our experiments.

Growth Assay

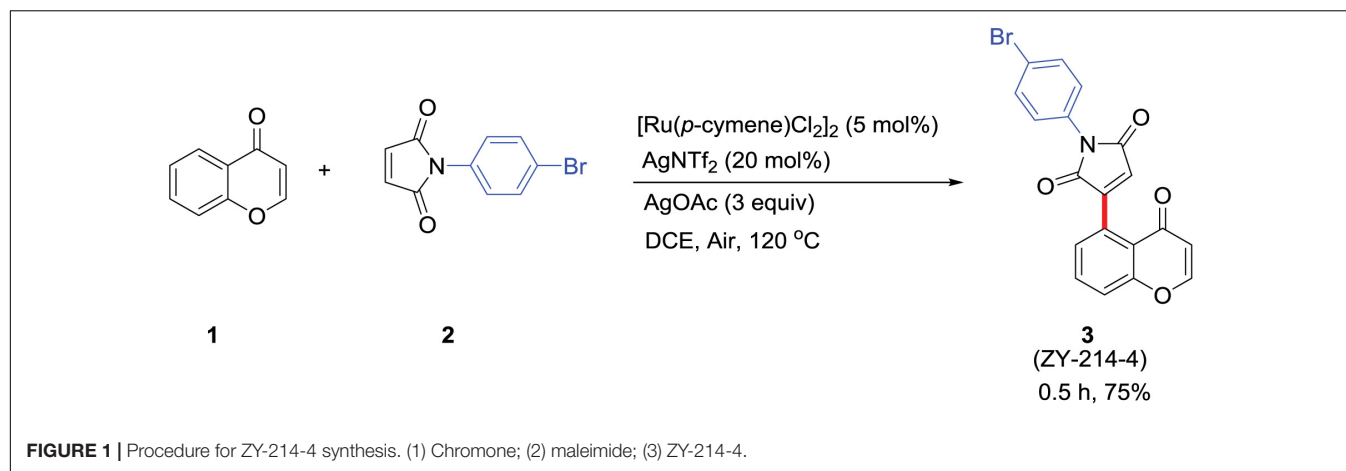
S. aureus strains were activated twice and added to tryptic soy broth (TSB) (BD Biosciences, Franklin Lakes, NJ, United States) at 1:200 and cultured to an optical density at 600 nm (OD $_{600}$) of 0.3. Appropriate amounts of ZY-214-4 were added to the culture to achieve final concentrations of 2, 4, and 8 µg/ml. An equivalent volume of DMSO was also tested to ensure that the vehicle did not affect cell growth, and cultures with TSB only served as the blank control. All cultures were incubated at 37°C with shaking at 220 rpm. And the OD $_{600}$ values were measured every hour for a total of 24 h. The assay was performed in triplicate.

Effect of ZY-214-4 on *S. aureus* Biofilm Formation

ZY-214-4 was dissolved in dimethyl sulfoxide (DMSO) to a concentration of 20 mg/ml. *S. aureus* was inoculated in 5 ml TSB and cultured at 37°C and 220 rpm. ZY-214-4 solutions were prepared at different concentrations in TSB containing 1% glucose (Kranjec et al., 2020) and was added to bacterial cultures (1:100) in 96-well plates, with 3 parallel wells at each concentration. An equivalent volume of DMSO was also tested. After incubation for 24 h, the supernatant was discarded and the wells were washed 3 times with phosphate-buffered saline (PBS). The biofilms were fixed with 99% methanol for 15 min; after discarding the supernatant, they were stained with 2% crystal violet for 10 min and rinsed under running water until the water

TABLE 1 | Strains used in this study.

Strain	MIC (µg/ml)	Source
SA21	64	Tissue
SA882	64	Wound exudate
SA923	64	Sputum



was colorless. OD₅₇₀ was measured after adding 70% glacial acetic acid (Kannappan et al., 2017). TSB was used as a blank control. The assay was repeated 3 times.

Scanning Electron Microscopy (SEM) Analysis

A colony of *S. aureus* was picked from a blood agar plate and cultured overnight in 5 ml TSB medium at 37°C with shaking at 220 rpm (Kranjec et al., 2020). The culture was inoculated at 1:200 into 20 ml of TSB. A 3 ml volume of diluted bacterial solution was added to 6-well cell culture plates containing coverslips in each well and ZY-214-4 was added to achieve a final concentration 4 µg/ml, followed by incubation at 37°C for 24 h. Cultures without ZY-214-4 served as a control. The cells were cultured under the same conditions as for colony counting to ensure that the same number of bacteria were obtained. After removing the supernatant, the coverslip was washed 3 times with sterile PBS and freeze-dried for 2 h, then sputter-coated with gold for 3 min for SEM (Hitachi, Tokyo, Japan) observation.

Confocal Laser Scanning Microscopy (CLSM)

Strains were cultured in TSB in a glass-bottomed cell culture dish (NEST Biotechnology, Wuxi, China) without shaking for 24 h (Kannappan et al., 2017), in the presence of 4 µg/ml ZY-214-4; untreated samples served as a positive control. After rinsing with 0.85% saline, the dish was air-dried and 300 µl of SYTO-9 [0.02%; component A of the LIVE/DEAD BacLight Bacterial Viability kit (Thermo Fisher Scientific, Waltham, MA, United States)] and propidium iodide (0.067%) were added for 30 min in the dark at room temperature. Optical sections were scanned by CLSM (Nikon, Tokyo, Japan) using a 60 × oil-immersion objective lens. 3D reconstruction of the images was performed using NIS-Elements software (Nikon). The assay was performed in triplicate.

Cell Aggregation Assay

Cell aggregation was analyzed as previously described (Feldman et al., 2018). Briefly, five strains of *S. aureus* were added

to 2 ml TSB at 1:200 and ZY-214-4 was added at a final concentration 4 µg/ml. The cells were cultured at 37°C and 250 rpm for 24 h; untreated samples served as the control. The cells were collected by centrifugation at 16,600×g for 2 min, washed 3 times with PBS, and resuspended in 3 ml PBS; OD₅₉₅ was adjusted to 1.5 (initial OD) in a clean glass tube, and the sample was allowed to stand at room temperature for 24 h. The supernatant was removed by aspiration and the cell pellet was resuspended in 3 ml PBS. OD₅₉₅ (final OD) was measured and the percentage of cell aggregation was determined as (final OD/initial OD) × 100%. The relative aggregation of ZY-214-4-treated samples is expressed as a percentage of the value for untreated controls (100%). The assay was performed in triplicate.

Enzyme-Linked Dot Immunoblot Assay for PIA

S. aureus was inoculated on a blood agar plate and cultured at 37°C for 14–18 h. The culture was diluted to 10⁷ CFU/ml and added to a 6-well plate (2 ml per well) (Schlag et al., 2007). ZY-214-4 was then added to a final concentration 4 µg/ml, followed by incubation at 37°C for 24 h. Bacterial solution without ZY-214-4 served as a control. The culture medium was removed and 3 ml of EDTA was added to each well for resuspension of the biofilm attached to the bottom of the plate. The cells were transferred to a 1.5 ml centrifuge tube and incubated at 100°C for 5 min. After centrifugation at 8,000 rpm for 1 min, the supernatant was removed and 10 µl of 20 mg/ml proteinase K was added to 40 µl of supernatant, followed by incubation at 37°C for 2 h. A polyvinylidene difluoride membrane cut to an appropriate size was immersed in methanol for 3 min and deionized water for 15 min to activate functional groups on the membrane. A 10 µl volume of the extracted PIA sample was spotted onto the membrane, which was kept moist during the procedure. After the membrane had completely dried it was transferred to blocking solution [PBS with 0.1% Triton X100 (PBST) containing 3.5% bovine serum albumin] and incubated overnight at 4°C. The membrane was transferred to a Petri dish containing wheat germ agglutinin-conjugated horseradish

peroxidase and incubated at 37°C for 1 h, then washed twice with PBST for 12 min each time followed by PBS before visualizing the signal by enhanced chemiluminescence (Affinity Bio, San Francisco, United States).

Real-Time (RT)-PCR

S. aureus strains were cultured in TSB containing ZY-214-4 at an inhibitory concentration (4 µg/ml). After 12 h, total RNA was extracted from the cells and cDNA was synthesized using an RNA PCR kit (Takara Bio, Otsu, Japan). PCR was performed in a 20 µl reaction volume using Luna Universal qPCR Master Mix (New England Biolabs, Ipswich, MA, United States). The primer pairs used for RT-PCR are shown in **Table 2**. The assay was performed in triplicate.

Cytotoxicity Analysis

The cytotoxicity of ZY-214-4 was evaluated with the Cell Counting Kit (CCK)-8 assay using Bease-2B human normal bronchial epithelial cells. The cells were seeded in a 96-well plate containing Dulbecco's Modified Eagle's Medium (DMEM)/F12 at 4,000 cells/well, and 10% fetal bovine serum (FBS) was added to each well, followed by incubation at 37°C and 5% CO₂ in a humid environment for 12 h. The supernatant was discarded and the wells were washed 3 times with PBS. ZY-214-4 solution (2–8 µg/ml) was added for 24 h, with untreated cells serving as a control. The supernatant was discarded and cells were washed 3 times with PBS; DMEM/12 was added to each well along with CCK-8 reagent, followed by incubation for 1.5 h at 37°C and measurement of OD₄₅₀. The assay was repeated 5 times. Relative cell viability (%) was determined by comparing the OD₄₅₀ value with that of the control well containing only cell culture medium.

TABLE 2 | Primers used for real-time RT-PCR.

Primer name	Sequence (5'–3')
<i>gyrB</i> -RT-F	ACATTACAGCAGCGTATTAG
<i>gyrB</i> -RT-R	CTCATAGTGATAGGAGTCTTCT
<i>icaA</i> -RT-F	GTTGGTATCCGACAGTATA
<i>icaA</i> -RT-R	CACCTTTCTTACGTTTAAATG
<i>psmA</i> -RT-F	ATGGAATTCGTAGCAAAATTATTC
<i>psmA</i> -RT-R	TAGTTGTTACCTAAAAATTTACC
<i>psmβ</i> -RT-F	CCTAGTAAACCCACACCG
<i>psmβ</i> -RT-R	GCTGCACAACAACATGATA
<i>clfA</i> -RT-F	CAGCGATTGAGAATCAGA
<i>clfA</i> -RT-R	GGCGGAACCTACATTATTG
<i>clfB</i> -RT-F	CTGAGTCACTGTCTGAATC
<i>clfB</i> -RT-R	CTCAGACAGCGATTGAGA
<i>fnbB</i> -RT-F	GCGAAGTTTCTACTTTTG
<i>fnbB</i> -RT-R	CAACCATCACAATCAACA
<i>eno</i> -RT-F	CTCCAATTGCATTCCAAG
<i>eno</i> -RT-R	GCATCTTCAGTACCTTCA
<i>ebpS</i> -RT-F	GTGTGATGATTGACTTGG
<i>ebpS</i> -RT-R	CAGGATACAATAGAGAATACG
<i>fib</i> -RT-F	GCTGTAACTTGTTCAAAC
<i>fib</i> -RT-R	CTGTGTTGGAAATGAATTAAG

Statistical Analysis

Prism 6 software (GraphPad, La Jolla, CA, United States) was used to analyze experimental data. Growth curves were analyzed with the *t*-test and one-way analysis of variance was used for all other data. A *p* < 0.05 was considered statistically significant.

RESULTS

ZY-214-4 Suppresses *S. aureus* Growth

The MIC of ZY-214-4 for *S. aureus* strains SA21, SA882, and SA923 was 64 µg/ml. We generated growth curves for cells treated with various concentrations of ZY-214-4 and found that at the subinhibitory concentration of 4 µg/ml, the number of cells in the late logarithmic growth phase was consistent across strains (**Figure 2**). Therefore, 4 µg/ml ZY-214-4 was used for subsequent experiments.

ZY-214-4 Prevents *S. aureus* Biofilm Formation

S. aureus forms biofilm, which protects it against the action of anti-bacterial drugs. We used a semi-quantitative method to evaluate the effect of ZY-214-4 on *S. aureus* biofilm formation. *S. aureus* treated with ZY214-4 (4 µg/ml) had a 7.5–13 times lower OD₅₇₀ than untreated cells (0.2–0.4 vs. 2.6–3.0), with biofilm formation reduced by 83.3–91.5% (**Figure 3**). SEM analysis of *S. aureus* biofilms showed a high degree of aggregation of SA21 and SA923 in the absence of treatment. However, in ZY-214-4-treated samples, cell aggregates covered a smaller area and were scattered, with greater distance between colonies (**Figures 4A,B**). Examination of 3D biofilm morphology by CLSM showed that compared to the control sample, the thickness of the biofilm was decreased and the area covered by the biofilm was reduced by ZY-214-4 treatment (**Figures 4C,D**).

ZY-214-4 Prevents *S. aureus* Aggregation

Cell aggregation plays an important role in biofilm formation. Autoaggregation was observed after incubating *S. aureus* strains for 24 h under static conditions (**Figure 5A**). The cell aggregation rate was significantly decreased by treatment with ZY-214-4 to 68.81–83.14% of the value in untreated control samples (**Figure 5B**).

ZY-214-4 Inhibits PIA Production by *S. aureus*

Extracellular PIA is the main component of staphylococcal biofilms. To investigate the effect of ZY-214-4 on the production of biofilm matrix, we measured PIA release in cultures. As shown in the **Figure 6**, when the PIA antigen was diluted to 5,000-fold, as determined by the semi-quantitative determination of the WGA-HRP conjugate using the dot blot 96 system, among the strains treated with

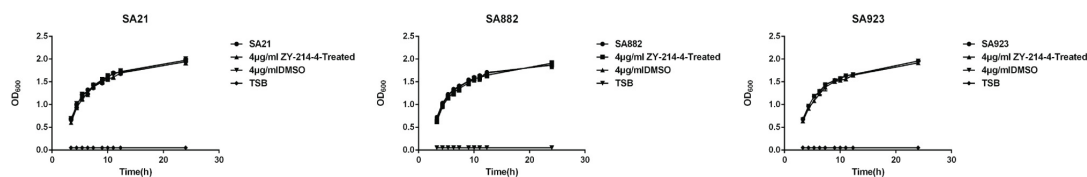


FIGURE 2 | Growth curves of *S. aureus* strains cultured with ZY-214-4. TSB served as a blank control, and growth in the presence of DMSO was evaluated to eliminate the possibility that inhibition of biofilm formation is due to suppression of cell growth.

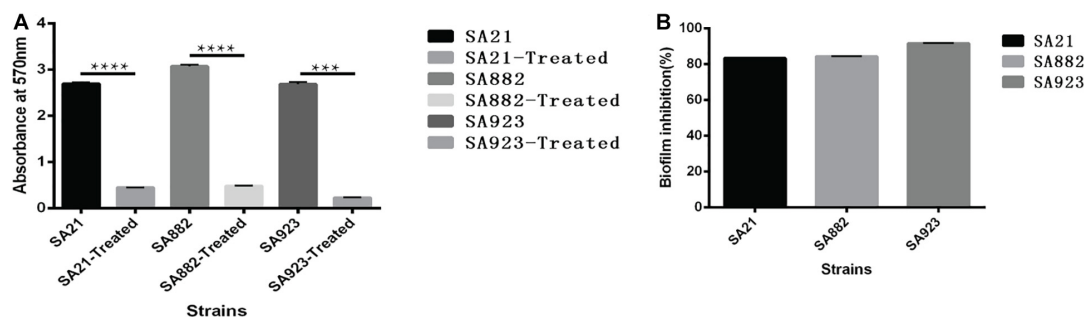


FIGURE 3 | Effect of subinhibitory ZY-214-4 concentration (4 $\mu\text{g/ml}$) on *S. aureus* biofilm formation. **(A)** OD_{570} of each strain differed significantly from that of the control group (grown in the absence of ZY-214-4). **(B)** Biofilm inhibition rate of 3 *S. aureus* strains. * $P < 0.05$.

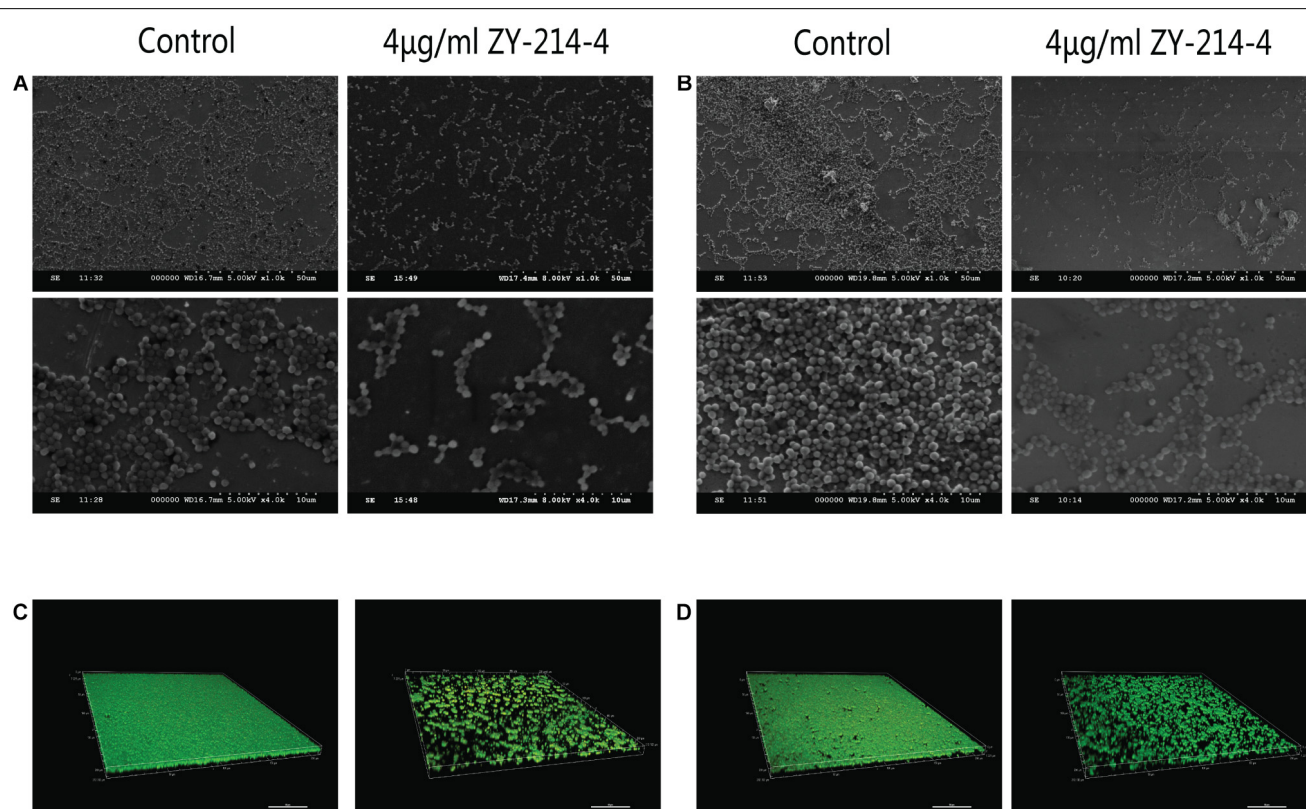
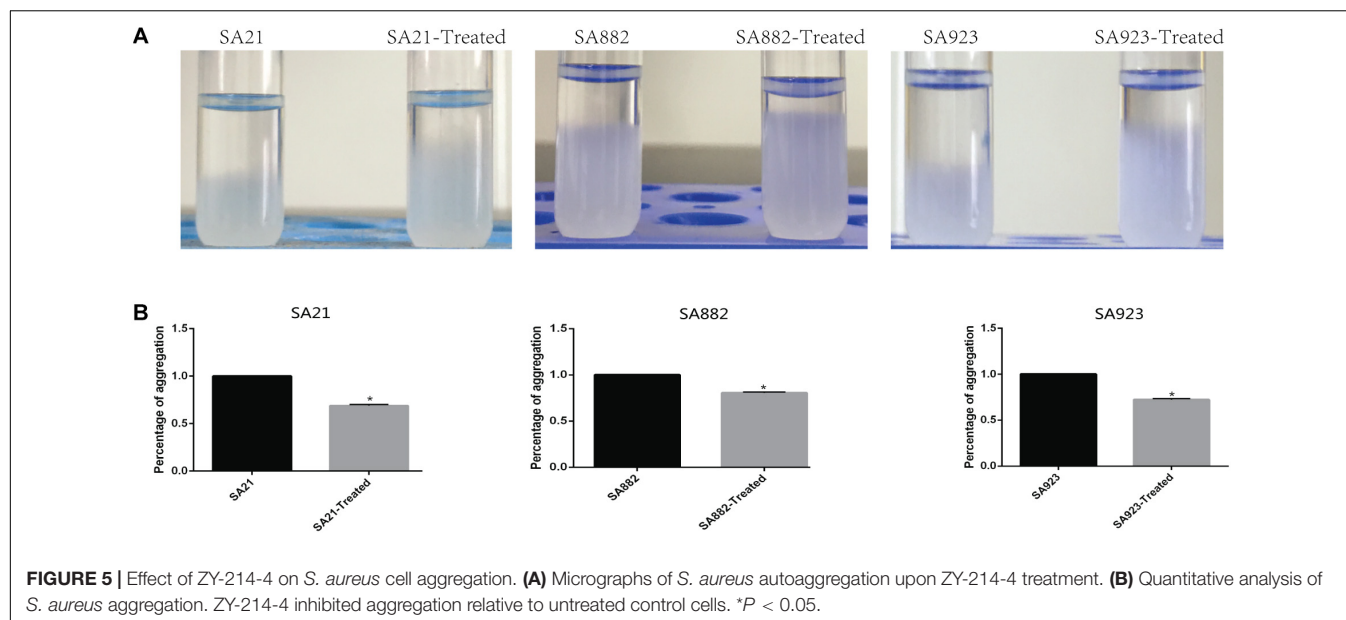


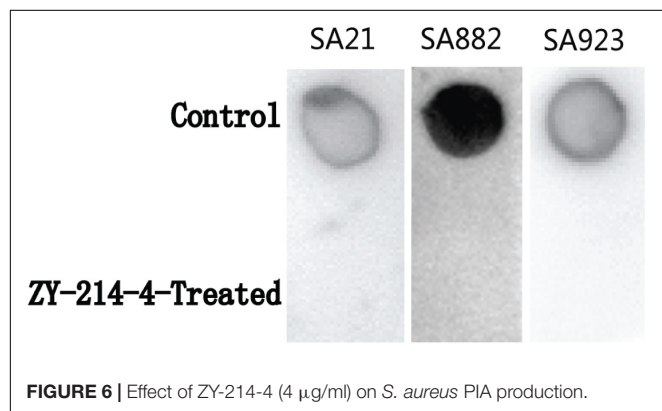
FIGURE 4 | Effect of ZY-214-4 on *S. aureus* biofilm formation evaluated by microscopy. **(A–D)** The antibiofilm potential of ZY-214-4 against *S. aureus* clinical isolates SA21 **(A,C)** and SA923 **(B,D)** was visualized by SEM **(A,B)** and CLSM **(C,D)**.



ZY-214-4 and untreated strains. This indicates that ZY-214-4 prevented *S. aureus* biofilm formation by inhibiting the production of PIA.

ZY-214-4 Suppresses the Expression of *S. aureus* Biofilm-Related Genes

PIA synthesis depends on the expression of the *icaA* gene, but genes encoding microbial surface components that recognize MSCRAMM also play a key role in biofilm formation. PSMs influence bacterial cell aggregation, and their absence can affect biofilm maturation and dissociation. To clarify the mechanism by which ZY-214-4 blocks *S. aureus* biofilm formation, we compared the expression of biofilm-related genes between untreated and ZY-214-4-treated *S. aureus* by RT-PCR. The results showed that the expression of *icaA*, *eno*, *clfA/B*, *fmbB*, *fib*, *ebpS*, *psmA*, and *psmB* genes was downregulated to varying degrees in the latter cells (Figure 7).



ZY-214-4 Is Nontoxic to Bease-2b Cells

We evaluated the cytotoxicity of ZY-214-4 with the CCK-8 assay using Bease-2B human normal bronchial epithelial cells. There was no difference in viability between control and ZY-214-4 treated groups (Figure 8A) and microscopic observation revealed no differences in cell morphology (Figure 8B), indicating that ZY-214-4 is not cytotoxic at a subinhibitory concentration.

DISCUSSION

Biofilms are fixed communities of bacterial cells attached to each other and embedded in a self-produced extracellular polymer (EPS) matrix (Flemming and Wingender, 2010). Biofilms can be formed on various surfaces including ducts, implants, prosthetics, and implanted medical devices (Costerton et al., 1999). There is evidence that cells in biofilms on biotic or abiotic surfaces are 1,000 times more resistant to conventional drugs than planktonic cells (Parsek and Singh, 2003; Verderosa et al., 2019). Once formed, a biofilm is difficult to eliminate and can develop into a chronic and persistent infection.

In this study, we synthesized the small-molecule compound ZY-214-4 and evaluated its antibacterial efficacy against clinical isolates of *S. aureus* obtained from different infection sites. A high concentration of ZY-214-4 inhibited the growth of *S. aureus* (Supplementary Figure S1) while no effect was observed at the subinhibitory concentration of 4 µg/ml. We therefore used the latter in our experiments in order to exclude the possibility that ZY-214-4 prevents *S. aureus* biofilm formation by suppressing cell proliferation.

Downregulation of the *ica* gene encoding PIA is a known mechanism of *S. aureus* biofilm inhibition (Cramton et al., 1999). We found that PIA production by *S. aureus* was

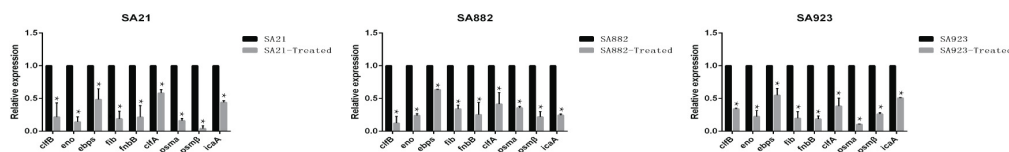


FIGURE 7 | Effect of ZY-214-4 on relative expression of biofilm-related genes in *S. aureus*. Values represent mean \pm SD. Cells grown without ZY-214-4 served as a control. * $P < 0.05$.

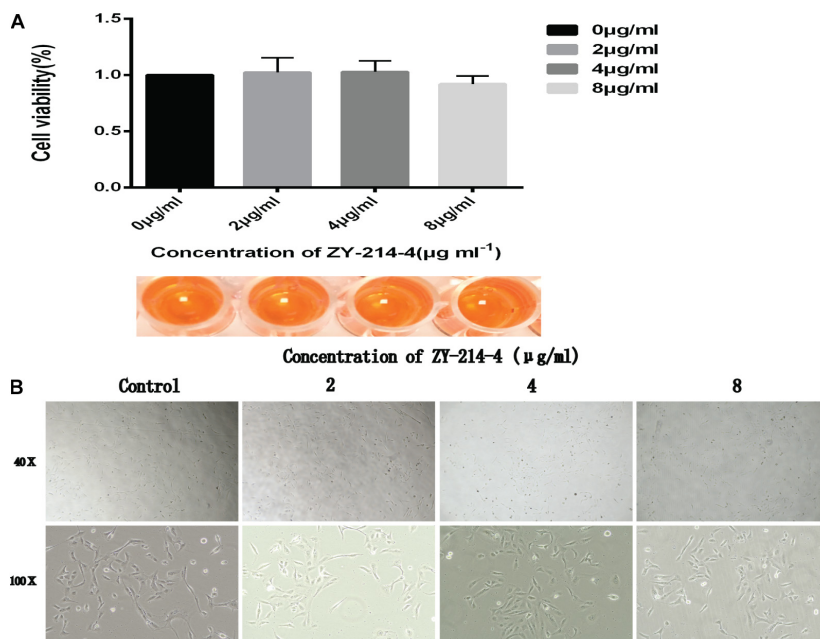


FIGURE 8 | Effect of ZY-214-4 on the growth and morphology of Bease-2B human normal bronchial epithelial cells. **(A)** CCK-8 assay. **(B)** Cell morphology and number evaluated by light microscopy.

decreased by treatment with 4 $\mu\text{g/ml}$ ZY-214-4. This is consistent with the relevant research results of Lee et al. (2013, 2014) on compounds inhibiting the formation of bacterial biofilms. Bacterial cell aggregation is an initial step in biofilm formation (Arciola et al., 2012). In staphylococci, PIA promotes cell-cell adhesion, which is important for cell aggregation following attachment to a surface (Mack et al., 1994; Heilmann et al., 1996). PSMs—especially PSM β —play an important role in cell aggregation (Periasamy et al., 2012; Kim et al., 2020). In this study we found that downregulation of the *psm* gene in the presence of ZY-214-4 was associated with a reduction in *S. aureus* cell aggregation. A consistent conclusion can be found in the relevant research of Lee et al. (2016). Additionally, the expression of genes involved in the initial attachment of cells to each other (*eno*, *clfA/B*, *fnbB*, *fib*, and *ebpS*) was also decreased. Thus, ZY-214-4 prevents biofilm formation by *S. aureus* by blocking the production of PIA and cell aggregation.

Importantly, ZY-214-4 had no cytotoxicity in Bease-2B epithelial cells at a subinhibitory concentration, suggesting that it is safe for use in humans.

This study had some limitations. For example, the mechanism by which ZY-214-4 regulates the expression of *icaA*, *psm*, and other biofilm-related genes remains to be determined. Nonetheless, we demonstrated that the small-molecule ZY-214-4 is non-toxic to human cells and effective in preventing biofilm formation by *S. aureus* at a subinhibitory concentration. These findings highlight the clinical potential of ZY-214-4 for the prevention and treatment of chronic *S. aureus* infections.

DATA AVAILABILITY STATEMENT

The raw data supporting the conclusions of this article will be made available by the authors, without undue reservation.

ETHICS STATEMENT

Written informed consent was obtained from the individual(s) for the publication of any potentially identifiable images or data included in this article.

AUTHOR CONTRIBUTIONS

JY, LR, and YZ designed the work and analyzed and interpreted the data for the work. JY and YG drafted the work and revised it critically for important intellectual content. FY provided approval for publication of the content. LZ, ZS, and XW participated in the experimental design and data analysis. FY agreed to be accountable for all aspects of the work in ensuring that questions related to the accuracy or integrity of any part of the work are appropriately investigated and resolved. All authors read and approved the final manuscript.

FUNDING

This study was supported by the National Natural Science Foundation of China (81871704).

REFERENCES

- Arciola, C. R., Campoccia, D., Speziale, P., Montanaro, L., and Costerton, J. W. (2012). Biofilm formation in *Staphylococcus* implant infections. A review of molecular mechanisms and implications for biofilm-resistant materials. *Biomaterials* 33, 5967–5982. doi: 10.1016/j.biomaterials.2012.05.031
- Atshan, S. S., Nor Shamsudin, M., Sekawi, Z., Lung, L. T., Hamat, R. A., Karunanidhi, A., et al. (2012). Prevalence of adhesion and regulation of biofilm-related genes in different clones of *Staphylococcus aureus*. *J. Biomed. Biotechnol.* 2012:976972.
- Bauer, P. R., and Sampathkumar, P. (2017). Methicillin-resistant *Staphylococcus aureus* infection in ICU: what is the best prevention strategy? *Crit. Care Med.* 45, 1413–1414. doi: 10.1097/ccm.0000000000002516
- Boles, B. R., and Horswill, A. R. (2011). *Staphylococcal* biofilm disassembly. *Trends Microbiol.* 19, 449–455. doi: 10.1016/j.tim.2011.06.004
- Cegelski, L., Marshall, G. R., Eldridge, G. R., and Hultgren, S. J. (2008). The biology and future prospects of antivirulence therapies. *Nat. Rev. Microbiol.* 6, 17–27. doi: 10.1038/nrmicro1818
- Costerton, J. W., Stewart, P. S., and Greenberg, E. P. (1999). Bacterial biofilms: a common cause of persistent infections. *Science* 284, 1318–1322. doi: 10.1126/science.284.5418.1318
- Craft, K. M., Nguyen, J. M., Berg, L. J., and Townsend, S. D. (2019). Methicillin-resistant *Staphylococcus aureus* (MRSA): antibiotic-resistance and the biofilm phenotype. *Medchemcomm* 10, 1231–1241. doi: 10.1039/c9md00044e
- Cramton, S. E., Gerke, C., Schnell, N. F., Nichols, W. W., and Götz, F. (1999). The intercellular adhesion (ica) locus is present in *Staphylococcus aureus* and is required for biofilm formation. *Infect. Immun.* 67, 5427–5433. doi: 10.1128/iai.67.10.5427-5433.1999
- Dayan, G. H., Mohamed, N., Scully, I. L., Cooper, D., Begier, E., Eiden, J., et al. (2016). *Staphylococcus aureus*: the current state of disease, pathophysiology and strategies for prevention. *Expert Rev. Vaccines* 15, 1373–1392. doi: 10.1080/14760584.2016.1179583
- Escaich, S. (2008). Antivirulence as a new antibacterial approach for chemotherapy. *Curr. Opin. Chem. Biol.* 12, 400–408. doi: 10.1016/j.cbpa.2008.06.022
- Feldman, M., Smoum, R., Mechoulam, R., and Steinberg, D. (2018). Antimicrobial potential of endocannabinoid and endocannabinoid-like compounds against methicillin-resistant *Staphylococcus aureus*. *Sci. Rep.* 8:17696.
- Flemming, H. C., and Wingender, J. (2010). The biofilm matrix. *Nat. Rev. Microbiol.* 8, 623–633.
- Gaspar, A., Matos, M. J., Garrido, J., Uriarte, E., and Borges, F. (2014). Chromone: a valid scaffold in medicinal chemistry. *Chem. Rev.* 114, 4960–4992. doi: 10.1021/cr400265z
- Gordon, C. P., Williams, P., and Chan, W. C. (2013). Attenuating *Staphylococcus aureus* virulence gene regulation: a medicinal chemistry perspective. *J. Med. Chem.* 56, 1389–1404.

ACKNOWLEDGMENTS

We are grateful to Professor Liangxing Wang and Professor Xiaoying Huang of Wenzhou Medical University for providing an experimental platform for this study.

SUPPLEMENTARY MATERIAL

The Supplementary Material for this article can be found online at: <https://www.frontiersin.org/articles/10.3389/fmicb.2021.618922/full#supplementary-material>

Supplementary Figure 1 | Growth curves of *S. aureus* strains cultured with ZY-214-4 (>4 µg/ml).

Supplementary Figure 2 | NMR identification of ZY-214-4.

- Heilmann, C., Schweitzer, O., Gerke, C., Vanittanakom, N., Mack, D., and Götz, F. (1996). Molecular basis of intercellular adhesion in the biofilm-forming *Staphylococcus epidermidis*. *Mol. Microbiol.* 20, 1083–1091. doi: 10.1111/j.1365-2958.1996.tb02548.x
- Kannappan, A., Gowrishankar, S., Srinivasan, R., Pandian, S. K., and Ravi, A. V. (2017). Antibiofilm activity of *Vetiveria zizanioides* root extract against methicillin-resistant *Staphylococcus aureus*. *Microb. Pathog.* 110, 313–324. doi: 10.1016/j.micpath.2017.07.016
- Kim, D. R., Lee, Y., Kim, H. K., Kim, W., Kim, Y. G., Yang, Y. H., et al. (2020). Phenol-soluble modulins-mediated aggregation of community-associated methicillin-resistant *Staphylococcus aureus* in human cerebrospinal fluid. *Cells* 9:788. doi: 10.3390/cells9030788
- Kranjec, C., Ovchinnikov, K. V., Grønseth, T., Ebineshan, K., Srikantam, A., and Diep, D. B. (2020). A bacteriocin-based antimicrobial formulation to effectively disrupt the cell viability of methicillin-resistant *Staphylococcus aureus* (MRSA) biofilms. *NPJ Biofilms Microbiomes* 6:58.
- Lee, J. H., Kim, Y. G., Yong Ryu, S., and Lee, J. (2016). Calcium-chelating alizarin and other anthraquinones inhibit biofilm formation and the hemolytic activity of *Staphylococcus aureus*. *Sci Rep* 6:19267.
- Lee, J. H., Park, J. H., Cho, H. S., Joo, S. W., Cho, M. H., and Lee, J. (2013). Antibiofilm activities of quercetin and tannic acid against *Staphylococcus aureus*. *Biofouling* 29, 491–499. doi: 10.1080/08927014.2013.788692
- Lee, K., Lee, J. H., Ryu, S. Y., Cho, M. H., and Lee, J. (2014). Stilbenes reduce *Staphylococcus aureus* hemolysis, biofilm formation, and virulence. *Foodborne Pathog. Dis.* 11, 710–717.
- Lowy, F. D. (2003). Antimicrobial resistance: the example of *Staphylococcus aureus*. *J. Clin. Invest.* 111, 1265–1273. doi: 10.1172/jci18535
- Mack, D., Nedelmann, M., Krokotsch, A., Schwarzkopf, A., Heesemann, J., and Laufs, R. (1994). Characterization of transposon mutants of biofilm-producing *Staphylococcus epidermidis* impaired in the accumulative phase of biofilm production: genetic identification of a hexosamine-containing polysaccharide intercellular adhesin. *Infect. Immun.* 62, 3244–3253. doi: 10.1128/iai.62.8.3244-3253.1994
- Martinez, A., Alonso, M., Castro, A., Dorronsoro, I., Gelpi, J. L., Luque, F. J., et al. (2005). SAR and 3D-QSAR studies on thiazolidinone derivatives: exploration of structural requirements for glycogen synthase kinase 3 inhibitors. *J. Med. Chem.* 48, 7103–7112. doi: 10.1021/jm040895g
- O’Gara, J. P. (2007). ica and beyond: biofilm mechanisms and regulation in *Staphylococcus epidermidis* and *Staphylococcus aureus*. *FEMS Microbiol. Lett.* 270, 179–188.
- Parsek, M. R., and Singh, P. K. (2003). Bacterial biofilms: an emerging link to disease pathogenesis. *Annu. Rev. Microbiol.* 57, 677–701. doi: 10.1146/annurev.micro.57.030502.090720
- Periasamy, S., Joo, H. S., Duong, A. C., Bach, T. H., Tan, V. Y., Chatterjee, S. S., et al. (2012). How *Staphylococcus aureus* biofilms develop their characteristic

- structure. *Proc. Natl. Acad. Sci. U.S.A.* 109, 1281–1286. doi: 10.1073/pnas.1115006109
- Queck, S. Y., Khan, B. A., Wang, R., Bach, T. H., Kretschmer, D., Chen, L., et al. (2009). Mobile genetic element-encoded cytolyisin connects virulence to methicillin resistance in MRSA. *PLoS Pathog.* 5:e1000533. doi: 10.1371/journal.ppat.1000533
- Reis, J., Gaspar, A., Milhazes, N., and Borges, F. (2017). Chromone as a privileged scaffold in drug discovery: recent advances. *J. Med. Chem.* 60, 7941–7957. doi: 10.1021/acs.jmedchem.6b01720
- Schlag, S., Nerz, C., Birkenstock, T. A., Altenberend, F., and Götz, F. (2007). Inhibition of staphylococcal biofilm formation by nitrite. *J. Bacteriol.* 189, 7911–7919. doi: 10.1128/jb.00598-07
- Thoma, G., Nuninger, F., Falchetto, R., Hermes, E., Tavares, G. A., Vangrevelinghe, E., et al. (2011). Identification of a potent Janus kinase 3 inhibitor with high selectivity within the Janus kinase family. *J. Med. Chem.* 54, 284–288. doi: 10.1021/jm101157q
- Tsompanidou, E., Denham, E. L., Becher, D., de Jong, A., Buist, G., van Oosten, M., et al. (2013). Distinct roles of phenol-soluble modulins in spreading of *Staphylococcus aureus* on wet surfaces. *Appl. Environ. Microbiol.* 79, 886–895. doi: 10.1128/aem.03157-12
- Verderosa, A. D., Totsika, M., and Fairfull-Smith, K. E. (2019). Bacterial biofilm eradication agents: a current review. *Front. Chem.* 7:824. doi: 10.3389/fchem.2019.00824
- Verma, A. K., and Pratap, R. (2010). The biological potential of flavones. *Nat. Prod. Rep.* 27, 1571–1593. doi: 10.1039/c004698c
- Wagner, J., von Matt, P., Sedrani, R., Albert, R., Cooke, N., Ehrhardt, C., et al. (2009). Discovery of 3-(1H-indol-3-yl)-4-[2-(4-methylpiperazin-1-yl)quinazolin-4-yl]pyrrole-2,5-dione (AEB071), a potent and selective inhibitor of protein kinase C isotypes. *J. Med. Chem.* 52, 6193–6196. doi: 10.1021/jm901108b
- Waksman, S. A. (1947). What is an antibiotic or an antibiotic substance? *Mycologia* 39, 565–569. doi: 10.2307/3755196
- Zhou, Y., Liang, H., Sheng, Y., Wang, S., Gao, Y., Zhan, L., et al. (2020). Ruthenium(II)-catalyzed C–H activation of chromones with maleimides to synthesize succinimide/maleimide-containing chromones. *J. Org. Chem.* 85, 9230–9243. doi: 10.1021/acs.joc.0c01223

Conflict of Interest: The authors declare that the research was conducted in the absence of any commercial or financial relationships that could be construed as a potential conflict of interest.

Copyright © 2021 Yu, Rao, Zhan, Zhou, Guo, Wu, Song and Yu. This is an open-access article distributed under the terms of the Creative Commons Attribution License (CC BY). The use, distribution or reproduction in other forums is permitted, provided the original author(s) and the copyright owner(s) are credited and that the original publication in this journal is cited, in accordance with accepted academic practice. No use, distribution or reproduction is permitted which does not comply with these terms.



The Bactericidal Tandem Drug, AB569: How to Eradicate Antibiotic-Resistant Biofilm *Pseudomonas aeruginosa* in Multiple Disease Settings Including Cystic Fibrosis, Burns/Wounds and Urinary Tract Infections

OPEN ACCESS

Edited by:

Rustam Aminov,
University of Aberdeen,
United Kingdom

Reviewed by:

Scott Rice
Nanyang Technological University,
Singapore
Naresh Kumar,
University of New South Wales,
Australia
Liang Yang,
Southern University of Science
and Technology, China

*Correspondence:

Daniel J. Hassett
Daniel.Hassett@UC.Edu

Specialty section:

This article was submitted to
Antimicrobials, Resistance
and Chemotherapy,
a section of the journal
Frontiers in Microbiology

Received: 08 December 2020

Accepted: 07 April 2021

Published: 17 June 2021

Citation:

Hassett DJ, Kovall RA, Schurr MJ,
Kotagiri N, Kumari H and Satish L
(2021) The Bactericidal Tandem Drug,
AB569: How to Eradicate
Antibiotic-Resistant Biofilm
Pseudomonas aeruginosa in Multiple
Disease Settings Including Cystic
Fibrosis, Burns/Wounds and Urinary
Tract Infections.
Front. Microbiol. 12:639362.
doi: 10.3389/fmicb.2021.639362

Daniel J. Hassett^{1*}, Rhett A. Kovall¹, Michael J. Schurr², Nalinikanth Kotagiri³,
Harshita Kumari³ and Latha Satish^{4,5}

¹ Department of Molecular Genetics, Biochemistry and Microbiology, Cincinnati, OH, United States, ² Department of Immunology and Microbiology, University of Colorado Health Sciences, Denver, CO, United States, ³ Division of Pharmacy, University of Colorado Health Sciences, Denver, CO, United States, ⁴ Department of Pathology and Laboratory Medicine, University of Cincinnati College of Medicine, Cincinnati, OH, United States, ⁵ Shriners Hospitals for Children—Cincinnati, Cincinnati, OH, United States

The life-threatening pandemic concerning multi-drug resistant (MDR) bacteria is an evolving problem involving increased hospitalizations, billions of dollars in medical costs and a remarkably high number of deaths. Bacterial pathogens have demonstrated the capacity for spontaneous or acquired antibiotic resistance and there is virtually no pool of organisms that have not evolved such potentially clinically catastrophic properties. Although many diseases are linked to such organisms, three include cystic fibrosis (CF), burn/blast wounds and urinary tract infections (UTIs), respectively. Thus, there is a critical need to develop novel, effective antimicrobials for the prevention and treatment of such problematic infections. One of the most formidable, naturally MDR bacterial pathogens is *Pseudomonas aeruginosa* (PA) that is particularly susceptible to nitric oxide (NO), a component of our innate immune response. This susceptibility sets the translational stage for the use of NO-based therapeutics during the aforementioned human infections. First, we discuss how such NO therapeutics may be able to target problematic infections in each of the aforementioned infectious scenarios. Second, we describe a recent discovery based on years of foundational information, a novel drug known as AB569. AB569 is capable of forming a “time release” of NO from S-nitrosothiols (RSNO). AB569, a bactericidal tandem consisting of acidified NaNO₂ (A-NO₂⁻) and Na₂-EDTA, is capable of killing all pathogens that are associated with the aforementioned disorders. Third, we described each disease state in brief, the known or predicted effects of AB569 on the viability of PA, its potential toxicity and highly

remote possibility for resistance to develop. Finally, we conclude that AB569 can be a viable alternative or addition to conventional antibiotic regimens to treat such highly problematic MDR bacterial infections for civilian and military populations, as well as the economical burden that such organisms pose.

Keywords: bactericidal, AB569, cystic fibrosis, burns/wounds, urinary tract infections

Pseudomonas Aeruginosa

Pseudomonas aeruginosa (PA) is an opportunistic pathogen of multiple human infections including but are not limited to cystic fibrosis (CF) airway disease, chronic obstructive pulmonary disease (COPD), wounds (lacerations, abrasions, burns, blast, diabetic), bone, catheter, implant/prosthetic devices, inner ear, urinary tract (UTI), heart valve, and many others. PA is also a member of the six notorious ESKAPE pathogens (*E. faecium*, *S. aureus*, *K. pneumoniae*, *A. baumannii*, PA, and *Enterobacter* sp.), organisms representing those that are multi-drug resistant (MDR) and highly problematic to overall global health. In this review, we will focus on three disease states, CF, burns and UTIs, where MDR-PA is a significant problem pathogen, and within the past several decades, highly refractory to conventional antibiotic regimens.

Despite the relative success of early, aggressive (“eradication”) treatments, *P. aeruginosa* (especially MDR-PA) remains the leading and, arguably, the most formidable pathogen in CF. The majority of individuals with CF becomes chronically infected by adulthood—and although chronic suppressive antimicrobial therapy, primarily with inhaled agents such as tobramycin, aztreonam and colistin, has clear benefits in slowing the progression of lung disease, this intensive antimicrobial exposure drives antibiotic resistance. Approximately one-third of PA recovered from adults with CF have an MDR phenotype (Cystic Fibrosis Foundation Patient Registry, 2019 Annual Data Report Bethesda, MD), presenting an enormous challenge to effective antimicrobial therapy, particularly in those with advanced disease.

CYSTIC FIBROSIS (CF)

Although a multi-organ disease, CF is most commonly associated with lung abnormalities, particularly CFTR-mediated Cl[−] secretion across the apical membrane of secretory epithelial cells. CFTR is a multi-transmembrane spanning ABC transporter, the primary function of which is Cl[−] transport across secretory epithelia (Fenker et al., 2018). Greater than 2000 mutations in *cftr* have been identified (Egan, 2016; Lopes-Pacheco, 2016). These result in several classes of protein dysfunction, affecting CFTR (I) synthesis, (II) maturation, (III) regulation, (IV) conductance, (V) quantity, and (VI) stability (**Figure 1**; Tildy and Rogers, 2015). The most common mutation is F508del (class II), which exists in ~70% of CF patients (Rowntree and Harris, 2003). Others such as G542X (class I) and G551D (class III) represent only ~1–3% of all mutations world-wide (Rogan et al., 2011). Each class of mutations is associated with different degrees of

clinical manifestation of CF ranging from severe disease (classes I–III, and VI, (Kerem and Kerem, 1996; Yeh et al., 2019) to moderate or mild disease (classes IV–VI). CFTR class also dictates the quantity and composition of mucins expressed in airways (Thornton et al., 2008) that is likely also mediated by the NPo (number of channels open probability). Generally, CF mucus is 2/3 of the mucins MUC5B and 1/3 MUC5AC in large airways, whereas MUC5B dominates the small airways where the most notable disease is evident. MUC5B is essential for muco-ciliary clearance and bacterial infection control while MUC5AC appears dispensable for the latter functions (Roy et al., 2014). One key feature of normal vs. CF mucus is that the former contains 2% solids, with the latter containing 8–10% (Martens et al., 2011). These mucin proportions represent huge differences of readily available and degradable proteinaceous substrate for metabolism and growth by pathogenic bacteria residing as biofilms within the airway mucus. An underappreciated, yet important feature of this variation in airway mucus is the impact this has on the antibiotic-resistance properties of bacteria residing in the airways in the form of what the corresponding author has coined “Mode II” biofilms (organisms enmeshed in thick mucus as opposed to surface-attached Mode I) (**Figure 2B** vs. **Figure 2A**). Metabolism of carbon-rich moieties (including mucin) within such biofilms allows PA (Henke et al., 2011), and many other MDR pathogens such as *Burkholderia cepacia* (Schwab et al., 2014) and *Mycobacterium abscessus* complex (Hunt-Serracin et al., 2019) to thrive in such a niche. The metabolism of mucins in CF can be by serine proteases including those from neutrophils and by PA elastase B (pseudolysin) (Henke et al., 2011) and protease PA3247 (Alrahman and Yoon, 2017). Rather, mucins are fermented by anaerobes in CF to form the readily metabolizable acid, propionate (Flynn et al., 2016), that is readily utilized as a viable carbon source for PA metabolism.

Problematic Bacterial Infections in CF and a Dearth of Novel Antimicrobials

Despite the tremendous early success of CFTR modifier drug therapy, current evidence indicates that airway infection will continue to be a cause of morbidity and premature mortality in CF. This is especially true for the large proportion of persons with CF whose lung disease preceded the advent of CFTR modifier therapy [for recent review, see Egan (2020)]. In these individuals, particularly those with moderate to severe lung disease, chronic infection, often with MDR-PA bacteria, presents an important and serious challenge to clinical care. Unfortunately, the development of novel antibiotics to meet this challenge has faltered, with no new classes of antibiotics being developed in the last 20 years. Although new combination

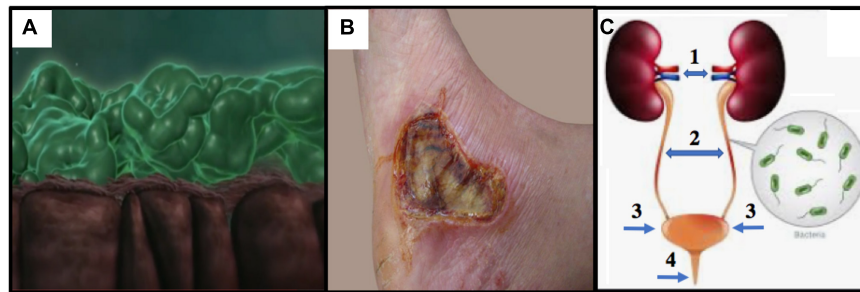


FIGURE 1 | (A) CF lung epithelium (brown) with flattened cilia and thick PA Mode II biofilms (green mats) clogging the airway lumen (snapshot from video at <https://www.youtube.com/watch?v=YzjnxegMWfk>). **(B)** Third degree burn on right foot of male. Note the burn breached the dermis, thereby exposing the hypodermis (from <https://www.verywellhealth.com/burn-pictures-4020409>). **(C)** The human urinary tract and the potential for (1) pyelonephritis, (2,3) cystitis and (4) urethritis (numbering and arrows added from <https://projectheartbeat.com/how-to-a-prevent-urinary-tract-infection-in-the-elderly>).

of β -lactam/ β -lactamase drugs (e.g., ceftazidime/avibactam and meropenem/vaborbactam) showed promise in filling this gap, resistance of bacteria recovered from CF patients to these agents is also on the rise (Caverly et al., 2019).

Multidrug-Resistant (MDR) Epidemic Strains of *P. aeruginosa* in CF Airway Disease, Hypoxic/Anaerobic Biofilms, and Relationships to Nitric Oxide (NO)

Our seminal past findings (Yoon et al., 2002) coupled with those of Worlitzsch et al. (2002) demonstrated an unappreciated yet important clinical feature of the thick mucus lining the CF airways. We discovered that this mucus is hypoxic or even anaerobic, representing an ideal growth environment for a myriad of opportunistic bacteria that form antibiotic-refractory Mode II biofilms enmeshed in the mucus as “soccerball”-like structures (Figures 2C,D, chronic CF Mode II biofilms; Su and Hassett, 2012). For over 50 years, the most prevalent CF airway pathogen has been *PA*, that exists in about 70–80% of adult patients (O’Toole, 2018), and can grow under both aerobic and anaerobic conditions (Hassett et al., 2004, 2009). Established pulmonary physiology research indicates that nitric oxide (NO), an important antimicrobial component of our innate immune system (Fang, 1997) and potentially toxic bacterial metabolite during anaerobic growth (Yoon et al., 2002), is present at lower levels in CF airways compared to normal individuals (Grasemann et al., 1998; Grasemann and Ratjen, 2012). The diminished production of NO in CF lungs may be an important factor accounting for hypersusceptibility to infections by *PA*. Still, despite such reduced NO levels, its oxidation to the alternative electron acceptors nitrate (NO_3^-) and nitrite (NO_2^-) likely contributes to microaerobic/anaerobic biofilm growth in the thick mucus (Hassett, 1996; Jones et al., 2000; Palmer et al., 2007a). The importance of these findings, especially in the context of the ever-burgeoning global antibiotic resistance pandemic, is that the most problematic CF infections currently involve multidrug-resistant *PA* strains (MDR-*PA*) that often acquire adaptive mutations *in vivo*. Clinically, the presence of such strains often triggers a prolonged course of antibiotics, which have

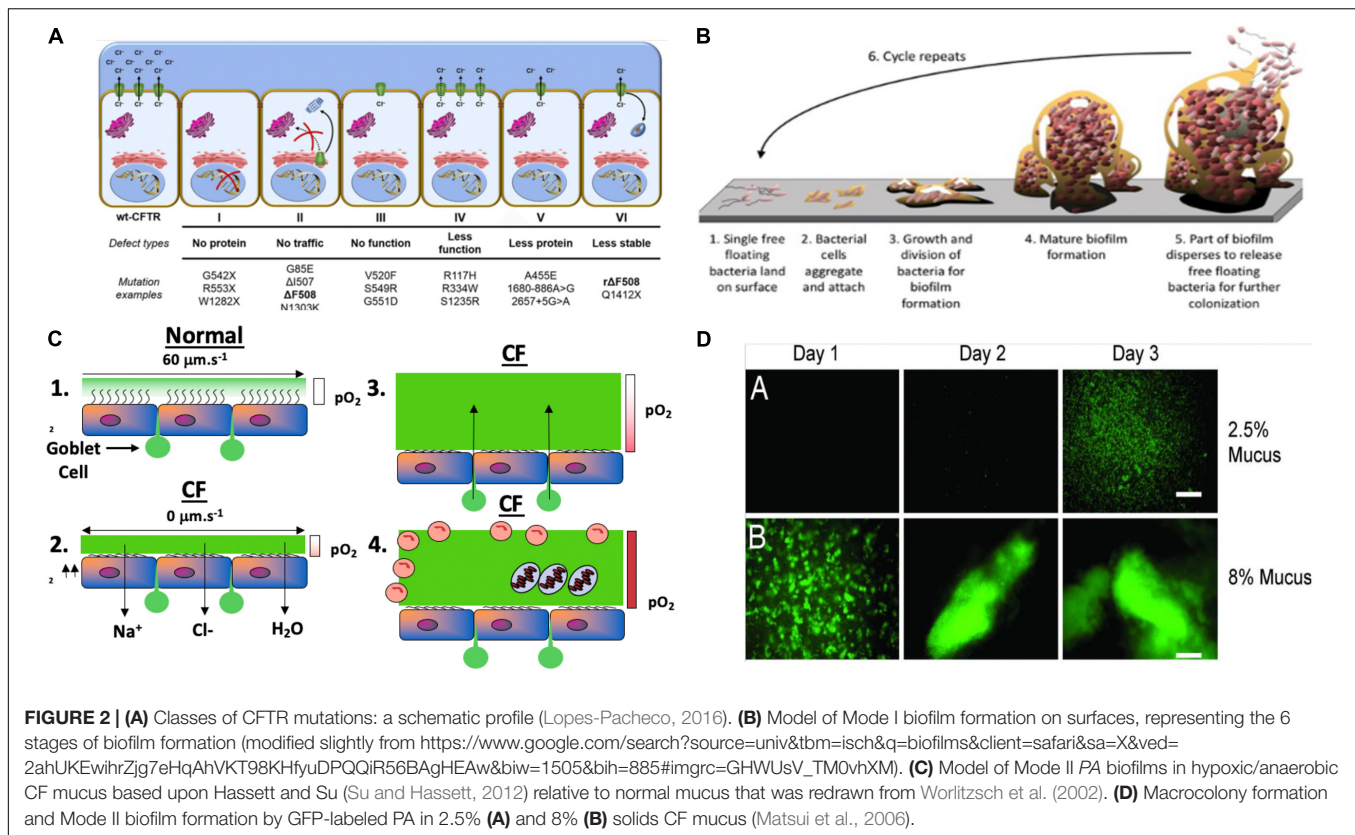
promoted the development of resistance to virtually all antibiotic classes. Thus, the impact of antimicrobial NO, NO donors and AB569 will be discussed later in this review.

BURN WOUNDS

Burn wounds represent various breaches of the skin mediated by thermal injury. First degree burns often do not breach the skin, causing some redness, pain, and swelling (e.g., sunburn). In contrast, second degree burns can affect both the epidermis and dermis via contact with stoves, boiling water/oil or fire exposure. Severe pain and infections can ensue, especially when the burn covers large surface areas. Finally, third degree burns essentially remove the dermal and epidermal layers, and perhaps part of the hypodermis. Such burns may surprisingly not be painful, due to extensive nerve damage. These burns may be hard in consistency, be moisture-free, and have a leathery consistency.

Several thousand people die each year because of complications from burn wounds (Mayhall, 2003). Although some burn patients die of burn shock during the first hours, the major course of death is infections, and it is estimated that 75% of all deaths following burns are directly correlated to infection (O’Sullivan and O’Connor, 1997). Burns and wounds occurring in the civilian population are very different from those encountered by the military population. Sir William Osler noted 105 years ago during the artillery war treating casualties that “*shrapnel does the damage, tearing flesh, breaking bones, and always causing jagged, irregular wounds. And here comes in the great tragedy- sepsis everywhere, unavoidable sepsis*” (Osler, 1914). Severe injury of the skin followed by burn/wound infection and sepsis is a serious threat to the life of the patient, as the skin is the largest organ in the body. Sepsis is still a major issue because of its complex pathophysiology (Russell, 2006). Infection leads to complications from sepsis and poses problems to wound healing resulting in significant morbidity. More than 52,000 U.S. military personnel were wounded in action in Iraq [Operation Iraqi Freedom (OIF)] and Afghanistan [Operation Enduring Freedom (OEF)]¹. The type of infections complicating combat injuries

¹www.defense.gov/casualty.pdf



during OIF/OEF was mainly wound infections (84%) followed by blood stream infections (38%). *Acinetobacter* spp. was the most common bacteria associated with infection followed by *Escherichia coli* and *Pseudomonas* spp. (Petersen et al., 2007). However, within a few days, 14–33% of burn wounds are colonized with PA (Steinstraesser et al., 2010; Nagoba et al., 2013). PA secretes many proinflammatory virulence factors, including elastase, exotoxin A, phospholipase, pyocyanin, rhamnolipid, and homoserine lactones (McCarthy et al., 2014). In addition, this organism possesses a variety of drug resistance mechanisms: inactivation or suppression of enzyme production, increased expression of an active efflux pump system, biofilm formation, and loss or decreased expression of outer membrane proteins or flagella (Livermore, 2002; Lewis, 2008). Burn patients infected with PA show a higher mortality rate (Mahar et al., 2010). Biofilms are also an important factor in burn wounds, a process found independent of quorum sensing (QS) (Schaber et al., 2007). It was later found that PA requires long chain fatty acids as substrates during acute burn infections (Turner et al., 2014).

Sepsis is often preceded by infectious complications (van Langeveld et al., 2017). Infection is the main cause of delayed wound healing in various types of wounds, including burns (Leaper, 2006). Wound healing is another major issue in the chronology of burn-related disease. Healing is, in part, impeded by the QS-dependent production of PA virulence factors that trigger elevated levels of proinflammatory IL-6, TGF- β , and G-CSF (Rumbaugh et al., 2004). Without rapid and optimal control, patients with severely extensive burns and sepsis

can rapidly develop systemic inflammatory response syndrome (SIRS), which results in the damage of many organs, such as the lung, liver and kidney. This leads to the development of multiple organ dysfunction syndrome (Martin et al., 2003; Seymour et al., 2010). Despite improvements in early treatment, survival following burn injury remains challenged, due largely to sepsis, the leading cause of death in both civilian and military populations. As such, antibiotic regimens are predictably and commonly prescribed in the burn population (Rex, 2012). This antibiotic exposure combined with other risk factors increases the risk for acquisition of multidrug-resistant (MDR) bacteria, a global pandemic which poses a formidable threat to human health. These infections are of particular importance to wounded military personnel and veterans, as hospital-associated transmissions of MDR bacteria are common in the settings of surgical sites and trauma units. Thus, given all of the aforementioned issues, burn injuries can frequently result in life-threatening complications (Calhoun et al., 2008). In fact, deaths from drug-resistant infections are projected to increase from 700,000 currently to 10 million annually, and cost estimates are projected to be as high as \$100 trillion (US) world-wide by 2050 (Jasovsky et al., 2016). Developing new antibiotics alone cannot fully address the problem, as bacteria inevitably develop resistance to them (Coates and Hu, 2007). Therefore, there have been tremendous efforts to develop alternative approaches to conventional antibiotics for the prevention and treatment of microbial infections. Indeed, the US government has announced a National Strategy to address the problem of antimicrobial

resistance². Current topical antimicrobial agents suffer from multiple issues including (a) bacterial resistance (b) lack of penetration into the burn eschar tissues (c) wound healing inhibition and (d) pain upon application that poses adverse systemic effects (Cartotto, 2017). Therefore, it is imperative to develop an agent that can surpass all the aforementioned problems, and can be applied immediately after burn injury in the battlefield and to the civilian patients to prevent biofilm formation while simultaneously promoting wound healing.

URINARY TRACT INFECTIONS AND PA

Urinary tract infections (UTIs) affect an estimated 150 million people worldwide per year and are the leading cause of nosocomial infections in the U.S. In fact, UTIs account for an astounding 40% of all nosocomial infections. Bacterial UTI pathogens include *Escherichia coli*, *Klebsiella pneumoniae*, *Proteus mirabilis*, *Enterococcus* spp., and PA. The most frequent cause of problematic UTIs and catheter associated UTI (CAUTI) which is one of the most common infections acquired by patients in health care facilities is *E. coli*, particularly those exhibiting Extended Spectrum β -Lactamase (ESBL) resistance. However, PA is associated with chronic UTI especially with CAUTI and most PA isolates are resistant to conventional antibiotics used for treatment (Newman et al., 2017). Despite improvements in early therapeutic intervention, increased mortality rates due to antibiotic-resistant bacteria is an ever-burgeoning global health problem. The CDC estimates antibiotic resistant ESKAPE pathogens such as PA cause 2.8 million illnesses and approximately 35,000 deaths per year. PA (especially MDR-PA) remains a formidable pathogen in UTIs (Jarvis and Martone, 1992). The CDC considers antibiotic resistance to be among the “biggest threats” because pathogens rapidly evolve new mechanisms to combat drug therapy. PA is especially linked with CAUTI and most clinical isolates are resistant to antibiotic treatment regimens. Given these important issues, it is crucial for developing novel antimicrobial agents or alternative tools to combat MDR-PA in UTIs, a huge public health challenge, especially in the highly vulnerable elderly population (Ismail et al., 1997). Bacterial biofilms forming on catheters can cause complicated treatment of CAUTI. Such biofilm catheter infections can lead to pyelonephritis and are nearly impossible to kill because they are up to 1,000-fold more resistant to antibiotics compared to their planktonic (free-living) counterparts due to acquired or inherent antibiotic resistance but also because of poor penetration issues (Stewart, 1996). Generally, the elderly and women are most susceptible to PA UTIs and require costly, intensive treatment strategies. The contribution of other host factors and bacterial virulence factors (Newman et al., 2017) to successful infection remains relatively understudied. Thus, there is still a critical and unmet need for effective antimicrobials that (i) prevent, (ii) treat and (iii) eradicate problematic MDR-PA biofilms in UTIs.

²<https://www.cdc.gov/drugresistance/us-activities.html>

Given the urgent need for the treatment of MDR-PA infections for the aforementioned 3 disease states, we will now shift our course to (i) a brief description of the novel drug, AB569, (ii) to a detailed step-by-step research progression behind the fascinating scientific path that led to its discovery and (iii) some proposed mechanisms of bactericidal action.

REVISITING NO, ITS PHYSIOLOGICAL SOURCES, AND REGULATION OF ITS PRODUCTION IN CF, BURNS AND UTIS

NO itself is antimicrobial, yet it has only a very short half-life in blood (<2 ms). In contrast, NO_2^- has 1.2 million-fold higher half-life (~40 min, Borlaug et al., 2016) and is reduced to NO from A- NO_2^- (Yoon et al., 2006; Major et al., 2010) or under hypoxic conditions (e.g., heart failure, Simon et al., 2016). The primary sources of NO in the human body are through its generation by three different NO synthases (NOS). Two NOS enzymes, the neuronal NOS (nNOS) and the epithelial NOS (eNOS), are expressed constitutively (Asano et al., 1994). Arguably the most influential with respect to combating pathogen infection is the inducible class of NOS (iNOS) (Fan et al., 1997; Ricciardolo et al., 2004). iNOS is inducible by a number of factors that include bacterial LPS (Nathan and Xie, 1994) and proinflammatory cytokines such as the T-cell generated cytokine IFN- γ (Remy et al., 2017). In CF, iNOS2 activity is dramatically reduced (Wooldridge et al., 2004; Moeller et al., 2006). Such reduced activity is thought to contribute to airway colonization and persistence in the CF airway luminal mucus. Similarly, patients suffering from burns also have reduced neutrophilic iNOS2 activity (Kartchner et al., 2019). In contrast with CF and burn infections, NO synthase activity was significantly increased during UTI (Smith et al., 1996).

PHAGOCYTE CONTRIBUTIONS OF NO-MEDIATED KILLING OR GROWTH INHIBITION OF PA

The respiratory burst of human phagocytic cells NADPH oxidase-catalyzed by the can generate a number of oxygen-centered radicals including the superoxide anion (O_2^-), hydrogen peroxide (H_2O_2), hydroxyl radical ($\text{HO}\cdot$), singlet oxygen ($^1\text{O}_2$) and hypochlorous acid (HOCl). Given that O_2^- is the first radical generated by this process, it can rapidly react with NO in the presence of oxygen to generate highly reactive, diffusion-limited oxidant peroxynitrite (ONOO^-). In addition to many other cell types in the body, NO can also be generated via iNOS enzymes in both macrophages and neutrophils (MacMicking et al., 1997; Saini and Singh, 2019). However, this event requires accessory contributions by either bacterial LPS or various cytokines (e.g., TNF- α , IL-1, INF- γ). Regarding CF, the versatile chemistry of nitrogen is of central importance to pulmonary physiology, as nitrogen oxidation and reduction occur continuously in both normal and CF lungs. NO is an important antimicrobial component of our innate

immune system (Fang, 1997) and a member of what are termed reactive nitrogen species (RNS). Of many conflicting reports, the majority indicate that exhaled NO from CF patients is lower than that produced by normal individuals (Grasemann et al., 1998; Grasemann and Ratjen, 2012). Thus, despite low CF airway NO, one likely reason why concentrations of the dominant CF pathogen, PA (Yoon et al., 2002; Palmer et al., 2007b), can approach 10^8 CFU/ml within microaerobic or anaerobic CF mucus is that it is rich in the alternative electron acceptors NO_3^- (383 ± 42 mM) and NO_2^- (125 ± 55 mM) (Jones et al., 2000), levels which are 2–3 fold higher than in normal individuals (Hassett, 1996; Palmer et al., 2007a).

HOW DOES PA SENSE AND COMBAT NO?

Arguably, the most influencing proteins involved in NO metabolic are enzymes which detoxify it, including NOR (Arai et al., 1995) and the hemoglobin/NO dioxygenase, Hmp (Yoon et al., 2007). As expected, bacteria lacking NOR grow abysmally slowly under anaerobic conditions (Yoon et al., 2007). This is due to the NO-mediated inactivation of the 4Fe-4S cluster of the master anaerobic regulator, ANR (Yoon et al., 2007). Without ANR, the NO-responsive second-tier regulator, DNR, is incapable of activating downstream *nar*, *nir*, *nor*, and *nos* genes (Schreiber et al., 2007). Elegant recent work by Boon and colleagues have illuminated previously unrecognized NO binding proteins (Hossain and Boon, 2017; Bacon et al., 2018; Williams et al., 2018; Williams and Boon, 2019). NosP, an NO-sensing protein, was discovered by Boon and colleagues as a critical protein involved in the dispersal of mature PA biofilms (Hossain and Boon, 2017). NosP was actually a protein that was anticipated to exist, for the majority of bacteria NO sensing protein are of the H-NOX variety (Williams et al., 2018; Williams and Boon, 2019). NosP is also a regulator of a histidine kinase signal transduction pathway that paradoxically is also critical for optimal biofilm formation (Williams et al., 2018).

NO GENERATORS AND CONTROL AND/OR KILLING OF PA IN BIOFILMS

NO, or their chemical generators, have also been used in the treatment of biofilms from two different fronts. First, there is the antimicrobial end. NO itself or compounds that generate it by hydrolysis or reduction, is capable of killing not only PA biofilms, but also a myriad of other problematic pathogens. Regarding biofilm control, dispersal and/or killing of resident bacteria, many compounds that are not NO or acidified nitrite have been used. For examples, please refer to **Table 1**. In an *ex vivo* model of PA dispersion, submicromolar NO disrupted biofilms in CF sputum (Howlin et al., 2017). Another example Barraud and colleagues ion 2006 (Barraud et al., 2006) demonstrated that NO-generating compounds are capable of dispersing mature PA biofilms. The addition of NO release significantly improved the antibiofilm action of

the hyperbranched polymers, with NO-releasing hyperbranched polyamidoamines of largest NO payloads being more effective than hyperbranched polykanamycins. Furthermore, the NO-releasing hyperbranched polymers reduced the biofilm metabolic activity in a dose-dependent manner, killing biofilm-detached bacteria under both aerobic and anaerobic conditions, with greater antimicrobial efficacy observed under aerobic conditions (Yang et al., 2020). Other similar NO-generating compounds include sodium nitroprusside (SNP, Barraud et al., 2006), S-nitrosoglutathione (GSNO Neufeld and Reynolds, 2016), spermine NON-Oate (Cai and Webb, 2020), NO-releasing alginates (Ahonen et al., 2018), and chitosan oligosaccharides (Reighard et al., 2015). Cephalosporin-based NO donor prodrugs (cephalosporin-3'-diazoniumdiolates) not only release NO, but possess direct β -lactam mediated antibacterial activity and antibiofilm effects (Yepuri et al., 2013; Rineh et al., 2020). Cephalosporin NO-donor prodrug DEA-C3D (diethylamin-cephalosporin-3'-diazoniumdiolate) has also been shown to disperse PA biofilms formed by cystic CF isolates (Soren et al., 2020). Finally, additional biocompatible compounds oligoethylene glycol, hydrophobic ethylhexyl, cationic primary amine, and nitric oxide (NO)-releasing functional groups have been not only shown to disperse mature biofilms, but also puncture membranes (18).

WHY INHALED OR TOPICAL NO IS LIKELY NOT NEARLY AS EFFECTIVE AS AB569

First, inhaled NO can rapidly react with O_2 in the lung to form nitrogen dioxide (NO_2), a known potent pulmonary irritant. Second, the vast majority of inhaled NO is exhaled. In the case of pulmonary hypertension, inhaled NO was considered a potential therapy, yet the short half-life of NO requires essentially constant inhalation for a sustained positive effect (Amdahl et al., 2019). In infected airways, AB569 would be aerosolized as a *mist*. In the case of CF, the mucus pH is already acidic (pH 6.3–6.5) where a buffer is not required, thus triggering the production of NO *within* (and not above) the infected airway mucus. In the case of topical use of AB569, the A- NO_2^- component has been used safely to kill other organisms (Weller et al., 1998; Ormerod et al., 1999; Phillips et al., 2004; Jowkar et al., 2010). An A- NO_2^- emollient or cream at 430 mM NaNO_2 has been shown to improve the rate and extent of incision wound healing in normal and diabetic mice (Weller and Finnen, 2006). We have shown that A- NO_2^- (McDonald and Thornton, 1994; McDaniel et al., 2016, 2020), the NO donor sodium nitroprusside (SNP) (Barraud et al., 2009), and an absence of endogenous NO reductase (NOR) (Barraud et al., 2009), triggers PA biofilm dispersion, rendering such organisms now vastly more susceptible to antibiotics. Similarly, the amount of EDTA typically used in nebulized bronchodilators does not induce bronchospasm (Asmus et al., 2001). Some additional benefits of EDTA is that it can disperse and kill mature PA in biofilms (Banin et al., 2006) and can achieve complete eradication of 7 bacterial pathogens (including 5 ESKAPE members) in skin,

TABLE 1 | NO, A-NO₂⁻, GSNO, AB569, and other NO-related anti-pseudomonas compounds and their effects on *P. aeruginosa*.

Agent	Organism	Growth/Biofilm inhibition	Killing	Biofilm dispersion	References
Acidified nitrite	<i>P. aeruginosa</i> PAO1 <i>P. aeruginosa</i> PAO1 <i>mucA22</i> <i>P. aeruginosa</i> FRD1 <i>mucA22</i>	Yes/ND	Yes	ND	Yoon et al., 2006; Major et al., 2010; McDaniel et al., 2016, 2020
Acidified nitrite	<i>P. aeruginosa</i> PAO1	Yes/Yes	Yes	ND	Major et al., 2010
NO donor (SNP)	<i>P. aeruginosa</i> PAO1	ND	ND	Yes	Barraud et al., 2006
EDTA	<i>P. aeruginosa</i> PAO1	Yes/Yes	Yes	Yes	Banin et al., 2006
Na4-EDTA	<i>P. aeruginosa</i>		Yes		Percival and Salisbury, 2018
Acidified Nitrite + Na ₂ -EDTA	All tested Gram-negative and Gram-positive bacteria	Yes/Yes	Yes	Yes	McDaniel et al., 2020
S-nitrosoglutathione (GSNO)	<i>P. aeruginosa</i>	ND/ND	Yes	ND	Neufeld and Reynolds, 2016
Spermine NON-Oate, Sodium nitroprusside	<i>P. aeruginosa</i>	Yes/Yes	No	Yes	Cai and Webb, 2020
NO-releasing alginates	<i>P. aeruginosa</i>	ND/ND	Yes	ND	Ahonen et al., 2018
DEA-C3D (diethylamin-cephalosporin-3'-diazoniumdiolate)	<i>P. aeruginosa</i>	ND	ND	Yes	Yepuri et al., 2013
NO-releasing chitosan oligosaccharides	<i>P. aeruginosa</i>	Yes	ND	Yes	Rineh et al., 2020
	<i>P. aeruginosa</i> PAK <i>fliC pilA</i> , <i>mucA22</i>	Yes/Yes	ND	Yes	Reighard et al., 2015

ND, not determined.

bone, implant infections (Deng et al., 2019). In UTIs, based upon the low pH of morning voided urine, the acidification of nitrite has been shown to kill nitrate reducing bacteria such as *E. coli* and *PA* (Carlsson et al., 2003, 2005). Similarly, Mir and colleagues recently showed that the 3-pronged combination of ceftriaxone, sublactam, and Na₂-EDTA killed infectious bacteria caused by extended spectrum β-lactamase (ESBL)-producing Gram-negative bacteria (Mir et al., 2019).

THE EXPERIMENTAL CHRONOLOGY LEADING TO THE DISCOVERY OF AB569, AN ALTERNATIVE TO STRICTLY NO-BASED THERAPEUTICS

Two Epidemic Mutant Strains of *PA* Emerge During CF Lung Disease: *lasR/rhlR* QS and Mucoid *mucA* Clinical Isolates

PA, like many Gram-negative and Gram-positive bacteria, engages in a form of intercellular communication known as quorum sensing (QS) (Whitehead et al., 2001). QS in *PA* regulates many bacterial processes including virulence factor production (Gambello and Iglewski, 1991; Brint and Ohman, 1995) and animal (Rumbaugh et al., 1999), nematode (Papaioannou et al., 2009), and insect (Park et al., 2014) pathogenesis. *PA* encodes two acyl-homoserine lactone (AHL) QS circuits, LasI/LasR and RhII/RhIR. During *in vivo* evolution in early CF, *lasR/rhlR* mutants in QS circuitry are frequently isolated (Bjarnsholt et al., 2010; Feliziani et al., 2010), especially in the early stages of

the disease. The Liverpool epidemic strain, LES400, is a *lasR* mutant that overproduces the redox-active virulence factor pyocyanin, is highly antibiotic-resistant, and is hyper-virulent (Salunkhe et al., 2005). In addition to QS inactivation, CF isolates during late-stage chronic disease are often mucoid (alginate overproduction) during the late, chronic disease stages, resulting from mutations in the anti-sigma factor gene, *mucA* (Martin et al., 1993; Bjarnsholt et al., 2010; Feliziani et al., 2010). Alginate is a highly viscous exopolysaccharide the production of which causes a precipitous decline in overall airway oxygen processing (Sanderson et al., 2008). Below is an intriguing chronology of why we believe that *lasR/rhlR* and ultimately *mucA* mutants emerge during the course of CF lung disease—a direct connection to the low nitric oxide (NO) levels produced in CF lung disease. Finally, the diminished production of innate NO in CF lungs may be an important factor accounting for hypersusceptibility to infection by *lasR/rhlR* and *mucA* mutant *PA* strains *in vivo*.

lasR and *rhlR* QS Mutants Perish in Anaerobic Biofilms Due to Overproduction of Endogenous, Metabolic Nitric Oxide (NO)

A seminal study in 1998 performed under aerobic conditions indicated that QS was essential for optimal biofilm formation, matrix development and maturation (Davies et al., 1998). We coined such surface attached bacterial structures as Mode I biofilms (Su and Hassett, 2012). A *lasI/rhlI* mutant was found to produce thin and densely packed biofilms relative to the mature, well-developed biofilms of wild-type bacteria. In contrast, those enmeshed within the thick CF mucus are termed Mode II (Su and Hassett, 2012) biofilms (**Figures 2A,B**). In chronic CF lung

disease, there is progressively poor airway oxygenation, resulting in what is termed pulmonary insufficiency (Elborn, 2016). Such events trigger markedly reduced oxygen tension for both the host and resident airway bacteria such as *PA* (Worlitzsch et al., 2002; Yoon et al., 2002). Until 2002, biofilm formation in the context of chronic CF airway disease was poorly understood, especially the role of oxygen tension. Subsequently, Worlitzsch et al. (2002) and Yoon et al. (2002) demonstrated not only hypoxic gradients within the thick mucus, but also anaerobic conditions. Given these discoveries coupled with the near crippling CF airway oxygenation of chronic CF patients, we elected to examine the role of QS under strict anaerobic conditions. First, wild-type bacteria were discovered to form far better (>3-fold) biofilms during anaerobic relative to aerobic growth (Figure 3A). When a *rhlR* mutant was grown anaerobically as biofilms virtually all organisms were dead, an event that initially puzzled us until we revisited the anaerobic respiratory pathway of *PA*. Although nitrate and nitrite can serve as terminal electron acceptors during anaerobic growth and have ATP-generating coupling steps, the remaining 3 gases produced are NO, nitrous oxide (N₂O) and N₂. Because NO can be powerfully antimicrobial, our first hypothesis was that the *lasR* and *rhlR* mutants perished due to overproduction of endogenous NO in biofilms. Surprisingly, *rhlR* mutant bacteria generated nearly 40-fold higher endogenous NO than wild-type bacteria resulting in anaerobic biofilm death. This was proven first biochemically when we added C-PTIO, a NO scavenger, that protected the bacteria. This was followed genetically when we created a *rhlR nirS* double mutant that is incapable of producing endogenous NO that was viable in anaerobic biofilms. With this discovery, it became obvious that paralysis of anaerobic QS could be one mechanism to kill *PA* during chronic CF.

Our previous work demonstrates that *rhl* QS is critical for anaerobic biofilm survival as *rhlR* mutant bacteria die as a result of overproduction of endogenous metabolic NO (Yoon et al., 2002). Still, it was unclear how the inactivation of *rhl* QS results in increased levels of endogenous NO that result in killing. Finally, our results became clearer when it was discovered that RhlR represses the anaerobic denitrification genes *nar*, *nir*, *nor*, and *nos* (Toyofuku et al., 2007, 2012; Figure 3B). Upon revisiting the overall bacterial integrity on anaerobic biofilms, we observed that wild-type bacteria had elongate rods and were mostly viable (Figure 3C1). In contrast, the integrity of bacteria on *rhlR* mutant biofilms almost represented a “war zone,” with what appears to be organisms literally exploding, leaving only a bacterial “skeleton” or “corpse” (Figure 3C2). An additional factor involved in anaerobic biofilm survival is the major catalase, KatA (Ma et al., 1999; Hassett and Imlay, 2006). KatA is a tetrameric catalase (Figure 3D1) that is responsive to both H₂O₂ in a QS (Hassett et al., 1999) and OxyR-dependent (Heo et al., 2010) fashion and anaerobic conditions in an ANR-dependent fashion (Trunk et al., 2010; Su et al., 2014; Kim et al., 2019). In each monomer, KatA has a methionine sulfone group that helps “buffer” NO (Figure 3D2), thus protecting it from NO generated from A-NO₂⁻ (Su et al., 2014). When we constructed a *rhlR katA* double mutant, we observed high levels of damaging dinitrosyliron complexes (DNICs, Su et al., 2014), far more than

that of the wild-type and *rhlR* mutant alone (Figure 3D3). Thus, the logical correlate from an absence of RhlR is a dramatic overproduction of lethal NO. When coupled with an absence of KatA, anaerobic *rhlR katA* bacteria are severely stressed by substantially elevated NO during anaerobic biofilm growth, resulting in overproduction of NO and concomitant DNICs, resulting in cell death.

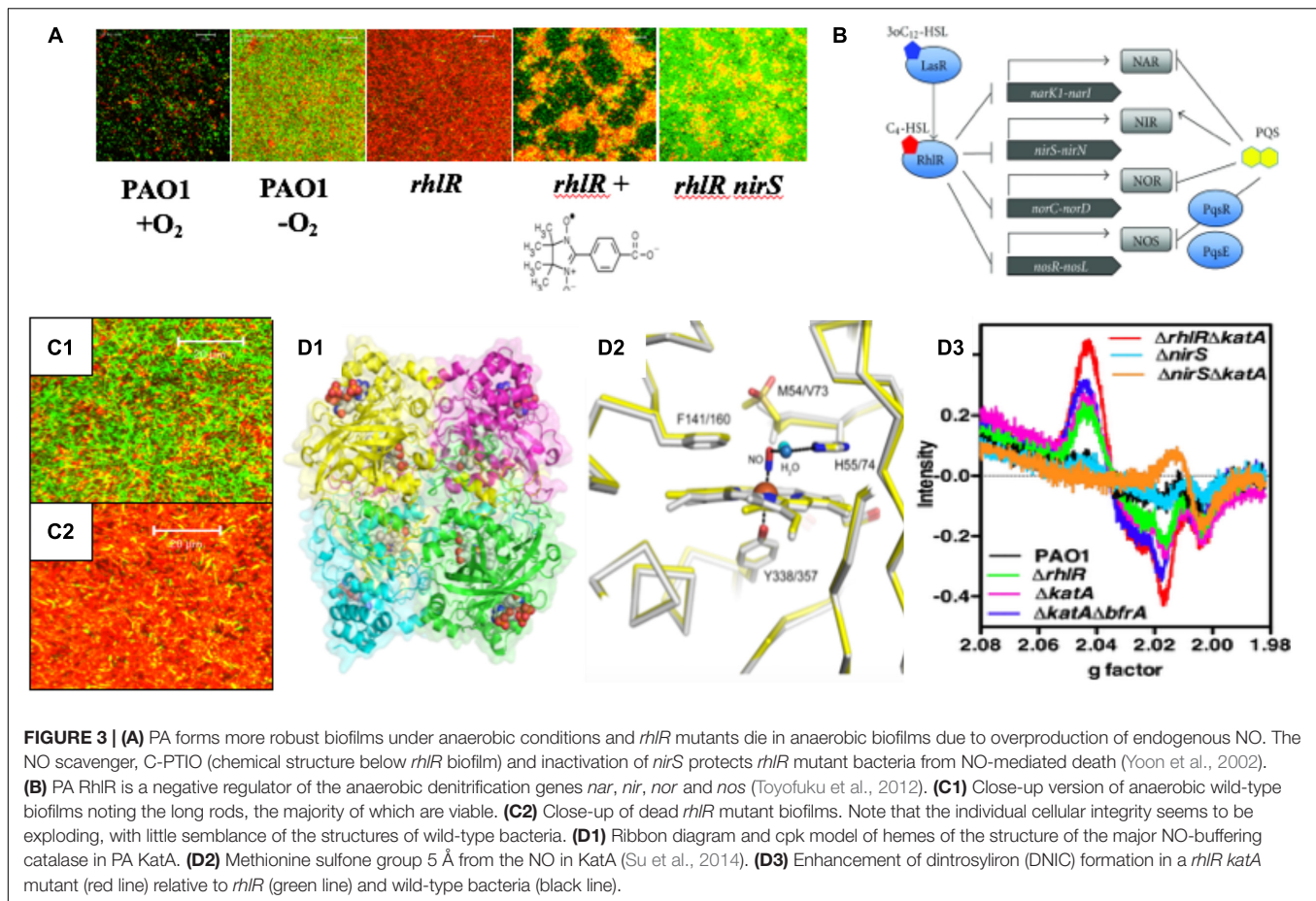
Mucoid, *mucA* Mutant Bacteria Have an Inherent Sensitivity to Acidified Nitrite, an NO Generator Under the Acidic Conditions of the CF Airway Mucus

In 2006, we discovered that alginate-overproducing *mucA* mutants (Figure 4A2 vs. nonmucoid 4A1) devoid of the anti-sigma factor MucA are more susceptible to exogenous NO produced by acidified nitrite (A-NO₂⁻) than wild-type bacteria at the pH of the CF airway mucus (Yoon et al., 2006). This is under planktonic (Figure 4B), biofilm (Figure 4C), and during chronic infection in mice (Figure 4D). However, unlike the mechanism underlying endogenous NO-mediated biofilm death of *rhlR* mutant bacteria described above, *mucA* mutant bacteria are sensitive to exogenous NO mediated by A-NO₂⁻ reduction (Yoon et al., 2006). Inactivation of *mucA* allows for the sigma factor, AlgT(U) to regulate and transcribe genes involved in alginate production (Martin et al., 1993). However, after scanning the literature for potential effects of AlgT(U) on anaerobic respiratory genes, we only found evidence that a *mucA22 sup-2* mutant that generates reduced alginate production demonstrated increased transcription of *norB*, *norC*, and *norD* (Firoved et al., 2004). The identity of the *sup-2* mutation remains unknown. Furthermore, *mucA22* mutants lacking AlgD (no alginate) or AlgT(U) were still sensitive to A-NO₂⁻. Still, the reason why *mucA22* mutant bacteria are sensitive to A-NO₂⁻ was only elucidated after examining anaerobic NAR, NIR and NOR activities in *mucA22* vs. wild-type bacteria. We noted an ~16-fold reduction in NIR and 4.5-fold reduction in NOR activity (Yoon et al., 2006).

How Else Might *las/rhl* and *mucA* Mutants Die From NO Derivatives? the Potential Relationship Between *PA* Denitrification, Biofilms, and Filamentous Pf Bacteriophages

Bacteria respond to nitrosative and oxidative stress by activating hundreds of genes. In *PA*, one of these genes is *oxyR*, which encodes a LysR-type transcriptional regulator that positively regulates several dozen genes involved in RNS (e.g., RSNO) and ROS (O₂⁻, H₂O₂, HO₂[·], ¹O₂) metabolism, such as catalases, alkylhydroperoxide reductases and superoxide dismutases (Ochsner et al., 2000; Vazquez-Torres, 2012; Wei et al., 2012). OxyR also binds to the Pf4 prophage in the intergenic region between *PA0716* and *PA0717* (Wei et al., 2012), suggesting that both nitrosative and oxidative stress may induce Pf4.

In contrast to lytic phages that must lyse and kill the host bacterium to complete their lifecycle, filamentous Inoviruses such

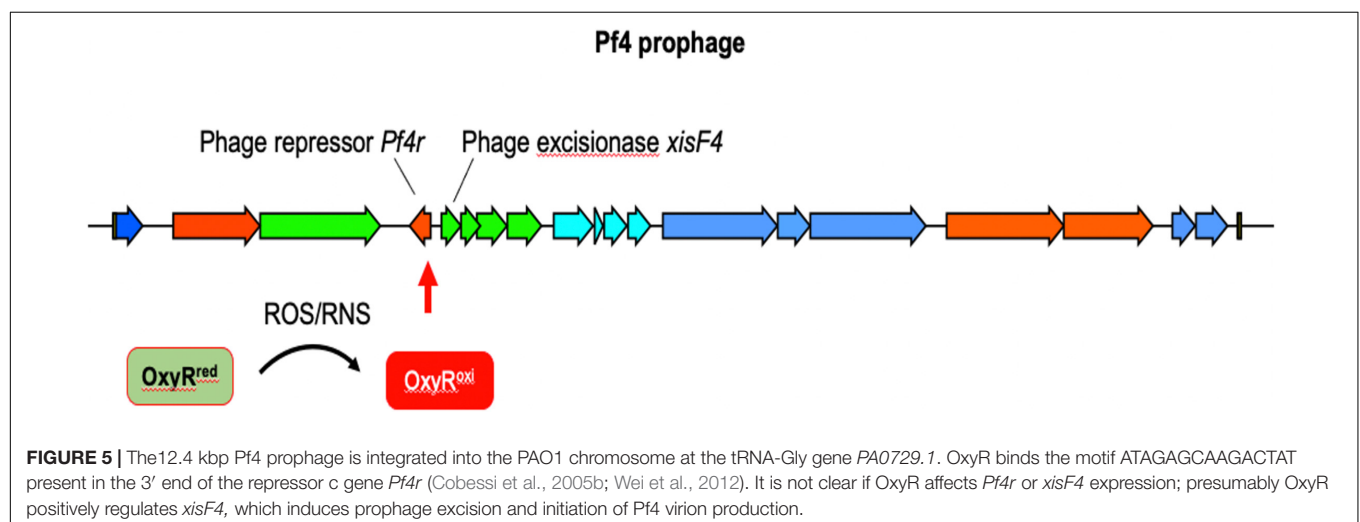
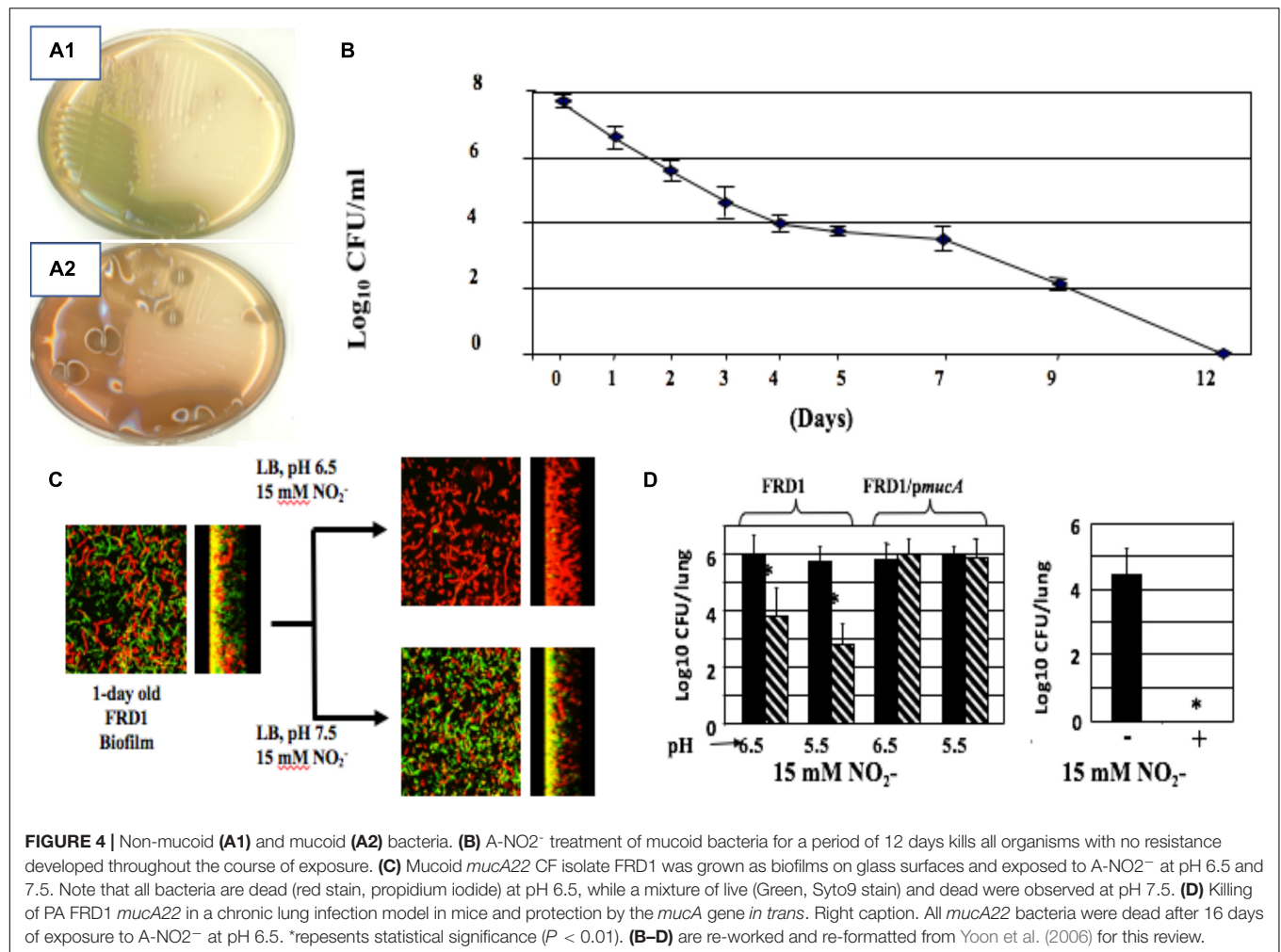


as Pf4 (Figure 5) are extruded from the cell without causing lysis (Rakonjac et al., 2011; Mai-Prochnow et al., 2015; Secor et al., 2020). However, *PA* biofilms routinely generate superinfective Pf4 variants that are capable of lysing their host. Pf4-induced cell lysis occurs in the center of biofilms where anaerobic conditions necessitate the use of nitrogen oxides (e.g., NO_3^- , NO_2^-) as alternative electron acceptors, which produces RNS in the form of NO (Hassett et al., 2004; Yoon et al., 2007; Arai, 2012). We have shown that Pf4 genes are some of the most activated genes when *PA* is grown under anaerobic conditions using NO_3^- or NO_2^- as terminal electron acceptors (Platt et al., 2008). After induction, the Pf4 excisionase XisF4 promotes the transcription of the recombinase IntF, excising the prophage from the chromosome forming a circular dsDNA species called the replicative form (RF) (Li et al., 2019). The RF replicates via rolling circle replication producing one dsDNA and one ssDNA copy (Martinez and Campos-Gomez, 2016). The ssDNA species can either be converted into a dsDNA RF or packaged into filamentous virions. When Pf4 is actively replicating, mutations in the phage repressor C gene *Pf4r* occur at high frequencies (McElroy et al., 2014). These mutations are thought to inactivate the repressor, resulting in a runaway superinfection that lyses *PA*. Cell lysis increases levels of extracellular DNA and the emergence of superinfective Pf4 variants is associated with biofilm dispersal,

both important components of the biofilm lifecycle (Webb et al., 2003, 2004; Rice et al., 2009; Petrova et al., 2011).

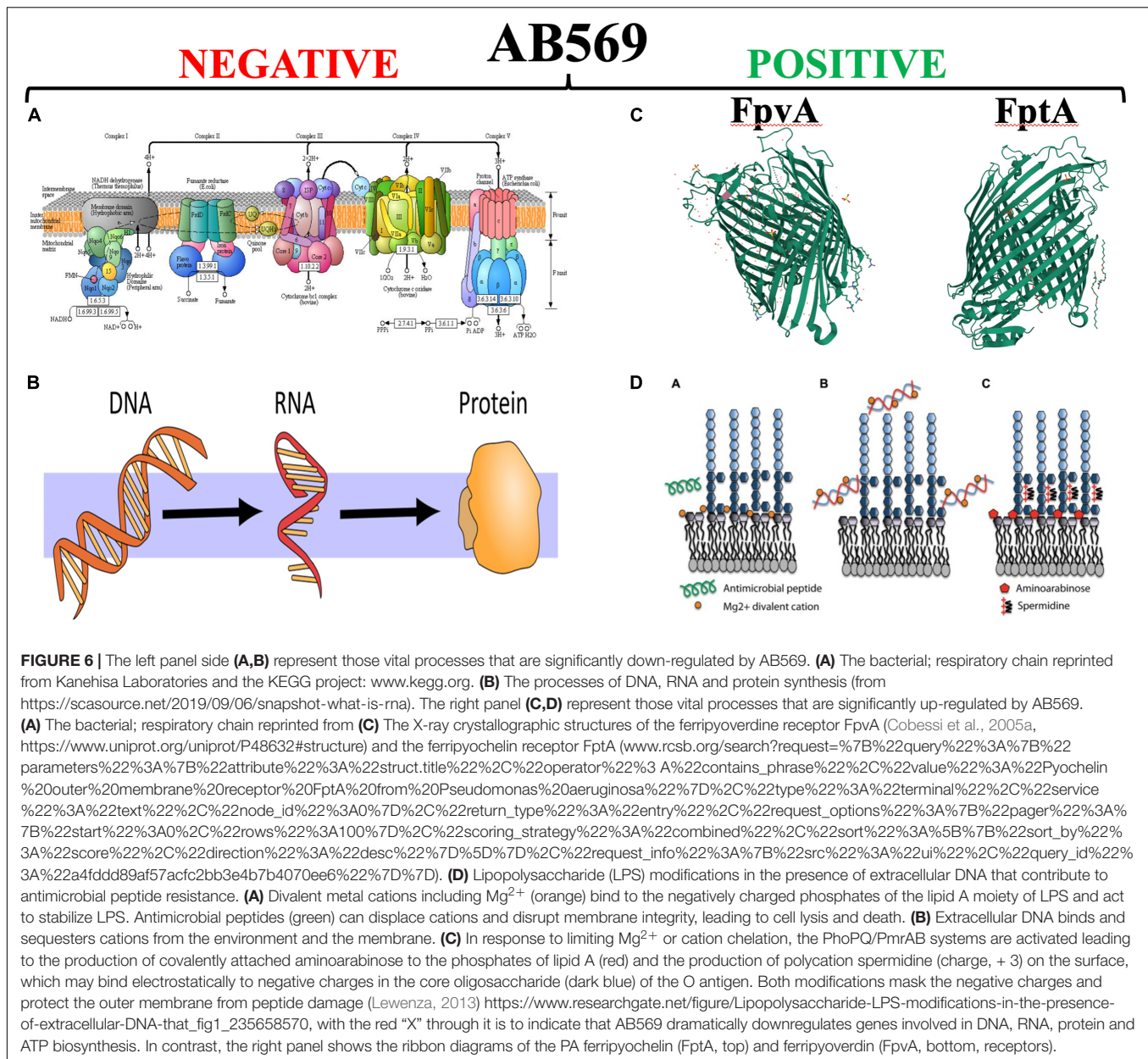
In the laboratory, *PA* biofilms consistently produce as many as 10^{10} infectious virions per ml (Webb et al., 2003, 2004; Rice et al., 2009; McElroy et al., 2014). As these filamentous virions accumulate in the biofilm matrix, they spontaneously align and assemble a liquid crystal (Secor et al., 2015a). The highly ordered liquid crystalline matrix promotes water retention, allowing *PA* to better withstand desiccation (Secor et al., 2015a). Pf4 virions also bind and sequester cationic antimicrobials away from *PA*, increasing antimicrobial tolerance and ensuring viability of its host (Janmey et al., 2014; Secor et al., 2015a,b). In animal models of infection, Pf4 phages increase the virulence potential of *PA* in both lung (Rice et al., 2009) and wound infection models (Sweere et al., 2019). Recent work demonstrates that Pf4 virions have immunomodulatory properties that steer the infection response toward a maladaptive type I interferon antiviral response that suppresses phagocytic uptake of bacteria, promoting infection initiation (Sweere et al., 2019).

Pf4 and related Pf prophages are prevalent amongst *PA* clinical isolates (Mooij et al., 2007; Knezevic et al., 2015; Burgener et al., 2019; Secor et al., 2020) and Pf virions are produced in abundance at sites of human infection (Secor et al., 2015b;



Burgener et al., 2019; Sweere et al., 2019). Pf phages represent a therapeutic target to treat or prevent *PA* infections, especially were AB569 to trigger Pf4 excision events. Indeed, vaccinating against the Pf4 coat protein prevents *PA* infections in mice

(Sweere et al., 2019). Future studies exploring the relationship between the anaerobic respiration (e.g., denitrification) processes and Pf phage induction may reveal additional therapeutic strategies to treat *PA* infections.



A New Clue to the Puzzle That Helped the Discovery of AB569: PA4455, a Putative ABC Transporter Permease

In 2016, we were interested in additional genes involved in A- NO_2^- sensitivity. We embarked on a screen of previously constructed isogenic and Tn mutants of *PA* PAO1. Among several mutants that were sensitive to A- NO_2^- , the most prominent including *muca* (described above) and PA4455. The latter strain was devoid of PA4455, encoding a 6-membrane spanning ABC transporter permease (McDaniel et al., 2016) which was also found to be sensitive to the membrane perturbing agent EDTA. In fact, killing of both *PA* PAO1 and especially the PA4455 mutant was even more sensitive to A- NO_2^- plus EDTA. Since

EDTA can destabilize the LPS layer of the outer membrane, specifically by stripping the structurally essential cations Ca^{2+} and Mg^{2+} , we also examined sensitivity of various A-band and/or B-band mutants. Two B-band LPS mutants *wbpM* (A^+ , B^-) and especially *rmlC* (A^- , B^-) were susceptible to A- NO_2^- , EDTA and especially A- NO_2^- + EDTA under both aerobic and even more so under anaerobic conditions (McDaniel et al., 2016). Interestingly, the *rmlC* mutant could not grow anaerobically (McDaniel et al., 2016).

Upon the discovery of the PA4455 mutant being uniquely susceptible to both A- NO_2^- and EDTA, we literally raided our collection of nearly 6000 bacterial frozen stocks for both Gram-negative and Gram-positive bacterial pathogens, especially those that were deemed MDR. First, however, we found two

PA MDR strains called “Andrea” and “BAMF” (McDaniel et al., 2020). The Andrea strain was isolated from a woman with a $\Delta F508$ that passed away at 35 years of age that was resistant to every antibiotic except colistin. In contrast, the BAMF strain was isolated from an 8-year-old girl after a small bowel-liver transplantation that was resistant to all antibiotics including colistin. Both had fractional inhibitory concentrations values of ~ 0.5 , indicative of synergy between $A\text{-NO}_2^-$ and EDTA. A transcriptomic and rigorous biochemistry and biophysics-based research strategy rapidly ensued using PA as a model organism and anaerobic conditions, representative of chronic, late-stage CF airway disease (Worlitzsch et al., 2002; Yoon et al., 2002). First, using RNA-seq analysis, we found a dramatic downregulation of a plethora of essential genes involving the biosynthesis of DNA, RNA, protein and ATP (Figure 5, red minus sign) coupled with a significant upregulation of genes involved in iron acquisition (Figure 5, green plus sign). In addition, we unexpectedly found a decrease in the transcription of the *fur* gene, encoding the ferric uptake regulator, by treatment with anaerobic $A\text{-NO}_2^-$ alone. In *E. coli*, purified iron (Fe)-Fur to form a $S = 1/2$ low-spin Fe-Fur-NO complex with a $g = 2.03$ EPR signal (D’Autreaux et al., 2002). However, NO derived from the HONO generated by $A\text{-NO}_2^-$ could react with Fe^{2+} in the Fur protein, thereby creating a flux of Fe^{2+} -Fur and Fe^{3+} -Fur, resulting in a derepression of genes that are normally tightly repressed by Fe^{2+} -Fur such as the *fprA* and *ftpA* genes encoding the ferripyoverdine and ferripyochelin receptors, respectively (Ochsner and Vasil, 1996; Figure 5, right panel, ribbon structures) as well as a myriad of siderophore biosynthetic and regulatory genes (McDaniel et al., 2020).

Regarding the chemistry of AB569, we have only just scraped the surface. Using three different techniques including NO polarographic measurements, cyclic voltammetry and electron paramagnetic resonance spectroscopy, we found a number of interesting features of AB569. However, these studies were only performed as yet in laboratory media or buffered solutions and not in human-relevant reagents such as airway surface liquid (e.g., CF/COPD), blood or serum (e.g., burns/wounds) or urine (e.g., UTIs). Thus, the mechanistic effect of AB569 at various oxygen tensions and human tissues remains a mystery. Still, we offer some glimpses of planned future work involving AB569 mechanism. Obviously, RNA-seq analysis of maximally down-regulated genes revealed in organisms exposed to AB569 in respective fluids coupled with an isogenic mutant analysis and followed by AB569 sensitivity measurements would be a logical start. Because EDTA can redox-cycling iron from the $\text{Fe}^{2+}/\text{Fe}^{3+}$ couple, substitution of diethylenetriamine pentaacetic acid (DTPA) which only chelates the reduced form for EDTA would indicate that redox-cycling is required for bactericidal activity if DTPA is not synergistic. Second, oxygen tension is likely also a major player in AB569 activity. For example, human urine has ~ 55 mM O_2 , where oxygen saturated water is 260 mM (Jalali et al., 2009).

AB569: A Novel Bactericidal Agent Against All MDR Gram-Negative and Gram-Positive Bacteria Including the ESKAPE Pathogens

Finally, AB569 is an innovative bactericidal combination of acidified nitrite ($A\text{-NO}_2^-$) and $\text{Na}_2\text{-EDTA}$, was patented by the corresponding author in 2018 (USPTO 9,925,206) and has great potential as a novel antimicrobial with broad spectrum activity against virtually all pathogenic bacteria. Regarding human use, the NaNO_2 and/or EDTA component(s) of AB569 have separately been proven safe in studies related to the treatment of cyanide poisoning (Bebarta et al., 2017), burn wounds (Wang et al., 2015), CF lung infection (Brown et al., 1985), urinary tract infection (Birkhauser et al., 2011), chelation therapy (Lanigan and Yamarik, 2002), and cosmetics (Juzeniene et al., 2007). Furthermore, both components of AB569 have been reported to increase the efficacy of certain antibiotics that are commonly used to treat a variety of infections (Zemke et al., 2014; Lebeaux et al., 2015; McDaniel et al., 2016), and individually to enhance the process of wound healing (Weller and Finnen, 2006; Wang et al., 2015). Our recent work in Proc. Natl. Acad. Sci. (McDaniel et al., 2020) showed that AB569 has excellent bactericidal activity against all tested Gram-positive (G^+) and Gram-negative (G^-) bacteria including those that are MDR. Importantly, in that study, we also observed no discernable toxicity of AB569 to human airway (e.g., CF), skin (e.g., burn), or bladder (e.g., UTIs) cells or in a mouse model of PA airway infection and no development of resistance by bacteria cultured *in vitro* (McDaniel et al., 2016, 2020).

CONCLUSION

The global pandemic of antibiotic resistance has been an ever-increasing problem for decades and has been nearly “forgotten” due to the COVID-19 pandemic which has taken scientific and political priority for nearly ~ 1.5 years (statement as of 3-27-21 based upon the “discovery” of SARS-CoV-2 in 2019). Drug companies have seemingly always been “behind the eight ball” in the development of novel antimicrobials that are not only bactericidal or bacteriostatic, but also offer the organisms little hope for development of resistance to them. The organisms inevitably are always a few “steps ahead” of the substantial creative brain power of the world’s best scientists. Thus, there is only a paltry glimmer of hope for control and, above all, eradication of such life-threatening organisms. We strongly believe that AB569 holds such promise.

AB569 is potentially one solution to the above problem. Although many organisms can metabolize nitrite, they are generally sensitive to it even under slight acidic conditions (e.g., pH 6.5). Organisms that cannot or have difficulty metabolizing nitrite are even more susceptible (Yoon et al., 2006). In contrast, there are only $\sim 4\text{--}8$ organisms that have been shown to degrade EDTA including *Chelativorans multitrophicus*

(Doronina et al., 2010), *C. oligotrophicus* (Doronina et al., 2010), *Aminobacter aminovorans* (Yuan and VanBriesen, 2008), and *Mesorhizobium*, none of which are considered human pathogens and are only capable of aerobic respiration (denitrification does not occur) (Willems, 2014).

Finally, the level of mechanistic complexity of AB569 bactericidal activity is multifactorial. Upon exposure of anaerobically grown PA (reminiscent of late-stage chronic CF airway infections), RNA-seq analyses clearly indicate a dramatic and paralyzing decrease in transcription of essential genes involved in DNA (e.g., ribonucleotide reductase), RNA, protein (e.g., ribosomal proteins), electron transport chain enzymes (e.g., cytochrome c oxidase, succinate dehydrogenase) and ATP synthesis (Figure 6, red minus sign). In contrast, there was a marked up-regulation of genes involved in iron regulation, and siderophore synthesis/acquisition machinery (McDaniel et al., 2020). We are currently trying to secure support to move the AB569 technology forward toward animal toxicology,

pharmacodynamic/pharmacokinetic data and ultimately human clinical trials.

AUTHOR CONTRIBUTIONS

DH wrote the initial and final draft. LS provided various segments on burns and wounds. PS, RK, NK, and HK provided expertise in quorum sensing, and structural biology and translational medicine. All authors contributed to the article and approved the submitted version.

FUNDING

This work was supported by the ARCH Biopartners, Inc. (Toronto, Canada). The funder was not involved in the study design, collection, analysis, interpretation of data, the writing of this article or the decision to submit it for publication.

REFERENCES

- Ahonen, M. J. R., Suchyta, D. J., Zhu, H., and Schoenfish, M. H. (2018). Nitric oxide-releasing alginates. *Biomacromolecules* 19, 1189–1197. doi: 10.1021/acs.biomac.8b00063
- Alrahman, M. A., and Yoon, S. S. (2017). Identification of essential genes of *Pseudomonas aeruginosa* for its growth in airway mucus. *J. Microbiol.* 55, 68–74. doi: 10.1007/s12275-017-6515-3
- Amdahl, M. B., DeMartino, A. W., and Gladwin, M. T. (2019). Inorganic nitrite bioactivation and role in physiological signaling and therapeutics. *Biol. Chem.* 401, 201–211. doi: 10.1515/hsz-2019-0349
- Arai, H. (2012). Regulation and function of versatile aerobic and anaerobic respiratory metabolism in *Pseudomonas aeruginosa*. *Front. Microbiol.* 2:103. doi: 10.3389/fmicb.2011.00103
- Arai, H., Igarashi, Y., and Kodama, T. (1995). The structural genes for nitric oxide reductase from *Pseudomonas aeruginosa*. *Biochim. Biophys. Acta* 1261, 279–284.
- Asano, K., Chee, C. B., Gaston, B., Lilly, C. M., Gerard, C., Drazen, J. M., et al. (1994). Constitutive and inducible nitric oxide synthase gene expression, regulation, and activity in human lung epithelial cells. *Proc. Natl. Acad. Sci. U.S.A.* 91, 10089–10093. doi: 10.1073/pnas.91.21.10089
- Asmus, M. J., Barros, M. D., Liang, J., Chesrown, S. E., and Hendeles, L. (2001). Pulmonary function response to EDTA, an additive in nebulized bronchodilators. *J. Allergy Clin. Immunol.* 107, 68–72. doi: 10.1067/mai.2001.111591
- Bacon, B. A., Liu, Y., Kincaid, J. R., and Boon, E. M. (2018). Spectral characterization of a novel no sensing protein in bacteria: NosP. *Biochemistry* 57, 6187–6200. doi: 10.1021/acs.biochem.8b00451
- Banin, E., Brady, K. M., and Greenberg, E. P. (2006). Chelator-induced dispersal and killing of *Pseudomonas aeruginosa* cells in a biofilm. *Appl. Environ. Microbiol.* 72, 2064–2069. doi: 10.1128/AEM.72.3.2064-2069.2006
- Barraud, N., Hassett, D. J., Hwang, S. H., Rice, S. A., Kjelleberg, S., and Webb, J. S. (2006). Involvement of nitric oxide in biofilm dispersal of *Pseudomonas aeruginosa*. *J. Bacteriol.* 188, 7344–7353.
- Barraud, N., Schleheck, D., Klebensberger, J., Webb, J. S., Hassett, D. J., Rice, S. A., et al. (2009). Nitric oxide signaling in *Pseudomonas aeruginosa* biofilms mediates phosphodiesterase activity, decreased cyclic di-GMP levels, and enhanced dispersal. *J. Bacteriol.* 191, 7333–7342. doi: 10.1128/JB.00975-09
- Bebarta, V. S., Brittain, M., Chan, A., Garrett, N., Yoon, D., Burney, T., et al. (2017). Sodium Nitrite and sodium thiosulfate are effective against acute cyanide poisoning when administered by intramuscular injection. *Ann. Emerg. Med.* 69, 718–725.e714. doi: 10.1016/j.annemergmed.2016.09.034
- Birkhauser, F. D., Zehnder, P., Roth, B., Schurch, L., Ochsner, K., Willener, R., et al. (2011). Irrigation of continent catheterizable ileal pouches: tap water can replace sterile solutions because it is safe, easy, and economical. *Eur. Urol.* 59, 518–523. doi: 10.1016/j.eururo.2011.01.003
- Bjarnsholt, T., Jensen, P. O., Jakobsen, T. H., Phipps, R., Nielsen, A. K., Rybtke, M. T., et al. (2010). Quorum sensing and virulence of *Pseudomonas aeruginosa* during lung infection of cystic fibrosis patients. *PLoS One* 5:e10115. doi: 10.1371/journal.pone.0010115
- Borlaug, B. A., Melenovsky, V., and Koeppe, K. E. (2016). Inhaled sodium nitrite improves rest and exercise hemodynamics in heart failure with preserved ejection fraction. *Circ. Res.* 119, 880–886. doi: 10.1161/CIRCRESAHA.116.309184
- Brint, J. M., and Ohman, D. E. (1995). Synthesis of multiple exoproducts in *Pseudomonas aeruginosa* is under the control of RhIR-RhII, another set of regulators in strain PAO1 with homology to the autoinducer-responsive LuxR-LuxI family. *J. Bacteriol.* 177, 7155–7163.
- Brown, J., Mellis, C. M., and Wood, R. E. (1985). Edetate sodium aerosol in *Pseudomonas* lung infection in cystic fibrosis. *Am. J. Dis. Child* 139, 836–839.
- Burgener, E. B., Sweere, J. M., Bach, M. S., Secor, P. R., Haddock, N., Jennings, L. K., et al. (2019). Filamentous bacteriophages are associated with chronic *Pseudomonas* lung infections and antibiotic resistance in cystic fibrosis. *Sci. Transl. Med.* 11:aa9748.
- Cai, Y. M., and Webb, J. S. (2020). Optimization of nitric oxide donors for investigating biofilm dispersal response in *Pseudomonas aeruginosa* clinical isolates. *Appl. Microbiol. Biotechnol.* 104, 8859–8869. doi: 10.1007/s00253-020-10859-7
- Calhoun, J. H., Murray, C. K., and Manning, M. M. (2008). Multidrug-resistant organisms in military wounds from Iraq and Afghanistan. *Clin. Orthop. Relat. Res.* 466, 1356–1362. doi: 10.1007/s11999-008-0212-9
- Carlsson, S., Govoni, M., Wiklund, N. P., Weitzberg, E., and Lundberg, J. O. (2003). In vitro evaluation of a new treatment for urinary tract infections caused by nitrate-reducing bacteria. *Antimicrob. Agents Chemother.* 47, 3713–3718. doi: 10.1128/aac.47.12.3713-3718.2003
- Carlsson, S., Weitzberg, E., Wiklund, P., and Lundberg, J. O. (2005). Intravesical nitric oxide delivery for prevention of catheter-associated urinary tract infections. *Antimicrob. Agents Chemother.* 49, 2352–2355. doi: 10.1128/AAC.49.6.2352-2355.2005
- Cartotto, R. (2017). Topical antimicrobial agents for pediatric burns. *Burns Trauma* 5:33. doi: 10.1186/s41038-017-0096-6
- Caverly, L. J., Spilker, T., Kalikin, L. M., Stillwell, T., Young, C., Huang, D. B., et al. (2019). In vitro activities of beta-lactam-beta-lactamase inhibitor antimicrobial agents against cystic fibrosis respiratory pathogens. *Antimicrob. Agents Chemother.* 64:e01595-19. doi: 10.1128/AAC.01595-19

- Coates, A. R., and Hu, Y. (2007). Novel approaches to developing new antibiotics for bacterial infections. *Br. J. Pharmacol.* 152, 1147–1154. doi: 10.1038/sj.bjp.0707432
- Cobessi, D., Celia, H., Folschweiller, N., Schalk, I. J., Abdallah, M. A., and Pattus, F. (2005a). The crystal structure of the pyoverdine outer membrane receptor FpvA from *Pseudomonas aeruginosa* at 3.6 angstroms resolution. *J. Mol. Biol.* 347, 121–134. doi: 10.1016/j.jmb.2005.01.021
- Cobessi, D., Celia, H., and Pattus, F. (2005b). Crystal structure at high resolution of ferric-pyochelin and its membrane receptor FptA from *Pseudomonas aeruginosa*. *J. Mol. Biol.* 352, 893–904. doi: 10.1016/j.jmb.2005.08.004
- D'Autreaux, B., Touati, D., Bersch, B., Latour, J. M., and Michaud-Soret, I. (2002). Direct inhibition by nitric oxide of the transcriptional ferric uptake regulation protein via nitrosylation of the iron. *Proc. Natl. Acad. Sci. U.S.A.* 99, 16619–16624. doi: 10.1073/pnas.252591299
- Davies, D. G., Parsek, M. R., Pearson, J. P., Iglewski, B. H., Costerton, J. W., and Greenberg, E. P. (1998). The involvement of cell-to-cell signals in the development of a bacterial biofilm. *Science* 280, 295–298.
- Deng, Z., Liu, F., and Li, C. (2019). Therapeutic effect of ethylenediaminetetraacetic acid irrigation solution against wound infection with drug-resistant bacteria in a rat model: an animal study. *Bone Joint Res.* 8, 189–198. doi: 10.1302/2046-3758.85.BJR-2018-0280.R3
- Doronina, N. V., Kaparullina, E. N., Trotsenko, Y. A., Nortemann, B., Bucheli-Witschel, M., Weilenmann, H. U., et al. (2010). *Chelativorans multitrophicus* gen. nov., sp. nov. and *Chelativorans oligotrophicus* sp. nov., aerobic EDTA-degrading bacteria. *Int. J. Syst. Evol. Microbiol.* 60, 1044–1051. doi: 10.1099/ijms.0.003152-0
- Egan, M. E. (2016). Genetics of cystic fibrosis: clinical implications. *Clin. Chest Med.* 37, 9–16. doi: 10.1016/j.ccm.2015.11.002
- Egan, M. E. (2020). Cystic fibrosis transmembrane conductance receptor modulator therapy in cystic fibrosis, an update. *Curr. Opin. Pediatr.* 32, 384–388. doi: 10.1097/MOP.0000000000000892
- Elborn, J. S. (2016). Cystic fibrosis. *Lancet* 388, 2519–2531. doi: 10.1016/S0140-6736(16)00576-6
- Fan, B., Wang, J., Stuehr, D. J., and Rousseau, D. L. (1997). NO synthase isozymes have distinct substrate binding sites. *Biochemistry* 36, 12660–12665. doi: 10.1021/bi9715369
- Fang, F. C. (1997). Perspective series: host/pathogen interactions. Mechanisms of nitric oxide-related antimicrobial activity. *J. Clin. Invest.* 99, 2818–2825.
- Feliziani, S., Lujan, A. M., Moyano, A. J., Sola, C., Bocco, J. L., Montanaro, P., et al. (2010). Mucoidy, quorum sensing, mismatch repair and antibiotic resistance in *Pseudomonas aeruginosa* from cystic fibrosis chronic airways infections. *PLoS One* 5:e012669. doi: 10.1371/journal.pone.0012669
- Fenker, D. E., McDaniel, C. T., Panmanee, W., Panos, R. J., Sorscher, E. J., Sabusap, C., et al. (2018). A comparison between two pathophysiologically different yet microbiologically similar lung diseases: cystic fibrosis and chronic obstructive pulmonary disease. *Int. J. Respir. Pulm. Med.* 5:98. doi: 10.23937/2378-3516/1410098
- Firoved, A. M., Wood, S. R., Ornatowski, W., Deretic, V., and Timmins, G. S. (2004). Microarray analysis and functional characterization of the nitrosative stress response in nonmucoid and mucoid *Pseudomonas aeruginosa*. *J. Bacteriol.* 186, 4046–4050.
- Flynn, J. M., Niccum, D., Dunitz, J. M., and Hunter, R. C. (2016). Evidence and role for bacterial mucin degradation in cystic fibrosis airway disease. *PLoS Pathog.* 12:e1005846. doi: 10.1371/journal.ppat.1005846
- Gambello, M. J., and Iglewski, B. H. (1991). Cloning and characterization of the *Pseudomonas aeruginosa lasR* gene, a transcriptional activator of elastase expression. *J. Bacteriol.* 173, 3000–3009.
- Grasemann, H., Ioannidis, I., Tomkiewicz, R. P., de Groot, H., Rubin, B. K., and Ratjen, F. (1998). Nitric oxide metabolites in cystic fibrosis lung disease. *Arch. Dis. Child* 78, 49–53.
- Grasemann, H., and Ratjen, F. (2012). Nitric oxide and L-arginine deficiency in cystic fibrosis. *Curr. Pharm. Des.* 18, 726–736. doi: 10.2174/138161212799315911
- Hassett, D. J. (1996). Anaerobic production of alginate by *Pseudomonas aeruginosa*: alginate restricts diffusion of oxygen. *J. Bacteriol.* 178, 7322–7325.
- Hassett, D. J., Lymar, S. V., Rowe, J. J., Schurr, M. J., Passador, L., Herr, A. B., et al. (2004). “Anaerobic metabolism by *Pseudomonas aeruginosa* in cystic fibrosis airway biofilms: role of nitric oxide, quorum sensing and alginate production,” in *Strict and Facultative Anaerobes: Medical and Environmental Aspects*, eds M. M. Nakano and P. Zuber (London: Horizon Biosciences), 87–108.
- Hassett, D. J., Ma, J.-F., Elkins, J. G., McDermott, T. R., Ochsner, U. A., West, S. E. H., et al. (1999). Quorum sensing in *Pseudomonas aeruginosa* controls expression of catalase and superoxide dismutase genes and mediates biofilm susceptibility to hydrogen peroxide. *Mol. Microbiol.* 34, 1082–1093.
- Hassett, D. J., Sutton, M. D., Schurr, M. J., Herr, A. B., Caldwell, C. C., and Matu, J. O. (2009). *Pseudomonas aeruginosa* hypoxic or anaerobic biofilm infections within cystic fibrosis airways. *Trends Microbiol.* 17, 130–138. doi: 10.1016/j.tim.2008.12.003
- Hassett, D. J., and Imlay, J. A. (2006). “Chapter 14, Oxidative stress systems in bacteria: four model systems,” in *Molecular Paradigms of Infectious Disease*, eds C. Nickerson and M. J. Schurr (Dordrecht: Kluwer Academic-Plenum), 544–573.
- Henke, M. O., John, G., Rheineck, C., Chillappagari, S., Naehrich, L., and Rubin, B. K. (2011). Serine proteases degrade airway mucins in cystic fibrosis. *Infect. Immun.* 79, 3438–3444. doi: 10.1128/IAI.01252-10
- Heo, Y. J., Chung, I. Y., Cho, W. J., Lee, B. Y., Kim, J. H., Choi, K. H., et al. (2010). The major catalase gene (*kata*) of *Pseudomonas aeruginosa* PA14 is under both positive and negative control of the global transactivator OxyR in response to hydrogen peroxide. *J. Bacteriol.* 192, 381–390. doi: 10.1128/JB.00980-09
- Hossain, S., and Boon, E. M. (2017). Discovery of a novel nitric oxide binding protein and nitric-oxide-responsive signaling pathway in *Pseudomonas aeruginosa*. *ACS Infect. Dis.* 3, 454–461. doi: 10.1021/acinfed.7b00027
- Howlin, R. P., Cathie, K., Hall-Stoodley, L., Cornelius, V., Duignan, C., Allan, R. N., et al. (2017). Low-dose nitric oxide as targeted anti-biofilm adjunctive therapy to treat chronic *Pseudomonas aeruginosa* infection in cystic fibrosis. *Mol. Ther.* 25, 2104–2116. doi: 10.1016/j.jymthe.2017.06.021
- Hunt-Serracin, A. C., Parks, B. J., Boll, J., and Boutte, C. C. (2019). *Mycobacterium abscessus* cells have altered antibiotic tolerance and surface Glycolipids in artificial cystic fibrosis sputum medium. *Antimicrob. Agents Chemother.* 63:e02488-18. doi: 10.1128/AAC.02488-18
- Ismail, N. H., Lieu, P. K., Lien, C. T., and Ling, M. L. (1997). Bacteraemia in the elderly. *Ann. Acad. Med. Singap.* 26, 593–598.
- Jalali, F., Ashrafi, A. M., and Nematollahi, D. (2009). Measurement of dissolved oxygen in biological fluids by using a modified carbon paste electrode. *Electroanalysis* 21, 201–205.
- Janmey, P. A., Slochower, D. R., Wang, Y. H., Wen, Q., and Cebers, A. (2014). Polyelectrolyte properties of filamentous biopolymers and their consequences in biological fluids. *Soft Matter* 10, 1439–1449. doi: 10.1039/c3sm50854d
- Jarvis, W. R., and Martone, W. J. (1992). Predominant pathogens in hospital infections. *J. Antimicrob. Chemother.* 29(Suppl. A), 19–24.
- Jasovsky, D., Littmann, J., Zorzet, A., and Cars, O. (2016). Antimicrobial resistance—a threat to the world's sustainable development. *Ups. J. Med. Sci.* 121, 159–164. doi: 10.1080/03009734.2016.1195900
- Jones, K. L., Hegab, A. H., Hillman, B. C., Simpson, K. L., Jenkins, P. A., Grisham, M. B., et al. (2000). Elevation of nitrotyrosine and nitrate concentrations in cystic fibrosis sputum. *Pediatr. Pulmonol.* 30, 79–85.
- Jowkar, F., Jamshidzadeh, A., Pakniyat, S., and Namazi, M. R. (2010). Efficacy of nitric oxide-liberating cream on pityriasis versicolor. *J. Dermatolog. Treat.* 21, 93–96. doi: 10.3109/09546630902887229
- Juzeniene, A., Juzenas, P., Iani, V., and Moan, J. (2007). Topical applications of iron chelators in photosensitization. *Photochem. Photobiol. Sci.* 6, 1268–1274. doi: 10.1039/b703861e
- Kartchner, L. B., Gode, C. J., Dunn, J. L. M., Glenn, L. I., Duncan, D. N., Wolfgang, M. C., et al. (2019). One-hit wonder: late after burn injury, granulocytes can clear one bacterial infection but cannot control a subsequent infection. *Burns* 45, 627–640. doi: 10.1016/j.burns.2018.08.019
- Kerem, E., and Kerem, B. (1996). Genotype-phenotype correlations in cystic fibrosis. *Pediatr. Pulmonol.* 22, 387–395.
- Kim, B. O., Chung, I. Y., and Cho, Y. H. (2019). Differential expression of the major catalase, *KatA* in the two wild type *Pseudomonas aeruginosa* strains, PAO1 and PA14. *J. Microbiol.* 57, 704–710. doi: 10.1007/s12275-019-9225-1
- Knezevic, P., Voet, M., and Lavigne, R. (2015). Prevalence of Pfl-like (pro)phage genetic elements among *Pseudomonas aeruginosa* isolates. *Virology* 483, 64–71. doi: 10.1016/j.virol.2015.04.008
- Lanigan, R. S., and Yamarik, T. A. (2002). Final report on the safety assessment of EDTA, calcium disodium EDTA, diammonium EDTA, dipotassium EDTA, disodium EDTA, TEA-EDTA, tetrasodium EDTA, tripotassium EDTA,

- trisodium EDTA, HEDTA, and trisodium HEDTA. *Int. J. Toxicol.* 21(Suppl. 2), 95–142. doi: 10.1080/10915810290096522
- Leaper, D. J. (2006). Silver dressings: their role in wound management. *Int. Wound J.* 3, 282–294. doi: 10.1111/j.1742-481X.2006.00265.x
- Lebeaux, D., Leflon-Guibout, V., Ghigo, J. M., and Beloin, C. (2015). In vitro activity of gentamicin, vancomycin or amikacin combined with EDTA or L-arginine as lock therapy against a wide spectrum of biofilm-forming clinical strains isolated from catheter-related infections. *J. Antimicrob. Chemother.* 70, 1704–1712. doi: 10.1093/jac/dkv044
- Lewenza, S. (2013). Extracellular DNA-induced antimicrobial peptide resistance mechanisms in *Pseudomonas aeruginosa*. *Front. Microbiol.* 4:21. doi: 10.3389/fmicb.2013.00021
- Lewis, K. (2008). Multidrug tolerance of biofilms and persister cells. *Curr. Top. Microbiol. Immunol.* 322, 107–131.
- Li, Y., Liu, X., Tang, K., Wang, P., Zeng, Z., Guo, Y., et al. (2019). Excisionase in Pf filamentous prophage controls lysis-lysogeny decision-making in *Pseudomonas aeruginosa*. *Mol. Microbiol.* 111, 495–513. doi: 10.1111/mmi.14170
- Livermore, D. M. (2002). Multiple mechanisms of antimicrobial resistance in *Pseudomonas aeruginosa*: our worst nightmare? *Clin. Infect. Dis.* 34, 634–640. doi: 10.1086/338782
- Lopes-Pacheco, M. (2016). CFTR modulators: shedding light on precision medicine for cystic fibrosis. *Front. Pharmacol.* 7:275. doi: 10.3389/fphar.2016.00275
- Ma, J.-F., Ochsner, U. A., Klotz, M. G., Nanayakkara, V. K., Howell, M. L., Johnson, Z., et al. (1999). Bacterioferritin A modulates catalase A (KatA) activity and resistance to hydrogen peroxide in *Pseudomonas aeruginosa*. *J. Bacteriol.* 181, 3730–3742.
- MacMicking, J., Xie, Q. W., and Nathan, C. (1997). Nitric oxide and macrophage function. *Annu. Rev. Immunol.* 15, 323–350. doi: 10.1146/annurev.immunol.15.1.323
- Mahar, P., Padiglione, A. A., Cleland, H., Paul, E., Hinrichs, M., and Wasiak, J. (2010). *Pseudomonas aeruginosa* bacteraemia in burns patients: risk factors and outcomes. *Burns* 36, 1228–1233. doi: 10.1016/j.burns.2010.05.009
- Mai-Prochnow, A., Hui, J. G., Kjelleberg, S., Rakonjac, J., McDougald, D., and Rice, S. A. (2015). 'Big things in small packages: the genetics of filamentous phage and effects on fitness of their host'. *FEMS Microbiol. Rev.* 39, 465–487. doi: 10.1093/femsre/fuu007
- Major, T. A., Panmanee, W., Mortensen, J. E., Gray, L. D., Hoglen, N., and Hassett, D. J. (2010). Sodium nitrite-mediated killing of the major cystic fibrosis pathogens *Pseudomonas aeruginosa*, *Staphylococcus aureus*, and *Burkholderia cepacia* under anaerobic planktonic and biofilm conditions. *Antimicrob. Agents Chemother.* 54, 4671–4677. doi: 10.1128/AAC.00379-10
- Martens, C. J., Inglis, S. K., Valentine, V. G., Garrison, J., Conner, G. E., and Ballard, S. T. (2011). Mucous solids and liquid secretion by airways: studies with normal pig, cystic fibrosis human, and non-cystic fibrosis human bronchi. *Am. J. Physiol. Lung Cell Mol. Physiol.* 301, L236–L246. doi: 10.1152/ajplung.00388.2010
- Martin, D. W., Schurr, M. J., Mudd, M. H., Govan, J. R., Holloway, B. W., and Deretic, V. (1993). Mechanism of conversion to mucoidy in *Pseudomonas aeruginosa* infecting cystic fibrosis patients. *Proc. Natl. Acad. Sci. U.S.A.* 90, 8377–8381.
- Martin, G. S., Mannino, D. M., Eaton, S., and Moss, M. (2003). The epidemiology of sepsis in the United States from 1979 through 2000. *N. Engl. J. Med.* 348, 1546–1554. doi: 10.1056/NEJMoa022139
- Martinez, E., and Campos-Gomez, J. (2016). Pf filamentous phage requires UvrD for replication in *Pseudomonas aeruginosa*. *mSphere* 1:e00104-15. doi: 10.1128/mSphere.00104-15
- Matsui, H., Wagner, V. E., Hill, D. B., Schwab, U. E., Rogers, T. D., Button, B., et al. (2006). A physical linkage between cystic fibrosis airway surface dehydration and *Pseudomonas aeruginosa* biofilms. *Proc. Natl. Acad. Sci. U.S.A.* 103, 18131–18136.
- Mayhall, C. G. (2003). The epidemiology of burn wound infections: then and now. *Clin. Infect. Dis.* 37, 543–550. doi: 10.1086/376993
- McCarthy, R. R., Mooij, M. J., Reen, F. J., Lesouhaitier, O., and O'Gara, F. (2014). A new regulator of pathogenicity (bvlR) is required for full virulence and tight microcolony formation in *Pseudomonas aeruginosa*. *Microbiology* 160, 1488–1500. doi: 10.1099/mic.0.075291-0
- McDaniel, C., Su, S., Panmanee, W., Lau, G. W., Browne, T., Cox, K., et al. (2016). A putative ABC transporter permease is necessary for resistance to acidified nitrite and EDTA in *Pseudomonas aeruginosa* under aerobic and anaerobic Planktonic and Biofilm conditions. *Front. Microbiol.* 7:291. doi: 10.3389/fmicb.2016.00291
- McDaniel, C. T., Panmanee, W., Winsor, G. L., Gill, E., Bertelli, C., Schurr, M. J., et al. (2020). AB569, a nontoxic chemical tandem that kills major human pathogenic bacteria. *Proc. Natl. Acad. Sci. U.S.A.* 117, 4921–4930. doi: 10.1073/pnas.1911927117
- McDonald, I. K., and Thornton, J. M. (1994). Satisfying hydrogen bonding potential in proteins. *J. Mol. Biol.* 238, 777–793.
- McElroy, K. E., Hui, J. G., Woo, J. K., Luk, A. W., Webb, J. S., Kjelleberg, S., et al. (2014). Strain-specific parallel evolution drives short-term diversification during *Pseudomonas aeruginosa* biofilm formation. *Proc. Natl. Acad. Sci. U.S.A.* 111, E1419–E1427. doi: 10.1073/pnas.1314340111
- Mir, M. D. A., Chaudhary, S., Payasi, A., Sood, R., Mavuduru, R. S., and Shameem, M. (2019). CSE (Ceftriaxone+ Sulbactam+ Disodium EDTA) Versus meropenem for the treatment of complicated urinary tract infections, including acute pyelonephritis: PLEA, a Double-blind, randomized noninferiority trial. *Open Forum Infect. Dis.* 6:ofz373. doi: 10.1093/ofid/ofz373
- Moeller, A., Horak, F. Jr., Lane, C., Knight, D., Kicic, A., Brennan, S., et al. (2006). Inducible NO synthase expression is low in airway epithelium from young children with cystic fibrosis. *Thorax* 61, 514–520. doi: 10.1136/thx.2005.054643
- Mooij, M. J., Drenkard, E., Llamas, M. A., Vandenbroucke-Grauls, C., Savelkoul, P. H. M., Ausubel, F. M., et al. (2007). Characterization of the integrated filamentous phage Pf5 and its involvement in small-colony formation. *Microbiology* 153, 1790–1798. doi: 10.1099/mic.0.2006/003533-0
- Nagoba, B. S., Selkar, S. P., Wadher, B. J., and Gandhi, R. C. (2013). Acetic acid treatment of pseudomonal wound infections—a review. *J. Infect. Public Health* 6, 410–415. doi: 10.1016/j.jiph.2013.05.005
- Nathan, C., and Xie, Q. W. (1994). Nitric oxide synthases: roles, tolls, and controls. *Cell* 78, 915–918. doi: 10.1016/0092-8674(94)90266-6
- Neufeld, B. H., and Reynolds, M. M. (2016). Critical nitric oxide concentration for *Pseudomonas aeruginosa* biofilm reduction on polyurethane substrates. *Biointerphases* 11:031012. doi: 10.1116/1.4962266
- Newman, J. W., Floyd, R. V., and Fothergill, J. L. (2017). The contribution of *Pseudomonas aeruginosa* virulence factors and host factors in the establishment of urinary tract infections. *FEMS Microbiol. Lett.* 364:fnx124. doi: 10.1093/femsle/fnx124
- Ochsner, U. A., and Vasil, M. L. (1996). Gene regulation by the ferric uptake regulator (Fur) in *Pseudomonas aeruginosa*: cycle selection of iron-regulated genes. *Proc. Natl. Acad. Sci. U.S.A.* 93, 4409–4414.
- Ochsner, U. A., Vasil, M. L., Alsabbagh, E., Parvatiyar, K., and Hassett, D. J. (2000). Role of the *Pseudomonas aeruginosa oxyR-recG* operon in oxidative stress defense and DNA repair: OxyR-dependent regulation of *katB*, *ahpB*, and *ahpCF*. *J. Bacteriol.* 182, 4533–4544.
- Ormerod, A. D., White, M. I., Shah, S. A., and Benjamin, N. (1999). Molluscum contagiosum effectively treated with a topical acidified nitrite, nitric oxide liberating cream. *Br. J. Dermatol.* 141, 1051–1053. doi: 10.1046/j.1365-2133.1999.03204.x
- Osler, W. (1914). Medical notes on England at war. *Science* 63, 2303–2305.
- O'Sullivan, S. T., and O'Connor, T. P. (1997). Immunosuppression following thermal injury: the pathogenesis of immunodysfunction. *Br. J. Plast. Surg.* 50, 615–623. doi: 10.1016/s0007-1226(97)90507-5
- O'Toole, G. A. (2018). Cystic fibrosis airway microbiome: overturning the old, opening the way for the new. *J. Bacteriol.* 200:e0561-17. doi: 10.1128/JB.00561-17
- Palmer, K. L., Aye, L. M., and Whiteley, M. (2007a). Nutritional cues control *Pseudomonas aeruginosa* multicellular behavior in cystic fibrosis sputum. *J. Bacteriol.* 189, 8079–8087.
- Palmer, K. L., Brown, S. A., and Whiteley, M. (2007b). Membrane-bound nitrate reductase is required for anaerobic growth in cystic fibrosis sputum. *J. Bacteriol.* 189, 4449–4455.
- Papaioannou, E., Wahjudi, M., Nadal-Jimenez, P., Koch, G., Setroikromo, R., and Quax, W. J. (2009). Quorum-quenching acylase reduces the virulence of *Pseudomonas aeruginosa* in a *Caenorhabditis elegans* infection model. *Antimicrob. Agents Chemother.* 53, 4891–4897. doi: 10.1128/AAC.00380-09

- Park, S. J., Kim, S. K., So, Y. I., Park, H. Y., Li, X. H., Yeom, D. H., et al. (2014). Protease IV, a quorum sensing-dependent protease of *Pseudomonas aeruginosa* modulates insect innate immunity. *Mol. Microbiol.* 94, 1298–1314. doi: 10.1111/mmi.12830
- Percival, S. L., and Salisbury, A. M. (2018). The efficacy of tetrasodium EDTA on biofilms. *Adv. Exp. Med. Biol.* 1057, 101–110. doi: 10.1007/5584_2017_134
- Petersen, K., Riddle, M. S., Danko, J. R., Blazes, D. L., Hayden, R., Tasker, S. A., et al. (2007). Trauma-related infections in battlefield casualties from Iraq. *Ann. Surg.* 245, 803–811. doi: 10.1097/01.sla.0000251707.32332.c1
- Petrova, O. E., Schurr, J. R., Schurr, M. J., and Sauer, K. (2011). The novel *Pseudomonas aeruginosa* two-component regulator BfmR controls bacteriophage-mediated lysis and DNA release during biofilm development through PhdA. *Mol. Microbiol.* 81, 767–783. doi: 10.1111/j.1365-2958.2011.07733.x
- Phillips, R., Adjei, O., Lucas, S., Benjamin, N., and Wansbrough-Jones, M. (2004). Pilot randomized double-blind trial of treatment of *Mycobacterium ulcerans* disease (Buruli ulcer) with topical nitrogen oxides. *Antimicrob. Agents Chemother.* 48, 2866–2870. doi: 10.1128/AAC.48.8.2866-2870.2004
- Platt, M. D., Schurr, M. J., Sauer, K., Vazquez, G., Kukavica-Ibrulj, I., Potvin, E., et al. (2008). Proteomic, microarray, and signature-tagged mutagenesis analyses of anaerobic *Pseudomonas aeruginosa* at pH 6.5, likely representing chronic, late-stage cystic fibrosis airway conditions. *J. Bacteriol.* 190, 2739–2758.
- Rakonjac, J., Bennett, N. J., Spagnuolo, J., Gagic, D., and Russel, M. (2011). Filamentous bacteriophage: biology, phage display and nanotechnology applications. *Curr. Issues Mol. Biol.* 13, 51–76.
- Reighard, K. P., Hill, D. B., Dixon, G. A., Worley, B. V., and Schoenfisch, M. H. (2015). Disruption and eradication of *P. aeruginosa* biofilms using nitric oxide-releasing chitosan oligosaccharides. *Biofouling* 31, 775–787. doi: 10.1080/08927014.2015.1107548
- Remy, M. M., Sahin, M., Flatz, L., Regen, T., Xu, L., Kreutzfeldt, M., et al. (2017). Interferon-gamma-driven iNOS: a molecular pathway to terminal shock in arenavirus hemorrhagic fever. *Cell Host Microb.* 22, 354–365.e355. doi: 10.1016/j.chom.2017.07.008
- Rex, S. (2012). Burn injuries. *Curr. Opin. Crit. Care* 18, 671–676. doi: 10.1097/MCC.0b013e328359fd6e
- Ricciardolo, F. L., Sterk, P. J., Gaston, B., and Folkerts, G. (2004). Nitric oxide in health and disease of the respiratory system. *Physiol. Rev.* 84, 731–765.
- Rice, S. A., Tan, C. H., Mikkelsen, P. J., Kung, V., Woo, J., Tay, M., et al. (2009). The biofilm life cycle and virulence of *Pseudomonas aeruginosa* are dependent on a filamentous prophage. *ISME J.* 3, 271–282. doi: 10.1038/ismej.2008.109
- Rineh, A., Soren, O., McEwan, T., Ravikumar, V., Poh, W. H., Azamifar, F., et al. (2020). Discovery of Cephalosporin-3'-diazeniumdiolates that show dual antibacterial and antibiofilm effects against *Pseudomonas aeruginosa* clinical cystic fibrosis isolates and efficacy in a murine respiratory infection model. *ACS Infect. Dis.* 6, 1460–1479. doi: 10.1021/acsinfecdis.0c00070
- Rogan, M. P., Stoltz, D. A., and Hornick, D. B. (2011). Cystic fibrosis transmembrane conductance regulator intracellular processing, trafficking, and opportunities for mutation-specific treatment. *Chest* 139, 1480–1490. doi: 10.1378/chest.10-2077
- Rowntree, R. K., and Harris, A. (2003). The phenotypic consequences of CFTR mutations. *Ann. Hum. Genet.* 67, 471–485. doi: 10.1046/j.1469-1809.2003.00028.x
- Roy, M. G., Livraghi-Butrico, A., Fletcher, A. A., McElwee, M. M., Evans, S. E., Boerner, R. M., et al. (2014). Muc5b is required for airway defence. *Nature* 505, 412–416. doi: 10.1038/nature12807
- Rumbaugh, K. P., Griswold, J. A., Iglewski, B. H., and Hamood, A. N. (1999). Contribution of quorum sensing to the virulence of *Pseudomonas aeruginosa* in burn wound infections. *Infect. Immun.* 67, 5854–5862.
- Rumbaugh, K. P., Hamood, A. N., and Griswold, J. A. (2004). Cytokine induction by the *P. aeruginosa* quorum sensing system during thermal injury. *J. Surg. Res.* 116, 137–144. doi: 10.1016/j.jss.2003.08.009
- Russell, J. A. (2006). Management of sepsis. *N. Engl. J. Med.* 355, 1699–1713. doi: 10.1056/NEJMra043632
- Saini, R., and Singh, S. (2019). Inducible nitric oxide synthase: an asset to neutrophils. *J. Leukoc. Biol.* 105, 49–61. doi: 10.1002/JLB.4RU0418-161R
- Salunkhe, P., Smart, C. H., Morgan, J. A., Panagea, S., Walslow, M. J., Hart, C. A., et al. (2005). A cystic fibrosis epidemic strain of *Pseudomonas aeruginosa* displays enhanced virulence and antimicrobial resistance. *J. Bacteriol.* 187, 4908–4920. doi: 10.1128/JB.187.14.4908-4920.2005
- Sanderson, K., Wescombe, L., Kirov, S. M., Champion, A., and Reid, D. W. (2008). Bacterial cyanogenesis occurs in the cystic fibrosis lung. *Eur. Respir. J.* 32, 329–333. doi: 10.1183/09031936.00152407
- Schaber, J. A., Triffo, W. J., Suh, S. J., Oliver, J. W., Hastert, M. C., Griswold, J. A., et al. (2007). *Pseudomonas aeruginosa* forms biofilms in acute infection independent of cell-to-cell signaling. *Infect. Immun.* 75, 3715–3721. doi: 10.1128/IAI.00586-07
- Schreiber, K., Krieger, R., Benkert, B., Eschbach, M., Arai, H., Schobert, M., et al. (2007). The anaerobic regulatory network required for *Pseudomonas aeruginosa* nitrate respiration. *J. Bacteriol.* 189, 4310–4314.
- Schwab, U., Abdullah, L. H., Perlmutter, O. S., Albert, D., Davis, C. W., Arnold, R. R., et al. (2014). Localization of *Burkholderia cepacia* complex bacteria in cystic fibrosis lungs and interactions with *Pseudomonas aeruginosa* in hypoxic mucus. *Infect. Immun.* 82, 4729–4745. doi: 10.1128/IAI.01876-14
- Secor, P. R., Burgener, E. B., Kinnersley, M., Jennings, L. K., Roman-Cruz, V., Popescu, M., et al. (2020). Pf bacteriophage and their impact on *Pseudomonas* Virulence, mammalian immunity, and chronic infections. *Front. Immunol.* 11:244. doi: 10.3389/fimmu.2020.00244
- Secor, P. R., Jennings, L. K., Michaels, L. A., Sweere, J. M., Singh, P. K., Parks, W. C., et al. (2015a). Biofilm assembly becomes crystal clear - filamentous bacteriophage organize the *Pseudomonas aeruginosa* biofilm matrix into a liquid crystal. *Microb. Cell* 3, 49–52. doi: 10.15698/mic2016.01.475
- Secor, P. R., Sweere, J. M., Michaels, L. A., Malkovskiy, A. V., Lazzareschi, D., Katznelson, E., et al. (2015b). Filamentous Bacteriophage promote Biofilm assembly and function. *Cell Host Microb.* 18, 549–559. doi: 10.1016/j.chom.2015.10.013
- Seymour, C. W., Iwashyna, T. J., Cooke, C. R., Hough, C. L., and Martin, G. S. (2010). Marital status and the epidemiology and outcomes of sepsis. *Chest* 137, 1289–1296. doi: 10.1378/chest.09-2661
- Simon, M. A., Vanderpool, R. R., Nouraie, M., Bachman, T. N., White, P. M., Sugahara, M., et al. (2016). Acute hemodynamic effects of inhaled sodium nitrite in pulmonary hypertension associated with heart failure with preserved ejection fraction. *JCI Insight* 1:e89620. doi: 10.1172/jci.insight.89620
- Smith, S. D., Wheeler, M. A., Foster, H. E. Jr., and Weiss, R. M. (1996). Urinary nitric oxide synthase activity and cyclic GMP levels are decreased with interstitial cystitis and increased with urinary tract infections. *J. Urol.* 155, 1432–1435.
- Soren, O., Rineh, A., Silva, D. G., Cai, Y., Howlin, R. P., Allan, R. N., et al. (2020). Cephalosporin nitric oxide-donor prodrug DEA-C3D disperses biofilms formed by clinical cystic fibrosis isolates of *Pseudomonas aeruginosa*. *J. Antimicrob. Chemother.* 75, 117–125. doi: 10.1093/jac/dkz378
- Steinstraesser, L., Schubert, C., Jacobsen, F., and Al-Benna, S. (2010). Editorial: glycyrrhizin against multi-resistant bacteria? *J. Leukoc. Biol.* 87, 7–8. doi: 10.1189/jlb.0809567
- Stewart, P. S. (1996). Theoretical aspects of antibiotic diffusion into microbial biofilms. *Antimicrob. Agents Chemother.* 40, 2517–2522.
- Su, S., and Hassett, D. J. (2012). Anaerobic *Pseudomonas aeruginosa* and other obligately anaerobic bacterial biofilms growing in the thick airway mucus of chronically infected cystic fibrosis patients: an emerging paradigm or "Old Hat"? *Expert. Opin. Ther. Targets* 16, 859–873. doi: 10.1517/14728222.2012.708025
- Su, S., Panmanee, W., Wilson, J. J., Mahtani, H. K., Li, Q., Vanderwielen, B. D., et al. (2014). Catalase (KatA) plays a role in protection against anaerobic nitric oxide in *Pseudomonas aeruginosa*. *PLoS One* 9:e91813. doi: 10.1371/journal.pone.0091813
- Sweere, J. M., Van Belleghem, J. D., Ishak, H., Bach, M. S., Popescu, M., Sunkari, V., et al. (2019). Bacteriophage trigger antiviral immunity and prevent clearance of bacterial infection. *Science* 363:eaat9691. doi: 10.1126/science.aat9691
- Thornton, D. J., Rousseau, K., and McGuckin, M. A. (2008). Structure and function of the polymeric mucins in airways mucus. *Annu. Rev. Physiol.* 70, 459–486. doi: 10.1146/annurev.physiol.70.113006.100702
- Tildy, B. E., and Rogers, D. F. (2015). Therapeutic options for hydrating airway mucus in cystic fibrosis. *Pharmacology* 95, 117–132. doi: 10.1159/000377638
- Toyofuku, M., Nomura, N., Fujii, T., Takaya, N., Maseda, H., Sawada, I., et al. (2007). Quorum sensing regulates denitrification in *Pseudomonas aeruginosa* PAO1. *J. Bacteriol.* 189, 4969–4972. doi: 10.1128/JB.00289-07

- Toyofuku, M., Uchiyama, H., and Nomura, N. (2012). Social behaviours under anaerobic conditions in *Pseudomonas aeruginosa*. *Int. J. Microbiol.* 2012:405191. doi: 10.1155/2012/405191
- Trunk, K., Benkert, B., Quack, N., Munch, R., Scheer, M., Garbe, J., et al. (2010). Anaerobic adaptation in *Pseudomonas aeruginosa*: definition of the Anr and Dnr regulons. *Environ. Microbiol.* 12, 1719–1733. doi: 10.1111/j.1462-2920.2010.02252.x
- Turner, K. H., Everett, J., Trivedi, U., Rumbaugh, K. P., and Whiteley, M. (2014). Requirements for *Pseudomonas aeruginosa* acute burn and chronic surgical wound infection. *PLoS Genet.* 10:e1004518. doi: 10.1371/journal.pgen.1004518
- van Langeveld, I., Gagnon, R. C., Conrad, P. F., Gamelli, R. L., Martin, B., Choudhry, M. A., et al. (2017). Multiple-drug resistance in burn patients: a retrospective study on the impact of antibiotic resistance on survival and length of stay. *J. Burn Care Res.* 38, 99–105. doi: 10.1097/BCR.0000000000000479
- Vazquez-Torres, A. (2012). Redox active thiol sensors of oxidative and nitrosative stress. *Antioxid. Redox Signal.* 17, 1201–1214. doi: 10.1089/ars.2012.4522
- Wang, C. Z., Ayadi, A. E., Goswamy, J., Finnerty, C. C., Mifflin, R., Sousse, L., et al. (2015). Topically applied metal chelator reduces thermal injury progression in a rat model of brass comb burn. *Burns* 41, 1775–1787. doi: 10.1016/j.burns.2015.08.012
- Webb, J. S., Lau, M., and Kjelleberg, S. (2004). Bacteriophage and phenotypic variation in *Pseudomonas aeruginosa* biofilm development. *J. Bacteriol.* 186, 8066–8073. doi: 10.1128/JB.186.23.8066-8073.2004
- Webb, J. S., Thompson, L. S., James, S., Charlton, T., Tolker-Nielsen, T., Koch, B., et al. (2003). Cell death in *Pseudomonas aeruginosa* biofilm development. *J. Bacteriol.* 185, 4585–4592.
- Wei, Q., Le Minh, P. N., Dotsch, A., Hildebrand, F., Panmanee, W., Elfarash, A., et al. (2012). Global regulation of gene expression by OxyR in an important human opportunistic pathogen. *Nucleic Acids Res.* 40, 4320–4333. doi: 10.1093/nar/gks017
- Weller, R., and Finnen, M. J. (2006). The effects of topical treatment with acidified nitrite on wound healing in normal and diabetic mice. *Nitric Oxide* 15, 395–399. doi: 10.1016/j.niox.2006.04.002
- Weller, R., Ormerod, A. D., Hobson, R. P., and Benjamin, N. J. (1998). A randomized trial of acidified nitrite cream in the treatment of tinea pedis. *J. Am. Acad. Dermatol.* 38, 559–563. doi: 10.1016/s0190-9622(98)70117-3
- Whitehead, N. A., Barnard, A. M., Slater, H., Simpson, N. J., and Salmond, G. P. (2001). Quorum-sensing in gram-negative bacteria. *FEMS Microbiol. Rev.* 25, 365–404.
- Willems, A. (2014). “The family Pylobacteriaceae,” in *The Prokaryotes*, eds A. Balows, H. G. Troper, M. Dworkin, W. Harder, and D. K.-H. Schleifer (Cham: Springer), 335–418.
- Williams, D. E., and Boon, E. M. (2019). Towards understanding the molecular basis of nitric oxide-regulated group behaviors in pathogenic bacteria. *J. Innate Immun.* 11, 205–215. doi: 10.1159/000494740
- Williams, D. E., Nisbett, L. M., Bacon, B., and Boon, E. (2018). Bacterial heme-based sensors of nitric oxide. *Antioxid. Redox Signal.* 29, 1872–1887. doi: 10.1089/ars.2017.7235
- Wooldridge, J. L., Deutsch, G. H., Sontag, M. K., Osberg, I., Chase, D. R., Silkoff, P. E., et al. (2004). NO pathway in CF and non-CF children. *Pediatr. Pulmonol.* 37, 338–350.
- Worlitzsch, D., Tarran, R., Ulrich, M., Schwab, U., Cekici, A., Meyer, K. C., et al. (2002). Reduced oxygen concentrations in airway mucus contribute to the early and late pathogenesis of *Pseudomonas aeruginosa* cystic fibrosis airway infection. *J. Clin. Invest.* 109, 317–325.
- Yang, L., Teles, F., Gong, W., Dua, S. A., Martin, L., and Schoenfisch, M. H. (2020). Antibacterial action of nitric oxide-releasing hyperbranched polymers against ex vivo dental biofilms. *Dent. Mater.* 36, 635–644. doi: 10.1016/j.dental.2020.03.012
- Yeh, J. T., Yu, Y. C., and Hwang, T. C. (2019). Structural mechanisms for defective CFTR gating caused by the Q1412X mutation, a severe Class VI pathogenic mutation in cystic fibrosis. *J. Physiol.* 597, 543–560. doi: 10.1113/JP277042
- Yepuri, N. R., Barraud, N., Mohammadi, N. S., Kardak, B. G., Kjelleberg, S., Rice, S. A., et al. (2013). Synthesis of cephalosporin-3'-diazoniumdiolates: biofilm dispersing NO-donor prodrugs activated by beta-lactamase. *Chem. Commun.* 49, 4791–4793. doi: 10.1039/c3cc40869h
- Yoon, S. S., Coakley, R., Lau, G. W., Lymar, S. V., Gaston, B., Karabulut, A. C., et al. (2006). Anaerobic killing of mucoid *Pseudomonas aeruginosa* by acidified nitrite derivatives under cystic fibrosis airway conditions. *J. Clin. Invest.* 116, 436–446.
- Yoon, S. S., Hennigan, R. F., Hilliard, G. M., Ochsner, U. A., Parvatiyar, K., Kamani, M. C., et al. (2002). *Pseudomonas aeruginosa* anaerobic respiration in biofilms: relationships to cystic fibrosis pathogenesis. *Dev. Cell* 3, 593–603.
- Yoon, S. S., Karabulut, A. C., Lipscomb, J. D., Hennigan, R. F., Lymar, S. V., Groce, S. L., et al. (2007). Two-pronged survival strategy for the major cystic fibrosis pathogen, *Pseudomonas aeruginosa*, lacking the capacity to degrade nitric oxide during anaerobic respiration. *EMBO J.* 26, 3662–3672.
- Yuan, Z., and VanBriesen, J. M. (2008). Bacterial growth yields on EDTA, NTA, and their biodegradation intermediates. *Biodegradation* 19, 41–52. doi: 10.1007/s10532-007-9113-y
- Zemke, A. C., Shiva, S., Burns, J. L., Moskowitz, S. M., Pilewski, J. M., Gladwin, M. T., et al. (2014). Nitrite modulates bacterial antibiotic susceptibility and biofilm formation in association with airway epithelial cells. *Free Radic. Biol. Med.* 77, 307–316. doi: 10.1016/j.freeradbiomed.2014.08.011

Conflict of Interest: The authors declare that the research was conducted in the absence of any commercial or financial relationships that could be construed as a potential conflict of interest.

Copyright © 2021 Hassett, Kovall, Schurr, Kotagiri, Kumari and Satish. This is an open-access article distributed under the terms of the Creative Commons Attribution License (CC BY). The use, distribution or reproduction in other forums is permitted, provided the original author(s) and the copyright owner(s) are credited and that the original publication in this journal is cited, in accordance with accepted academic practice. No use, distribution or reproduction is permitted which does not comply with these terms.



Characterization of Binary Biofilms of *Listeria monocytogenes* and *Lactobacillus* and Their Response to Chlorine Treatment

Magdalena A. Olszewska^{1,2*} and Francisco Diez-Gonzalez¹

¹ Center for Food Safety, College of Agricultural and Environmental Sciences, University of Georgia, Griffin, GA, United States, ² Department of Industrial and Food Microbiology, Faculty of Food Science, University of Warmia and Mazury in Olsztyn, Olsztyn, Poland

OPEN ACCESS

Edited by:

Luis Cláudio Nascimento da Silva,
Universidade Ceuma, Brazil

Reviewed by:

Antonio Valero,
University of Córdoba, Spain
Prem Saran Tirumalai,
Dayalbagh Educational Institute, India
Valério Monteiro-Neto,
Universidade Federal do Maranhão,
Brazil

Pedro Rodríguez-López,
University of Parma, Italy

*Correspondence:

Magdalena A. Olszewska
magolsz@uga.edu;
magdalena.olszewska@uwm.edu.pl

Specialty section:

This article was submitted to
Antimicrobials, Resistance
and Chemotherapy,
a section of the journal
Frontiers in Microbiology

Received: 07 December 2020

Accepted: 14 June 2021

Published: 14 July 2021

Citation:

Olszewska MA and
Diez-Gonzalez F (2021)
Characterization of Binary Biofilms
of *Listeria monocytogenes*
and *Lactobacillus* and Their Response
to Chlorine Treatment.
Front. Microbiol. 12:638933.
doi: 10.3389/fmicb.2021.638933

In nature, *Listeria* may interact competitively and cooperatively with other organisms, resulting in unique spatial organization and functions for cells within the community. This study was undertaken to characterize the biofilm architecture of binary biofilms of *Listeria monocytogenes* and *Lactobacillus* species and to assess their effect on the survival of *Listeria* during exposure to hypochlorite. Three *L. monocytogenes* strains, ATCC 19115 (Lm5), ATCC 19117 (Lm7), and Coleslaw (LmC), were selected and combined individually with three *Lactobacillus* strains: *L. fermentum* (Lf), *L. bavaricus* (Lb), and *L. plantarum* (Lp). In binary Lm-Lp biofilms, the Lm cell counts were similar to single-species biofilms (8.5 log CFU/well), and the Lp cell numbers declined by 1.0 log CFU/well. In the presence of Lb, the Lm cell counts were reduced by 1.5 log CFU/well ($p < 0.05$), whereas the Lf cell counts increased at least by 3.5 log CFU/well. Confocal laser scanning microscopy (CLSM) determined that interspecies interactions significantly affected the spatial organization of three binary biofilms. Biofilm surface-to-volume ratio increased from $0.8 \mu\text{m}^2/\mu\text{m}^3$ for Lm5 in the monoculture to $2.1 \mu\text{m}^2/\mu\text{m}^3$ for Lm5-Lp in the dual-species model ($p < 0.05$), and was characterized by a thicker structure with a largely increased surface area. Biofilm roughness increased from 0.2 for Lm7 to 1.0 for Lm7-Lb biofilms ($p < 0.05$), which appeared as interspecific segregation. Biofilm thickness increased from $34.2 \mu\text{m}$ for LmC to $46.3 \mu\text{m}$ for LmC-Lf ($p < 0.05$), which produced flat and compact structures that covered the entire surface available. The biomass of the extracellular matrix was higher in the case of some binary biofilms ($p < 0.05$); however, this effect was dependent upon the species pair. When treated with hypochlorite, Lm5 in binary biofilms had an approximately 1.5 log CFU/well greater survival than individually. The unique spatial organization and greater protein production may explain the protective effect of Lp after hypochlorite exposure.

Keywords: *Listeria monocytogenes*, *Lactobacillus*, biofilm structure, microbial interaction, hypochlorite treatment, matrix composition

INTRODUCTION

In nature, microbes exist predominantly as communities of sessile cells known as biofilms (Donlan, 2002). Biofilms can be defined as aggregated microbial communities surrounded by a matrix of self-produced extracellular polymeric substances (EPS), which form on a wide variety of surfaces (O'Toole et al., 2000; Kim and Lee, 2016). In these distinctly structured and organized communities, cells coordinate their behavior and are capable of demonstrating specific functions (Rutherford and Bassler, 2012). Biofilms can play a positive role and are beneficial commercially for the immobilization technology, e.g., for the removal of crude oil from wastewaters (Nie et al., 2016). In contrast, biofilms can also have detrimental effects due to their strong antimicrobial tolerance and contribution to the persistence of pathogenic microorganisms in the food processing environment, thus, biofilms of *Escherichia coli* O157:H7 (e.g., Zhao et al., 2013), *Salmonella* spp. (e.g., Yang et al., 2016), *Pseudomonas aeruginosa* (Kim et al., 2008), *Bacillus cereus* (Ryu and Beuchat, 2005), and *Listeria monocytogenes* (e.g., Guilbaud et al., 2015) have attracted special attention over the years.

Cells originating from the biofilms formed in different locations of a food processing facility represent a potential source of food contamination, and *L. monocytogenes* is a bacterium of the greatest concern because of the high morbidity and mortality rate of foodborne listeriosis. Despite the thorough cleaning and disinfection applied, *Listeria* is repeatedly found at such a facility. Various studies have reported that *L. monocytogenes* can be present in food processing areas for very long periods (Saá Ibusquiza et al., 2012; Nowak et al., 2017; Rodríguez-Campos et al., 2019) and these persistent isolates may produce more biofilm than transient ones (Rieu et al., 2008; Kostaki et al., 2012). In addition, *L. monocytogenes* is able to form biofilms on different surfaces (Zhao et al., 2013; Alonso et al., 2014), representing a serious concern for the food industry.

The presence of other bacterial species along with a pathogenic bacterium may increase biofilm formation to the benefit of the pathogen by providing protection. However, different interactions, including synergistic and antagonistic, have been reported for *L. monocytogenes* biofilms with *Pseudomonas putida* (Saá Ibusquiza et al., 2012), *Salmonella enterica* (Kostaki et al., 2012), *Staphylococcus aureus* (Rieu et al., 2008), and *Vibrio parahaemolyticus* (Chen et al., 2019). Certainly, there is a correlation between the interspecific interactions and spatial organization of microorganisms in multi-species biofilms. According to the latest literature, a strong interdependence favors intermixing or layered structure, whereas weak interdependence is reflected in interspecific segregation and layered structure with patchy patterning, and finally, mutual inhibition resulted in a decreased biomass with patchy patterning or interspecific segregation (Liu et al., 2016). Moreover, functional properties like antimicrobial tolerance may be associated with the spatial architecture of biofilms. The limitation of agent penetration reflects the importance of the matrix shape and the three-dimensional organization of cells in protecting biofilm inhabitants (Kim et al., 2008). Evidence of spatial organization of mixed-species biofilms carrying *L. monocytogenes* and how and if the pathogen can be privileged

in surviving environmental challenges like disinfection measures is unfortunately very limited, hence, further studies with various bacterial species are needed.

Obtaining knowledge on biofilms composed of multiple bacterial species can be accomplished by confocal laser scanning microscopy (CLSM) as it offers the direct *in situ* and non-damaging investigation of native multicellular structures (Bridier et al., 2010). CLSM proved to be suitable for the characterization of the single-species biofilms of *L. monocytogenes* and opportunistic pathogens such as *E. coli*, *P. aeruginosa*, *S. aureus*, and *Enterococcus faecalis* (Bridier et al., 2010). In addition to the biofilm architecture of *L. monocytogenes*, this study aimed to correlate the genetic lineages of the isolates with structural diversity of their biofilms (Guilbaud et al., 2015). Given the importance of the co-existing microbiota for *L. monocytogenes* establishment and survival, we were particularly interested in the characterization of biofilms harboring *L. monocytogenes* in the presence of commensal or spoilage-associated genera such as *Lactobacillus*. *Lactobacilli* often share the same niche with *Listeria*, i.e., soil, plant material, and the food-processing environment including meat and dairy-related industrial environments where non-starter *lactobacilli* are introduced. Resident *lactobacilli* were shown to either protect or inhibit *L. monocytogenes* in the biofilms (Van der Veen and Abee, 2011; Pérez-Ibarreche et al., 2016). This ambiguous behavior prompted us to further investigate the characteristics of the binary biofilms of *L. monocytogenes* (Lm) with *Lactobacillus* spp., all selected on the basis of their biofilm formation capacity, and to assess the effect of cohabitation on the survival of *Listeria* during exposure to hypochlorite. Our approach specifically aimed at describing the spatial parameters to provide more knowledge on the architecture of Lm-carrying biofilms and if and how Lm can survive chemical disinfection depending on the *Lactobacillus* species present in the system. *Lactobacillus* species, such as *L. fermentum*, *L. bavaricus*, *L. sakei*, or *L. plantarum*, used here for biofilm formation screening represent the non-starter and resident *lactobacilli* found in the food-related industrial environments. The variability between the biomass (cell counts), structural parameters, and matrix production of binary biofilms was shown and comprehensively discussed as to if particular characteristics are involved in the hypochlorite tolerance of Lm.

RESULTS

Screening Biofilm Formation

L. monocytogenes strains (Table 1) and *Lactobacillus* species (Table 2) were tested for their biofilm formation abilities, and results indicated that both bacteria were better able to form biofilms aerobically than anaerobically (Supplementary Tables 1, 2). Average OD readings of *L. monocytogenes* biofilms grown aerobically and stained with crystal violet were very different among strains (Figure 1A), which suggested diverse biofilm-forming capabilities. These results allowed us to select three biofilm producers, i.e., *L. monocytogenes* ATCC 19115 (Lm5), *L. monocytogenes* ATCC 19117 (Lm7), and *L. monocytogenes* Coleslaw (LmC), for biofilm architecture and matrix localization studies. Also, three were selected

TABLE 1 | The 27 *Listeria monocytogenes* strains used in this study.

Strain	Isolate origin (if known)	Serotype (if known)	References
F8027	Food (celery)	4b	UGA
19115	Human	4b	ATCC
ScottA	Food (raw milk)	4b	UGA
Jalisco	Food (cheese)		UGA
Bilmar	Food (hot dog)		UGA
G1091	Coleslaw outbreak	4b	UGA
12443		1/2a	UGA
51774	Human	1/2a	ATCC
FSLJ1-101		1/2a	UGA
F8385		1/2a	UGA
2011L-2626	Cantaloupe outbreak		CDC
51782	Food (dairy)	3a	ATCC
51779	Food (dairy)	1/2c	ATCC
108M	Food (meat)		UGA
F6900	Clinical isolate, deli meat		UGA
Coleslaw	Food (Coleslaw)	4b	UGA
19117	Animal (sheep)	4d	ATCC
F8369	Food (corn)	1/2a	UGA
F8385	Food (carrots)	1/2b	UGA
G3982	Human, outbreak linked to Mexican-style cheese	4b	UGA
101M	Food (beef)		UGA
G3990	Human, outbreak linked to hot dog	4b	UGA
19114	Animal	4a	ATCC
G6006	Human, outbreak, IL, United States	1/2b	UGA
51780	Food (cheese)	1/2b	ATCC
19116	Animal (chicken)	4c	ATCC
F8255	Food (peach/plum)	1/2b	UGA

UGA, University of Georgia; ATCC, American Type Culture Collection; CDC, Centers for Disease Control and Prevention.

among the *Lactobacillus* species, *L. fermentum* ATCC 14931 (Lf), *L. bavaricus* LB5 (Lb), and *L. plantarum* CaTC2 (Lp) (**Figure 1B**), and used as secondary species for *Listeria* cells in binary biofilms.

Biofilm Growth Observation in Monoculture Biofilms

As monocultures, there was no difference in the biofilm cell counts among the Lm strains, reaching levels of 8.4 log CFU/well (Lm5) and 8.5 log CFU/well (Lm7, LmC) in BHI ($p > 0.05$) (**Figure 2**). Lb and Lp formed their biofilms at the levels of 7.7 and 7.3 log CFU/well, respectively, whereas Lf failed to develop biofilms (~2.0 log CFU/well) despite its abundant planktonic growth in BHI (data not shown) and biofilm formation in MRS (~8.0 log CFU/well).

Biofilm Growth Observation in Binary Biofilms

However, when Lf was grown in combination with Lm strains, its final cell counts increased by 3.5 log CFU/well. Still, all

TABLE 2 | The *Lactobacillus* spp. strains used in this study.

Species	Strain	Other code	Isolate origin (if known)	References
<i>L. fermentum</i>	14931	B1 28		ATCC
	36	B-9338		UGA
<i>L. bavaricus</i>		LB5		UGA
<i>L. plantarum</i>	2234			Silliker
	17-5	LB3 8014		UGA
	CaTC2	LB7	Animal-derived foodstuff	USDA ARS
<i>L. coprophilus</i>	2233			Silliker
<i>L. buchneri</i>	NCDO110	B-1837	Food (tomato pulp)	USDA ARS
<i>L. malefermentans</i>	NCIB8516	B-1861	Food (fermented beverages)	USDA ARS
<i>L. sakei</i>		LB706		UGA

ATCC, American Type Culture Collection; UGA: University of Georgia; USDA ARS, Agricultural Research Service United States Department of Agriculture Silliker-Silliker Laboratories.

the binary Lm–Lf biofilms had from 1.4 to 3.3 log CFU/well more *Listeria* than Lf ($p < 0.05$) (**Figure 2**). Likewise, binary biofilms with Lp also resulted in a greater contribution of *Listeria* (from 1.2 to 1.6 log CFU/well; $p < 0.05$). However, Lp analyses did not show significant differences in the cell counts between its single-species derivative and in combination with Lm5 ($p > 0.05$). In contrast, Lb had a higher contribution to the mixed-species biofilm than any *Listeria* (0.8–1.5 log CFU/well; $p < 0.05$), and its cell count was slightly higher than in the single-species counterpart.

Biofilm Resistance to Chlorine Treatment

The inactivation of mono and binary biofilms by chlorine is shown in **Figure 3**. Three Lm strains (Lm5/Lm7/LmC) individually and in combination with Lb/Lp/Lf were tested. A concentration of 50 ppm chlorine reduced the count of Lm5 and Lm7 by 4.4 and 2.9 log CFU, respectively, in the monocultures, but no more than 3.3 log CFU were killed in the binary biofilms. In dual-species models, Lm5 increased its survival by 1.5 and 1.0 log when co-cultured with Lp and Lb, respectively. Lp was the most resistant to chlorine, resulting in a reduction of 1.1 log CFU, however, it declined greatly (4.4 log CFU) in combination with Lm5. No such protective effect was observed for Lm7, with a reduction of approx. 3.0 log CFU. However, once in combination with Lf, the reduction of Lm7 decreased to 1.9 log CFU and the inactivation of Lf was comparatively high. Note that this pair scored first in terms of Lf cell contribution (**Figure 2**) and second in SVR increase (**Figure 4**). LmC itself yielded the lowest reduction (1.5 log CFU), and no increase in survival was observed when in the binary biofilms but with equal reduction levels between 3.0 and 3.5 log CFU instead.

3-D Biofilm Architecture

To determine which Lm biofilms were associated with which structural parameters, a Principal Component Analysis (PCA) was performed. The PCA revealed a separation of Lm biofilms

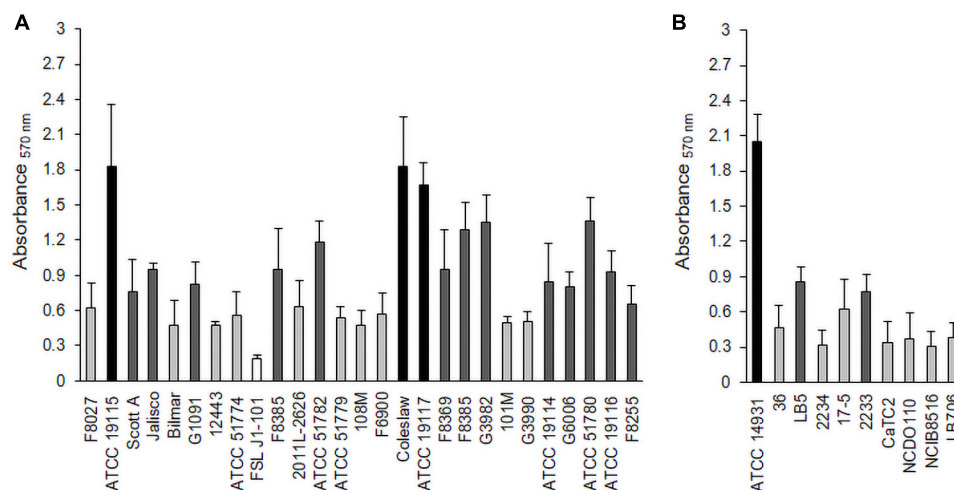


FIGURE 1 | Biofilm formation by *L. monocytogenes* strains (A) and *Lactobacillus* species (B) under aerobic conditions. Biofilms were quantified by the crystal violet (CV) assay at 570 nm. Black bars represent strong biofilm producers; dark gray, moderate biofilm producers; light gray, weak biofilm producers; and white, non-adherent.

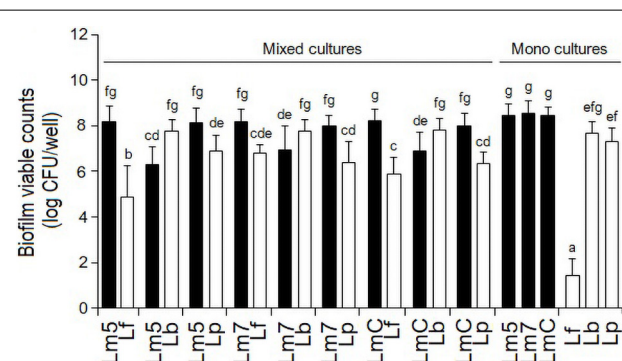


FIGURE 2 | Biofilm viable counts of *L. monocytogenes* strains and *Lactobacillus* species in mono and binary culture conditions grown in brain heart infusion supplemented with 0.005% manganese sulfate. Biofilm cells were quantified by enumeration following detachment, re-suspension, and agar plating. Different letters indicate a significant difference at a p -value of 0.05. *L. monocytogenes* strains ATCC 19115 (Lm5), ATCC 19117 (Lm7), and Coleslaw (LmC); *Lactobacillus fermentum* ATCC 14931 (Lf), *L. bavaricus* LB5 (Lb), and *L. plantarum* CaTC2 (Lp).

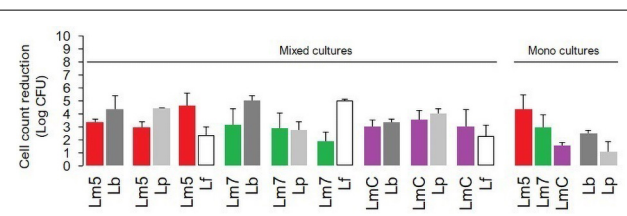


FIGURE 3 | The impact of chlorine (50 ppm) on the viability of *L. monocytogenes* strains (Lm5/Lm7/LmC) and their combinations with *Lactobacillus* species (Lb/Lp/Lf) in mono and binary culture biofilms assessed with the plate counting method and exhibited as log cell reductions. Lf is not represented as a monoculture (data not obtained). Results were means of at least three independent experiments conducted on different days. Abbreviations: see Figure 2.

along with their loadings in PC 1 and PC 2 (Supplementary Table 3). Given that the specific patterning of bacteria may lead to an increased biomass and enhanced tolerance toward antimicrobials compared to their component species individually, three binary biofilms were the most noteworthy. Lm5 when grown in combination with Lp yielded the closest proximity to the surface-to-volume ratio (SVR), whereas Lm7 when grown with Lb approached roughness. In contrast, LmC with Lf was strongly attributed to maximum thickness. Accordingly, differences were observed between these biofilms and those formed individually. The SVR increased from $0.8 \mu\text{m}^2/\mu\text{m}^3$ for Lm5 in monoculture to $2.1 \mu\text{m}^2/\mu\text{m}^3$ in the binary culture biofilm ($p < 0.05$) (Figure 4A). For the

monoculture biofilm, the roughness coefficient was 0.2 for Lm7, whereas in the binary biofilm, the roughness was 1.0 ($p < 0.05$) (Figure 4B). Considering the thickness for LmC biofilms, values of 34.2 and 46.3 μm in the mono and binary cultures, respectively, were obtained ($p < 0.05$) (Figure 4C). However, we also found that in the case of Lm5, the thickness increased from 13.8 to 26.6 μm in its binary biofilm with Lp ($p < 0.05$). This was not the case for Lm7 in the binary biofilm with Lb, but rather a contrary tendency was observed.

Representative biofilm structures for three Lm strains and their binary combinations (Lm5-Lp, Lm7-Lb, and LmC-Lf) are presented in Figure 5. The images correspond to the 3-D reconstructions acquired from confocal stacks, with shadow projections on the right. In the monoculture, LmC colonized the entire substratum and its biofilm was the thickest, whereas Lm5 formed small scattered cell clusters and overall thin biofilms. Lm5 with Lp formed denser structures, closely associated with one another. Lm7 and Lb grew independently and often formed separate microcolonies, despite the ability of Lm7 to cover the

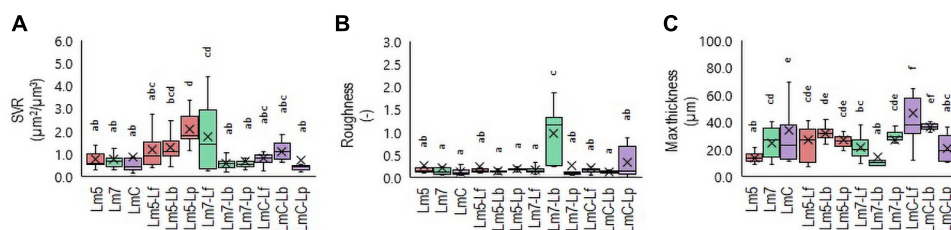


FIGURE 4 | Box plots of the biofilm structural parameters: surface-to-volume ratio (SVR) **(A)**, roughness average **(B)**, and maximum thickness **(C)** obtained for *L. monocytogenes* strains and their combinations with *Lactobacillus* species after confocal data processing of Syto® 9-labeled biofilms. The boxes range from the 25th to the 75th percentile and are intersected by the median line. Whiskers extend below and above the box range, from the lowest to the highest values, respectively. Averages are indicated by a cross symbol (x). Different letters indicate a significant difference at a *p*-value of 0.05. Abbreviations: see **Figure 2**.

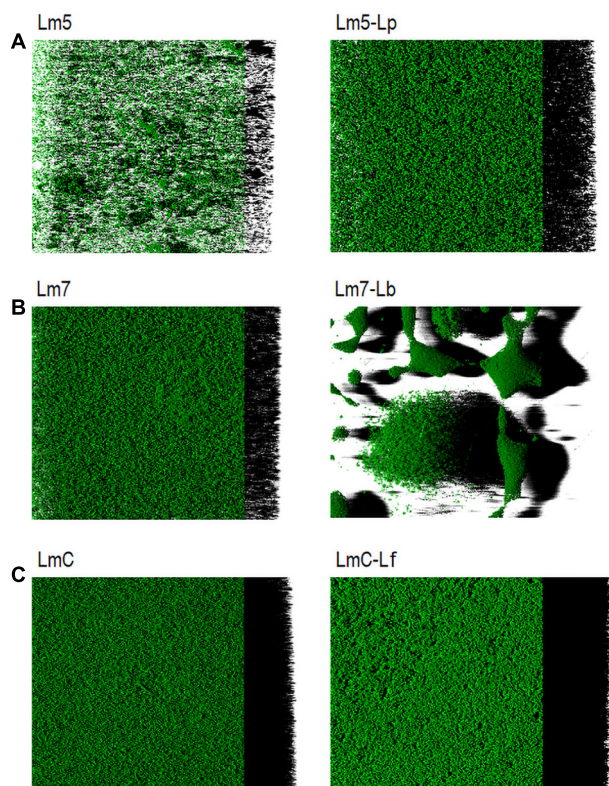


FIGURE 5 | Three-dimensional biofilm structures of *L. monocytogenes* strains in mono and binary culture conditions with different *Lactobacillus* species obtained from confocal z-stacks using the ZEN 2.3 software. **(A)** Lm5 individually and in combination with Lp. **(B)** Lm7 individually and in combination with Lb. **(C)** LmC individually and in combination with Lf. These images present the shadow projection on the right. The biofilms were labeled with Syto® 9, a cell permeant green fluorescent nucleic acid marker. Abbreviations: see **Figure 2**.

entire surface as in the monoculture. LmC with Lf formed flat and thick structures. The biofilms of *Lactobacillus* species had variable structures (**Supplementary Figure 1**). Lp developed thin biofilms that covered almost the entire surface, whereas the biofilm image of Lb showed an uneven coverage since the cells tended to create clumps. Lf produced rough structures, but only in the MRS

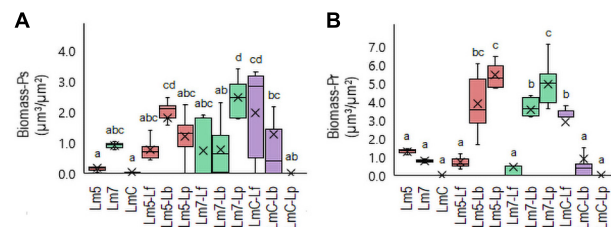
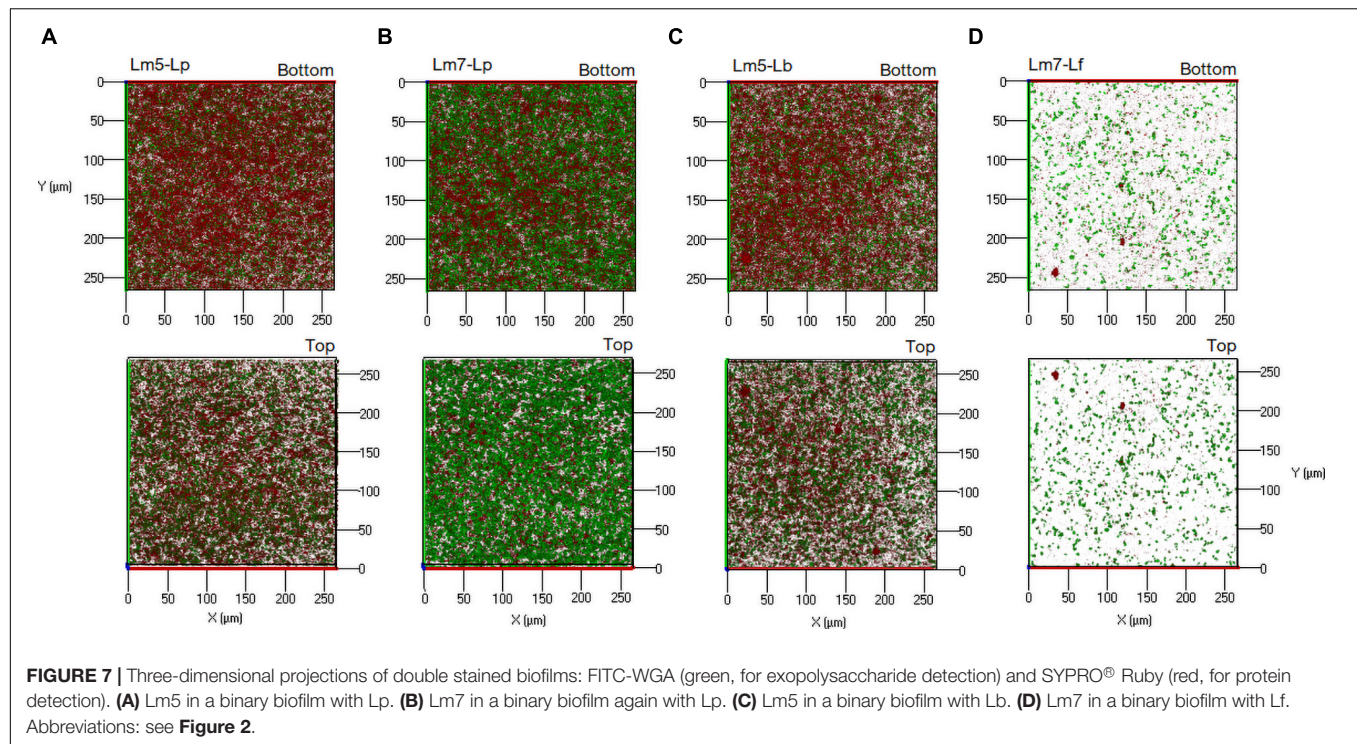


FIGURE 6 | Box plots of the biomass: polysaccharides (Ps-**A**) and proteins (Pr-**B**) obtained for *L. monocytogenes* strains and their combinations with *Lactobacillus* species after confocal data processing of FITC-WGA and SYPRO® Ruby-labeled biofilms. Box and whisker description: **Figure 3**. Different letters indicate a significant difference at a *p*-value of 0.05. Abbreviations: see **Figure 2**.

broth. For review, their structural parameters are also available in **Supplementary Figure 2**.

3-D Biofilm Matrix Localization

New staining revealed the 3-D biofilms based on the non-cellular biomass components polysaccharide and protein (**Figures 6, 7**). Some binary biofilm pictures displayed a substantial boost in the matrix production since they were variables with closer proximity to biomass variables (**Supplementary Table 4**). In particular, Lm5 and Lm7 in the binary biofilms with the same secondary species, Lp, stood out from the other biofilms (**Figure 6**). Individually, Lm5 produced more proteins and Lm7 more polysaccharides. Then, polysaccharide biomass increased from 0.2 to 1.2 $\mu\text{m}^3/\mu\text{m}^2$ and from 0.9 to 2.5 $\mu\text{m}^3/\mu\text{m}^2$ (**Figure 6A**), and protein biomass from 1.3 to 5.4 $\mu\text{m}^3/\mu\text{m}^2$ and from 0.8 to 4.9 $\mu\text{m}^3/\mu\text{m}^2$ in Lm5-Lp and Lm7-Lp biofilms, respectively ($p < 0.05$) (**Figure 6B**). LmC itself was not capable of producing the matrix under the conditions tested, nor the stimulation by Lp was observed. However, more matrices were observed when Lf was present, since values of 1.9 and 3.5 $\mu\text{m}^3/\mu\text{m}^2$ were obtained for polysaccharides and proteins, respectively ($p < 0.05$). Visual inspection revealed the presence of highly fluorescent red-stained aggregates, thus, more protein than polysaccharide fraction for Lm5-Lp (**Figure 7A**) and brightly green-labeled components and, thus, an opposite relationship for Lm7-Lp (**Figure 7B**). Another best matrix producer was again Lm5, this time with Lb, because



an increase to 1.8 and 3.9 $\mu\text{m}^3/\mu\text{m}^2$ (polysaccharide and protein) was observed and the visual inspection also showed that red-stained aggregates prevailed (**Figure 7C**). In contrast, the biomass of protein and polysaccharide obtained for the Lm7-Lf pair was comparatively small, with no indication of a stimulating effect (**Figure 6**).

DISCUSSION

The use of high throughput methods which allow the detailed characterization of the native architecture of biofilms is crucial to contribute to the understanding of microbial interactions and advancement in the field of biofilm research (Azeredo et al., 2017). Previous studies have discussed the significance of biofilm formation by *L. monocytogenes* (Borucki et al., 2003; Pilchová et al., 2014; Renier et al., 2014; Heredia and García, 2018) and 3-D structures have been previously described, i.e., a monolayer of cells, unstructured multilayers, a knitted-chain network, or honeycomb-like structures (Bridier et al., 2010; Renier et al., 2014; Guilbaud et al., 2015). Here, we applied a high throughput microscopic method for a high-resolution imaging of the biofilms of *L. monocytogenes* strains in mono and binary culture conditions with *Lactobacillus* species. We were especially interested in deciphering biofilms based on the different structural and functional parameters. They were important to better understand the complex behavioral and survival strategies of *L. monocytogenes* biofilms.

In this work, *L. monocytogenes* formed biofilms containing several small aggregates and the emergence of cell clusters

with a high degree of substratum coverage as single strain biofilms. The architecture of mixed communities was diverse in particular within three combinations, as emphasized by the SVR, roughness, and thickness parameters (**Figure 4**). As reflected in the increased thickness and SVR, cells of Lm5 and Lp arranged together indicates that when biofilms became thicker, the surface area of the biofilm actually increased (**Figure 5A**). Note that cooperation or exploitation results in an increased biomass, while competition leads to a decreased biomass in the mixed-species compared to single-species biofilms; the Lm5-Lp pair corresponded to the former. Although Lm5 was dominant in the biofilm, this particular combination had the lowest difference in the cell counts between the two species and the highest overall cell contribution than any other binary community. Considering the structural parameters, the surface-to-volume ratio was closely associated with the Lm5-Lp pair (**Figure 4A**).

The surface-to-volume ratio reflects what fraction of the biofilm is exposed to the nutrient flow, hence indicating how the biofilm adapts to the environment (Heydorn et al., 2000). Also, single cells and small cell aggregates naturally have a higher surface-to-volume ratio than larger microcolonies, suggesting that Lm5-Lp tended to mix together to a certain degree and form packed clusters decorated with loosely attached cells. Lm5-Lp pair also had strong matrix-producing abilities, in particular, toward proteins. Interesting observations on the interactions could be seen between Lm strains and Lf, where lactobacilli were markedly stimulated in the presence of *Listeria*. Depending on the Lm strain, these communities revealed differences in their 3-D architectures, suggesting the most compact structure with LmC.

Certainly, microbial interactions among different species have a significant impact on the growth potential, survival, individual behavior of each species, and the biofilm structure-function relationships (Kostaki et al., 2012). In our study, Lm tend to cooperate, compete, and communicate with Lp, Lb, and Lf in the binary biofilms. Interactions are cooperative, when interspecies interactions lead to benefits for one or all interacting species and are crucial for the overall biofilm fitness. Cooperative interactions include the secretion of enzymes or metabolic cross-feeding, and often lead to the specific spatial organization of different species in biofilms (Tan et al., 2017). Hence, this scenario matched the Lm-Lp pair than any other pair. Competition results in a decreased productivity for all or some interacting species. They compete for space and nutrients in an indirect strategy where fast growers deplete resources from slow competitors or in a direct fight with competing species, for example, by secretion of antimicrobials (Yang et al., 2011). This was the most likely scenario when Lb was present in the system.

To further continue, Lb competed with Lm strains and cells of Lm7 and Lb most probably attached as separate microcolonies in a spatial organization known as interspecific segregation (Figure 5B). Their structure generally presented the greatest roughness and the smallest bacterial thickness, thus, biomass resulting in a spatial structure with initial species segregation driven by exploitative or competitive interactions. Because *Listeria* residing in a binary community greatly suffered from the interaction with Lb, this might also fall into interference competition, hence, further studies need to be carried out to identify the compounds promoting this phenomenon. Such spatial organization where Lm forms its own microcolonies has been found in biofilms with the Gram-negative bacterium, *Comamonas testosteroni* (Carpentier and Chassaing, 2004). Similarly, competitive advantage was demonstrated for *V. parahaemolyticus* when with Lm cells because its favorable location on the surface layers resulted in overgrowing the partner strain (Chen et al., 2019). Likewise, in the presence of the antagonist produced by *B. cereus*, the number of Lm cells was lower, contributing to competitive interactions (Alonso et al., 2020). However, the number of cells was again higher in the presence of non-antagonist producers, suggesting a cooperative behavior between species. Lm was also dominant in the presence of *S. aureus*, showing an intimate association and an increase in the number of cells in the cell-free supernatant (Rieu et al., 2008).

In addition, signaling molecules-based communication known as quorum sensing (QS) plays an important role in intra- and interspecies interactions. Since biofilms comprise high concentrations of cells, QS is considered a crucial form of interaction leading to specific physiological activities for the cells (Rutherford and Bassler, 2012). Cells secrete autoinducers (AIs), which accumulate in the environment as the population density increases and further govern the gene expression like *luxS*. It has been demonstrated that *luxS* in *Lactobacillus acidophilus* is upregulated in response to viable cells and cell-free supernatant of Lm (Moslehi-Jenabian et al., 2011). This triggered important effects on the behavior and functionality

of co-existing bacteria. It could be hypothesized that a higher transcription of the gene might affect the adherence of lactobacilli to the substratum positively and competitive exclusion might affect the adherence of Lm. This could largely explain the observations made about Lm-carrying biofilms when Lf was present in the system.

Antimicrobial tolerance resulting from different interspecific interactions and the spatial organization of cells in multi-species biofilms has not been fully elucidated. In our study, a link has been found between microbial interactions and matrix production capacity by cells. This positive effect was the greatest in Lm-carrying biofilms when co-cultured with Lp, with only one exception, i.e., much production did not occur for LmC. This signifies the important stimulating role of a secondary species in a strict strain-dependent manner as well as an essential role of the matrix in providing a favorable habitat for bacteria to co-exist and protect against antimicrobial action.

In our disinfection experiment, we used chlorine due to its broad-spectrum bactericidal activity, which is recommended to be used at a concentration of at least 50 ppm to achieve a safe and effective sanitizing effect. Limited reports have been published on the hypochlorite resistance of Lm in a mixed-species biofilm, nor comparison with results of a single species biofilm, making it difficult to judge upon the protection of secondary species over Lm. Previous work on disinfectant resistance of Lm-carrying biofilms showed that it obtained a higher resistance to benzalkonium chloride (BAC) when co-cultured with *P. putida* (Saá Ibusquiza et al., 2012) or *L. plantarum* (Van der Veen and Abee, 2011). In the latter study, both species were more resistant to the disinfection treatments whereas in our study, it was just one of them.

We observed that Lm5 was more resistant to hypochlorite than its single species counterpart while Lp was largely diminished. The Lm5-Lp pair was characterized by a thicker structure with an increased surface area and increased matrix production, in particular, the protein fraction. We could hypothesize that the close association with its partner species, Lp, provided protection toward Lm as well as the elevated protein production created a diffusion barrier to hypochlorite penetration. In addition to physical barrier, the antimicrobial can be inactivated due to chemical interaction with proteins, thus reducing its effect on the underlying cells. The former scenario makes more sense for the Lm 7-Lf pair where Lf reached the greatest cell counts while in co-culture with Lm7, and this pair was also characterized by a high surface-to-volume ratio.

An intimate association between Lm7 and Lf comparable to that of Lm5-Lp indicates that the increased resistance of Lm in the binary biofilm is closely related to the 3-D organization of cells and here, refers to the localization of partner species. Peripheral species may be more susceptible to antimicrobial treatments, and no benefit is provided for the killed species, i.e., Lf. The fact that Lf was significantly increased when with Lm and reduced after the treatment suggests the shielding effect of Lf toward privileged Lm in the biofilm.

Another species that provided protection for Lm5 was Lb and this association resulted in an abundant protein production. Given that Lm5 was overgrown by Lb like any other Lm strain,

a key role here may be played by still the favorable localization of Lm and the reaction-diffusion limitation of the protein matrix. Of note, Lm7 when co-cultured with Lb, which revealed confluent growth areas where bacteria formed clumps separated from each other, was not more tolerant to hypochlorite. This indicates that Lb directly fights Lm7 either by secreting anti-listerial compounds or creating an environment suitable for the emergence of antimicrobial susceptible cells. It again proves that an intimate association leading to a particular organization of cells with a greater surface area confers the privilege to one of the species, Lm. This way, the generation of structural data can enable a clearer understanding of biofilm traits.

CONCLUSION

L. monocytogenes exhibits co-dependence with other bacteria that may help avoid the removal or inactivation by disinfectants in food processing environments. We argued that the cohabitation with *Lactobacillus* spp. may result in an increased survival against hypochlorite. Most importantly, the intimate association related to the certain spatial organization of cells and matrix production rich in protein fraction may explain the protective effect of *Lactobacillus* over *Listeria*. Thus, this study contributes to a better understanding of the behavior of this pathogen and it may help to inform better strategies for the use of antimicrobial treatments against *Listeria* biofilms. Obtained results also highlight that to improve disinfection, it is crucial to further characterize those bacterial associations that occur in nature. Yet, a special focus on the spatial organization of cells within multi-species biofilms may help reveal the molecular mechanisms underlying the interspecies interactions.

MATERIALS AND METHODS

Bacterial Strains, Media, and Preparation of Inoculum

Bacterial strains used in this study are listed in **Tables 1, 2**. They include 27 *L. monocytogenes* strains and 10 *Lactobacillus* spp. isolated from different origins and stored in the collection of the Center for Food Safety, University of Georgia, United States. Before use, *Listeria* strains were resuscitated from -80°C stocks in a tryptic soy broth (TSB; Difco Laboratories, Sparks, MD, United States) and incubated for 24 h at 34°C . *Lactobacilli* strains were transferred to De Man, Rogosa, and Sharpe broth (MRS; Acumedia, Lansing, MI) and incubated for 24 h anaerobically at 30°C . Anaerobic conditions were obtained by incubating the cultures inside sealed jars containing anaerobic atmosphere packs (MitsubishiTM AnaeroPack, Thermo Fisher, Waltham, MA). Working cultures were prepared by adding 100 μL of each pre-culture to 10 mL of TSB or MRS broths and incubating at 34°C or 30°C for 18 h and, finally, diluting it down in 0.1% buffered peptone water (BPW; Difco) (ca. 10^6 CFU mL^{-1}), in order to be used as the inoculum for the biofilm development assays. For the binary culture conditions, the inocula of *L. monocytogenes* and *Lactobacillus* spp. (1:1) were mixed so that a cocktail was used.

Screening Biofilm Formation

To select the best biofilm producers, the biofilm formation of 37 strains altogether was evaluated with a crystal violet assay. Different oxygen requirements for *Listeria* and lactobacilli were used when biofilms were grown under aerobic and anaerobic incubation conditions. Aliquots (200 μL) of each bacterial suspension (in BPW) were transferred into wells of 96-well polystyrene (PS) microtiter plates (Costar, Corning, NY) and plates were incubated for 3 h at 34°C , under static conditions. Subsequently, the liquid cultures were removed with a pipette and each well was washed twice with BPW to remove unattached cells. Volumes of 200 μL of the TSB or MRS were added, and plates were incubated in an aerobic atmosphere and the added vent or inside of sealed jars containing anaerobic atmosphere packs (MitsubishiTM AnaeroPack, Thermo Fisher, Waltham, MA) for 24 h at 34°C under static conditions. Liquid cultures were once again removed and each well was washed with BPW. For biofilm fixation, 200 μL of ethanol ($\geq 99.5\%$, v/v) were loaded. After 15 min, ethanol was pipetted and plates were air-dried. Subsequently, 200 μL of 1% (wt/vol) crystal violet solution (Sigma-Aldrich, St. Louis, MO, United States) were added to each well, and plates were incubated for 15 min at room temperature. After washing with water, the plates were dried and the wells were loaded with 200 μL of acetic acid 33% (v/v) (Merck) to release and dissolve the stain. Absorbance was read using a CytationTM 3 imaging reader (BioTek Instruments, Inc. Winooski, VT, United States) at 570 nm. The experiment included up to four replicate wells and was repeated three times. Optical density (ODs) readings were measured and compared with the cut-off OD (OD_c), which was described as three standard deviations above the mean OD of the negative controls containing only media. For the interpretation, the following classifications were used: no biofilm producers ($\text{OD} \leq \text{OD}_c$), weak biofilm producers ($\text{OD}_c < \text{OD} \leq 2 \times \text{OD}_c$), moderate biofilm producers ($2 \times \text{OD}_c < \text{OD} \leq 4 \times \text{OD}_c$), and strong biofilm producers ($4 \times \text{OD}_c < \text{OD}$) (Stepanović et al., 2000).

Biofilm Growth and Chlorine Treatment

The bacterial growth of the best biofilm producers of *L. monocytogenes* strains (3) and *Lactobacillus* species (3) on PS microtiter plates under mono and binary culture conditions was evaluated by using the drop plate (DP) method. All six strains were selected for assessing the chlorine effect. The biofilms on PS microtiter plates were first grown as described in the previous section. We used brain heart infusion (BHI; Neogen, Lansing, MI, United States) broth for the co-cultures and supplemented it with 0.005% manganese sulfate (MnSO_4 ; Merck) to meet the high Mn requirements of *L. plantarum* for growth (Van der Veen and Abee, 2011). After growth, liquid cultures were removed and wells were washed with BPW to obtain mature biofilms. Wells receiving in-well treatments were added with 200 μL of sodium hypochlorite solution (Fisher Scientific) at 50 ppm and incubated for 1 min. After this time, solutions were removed, incubated for 5 min with a Dey/Engley (D/E) neutralizing broth (Becton Dickinson, Sparks, MD, United States) to neutralize the residual

chlorine solution, and replaced with BPW. After that, biofilms were scraped from the wells with a pipette tip (three times for periods of 1 min each) and resuspended in BPW (Borges et al., 2017). Biofilm viable counts were measured by standard dilution, plating on Oxford-agar (Oxoid, Lenexa, KS, United States) and MRS-agar, and incubating for 24 and 48 h at 34 and 30°C under aerobic and anaerobic conditions, respectively. The impact of chlorine on cell viability was expressed as the logarithmic value of a relative survivor fraction ($\log N \text{ No}^{-1}$), where N refers to the bacterial count following treatments and No refers to the bacterial count avoiding chlorine exposure. The experiment included three replicate wells and was repeated at least three times using independent bacterial cultures.

Biofilm Growth in Chamber Slides and Fluorescent Labeling

As described above, the inoculum of the best biofilm producers under mono and binary culture conditions was added to 8-well chamber slides (Nunc™ II; Lab-Tek™; Fisher Scientific) at 400 μL per well and let to attach at 34°C for 3 h and then to form biofilms at 34°C for 24 h under aerobic conditions. Each experiment included two replicate chambers and was repeated three times using independent bacterial cultures. After this, the chambers were rinsed with NaCl (8.5 g L^{-1}) and refilled with NaCl containing 5 μM Syto®9 (1:1,000 dilution from a Syto®9 stock solution of the LIVE/DEAD BacLight™ viability kit, Molecular Probes, LifeTechnologies, Eugene, OR), a cell-permeant green fluorescent DNA label. The slide was then incubated in the dark at room temperature for 30 min to enable the fluorescent labeling of the bacteria. Separately (using different chambers), we performed double staining with FITC-WGA (for exopolysaccharide) and SYPRO® Ruby (for proteins). First, FITC-WGA (Sigma-Aldrich) (10 $\mu\text{g mL}^{-1}$) was applied and incubated in the dark at room temperature for 1.5 h. The solution was then removed and the chambers were washed three times with PBS (0.1 M; Sigma-Aldrich). After that, the undiluted FilmTracer™ SYPRO® Ruby Biofilm Matrix Stain (Invitrogen, Carlsbad, CA, United States) was applied and incubated in the dark at room temperature for 30 min. The solution was then removed and the chambers were washed three times with PBS (200 μL each time).

Confocal Laser Scanning Microscopy (CLSM)

Prior to image acquisition, the plastic chambers were removed from the glass slides and the NaCl solution was applied to the biofilms separated from each other with a gasket. Coverslips were then placed on the gaskets and BacLight™ mounting oil (Molecular Probes) was used to seal their corners, and finally, nail polish was applied to seal the slides. The slides were left overnight at 4°C and observed the day after. Images were acquired with a Zeiss LSM 700 confocal laser scanning microscope (Carl Zeiss Microscopy, Thornwood, NY, United States). All biofilms were scanned using a water-immersion objective lens (Zeiss, 40 \times C Pan-Apochromat, NA 1.3) with a 488-nm argon laser and a 561-nm diode-pumped solid-state laser. The fluorescence was

recorded within the range from 500 to 600 nm to collect green fluorescence and from 610 to 710 nm to collect red fluorescence. Up to ten stacks of horizontal plane images (260 \times 260 μm) with a z-step of 0.4 μm were acquired for each chamber in its different areas. Serial images were captured and processed by the Zeiss Zen 2.3 software (Carl Zeiss).

Image Analysis

Quantitative structural parameters (biomass, biovolume, maximum thickness, average thickness, roughness coefficient, surface to volume ratio (SVR), number of colonies at the substratum, and average colony size at the substratum) were extracted from confocal image series with COMSTAT 2, an image analysis software¹ (Heydorn et al., 2000; Vorregaard, 2008). Following preliminary analyses, to describe the biofilms under study, we proceeded with the SVR, roughness, and maximum thickness for biofilm architecture and biomass for matrix localization studies.

Statistical Analysis

All statistical analyses [Principal Component Analysis (PCA), analysis of variance—one-way ANOVA, followed by HSD *post hoc* test] were performed using the Statistica software ver. 13.1 (StatSoft Inc., Tulsa, OK). Differences were considered significant at a $p < 0.05$ level of probability.

DATA AVAILABILITY STATEMENT

The original contributions presented in the study are included in the article/**Supplementary Material**, further inquiries can be directed to the corresponding author.

AUTHOR CONTRIBUTIONS

MO designed the study, performed the experimental work, analyzed the data, and drafted the manuscript. FD-G revised the manuscript. Both authors contributed to the interpretation of the results, reviewed, and approved the final version of the manuscript.

FUNDING

MO was supported by a Fulbright Senior Award sponsored jointly by the Polish Ministry of Education and Science and the United States Department of State and administered by the Polish-United States Fulbright Commission and the Institute of International Education.

SUPPLEMENTARY MATERIAL

The Supplementary Material for this article can be found online at: <https://www.frontiersin.org/articles/10.3389/fmicb.2021.638933/full#supplementary-material>

¹www.comstat.dk

REFERENCES

- Alonso, A. N., Perry, K. J., Regeimbal, J. M., Regan, P. M., and Higgins, D. E. (2014). Identification of *Listeria monocytogenes* determinants required for biofilm formation. *PLoS One* 9, 1–16. doi: 10.1371/journal.pone.0113696
- Alonso, V. P. P., Harada, A. M. M., and Kabuki, D. Y. (2020). Competitive and/or Cooperative Interactions of *Listeria monocytogenes* With *Bacillus cereus* in Dual-Species Biofilm Formation. *Front. Microbiol.* 11, 1–10. doi: 10.3389/fmicb.2020.00177
- Azeredo, J., Azevedo, N. F., Briandet, R., Cerca, N., Coenye, T., Costa, A. R., et al. (2017). Critical review on biofilm methods. *Crit. Rev. Microbiol.* 43, 313–351. doi: 10.1080/1040841X.2016.1208146
- Borges, A., Lopez-Romero, J. C., Oliveira, D., Giaouris, E., and Simões, M. (2017). Prevention, removal and inactivation of *Escherichia coli* and *Staphylococcus aureus* biofilms using selected monoterpenes of essential oils. *J. Appl. Microbiol.* 123, 104–115. doi: 10.1111/jam.13490
- Borucki, M. K., Peppin, J. D., White, D., Loge, F., and Call, D. R. (2003). Variation in Biofilm Formation among Strains of. *Society* 69, 7336–7342. doi: 10.1128/AEM.69.12.7336
- Bridier, A., Dubois-Brissonnet, F., Boubetra, A., Thomas, V., and Briandet, R. (2010). The biofilm architecture of sixty opportunistic pathogens deciphered using a high throughput CLSM method. *J. Microbiol. Methods* 82, 64–70. doi: 10.1016/j.mimet.2010.04.006
- Carpentier, B., and Chassaing, D. (2004). Interactions in biofilms between *Listeria monocytogenes* and resident microorganisms from food industry premises. *Int. J. Food Microbiol.* 97, 111–122. doi: 10.1016/j.ijfoodmicro.2004.03.031
- Chen, P., Wang, J. J., Hong, B., Tan, L., Yan, J., Zhang, Z., et al. (2019). Characterization of Mixed-Species Biofilm Formed by *Vibrio parahaemolyticus* and *Listeria monocytogenes*. *Front. Microbiol.* 10, 1–15. doi: 10.3389/fmicb.2019.02543
- Donlan, R. M. (2002). Biofilms: Microbial life on surfaces. *Emerg. Infect. Dis.* 8, 881–890. doi: 10.3201/eid0809.020063
- Guilbaud, M., Piveteau, P., Desvaux, M., Brisse, S., and Briandet, R. (2015). Exploring the diversity of *Listeria monocytogenes* biofilm architecture by high-throughput confocal laser scanning microscopy and the predominance of the honeycomb-like morphotype. *Appl. Environ. Microbiol.* 81, 1813–1819. doi: 10.1128/AEM.03173-14
- Heredia, N., and García, S. (2018). Animals as sources of food-borne pathogens: A review. *Anim. Nutr.* 4, 250–255. doi: 10.1016/j.aninu.2018.04.006
- Heydorn, A., Nielsen, A. T., Hentzer, M., Sternberg, C., Givskov, M., Ersboll, B. K., et al. (2000). Quantification of biofilm structures by the novel computer program COMSTAT. *Microbiology* 146, 2395–2407. doi: 10.1099/00221287-146-10-2395
- Kim, J., Pitts, B., Stewart, P. S., Camper, A., and Yoon, J. (2008). Comparison of the antimicrobial effects of chlorine, silver ion, and tobramycin on biofilm. *Antimicrob. Agents Chemother.* 52, 1446–1453. doi: 10.1128/AAC.00054-07
- Kim, S. K., and Lee, J. H. (2016). Biofilm dispersion in *Pseudomonas aeruginosa*. *J. Microbiol.* 54, 71–85. doi: 10.1007/s12275-016-5528-7
- Kostaki, M., Chorianopoulos, N., Braxou, E., Nychas, G. J., and Giaouris, E. (2012). Differential biofilm formation and chemical disinfection resistance of sessile cells of *Listeria monocytogenes* strains under monospecies and dual-species (with *Salmonella enterica*) conditions. *Appl. Environ. Microbiol.* 78, 2586–2595. doi: 10.1128/AEM.07099-11
- Liu, W., Røder, H. L., Madsen, J. S., Bjarnsholt, T., Sørensen, S. J., and Burmølle, M. (2016). Interspecific bacterial interactions are reflected in multispecies biofilm spatial organization. *Front. Microbiol.* 7, 1–8. doi: 10.3389/fmicb.2016.01366
- Moslehi-Jenabian, S., Vogensen, F. K., and Jespersen, L. (2011). The quorum sensing luxS gene is induced in *Lactobacillus acidophilus* NCFM in response to *Listeria monocytogenes*. *Int. J. Food Microbiol.* 149, 269–273. doi: 10.1016/j.ijfoodmicro.2011.06.011
- Nie, M., Nie, H., He, M., Lin, Y., Wang, L., Jin, P., et al. (2016). Immobilization of biofilms of *Pseudomonas aeruginosa* NY3 and their application in the removal of hydrocarbons from highly concentrated oil-containing wastewater on the laboratory scale. *J. Environ. Manage.* 173, 34–40. doi: 10.1016/j.jenvman.2016.02.045
- Nowak, J., Cruz, C. D., Tempelaars, M., Abee, T., van Vliet, A. H. M., Fletcher, G. C., et al. (2017). Persistent *Listeria monocytogenes* strains isolated from mussel production facilities form more biofilm but are not linked to specific genetic markers. *Int. J. Food Microbiol.* 256, 45–53. doi: 10.1016/j.ijfoodmicro.2017.05.024
- O'Toole, G., Kaplan, H. B., and Kolter, R. (2000). Biofilm formation as microbial development. *Annu. Rev. Microbiol.* 54, 49–79. doi: 10.1146/annurev.micro.54.1.49
- Pérez-Ibarreche, M., Castellano, P., Leclercq, A., and Vignolo, G. (2016). Control of *Listeria monocytogenes* biofilms on industrial surfaces by the bacteriocin-producing *Lactobacillus sakei* CRL1862. *FEMS Microbiol. Lett.* 363, 1–6. doi: 10.1093/femsle/fnw118
- Pilchová, T., Hernould, M., Prévost, H., Demnerová, K., Pazlarová, J., and Tresse, O. (2014). Influence of food processing environments on structure initiation of static biofilm of *Listeria monocytogenes*. *Food Control* 35, 366–372. doi: 10.1016/j.foodcont.2013.07.021
- Renier, S., Chagnot, C., Deschamps, J., Caccia, N., Szlavik, J., Joyce, S. A., et al. (2014). Inactivation of the SecA2 protein export pathway in *Listeria monocytogenes* promotes cell aggregation, impacts biofilm architecture and induces biofilm formation in environmental condition. *Environ. Microbiol.* 16, 1176–1192. doi: 10.1111/1462-2920.12257
- Rieu, A., Lemaître, J. P., Guzzo, J., and Piveteau, P. (2008). Interactions in dual species biofilms between *Listeria monocytogenes* EGD-e and several strains of *Staphylococcus aureus*. *Int. J. Food Microbiol.* 126, 76–82. doi: 10.1016/j.ijfoodmicro.2008.05.006
- Rodríguez-Campos, D., Rodríguez-Melcón, C., Alonso-Calleja, C., and Capita, R. (2019). Persistent *Listeria monocytogenes* isolates from a poultry-processing facility form more biofilm but do not have a greater resistance to disinfectants than sporadic strains. *Pathogens* 8:8040250. doi: 10.3390/pathogens8040250
- Rutherford, S. T., and Bassler, B. L. (2012). Bacterial quorum sensing: Its role in virulence and possibilities for its control. *Cold Spring Harb. Perspect. Med.* 2, 1–25. doi: 10.1101/cshperspect.a012427
- Ryu, J. H., and Beuchat, L. R. (2005). Biofilm formation and sporulation by *Bacillus cereus* on a stainless steel surface and subsequent resistance of vegetative cells and spores to chlorine, chlorine dioxide, and a peroxyacetic acid-based sanitizer. *J. Food Prot.* 68, 2614–2622. doi: 10.4315/0362-028X-68.12.2614
- Saá Ibusquiza, P., Herrera, J. J. R., Vázquez-Sánchez, D., and Cabo, M. L. (2012). Adherence kinetics, resistance to benzalkonium chloride and microscopic analysis of mixed biofilms formed by *Listeria monocytogenes* and *Pseudomonas putida*. *Food Control* 25, 202–210. doi: 10.1016/j.foodcont.2011.10.002
- Stepanović, S., Vuković, D., Dakić, I., Savić, B., and Švabić-Vlahović, M. (2000). A modified microtiter-plate test for quantification of staphylococcal biofilm formation. *J. Microbiol. Methods* 40, 175–179. doi: 10.1016/S0167-7012(00)00122-6
- Tan, C. H., Lee, K. W. K., Burmølle, M., Kjelleberg, S., and Rice, S. A. (2017). All together now: experimental multispecies biofilm model systems. *Environ. Microbiol.* 19, 42–53. doi: 10.1111/1462-2920.13594
- Van der Veen, S., and Abee, T. (2011). Mixed species biofilms of *Listeria monocytogenes* and *Lactobacillus plantarum* show enhanced resistance to benzalkonium chloride and peracetic acid. *Int. J. Food Microbiol.* 144, 421–431. doi: 10.1016/j.ijfoodmicro.2010.10.029
- Vorregaard, M. (2008). *Comstat2 - a modern 3D image analysis environment for biofilms*. PhD thesis, Denmark, CA: Technical University of Denmark.
- Yang, L., Liu, Y., Wu, H., Hoiby, N., Molin, S., and Song, Z. J. (2011). Current understanding of multispecies biofilms. *Int. J. Oral Sci.* 3, 74–81. doi: 10.4248/IJOS11027
- Yang, Y., Mikš-Krajnc, M., Zheng, Q., Lee, S. B., Lee, S. C., and Yuk, H. G. (2016). Biofilm formation of *Salmonella* Enteritidis under food-related environmental stress conditions and its subsequent resistance to chlorine treatment. *Food Microbiol.* 54, 98–105. doi: 10.1016/j.fm.2015.10.010
- Zhao, T., Teresa, C. P., Zhao, P., Chen, D., Baker, D. A., Cords, B., et al. (2013). Reduction by competitive bacteria of *Listeria monocytogenes* in biofilms and *Listeria* bacteria in floor drains in a ready-to-eat poultry processing plant. *J. Food Prot.* 76, 601–607. doi: 10.4315/0362-028X.JFP-12-323

Conflict of Interest: The authors declare that the research was conducted in the absence of any commercial or financial relationships that could be construed as a potential conflict of interest.

Copyright © 2021 Olszewska and Diez-Gonzalez. This is an open-access article distributed under the terms of the Creative Commons Attribution License (CC BY). The use, distribution or reproduction in other forums is permitted, provided the original author(s) and the copyright owner(s) are credited and that the original publication in this journal is cited, in accordance with accepted academic practice. No use, distribution or reproduction is permitted which does not comply with these terms.

Advantages of publishing in Frontiers



OPEN ACCESS

Articles are free to read
for greatest visibility
and readership



FAST PUBLICATION

Around 90 days
from submission
to decision



HIGH QUALITY PEER-REVIEW

Rigorous, collaborative,
and constructive
peer-review



TRANSPARENT PEER-REVIEW

Editors and reviewers
acknowledged by name
on published articles

Frontiers

Avenue du Tribunal-Fédéral 34
1005 Lausanne | Switzerland

Visit us: www.frontiersin.org

Contact us: frontiersin.org/about/contact



REPRODUCIBILITY OF RESEARCH

Support open data
and methods to enhance
research reproducibility



DIGITAL PUBLISHING

Articles designed
for optimal readership
across devices



FOLLOW US

@frontiersin



IMPACT METRICS

Advanced article metrics
track visibility across
digital media



EXTENSIVE PROMOTION

Marketing
and promotion
of impactful research



LOOP RESEARCH NETWORK

Our network
increases your
article's readership